

Archean to Early Paleoproterozoic Tectono-Magmatic Evolution of the Western Rae Craton

by

Benjamin Neil

A thesis submitted in partial fulfillment of the requirements for the degree of

Doctor of Philosophy

Department of Earth and Atmospheric Sciences
University of Alberta

© Benjamin Neil, 2024

Abstract

The Rae craton is one of the largest Archean–Paleoproterozoic age terranes on Earth and preserves >1.6 billion years of the planet’s history. However, significant uncertainty remains regarding how and when the crust of this craton was created and reworked. This thesis investigates the nature and evolution of continental crust in the western Rae craton, with a focus on the Nonacho Lake area (“Nonacho area”) of the Northwest Territories. The techniques used in this study include bedrock mapping, whole-rock geochemical and isotopic analyses, and accessory mineral trace-element and isotopic analyses.

Granitoid and orthogneiss rocks (“granitoids”) with zircon U-Pb dates >3.0 Ga and whole-rock Sm-Nd depleted mantle model ages ≥ 3.2 Ga are shown to be widely distributed throughout the western Rae craton. They define a large (~1000 x 100 km) basement block referred to herein as the Perry River terrane (PRT). The PRT primarily comprises 3.3–3.1 Ga sodic tonalites and granodiorites that have chondritic to suprachondritic zircon initial ϵ_{Hf} (ϵ_{Hf_i}) values and mantle-like zircon oxygen isotope compositions. These granitoids were derived from partial melting of mantle-derived basaltic rocks that had resided in the crust for a relatively short period of time, potentially at the base of a magmatic arc. The 3.3–3.1 Ga PRT granitoids appear to reflect a global period of enhanced continental growth. The juvenile nature of most 3.3–3.1 Ga granitoids worldwide argues that only small amounts of older continental crust were present, and thus available for magmatic reworking, on Earth at that time. This observation is at odds with models that suggest large volumes of continental crust were established on the early (>3.5 Ga) Earth.

The Nonacho area basement comprises variably deformed and heterogeneous granitoids, and rare metasedimentary rocks. Zircon U-Pb geochronology documents at least seven episodes of granitoid magmatism in the Nonacho area, at: ca. 3.25, 2.78, 2.71–2.68, 2.58–2.57, 2.52–2.48, 2.43–2.38 and 2.32–2.31 Ga. Zircon and monazite U-Pb age and trace-element data show that the protoliths to the metasedimentary rocks were deposited after ~2.52 Ga and underwent high-grade metamorphism/migmatization during the Arrowsmith orogeny at ~2.38 Ga. Geochemical and isotopic

data indicate that the granitoids emplaced prior to ~2.45 Ga primarily represent juvenile crustal additions, whereas those emplaced after ~2.45 Ga reflect reworking of older (Archean) continental crust.

The geochemical and petrogenetic characteristics of the ca. 2.52–2.48 (2.5), 2.43–2.38 (2.4) and 2.32–2.31 (2.3) Ga granitoids from the Nonacho area were studied in detail. The 2.5 Ga granitoids range from mafic to felsic, comprise a high-K calc-alkaline series, are light rare earth element (LREE)-enriched and have “subduction-like” trace-element patterns. They also yield consistently chondritic whole-rock initial ϵNd (ϵNd_i) and near-chondritic zircon ϵHf_i values. The homogeneous chondritic isotopic compositions suggest that all components of the suite (mafic to felsic) represent, at least in part, juvenile crustal additions. The mafic 2.5 Ga magmas are interpreted to have derived from a subduction-enriched lithospheric mantle source. Geochemical comparisons with possible Phanerozoic-age analogues suggest that the 2.5 Ga granitoids were emplaced in a post-collisional setting, potentially associated with the accretion of the PRT to the Rae craton.

Both the ca. 2.43–2.38 and 2.32–2.31 Ga granitoid suites are characterized by >69 wt.% SiO_2 and negative ϵNd_i values (-1 to -11). The former are strongly heavy rare earth element (HREE)-depleted, characterized by steeply-sloping REE patterns and in some cases contain abundant inherited zircon. The latter have comparatively shallow-sloping REE patterns, are strongly LREE-, Th- and Zr-enriched, contain little-to-no inherited zircon, and yield relatively high zircon saturation and Ti-in-zircon temperatures. The 2.4 Ga granitoids are interpreted to reflect crustal thickening and partial melting of garnet-bearing rocks in the mid- to lower-crust during the collisional phase of the 2.4–2.3 Ga Arrowsmith orogeny. The 2.3 Ga granites are interpreted to reflect high-temperature partial melting of tonalitic/granodioritic rocks at relatively shallow levels, associated with post-orogenic extension and the intrusion of hot mantle-derived magmas. Geochemically analogous Phanerozoic or Paleoproterozoic granitoids from orogenic and post-orogenic settings are identified for all three of the 2.5–2.3 Ga granitoid suites, which is consistent with the operation of “modern-style” plate tectonics by at least the end of the Archean.

Preface

This thesis contains four manuscripts based on the author's (B. Neil) Ph.D research, which was conducted under the supervision of Drs. Tom Chacko and Larry M. Heaman. The project was designed by B. Neil, T. Chacko, L.M. Heaman and Edith Martel. Bedrock sampling and mapping was completed by B. Neil, E. Martel, Rebecca Canam, T. Chacko and L.M. Heaman. Field assistance was provided by Laurén Langlois, Kerstin Landry, Andree Roy-Garand and Gordon Cumming. The author collected, or was present for the collection of, the majority of the samples used in the research. Additional samples were provided by the University of Alberta (Dan Tersmette's MSc thesis collection) and the Geological Survey of Canada (collections of Bruce A. Kjarsgaard, Subhas Tella, Vicki J. McNicoll and John B. Henderson). Field work was facilitated by the Northwest Territories Geological Survey (NTGS). Funding was provided by the NTGS, the Polar Continental Shelf Program, and by Natural Sciences and Engineering Research Council Discovery grants to T. Chacko and L.M. Heaman. The author received financial support from the George and Eva Cumming Memorial, Christopher Scarfe Memorial, Steve and Elaine Antoniuk, and Alberta Graduate Excellence Scholarships.

Samples were prepared (whole-rock powders, mineral separates and grain mounts) for analyses by the author, with assistance from James Leblanc, Robert Fuchs, Dr. Andy Dufrane, Robert Dokken and Thomasina Kastendieck. LA-ICPMS data were collected by B. Neil, Dr. Andy Dufrane and Dr. Yan Luo. Electron microprobe data were collected by B. Neil and Dr. Andrew Locock. Whole-Rock Sm-Nd isotope data were acquired by Dr. Robert Creaser, Krystle Moore and Dr. Andy Dufrane. The author completed the Sm-Nd chemistry for some samples. SIMS zircon oxygen isotope data were acquired by Dr. Richard Stern with assistance from B. Neil. Whole-rock powders were sent to external laboratories (Activation Laboratories Ltd., Peter Hooper GeoAnalytical Lab – Washington State University, Dr. Stan Mertzman's lab – Franklin and Marshall College) for major- and trace-element analyses. The writing, figures and ideas presented in this thesis are the original work of the author. The final product has, however, been refined through discussions with, and edits from, supervisors and collaborators.

An earlier version of Chapter 2 was published in *Geology* as: Neil, B.J.C., Tersmette, D.B., Chacko, T., Heaman, L.M., Kjarsgaard, B.A., Martel, E., Creaser, R.A., Pearson, D.G., Stern, R.A., Dufrane, S.A., and Luo, Y., 2023. *Discovery of a giant 3.3–3.1 Ga terrane in the Rae craton, Canada: Implications for the timing and extent of ancient continental growth*, *Geology*, 51, 597–601. All authors were involved in sample collection, data collection, data interpretation and manuscript revision. B. Neil was responsible for writing the initial manuscript draft and making revisions.

Some zircon crystals were harmed in the making of this thesis.

Acknowledgements

I would like to express my sincere gratitude to my supervisors Tom Chacko and Larry Heaman, and my unofficial supervisor Edith Martel. Tom, Larry and Edith are responsible for initiating this project and for securing the necessary funds. They never refused me a moment of their time, listened carefully to my ideas, provided quick and sound feedback, and always employed a “student first” mentality that prioritized my goals above their own. I cannot imagine a better team of supervisors and role models. Tom, thanks for your open-door policy, for enduring our sometimes daily discussions (and my rants) and for pushing me to dig a bit deeper when I didn’t want to. When faced with the stickier aspects of academic life I, probably like many students before me, often ask “what would Chacko do?”. Larry, thanks for giving me confidence in my data and interpretations, for reminding me to look at the bigger picture and for your words of encouragement near the end when they were needed most. Edith, thanks for showing me how to do field work in the NWT, for keeping it fun and for suggesting calf implants – I think they look great.

Thank you to all of those involved in the Nonacho Lake project for great company in and out of the field. Thanks to Becca Canam for discussions on the Rae craton and future research plans, for helping to make sure my field camps didn’t end in disaster and for packing my entire camp during COVID. Thanks to my field assistants Laurén Langlois, Kerstin Landry, Andree Roy-Garand and Gordon Cumming for taking part in some type-2 and -3 fun, and for doing the best with my unclear instructions.

I am extremely grateful for the committed Staff and Faculty in the U. Alberta EAS department. Graham Pearson provided sound advice as a member of my supervisory committee, offered full access to his labs and waited patiently for me to finish this thesis. Robert Creaser oversaw the Sm-Nd isotopic analysis of ~100 samples and took his own time to show me the technique. Andy Dufrane endured many long days and nights of ablating zircons, didn’t get annoyed when I pestered him for more instrument time, gave advice on uncertainty propagation, and (re)explained details of mass spectrometry that may or may not have been retained. A special thanks to Andy for keeping the Nu Plasma MC-ICPMS, the workhorse of this thesis, in smooth operating condition. Andrew Locock facilitated efficient EPMA data acquisition, and made special efforts for the zircon U-Hf-Ca and monazite U-Th-Pb analyses. Yan Luo facilitated efficient collection of zircon trace-element and Hf isotope data. Richard Stern and Robert Dokken facilitated efficient collection of zircon O isotope data. Mark Labbe prepared countless thin-sections on short notice and kept all rock cutting/crushing equipment in top shape. Marilyn Huff made my job as a TA easy.

Thank you to Drs. Jonathan O’Neil and Chris Herd for examining this work.

Thank you to the families of George Cumming, Christopher Scarfe and Steve Antoniuk for their generous donations in the form of EAS student scholarships.

This would not have been possible without the support of my family. Thank you to my parents (Mary Collyer and John Neil), who worked extremely hard so that I could pursue my interests and have been my biggest supporters every step of the way. Thank you to my sister (Kate Neil) for the encouragement and comedic relief. Thank you to my dog-sister (Nerys) for being a source of joy and distraction, even when she is in a huff. Finally, my greatest thanks to my partner (Erin Macdonald) for your love, support and sacrifice, for putting up with my strange/long work hours and time away from home, and for listening to talk about the Rae craton and rants about Academia.

Table of Contents

Abstract	II
Preface	IV
Acknowledgements	V
Chapter 1: Introduction	1
1.1 Motivation.....	1
1.2 The Rae craton	2
1.3 Thesis objectives and outline	3
Chapter 2: Discovery of a giant 3.3–3.1 Ga terrane in the Rae craton, Canada: Implications for the timing and extent of ancient continental growth	6
2.1 Introduction	6
2.2 Geological context	7
2.3 Extent of ancient crust in the western Rae craton.....	9
2.4 Nature and origin of the Perry River terrane	10
2.5 Possible geodynamic setting	11
2.6 Implications for ancient continental growth	14
Chapter 3: 2.5 Ga high-K calc-alkaline granitoids of the Rae craton, Canada: Latest Archean continental growth in a post-collisional setting	18
3.1 Introduction	18
3.2 Geological Context	21
3.3 Local geology and current study.....	22
3.3.1 Map units	25
3.4 Samples and Methods	29
3.5 Results	32
3.5.1 Zircon U-Pb geochronology	32
3.5.2 Whole-rock geochemistry.....	37
3.5.2.1 2.7 Ga granitoids.....	39
3.5.2.2 2.6 Ga granitoids.....	39
3.5.2.3 2.5 Ga granitoids.....	42
3.5.3 Isotope geochemistry	45
3.5.3.1 Whole-rock Sm-Nd isotope data.....	45
3.5.3.2 Zircon Lu-Hf isotope results data.....	45

3.6 Discussion.....	47
3.6.1 Granitoid classification	47
3.6.2 Petrogenesis of the 2.7 and 2.6 Ga granitoids	49
3.6.3 Petrogenesis of the 2.5 Ga granitoids.....	50
3.6.3.1 Geochemical constraints on mantle source.....	50
3.6.3.2 Isotopic constraints on mantle source	53
3.6.3.3 Mantle metasomatism and metasomatic agents	56
3.6.3.4 Differentiation and involvement of older continental crust.....	57
3.6.4 Tectonic setting of the 2.5 Ga granitoids.....	59
3.6.5 Conclusions and broader implications	63
Chapter 4: 2.53–2.38 Ga metasedimentary rocks in the Nonacho Lake area, Rae craton, Canada: Regional correlations and tectonic implications	65
4.1 Introduction	65
4.2 Rock types: description and interpretation	68
4.3 Zircon and monazite data: methods and results	71
4.3.1 LA-ICPMS zircon U-Pb age and trace-element data	71
4.3.2 LA-ICPMS monazite U-Pb age data	76
4.3.3 Electron microprobe monazite U-Th-Pb _{total} age data	76
4.4 Discussion.....	79
4.4.1 Age of metamorphism and migmatization.....	79
4.4.2 Depositional age of the sedimentary protoliths	80
4.4.3 Detrital zircon provenance	80
4.4.4 Regional correlation	80
4.4.5 Tectonic implications	82
Chapter 5: 2.4–2.3 Ga granitic magmatism of the southwestern Rae craton: Modern-style collisional orogenesis in the earliest Paleoproterozoic	84
5.1 Introduction	84
5.2 Geological context	87
5.3 Local geology and samples	88
5.3.1 Leucogranitoids	92
5.3.2 Biotite granites.....	93
5.3.3 Migmatitic mafic gneiss: garnet-leucosome	93
5.4 Analytical methods.....	96
5.5 Zircon U-Pb age and trace-element data	97

5.5.1 Leucotondhjemite.....	97
5.5.2 Two-mica leucogranite	98
5.5.3 Pink leucogranite.....	98
5.5.4 Biotite granites.....	99
5.5.5 Migmatitic mafic gneiss: garnet-leucosome	100
5.6 Whole-rock geochemical and isotopic data.....	104
5.7 Discussion.....	110
5.7.1 Granitoid petrogenesis	110
5.7.2 The North Shore granites revisited	113
5.7.3 Tectonic implications	114
5.7.4 Extent of crustal shortening during the Arrowsmith orogeny	117
5.7.5 A late Paleoproterozoic analogue: The Trans-Hudson orogen.....	118
Chapter 6: Summary and Conclusions.....	121
6.1 Chapter 2	121
6.2 Chapter 3	122
6.3 Chapter 4	123
6.4 Chapter 5	124
6.5 Overall conclusions.....	125
References	127
References for chapters 1–6 and appendices A–E:	127
Appendix A: Analytical methods and data verification results.....	165
Appendix B: Supporting information for chapter 2	211
Appendix C: Supporting information for chapter 3	271
Appendix D: Supporting information for chapter 4	313
Appendix E: Supporting information for chapter 5	331

List of Figures

Chapter 1

Figure 1-1. Simplified tectonic domain map of the Canadian Shield. Shows the location of the Nonacho lake area, and the location of >3 Ga and 2.5–2.3 Ga plutonic rocks in the western Rae craton.5

Chapter 2

Figure 2-1. Simplified geology, and aeromagnetic anomaly map, of the Rae craton and surrounding cratons/terranes. Maps are overlain by compilations of Sm-Nd depleted mantle model ages and igneous rocks with U-Pb zircon crystallization ages >3.0 Ga.....8

Figure 2-2. Whole-rock geochemical and zircon O isotope data for 3.3–3.1 Ga Perry River terrane granitoids..... 13

Figure 2-3. Zircon Hf isotope composition of 3.3–3.1 Ga Perry River terrane granitoids, and 3.5–3.0 Ga igneous rocks globally..... 17

Chapter 3

Figure 3-1. Simplified geology of the Rae craton and surrounding cratons/terranes. A cut-out of the Rae craton is overlain by a compilation of U-Pb zircon crystallization ages for 2.74–2.46 Ga igneous rocks.....20

Figure 3-2. Aeromagnetic anomaly and geology maps of the Nonacho Lake area, with sample locations indicated.....24

Figure 3-3. Representative outcrop photos of 2.7–2.5 Ga granitoids in the Nonacho Lake area..28

Figure 3-4. LA-ICPMS zircon U-Pb isotope data for 2.7–2.5 Ga granitoids for 2.7–2.5 Ga granitoids in the Nonacho lake area.....34

Figure 3-5. Standard granitoid geochemical classification plots for 2.7–2.5 Ga granitoids in the Nonacho lake area.....38

Figure 3-6. Major element Harker variation diagrams for 2.7–2.5 Ga granitoids in the Nonacho lake area.....40

Figure 3-7. Primitive mantle normalized trace-element plots and chondrite normalized rare earth element plots for 2.7–2.5 Ga granitoids in the Nonacho lake area.41

Figure 3-8. Harker variation diagrams for select trace elements (ppm) and trace element ratios for 2.7–2.5 Ga granitoids in the Nonacho lake area.44

Figure 3-9. Whole-rock Nd and zircon Hf isotope data for 2.7–2.5 Ga granitoids in the Nonacho lake area.....	46
Figure 3-10. Trace-element modelling plots, constraining the origin of the most primitive mantle-derived 2.5 Ga granitoids.....	52
Figure 3-11. SiO ₂ wt.% vs. εNd _i and εHf _i values for 2.5 Ga granitoids. Assimilation fractional crystallization models constraining the isotopic systematics of the 2.5 Ga granitoids.....	55
Figure 3-12. Summary tectono-magmatic discrimination plots for the 2.5 Ga granitoids.....	61
Figure 3-13. Tectonic cartoon illustrating the possibility tectonic setting of ca. 2.5 Ga magmatism in the western Rae craton.....	63
Chapter 4	
Figure 4-1. Simplified geology of the Rae craton and surrounding cratons/terrane. Inset aeromagnetic anomaly map of the Nonacho Lake area with sample locations indicated.....	68
Figure 4-2. Representative outcrop photographs of the migmatitic quartzofeldspathic (metasedimentary) gneiss, and cross-cutting two-mica leucogranite dyke, in the Nonacho Lake area.....	70
Figure 4-3. LA-ICPMS Zircon U-Pb age and trace element (TE) data for two samples of the migmatitic quartzofeldspathic gneiss samples.....	74
Figure 4-4. LA-ICPMS monazite U-Pb isotope data, and electron microprobe monazite chemical U-Th-Pb(total) age data, for samples of the quartzofeldspathic gneiss and the cross-cutting two-mica leucogranite dyke.....	78
Figure 4-5. Zircon age spectra (Kernel density estimate plots) for the quartzofeldspathic gneiss in the Nonacho Lake area, and broadly broadly correlative metasedimentary rocks on Boothia Peninsula and in the Queen Maud block.....	82
Chapter 5	
Figure 5-1. Tectonic domain map of the western Canadian Shield modified. Map is overlain by a compilation of igneous rocks with 2.4–2.3 Ga crystallization ages.....	86
Figure 5-2. Aeromagnetic anomaly map and geology map of the Nonachoa Lake area, with sample locations indicated.....	90
Figure 5-3. Representative outcrop photographs of ca. 2.43–2.38 Ga leucogranitoids in the Nonacho Lake area.....	94

Figure 5-4. Representative outcrop photos of the ca. 2.32–2.31 Ga biotite granites and the migmatitic mafic gneiss (including ca. 2.38 Ga garnet-bearing leucosome) in the Nonacho Lake area.	95
Figure 5-5. Representative backscattered electron images of zircon grains from 2.4–2.3 Ga granitoids and the ca. 2.38 Ga garnet-bearing leucosome.	101
Figure 5-6. LA-ICPMS zircon U-Pb isotope data for 2.4–2.3 Ga granitoids and the ca. 2.38 Ga garnet-bearing leucosome.	102
Figure 5-7. Bivariate zircon trace-element data plots and Ti-in-zircon temperatures.....	103
Figure 5-8. Standard granitoid classification diagrams and select major-element Harker variation diagrams for 2.4–2.3 Ga granitoids in the Nonacho Lake area.....	106
Figure 5-9. Primitive mantle normalized extended element plots (left panel) and chondrite normalized rare earth element plots (right panel) for 2.4–2.3 Ga granitoids in the Nonacho Lake area.....	107
Figure 5-10. Bivariate trace-element plots and zircon saturation temperatures for 2.4–2.3 Ga granitoids in the Nonacho Lake area.....	108
Figure 5-11. Whole-rock Nd isotope data for 2.4–2.3 Ga granitoids in the Nonacho Lake area.	109
Figure 5-12. Standard granitoid trace-element discrimination diagrams for 2.4–2.3 Ga granitoids in the Nonacho Lake area.....	114
Figure 5-13. Tectonic cartoons illustrating the inferred tectonic settings in which the ca. 2.43–2.28 Ga leucogranitoids and ca. 2.32–2.31 Ga biotite granites in the Nonacho Lake area.	117

List of Tables

Table 2-1. Summary sample information for chapter 2.....	10
Table 3-1. Summary sample information for chapter 3.....	31
Table 3-2. Summary of key geochemical parameters in different types of Archean granitoids and the granitoids in chapter 3.....	49
Table 5-1. Summary sample information for chapter 5.....	91

Chapter 1: Introduction

1.1 Motivation

Continental crust plays a key role in regulating Earth's climate and in making the planet habitable (e.g., Lee et al., 2016). It also provides a substrate for the evolution of terrestrial life and contains most of the mineral resources that sustain modern civilization. It is therefore important to understand how and when the continental crust formed and evolved. Presently, continental crust covers ~41% of Earth's surface (Cogley, 1984) and is primarily created at convergent plate margins by processes related to plate tectonics (Condie, 2021). How far back in time this present situation extends, however, is unclear. For instance, there is considerable debate surrounding the extent and manner in which the volume of continental crust has increased with time. Some authors contend that continents reached their present volume early in Earth's history, and that there has been a near balance of new crust formation and crust recycling ever since (Armstrong, 1991; Guo and Korenaga, 2023). Others argue that the volume of continental crust has increased with time, either semi-continuously (e.g., Reymmer and Schubert, 1984; Belousova et al., 2010; Reimink et al., 2023) or episodically (e.g., McCulloch and Bennett, 1994; Taylor and McLennan, 1995; Condie et al., 2017). When plate tectonics became the dominant driver of continental crust formation is also disputed. Hypotheses as to when plate tectonics began range from as early ~4.2 Ga (Hopkins et al., 2008) to as late as ~1.0 Ga (Stern, 2005; Hamilton, 2011), although most estimates fall somewhere between ~3.6 and 2.5 Ga (Palin and Santosh, 2021).

Several factors contribute to the uncertainties described above. One is the incomplete nature of the ancient rock record. For instance, the Archean Eon (4.0–2.5 Ga) spans >30% of Earth's history, and conservative estimates of continental growth indicate that at least 30% of the present continental volume was generated during this eon (Condie and Aster, 2010). However, less than 7% of the continental crust exposed today is Archean in age (Goodwin, 1996). Therefore, a significant amount of Archean continental crust has probably been reworked (its age is overprinted, but its mass is retained in the crust) by processes such as partial melting and sedimentary erosion, or recycled (its mass is returned to the mantle) by processes such as lower crustal delamination and sediment subduction. This raises the potential for preservation bias in the ancient rock record (e.g., Hawkesworth et al., 2009). Another reason is the complexity of Archean terranes. Much of the preserved Archean continental crust has been partially overprinted by younger episodes of deformation, metamorphism and magmatism. The Rae craton (described below) is an example of an Archean terrane that was extensively reworked in the Paleoproterozoic. Finally, the majority of research on Archean terranes has been directed towards those that are exceptionally well preserved (e.g., Pilbara craton, Australia) and those that are comparatively accessible (e.g., southern Superior

craton, Canada). There are still large tracts of Archean continental crust that are significantly understudied (e.g., western Rae craton). Altogether, the incomplete and complex nature of the ancient rock record, along with a dearth of data from parts of it, leaves room for many different interpretations.

In light of the issues described above, it is popular to exploit “proxy” records of continental evolution, such as detrital zircon U-Pb-Hf isotope data (e.g., Belousova et al., 2010; Dhuime et al., 2012), and the bulk chemical and isotopic composition of terrigenous sediments and sedimentary rocks (e.g., Taylor and McLennan, 1985; Tang et al., 2016; Garçon, 2021). The terrigenous sedimentary record provides a bulk sampling of eroded continental crust through time, and thus proxy data derived from it arguably provide a more complete view of crustal evolution than the extant igneous rock record. A sometimes overlooked caveat, however, is that the sedimentary record is also subject to preservation bias. How that bias translates into proxy data derived from it, and whether it is more or less severe than preservation bias in the igneous rock record, is not known. Large global compilations of detrital and igneous zircon U-Pb-Hf isotope data reveal the same general patterns (e.g., Condie and Puetz, 2019), which suggests that the igneous rock record is a no less reliable monitor of crustal evolution than the detrital zircon record.

To fully understand the evolution of Earth’s continental crust, detailed regional-scale studies of complex Archean terranes, in which geochronological and isotopic data can be tied directly to the chemical composition and petrogenesis of igneous rocks, are required. On their own, regional-scale studies cannot necessarily address global questions, such as how much continental crust existed in the Eoarchean and when plate tectonics began? However, regional studies are the template upon which global proxy datasets must be interpreted, and their aggregation will ultimately lead to more robust global models. In the words of Hugh Rollinson (2017): “Of course, ultimately, a global picture is what we want to obtain, but this will better come through first understanding processes at a regional level”.

1.2 The Rae craton

The subject of this thesis is the Rae craton of the Canadian Shield (Figure 1-1). The geological history of this craton is described in detail in sections 3.2 and 5.2, and only a brief overview is given here. The Rae craton stretches for >2000 km from central Canada, through Baffin Island and into western Greenland (Figure 1-1). It preserves a protracted history of Paleoproterozoic to Neoproterozoic (3.4–2.6 Ga) crust formation and greenstone belt development (e.g., Hartlaub et al., 2005; Sanborn-Barrie et al., 2014; Skipton et al., 2019; Thrane, 2021; Davis et al., 2021; Neil et al., 2023). From ~2.62 to 2.58 Ga, most of the craton was intruded by granitoid magmas in what can be described as a “granite bloom” (Hinchey et al., 2011; Regis et al., 2017a; Peterson et al., 2024). This Archean

history is similar to some “prototypical” Archean terrains, such as the Slave and Superior cratons (e.g., Bleeker, 2003). The Rae craton differs from those terrains, however, in that it has not remained stable since the end of the Archean. Instead, it was subject to extensive reworking during several latest Neoproterozoic to Paleoproterozoic tectono-magmatic and -metamorphic events (see Berman, 2010 for a review). Only after pervasive deformation, metamorphism and intraplate granitic magmatism associated with the 1.9–1.8 Ga Trans-Hudson orogeny did the Rae craton achieve long-term stability (e.g., Peterson et al., 2002; Regis et al., 2021). Altogether, the Rae craton is one of the largest Archean–Paleoproterozoic terranes on Earth and its crust preserves >1.6 Byr (3.4–1.8 Ga) of Earth’s history. Due in part to its remote location, sheer size and complex history, however, considerable uncertainty remains about the exact timing, duration and nature of the various events involved in its growth and reworking.

1.3 Thesis objectives and outline

The overarching goal of this thesis is to constrain the Archean to Paleoproterozoic history of crust formation and reworking in the western Rae craton. Two main objectives were defined with this goal in mind. The first is to evaluate the extent, geochemical character and petrogenesis of pre-3 Ga granitoid rocks in the western Rae craton. Previous work identified remnants of >3 Ga crust in the western Rae (Figure 1-1; Henderson and Thériault, 1994; McNicoll et al., 2000; Tersmette, 2012; Davis et al., 2014), but the full extent of that ancient crust, a potentially important archive of the early Earth, remains unknown. Moreover, little-to-no geochemical and isotopic data constraining the petrogenesis of pre-3 Ga granitoid rocks, from any part of the Rae craton, has been reported. The second objective is to evaluate the geochemical character, petrogenesis and tectonic significance of 2.5–2.3 Ga granitoid rocks in the western Rae craton (Figure 1-1). Magmatic rocks with crystallization ages between ~2.5 and 2.3 Ga are comparatively rare on a global scale (e.g., Condie et al., 2009, 2022), and the Rae craton is one of the few places where volumetrically significant 2.5–2.3 Ga granitoids are available for study (Figure 1-1). Despite this, relatively little geochemical and isotopic data have been acquired for those rocks (e.g., Hartlaub et al., 2007; Schultz et al., 2007; Cloutier et al., 2021), and in some cases their tectonic setting of formation is debated (cf. Schultz et al., 2007; Berman et al., 2013).

In pursuit of these objectives, 12 weeks of bedrock mapping and sampling were conducted over the course of three field seasons (2018, 2019 and 2021) in the Nonacho Lake area (“Nonacho area” hereafter) of the southwestern Rae craton (Figure 1-1). Until recently (Canam, 2023; this thesis), the basement rocks in the Nonacho area had not been studied with modern geochemical or geochronological techniques, and were largely mapped as undifferentiated orthogneiss and granitoid rocks (Taylor, 1958). Although little baseline geological information was available for the Nonacho

area at the outset of this project, it was recognized that conducting research in this region would likely lead to better constraints on the regional extent, character and diversity of the >3 Ga and 2.5–2.3 Ga plutonic rocks described above (Figure 1-1). Moreover, a network of lakes and rivers in the Nonacho area permitted boat access to shoreline bedrock exposure for an ~100 km east-west transect across the structural grain of the craton. Reconnaissance U-Pb zircon geochronology conducted in 2018 and 2019 showed that the basement rocks in the Nonacho area have a wide range of igneous crystallization ages (3.2 to 1.9 Ga), and that the >3 Ga and 2.5–2.3 Ga granitoids of interest are indeed present. This reconnaissance geochronology allowed for more targeted sampling and mapping during the 2019 and 2021 field seasons.

In chapter 2, I address the first objective of the thesis using samples from the Nonacho area and archival samples from other parts of the western Rae craton. Whole-rock Nd isotope and zircon U-Pb age data from granitoid rocks are used to constrain the extent of pre-3 Ga crust in the western Rae craton. Then whole-rock geochemical, and zircon Hf and O isotope data are employed to evaluate the origin of that ancient crust. Aspects of the second objective are addressed throughout chapters 3, 4 and 5, using field data and samples collected from the Nonacho area. In chapter 3, I document three suites (2.7, 2.6 and 2.5 Ga) of Late Archean granitoids. The petrogenesis and tectonic significance of the 2.5 Ga granitoid is evaluated in detail using whole-rock geochemical, and whole-rock Nd and zircon Hf isotope data. In chapter 4, I divert from the granitoid theme to investigate two occurrences of quartzofeldspathic metasedimentary rocks. Zircon and monazite U-Pb age and trace-element data constrain the provenance, depositional age and metamorphic age of those rocks. The results bear on the tectonic setting of the western Rae craton at ~2.4 Ga, and indirectly help to constrain the petrogenesis some granitic rocks in chapter 5. In chapter 5, I document multiple suites of 2.4–2.3 Ga granitic rocks. Whole-rock geochemical and Nd isotope data, and zircon trace-element data, are used to constrain the petrogenesis of those granites. The results have important implications for the tectonic evolution of the Rae craton from 2.4 to 2.3 Ga. In the final chapter, I summarize the key findings of chapters 2–5 and suggest avenues for future research that arise from these findings.

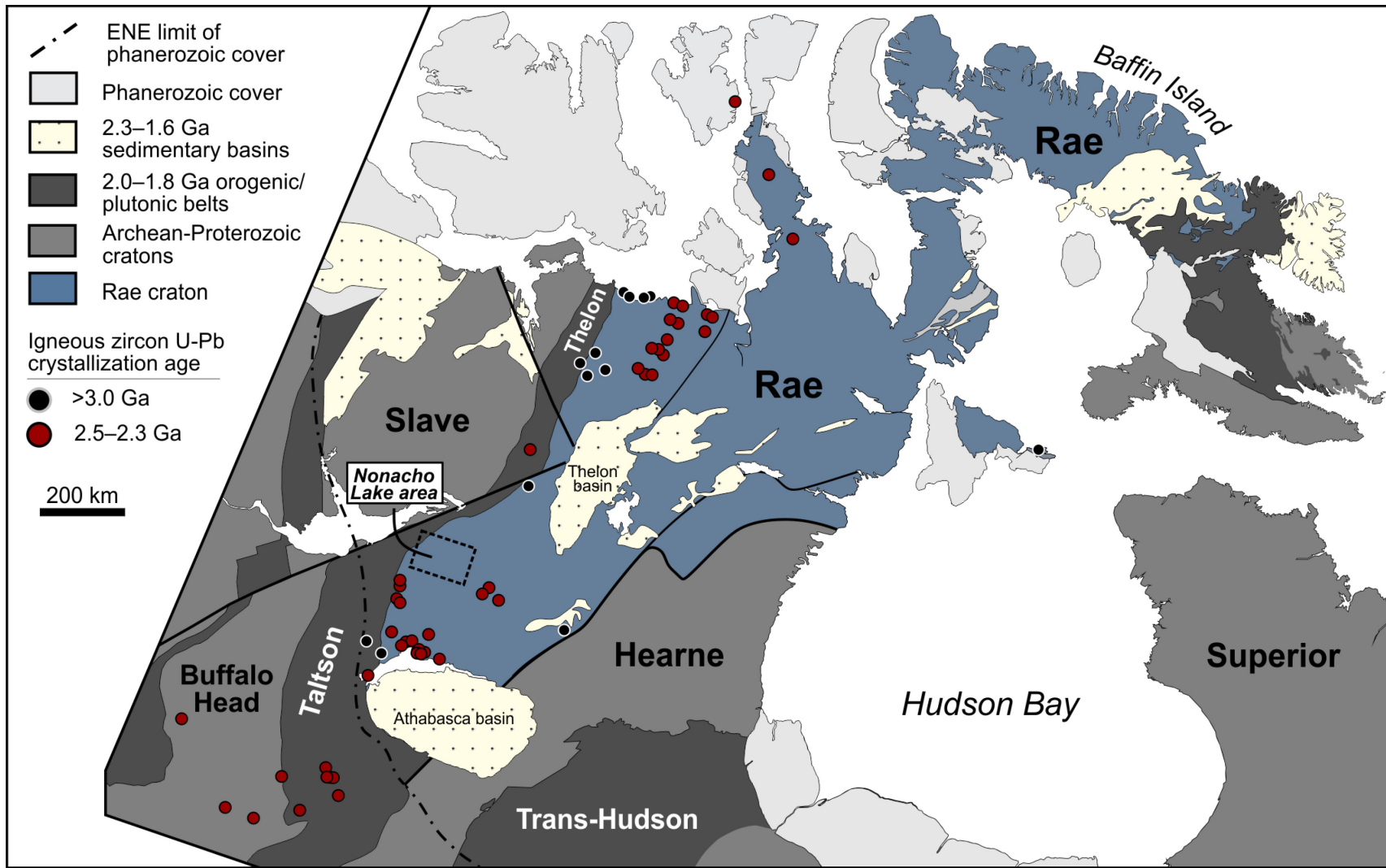


Figure 1-1. Simplified tectonic domain map for part of the Canadian shield. Modified after Berman et al. (2005). Igneous rocks in the Rae craton and Buffalo Head terrane with crystallization ages of >3.0, 2.5–2.3 Ga are shown. Locations are approximate. See chapters 2, 3 and 5 for compiled data sources.

Chapter 2: Discovery of a giant 3.3–3.1 Ga terrane in the Rae craton, Canada: Implications for the timing and extent of ancient continental growth

2.1 Introduction

The timing, extent and nature of continental growth prior to 3 Ga is poorly understood (Rollinson, 2017; Condie et al., 2018; Hawkesworth et al., 2019). The greatest obstacle in addressing these topics is the paucity of preserved ancient (>3 Ga) continental crust. To mitigate this issue, researchers have exploited proxy records, such as the Sm-Nd isotope composition of terrigenous sedimentary rocks (e.g., Garçon, 2021), and the U-Pb-Hf isotope composition of detrital zircon (e.g., Dhuime et al., 2012). These proxies arguably provide a more complete view of crustal evolution than the extant igneous rock record. They are limited, however, by a lack of information on the composition and petrogenesis of the source rocks, and by an indirect and in some cases questionable link to continental volume (Korenaga, 2018). The reliability of the ancient detrital zircon record, in particular, is plagued by the effects of non-zero-aged Pb loss (e.g., Guitreau et al., 2012; Fisher and Vervoort, 2018). These limitations place a premium on the discovery and direct characterization of new ancient crustal terranes. Identifying such terranes will lead to an increase in the minimum amount of continental crust that was present before 3 Ga and to more robust constraints on pre-3 Ga continental growth.

Despite the considerable size of the Rae craton (Figure 2-1A), the record of its ancient crust is virtually unscrutinized. Previous work has hinted at the presence of pre-3 Ga crust at the western (Henderson and Thériault, 1994; McNicoll et al., 2000; Davis et al., 2014) and southern (Hartlaub et al., 2005; Ashton et al., 2016) margins of the craton, and it has been speculated that this crust may constitute a single large terrane (Henderson and Thériault, 1994; Hartlaub et al., 2005). However, the true areal extent, age and character of pre-3 Ga crust in the Rae craton remains unconstrained. In this chapter, I present new data for granitoid and orthogneiss rocks (“granitoids” hereafter) from the western Rae craton, including whole-rock Sm-Nd isotope data for 82 samples, and whole-rock elemental plus zircon U-Pb-Hf-O isotope data for a subset of samples. These data and compilations of existing data are used to: 1) document one of the largest ancient crustal terranes on Earth; 2) characterize that terrane; and 3) discuss implications for global pre-3 Ga continental growth. Detailed descriptions of the analytical methods used are given in Appendix A. All of the new and compiled data can be found in Appendix B, along with a sample-by-sample description of the zircon U-Pb-Hf-O isotope data results.

2.2 Geological context

This study focuses on the Rae craton in mainland Canada, the western and eastern boundaries of which are defined by the 2.0–1.9 Ga Taltson-Thelon orogen and the Snowbird tectonic zone, respectively (Figure 2-1A). The interior of the Rae craton is characterized by abundant 2.7–2.6 Ga granitoids and subordinate ca. 2.7 Ga greenstone belts (Sanborn-Barrie et al., 2014; Regis et al., 2017a). Exposures of 3.4–3.0 Ga crust occur at the margins of the craton, in the Queen Maud block, Taltson basement complex, Snowbird tectonic zone and on Southhampton Island (Figure 2-1). Archean crust in the Rae craton has been overprinted by widespread deformation, metamorphism and magmatism related to both the 2.5–2.3 Ga Arrowsmith (Berman et al., 2013) and 1.9–1.8 Ga Trans-Hudson (Regis et al., 2021) orogenic events.

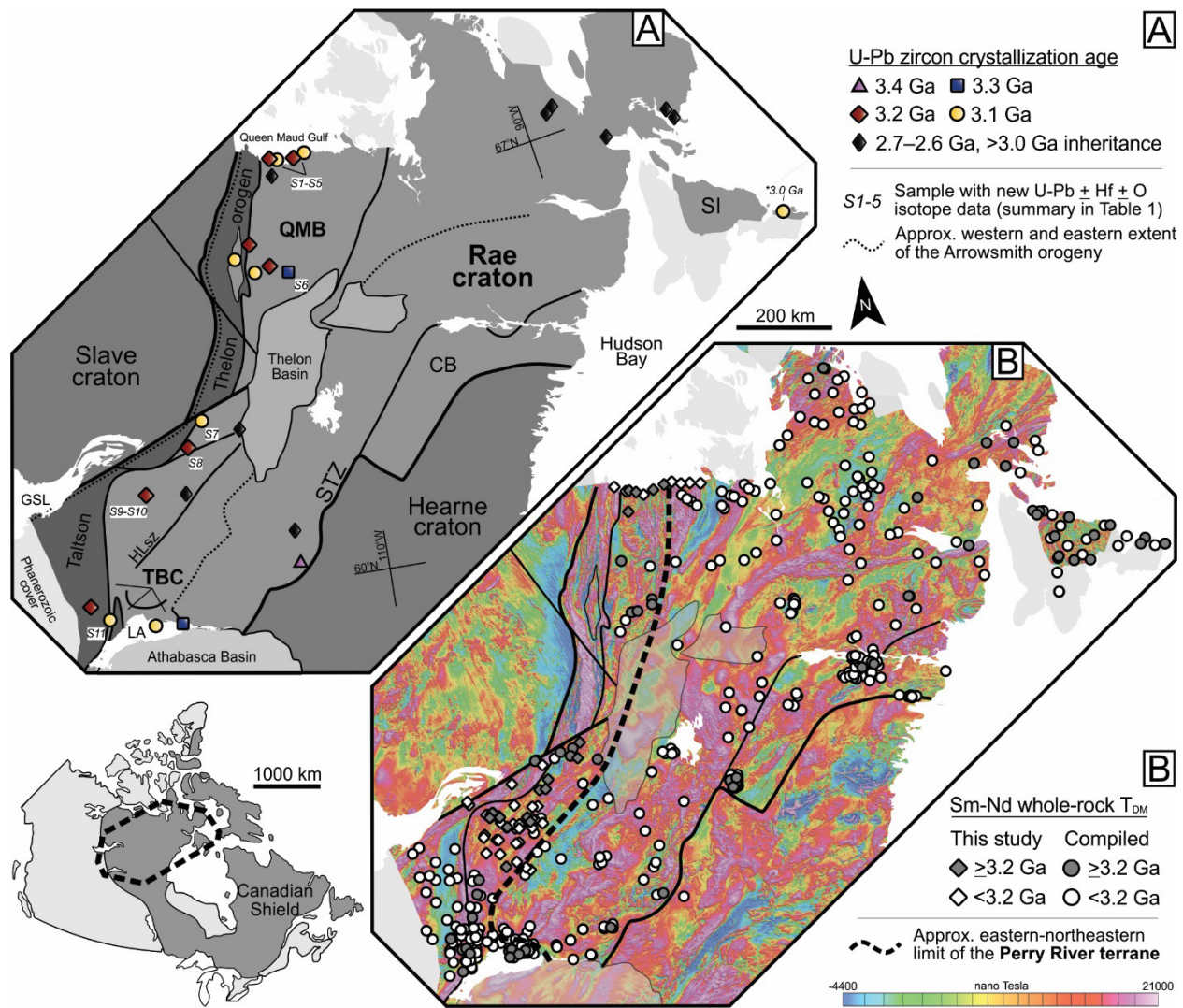


Figure 2-1. (A) Simplified geology of part of the Canadian Shield, adapted after Pehrsson et al. (2013a), Davis et al. (2014) and Ashton et al. (2016). CB: Chesterfield block; GSL: Great Slave Lake; HLSz: Howard Lake shear zone; LA: Lake Athabasca; QMB: Queen Maud block; SI: Southampton Island; STZ: Snowbird tectonic zone; TBC: Taltson basement complex. (B) Total field aeromagnetic anomaly map (Miles and Oneschuck, 2016). T_{DM} are single stage Sm-Nd depleted mantle model ages, calculated using the linear depleted mantle model of Goldstein et al. (1984). See Appendix B for compiled data sources.

2.3 Extent of ancient crust in the western Rae craton

Zircon U-Pb crystallization ages and whole-rock Sm-Nd depleted mantle model ages (T_{DM}) from (meta)igneous rocks are used to characterize the extent of ancient crust in the Rae craton (Figure 2-1). All samples with crystallization ages >3.0 Ga, and for which Sm-Nd data are available, yield a $T_{DM} \geq 3.2$ Ga. Therefore, $T_{DM} \geq 3.2$ Ga are used to identify rocks that are, or may have derived in part from crust that is, >3.0 Ga in age. Sixteen samples with crystallization ages >3.0 Ga and 46 with $T_{DM} \geq 3.2$ Ga are distributed along the western and southwestern margin of the craton (Figure 2-1). These samples appear to define a belt of ancient crust that stretches for >1000 km from central Canada to the Arctic coast. The existence of this ancient belt is strongly supported by along strike similarities in the zircon U-Pb age data. Granitoids from both the northern and southern portions of the belt yield crystallization ages of ca. 3.3, 3.2 and 3.1 Ga, and contain rare ca. 3.3 Ga inherited zircon (Figure 2-1, Table 2-1). We refer to this belt as the Perry River terrane (PRT), after a major north-flowing river that empties into the Queen Maud Gulf (Figure 2-1).

The full extent of the PRT is a challenge to evaluate. The western boundary of the terrane appears to lie within the Taltson-Thelon orogen (Figure 2-1). In the Queen Maud block, the eastern boundary is clearly defined by a sharp transition from a mottled aeromagnetic anomaly pattern and abundant $T_{DM} \geq 3.2$ Ga in the west, to a linear aeromagnetic anomaly pattern and T_{DM} exclusively <3.2 Ga in the east (Figure 2-1). South of the Queen Maud block, the eastern-northeastern boundary of the terrane may coincide with the Howard Lake shear zone, and the northeastern extent of the Taltson basement complex (Ashton et al., 2016) (Figure 2-1). The Howard Lake shear zone lies along strike of the well-defined eastern boundary in the Queen Maud block, and there is no evidence for ancient crust immediately east of it, or northeast of the Taltson basement complex (Figure 2-1). Furthermore, although deformation in the Howard Lake shear zone is Paleoproterozoic in age, it has been interpreted as a reactivated Meso to Neoproterozoic lithospheric boundary (Thiessen et al., 2022). In the Queen Maud block, the ancient crust appears to dominate an area of $\sim 50,000$ km² (Figure 2-1B). To the south of the Queen Maud block, however, numerous $T_{DM} < 3.2$ Ga indicate that the ancient crust has been added to by a substantial amount of younger and relatively juvenile magmatism (Figure 2-1B). Nevertheless, the spatial distribution of samples with crystallization ages >3.0 Ga and/or $T_{DM} \geq 3.2$ Ga (Figure 2-1) suggest that the PRT once occupied an area up to $\sim 100,000$ km², or more. Based on this, its >1000 km length and its minimum extent of $\sim 50,000$ km², we conclude that the PRT is one of the largest remnants of ancient crust on Earth. For comparison, the areal extent of exposed pre-3.0 Ga crust in each of the well-studied Kaapvaal (South Africa) and Pilbara (Western Australia) cratons is $\sim 60,000$ km² (e.g., Eglington and Armstrong, 2004; Kemp et al., 2015).

Table 2-1. New zircon U-Pb-Hf-O isotope results from pre-3 Ga granitoids of the Perry River terrane, Rae craton, Canada.

Sample ID	Latitude (°N)	Longitude (°W)	Rock type	Crystallization age $\pm 2\sigma$ (Ga)	Inherited zircon (Ga)	Weighted mean $\epsilon\text{Hf}_i \pm 2\text{SE}/2\text{SD}$	Median $\delta^{18}\text{O}$ (‰) $\pm 2\text{SE}/2\text{SD}$
S1	67.8312	-102.3724	Gneissic tonalite	3.225 \pm 0.008	---	2.7 \pm 0.4/2.3	5.5 \pm 0.1/0.2
S2	67.7851	-102.0548	Foliated tonalite	3.123 \pm 0.007	---	0.5 \pm 0.5/1.9	5.6 \pm 0.1/0.2
S3	67.7847	-101.2144	Gneissic diorite	3.224 \pm 0.009	---	0.6 \pm 0.5/1.7	5.7 \pm 0.1/0.2
S4	67.7840	-101.2144	Gneissic tonalite	*3.200 \pm 0.023	3.3	---	---
S5	67.8502	-100.6521	Gneissic granodiorite	3.140 \pm 0.009	---	0.0 \pm 0.3/1.6	5.6 \pm 0.1/0.5
S6	65.6833	-102.0583	Gneissic tonalite	3.314 \pm 0.006	---	0.4 \pm 0.4/1.3	---
S7	63.1400	-106.6120	Gneissic tonalite	3.122 \pm 0.006	3.3, 3.2	0.0 \pm 0.3/2.0	5.5 \pm 0.1/0.3
S8	62.6544	-101.1990	Gneissic tonalite	3.215 \pm 0.006	---	1.2 \pm 0.3/1.3	---
S9	61.8085	-108.9588	Gneissic tonalite	3.238 \pm 0.008	---	1.6 \pm 0.4/1.9	5.1 \pm 0.2/0.7
S10	61.8093	-108.9579	Foliated monzodiorite	*3.185 \pm 0.011	---	---	---
S11	59.4707	-110.4058	Gneissic granitoid	3.074 \pm 0.007	3.3, 3.1	-1.7 \pm 0.5/1.5	5.5 \pm 0.1/0.5

Note: Crystallization ages are weighted mean $^{207}\text{Pb}/^{206}\text{Pb}$ ages with 2σ uncertainties including internal 2SE and long-term external reproducibility. SE is standard error, SD is standard deviation, * indicates a minimum age estimate, --- indicates no data. Samples S7 and S11 were originally dated by Henderson and Thériault (1994) and McNicoll et al. (2000), respectively. All samples yield initial ϵHf values with 2SD similar to the analyzed homogeneous reference materials (~1-2 ϵHf units), indicating that at the precision level of the data, they have homogeneous Hf isotope compositions.

2.4 Nature and origin of the Perry River terrane

Most of the 3.3–3.1 Ga granitoids from the PRT are sodic tonalites ($\text{K}_2\text{O}/\text{Na}_2\text{O} < 0.6$), with major- and trace-element compositions that are typical of Archean TTGs (tonalite-trondjemite-granodiorites) (Figures 2-2A-C; Moyen and Martin, 2012). Although some mafic (~53 wt. % SiO_2) and potassic ($\text{K}_2\text{O}/\text{Na}_2\text{O} > 0.6$) granitoids are also present (Figures 2-2A-B). Archean TTGs are generally thought to originate through partial melting of hydrated metabasaltic rocks (e.g., Rapp et al., 1991; Nair and Chacko, 2008; Moyen, 2011; Moyen and Martin, 2012). With increasing depths of partial melting, the amounts of residual garnet and plagioclase left in the metabasaltic source rocks increase and decrease, respectively. As such, steeper rare earth element patterns (higher $\text{La}_{\text{CN}}/\text{Yb}_{\text{CN}}$ ratios; CN: chondrite normalized) and higher Sr/Y ratios in TTGs are generally thought to reflect greater depths of magma generation (e.g., Moyen, 2011). The TTGs from the PRT have $\text{La}_{\text{CN}}/\text{Yb}_{\text{CN}}$ and Sr/Y ratios (Figure 2-2C) similar to the “low- and medium-pressure” TTGs of Moyen (2011), which is consistent with magma generation at depths of 35 km or more (Moyen, 2011; Moyen and Martin, 2012). On average, the 3.1 Ga granitoids have more evolved major-element compositions (higher $\text{K}_2\text{O}/\text{Na}_2\text{O}$), and higher Sr/Y and $\text{La}_{\text{CN}}/\text{Yb}_{\text{CN}}$ ratios, than the 3.3–3.2 Ga granitoids (Figs. 2A and 2B). All samples that were analysed for their zircon O isotope compositions yield $\delta^{18}\text{O}$ values dominantly within the mantle-zircon field, regardless of their age (Figure 2-2D). By contrast, weighted mean initial zircon ϵHf (ϵHf_i) values do vary with granitoid age, and are described in detailed below.

Zircon Hf isotope data were acquired for five 3.3–3.2 Ga and four 3.1 Ga granitoids (Table 2-1). The older group includes ca. 3.31 Ga and ca. 3.24–3.21 Ga sodic tonalites with ϵHf_i values of +0.5 to +2.7, and a ca. 3.22 Ga mafic granitoid (53 wt.% SiO_2) with an ϵHf_i value of +0.6 (Figure 2-3A; Table 2-1). The former are interpreted to have derived from partial melting of mafic rocks with relatively short crustal residence times, whereas the latter may be a direct mantle melt. The variable ϵHf_i values from the ca. 3.24–3.21 Ga granitoids (Figure 2-3A) probably reflects mixing between juvenile and older, more evolved, crustal components. This interpretation is consistent with the presence of rare 3.3 Ga inherited zircon (Table 2-1) and with the Hf isotope composition of the ca. 3.31 Ga tonalite, which would have been sub-chondritic by 3.24 Ga (Figure 2-3A). The younger group includes three samples of ca. 3.13 Ga sodic tonalite-granodiorite with ϵHf_i values of ~ 0 and a ca. 3.07 Ga granitoid (no whole-rock elemental data) with an ϵHf_i value of -1.5 (Figure 2-3A; Table 2-1). These granitoids may have derived from partial melting of broadly similar mafic crustal rocks that gave rise to the ca. 3.3–3.2 Ga tonalites (Figure 2-3A), although the presence of inherited zircon in two of them (Table 2-1), indicates that at least some felsic-intermediate crustal material was also involved as a magma source or contaminant.

The geochemical and isotopic data summarized above are consistent with the PRT being a relatively juvenile 3.3–3.2 Ga terrane that was partially reworked to produce more evolved 3.1 Ga granitoid melts. The extent to which the PRT granitoids are juvenile depends in part on the isotopic composition of the mantle reservoir from which they formed. There is significant evidence that, on a global scale, juvenile Eo to Mesoarchean magmas were primarily extracted from mantle reservoirs with chondritic to only moderately radiogenic Hf isotope compositions (Guitreau et al., 2012; Fisher and Vervoort, 2018; Kemp et al., 2023), broadly similar to the 3.8 Ga depleted mantle model (Figure 2-3A). Considering this, and the fact that there is no direct evidence (igneous or inherited zircon) for crust older than ~ 3.3 Ga in the PRT (Table 2-1), I argue that the mafic source rocks to the sodic 3.3–3.1 Ga PRT granitoids are unlikely to have been extracted from the mantle earlier than ~ 3.45 – 3.23 Ga (Figure 2-3A).

2.5 Possible geodynamic setting

The dominantly TTG-like geochemical characteristics of the 3.3–3.1 Ga PRT granitoids do not place unique constraints on their geodynamic setting of formation. The tectonic setting or settings in which Archean TTGs were generated is a topic of considerable debate (see Moyen and Martin, 2012 and Condie, 2014 for reviews). It has been argued that Archean TTGs formed through the partial melting of metabasaltic rocks: 1) in subducted oceanic crust (e.g., Martin, 1986); 2) at the base of thick magmatic arcs (e.g., Nagel et al., 2012; Polat, 2012); 3) at the base of thick, oceanic plateau-like, mafic crust (e.g., Willbold et al., 2009; Smithies et al., 2009); or 4) in the delaminated roots of

oceanic plateau-like mafic crust as it foundered into the underlying mantle (e.g., Bédard, 2006). Despite this debate, a subduction-related origin for TTGs, and thus for the PRT, is preferred here for three reasons. First, subduction provides a straight-forward explanation for the presence of hydrous basaltic rocks at the depths necessary for TTG genesis (>35 km; e.g., Nair and Chacko, 2008; Moyen, 2011; Moyen and Martin, 2012). By contrast, the rocks at the base of oceanic plateaus are typically anhydrous mafic to ultramafic cumulates (e.g., Nair and Chacko, 2008; Arndt, 2023). Second, only small volumes of felsic magmatic rocks are present in modern oceanic plateaus (e.g., Martin et al., 2014; Arndt, 2023). Third, the modern magmatic rocks that are geochemically most similar to Archean TTGs (i.e., high-silica adakites; Martin et al., 2005) are found in island and continental-margin arc settings (e.g., Petford and Atherton, 1996; Martin et al., 2005; Martin et al., 2014).

In a subduction setting, the mantle-like zircon $\delta^{18}\text{O}$ values of the PRT TTGs may be reconciled if the source rocks were hydrated basaltic rocks that were emplaced at the base of a magmatic arc. Arc basalts owe their genesis in part to fluids or melts liberated from subducted oceanic crust, and such fluids may have non-mantle $\delta^{18}\text{O}$ values (e.g., Eiler et al., 2000). Nevertheless, the O isotope compositions of arc basalts are strongly controlled by their mantle source, and they commonly retain mantle-like $\delta^{18}\text{O}$ values (e.g., Eiler et al., 2000; Jones et al., 2015). Alternatively, partial melting of multiple layers of seawater-altered subducted oceanic crust, including layers with $\delta^{18}\text{O}$ values both above and below the mantle field, could produce hybrid TTG magmas with $\delta^{18}\text{O}$ values overlapping the mantle field. Both of the scenarios considered above have been proposed as explanations for the mantle-like O isotope compositions of some modern adakites (Bindeman et al., 2005). Finally, the comparatively evolved major-element compositions (on average), less radiogenic zircon Hf isotope compositions, and higher $\text{La}_{\text{CN}}/\text{Yb}_{\text{CN}}$ and Sr/Y ratios of the younger (ca. 3.1 Ga) PRT granitoids could be explained through the progressive thickening and maturation of a magmatic arc. As the thickness of the arc crust increased, metabasaltic rocks that had resided in the crust for some time may have been buried and partially melted, generating the ca. 3.1 Ga sodic tonalites with zircon ϵHf_i values of ~ 0 . Thickening of the arc crust could also have resulted in the burial and partial melting of more evolved (i.e., tonalitic) infracrustal rocks, or greater degrees of crustal assimilation, in order to account for the relatively potassic composition of some ca. 3.1 Ga PRT granitoids.

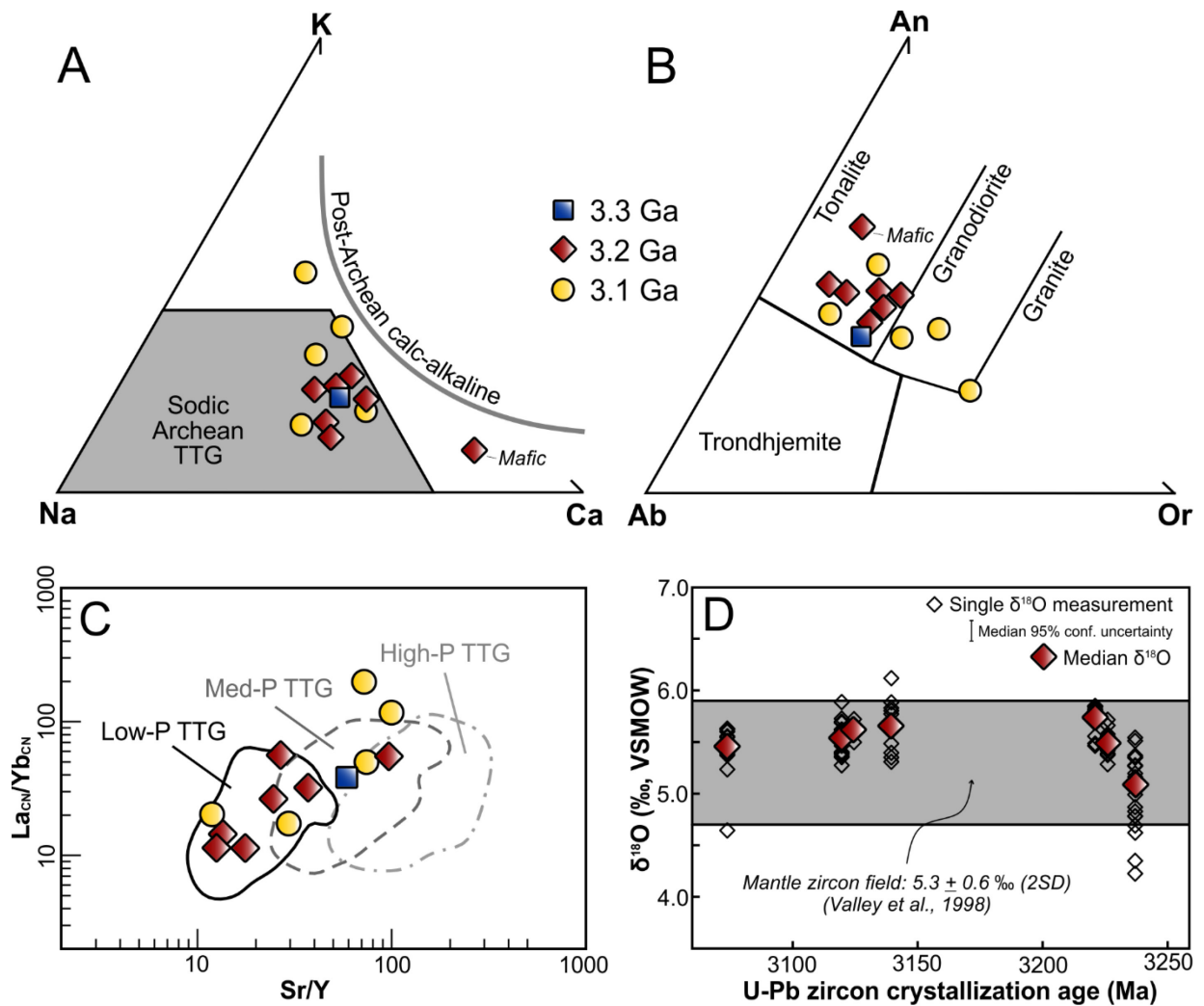


Figure 2-2. (A) Molar K-Na-Ca plot (Moyen and Martin, 2012). (B) Normative An-Ab-Or plot (Barker, 1979). Geochemical data for three 3.1 Ga samples are from Whalen et al. (2018), and the U-Pb ages for those samples are from Davis et al. (2014). (C) Sr/Y vs. La_{CN}/Yb_{CN} (CN: chondrite normalized). Chondrite normalizing values from Sun and McDonough (1989). Low-, medium- and high-P TTG fields are 75% kernel density contours of the data compiled by Moyen (2011). (D) Crystallization age vs. zircon δ¹⁸O_{VSMOW}. VSMOW: Vienna standard mean ocean water.

2.6 Implications for ancient continental growth

The discovery of an ancient terrane, similar or greater in size to some of the best studied pre-3.0 Ga crustal blocks, warrants a reassessment of the timing and extent of continental growth on the early Earth. I have therefore integrated our new data from the PRT with a global compilation of zircon ϵHf_i values from 3.6–3.0 Ga igneous rocks (Figure 2-3A). Several studies have highlighted the importance of using the comparably robust igneous zircon Hf isotope record, instead of or in addition to detrital zircon Hf isotope data, to constrain ancient continental growth (Guitreau et al., 2012; Vervoort and Kemp, 2016; Fisher and Vervoort, 2018). Two important observations are discussed.

First, the compilation reveals clusters of relatively juvenile (ϵHf_i : -2 to +3) igneous rocks at ca. 3.45, 3.31 and 3.23 Ga. The ca. 3.45 Ga cluster dominantly consists of samples from the Pilbara and Kaapvaal cratons. By contrast, when considered together, the ca. 3.31 and 3.23 Ga modes comprise samples from the PRT and 13 other cratons or crustal blocks (Figure 2-3A and B-2 in Appendix B). Similar patterns emerge from other global zircon datasets. A detrital zircon U-Pb-Hf isotope compilation reveals a cluster of broadly chondritic ϵHf_i values at \sim 3.2 Ga (Figure 2-3B). Furthermore, two igneous zircon U-Pb age compilations document density peaks between \sim 3.33 and 3.20 Ga (Figure 2-3C) that mirror the ca. 3.31 and 3.23 Ga modes in the igneous zircon U-Pb-Hf isotope dataset (Figure 2-3A). These findings suggest that ca. 3.33–3.20 Ga was a period of increased net continental growth, and the PRT may be one of the largest terranes created during that period. This conclusion is independent of whether that net continental growth reflects a period of enhanced continental crust production (Condie et al., 2018) or a period of enhanced continental crust preservation (Hawkesworth et al., 2019).

The second observation pertains to how much continental crust existed on the early Earth. Detrital zircon U-Pb-Hf isotope data have been used to argue that \sim 40% of present-day continental crust volume was established by 3.6 Ga (Dhuime et al., 2012; Hawkesworth et al., 2019), although the methods that were used to convert those data into a measure of crustal volume have been challenged (Korenega, 2018). If such a large amount of continental crust was present by 3.6 Ga, then on a global scale, it is reasonable to infer that a significant fraction of igneous rocks emplaced from 3.5–3.0 Ga should bear the isotopic fingerprint of that voluminous pre-3.6 Ga crust. This is not the case. Rather, the overwhelming majority of 3.5–3.0 Ga igneous rocks, worldwide, yield ϵHf_i values well above the modelled evolution of 3.6 Ga felsic crust and above the modeled evolution of 3.6 Ga mafic crust (Figure 2-3A). An important consideration is that ancient continental crust may have been more mafic, on average, than modern continental crust (Tang et al., 2016; Hawkesworth and Jaupart, 2021; cf. Garcon, 2021), which would make its interaction with younger magmas less perceptible in Hf isotope data (Figure 2-3A). However, the Hf budget of continental crust is strongly

weighted towards felsic rocks. For instance, mass balance calculations indicate that if ~70% of ancient continental crust were mafic (<57 wt. % SiO₂; Hawkesworth and Jaupart, 2021), ~49% of the Hf in the total continental crust would still reside in the felsic component (Table B-2), and that felsic component would evolve to very negative ϵ_{Hf} values with time (Figure 2-3A). Yet there is a striking paucity of evidence for reworking of pre-3.6 Ga felsic crust in the 3.5–3.0 Ga igneous zircon Hf isotope record (Figure 2-3A). Furthermore, the samples that do have ϵ_{Hf_i} values consistent with reworking of pre-3.6 Ga crust are largely from the Acasta gneiss complex (Northwest Territories, Canada) (Figure 2-3A), a tiny area that has been sampled extensively due to the known presence of Hadean to Eoarchean rocks (Reimink et al., 2019). These points, along with other evaluations of the zircon Hf isotope (Kemp et al., 2015; Fisher and Vervoort, 2018), detrital zircon U-Pb age (Parman, 2015) and rock (Rollinson, 2017) records, suggests that the volume of continental crust established by the end of the Eoarchean was relatively small.

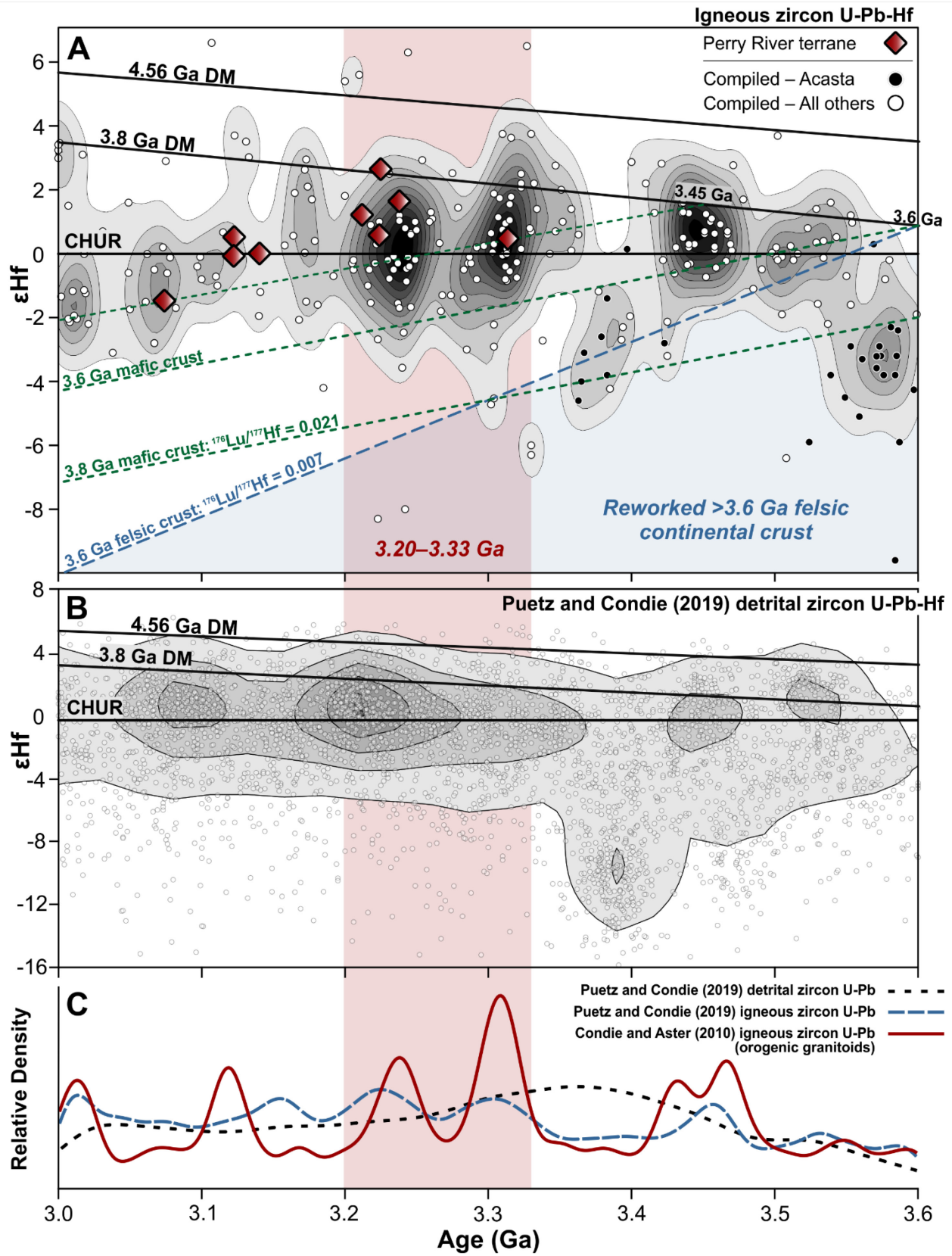


Figure 2-3. (A) Age vs. zircon ϵ_{Hf} for PRT granitoids and igneous rocks globally. Each data point is the age and weighted mean, mean or median zircon initial ϵ_{Hf} value of one rock. DM: depleted mantle; CHUR: chondritic uniform reservoir. DM models are from Vervoort et al. (2018) and Fisher and Vervoort (2018). (B) Published detrital zircon U-Pb-Hf isotope data compilation (Puetz and Condie, 2019). Data in (A) and (B) are contoured by their bivariate KDE (kernel density estimate) using the MATLAB code of Spener et al. (2020). Bandwidths were set at 10 Myr and 1 ϵ_{Hf} unit, and 20 Myr and 2 ϵ_{Hf} units, for (A) and (B), respectively. (C) KDE of published detrital zircon (Puetz and Condie, 2019) and igneous zircon (Condie and Aster, 201) U-Pb ages, with bandwidths of 20 Myr and 10 Myr, respectively. See Appendix B for compiled data sources. See Table B-2 for sources of mafic and felsic crust $^{176}\text{Lu}/^{177}\text{Hf}$ ratios. See Figure B-2 for all single zircon ϵ_{Hf} values from the PRT granitoids. See figure B-3 for compiled zircon ϵ_{Hf} values coded by location.

Chapter 3: 2.5 Ga high-K calc-alkaline granitoids of the Rae craton, Canada: Latest Archean continental growth in a post-collisional setting

3.1 Introduction

The presence of voluminous continental crust distinguishes Earth from all other planets in our solar system (Campbell and Taylor, 1983), and it is therefore of intrinsic importance to understand how and when that crust was created. A widely held view is that on the modern (Phanerozoic) Earth, new continental crust is largely generated in continental margin arcs, or in island arcs that are eventually accreted to a continental margin (e.g., Taylor and McLennan, 1985; Rudnick, 1995; Lee et al., 2007; Ducea et al., 2015; Jagoutz and Kelemen, 2015). The juvenile crust generated in such settings is often identified with relative ease, because the mantle sources from which primitive arc magmas derive commonly bear long-term depleted (suprachondritic) Nd and Hf isotope signatures (e.g., DePaolo, 1981a; Chapman et al., 2021). Juvenile magmas are also emplaced at sites of intracontinental extension, however, and their contribution to crustal growth may be less apparent when long-term enriched (subchondritic) lithospheric mantle sources are involved (e.g., Johnson, 1993). Moreover, it has increasingly been suggested that syn- to post-collisional or “late-orogenic” magmas that follow the cessation of subduction, and which are often derived in part from subchondritic mantle sources, are important contributors to continental growth (e.g., Liégeois et al., 1998; Bonin, 2004; Moyen et al., 2017; Gómez-Frutos et al., 2023).

While the processes outlined above apply to continental growth on the modern Earth, at least 30% of the preserved continental crust was generated in the late Archean (3.0–2.5 Ga) (Condie and Aster, 2010), and how that late Archean continental crust formed is much less well understood (e.g., Moyen and Laurent, 2018). Geochemical and petrogenetic studies of Archean magmatic rocks, and comparisons with their modern counterparts, help to constrain the continental crust forming processes that operated in the Archean (e.g., Polat and Kerrich, 2004; Martin et al., 2005; Fowler and Rollinson, 2012). A large amount of research has been dedicated to the voluminous 2.7–2.6 Ga granitoids and greenstone belts that are exposed in many Archean cratons around the world (e.g., Bleeker, 2003; Heilimo et al., 2010; Laurent et al., 2014a). The importance of those rocks is reflected in global igneous and detrital zircon datasets, which since the 1990’s have documented prominent U-Pb age peaks at ~2.7 Ga (Condie, 1998). As global zircon data sets have grown, however, a prominent age peak has also appeared at ~2.5 Ga (e.g., Voice et al., 2011; Puetz and Condie, 2019), and volumetrically significant 2.5 Ga mafic rocks and granitoids are now recognized in at least eight cratons (Heaman, 1997; Pehrsson et al., 2013a). Apart from in the North China and Dharwar cratons (e.g., Zhai, 2014; Jayananda et al., 2020), however, the nature of 2.5 Ga granitoid

magmatism and its relevance with respect to continental growth, has been the subject of relatively little investigation.

Another place with a significant 2.5 Ga magmatic record is the Rae craton of the Canadian Shield (Figure 3-1A). Mafic plutonic rocks and granitoids with ages between ~2.52 and 2.47 Ga have been documented on the western and southwestern margins of the craton (Figure 3-1B; Schultz et al., 2007; Davis et al., 2014; Cloutier et al., 2021). Those rocks have been used as a “bar-code” in the reconstruction of a proposed Neoproterozoic supercraton (Pehrsson et al., 2013a), and have been implicated in large-scale tectonic models for the craton (Berman et al., 2013). Yet the petrogenesis of those rocks has not been studied in detail, and their tectonic setting of formation is debated (Schultz et al., 2007; Berman et al., 2013; Cloutier et al., 2021). In this paper, we present new mapping, U-Pb zircon geochronology, and geochemical plus isotopic data, for basement rocks in an understudied portion of the southwestern Rae craton (Figure 3-1A). The data reveal three late Archean (2.7, 2.6 and 2.5 Ga) granitoid suites, and significantly expand the known extent of 2.5 Ga magmatism in the Rae craton. The geochemical and isotopic characteristics of the 2.5 Ga granitoids are investigated in detail to constrain their petrogenesis and tectonic setting of formation. Data from the 2.7 and 2.6 Ga granitoids are primarily employed to characterize the chemical and isotopic composition of the local basement, and thus better constrain the petrogenesis of the 2.5 Ga suite. The results have implications for the tectonic evolution of the Rae craton and for Archean crustal evolution in general.

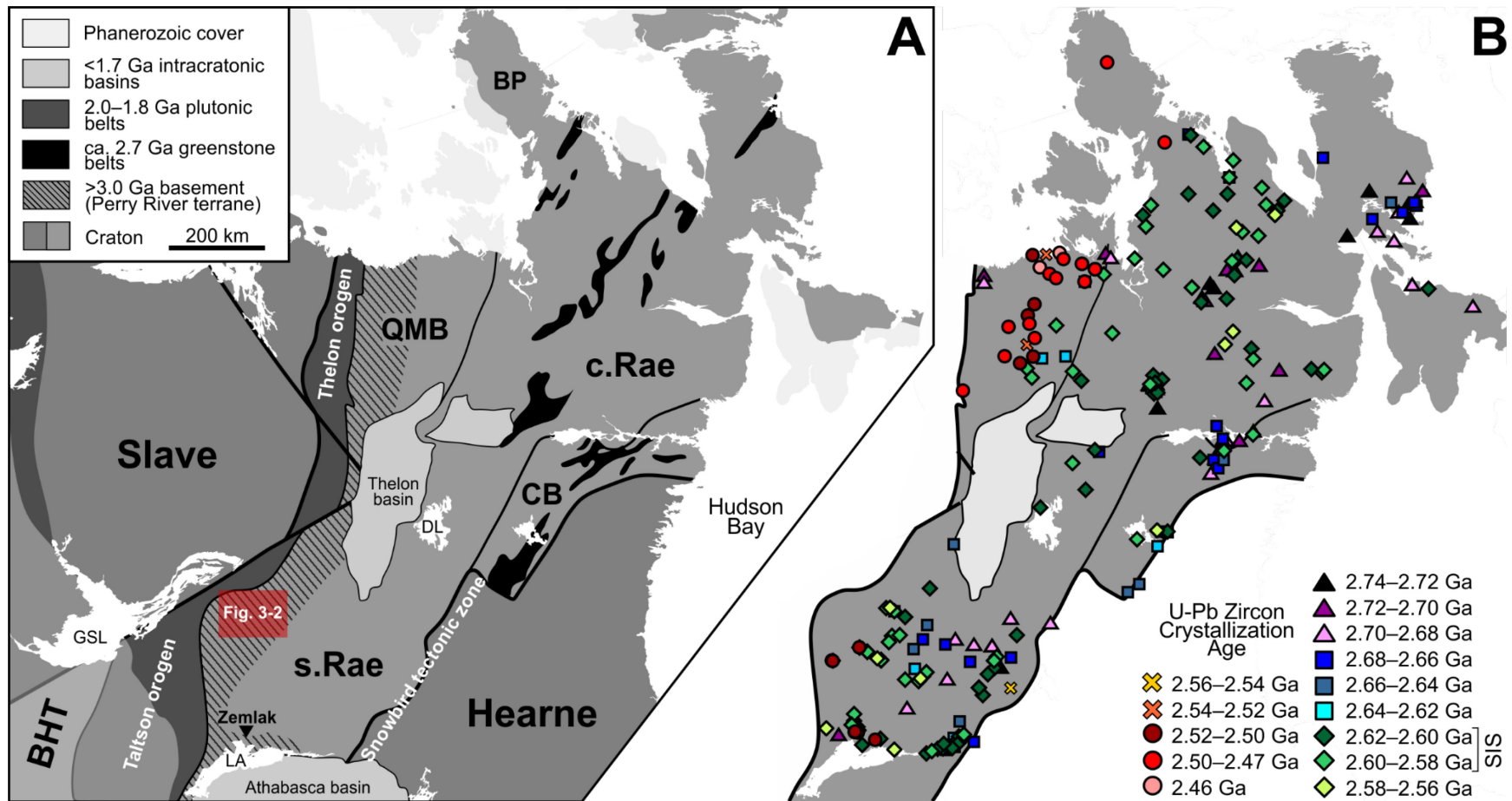


Figure 3-1. (A) Simplified geology of the Rae craton and surrounding cratons/terrane, adapted after Pehrsson et al. (2013a) and Neil et al. (2023). BHT: Buffalo Head terrane; BP: Boothia Peninsula; CB: Chesterfield block; DL: Dubawnt Lake; GSL: Great Slave lake; LA: Lake Athabasca; QMB: Queen Maud block; c.Rae: central Rae; s.Rae: southern Rae. Red rectangle indicates the location of this study and figure 3-2. (B) Cut out of the Rae craton overlain by a compilation of U-Pb zircon crystallization ages for 2.74–2.46 Ga igneous rocks. SIS: Snow Island suite. See Appendix C for compiled data sources.

3.2 Geological Context

The part of the Rae craton under investigation is located in mainland Canada, where it is separated from the Hearne craton to the east by the Snowbird tectonic zone, and from the Slave craton and Buffalo Head terrane to the west by the 2.0–1.9 Ga Thelon and Taltson orogens (Figure 3-1A). Basement rocks in the Rae craton are dominated by Mesoarchean to Neoarchean (2.9–2.7 Ga) tonalitic to granodioritic orthogneiss (e.g., Regis et al., 2017a; Davis et al., 2021). Remnants of older (>3 Ga) crust occur at the margins of the craton (e.g., Hartlaub et al., 2005; Whalen et al., 2011; Neil et al., 2023), and northeast-striking 2.7 Ga komatiite-bearing greenstone belts are preserved in the central part of the craton (Sanborn-Barrie et al., 2014; Hunter et al., 2018) (Figure 3-1A). From ~2.62–2.58 Ga most of the craton was intruded by voluminous, dominantly quartz-dioritic to monzogranitic, magmas of the so-called Snow Island suite (LeCheminant and Roddick, 1991; Hinchey et al., 2011; Peterson et al., 2024) (Figure 3-1B).

Two domains in the Rae craton, the Chesterfield block and the Queen Maud block (QMB), are of note (Figure 3-1A). The former is characterized by isotopically juvenile 2.7 Ga tonalitic rocks and greenstone belts, which in contrast to the central Rae craton, lack komatiite (Davis et al., 2006; Sandeman et al., 2006). The latter is typified by the widespread occurrence of granulite-facies mineral assemblages related to the Arrowsmith orogeny (see below), and by a paucity of Snow Island suite rocks (Schultz et al., 2007; Tersmette, 2012). Internally, the QMB is divided into an eastern domain dominated by 2.5–2.4 Ga metasedimentary rocks and 2.5 Ga granitoids (Schultz et al., 2007; Regis and Sanborn-Barrie, 2022), and a western domain dominated by 3.3–3.1 Ga orthogneiss rocks (Tersmette, 2012; Davis et al., 2014). Isotopic data indicate that the 3.3–3.1 Ga rocks of the western QMB extend to the south and are part of a larger basement terrane called the Perry River terrane (PRT) (Thériault and Henderson, 1994; Hartlaub et al., 2005; Neil et al., 2023; chapter 2; Figure 3-1A). Both the western and eastern domains of the QMB are stitched to the Rae craton by 2.5 Ga granitoids (Davis et al., 2014; Berman et al., 2015), whereas the Chesterfield block is thought to have accreted to the Rae craton by ~2.64 Ga, prior to Snow Island suite plutonism (Davis et al., 2006; Berman et al., 2007).

The Rae craton was not stabilized until after the 1.9–1.8 Ga Trans-Hudson orogeny (Corrigan et al., 2009; Regis et al., 2021), and consequently, the Archean history described above has been overprinted by several latest Archean to Paleoproterozoic tectono-metamorphic and -magmatic events (see Berman, 2010 for a review). Most pertinent to this study are the 2.56–2.50 Ga MacQuoid and the 2.5–2.3 Ga Arrowsmith orogenies (Schultz et al., 2007; Berman, 2010; Berman et al., 2013). Deformation and moderate- to high-pressure (5–15 kbar) metamorphism related to the former has been identified along the eastern margin of the craton, immediately adjacent the

Snowbird tectonic zone and within the Chesterfield block (Figure 3-1A) (Berman et al., 2002; MacLachlan et al., 2005; Davis et al., 2006; Mahan et al., 2006; Baldwin et al., 2006; Flowers et al., 2008; Regis et al., 2019). Some authors have suggested that northwest-dipping subduction beneath eastern margin of the Rae craton generated the widespread 2.62–2.58 Ga Snow Island suite plutons, and subsequently lead to the collision of an unknown block, or the Hearne craton, with the Rae craton during the MacQuoid orogeny (Berman, 2010; Peterson et al., 2024). Others have pointed to the widespread nature of the 2.62–2.58 Ga plutonism, and the lack of a systematic variation in its age across the craton (Figure 3-1B), as evidence against a subduction model (Hinchey et al., 2011).

With respect to the Arrowsmith orogeny, granitoid magmatism, deformation and low- to moderate-pressure (4–8 kbar) metamorphism is documented in the western and central parts of the craton (Hartlaub et al., 2007; Schultz et al., 2007; Tersmette, 2012; Berman et al., 2005, 2013). Amphibolite- to granulite-facies metamorphism and granitic magmatism was particularly widespread between ~2.4 and 2.3 Ga, and most investigators agree that this reflects the collision of the Slave craton, or another unidentified block, with the Rae craton (Hartlaub et al., 2007; Schultz et al., 2007; Berman et al., 2005, 2013). The 2.5 Ga plutonic rocks in the QMB (Figure 3-1B) were initially interpreted as being emplaced in a failed continental rift that preceded the onset of Arrowsmith orogenesis (Schultz et al., 2007; Schultz, 2007). Later, Berman et al. (2013) documented metamorphism between ~2.54 and 2.44 Ga on the western side of the craton, and ca. 2.54–2.49 Ga regional deformation immediately south of Boothia Peninsula (Figure 3-1A), which they related to an early “Andean-style” convergent margin phase of the Arrowsmith orogeny. In this context, Berman et al. interpreted 2.5 Ga plutonic rocks in the western Rae as being emplaced in continental margin arc and/or back-arc settings. This model has received support from reports of ca. 2.52 Ga granitoids with some arc-like geochemical characteristics in the Zemplak domain of northern Saskatchewan (Cloutier et al., 2021; Figure 3-1). It is notable, however, that the putative early phase of the Arrowsmith orogeny overlaps in time with, and could also be related to, MacQuoid orogenesis on the eastern side of the Rae craton (Berman et al., 2013; Pehrsson et al., 2013a). Thus, the 2.5 Ga plutonic rocks of the western Rae craton lie at the centre of debates surrounding the tectonic evolution of the craton between ~2.56 and 2.4 Ga.

3.3 Local geology and current study

This study is based on field work conducted in the Nonacho Lake area (“Nonacho area” hereafter) (Figures 3-1A and 3-2) of the southwestern Rae craton (Figure 3-1A and 3-2). The Nonacho area was selected for this study because: reconnaissance geochronology indicated the presence of widespread 2.5 Ga plutonic rocks in the area; its location is ideal for testing possible linkages

between the 2.5 Ga granitoids in the Zemplak domain to the south and the QMB to the north (Figure 3-1); and a network of lakes and rivers in the area allowed boat access to a ~100 km east-west transect across the structural and aeromagnetic grain of the craton, from Sparrow Bay to the east end of Gray Lake (Figure 3-2).

Previous work on basement rocks in the Nonacho area was largely limited to 1:250,000 scale mapping conducted in the 1950's (Taylor, 1958). More recently, detailed structural mapping, petrochronology and thermochronology of the region has revealed a complex history of Paleoproterozoic (2.3–1.8 Ga) shear zone development and exhumation (Canam, 2023). In addition, a regional-scale study of the Rae craton documented isotopic evidence for pre-3.0 Ga basement rocks of the PRT in the area (Neil et al., 2023; Figure 3-1A). That study also noted, however, an abundance of younger (<3.0 Ga) granitoids with relatively juvenile Nd isotope compositions. As will be shown in this chapter, those comparatively juvenile post-3.0 Ga granitoids are in large part late Archean in age. Chapter 5 addresses the occurrence and nature of younger (<2.4 Ga) granitic rocks that yield isotopic evidence for pre-3.0 Ga crustal sources.

On existing geological maps of the Nonacho area, the basement rocks are mostly depicted as undifferentiated orthogneiss and granitoid rocks. I therefore produced a new map for the ~100 km transect along which the majority of my field work and sampling was conducted (Figure 3-2B). The area is indeed dominated by variably deformed granitoid and orthogneiss rocks, which are a challenge to distinguish on the basis of field observations alone. The units shown on this map are therefore based on a combination of field observations, aeromagnetic data (Figure 3-2A), zircon U-Pb age data and whole-rock geochemical data. Some of the U-Pb age and geochemical data upon which the map is based are part of the present study and some are presented in chapters 2 and 5. In the following section, I summarize the pertinent geology of units 1 through 3 (Figure 3-2B), which contain the late Archean rocks under investigation. Unless specified otherwise, these late Archean rocks have been metamorphosed to amphibolite-facies conditions. This inference is based on their moderately foliated to gneissic texture, and the abundance of hornblende but lack of pyroxene in the mafic to intermediate rocks. Igneous rock names (e.g., diorite) are used and the prefix “meta-“ has been dropped for simplicity.

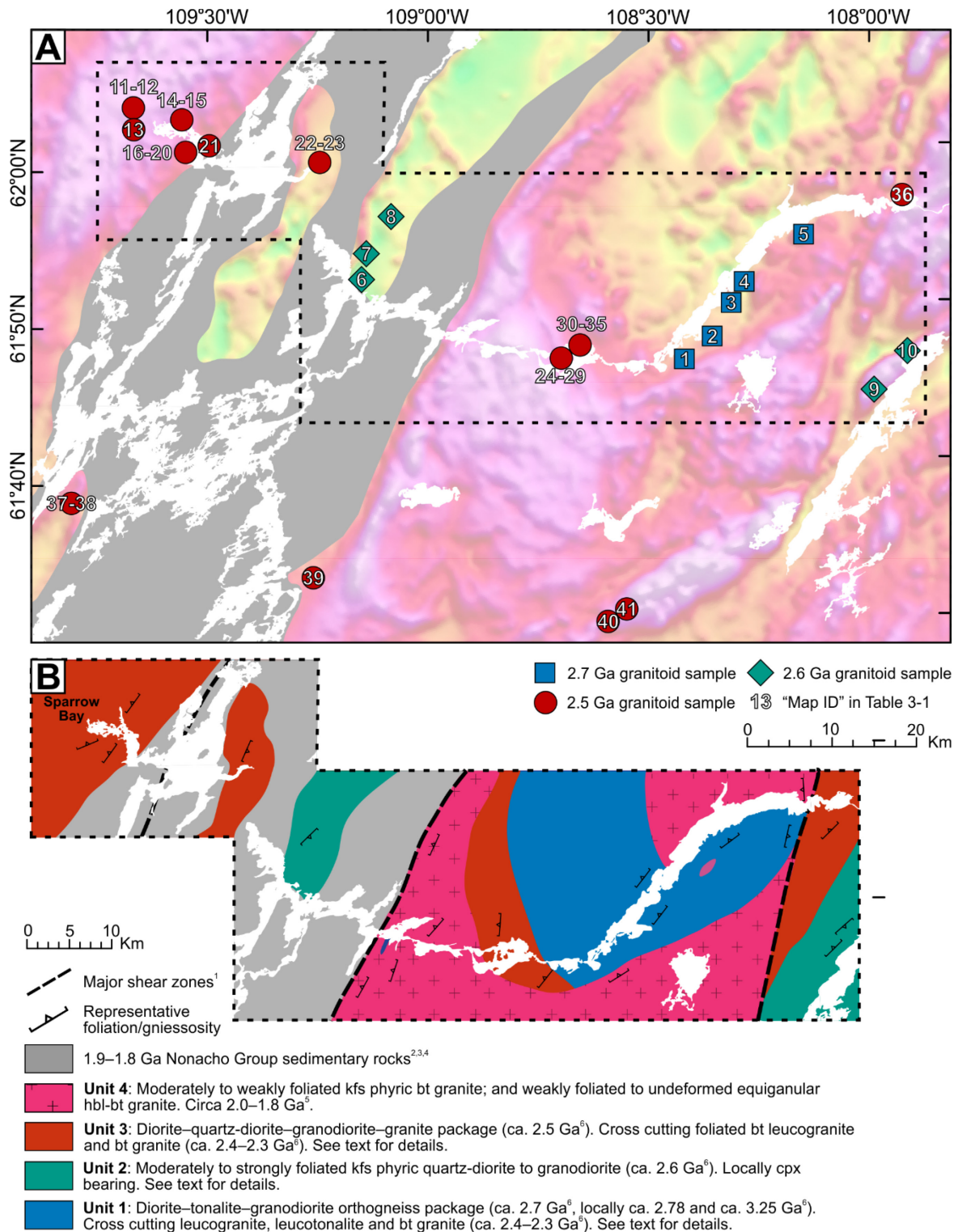


Figure 3-2. (A) Aeromagnetic map with sample locations. Samples are indicated by their "Map ID" in Table 3-1. (B) Sketch geology map of the main study area. In general, map constraints within ~5 km of shoreline are moderate to high confidence, those further from shoreline are inferred on the basis of aeromagnetic data and widely spaced helicopter stops. References: 1. Canam (2023); 2. Aspler (1985); 3. Bostock and van Breemen (1992); 4. van Breemen et al. (2013); 5. Neil, unpublished; 6. This thesis; Mineral abbreviations after Kretz (1983).

3.3.1 Map units

The dominant component of map unit 1 is a diorite–tonalite–granodiorite orthogneiss package (Figure 3-2B). In detail, this package includes moderately foliated to gneissic hornblende diorite (amphibolite *sensu stricto*), biotite tonalite and granodiorite, and lesser hornblende quartz-monzodiorite and quartz-ribbon granite. These rock types commonly together in the same outcrop as transposed and tightly folded layers, with layering on a decimetre to metre scale (Figure 3-3A), but homogeneous outcrops are also observed (Figure 3-3B and C). Garnet is locally present (one occurrence) in a biotite-bearing quartz-diorite. The orthogneiss package is cross-cut by moderately foliated 2.4–2.3 Ga leucotondhjemite, leucogranite and biotite granite (chapter 5). The leucotondhjemite also occurs as partially transposed layers within the gneiss package. Most rock types are equigranular and medium-grained, whereas the leucotondhjemite is coarse-grained. All components of unit 1 are intruded by granitic rocks of unit 4 (Figure 3-2B).

Map unit 2 is the least well constrained, due in part to its lack of shoreline exposure (Figure 3-2B). Nevertheless, the unit appears to be dominated by moderately to strongly foliated, medium to coarse-grained, K-feldspar phyric, quartz-monzodiorite and granodiorite (Figures 3-3D and E). In some cases these granitoids contain relict clinopyroxene cores surrounded by biotite and hornblende, whereas in others they are simply biotite bearing. The K-feldspar phenocrysts are typically ~2–4 cm, and up to ~7 cm, in length. Fine-grained dioritic rocks are observed as inclusions in (Figure 3-3E), and in places, appear to be intermingled with, the K-feldspar-phyric granitoids. Some of the K-feldspar phyric granitoids exhibit a distinctive outcrop appearance in which chalky white feldspar grains are surrounded by smoky grey interstitial quartz (Figure 3-3D). This unit, and the description of it, draws in part from earlier mapping to the east of Gray Lake (Figure 3-2B) by Martel et al. (2020).

The main component of map unit 3, and the primary focus of this study, is a diorite–quartz-diorite–granodiorite–granite package (Figure 3-2B). In detail, this package of rocks includes moderately foliated to locally gneissic hornblende ± biotite (monzo)diorite, hornblende-biotite quartz-(monzo)diorite, biotite ± hornblende granodiorite and biotite granite (Figures 3-3F-I). The (monzo)diorite and quartz-(monzo)diorite are fine- to medium-grained and equigranular, whereas the granodiorite and granite are medium to coarse-grained and range from equigranular to K-feldspar porphyritic and porphyroclastic (Figures 3-3F-I). The K-feldspar phenocrysts are typically ~2–3 cm, and up ~5 cm, in length. In the Sparrow Bay area, these rock types are commonly transposed and interlayered on a decimetre to meter scale, whereas elsewhere they tend to comprise homogeneous meter scale units. Ultramafic cumulates (>90% amphibole) are locally associated with the dioritic and quartz-dioritic rocks. This package of rocks is cross-cut by moderately foliated to undeformed

leucogranite and biotite granite that are 2.4–2.3 Ga in age (Chapter 5). These cross-cutting granites are a major component (~50%) of the unit in the Sparrow Bay area (Figure 3-2) but are subordinate elsewhere. Migmatitic granulite-facies mafic gneisses containing layers (centimeter- to decimetre-scale) and lenses (decimeter to metre scale) of garnet-bearing leucosome occur at the easternmost end of Gray lake (Figure 3-2B). The mafic protolith to these rocks is correlated to unit 3 on the basis of geochronology (sample 19BC02A, see below), but given that they have been partially melted and metamorphosed to granulite-facies conditions, no geochemical or isotopic data were acquired from them.

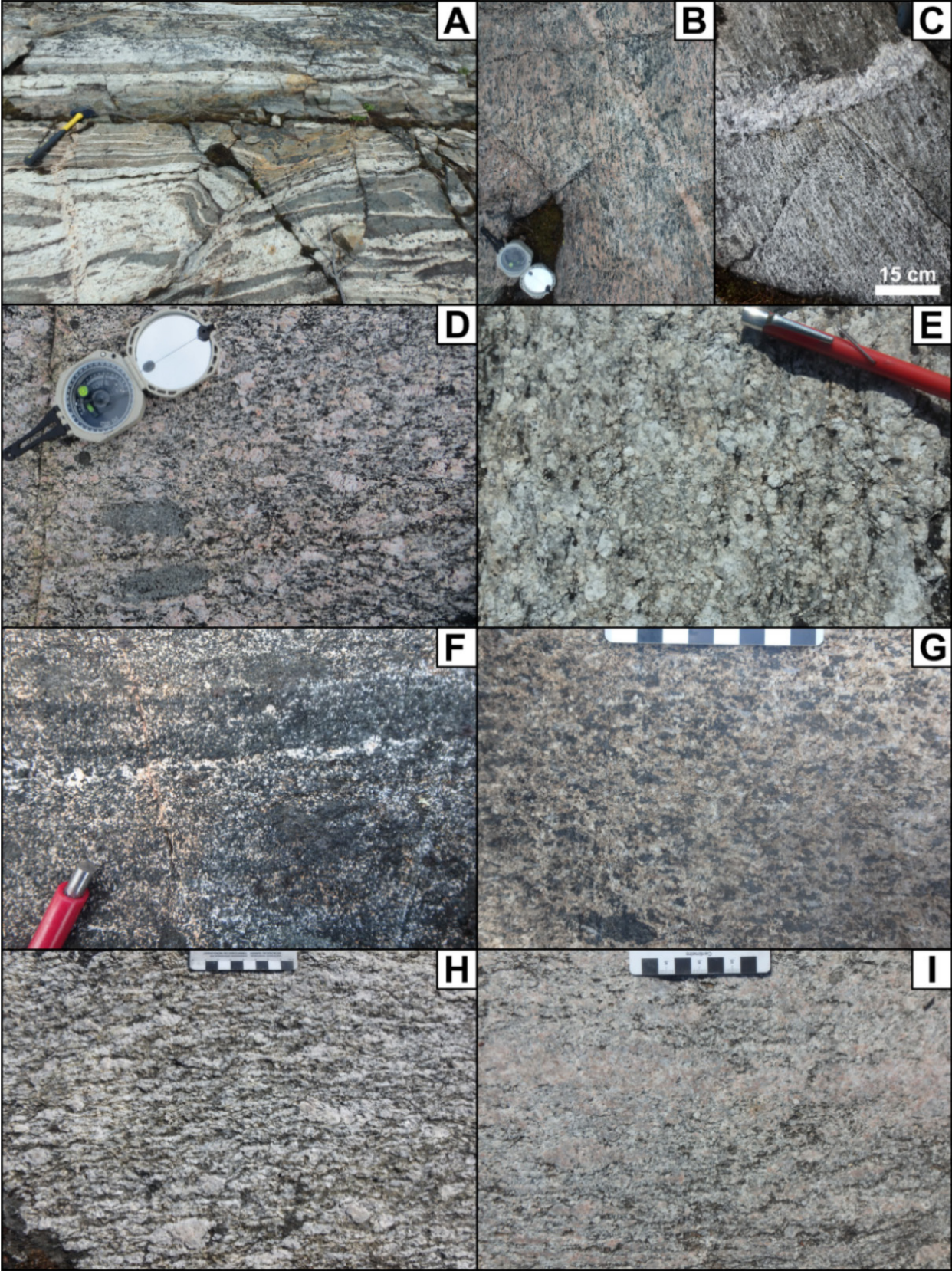


Figure 3-3. Representative outcrop photos for map units 1 (A–C), 2 (D and E) and 3 (F–I). (A) Multi-component orthogneiss outcrop. (B) 2.7 Ga granodiorite, sample 19BN07B. (C) 2.7 Ga tonalite (sample 19BN38A) cross-cut by a small leucotondhemite dyke. (D) 2.6 Ga K-feldspar phyric granodiorite with fine-grained diorite inclusions, sample 16BK374A. (E) 2.6 Ga K-feldspar-phyric quartz-monzodiorite with smoky grey interstitial quartz, sample 19BN106B. (F) 2.5 Ga diorite, sample 18BN56A. (G) 2.5 Ga quartz-monzodiorite, sample 19BN173A. (H) 2.5 Ga K-feldspar-phyric granodiorite, sample 21BN28A. (I) 2.5 Ga equigranular to weakly K-feldspar-phyric monzogranite, sample 21BN30A.

3.4 Samples and Methods

The sampling strategy focused on outcrops where rock units that are homogeneous on at least the decimeter scale, and typically the metre scale, could be identified (Figures 3-3B-I). Samples returned from the field were inspected in thin section and in cut slab, and only those that were minimally altered and devoid of cross-cutting dykes or veins were selected for further work. In total, 41 samples were processed for some combination U-Pb zircon geochronology, whole-rock elemental, and whole-rock Sm-Nd isotope and zircon Hf isotope analyses (Figure 3-2A; Table 3-1). Appendix A contains the details of sample preparation, analytical methods and data reduction protocols, along with the secondary reference material results. Appendix C contains individual sample descriptions and complete data tables. A brief summary of sample preparation and methods is provided below.

Whole-rock grits for zircon separations, and whole-rock powders for geochemical and isotopic analyses, were prepared in a tungsten-carbide puck mill. Zircon grains were separated using a modified version of the “water-based” baddeleyite separation technique (Söderlund and Johansson, 2002). Zircon grains were picked for quality and approximately 75–125 grains from each sample were cast in an epoxy mount, and polished to their mid-sections. Back scattered electron (BSE) and/or cathodoluminescence (CL) images of the grains were acquired prior to analyses, using a scanning electron microscope or electron microprobe. Higher resolution images of some grains were acquired after analysis, such that the laser ablation pits are visible (Figure 3-4).

All isotopic analyses were made at the University of Alberta. U-Pb zircon geochronology was conducted by LA-MC-ICPMS (laser ablation–multi-collector–inductively coupled plasma mass spectrometry) using a 213 nm Nd:YAG laser ablation system, a 25 µm diameter laser beam and a Nu Plasma MC-ICPMS. Whole-rock Sm-Nd isotope data were acquired by isotope dilution MC-ICPMS using the same Nu Plasma. Zircon Hf isotope measurements were made by LA-MC-ICPMS using a RESOLUTION 193 nm ArF laser ablation system, a 33 µm diameter laser beam and a Neptune Plus MC-ICPMS. The Hf isotope analyses were made in the same zircon growth domain from which the U-Pb data were acquired, either directly overlapping or adjacent the U-Pb pit (Figure 3-4). All time-resolved zircon U-Pb and Hf isotope measurements were inspected and rare analyses were excluded for reasons given in Appendix A. These analyses are included in the data tables (Appendix C), with a note stating the reason for their exclusion. Whole-rock major-element data were acquired by fusion-dissolution ICP-OES (optical emission spectrometry) at Activation Laboratories in Ancaster, Ontario. Whole-rock trace-element data were acquired by fusion-dissolution ICP-MS in the Peter Hooper Geoanalytical Laboratory at Washington State University and by pressed-powder briquette XRF (X-ray fluorescence) in Dr. Stan Mertzman’s laboratory at Franklin and Marshall College.

All uncertainties in this paper are reported at the 95% confidence level, and all dates referred to in the text are $^{207}\text{Pb}/^{206}\text{Pb}$ dates. Uncertainties on weighted mean $^{207}\text{Pb}/^{206}\text{Pb}$ ages are shown at two levels (Table 3-1). The first is the 2SE on the weighted mean calculated in ISOPLOT (Ludwig, 2009). The second uncertainty, denoted as 2σ , combines the first with the long-term external reproducibility of the *weighted mean* $^{207}\text{Pb}/^{206}\text{Pb}$ ratio (Horstwood et al., 2016; Sliwinski et al. 2022), which is $\sim 0.3\%$ (2σ ; Appendix A). The 2σ uncertainties on initial ϵNd values (Table 3-1) include the long-term reproducibility of the $^{147}\text{Sm}/^{144}\text{Nd}$ and $^{143}\text{Nd}/^{144}\text{Nd}$ ratios, and uncertainty in the samples age. An age uncertainty of ± 10 Myr was assumed for samples that were not dated directly.

Table 3-1. Summary of samples in this study, their locations, igneous zircon U-Pb crystallization ages and isotope geochemistry results.

Map ID	Sample ID	Northing	Easting	Rock type	SiO ₂ wt. %	Age (Ma) ± 2SE/2σ	Whole Rock εNd _i ± 2σ	Zircon εHf _i ± 2SE/2SD
2.7 Ga Granitoids								
1	19BN38A	6852910	634468	Bt tonalite	68	2700	-0.2 ± 0.4	
2	19BN07B	6854840	637652	Bt-Hbl granodiorite	67	2707 ± 6/8	-0.2 ± 0.3	
3	19BN45B	6859902	640340	Bt granodiorite	64	2700	0.1 ± 0.4	
4	19BN01A	6862107	641794	Bt granodiorite	67	2698 ± 4/6	0.6 ± 0.3	
5	19BC52A	6867703	648869	Bt-Hbl quartz-monzodiorite	61	2688 ± 4/7	0.5 ± 0.3	
2.6 Ga Granitoids								
6	19BN106B	6863093	596654	Bt quartz-monzodiorite	61	2580 ± 3/6	0.5 ± 0.4	
7	19BN98A	6864746	597097	Bt-Hbl diorite	52	2580	-0.2 ± 0.4	
8	18EM31B	6869953	602152	Bt granodiorite	65	2582 ± 4/6	-0.3 ± 0.3	
9	16BK366A	6849048	340556	Bt-Hbl-Cpx granodiorite		2569 ± 3/6		
10	16BK374A	6853739	345204	Bt-Hbl-Cpx granodiorite	67	2578 ± 2/5	0.2 ± 0.4	
2.5 Ga Granitoids								
11	21BN34A	6881604	570102	Bt-Hbl-monzodiorite	56	2500 ± 3/6	-0.1 ± 0.3	-0.1 ± 0.3/1.2
12	21BN34C	6881609	570104	Hbl-Bt diorite	50	2499 ± 4/6	0.6 ± 0.4	0.8 ± 0.4/1.7
13	18BN114A	6879842	569670	Hbl-Bt diorite	53	2476 ± 4/6	-0.2 ± 0.4	
14	18BN27A	6879891	575600	Hbl-Bt monzodiorite	50	2500	-0.4 ± 0.4	
15	18BN56A	6880633	575831	Hbl-Bt diorite	50	2500	0.2 ± 0.4	
16	18BN18B-M	6877576	576422	Bt-Hbl quartz-diorite	61	2500	-0.4 ± 0.4	
17	18BN18B-F	6877576	576422	Bt monzogranite	70	2500		
18	18BN31A	6877070	576567	Bt monzogranite	71	2500	0.4 ± 0.4	
20	19BN173A	6877692	576422	Bt-Hbl quartz-monzodiorite	62	2502 ± 4/7	-0.5 ± 0.3	
19	18BN113A	6877586	576215	Bt granodiorite	72	2512 ± 5/7	-0.4 ± 0.4	
21	18BN20B	6877062	578638	Bt-Hbl quartz-monzodiorite	58	2500	-0.1 ± 0.4	
22	19BN154A	6875584	589895	Bt granodiorite	63	2505 ± 3/6	0.1 ± 0.3	-1.2 ± 0.4/1.6
23	19BN166A	6877082	592089	Bt granodiorite	67	2499 ± 3/6	-0.4 ± 0.4	-0.9 ± 0.7/2.6
24	21BN32A	6852211	619764	Hbl quartz-diorite	58	2494 ± 3/6	0.1 ± 0.4	-0.8 ± 0.4/1.3
25	21BN15A	6852788	620851	Hbl diorite	51	2500 ± 8/9	0.2 ± 0.4	1.5 ± 1.1/2.3
26	19BN79A	6853131	620700	Bt-Hbl quartz-monzodiorite	56	2500	-0.2 ± 0.4	
27	21BN09A	6853272	620765	Bt-Hbl quartz-monzodiorite	56	2504 ± 4/6	-0.1 ± 0.4	
28	21BN16A	6853889	620453	Hbl-Bt quartz-monzodiorite	59	2500	0.0 ± 0.4	
29	19BN88A	6853061	622311	Bt-Hbl quartz-monzodiorite	63	2502 ± 3/6	0.2 ± 0.3	1.0 ± 0.5/1.7
30	21BN20D	6854554	621787	Bt monzogranite	74	2500	-0.4 ± 0.4	
31	21BN20C	6854564	621810	Bt-Hbl quartz monzodiorite	60	2500	0.2 ± 0.4	
32	21BN28A	6853291	622298	Bt granodiorite	66	2500	0.3 ± 0.4	
33	21BN29A	6853349	622112	Bt monzogranite	71	2500	-0.3 ± 0.4	
34	21BN30A	6854617	622608	Bt monzogranite	72	2500	0.2 ± 0.4	
35	19BN53A	6854520	622613	Bt granodiorite	69	2497 ± 3/6	-0.1 ± 0.4	0.5 ± 0.3/1.1
36	19BC02A	6871892	660494	Retrogressed mafic granulite		2516 ± 5/7		
37	19BN126B	6835534	563443	Bt granodiorite	66	2496 ± 4/6	0.2 ± 0.4	-0.2 ± 0.4/1.5
38	19BN127A	6835281	563626	Hbl-Bt monzodiorite	47	2497 ± 4/6	0.3 ± 0.4	
39	18BN14B	6827611	590700	Hbl quartz-diorite	56	2518 ± 2/5	-0.3 ± 0.4	-0.7 ± 0.6/2.4
40	21BN45A	6821694	625686	Bt monzodiorite	56	2507 ± 3/6	-0.1 ± 0.4	-1.1 ± 0.3/1.4
41	18EM33A	6822292	626834	Bt-Hbl monzodiorite	55	2500	-0.4 ± 0.4	

See "Map ID" on figure 3-2A for sample locations. UTM zones are 13 (16BK374A and 19BC02A) and 12 (all others). Rock names are from the Q-ANOR geochemical plot (Streckeisen and LeMaitre, 1979). Minerals are listed in order of decreasing abundance, with abbreviations after Kretz (1983). SE: standard error. SD: standard deviation. **Water levels on the Taltson River system fluctuate dramatically. As of 2021, several 2018 and 2019 sample sites were under water.**

3.5 Results

3.5.1 Zircon U-Pb geochronology

In general, the U-Pb age data were treated in the following manner. Analyzed zircon domains/grains were classified as igneous, metamorphic or inherited on the basis of internal zoning, external morphology and core-rim relationships (e.g., Corfu et al, 2003). These classifications are included alongside the data in Appendix C. Igneous crystallization ages were then assigned from the oldest cluster of concordant to near concordant igneous zircon $^{207}\text{Pb}/^{206}\text{Pb}$ dates that yield a weighted mean age with a reasonably low MSWD (mean squared weighted deviates), which was typically <2 and always <3 (Figure 3-4). Igneous zircon dates that are younger than the oldest cluster are interpreted to be the product of Pb-loss, or to reflect mixed analyses of igneous and metamorphic domains that were not detected during data reduction. This is a reasonable assumption for Archean samples. It is also supported in cases where the younger $^{207}\text{Pb}/^{206}\text{Pb}$ dates originate from zircon domains yielding comparatively high ^{238}U cps (counts per second), as these higher U zircon domains would likely be more radiation damaged and more susceptible to Pb-loss.

Three samples from the diorite-tonalite-granodiorite gneiss package in map unit 1 (Figure 3-2) were selected for geochronology (Table 3-1). The majority of the igneous zircon analyses from each sample are spread along or just below the concordia curve from ~ 2710 to 2650 Ma (Figure 3-4). Crystallization ages calculated from the oldest clusters of igneous dates are 2707 ± 8 , 2698 ± 6 and 2688 ± 7 Ma (Table 3-1; Figure 3-4). The interpretation that the younger igneous dates reflect Pb loss is well supported in sample 19BN01A, where there is a clear correlation between $^{207}\text{Pb}/^{206}\text{Pb}$ date and ^{238}U cps (Figure 3-4). All three samples also contain unzoned grains or rim domains that are interpreted as metamorphic and yield dates between ~ 2450 and 2400 Ma (Figure 3-4). Sample 19BN01A yields a relatively tight cluster of metamorphic zircon analyses with a weighted mean age of 2421 ± 7 Ma (Figure 3-4). This ca. 2420 Ma zircon population cannot be igneous in origin because the diorite-tonalite-granodiorite gneiss package is intruded by a ca. 2430 Ma leucotrochite (chapter 5).

Four samples of K-feldspar-phyric quartz-monzodiorite to granodiorite from map unit 2 (Figure 3-2) were selected for geochronology (Table 3-1). Igneous zircon analyses from all four samples yield relatively tight clusters (Figure 3-4). The crystallization ages determined are between 2582 ± 6 and 2569 ± 6 Ma, and are almost indistinguishable within analytical uncertainty (Table 3-1; Figure 3-4). Zircon domains or grains of clear inherited or metamorphic origin were not identified in any of the samples. However, many of the grains from sample 16BK374A do have distinct core and rim domains (Figure 3-4). The cores exhibit fine-scale oscillatory zoning, whereas the rims exhibit broad zoning that roughly parallels the zoning in the cores. All of the core-rim pairs yield dates that are

indistinguishable within uncertainty. The cores and rims are therefore interpreted to reflect two, analytically indistinguishable, stages of igneous zircon growth.

Thirteen samples spanning the full compositional range of the diorite–quartz-diorite–granodiorite–granite package in map unit 3 (Figure 3-2), were selected for geochronology (Table 3-1). Four samples to the south of the main study area that are correlated to this rock package were also dated (Figure 3-2; Table 3-1). Most of the igneous zircon analyses from these samples yield consistent data clusters, and the crystallization ages determined range from 2518 ± 5 to 2476 ± 6 Ma (Table 3-1; Figure 3-1A). Rare zircon core domains and grains ($n=4$) yielding dates of ~ 2570 Ma and ~ 2530 Ma from samples 21BN34A and 19BN166A are interpreted as inherited (Figure 3-4). Three samples (18BN114A, 19BN173A and 18BN113A) contain unzoned rims and irregularly zoned and shaped grains that yield dates of ~ 2400 Ma, which are interpreted as metamorphic (Figure 3-4). Regarding samples 19BN173A and 18BN113A in particular, there is a clear relationship between $^{207}\text{Pb}/^{206}\text{Pb}$ date and ^{238}U cps (Figure 3-4). The ^{238}U cps from igneous zircon analyses tend to increase with decreasing $^{207}\text{Pb}/^{206}\text{Pb}$ date, supporting the interpretation that dates younger than the main clusters reflect ancient Pb-loss. By contrast, the ca. 2400 Ma analyses yield relatively low ^{238}U cps, which is consistent with the interpretation that they represent distinct metamorphic zircon populations.

In summary, zircon U-Pb geochronology has identified three late Archean granitoid suites in the Nonacho area, with crystallization ages of ca. 2.71–2.69, 2.58–2.57 and 2.52–2.48 Ga (Table 3-1). These three suites are referred to as the 2.7, 2.6 and 2.5 Ga granitoids hereafter. As it is used here, the term granitoid includes mafic (dioritic) plutonic rocks that are associated with more evolved (quartz-dioritic to granitic) plutonic rocks. Note that although the 2.5 Ga granitoids include samples with crystallization ages between 2.52 and 2.48 Ga, the majority of the dated samples in this suite are 2.50 ± 0.01 Ga in age (Table 3-1; Figure 3-4).

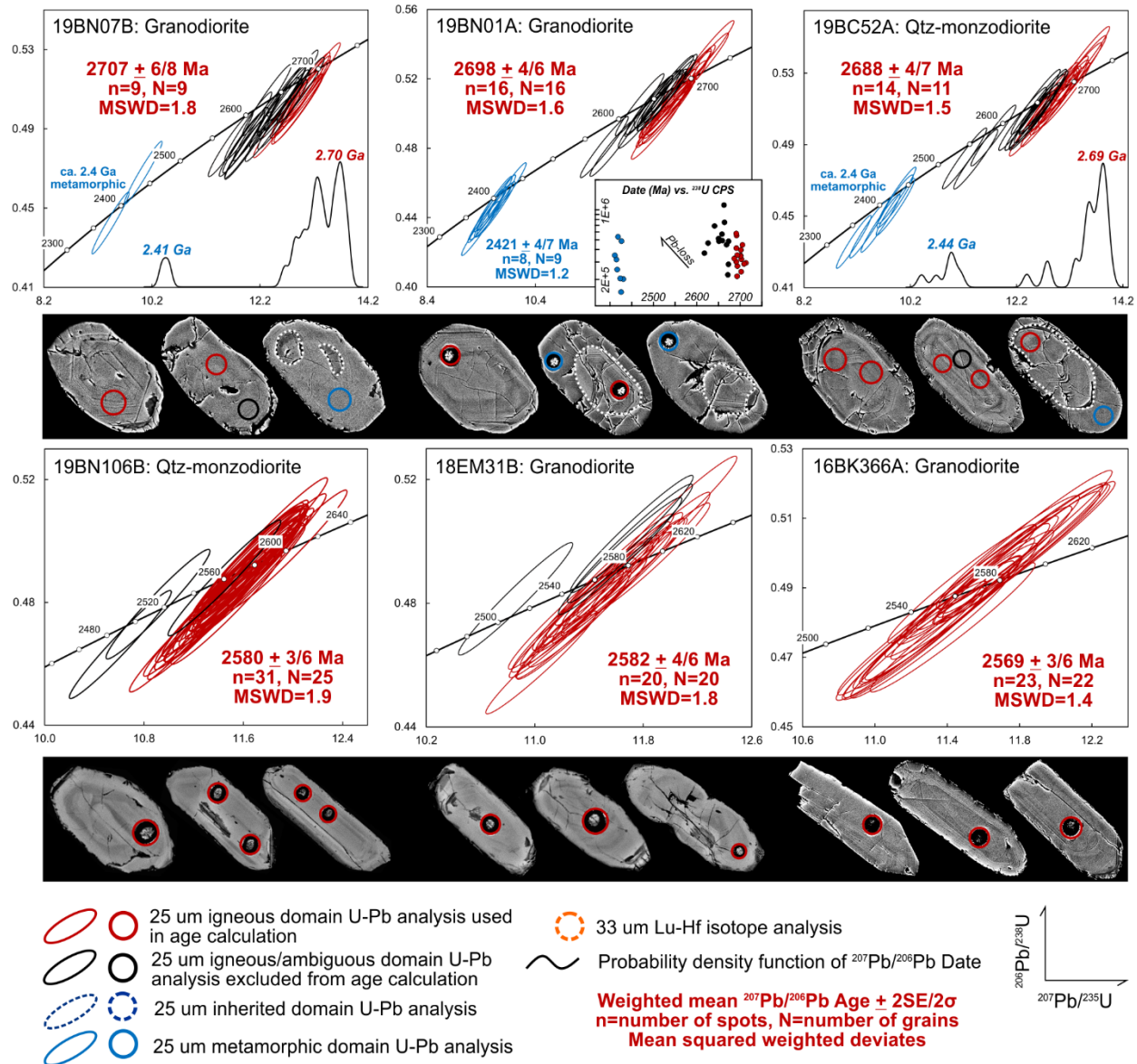


Figure 3-4. Wetherill Concordia diagrams and representative BSE or CL zircon images with analytical spot locations. Uncertainty ellipses are 2σ. Probability density plots of ²⁰⁷Pb/²⁰⁶Pb dates and plots of ²⁰⁷Pb/²⁰⁶Pb Date vs. ²³⁸U cps (counts per second) plots are included for select samples. White dashed lines highlight core-rim boundaries.

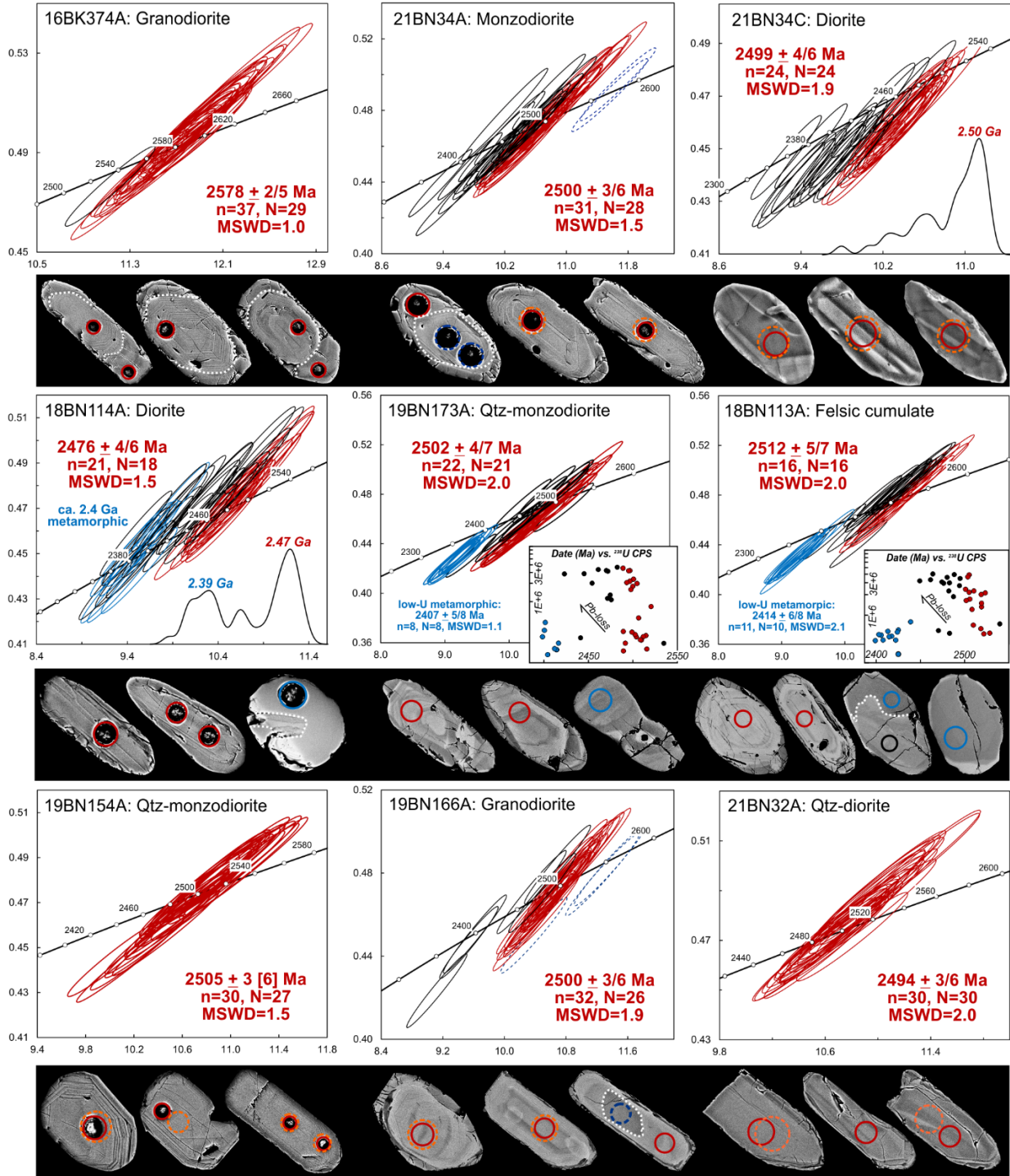


Figure 3-4. Continued.

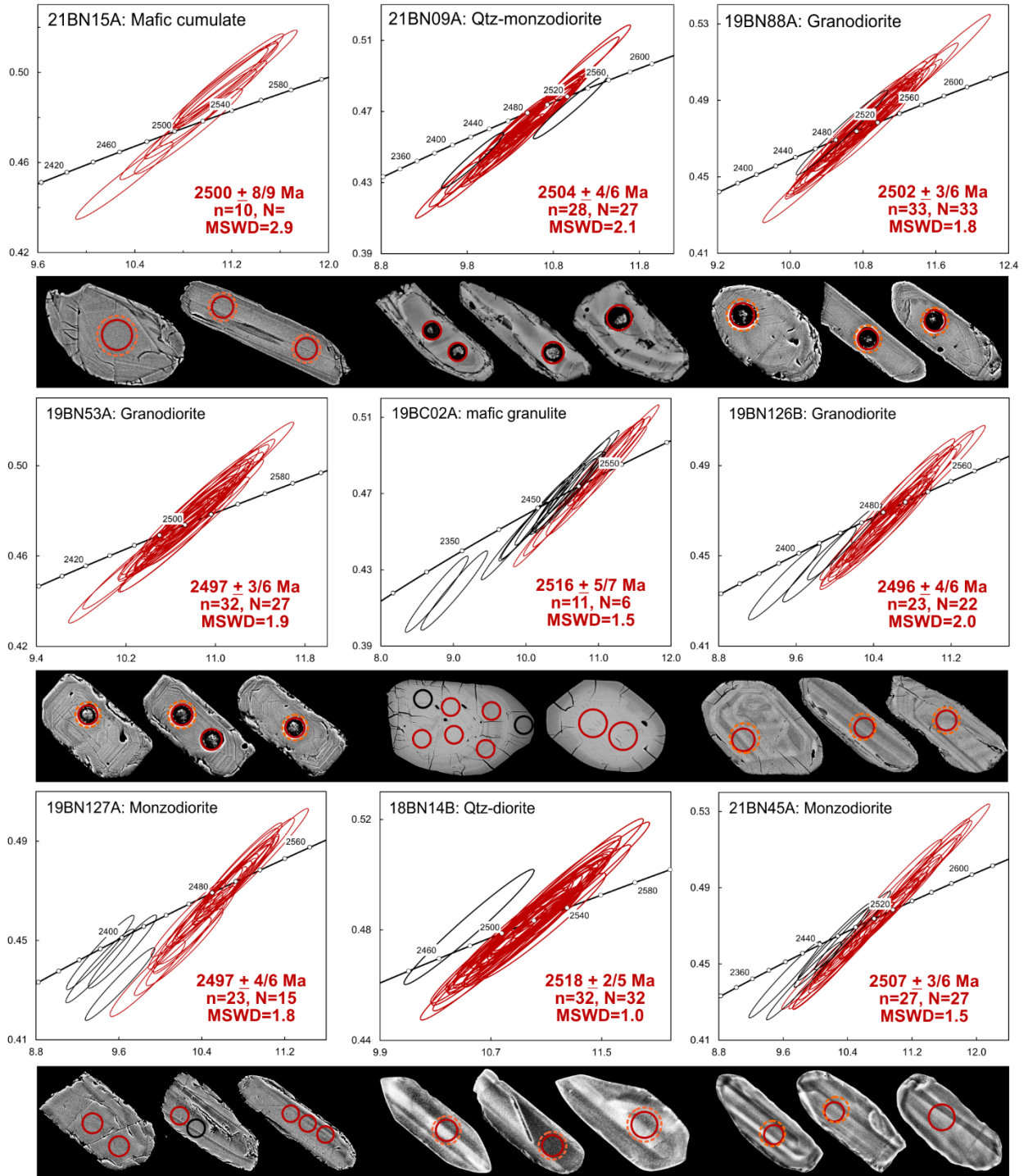


Figure 3-4. Continued.

3.5.2 Whole-rock geochemistry

Here I describe and compare the geochemical characteristics of the three late Archean granitoid suites identified above. The focus is on characterizing the 2.5 Ga granitoids, but the 2.7 and 2.6 Ga granitoids are also considered in order to contrast them with the 2.5 Ga rocks, and to constrain the geochemical and isotopic composition of the basement into which the 2.5 Ga magmas may have intruded. Samples that were not dated directly via U-Pb zircon geochronology were correlated to their respective suite on the basis of field mapping, petrography, and their geochemical and isotopic composition.

The major-element data are presented on conventional granitoid classification diagrams (Figure 3-5) and on Harker variation diagrams (Figure 3-6). The trace-element, and some minor- and major-element data are presented on primitive mantle-normalized extended element plots (Figure 3-7), chondrite-normalized rare earth element (REE) plots (Figure 3-7), and on select variation diagrams (Figure 3-8). All three granitoid suites comprise samples that are broadly calc-alkalic to calcic (rarely alkali-calcic), dominantly magnesian, and metaluminous to weakly peraluminous (Figure 3-5). Another common feature of the three suites is the overall enrichment of elements that are traditionally considered incompatible. The large ion lithophile elements (LILE) Rb, Ba and K are typically present in concentrations of ~100x primitive mantle, and the light REE (LREE) are typically present in concentrations $\geq 100x$ chondrite (Figure 3-7).

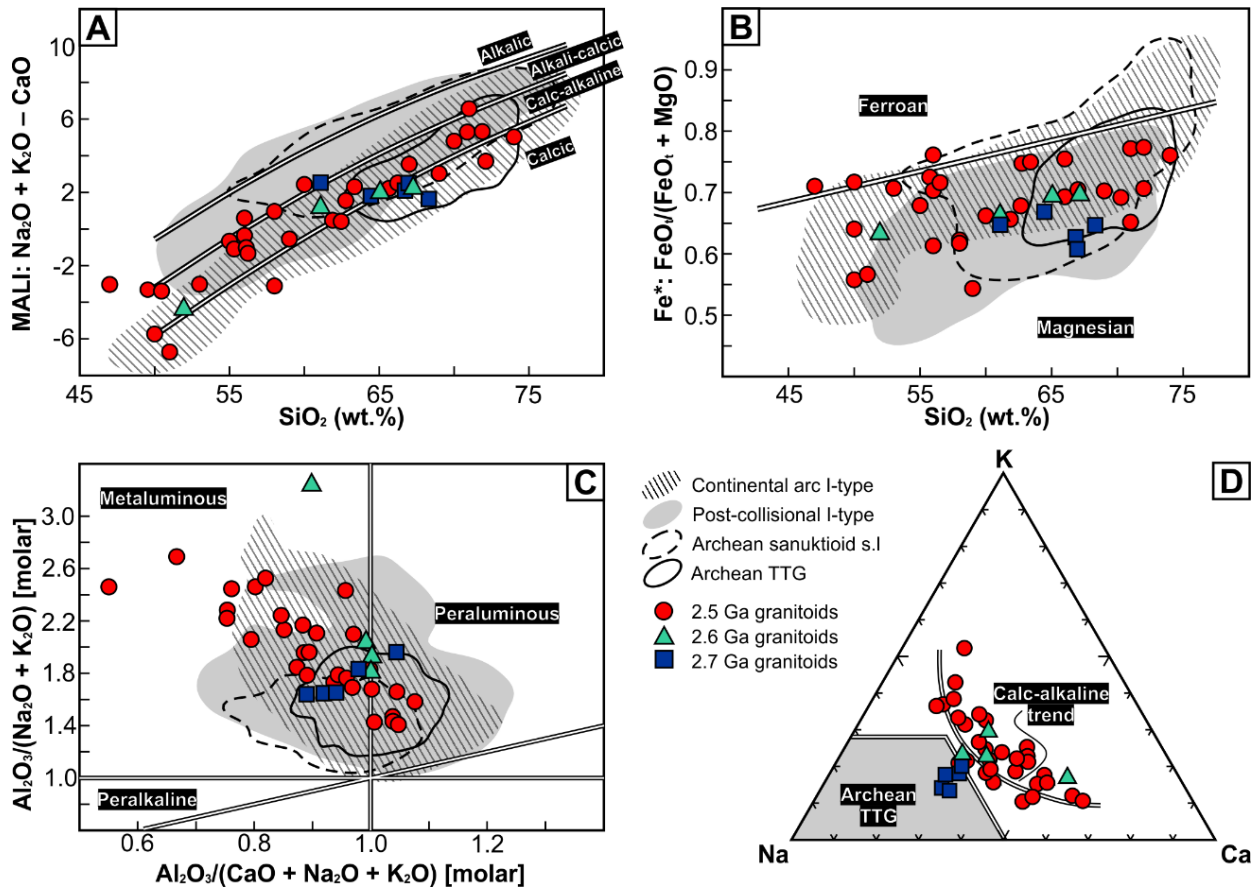


Figure 3-5. Standard granitoid geochemical classification diagrams. (A) SiO_2 vs. MALI (modified alkali-lime index) (Frost et al., 2001); (B) SiO_2 vs. Fe^* (Frost et al., 2001); (C) Shand's index (Maniar and Piccoli, 1989); (D) Na-K-Ca ternary after Barker and Arth (1976) and Martin (1994). Comparative data fields on (A)–(C) (e.g., Continental arc I-type) are 75% Kernel density contours, see Appendix C for compiled data sources.

3.5.2.1 2.7 Ga granitoids

The 2.7 Ga granitoids contain 61 to 68 wt.% SiO₂. Although these rocks are calc-alkalic to calcic in the classification scheme of Frost et al. (2001), on the ternary Na-K-Ca plot of Barker and Arth (1976), they do not define a calc-alkaline trend, but rather plot at the edge of the Archean TTG (tonalite-trondhjemite-granodiorite) field (Figure 3-5A). At comparable SiO₂ contents, these granitoids have the lowest K₂O (1.5–2.5 wt.%) contents, highest Na₂O (3.9–5.3 wt.%) contents and highest Mg-numbers (47–54) of the three suites (Figure 3-6). Trace-element patterns are characterized by prominent negative Nb anomalies, small negative Sr and Ti anomalies, and nearly absent Eu and Zr-Hf anomalies (Figure 3-7). The LREE are strongly enriched ($La_{CN} = 200\text{--}300$; CN=chondrite normalized) and the HREE are strongly depleted ($Yb_{CN} = 4\text{--}5$), giving rise to very steep REE patterns ($La_{CN}/Yb_{CN} = 45\text{--}60$). These rocks have the steepest REE patterns and are the most HREE depleted of the three suites. They also have the highest Ni (24–33 ppm) concentrations at comparable SiO₂ contents (Figure 3-8). The high Ni contents and Mg-numbers of these rocks are notable considering their relatively evolved nature.

3.5.2.2 2.6 Ga granitoids

Three of the 2.6 Ga granitoids contain between 61 and 67 wt.% SiO₂, whereas a fourth sample (hornblende diorite) contains 52 wt.% SiO₂. These rocks fall outside the TTG field on the Na-K-Ca plot (Figure 3-5), distinguishing them from the 2.7 Ga granitoids. They are also separated from the 2.7 Ga suite by their higher K₂O contents (2.2–3.5 wt.%), lower Na₂O contents (2.2–3.6 wt.%), slightly lower Mg-numbers (44–51) and lower Ni contents (Figures 3-6 and 3-8). The three more siliceous granitoids are characterized by prominent negative Nb and Ti anomalies, moderate negative Sr anomalies, and a lack of significant Eu and Zr-Hf anomalies (Figure 3-7). In addition, their REE patterns are moderately steep ($La_{CN}/Yb_{CN} = 24\text{--}35$) and their HREE contents are moderately depleted ($Yb_{CN} = 7\text{--}8$); in this sense they are intermediate between the 2.7 Ga and 2.5 Ga granitoids (Figure 3-7). The absence of significant Eu anomalies also distinguish the 2.6 Ga granitoids from the 2.5 Ga granitoids. The hornblende diorite is distinct in that it exhibits negative Zr-Hf anomalies, a positive Sr anomaly, no Ti anomaly, and a concave down LREE pattern (Figure 3-7).

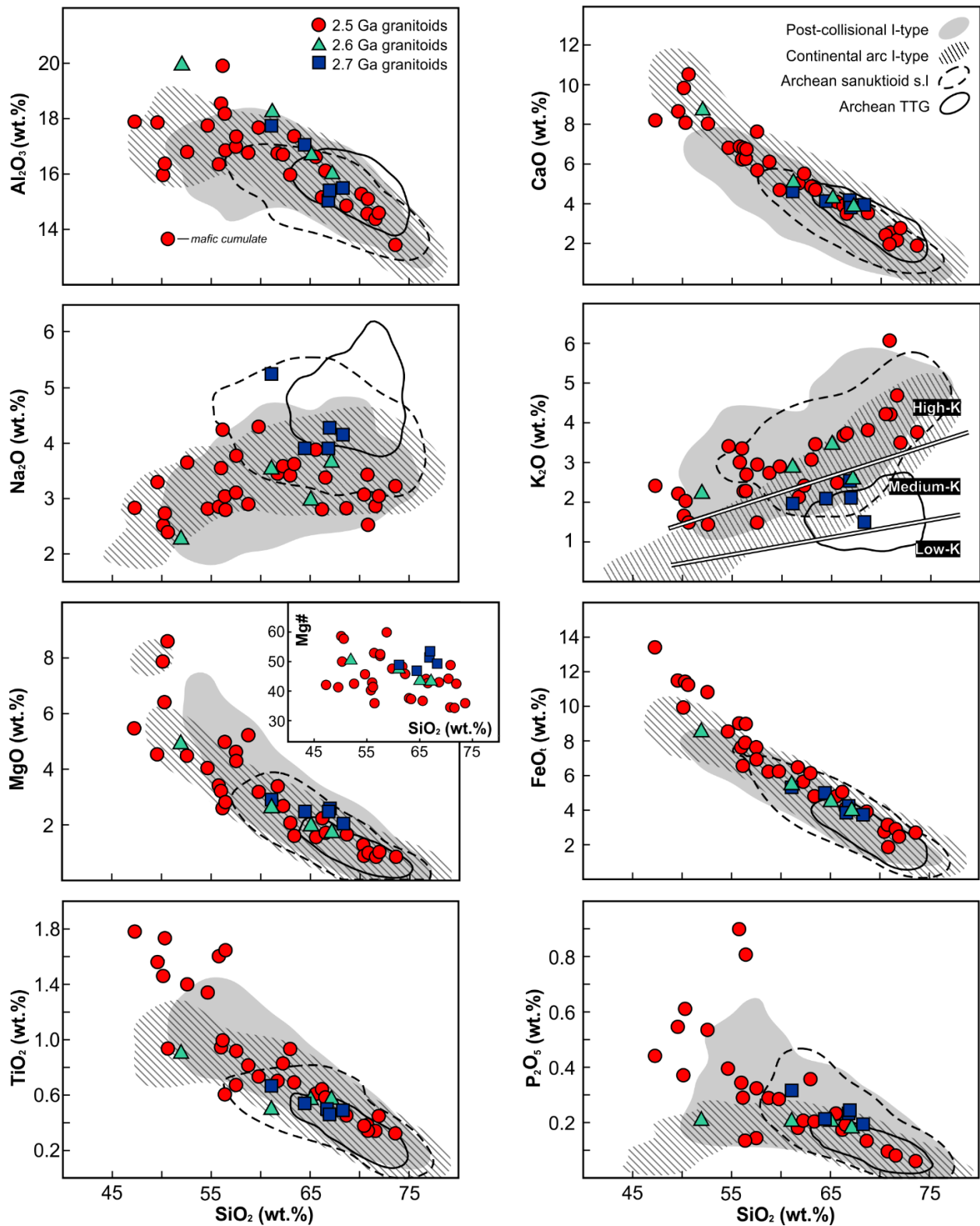


Figure 3-6. Major element Harker variation diagrams. Comparative data fields are as in Figure 3-5. Series fields on the SiO_2 vs. K_2O plot (i.e., high-K) are from Gill (1981). Mg# (Mg-number) is calculated as molecular $\text{Mg}/(\text{Mg}+\text{Fe}^{2+})$, with all Fe expressed as Fe^{2+} .

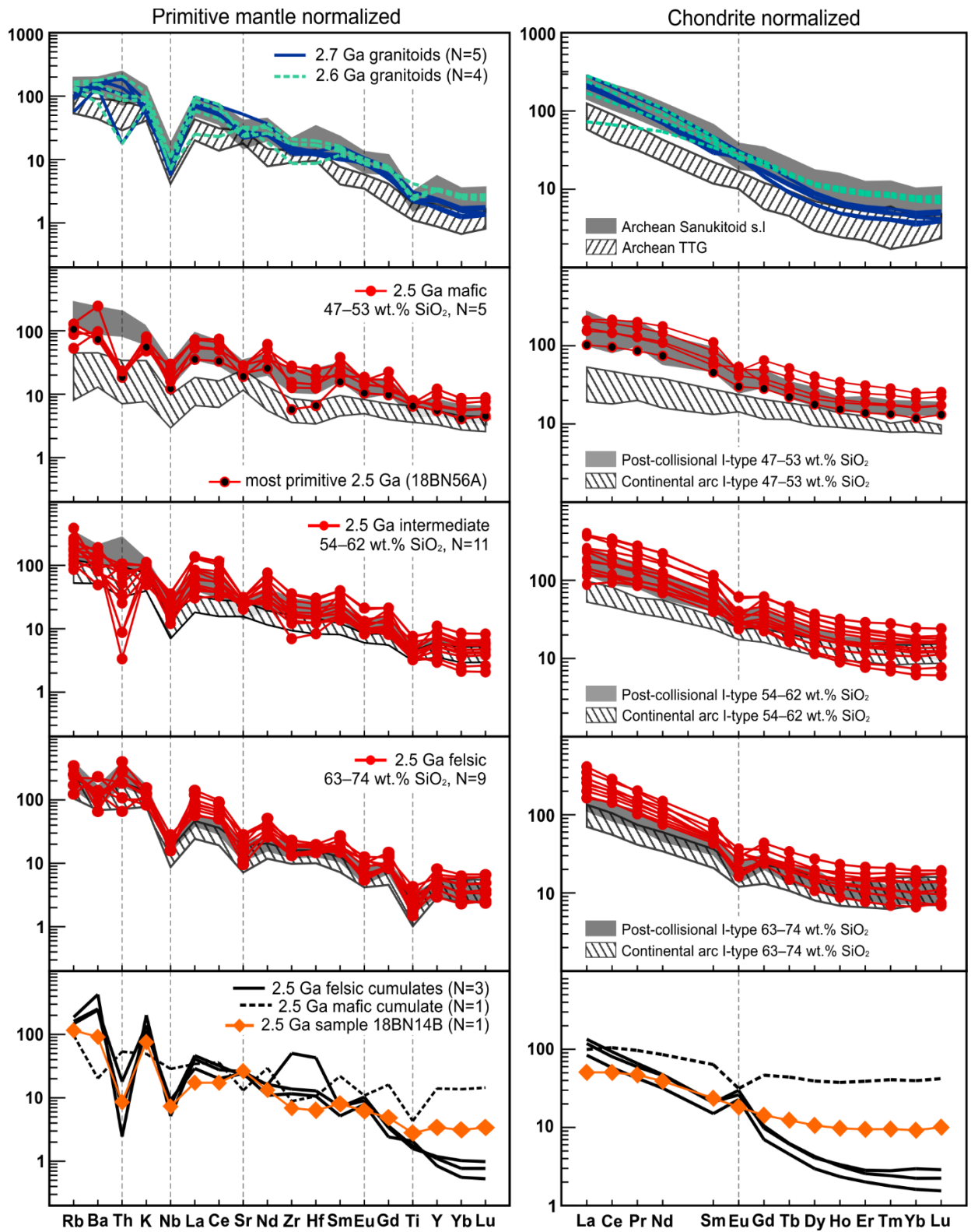


Figure 3-7. Primitive mantle normalized trace-element plots and chondrite normalized REE plots. Normalizing values are from Sun and McDonough (1989). Comparative data fields (e.g., Archean TTG field) are interquartile ranges. N = number of samples. Data sources are as in Figure 3-3.

3.5.2.3 2.5 Ga granitoids

The 2.5 Ga granitoids range in a near continuous fashion from 47 to 74 wt.% SiO₂, and define very clear calc-alkaline trends on both the MALI (modified alkali-lime index) plot (Figure 3-5A) and the Na-K-Ca ternary plot (Figure 3-5D). On Harker variation diagrams most major and minor oxides are negatively (CaO, FeO_t, MgO, TiO₂ and P₂O₅) or positively (K₂O) correlated with SiO₂ (Figure 3-6). The oxides Al₂O₃ and Na₂O display poorly defined inflections (change to compatible behavior) at ~60 wt.% SiO₂ (Figure 3-6). The Mg-numbers range from 60 to 34 and decreases, on average, with increasing SiO₂ content (Figure 3-6). The least siliceous samples have rather high TiO₂ and P₂O contents of more than ~1.2 and ~0.3 wt.%, respectively (Figure 3-6). On the SiO₂ vs. K₂O plot, almost all 2.5 Ga samples fall within the high-K field (Figure 3-6), and thus, the suite can be referred to as high-K calc-alkaline. Potassium and other fluid mobile LILE are susceptible to alteration. However, the fact that the 2.5 Ga samples plot rather consistently within the high-K field (Figure 3-6), and are also enriched in other less mobile incompatible elements such as the LREE (see below), suggests that the enrichment is a primary igneous feature.

Given the broad range of silica contents in the 2.5 Ga suite, the trace-element data are presented in three groups referred to as the mafic (47–53 wt.% SiO₂), intermediate (53–63 wt.% SiO₂) and felsic (63–74 wt.% SiO₂) rocks (Figure 3-7). The overall trace-element patterns of the three groups are similar, and consist of moderate negative Nb, Zr, Hf, Ti, Sr and Eu anomalies, and moderately steeply sloping REE patterns (Figure 3-7). The mafic rocks and some of the intermediate rocks are also depleted in Th relative to K and La, and in some cases even relative to Nb (Figure 3-7). Some trace-element characteristics of the suite are better visualized on variation diagrams (Figure 3-8). The LREE data are scattered and show little-to-no correlation with SiO₂, whereas the middle REE and HREE tend to decrease in concentration, on average, with increasing SiO₂ (Figure 3-8). Consequently the felsic rocks tend to have steeper REE patterns (average La_{CN}/Yb_{CN} = 24) than the intermediate (average La_{CN}/Yb_{CN} = 15) and mafic (average La_{CN}/Yb_{CN} = 9) rocks. Strontium contents and Sr/Sr* and Eu/Eu* values do not decrease systematically until above ~60 wt.% SiO₂. Hafnium and Zr (not plotted) contents are variable, but some samples in the 47–57 wt.% SiO₂ range contain as much as 6–9 ppm Hf and 285–398 ppm Zr (Figure 3-8). Niobium contents are elevated (typically >10 ppm) throughout the full compositional range of the suite (Figure 3-8), and the highest concentrations (18–27 ppm) are in samples with 50–56 wt.% SiO₂ (Figure 3-8). The compatible elements V and Sc (not plotted) exhibit strong negative correlations with SiO₂, and reach abundances in line with those of primitive MORB or arc basalts (Kelemen et al., 2014). By contrast, Ni and Cr (not plotted) abundances are relatively low and their correlations with SiO₂ are weak (Figure 3-8). Altogether, trace-element characteristics that distinguish the 2.5 Ga granitoids from the

2.7 Ga and 2.6 Ga granitoids are their higher Nb contents, less steep REE patterns, and sizeable negative Eu and Sr anomalies (Figures 3-7 and 3-8).

The most primitive sample in the mafic group, which is likely the closest in composition to a primary mantle-derived parent magma, is 18BN56A (Table 3-1; Figure 3-7). This sample contains 50 wt.% SiO₂, 346 ppm Cr and 105 ppm Ni, and has an Mg-number of 59. 18BN56A was collected from a ~1-metre-thick layer (transposed dyke?) of relative fine-grained diorite in a complex orthogneiss outcrop (Figure 3-3F). The relatively fine-grained nature of the sample suggests that it likely approximates a liquid composition, rather than being a crystal cumulate. This interpretation is supported by its textural and geochemical similarity to another mafic 2.5 Ga sample (21BN34C), which was collected from a discrete ~30–50 cm wide dyke of fine-grained diorite that cross-cuts a coarser grained and more evolved 2.5 Ga granitoid (sample 21BN34A).

A fourth set of plots (bottom row, Figure 3-7) presents data for five 2.5 Ga samples that do not fit into the mafic, intermediate or felsic groups, including four that are suspected to be dominated by cumulate crystals. One mafic cumulate (21BN15A) has a high modal abundance of hornblende, and substantially lower Al₂O₃ (14 wt.%), higher HREE and higher Sc contents, than all other 2.5 Ga granitoids. These features are suggestive of amphibole or clinopyroxene accumulation. Three felsic cumulates (18BN31A; 18BN113A; 18BN18B-F) are characterised by high feldspar modal abundances, large positive Eu anomalies, and much lower REE contents than all other 2.5 Ga rocks. These characteristics are consistent with feldspar accumulation (e.g., Rollinson, 2021). Finally, one quartz-diorite (sample 18BN14B) is plotted separately (Figure 3-7 and 3-8) because, in contrast to the other 2.5 Ga granitoids, it has substantially lower REE and HFSE contents, no Eu anomaly and a large positive Sr anomaly (Figures 3-7 and 3-8). This sample is also measurably older (ca. 2.52 Ga) than the other dated 2.5 Ga suite samples, with the exception of one felsic cumulate (18BN113A; Table 3-1) and a mafic granulite (19BC02A; Table 3-1).

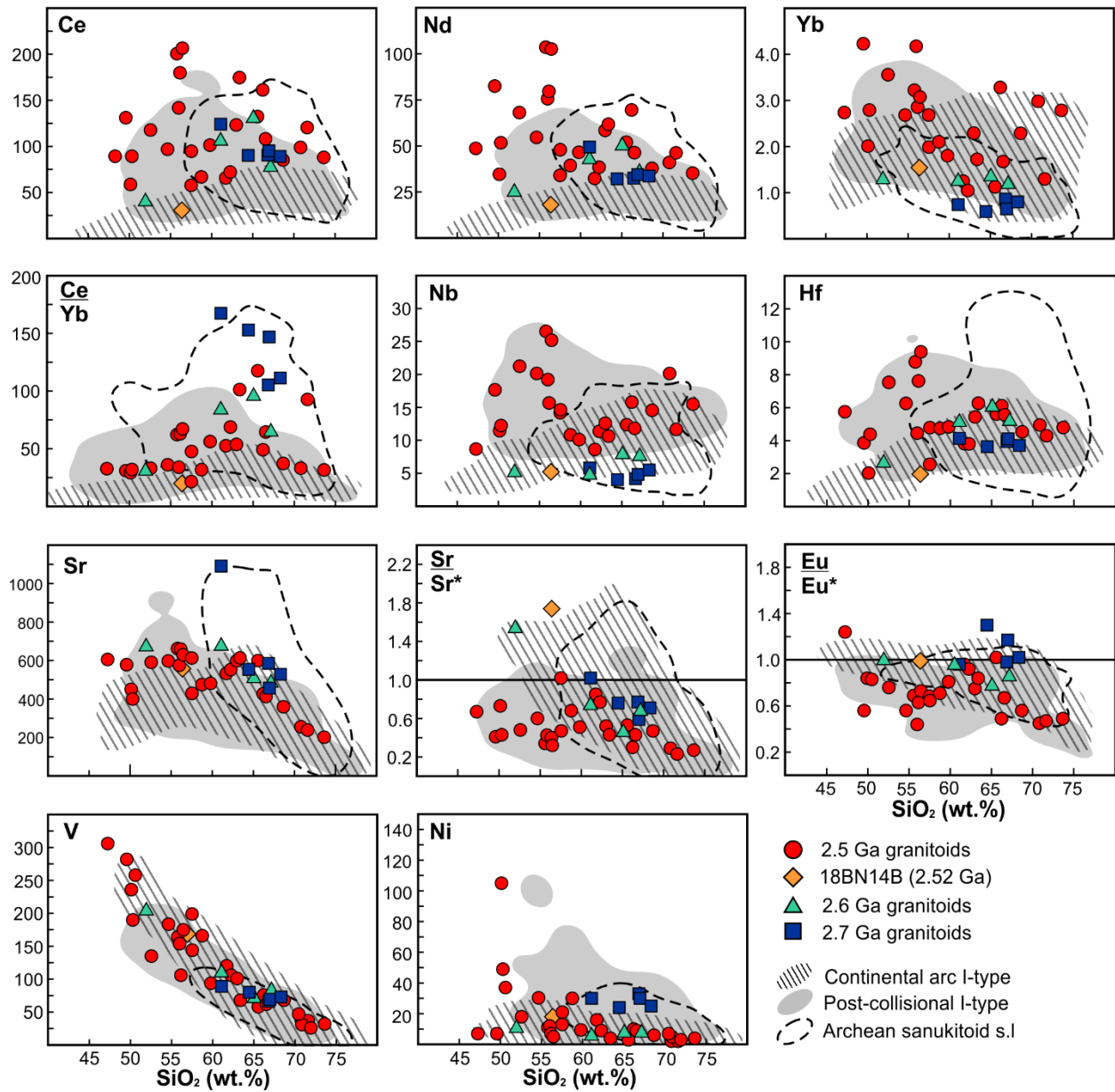


Figure 3-8. Harker variation diagrams for select trace elements (ppm) and trace element ratios. Comparative data fields (e.g., Archean sanukitoid s.l) are as in Figures 3-5 and 3-6. The TTG fields have been excluded for clarity. $Eu/Eu^* = Eu_{CN}/(Sm_{CN} \times Gd_{CN})^{0.5}$. $Sr/Sr^* = Sr_{N}/(Ce_{N} \times Nd_{N})^{0.5}$. CN=chondrite normalized, N=primitive mantle normalized. Normalizing values from Sun and McDonough (1989).

3.5.3 Isotope geochemistry

3.5.3.1 Whole-rock Sm-Nd isotope data

The results of 38 whole-rock Sm-Nd isotope analyses are strikingly consistent. All three plutonic suites yield approximately chondritic initial ϵNd (ϵNd_i) values (Table 3-1; Figure 3-9A). The ϵNd_i values range from +0.6 to -0.2 for the 2.7 Ga granitoids, +0.5 to -0.3 for the 2.6 Ga granitoids, and +0.6 to -0.5 for the 2.5 Ga granitoids (Table 3-1). The Nd isotope homogeneity of the 2.5 Ga granitoid suite is especially remarkable considering its compositional diversity. The ϵNd_i values from the 2.5 Ga suite as a whole yield a 2SD of 0.6, which is only slightly greater than the long-term reproducibility of the technique (~ 0.3 ϵNd , Appendix A). Thus, half of the already miniscule Nd isotope variability in the suite can be attributed to analytical uncertainty. In addition, the 2.5 Ga rocks yield a Sm-Nd isochron age of 2485 ± 69 Ma with an ϵNd_i of -0.1 ± 1.0 (Figure 3-9B). The coherence of the 2.5 Ga suite Sm-Nd isotope data and the consistency of this isochron age with the U-Pb age data is evidence that the REE, and presumably the other relatively immobile trace elements (e.g. Th, Nb, Zr and Y), were not significantly affected by metamorphism or alteration.

3.5.3.2 Zircon Lu-Hf isotope results data

To further examine the isotopic homogeneity of the 2.5 Ga suite, zircon Hf isotope data were acquired for eleven samples (Table 3-1). Hafnium isotope analyses primarily targeted homogeneous zircon domains that yielded “concordant” U-Pb data and $^{207}\text{Pb}/^{206}\text{Pb}$ ages that were included in the crystallization age calculations (Figure 3-4). Individual ϵHf measurements are plotted at the $^{207}\text{Pb}/^{206}\text{Pb}$ date of the corresponding zircon domain. These data cluster within ~ 2 ϵHf units of CHUR, and largely overlap it within uncertainty (Figure 3-9). A small number of analyses plotting to the left of the main cluster (Figure 3-9) are from igneous domains in sample 21BN34C that are interpreted to have undergone ancient-Pb loss (Figure 3-4). Indeed, these analyses fall on a Pb-loss trajectory projected from the initial ϵHf of 21BN34C (Figure 3-9). Prior to calculating weighted mean initial ϵHf_i values, all individual ϵHf values were recalculated at their respective samples crystallization age (Table 3-1). The weighted mean ϵHf_i values range from $+1.5 \pm 2.3$ to -1.1 ± 1.4 (2SD) (Table 3-1; Figure 3-9C). Most samples have relatively homogeneous zircon ϵHf_i populations, with MSWDs of ~ 1 – 2 . For samples 18BN14B and 19BN166A, there is more dispersion (MSWDs of ~ 3 – 4), implying that to some extent, isotopically heterogeneous magma sources or assimilants were involved in their genesis. Altogether, the Hf isotope data confirm the chondritic character of the 2.5 Ga granitoids, revealed by the Nd isotope data. The somewhat greater dispersion in ϵHf_i values compared to ϵNd_i values is not surprising given that: 1) laser ablation Hf isotope data are inherently less precise than isotope dilution Nd isotope data; and 2) in most crust-mantle differentiation processes, the fractionation between Lu and Hf is greater than that between Sm and Nd. All samples

for which both Nd and Hf isotope data were acquired plot within the “terrestrial array” envelope of Vervoort et al. (2011), and thus provide no indication of Nd-Hf isotope decoupling (Figure 3-9D).

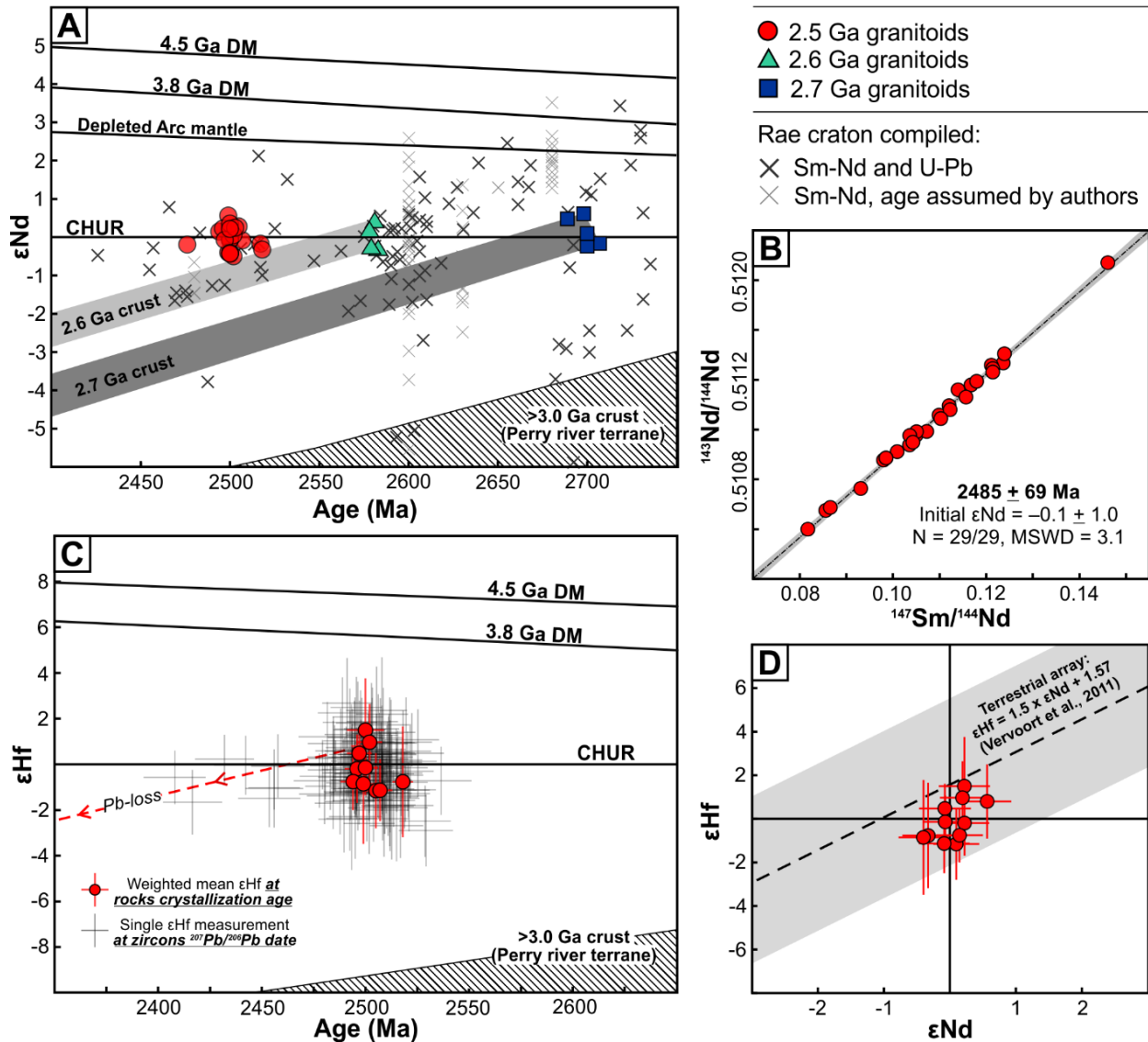


Figure 3-9. Isotope geochemistry results. (A) Age vs. initial ϵ_{Nd} . 4.5 Ga and 3.8 Ga depleted mantle (DM) lines after Goldstein et al. (1984) and Fisher and Vervoort (2018), respectively. Depleted Arc mantle model from DePaolo (1981a). See appendix C for compiled data sources. (B) Sm-Nd whole-rock isochron for all 2.5 Ga suite samples (cumulates and 18BN14B included). Uncertainties are smaller than the data points. (C) Age vs. zircon ϵ_{Hf} . Single ϵ_{Hf} measurements plotted at the zircon domains $^{207}Pb/^{206}Pb$ date. Weighted mean ϵ_{Hf} values calculated at the rocks interpreted crystallization age. Weighted mean, mean and median ϵ_{Hf} values are indistinguishable for all samples. The Pb-loss vector is the time integrated ϵ_{Hf} evolution of zircon ($^{176}Lu/^{177}Hf=0.001$), starting at the ϵ_{Hf} of sample 21BN34C. (D) Initial ϵ_{Nd} vs. weighted mean initial ϵ_{Hf} for samples with both Nd and Hf isotope data. Uncertainties shown for the weighted mean ϵ_{Hf} are 2SD.

3.6 Discussion

3.6.1 Granitoid classification

Prior to discussing the petrogenesis of the 2.7–2.5 Ga granitoids, it is instructive to consider how they compare to established Archean granitoid types. Archean granitoid classification schemes typically include three main divisions: 1) siliceous (>65 wt.% SiO₂) and sodic (K₂O/Na₂O <0.6) tonalite-trondhjemite-granodiorite (TTG) suites; 2) high-Mg mafic to felsic sanukitoids; and 3) potassic (K₂O/Na₂O >0.8) biotite ± muscovite granites (Moyen et al., 2003; Halla et al., 2009; Laurent et al., 2014a). Sanukitoids were originally defined as high-Mg quartz-diorites (Mg#>60) with the unique combination of elevated compatible (e.g., Cr and Ni) and incompatible (e.g., LILE and LREE) element concentrations (Shirey and Hanson, 1984; Stern et al., 1989). The sanukitoid definition has since been expanded to include more evolved granitoids (up to ~70 wt.% SiO₂) that are genetically related to incompatible element rich high-Mg mafic rocks, and have higher concentrations of compatible and incompatible elements by comparison to TTGs of similar SiO₂ content (Stern and Hanson, 1991; Martin et al., 2009; Heilimo et al., 2010). Some authors also distinguish between sanukitoids *sensu stricto* (s.s) and sanukitoids *sensu lato* (s.l) (Laurent et al., 2014a; Moyen, 2020a). The sanukitoid s.l umbrella includes the sanukitoids s.s and a group of rocks sometimes referred as high-Ti sanukitoids (Martin et al., 2009). The latter have also been referred to as to as Closepet-type granitoids (Martin et al., 2005) and high-K calc-alkaline granitoids (Moyen, 2020a). High-Ti sanukitoids are less well documented than sanukitoids s.s and most geochemical data for them come from two locations, the Closepet Batholith of southern India (Moyen et al., 2001, 2003) and the Bulai pluton of South Africa (Laurent et al., 2011, 2013). These rocks differ from sanukitoids s.s in that they tend to be more evolved (higher K₂O/Na₂O, lower Mg#, and lower Ni and Cr contents), exhibit negative Eu and Sr anomalies, and have greater Ti and Nb contents (Moyen et al., 2003; Martin et al., 2005; Martin et al., 2009; Laurent et al., 2011; Moyen, 2020a). It must be emphasized that continuums likely exist between some or all of the granitoid types describe above, especially at the evolved end of the compositional spectrum (Moyen, 2020a).

For comparison to the rocks in this study, compositional fields for TTGs and sanukitoids s.l (sanukitoids s.s plus high-Ti sanukitoids) have been included on Figures 3-5 through 3-8. The sanukitoids s.s and high-Ti sanukitoids were grouped on these plots for simplicity, but have been separated in Table 3-2. Table 3-2 contains median values for a set of distinguishing chemical parameters in TTGs, sanukitoids s.s and high-Ti sanukitoids, along with median values from the 2.7, 2.6 and 2.5 Ga suites. The sanukitoids s.s, high-Ti sanukitoids and 2.5 Ga granitoids are compared at both >62 wt.% SiO₂ and ≤62 wt.% SiO₂ (Table 3-2), because the distinguishing compositional features of these rocks are more apparent at lower degrees of differentiation (e.g., Martin et al., 2009).

None of the rocks in this study can be classified as TTGs. Some aspects of the 2.7 Ga granitoids, such as their moderately low K₂O/Na₂O ratios, steep REE patterns and negligible Eu anomalies, are similar to TTGs. However, when these TTG-like characteristics are combined with other traits, such as their comparably high Mg#, and Cr, Ni and LREE contents, it is clear that the 2.7 Ga granitoids are best classified as sanukitoids s.s. The four 2.6 Ga rocks from this study have equivocal geochemical characteristics, and it is hardly justifiable to “classify” them. However, they are probably part of the much larger, pan-Rae, 2.62–2.58 Ga SIS (Figure 3-1B), which has been described as “sanukitoidal” (Peterson et al., 2024). Although not a perfect match, several characteristics of the 2.5 Ga granitoids liken them to the high-Ti sanukitoids (Table 3-2). This includes their elevated HFSE (especially Ti and Nb) contents, their negative Eu and Sr anomalies, and their comparatively high K₂O/Na₂O ratios, low Mg#, and low Ni and Cr contents. The elevated Ti and Nb contents, in particular, appear to be a relatively diagnostic feature of high-Ti sanukitoids (Martin et al., 2005, 2009; Table 3-2). Having established some similarities with different types of sanukitoids, the petrogenesis of the 2.7–2.5 Ga granitoids is discussed below.

Table 3-2. Comparison of median values for select chemical parameters in TTGs, sanukitoids s.s, and high-Ti sanukitoids, and the granitoid suites in this study.

	TTG N=1454	Sanukitoid s.l				This study			
		Sanukitoid s.s		High-Ti sanukitoid		2.7 Ga suite N=5	2.6 Ga suite N=4	2.5 Ga suite	
		>62 wt.% SiO ₂ N=226	<62 wt.% SiO ₂ N=90	>62 wt.% SiO ₂ N=245	<62 wt.% SiO ₂ N=79			>62 wt.% SiO ₂ N=10	<62 wt.% SiO ₂ N=15
SiO₂ wt.%	69.66	66.39	59.03	70.45	57.26	66.84	63.07	66.37	55.99
MgO wt.%	0.99	1.76	3.93	0.65	2.90	2.48	2.38	1.63	4.30
TiO₂ wt.%	0.34	0.43	0.62	0.39	1.39	0.49	0.57	0.60	1.34
K₂O/Na₂O	0.33	0.67	0.60	1.10	0.73	0.49	0.90	1.14	0.55
Mg#	42	48	55	32	40	49	46	37	46
Cr ppm	24	44	116	16	56	39	7	13	49
Ni ppm	11	22	55	11	32	30	8	4	13
Ce ppm	38.1	72.8	106.9	114.9	172.5	90.6	92.5	114.3	96.9
Yb ppm	0.57	0.86	1.57	2.22	2.72	0.74	1.28	2.01	2.74
Nb ppm	4.5	5.9	7.3	14.1	18.8	4.6	6.5	12.5	14.6
Ce/Yb	66.8	84.7	68.1	51.7	63.4	122.2	72.1	59.1	35.4
Eu/Eu*	1.05	0.87	0.90	0.72	0.79	1.02	0.91	0.62	0.71
Sr/Sr*	1.55	1.01	0.98	0.36	0.37	0.76	0.71	0.49	0.43

Note: TTG, sanukitoid s.s and high-Ti sanukitoid data are from Moyen (2020a), minus data from the ferroan Matok pluton (Laurent et al., 2014b) and plus data from sanukitoids s.s in the Slave craton (Davis et al., 1994). High-Ti sanukitoids have also been referred to as “Closepet-type” or “high-K calc-alkaline” granitoids (Moyen, 2019).

3.6.2 Petrogenesis of the 2.7 and 2.6 Ga granitoids

As noted above, the 2.7 Ga granitoids can be unequivocally described as sanukitoids s.s. The prevailing interpretation of sanukitoid s.s suites is that they reflect the interaction between melts of subducted basalt (TTG-like melts) and mantle peridotite, and that this interaction gives rise to magmas that have high Mg-numbers, and Cr and Ni contents, but which are also LILE and LREE enriched (e.g., Smithies and Champion, 2000; Moyen, 2003; Martin et al., 2009). Specifically, two models have been proposed: 1) that sanukitoids s.s are slab melts that were contaminated by mantle peridotite during their ascent (e.g., Rapp et al., 1999); or 2) that sanukitoids s.s derive from partial melting of a mantle source that was metasomatized by slab melts (e.g., Smithies and Champion, 2000). The two models may apply to different sanukitoid s.s suites (e.g., Martin et al., 2009). The latter model seems more applicable to the 2.7 Ga granitoids, because they are more LREE enriched than typical TTGs (Figure 3-7), and the contamination of a TTG melt by mantle peridotite could only serve to decrease its LREE content. This interpretation implies that the evolved (>60 wt.% SiO₂) 2.7 Ga granitoids identified here are the derivatives of less evolved (i.e., dioritic) sanukitoid s.s parent magmas that have yet to be identified.

Given that the 2.6 Ga granitoids do not bear any particularly diagnostic geochemical features, less can be said about their petrogenesis. However, one point worth making is that both the 2.7 and 2.6 Ga suites represent, at least in part, juvenile additions to the continental crust. For the 2.7 Ga granitoids this is evidenced by their high Ni contents and Mg-numbers, and for the 2.6 Ga granitoids it is evidenced by the presence of coeval mafic (~52 wt.%) magmatic rocks (sample 19BN98A; Table 3-1). Furthermore, the consistently chondritic Nd isotope compositions of the 2.7 and 2.6 Ga granitoids cannot be explained by partial melting of any known older crustal reservoirs in the Nonacho area (Figure 3-9A). Rather, the chondritic isotopic compositions could reflect: 1) crustal contamination of parent magmas that were derived from a suprachondritic mantle source; or 2) parent magmas and/or juvenile mafic source rocks that were derived from a chondritic mantle source, as is proposed for the 2.5 Ga granitoids below. Further isotopic data on less compositionally evolved components of the 2.7 and 2.6 Ga suites, assuming they exist, would be required to discriminate between these two possibilities.

3.6.3 Petrogenesis of the 2.5 Ga granitoids

Given that the 2.5 Ga granitoids bear a geochemical resemblance to high-Ti sanukitoids, they may also be similar in their petrogenesis. Similar to sanukitoid s.s suites, high-Ti sanukitoid parent magmas are thought to derive from subduction-enriched mantle sources (Martin et al., 2005, 2009; Laurent et al., 2009). The compositional differences between high-Ti sanukitoids and sanukitoids s.s have been attributed to differences in the degree of mantle metasomatism and/or mantle melting, and to differences in the nature of the metasomatic agent. Martin et al. (2009) proposed that high-Ti sanukitoids reflect lower degrees of mantle melting and/or melting of mantle that had experience a greater degree of metasomatism, such that the breakdown of hydrous metasomatic phases during partial melting exerts a greater control on the melts composition. Specifically, Martin et al. argued that the preferential breakdown of metasomatic amphibole, which tends to contain significant amounts of Ti and Nb (e.g., Grégoire et al., 2002), accounts for Ti- and Nb-rich character of high-Ti sanukitoids. Additionally, Laurent et al. (2011) argued that higher K₂O contents, and negative Sr and Eu anomalies, in high-Ti sanukitoids from the Bulai pluton reflect a mantle source that was metasomatized by partial melts of subducted terrigenous sediment, rather than subducted basalt. The more differentiated (i.e., granodioritic to granitic) components of high-Ti sanukitoid suites have been attributed to various processes, including (assimilation-)fractional crystallization, magma mixing, or partial melting of mafic crustal rocks (Moyen et al., 2001; Laurent et al., 2013).

It must be born in mind that the petrogenetic constraints on high-Ti sanukitoids summarized above come almost entirely from two locations, the Closepet batholith and the Bulai pluton. Additionally, the 2.5 Ga granitoids of the present study are not geochemically identical to the Closepet and Bulai granitoids. Therefore, the following sections aim to independently evaluate the petrogenesis of the 2.5 Ga granitoids, while drawing on previous studies of high-Ti sanukitoids when relevant. The main questions we attempt to address are: 1) what was the chemical and isotopic character of the mantle source?; and 2) to what extent was older, isotopically evolved, continental crust involved in the petrogenesis of the 2.5 Ga suite?

3.6.3.1 Geochemical constraints on mantle source

The mafic, and to a lesser extent, the intermediate, 2.5 Ga granitoids provide constraints on the nature of the mantle source. An important characteristic of these rocks is their overall enrichment in incompatible elements (LILE, LREE and some HFSE). There are three main processes that could have contributed to this enrichment: 1) assimilation of incompatible element-rich crust; 2) fractional crystallization of minerals with low mineral/melt partition coefficients for the incompatible elements, such as olivine and pyroxene; and 3) derivation of mantle-derived parent magmas from an enriched mantle source.

Although some crustal assimilation may have occurred (section 3.6.3.4), it is not thought to have had a major impact on the incompatible element contents of the 2.5 Ga magmas, for a number of reasons. First, the mafic and intermediate rocks tend to be equally or more LREE and HFSE enriched when compared to the felsic rocks (Figure 3-8), even though the latter would presumably reflect the greatest degree of crustal assimilation. Second, for some elements (e.g., Nd and Nb), local crustal sources with sufficiently high concentrations of these elements be suitable contaminants have not been identified (Figure 3-8). Third, several of the mafic/intermediate samples exhibit negative Th anomalies relative to $La \pm Nb$ (Figure 3-7), which is typically regarded a sign of minimal crustal assimilation (e.g., Pearce, 2014). Fractional crystallization may have contributed to the incompatible enrichment, because many of the mafic/intermediate granitoids have relatively low Mg-numbers (<60), Cr contents (<346 ppm) and Ni contents (<105 ppm), which indicates that their mantle-derived parent magmas did indeed undergo fractional crystallization of minerals like olivine and pyroxene. However, basic trace-element modelling summarized below (Figure 3-10), indicates that fractional crystallization alone cannot explain the degree of enrichment in the mafic samples.

Figure 3-10A models 5% batch melting of primitive mantle leaving a lherzolite residue (58% olivine, 29% orthopyroxene and 13% clinopyroxene), followed by 10–30% fractionation of a typical primitive arc basalt crystallizing assemblage (65% clinopyroxene and 35% olivine; e.g., Nandekar et al., 2014). An arc basalt fractionation assemblage was chosen for the modeling based on the broad major-element similarities between the 2.5 Ga granitoids and continental arc granitoids (Figures 3-5 and 3-6). The absence of plagioclase in this assemblage is consistent with the lack of a systematic decrease in Al_2O_3 and Sr contents, or Sr/Sr^* and Eu/Eu^* values, until >60 wt.% SiO_2 (Figures 3-6 and 3-8). The calculations show that even in this favorable scenario, which assumes a primitive (i.e., non-depleted) mantle source and a low degree of mantle melting, it is difficult to generate the high LILE and LREE contents of the most primitive 2.5 Ga sample via fractional crystallization without producing compatible element (e.g., Sc, V, Cr, Ni) contents that are too low (Figure 3-10A). This point is even more clear on a plot of Ni versus Nd where the same 5% batch melt and 10–30% fractional crystallization sequence is shown (Figure 3-10B). Here, it can be seen that the model can easily explain the range of Ni contents in the mafic rocks, but it cannot account for their high Nd contents. Assimilation-fractional crystallization (AFC) models, involving fractionation of the same crystal assemblage from the same batch melt, and assimilation of a median local crustal composition, also cannot account for the Nd contents in the mafic rocks (Figure 3-10B). The mantle-derived 2.5 Ga parent magmas must therefore have been more enriched than the modeled batch melt of primitive mantle, and thus, their source was likely more enriched than that of primitive mantle. The degree of enrichment experienced by the source would need to be very significant if the ambient

mantle (mantle prior to enrichment) was depleted (e.g., Workman and Hart, 2005; Figure 3-10A), rather than the primitive mantle starting composition used in the modelling.

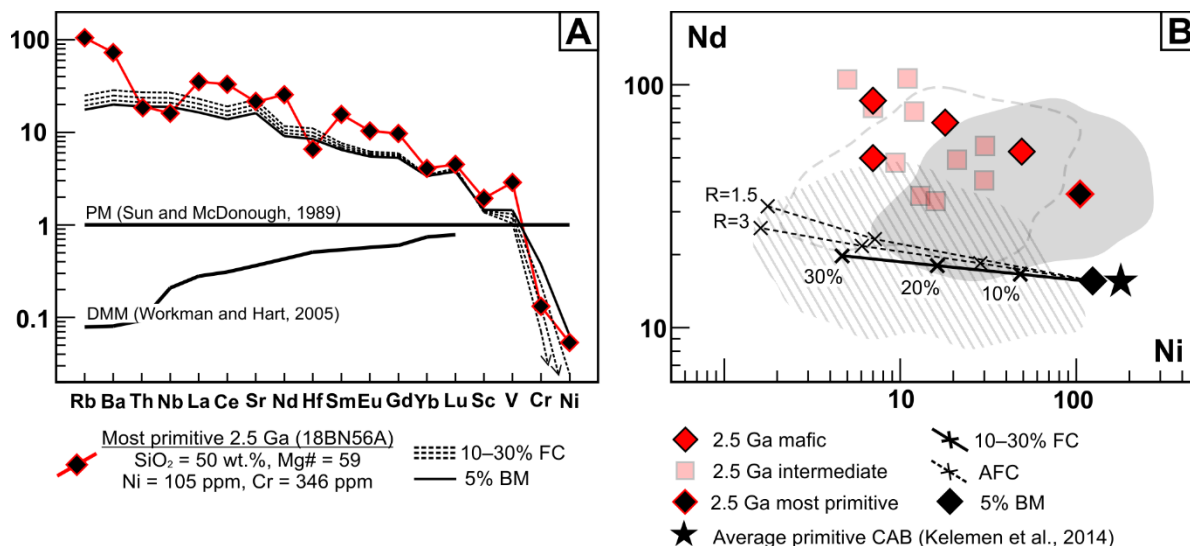


Figure 3-10. (A) Solid black line represents a 5% batch melt of primitive mantle leaving a lherzolite (58% olivine, 29% orthopyroxene and 13% clinopyroxene) residue, followed by 10–30 % fractional crystallization of an assemblage containing 65% clinopyroxene and 35% olivine (dashed black lines). PM: primitive mantle; DMM: depleted MORB mantle; FC: fractional crystallization; BM: Batch melt. (B) Log Ni ppm vs. log Nd ppm. Solid and dashed black lines show the results of fractional crystallization and AFC from the 5% batch melt of primitive mantle, using the same fractionation assemblage as in (A). Crosses indicate the % of solids removed, in 10% increments. The AFC calculations assume assimilation of the median local 2.7 and 2.6 Ga granitoid composition (34 ppm Nd, 24 ppm Ni). R values (mass cumulates/mass assimilants) of 1.5 and 3 represent lower and upper crustal AFC scenarios (DePaolo, 1981b), respectively. All calculations employ partition coefficients for basaltic magmas from Rollinson and Pease (2021). Bulk D values for Nd and Ni are 0.3 and 10, respectively. AFC equations from DePaolo (1981b) were used. Comparative data fields in (B) are as in Figure 3-8. The average primitive continental arc basalt (CAB) of Kelemen et al. (2014) is shown for reference.

Another characteristic of the mafic/intermediate granitoids that suggests they derived from an enriched mantle source is their depletion in Nb relative to the adjacent LREE and LILE (Figure 3-7). Mantle-derived magmatic rocks that exhibit this characteristic are widely interpreted to originate from peridotite that was metasomatized (enriched) by fluids or melts derived from subducted oceanic crust and/or subducted sediments (e.g., McCulloch and Gamble, 1991; Pearce and Peate, 1995; Elliott, 2003). This is true of both modern arc magmatic rocks and the Archean sanukitoids described above (e.g., Pearce and Peate, 1995; Martin et al., 2009). The general thinking is that the LILE and LREE are more mobile in the fluids or melts liberated from the subducted slab than Nb, and/or that residual rutile in the slab preferentially retains Nb (e.g., McCulloch and Gamble, 1991; Pearce and Peate, 1995; Elliott, 2003). Alternatively, this geochemical signature can be produced through crustal

assimilation. Here again, crustal assimilation is not the favored explanation because the most primitive sample exhibits the same overall trace-element patterns as the rest of the mafic/intermediate samples, including a negative Nb anomaly (Figure 3-7).

3.6.3.2 Isotopic constraints on mantle source

There are two main ways to explain the uniformly chondritic Nd, and largely chondritic Hf, isotopic compositions of the 2.5 Ga granitoids. The first is that the parent magmas derived from a chondritic mantle and any crustal assimilation that occurred had no measurable impact on the isotopic composition of the differentiated magmas. The second is that the parent magmas originated from a long-term depleted (suprachondritic) mantle, and the differentiated magmas attained chondritic isotopic compositions through crustal assimilation. The former is clearly the most straight forward interpretation, given that there is no correlation between SiO₂ contents and isotopic compositions (Figures 3-11A and B), and that the most primitive sample is chondritic (18BN56A; Table 3-1). Nevertheless, the second option can be evaluated through AFC modelling.

Figure 3-11C presents AFC models in which the parent magma has an ϵ Nd value equivalent to the DePaolo et al. (1981a) depleted mantle model at 2.5 Ga (+2.6). The potential crustal assimilants are represented by median isotopic and chemical compositions of the >3 Ga PRT granitoids (Neil et al., 2023), and the 2.7 and 2.6 Ga granitoids identified herein (Figure 3-11C). Lower and upper crustal AFC scenarios are modelled using R values (mass of cumulates/mass of assimilants) of 1.5 and 3, respectively (Figure 3-11C). The Nd content of the parent magma was set to 15 ppm, which is equivalent to the average primitive continental arc basalt (CAB) of Kelemen et al. (2014). As can be seen in Figure 3-10B, the 2.5 Ga parent magmas were probably more enriched (higher Nd contents) than the average primitive CAB. However, if the Nd content of the parent magma is set much higher than 15 ppm (e.g., ~20 ppm), the AFC models fail because chondritic isotope ratios are not reached until the Nd content of the liquid is greater than the most primitive 2.5 Ga sample (~35 ppm Nd). This is a sign in itself that a suprachondritic mantle source may not be feasible. Nevertheless, for the purpose of argument, the results of models that start with a primitive CAB magma (15 ppm Nd) and a depleted mantle Nd isotope composition are considered below.

The AFC models show that upper crustal assimilation of the 2.7 or 2.6 Ga granitoids cannot explain the chondritic isotopic compositions of the 2.5 Ga granitoids. In these scenarios, more than 40% fractional crystallization (60% liquid remaining) is required for the melt to reach chondritic isotope ratios (Figure 3-11C). After 40% fractional crystallization from a primitive CAB, the Ni content of the liquid would be lower than the Ni contents of the mafic/intermediate granitoids (Figure 3-10B). Assimilation of >3 Ga PRT crust is also considered unlikely, because both the upper and lower crustal calculations result in AFC curves that are nearly orthogonal to the horizontal data array of the

2.5 Ga granitoids (Figure 3-11C). Therefore, much greater dispersion of ϵNd_i values amongst the 2.5 Ga granitoids would be expected if any significant assimilation of >3 Ga crust occurred. Assimilation of 2.7 or 2.6 Ga granitoids in the lower crust may be a more realistically scenario. The calculations show that lower crustal AFC involving those granitoids will result in chondritic isotopic compositions after ~20–15% fractional crystallization, and if the 2.6 Ga granitoids are assimilated, the AFC curve eventually becomes subparallel to the horizontal array of 2.5 Ga granitoid ϵNd_i values (Figure 3-11C). Here again, however, an AFC process results in a liquid with that has a lower Ni content than the most primitive 2.5 Ga sample after only 10% fractional crystallization (Figure 3-10B). Altogether, this modelling re-emphasizes that the simplest interpretation of the data is that the 2.5 Ga parent magmas derived from an isotopically chondritic mantle source.

There are at least three possible reasons for the mantle source to have been chondritic at 2.5 Ga: 1) the ambient mantle beneath the Rae craton was not subject to long-term depletion or enrichment (it was primitive), and the subduction-related enrichment described above occurred during or shortly before the 2.5 Ga magmatism; 2) the ambient mantle was subject to long-term depletion, but its Nd isotopic composition was completely overwhelmed by the metasomatic agent; and 3) the mantle was subject to long-term enrichment, such that it evolved with a low Sm/Nd ratio from a suprachondritic to a chondritic composition by 2.5 Ga. The first scenario seems unlikely because, although not registered in our data set, there is ample evidence for a long-term depleted mantle in the pre-2.6 Ga Rae craton magmatic record (Figure 3-9A). The second scenario is plausible because the Nd (or Hf) content of metasomatized mantle can be strongly weighted towards that of the metasomatic agent, which could be chondritic or subchondritic if subducted sediments were involved (e.g., Couzinie et al., 2016). However, on the basis of the data compiled in Figure 3-9A, subducted material derived from >2.6 Ga Rae craton crust would likely have an average ϵNd value of -1.6 at 2.5 Ga. Thus, if the Nd in the depleted mantle was completely overwhelmed by Nd from subducted sediments, at least some of the mantle-derived 2.5 Ga granitoids would be expected to yield subchondritic, rather than consistently chondritic, ϵNd_i values. The third scenario is therefore preferred, which importantly implies that the subduction-like trace-element characteristics of the rocks highlighted above, need not be related to subduction that was concomitant with 2.5 Ga magmatism, but could reflect a lithospheric mantle source that was modified by subduction at some earlier time.

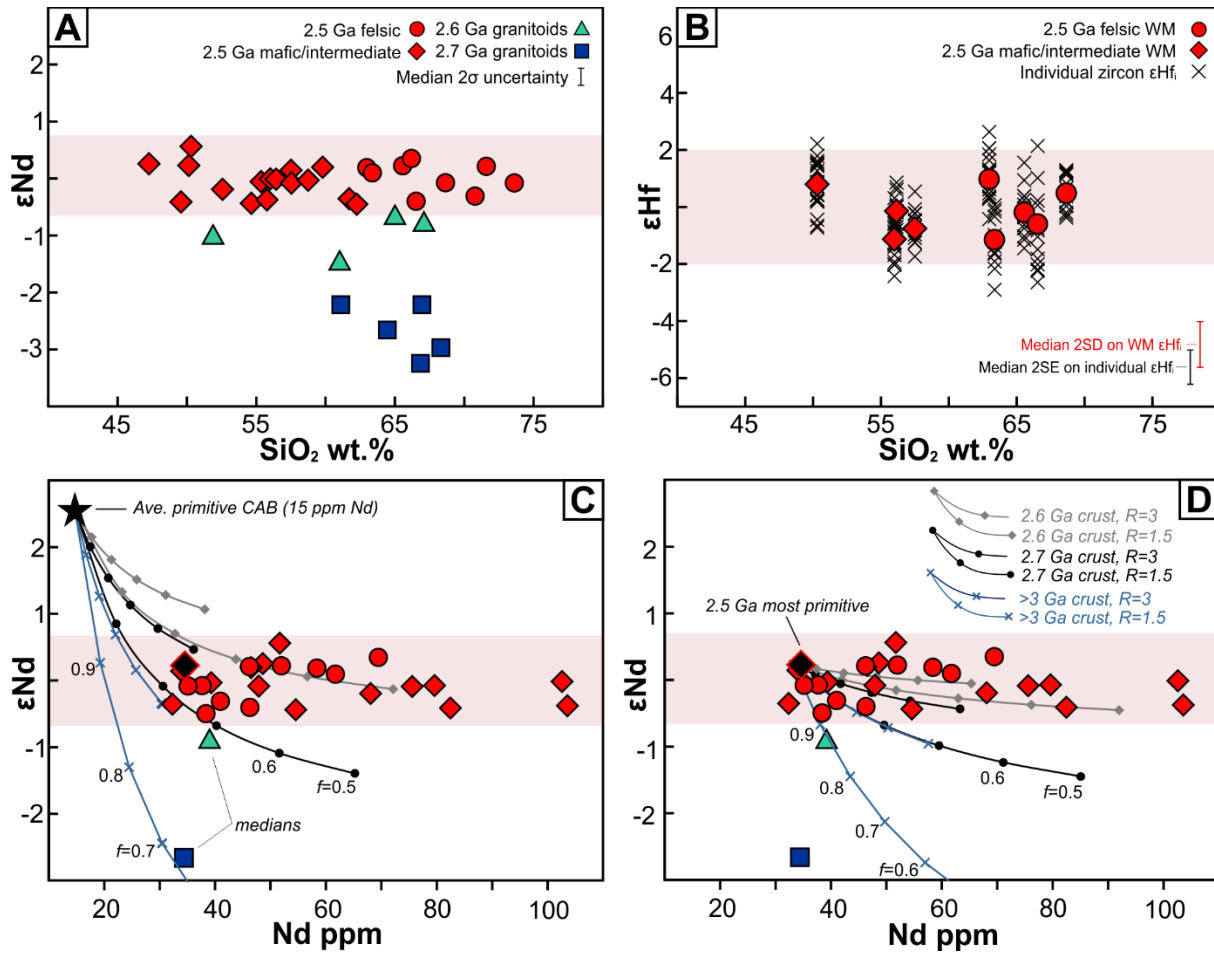


Figure 3-11. (A) SiO_2 wt.% vs. ϵ_{Nd} . ϵ_{Nd_i} values plotted for 2.5 Ga granitoids, $\epsilon_{Nd_{2.5 Ga}}$ values plotted for 2.7 and 2.6 Ga granitoids. (B) SiO_2 wt.% vs. ϵ_{Hf} . (C) Nd ppm vs. ϵ_{Nd} . AFC models use a starting composition with the ϵ_{Nd} value of the DePaolo et al. (1981a) depleted mantle model at 2.5 Ga (+2.6), and the Nd concentration (15 ppm) of an average primitive CAB (Kelemen et al., 2014). (D) Nd ppm vs. ϵ_{Nd} . AFC models use the most primitive 2.5 Ga sample as the starting composition. A bulk D_{Nd} of 0.3 was assumed for all AFC calculations (Nielsen, 1989). AFC equations from DePaolo et al. (1981b). Markers on curves indicate the wt.% fraction of liquid remaining (f), in 10% increments. Cumulate 2.5 Ga samples and sample 18BN14B excluded for clarity.

3.6.3.3 Mantle metasomatism and metasomatic agents

If the mantle-derived parent magmas to the 2.5 Ga suite originated from a subduction-enriched source, then what was the nature of the metasomatic agent(s)? This is not a straightforward question to answer. In modern arc settings, for example, better constraints on the composition of metasomatic agents and the ambient mantle are available, and there is considerable debate as to which metasomatic agents (e.g., aqueous fluids, partial melts of subducted sediments, or partial melts of subducted basalt) are important (Kelemen et al., 2014; Turner and Langmuir, 2022). The issue is also complicated by the details of how mantle metasomatism takes place and how melting of metasomatized mantle proceeds. For instance, the mantle may act a chromatographic separation column, preferentially retaining the elements that are stable in the metasomatic mineral assemblage while others pass through to higher levels of the mantle or crust (Nielson et al., 1993). Furthermore, at low degrees of melting and/or high degrees of metasomatism, the break-down of hydrous metasomatic phases (e.g., phlogopite or amphibole) may have a disproportionate influence on the incompatible element characteristics of the melt (Martin et al., 2009). In other words, there can be selective incompatible element enrichments and depletions in melts of metasomatized mantle, depending on which minerals form the metasomatic assemblage and which metasomatic phases melt out. There is also the potential for more than one metasomatic agent/event, especially if the source was in the lithospheric mantle. Despite these potential complications, it is useful to discuss some of the possibilities.

Although the mafic/intermediate granitoids are depleted in the HFSE relative to the LREE and LILE, the HFSE concentrations (especially Ti and Nb) in these rocks tend to be higher than modern arc granitoids (Figures 3-6 and 3-8). Similarly elevated Ti and Nb contents have been documented in high-Ti sanukitoids (Martin et al., 2009), modern low-silica adakites (Martin et al., 2005), and modern “high-Nb basalts” (>20 ppm Nb) and “Nb enriched basalts” (>7 ppm Nb) (Sajona et al., 1996). Given that the HFSE are relatively immobile in aqueous fluids (Kessell et al., 2005), the high Nb and Ti concentrations in these rocks has been interpreted to reflect a mantle source that was metasomatized by partial melts of subducted basalt or sediment, rather than by aqueous fluids (Sajona et al., 1996; Martin et al., 2005, 2009; Laurent et al., 2011). Partial melts of subducted basalt (high-silica adakites and TTGs; Martin et al., 2005) tend to be sodic and to have neutral or positive Sr and Eu anomalies, and these characteristics are carried forward into magmas derived from peridotite metasomatized by such melts (low-silica adakites and sanukitoids s.s; Martin et al., 2005; Table 3-2). By contrast, the 2.5 Ga mafic and intermediate rocks are typified by high K_2O/Na_2O ratios (Figure 3-6), and consistently negative Sr and Eu anomalies (Figures 3-6 and 3-8). The negative Sr and Eu anomalies in these rocks are not easily attributed to plagioclase fractionation, because these anomalies do not become more pronounced until above ~60 wt.% SiO_2 (Figure 3-8), indicating that

plagioclase was not a major component of the fractionating assemblage until that point. Thus, melts from a basaltic slab may not be suitable metasomatic agents. Terrigenous sediments from oceanic trenches on the other hand tend to have negative Eu and Sr anomalies, and high K₂O contents (Plank and Langmuir, 1998). Therefore, a peridotite source metasomatized by partial melts of subducted sediments, as has been proposed for some high-Ti sanukitoids (Laurent et al., 2011), could potentially explain multiple characteristics of the mafic and intermediate granitoids. One issue with this proposal is that many of the mafic and intermediate granitoids exhibit negative or neutral Th anomalies relative to La and Nb (Figure 3-7), whereas sediment subduction is thought to be responsible for high Th/La and Th/Nb ratios in arc magmas (Plank, 2005; cf. Cloutier et al., 2021).

Some of the seemingly contradictory characteristics of the 2.5 Ga mafic and intermediate granitoids (e.g., negative Th vs. negative Sr anomalies) might be reconciled by considering how the breakdown of certain metasomatic phases during dehydration melting of the mantle could have influenced the incompatible element contents of the melts. As an example, anomalously low Th and Rb concentrations in some modern high-Mg andesites are attributed to the preferential break-down of low-Th and -Rb metasomatic amphibole during mantle melting (Rogers and Saunders, 1989; Calmus et al., 2003). Metasomatic amphibole with these characteristics cannot be the reason for the Th depletion in the mafic and intermediate rocks, because they have relatively high Rb contents (Figure 3-7). However, the presence of phlogopite in the source, another common mantle metasomatic phase, would be consistent with their high K₂O and Rb contents (Figures 3-6 and 3-7). Studies of metasomatized peridotite xenoliths have shown metasomatic phlogopite to contain substantial K, Rb, Nb, and Ti, but relatively little Sr and very little (<0.1 ppm) Th (Grégoire et al., 2002). Thus, dehydration melting of phlogopite-bearing peridotite, in which phlogopite is consumed in the melting reaction, could potentially account for the low relative Th contents of the rocks, while also being consistent with their other incompatible element characteristics. Whether or not this suggestion permits metasomatism of the mantle by partial melts of subducted sediments will require further isotopic data (e.g., oxygen isotopes) to determine.

3.6.3.4 Differentiation and involvement of older continental crust

It was argued above that crustal assimilation is unlikely to explain the chondritic isotopic compositions of the 2.5 Ga granitoids. This does not necessarily mean that no crustal assimilation occurred during the differentiation of the suite, just that it did not have a major impact on the isotopic compositions of the magmas. Figure 3-11D presents the same set of AFC models as in Figure 3-11C, but in this case with the most primitive 2.5 Ga sample set as the initial magma composition. The results show that when starting with a chondritic parent magma, the assimilation of 2.6 Ga and 2.7 Ga crust is difficult to detect in the Nd isotope data. Only assimilation of >3 PRT granitoids, or

lower crustal ($R=1.5$) assimilation of 2.7 Ga granitoids, produces AFC curves that deviate significantly from the horizontal array of 2.5 Ga granitoid ϵNd_i values (Figure 3-11E). Note that Nd concentrations in the 2.5 Ga suite do not vary monotonically. Instead, the highest Nd contents are in intermediate (~57 wt.% SiO_2) samples, implying that Nd may have been a compatible element ($D_{\text{Nd}} > 1$) during the later stages of differentiation, potentially due to the fractionation of LREE-rich accessory phases, such as titanite and/or allanite, which are common in the 2.5 Ga granitoids (Appendix C). As such, the AFC models presented in Figure 3-11D cannot apply to the full range of compositions in the 2.5 Ga suite. Nevertheless, if a more Nd enriched sample is chosen as the starting composition, and D_{Nd} is varied within reason (e.g., 1.5–3.0) the same general conclusions apply. The reasons for this are: 1) the high Nd contents of the 2.5 Ga granitoids buffer their Nd isotopic compositions against those of the assimilants; and 2) some of the potential assimilants (i.e., the local 2.7 and 2.6 Ga granitoids) have only slightly negative ϵNd values at 2.5 Ga (Figure 3-11A). Thus, differentiation of the 2.5 Ga suite to produce its intermediate and felsic components could have involved assimilation of the local 2.7 Ga and 2.6 Ga crust, and this would be consistent with the slight heterogeneity of zircon ϵHf_i values in some 2.5 Ga samples (section 3.5.3.2). That being said, of the 563 zircon grains analyzed from 17 different 2.5 Ga granitoids, only 4 inherited grains/cores were identified (Figure 3-4). Such a small amount of zircon inheritance suggests that any crustal assimilation that did occur was minor.

Although the Nd isotope data do not yield clear constraints on the extent of crustal assimilation that occurred during the differentiation of the 2.5 Ga suite, one thing that is clear from these data is that the felsic 2.5 Ga rocks did not derive from direct partial melting of older (i.e., ≥ 2.6 Ga) continental crust. If that were the case, the felsic rocks would be expected to have $\epsilon\text{Nd}_{2.5 \text{ Ga}}$ values similar to the local 2.7 Ga or 2.6 Ga granitoids (Figure 3-11A), or even as negative (-7 or lower) as the >3 Ga PRT granitoids. The most mafic, and thus the most melt fertile, 2.6 Ga granitoids have $\epsilon\text{Nd}_{2.5 \text{ Ga}}$ values of -1 (Figure 3-11A). The potential for unidentified older crustal sources with $\epsilon\text{Nd}_{2.5 \text{ Ga}}$ values of ~ 0 exists, but the similar trace-element patterns of the mafic, intermediate and felsic 2.5 Ga granitoids (Figure 3-7) strongly suggest that, if the latter did originate via crustal anatexis, the source was juvenile 2.5 Ga crust. Importantly, this implies that all components of the 2.5 Ga suite, felsic rocks included, are at least in part juvenile additions to the continental crust.

3.6.4 Tectonic setting of the 2.5 Ga granitoids

There is considerable debate surrounding the tectonic setting of 2.5 Ga magmatism in the western Rae craton. Arguments have been advanced for continental rift, continental back-arc and continental margin arc settings (Schultz et al., 2007; Berman et al., 2013; Cloutier et al., 2021). These different tectonic settings can be evaluated in light of the dataset presented here, and by comparison with modern analogues. In contrast to the 2.5 Ga suite, magmatic rocks from continental rifts tend to be bimodal, alkalic and ferroan, and to have “A-type” trace-element characteristics (e.g., Whalen et al., 1987; Maniar and Piccoli, 1989; Barbarin, 1999; Frost and Frost, 2011). Magmatic rocks from continental back-arcs are more variable, but again these rocks tend to be bimodal and to include ferroan or “A-type” varieties (e.g., Shinjo and Kato, 2000; Ma et al., 2015; Collins et al., 2020). Put simply, the two places in which voluminous mafic, intermediate and felsic plutonic rocks with broad compositional similarities to the 2.5 Ga suite are most commonly found are in continental arcs and in post-collisional terranes. Examples of the former are the Cordilleran batholiths of western North and South America (Frost et al., 2001; Ducea et al., 2015), and examples of the latter are the high-K I-type granitoids (including associated mafic rocks) of the Caledonian, Variscan and Pan-African orogens (Liégeois et al., 1998; Barbarin, 1999; Castro, 2020; Jacob et al., 2021; Gómez-Frutos et al., 2023). This type of post-collisional magmatism takes place shortly after collisional orogenesis; it is distinct from truly post-orogenic magmatism that occurs several 10's of Myr after collision and tends to be bimodal in nature (Finger et al., 1997; Bonin, 2004; Jacob et al., 2021). Some authors refer to this magmatism as syn-collisional or late orogenic (e.g., Atherton and Ghani, 2002). The tectonic mechanisms that have been proposed for this post-collisional magmatism include slab break-off, orogenic collapse and lithospheric delamination (e.g., Atherton and Ghani, 2002; Neilson et al., 2009; Miles et al., 2016; Jacob et al., 2021). In an effort to constrain the tectonic setting of the 2.5 Ga suite, composition fields for modern continental arc granitoids and post-collisional I-type granitoids from the Caledonian and Variscan orogens, have been included in figures 3-5 through 3-8.

There is substantial overlap of the continental arc and post-collisional fields on most major-element plots (Figures 3-5 and 3-6), and some major-element characteristics of the 2.5 Ga granitoids yield contradictory evidence as to which of these settings is supported by the data (Figures 3-5 to 3-8). On several plots, such as SiO₂ vs. MALI, Fe*, and CaO, the 2.5 Ga granitoids show slightly more overlap with the continental arc fields than the post-collisional fields. By contrast, the high K₂O contents of the 2.5 Ga suite are more similar to those of the post-collisional granitoids (Figure 3-6). The calc-alkalic composition of the 2.5 Ga suite is notable because this is widely regarded as a key characteristics of arc magmatism, whereas post-collisional magmas tend to be alkali-calcic (e.g., Frost et al., 2001; Figure 3-5). It should be noted, however, that volumetrically significant high-K calc-alkaline (*sensu stricto*) granitoid suites, similar to the 2.5 Ga suite, have also been documented

in post-collisional settings (Jacob et al., 2021). The somewhat equivocal nature of the major-element data is summarized on the multi-cation plot of De la Roche et al. (1980), which incorporates all major elements, plus Ti (Figure 3-12A). The overlap of continental arc and post-collisional granitoids in terms of major elements is apparent on this plot, and here the mafic and intermediate (≤ 62 wt.% SiO_2) 2.5 Ga granitoids actually show slightly more overlap with the post-collisional field.

There is greater separation between continental arc and post-collisional granitoids in terms of minor- and trace-elements, and on the plots showing the greatest separation, the post-collisional affinity of the 2.5 Ga suite is apparent (Figures 3-6 to 3-8). In particular, the high P_2O_5 , LREE and HFSE contents of the 2.5 Ga granitoids are much more similar to post-collisional granitoids than continental arc granitoids (Figures 3-6 to 3-8). The relatively high Ce/Yb ratios, and the low Eu/Eu* and Sr/Sr* values (negative Eu and Sr anomalies) of the 2.5 Ga granitoids also show more overlap with the post-collisional fields. These distinguishing minor- and trace-element characteristics are most apparent in the mafic and intermediate (≤ 62 wt.% SiO_2) samples (Figures 3-6 to 3-8), and the post-collisional trace-element affinity of these rocks is summarized best on a plot of Nd ppm vs Nb ppm (Figure 3-12B). Another reason to favor a post-collisional setting for the 2.5 Ga granitoids is their consistently chondritic Nd and Hf isotope compositions. Primitive continental arc magmas commonly yield at least some evidence for input from a long-term depleted (suprachondritic) mantle (e.g., Chapman et al., 2021). By contrast, mantle-derived post-collisional rocks from the Caledonian and Variscan orogens have dominantly chondritic to subchondritic Nd and Hf isotopic compositions (e.g., Fowler and Rollinson, 2012; Couzinié et al., 2016; Moyen et al., 2017). This last argument is tempered by the fact that depleted mantle reservoirs would have been substantially less radiogenic in the late Archean than they are today, potentially making the input from such a reservoir more difficult to detect.

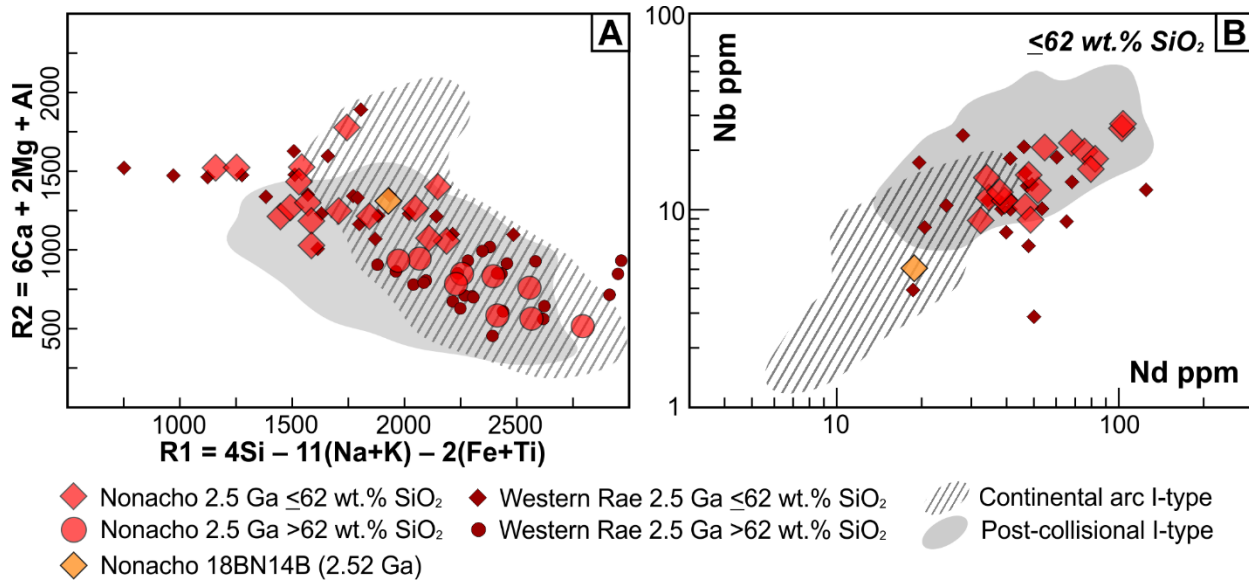


Figure 3-12. Summary tectono-magmatic discrimination plots. (A) multi-cation major-element plot of De la Roche et al. (1980). (B) log Nd ppm vs. log Nb ppm for samples with ≤ 62 wt.% SiO_2 . Western Rae 2.5 Ga data includes plutonic rocks from QMB (Schultz, 2007; Berman et al., 2015) and Zemplak domain (Cloutier et al., 2021). Circa 2.52–2.48 Ga plutonic rocks from Boothia Peninsula are also included, but note that U-Pb age data for these samples are unpublished (Sanborn-Barrie and Regis, 2023). Continental arc and post-collisional granitoid data fields are 75% Kernel density contours, as in preceding plots.

In summary, I find the geochemical and isotopic characteristics of the 2.5 Ga suite to be most consistent with a post-collisional setting. At the very least, a post-collisional model is a viable alternative to the continental margin arc/back-arc models that have been proposed for these rocks (Berman et al., 2013; Cloutier et al., 2021). Also plotted on figures 3-12A and B are ca. 2.52–2.47 Ga granitoids from elsewhere in the western Rae craton, including the QMB (Schultz, 2007; Berman et al., 2015), the Zemplak domain (Cloutier et al., 2021) and Boothia Peninsula (Sanborn-Barrie and Regis, 2023). The broad similarity between these rocks and the 2.5 Ga suite from Nonacho suggest that they too could have been generated in a post-collisional setting. The 2.5 Ga granitoids of the western Rae craton may therefore be better regarded as reflecting a late Archean orogenic event that was separate from the Arrowsmith orogeny, rather than an early “Andean-style” convergent margin phase of the Arrowsmith orogeny (Berman et al., 2013).

If 2.52–2.47 Ga magmatism in the western Rae craton occurred in a post-collisional setting, then this requires a ≥ 2.52 Ga collisional event, and there are at least two candidates for such an event. First, the Hearne craton or an unidentified block may have collided with the eastern side of the Rae craton during the 2.56–2.50 Ga MacQuoid orogeny (e.g., Berman, 2010; Regis et al., 2019). If this is the collisional event that triggered the post-collisional magmatism, then the occurrence of 2.5 Ga granitoids in a linear belt on the western side of the craton (Figure 3-1B), would need to be explained

by mantle upwelling and magmatism that was concentrated along a pre-existing lithospheric discontinuity between the PRT and the interior of the Rae craton (Figure 3-1A). The second option is a less well documented orogenic event on the western margin of the craton (Figure 3-13). Berman et al. (2015) argued that the Mesoarchean domain of the western QMB, which I consider to be part of the PRT (Neil et al., 2023; Figure 3-1A), collided with the interior of the Rae craton sometime between 2.6 and 2.5 Ga. The basis for their argument is that: 1) rare 2.5 Ga granitoids have been documented in the western QMB, but the otherwise widespread 2.62–2.58 Ga Snow Island suite granitoids have not; and 2) some deformation and metamorphism in the northwestern Rae craton occurred between ~2.54 and 2.49 Ga (Berman et al., 2013). These two scenarios are not mutually exclusive, but if one is to be preferred, the latter provides a more simple explanation for the geographic location of the 2.5 Ga granitoids.

Figure 3-13 illustrates one way in which the 2.5 Ga post-collisional magmas could have been produced. In this model, collision of the PRT with the western margin of the Rae craton leads to slab breakoff, and the asthenosphere upwells to induce melting of a subcontinental lithospheric mantle that had been enriched by earlier subduction. Here, the enriched lithospheric mantle had evolved to ϵNd and ϵHf values of ~0, thus accounting for the chondritic isotopic signature of the 2.5 Ga suite. Slab breakoff is the preferred catalyst for asthenosphere upwelling, because in other post-collisional scenarios, such as lithospheric delamination, significant anatexis of older continental crust might be expected (e.g., Jacob et al., 2021).

One question that arises from the post-collisional model presented above is, where is the record of pre-collisional continental arc magmatism? This pre-collisional magmatism could be preserved in ≥ 2.52 Ga arc magmatic rocks that are yet to be widely identified. For instance, sample 18BN14B from this study is slightly older (ca. 2.52) Ga than the majority of the 2.5 Ga suite granitoids, and has trace-element characteristics that are more consistent with an arc setting, such as a large positive Sr anomaly, lower overall REE contents and the lack of a Eu anomaly (Figures 3-7, 3-8 and 3-12B). Alternatively, the pre-collisional magmatism could be preserved in the 2.62–2.58 Ga Snow Island suite granitoids (Figure 3-1B, Peterson et al., 2024). However, I tend to agree with the arguments against a supra-subduction zone model for the Snow Island suite (Hinchey et al., 2011). Other possibilities are that the pre-collisional magmatism was never volumetrically significant or is not well preserved. In the modern analogues of the Variscan and Caledonian orogens, the pre-collisional magmatic record is volumetrically insignificant in comparison to the post-collisional record (Jacob et al., 2021), or seemingly absent altogether (Miles et al., 2016). Thus, an apparent paucity or absence of subduction-related magmatism preceding the post-collisional magmatism, should not be perceived as a serious weakness in the model or as a strong argument against it.

2.52–2.47 Ga

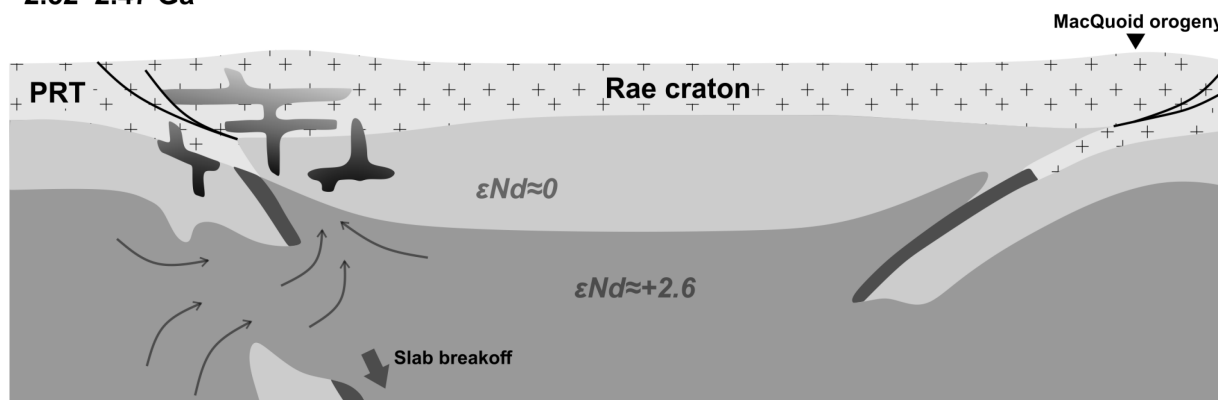


Figure 3-13. Tectonic cartoon illustrating the possibility tectonic setting of ca. 2.5 Ga magmatism in the western Rae craton. A minor amount of magmatism takes place on the PRT (lower plate) side, to explain the rare occurrence of 2.5 Ga granitoids in the western QMB portion of the PRT (Figure 3-1B; Davis et al., 2013, 2014). Artistic inspiration from diagrams in Laurent et al. (2014b).

3.6.5 Conclusions and broader implications

Three late Archean granitoid suites with crystallization ages of ca. 2.71–2.69, 2.58–2.57 and 2.52–2.48 Ga were documented in the Nonacho area of the southwestern Rae craton. The geochemical and isotopic data indicate that all three suites represent, at least in part, juvenile additions to the continental crust. Field and analytical efforts were focused on characterizing the 2.5 Ga granitoids. These granitoids range from mafic to felsic, comprise a high-K calc-alkaline series, are light rare earth element (LREE)-enriched and have “subduction-like” trace-element patterns. The mafic 2.5 Ga granitoids are interpreted to have derived from a subduction-enriched lithospheric mantle source that had evolved to chondritic Nd and Hf isotopic compositions by 2.5 Ga. Differentiation to produce the intermediate and felsic 2.5 Ga granitoids could have involved fractional crystallization, AFC and/or partial melting of juvenile 2.5 Ga mafic rocks. Although all of the granitoids in the suite yield chondritic ϵNd_i and near chondritic ϵHf_i values, AFC modeling indicates that some assimilation of older (i.e. ≥ 2.6 Ga) continental crust cannot be ruled out. Geochemically, the 2.5 Ga granitoids are analogous to post-collisional high-K, I-type granitoids from the Caledonian and Variscan orogens. These granitoids may therefore have been emplaced in a post-collisional setting related to ca. 2.56–2.50 Ga MacQuoid orogeny on the eastern side of the Rae craton, or the accretion of the PRT to the western Rae between ~ 2.6 and 2.5 Ga (Figure 3-13).

The characteristics of the late Archean granitoids identified here also have broader implications for Archean crustal evolution. First, it is widely recognized that juvenile magmas may be extracted from chondritic or subchondritic mantle reservoirs, but a tacit assumption of continental growth models that rely on depleted mantle model ages (T_{DM}) is that such magmatism only contributes to

continental growth in a minor way (e.g., see review by Payne et al., 2016). Although all three 2.7–2.5 Ga granitoid suites appear to represent juvenile additions to the continental crust, little-to-no evidence for input from a long-term depleted mantle source has been identified in any of them (Figure 3-9A). Similar isotopic characteristics have been identified in late Archean sanukitoids s.l from other cratons (Laurent et al., 2011, 2014a). Therefore, T_{DM} -based approaches may significantly underestimate the amount of late Archean continental growth on a regional scale (i.e., western Rae craton), and potentially on a global scale. Second, several other authors have also proposed a post-collisional setting for late Archean sanukitoid s.l suites in other cratons, based both on their late- to post-tectonic occurrence in those cratons and on their geochemical similarities with modern post-collisional granitoids (e.g., Whalen et al., 2004; Halla et al., 2009; Fowler and Rollinson, 2011; Laurent et al., 2014a; Moyen and Laurent, 2018). A substantial amount of late Archean continental growth therefore may have occurred in post-collisional environments. Finally, zircon Hf isotope data are increasingly used in favor of whole-rock Nd (or Hf) isotope data to study Archean rocks, because the former are less susceptible to post-magmatic disturbance than the latter (e.g., Vervoort and Kemp, 2016). However, each late Archean granitoid suite in this study yields consistent ϵNd_i values, which suggests that their Sm-Nd isotope systematics are unperturbed at the whole-rock scale (Figure 3-9A). The 2.5 Ga granitoids in particular yield a Sm-Nd isochron age that is consistent with zircon U-Pb crystallization ages (Figure 3-9B), and whole-rock ϵNd_i values that are consistent with zircon ϵHf_i values (Figure 3-9D). It is therefore argued that whole-rock Sm-Nd isotope analyses should not be routinely abandoned in favor of zircon Hf isotope analyses, but rather that the two techniques should be used in tandem. The advantage of the whole-rock data are that they can be obtained from numerous samples without the need for laborious mineral separations, and from samples that are devoid of zircon.

Chapter 4: 2.53–2.38 Ga metasedimentary rocks in the Nonacho Lake area, Rae craton, Canada: Regional correlations and tectonic implications

4.1 Introduction

Accessory mineral U-Pb age and trace-element data from metasedimentary rocks provide important constraints on the provenance of sedimentary systems, the maximum age of sediment deposition, and the timing and conditions of metamorphism (e.g., Fedo et al., 2003; Gehrels, 2014; Engi et al., 2017; Rubatto, 2017). These constraints can be used to link the deposition and metamorphism of the sedimentary protoliths to tectonic events, and to assist in the regional correlation of supracrustal sequences. Moreover, in deeply-eroded terranes, detrital zircon grains from metasedimentary rocks may be the only remaining evidence of the crust that was exposed and undergoing erosion during a given time period.

The Rae craton of the Canadian Shield (Figure 4-1A) preserves a complex history of crust formation that spans the Paleoproterozoic to latest Neoproterozoic (ca. 3.3–2.5 Ga) (e.g., Hinchey et al., 2011; Sanborn-Barrie et al., 2014; Peterson et al., 2024; Neil et al., 2023; Chapter 3). The Archean history of the craton is obscured by several Paleoproterozoic tectono-magmatic and -metamorphic events, including: the 2.5–2.3 Ga Arrowsmith orogeny (e.g., Schultz et al., 2007; Berman et al., 2013); the 2.0–1.9 Ga Taltson-Thelon orogeny (e.g., McDonough et al., 2000; Card et al., 2014; Berman et al., 2023), and the 1.9–1.8 Ga Snowbird and Trans-Hudson orogenic events (e.g., Berman et al., 2007; Regis et al., 2021). The poly-metamorphic history of the craton makes constraining the extent and character of any one tectonic event difficult. This is particularly true in the case of the Arrowsmith orogeny, where the potential for overprinting by younger tectonic events is great. Nevertheless, there is now substantial evidence for granitic magmatism, moderate-pressure (<8 kbar) metamorphism, and deformation related to the Arrowsmith orogeny along the western side of the craton (Figure 4-1A), and the existing data suggest that peak metamorphic conditions were reached between ~2.40 and 2.35 Ga (Schultz et al., 2007; Hartlaub et al., 2007; Tersmette, 2012; Berman et al., 2013).

Extensive 2.5–2.4 Ga metasedimentary sequences are preserved in the northwestern Rae craton, in the Queen Maud block (QMB) and on Boothia Peninsula (Figure 4-1A; Schultz, 2007; Schultz et al., 2007; Regis and Sanborn-Barrie, 2022, 2023). In the QMB, these sequences have been metamorphosed to granulite-facies conditions, and are referred to as the Sherman group (Schultz et al., 2007; Schultz, 2007; Regis and Sanborn-Barrie, 2023; Figure 4-1A). Zircon and monazite geochronology of these metasedimentary rocks have played an important role in deciphering the 2.5–2.3 Ga tectonic evolution of the western Rae craton, in particular with respect to the timing and conditions of Arrowsmith-aged metamorphism (e.g., Schultz et al., 2007; Berman et al., 2013; Regis and Sanborn-Barrie, 2023). In the southern portions of Rae craton, however, metasedimentary rocks

overlapping in age with the Arrowsmith orogeny appear to be either absent altogether, or rarely preserved and younger than ~2.33 Ga (e.g., Murmac Bay group; Ashton et al., 2013; Figure 4-1A).

This chapter presents new zircon and monazite U-(Th)-Pb age data, and zircon trace-element data, for two samples of migmatitic quartzofeldspathic gneiss from the Nonacho Lake area of the southwestern Rae craton (Figure 4-1). The quartzofeldspathic gneiss is inferred to be of metasedimentary origin, and the zircon and monazite data place robust constraints on the age of deposition and migmatization of the sedimentary protoliths. These age constraints, along with the provenance and inferred metamorphic grade of the rocks, are used to suggest an along-strike correlation with Sherman group rocks to the north (Figure 4-1A). Furthermore, the age and trace-element composition of metamorphic zircon domains in these rocks have implications for the timing, nature and extent of Arrowsmith orogenesis in the western Rae craton.

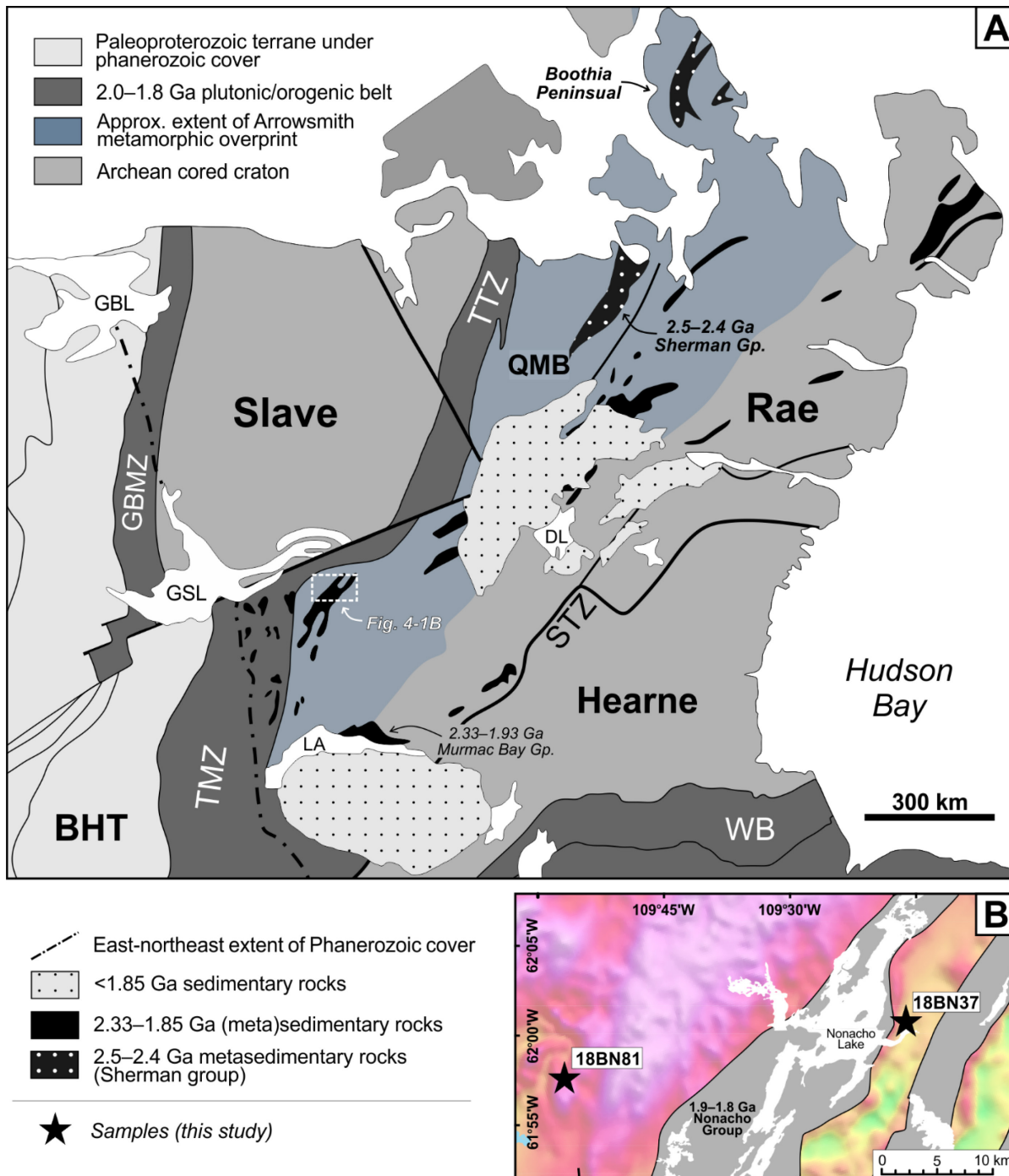


Figure 4-1. (A) Tectonic domain map of the western Canadian shield modified after Aspler and Chiarenzelli (1998); Rainbird et al. (2010), Ashton et al. (2013) and Berman et al. (2013). BHT: Buffalo Head terrane; GBMZ: Great Bear magmatic zone; GBL: Great Bear Lake; GSL: Great Slave Lake; QMB: Queen Maud block; STZ: Snowbird tectonic zone; TTZ: Thelon tectonic zone; TMZ: Taltson magmatic zone; WB: Wathaman Batholith. (B) Aeromagnetic anomaly map of the study area with sample locations indicated by black stars. Grey polygon: 1.9–1.8 Ga Nonacho Group sedimentary rocks (Aspler, 1985; van Breemen et al., 2013). 18BN81: 554826E, 6870902N UTM zone 12; 18BN37: 589632E, 6875763N, UTM zone 12.

4.2 Rock types: description and interpretation

Two relatively small occurrences of migmatitic quartzofeldspathic gneiss were identified in the Nonacho Lake area (Figure 4-1B). The rocks exhibit a strong fabric with compositional layering occurring on the millimeter to decimeter scale (Figure 4-2). Millimeter- to decimeter-scale layers, lenses and patches of white, quartz and K-feldspar rich material are interpreted as leucosomes (Figure 4-2). Darker, beige and rusty portions of the rock are rich in biotite, muscovite and chlorite, and are interpreted as relict melanosomes (Figure 4-2). At site 18BN81 (Figure 4-1B), the compositional banding in the quartzofeldspathic gneiss is cross-cut by an undeformed dyke of beige, fine-grained, two-mica leucogranite (Figure 4-2A). The contacts between this dyke and the quartzofeldspathic gneiss are sharp, which suggests that the two-mica leucogranite was not produced during the same episode of anatexis that gave rise to the leucosome in the quartzofeldspathic gneiss. Two samples of the quartzofeldspathic gneiss (18BN81A and 18BN37B) and one of the two-mica leucogranite (18BN81B) were collected (Figure 4-2). Both samples of the quartzofeldspathic gneiss contain zircon and monazite. Ilmenite was identified in 18BN81A and rutile was found in 18BN37B. Accessory phases in the two-mica leucogranite include zircon, monazite and unidentified oxides.

The presence of partial melt (leucosome) in the quartzofeldspathic gneiss indicates that metamorphic conditions reached at least the uppermost amphibolite-facies. This implies that the current metamorphic mineral assemblage in the rocks (K-feldspar, muscovite, biotite and chlorite) does not reflect peak metamorphic conditions. Rather, the muscovite, chlorite and potentially the biotite, must reflect retrograde metamorphism, unrelated lower-grade metamorphism, hydrothermal alteration, or a combination of these processes. This interpretation is consistent with the textural occurrence of the muscovite and chlorite. The muscovite occurs as relatively coarse crystals (mm-scale), but also as fine-grained aggregates (sericite) that comprise cm-scale pale blue stringers in outcrop (Figure 4-2). Chlorite occurs primarily as a secondary phase replacing biotite, and locally as cm-scale sub-equant “clots” in the leucosome at 18BN37 (Figure 4-2B). Given that chlorite does not have an equant crystal habit, and there is no reason for it to occur preferentially in the leucosome, these “clots” are suspected to be pseudomorphs of peritectic garnet.

To help interpret the origin of the quartzofeldspathic gneiss, whole-rock geochemical data were acquired for samples 18BN81A and 18BN37B (see Appendix A for whole-rock geochemical methods). The quartzofeldspathic gneiss is strongly peraluminous, with ASI (alumina saturation index) values of 2.1 and 1.6 for samples 18BN37B and 18BN81A, respectively. The strongly peraluminous composition of the quartzofeldspathic gneiss, and the broad spectrum of zircon ages recovered from it (section 4.3.1 below), are features consistent with a sedimentary protolith. It is

possible that the strongly peraluminous composition of the quartzofeldspathic gneiss unit is due, in part, to hydrothermal alteration. However, one particularly convincing piece of evidence in favor of a sedimentary protolith is the presence of an extremely zircon-rich layer in a thin section of 18BN37B (Figure 4-2C). The layer is <1 cm thick, contains more than 100 zircon grains in the thin section, and is interpreted as a relict heavy mineral laminae. No igneous (i.e., crystal accumulation) or metamorphic (i.e., mineral segregation) processes are expected to produce such a thin and discrete band of zircon concentrate. Thus, the quartzofeldspathic gneiss is interpreted to be of metasedimentary origin.

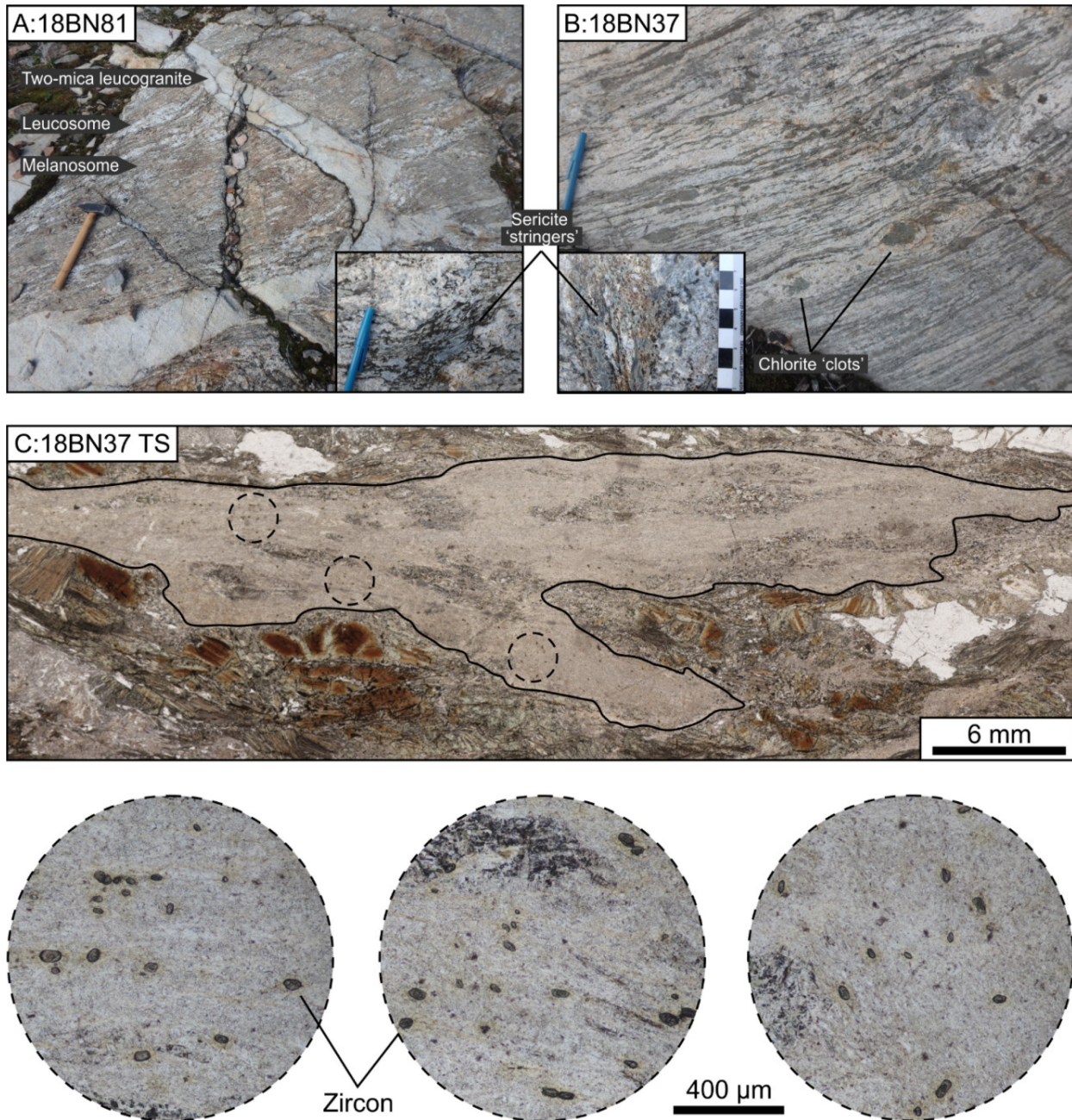


Figure 4-2. Representative outcrop photographs. (A) Quartzofeldspathic gneiss (sample 18BN81A) with leucosome and melanosome cross-cut by two-mica leucogranite dyke (sample 18BN81B). (B) Quartzofeldspathic gneiss (sample 18BN37B). Note the euhedral chlorite “clots” in the leucosome, which are interpreted as pseudomorphs of peritectic garnet. Inset images show pale blue sericite “stringers”. (C) Photomicrograph of a zircon-rich layer in a thin section from sample 18BN37B, which is interpreted as a relict heavy mineral lamella. Solid black lines outline the layer. Inset images are of particularly zircon-rich sections.

4.3 Zircon and monazite data: methods and results

Both samples of the quartzofeldspathic gneiss (18BN81A and 18BN37B) were processed for zircon geochronology. No attempt was made to separate the melanosome and leucosome because the two components are intimately mixed. Zircon grains were separated using a modified version of the water-based mineral separation technique of Söderlund and Johansson (2002). Selected grains were mounted in epoxy and polished to their mid sections. An effort was made to pick high-quality grains of variable size, morphology and colour. Monazite grains from samples 18BN81A, 18BN81B and 18BN37B were analyzed in petrographic thin sections. Backscattered electron (BSE) images of all zircon and monazite grains were acquired with a Zeiss Sigma 3000 SEM (scanning electron microscope) or a JEOL JXA-8900R electron microprobe. Yttrium X-Ray maps of monazite grains in samples 18BN81A and 18BN37B were acquired using the JEOL JXA-8900R microprobe. The details of sample preparation and analytical techniques are given in Appendix A, along with the secondary reference material data. The complete data tables for the samples analyzed are in Appendix D.

4.3.1 LA-ICPMS zircon U-Pb age and trace-element data

Zircon U-Pb age data from the two quartzofeldspathic gneiss samples (18BN81A and 18BN37B) were initially acquired by LA-MC-ICPMS (Laser ablation–multi-collector–inductively coupled plasma mass spectrometry). These data were acquired with a 25 µm diameter laser beam, using a 213 nm Nd:YAG laser ablation system and Nu Plasma MC-ICPMS. Zircon trace-element data can be an important tool in identifying different zircon populations (e.g., Rubatto, 2017), so coupled U-Pb age and trace-element (TE) concentration data were also acquired on *additional zircon grains* from samples 18BN81A and 18BN37B. These zircon U-Pb-TE data were acquired with a 25 µm diameter laser beam, using a RESOLUTION 193 nm ArF laser ablation system and an Element XR SC-(single-collector)-ICPMS. The fast-scanning magnet on the Element XR was used to measure ^{49}Ti , ^{157}Gd , ^{172}Yb , ^{202}Hg , $^{204}\text{Pb}+\text{Hg}$, ^{202}Hg , ^{206}Pb , ^{207}Pb , ^{208}Pb , ^{232}Th and ^{238}U during a single ablation. The LA-MC- and LA-ICPMS U-Pb data are combined in the histogram and kernel density estimate (KDE) plots (Figure 4-3), so as to increase the number of data points and the robustness of the age spectra. However, the LA-SC-ICPMS U-Pb-TE data are considered on their own in identifying specific zircon populations and in calculating weighted mean ages (Figure 4-3).

The zircon age spectra of the two quartzofeldspathic gneiss samples are similar (Figure 4-3). Both samples are characterized prominent density peaks at ca. 2.38 Ga and ca. 2.53–2.52 Ga. In addition, sample 18BN81A exhibits a shoulder peak at ca. 2.56 Ga and a minor peak at ca. 2.80 Ga, whereas 18BN37B exhibits prominent modes at ca. 2.60 Ga and ca. 2.70 Ga. Rare grains older than 3.0 Ga (two from 18BN81A and three from 18BN37B) are not plotted. In both samples, there are systematic differences in the morphology, zoning and trace-element composition of zircon domains

that are older than ~2.45 Ga, compared to those that yield dates between ~2.42 and 2.36 Ga and comprise the ca. 2.38 Ga density peaks (Figures 4-3 and 4-4). These differences are described below. The morphology and zoning descriptions apply to both the LA-MC- and LA-SC-ICPMS data sets, whereas the trace element descriptions only apply to grains analyzed by LA-SC-ICPMS.

Zircon dates older than ~2.45 Ga derive almost exclusively from grains with fine-scale oscillatory zoning and prismatic shapes (Figure 4-4). These grains yield moderate Th/U ratios (dominantly between 0.2 and 0.8), moderate to high Yb contents (dominantly >200 ppm), and consistently low Gd_N/Yb_N ratios of ~0.05 to 0.2 (grey circles, Figure 4-3). Such low Gd_N/Yb_N ratios equate to steep positive chondrite normalized HREE (heavy rare earth element) slopes. These physical and trace element characteristics are consistent with a detrital-igneous origin (e.g., Corfu et al., 2003; Hoskin and Schaltegger, 2003).

The ca. 2.38 Ga (~2.42–2.36 Ga) dates originate from ovoid grains and rim domains that are unzoned or faintly zoned (Figure 4-4). In terms of trace-element compositions, they can be divided into two categories, those that have high Yb contents (>490 ppm, grey diamonds) and those that have very low Yb contents (typically <100 ppm, blue diamonds) (Figure 4-3). Given that only three of the former were identified, their significance is unclear and they are not discussed further. The low-Yb domains are also characterized by Th/U ratios of ~0.1 to 0.5, which are lower, on average, than those of the >2.45 Ga grains (Figure 4-3). In addition, they have high Gd_N/Yb_N ratios that are always >0.1 and often >1 (Figure 4-3). Such high Gd_N/Yb_N ratios equate to shallow positive, flat or negative chondrite normalized HREE slopes. Altogether, the trace-element and physical characteristics of the low-Yb ca. 2.38 Ga domains are consistent with a metamorphic origin (e.g., Corfu, 2003; Hoskin and Schaltegger, 2003). In particular, the low Yb contents and high Gd_N/Yb_N ratios, suggest that these zircon domains were crystallized or recrystallized in the presence of garnet (e.g., Rubatto, 2002, 2017). Weighted mean $^{207}Pb/^{206}Pb$ dates calculated from the low-Yb zircon domains are 2396 ± 7 Ma ($n=27$, MSWD=1.3) and 2381 ± 7 Ma ($n=18$, MSWD=1.0) for samples 18BN81A and 18BN37B, respectively (Figure 4-3).

If the low-Yb ca. 2.38 Ga zircon domains described above are a product of *in situ* metamorphic growth (i.e., they are not detrital, see section 4.4.1), then titanium-in-zircon temperatures derived from them may help to constrain the metamorphic conditions experienced by the quartzofeldspathic gneiss. Titanium-in-zircon temperatures were calculated using the calibration of Ferry and Watson (2007), and by assuming the activities of SiO_2 (a_{SiO_2}) and TiO_2 (a_{TiO_2}) were both equal to 1. The presence of quartz in both quartzofeldspathic gneiss samples supports the assumption that $a_{SiO_2} \approx 1$, and the presence of rutile in sample 18BN37B is consistent with the assumption that $a_{TiO_2} \approx 1$. However, no rutile was identified in 18BN81A, and therefore, the Ti-in-zircon temperatures from that

sample should be taken as minimum estimates (Ferry and Watson, 2007). Despite this, the low-Yb ca. 2.38 Ga zircon domains from sample 18BN81A yield higher Ti-in-zircon temperatures, on average, compared to those from sample 18BN37B. The temperatures from 18BN81A are between 750 and 823 °C, with a median value of 780 °C and a standard deviation of 18 °C. By contrast, the temperatures from 18BN37B are between 700 to 780°C, with a median value of 715°C and a standard deviation of 30°C.

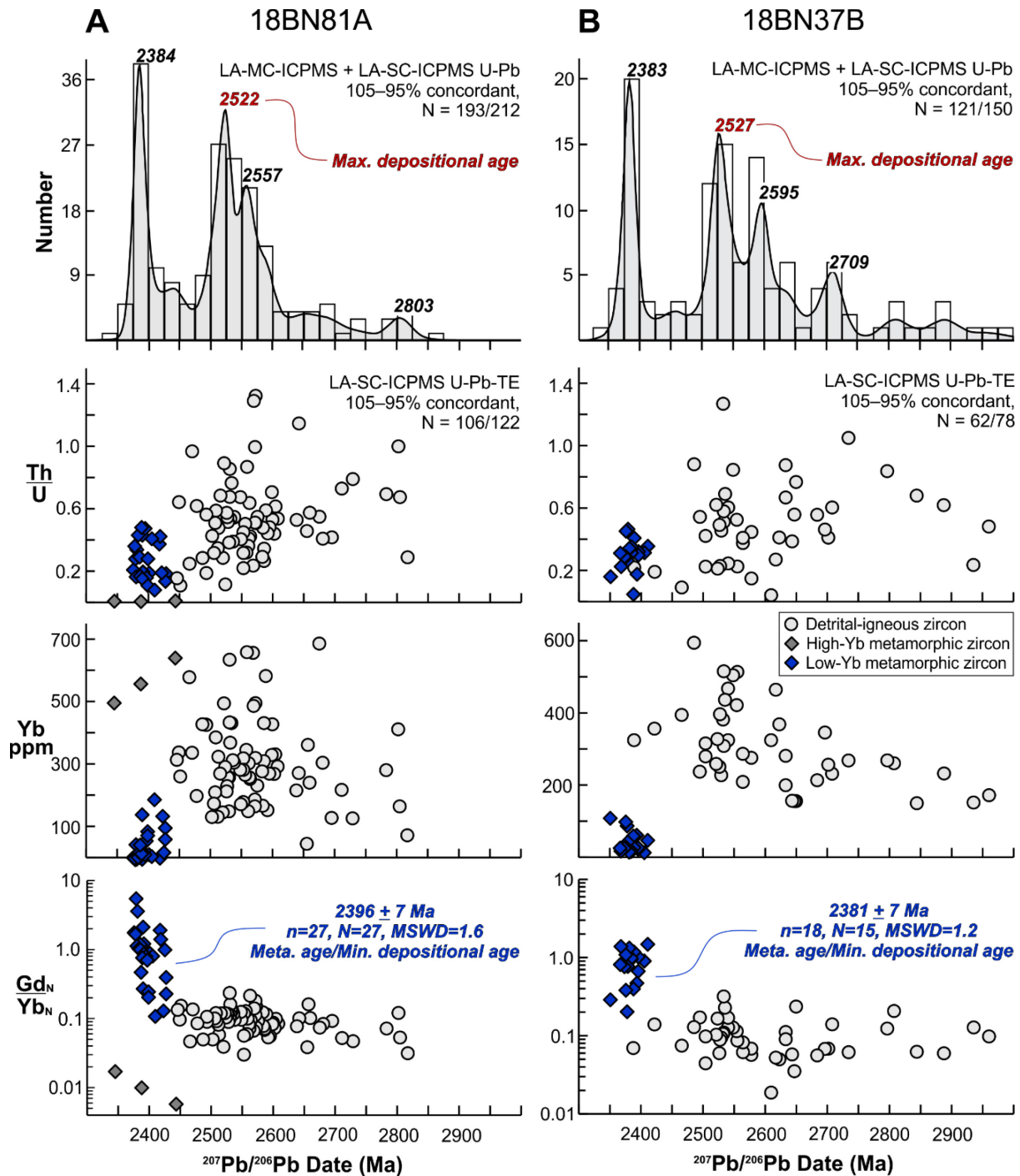


Figure 4-3. Zircon U-Pb age and trace element (TE) data for quartzofeldspathic gneiss samples 18BN81A (A) and 18BN37B (B). Uppermost plots are histograms and kernel density estimate (KDE) curves for 105–95% concordant dates. N=number of 105–95% concordant dates/number of dates. If multiple analyses of the same zircon domain were made, only one date was included in the histogram and KDE. Histogram binwidths are 25 my. KDE curves were produced in DensityPlotter (Vermeesch, 2012) using an adaptive bandwidth. Gd_N/Yb_N ratios are normalized to the chondrite values of Sun and McDonough (1989). Uncertainties on weighted mean $^{207}Pb/^{206}Pb$ ages are 2SE (two standard errors). n=number of dates, N=number of grains.

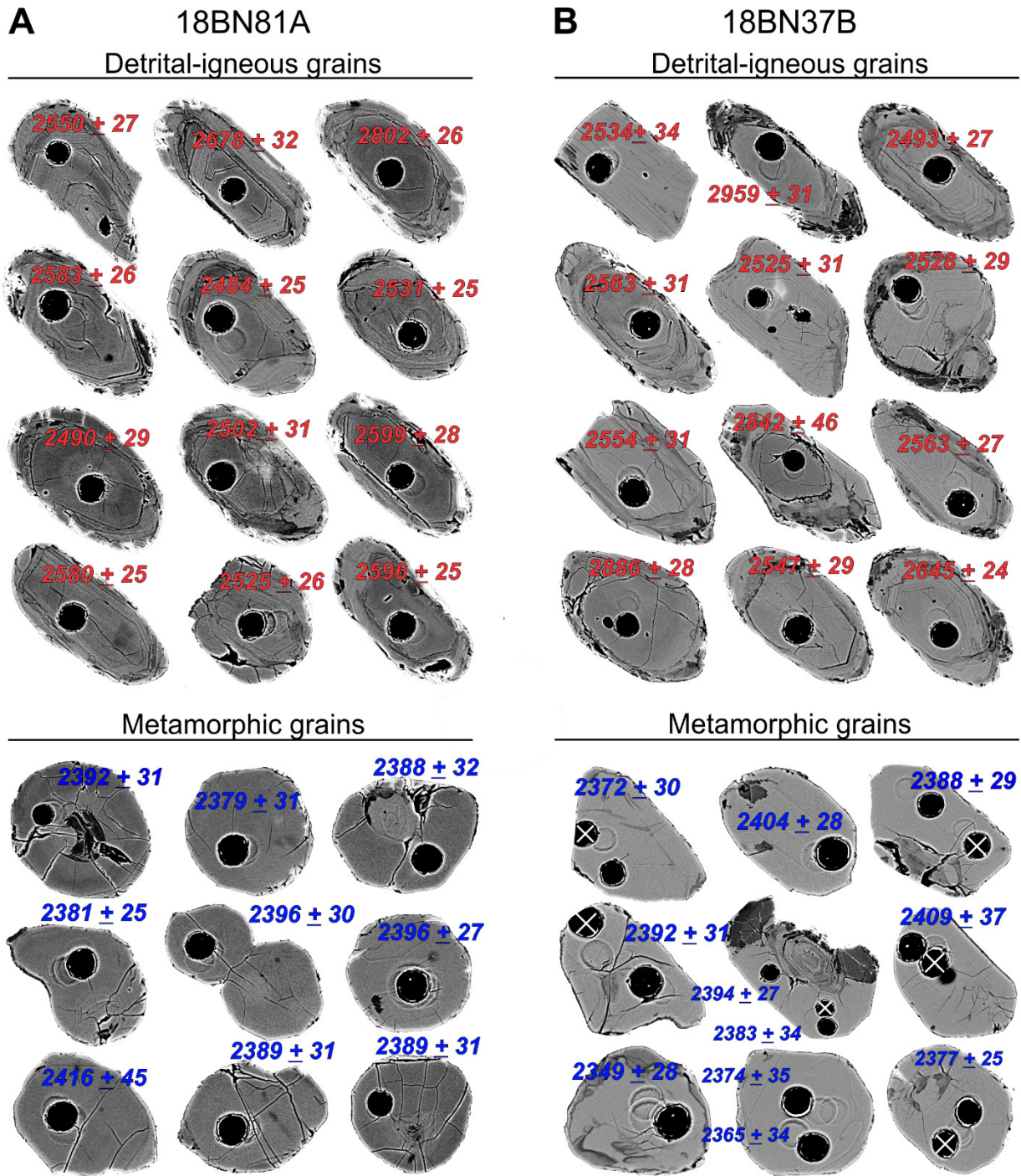


Figure 4-4. Representative BSE images of detrital-igneous and metamorphic zircon from quartzofeldspathic gneiss samples 18BN81A (A) and 18BN37B (B). Examples are from the LA-SC-ICPMS data set. Laser ablation pits are 25 μ m in diameter. Shallow pits on some grains are test ablations from calibrating the automated stage. The "X" over some pits indicates analyses that failed because the plasma went out during an automated run.

4.3.2 LA-ICPMS monazite U-Pb age data

Monazite grains from samples 18BN81B (two-mica leucogranite dyke) and 18BN81A (quartzofeldspathic gneiss) were analyzed for their U-Pb isotopic compositions by LA-MC-ICPMS. These data were acquired with a 12 μm diameter laser beam, using a 213 nm Nd:YAG laser ablation system and a Nu Plasma MC-ICPMS.

Thirteen analyses on eleven monazite grains from sample 18BN81B yield a weighted mean $^{207}\text{Pb}/^{206}\text{Pb}$ date of 1937 ± 5 Ma (N=13, MSWD=1.0) (Figure 4-5A). This date is interpreted as the igneous crystallization age of the cross-cutting leucogranite dyke (Figure 4-2A), which establishes an absolute minimum age for the quartzofeldspathic gneiss. Twelve analyses on three grains from sample 18BN81A yield a weighted mean $^{207}\text{Pb}/^{206}\text{Pb}$ date of 1945 ± 5 Ma (N=13, MSWD=1.0) (Figure 4-5B), which is indistinguishable from the crystallization age of the leucogranite dyke. All monazite analyses from sample 18BN81A are normally discordant (Figure 4-5B). The clustering of the data (Figure 4-5B), and the lack of measurable variation in $^{207}\text{Pb}/^{206}\text{Pb}$ dates, suggests that this discordance is not the product of ancient-Pb loss. Rather, the discordance may reflect recent (zero-aged) Pb-loss, or laser induced U/Pb fractionation that was not adequately corrected for due to an imperfect matrix match between the sample and the primary monazite standard. Neither of these possibilities would impact the accuracy of the measured $^{207}\text{Pb}/^{206}\text{Pb}$ dates, and the weighted mean $^{207}\text{Pb}/^{206}\text{Pb}$ date is therefore considered to be accurate.

4.3.3 Electron microprobe monazite U-Th-Pb_{total} age data

Backscattered electron images and Y X-Ray maps of monazite grains in sample 18BN37B revealed complex zoning on a scale of <10 μm (Figure 4-5C). In an effort to resolve any age variability accompanying this zoning, the electron microprobe U-Th-Pb_{total} dating technique was used. The data were obtained with a JEOL JXA-8900R electron microprobe, following the procedures recommended by Allaz et al. (2020). Monazite domains were analyzed with a fully-focused (<1 μm diameter) beam at an accelerating voltage of 15 kV and a beam current 100 nA. Repeat analyses of the in-house monazite standards “western Australia” (2843 Ma; L. Heaman, unpublished ID-TIMS U-Pb data) and “Madagascar” (512 Ma; L. Heaman, unpublished ID-TIMS U-Pb data) yielded mean dates of 2792 ± 83 Ma (1SD, n=7) and 515 ± 24 Ma (1SD, n=4), indicating that the data are imprecise, but accurate.

Ninety-three analyses on 7 monazite grains in 18BN37B were made. The U-Th-Pb_{total} dates range from 2625 to 2264 Ma, but are dominantly (71/93) between 2475 and 2350 Ma (Figure 4-5C). No systematic variation between the dates and the chemical composition of the analyzed domains can be identified, and this is apparent in the Y map of the most complexly zoned grain (Figure 4-5C). The lack of a correlation between the dates and the compositional zoning could, in part, reflect the imprecise nature of the U-Th-Pb_{total} data, and it is possible that more precise data would yield

multiple age populations. Nevertheless, the data yield a prominent KDE peak at 2405 Ma (Figure 4-5C), suggesting that significant monazite (re)crystallization occurred at ~2.40 Ga. This age result for monazite is consistent with the ca. 2.38 Ga low-Yb metamorphic zircon population identified in the same sample (Figure 4-3C).

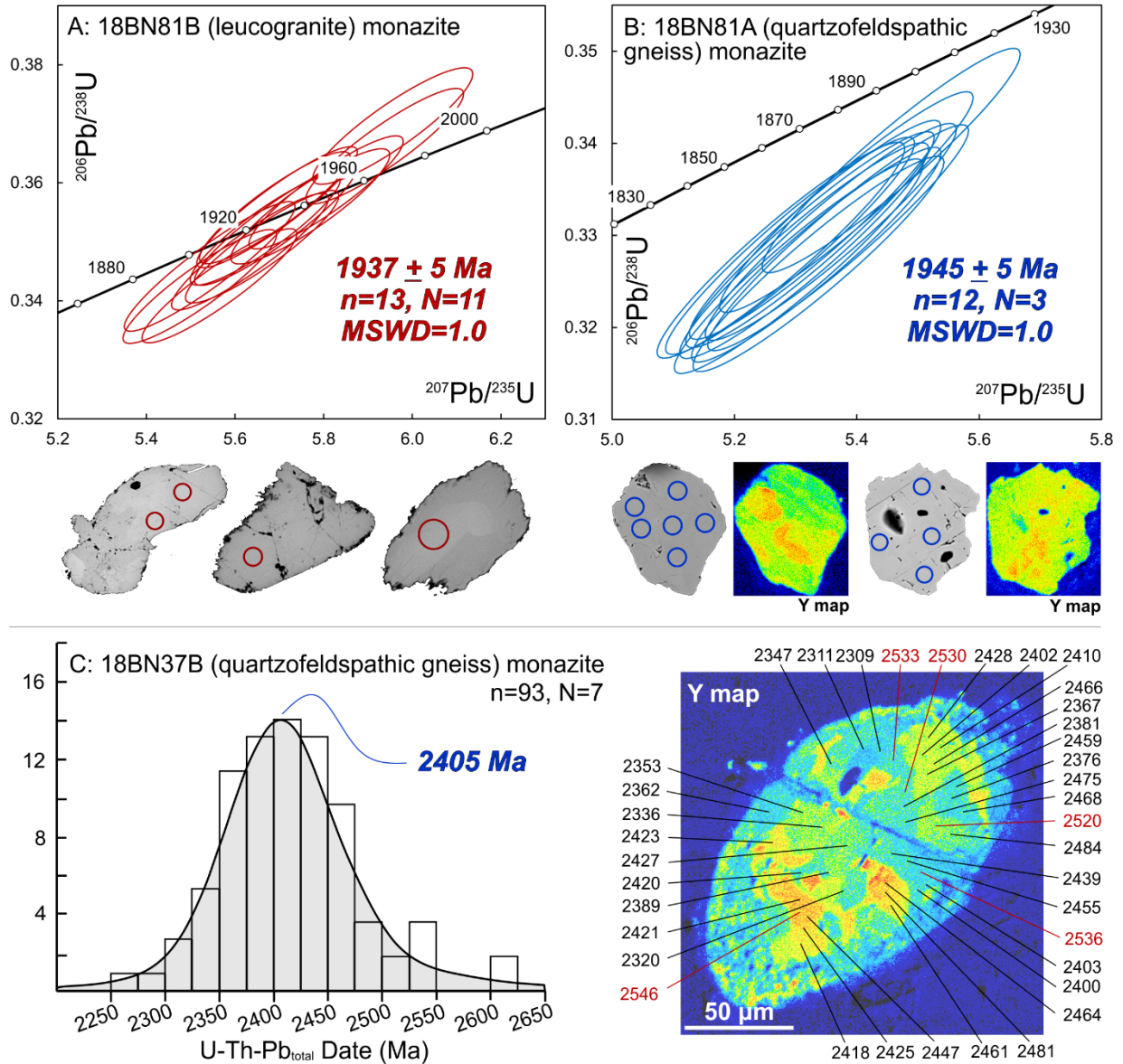


Figure 4-4. (A-B) Wetherill concordia plots for the LA-MC-ICPMS monazite U-Pb age data from samples 18BN81A (two-mica leucogranite dyke) and 18BN81B (quartzofeldspathic gneiss). Representative BSE images of monazite with 12 μm diameter laser spots are shown. Accompanying Y-maps are shown for monazite from 18BN81A. Weighted mean age uncertainties are 2SE. C) KDE curve and histogram for electron microprobe U-Th-Pb_{total} monazite dates from sample 18BN37B. Histogram bin widths are 25 My. The KDE curve was produced in DensityPlotter (Vermeesch, 2012) using an adaptive bandwidth. An Y-map for the most complexly zoned monazite grain from 18BN37B is shown, with analytical spots and associated dates (Ma) labelled. Dates notably older than the rest (>2500 Ma) are indicated in red. Relative Y content on X-ray maps: red>orange>yellow>green>blue. n=number of dates, N=number of grains.

4.4 Discussion

4.4.1 Age of metamorphism and migmatization

Establishing an age for the metamorphism and migmatization of the quartzofeldspathic gneiss hinges on the interpretation of the low-Yb ca. 2.38 Ga zircon populations (Figure 4-3). There are two possibilities: 1) the ca. 2.38 Ga zircon domains are of detrital-metamorphic origin; or 2) they are the product of *in situ* metamorphic zircon growth. The first scenario is highly unlikely for several reasons. First, it would imply that during post-2.38 Ga deformation, metamorphism and migmatization of these rocks, no zircon (re)crystallization, and in the case of sample 18BN37B no monazite (re)crystallization, occurred. Second, the ca. 2.38 Ga zircon domains are relatively abundant, in sample 18BN81A they make up 25% of all analyzed domains (Figure 4-3). Thus, a detrital-metamorphic origin would require a source region that was unusually metamorphic zircon rich. Third, the ca. 2.38 Ga zircon domains have relatively consistent trace-element characteristics, in particular with respect to their low Yb contents (Figure 4-3). If these zircon domains were of detrital-metamorphic origin, multiple source rocks with varying garnet abundances would be expected and this would presumably be reflected in more variable zircon Yb contents. Fourth, widespread ca. 2.32 Ga granites in the Nonacho Lake area are only moderately to weakly foliated (Chapter 5). Thus, a detrital-metamorphic origin would require that deformation and migmatization of the quartzofeldspathic gneiss occurred between ~2.38 and 2.32 Ga, but no high-grade metamorphic event in that time frame has been identified in the Nonacho Lake area (this thesis; Canam, 2023). For these reasons, the ca. 2.38 Ga zircon domains, and the ca. 2.4 Ga monazite in 18BN37B (Figure 4-5C), are interpreted to reflect *in situ* metamorphic growth.

Although no garnet is preserved in the rocks today, the HREE-depleted nature of the low-Yb ca. 2.38 Ga zircon domains (Figure 4-3) is consistent with the inference that the rocks once contained peritectic garnet that has since been replaced by chlorite (section 4.2). Furthermore, the median Ti-in-zircon temperature of 780 °C obtained for the low-Yb population in sample 18BN81A is consistent with typical dehydration melting temperatures in muscovite- and biotite-bearing metasedimentary rocks (e.g., Pattison et al., 2003). Therefore, the interpretation that the ca. 2.38 Ga zircon domains formed *in situ* is advanced further to suggest that they specifically date the migmatization of the sedimentary protoliths, and that the migmatization involved a melting reaction that produced garnet as a peritectic phase.

The interpretation presented for the ca. 2.38 Ga zircon domains implies that the ca. 1.94 Ga monazite age from quartzofeldspathic gneiss sample 18BN81A records a second metamorphic or hydrothermal event, possibly related to heat and/or fluids associated with the intrusion of the ca. 1.94 Ga leucogranite dyke (Figures 4-2A and 4-5). The absence of ca. 1.9 Ga dates in the electron

microprobe U-Th-Pb_{total} monazite age data acquired for 18BN37B indicate that this second event did not affect that sample (Figure 4-5C). This difference in the metamorphic history of the two quartzofeldspathic gneiss samples is consistent with the fact that: 1) no ca. 1.94 Ga leucogranite dykes were identified in the vicinity of sample 18BN37B; and 2) sample 18BN81A is located closer to the Taltson magmatic zone (Figure 4-1), where metamorphism associated with the 2.0–1.9 Ga Taltson-Thelon orogeny is more likely to have occurred.

4.4.2 Depositional age of the sedimentary protoliths

Assuming the interpretation of the ca. 2.38 Ga zircon domains is correct, then the minimum depositional ages for samples 18BN81A and 18BN37B are 2396 ± 7 Ma and 2381 ± 7 Ma, respectively (Figure 4-2). Maximum depositional ages (MDAs) can then be calculated using the detrital-igneous zircon dates, and there are a variety of approaches to establishing such maximum ages (e.g., Dickinson and Gehrels, 2009; Coutts et al., 2019; Herriott et al., 2019). Given the potential for ancient-Pb loss, or for undetected mixing of analyses between detrital-igneous and metamorphic zircon domains, a conservative approach is adopted here and MDAs are assigned from the youngest detrital-igneous KDE peaks, which are 2522 Ma and 2527 Ma for samples 18BN81A and 18BN37B, respectively (Figure 4-3). Altogether, the sedimentary protoliths to the quartzofeldspathic gneiss are interpreted to have been deposited between ~2.53 and 2.38 Ga.

4.4.3 Detrital zircon provenance

The prominent ca. 2.53–2.52 Ga detrital zircon modes in both samples are suggestive of a provenance on the western side of the Rae craton. Plutonic rocks with crystallization ages between ~2.53 and 2.47 Ga are abundant all along the western side of the Rae craton, from northern Saskatchewan to Boothia Peninsula (Schultz et al., 2007; Cloutier et al., 2021; Regis and Sanborn-Barrie, 2023; Figure 4-1; see also Figure 3-1B in chapter 3), and this includes the Nonacho Lake area (Chapter 3). It is difficult to constrain exactly where on the western side of the craton the ca. 2.53–2.52 Ga zircon grains originated from. However, sample 18BN37B exhibits a particularly distinct detrital zircon signature, with well-defined peaks at ca. 2.53, 2.60 and 2.70 Ga (Figure 4-3b). These three age peaks correspond closely to three late Archean granitoid suites in the local basement, which have crystallization ages of 2.52–2.48 (dominantly ca. 2.50 Ga), ca. 2.58 and ca. 2.70 Ga (Chapter 3). Thus, the simplest interpretation is that the detritus was derived primarily from the erosion of local Nonacho Lake area basement rocks.

4.4.4 Regional correlation

The Sherman group is loosely defined as a north-northeast trending belt of metasedimentary rocks in the eastern QMB (Figure 4-1A) that is associated with a distinctive low aeromagnetic anomaly

(Schultz et al., 2007; Regis and Sanborn-Barrie, 2022). The Sherman group rocks described by Schultz et al. (2007) are pelitic and semipelitic in composition, contain garnet-bearing leucosomes, and preserve a low- to moderate-pressure granulite-facies assemblage of garnet, cordierite and K-feldspar (Schultz et al., 2007). Schultz et al. (2007) carried out zircon and monazite U-Pb geochronology on two Sherman group samples. They assigned a MDA of ~ 2.44 Ga on the basis of the two youngest detrital igneous zircon grains recovered from the rocks, and interpreted ca. 2.39 Ga monazite in the garnet-bearing leucosomes (low-Y monazite, T. Chacko, pers. comm) to reflect the timing of granulite-facies metamorphism and migmatization. More recently, Regis and Sanborn-Barrie (2022) conducted detrital zircon U-Pb geochronology on a psammitic sample of the Sherman group, which was collected ~ 20 km south of the samples investigated by Schultz et al. (2007). They established a MDA of 2494 ± 12 Ma (2σ) for that sample, and interpreted a 2504 ± 5 Ma (2σ) monazite date from the same locality (Berman et al., 2015) to record *in situ* metamorphic growth. If correct, this would constrain Sherman group deposition to a very narrow time interval (Regis and Sanborn-Barrie, 2022). However, the ca. 2.50 Ga monazite could also be interpreted as detrital in origin, in which case the minimum age of the Sherman group sample investigated by Regis and Sanborn-Barrie would be unconstrained. Widespread semipelitic and psammitic metasedimentary rocks have also been documented on Boothia Peninsula (Figure 4-1A), and are thought to be broadly correlative with the Sherman group (Regis and Sanborn-Barrie, 2023). The depositional age of those rocks is tightly constrained to between ~ 2.51 and 2.49 Ga, on the basis of the youngest detrital zircon grains and the age of cross-cutting plutonic rocks (Regis and Sanborn-Barrie, 2023).

It is evident from the summary above that there is some uncertainty surrounding the exact depositional age of the Sherman group rocks in the QMB. Moreover, as the Sherman group is currently loosely defined, there is the obvious potential for it to contain multiple sedimentary packages that were deposited at various times between ~ 2.5 and 2.4 Ga (Schultz et al., 2007; Regis and Sanborn-Barrie, 2022). Regardless, the ca. 2.53–2.38 Ga depositional age established for the metasedimentary rocks in the Nonacho Lake area permits their broad correlation to the Sherman group rocks in the QMB, and their equivalents on Boothia Peninsula (Figure 4-1A). One piece of evidence that strengthens this correlation is the similarity in the detrital zircon age spectra of the metasedimentary rocks from the three locations (Figure 4-6). The youngest (and only) detrital zircon age peaks in the Boothia Peninsula and QMB samples are ~ 2.50 Ga, which is slightly younger than the ca. 2.53–2.52 Ga detrital zircon age peaks in the Nonacho samples (Figures 4-3 and 4-6). This relatively minor difference could reflect local differences in the ages of rocks exposed in the source regions, or as suggested below, it could be that the metasedimentary rocks in the Nonacho area were deposited a bit earlier (~ 10 – 20 Myr) than those on Boothia Peninsula and in the QMB. In either

case, the data show that metasedimentary rocks of similar age and detrital zircon provenance, separated by distances of >1000 km, are present in the western Rae craton (Figures 4-1 and 4-6).

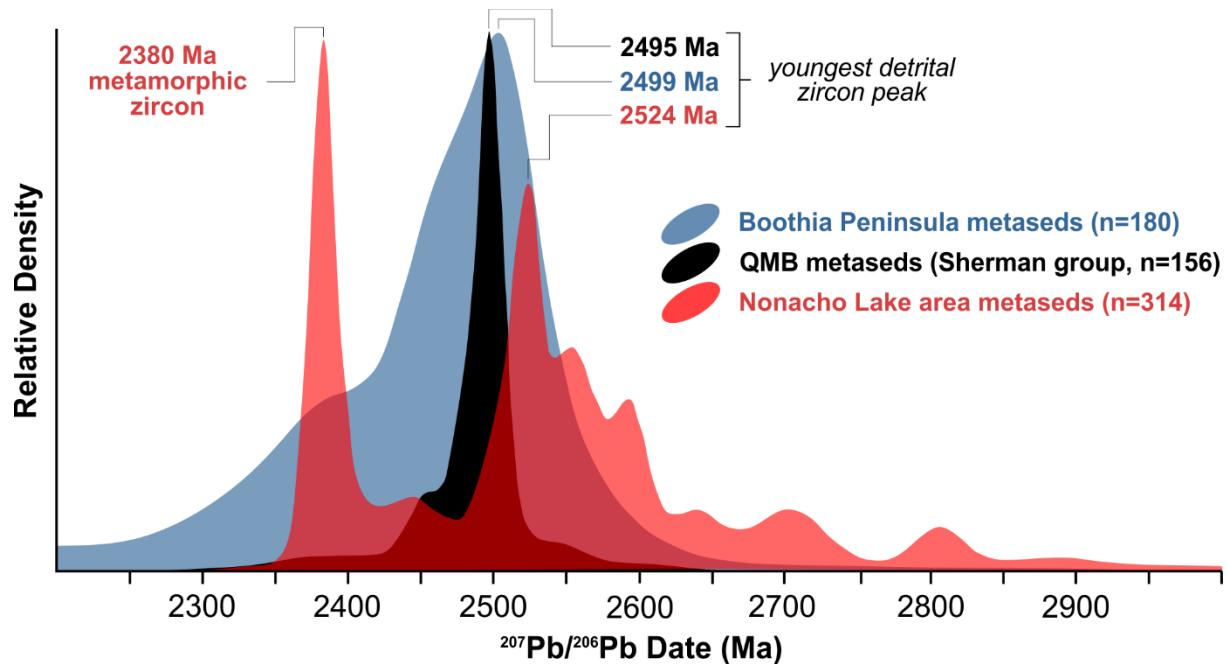


Figure 4-5. Zircon age spectra (KDE) for the broadly correlative (proposed here) metasedimentary rocks from Boothia Peninsula, the Queen Maud block (QMB) and the Nonacho Lake area. Only <5% discordant U-Pb data are plotted. KDE curves were produced in DensityPlotter (Vermeesch, 2012) using an adaptive bandwidth. Boothia Peninsula data: Regis and Sanborn-Barrie, 2023; QMB data: Schultz et al., 2007; Regis and Sanborn-Barrie, 2022; Nonacho Lake area data: this study; n = number of zircon analyses. Note the similarity in the youngest and most prominent detrital zircon modes from the three locations.

4.4.5 Tectonic implications

Without stratigraphic and sedimentological information, and without tighter depositional age constraints, it is difficult to speculate on the tectonic setting in which the sedimentary protoliths to the quartzofeldspathic gneiss were deposited. One possibility, however, is that sedimentation took place during extension or trans-tension related to the post-collisional ca. 2.50 Ga magmatic event documented in chapter 3. Some support for this scenario comes from the detrital zircon age spectra of the rocks. It is interesting that in both samples, the youngest detrital zircon modes are ca. 2.53–2.52 Ga, with relatively few dates in the 2.50–2.48 Ga range (Figure 3-4). This stands in contrast to the local basement, and the western Rae craton in general, where 2.50 Ga granitoids appear to be more abundant than 2.53–2.52 Ga granitoids (Chapter 3). I argue that this is most consistent with a depositional age that is close to the MDA's, perhaps between ~2.53 and 2.50 Ga. If the rocks were deposited much later than 2.50 Ga, the youngest detrital zircon mode might be expected to be centered about 2.50 Ga, rather than 2.53–2.52 Ga. However, this argument assumes that a

significant volcanic record was associated with the 2.50 Ga granitoids, or that the 2.50 Ga plutons were unroofed soon after their emplacement, and the validity of these assumptions is difficult to assess.

The ca. 2.38 Ga high-grade metamorphism and migmatization of the metasedimentary rocks documented here significantly expands the known spatial extent of high-grade metamorphism and anatexis related to the Arrowsmith orogeny (Schultz et al., 2007; Berman et al., 2013). In chapter 5, I also present evidence for the ca. 2.39 Ga granulite-facies metamorphism and migmatization of metabasic rocks, and for the ca. 2.43–2.38 Ga intrusion of HREE-depleted leucogranitic rocks that likely derived from garnet-bearing crustal sources. Thus, there is now abundant evidence for ca. 2.43–2.38 Ga crustal anatexis and granulite-facies metamorphism not only in the QMB (Schultz et al., 2007; Tersmette, 2012), but also in the Nonacho Lake area ~750 km to the south. The scale of this high-grade metamorphic and anatectic event is consistent with models for the Arrowsmith orogeny that involve continent-continent collision at ~2.4 Ga (Schultz et al., 2007; Berman et al., 2013).

Chapter 5: 2.4–2.3 Ga granitic magmatism of the southwestern Rae craton: Modern-style collisional orogenesis in the earliest Paleoproterozoic

5.1 Introduction

When plate tectonics started on Earth is a topic of constant debate. Many authors argue that lateral plate motions and subductions began in the early Archean (>3 Ga) (e.g., Pease et al., 2008; van Kranendonk, 2010; Shirey and Richardson, 2011; Naeraa et al., 2012; Bauer et al., 2020; Nutman et al., 2021). A commonly associated point of view is that the Earth underwent a gradual transition from a primitive (i.e., mobile-lid) form of plate tectonics to a modern-style of plate tectonics sometime between the early Archean and the Paleoproterozoic (e.g., Brown, 2008; Laurent et al., 2014a; Condie, 2018). However, there is no consensus as to when that transition started or was complete (e.g., Condie, 2018; Windley, 2021; Palin and Santosh, 2021). Others argue that plate-tectonics did not start until the Neoproterozoic (Hamilton, 2011), or that it operated only intermittently prior to that time (Stern, 2008; 2023). Amongst this controversy, a point that most investigators appear to agree upon is that late Paleoproterozoic (2.0–1.8 Ga) orogenic belts the world over reflect modern-style accretionary and collisional orogenic processes associated with the assembly of supercontinent Nuna (e.g., Hoffman, 1988; Rogers and Santosh, 2002; Evans and Mitchell, 2011; Stern, 2023). The largest and best preserved example of such an orogenic belt is the 1.9–1.8 Ga Trans-Hudson orogen (THO) in the Canadian Shield (Figure 5-1A; St-Onge et al., 2006; Corrigan et al., 2009; Regis et al., 2021).

One period of Earth's history that stands out in this debate is the 2.4–2.2 Ga tectono-magmatic lull (TML; Condie et al., 2009; 2022). The TML is defined by an apparent drop in the global frequency of orogenic granitoids, large igneous provinces and tectonic activity in general. This lull has been interpreted to reflect the slowdown of plate tectonics (Pehrsson et al., 2014; Condie et al., 2022) or the shutdown of plate tectonics during a transient period of stagnant- or single-lid tectonics (Condie et al., 2009; Stern, 2023). The importance of the TML lies in its occurrence after the Archean, a period for which the operation of modern-style plate tectonics is controversial, and before ~2.0–1.8 Ga, a period for which the operation of modern-style plate tectonics is widely, though not universally, accepted. Constraints on the geochemical character, petrogenesis and tectonic setting of magmatic rocks produced during the TML are therefore central to understanding the transition to modern-style plate tectonics. However, efforts to study such rocks are hampered by their global paucity.

At the centre of the Canadian Shield is the western Churchill Province and its core building blocks, the Rae and Hearne cratons (Figure 5-1). The Rae craton is one of only a few places in the world with a substantial record of tectonic and magmatic activity in the TML (Figure 5-1). Evidence of 2.4–2.3 Ga deformation, metamorphism and granitoid magmatism has been documented along the

western side of the craton (Figure 5-1), and is typically attributed to convergent margin or collisional orogenic processes, in an event dubbed the Arrowsmith orogeny (Berman et al., 2005, 2013; Hartlaub et al., 2007; Schultz et al., 2007). The western Rae craton is therefore an ideal place to study tectonic and magmatic processes in the TML. Despite this, constraints on the geochemical character and petrogenesis of 2.4–2.3 Ga magmatic rocks in the western Rae are limited almost entirely to one suite of rocks on the north shore of Lake Athabasca, the North Shore granites (Figure 5-1; Hartlaub et al., 2007; Partin and Sylvester, 2024). This chapter presents new whole-rock geochemical and Sm-Nd isotope data, and zircon U-Pb age and trace-element data, from granitoid and migmatitic rocks in a previously understudied portion of the southwestern Rae craton (Figure 5-1). The data are used to document multiple 2.4–2.3 Ga granitoid suites that differ in age, geochemical character, petrogenesis and tectonic setting. These granitoids are then compared to syn- and post-orogenic ca. 1.85–1.75 Ga granitoids from the upper plate of the THO in the western Churchill Province (Figure 5-1). The results have implications for the tectonic evolution of the Rae craton, and for our understanding of the transition to modern-style plate tectonics in general.

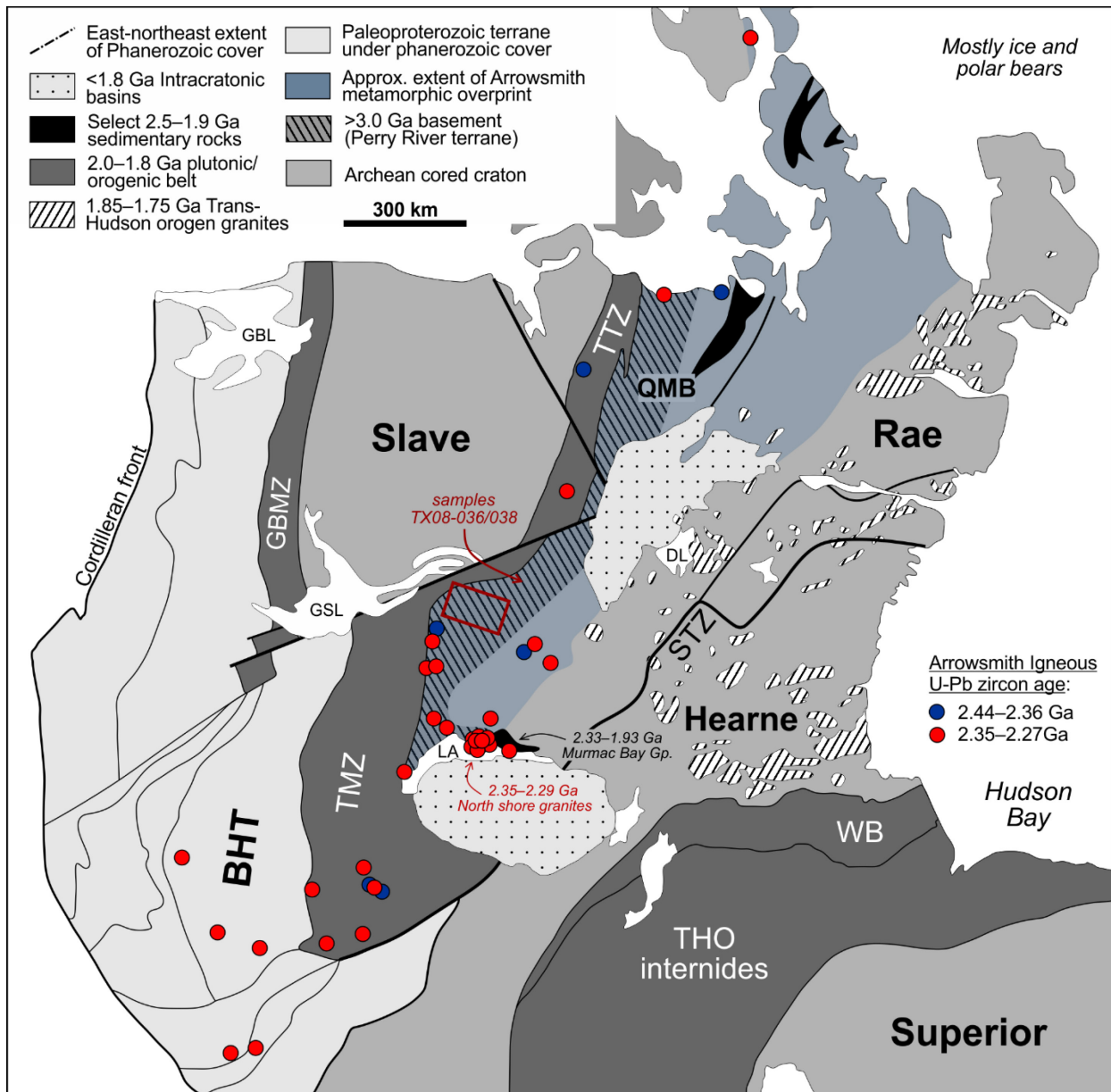


Figure 5-1. Tectonic domain map of the western Canadian Shield modified after Aspler and Chiarenzelli (1998), van Breemen et al. (2005) and Hartlaub et al. (2007). Circles indicate igneous rocks with 2.44–2.27 Ga U-Pb zircon crystallization ages from: Bostock and Loveridge (1988); Bostock et al. (1991); Frish and Hunt (1993); Villeneuve et al. (1993); Roddick and van Breemen (1994); van Breemen and Bostock (1994); McNicoll et al. (2000); Hartlaub et al. (2007); Ashton et al. (2007a,b); Tersmette (2012); Ashton et al. (2013); Walsh (2013); Davis et al. (2015); Ashton et al. (2017c); Berman and Camacho (2020). Some 2.44–2.27 Ga zircon ages of uncertain origin are excluded. Extent of Arrowsmith metamorphic overprint after Berman et al. (2013). BHT: Buffalo Head terrane; THO: Trans-Hudson orogen; TMZ: Taltson magmatic zone; TTZ: Thelon tectonic zone; WB: Wathaman batholith; QMB: Queen Maud block; STZ: Snowbird tectonic zone. Red box is the Nonacho Lake area and the outline of Figure 5-2.

5.2 Geological context

The Rae craton is separated from the Hearne craton to the east by the Snowbird tectonic zone, and from the Slave craton and Buffalo Head terrane (BHT) to the west by the 2.0–1.9 Ga Thelon tectonic and Taltson magmatic zones, respectively (Figure 5-1). Basement rocks in the Rae craton are dominated by Mesoarchean to Neoproterozoic (2.9–2.5 Ga) orthogneisses and granitoids (Hinchey et al., 2011; Regis et al., 2017a; Davis et al., 2021; Peterson et al., 2024; chapter 3). Northeast-striking 2.7 Ga greenstone belts are preserved in the central part of the craton (Sanborn-Barrie et al., 2014; Hunter et al., 2018) and remnants of pre-3 Ga crust occur at the peripheries of the craton (Thériault et al., 1994; Hartlaub et al., 2005; Whalen et al., 2011; Neil et al., 2023). Isotopic data indicate that an extensive >3 Ga basement terrane, referred to as the Perry River terrane (PRT), is present along the western and southern margin of the craton (Figure 5-1; Neil et al., 2023). The Archean nucleus of the Rae craton was variably reworked by a number of late Archean to Paleoproterozoic tectono-magmatic and -metamorphic events, including the: ca. 2.56–2.50 Ga MacQuoid; 2.5–2.3 Ga Arrowsmith; 2.0–1.9 Ga Taltson and Thelon; and 1.9–1.8 Ga Snowbird and Trans-Hudson orogens (see Berman, 2010 for a review). Far-field effects of the 1.9–1.8 Ga Trans-Hudson orogen (THO) are documented well into the interior of the craton, where greenschist- to granulite-facies metamorphism occurred from ~1.86 to 1.83 Ga, and intraplate magmatism and sedimentation occurred from ~1.85 to 1.75 Ga (e.g., Peterson et al., 2002; Rainbird and Davis, 2007; Pehrsson et al., 2013b; Regis et al., 2021).

Most pertinent to this paper is the Arrowsmith orogeny. There is uncertainty as to whether the Arrowsmith orogeny should be regarded as spanning the ~2.5–2.3 Ga, or only the ~2.4–2.3 Ga time interval (Berman et al., 2013; Pehrsson et al., 2013a; chapter 3). Mafic to felsic calc-alkaline granitoids were emplaced along the western side of the Rae craton between ~2.53 and 2.47 Ga (Schultz et al., 2007; Cloutier et al., 2021; chapter 3). One interpretation is that these rocks represent continental arc or back-arc magmatism in an early convergent margin phase of the Arrowsmith orogeny (Berman et al., 2013; Cloutier et al., 2021). Another interpretation, however, is that they reflect post-collisional magmatism related to ca. 2.56–2.50 Ga MacQuoid orogenesis on the eastern margin of the craton, or to the ca. 2.5 Ga accretion of the PRT to the western Rae craton, and that the Arrowsmith orogeny is a separate and later tectonic event (chapter 3). Regardless, the focus of this paper on the 2.4–2.3 Ga tectonic evolution of the western Rae craton.

Widespread evidence of 2.4–2.3 Ga granitic magmatism, metamorphism and deformation related to the Arrowsmith orogeny has been documented throughout the western Rae craton (Hartlaub et al., 2007; Schultz et al., 2007; Tersmette, 2012; Berman et al., 2005, 2013; Bethune et al., 2013; Figure 5-1). Upper amphibolite- to granulite-facies metamorphism occurred between ~2.40 and 2.35 Ga,

and has been interpreted to reflect the collision of one or more terranes with the western Rae craton at ~2.4 Ga (Schultz et al., 2007; Tersmette, 2012; Berman et al., 2013; chapter 4). It remains unclear what terrane(s) collided with the Rae craton, and whether that collision took place on the present-day western margin of the craton, or outboard of it (Schultz et al., 2007; Berman et al., 2013). Possible colliding blocks include the Slave craton, the Buffalo Head terrane (BHT), or an unidentified terrane that was rifted away at ~2.1 Ga (Schultz et al., 2007; Berman et al., 2013). The ca. 2.35–2.29 Ga North Shore granites (Figure 5-1) are potassic and siliceous (>70 wt.% SiO₂) rocks that have been interpreted as syn- to post-collisional (Hartlaub et al., 2007), or strictly post-collisional (Ashton et al., 2013; Partin and Sylvester, 2024), with respect to the Arrowsmith orogeny. Mafic volcanic and sedimentary rocks of the lower Murmac Bay group (Figure 5-1) are thought to comprise a post-collisional rift succession that was deposited roughly coeval with emplacement of the North Shore granites (Ashton et al., 2013). Circa 2.33–2.28 Ga plutonic rocks have also been documented beneath Phanerozoic cover in the BHT (Villeneuve et al., 1993; Figure 5-1), suggesting that the BHT and Rae craton were likely united by ~2.3 Ga (Hartlaub et al., 2007).

5.3 Local geology and samples

This study is based on field work conducted in the Nonacho Lake area (“Nonacho area” hereafter) of the southwestern Rae craton (Figure 5-1 and 5-2). Existing models for the Arrowsmith orogeny predict that basement rocks in the Nonacho area (Figure 5-1) should preserve a significant record of 2.4–2.3 Ga magmatism, metamorphism and deformation. However, until recently (this thesis; Canam, 2023), no modern geochronological and geochemical studies on the Nonacho area basement had been carried out. It was therefore recognized that investigating the age, geochemical character and petrogenesis of granitoids in the Nonacho area would provide important new constraints on the regional extent and tectonic evolution of the Arrowsmith orogeny.

Figure 5-2 presents a geological sketch map of the transect along which the majority of my field work and sampling was conducted. Map units 1–3 are dominated by strongly-foliated to gneissic mafic to felsic meta-plutonic rocks that are collectively referred to as “granitoids” hereafter. The mafic and intermediate rocks primarily preserve amphibolite-facies mineral assemblages. Zircon U-Pb age data show that these rocks are dominantly ca. 2.70, ca. 2.58 or ca. 2.50 Ga in age, and locally ca. 3.25 or ca. 2.78 Ga in age (chapters 2 and 3; Appendix C). Map unit 3 also includes local occurrences of a migmatitic quartzofeldspathic paragneiss in the Stewart River area, and a granulite-facies migmatitic mafic orthogneiss at the east end of Gray Lake (Figure 5-2). Zircon and monazite U-Pb age and trace-element data from the former suggest that sedimentation took place after ~2.53 Ga, and that migmatization took place at ~2.38 Ga (chapter 4). The Archean rocks of map units 1 and 3 are also cross-cut by, and locally interlayered with, a variety of weakly to strongly foliated Paleoproterozoic

granitoids. Finally, map unit 4 comprises fairly homogeneous, weakly foliated to undeformed, 2.0–1.8 Ga granites that are younger than, and unrelated to, the Paleoproterozoic granitoids in units 1–3.

The focus of this study is the Paleoproterozoic granitoids in map units 1 and 3, and the migmatitic mafic gneiss at the easternmost end of Gray Lake. The Paleoproterozoic granitoids are divided into two groups referred to as the leucogranitoids and the biotite granites (Table 5-1). In general the leucogranitoids are coarser-grained and more strongly deformed than the biotite granites. However, there were multiple episodes of deformation in the Nonacho area (Canam, 2023) and the deformation is heterogeneously distributed, such that in some outcrops a biotite granite may be more deformed than a typical leucogranitoid, and vice-versa. Detailed descriptions of these granitoids, and the migmatitic mafic gneiss, are given below.

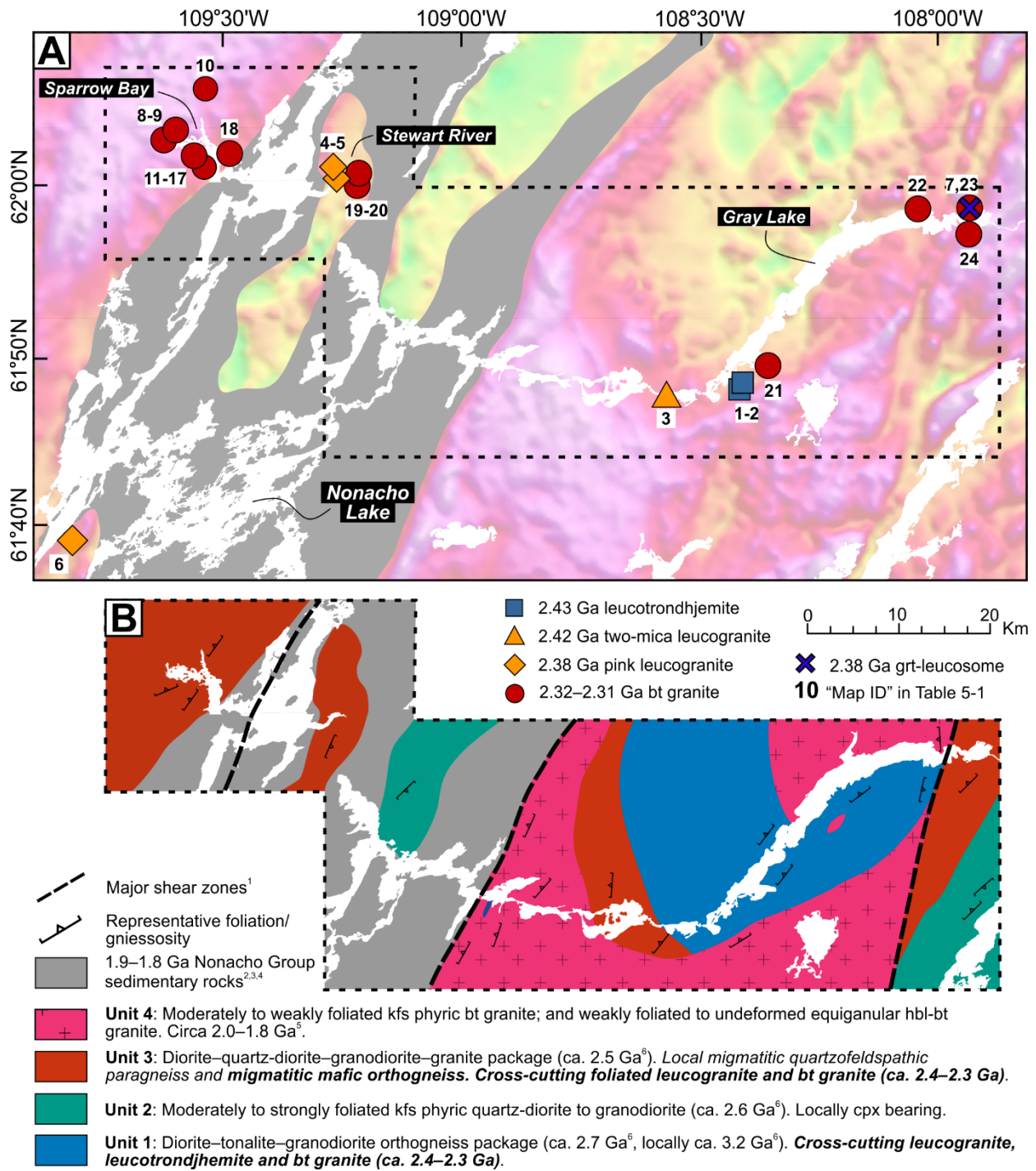


Figure 5-2. (A) Aeromagnetic anomaly map with sample locations. Samples are indicated by their "Map ID" in Table 5-1. (B) Sketch geology map of the inset area. Bold text in the legend highlights map unit components in this study. References: 1: Canam (2013); 2: Aspler (1985); 3: Bostock and van Breemen (1992); 4: van Breemen et al. (2013); 5: Neil, unpublished data; 6: This thesis. Mineral abbreviations after Kretz (1983).

Table 5-1. Summary of samples in this study.

Map ID	Sample ID	Northing	Easting	Rock type	Age $\pm 2\sigma$ (Ma)	Inhrt Zrc (Ga)	WR ϵNd_i	Tsat ($^{\circ}C$)	Ti-in-Zrc ($^{\circ}C$)
ca. 2.43–2.38 Ga leucogranitoids									
1	18EM35B	6852872	634658	Leucotondhemite	2432 \pm 6		–5.3	805	782
2	19BN32A	6852789	634585	Leucotondhemite	<i>2430</i>		–4.6	665	
3	19BN51A	6851686	626451	Two-mica leucogranite	2420 \pm 8		–3.7	828	
4	19BN150A	6876240	589293	Pink leucogranite	2379 \pm 7	2.52–2.47	–1.7	784	774
5	19BN154C	6875568	589894	Pink leucogranite	2374 \pm 9	2.53–2.45	–2.4	748	755
6	19BN123A	6836435	562017	Pink leucogranite	2382 \pm 7	2.54–2.48	–0.7	799	712
7	21BN52B	660555	660555	Grt-bearing leucosome	2385 \pm 7	2.67–2.44			871
ca. 2.32–2.31 Ga biotite granites									
8	18BN16A	6880181	571864	Bt syenogranite	<i>2320</i>		–10.1	873	
9	19BN17E	6879677	571818	Bt syenogranite	2321 \pm 6		–7.3	905	
10	21BN35A	576396	576396	Bt monzogranite	<i>2320</i>		–4.7	868	
11	18BN18C	6877717	576407	Bt syenogranite	<i>2320</i>		–8.0	870	
12	18-002E	6877567	576031	Bt monzogranite	2312 \pm 6		–9.3	887	
13	17-13A	6877546	576375	Bt syenogranite	<i>2320</i>		–9.8	868	
14	17-13B	6877575	576424	Bt monzogranite	<i>2320</i>		–6.2	852	
15	17-13C	6877575	576424	Bt monzogranite	<i>2320</i>		–9.4	877	
16	18BN31C	6877031	576538	Bt syenogranite	2316 \pm 6		–5.6	872	
17	17-12A	6875725	576510	Bt syenogranite	<i>2320</i>		–4.6	904	
18	18BN20C	6877076	578608	Bt syenogranite	2323 \pm 6		–9.7	893	899
19	19BN168A	6875600	592218	Bt syenogranite	2316 \pm 25		–11.2	809	
20	21BN39A	6874777	592951	Bt syenogranite	<i>2320</i>			842	
21	19BN07E	6854848	637662	Bt syenogranite	2314 \pm 6	2.74	–9.4	835	861
22	19BN43B	6871804	653821	Bt syenogranite	2322 \pm 6	2.64	–9.9	840	
23	21BN48D	6871649	659976	Bt syenogranite	2305 \pm 6		–6.0	864	
24	19BC37A	6869093	659872	Bt monzogranite	<i>2320</i>		–9.8	886	
	TX08-036	6929938	369611	Bt alkali-feldspar granite	<i>2320</i>		–9.5	845	
	TX08-038	6929726	379113	Bt syenogranite	<i>2320</i>		–10.8	785	

See Map ID on figure 5-2 for sample location. See figure 5-1 for location of samples TX08-036 and TX08-038. UTM zones are 13 (TX08-036 and TX08-038) and 12 (all others). Route rock names for the bt granites are from the Q-ANOR diagram (Steckeisen and LeMaitre, 1979). Ages in bold are weighted mean $^{207}Pb/^{206}Pb$ dates or upper intercept dates (Figure 5-6). Ages in *italics* are assumed. Inhrt Zrc: $^{207}Pb/^{206}Pb$ dates or range of dates from inherited zircon domains. WR: whole-rock. Ti-in-Zrc: Median Ti-in-zircon temperatures corrected for $aTiO_2$ and $aSiO_2 \leq 1$, see text for explanation. Note the higher zircon saturation and Ti-in-zircon temperatures of the biotite granites compared to the leucogranitoids. **Water levels on the Taltson River system fluctuate dramatically. As of 2021, several 2017, 2018 and 2019 sample sites were under water.**

5.3.1 Leucogranitoids

Three varieties of leucogranitoid were identified. The first is a **leucotrondhjemite** that is light grey, equigranular, medium grained and weakly to strongly foliated (Figure 5-3A and B). It is characterized by purple-grey or “smoky” quartz (Figures 5-3A and B), and contains minor amounts (<5%) of partially chloritized biotite, and trace amounts (<1%) of actinolite, zircon and opaque minerals. The foliation is defined by deformed/recrystallized quartz. This granitoid is found in map unit 1 (Figure 5-2), where it occurs as decimetre-scale dykes and transposed layers, and rarely as meter-scale bodies (Figure 5-3A). Small leucotrondhjemite dykes commonly occur within ca. 2.7 Ga granodioritic rocks (Figure 5-3B). Two samples were collected from a series of sizable (up to ~3 metres) leucotrondhjemite bodies that are in intrusive contact with tonalitic and amphibolitic gneisses (18EM35B and 19BN32A; Figures 5-2; Table 5-1).

The second variety is a **two-mica leucogranite** that is light-grey, equigranular, medium grained and strongly lineated. This rock contains relatively abundant biotite (~10%), minor amounts of muscovite, and trace amounts monazite, zircon and opaque minerals. The lineation is defined by aligned biotite and strongly deformed/recrystallized quartz. The presence of muscovite and monazite distinguishes this rock from all of the other granitoids in this study. This leucogranite was found in one outcrop near the boundary between map units 1 and 3 (Figure 5-2), and one sample (19BN51A; Table 5-1) was collected.

The third variety is a **pink leucogranite** that is equigranular, medium grained and ranges from weakly to moderately foliated (Figures 5-3C–E). It contains minor amounts of partially chloritized biotite, and trace amounts of allanite, apatite, zircon and ilmenite. The foliation is defined by deformed/recrystallized quartz. This leucogranite primarily occurs as centimeter- to meter-scale bodies in the Stewart River area (Figure 5-2), and is commonly found in intrusive contact with strongly-foliated to gneissic ca. 2.50 Ga granodiorites (Figure 5-3E). It also occurs in close proximity to the migmatitic quartzofeldspathic paragneiss. No direct field relationship between the paragneiss and the pink leucogranite was observed. However, some of the ca. 2.38 Ga leucosomes within the paragneiss are texturally similar to the pink leucogranite (Figure 5-3F), suggesting that the latter may have derived from partial melting of the former. Two pink leucogranite samples were collected from the Stewart River area (19BN154A and 19BN150A; Figures 5-2; Table 5-1). A third sample collected to the southwest of the map area (19BN123A, Figure 5-2; Table 5-1) is correlated to the pink leucogranite on the basis of its petrographic, geochronological (section 5.5) and geochemical (section 5.6) similarity.

5.3.2 Biotite granites

The biotite granites are medium grained and range from equigranular to slightly K-feldspar porphyritic (Figures 5-4A-D). These rocks typically exhibit a weak foliation that is defined by aligned biotite. The biotite ranges ~5 to 20% in modal abundance, and from being pristine to almost entirely chloritized. The feldspars range from pristine to strongly sericitized. Accessory minerals are far more abundant in the biotite granites than in the leucogranitoids; they include allanite, titanite, apatite, zircon, magnetite and ilmenite. Allanite is particularly ubiquitous and is commonly rimmed by epidote. These granites were documented in map units 1 and 3, where they cross-cut strongly foliated ca. 2.52–2.50 Ga and ca. 2.70 Ga granitoids, and the migmatitic mafic gneiss at the east end of Gray Lake (Figures 5-4B-D). In the Sparrow Bay area (Figure 5-2), they occur as sizable bodies that make-up ~50% of the outcropping area (Figure 5-4B). Elsewhere, they occur as small (<5 metres wide) dykes. Seventeen samples of the biotite granites were collected from the map area (Figure 5-2; Table 5-1). In addition, two samples from the region immediately north of the study area (TX08-036 and TX08-038; Figure 5-1; Table 5-1) are correlated to the biotite granites on the basis of their petrographic, geochemical and isotopic (section 5.6) similarity.

5.3.3 Migmatitic mafic gneiss: garnet-leucosome

The mafic gneiss at the eastern end of Gray Lake is heterogeneous (Figure 5-4E). Some layers contain orthopyroxene, clinopyroxene and garnet, which in addition to plagioclase, are interpreted to comprise a peak granulite-facies mineral assemblage. Where present, the pyroxene and garnet are partially resorbed and rimmed by amphibole, biotite, chlorite and epidote. In other layers, amphibole, biotite and chlorite are the only ferromagnesian minerals present, which is interpreted to reflect the locally complete retrograde replacement of the granulite-facies assemblage. One such layer yielded an igneous zircon age of ca. 2.52 Ga (19BC02A, chapter 3), which establishes a protolith age for at least some components of the gneiss. Centimetre-scale layers and metre-scale lenses of garnet-rich leucosome within the mafic gneiss (Figures 5-4E-F) are interpreted to reflect partial melting and peritectic garnet growth that was coeval with the granulite-facies metamorphism. One sample of a garnet-rich leucosome (21BN52B; Figure 5-2; Table 5-1) was investigated to constrain the age of granulite-facies metamorphism and migmatization. The sample contains abundant (~25% modal) garnet that is extensively fractured, and partially replaced by biotite and chlorite. For accessory phases, it contains zircon, monazite, apatite and opaque minerals.

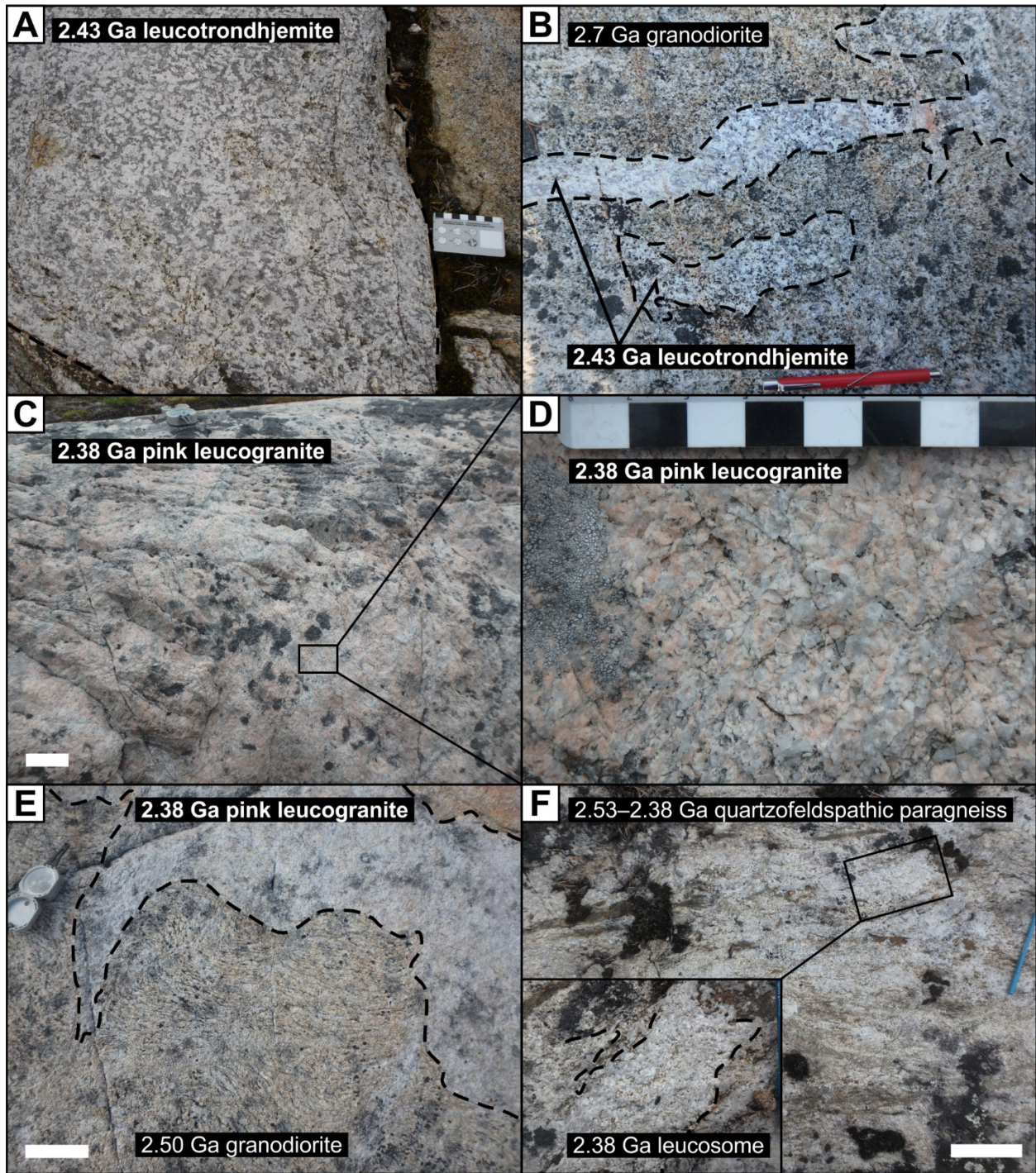


Figure 5-3. Representative outcrop photographs of the leucogranitoids. (A) Leucotondhjemite, location of sample 18EM35B. (B) Leucotondhjemite lenses within 2.7 Ga granodiorite. (C) Pink leucogranite, location of sample 19BN150A. (D) Close-up of the pink leucogranite. (E) Pink leucogranite in intrusive contact with strongly foliated 2.50 Ga granodiorite. Location of sample 19BN154C. (F) Quartzofeldspathic paragneiss. Inset shows the textural similarity between the leucosome in this paragneiss and the pink leucogranite. White scale bars are 15 cm.

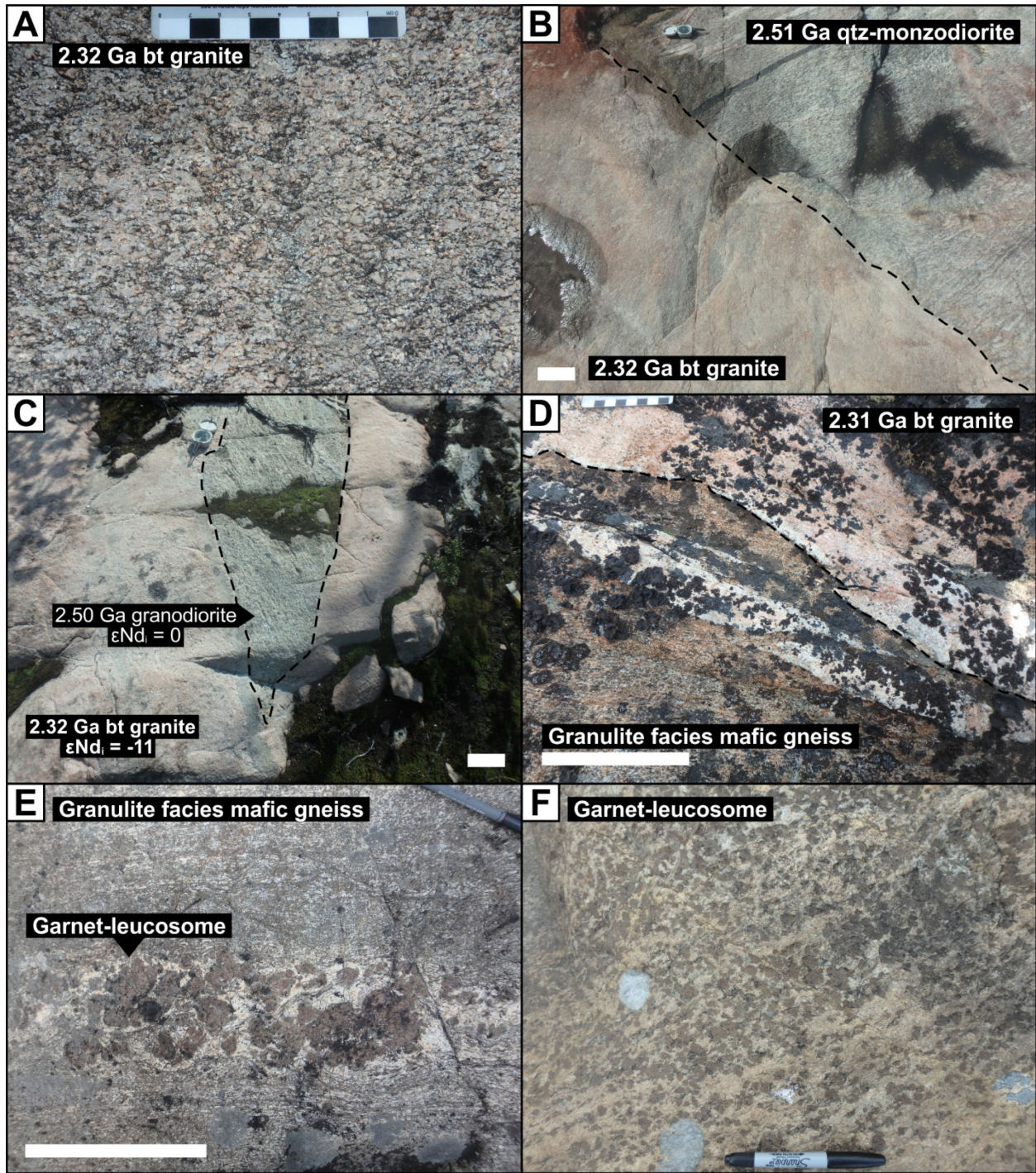


Figure 5-4. Representative outcrop photos of the biotite granites and the migmatitic mafic gneiss. (A) Close-up of a typical biotite granite, near sample 18BN17E. (B) 2.32 Ga biotite granite (near sample 18BN31C) cross-cutting strongly foliated 2.51 Ga quartz-monzodiorite. (C) 2.32 Ga biotite granite (sample 19BN168A) cross-cutting strongly foliated 2.50 Ga granodiorite. (D) 2.31 Ga biotite granite (sample 21BN48D) cross-cutting the granulite-facies mafic gneiss. (E) granulite-facies mafic gneiss with a layer of garnet-rich leucosome. (F) Large lens of garnet-rich leucosome (sample 21BN52B) in the granulite-facies mafic gneiss. White scale bars are 15 cm.

5.4 Analytical methods

A brief summary of the analytical techniques used in this study is given below. The complete details of sample preparation, analytical methods and data reduction protocols can be found in Appendix A. The complete data tables for the secondary reference materials and samples analyzed in this study can be found in Appendices A and E, respectively.

Zircon U-Pb age and trace-element data were acquired by LA-ICPMS (laser ablation – inductively coupled plasma mass spectrometry) at the University of Alberta. The U-Pb isotope analyses were made with a 213 nm Nd:YAG laser ablation system and a Nu Plasma MC-ICPMS (MC: multi-collector). Zircon was typically analyzed in epoxy grain mount with a 25 μm diameter laser beam. Zircon from sample 19BN51A was analyzed with a 15 μm laser beam that was rastered for $\sim 30 \mu\text{m}$, and zircon from 21BN52B was analyzed in petrographic thin-section. Select zircon domains were analyzed for their trace-element composition using a RESOLUTION 193 nm ArF laser ablation system and an Element XR ICPMS. These data were acquired with 25 μm diameter laser spots that were placed within the ablation pits from the U-Pb analyses, or adjacent to them and within the same zircon growth domain. All time-resolved U-Pb and trace-element measurements were inspected offline, and rare analyses were excluded for reasons given in Appendix A. These analyses are included in the data tables (Appendix E), with a note stating the reason for their exclusion. Whole-rock major-element data were acquired by fusion-dissolution ICP-OES (optical emission spectrometry) at Activation Laboratories in Ancaster, Ontario. Whole-rock trace-element data were acquired by fusion-dissolution ICP-MS in the Peter Hooper Geoanalytical Laboratory at Washington State University and by pressed-powder briquette XRF (X-ray fluorescence) in Dr. Stan Mertzman's laboratory at Franklin and Marshall College. Finally, whole-rock Sm-Nd isotope data were acquired by isotope dilution MC-ICPMS using a Nu Plasma MC-ICPMS at the University of Alberta.

Titanium-in-zircon temperatures were calculated using the calibration of Ferry and Watson (2007). “Uncorrected” Ti-in-zircon temperatures were calculated with the activities of both TiO_2 ($a\text{TiO}_2$) and SiO_2 ($a\text{SiO}_2$) set as one. “Corrected” Ti-in-zircon temperatures were adjusted for $a\text{SiO}_2$ and/or $a\text{TiO}_2$ values below unity following the recommendations of Schiller and Finger (2019). For the granitoid samples, this involved using the whole-rock composition and Excel-based Rhyolite MELTS v.1.1 (Gualda and Ghiorso, 2015) to model the evolution of $a\text{TiO}_2$ and $a\text{SiO}_2$ in the melt during isobaric equilibrium crystallization. Calculations were performed at 4 kbar with $f\text{O}_2$ constrained to the QFM buffer and initial melt H_2O contents set at 3 wt.%. The model results were combined with the measured whole-rock Zr content, and the zircon saturation model of Watson and Harrison (1983), to estimate $a\text{SiO}_2$ and $a\text{TiO}_2$ over the ideal temperature interval of zircon crystallization (Schiller and Finger, 2019). The $a\text{TiO}_2$ and $a\text{SiO}_2$ values corresponding to the temperature at which 50% of zircon

would have theoretically crystallized were used to calculate the corrected Ti-in-zircon temperatures (Table E-1). For the garnet-leucosome (sample 21BN52B), a simple +70°C correction was applied to the uncorrected Ti-in-zircon temperatures, as Schiller and Finger (2019) suggest this is a reasonable approximate upward correction for a broad range of granitoid compositions. Both the uncorrected and corrected temperatures are plotted below, however, only the corrected Ti-in-zircon temperatures are discussed in the text.

All uncertainties in this paper are reported at the 95% confidence level, and all dates referred to in the text are $^{207}\text{Pb}/^{206}\text{Pb}$ dates. Uncertainties on weighted mean $^{207}\text{Pb}/^{206}\text{Pb}$ ages are shown at two levels (Table 5-1). The first is the 2SE on the weighted mean calculated in ISOPLOT (Ludwig, 2009). The second uncertainty, denoted as 2σ , combines the first with the long-term external reproducibility of the *weighted mean* $^{207}\text{Pb}/^{206}\text{Pb}$ ratio, which is $\sim 0.3\%$ (2σ ; Appendix A).

5.5 Zircon U-Pb age and trace-element data

5.5.1 Leucotrandhjemite

One sample of the leucotrandhjemite (18EM35B; Figure 5-3A) was processed for U-Pb zircon geochronology. The zircon grains recovered range from prismatic to sub-equant (Figure 5-5). Two distinct domain types were recognized. First are several grains and core domains with fine-scale oscillatory zoning that is consistent with an igneous origin (e.g., Corfu et al., 2003). Second are a number of grains and rim domains that are unzoned or broadly zoned (Figure 5-5). The latter might typically be interpreted as metamorphic in origin (e.g., Corfu et al., 2003). However, there is no systematic relationship between the $^{207}\text{Pb}/^{206}\text{Pb}$ dates of the zircon domains and their zoning characteristics. Therefore, the variation in zoning, and the presence of cores and rims, may simply reflect different phases of igneous zircon growth from a single magma. Alternatively, metamorphism could have occurred shortly after magma crystallization, such that the two events cannot be resolved at the precision level of these data. In either case, the data should provide a reasonable crystallization age estimate. The 6 youngest analyses are slightly discordant (2-4%), which may reflect minor Pb-loss (Figure 5-6). The 40 oldest analyses largely overlap concordia and yield a weighted mean date of 2432 ± 6 Ma with an MSWD (mean squared weighted deviation) of 2.2 (Figure 5-6), which is taken as the best igneous crystallization age estimate.

Trace-element data were acquired for both zircon domain types (Figure 5-7). The finely-zoned cores and grains yield lower Th/U ratios (average = 0.1) than the unzoned/broadly zoned rims and grains (average = 0.5) (Figure 5-7A). This is the opposite of what is expected for co-existing igneous and metamorphic zircon populations (Hoskin and Schaltegger, 2003; Rubatto, 2017), and is arguably more consistent with the interpretation of multiple igneous zircon growth phases presented above. Apart from Th and U, however, there is no perceptible difference in the trace-element character of

the two domain types. Both domain types have positive sloping heavy rare earth element (HREE) patterns, but low total HREE contents (Figures 5-7C). The low HREE contents of these zircon domains/grains is consistent with their direct crystallization from the leucotondhjemite magma, because the leucotondhjemite itself has very low HREE contents (section 5.6). The finely-zoned domains yield Ti-in-zircon temperatures of 738–792°C, the unzoned/broadly zoned domains yield Ti-in-zircon temperatures of 722–835°C, and collectively they give a median value of 782°C (Figure 5-7D; Table 5-1).

5.5.2 Two-mica leucogranite

Many of the zircon grains recovered from the two-mica leucogranite contain thin (<30 µm) rims on metamict cores (19BN51A; Figure 5-5). An initial attempt to date these grains with a static 25 µm laser spot resulted in data that were largely mixed (inconsistent $^{207}\text{Pb}/^{206}\text{Pb}$ signals) and unresolvable. A second attempt employed ~15 x 30 µm line raster's and resulted in a more coherent dataset (Figure 5-6). The fifteen oldest raster analyses are from rim domains and prismatic grains that exhibit fine-scale oscillatory zoning. These fifteen analyses yield a weighted mean date of 2420 ± 8 Ma (MSWD=2.5; Figure 5-6), which is taken as the best igneous crystallization age estimate. Five younger dates (2396 ± 14 to 2374 ± 14 Ma) come from one oscillatory zoned rim domain, and three faintly zoned or unzoned rim domains. These younger dates are interpreted to reflect Pb-loss or metamorphic zircon (re)crystallization. No zircon trace-element data were obtained for this sample.

5.5.3 Pink leucogranite

All three samples of the pink leucogranite (19BN150A, 19BN154C and 19BN123A; Figure 5-2A) were processed for U-Pb zircon geochronology. Two distinct and broadly concordant age clusters were obtained from each sample, one at ~2.50 Ga and one at ~2.38 Ga (Figure 5-6). The ca. 2.50 Ga dates originate from grains and core domains with oscillatory zoning (Figure 5-5). The ca. 2.38 Ga dates from samples 19BN150A and 19BN154C are associated with rim domains and grains that are unzoned or faintly zoned (Figure 5-5). Most ca. 2.38 Ga rim domains and a single ca. 2.38 Ga grain from sample 19BN123A exhibit clear fine-scale oscillatory zoning that is consistent with an igneous origin (Figure 5-5). The ca. 2.38 Ga rims and grains from all three samples also tend to be relatively well-faceted, whereas the ca. 2.50 Ga grains tend to be rounded (Figure 5-5). Therefore, the ca. 2.50 Ga grains and cores are interpreted as xenocrysts from the ca. 2.50 Ga granodiorite wall rocks (Figure 5-3E), and the ca. 2.38 Ga domains are interpreted as igneous zircon that crystallized in the leucogranite melts. This interpretation is also supported by the fact that sample 19BN150A is nearly undeformed (Figure 5-3F), such that it is unlikely to contain metamorphic zircon. Weighted mean dates from the ca. 2.38 Ga domains provide igneous crystallization ages of 2374 ± 9

Ma (19BN154C), 2379 ± 7 Ma (19BN150A) and 2382 ± 7 Ma (19BN123A), which are indistinguishable within analytical uncertainty (Figure 5-4).

To evaluate the age interpretation presented above, zircon trace-element data were acquired for all three samples of the pink leucogranite, and two samples of the ca. 2.50 Ga granodiorite wall rocks (samples 19BN154A and 19BN126B in chapter 3). The Th and U contents of the ca. 2.50 Ga zircon domains/grains from the pink leucogranite and the wall rocks overlap almost entirely (Figure 5-7A), and their Hf and Σ HREE contents overlap in large part (Figure 5-7A). By contrast, the ca. 2.38 Ga domains from the pink leucogranite are, on average, offset to higher U contents (lower Th/U ratios), higher Hf contents and lower Σ HREE contents (Figures 5-7A and B). These results are consistent with the ca. 2.50 Ga zircon domains in the pink leucogranite being inherited from the local wall rocks, and the ca. 2.38 Ga domains being magmatic rather than metamorphic. Ti-in-zircon temperatures from the ca. 2.38 Ga domains therefore provide constraints on the petrogenesis of the pink leucogranite. Individual Ti-in-zircon temperatures range from 680 to 786°C, with three outlying analyses >800°C (Figure 5-7C). Median values for the three samples are 712°C (19BN123A), 755°C (19BN154C) and 774°C (19BN150A) (Figure 5-7C; Table 5-1).

5.5.4 Biotite granites

Eight samples of the biotite granites were processed for U-Pb zircon geochronology (Figure 5-2A). Zircon grains from these samples are, for the most part, prismatic with fine- to broad-scale oscillatory zoning that is consistent with an igneous origin (Figure 5-5). In rare cases, oscillatory zoned domains are transected by unzoned (recrystallized?) domains (e.g., sample 18-002E; Figure 5-5), but the two domains always yield indistinguishable dates. For seven of eight samples, weighted mean dates from largely concordant data clusters are interpreted as igneous crystallization ages (Figure 5-6). Six of these samples yield indistinguishable crystallization ages between 2323 ± 6 Ma and 2312 ± 6 Ma (Figure 5-6). Sample 21BN48D yields a slightly younger crystallization age of 2305 ± 6 Ma (Figure 5-6), and establishes a minimum age for the granulite-facies metamorphism and migmatization of the mafic gneiss at the east end of Gray Lake, which this granite cross-cuts (Figure 5-4D). Two core domains from samples 19BN07E and 19BN43B (Figure 5-5) yield discordant dates of 2739 ± 14 Ma and 2635 ± 12 Ma, and are interpreted as inherited (Figure 5-6). Rare discordant (4–6%) igneous zircon analyses from samples 18BN07E and 19BN48D (Figure 5-6) are younger than the main data clusters in their corresponding sample, and are interpreted to reflect minor Pb-loss.

The zircon U-Pb systematics of one biotite granite sample, 19BN168A, are more complex than the rest (Figure 5-6). The zircon grains recovered from this sample are of poor quality. They are typically prismatic with convolute or oscillatory zoning (Figure 5-5). The zoning is marked by dark (in BSE response) bands that are U-rich and strongly radiation damaged (Figure 5-5). The analyses range

from concordant to 37% discordant (Figure 5-5). A regression through all of the data yields an upper intercept of 2344 ± 39 Ma (MSWD=11.4). Two analyses fall to the right of the main data array (Figure 5-6) and come from the central parts (cores?) of two grains, which may be inherited. Excluding these two analyses, the data yield an imprecise upper intercept of 2316 ± 25 Ma (MSWD=5.5), which is taken as the best crystallization age estimate (Figure 5-6).

Zircon grains from samples 18BN20C and 19BN07E were analyzed for their trace-element composition. The zircon grains from these two samples are by far the highest quality of those found in all the biotite granite samples and contain the fewest inclusions. The Th/U ratios of these grains range from 0.4 to 1.8, but the majority (27/34) are >1.0 (Figure 5-7A). These Th/U ratios are higher than is typical of zircon from granitic rocks (Kirkland et al., 2015), which is not surprising because the biotite granites themselves have high whole-rock Th/U ratios (section 5.6). Individual Ti-in-zircon temperatures range from 748 to 952°C, but are dominantly (27/34) $>850^\circ\text{C}$ (Figure 5-7C). Median values of 899°C and 861°C were obtained for samples 18BN20C and 19BN07E, respectively (Figure 5-7C; Table 5-1).

5.5.5 Migmatitic mafic gneiss: garnet-leucosome

The garnet-leucosome (sample 21BN52B) contains zircon grains that are either monophase and unzoned, or have a core with fine-scale oscillatory zoning and an unzoned rim (Figure 5-5). Some grains with unzoned rims are included in garnet (Figure 5-5), indicating that the rim domains formed before or at the same time as the garnet. The finely zoned zircon cores yield dates between 2668 ± 13 and 2441 ± 13 Ma, whereas the unzoned rims and grains yield dates between 2413 ± 13 and 2363 ± 13 Ma (Figure 5-6). Both the cores and unzoned domains were analyzed for their trace-element composition. There is no systematic difference in Th/U ratios between the cores and unzoned domains, which range from 0.2 to 1.1 (not plotted). By contrast, the cores have steep positive sloping HREE patterns, whereas the rims have flat or negative sloping HREE patterns (Figure 5-7D), indicating that the latter formed in the presence of garnet (e.g., Rubatto, 2017). Ti-in-zircon temperatures from the unzoned domains range from 821 to 906°C (median = 871°C; Figure 5-7C), which is consistent with the temperatures of amphibole dehydration melting reactions in mafic and intermediate rocks (e.g., Pattison et al., 2003). Therefore, the core domains are regarded as inherited, and the unzoned domains are interpreted to reflect magmatic zircon that formed with peritectic garnet during granulite-facies metamorphism and partial melting of the mafic gneiss. All unzoned domain analyses yield a weighted mean date of 2385 ± 7 Ma with an MSWD of 3.6 (Figure 5-6). Excluding the two oldest and two youngest dates yields an identical weighted mean while reducing the MSWD to 1.6. Thus, 2385 ± 7 Ma is taken as the age of partial melting, peritectic garnet growth and granulite-facies metamorphism at the east end of Gray Lake.

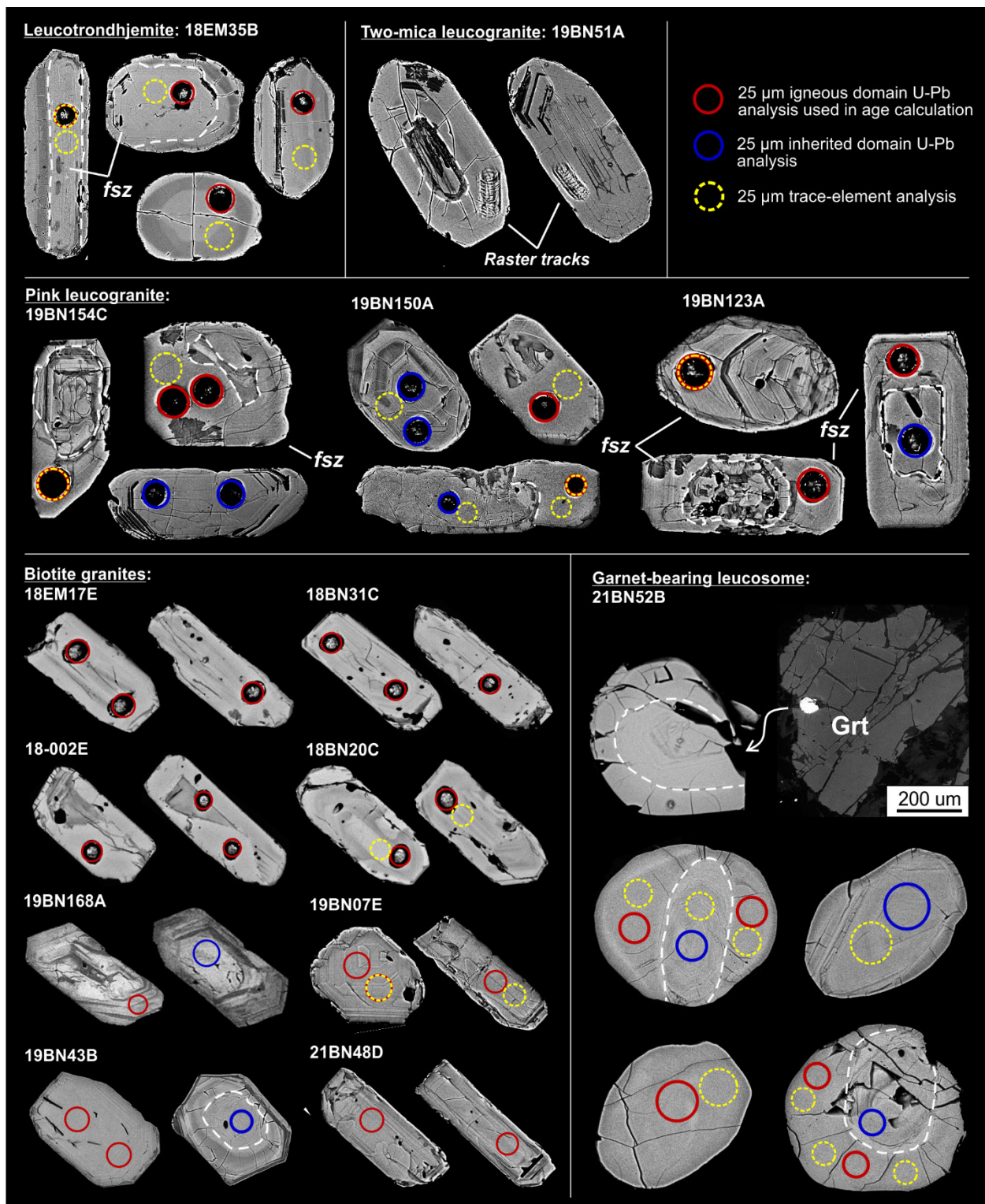


Figure 5-5. Representative backscattered electron images of zircon with analytical spots. White dashed lines highlight core-rim boundaries. Grt: garnet; fsz: fine-scale zoning. Higher resolution images of some grains were acquired after analyses, such that the laser ablation pits are visible.

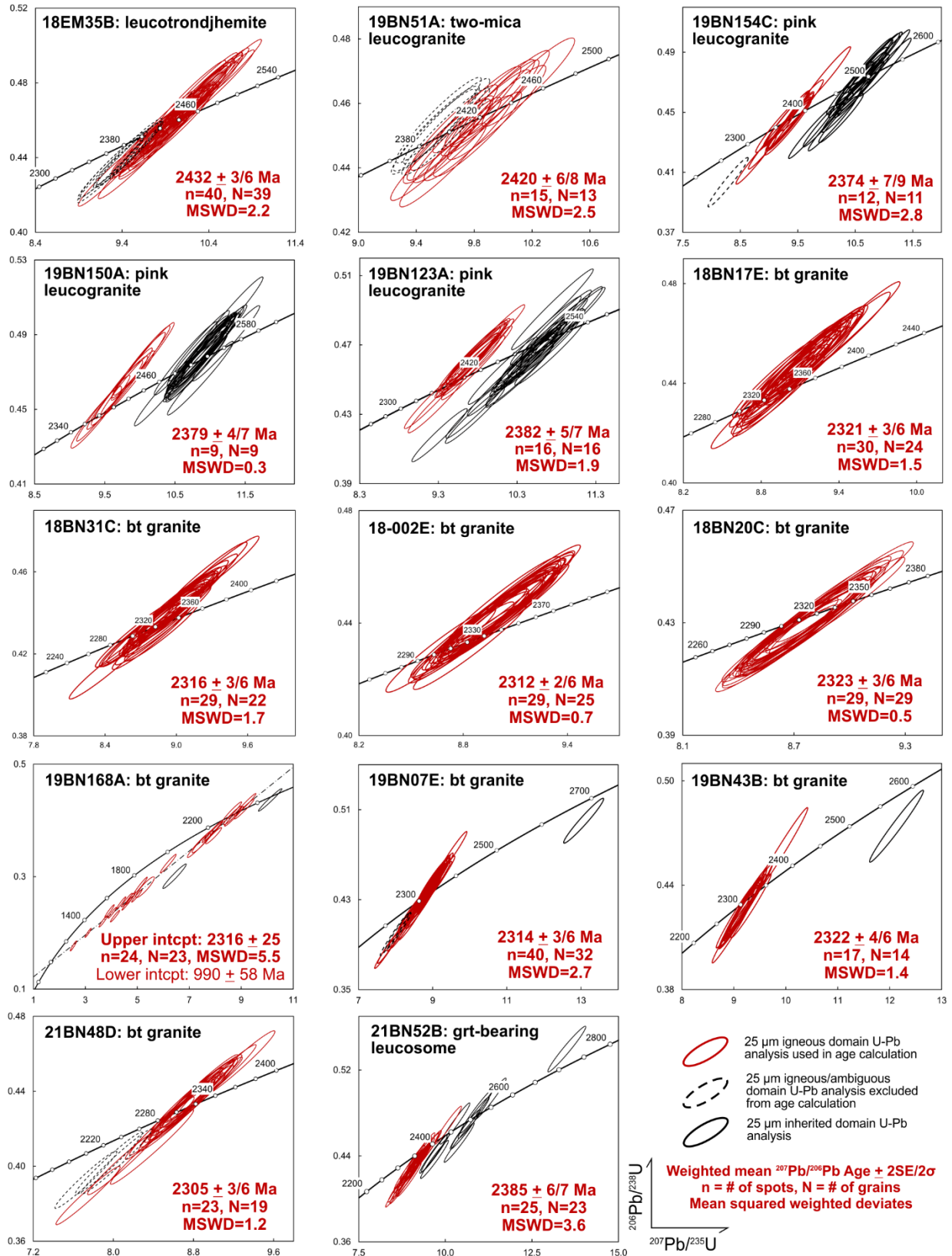


Figure 5-6. Wetherill concordia diagrams for LA-ICPMS zircon U-Pb isotope data. Uncertainty ellipses are 2σ.

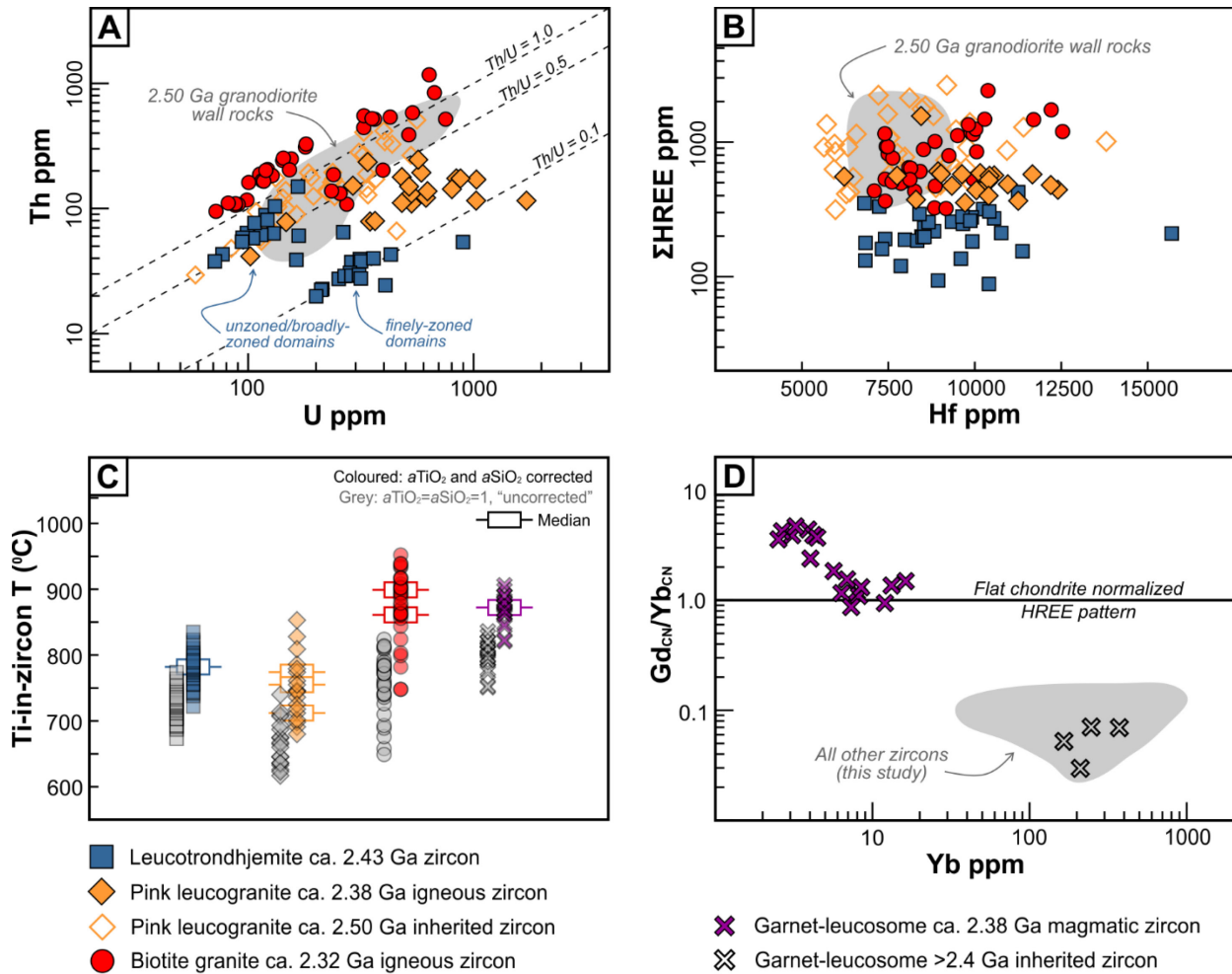


Figure 5-7. Zircon trace-element data. (A) U ppm vs. Th ppm. (B) Hf ppm vs. $\Sigma HREE$ ppm. (C) Yb ppm vs. Gd_{CN}/Yb_{CN} . (D) Ti-in-zircon temperatures. CN = chondrite normalized. Chondrite normalizing values from Sun and McDonough (1989). Grey fields in (A) and (B) outline the composition of igneous ca. 2.50 Ga zircon from the wall rocks to the ca. 2.38 Ga pink leucogranite. Data from the garnet-bearing leucosome are excluded from (A) and (B) for clarity. Grey field in (C) outlines the composition of all analyzed zircons other than those from the garnet-bearing leucosome. Grey symbols in (D) indicate "uncorrected" ($aTiO_2 = aSiO_2 = 1$) Ti-in-zircon temperatures. Coloured symbols are Ti-in-zircon temperatures corrected for $aTiO_2$ and $aSiO_2$ (Table E-1).

5.6 Whole-rock geochemical and isotopic data

All of the granitoids documented in this study contain more than 69 wt.% SiO₂, and most of them are weakly to moderately peraluminous with ASI (aluminium saturation index) values between 1.0 and 1.1 (Figure 5-8). Apart from these similarities, there are substantial geochemical and isotopic differences between the different suites.

The two **leucotrondhjemite** samples are calcic and calc-alkalic, magnesian, and plot within the trondhjemite field on the normative albite(Ab)-anorthite(An)-orthoclase(Or) ternary diagram (Figure 5-8). They have relatively high CaO, Al₂O₃ and Na₂O contents, and low K₂O (≤ 2 wt.%) contents (Figure 5-8). Both samples exhibit prominent negative Th, Nb and P anomalies on primitive mantle normalized plots, and steep REE patterns (median La_{CN}/Yb_{CN} = 189) with large positive Eu anomalies on chondrite-normalized plots (Figure 5-9). One sample exhibits a concave upward HREE pattern (Figure 5-9). These rocks are also characterized by high Sr contents (419 and 610 ppm), very high Sr/Y ratios (524 and 582) (Figure 5-10A), and very low overall REE and high-field strength (HFSE) element contents (Figures 5-9 and 5-10B-C). For instance, Yb and Nb are present in abundances of ~1x chondrite and ~1x primitive mantle, respectively (Figure 5-9). Both samples yield similar initial ϵ Nd (ϵ Nd_i) values of -6.7 and -5.3 (Figure 5-11A; Table 5-1).

The **two-mica and pink leucogranite** samples (collectively referred to as the leucogranites) are calcic to alkali-calcic, magnesian, plot within the granite field on the Ab-An-Or ternary, and have high K₂O contents of ~5–6 wt.% (Figure 5-8). They exhibit prominent negative Nb, Sr and P anomalies on primitive mantle-normalized plots, and steep REE patterns on chondrite-normalized plots (Figure 5-9). Europium anomalies are variable but relatively small, and Sr/Y ratios range from 41 to 54 (Figures 5-9 and 5-10A). The two-mica leucogranite is more light REE (LREE) enriched and has a steeper REE pattern (La_{CN}/Yb_{CN} = 311) than the pink leucogranite (median La_{CN}/Yb_{CN} = 123) (Figures 5-9 and 5-10A). The LREE and HFSE contents of these rocks are intermediate between those of the leucotrondhjemite and the biotite granites (Figures 5-9 and 5-10A-B). Initial ϵ Nd values of -3.6 and -2.4 to -0.7 were obtained for the two-mica leucogranite and the pink leucogranite, respectively (Figure 5-11A; Table 5-1).

The **biotite granites** range from 70 to 75 wt.% SiO₂, are alkali-calcic, straddle the ferroan-magnesian boundary and fall within the granite field on the Ab-An-Or ternary (Figure 5-8). Four samples yield ASI values >1.1 (Figure 5-8), which are thought to reflect sericite alteration because no strongly peraluminous primary minerals (e.g., muscovite) were observed in these granites. All major- and minor-oxides concentrations, except for K₂O and Na₂O, are negatively correlated with SiO₂ (examples in Figure 5-8). K₂O contents are high (5-6 wt.%), similar to the leucogranites (Figure 5-8). The concentrations of several trace-elements (Ba, Sr, Zr and the LREE) also exhibit negative

correlations with SiO_2 , as do the Eu/Eu^* values (examples in Figure 5-10B-E). Primitive mantle-normalized trace-element patterns are characterized by prominent negative Nb, Sr, P, Ti and Eu anomalies, small negative Zr and Hf anomalies, and positive Th anomalies (Figure 5-9). On average, these granites have more shallowly-sloping REE patterns (median $\text{La}_{\text{CN}}/\text{Yb}_{\text{CN}} = 59$), and lower Sr/Y ratios (median = 7.5) than the leucogranitoids (Figures 5-9 and 5-10A). They are also distinguished from the leucogranitoids by their elevated HFSE and LREE contents. Thorium is present in abundances up to 1000x primitive mantle, La is present in abundances up to 1000x chondrite, and Zr ranges from 148 to 590 ppm (median = 388) (Figures 5-9 and 5-10C). The high Zr contents translate into rather high zircon saturation temperatures (Watson and Harrison, 1983) of 905 to 785°C (Figure 5-10E; Table 5-1). Many of the biotite granites also have unusually high Th/U ratios of ~30 to 50 (Figure 5-10F). For comparison, the average upper continental crust has Th/U ratio is 4 (Rudnick and Gao, 2014; Figure 5-10F). Finally, the biotite granites yield ϵNd_i values between -11.2 and -4.6 (Figure 5-11A; Table 5-1). There is not a strong correlation between ϵNd_i and SiO_2 (Figure 5-11B), particularly if the two highest SiO_2 samples are excluded (Figure 5-11B). There does, however, appear to be a negative correlation between ϵNd_i and Fe-number, with more negative ϵNd_i values associated with more ferroan compositions (Figure 5-11C).

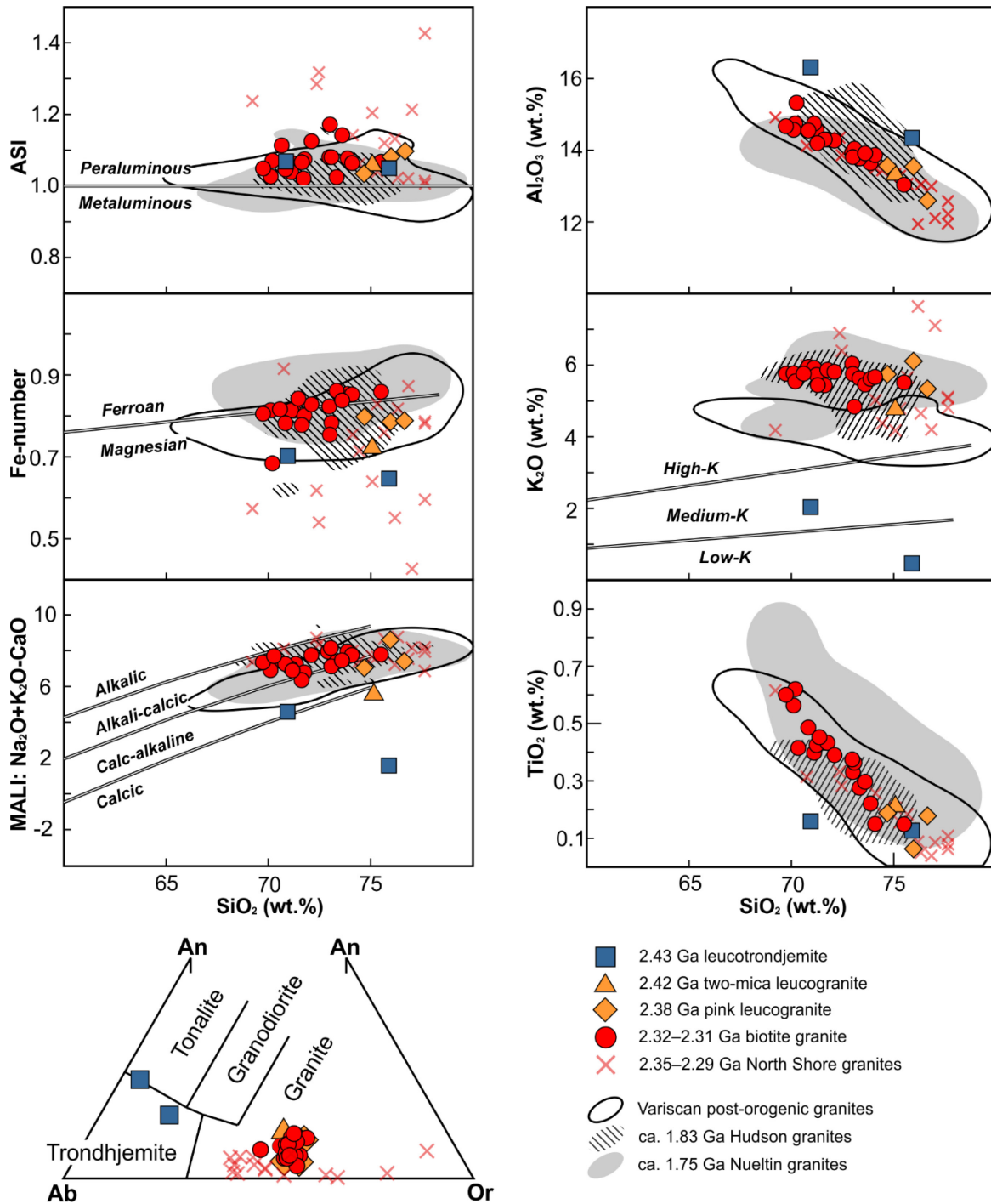


Figure 5-8. Left panel: granitoid classification diagrams of Frost et al. (2001) and Barker (1979). ASI (Aluminum saturation index) $[Al_2O_3/(Na_2O + K_2O + CaO - 3.33 \cdot P_2O_5)]$ calculated on a molar basis. Fe-number $[FeO_{total}/(FeO_{total} + MgO)]$ and MALI (modified alkali-lime index) are calculated in wt.%. Right panel: select Harker variation diagrams. Low-, medium and high-K fields from Gill (1981). Comparative data fields (e.g., ca. 1.83 Ga Hudson granitoids) are 75% kernel density contours. Variscan post-orogenic granite data from compilation of Jacob et al. (2021). Hudson and Nueltin granitoid data from Peterson et al. (2002; 2015), Scott (2012) and T.D. Peterson (unpublished data).

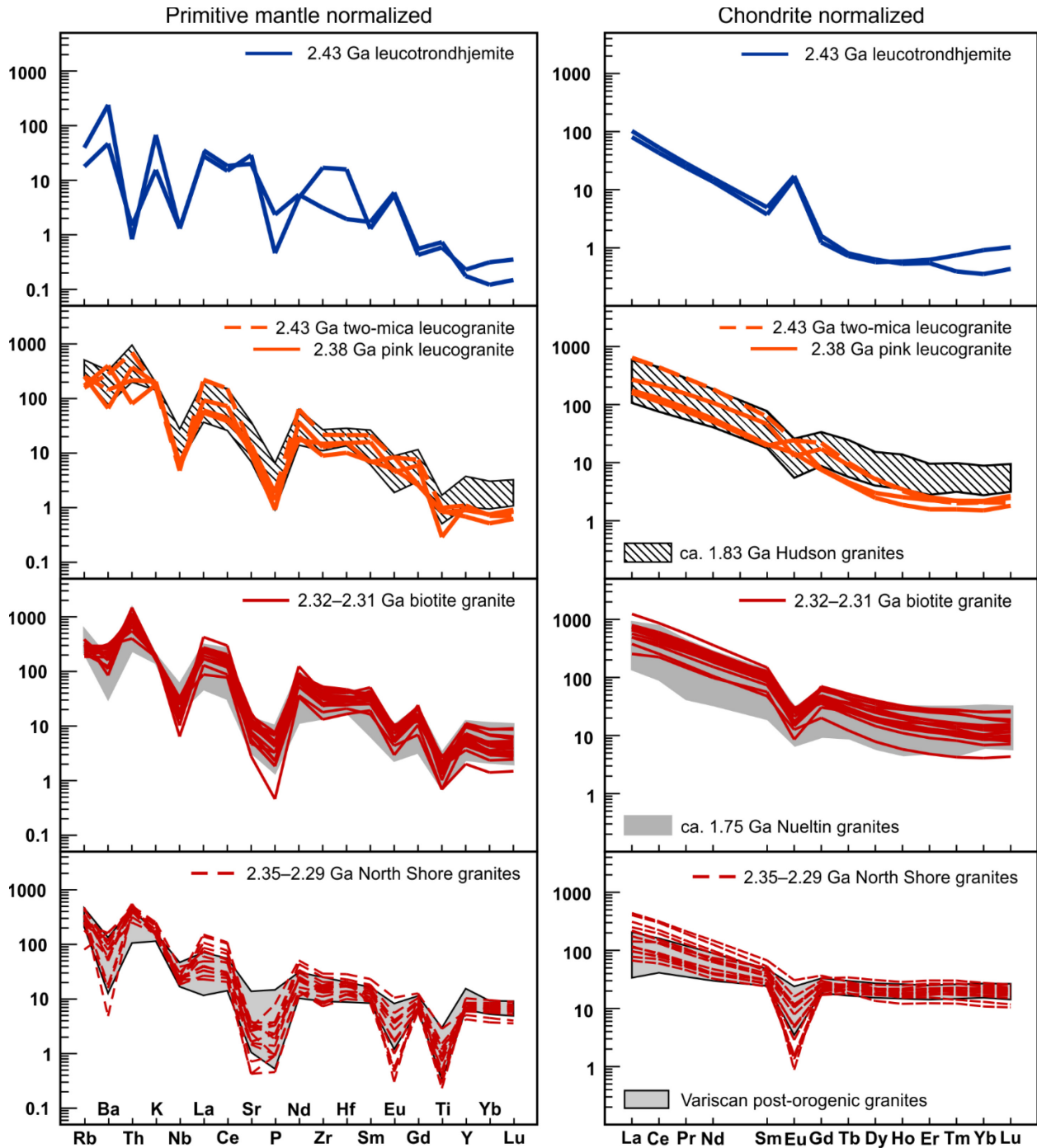


Figure 5-9. Primitive mantle normalized extended element plots (left panel) and chondrite normalized rare earth element plots (right panel) for the granitoids of this study and the North Shore granites (Hartlaub et al., 2007). Two (of 16) North Shore pluton samples with distinct trace-element patterns excluded for clarity (Hartlaub et al., 2007). Primitive mantle and chondrite normalizing values are from Sun and McDonough (1989). Comparative data fields (e.g., ca. 1.83 Ga Hudson granites) are the middle 75% of the data. Data sources are as in Figure 5-8.

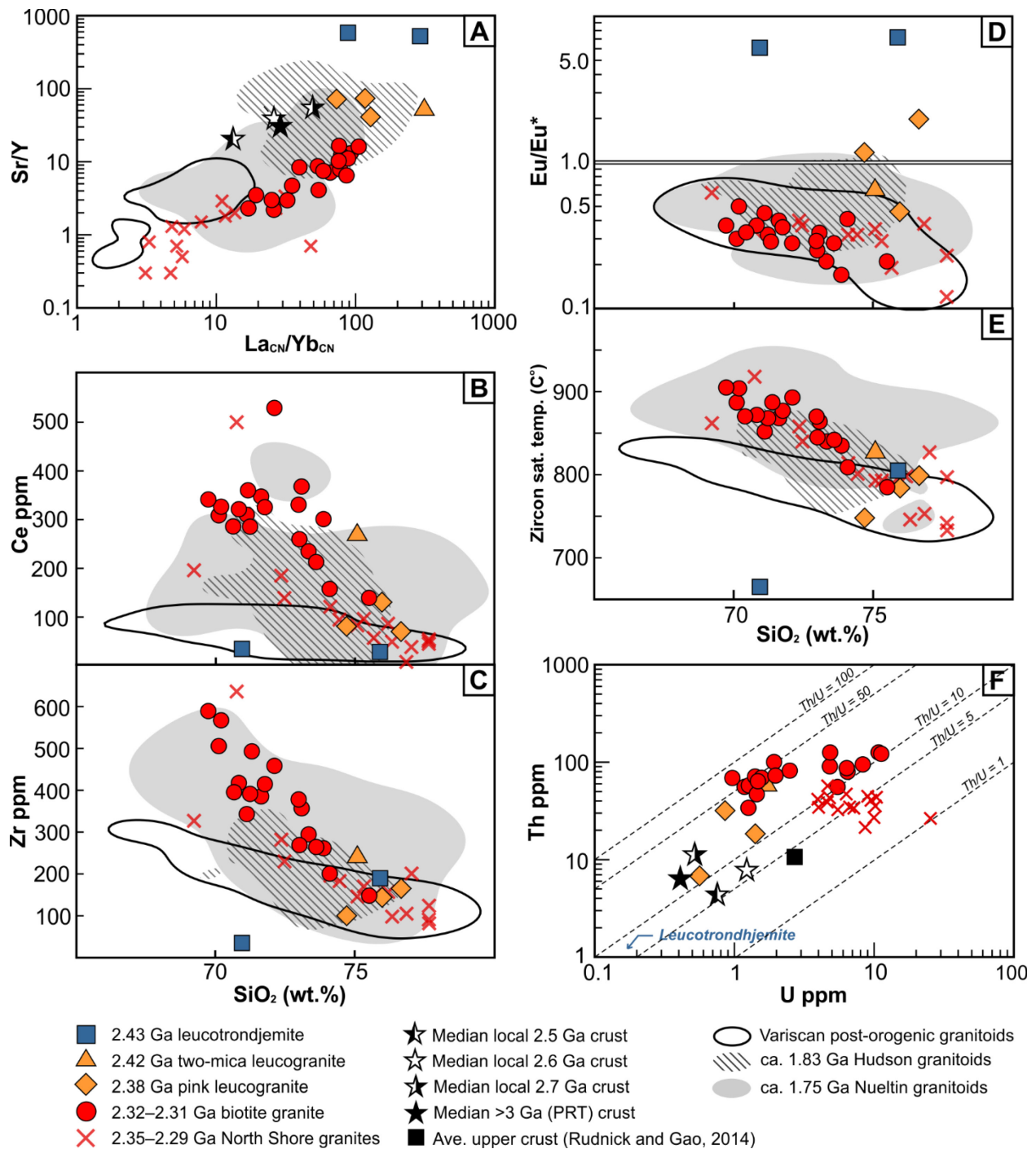


Figure 5-10. Bivariate trace-element plots. (A) La_{CN}/Yb_{CN} vs. Sr/Y. (B-E) SiO₂ vs. select trace-elements and trace-element parameters. Eu/Eu* = Eu_{CN}/√(Sm_{CN}XGd_{CN}). CN: chondrite normalized. Normalizing values from Sun and McDonough (1989). Zircon saturation temperatures calculated with calibration of Watson and Harrison (1983). (F) U ppm vs. Th ppm. Median values (stars) for local granitoids and PRT granitoids calculated from the data in chapters 2 and 3. Comparative data fields (e.g., ca. 1.83 Ga Hudson granitoids) as in Figure 5-8. Fields excluded from (F) for clarity.

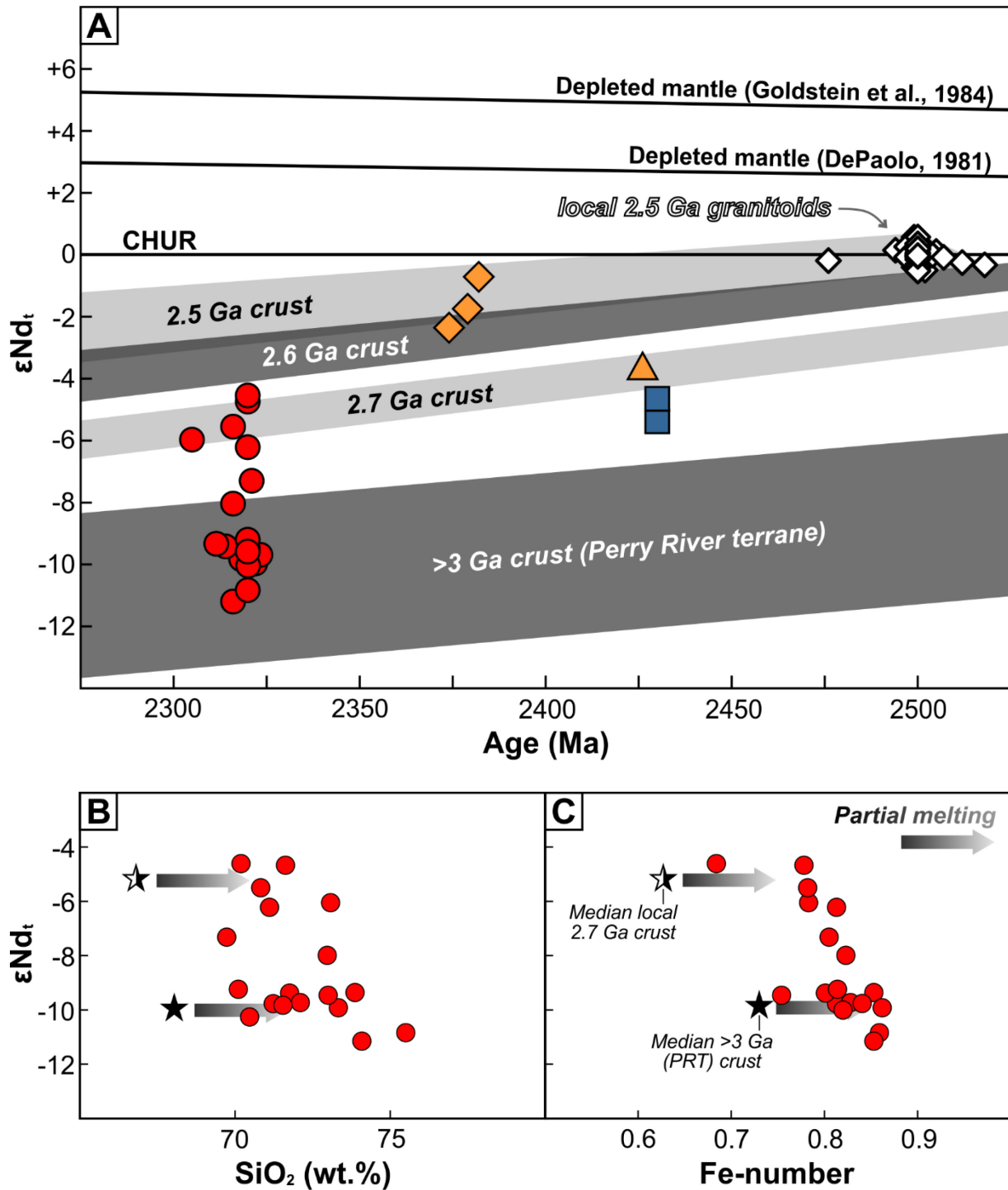


Figure 5-11. (A) Age vs. ϵNd_t for Paleoproterozoic (2.4–2.3 Ga) granitoids of this study. Isotopic evolution fields for local 2.7, 2.6 and 2.5 Ga granitoids, and >3 Ga PRT granitoids, are from data in chapters 2 and 3. CHUR: chondritic uniform reservoir. Plotted for comparison are ϵNd_t values from the local 2.5 Ga granitoids. (B) SiO₂ vs. ϵNd_t . (C) Fe-number vs. ϵNd_t . Initial values plotted for ca. 2.32–2.31 Ga biotite granites. Median $\epsilon Nd_{2.32\text{ Ga}}$ values plotted for local 2.7 Ga crust (black/white star) and >3 Ga PRT crust (black star) are also shown in (B) and (C). Data point symbols are the same as in previous figures.

5.7 Discussion

5.7.1 Granitoid petrogenesis

All of the 2.43–2.31 Ga granitoids documented in this study are highly evolved in that they contain more than 69 wt.% SiO₂ and have negative ϵNd_i values (Figures 5-8 and 5-11; Table 5-1). In addition, no field evidence was observed for the direct involvement of mantle-derived mafic magmas in their genesis (Figures 5-3 and 5-4). When mafic magmas contribute directly to the genesis of felsic granitoids, evidence for this process can typically be seen in the presence of mafic microgranular enclaves or magma mixing textures (e.g., Barbarin and Didier, 1992; Pitcher, 1997); such evidence is conspicuously absent in the leucogranitoids and biotite granites of the Nonacho area. The granitoids in this study are therefore regarded as having derived entirely, or almost entirely, from partial melting of crustal rocks. Thus, the following discussion focuses on identifying the crustal source rocks and melting conditions (i.e., temperatures and pressures) that were involved in magma genesis. This does not, however, rule out the indirect involvement of mantle-derived magmas as a source of heat for crustal melting.

Sodic granitoids, similar in composition to the **ca. 2.43 Ga leucotronthjemite**, can be generated through partial melting of low-K metabasaltic rocks, as is commonly proposed for Archean TTG (tonalite-trondhjemite-granodiorite) suites (e.g., Rapp et al., 1991; Moyen and Stevens, 2006). This is certainly a plausible explanation for the leucotronthjemite. Although its ϵNd_i values do not match the isotopic composition of any older igneous suites documented in the area so far (Figure 5-11A), they clearly require an Archean source, and low-K mafic rocks are a common component of Archean terranes in general (e.g., Moyen and Martin, 2012). The high Al₂O₃, CaO, Na₂O and Sr contents, and large positive Eu anomalies, in the leucotronthjemite (Figures 5-8 to 5-10) may reflect plagioclase accumulation. Alternatively, the enrichment in these elements could reflect the presence of excess water during partial melting (fluid-present melting), which would favor the breakdown of plagioclase in the source (e.g., Beard and Lofgren, 1991; Frost et al., 2016). The experiments of Beard and Lofgren (1991) also suggest that fluid-present melting of mafic rocks leaves an amphibole-rich residue, which would explain the concave upward HREE pattern of one leucotronthjemite sample (Figure 5-9). In either scenario, plagioclase exerts a strong control on the major- and trace-element budget of the leucotronthjemite, and this likely accounts, at least in part, for its very steep REE patterns and high Sr/Y ratios (e.g., Rollinson, 2021; Kendrick et al., 2022). Thus, the steep REE patterns and high Sr/Y ratios of the leucotronthjemite do not necessarily reflect abundant garnet in the melt residue, and a robust assessment of the pressure/depth at which melting occurred is precluded.

Evolved granitic rocks that are weakly peraluminous and potassic, such as the **ca. 2.42 Ga two-mica leucogranite** and the **ca. 2.38 Ga pink leucogranite**, can form through low degrees of partial melting in metasedimentary rocks or potassic metaigneous rocks (e.g., Chappell and White, 1992). The Sm-Nd isotope data point to deeper seated equivalents of the local 2.6 and 2.5 Ga granitoids as potential source rocks for the pink leucogranite (Figure 5-11A). Similarly, the ϵ_{Nd_i} value from the two-mica leucogranite is consistent with its derivation from a deeper seated equivalent to the local 2.7 Ga granitoids (Figure 5-11A). Any sedimentary rocks derived chiefly from erosion of those Archean granitoids would also be viable source rocks. In the case of the pink leucogranite, there is direct evidence for coeval partial melting of both metaigneous and metasedimentary rocks, in the form of the garnet-bearing leucosome (Figure 5-4E) and the migmatitic quartzofeldspathic paragneiss (Figure 5-3F), respectively. The abundance of zircon xenocrysts in the pink leucogranite (Figure 5-6), and its relatively low zircon saturation and Ti-in-zircon temperatures (Figure 5-7C; Table 5-1), suggest that the pink leucogranite magmas were relatively cool, at least at their level of emplacement. This arguably favors a muscovite-rich metasedimentary source, since muscovite dehydration melting occurs at lower temperatures than biotite and amphibole dehydration melting (e.g., Clemens and Vielzeuf, 1987; Pattison et al., 2013). Either way, the REEs tend not to be strongly fractionated during sedimentary processes (e.g., Taylor and McLennan, 1985), and therefore, the La/Yb ratios of the local 2.7–2.5 Ga granitoids should be similar to any sediments that were derived from them. This is a useful constraint in evaluating the pressure and depth at which the leucogranite melts were generated. The pink leucogranite has higher La/Yb ratios than the local 2.6 and 2.5 Ga granitoids, and the two-mica leucogranite has a much higher La/Yb ratio than the local 2.7 Ga granitoids (Figure 5-10E). Thus, the source rocks likely contained a significant amount of residual garnet, and the leucogranite melts were probably generated in the mid- to lower-crust, at pressures ≥ 6 kbar and depths ≥ 20 km (e.g., Moyen, 2009).

Considerably more data are available for the **ca. 2.32–2.31 Ga biotite granites** and their petrogenesis can be discussed in greater detail. The weakly peraluminous and alkali-calcic character of the biotite granites, along with their enrichments in certain HFSE (Th and Zr) and the LREEs (Figures 5-9, 5-10 and 5-11A), liken them to some crust-derived Phanerozoic and Proterozoic “A-type” granites. Examples include the “Aluminous A-type” granites in the Lachlan Fold belt (Australia; Collins et al., 1982; Eby, 1990; King et al., 1997; 2001), the Mesoproterozoic Roxby Downs granite in the Gawler craton (Australia; Creaser, 1996), and the Paleoproterozoic Nueltin granitoids of the western Churchill province (Canada; Peterson et al., 2015). Granitoids of this nature are commonly interpreted to originate through high-temperature melting of refractory (low hydrous mineral content) crustal sources (Collins et al., 1982; Whalen et al., 1987; Creaser et al., 1991). The refractory source can come in the form of granulite-facies rocks that were depleted during an earlier melt generating

event (e.g., Collins et al., 1982; Clemens et al., 1986; Whalen et al., 1987), or in the form of siliceous tonalitic to granodioritic rocks that naturally have low water contents (Creaser et al., 1991; Skjerlie and Johnston, 1992, 1993; King et al., 1997, 2001). Experimental data indicate that dehydration melting of tonalites and granodiorites can generate metaluminous to weakly peraluminous granitic melts, similar in composition to some “A-type” granites and the Nonacho biotite granites, but that high temperatures (>900°C) are required to produce melts that would be of sufficient volume to migrate from their source (e.g., Rutter and Wyllie, 1988; Skjerlie and Johnston, 1992, 1993; Patiño Douce, 1997; Watkins et al., 2007). It is these high temperatures that promote the breakdown of accessory phases (e.g., zircon, apatite, allanite and titanite) in the source rocks, which leads to HFSE and REE enrichment of the melt (e.g., Collins et al., 1982; Whalen et al., 1987; Creaser et al., 1991; King et al., 1997, 2001). In the case of the biotite granites, the breakdown of zircon in the source explains their high Zr contents, whereas the breakdown of allanite could account for their extremely high Th and LREE contents. Melting allanite in the source may also help to explain the unusually high Th/U ratios of these rocks, given that allanite commonly contains >5x more Th than U (e.g., Hermann, 2002).

A high-temperature origin for the biotite granites is supported by their near absence of inherited zircon (Figure 5-6), their relatively high zircon saturation temperatures (up to 905°C; Figure 5-10; Table 5-1), and by the relatively high Ti-in-zircon temperatures obtained for samples 18BN20C and 19BN07E (Figure 5-7C; Table 5-1). Moreover, the refractory source model described above is consistent with the Sm-Nd isotope data (Figure 5-11A). The spread of ϵNd_i values from the biotite granites suggests that they derived from a mixture of crustal sources that included deeper seated equivalents of the local 2.7 Ga granitoids, and the >3 Ga granitoids of the PRT (Figure 5-11A). Both the local 2.7 Ga granitoids, and the >3 Ga PRT granitoids, are dominantly siliceous (>65 wt.% SiO_2) tonalites and granodiorites with relatively low overall hydrous mineral (biotite and amphibole) contents (chapters 2 and 3). Moreover, the 2.7 Ga granitoids have lower Fe-numbers than the >3 Ga PRT granitoids, such that mixing of melts derived from these two crustal sources can explain the apparent correlation between ϵNd_i value and Fe-number in the biotite granites (Figure 5-11C). These proposed source rocks also further help to explain the unusually high Th/U ratios of the biotite granites, because both the 2.7 Ga and >3 Ga granitoids have rather high whole-rock Th/U ratios themselves (Figure 5-10F), with median values of 22 and 16, respectively.

Finally, as with the leucogranites, it is possible to compare the trace-element characteristics of the biotite granites to those of their proposed source rocks, in order to constrain the depth and pressure at which partial melting occurred. In isolation, the relatively steep REE patterns of the biotite granites (Figure 5-9) might be interpreted to reflect partial melting at great depths, leaving a garnet-rich residue. Herein lies the importance of independent source rock constraints to understanding the

petrogenesis of any crust-derived granitoids (e.g., Moyen, 2009). The La/Yb ratios of the biotite granites are similar to those of the >3 and 2.7 Ga granitoids, and their Sr/Y ratios are lower than those of the >3 and 2.7 Ga granitoids (Figure 5-10E). Combined with the presence of a sizable negative Eu anomalies in even the least fractionated samples (Figure 5-10C), these trace-element characteristics are consistent with partial melting at comparatively shallow levels where substantial plagioclase, but little or no garnet, was left in the residue.

5.7.2 The North Shore granites revisited

Considering that the ca. 2.35–2.29 Ga North Shore granites (Lake Athabasca area; Figure 5-1) and the ca. 2.32–2.31 Ga biotite granites (this study) overlap in age, it is instructive to examine the similarities and differences between these granite suites. The two suites are similar in that they are both characterized by high SiO₂ contents (>69 wt.%) and exclusively negative whole-rock ϵNd_i (and zircon ϵHf_i for the North Shore granites) values (Hartlaub et al., 2007; Partin and Sylvester, 2024). Moreover, the primitive mantle- and chondrite-normalized trace-element patterns of the North Shore granites mirror those of the biotite granites (Figure 5-9). One difference is that the North Shore granites exhibit considerably more variation in certain major-element parameters (e.g., ASI and Fe-number; (Figure 5-8). This is at least in part a consequence of alteration because the primary mineralogy of the North Shore granites (Hartlaub et al., 2007) cannot account for the very high ASI (>1.2) values and low Fe-numbers (<0.6) in some of them (Figure 5-8). Another difference is that, on average, the North Shore granites are also more evolved (higher SiO₂ contents), and have lower Zr and LREE contents (Figure 5-10). That said, some of the less evolved North Shore granites do have LREE and Zr contents, and zircon saturation temperatures, as high as the biotite granites (Figure 5-10). In light of this comparison, it is reasonable to infer that the North Shore granites originated through petrogenetic processes akin to those described for the biotite granites above. The typically more evolved nature of the North Shore granites may simply reflect greater degrees of fractional crystallization, lower temperatures (and extents) of crustal melting, differences in source rock composition, or a combination of these factors.

Partin and Sylvester (2024) evaluated the petrogenesis of the North Shore granites using geochemical and isotopic data from Hartlaub et al. (2007) and Partin et al. (2014). Partin and Sylvester argue that the North Shore granites originated through mixing of crust- and mantle-derived magmas with “minor recycling of crustal sources”. The sole basis for their argument appears to be that there is substantial variability in zircon ϵHf_i (dominantly -2 to -12) and $\delta^{18}\text{O}$ (dominantly 5.4 to 6.6 ‰) values within and between samples of the North Shore granites. However, such isotopic heterogeneity can instead be explained by mixing of magmas derived from different crustal sources, similar to how the range of whole-rock ϵNd_i values in the biotite granites was explained in the

previous section. Partin and Sylvester also classified the North Shore granites as “A₂-type” granites, a specific variety of “A-type” granite defined by Eby (1992). The North Shore granites and the biotite granites exhibit some characteristics of “A-type” granites, and plot in the “A-type” fields on some discrimination diagrams (Figure 5-12A). However, they should not be referred to as “A₂-types” because Eby (1992) states that the A₁- and A₂-type classification scheme is only for samples that plot in the within-plate field on the discrimination diagrams of Pearce et al. (1984). Most of the North Shore granites and the biotite granites of the present study do not plot in that field (Figure 5-12B).

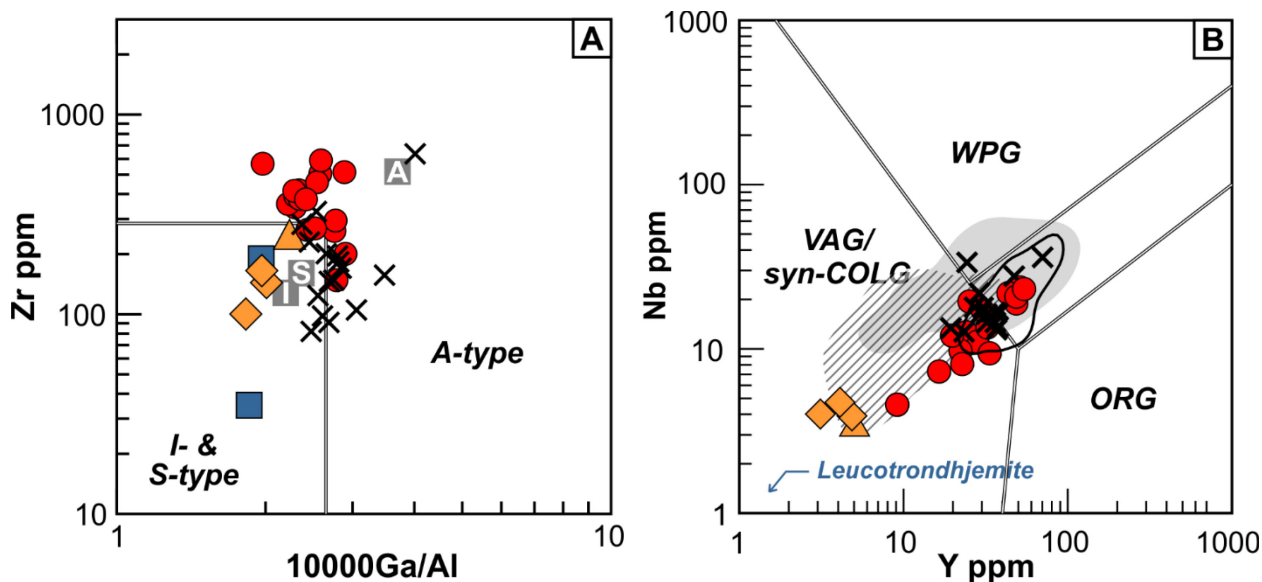


Figure 5-12. Granitoid discrimination diagrams. (A) A- and I/S-type discrimination diagram of Whalen et al. (1987). Grey squares are average A-, I- and S-type granitoids of Whalen et al. (1987). (B) tectonic discrimination diagram of Pearce et al. (1984). VAG: volcanic arc granitoid; syn-COLG: syn-collisional granitoid; WPG: within-plate granitoid; ORG: ocean ridge granitoid. Data point symbols as in previous plots, except the North Shore pluton X's are black. Comparative data fields and data sources are as in Figure 5-8. Fields are excluded from (A) because most compiled data do not include Ga measurements.

5.7.3 Tectonic implications

The contrasting geochemical and petrogenetic characteristics of the different granitoid suites described above document an evolving tectonic regime from ~2.4 to 2.3 Ga. Between ~2.43 and 2.38 Ga, leucogranitoids and migmatites were generated in the mid to lower crust, by partial melting of both metasedimentary and mafic metaigneous rocks. There is no evidence from the Nonacho area, or any other part of the western Rae craton, for significant mantle-derived magmatism in the 2.43–2.38 Ga period. The heat (or fluid, see below) required for this anatexis is therefore interpreted to have been provided largely or entirely through crustal thickening (e.g., Le Fort et al., 1987; Searle et al., 2009; Moyén, 2020b; Figure 5-13A). Coeval migmatites and leucogranites generated in

response to crustal thickening are a hallmark of collisional orogens (e.g., Harris et al., 1986; Searle et al., 2009; Weller et al., 2021; Frost et al., 2016). The recognition of such rocks in the Nonacho area therefore supports models for the Arrowsmith orogeny that involve collisional orogenesis at ~2.4 Ga (Schultz et al., 2007; Berman et al., 2005; 2013; Figure 5-13A).

The ca. 2.43 leucotondhemite and ca. 2.42 Ga two-mica leucogranite may mark an early phase of anatexis near the onset of collisional orogenesis. It would be unlikely for the crust to have accumulated a significant amount of radiogenic heat early in the evolution of the orogen, and some characteristics of the leucotondhemite suggest that it could have originated via fluid-present melting. It is therefore speculated that this early phase of crustal anatexis was facilitated in part by the presence of excess water (e.g., Reichardt and Weinberg, 2012). Fluid-present or “water-excess” melting can occur in collisional orogens when relatively cool and hydrous rocks are thrust beneath hotter rocks from lower crustal levels, such that devolatilization of the lower plate releases water into the hotter upper plate (e.g., Le Fort et al., 1987; Frost et al., 2016). The ca. 2.38 Ga leucogranites and migmatites may then reflect a second phase of anatexis that followed ~50–40 Myr of radiogenic heat accumulation in the thickened orogenic crust, such that a significant amount of fluid-absent dehydration melting could occur. A ca. 50–40 Myr incubation period, between the start of collision and the occurrence of substantial dehydration melting in the crust, would be broadly consistent with the ca. 20–40 Myr gap between collision and the peak of metamorphism and anatexis that is typical of modern orogens (e.g., Thompson et al., 1997; Weller et al., 2021).

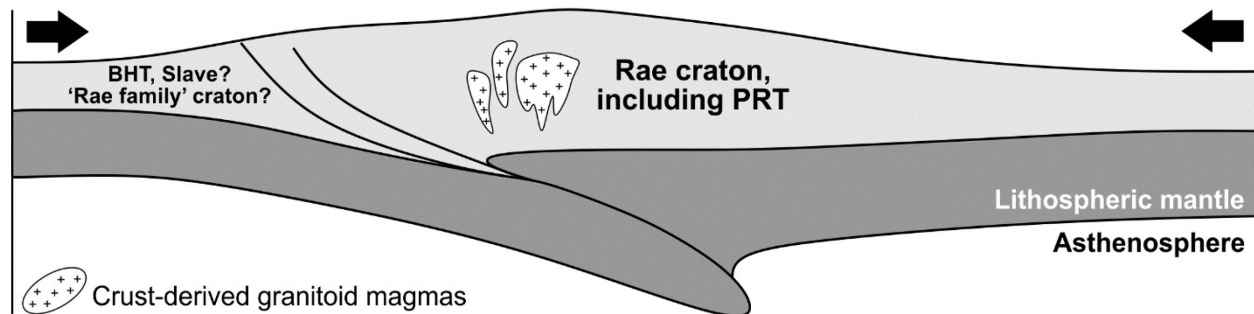
The geochemical and petrogenetic characteristics of the ca. 2.32–2.31 Ga biotite granites require a very different tectonic setting than the leucogranitoids. The inferred origin of these rocks through high-temperature (>900°C) melting of tonalitic and granodioritic rocks likely requires that heat was transferred to the crust through the intrusion and crystallization of mantle-derived mafic magmas (e.g., Rutter and Wyllie, 1988; Creaser et al., 1991). No mafic plutonic rocks associated with the biotite granites were documented in the Nonacho area (Figure 5-1), but there is evidence for broadly coeval (2.35–2.30 Ga) mafic magmatism in other parts of the western and southern Rae craton (van Breemen and Bostock, 1994; Ashton et al., 2007b; Tersmette, 2012; Davis et al., 2015; Ashton et al., 2013). In particular, Tersmette (2012) documented bimodal ca. 2.32 Ga granitic and gabbroic rocks in the northern QMB (Figure 5-1). Thus, on a regional scale, the ca. 2.32–2.31 Ga magmatism was likely bimodal in nature. The biotite granites also appear to have originated at shallower crustal levels than the leucogranites. Collectively these characteristics signal the transition from an overall compressional tectonic regime at ~2.4 Ga, to one of extension and crustal thinning by ~2.32 Ga or earlier. The biotite granites are therefore interpreted to have formed when post-orogenic extension led to mantle upwelling and the intrusion of mafic magmas, which in turn triggered high temperature crustal melting at comparatively shallow levels (Figure 5-13B). These findings are generally

consistent with the post-collisional setting previously proposed for the ca. 2.35–2.29 Ga North Shore granites (Hartlaub et al., 2007; Ashton et al., 2013; Partin and Sylvester, 2024). However, the term post-orogenic rather than post-collisional is used here for a reason.

The distinction between post-collisional and post-orogenic magmatism is not always made, but is useful when comparing the biotite granites to potential modern analogues. One place where the difference between the two is well defined is the Variscan orogen of central and western Europe (Finger et al., 1997; Bonin et al., 1998; Bonin, 2004; Jacob et al., 2021). There, post-collisional magmatic rocks were emplaced soon after collision and include abundant high-K I-type granitoids that span a wide range of SiO₂ contents and are not bimodal (Bonin, 2004; Jacob et al., 2021), similar to the 2.5 Ga granitoids documented in chapter 3. By contrast, post-orogenic granitoids related to the final stages of orogenic collapse were emplaced ≥ 50 Myr after collision (Bonin, 2004; Jacob et al., 2021). Those granitoids tend to be more siliceous (>65 wt.% SiO₂) on average, and to form bimodal associations with mafic magmatic rocks (Bonin et al., 2004; Jacob et al., 2021). They also tend to exhibit trace-element characteristics similar to those of A-type or “within-plate” granites (Finger et al., 1997; Bonin et al., 1998; Bonin, 2004; Jacob et al., 2021). The major-element characteristics of the Nonacho biotite granites are very similar to the post-orogenic Variscan granitoids (Figure 5-8), and considering their occurrence >60 Myr after the inferred collisional phase of the Arrowsmith orogeny, the term post-orogenic seems like an appropriate description of their tectonic setting. Furthermore, the trace-element patterns of the North Shore granites almost completely overlap those of the post-orogenic Variscan granitoids (Figure 5-9), emphasizing the post-orogenic character of ca. 2.35–2.29 Ga granitic magmatism in the Rae craton in general.

A: ca. 2.43–2.38 Ga continent-continent collision

Crustal thickening and anatexis generating the leucogranitoids



B: ca. 2.32–2.31 Ga post-orogenic extension

Crustal thinning, mantle upwelling/melting and high-temperature anatexis generating the biotite granites

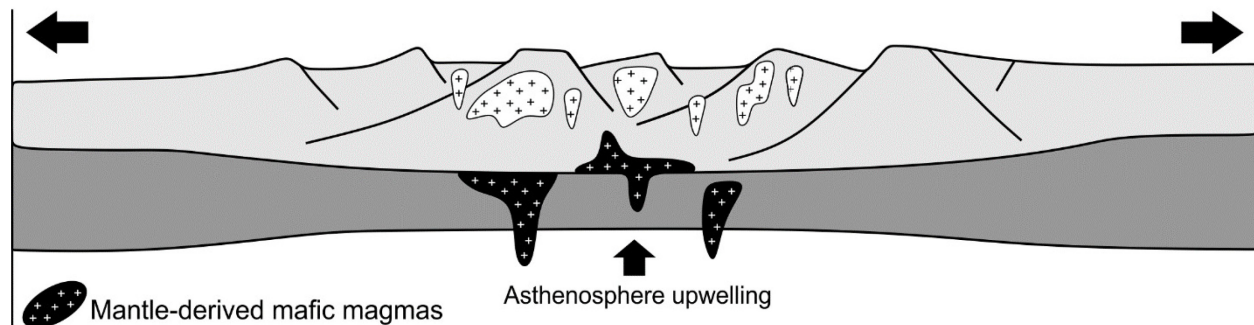


Figure 5-13. Tectonic cartoons illustrating the inferred tectonic settings in which the ca. 2.43–2.28 Ga leucogranitoids (A) and ca. 2.32–2.31 Ga biotite granites (B) were generated. Terranes that might have collided with the western Rae at ~2.4 Ga are indicated in (A). BHT: Buffalo Head terrane; Slave: Slave craton; and “Rae family” craton: A group of cratons (Dharwar craton, North China craton and others) that Pehrsson et al. (2013a) argue formed a late Neoproterozoic to early Paleoproterozoic supercraton with the Rae craton. One such craton could potentially have collided with the western Rae at ~2.4 Ga and have subsequently been rifted away (Berman et al., 2013).

5.7.4 Extent of crustal shortening during the Arrowsmith orogeny

A collisional model for the Arrowsmith orogeny predicts a significant amount of crustal shortening in the western Rae craton at ~2.4 Ga (Figure 5-13A). Evidence for widespread deformation of that age has been documented by Berman et al. (2005; 2013). The field relationships, U-Pb ages and Nd isotopic compositions of the granitoids in the Nonacho area also provide constraints on the timing and extent of deformation. In many places, strongly foliated to gneissic ca. 2.50 Ga granitoids are cross-cut by weakly foliated ca. 2.38 Ga leucogranites and ca. 2.32 Ga biotite granites (Figures 5-3E and 5-4B-D), indicating that substantial deformation occurred between ~2.50 Ga and 2.32 Ga, and at least locally between ~2.50 and 2.38 Ga (Figures 5-3E and 5-4B-D). More noteworthy is the

contrasting Nd isotopic compositions of the ca. 2.50 and ca. 2.32 Ga granitoids (Figure 5-11A). Many of the ca. 2.32 Ga granites yield Nd isotope evidence for re-working of >3 Ga PRT crust (Figure 5-11A), and in several places those granites cross-cut ca. 2.50 Ga granitoids (e.g., Figure 5-4C). However, the ca. 2.50 Ga granitoids, which include a significant mafic component, return no evidence for assimilation of PRT crust (Figure 5-11A). It seems unlikely that hot mafic magmas could traverse PRT crust, which had an ϵNd value at least as low as -7 at 2.5 Ga (Figure 5-11A), without registering its isotopic signal. The simplest explanation is that the 2.5 Ga magmas did not intrude the PRT. This implies that the PRT and the local ca. 2.50 Ga granitoids were tectonically intercalated sometime after ~2.50 Ga, but before intrusion of the biotite granites at ~2.32 Ga. This points to a very significant amount of crustal shorting between ~2.50 and 2.32 Ga, which I suggest occurred during the 2.4 Ga collisional phase of the Arrowsmith orogeny. This does not require that the PRT and ca. 2.50 Ga granitoids were entirely separate at ~2.5 Ga, as there is local evidence in the Queen Maud block (Figure 5-1) that some ca. 2.50 Ga granitoids did intrude the PRT (Davis et al., 2014; Berman et al., 2015). Rather, the ca. 2.50 Ga granitoids in the Nonacho area are thought to have originally been emplaced immediately east of the PRT, similar to how most of the ca. 2.50 Ga granitoids in the Queen Maud block presently occur (Schultz et al., 2007; Davis et al., 2014; see Figure 3-1B).

5.7.5 A late Paleoproterozoic analogue: The Trans-Hudson orogen

A potential late Paleoproterozoic analogue for the Arrowsmith orogeny is the 1.9–1.8 Ga THO (Figure 5-1; St-Onge et al., 2006; Corrigan et al., 2009; Regis et al., 2021). The THO involved the accretion of several Archean and early Paleoproterozoic continental blocks during the closure of a large ocean basin from ~1.92 to 1.83 Ga, and terminated with ca. 1.83–1.80 Ga collision between the Superior craton and the western Churchill province (Corrigan et al., 2009; Regis et al., 2021). Berman et al. (2013) noted that the magmatic and metamorphic footprint of the Arrowsmith orogeny (Figure 5-1) is similar in scale to that of the THO. Here, I specifically draw attention to similarities between syn- and post-orogenic granitoids in the hinterland of the THO (Figure 5-1), and the 2.4–2.3 Ga Arrowsmith granitoids.

Two different suites of THO-related granitoids are recognized in the western Churchill Province, the ca. 1.85–1.80 Ga Hudson granitoids and the ca. 1.77–1.75 Ga, locally rapakivi-textured, Nueltin granitoids (Figure 5-1; Peterson et al., 2002; van Breemen et al., 2005; Regis et al., 2021). Generation of the Hudson granitoids was contemporaneous with ca. 1.85 Ga accretion of the Sask craton and Sugluk block to the western Churchill province, and with ca. 1.83–1.80 Ga collision of the Superior craton and the western Churchill Province (Peterson et al., 2002; van Breemen et al., 2005; Corrigan et al., 2009). These granitoids are interpreted as mid to lower crustal melts, and this melting

is thought to reflect enhanced radiogenic heat production and/or isotherm relaxation in thickened orogenic crust (Peterson et al., 2002). The younger Nueltin granitoids on the other hand are associated with basaltic and anorthositic rocks, and are thought to have been generated by higher-temperature crustal melting, when mantle-derived magmas intruded in an extensional setting (Peterson et al., 2002, 2015). Peterson et al. (2002; 2015) referred to the Nueltin granitoids as anorogenic, and likened them to the Proterozoic rapakivi granites of Fennoscandia (Ramo and Haapalo, 1995). Although such rocks are frequently described as anorogenic, a temporal link between their generation and large-scale orogenesis associated with supercontinent assembly is commonly recognized (Windley, 1993; Ramo and Haapalo, 1995; Peterson et al., 2015; Condie et al., 2023). Moreover, the emplacement of the Nueltin granitoids ~60–80 Myr after a major continent-continent collision is consistent with usage of the term post-orogenic (e.g., Condie, 1991), and they have recently been described as such (Regis et al., 2021).

The ca. 1.85–1.75 Ga THO granitoids described above present an ideal comparison for the 2.4–2.3 Ga Arrowsmith granitoids. Similar to the Arrowsmith granitoids, the Hudson and Nueltin granitoids are interpreted to have derived from partial melting of Archean crustal source rocks (Peterson et al., 2002; van Breemen et al., 2005). Therefore, any compositional differences between the Arrowsmith and THO granitoids that are related to the secular geochemical evolution of the continental crust, and in turn the nature of their source rocks, should be minimized. Moreover, due to the secular decrease in the concentration of heat-producing isotopes, the amount of crustal heat production during the ca. 2.4 Ga Arrowsmith orogeny would have been closer to that of the ca. 1.8 Ga THO than it would to that of a Phanerozoic collisional orogen. Finally, the inferred petrogenetic origins of the Hudson and Nueltin suites are very similar to those of the ca. 2.4 Ga leucogranites and ca. 2.32–2.31 Ga biotite granites, respectively.

There is substantial overlap in the major- and trace-element compositions of the Hudson and Nueltin suites (Figures 5-8 to 5-10). Consequently, the Arrowsmith granitoids commonly overlap with the fields for both (Figures 5-8 to 5-10). Such compositional overlap is expected in evolved granitoid suites such as these, because all granitic melts either start with a composition near the granite minimum during partial melting (leucogranites), or evolve towards it during fractional crystallization. It is therefore the subtle differences amongst the granitoid suites, not their similarities, that are significant. On average, the Nueltin suite extends to higher HFSE (e.g., Th, Ti and Zr) and LREE contents, whereas the Hudson granitoids tend to have steeper REE patterns and higher Sr/Y ratios (Figures 5-9 and 5-10). These differences are mirrored in the Arrowsmith granitoids, where the biotite granites have greater HFSE and LREE contents, but lower Sr/Y ratios and less steep REE patterns, compared to the leucogranites (Figures 5-9 and 5-10). Another difference between the Hudson and Nueltin granitoids is that the former tend to contain abundant inherited zircon, whereas

the latter contain little to no inherited zircon (van Breemen et al., 2005). This difference is again mirrored by the inheritance-rich ca. 2.38 Ga leucogranites and the inheritance-poor ca. 2.32 Ga biotite granites (Figure 5-6). Finally, the ca. 60–80 Myr gap between emplacement of the Hudson and Nuelin granitoids is similar to the gap between emplacement of the ca. 2.43–2.38 Ga leucogranitoids and the ca. 2.32–2.31 Ga biotite granites

Based on the petrogenetic and geochemical similarities between the 2.4–2.3 Ga Arrowsmith granitoids, and the ca. 1.85–1.75 Ga THO granitoids (Figures 5-8 to 5-10), I argue that similar syn- and post-orogenic granitoid producing processes associated with the THO occurred during and after the Arrowsmith orogeny. This interpretation is consistent with the transition to a modern-style plate tectonics having taken place by the end of the Archean, and with the continuous operation of plate tectonics throughout the TML (Pehrsson et al., 2014; Condie et al., 2022). A similar argument has been made based on the geochemical and petrogenetic study of late Archean leucogranitoids in the Teton Range of Wyoming, which Frost et al. (2016) argue formed through the same general processes that produce leucogranites in modern collisional orogens. In the case of the Arrowsmith orogeny, however, the scale of magmatism and metamorphism (Figure 5-1) appears more similar to that of the modern collisional orogen, and a record of both syn- and post-orogenic granitic magmatism is preserved.

The hypothesis that the Arrowsmith orogen was a modern- or THO-style collisional orogen could be tested further through detailed petrochronological and thermobarometric studies of samples preserving ca. 2.4 Ga metamorphic mineral assemblages, such as the mafic granulite-facies gneiss documented here (Figure 5-4E), and the upper amphibolite- to granulite-facies metasedimentary and metaigneous rocks in the Queen Maud block (Schultz et al., 2007; Tersmette, 2012). A common phenomenon in Phanerozoic collisional orogens is the relatively rapid cooling and exhumation of high-grade metamorphic rocks, on the order of ~5–50°C/Myr (Scibiorski et al., 2015 and references therein). Regis et al. (2021) documented cooling rates up to ~25°C/Myr for THO metamorphic rocks in the south Rae craton. However, the cooling and exhumation rates associated with the Arrowsmith orogeny have yet to be examined.

Chapter 6: Summary and Conclusions

Two main objectives were laid out at the start of this thesis. The first was to constrain the extent, geochemical character and origin of “ancient” (>3 Ga) crust in the western Rae craton; the second was to constrain the geochemical character, petrogenesis, and tectonic setting(s) of 2.5–2.3 Ga granitoids in the western Rae. The work presented in chapter 2 and published in Neil et al. (2023) contributed to the first objective, whereas chapters 3–5 addressed the second. The following sections describe the key findings of each chapter and avenues for future research that emerged from these findings.

6.1 Chapter 2

Whole-rock Sm-Nd isotope and U-Pb zircon age data from granitoids were used to document an extensive (~1000 x 100 km) 3.3–3.1 Ga basement terrane in the western Rae craton, referred to as the Perry River terrane (PRT). The 3.3–3.1 Ga granitoids from this terrane have the major- and trace-element characteristics of “low- to medium-pressure” Archean TTGs (tonalites-trondhjemites-granodiorites) (Moyen, 2011; Moyen and Martin, 2012), dominantly mantle-like zircon $\delta^{18}\text{O}$ values and weighted-mean zircon initial ϵHf_i (ϵHf_i) values of -1 to +3. Accounting for these geochemical characteristics, it was proposed that the PRT formed in a subduction setting, and that the TTGs were generated by partial melting of hydrous basaltic rocks at the base of a magmatic arc. After combining the data from the PRT with a global compilation of igneous zircon ϵHf_i values, it was found that 3.3–3.2 Ga was likely a period of enhanced continental growth on Earth, with the great majority of rocks from this time period being characterized by near chondritic to suprachondritic isotopic values. Importantly, 3.5–3.0 Ga igneous rocks the world over record little zircon Hf isotope evidence for interaction with evolved Hadean–Eoarchean crust. This latter observation is best explained if only small amounts of continental crust were established, and thus available for reworking, by the end of the Eoarchean.

The findings of chapter 2 raise a fundamental question: what is the relationship between the PRT and the dominantly 2.7–2.6 Ga granitoid rocks that make up the interior of the Rae craton? In Neil et al. (2023) I suggested that the PRT may have been a nucleus upon which the Neoproterozoic crust of the Rae craton formed, based on the presence of rare >3 Ga inherited zircons in some 2.7–2.6 Ga granitoids. For the following reasons, I have changed my thinking and now consider it likely that the PRT accreted to the rest of the Rae craton sometime between ~2.58 and 2.49 Ga: 1) ca. 2.62–2.58 Ga Snow Island suite granitoids are widespread within most of the Rae craton, but are rare within the vicinity of the PRT; 2) no direct evidence that Snow Island suite granitoids intruded the PRT has been documented, apart from a single 3.4 Ga zircon xenocryst in a ca. 2.62 Ga granitoid (Regis et al., 2017), which could have derived from >3 Ga crust that is unrelated to that of the PRT; 3) ca. 2.49

Ga granitoids have been documented within the PRT portion of the Queen Maud block (Davis et al., 2014), and one of those granitoids yields the most negative ϵNd_i value (-4) of any 2.5 Ga magmatic rock in the Rae craton (Berman et al., 2015), clearly indicating that it did intrude PRT crust. These observations suggest that the PRT may not have been proximal to the Rae craton during intrusion of ca. 2.62–2.58 Ga Snow Island suite granitoids, but was in the vicinity of the craton by at least ca. 2.49 Ga. One way to address this question would be to complete a detailed whole-rock Nd and/or zircon Hf isotope transect across the Rae craton, focusing solely on 2.7–2.6 Ga granitoids. If the PRT was a nucleus upon which the Neoproterozoic crust of the Rae craton formed, then a systematic westward decrease in the ϵNd_i and ϵHf_i values of the 2.7–2.6 Ga granitoids would be expected (e.g., Davis and Hegner, 1992).

6.2 Chapter 3

Three late Archean granitoid suites with crystallization ages of ca. 2.71–2.69, ca. 2.58–2.57 and ca. 2.52–2.48 Ga were documented in the Nonacho area. Field and analytical efforts were focused on characterizing the 2.5 Ga suite. The 2.5 Ga granitoids range from mafic to felsic, comprise a high-K calc-alkaline series, are light rare earth element (LREE)-enriched and have “subduction-like” trace-element patterns. They also yield consistently chondritic whole-rock initial ϵNd (ϵNd_i) and near-chondritic zircon ϵHf_i values. The characteristics of the mafic granitoids can be explained if they derived from a subduction-enriched lithospheric mantle source that had evolved to chondritic Nd and Hf isotopic compositions by 2.5 Ga. Differentiation to produce the intermediate and felsic 2.5 Ga granitoids could have involved a variety of processes, and some assimilation of older (i.e. ≥ 2.6 Ga) continental crust cannot be ruled out. Importantly, however, the isotopic data require that all components of the suite (mafic to felsic) are at least in part juvenile crustal additions. Geochemically, the 2.5 Ga granitoids are analogous to post-collisional high-K I-type granitoids from the Caledonian and Variscan orogens, and the interpretation that the mafic magmas originated from an enriched lithospheric mantle source is consistent with a post-collisional setting (e.g., Couzinié et al., 2016). The 2.5 Ga granitoids may therefore have been emplaced in a post-collisional setting related to ca. 2.56–2.50 Ga MacQuoid orogeny on the eastern side of the Rae craton, or the accretion of the PRT to the western Rae between ~ 2.6 and 2.5 Ga.

A finding that was not fully explored in chapter 3 is that all three late Archean (2.7, 2.6 and 2.5 Ga) granitoid suites in the Nonacho area are of sanukitoid affinity. The 2.7 Ga and 2.5 Ga granitoids can be classified as sanukitoids *sensu stricto* (s.s) and high-Ti sanukitoids, respectively. The latter are also called “Closepet-type” granitoids (Moyen et al., 2003) or “high-K calc-alkaline” granitoids (Moyen, 2020a). The exact classification of the 2.6 Ga granitoids is unclear, but they are likely part of a sanukitoid suite. Interestingly, a similar pattern can be found in the global Archean granitoid record,

where 2.7 Ga sanukitoids s.s give way to younger high-Ti sanukitoids (Moyen and Laurent, 2018). However, the petrogenetic differences between sanukitoids s.s and high-Ti sanukitoids are not fully understood, and thus, neither is the reason for the apparent global transition between them. One possibility is that sanukitoids s.s derived from mantle sources that were metasomatized by partial melts of subducted basalt (TTGs), whereas the high-Ti sanukitoids derived from a mantle sources that were metasomatized by partial melts of subducted sediments (Laurent et al., 2011). Alternatively or in addition, the mantle sources for high-Ti sanukitoids may have been subject to lower degrees of metasomatism than those for sanukitoids s.s (Martin et al., 2009). Both explanations are compatible with the progressive cooling of the Earth and the lowering of geothermal gradients in subduction zones (Martin et al., 2009).

The Nonacho area is an ideal location to examine the evolution of sanukitoid magmatism from 2.7 to 2.5 Ga. Doing so will require more field-work and sampling to better characterize the 2.7 and 2.6 Ga suites. It will be important to determine what variety of sanukitoid the 2.6 Ga granitoids represent, and to identify the least evolved mantle-derived components of the 2.7 Ga and 2.6 Ga suites. By comparing geochemical and isotopic (e.g., zircon Hf and O isotopes) data from the least evolved samples in all three suites, it may be possible to constrain the extent to which differences between sanukitoids s.s and high-Ti sanukitoids are related differences in the metasomatic agents (partial melts of subducted basalt vs. subducted sediment) that enriched their mantle sources.

6.3 Chapter 4

Two occurrences of migmatitic quartzofeldspathic metasedimentary rocks were identified in the Nonacho area. These rocks were investigated to constrain their depositional age and provenance. Zircon and monazite U-Pb age and trace-element data show that the metasedimentary protoliths were deposited after ~2.52 Ga, and underwent high-grade metamorphism and migmatization at ~2.38 Ga. Similar ca. 2.42–2.39 Ga metamorphic zircon ages were obtained from metaplutonic rocks in chapter 3, and ca. 2.43–2.38 Ga leucogranitoids were documented in chapter 5. Collectively, these results show that most of the metamorphism in the Nonacho basement is related to the Arrowsmith orogeny (e.g., Berman et al., 2013). The detrital zircon data are consistent with a local derivation primarily from ca. 2.70, 2.60 and 2.53–2.52 Ga igneous source rocks. The depositional age (2.52–2.38 Ga), provenance and migmatitic nature of the these metasedimentary rocks permit their correlation with 2.5–2.4 Ga metasedimentary rocks >700 km to the north, in the Queen Maud block (Schultz et al., 2007) and on Boothia Peninsula (Regis and Sanborn-Barrie, 2023). Collectively, these observations indicate the presence of large sedimentary basin in the western Rae craton, the Sherman basin (Schultz et al., 2007), that formed during or after the

intrusion of the 2.5 Ga granitoid suite but prior to the collisional phase of the Arrowsmith orogeny (see below).

Unfortunately, the peak metamorphic mineral assemblages in these metasedimentary rocks are not preserved. Presently, the rocks contain quartz, K-feldspar, biotite, muscovite (including sericite) and K-feldspar. However, the migmatitic character of the rocks suggests that they were metamorphosed to upper amphibolite- or granulite-facies conditions. Moreover, the Yb-depleted composition of the ca. 2.38 Ga metamorphic zircons recovered from them, and the presence of equant chlorite “clots” in their leucosome, suggests that these rocks at one point contained garnet. Future work should focus on documenting better preserved (less retrogressed) occurrences of these metasedimentary rocks, or similar metasedimentary rocks, so that the pressure and temperature conditions associated with Arrowsmith metamorphism in the southwestern Rae craton can be better constrained.

6.4 Chapter 5

Two groups of 2.4–2.3 Ga granitoids related to the Arrowsmith orogeny were documented in the Nonacho area. The first are the ca. 2.43–2.38 Ga leucogranitoids and the second are the ca. 2.32–2.31 Ga biotite granites. The isotopic and geochemical characteristics of the former are consistent with their derivation from partial melting of metagneous and/or metasedimentary sources in the garnet stability field. The geochemical and isotopic characteristics of the latter suggest an origin through high-temperature (>900°C) partial melting of tonalitic/granodioritic rocks at relatively shallow levels where plagioclase, but little or no garnet, was stable. In particular, their ϵNd_i values are consistent with partial melting of deeper seated equivalents to the local 2.7 Ga tonalites/granodiorites (chapter 3), and the 3.3–3.1 Ga tonalites/granodiorites of the PRT (chapter 2). A high-temperature origin for the ca. 2.32–2.31 Ga granites is also supported by their relatively high zircon saturation (up to ~900°C) and Ti-in-zircon (~860–900°C) temperatures. The ca. 2.43–2.38 Ga leucogranitoids are interpreted to reflect crustal thickening during the collisional phase of the Arrowsmith orogeny. The ca. 2.32–2.31 Ga granites are interpreted to reflect post-orogenic collapse or lithospheric delamination, which resulted in crustal thinning, asthenosphere upwelling, and the intrusion of hot mantle-derived magmas, such that high-temperature melting of tonalitic/granodioritic rocks occurred at relatively shallow levels.

Interestingly, the two granitoid suites described above are mirrored in two granitoid suites associated with the 1.9–1.8 Ga Trans-Hudson orogeny. The 2.43–2.38 Ga leucogranitoids (leucotondhjemite excluded) are broadly similar to the ca. 1.85–1.80 Ga syn-collisional Hudson granitoids, and the ca. 2.32–2.31 Ga granites are very similar to the ca. 1.77–1.75 Ga post-orogenic Nueltin granitoids (Peterson et al., 2002; van Breemen et al., 2005; Scott, 2012; Peterson et al., 2015; Regis et al., 2021). Many workers (e.g., St-Onge et al., 2006; Corrigan et al., 2009; Regis et al., 2021; Weller et

al., 2021) interpret the Trans-Hudson as a collisional orogen that formed by tectonic, metamorphic and magmatic processes analogous in character and scale to those that operate in modern collisional orogens, such as the Himalayas. Therefore, the similarity between the Trans-Hudson and Arrowsmith granitoids suggests that the Arrowsmith is an early Paleoproterozoic example of a “modern-style” collisional orogen and may be one of the earliest examples of such an orogen on Earth.

Two directions for future work emerge from this chapter. First, an effort should be made to identify and characterize ca. 2.32–2.31 Ga mafic plutonic rocks in the western Rae craton. Such rocks are known to exist (Tersmette, 2012; Ashton et al., 2007b), but a better understanding of their regional extent and geochemical character is required to further evaluate the petrogenetic and tectonic models proposed for the ca. 2.32–2.31 Ga Nonacho granites. Second, the economic significance of the ca. 2.32–2.31 Ga granites should be explored. Geochemically similar “A-type” granites occur in association with large Sn deposits and Iron oxide-copper-gold (IOCG)-type deposits (e.g., Dall-Agnol et al., 2012). In particular, the ca. 2.32–2.31 Ga Nonacho granites are similar to the 1.6 Ga Roxby Downs granite (Creaser, 1996), which hosts the giant Olympic dam IOCG-U-REE deposit. Furthermore, the ca. 2.32–2.31 Ga Nonacho granites are correlated to the ca. 2.35–2.29 Ga North Shore granites (Uranium City/Lake Athabasca region), which occur in the Beaverlodge uranium district (Hartlaub et al., 2007; Ashton et al., 2017c). Some of the North Shore granites are known to host U mineralization (Ashton et al., 2017c), and at least some U mineralization in the Beaverlodge district is 2.3 Ga in age (Dieng et al., 2013). Uranium mineralization has also been identified in albitized and potassic-altered granitoids in the Nonacho area (Landry et al., 2022), but the age of those granitoids is unknown. A geochronology study of granitoids hosting U-mineralization in the Nonacho area should be carried out, to test a correlation with the ca. 2.32–2.31 Ga granites identified in this study.

6.5 Overall conclusions

The primary contribution of this thesis is an improved understanding of how and when the continental crust of the western Rae craton was formed and reworked, from the Paleoproterozoic to the early Paleoproterozoic. A large 3.3–3.1 Ga basement terrane was recognized in the western Rae craton, and at least seven episodes of granitoid magmatism were identified in the Nonacho Lake area, at ca. 3.25, 2.78, 2.71–2.68, 2.58–2.57, 2.52–2.48, 2.43–2.38 and 2.32–2.31 Ga. Geochemical and isotopic data indicate that the granitoids emplaced between ~3.25 and 2.48 Ga largely represent new additions to the continental crust. That is, they derived from fractional crystallization or combined assimilation-fractional crystallization (AFC) of mantle-derived magmas, or from partial melting of mafic to intermediate rocks that had only resided in the crust for a short period of time

prior to partial melting. By contrast, the granitoids emplaced between ~2.43 and 2.31 Ga derived entirely, or almost entirely, from partial melting of older (Archean) crustal rocks. In other words, the western Rae craton underwent a transition from a long period characterized by crustal growth to one characterized by crustal reworking at ~2.45 Ga. Similar transitions occurred slightly earlier (~2.55–2.50 Ga) in the North China and Dharwar cratons, and significantly earlier (>2.55 Ga) in most other cratons (e.g., Laurent et al., 2014a). The geochemical and petrogenetic characteristics of the ca. 2.52–2.47, 2.43–2.38 and 2.32–2.31 Ga granitoid suites from the Nonacho area were studied in detail. In all three cases, geochemically analogous granitoids from well-constrained Phanerozoic or Paleoproterozoic orogenic and post-orogenic settings can be identified. These observations are consistent with the operation of “modern-style” or “Paleoproterozoic-style” plate-tectonic processes by at least 2.5 Ga in the western Rae craton.

References

References for chapters 1–6 and appendices A–E:

- Acosta-Góngora, P., Pehrsson, S. P., Knox, B., Regis, D., Hulbert, L., Creaser, R. A., and Ashton, K. (2018). Neoproterozoic convergent margin Ni-Cu mineralization? Axis Lake and Nickel King Ni-Cu deposits in the south Rae craton of the Canadian Shield. *Precambrian Research*, 316, 305-323.
- Ahmad, T., VC, T., Islam, R., Khanna, P.P., and Mukherjee, P.L. (1998). Geochemistry and geodynamic implications of magmatic rocks from the Trans-Himalayan arc. *Geochemical Journal*, 32(6), 383-404.
- Allaz, J. M., Jercinovic, M. J., and Williams, M. L. (2020). U-Th-Pb total dating of REE-phosphate by electron microprobe: review and progress. In *IOP Conference Series: Materials Science and Engineering*, 891, 012001.
- Allaz, J.M., Williams, M.L., Jercinovic, M.J., Goemann, K., and Donovan, J. (2019). Multipoint background analysis: Gaining precision and accuracy in microprobe trace element analysis. *Microscopy and Microanalysis*, 25, 30-46.
- Armstrong, J.T. (1988) Quantitative analysis of silicate and oxide materials: Comparison of Monte Carlo, ZAF and $\phi(\rho z)$ procedures. *Microbeam Analysis* 1, 239-246.
- Armstrong, R. L. (1991). The persistent myth of crustal growth. *Australian Journal of Earth Sciences*, 38(5), 613-630.
- Ashton, K.E., Card, C.D., Davis, W., and Heaman, L.M. (2007a). New U-Pb zircon age data from the Tazin Lake map area (NTS 74N); in summary of investigations 2007, Volume 2, Saskatchewan Geological Survey, Saskatchewan Ministry of Energy and Resources, Misc. Rep. 2007-4.2, Paper A-11, 8p.
- Ashton, K.E., Creaser, R.A., and Bethune, K. (2016): New Sm-Nd data from the Zemplin Domain: testing the model for tectonically amalgamated Taltson basement complex and proto-Rae cratonic blocks within the Rae Province of northwestern Saskatchewan; in Summary of Investigations 2016, Volume 2, Saskatchewan Geological Survey, Saskatchewan Ministry of the Economy, Miscellaneous Report 2016-4.2, Paper A-7, 12p.
- Ashton, K. E., Hartlaub, R. P., Bethune, K. M., Heaman, L. M., Rayner, N., and Niebergall, G. R. (2013). New depositional age constraints for the Murmac Bay group of the southern Rae craton, Canada. *Precambrian Research*, 232, 70-88.

- Ashton, K. E., Heaman, L. M., Lewry, J. F., Hartlaub, R. P., and Shi, R. (1999). Age and origin of the Jan Lake Complex: a glimpse at the buried Archean craton of the Trans-Hudson Orogen. *Canadian Journal of Earth Sciences*, 36(2), 185-208.
- Ashton, K.E, Knox, B., Rayner, N., Creaser, R., and Bethune, K. (2017b). New U-Pb and Sm-Nd results from the Tantato Domain, southeastern Rae Province, Saskatchewan; in Summary of Investigations 2017, Volume 2, Saskatchewan Geological Survey, Saskatchewan Ministry of the Economy, Miscellaneous Report 2017-4.2, Paper A-14, 27p.
- Ashton, K.E, Rayner, N., Creaser, R., and Bethune, K. (2017c): A new U-Pb age for pink leucogranite hosting mineralization in the Beaverlodge uranium district, and new Sm-Nd results from the Nolan, Zemlak and Beaverlodge domains; in Summary of Investigations 2017, Volume 2, Saskatchewan Geological Survey, Saskatchewan Ministry of the Economy, Miscellaneous Report 2017-4.2, Paper A-5, 18p.
- Ashton, K.E. (1988). Precambrian geology of the southeastern Amer Lake area (66H/1), near Baker Lake, N.W.T.: a study of the Woodburn Lake Group, an Archean orthoquartzite-bearing sequence in the Churchill structural province. Unpublished Ph.D. thesis, Queen's University, Kingston, Ontario, 335 p.
- Ashton, K.E., Knox, B., Card, C., Rayner, N., Davis, B., Heaman, L., and Creaser, R. (2017a). Synthesis of U-Pb and Sm-Nd geochronological results from the Dodge Domain, southeastern Rae Province; in Summary of Investigations 2017, Volume 2, Saskatchewan Geological Survey, Saskatchewan Ministry of the Economy, Miscellaneous Report 2017-4.2, Paper A-12, 31p.
- Ashton, K.E., Knox, B.R., Bethune, K.M., and Rayner, N. (2007b). Geochronological update and basement geology along the northwestern margin of the Athabasca Basin east of Fond-du-Lac (NTS 74O/06 and 07), southeastern Beaverlodge-southwestern Tantato domains, Rae Province; in Summary of Investigations 2007, Volume 2, Saskatchewan Geological Survey, Saskatchewan Ministry of Energy and Resources, Misc. Rep. 2007-4.2, Paper A-9, 22p.
- Ashton, K.E., Rayner, N.M., and Bethune, K.M., 2009. Meso- and Neoproterozoic (2.37 and 1.93 Ga) metamorphism and 2.17 Ga provenance ages in the Murmac Bay Group pelite; U-Pb SHRIMP ages from the Uranium City area; in Summary of Investigations 2009, Volume 2, Saskatchewan Geological Survey, Sask. Ministry of Energy and Resources, Misc. Rep. 2009-4.2, Paper A-5, 9p.
- Ashton, K.E., Rayner, N.M., Heaman, L.M., and Creaser, R.A. (2014). New Sm-Nd and U-Pb ages from the Zemlak and south-central Beaverlodge domains: a case for amalgamated Taltson

- basement complex and proto-Rae cratonic blocks within the Rae Province of northwestern Saskatchewan;NAin Summary of Investigations 2014, Volume 2, Saskatchewan Geological Survey, Saskatchewan Ministry of the Economy, Miscellaneous Report 2014-4.2, Paper A-6, 28p.
- Aspler, L. B., and Chiarenzelli, J. R. (1998). Two Neoproterozoic supercontinents? evidence from the Paleoproterozoic. *Sedimentary Geology*, 120(1-4), 75-104.
- Aspler, L.B., 1985. Geology of the Nonacho Basin (Early Proterozoic), NWT. Unpublished PhD Thesis, Carleton University, Ottawa, Ontario, Canada.
- Atherton, M. P., and Ghani, A. A. (2002). Slab breakoff: a model for Caledonian, Late Granite syn-collisional magmatism in the orthotectonic (metamorphic) zone of Scotland and Donegal, Ireland. *Lithos*, 62(3-4), 65-85.
- Baldwin, J. A., Bowring, S. A., and Williams, M. L. (2003). Petrological and geochronological constraints on high pressure, high temperature metamorphism in the Snowbird tectonic zone, Canada. *Journal of Metamorphic Geology*, 21(1), 81-98.
- Baldwin, J. A., Bowring, S. A., Williams, M. L., and Mahan, K. H. (2006). Geochronological constraints on the evolution of high-pressure felsic granulites from an integrated electron microprobe and ID-TIMS geochemical study. *Lithos*, 88(1-4), 173-200.
- Barbarin, B. (1999). A review of the relationships between granitoid types, their origins and their geodynamic environments. *Lithos*, 46(3), 605-626.
- Barbarin, B., and Didier, J. (1992). Genesis and evolution of mafic microgranular enclaves through various types of interaction between coexisting felsic and mafic magmas. *Earth and Environmental Science Transactions of the Royal Society of Edinburgh*, 83(1-2), 145-153.
- Barker, F. (1979). Trondhjemite: definition, environment and hypotheses of origin. In F. Barker (ed.), *Trondhjemites, Dacites and Related Rocks, Developments in petrology* (Vol. 6, pp. 1-12). Elsevier.
- Barker, F., and Arth, J. G. (1976). Generation of trondhjemitic-tonalitic liquids and Archean bimodal trondhjemite-basalt suites. *Geology*, 4(10), 596-600.
- Barth, A. P., Walker, J. D., Wooden, J. L., Riggs, N. R., and Schweickert, R. A. (2011). Birth of the Sierra Nevada magmatic arc: Early Mesozoic plutonism and volcanism in the east-central Sierra Nevada of California. *Geosphere*, 7(4), 877-897.

- Bauer, A. M., Reimink, J. R., Chacko, T., Foley, B. J., Shirey, S. B., and Pearson, D. G. (2020). Hafnium isotopes in zircons document the gradual onset of mobile-lid tectonics. *Geochemical Perspectives Letters*, 14, 1-6.
- Beard, J. S., and Lofgren, G. E. (1991). Dehydration melting and water-saturated melting of basaltic and andesitic greenstones and amphibolites at 1, 3, and 6.9 kb. *Journal of Petrology*, 32(2), 365-401.
- Bédard, J. H. (2006). A catalytic delamination-driven model for coupled genesis of Archaean crust and sub-continental lithospheric mantle. *Geochimica et cosmochimica acta*, 70(5), 1188-1214.
- Belousova, E. A., Kostitsyn, Y. A., Griffin, W. L., Begg, G. C., O'reilly, S. Y., and Pearson, N. J. (2010). The growth of the continental crust: constraints from zircon Hf-isotope data. *Lithos*, 119(3-4), 457-466.
- Berman, R. G., Cutts, J. A., Davis, W. J., Camacho, A., Sanborn-Barrie, M., and Smit, M. A. (2023). The tectonic evolution of Thelon tectonic zone, Canada: a new model based on petrological modeling linked with Lu–Hf garnet and U–Pb accessory mineral geochronology. *Canadian Journal of Earth Sciences*, 60(5), 550-582.
- Berman, R. G., Davis, W. J., and Pehrsson, S. (2007). Collisional Snowbird tectonic zone resurrected: Growth of Laurentia during the 1.9 Ga accretionary phase of the Hudsonian orogeny. *Geology*, 35(10), 911-914.
- Berman, R. G., Pehrsson, S., Davis, W. J., Ryan, J. J., Qui, H., and Ashton, K. E. (2013). The Arrowsmith orogeny: Geochronological and thermobarometric constraints on its extent and tectonic setting in the Rae craton, with implications for pre-Nuna supercontinent reconstruction. *Precambrian Research*, 232, 44-69.
- Berman, R. G., Sanborn-Barrie, M., Stern, R. A., and Carson, C. J. (2005). Tectonometamorphism at ca. 2.35 and 1.85 Ga in the Rae domain, western Churchill Province, Nunavut, Canada: insights from structural, metamorphic and in situ geochronological analysis of the southwestern Committee Bay Belt. *Canadian Mineralogist*, 43(1), 409-442.
- Berman, R.G. (2010). Metamorphic map of the western Churchill Province, Canada; Geological Survey of Canada, Open File 5279.
- Berman, R.G., and Camacho, A. (2020). U-Pb zircon ages of plutonic rocks in the eastern Slave Craton and adjacent Thelon tectonic zone, Nunavut, determined by laser-ablation inductively coupled multi-collector mass spectrometry; Geological Survey of Canada, Open File 8703.

- Berman, R.G., Davis, W.J., Aspler, L.B., and Chiarenzelli, J.R. (2002). SHRIMP U-Pb ages of multiple metamorphic events in the Angikuni Lake area, western Churchill Province, Nunavut; Radiogenic Age and Isotopic Studies: Report 15; Geological Survey of Canada, Current Research 2002-F3, 9p.
- Berman, R.G., Nadeau, L., Percival, J.A., Harris, J., Girard, É., Whalen, J.B., Davis, W.J., Kellett, D., Jefferson, C.W., Camacho, A., and Bethune, K. (2015). Geo-Mapping Frontiers' Chantrey project: bedrock geology and multidisciplinary supporting data of a 550 kilometre transect across the Thelon tectonic zone, Queen Maud block, and adjacent Rae craton; Geological Survey of Canada, Open File 7698.
- Bethune, K. M., Berman, R. G., Rayner, N., and Ashton, K. E. (2013). Structural, petrological and U–Pb SHRIMP geochronological study of the western Beaverlodge domain: Implications for crustal architecture, multi-stage orogenesis and the extent of the Taltson orogen in the SW Rae craton, Canadian Shield. *Precambrian Research*, 232, 89-118.
- Bethune, K.M., and Scammell, R.J. (2003). Geology, geochronology, and geochemistry of Archean rocks in the Ege Bay area, north-central Baffin Island, Canada: constraints on the depositional and tectonic history of the Mary River Group of northeastern Rae Province. *Can. J. Earth Sci.* 40, 1137-1167.
- Bindeman, I. N., Eiler, J. M., Yogodzinski, G. M., Tatsumi, Y., Stern, C. R., Grove, T. L., Portnyagin, M., Hoernle, K., and Danyushevsky, L. V. (2005). Oxygen isotope evidence for slab melting in modern and ancient subduction zones. *Earth and Planetary Science Letters*, 235(3-4), 480-496.
- Black, L. P., Kamo, S. L., Allen, C. M., Davis, D. W., Aleinikoff, J. N., Valley, J. W., Mundil, R., Campbell, I.H., Korsch, R.J., Williams, I.S., and Foudoulis, C. (2004). Improved $^{206}\text{Pb}/^{238}\text{U}$ microprobe geochronology by the monitoring of a trace-element-related matrix effect; SHRIMP, ID–TIMS, ELA–ICP–MS and oxygen isotope documentation for a series of zircon standards. *Chemical Geology*, 205(1-2), 115-140.
- Bleeker, W. (2003). The late Archean record: a puzzle in ca. 35 pieces. *Lithos*, 71(2-4), 99-134.
- Blichert-Toft, J. (2008). The Hf isotopic composition of zircon reference material 91500. *Chemical Geology*, 253(3-4), 252-257.
- Bonin, B. (2004). Do coeval mafic and felsic magmas in post-collisional to within-plate regimes necessarily imply two contrasting, mantle and crustal, sources? A review. *Lithos*, 78(1-2), 1-24.

- Bonin, B., Azzouni-Sekkal, A., Bussy, F., and Ferrag, S. (1998). Alkali-calcic and alkaline post-orogenic (PO) granite magmatism: petrologic constraints and geodynamic settings. *Lithos*, 45(1-4), 45-70.
- Bostock, H.H., and Loveridge, W.D. (1988). Geochronology of the Talston Magmatic zone and its eastern cratonic margin, District of Mackenzie; in *Radiogenic Age and Isotopic Studies: Report 2*, Geological Survey of Canada, Paper 88-2, p. 59-65.
- Bostock, H.H., van Breemen, O. (1992). The timing of emplacement and distribution of the Sparrow diabase dyke swarm, District of Mackenzie, Northwest Territories; in *Radiogenic Age and Isotopic Studies: Report 6*; Geological Survey of Canada, Paper 92-2, p. 49-55.
- Bostock, H.H., van Breemen, O., and Loveridge, W.D. (1991). Further geochronology of plutonic rocks in northern Taltson Magmatic Zone, District of Mackenzie, N.W.T.; in *Radiogenic Age and Isotopic Studies: Report 4*, Geological Survey of Canada, paper 90-2, p. 67-78.
- Bouvier, A., Vervoort, J. D., and Patchett, P. J. (2008). The Lu–Hf and Sm–Nd isotopic composition of CHUR: constraints from unequilibrated chondrites and implications for the bulk composition of terrestrial planets. *Earth and Planetary Science Letters*, 273(1-2), 48-57.
- Breemen, O. V., Peterson, T. D., and Sandeman, H. A. (2005). U Pb zircon geochronology and Nd isotope geochemistry of Proterozoic granitoids in the western Churchill Province: intrusive age pattern and Archean source domains. *Canadian Journal of Earth Sciences*, 42(3), 339-377.
- Brown, M. (2008). Characteristic thermal regimes of plate tectonics and their metamorphic imprint throughout Earth history: When did Earth first adopt a plate tectonics mode of behavior. *When did plate tectonics begin on planet Earth*, 440(97), 05.
- Calmus, T., Aguillón-Robles, A., Maury, R. C., Bellon, H., Benoit, M., Cotten, J., Bourgois, J., and Michaud, F. (2003). Spatial and temporal evolution of basalts and magnesian andesites (“bajaites”) from Baja California, Mexico: the role of slab melts. *Lithos*, 66(1-2), 77-105.
- Campbell, I. H., and Taylor, S. R. (1983). No water, no granites-No oceans, no continents. *Geophysical Research Letters*, 10(11), 1061-1064.
- Canam, R. (2023). Paleoproterozoic structural evolution of the southwestern margin of the Rae craton, Northwest Territories. Unpublished MSc thesis. Simon Fraser University.
- Card, C. D., Bethune, K. M., Davis, W. J., Rayner, N., and Ashton, K. E. (2014). The case for a distinct Taltson orogeny: Evidence from northwest Saskatchewan, Canada. *Precambrian Research*, 255, 245-265.

- Card, C.D., Rayner, N.M., and Creaser, R.A. (2016). U-Pb geochronology, Sm-Nd isotopic analysis and geochemistry for a diorite from the Nisikkatch Lake area of the northeastern Zemplin Domain; in Summary of Investigations 2016, Volume 2, Saskatchewan Geological Survey, Saskatchewan Ministry of the Economy, Miscellaneous Report 2016-4.2, Paper A-9, 9p.
- Carr, M. J., and Gazel, E. (2017). Iqpet software for modeling igneous processes: examples of application using the open educational version. *Mineralogy and Petrology*, 111, 283-289.
- Castro, A. (2020). The dual origin of I-type granites: the contribution from experiments. Geological Society, London, Special Publications, 491(1), 101-145.
- Castro, A., Rodríguez, C., Gutiérrez-Alonso, G., and de la Rosa, J. D. (2023). A post-collisional batholith from Southern Iberia rooted in the Earth's mantle: Los Pedroches batholith. *Lithos*, 107245.
- Cecil, M. R., Rotberg, G. L., Ducea, M. N., Saleeby, J. B., and Gehrels, G. E. (2012). Magmatic growth and batholithic root development in the northern Sierra Nevada, California. *Geosphere*, 8(3), 592-606.
- Chapman, A. D., Ducea, M. N., Kidder, S., and Petrescu, L. (2014). Geochemical constraints on the petrogenesis of the Salinian arc, central California: Implications for the origin of intermediate magmas. *Lithos*, 200, 126-141.
- Chapman, J. B., Shields, J. E., Ducea, M. N., Paterson, S. R., Attia, S., and Ardill, K. E. (2021). The causes of continental arc flare ups and drivers of episodic magmatic activity in Cordilleran orogenic systems. *Lithos*, 398, 106307.
- Chappell, B. W., and White, A. J. R. (1992). I- and S-type granites in the Lachlan Fold Belt. *Earth and Environmental Science Transactions of the Royal Society of Edinburgh*, 83(1-2), 1-26.
- Clemens, J. D., and Vielzeuf, D. (1987). Constraints on melting and magma production in the crust. *Earth and Planetary Science Letters*, 86(2-4), 287-306.
- Clemens, J. D., Darbyshire, D. P. F., and Flinders, J. (2009). Sources of post-orogenic calcalkaline magmas: the Arrochar and Garabal Hill–Glen Fyne complexes, Scotland. *Lithos*, 112(3-4), 524-542.
- Clemens, J. D., Holloway, J. R., and White, A. J. R. (1986). Origin of an A-type granite; experimental constraints. *American mineralogist*, 71(3-4), 317-324.
- Cloutier, M. A., Bethune, K. M., Ashton, K. E., and Deane, J. M. K. (2021). U-Pb geochronology, geochemistry, and isotopic composition of granitoids across the Nolan-Zemplin domain

- boundary in the SW Rae craton, Laurentia: Evidence for a late Neoproterozoic suture reworked during Arrowsmith orogeny. *Precambrian Research*, 362, 106303.
- Cogley, J. G. (1984). Continental margins and the extent and number of the continents. *Reviews of Geophysics*, 22(2), 101-122.
- Coleman, D. S., Bartley, J. M., Glazner, A. F., and Pardue, M. J. (2012). Is chemical zonation in plutonic rocks driven by changes in source magma composition or shallow-crustal differentiation?. *Geosphere*, 8(6), 1568-1587.
- Collins, W. J., Beams, S. D., White, A. J. R., and Chappell, B. W. (1982). Nature and origin of A-type granites with particular reference to southeastern Australia. *Contributions to mineralogy and petrology*, 80, 189-200.
- Collins, W. J., Huang, H. Q., Bowden, P., and Kemp, A. I. S. (2020). Repeated S-I-A-type granite trilogy in the Lachlan Orogen and geochemical contrasts with A-type granites in Nigeria: implications for petrogenesis and tectonic discrimination. *Geological society, london, special publications*, 491(1), 53-76.
- Condie, K. (2014). How to Make a Continent: Thirty-five Years of TTG Research. In: Dilek, Y., Furnes, H. (eds) *Evolution of Archean Crust and Early Life. Modern Approaches in Solid Earth Sciences*, vol 7. Springer, Dordrecht.
- Condie, K. C. (1991). Precambrian granulites and anorogenic granites: are they related?. *Precambrian research*, 51(1-4), 161-172.
- Condie, K. C. (1998). Episodic continental growth and supercontinents: a mantle avalanche connection?. *Earth and Planetary Science Letters*, 163(1-4), 97-108.
- Condie, K. C. (2018). A planet in transition: The onset of plate tectonics on Earth between 3 and 2 Ga? *Geoscience Frontiers*, 9(1), 51-60.
- Condie, K. C. (2021). *Earth as an evolving planetary system*. Academic Press, Elsevier.
- Condie, K. C., and Aster, R. C. (2010). Episodic zircon age spectra of orogenic granitoids: the supercontinent connection and continental growth. *Precambrian Research*, 180(3-4), 227-236.
- Condie, K. C., and Puetz, S. J. (2019). Time series analysis of mantle cycles Part II: The geologic record in zircons, large igneous provinces and mantle lithosphere. *Geoscience Frontiers*, 10(4), 1327-1336.
- Condie, K. C., Arndt, N., Davaille, A., and Puetz, S. J. (2017). Zircon age peaks: Production or preservation of continental crust?. *Geosphere*, 13(2), 227-234.

- Condie, K. C., O'Neill, C., and Aster, R. C. (2009). Evidence and implications for a widespread magmatic shutdown for 250 My on Earth. *Earth and Planetary Science Letters*, 282(1-4), 294-298.
- Condie, K. C., Pisarevsky, S. A., Puetz, S. J., Roberts, N. M., and Spencer, C. J. (2023). A-type granites in space and time: Relationship to the supercontinent cycle and mantle events. *Earth and Planetary Science Letters*, 610, 118125.
- Condie, K. C., Pisarevsky, S. A., Puetz, S. J., Spencer, C. J., Teixeira, W., and Faleiros, F. M. (2022). A reappraisal of the global tectono-magmatic lull at ~ 2.3 Ga. *Precambrian research*, 376, 106690.
- Condie, K. C., Puetz, S. J., and Davaille, A. (2018). Episodic crustal production before 2.7 Ga. *Precambrian Research*, 312, 16-22.
- Corfu, F., Hanchar, J. M., Hoskin, P. W., and Kinny, P. (2003). Atlas of zircon textures. *Reviews in mineralogy and geochemistry*, 53(1), 469-500.
- Corrigan, D., Pehrsson, S., Wodicka, N., and De Kemp, E. (2009). The Palaeoproterozoic Trans-Hudson Orogen: a prototype of modern accretionary processes. Geological Society, London, *Special Publications*, 327(1), 457-479.
- Coutts, D. S., Matthews, W. A., and Hubbard, S. M. (2019). Assessment of widely used methods to derive depositional ages from detrital zircon populations. *Geoscience Frontiers*, 10, 1421–1435.
- Couzinié, S., Laurent, O., Moyen, J. F., Zeh, A., Bouilhol, P., and Villaros, A. (2016). Post-collisional magmatism: Crustal growth not identified by zircon Hf–O isotopes. *Earth and Planetary Science Letters*, 456, 182-195.
- Crawford, M. B., and Searle, M. P. (1992). Field relationships and geochemistry of pre-collisional (India-Asia) granitoid magmatism in the central Karakoram, northern Pakistan. *Tectonophysics*, 206(1-2), 171-192.
- Creaser, R. A. (1996). Petrogenesis of a Mesoproterozoic quartz latite-granitoid suite from the Roxby Downs area, South Australia. *Precambrian Research*, 79(3-4), 371-394.
- Creaser, R. A., Erdmer, P., Stevens, R. A., and Grant, S. L. (1997). Tectonic affinity of Nisutlin and Anvil assemblage strata from the Teslin tectonic zone, northern Canadian Cordillera: Constraints from neodymium isotope and geochemical evidence. *Tectonics*, 16(1), 107-121.
- Creaser, R. A., Price, R. C., and Wormald, R. J. (1991). A-type granites revisited: assessment of a residual-source model. *Geology*, 19(2), 163-166.

- Dall'Agnol, R., Frost, C. D., and Rämö, O. T. (2012). IGCP Project 510 "A-type Granites and Related Rocks through Time": Project vita, results, and contribution to granite research. *Lithos*, 151, 1-16.
- Davies, J. H., Stern, R. A., Heaman, L. M., Rojas, X., and Walton, E. L. (2015). Resolving oxygen isotopic disturbance in zircon: A case study from the low $\delta^{18}\text{O}$ Scourie dikes, NW Scotland. *American Mineralogist*, 100(8-9), 1952-1966.
- Davis, W. J., and Hegner, E. (1992). Neodymium isotopic evidence for the tectonic assembly of Late Archean crust in the Slave Province, northwest Canada. *Contributions to Mineralogy and Petrology*, 111(4), 493-504.
- Davis, W. J., Fryers, B. J., and King, J. E. (1994). Geochemistry and evolution of Late Archean plutonism and its significance to the tectonic development of the Slave craton. *Precambrian Research*, 67(3-4), 207-241.
- Davis, W. J., Hanmer, S., Tella, S., Sandeman, H. A., and Ryan, J. J. (2006). U–Pb geochronology of the MacQuoid supracrustal belt and Cross Bay plutonic complex: key components of the northwestern Hearne subdomain, western Churchill Province, Nunavut, Canada. *Precambrian Research*, 145(1-2), 53-80.
- Davis, W.J. and Zaleski, E. (1998). Geochronological investigations of the Woodburn Lake Group, western Churchill Province, Northwest Territories: preliminary results; in *Radiogenic Age and Isotopic Studies: Report 11*; Geological Survey of Canada, Current Research 1998-F, p. 89–97.
- Davis, W.J., Berman, R.G., and MacKinnon, A. (2013). U-Pb Geochronology of archival rock samples from the Queen Maud block, Thelon tectonic zone and Rae Craton, Kitikmeot Region, Nunavut, Canada; Geological Survey of Canada, Open File 7409.
- Davis, W.J., Berman, R.G., Nadeau, L., and Percival, J.A. (2014). U-Pb zircon geochronology of a transect across the Thelon tectonic zone, Queen Maud region, and adjacent Rae craton, Kitikmeot Region, Nunavut, Canada; Geological Survey of Canada, Open File 7652.
- Davis, W.J., Hanmer, S., Tella, S., Sandeman, H.A., Ryan, J.J. (2006). U-Pb geochronology of the MacQuoid supracrustal belt and Cross Bay plutonic complex: Key components of the northwestern Hearne subdomain, western Churchill Province, Nunavut, Canada. *Precambrian Research*, 145, 53-80.
- Davis, W.J., Pehrsson, S.J., and Percival, J.A. (2015). Results of a U-Pb zircon geochronology transect across the southern Rae craton, Northwest Territories, Canada; Geological Survey of Canada, Open File 7655.

- Davis, W.J., Pestaj, T., Rayner, N., and MicNicoll, V.M. (2019). Long-term reproducibility of $^{207}\text{Pb}/^{206}\text{Pb}$ age at the GSC SHRIMP lab based on the GSC Archean reference zircon z1242; Geological Survey of Canada, Scientific Presentation 111, 1 poster.
- Davis, W.J., Zaleski, E., and Emon, Q. (2021). U-Pb geochronology of volcanic and plutonic rocks from the White Hills Lake to Meadowbank River area, Rae Province, Nunavut, Canada; Geological Survey of Canada, Open File 8766.
- De la Roche, H. D., Leterrier, J. T., Grandclaude, P., and Marchal, M. (1980). A classification of volcanic and plutonic rocks using R1R2-diagram and major-element analyses—its relationships with current nomenclature. *Chemical geology*, 29(1-4), 183-210.
- Debon, F., Le Fort, P., Dautel, D., Sonet, J., and Zimmermann, J. L. (1987). Granites of western Karakorum and northern Kohistan (Pakistan): a composite Mid-Cretaceous to upper Cenozoic magmatism. *Lithos*, 20(1), 19-40.
- Debon, F., Le Fort, P., Sheppard, S. M., and Sonet, J. (1986). The four plutonic belts of the Transhimalaya-Himalaya: A chemical, mineralogical, isotopic, and chronological synthesis along a Tibet-Nepal section. *Journal of Petrology*, 27(1), 219-250.
- DePaolo, D. J. (1981). Neodymium isotopes in the Colorado Front Range and crust–mantle evolution in the Proterozoic. *Nature*, 291(5812), 193-196.
- DePaolo, D. J. (1981). Trace element and isotopic effects of combined wallrock assimilation and fractional crystallization. *Earth and planetary science letters*, 53(2), 189-202.
- Dhuime, B., Hawkesworth, C. J., Cawood, P. A., and Storey, C. D. (2012). A change in the geodynamics of continental growth 3 billion years ago. *Science*, 335(6074), 1334-1336.
- Dhuime, B., Hawkesworth, C. J., Delavault, H., and Cawood, P. A. (2018). Rates of generation and destruction of the continental crust: implications for continental growth. *Philosophical Transactions of the Royal Society A: Mathematical, Physical and Engineering Sciences*, 376(2132), 20170403.
- Dickinson, W. R., and Gehrels, G. E. (2009). Use of U–Pb ages of detrital zircons to infer maximum depositional ages of strata: a test against a Colorado Plateau Mesozoic database. *Earth and Planetary Science Letters*, 288(1-2), 115-125.
- Dieng, S., Kyser, K., and Godin, L. (2013). Tectonic history of the North American shield recorded in uranium deposits in the Beaverlodge area, northern Saskatchewan, Canada. *Precambrian Research*, 224, 316-340.

- Donaire, T., Pascual, E., Pin, C., and Duthou, J. L. (1999). Two-stage granitoid-forming event from an isotopically homogeneous crustal source: the Los Pedroches batholith, Iberian Massif, Spain. *Geological Society of America Bulletin*, 111(12), 1897-1906.
- Donaire, T., Pascual, E., Pin, C., and Duthou, J. L. (2005). Microgranular enclaves as evidence of rapid cooling in granitoid rocks: the case of the Los Pedroches granodiorite, Iberian Massif, Spain. *Contributions to Mineralogy and Petrology*, 149, 247-265.
- Donovan, J.J., and Tingle, T.N. (1996) An improved mean atomic number correction for quantitative microanalysis. *Microscopy and Microanalysis* 2, 1-7.
- Donovan, J.J., Kremser, D., Fournelle, J.H., and Goemann, K. (2015) Probe for EPMA: Acquisition, automation and analysis. Eugene, Oregon, Probe Software Inc. www.probesoftware.com.
- Donovan, J.J., Singer, J.W., and Armstrong, J.T. (2016) A new EPMA method for fast trace element analysis in simple matrices. *American Mineralogist* 101, 1839-1853.
- Donovan, J.J., Snyder, D.A., and Rivers, M.L. (1993) An improved interference correction for trace element analysis. *Microbeam Analysis* 2, 23-28.
- Ducea, M. N., Saleeby, J. B., and Bergantz, G. (2015). The architecture, chemistry, and evolution of continental magmatic arcs. *Annual Review of Earth and Planetary Sciences*, 43, 299-331.
- Dudas, F.O., LeCheminant, A.N., and Sullivan, R.W. (1991). Reconnaissance Nd isotopic study of granitoid rocks from the Baker Lake region, District of Keewatin, N.W.T., and observations on analytical procedures; In radiogenic and isotopic Studies: Report 4, Geological Survey of Canada Paper 90-2, p. 101-112.
- Eby, G. N. (1990). The A-type granitoids: a review of their occurrence and chemical characteristics and speculations on their petrogenesis. *Lithos*, 26(1-2), 115-134.
- Eby, G. N. (1992). Chemical subdivision of the A-type granitoids: petrogenetic and tectonic implications. *Geology*, 20(7), 641-644.
- Eglington, B. M., and Armstrong, R. A. (2004). The Kaapvaal Craton and adjacent orogens, southern Africa: a geochronological database and overview of the geological development of the craton. *South African Journal of Geology*, 107(1-2), 13-32.
- Eiler, J. M., Crawford, A., Elliott, T. I. M., Farley, K. A., Valley, J. W., and Stolper, E. M. (2000). Oxygen isotope geochemistry of oceanic-arc lavas. *Journal of Petrology*, 41(2), 229-256.
- Elliott, T. (2003). Tracers of the slab. In: Eiler, J. (ed.) *Inside the Subduction Factory* (Geophysical Monograph 138), pp. 23-45. Washington DC: American geophysical Union.

- Engi, M., Lanari, P., and Kohn, M. J. (2017). Significant ages—An introduction to petrochronology. *Reviews in Mineralogy and Geochemistry*, 83(1), 1-12.
- Evans, D. A., and Mitchell, R. N. (2011). Assembly and breakup of the core of Paleoproterozoic–Mesoproterozoic supercontinent Nuna. *Geology*, 39(5), 443-446.
- Fedo, C. M., Sircombe, K. N., and Rainbird, R. H. (2003). Detrital zircon analysis of the sedimentary record. *Reviews in mineralogy and geochemistry*, 53(1), 277-303.
- Ferry, J. M., and Watson, E. B. (2007). New thermodynamic models and revised calibrations for the Ti-in-zircon and Zr-in-rutile thermometers. *Contributions to Mineralogy and Petrology*, 154(4), 429-437.
- Finger, F., Roberts, M. P., Haunschmid, B., Schermaier, A., and Steyrer, H. P. (1997). Variscan granitoids of central Europe: their typology, potential sources and tectonothermal relations. *Mineralogy and Petrology*, 61(1-4), 67.
- Fisher, C. M., and Vervoort, J. D. (2018). Using the magmatic record to constrain the growth of continental crust—The Eoarchean zircon Hf record of Greenland. *Earth and Planetary Science Letters*, 488, 79-91.
- Fisher, C. M., Hanchar, J. M., Samson, S. D., Dhuime, B., Blichert-Toft, J., Vervoort, J. D., and Lam, R. (2011). Synthetic zircon doped with hafnium and rare earth elements: A reference material for in situ hafnium isotope analysis. *Chemical Geology*, 286(1-2), 32-47.
- Fisher, C. M., Paton, C., Pearson, D. G., Sarkar, C., Luo, Y., Tersmette, D. B., and Chacko, T. (2017). Data reduction of laser ablation split-stream (LASS) analyses using newly developed features within iolite: with applications to Lu-Hf+ U-Pb in detrital zircon and Sm-Nd+ U-Pb in igneous monazite. *Geochemistry, Geophysics, Geosystems*, 18(12), 4604-4622.
- Flowers, R. M., Bowring, S. A., Mahan, K. H., Williams, M. L., and Williams, I. S. (2008). Stabilization and reactivation of cratonic lithosphere from the lower crustal record in the western Canadian shield. *Contributions to Mineralogy and Petrology*, 156, 529-549.
- Fowler, M. B., Henney, P. J., Darbyshire, D. F., and Greenwood, P. B. (2001). Petrogenesis of high Ba–Sr granites: the Rogart pluton, Sutherland. *Journal of the Geological Society*, 158(3), 521-534.
- Fowler, M. B., Kocks, H., Darbyshire, D. P. F., and Greenwood, P. B. (2008). Petrogenesis of high Ba–Sr plutons from the northern highlands Terrane of the British Caledonian Province. *Lithos*, 105(1-2), 129-148.

- Fowler, M., and Rollinson, H. (2012). Phanerozoic sanukitoids from Caledonian Scotland: implications for Archean subduction. *Geology*, 40(12), 1079-1082.
- Frisch, T. and Hunt, P. (1993). Reconnaissance U-Pb geochronology of the crystalline core of the Boothia Uplift, District of Franklin, Northwest Territories.; in *Radiogenic Age and Isotopic Studies: Report 7*; Geological Survey of Canada, Paper 93-2, p. 3-22.
- Frisch, T. and Hunt, P.A. (1988). U-Pb zircon and monazite ages from the Precambrian Shield of Ellesmere and Devon islands, Arctic Archipelago.; in *Radiogenic and Isotopic Studies: Report 2*, Geological Survey of Canada, Paper 88-2, p. 117-125.
- Frisch, T. and Parrish, R.R. (1992). U-Pb zircon ages from the Chantrey Inlet area, northern District of Keewatin, Northwest Territories; in *Radiogenic Age and Isotopic Studies: Report 5*; Geological Survey of Canada, Paper 91-2, p. 35-41.
- Frisch, T., and Hunt, P. (1993). Reconnaissance U-Pb geochronology of the crystalline core of the Boothia Uplift, District of Franklin, Northwest Territories.; in *Radiogenic Age and Isotopic Studies: Report 7*; Geological Survey of Canada, Paper 93-2, p. 3-22.
- Frost, B. R., Barnes, C. G., Collins, W. J., Arculus, R. J., Ellis, D. J., and Frost, C. D. (2001). A geochemical classification for granitic rocks. *Journal of petrology*, 42(11), 2033-2048.
- Frost, C. D., and Frost, B. R. (2011). On ferroan (A-type) granitoids: their compositional variability and modes of origin. *Journal of petrology*, 52(1), 39-53.
- Frost, C. D., Swapp, S. M., Frost, B. R., Finley-Blasi, L., and Fitz-Gerald, D. B. (2016). Leucogranites of the Teton Range, Wyoming: A record of Archean collisional orogeny. *Geochimica et Cosmochimica Acta*, 185, 528-549.
- Ganderton, N.B. (2013). Mapping and zircon geochronology of the Lyon Inlet boundary zone, Nunavut; a crustal-scale break in the Churchill province; unpublished M.Sc. thesis, University of Western Ontario, London, Ontario, 87 p.
- Garçon, M. (2021). Episodic growth of felsic continents in the past 3.7 Ga. *Science advances*, 7(39), eabj1807.
- Garçon, M., Boyet, M., Carlson, R. W., Horan, M. F., Auclair, D., and Mock, T. D. (2018). Factors influencing the precision and accuracy of Nd isotope measurements by thermal ionization mass spectrometry. *Chemical Geology*, 476, 493-514.
- Gehrels, G. (2014). Detrital zircon U-Pb geochronology applied to tectonics. *Annual Review of Earth and Planetary Sciences*, 42, 127-149.

- Gerdes, A., Wörner, G., and Finger, F. (2000). Hybrids, magma mixing and enriched mantle melts in post-collisional Variscan granitoids: the Rastenberg Pluton, Austria. *Geological Society, London, Special Publications*, 179(1), 415-431.
- Gill, J. B. (2012). *Orogenic andesites and plate tectonic: Minerals and Rocks (Vol. 16)*. Springer Science and Business Media.
- Girardi, J. D., Patchett, P. J., Ducea, M. N., Gehrels, G. E., Cecil, M. R., Rusmore, M. E., Woodsworth, G.J., Pearson, D.M., Manthei, C. and Wetmore, P. (2012). Elemental and isotopic evidence for granitoid genesis from deep-seated sources in the Coast Mountains batholith, British Columbia. *Journal of Petrology*, 53(7), 1505-1536.
- Goldstein, S.L., O'nions, R.K., and Hamilton, P.J. (1984). A Sm-Nd isotopic study of atmospheric dusts and particulates from major river systems. *Earth and planetary Science letters*, 70(2), 221-236.
- Gómez-Frutos, D., Castro, A., and Gutiérrez-Alonso, G. (2023). Post-collisional batholiths do contribute to continental growth. *Earth and Planetary Science Letters*, 603, 117978.
- Goodwin, A. M. (1996). *Principles of Precambrian geology*. Elsevier.
- Grégoire, M., Bell, D., and Le Roex, A. (2002). Trace element geochemistry of phlogopite-rich mafic mantle xenoliths: their classification and their relationship to phlogopite-bearing peridotites and kimberlites revisited. *Contributions to Mineralogy and Petrology*, 142, 603-625.
- Gualda, G. A., and Ghiorso, M. S. (2015). MELTS_E xcel: A Microsoft Excel-based MELTS interface for research and teaching of magma properties and evolution. *Geochemistry, Geophysics, Geosystems*, 16(1), 315-324.
- Guitreau, M., Blichert-Toft, J., Martin, H., Mojzsis, S. J., and Albarède, F. (2012). Hafnium isotope evidence from Archean granitic rocks for deep-mantle origin of continental crust. *Earth and Planetary Science Letters*, 337, 211-223.
- Guo, M., and Korenaga, J. (2023). The combined Hf and Nd isotope evolution of the depleted mantle requires Hadean continental formation. *Science Advances*, 9, 1-13.
- Halla, J., and Heilimo, E. (2009). Deformation-induced Pb isotope exchange between K-feldspar and whole rock in Neoproterozoic granitoids: Implications for assessing Proterozoic imprints. *Chemical Geology*, 265(3-4), 303-312.
- Hamilton, W. B. (2011). Plate tectonics began in Neoproterozoic time, and plumes from deep mantle have never operated. *Lithos*, 123(1-4), 1-20.

- Hanmer, S., Parrish, R., Williams, M., and Kopf, C. (1994). Striding-Athabasca mylonite zone: Complex Archean deep-crustal deformation in the East Athabasca mylonite triangle, northern Saskatchewan. *Canadian Journal of Earth Sciences*, 31(8), 1287-1300.
- Harris, N. B., Pearce, J. A., and Tindle, A. G. (1986). Geochemical characteristics of collision-zone magmatism. Geological Society, London, Special Publications, 19(1), 67-81.
- Hartlaub, R. P., Chacko, T., Heaman, L. M., Creaser, R. A., Ashton, K. E., and Simonetti, A. (2005). Ancient (Meso- to Paleoproterozoic) crust in the Rae Province, Canada: evidence from Sm–Nd and U–Pb constraints. *Precambrian Research*, 141(3-4), 137-153.
- Hartlaub, R. P., Heaman, L. M., Chacko, T., and Ashton, K. E. (2007). Circa 2.3-Ga magmatism of the Arrowsmith orogeny, Uranium City region, western Churchill craton, Canada. *The Journal of Geology*, 115(2), 181-195.
- Hawkesworth, C., and Jaupart, C. (2021). Heat flow constraints on the mafic character of Archean continental crust. *Earth and Planetary Science Letters*, 571, 117091.
- Hawkesworth, C., Cawood, P., Kemp, T., Storey, C., and Dhuime, B. (2009). A matter of preservation. *Science*, 323(5910), 49-50.
- Hawkesworth, C.J., Cawood, P.A., and Dhuime, B. (2019). Rates of generation and growth of the continental crust. *Geoscience Frontiers*, 10, 165-173.
- Heaman, L. M. (1997). Global mafic magmatism at 2.45 Ga: Remnants of an ancient large igneous province? *Geology*, 25, 299-302.
- Heilimo, E., Halla, J., and Hölttä, P. (2010). Discrimination and origin of the sanukitoid series: geochemical constraints from the Neoproterozoic western Karelian Province (Finland). *Lithos*, 115(1-4), 27-39.
- Henderson, J.B., and Thériault, R.J. (1994). U-Pb zircon evidence for ancient crust south of the McDonald Fault, northwestern Canadian Shield, Northwest Territories; in *Radiogenic Age and Isotopic Studies: Report 8; Current Research 1994-F*; Geological Survey of Canada, p. 43-47.
- Hermann, J. (2002). Allanite: thorium and light rare earth element carrier in subducted crust. *Chemical geology*, 192(3-4), 289-306.
- Herriott, T. M., Crowley, J. L., Schmitz, M. D., Wartes, M. A., and Gillis, R. J. (2019). Exploring the law of detrital zircon: LA-ICP-MS and CA-TIMS geochronology of Jurassic forearc strata, Cook Inlet, Alaska, USA. *Geology*, 47(11), 1044-1048.

- Herve, F., Pankhurst, R. J., Fanning, C. M., Calderón, M., and Yaxley, G. M. (2007). The South Patagonian batholith: 150 my of granite magmatism on a plate margin. *Lithos*, 97(3-4), 373-394.
- Hildreth, W., and Moorbath, S. (1988). Crustal contributions to arc magmatism in the Andes of Central Chile. *Contributions to mineralogy and petrology*, 98, 455-489.
- Hinchev, A. M., Davis, W. J., Ryan, J. J., and Nadeau, L. (2011). Neoproterozoic high-potassium granites of the Boothia mainland area, Rae domain, Churchill Province: U–Pb zircon and Sm–Nd whole rock isotopic constraints. *Canadian Journal of Earth Sciences*, 48(2), 247-279.
- Hoffman, P. F. (1988). United plates of America, the birth of a craton: Early Proterozoic assembly and growth of Laurentia. *Annual Review of Earth and Planetary Sciences*, 16(1), 543-603.
- Holland, J. E., Surpless, B., Smith, D. R., Loewy, S. L., and Lackey, J. S. (2013). Intrusive history and petrogenesis of the Ash Mountain Complex, Sierra Nevada batholith, California (USA). *Geosphere*, 9(4), 691-717.
- Honegger, K., Dietrich, V., Frank, W., Gansser, A., Thöni, M., and Trommsdorff, V. (1982). Magmatism and metamorphism in the Ladakh Himalayas (the Indus-Tsangpo suture zone). *Earth and Planetary Science Letters*, 60(2), 253-292.
- Hopkins, M., Harrison, T. M., and Manning, C. E. (2008). Low heat flow inferred from > 4 Gyr zircons suggests Hadean plate boundary interactions. *Nature*, 456(7221), 493-496.
- Horstwood, M. S. A., Košler, J., Gehrels, G., Jackson, S. E., McLean, N. M., Paton, C., Pearson, N.J., Sircombe, K., Sylvester, P., Vermeesch, P., Bowring, J.F., Condon, D.J., and Schoene, B. (2016). Community-Derived Standards for LA-ICP-MS U-(Th-)Pb Geochronology – Uncertainty Propagation, Age Interpretation and Data Reporting. *Geostandards and Geoanalytical Research*, 40, 311–332
- Hoskin, P. W., and Schaltegger, U. (2003). The composition of zircon and igneous and metamorphic petrogenesis. *Reviews in mineralogy and geochemistry*, 53(1), 27-62.
- Hunter, R. C., Lafrance, B., Heaman, L. M., and Thomas, D. (2021). Long-lived deformation history recorded along the Precambrian Thelon and Judge Sissons faults, northeastern Thelon Basin, Nunavut. *Canadian Journal of Earth Sciences*, 58(5), 433-457.
- Hunter, R. C., Lafrance, B., Heaman, L. M., Zaluski, G., and Thomas, D. (2018). Geology, litho-geochemistry and U-Pb geochronology of the Aberdeen Lake area, Nunavut: New insights into the Neoproterozoic tectonic evolution of the central Rae domain. *Precambrian Research*, 310, 114-132.

- Jackson, G.D., Hunt, P.A., Loveridge, W.D. and Parrish, R.R. (1990). Reconnaissance geochronology of Baffin Island, N.W.T.; in *Radiogenic Age and Isotopic Studies: Report 3*; Geological Survey of Canada, Paper 89-2, p. 123-148.
- Jacob, J. B., Moyen, J. F., Fiannacca, P., Laurent, O., Bachmann, O., Janoušek, V., Farina, F., and Villaros, A. (2021). Crustal melting vs. fractionation of basaltic magmas: Part 2, Attempting to quantify mantle and crustal contributions in granitoids. *Lithos*, 402, 106292.
- Jagoutz, O., and Kelemen, P. B. (2015). Role of arc processes in the formation of continental crust. *Annual Review of Earth and Planetary Sciences*, 43, 363-404.
- Janoušek, V., Bowes, D. R., Rogers, G., Farrow, C. M., and Jelínek, E. (2000). Modelling diverse processes in the petrogenesis of a composite batholith: the Central Bohemian Pluton, Central European Hercynides. *Journal of Petrology*, 41(4), 511-543.
- Jayananda, M., Aadhisesan, K. R., Kusiak, M. A., Wilde, S. A., Sekhmo, K. U., Guitreau, M., Santosh, M., and Gireesh, R. V. (2020). Multi-stage crustal growth and Neoproterozoic geodynamics in the Eastern Dharwar Craton, southern India. *Gondwana Research*, 78, 228-260.
- Jochum, K. P., Weis, U., Schwager, B., Stoll, B., Wilson, S. A., Haug, G. H., Andreae, M.O., and Enzweiler, J. (2016). Reference values following ISO guidelines for frequently requested rock reference materials. *Geostandards and Geoanalytical Research*, 40(3), 333-350.
- Johnson, C. M. (1993). Mesozoic and Cenozoic contributions to crustal growth in the southwestern United States. *Earth and Planetary Science Letters*, 118(1-4), 75-89.
- Johnson, D.M., Hooper, P.R., and Conrey, R.M. (1999). XRF analyses of rocks and minerals for major and trace elements on a single low dilution Li-tetraborate fused bead. *Geoanalytical laboratory*. Washington State University.
- Johnstone, S. (2002). Structural and geochronological constraints on the tectonic evolution of the Walker Lake area, Committee Bay belt, Nunavut; unpublished M.Sc. thesis, University of Waterloo, Waterloo, Ontario, 376 p.
- Jones, R. E., Kirstein, L. A., Kasemann, S. A., Dhuime, B., Elliott, T., Litvak, V. D., Alonso, R., Hinton, R., and Facility, E. I. M. (2015). Geodynamic controls on the contamination of Cenozoic arc magmas in the southern Central Andes: Insights from the O and Hf isotopic composition of zircon. *Geochimica et Cosmochimica Acta*, 164, 386-402.
- Kamber, B. S. (2015). The evolving nature of terrestrial crust from the Hadean, through the Archaean, into the Proterozoic. *Precambrian Research*, 258, 48-82.

- Kelemen, P. B., Hanghøj, K., and Greene, A. R. (2014). One view of the geochemistry of subduction-related magmatic arcs, with an emphasis on primitive andesite and lower crust. In H.D. Holland and K.K. Turekian (Eds.), *Treatise on Geochemistry* (2nd ed., pp. 749-806), Elsevier.
- Kemp, A. I., Hickman, A. H., Kirkland, C. L., and Vervoort, J. D. (2015). Hf isotopes in detrital and inherited zircons of the Pilbara Craton provide no evidence for Hadean continents. *Precambrian Research*, 261, 112-126.
- Kemp, A. I., Vervoort, J. D., Bjorkman, K. E., and Iaccheri, L. M. (2017). Hafnium isotope characteristics of palaeoarchean zircon OG1/OGC from the Owens Gully Diorite, Pilbara Craton, Western Australia. *Geostandards and Geoanalytical Research*, 41(4), 659-673.
- Kemp, A. I., Vervoort, J. D., Petersson, A., Smithies, R. H., and Lu, Y. (2023). A linked evolution for granite-greenstone terranes of the Pilbara Craton from Nd and Hf isotopes, with implications for Archean continental growth. *Earth and Planetary Science Letters*, 601, 117895.
- Kendrick, J., Duguet, M., and Yakymchuk, C. (2022). Diversification of Archean tonalite-trondhjemite-granodiorite suites in a mushy middle crust. *Geology*, 50(1), 76-80.
- Kessel, R., Schmidt, M.W., Ulmer, P., and Pettke, T. (2005). Trace element signature of subduction-zone fluids, melts and supercritical liquids at 120-180 km depth. *Nature*, 437, 724-727.
- King, P. L., Chappell, B. W., Allen, C. M., and White, A. J. R. (2001). Are A-type granites the high-temperature felsic granites? Evidence from fractionated granites of the Wangrah Suite. *Australian Journal of Earth Sciences*, 48(4), 501-514.
- King, P. L., White, A. J. R., Chappell, B. W., and Allen, C. M. (1997). Characterization and origin of aluminous A-type granites from the Lachlan Fold Belt, southeastern Australia. *Journal of Petrology*, 38(3), 371-391.
- Klein, B. Z., and Jagoutz, O. (2021). Construction of a trans-crustal magma system: building the Bear Valley Intrusive Suite, southern Sierra Nevada, California. *Earth and Planetary Science Letters*, 553, 116624.
- Knaack, C., Cornelius, S., and Hooper, P.R. (1994). Trace element analyses of rocks and minerals by ICP-MS. Open File Report. Department of Geology. Washington State University.
- Korenaga, J. (2018). Crustal evolution and mantle dynamics through Earth history. *Philosophical Transactions of the Royal Society A: Mathematical, Physical and Engineering Sciences*, 376(2132), 20170408.
- Kretz, R. (1983). Symbols for rock-forming minerals. *American mineralogist*, 68(1-2), 277-279.

- Lackey, J. S., Cecil, M. R., Windham, C. J., Frazer, R. E., Bindeman, I. N., and Gehrels, G. E. (2012). The Fine Gold Intrusive Suite: The roles of basement terranes and magma source development in the Early Cretaceous Sierra Nevada batholith. *Geosphere*, 8(2), 292-313.
- Lackey, J. S., Valley, J. W., Chen, J. H., and Stockli, D. F. (2008). Dynamic magma systems, crustal recycling, and alteration in the central Sierra Nevada batholith: the oxygen isotope record. *Journal of Petrology*, 49(7), 1397-1426.
- LaFlamme, C., McFarlane, C. R., and Corrigan, D. (2014a). U–Pb, Lu–Hf and REE in zircon from 3.2 to 2.6 Ga Archean gneisses of the Repulse Bay block, Melville Peninsula, Nunavut. *Precambrian Research*, 252, 223-239.
- LaFlamme, C., McFarlane, C. R., Corrigan, D., and Wodicka, N. (2014b). Origin and tectonometamorphic history of the Repulse Bay block, Melville Peninsula, Nunavut: exotic terrane or deeper level of the Rae craton?. *Canadian Journal of Earth Sciences*, 51(12), 1097-1122.
- Landry, K., Adlakha, E., Roy-Garand, A., Terekhova, A., Hanley, J., Falck, H., and Martel, E. (2022). Uranium Mineralization in the MacInnis Lake Area, Nonacho Basin, Northwest Territories: Potential Linkages to Metasomatic Iron Alkali-Calcic Systems. *Minerals*, 12(12), 1609.
- Laurent, O., Doucelance, R., Martin, H., and Moyen, J. F. (2013). Differentiation of the late-Archaean sanukitoid series and some implications for crustal growth: insights from geochemical modelling on the Bulai pluton, Central Limpopo Belt, South Africa. *Precambrian Research*, 227, 186-203.
- Laurent, O., Martin, H., Doucelance, R., Moyen, J. F., and Paquette, J. L. (2011). Geochemistry and petrogenesis of high-K “sanukitoids” from the Bulai pluton, Central Limpopo Belt, South Africa: Implications for geodynamic changes at the Archaean–Proterozoic boundary. *Lithos*, 123(1-4), 73-91.
- Laurent, O., Martin, H., Moyen, J. F., and Doucelance, R. (2014). The diversity and evolution of late-Archaean granitoids: Evidence for the onset of “modern-style” plate tectonics between 3.0 and 2.5 Ga. *Lithos*, 205, 208-235.
- Laurent, O., Rapopo, M., Stevens, G., Moyen, J. F., Martin, H., Doucelance, R., and Bosq, C. (2014). Contrasting petrogenesis of Mg–K and Fe–K granitoids and implications for post-collisional magmatism: case study from the Late-Archaean Matok pluton (Pietersburg block, South Africa). *Lithos*, 196, 131-149.

- Le Fort, P., Cuney, M., Deniel, C., France-Lanord, C., Sheppard, S. M. F., Upreti, B. N., and Vidal, P. (1987). Crustal generation of the Himalayan leucogranites. *Tectonophysics*, 134(1-3), 39-57.
- LeCheminant, A.N., and Roddick, J.C. (1991). U-Pb zircon evidence for widespread 2.6 Ga felsic magmatism in the central District of Keewatin, NWT.; in *Radiogenic and Isotopic Studies: Report 4, Geological Survey of Canada Paper 90-2*, p. 91-99.
- Lee, C. T. A., Morton, D. M., Kistler, R. W., and Baird, A. K. (2007). Petrology and tectonics of Phanerozoic continent formation: From island arcs to accretion and continental arc magmatism. *Earth and Planetary Science Letters*, 263(3-4), 370-387.
- Lee, C. T. A., Yeung, L. Y., McKenzie, N. R., Yokoyama, Y., Ozaki, K., and Lenardic, A. (2016). Two-step rise of atmospheric oxygen linked to the growth of continents. *Nature Geoscience*, 9(6), 417-424.
- Liegeois, J. P., Navez, J., Hertogen, J., and Black, R. (1998). Contrasting origin of post-collisional high-K calc-alkaline and shoshonitic versus alkaline and peralkaline granitoids. The use of sliding normalization. *Lithos*, 45(1-4), 1-28.
- Ludwig, K.L. (2009). *ISOPLOT 3.70 A Geochronological Toolkit for Microsoft Excel*. Berkeley Geochronology Centre, Special Publication No. 4.
- Lugmair, G. W., and Marti, K. (1978). Lunar initial $^{143}\text{Nd}/^{144}\text{Nd}$: differential evolution of the lunar crust and mantle. *Earth and Planetary Science Letters*, 39(3), 349-357.
- Ma, L., Wang, Q., Wyman, D. A., Jiang, Z. Q., Wu, F. Y., Li, X. H., Yang, J.H., Gou, G.N., and Guo, H. F. (2015). Late Cretaceous back-arc extension and arc system evolution in the Gangdese area, southern Tibet: Geochronological, petrological, and Sr-Nd-Hf-O isotopic evidence from Dagze diabases. *Journal of Geophysical Research: Solid Earth*, 120(9), 6159-6181.
- MacHattie, T.G. (2008). *Geochemistry and Geochronology of the late Archean Prince Albert group, Nunavut, Canada*; unpublished Ph.D. thesis, University of Alberta, Edmonton, Alberta, 339 p.
- MacLachlan, K., Davis, W. J., and Relf, C. (2005). U/Pb geochronological constraints on Neoproterozoic tectonism: multiple compressional events in the northwestern Hearne Domain, Western Churchill Province, Canada. *Canadian Journal of Earth Sciences*, 42(1), 85-109.
- Mahan, K. H., Goncalves, P., Williams, M. L., and Jercinovic, A. M. (2006). Dating metamorphic reactions and fluid flow: Application to exhumation of high-P granulites in a crustal-scale shear zone, western Canadian Shield. *Journal of Metamorphic Geology*, 24(3), 193-217.

- Maniar, P. D., and Piccoli, P. M. (1989). Tectonic discrimination of granitoids. *Geological society of America bulletin*, 101(5), 635-643.
- Martel, E., Pehrsson, S.J., Regis, D., Thiessen, E.J., Jamison, D., Percival, J., Pierce, K.L., and Acosta-Gongora, P. (2020). Geology of the McCann Lake area, South Rae craton, Northwest Territories (NTS 75G); Northwest Territories Geological Survey, NWT Open File 2020-01, 1 map, 1:250 000 scale, and digital files.
- Martel, E., van Breemen, O., Berman, R. G., and Pehrsson, S. (2008). Geochronology and tectonometamorphic history of the Snowbird Lake area, Northwest Territories, Canada: New insights into the architecture and significance of the Snowbird tectonic zone. *Precambrian Research*, 161(3-4), 201-230.
- Martin, H. (1986). Effect of steeper Archean geothermal gradient on geochemistry of subduction-zone magmas. *Geology*, 14, 753-756.
- Martin, H. (1994). The Archean grey gneisses and the genesis of continental crust. In *Developments in Precambrian geology* (Vol. 11, pp. 205-259). Elsevier.
- Martin, H., Moyen, J. F., and Rapp, R. (2009). The sanukitoid series: magmatism at the Archaean–Proterozoic transition. *Earth and Environmental Science Transactions of the Royal Society of Edinburgh*, 100(1-2), 15-33.
- Martin, H., Moyen, J. F., Guitreau, M., Blichert-Toft, J., and Le Pennec, J. L. (2014). Why Archaean TTG cannot be generated by MORB melting in subduction zones. *Lithos*, 198, 1-13.
- Martin, H., Smithies, R. H., Rapp, R., Moyen, J. F., and Champion, D. (2005). An overview of adakite, tonalite–trondhjemite–granodiorite (TTG), and sanukitoid: relationships and some implications for crustal evolution. *Lithos*, 79(1-2), 1-24.
- McCulloch, M. T., and Bennett, V. C. (1994). Progressive growth of the Earth's continental crust and depleted mantle: geochemical constraints. *Geochimica et Cosmochimica Acta*, 58(21), 4717-4738.
- McCulloch, M. T., and Gamble, J. A. (1991). Geochemical and geodynamical constraints on subduction zone magmatism. *Earth and Planetary Science Letters*, 102(3-4), 358-374.
- McDonough, M. R., McNicoll, V. J., Schetselaar, E. M., and Grover, T. W. (2000). Geochronological and kinematic constraints on crustal shortening and escape in a two-sided oblique-slip collisional and magmatic orogen, Paleoproterozoic Taltson magmatic zone, northeastern Alberta. *Canadian Journal of Earth Sciences*, 37(11), 1549-1573.

- McDonough, W.F., and Sun, S.-s. (1989). Chemical and isotopic systematics of oceanic basalts: implications for mantle composition and processes: in *Magmatism in the Ocean basins*, Saunders, A.D., and Norry, M.J., (Eds.), Geological Society Special Publication, No. 42, p. 313-345.
- McNicoll, V. J., Thériault, R. J., and McDonough, M. R. (2000). Taltson basement gneissic rocks: U Pb and Nd isotopic constraints on the basement to the Paleoproterozoic Taltson magmatic zone, northeastern Alberta. *Canadian Journal of Earth Sciences*, 37(11), 1575-1596.
- Miles, A. J., Woodcock, N. H., and Hawkesworth, C. J. (2016). Tectonic controls on post-subduction granite genesis and emplacement: the late Caledonian suite of Britain and Ireland. *Gondwana Research*, 39, 250-260.
- Miles, W., and Oneschuk, D. (2016). Magnetic Anomaly Map, Canada; Geological Survey of Canada, Open File 7799; scale 1:7,5000,000.
- Mills, A. J., Berman, R. G., Davis, W. J., Tella, S., Roddick, C., and S. Carr, S. H. (2007). Thermobarometry and geochronology of the Uvauk complex, a polymetamorphic Neoproterozoic and Paleoproterozoic segment of the Snowbird tectonic zone, Nunavut, Canada. *Canadian Journal of Earth Sciences*, 44(2), 245-266.
- Moyen, J. F. (2009). High Sr/Y and La/Yb ratios: the meaning of the “adakitic signature”. *Lithos*, 112(3-4), 556-574.
- Moyen, J. F. (2011). The composite Archaean grey gneisses: petrological significance, and evidence for a non-unique tectonic setting for Archaean crustal growth. *Lithos*, 123(1-4), 21-36.
- Moyen, J. F. (2020a). Archaean granitoids: classification, petrology, geochemistry and origin. Geological Society, London, Special Publications, 489(1), 15-49.
- Moyen, J. F. (2020b). Granites and crustal heat budget. Geological Society, London, Special Publications, 491(1), 77-100.
- Moyen, J. F., and Laurent, O. (2018). Archaean tectonic systems: A view from igneous rocks. *Lithos*, 302, 99-125.
- Moyen, J. F., and Martin, H. (2012). Forty years of TTG research. *Lithos*, 148, 312-336.
- Moyen, J. F., Laurent, O., Chelle-Michou, C., Couzinié, S., Vanderhaeghe, O., Zeh, A., Villaros, A., and Gardien, V. (2017). Collision vs. subduction-related magmatism: two contrasting ways of granite formation and implications for crustal growth. *Lithos*, 277, 154-177.

- Moyen, J. F., Martin, H., and Jayananda, M. (2001). Multi-element geochemical modelling of crust–mantle interactions during late-Archaean crustal growth: the Closepet granite (South India). *Precambrian Research*, 112(1-2), 87-105.
- Moyen, J. F., Martin, H., Jayananda, M., and Auvray, B. (2003). Late Archaean granites: a typology based on the Dharwar Craton (India). *Precambrian Research*, 127(1-3), 103-123.
- Moyen, J., and Stevens, G. (2006). Experimental constraints on TTG petrogenesis: implications for Archean geodynamics. *Geophysical Monograph-American Geophysical Union*, 164, 149.
- Naeraa, T., Scherstén, A., Rosing, M. T., Kemp, A. I. S., Hoffmann, J. E., Kokfelt, T. F., and Whitehouse, M. J. (2012). Hafnium isotope evidence for a transition in the dynamics of continental growth 3.2 Gyr ago. *Nature*, 485(7400), 627-630.
- Nagel, T. J., Hoffmann, J. E., and Münker, C. (2012). Generation of Eoarchean tonalite-trondhjemite-granodiorite series from thickened mafic arc crust. *Geology*, 40(4), 375-378.
- Nair, R., and Chacko, T. (2008). Role of oceanic plateaus in the initiation of subduction and origin of continental crust. *Geology*, 36(7), 583-586.
- Nandedkar, R. H., Ulmer, P., and Müntener, O. (2014). Fractional crystallization of primitive, hydrous arc magmas: an experimental study at 0.7 GPa. *Contributions to Mineralogy and Petrology*, 167(6), 1015.
- Neil, B. J., Tersmette, D. B., Chacko, T., Heaman, L. M., Kjarsgaard, B. A., Martel, E., Creaser, R.A., Pearson, D.G., Stern, R.A., Dufrane, S.A., and Luo, Y. (2023). Discovery of a giant 3.3–3.1 Ga terrane in the Rae craton, Canada: Implications for the timing and extent of ancient continental growth. *Geology*, 51(6), 597-601.
- Neilson, J. C., Kokelaar, B. P., and Crowley, Q. G. (2009). Timing, relations and cause of plutonic and volcanic activity of the Siluro-Devonian post-collision magmatic episode in the Grampian Terrane, Scotland. *Journal of the Geological Society*, 166(3), 545-561.
- Neilson, J.C. (2008). From slab breakoff to triggered eruptions: Tectonic controls of Caledonian Post-orogenic magmatism. Unpublished PhD thesis. University of Liverpool. PhD thesis. pp. 512.
- Nelson, W. R., Dorais, M. J., Christiansen, E. H., and Hart, G. L. (2013). Petrogenesis of Sierra Nevada plutons inferred from the Sr, Nd, and O isotopic signatures of mafic igneous complexes in Yosemite Valley, California. *Contributions to Mineralogy and Petrology*, 165, 397-417.

- Nielsen, R. L. (1989). Phase equilibria constraints on liquid lines of descent generated by paired assimilation and fractional crystallization: trace elements and Sr and Nd isotopes. *Journal of Geophysical Research: Solid Earth*, 94(B1), 787-794.
- Nielson, J. E., Budahn, J. R., Unruh, D. M., and Wilshire, H. G. (1993). Actualistic models of mantle metasomatism documented in a composite xenolith from Dish Hill, California. *Geochimica et Cosmochimica Acta*, 57(1), 105-121.
- Nutman, A. P., Bennett, V. C., Friend, C. R., Polat, A., Hoffmann, E., and Van Kranendonk, M. (2021). Fifty years of the Eoarchean and the case for evolving uniformitarianism. *Precambrian Research*, 367, 106442.
- Paces, J. B., and Miller Jr, J. D. (1993). Precise U-Pb ages of Duluth complex and related mafic intrusions, northeastern Minnesota: Geochronological insights to physical, petrogenetic, paleomagnetic, and tectonomagmatic processes associated with the 1.1 Ga midcontinent rift system. *Journal of Geophysical Research: Solid Earth*, 98(B8), 13997-14013.
- Palin, R. M., and Santosh, M. (2021). Plate tectonics: What, where, why, and when?. *Gondwana Research*, 100, 3-24.
- Parman, S. W. (2015). Time-lapse zirconography: Imaging punctuated continental evolution. *Geochemical Perspectives Letters*, 1(1), 43-52.
- Partin, C. A., and Sylvester, P. J. (2023). Paleoproterozoic A-Type Postcollisional Granitic Magmatism Associated with the Arrowsmith Orogeny during the Global Tectonomagmatic Lull. *The Journal of Geology*, 131(1), 1-23.
- Partin, C. A., Bekker, A., Sylvester, P. J., Wodicka, N., Stern, R. A., Chacko, T., and Heaman, L. M. (2014). Filling in the juvenile magmatic gap: Evidence for uninterrupted Paleoproterozoic plate tectonics. *Earth and Planetary Science Letters*, 388, 123-133.
- Patiño Douce, A. E. (1997). Generation of metaluminous A-type granites by low-pressure melting of calc-alkaline granitoids. *Geology*, 25(8), 743-746.
- Paton, C., Hellstrom, J., Paul, B., Woodhead, J., and Hergt, J. (2011). Lolite: Freeware for the visualisation and processing of mass spectrometric data. *Journal of Analytical Atomic Spectrometry*, 26(12), 2508-2518.
- Paton, C., Woodhead, J. D., Hellstrom, J. C., Hergt, J. M., Greig, A., and Maas, R. (2010). Improved laser ablation U-Pb zircon geochronology through robust downhole fractionation correction. *Geochemistry, Geophysics, Geosystems*, 11(3).

- Pattison, D.R.M., Chacko, T., Farquhar, J., and McFarlane, C.R.M. (2003). Temperatures of granulite-facies metamorphism: constraints from experimental phase equilibria and thermobarometry corrected for retrograde exchange. *Journal of Petrology*, 44(5), 867-900.
- Payne, J. L., McInerney, D. J., Barovich, K. M., Kirkland, C. L., Pearson, N. J., and Hand, M. (2016). Strengths and limitations of zircon Lu-Hf and O isotopes in modelling crustal growth. *Lithos*, 248, 175-192.
- Pearce, J. A. (2014). Immobile element fingerprinting of ophiolites. *Elements*, 10, 101–108.
- Pearce, J. A., and Peate, D. W. (1995). Tectonic implications of the composition of volcanic arc magmas. *Annual review of Earth and planetary sciences*, 23(1), 251-285.
- Pearce, J. A., Harris, N. B., and Tindle, A. G. (1984). Trace element discrimination diagrams for the tectonic interpretation of granitic rocks. *Journal of petrology*, 25(4), 956-983.
- Pease, V., Percival, J., Smithies, H., Stevens, G., and Van Kranendonk, M. (2008). When did plate tectonics begin? Evidence from the orogenic record. In Condie, K.C. and Pease, V. (Eds.), *When Did Plate Tectonics Begin on Planet Earth?* (pp. 199-228), Geological Society of America.
- Pehrsson, S. J., Berman, R. G., and Davis, W. J. (2013b). Paleoproterozoic orogenesis during Nuna aggregation: a case study of reworking of the Rae craton, Woodburn Lake, Nunavut. *Precambrian Research*, 232, 167-188.
- Pehrsson, S. J., Berman, R. G., Eglington, B., and Rainbird, R. (2013a). Two Neoproterozoic supercontinents revisited: The case for a Rae family of cratons. *Precambrian Research*, 232, 27-43.
- Pehrsson, S. J., Buchan, K. L., Eglington, B. M., Berman, R. M., and Rainbird, R. H. (2014). Did plate tectonics shutdown in the Palaeoproterozoic? A view from the Siderian geologic record. *Gondwana Research*, 26(3-4), 803-815.
- Peterson, T. D., Scott, J. M., LeCheminant, A. N., Jefferson, C. W., and Pehrsson, S. J. (2015). The Kivalliq igneous suite: anorogenic bimodal magmatism at 1.75 Ga in the western Churchill Province, Canada. *Precambrian Research*, 262, 101-119.
- Peterson, T. D., Van Breemen, O., Sandeman, H., and Cousens, B. (2002). Proterozoic (1.85–1.75 Ga) igneous suites of the Western Churchill Province: granitoid and ultrapotassic magmatism in a reworked Archean hinterland. *Precambrian Research*, 119(1-4), 73-100.
- Peterson, T.D. (2006). *Geology of the Dubawnt Lake area, Nunavut-Northwest Territories*. Geological Survey of Canada Bulletin 580.

- Peterson, T.D., Pehrsson, S., Skulski, T., Sandeman, H. (2010). Compilation of Sm-Nd Isotope Analyses of Igneous Suites, Western Churchill Province; Geological Survey of Canada, Open File 6439.
- Peterson, T.D., Wodicka, N., Pehrsson, S.J., Acosta-Góngora, P., Tschirhart, V., Jefferson, C.W., Steenkamp, H.M., Martel, E., Percival, J.A., and Corrigan, D. (2024). Rae Province at 2.6 Ga: a sanukitoid storm on the Canadian Shield; in *Canada's northern shield: new perspectives from the Geo-mapping for Energy and Minerals program*, (ed.) S. Pehrsson, N. Wodicka, N. Rogers, and J.A. Percival; Geological Survey of Canada, Bulletin 612, p. 339–374.
- Petford, N., and Atherton, M. (1996). Na-rich partial melts from newly underplated basaltic crust: the Cordillera Blanca Batholith, Peru. *Journal of petrology*, 37(6), 1491-1521.
- Piazolo, S., Belousova, E., La Fontaine, A., Corcoran, C., and Cairney, J. M. (2017). Trace element homogeneity from micron-to atomic scale: Implication for the suitability of the zircon GJ-1 as a trace element reference material. *Chemical Geology*, 456, 10-18.
- Pitcher, W.J. (1997). *The Nature and Origin of Granite* (2nd ed.). Chapman and Hall.
- Pitcher, W.S., Atherton, M.P., Cobbing, E.J., and Beckensale, R.D. (eds.). (1985). *Magmatism at a Plate Edge. The Peruvian Andes*. Blackie. Glasgow.
- Plank, T. (2005). Constraints from thorium/lanthanum on sediment recycling at subduction zones and the evolution of the continents. *Journal of Petrology*, 46(5), 921-944.
- Plank, T., and Langmuir, C. H. (1998). The chemical composition of subducting sediment and its consequences for the crust and mantle. *Chemical geology*, 145(3-4), 325-394.
- Polat, A. (2012). Growth of Archean continental crust in oceanic island arcs. *Geology*, 40(4), 383.
- Polat, A., and Kerrich, R. (2004). Precambrian arc associations: Boninites, adakites, magnesian andesites, and Nb-enriched basalts. *Developments in Precambrian geology*, 13, 567-597.
- Puetz, S. J., and Condie, K. C. (2019). Time series analysis of mantle cycles Part I: Periodicities and correlations among seven global isotopic databases. *Geoscience Frontiers*, 10(4), 1305-1326.
- Putirka, K. D., Canchola, J., Rash, J., Smith, O., Torrez, G., Paterson, S. R., and Ducea, M. N. (2014). Pluton assembly and the genesis of granitic magmas: Insights from the GIC pluton in cross section, Sierra Nevada Batholith, California. *American Mineralogist*, 99(7), 1284-1303.
- Rainbird, R. H., and Davis, W. J. (2007). U-Pb detrital zircon geochronology and provenance of the late Paleoproterozoic Dubawnt Supergroup: Linking sedimentation with tectonic reworking of

- the western Churchill Province, Canada. *Geological Society of America Bulletin*, 119(3-4), 314-328.
- Rainbird, R. H., Davis, W. J., Pehrsson, S. J., Wodicka, N., Rayner, N., and Skulski, T. (2010). Early Paleoproterozoic supracrustal assemblages of the Rae domain, Nunavut, Canada: Intracratonic basin development during supercontinent break-up and assembly. *Precambrian Research*, 181(1-4), 167-186.
- Rämö, O. T., and Haapala, I. (1995). One hundred years of rapakivi granite. *Mineralogy and Petrology*, 52(3), 129-185.
- Rapp, R. P., Shimizu, N., Norman, M.D., and Applegate, G.S. (1999). Reaction between slab-derived melts and peridotite in the mantle wedge: experimental constraints at 3.8 GPa, *Chemical Geology*, 160, 335-356.
- Rapp, R. P., Watson, E. B., and Miller, C. F. (1991). Partial melting of amphibolite/eclogite and the origin of Archean trondhjemites and tonalites. *Precambrian Research*, 51(1-4), 1-25.
- Rayner, N., Chakungal, J., and Sanborn-Barrie, M. (2011). New U-Pb geochronological results from plutonic and sedimentary rocks of Southampton Island, Nunavut; Geological Survey of Canada, Current Research 2011-5, 23 p.
- Rayner, N., Stern, R. A., and Carr, S. D. (2005). Grain-scale variations in trace element composition of fluid-altered zircon, Acasta Gneiss Complex, northwestern Canada. *Contributions to Mineralogy and Petrology*, 148, 721-734.
- Regan, S. P., Williams, M. L., Chiarenzelli, J. R., Grohn, L., Mahan, K. H., and Gallagher, M. (2017). Isotopic evidence for Neoproterozoic continuity across the Snowbird tectonic zone, western Churchill Province, Canada. *Precambrian Research*, 300, 201-222.
- Regis, D. and Sanborn-Barrie, M. (2022). Delimiting the extent of 'Boothia terrane' crust, Nunavut: new U-Pb geochronological results; Geological Survey of Canada, Open File 8917.
- Regis, D., Acosta-Gongora, P., Davis, W. J., Knox, B., Pehrsson, S. J., Martel, E., and Hulbert, L. (2017b). Evidence for Neoproterozoic Ni-Cu-bearing mafic intrusions along a major lithospheric structure: a case study from the south Rae craton (Canada). *Precambrian Research*, 302, 312-339.
- Regis, D., and Sanborn-Barrie, M. (2023). U-Pb detrital zircon geochronological constraints on Siderian and Orosirian rocks of Boothia Peninsula and Somerset Island (Nunavut, Canada). *Precambrian Research*, 387, 106991.

- Regis, D., Canam, R., and Martel, E. (2022). U-Pb geochronological results from the Nonacho Lake area (NTS 75-F), Northwest Territories; Geological Survey of Canada, Open File 8880.
- Regis, D., Davis, W. J., Ryan, J. J., Berman, R. G., Pehrsson, S., Joyce, N. L., and Sandeman, H. A. (2019). Multiple burial–exhumation episodes revealed by accessory phases in high-pressure granulite-facies rocks (Rae craton, Nunavut, Canada). *Contributions to Mineralogy and Petrology*, 174, 1-25.
- Regis, D., Martel, E., Davis, W.J., Pehrsson, S.J. (2017a). U-Pb zircon geochronology of metaplutonic rocks across the southern Rae province, Northwest Territories; Geological Survey of Canada, Open File 8254.
- Regis, D., Pehrsson, S., Martel, E., Thiessen, E., Peterson, T., and Kellett, D. (2021). Post-1.9 Ga evolution of the south Rae craton (Northwest Territories, Canada): A Paleoproterozoic orogenic collapse system. *Precambrian Research*, 355, 106105.
- Reichardt, H., and Weinberg, R. F. (2012). Hornblende chemistry in meta- and diatexites and its retention in the source of leucogranites: an example from the Karakoram Shear Zone, NW India. *Journal of Petrology*, 53(6), 1287-1318.
- Reimink, J. R., Davies, J. H. F. L., Moyon, J. F., and Pearson, D. G. (2023). A whole-lithosphere view of continental growth. *Geochem. Persp. Lett.*, 26, 45-49.
- Reymer, A., and Schubert, G. (1984). Phanerozoic addition rates to the continental crust and crustal growth. *Tectonics*, 63-77.
- Roddick, J.C., and van Breemen, O. (1994). U-Pb zircon dating: a comparison of ion microprobe and single grain conventional analysis; in *Radiogenic Age and Isotopic Studies: Report 8*; Geological Survey of Canada, Current Research 1994-F, p. 1-9.
- Roddick, J.C., Henderson, J.R. and Chapman, H.J. (1992). U-Pb ages from the Archean Whitehills-Tehek lakes supracrustal belt, Churchill Province, district of Keewatin, Northwest Territories; in *Radiogenic Age and Isotopic Studies: Report 6*; Geological Survey of Canada, Paper 92-2, p. 31–40.
- Rogers, G., and Saunders, A.D. (1989). Magnesian andesites from Mexico, Chile and the Aleutian Islands: implications for magmatism associated with ridge–trench collisions. In: Crawford, A.J. (Ed.), *Boninites and Related Rocks*. Unwin Hyman, London, pp. 416–445.
- Rogers, J. J., and Santosh, M. J. G. R. (2002). Configuration of Columbia, a Mesoproterozoic supercontinent. *Gondwana Research*, 5(1), 5-22.

- Rollinson, H. (2017). There were no large volumes of felsic continental crust in the early Earth. *Geosphere*, v. 13, p. 235–246.
- Rollinson, H. (2021). Do all Archaean TTG rock compositions represent former melts?. *Precambrian Research*, 367, 106448.
- Rollinson, H., and Pease, V. (2021). Using Geochemical Data to Understand Geological Processes.
- Rubatto, D. (2002). Zircon trace element geochemistry: partitioning with garnet and the link between U–Pb ages and metamorphism. *Chemical geology*, 184(1-2), 123-138.
- Rubatto, D. (2017). Zircon: the metamorphic mineral. *Reviews in mineralogy and geochemistry*, 83(1), 261-295.
- Rudnick, R. L. (1995). Making continental crust. *Nature*, 378(6557), 571-578.
- Rudnick, R.L., and Gao, S. (2014). Composition of the Continental Crust. In H.D. Holland and K.K. Turekian (Eds.), *Treatise on Geochemistry* (2nd ed., pp. 1-51), Elsevier.
- Rutter, M. J., and Wyllie, P. J. (1988). Melting of vapour-absent tonalite at 10 kbar to simulate dehydration–melting in the deep crust. *Nature*, 331(6152), 159-160.
- Sajona, F. G., Maury, R. C., Bellon, H., Cotten, J., and Defant, M. (1996). High field strength element enrichment of Pliocene–Pleistocene Island arc basalts, Zamboanga peninsula, Western Mindanao (Philippines). *Journal of petrology*, 37(3), 693-726.
- Sanborn-Barrie, M., and Regis, D. (2023). Geochemical characterization of plutonic rocks and U-Pb ages of dykes, Boothia Peninsul–Somerset Island, Nunavut. Geological Survey of Canada, Open File 8972.
- Sanborn-Barrie, M., Davis, W. J., Berman, R. G., Rayner, N., Skulski, T., and Sandeman, H. (2014). Neoproterozoic continental crust formation and Paleoproterozoic deformation of the central Rae craton, Committee Bay belt, Nunavut. *Canadian Journal of Earth Sciences*, 51(6), 635-667.
- Sandeman, H. A., Hanmer, S., Tella, S., Armitage, A. A., Davis, W. J., and Ryan, J. J. (2006). Petrogenesis of Neoproterozoic volcanic rocks of the MacQuoid supracrustal belt: a back-arc setting for the northwestern Hearne subdomain, western Churchill Province, Canada. *Precambrian Research*, 144(1-2), 140-165.
- Schiller, D., and Finger, F. (2019). Application of Ti-in-zircon thermometry to granite studies: problems and possible solutions. *Contributions to Mineralogy and Petrology*, 174, 1-16.

- Schultz, M. E. (2007). The Queen Maud Block, Nunavut: genesis of a large felsic igneous province in the earliest Paleoproterozoic and implications for Laurentian geotectonic models. Unpublished MSc thesis. University of Alberta.
- Schultz, M. E., Chacko, T., Heaman, L. M., Sandeman, H. A., Simonetti, A., and Creaser, R. A. (2007). Queen Maud block: A newly recognized Paleoproterozoic (2.4–2.5 Ga) terrane in northwest Laurentia. *Geology*, 35(8), 707-710.
- Scibiorski, E., Tohver, E., and Jourdan, F. (2015). Rapid cooling and exhumation in the western part of the Mesoproterozoic Albany-Fraser Orogen, Western Australia. *Precambrian Research*, 265, 232-248.
- Scott, J.M.J. (2012). Paleoproterozoic (1.75 Ga) Granitoid Rocks and Uranium Mineralization in the Baker Lake – Thelon Basin region, Nunavut. Unpublished MSc thesis, Department of Earth Sciences, Carleton University.
- Searle, M. P., Cottle, J. M., Streule, M. J., and Waters, D. J. (2009). Crustal melt granites and migmatites along the Himalaya: melt source, segregation, transport and granite emplacement mechanisms. *Earth and Environmental Science Transactions of the Royal Society of Edinburgh*, 100(1-2), 219-233.
- Segal, I., Halicz, L., and Platzner, I. T. (2003). Accurate isotope ratio measurements of ytterbium by multiple collection inductively coupled plasma mass spectrometry applying erbium and hafnium in an improved double external normalization procedure. *Journal of Analytical Atomic Spectrometry*, 18(10), 1217-1223.
- Sherlock, R., Pehrsson, S., Logan, A.V., Hrabí, R.B., and Davis, W.J. (2004). Geological setting of the Meadowbank gold deposits, Woodburn Lake Group, Nunavut; *Exploration and Mining Geology*, v. 13, p. 67–107.
- Shinjo, R., and Kato, Y. (2000). Geochemical constraints on the origin of bimodal magmatism at the Okinawa Trough, an incipient back-arc basin. *Lithos*, 54(3-4), 117-137.
- Shirey, S. B., and Hanson, G. N. (1984). Mantle-derived Archaean monzodiorites and trachyandesites. *Nature*, 310(5974), 222-224.
- Shirey, S. B., and Richardson, S. H. (2011). Start of the Wilson cycle at 3 Ga shown by diamonds from subcontinental mantle. *Science*, 333(6041), 434-436.
- Simonetti, A., Heaman, L. M., Chacko, T., and Banerjee, N. R. (2006). In situ petrographic thin section U–Pb dating of zircon, monazite, and titanite using laser ablation–MC–ICP–MS. *International Journal of Mass Spectrometry*, 253(1-2), 87-97.

- Simonetti, A., Heaman, L. M., Hartlaub, R. P., Creaser, R. A., MacHattie, T. G., and Böhm, C. (2005). U–Pb zircon dating by laser ablation-MC-ICP-MS using a new multiple ion counting Faraday collector array. *Journal of Analytical Atomic Spectrometry*, 20(8), 677-686.
- Skipton, D.R., Wodicka, N., McNicoll, V., Saumur, B.M., St-Onge, M.R., and Young, M.D. (2019). U–Pb zircon geochronology of Archean greenstone belts (Mary River Group) and surrounding Archean to zircon geochronology of Archean greenstone belts (Mary River Group) and surrounding Archean to Paleoproterozoic rocks, northern Baffin Island, Nunavut; Geological Survey of Canada, Open File 8585, 1 .zip file. <https://doi.org/10.4095/314944>
- Skjerlie, K. P., and Johnston, A. D. (1992). Vapor-absent melting at 10 kbar of a biotite-and amphibole-bearing tonalitic gneiss: implications for the generation of A-type granites. *Geology*, 20(3), 263-266.
- Skjerlie, K. P., and Johnston, A. D. (1993). Fluid-absent melting behavior of an F-rich tonalitic gneiss at mid-crustal pressures: implications for the generation of anorogenic granites. *Journal of Petrology*, 34(4), 785-815.
- Skulski, T., Sandeman, H., Sanborn-Barrie, M., MacHattie, T., Young, M., Carson, C., Berman, R., Brown, J., Rayner, N., Panagapko, D., Byrne, D., and Deyell, C. (2003). Bedrock geology of the Ellice Hills map area and new constraints on the regional geology of the Committee Bay area, Nunavut; Geological Survey of Canada, Current Research 2003-C22, 11 p.
- Słaby, E., and Martin, H. (2008). Mafic and felsic magma interaction in granites: the Hercynian Karkonosze Pluton (Sudetes, Bohemian Massif). *Journal of Petrology*, 49(2), 353-391.
- Sláma, J., Košler, J., Condon, D. J., Crowley, J. L., Gerdes, A., Hanchar, J. M., Horstwood, M.S.A., Morris, G.A., Nasdala, L., Norberg, N., Schaltegger, U., Schoene, B., Tubrett, M.N., and Whitehouse, M. J. (2008). Plešovice zircon—a new natural reference material for U–Pb and Hf isotopic microanalysis. *Chemical geology*, 249(1-2), 1-35.
- Sliwinski, J. T., Guillong, M., Horstwood, M. S., and Bachmann, O. (2022). Quantifying Long-Term Reproducibility of Zircon Reference Materials by U–Pb LA-ICP-MS Dating. *Geostandards and Geoanalytical Research*, 46(3), 401-409.
- Smithies, R. H., and Champion, D. C. (2000). The Archaean high-Mg diorite suite: links to tonalite–trondhjemite–granodiorite magmatism and implications for early Archaean crustal growth. *Journal of Petrology*, 41(12), 1653-1671.
- Smithies, R. H., Champion, D. C., and Van Kranendonk, M. J. (2009). Formation of Paleoproterozoic continental crust through infracrustal melting of enriched basalt. *Earth and Planetary Science Letters*, 281(3-4), 298-306.

- Smithies, R.H., Champion, D.C., Van Kranendonk, M.J., and Hickman, A.H. (2007). Geochemistry of volcanic rocks of the northern Pilbara craton, Western Australia. Geological Survey of Western Australia, Report 104, 470.
- Söderlund, U., and Johansson, L. (2002). A simple way to extract baddeleyite (ZrO₂). *Geochemistry, Geophysics, Geosystems*, 3(2), 1-7.
- Söderlund, U., Patchett, P. J., Vervoort, J. D., and Isachsen, C. E. (2004). The ¹⁷⁶Lu decay constant determined by Lu–Hf and U–Pb isotope systematics of Precambrian mafic intrusions. *Earth and Planetary Science Letters*, 219(3-4), 311-324.
- Spencer, C. J., Kirkland, C. L., Roberts, N. M. W., Evans, N. J., and Liebmann, J. (2020). Strategies towards robust interpretations of in situ zircon Lu–Hf isotope analyses. *Geoscience Frontiers*, 11(3), 843-853.
- Stacey, J.S., and Kramers, J.D. (1975). Approximation of terrestrial lead isotope evolution by a two-stage model. *Earth and planetary science letters*, 26(2), 207-221.
- Stern, R.A., Card, C.D., Pana, D., and Rayner, N. (2003). SHRIMP U-Pb ages of granitoid basement rocks of the southwestern part of the Athabasca Basin, Saskatchewan and Alberta; Radiogenic Age and Isotopic Studies: Report 16; Geological Survey of Canada, Current Research 2003-F3, 20 p.
- Stern R.A., and Hanson, G.N. (1991). Archean high-Mg granodiorite: a derivative of light rare earth element-enriched monzodiorite of mantle origin. *Journal of Petrology*, 32(1), 201-238.
- Stern, R. A., Bodorkos, S., Kamo, S. L., Hickman, A. H., and Corfu, F. (2009). Measurement of SIMS instrumental mass fractionation of Pb isotopes during zircon dating. *Geostandards and Geoanalytical Research*, 33(2), 145-168.
- Stern, R. A., Hanson, G. N., and Shirey, S. B. (1989). Petrogenesis of mantle-derived, LILE-enriched Archean monzodiorites and trachyandesites (sanukitoids) in southwestern Superior Province. *Canadian Journal of Earth Sciences*, 26(9), 1688-1712.
- Stern, R. J. (2005). Evidence from ophiolites, blueschists, and ultrahigh-pressure metamorphic terranes that the modern episode of subduction tectonics began in Neoproterozoic time. *Geology*, 33(7), 557-560.
- Stern, R. J. (2008). Modern-style plate tectonics began in Neoproterozoic time: An alternative interpretation of Earth's tectonic history. In *When Did Plate Tectonics Begin on Planet Earth?* In Condie, K.C. and Pease, V. (Eds.), *When Did Plate Tectonics Begin on Planet Earth?* (pp. 265-280), Geological Society of America.

- Stern, R. J. (2023). The Orosirian (1800–2050 Ma) plate tectonic episode: Key for reconstructing the Proterozoic tectonic record. *Geoscience Frontiers*, 14(3), 101553.
- Stevenson, R., Henry, P., and Gariépy, C. (1999). Assimilation–fractional crystallization origin of Archean sanukitoid suites: Western Superior Province, Canada. *Precambrian Research*, 96(1-2), 83-99.
- St-Onge, M. R., Searle, M. P., and Wodicka, N. (2006). Trans-Hudson Orogen of North America and Himalaya-Karakoram-Tibetan Orogen of Asia: Structural and thermal characteristics of the lower and upper plates. *Tectonics*, 25(4).
- Streckeisen, A.L., and LeMaitre, R.W. (1979). Chemical approximation to modal QAPF classification of the igneous rocks: *Neues Jahrbuch für Mineralogie*, 136, 169-206.
- Sun, S. S., and McDonough, W. F. (1989). Chemical and isotopic systematics of oceanic basalts: implications for mantle composition and processes. Geological Society, London, Special Publications, 42(1), 313-345.
- Suzuki, K., and Adachi, M. (1991). Precambrian provenance and Silurian metamorphism of the Tsubonosawa paragneiss in the South Kitakami terrane, Northeast Japan, revealed by the chemical Th-U-total Pb isochron ages of monazite, zircon and xenotime. *Geochemical Journal*, 25(5), 357-376.
- Szymanowski, D., Fehr, M. A., Guillong, M., Coble, M. A., Wotzlaw, J. F., Nasdala, L., Ellis, B.S., Bachmann, O., and Schönbächler, M. (2018). Isotope-dilution anchoring of zircon reference materials for accurate Ti-in-zircon thermometry. *Chemical Geology*, 481, 146-154.
- Tanaka, T., Togashi, S., Kamioka, H., Amakawa, H., Kagami, H., Hamamoto, T., Yuhara, M.K., Orihashi, Y., Yoneda, S., Shimizu, H., Kunimaru, T., Takahashi, K., Yanagi, T., Nakano, T., Fujimaki, H., Shinjo, R., Asahara, Y., Tanimizu, M., and Dragusanu, C. (2000). JNdi-1: a neodymium isotopic reference in consistency with LaJolla neodymium. *Chemical Geology*, 168(3-4), 279-281.
- Tang, M., Chen, K., and Rudnick, R. L. (2016). Archean upper crust transition from mafic to felsic marks the onset of plate tectonics. *Science*, 351(6271), 372-375.
- Taylor, F.C. (1958). Nonacho Lake, District of Mackenzie, Northwest Territories. Geological Survey of Canada Map 1281A.
- Taylor, S. R., and McLennan, S. M. (1985). The continental crust: its composition and evolution. Blackwell Scientific Publications.

- Taylor, S.R., and McLennan, S.M. (1995). The geochemical evolution of the continental crust. *Reviews of Geophysics*, 33, 2241-265.
- Tepper, J. H., Nelson, B. K., Bergantz, G. W., and Irving, A. J. (1993). Petrology of the Chilliwack batholith, North Cascades, Washington: generation of calc-alkaline granitoids by melting of mafic lower crust with variable water fugacity. *Contributions to Mineralogy and Petrology*, 113, 333-351.
- Tersmette, D. B. (2012). Geology, geochronology, thermobarometry, and tectonic evolution of the Queen Maud block, Churchill craton, Nunavut, Canada. Unpublished MSc thesis. University of Alberta.
- Thériault, R.J., Henderson, J.B., and Roscoe, S.M. (1994). Nd isotopic evidence for early to mid-Archean crust in high graded gneisses from the Queen Maud Block and south of the McDonald Fault, western Churchill Province, Northwest Territories; in *Radiogenic Age and Isotopic Studies: Report 8; Geological Survey of Canada, Current Research 1994-F*, p. 37-42.
- Thiessen, E. J., Gibson, H. D., Pehrsson, S. J., and Regis, D. (2022). A lithospheric-scale Arrowsmith (2.4 Ga) detachment system with major Trans-Hudson (1.8 Ga) reactivation documented in the Howard Lake shear zone, Rae craton, Canada. *Precambrian Research*, 376, 106683.
- Thiessen, E.J., Regis, D., and Gibson, H.D. (2017). U-Pb zircon geochronology of the Paleoproterozoic Wholdaia Lake shear zone, south Rae craton, Northwest Territories; *Geological Survey of Canada, Open File 8193*, 27 p.
- Thompson, A. B., Schulmann, K., and Jezek, J. (1997). Thermal evolution and exhumation in obliquely convergent (transpressive) orogens. *Tectonophysics*, 280(1-2), 171-184.
- Thrane, K. (2021). The oldest part of the Rae craton identified in western Greenland. *Precambrian Research*, 357, 106139.
- Turner, S. J., and Langmuir, C. H. (2022). Sediment and ocean crust both melt at subduction zones. *Earth and Planetary Science Letters*, 584, 117424.
- Valley, J. W., Kinny, P. D., Schulze, D. J., and Spicuzza, M. J. (1998). Zircon megacrysts from kimberlite: oxygen isotope variability among mantle melts. *Contributions to mineralogy and petrology*, 133, 1-11.
- van Breemen, O., and Bostock, H.H. (1994). Age of emplacement of Thoa metagabbro, western margin of Rae Province, Northwest Territories: initiation of rifting prior to Taltson

- magmatism?; in Radiogenic Age and Isotope Studies: Report 8; Geological Survey of Canada, Current Research 1994-F, p. 61-68.
- van Breemen, O., Hanmer, S.K. and Parrish, R.R. (1990). Archean and Proterozoic mylonites along the southeastern margin of the Slave structural province, Northwest Territories; in Radiogenic Age and Isotopic Studies: Report 3, Geological Survey of Canada, Paper 89-2, p. 55-62.
- van Breemen, O., Kjarsgaard, B.A., Tella, S., Lemkow, D., and Aspler, L. (2013). U-Pb detrital zircon geochronology of clastic sedimentary rocks of the Paleoproterozoic Nonacho and East Arm basins, Thaidene Nene MERA study area, Chapter 4 in Mineral and Energy Resource Assessment for the Proposed Thaidene Nene National Park Reserve in the Area of the East Arm of Great Slave Lake, Northwest Territories, (eds.) D.F. Wright, E.J. Ambrose, D. Lemkow, and G.F. Bonham-Carter; Geological Survey of Canada, Open File 7196, p. 119-142.
- van Breemen, O., Pehrsson, S. and Peterson, T.D. (2007). Reconnaissance U-Pb SHRIMP geochronology and Sm-Nd isotope analyses from the Tehery-Wager Bay gneiss domain, western Churchill Province, Nunavut. Geological Survey of Canada, Current Research 2007-F2, 15 p.
- Van Kranendonk, M. J. (2010). Two types of Archean continental crust: Plume and plate tectonics on early Earth. *American Journal of Science*, 310(10), 1187-1209.
- Vermeesch, P. (2012). On the visualisation of detrital age distributions. *Chemical Geology*, 312, 190-194.
- Vervoort, J. D., and Kemp, A. I. (2016). Clarifying the zircon Hf isotope record of crust–mantle evolution. *Chemical Geology*, 425, 65-75.
- Vervoort, J.D., Kemp, A.I., and Fisher, C.M. (2018). Hf isotope constraints on evolution of the depleted mantle and growth of continental crust. American Geophysical Union, Fall Meeting 2018, abstract #V23A-07.
- Vervoort, J.D., Plank, T., and Prytulak, J. (2011) The Hf-Nd isotopic composition of marine sediments, *Geochimica et Cosmochimica Acta*, 75, 5903-5926.
- Vezelet, A., Pearson, D. G., Thomassot, E., Stern, R. A., Sarkar, C., Luo, Y., and Fisher, C. M. (2018). Hydrothermally-altered mafic crust as source for early Earth TTG: Pb/Hf/O isotope and trace element evidence in zircon from TTG of the Eoarchean Saglek Block, N. Labrador. *Earth and Planetary Science Letters*, 503, 95-107.

- Villeneuve, M.E., Ross, G.M., Theriault, R.J., Miles, W., Parrish, R.R., and Broome, J. (1993). Tectonic subdivision and U-Pb geochronology of the crystalline basement of the Alberta basin western Canada. Geological Survey of Canada, bulletin 447.
- Voice, P. J., Kowalewski, M., and Eriksson, K. A. (2011). Quantifying the timing and rate of crustal evolution: Global compilation of radiometrically dated detrital zircon grains. *The Journal of Geology*, 119(2), 109-126.
- Walsh, N.J. (2013). Geochemistry and geochronology of the Precambrian Basement Domains in the Vicinity of Fort McMurray, Alberta: A Geothermal Perspective. Unpublished MSc thesis. University of Alberta.
- Watkins, J. M., Clemens, J. D., and Treloar, P. J. (2007). Archean TTGs as sources of younger granitic magmas: melting of sodic metatonalites at 0.6–1.2 GPa. *Contributions to Mineralogy and Petrology*, 154(1), 91-110.
- Watson, E. B., and Harrison, T. M. (1983). Zircon saturation revisited: temperature and composition effects in a variety of crustal magma types. *Earth and Planetary Science Letters*, 64(2), 295-304.
- Weller, O. M., Mottram, C. M., St-Onge, M. R., Möller, C., Strachan, R., Rivers, T., and Copley, A. (2021). The metamorphic and magmatic record of collisional orogens. *Nature Reviews Earth and Environment*, 2(11), 781-799.
- Wendt, I., and Carl, C. (1991). The statistical distribution of the mean squared weighted deviation. *Chemical Geology*, 86, 275-285.
- Whalen, J. B., and Hildebrand, R. S. (2019). Trace element discrimination of arc, slab failure, and A-type granitic rocks. *Lithos*, 348, 105179.
- Whalen, J. B., Currie, K. L., and Chappell, B. W. (1987). A-type granites: geochemical characteristics, discrimination and petrogenesis. *Contributions to mineralogy and petrology*, 95, 407-419.
- Whalen, J. B., Percival, J. A., McNicoll, V. J., and Longstaffe, F. J. (2004). Geochemical and isotopic (Nd–O) evidence bearing on the origin of late-to post-orogenic high-K granitoid rocks in the Western Superior Province: implications for late Archean tectonomagmatic processes. *Precambrian Research*, 132(3), 303-326.
- Whalen, J.B., Berman, R.G., Davis, W.J., Sanborn-Barrie, M., and Nadeau, L. (2018). Bedrock geochemistry of the central Thelon tectonic zone, Nunavut. Geological Survey of Canada, Open File 8234.

- Whalen, J.B., Sanborn-Barrie, M., and Chakungal, J. (2011). Geochemical and Nd isotopic constraints from plutonic rocks on the magmatic and crustal evolution of Southhampton Island, Nunavut; Geological Survey of Canada, Current Research 2011-2, 11p.
- Wiedenbeck, M., Hanchar, J. M., Peck, W. H., Sylvester, P., Valley, J., Whitehouse, M., Kronz, A., Morishita, Y., Nasdala, L., Zheng, Y. F., Franchi, I., Girard, J.-P., Greenwood, R.C., Hinton, R., Kita, N., Mason, P.R.D., Norman, M., Ogasawara, M., Piccoli, P.M., Rhede, D., Satoh, H., Schulz-Dobrick, B., Skår, Ø., Spicuzza, M.J., Terada, K., Tindle, A., Togashi, S., Vennemann, T., Xie, Q., and Zheng, Y.-F. (2004). Further characterisation of the 91500 zircon crystal. *Geostandards and Geoanalytical Research*, 28(1), 9-39.
- Wiedenbeck, M., Webb, P.C., Glodny, J., and Meisel, T.C. (2022). An international proficiency test for U-Pb geochronology laboratories. Report on the 2021 Round of G-Chron based on Archean zircon Kara-18. G-Chron, International Association of Geoanalysts.
- Willbold, M., Hegner, E., Stracke, A., and Rocholl, A. (2009). Continental geochemical signatures in dacites from Iceland and implications for models of early Archaean crust formation. *Earth and Planetary Science Letters*, 279(1-2), 44-52.
- Windley, B. F. (1993). Proterozoic anorogenic magmatism and its orogenic connections: Fermor Lecture 1991. *Journal of the Geological Society*, 150(1), 39-50.
- Windley, B. F., Kusky, T., and Polat, A. (2021). Onset of plate tectonics by the Eoarchean. *Precambrian Research*, 352, 105980.
- Wodicka, N., St-Onge, M.R., Scott, D.J. and Corrigan, D. (2002). Preliminary report on the U-Pb geochronology of the northern margin of the Trans-Hudson Orogen, central Baffin Island, Nunavut; Radiogenic Age and Isotopic Studies: Report 15; Geological Survey of Canada, Current Research 2002-F7.
- Workman, R. K., and Hart, S. R. (2005). Major and trace element composition of the depleted MORB mantle (DMM). *Earth and Planetary Science Letters*, 231(1-2), 53-72.
- Zhai, M. (2014). Multi-stage crustal growth and cratonization of the North China Craton. *Geoscience Frontiers*, 5(4), 457-469.

Appendix A: Analytical methods and data verification results

A.1 Sample preparation (chapters 2–5)

Samples were processed for geochemical and geochronological analyses at the University of Alberta. Approximately 0.5–2 kg of rock sample was cut into ~1 cm-thick slabs using a rock saw with a diamond-tipped blade. Any visibly weathered or altered portions of the sample, or any cross-cutting dykes or veins, were removed at this stage. The slabs were then cleaned and left to dry. The clean slabs were placed in polypropylene bags and broken into <1 cm chips using a rock hammer and a steel plate. The sample chips were crushed for ~20 seconds in a tungsten carbide (WC) puck mill, to produce a fine sand-sized fraction for zircon separation. The sand-sized fraction was thoroughly mixed and an aliquot was crushed for a further 2–3 minutes in the same puck mill to produce a powder for whole-rock analyses. Between samples, the puck mill was cleaned with water, ethanol and compressed air, then an aliquot of quartz sand (>99 wt.% SiO₂) was crushed in it for two minutes, and then it was cleaned again. All rock crushing and mineral separation devices were thoroughly cleaned between samples.

For almost all samples, zircon grains were separated using a modified version of the “water-based” baddeleyite separation technique of Söderlund and Johansson (2002). The sample was loaded onto a Wilfley Table one spoonful at a time and two fractions were collected, a “heavy fraction” consisting of the material left on the table after ~60–100 seconds, and a “light fraction” consisting of everything else. Each spoonful of material was allowed to run off the Wilfley Table before repeating the process. Magnetite was removed from the “heavy fraction” with a hand magnet. Zircon grains were picked directly from the “heavy fraction”. Zircon grains from samples HBA-J-622-A-92 and MSB93-139 in chapter 2 were picked from the least magnetic fraction of mineral separates that had been prepared using conventional Wilfley Table, magnetic (Frantz™) and heavy-liquid separation techniques at the Geological Survey of Canada in Ottawa, Ontario (Henderson and Thériault, 1994; McNicoll et al., 2000). Zircon grains from samples 19BN127A and 21BN09A in Chapter 3 were picked from the least magnetic fraction of mineral separates that were prepared using conventional Wilfley Table, magnetic (Frantz™) and heavy liquid separation techniques at the University of Alberta. An effort was made to pick high-quality grains with minimal cracks, inclusions and radiation damage, and grains that were representative of any variation in grain size, morphology or colour. The picked grains were cast in epoxy mounts and polished to their midsections. Backscattered electron (BSE) and/or cathodoluminescence (CL) images of the mounted grains were acquired prior to laser ablation and ion microprobe analyses using a JEOL JXA-8900R electron microprobe, a Zeiss Sigma 3000 scanning electron microscope (SEM) or a Zeiss EVO MA15 SEM.

A.2 Whole-rock major- and trace-element data (chapters 2–5)

A.2.1 Actlabs major- and trace-element data

Whole-rock major- and trace-element data were initially acquired for all samples using the 4Lithoresearch analytical package at Activation Laboratories Ltd. (Actlabs) in Ancaster, Ontario. Using this analytical package, the powders were fused with a lithiumborate flux and then dissolved in nitric acid. The resulting solution was analysed for major-elements by ICP-OES (inductively coupled plasma optical emission spectroscopy) and trace-elements by ICP-MS (inductively coupled plasma mass spectrometry). A reference material (RM) granodiorite rock powder, OREAS-20a (COA-1330-OREAS20a-R0, 2018), was submitted as a blind standard along with the samples to evaluate the accuracy and precision of the data. Replicate analyses of OREAS-20a and some samples are given in tables A-1 and A-2, respectively. Replicate analyses started with the fusion of different aliquots of the same powder, i.e., the entire analytical processes from fusion to ICP analysis was repeated. The OREAS-20a data indicate that the reproducibility is better than 6% (2RSD: two relative standard deviations) for most major elements and better than 10% (2RSD) for most trace elements (Table A-1). Except for Nb and Ba, the average values obtained for OREAS-20a are within the 2SD range of the accepted values (Table A-1). The quality of the Actlabs data is clearly more than sufficient for almost all purposes. However, the accuracy of the Nb measurements (Table A-1), and the reproducibility of the Zr measurements for some samples (Table A-2) was slightly less than desired. Detection limits for Cr and Ni by ICP-MS are also rather high (20 ppm for both in the case of the Actlabs data). The elements Nb, Zr, Cr and Ni were of specific interest for the research reported in chapters 3 and 5, so improvements in the trace-element data were sought for those chapters (section A.2.2).

Table A-1. Actlabs major- and trace-element data for OREAS 20a.

	OREAS-20a						Average	2SD	2RSD(%)	Accepted ¹	2SD ¹
	1	2	3	4	5	6					
SiO2 (wt.%)	65.86	65.96	66.03	65.28	65.37	65.53	65.67	0.64	1	65.51	0.68
Al2O3	15.47	15.28	15.26	15.48	15.36	15.29	15.36	0.20	1	15.52	0.21
FeO(T)	4.82	4.91	4.85	5.00	5.00	5.01	4.93	0.17	3	4.87	0.05
MnO	0.071	0.073	0.072	0.072	0.072	0.072	0.072	0.001	1	0.071	0.002
MgO	2.40	2.41	2.42	2.41	2.41	2.42	2.41	0.01	1	2.44	0.06
CaO	3.50	3.54	3.54	3.70	3.69	3.79	3.63	0.23	6	3.67	0.04
Na2O	2.74	2.74	2.72	2.76	2.79	2.70	2.74	0.06	2	2.77	0.11
K2O	4.09	4.06	4.05	4.19	4.21	4.09	4.11	0.14	3	4.06	0.05
TiO2	0.836	0.830	0.832	0.854	0.852	0.854	0.843	0.022	3	0.841	0.022
P2O5	0.21	0.21	0.22	0.24	0.25	0.25	0.23	0.03	14	0.23	0.01
LOI	0.87	0.96	1.04	1.01	0.97	0.76					
Total	100.9	100.8	100.7	98.88	98.98	98.37					
Sc (ppm)	12	12	12	13	13	12	12	1	8	NR	NR
V	112	113	113	112	113	113	113	1	1	114	20
Ga	19	17	18	17	18	17	18	2	9	19	2
Rb	236	215	225	227	228	223	226	14	6	233	10
Sr	300	295	297	302	300	296	298	5	2	299	12
Y	29.6	27.5	28.4	29.3	29.8	28.5	28.9	1.7	6	29.2	1.0
Zr	297	299	306	293	302	302	300	9	3	303	23
Nb	18.1	16.3	18.0	17.6	18.3	16.8	17.5	1.6	9	20.4	1.1
Cs	15.0	14.1	14.3	14.3	14.7	14.3	14.5	0.7	5	NR	12.0
Ba	1148	1146	1143	1183	1185	1162	1161	38	3	1082	31
La	44.4	41.7	42.2	42.9	43.2	41.8	42.7	2.0	5	41.9	2.0
Ce	86.4	80.7	81.9	83.1	84.3	81.2	82.9	4.3	5	82.0	2.6
Pr	9.55	9.06	9.14	10.20	10.40	10.10	9.74	1.14	12	9.36	0.36
Nd	35.2	33.2	34.0	37.8	37.7	36.7	35.8	3.9	11	35.2	1.1
Sm	6.92	6.53	6.60	7.41	7.65	7.15	7.04	0.89	13	6.66	0.20
Eu	1.42	1.36	1.39	1.47	1.50	1.49	1.44	0.11	8	1.44	0.08
Gd	5.55	5.19	5.36	5.99	6.01	5.82	5.65	0.68	12	5.79	0.30
Tb	0.86	0.85	0.83	0.95	0.97	0.93	0.90	0.12	13	0.88	0.05
Dy	5.30	5.18	5.01	5.55	5.64	5.36	5.34	0.47	9	5.24	0.28
Ho	1.05	0.98	1.01	1.10	1.11	1.08	1.06	0.10	10	1.07	0.05
Er	2.92	2.89	2.83	3.23	3.30	3.12	3.05	0.39	13	3.08	0.14
Tm	0.440	0.404	0.414	0.457	0.471	0.461	0.441	0.054	12	0.450	0.015
Yb	2.91	2.81	2.81	3.08	3.19	3.16	2.99	0.34	12	2.96	0.20
Lu	0.455	0.432	0.445	0.454	0.519	0.504	0.468	0.070	15	0.450	0.028
Hf	7.4	6.9	7.1	6.5	6.8	6.7	6.9	0.6	9	7.9	0.4
Pb	25	24	23	22	23	20	23	3	15	21	2
Th	22.4	20.5	21.7	22.4	22.6	21.5	21.9	1.6	7	22.0	0.8
U	6.74	6.02	6.93	6.88	7.02	6.65	6.71	0.72	11	6.69	0.36

Major elements are normalized to 100% with all Fe expressed as FeO

Totals are reported as measured, with all Fe as Fe2O3

1: Accepted values and their 2SD are from the certificate of analysis, COA-1330-OREAS20a-RO (2018)

LOI: loss on ignition; SD: standard deviation; RSD: relative standard deviation; NR: not reported

Table A-2. Actlabs major- and trace-element data for sample duplicates/triplicates.

	18BN27A (Ch.3)				19BN126B (Ch.3)				19BN173A (Ch.3)				21BN09A (Ch.3)			
	1	2	Diff	%Diff	1	2	Diff	%Diff	1	2	Diff	%Diff	1	2	Diff	%Diff
SiO2 (wt.%)	49.57	49.13	0.44	1	65.56	65.40	0.17	0	61.27	62.25	0.97	2	56.44	56.37	0.07	0
Al2O3	17.86	18.20	0.34	2	16.62	17.12	0.51	3	17.78	16.70	1.08	6	16.86	17.05	0.19	1
FeO(T)	11.49	11.67	0.18	2	4.80	4.73	0.06	1	5.74	5.64	0.09	2	8.98	8.97	0.02	0
MnO	0.193	0.184	0.009	5	0.095	0.095	0.000	0	0.096	0.105	0.008	8	0.138	0.129	0.009	7
MgO	4.54	4.68	0.14	3	1.56	1.61	0.05	3	2.81	2.67	0.14	5	2.82	2.96	0.14	5
CaO	8.73	8.43	0.30	4	4.16	3.92	0.24	6	5.43	5.59	0.16	3	6.82	6.48	0.34	5
Na2O	3.30	3.29	0.01	0	3.88	3.83	0.06	1	3.53	3.59	0.06	2	2.80	2.88	0.08	3
K2O	2.22	2.23	0.02	1	2.49	2.47	0.01	1	2.29	2.42	0.13	5	2.70	2.77	0.08	3
TiO2	1.561	1.659	0.098	6	0.610	0.608	0.002	0	0.858	0.829	0.029	3	1.646	1.692	0.046	3
P2O5	0.55	0.51	0.03	6	0.23	0.22	0.01	5	0.20	0.21	0.01	6	0.81	0.71	0.10	13
LOI	1.55	1.66		7	0.99	1.19		17	1.26	1.29		2	1.13	1.10		3
Total	99.81	100.1		0	100.4	100.8		0	99.30	98.36		1	100.1	100.5		0
Sc (ppm)	35	35	0	0	12	12	0	0	17	17	0	0	23	23	0	0
V	291	278	13	5	61	59	2	3	109	112	3	3	194	188	6	3
Ga	27	25	2	8	20	21	1	5	21	21	0	0	25	24	1	4
Rb	80	80	0	0	74	78	4	5	92	88	4	5	151	158	7	4
Sr	536	549	13	2	592	612	20	3	549	524	25	5	620	638	18	3
Y	51.0	46.5	4.5	10	11.8	12.3	0.5	4	11.4	12.2	0.8	7	38.0	34.4	3.6	10
Zr	144	125	19	15	227	239	12	5	158	121	37	31	375	386	11	3
Nb	16.4	15.1	1.3	9	9.2	10.8	1.6	15	9.2	9.4	0.2	2	20.9	20.2	0.7	3
Cs	0.5	0.4	0.1	25	1.4	1.4	0.0	0	0.7	0.6	0.1	17	7.2	7.2	0.0	0
Ba	574	583	9	2	1681	1648	33	2	901	894	7	1	1149	1225	76	6
La	51.2	51.1	0.1	0	65.7	72.3	6.6	9	33.1	35.4	2.3	6	103.0	93.3	9.7	10
Ce	134.0	134.0	0.0	0	126.0	138.0	12.0	9	71.9	76.0	4.1	5	228.0	204.0	24.0	12
Pr	18.50	18.30	0.20	1	13.80	14.80	1.00	7	9.12	9.41	0.29	3	27.50	25.10	2.40	10
Nd	78.9	80.8	1.9	2	51.5	51.9	0.4	1	37.6	38.6	1.0	3	109.0	102.0	7.0	7
Sm	16.40	16.20	0.20	1	7.40	7.45	0.05	1	6.88	7.25	0.37	5	19.00	17.20	1.80	10
Eu	2.62	2.78	0.16	6	1.92	1.86	0.06	3	1.75	1.70	0.05	3	3.83	3.62	0.21	6
Gd	12.90	12.60	0.30	2	4.08	4.43	0.35	8	4.66	4.71	0.05	1	12.70	11.80	0.90	8
Tb	1.88	1.86	0.02	1	0.49	0.53	0.04	8	0.60	0.59	0.01	2	1.60	1.57	0.03	2
Dy	9.70	10.00	0.30	3	2.39	2.57	0.18	7	2.82	2.81	0.01	0	8.69	7.94	0.75	9
Ho	1.79	1.88	0.09	5	0.45	0.47	0.02	4	0.51	0.50	0.01	2	1.51	1.45	0.06	4
Er	4.78	5.14	0.36	7	1.23	1.21	0.02	2	1.25	1.34	0.09	7	4.03	3.69	0.34	9
Tm	0.647	0.702	0.055	8	0.167	0.163	0.004	2	0.156	0.165	0.009	5	0.529	0.508	0.021	4
Yb	4.07	4.36	0.29	7	1.09	1.06	0.03	3	0.97	1.00	0.03	3	3.35	3.04	0.31	10
Lu	0.624	0.614	0.010	2	0.185	0.194	0.009	5	0.148	0.160	0.012	8	0.499	0.436	0.063	14
Hf	3.8	3.1	0.7	23	4.8	5.2	0.4	8	3.5	3.1	0.4	13	5.2	7.8	2.6	33
Pb	13	12	1	8	12	15	3	20	9	10	1	10	13	12	1	8
Th	1.81	1.72	0.09	5	8.19	9.17	0.98	11	0.25	0.27	0.02	7	6.92	6.21	0.71	11
U	0.73	0.69	0.04	6	0.54	0.58	0.04	7	0.29	0.28	0.01	4	1.49	1.29	0.20	16

	18BN17E (Ch.5)				19BN154C (Ch.5)				TX08-036 (Ch.5)				18BN14B (Ch.3)				
	1	2	Diff	%Diff	1	2	Diff	%Diff	1	2	Diff	%Diff	1	2	3	2SD	2RSD(%)
SiO2 (wt.%)	69.73	69.72	0.01	0	74.69	75.29	0.60	1	73.00	73.86	0.86	1	56.37	56.43	56.34	0.08	0
Al2O3	14.67	14.93	0.26	2	13.57	13.06	0.50	4	13.81	13.26	0.55	4	18.18	18.15	18.45	0.33	2
FeO(T)	3.52	3.47	0.04	1	1.35	1.40	0.04	3	2.74	2.77	0.04	1	7.90	7.89	7.82	0.09	1
MnO	0.039	0.036	0.004	11	0.021	0.021	0.000	1	0.031	0.030	0.001	4	0.159	0.156	0.151	0.008	5
MgO	0.85	0.85	0.00	0	0.34	0.36	0.01	3	0.89	0.90	0.01	1	4.98	5.03	5.06	0.08	2
CaO	1.54	1.54	0.00	0	1.38	1.41	0.03	2	0.54	0.54	0.01	1	6.34	6.35	6.18	0.19	3
Na2O	3.13	3.02	0.11	4	2.675	2.578	0.097	4	2.84	2.74	0.10	3	3.04	2.94	3.00	0.11	4
K2O	5.76	5.69	0.07	1	5.74	5.67	0.07	1	5.75	5.48	0.27	5	2.28	2.31	2.27	0.05	2
TiO2	0.600	0.613	0.013	2	0.188	0.186	0.002	1	0.331	0.316	0.015	5	0.605	0.603	0.612	0.010	2
P2O5	0.16	0.13	0.03	23	0.03	0.02	0.01	49	0.07	0.08	0.01	12	0.13	0.15	0.11	0.03	25
LOI	1.17	1.00		17	0.81	0.84		4	1.19	1.19		0	2.75	2.83	2.81		3
Total	100.3	99.87		0	100.0	99.51		0	100.2	99.89		0	99.93	98.71	99.85		1
Sc (ppm)	5	4	1	25	2	2	0	0	4	4	0	0	24	24	24	0	0
V	47	46	1	2	14	14	0	0	29	24	5	21	165	156	156	10	7
Ga	23	22	1	5	15	16	1	6	19	19	0	0	20	18	18	2	12
Rb	194	203	9	4	171	173	2	1	173	180	7	4	75	72	73	3	4
Sr	228	230	2	1	235	238	3	1	103	101	2	2	537	547	540	10	2
Y	27.8	27.6	0.2	1	3.1	3.1	0.0	0	21.0	22.0	1.0	5	15.0	14.4	13.2	1.8	13
Zr	582	598	16	3	82	92	10	11	257	247	10	4	79	76	78	3	4
Nb	16.1	14.8	1.3	9	2.4	4.0	1.6	40	9.0	9.0	0.0	0	4.4	5.2	4.3	1.0	21
Cs	0.4	0.4	0.0	0	0.5	0.6	0.1	17		0.3	0.3		0.8	0.7	0.7	0.1	16
Ba	2135	2066	69	3	489	493	4	1	1463	1457	6	0	662	677	666	16	2
La	175.0	177.0	2.0	1	41.7	41.4	0.3	1	134.0	138.0	4.0	3	11.4	11.8	11.3	0.5	5
Ce	344.0	359.0	15.0	4	79.9	77.6	2.3	3	257.0	263.0	6.0	2	30.6	30.9	29.6	1.4	4
Pr	35.70	35.40	0.30	1	8.05	8.46	0.41	5	26.10	26.50	0.40	2	4.15	4.69	4.16	0.62	14
Nd	116.0	120.0	4.0	3	25.7	27.3	1.6	6	83.9	85.1	1.2	1	17.1	19.0	17.3	2.1	12
Sm	16.20	16.20	0.00	0	2.98	3.43	0.45	13	12.90	12.80	0.10	1	3.30	3.66	3.47	0.36	10
Eu	1.58	1.58	0.00	0	0.86	0.91	0.05	5	0.85	0.79	0.06	7	1.01	1.11	1.05	0.10	10
Gd	9.26	9.89	0.63	6	1.46	1.56	0.10	6	7.60	7.58	0.02	0	2.80	3.03	2.67	0.36	13
Tb	1.21	1.31	0.10	8	0.13	0.15	0.02	13	1.00	0.99	0.01	1	0.40	0.47	0.45	0.07	16
Dy	6.01	6.34	0.33	5	0.60	0.65	0.05	8	4.90	4.81	0.09	2	2.43	2.77	2.56	0.34	13
Ho	1.02	1.09	0.07	6	0.10	0.11	0.01	9	0.80	0.82	0.02	2	0.48	0.54	0.53	0.06	12
Er	2.60	2.83	0.23	8	0.26	0.30	0.04	13	2.10								

A.2.2 F&M XRF and WSU ICP-MS trace-element data

For all samples in chapters 3 and 5, the same rock powders that were submitted to Actlabs (above) were also analyzed for trace-elements by fusion-dissolution ICP-MS at Washington State University (WSU) in the Peter Hooper GeoAnalytical laboratory (REE, Ba, Rb, Cs, Sr, Pb, U, Th, Nb, Y, Zr, Hf and Sc), and by pressed-powder briquette XRF (X-ray fluorescence) at Franklin and Marshall (F&M) College in Dr. Stan Merztman's laboratory (La, Ce, Ba, Rb, Sr, Pb, U, Th, Nb, Y, Zr, Ni, Cr, V, Sc and Ga). The WSU ICP-MS technique is described in detail by Knaack et al. (1994). The RM OREAS-20a was submitted as a blind standard along with the samples to both laboratories. The WSU lab provided data for several other RMs that were also analyzed alongside the samples. The ICP-MS and XRF data for replicate analyses of the RMs and some samples are reported in tables A-3, A-4 and A-5. The replicate analyses of OREAS-20a and samples started with different aliquots of the same powder, i.e. the entire analytical processes from fusion/pressed-powder briquette production to ICP/XRF analysis was repeated. The reproducibility of the RMs analyzed at WSU is better than 4% (2RSD) for most elements and better than 6% (2RSD) for all elements, and the data are accurate at this level of precision (Table A-3). The F&M XRF data were procured primarily for the purpose of obtaining Ni and Cr concentrations at reasonably low detection limits (<2 ppm), and three measurements of OREAS-20a yielded reasonably accurate and precise results for both elements (Table A-5).

In all cases where trace-element data are available from multiple techniques (Actlabs ICP-MS, WSU ICP-MS and F&M XRF), the WSU data are favoured in light of the excellent accuracy and reproducibility of the data for multiple RMs and samples (Tables A-3 and A-4). ***The data used in chapters 3 and 5 are as follows: Major elements, TiO₂ and P₂O₅ by ICP-OES at Actlabs; Ni, Cr, V and Ga by XRF at F&M College; and all other trace elements by ICP-MS at WSU.***

Table A-3. Washington State University ICP-MS trace-element data for RMs.

	OREAS-20a										AGV-2			
	1	2	3	4	5	6	Ave.	2SD	2RSD(%)	Accpt. ¹	2SD ¹	1	Accpt. ²	2SD ²
La (ppm)	41.77	41.69	41.75	41.67	41.41	41.67	41.66	0.26	1	41.90	1.99	39.71	38.21	0.38
Ce	82.06	81.81	81.77	82.23	81.17	82.11	81.86	0.76	1	82.00	2.60	71.57	69.43	0.57
Pr	9.521	9.563	9.581	9.542	9.522	9.540	9.545	0.047	0	9.360	0.359	8.433	8.165	0.084
Nd	35.20	35.11	35.27	35.19	35.18	35.02	35.16	0.17	0	35.20	1.10	31.15	30.49	0.47
Sm	6.70	6.73	6.79	6.78	6.63	6.80	6.74	0.13	2	6.66	0.20	5.62	5.51	0.08
Eu	1.451	1.453	1.451	1.488	1.426	1.429	1.450	0.045	3	1.440	0.078	1.600	1.553	0.015
Gd	5.822	5.873	5.806	5.857	5.828	5.924	5.852	0.086	1	5.790	0.296	4.650	4.678	0.064
Tb	0.913	0.934	0.935	0.922	0.928	0.929	0.927	0.016	2	0.880	0.051	0.656	0.651	0.007
Dy	5.32	5.40	5.44	5.24	5.32	5.33	5.34	0.14	3	5.24	0.28	3.62	3.55	0.03
Ho	1.068	1.076	1.065	1.069	1.056	1.072	1.068	0.014	1	1.070	0.049	0.689	0.682	0.008
Er	2.933	2.972	3.011	2.988	2.986	3.055	2.991	0.081	3	3.080	0.140	1.788	1.825	0.013
Tm	0.4760	0.4671	0.4689	0.4732	0.4671	0.4713	0.4706	0.0071	2	0.4500	0.0150	0.2694	0.2623	0.0035
Yb	2.969	2.944	2.934	2.985	2.956	3.036	2.971	0.073	2	2.960	0.195	1.670	1.653	0.013
Lu	0.467	0.469	0.452	0.449	0.470	0.477	0.464	0.022	5	0.450	0.028	0.258	0.251	0.003
Ba	1081.7	1091.3	1091.3	1084.7	1085.5	1083.1	1086.3	8.2	1	1082	31	1148.0	1134.0	8.0
Th	22.58	22.66	22.69	22.27	22.30	22.40	22.48	0.37	2	22.00	0.82	6.43	6.17	0.06
Nb	20.99	20.84	21.05	20.87	21.00	20.96	20.95	0.16	1	20.40	1.13	14.24	14.12	0.22
Y	30.50	30.56	30.69	30.60	30.55	30.71	30.60	0.17	1	29.20	0.99	20.02	19.14	0.84
Hf	7.91	7.94	7.90	7.77	7.85	7.97	7.89	0.14	2	7.91	0.41	5.25	5.14	0.06
U	6.77	6.74	6.62	6.71	6.60	6.53	6.66	0.19	3	6.69	0.36	1.90	1.89	0.02
Pb	23.34	23.40	23.28	22.97	23.05	22.90	23.16	0.42	2	21.40	1.73	13.61	13.14	0.15
Rb	227.0	227.4	229.6	224.2	225.7	222.9	226.1	4.8	2	233	10	68.0	67.8	0.7
Cs	15.23	15.28	15.38	15.17	15.08	15.19	15.22	0.20	1	NR	NR	1.16	1.17	0.02
Sr	293.0	292.0	291.7	295.5	293.3	288.0	292.3	5.0	2	299	12	664.1	659.5	5.7
Sc	12.52	12.43	12.33	12.48	12.50	12.72	12.50	0.25	2	NR	NR	12.66	13.11	0.31
Zr	292.9	294.5	296.2	293.9	297.7	297.7	295.5	4.1	1	303	23	234.0	232.0	2.3

	BCR-2						BHVO-2				
	1	2	3	Ave.	2SD	2RSD(%)	Accpt. ²	2SD ²	1	Accpt. ²	2SD ²
La (ppm)	25.59	25.14	25.95	25.56	0.81	3	25.08	0.81	15.57	15.20	0.08
Ce	53.37	52.84	54.23	53.48	1.40	3	53.12	1.40	37.72	37.53	0.19
Pr	6.833	6.816	6.921	6.857	0.113	2	6.827	0.113	5.399	5.339	0.028
Nd	28.75	28.40	28.96	28.70	0.57	2	28.26	0.57	24.57	24.27	0.25
Sm	6.70	6.50	6.78	6.66	0.29	4	6.55	0.29	6.07	6.02	0.06
Eu	1.946	1.947	2.023	1.972	0.088	4	1.989	0.088	2.098	2.043	0.012
Gd	6.814	6.756	6.827	6.799	0.076	1	6.811	0.076	6.288	6.207	0.038
Tb	1.107	1.091	1.089	1.096	0.019	2	1.077	0.019	0.970	0.939	0.006
Dy	6.42	6.34	6.49	6.42	0.16	2	6.42	0.16	5.31	5.28	0.03
Ho	1.303	1.321	1.321	1.315	0.020	2	1.313	0.020	0.991	0.989	0.005
Er	3.635	3.519	3.607	3.587	0.122	3	3.670	0.122	2.439	2.511	0.014
Tm	0.5392	0.5233	0.5448	0.5357	0.0223	4	0.5341	0.0223	0.3393	0.3349	0.0031
Yb	3.262	3.258	3.299	3.273	0.045	1	3.392	0.045	1.931	1.994	0.027
Lu	0.529	0.510	0.515	0.518	0.020	4	0.505	0.020	0.281	0.275	0.002
Ba	665.8	664.7	678.6	669.7	15.4	2	683.9	15.4	129.9	130.9	1.0
Th	5.88	5.98	6.10	5.99	0.23	4	5.83	0.23	1.24	1.22	0.02
Nb	12.27	12.05	12.37	12.23	0.32	3	12.44	0.32	18.20	18.10	0.20
Y	35.59	35.19	36.14	35.64	0.95	3	36.07	0.95	26.10	25.91	0.28
Hf	4.89	4.84	4.85	4.86	0.05	1	4.97	0.05	4.48	4.47	0.03
U	1.66	1.67	1.69	1.67	0.03	2	1.68	0.03	0.42	0.41	0.04
Pb	10.24	10.34	10.47	10.35	0.23	2	10.59	0.23	1.71	1.65	0.04
Rb	44.5	44.9	46.9	45.4	2.6	6	46.0	2.6	9.2	9.3	0.1
Cs	1.18	1.21	1.21	1.20	0.03	3	1.16	0.03	0.11	0.10	0.00
Sr	326.4	328.1	341.5	332.0	16.5	5	337.4	16.5	394.0	394.1	1.7
Sc	32.91	32.10	33.05	32.69	1.03	3	33.53	1.03	32.27	31.83	0.34
Zr	181.0	178.8	184.9	181.6	6.2	3	186.5	6.2	168.7	171.2	1.3

1. Accepted values and their 2SD are from the certificat of analysis COA-1330-OREASa-RO (2018)

2. Accepted values and their 2SD are from Jochum et al. (2016)

Ave: average; Accpt: accepted; SD: standard deviation; RSD: relative standard deviation; Diff: difference; %Diff: percent difference

Table A-4. Washington State University ICP-MS trace-element data for sample duplicates.

	19BN154A (Ch.3)				21BN30A (Ch.3)				18BN27A				19BN173A			
	1	2	Diff	%Diff	1	2	Diff	%Diff	1	2	Diff	%Diff	1	2	Diff	%Diff
La (ppm)	97.55	97.15	0.40	0	60.72	61.28	0.56	1	51.01	51.58	0.57	1	33.68	31.55	2.13	7
Ce	174.64	176.06	1.42	1	120.44	121.41	0.97	1	131.08	134.30	3.22	2	72.07	67.50	4.57	7
Pr	18.427	18.321	0.106	1	13.379	13.410	0.031	0	19.030	19.151	0.121	1	9.452	8.791	0.661	8
Nd	61.77	60.99	0.78	1	46.26	46.09	0.17	0	82.47	82.79	0.32	0	38.44	36.37	2.07	6
Sm	8.31	8.41	0.10	1	7.50	7.42	0.08	1	16.85	17.12	0.26	2	7.05	6.72	0.33	5
Eu	1.867	1.870	0.003	0	0.959	0.996	0.038	4	2.740	2.772	0.033	1	1.763	1.679	0.084	5
Gd	5.537	5.564	0.027	0	5.164	5.237	0.073	1	13.313	13.732	0.419	3	4.879	4.615	0.264	6
Tb	0.749	0.735	0.015	2	0.711	0.725	0.015	2	1.917	1.937	0.021	1	0.615	0.559	0.057	10
Dy	3.81	3.85	0.04	1	3.64	3.63	0.00	0	10.24	10.28	0.04	0	2.92	2.71	0.21	8
Ho	0.724	0.701	0.023	3	0.652	0.662	0.010	1	1.935	1.947	0.012	1	0.510	0.483	0.027	6
Er	1.919	1.880	0.039	2	1.663	1.674	0.011	1	5.126	5.283	0.156	3	1.270	1.195	0.075	6
Tm	0.2740	0.2686	0.0054	2	0.2311	0.2303	0.0008	0	0.7213	0.7359	0.0146	2	0.1759	0.1666	0.0093	6
Yb	1.724	1.708	0.016	1	1.299	1.311	0.012	1	4.232	4.268	0.036	1	1.048	0.981	0.067	7
Lu	0.279	0.264	0.015	6	0.174	0.189	0.015	8	0.650	0.605	0.045	8	0.154	0.150	0.004	3
Ba	1525.5	1506.5	19.0	1	672.8	676.5	3.7	1	560.1	558.4	1.6	0	860.6	790.2	70.5	9
Th	15.96	15.85	0.12	1	21.91	21.83	0.08	0	1.91	2.01	0.10	5	0.28	0.37	0.09	24
Nb	10.64	10.42	0.22	2	11.66	11.68	0.02	0	17.66	17.55	0.11	1	11.37	10.59	0.78	7
Y	20.53	19.73	0.81	4	17.70	17.72	0.01	0	54.75	53.43	1.32	2	13.46	12.42	1.04	8
Hf	6.27	6.08	0.20	3	4.30	4.43	0.13	3	3.86	3.70	0.17	5	3.80	3.55	0.25	7
U	1.77	1.78	0.01	1	1.30	1.30	0.00	0	0.74	0.76	0.02	3	0.29	0.30	0.01	4
Pb	20.20	20.22	0.02	0	25.56	25.33	0.23	1	16.60	16.76	0.17	1	12.72	11.90	0.81	7
Rb	142.4	140.4	2.0	1	185.6	185.6	0.0	0	80.8	81.1	0.3	0	90.6	83.5	7.0	8
Cs	1.91	1.86	0.05	3	2.41	2.44	0.03	1	0.43	0.46	0.03	6	0.75	0.72	0.03	4
Sr	613.7	588.7	25.0	4	238.1	235.4	2.8	1	578.2	553.8	24.3	4	552.8	507.7	45.1	9
Sc	13.58	13.17	0.41	3	9.31	9.32	0.01	0	36.28	36.29	0.01	0	17.87	16.11	1.76	11
Zr	258.9	245.6	13.4	5	144.9	147.6	2.8	2	142.0	137.1	4.9	4	150.8	140.7	10.1	7

Diff: difference; %Diff: percent difference

Table A-5. Franklin and Marshall College XRF trace element data for OREAS-20a and a sample duplicate.

	OREAS-20a								17-12A (Ch.5)			
	1	2	3	Average	2SD	2RSD(%)	Accepted ¹	2SD ¹	1	2	Diff	%Diff
Rb (ppm)	223.7	223.5	224.1	223.8	0.6	0.3	233	10.0	137.3	138.6	1.3	0.9
Sr	280	280	280	280	0	0	299	12	308	310	2	1
Y	30.2	29.0	30.7	30.0	1.7	6	29.2	1.0	16.8	18.5	1.7	9
Zr	264	261	260	262	4	2	303	23	496	497	1	0
V	115	113	117	115	4	3	114	20	36	39	3	8
Ni	35	36	35	35	1	3	41	8	7	8	1	13
Cr	84	85	94	88	11	13	87	20	7	4	3	75
Nb	19.5	19.5	19.5	19.5	0	0	20.4	1	15.4	15.3	0.1	1
Ga	18.1	17.7	18.1	18.0	0.46	3	19.4	2.3	11.9	11.9	0	0
Ba	1026	1013	1043	1027	30	3	1082	31	1928	1979	51	3
La	38	45	37	40	9	22	42	2	167	175	8	5
Ce	90	86	92	89	6	7	82	3	322	371	49	13
U	6.9	7.2	6.9	7.0	0.3	5	6.7	0	1.1	0.7	0.4	57
Th	21.6	21.0	21.8	21.5	0.8	4	22	0.8	35.2	34.9	0.3	1
Sc	12	13	15	13	3	23	NR	NR	3	3	0	0
Pb	22	23	22	22	1	5	21	2	19	18	1	6

¹: Accepted values and their 2SD are from certificate of analysis COA-1330-OREAS20a-RO (2018)

SD: standard deviation; RSD: relative standard deviation; Diff: difference; %Diff: percent difference; NR: not reported

A.3 Tungsten carbide puck mill contamination test

Some tungsten carbide mills have been reported to cause Nb and Ta contamination (e.g., Johnson et al., 1999). To examine the contamination levels in the WC puck mill used here, one aliquot of the quartz cleaning sand was powdered in the WC puck mill, and another was powdered in an agate puck mill. Both powders were sent to the Peter Hooper Geoanalytical Laboratory at WSU for major-element analysis by XRF (X-ray fluorescence) and trace-element analysis by XRF and fusion-dissolution ICP-MS (inductively coupled plasma – mass spectrometry). The XRF and ICP-MS techniques are detailed in Johnson et al. (1999) and Knaack et al. (1994), respectively. The data for the two aliquots are compared in table A-6. The small difference in the Nb concentrations measured by ICP-MS (inductively coupled plasma-mass spectrometry) between the two aliquots (0.11 ppm; Table A-6) is less than the analytical reproducibility (2SD) for Nb (Table A-3), indicating that Nb contamination is either non-existent or negligible. On the other hand, the quartz sand crushed in WC yielded 0.14 ppm more Ta than the quartz sand crushed in agate (Table A-6), which is far greater than the analytical reproducibility (2SD) for this element (Table A-3). Considering the low Ta contents of the samples in the present study (average = 0.71 ppm), this is a significant level of contamination and therefore no Ta data are reported.

Table A-6. Major- and trace-element data for quartz cleaning sand crushed in tungsten carbide (Qtz Sand WC) and agate (Qtz Sand Agate).

XRF	Qtz Sand WC	Qtz Sand Agate	Difference	ICP-MS	Qtz Sand WC	Qtz Sand Agate	Difference
SiO2 (wt.%)	99.69	99.64	0.04	Ba (ppm)	5.2	5.5	-0.3
TiO2	0.020	0.021	0.001	Rb	0.5	0.4	0.1
Al2O3	0.09	0.12	0.02	Cs	0.01	0.01	0.00
FeO(T)	0.07	0.07	0.01	Sr	8.0	8.4	-0.3
MnO	0.001	0.001	0.000	Pb	0.82	0.90	-0.08
MgO	0.00	0.00	0.00	Th	0.46	0.45	0.01
CaO	0.10	0.10	0.00	U	0.23	0.21	0.02
Na2O	0.00	0.00	0.00	La	2.34	2.29	0.05
K2O	0.03	0.04	0.01	Ce	4.51	4.38	0.12
P2O5	0.005	0.005	0.001	Pr	0.529	0.529	0.000
Total	99.57	99.94		Nd	2.03	1.91	0.12
				Sm	0.36	0.41	-0.04
Ni (ppm)	1.6	6.6	5.0	Eu	0.075	0.076	-0.001
Cr	4.2	4.1	0.1	Gd	0.400	0.408	-0.008
Sc	0.0	0.0	0.0	Tb	0.066	0.063	0.002
V	1.6	2.1	0.5	Dy	0.38	0.37	0.01
Ba	0.0	3.6	3.6	Ho	0.078	0.073	0.004
Rb	1.0	1.4	0.4	Er	0.202	0.210	-0.008
Sr	10.0	10.6	0.6	Tm	0.0288	0.0315	-0.0027
Zr	49.9	51.0	1.1	Yb	0.199	0.195	0.004
Y	2.2	2.8	0.5	Lu	0.030	0.031	-0.001
Nb	0.0	0.0	0.0	Y	2.25	2.23	0.01
Ga	0.0	0.0	0.0	Nb	0.36	0.25	0.11
La	0.0	0.0	0.0	Ta	0.16	0.02	0.14
Ce	5.9	2.1	3.8	Zr	47.4	42.2	5.22
Th	0.8	0.7	0.1	Hf	1.28	1.17	0.11
Nd	3.8	2.2	1.6	Sc	0.11	0.13	-0.02
U	1.1	0.7	0.3				

XRF and ICPMS data from the Peter Hooper Geoanalytical laboratory at Washington State University

Major-elements are normalized to 100% with all Fe as FeO

Totals are reported as measured, with all Fe as Fe2O3

WC: tungsten carbide

A.4 Whole-rock Sm-Nd isotope data (chapters 2, 3 and 5)

Whole-rock Sm-Nd isotope data were acquired by isotope dilution MC-ICPMS in Dr. Rob Creaser's laboratory, University of Alberta. Samples powders were weighed and totally spiked with a known amount of mixed ^{150}Nd - ^{149}Sm tracer solution. Powders were dissolved in a mixture of 24N HF + 16N HNO_3 in sealed PFA Teflon vessels at 160 °C for 5 days. The fluoride residues were converted to chloride with HCl, and Nd and Sm were separated by conventional cation and HDEHP-based chromatography. Chemical processing blanks are <300 picograms for both Sm and Nd. Further details are given in Creaser et al. (1997).

The isotopic compositions of Sm and Nd were determined on a Nu Plasma MC-ICPMS (Nu instruments, UK). Instrumental mass bias was corrected using an exponential mass fractionation law, and $^{146}\text{Nd}/^{144}\text{Nd}$ and $^{152}\text{Sm}/^{154}\text{Sm}$ ratios of 0.7219 and 1.17537, respectively. The $^{143}\text{Nd}/^{144}\text{Nd}$ ratios are reported relative to a value of 0.511850 for the La Jolla Nd isotopic standard, which was monitored by measurements of an in-house Afla Nd isotopic standard in each analytical session. The Geological Survey of Japan isotope standard, J-Ndi-1 (Tanaka et al., 2000), was analyzed as an "unknown" in each analytical session. Over the period of this study, the laboratory average $^{143}\text{Nd}/^{144}\text{Nd}$ for J-Ndi-1 was 0.512094 ± 0.000011 (2SD, n=29), which is in agreement with the recommended value of 0.512099 ± 0.000005 (2SD) (Garçon et al., 2018). Measurements of the basalt RM BCR-1 yield $^{147}\text{Sm}/^{144}\text{Nd}$ ratios between 0.1380 and 0.1382, consistent with values reported from isotope dilution techniques in the literature. The long-term external reproducibility (2RSD) is ~0.2% for $^{147}\text{Sm}/^{144}\text{Nd}$ and ~0.003% (or ~0.3 ϵNd units) for $^{143}\text{Nd}/^{144}\text{Nd}$. Replicate analyses of three samples in this study reproduced within ≤ 0.3 initial ϵNd units (Table A-7).

Initial ϵNd values were calculated using the CHUR (chondritic uniform reservoir) values of Bouvier et al. (2008). Depleted mantle model ages (T_{DM}) were calculated using the linear model of Goldstein et al. (1984). Both calculations employed the ^{147}Sm decay constant of Lugmair and Marti (1978). Uncertainties on initial ϵNd values are propagated to include the long term external reproducibility of $^{147}\text{Sm}/^{144}\text{Nd}$ and $^{143}\text{Nd}/^{144}\text{Nd}$, the internal 2SE on $^{143}\text{Nd}/^{144}\text{Nd}$, and uncertainty in the samples age. An age uncertainty of +/- 10 Myr was assumed for samples that were not dated directly.

Table A-7. Sm-Nd isotope data for replicate analyses of three samples.

	19BN126B (Ch.3)		21BN15A (Ch.3)		18BN20C (Ch.5)	
	1	2	1	2	1	2
Sm (ppm)	7.151	7.158	9.298	9.316	20.99	21.90
Nd (ppm)	51.12	50.54	38.47	38.59	158.00	165.31
¹⁴⁷Sm/¹⁴⁴Nd	0.0846	0.0856	0.1461	0.1460	0.0803	0.0801
¹⁴³Nd/¹⁴⁴Nd(0)	0.510816	0.510825	0.511819	0.511800	0.510366	0.510366
2SE	0.000010	0.000010	0.000007	0.000008	0.000007	0.000009
t (Ma)	2500	2500	2500	2500	2320	2320
¹⁴³Nd/¹⁴⁴Nd(t)	0.509422	0.509414	0.509411	0.509394	0.509138	0.509142
εNd(t)	0.4	0.3	0.2	-0.1	-9.7	-9.7
T_{DM} (Ga)	2.75	2.77	3.01	3.05	3.17	3.17

¹⁴³Nd/¹⁴⁴Nd ratios are normalized to a value of 0.511850 for the La Jolla Nd isotopic standard

T_{DM} are from the linear depleted mantle model of Goldstein et al. (1984)

T_{DM}: depleted mantle model age; SE: standard error

A.5 LA-MC-ICPMS zircon and monazite U-Pb isotope data (Chapters 2–5)

Most of the U-Pb age data in this thesis were acquired by LA-MC-ICPMS (laser ablation multi-collector inductively coupled plasma mass spectrometry), using analytical procedures modified from Simonetti et al. (2005 and 2006). A New Wave 213 nm Nd:YAG laser ablation system (New Wave Research, USA) was used to ablate zircon and monazite for 30s with a repetition rate of 4 Hz, a fluence of 2–3 J/cm², and beam diameters of 25 µm (zircon) and 12 µm (monazite). Output from the ablation cell was joined to the output from a Nu plasma desolvating nebulizer (DSN-100) that aspirated a TI solution (NIST SRM 997). Data were collected in 30 1s integrations on a Nu Plasma MC-ICPMS (Nu Instruments, UK), which measured masses ²⁰³Tl, ²⁰⁴Pb+Hg, ²⁰⁵Tl, ²⁰⁶Pb, ²⁰⁷Pb and ²³⁸U statically (see Simonetti et al., 2005 for Faraday cup and ion counter configuration). Lead isotope mass bias was corrected by measuring ²⁰⁵Tl/²⁰³Tl in the aspirated TI solution, assuming a natural ²⁰⁵Tl/²⁰³Tl ratio of 2.3871 and using an exponential mass fractionation law. On peak gas + acid blanks (30s) were measured before every 10 unknown analyses. Primary (data calibration) and secondary (data verification) RMs were analyzed once or twice before every 10 unknowns.

The data were reduced offline using an in-house Excel-based program. Sample and secondary RM zircon data were normalized to the in-house zircon RM LH94-15 (1830 Ma; Ashton et al., 1999). Sample and secondary RM monazite data were normalized to the in-house monazite RM Western Australia (2843 Ma; L.M. Heaman, unpublished ID-TIMS date). Rare analyses were screened if they had: inconsistent and unresolvable (mixed) time-integrated ²⁰⁷Pb/²⁰⁶Pb or ²⁰⁶Pb/²³⁸U signals, >10% discordance, or 204 cps >100 and 206/204 <4000. The 204 cps and 206/204 ratio screen was employed to exclude data that may be influenced by common Pb. No common Pb correction was applied to the data. The screened analyses are included in the data tables, with a note stating the reason for their exclusion. The accuracy of the zircon data was verified in each analytical session by analyzing one or two of the following RMs as an unknown: OG1 (3465 Ma; Stern et al., 2009), Kara18 (2632 Ma; Wiedenbeck et al., 2022) and FC1 (1099 Ma; Paces and Miller, 1998) (Table A-8). The accuracy of the monazite data was verified in one of the two monazite sessions by analysing the in-house monazite RM TG09 (2555 Ma; R.A Stern, unpublished ID-TIMS date) as an unknown (Table A-8).

Table A-8. Secondary zircon and monazite RM results for the LA-MC-ICPMS U-Pb method.

		Secondary zircon reference materials														
Session	Chapters	OG1: 3465.4 +/- 0.6 Ma					Kara18: 2632.5 +/- 1.1 Ma					FC1: 1099.0 +/- 0.6 Ma				
		WM Age	2SE	2σ	n	MSWD	WM Age	2SE	2σ	n	MSWD	WM Age	2SE	2σ	n	MSWD
July 10 2020	Ch3	3469	5	7	5/5	0.22	<i>Not measured</i>					<i>Not measured</i>				
July 13 2020	Ch3	3463	5	7	4/4	0.06	<i>Not measured</i>					<i>Not measured</i>				
April 13 2021	Ch3	3467	3	6	10/10	0.35	<i>Not measured</i>					1102	7	9	10/10	1.40
April 15 2021	Ch3	3459	4	6	9/9	0.29	<i>Not measured</i>					1098	6	8	9/9	0.94
April 20 2021	Ch2	3467	3	6	11/11	0.81	<i>Not measured</i>					1108	8	10	10/11	1.60
April 21 2021	Ch2	3462	3	6	11/11	1.15	<i>Not measured</i>					1101	5	8	9/11	0.74
May 28 2021	Ch3, Ch4, Ch5	3466	3	5	15/15	1.12	<i>Not measured</i>					<i>Not measured</i>				
Nov 16 2021	Ch2	3462	3	6	13/13	0.28	<i>Not measured</i>					1091	4	7	12/12	0.53
Nov 17 2021	Ch2, Ch4	3463	3	6	13/14	0.62	<i>Not measured</i>					1097	4	7	14/14	0.62
Nov 18 2021	Ch5	3468	4	6	10/10	0.63	2638	4	7	8/8	0.56	<i>Not measured</i>				
Feb 28 2022	Ch3	3465	3	5	15/15	0.42	<i>Not measured</i>					1099	4	7	14/14	0.41
March 1 2022	Ch3, Ch5	3465	3	6	13/13	1.16	<i>Not measured</i>					1096	5	8	9/9	0.89
March 2 2022	Ch3, Ch5	3463	3	6	11/11	0.42	<i>Not measured</i>					1094	4	7	11/11	0.43
April 25 2022	Ch3	3462	3	5	16/16	1.03	<i>Not measured</i>					1090	5	8	10/10	0.08
April 26 2022	Ch3	3462	3	6	11/11	0.21	<i>Not measured</i>					1091	5	8	10/10	0.40
April 27 2022	Ch3	3465	3	6	11/11	0.80	<i>Not measured</i>					1099	9	11	9/9	2.50
April 28 2022	Ch3	3469	4	6	7/7	0.36	<i>Not measured</i>					1092	6	8	6/6	0.21
Aug 8 2022	Ch3, Ch5	3463	3	6	15/15	0.79	2635	4	6	16/16	1.16	<i>Not measured</i>				
Aug 9 2022	Ch5	3467	3	6	13/13	0.68	2639	4	6	13/13	0.89	<i>Not measured</i>				
Oct 25 2022	Ch3	3465	5	7	5/5	0.78	2636	9	11	5/5	1.50	<i>Not measured</i>				
Oct 24 2022	Ch2, Ch5	3464	3	5	17/17	0.31	2636	3	6	19/19	0.55	<i>Not measured</i>				
March 20 2023	Ch3	3464	3	5	17/17	0.54	2637	3	6	19/19	1.01	<i>Not measured</i>				
Sept 14 2023	Ch3, Ch5	3464	4	6	6/6	0.27	2635	3	6	13/13	0.27	1099	9	11	8/8	2.00
Aug 11 2022_R	Ch5	3469	4	6	11/11	0.7	2624	5	7	11/11	0.46	<i>Not measured</i>				

		Secondary monazite reference material				
Session	Chapters	TG09: 2554.5 +/- 1.4 Ma				
		WM Age	2SE	2σ	n	MSWD
June 20 2019	Ch4	<i>Not measured</i>				
Nov 19 2021	Ch4	2550	5	7	10/10	0.36

WM Age: weighted mean ²⁰⁷Pb/²⁰⁶Pb age in Ma; n: number of analyses used/number of analyses made

2σ uncertainties include long-term external reproducibility in the weighted mean ²⁰⁷Pb/²⁰⁶Pb ratio

Reference ages are from Stern et al. (2009) for OG1, Wiedenbeck et al. (2022) for Kara18 and Paces and Miller (1998) for FC1

In session "Aug 11 2022_R", sample and reference material zircon grains were analysed by rastering a ~15 μm laser beam for ~30 μm

A.6 Split-stream LA-ICPMS zircon U-Pb-Hf isotope data (Chapter 2)

Split-stream LA-ICPMS zircon U-Pb-Hf isotope data were acquired following the analytical methods described in Fisher et al. (2017) and Vezinet et al. (2018). Zircon grains were ablated with a RESOLUTION ArF 193 nm excimer laser ablation system (Applied Spectra, USA), using a 33 μm beam, a repetition rate of 8 Hz and a fluence of $\sim 6.5 \text{ J/cm}^2$. One half of the ablated material was sent to an Element II XR ICPMS (Thermo Fisher Scientific, USA) for U-Th-Pb isotope determination. The other half was sent to a Neptune Plus MC-ICPMS (Thermo Fisher Scientific, USA) for concurrent Lu-Yb-Hf isotope determination. Each analysis comprised a 30 s gas background measurement followed by 60 s of ablation and 40 s of sample washout. The Element monitored ^{202}Hg , $^{204}\text{Pb}+\text{Hg}$, ^{208}Pb , ^{232}Th , ^{206}Pb , ^{207}Pb and ^{238}U by peak-hopping, and the Neptune monitored ^{172}Yb , ^{173}Yb , ^{175}Lu , $^{176}\text{Hf}+\text{Yb}+\text{Lu}$, ^{177}Hf , ^{178}Hf , ^{179}Hf , ^{180}Hf and ^{181}Hf statically (see Vezinet et al., 2018 for Faraday cup configuration). Primary and secondary zircon RMs were analyzed one to three times before every twelve unknowns.

Data were reduced offline using the Lolite v3 software (Paton et al., 2011; Fisher et al., 2017). U-Pb isotope ratios were normalized to the in-house zircon RM LH94-15 (1830 Ma; Ashton et al., 1999) and Hf isotope ratios were normalized to Plésovice (Slama et al., 2008). Downhole fractionation of U and Pb was corrected by fitting an exponential curve to analyses of LH94-15 (Paton et al., 2010). Hafnium and Yb mass bias were determined using a $^{179}\text{Hf}/^{177}\text{Hf}$ ratio of 0.7325 and a $^{173}\text{Yb}/^{172}\text{Yb}$ ratio of 0.738891 (Segal et al., 2003), respectively. Isobaric Interference of ^{176}Yb on ^{176}Hf was corrected for by iteratively adjusting the $^{176}\text{Yb}/^{173}\text{Yb}$ ratio until both MUN1 and MUN3 synthetic zircon (Fisher et al., 2011) yielded identical and accurate $^{176}\text{Hf}/^{177}\text{Hf}$ ratios (Table A-9). The veracity of the Yb interference correction is confirmed by the lack of correlation between $^{176}\text{Yb}/^{177}\text{Hf}$ and $^{176}\text{Hf}/^{177}\text{Hf}$ for all sample and RM zircon analyses, and by the fact that MUN3 zircon yielded $^{176}\text{Yb}/^{177}\text{Hf}$ ratios greater than any of the samples (Figure A-1). Analyses were trimmed to only integrate sections with consistent U-Pb, Pb-Pb and Hf isotope compositions. Analyses were screened if they had: variable and unresolvable (mixed) $^{207}\text{Pb}/^{206}\text{Pb}$, $^{206}\text{Pb}/^{238}\text{U}$, or $^{176}\text{Hf}/^{177}\text{Hf}$ ratios; >10% discordance; an internal 2SE >3 ϵHf ; or >1% ^{206}Pb (fraction of ^{206}Pb that is common). No common Pb correction was applied to the data. The screened analyses are included in the data tables, with a note stating the reason for their exclusion. $^{176}\text{Hf}/^{177}\text{Hf}(t)$ calculations employed the ^{176}Lu decay constant of Söderlund et al. (2004) and $\epsilon\text{Hf}(t)$ values were calculated using the CHUR values of Bouvier et al. (2008). Uncertainties on $\epsilon\text{Hf}(t)$ values were propagated to include the internal 2SE on $^{176}\text{Lu}/^{177}\text{Hf}$ and $^{176}\text{Hf}/^{177}\text{Hf}$ ratios, and uncertainty on the $^{207}\text{Pb}/^{206}\text{Pb}$ date or the assigned rock age.

The accuracy of the U-Pb data was evaluated with the secondary zircon RM OG1 (Table A-10) (Stern et al., 2009), and the accuracy of Hf isotope data was evaluated with the secondary RMs

OG1 (Kemp et al., 2017) and 91500 (Blitchert-Toft, 2008) (Table A-9). All weighted mean $^{207}\text{Pb}/^{206}\text{Pb}$ ages are within 10 Myr of the accepted OG1 age (Table A-10), and all weighted mean $^{176}\text{Hf}/^{177}\text{Hf}$ ratios are within uncertainty of the accepted values (Table A-9).

A.7 Single-stream LA-MC-ICPMS zircon Hf isotope data

For chapter 3 and two samples in chapter 2 (RF-86-49A and TX08-027), zircon Hf isotope data were acquired by single-stream rather than split-stream LA-ICPMS. In this case, the Hf isotope analyses were made directly overlapping or adjacent to, and in the same zircon growth domain, as the ablation pits from LA-MC-ICPMS U-Pb dating (section A.5). The analytical methods were the same as those described for the split-stream LA-ICPMS U-Pb-Hf method (section A.6), except that all of the ablated material was sent to the Neptune MC-ICPMS for Lu-Yb-Hf isotope determination. When necessary, analyses were trimmed to only include a consistent $^{176}\text{Hf}/^{177}\text{Hf}$ signal that began at the start of the analysis (i.e., began during ablation of the same zircon domain from which the LA-MC-ICPMS U-Pb data were acquired). Again the effectiveness of the Yb interference correction is confirmed by the lack of a correlation between $^{176}\text{Hf}/^{177}\text{Hf}$ and $^{176}\text{Yb}/^{177}\text{Hf}$ for all sample and RM zircon analyzes, and by the fact that MUN3 zircon yields greater $^{176}\text{Yb}/^{177}\text{Hf}$ ratios than the samples (Figure A-1). All weighted mean $^{176}\text{Hf}/^{177}\text{Hf}$ ratios obtained for the secondary RMs 91500 and OG1 are within uncertainty of the accepted values (Table A-9).

Table A-9. Secondary zircon RM Hf isotope results for split-stream LA-ICPMS U-Pb-Hf and single-stream LA-MC-ICPMS Hf isotope methods.

			Secondary zircon reference materials							
Method	Session	Chapter	MUN1 $^{176}\text{Hf}/^{177}\text{Hf}$: 0.282135 +/- 7				MUN3 $^{176}\text{Hf}/^{177}\text{Hf}$: 0.282135 +/- 7			
			WM $^{176}\text{Hf}/^{177}\text{Hf}$	2SE	n	MSWD	WM $^{176}\text{Hf}/^{177}\text{Hf}$	2SE	n	MSWD
Split-stream U-Pb-Hf	June 25 2021	Ch2	0.282132	10	10	0.74	0.282136	17	10	1.4
Split-stream U-Pb-Hf	July 7 2021	Ch2	0.282143	11	8	0.55	0.282127	13	8	0.83
Split-stream U-Pb-Hf	July 9 2021	Ch2	0.282143	18	7	1.4	0.282134	17	7	1.1
Split-stream U-Pb-Hf	July 12 2021	Ch2	0.282127	11	7	0.70	0.282143	16	7	1.2
Single-stream Hf	July 6 2022	Ch2	0.282140	38	4	1.90	0.282133	21	4	0.05
Single-stream Hf	Dec 20 2022	Ch2, Ch3	0.282132	7	8	0.68	0.282138	9	8	1.7
Single-stream Hf	Dec 21 2022	Ch3	0.282137	16	9	4.90	0.282132	10	9	2.2
Method	Session	Chapter	91500 $^{176}\text{Hf}/^{177}\text{Hf}$: 0.282308 +/- 6				OG1 $^{176}\text{Hf}/^{177}\text{Hf}$: 0.280554 +/- 3			
			WM $^{176}\text{Hf}/^{177}\text{Hf}$	2SE	n	MSWD	WM $^{176}\text{Hf}/^{177}\text{Hf}$	2SE	n	MSWD
Split-stream U-Pb-Hf	June 25 2021	Ch2	0.282309	12	21	1.3	0.280566	12	21	1.4
Split-stream U-Pb-Hf	July 7 2021	Ch2	0.282307	15	19	1.5	0.280555	13	18	1.2
Split-stream U-Pb-Hf	July 9 2021	Ch2	0.282319	16	15	1.5	0.280561	15	15	1.4
Split-stream U-Pb-Hf	July 12 2021	Ch2	0.282310	18	16	1.9	0.280566	11	16	0.57
Single-stream Hf	July 6 2022	Ch2	0.282308	23	9	1.2	0.280554	16	9	0.72
Single-stream Hf	Dec 20 2022	Ch2, Ch3	0.282305	8	9	0.70	0.280552	10	9	1.2
Single-stream Hf	Dec 21 2022	Ch3	0.282306	14	10	2.3	0.280551	9	14	1.5

WM: weighted mean; n: number of analyses

2SE uncertainties are in the fifth or sixth decimal place

$^{176}\text{Hf}/^{177}\text{Hf}$ ratios for MUN1, MUN3 and 91500 are as measured.

$^{176}\text{Hf}/^{177}\text{Hf}$ ratios for OG1 are calculated at 3467 Ma

Reference values from Fisher et al. (2011) for MUN, Blichert-Toft (2008) for 91500, and Kemp et al. (2017) for OG1

Table A-10. Secondary zircon RM U-Pb age results for the split-stream LA-ICPMS U-Pb-Hf isotope method.

		Secondary zircon reference material				
		OG1: 3465.4 +/- 0.6				
Session	Chapter	WM Age	2SE	2 σ	n	MSWD
June 25 2021	Ch2	3459	2	5	21/21	0.93
July 7 2021	Ch2	3458	3	5	18/18	1.10
July 9 2021	Ch2	3454	3	6	15/15	0.56
July 12 2021	Ch2	3461	3	5	16/16	0.80

WM Age: weighted mean $^{207}\text{Pb}/^{206}\text{Pb}$ age in Ma; SE: standard error

n: number of analyses used/number of analyses made

2 σ uncertainties include estimated long-term reproducibility of the weighted mean $^{207}\text{Pb}/^{206}\text{Pb}$ ratio

Reference age for OG1 from Stern et al. (2009)

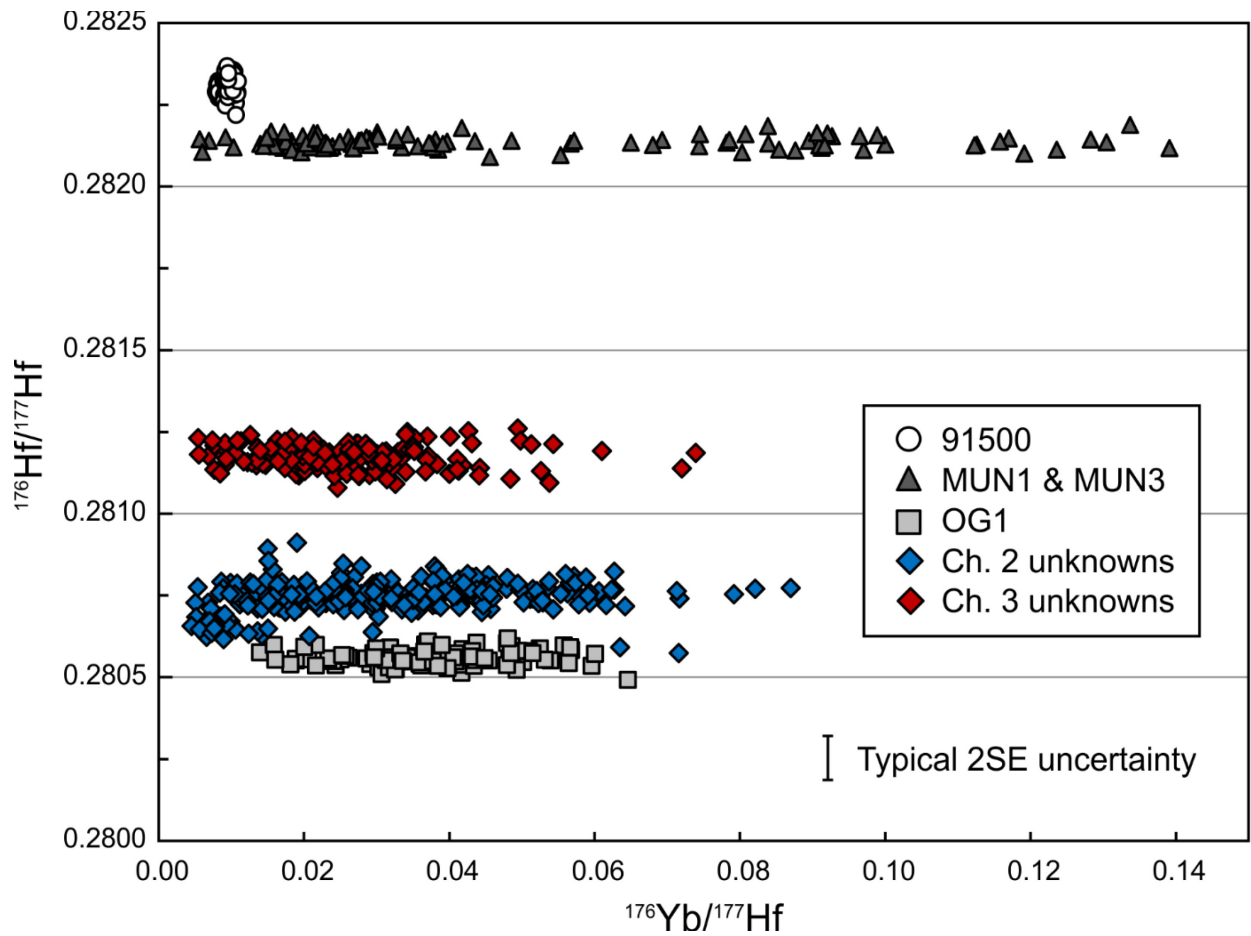


Figure A-1. $^{176}\text{Yb}/^{177}\text{Hf}$ vs. $^{176}\text{Hf}/^{177}\text{Hf}$ for unknown and secondary RM zircons analysed by split-stream LA-ICPMS U-Pb-Hf and single-stream LA-MC-ICPMS Hf isotope methods. $^{176}\text{Hf}/^{177}\text{Hf}$ values for MUN1 and MUN3 are as measured (present-day). $^{176}\text{Hf}/^{177}\text{Hf}$ values for 91500 and OG1 are calculated at their accepted ages. $^{176}\text{Hf}/^{177}\text{Hf}$ values for unknown zircons are calculated at the crystallization age of the sample.

A.8 LA-ICPMS zircon U-Pb-TE(trace-element) data (chapter 4)

Coupled LA-ICPMS zircon U-Pb age and trace-element (TE) data were acquired for two samples in chapter 4. Ablations were conducted with a RESOLUTION ArF 193 nm excimer laser ablation system (Applied Spectra, USA), using a 25 μm diameter laser beam, a repetition rate of 6 Hz and a fluence of $\sim 4 \text{ J/cm}^2$. An Element II-XR SC-ICPMS (Thermo Fisher Scientific, USA) was used to measure masses ^{49}Ti , ^{157}Gd , ^{172}Yb , ^{202}Hg , $^{204}\text{Pb}+\text{Hg}$, ^{206}Pb , ^{207}Pb , ^{208}Pb , ^{232}Th and ^{238}U . Each analysis comprised 50 s of washout and background measurement followed by 35 s of ablation. Primary and secondary RMs were analyzed 1–3 times before every 12 unknowns. Data were reduced offline using the *lolyte* v3 software (Paton et al., 2011). The trace-element data were calibrated internally using ^{29}Si (assumed zircon Si concentration 15.32%) and externally with NIST SRM 612. The U-Pb data were normalized to the in-house zircon RM LH94-15 (1830 Ma; Ashton et al., 1999). Analyses were trimmed to only integrate sections with consistent isotope ratios and trace-element signals. Analyses were screened if they: appeared to intersect inclusions (indicated by large positive excursions in $^{204}\text{Pb}+\text{Hg}$ or ^{49}Ti signals); exhibited inconsistent and unresolvable (mixed) isotope ratios; or had 204 cps >100 and 206/204 <4000 . The 204 cps and 206/204 ratio screen was employed to exclude data that may be influenced by common Pb. No common Pb correction was applied to the data. The screened analyses are included in the data tables, with a note stating the reason for their exclusion. Secondary zircon RMs OG1 and FC1 were used to confirm the accuracy of the U-Pb data (Table A-11). Zircon 91500 was used as a secondary RM to evaluate the quality of the trace-element data, and the average concentrations obtained in each session are within 2SD of the working or accepted values (Table A-12). Zircon 91500 was not used to evaluate the U-Pb data because its very low U content (Wiedenbeck et al., 2004) results in ^{206}Pb and ^{207}Pb count rates that are typically an order of magnitude lower than those of the sample zircons and the other RM zircons.

Table A-11. Zircon secondary RM U-Pb age results for the LA-ICPMS U-Pb-TE method.

Secondary zircon reference materials											
Session	Chapter	OG1: 3465.4 +/- 0.6 Ma					FC1: 1099.0 +/- 0.6 Ma				
		WM Age	2SE	2σ	n	MSWD	WM Age	2SE	2σ	n	MSWD
April 7 2022	Ch4	3468	7	8	9/9	0.13	1103	11	13	8/8	0.80
April 8 2022	Ch4	3466	8	10	7/7	0.49	1110	14	15	7/7	0.56
April 11 2022	Ch4	3457	8	10	12/12	1.3	1110	18	19	11/12	2.3
April 12 2022	Ch4	3450	22	22	6/6	2.7	1084	18	19	6/6	0.65

WM Age: weighted mean ²⁰⁷Pb/²⁰⁶Pb age in Ma; SE: standard error; n: number of analyses used/number of analyses made
 2σ uncertainties include estimated long-term external reproducibility in the weighted mean ²⁰⁷Pb/²⁰⁶Pb ratio
 Reference ages are from Stern et al. (2009) and Paces and Miller (1998) for FC1

Table A-12. Zircon 91500 trace-element results for the LA-ICPMS U-Pb-TE method, compared to working/accepted values.

Accepted/working zircon 91500 values											
	Ti ppm	2SD	Gd ppm	2SD	Yb ppm	2SD	Th ppm	2SD	U ppm	2SD	
Working LA-ICPMS values ¹	NR	NR	2.21	0.49	73.9	7.4	29.9	4.2	80	16	
Working SIMS values ¹	NR	NR	1.76	0.77	60.1	16.8	NR	NR	NR	NR	
Isotope-dilution value ²	4.76	0.15	NR	NR	NR	NR	NR	NR	NR	NR	

Average zircon 91500 values obtained												
Session	Chapter	n	Ti ppm	2SD	Gd ppm	2SD	Yb ppm	2SD	Th ppm	2SD	U ppm	2SD
April 7 2022	Ch4	8	5.9	2.0	2.00	0.60	58.0	5.4	25.8	2.8	71.2	4.6
April 8 2022	Ch4	7	5.4	1.9	2.00	0.60	60.3	1.3	26.1	1.4	72.2	1.8
April 11 2022	Ch4	12	5.5	2.9	2.00	0.40	59.9	2.2	26.4	0.6	71.7	2.8
April 12 2022	Ch4	6			1.70	0.50	54.8	5.1	24.1	2.7	68.4	5.6

1: working LA-ICPMS and SIMS values from Wiedenbeck et al. (2004)

2: Isotope-dilution Ti concentration from Szymanowski et al. (2018)

n: number of analyses made; SD: standard deviation; NR: not reported

No Ti data for April 12 2022 session, due to an analytical error

A.9 LA-ICPMS zircon trace-element data (chapter 5)

LA-ICPMS zircon trace-element data were acquired for samples in chapter 5. Ablations were conducted with a RESOLUTION ArF 193 nm excimer laser ablation system (Applied Spectra, USA), using a 25 μm diameter laser beam, a repetition rate of 8 Hz and a fluence of $\sim 4 \text{ J/cm}^2$. An Element II XR ICPMS (Thermo Fisher Scientific, USA) was used to measure masses ^{29}Si , ^{31}P , ^{43}Ca , ^{49}Ti , ^{91}Zr , ^{137}Ba , ^{139}La , ^{140}Ce , ^{141}Pr , ^{146}Nd , ^{147}Sm , ^{153}Eu , ^{157}Gd , ^{159}Tb , ^{163}Dy , ^{165}Ho , ^{166}Er , ^{169}Tm , ^{172}Yb , ^{175}Lu , ^{178}Hf , ^{232}Th and ^{238}U . Data were reduced offline using the Lolite v3 software (Paton et al., 2011). The trace-element data were calibrated internally using ^{29}Si (assumed zircon Si concentration of 15.32 wt. %) and externally with NIST SRM 612. See Vezinet et al. (2018) for further details. The time-resolved data were trimmed to only integrate consistent trace-element signals. Analyses that appeared to intersect inclusions or strongly altered zircons domains, as indicated by large positive deviations in P, Ti, Ca, Ba and/or La signals, were excluded from consideration. Some analyses showing signs of fluid alteration (elevated Ca, Ba and/or LREE contents) were retained because the elements of interest (Ti, Th, U and the HREE) appear unaffected. Zircon 91500 was used as a secondary RM to evaluate the quality of the trace-element data, and the average concentrations obtained are typically within 2SD of the working or accepted values (Table A-13).

Table A-13. Zircon 91500 trace-element results for the LA-ICPMS trace-element method.

Working/Accepted zircon 91500 values							Zircon 91500 values obtained	
	Working SIMS values ¹	2SD	Working LA-ICPMS values ₁	2SD	Isotope-dilution value ²	2SD	Average	2SD
P	NR		NR		NR		18	10
Ca	NR		NR		NR			
Ti	NR		NR		4.76	0.15	4.4	1.5
La	0.013	0.022	0.0060	0.0065	NR			
Ce	2.56	0.41	2.56	0.51	NR		2.11	0.26
Pr	0.020	0.011	0.024	0.030	NR			
Nd	0.250	0.095	0.240	0.077	NR		0.150	0.071
Sm	0.380	0.061	0.50	0.15	NR		0.32	0.11
Eu	0.190	0.042	0.240	0.058	NR		0.177	0.043
Gd	1.76	0.77	2.21	0.49	NR		1.77	0.40
Tb	0.78	0.23	0.86	0.14	NR		0.69	0.12
Dy	10.3	1.9	11.8	1.7	NR		8.90	0.12
Ho	4.60	0.92	4.84	0.68	NR		3.76	0.59
Er	23.7	5.2	24.6	4.9	NR		20.3	3.3
Tm	6.0	1.4	6.9	0.69	NR		5.00	0.80
Yb	60	17	73.9	7.4	NR		52.1	8.4
Lu	14.1	3.4	13.1	2.1	NR		10.7	1.9
Hf	NR		NR		NR		4608	825
Th	NR		29.9	4.2	NR		24.2	3.8
U	NR		80	16	NR		67	8

1: working LA-ICPMS and SIMS values from Wiedenbeck et al. (2004)

2: Isotope-dilution Ti concentration from Szymanowski et al. (2018)

n: number of analyses made; SD: standard deviation; NR: not reported

Ca and Pr measurements were typically below detection limit.

All La measurements were below detection limit.

A.10 SIMS zircon oxygen isotope data (chapter 2)

SIMS (secondary ion mass spectrometry) zircon oxygen isotope data were acquired for samples reported in chapter 2. The zircon grains, including RMs, were cast in a 25 mm diameter epoxy mount, then ground and polished to 1 μm finish using diamond grits. The mount was coated with 25 nm of high-purity Au prior to SEM imaging with a Zeiss EVO MA15 instrument equipped with a high-sensitivity, broadband CL detector. Both BSE and CL images were acquired prior to SIMS analyses. Beam conditions were 15kV and 3-5 nA sample current. A further 100 nm of Au was subsequently deposited prior to SIMS analysis.

Oxygen isotope (^{18}O , ^{16}O) measurements were made in two sessions, using a IMS 1280 multicollector ion microprobe (CAMECA Instruments Inc.). A $^{133}\text{Cs}^+$ primary beam was operated with impact energy of 20 keV and beam current of ~ 2.0 nA. The ~ 10 μm diameter primary was rastered (20×20 μm) at the analysis site for 30 s prior to acquisition, and then over a 3×3 μm area during analysis. The normal incidence electron gun was utilized for charge compensation. Negative secondary ions were extracted through 10 kV potential into the secondary (Transfer) column. Transfer conditions included a 122 μm entrance slit, a 5×5 mm pre-ESA (field) aperture, and 100x (MA80) sample magnification at the field aperture. The mass/charge separated oxygen ions were detected simultaneously in Faraday cups L'2 ($^{16}\text{O}^-$) and H'2 ($^{18}\text{O}^-$) at mass resolutions ($m/\Delta m$ at 10%) of 1950 and 2250, respectively. Secondary ion count rates for $^{16}\text{O}^-$ and $^{18}\text{O}^-$ were typically $\sim 2 \times 10^9$ and 4×10^6 counts/s utilizing $10^{10} \Omega$ and $10^{12} \Omega$ amplifier circuits, respectively. Faraday cup baselines were measured at the start of the analytical session. A single analysis took 240 s, including pre-analysis primary beam rastering, automated secondary ion tuning, and 75 s of continuous peak counting.

Instrumental mass fractionation (IMF) was monitored by repeated analysis of the primary zircon RM S0081 ($\delta^{18}\text{O}_{\text{VSMOW}} = 4.87$ ‰; R. Stern, unpublished laser fluorination data, University of Oregon), once after every four unknowns. The $^{18}\text{O}^-/^{16}\text{O}^-$ data set for S0081 was processed collectively for each analytical session, yielding standard deviations of 0.09 ‰ for the first session and 0.08 ‰ for the second session, following correction for systematic within-session drift. The individual spot uncertainties in $\delta^{18}\text{O}_{\text{VSMOW}}$ (VSMOW: Vienna standard mean ocean water) for the unknowns are typically $\sim \pm 0.2$ ‰ at 95% confidence, which include errors relating to within-spot counting statistics, between-spot (geometric) effects, and correction for instrumental mass fractionation. Data accuracy was verified with the secondary zircon RM TEM2 ($\sim \delta^{18}\text{O} \sim 8.2$ ‰; Black et al., 2004), which was analyzed after every 12 unknowns. Weighted mean TEM2 $\delta^{18}\text{O}$ values were 8.22 ± 0.05 ‰ ($n=21$, MSWD=1.3) for one session and 8.25 ± 0.04 ‰ ($n=24$, MSWD=1.1) for the other.

A.11 Electron microprobe zircon Ca, U and Hf concentration data (chapter 2)

The zircon grains analyzed for their oxygen isotope composition in chapter 2 were also analyzed for their Ca, U and Hf contents using a SX100 electron microprobe (CAMECA Instruments Inc.). The measurements were made immediately adjacent to SIMS oxygen isotope pits and within the same zircon growth domain. A 2 μm beam was used, with an accelerating voltage of 15 kV and a current of 200 nA. Five wavelength-dispersive spectrometers were used, one for Hf and two for each of Ca and U. Background and on-peak counting times were 30 seconds for Hf $M\alpha$, and 300 seconds for Ca $K\alpha$ and U $M\beta$. Limits of detection (3σ above background, calculated using the formula of Potts (1992) with the ZAF modification of John Fournelle (University of Wisconsin, Madison) are 105 ppm for Hf, 50 ppm for U and 12 ppm for Ca. The zircon RM GJ-1 (Piazolo et al., 2017) was analyzed as an “unknown” to evaluate the quality of the data. The average Hf, U and Ca ppm values obtained for GJ-1 are 7092 ± 66 ($n=39, 1SD$), 330 ± 32 ($n=39, 1SD$) and 14 ± 11 ($n=39, 1SD$), respectively. The average Hf and U contents are consistent with the GJ-1 values reported by Piazolo et al. (2017), and the Ca contents are at the detection limit, as is expected for a pristine zircon RM.

These data were acquired to assess the effect that radiation damage (indicated by elevated U contents) and subsequent fluid alteration (indicated by elevated Ca contents) may have had on the oxygen isotope composition of the zircon domains (e.g., Rayner et al., 2005; Davies et al., 2015). In general, there is more dispersion in $\delta^{18}\text{O}$ values above ~ 40 ppm Ca, and for one sample (19BN59A), there is a clear correlation between $\delta^{18}\text{O}$ and Ca content above ~ 40 ppm Ca (Figure A-2). For this reason, O isotope data from zircon domains with >40 ppm Ca were excluded from consideration. These data can be found in the data tables with a note stating their exclusion.

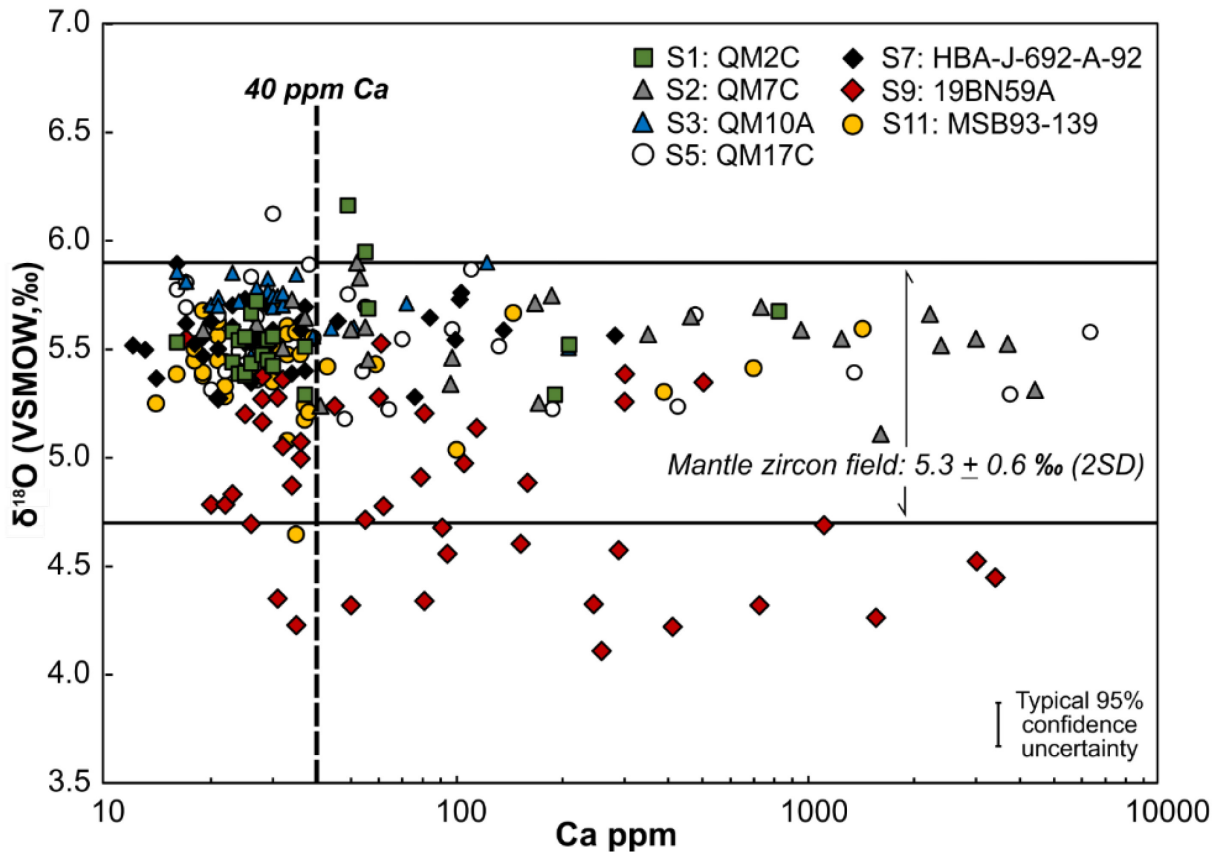


Figure A-2. Calcium content (ppm) vs. $\delta^{18}\text{O}$ (‰) for all igneous zircon domains analyzed in chapter 2. Inherited and metamorphic zircon analyses are not plotted, so that a clear comparison between the calcium content and O isotope composition of the igneous zircon populations can be made. Mantle zircon field from Valley et al. (1998). Abbreviated samples ID's (e.g., "S9") correspond to those on Figure 2-1 and in Table 2-1 in chapter 2.

A.12 Electron microprobe monazite total U-Th-Pb(total) chemical age data (chapter 4)

The U-Th-Pb_{total} dating of monazite was carried out following the methods of Allaz et al. (2020). A JXA-8900R electron microprobe (JEOL Ltd.) was run at 15 kV accelerating voltage using wavelength-dispersive spectrometry and Probe-for-EPMA software (Donovan et al. 2015), and corrected for the effects of dead-time. Thirteen X-ray lines were measured with the following diffraction crystals and 11 primary standards: U $M\beta$, PET (pentaerythritol), UO₂; Th $M\alpha$, PET, ThO₂; Pb $M\alpha$, PET, PbSiO₃ glass; Si $K\alpha$, TAP (thallium hydrogen phthalate), diopside; P $K\alpha$, PET, PrPO₄; S $K\alpha$, PET, anhydrite; Ca $K\alpha$, PET, anhydrite; Y $L\alpha$, PET, YVO₄; Ce $L\alpha$, LIF (lithium fluoride), CePO₄; La $L\alpha$, LIF, LaPO₄; Pr $L\beta$, LIF, PrPO₄; Nd $L\alpha$, LIF, NdPO₄; Sm $L\beta$, LIF, SmPO₄. For U-Th-Pb, multipoint exponential backgrounds were used following Allaz et al. (2019, 2020). For P, regular off-peak backgrounds with linear interpolation were used. For the remaining nine elements, mean-atomic-number backgrounds were used (Donovan and Tingle 1996, Donovan et al. 2016), with peak measurements on 6 to 13 of: plagioclase, Ni, Cu, Ge, Mo, Pd, Sb, Bi₂Te₃, and the 11 primary standards listed above. The mean-atomic-number backgrounds for each of these nine measured elements were optimized separately and corrected for absorption by the X-ray continuum. For the primary standards, the U-Th-Pb data were acquired with a beam current of 40 nA and a beam diameter of 2 μm with count times on peaks of 30 s and on multipoint backgrounds of 15 s. For measurement of the remaining elements on the standards, a beam current of 30 nA and beam diameter of 10 μm with count times on peaks of 30 s (and 15 s on backgrounds for P) were used. For the unknowns, a beam current of 100 nA and a fully-focused beam (<1 μm diameter) were used with count times for U-Th-Pb of 300 s on peak and 60 s on multipoint backgrounds; for measurement of other elements on the unknowns, a count time of 60 s on peaks and 30 s on backgrounds (P only) were used. The X-ray intensity data were reduced following Armstrong (1988); oxygen calculated by stoichiometry was included in the data reduction. Interference corrections were applied to U for interference by Th and Sm; and to Pb for interference by Y, Th, S and La; and to Si for interference by Nd; and to S for interference by Nd; and to Ce for interference by Th; and to La for interference by Nd; and to Nd for interference by Ce, La, and Pb (Donovan et al. 1993). Limits of detection (U-Th-Pb) determined in the Probe-for-EPMA software (Donovan et al. 2015) at 99% confidence were (rounded to the nearest 10 ppm): U 400 ppm, Th 400 ppm, and Pb 260 ppm. Analyses with totals >102 or <98 wt.% were excluded. U-Th-Pb_{total} dates were calculated by iteration using the equation of Suzuki and Adachi (1991). The in-house monazite RMs western Australia (2843 Ma; L. Heaman, unpublished ID-TIMS age) and Madagascar (512 Ma; L. Heaman, unpublished ID-TIMS age) analyzed as “unknowns”. Mean dates of 2792 ± 83 Ma (1SD, n=7) and 515 ± 24 Ma (1SD, n=4) were obtained for western Australia and Madagascar, respectively, indicating that the chemical age data are imprecise, but accurate.

A.13 Uncertainties on LA-ICPMS U-Pb ages

That largest component of uncertainty in LA-ICPMS U-Pb geochronology is typically the external reproducibility of the $^{207}\text{Pb}/^{206}\text{Pb}$ and $^{206}\text{Pb}/^{238}\text{U}$ ratios (Horstwood et al., 2016). This external reproducibility can be estimated from the “excess variance” (EV) in a set of RM measurements that have been corrected for instrument bias and drift (Horstwood et al., 2016). The EV is the amount of uncertainty that must be added to the internal 2SE of each data-point for the data-set to yield a weighted mean with an MSWD that, for the same size (n), is consistent with a single statistical population (Wendt and Carl, 1991).

The uncertainties on individual U-Pb ratios and dates reported in this thesis are the quadratic addition of the internal 2SE and the inter-session EV in measurements of the secondary RM OG1. For the LA-MC-ICPMS method (section A.5), the EV was calculated based on 329 analyses of OG1 made in 28 separate analytical sessions between 2018 and 2023. For the LASS-ICPMS U-Pb-Hf method (section A.6) it was calculated based on 70 measurements of OG1 over four analytical sessions in June–July 2020. Finally, for the LA-ICPMS U-Pb + trace-element method (section A.7), the EV was calculated based on 34 analyses of OG1 made over the course of four analytical sessions in April 2022. For all three techniques, the 2σ EV was $\sim 0.7\%$ for $^{207}\text{Pb}/^{206}\text{Pb}$ and $\sim 3\%$ for $^{206}\text{Pb}/^{238}\text{U}$.

It has been argued that for *igneous* zircon U-Pb data it is best to estimate the external reproducibility of individual measurements on an *intra-session* basis, so as to avoid *overestimating* data-point uncertainties prior to calculating group statistics (i.e., weighted means ages and their MSWDs) (Horstwood et al., 2016). That is, it is best to propagate an *intra-session* EV using only RM measurements that were made in the same analytical session as the sample. However, a large number of RM measurements are required to obtain a meaningful EV value, such that this may not be practical or advisable. This is because, at small n , there is uncertainty in the MSWD value itself (Wendt and Carl, 1991). For instance, at $\sim 95\%$ confidence, 15 measurements of a homogeneous population may be expected to yield an MSWD anywhere between 1.8 and 0.6 (Wendt and Carl, 1991). Thus, unless n is large, one cannot say with confidence what MSWD a set of homogeneous RM measurements should yield, or what amount of uncertainty should be added to each data point to achieve said MSWD. Therefore, uncertainties were propagated using *inter-session* EV values calculated from a large number of OG1 measurements that were made over the course of several analytical sessions. Importantly, sensitivity tests performed by propagating both *inter- and intra-session* EV values did not result in any meaningful difference in final age interpretations.

Most igneous and metamorphic U-Pb crystallization ages determined in this thesis are *weighted mean* $^{207}\text{Pb}/^{206}\text{Pb}$ ages. Uncertainties on these ages are quoted at two levels. The first is the 2SE on

the weighted mean calculated in ISOPLOT, which was multiplied by students-t and $\sqrt{\text{MSWD}}$, when appropriate (Ludwig, 2009). The second, larger uncertainty, incorporates the long-term external reproducibility of the *weighted mean* $^{207}\text{Pb}/^{206}\text{Pb}$ ratio. For the LA-MC-ICPMS method (section A.5), this reproducibility is estimated to be $\sim 0.3\%$ (2σ), on the basis of the EV in 28 OG1 *weighted mean* $^{207}\text{Pb}/^{206}\text{Pb}$ ratios from 28 analytical sessions conducted between 2018 and 2023. The 0.3% value is added in quadrature to the 2SE on the weighted mean $^{207}\text{Pb}/^{206}\text{Pb}$ ratio (as calculated in ISOPLOT), and then the ratio and its uncertainty are converted to an age and age uncertainty. It is important that this 0.3% value is propagated *after* calculating the weighted mean ratio, so that it is not reduced through the weighted mean calculation (Horstwood et al., 2016). The same 0.3% value was assumed for weighted mean split-stream LA-ICPMS $^{207}\text{Pb}/^{206}\text{Pb}$ dates in chapter 2. The same approach has been used by others to determine the long-term external reproducibility of *weighted mean* LA-ICPMS dates (Sliwinski et al., 2022) and weighted mean SHRIMP (sensitive high-resolution ion-microprobe) dates (Davis et al., 2019).

A.14 Plots and calculations

Weighted mean ages, weighted mean isotope ratios, and the excess variance parameter referred to above were calculated in ISOPLOT v. 4.15 (Ludwig, 2009). Concordia, isochron and probability density plots were also made in ISOPLOT v. 4.15. One dimensional kernel density estimate (KDE) curves were generated in DensityPlotter (Vermeesch, 2012) or in R. The two dimensional KDE contour plots in chapters 2 and 3 were made in MATLAB and R. Standard major- and trace-element plots were made in IgPet (Carr and Gazel, 2017).

A.15 Complete secondary reference material data

Table A-14. Secondary reference material data for the LA-MC-ICPMS U-Pb method (section A.5).

Session	Spot ID	206Pb cps	204 cps	Ratios						Dates (Ma)				Disc. %	
				207Pb 206Pb	2σ	207Pb 235U	2σ	206Pb 238U	2σ	ρ	207Pb 206Pb	2σ	206Pb 238U		2σ
July 10 2020	OG1-1	274646	101	0.3005	0.0022	28.49	1.11	0.688	0.026	0.983	3473	11	3375	100	3
July 10 2020	OG1-2	409184	120	0.2995	0.0022	29.07	1.12	0.704	0.027	0.982	3468	11	3436	100	1
July 10 2020	OG1-3	421971	53	0.2999	0.0021	29.29	1.14	0.709	0.027	0.984	3470	11	3453	102	0
July 10 2020	OG1-4	464092	35	0.2991	0.0022	29.34	1.09	0.712	0.026	0.981	3466	11	3465	97	0
July 10 2020	OG1-5	461038	44	0.2994	0.0021	28.81	1.05	0.698	0.025	0.981	3467	11	3414	94	2
July 13 2020	OG1-1	423412	48	0.2987	0.0021	28.92	0.96	0.703	0.023	0.977	3463	11	3431	85	1
July 13 2020	OG1-2	355154	51	0.2984	0.0022	28.97	0.93	0.704	0.022	0.974	3462	11	3437	82	1
July 13 2020	OG1-3	298958	19	0.2990	0.0021	28.60	0.93	0.694	0.022	0.975	3465	11	3399	83	2
July 13 2020	OG1-4	446151	67	0.2985	0.0021	28.69	0.94	0.697	0.022	0.976	3462	11	3411	84	2
April 13 2021	OG1-1	361880	40	0.2999	0.0021	29.39	0.96	0.711	0.023	0.976	3470	11	3462	85	0
April 13 2021	OG1-2	522519	47	0.2984	0.0021	29.87	0.94	0.726	0.022	0.974	3462	11	3520	83	-2
April 13 2021	OG1-3	437051	57	0.2987	0.0021	29.62	0.90	0.720	0.021	0.972	3463	11	3494	79	-1
April 13 2021	OG1-4	252845	42	0.3002	0.0021	29.48	0.92	0.713	0.022	0.974	3471	11	3468	81	0
April 13 2021	OG1-5	444710	35	0.2992	0.0021	29.55	0.87	0.717	0.020	0.970	3466	11	3484	76	-1
April 13 2021	OG1-6	347679	41	0.2996	0.0021	29.30	0.94	0.710	0.022	0.975	3468	11	3457	83	0
April 13 2021	OG1-7	325560	47	0.2995	0.0022	29.63	0.94	0.718	0.022	0.974	3467	11	3488	83	-1
April 13 2021	OG1-8	228488	40	0.2995	0.0022	29.30	0.90	0.710	0.021	0.972	3468	11	3458	80	0
April 13 2021	OG1-9	247699	41	0.2993	0.0021	29.49	0.93	0.715	0.022	0.974	3466	11	3477	82	0
April 13 2021	OG1-10	260917	74	0.3005	0.0022	29.12	0.84	0.703	0.020	0.967	3473	11	3432	74	1
April 15 2021	OG1-1	568572	27	0.2981	0.0021	29.55	0.96	0.719	0.023	0.976	3460	11	3493	85	-1
April 15 2021	OG1-2	569802	15	0.2972	0.0021	29.44	0.95	0.719	0.023	0.976	3456	11	3491	84	-1
April 15 2021	OG1-3	530116	53	0.2976	0.0021	29.48	0.94	0.719	0.022	0.974	3458	11	3491	83	-1
April 15 2021	OG1-4	471669	76	0.2971	0.0021	29.39	0.91	0.718	0.022	0.974	3455	11	3488	81	-1
April 15 2021	OG1-5	247401	43	0.2984	0.0021	29.21	0.92	0.710	0.022	0.973	3462	11	3459	81	0
April 15 2021	OG1-6	343386	45	0.2987	0.0022	28.29	0.94	0.687	0.022	0.976	3463	11	3372	84	3
April 15 2021	OG1-7	254914	77	0.2977	0.0022	29.35	1.00	0.715	0.024	0.976	3459	11	3478	89	-1
April 15 2021	OG1-8	318653	43	0.2980	0.0021	29.30	0.97	0.713	0.023	0.977	3460	11	3471	86	0
April 15 2021	OG1-9	268565	96	0.2986	0.0021	29.37	0.93	0.714	0.022	0.974	3463	11	3473	82	0
April 20 2021	OG1-1	393071	5	0.2987	0.0021	28.77	0.87	0.699	0.020	0.971	3463	11	3417	77	1
April 20 2021	OG1-2	305926	33	0.2988	0.0022	28.46	0.86	0.691	0.020	0.970	3464	11	3387	76	2
April 20 2021	OG1-3	331880	26	0.2980	0.0022	28.58	0.86	0.696	0.020	0.971	3460	11	3405	77	2
April 20 2021	OG1-4	322066	33	0.2985	0.0022	28.95	0.85	0.704	0.020	0.969	3462	11	3435	75	1
April 20 2021	OG1-5	290427	54	0.2993	0.0022	28.81	0.83	0.698	0.019	0.968	3467	11	3415	73	2
April 20 2021	OG1-6	342373	22	0.2989	0.0022	28.29	0.90	0.687	0.021	0.974	3465	11	3371	81	3
April 20 2021	OG1-7	378871	25	0.2994	0.0022	29.74	0.87	0.721	0.020	0.969	3467	11	3499	76	-1
April 20 2021	OG1-8	298653	68	0.3000	0.0022	29.59	0.87	0.716	0.020	0.969	3470	11	3480	76	0
April 20 2021	OG1-9	340267	53	0.3004	0.0022	29.82	0.85	0.720	0.020	0.966	3472	11	3498	74	-1
April 20 2021	OG1-10	285793	49	0.3010	0.0022	29.56	0.87	0.713	0.020	0.969	3475	11	3468	76	0
April 20 2021	OG1-11	318188	39	0.3008	0.0022	29.63	0.82	0.715	0.019	0.966	3474	11	3477	71	0
April 21 2021	OG1-1	279022	43	0.2988	0.0022	29.46	0.83	0.716	0.020	0.965	3464	11	3479	73	0
April 21 2021	OG1-2	375664	40	0.2988	0.0022	28.78	0.83	0.704	0.020	0.967	3454	11	3434	74	1
April 21 2021	OG1-3	608103	67	0.2966	0.0022	28.42	0.85	0.695	0.020	0.969	3452	11	3403	76	1
April 21 2021	OG1-4	516776	51	0.2982	0.0022	28.79	0.79	0.701	0.019	0.964	3461	11	3423	70	1
April 21 2021	OG1-5	350362	22	0.2981	0.0022	29.17	0.86	0.710	0.020	0.969	3461	11	3458	76	0
April 21 2021	OG1-6	334458	37	0.2980	0.0022	29.06	0.80	0.707	0.019	0.962	3460	12	3449	71	0
April 21 2021	OG1-7	290033	137	0.2979	0.0022	29.72	0.93	0.724	0.022	0.971	3459	11	3511	82	-1
April 21 2021	OG1-8	192081	60	0.2992	0.0022	29.07	0.85	0.705	0.020	0.967	3466	11	3440	75	1
April 21 2021	OG1-9	333670	40	0.3008	0.0022	29.42	0.87	0.710	0.020	0.968	3474	11	3457	76	1
April 21 2021	OG1-10	337313	32	0.2993	0.0022	29.14	0.88	0.706	0.021	0.970	3467	11	3445	78	1
April 21 2021	OG1-11	317931	42	0.2988	0.0022	28.71	0.79	0.697	0.019	0.964	3464	11	3409	70	2
May 28 2021	OG1-1	607948	81	0.2981	0.0022	27.55	0.86	0.671	0.020	0.973	3460	11	3308	78	5
May 28 2021	OG1-2	374726	61	0.2999	0.0021	28.71	0.94	0.695	0.022	0.976	3470	11	3401	84	2
May 28 2021	OG1-3	475676	73	0.2985	0.0022	29.57	1.08	0.719	0.026	0.980	3462	11	3492	95	-1
May 28 2021	OG1-4	562277	64	0.2977	0.0021	28.99	1.07	0.707	0.026	0.982	3458	11	3445	96	0
May 28 2021	OG1-5	574009	31	0.3003	0.0021	29.22	1.05	0.706	0.025	0.981	3472	11	3443	94	1
May 28 2021	OG1-6	536393	59	0.3002	0.0021	28.52	0.97	0.689	0.023	0.979	3471	11	3381	87	3
May 28 2021	OG1-7	436051	60	0.3015	0.0022	28.98	1.00	0.697	0.024	0.978	3478	11	3411	89	2
May 28 2021	OG1-8	643184	78	0.2978	0.0021	29.84	0.99	0.727	0.024	0.978	3459	11	3522	88	-2
May 28 2021	OG1-9	545849	44	0.2986	0.0021	29.80	1.00	0.724	0.024	0.978	3463	11	3512	88	-1
May 28 2021	OG1-10	564384	43	0.2990	0.0021	29.79	0.98	0.723	0.023	0.976	3465	11	3508	86	-1
May 28 2021	OG1-11	683048	62	0.2980	0.0021	30.07	1.01	0.732	0.024	0.978	3460	11	3542	89	-2
May 28 2021	OG1-12	681317	43	0.2991	0.0021	29.63	1.01	0.719	0.024	0.978	3466	11	3492	89	-1
May 28 2021	OG1-13	514557	67	0.3001	0.0021	28.85	1.00	0.697	0.024	0.979	3471	11	3411	89	2
May 28 2021	OG1-14	563290	27	0.2999	0.0021	28.93	0.99	0.700	0.023	0.978	3470	11	3421	88	1
May 28 2021	OG1-15	423007	65	0.2985	0.0022	29.21	0.93	0.710	0.022	0.974	3462	11	3459	83	0

Disc.: Percent discordance calculated as $[(207\text{Pb}/206\text{Pb date} / 206\text{Pb}/238\text{U date}) - 1] * 100\%$

Session	Spot ID	Ratios									Dates (Ma)				Disc. %
		206Pb	204	207Pb	207Pb		206Pb	206Pb		ρ	207Pb	206Pb		2σ	
		cps	cps	206Pb	2σ	235U	2σ	238U	2σ		206Pb	2σ	238U		
Nov 16 2021	OG1-1	480545	53	0.2989	0.0022	28.93	0.90	0.702	0.021	0.972	3465	11	3429	80	1
Nov 16 2021	OG1-2	398294	35	0.2997	0.0022	28.73	0.87	0.696	0.020	0.970	3468	11	3404	77	2
Nov 16 2021	OG1-3	475867	49	0.2981	0.0022	28.49	0.84	0.693	0.020	0.969	3460	11	3395	75	2
Nov 16 2021	OG1-4	310180	41	0.2986	0.0022	28.81	0.84	0.700	0.020	0.968	3463	11	3421	74	1
Nov 16 2021	OG1-5	391069	29	0.2980	0.0022	28.67	0.86	0.698	0.020	0.971	3460	11	3414	77	1
Nov 16 2021	OG1-6	453565	30	0.2980	0.0022	27.77	0.86	0.676	0.020	0.972	3460	11	3329	78	4
Nov 16 2021	OG1-7	466250	50	0.2981	0.0021	28.36	0.82	0.690	0.019	0.968	3460	11	3384	73	2
Nov 16 2021	OG1-1	468886	98	0.2990	0.0022	29.89	0.92	0.725	0.022	0.971	3465	11	3516	80	-1
Nov 16 2021	OG1-2	445291	62	0.2984	0.0022	29.66	0.87	0.721	0.021	0.969	3462	11	3500	77	-1
Nov 16 2021	OG1-3	613018	66	0.2991	0.0022	28.99	0.82	0.703	0.019	0.965	3466	12	3433	72	1
Nov 16 2021	OG1-4	452803	93	0.2988	0.0022	29.30	0.85	0.712	0.020	0.968	3464	11	3464	75	0
Nov 16 2021	OG1-5	310343	100	0.2981	0.0022	28.99	0.81	0.706	0.019	0.966	3461	11	3442	72	1
Nov 16 2021	OG1-6	434533	73	0.2976	0.0022	29.24	0.83	0.713	0.019	0.967	3458	11	3470	73	0
Nov 17 2021	OG1-1	441476	6	0.2994	0.0022	29.39	0.83	0.712	0.019	0.965	3467	11	3467	73	0
Nov 17 2021	OG1-2	378047	11	0.2995	0.0022	29.48	0.83	0.714	0.019	0.965	3467	11	3474	73	0
Nov 17 2021	OG1-3	386140	64	0.2995	0.0022	28.88	0.82	0.700	0.019	0.966	3468	11	3420	73	1
Nov 17 2021	OG1-4	446803	62	0.2990	0.0022	29.49	0.87	0.716	0.020	0.969	3465	11	3479	76	0
Nov 17 2021	OG1-5	411317	32	0.2990	0.0022	29.02	0.83	0.704	0.019	0.967	3465	11	3437	73	1
Nov 17 2021	OG1-6	501261	60	0.2987	0.0022	29.32	0.83	0.712	0.020	0.966	3463	11	3467	73	0
Nov 17 2021	OG1-7	349965	68	0.2992	0.0022	29.33	0.80	0.711	0.019	0.964	3466	11	3464	70	0
Nov 17 2021	OG1-8	494527	87	0.2975	0.0022	29.21	0.82	0.712	0.019	0.965	3457	11	3468	72	0
Nov 17 2021	OG1-10	531908	57	0.2973	0.0022	29.18	0.80	0.712	0.019	0.964	3456	11	3466	71	0
Nov 17 2021	OG1-11	367143	64	0.2976	0.0022	29.41	0.81	0.717	0.019	0.964	3458	11	3484	71	-1
Nov 17 2021	OG1-12	468477	50	0.2975	0.0022	29.23	0.81	0.713	0.019	0.964	3457	11	3470	71	0
Nov 17 2021	OG1-13	483141	68	0.2976	0.0022	29.32	0.80	0.715	0.019	0.963	3458	11	3476	71	-1
Nov 17 2021	OG1-14	391799	82	0.2933	0.0022	27.28	0.74	0.675	0.018	0.963	3435	11	3324	68	3
Nov 17 2021	OG1-15	243016	65	0.2992	0.0022	29.06	0.82	0.705	0.019	0.965	3466	11	3439	73	1
Nov 18 2021	OG1-1	244971	58	0.3008	0.0023	30.84	1.03	0.744	0.024	0.975	3474	12	3585	89	-3
Nov 18 2021	OG1-2	281453	31	0.3005	0.0022	29.75	0.94	0.718	0.022	0.972	3473	11	3490	82	0
Nov 18 2021	OG1-3	437560	50	0.2987	0.0022	29.65	0.93	0.720	0.022	0.971	3464	12	3497	82	-1
Nov 18 2021	OG1-4	266229	22	0.2996	0.0022	30.00	0.97	0.727	0.023	0.974	3468	11	3521	85	-1
Nov 18 2021	OG1-5	278597	30	0.3000	0.0023	30.23	0.97	0.731	0.023	0.972	3470	12	3538	85	-2
Nov 18 2021	OG1-6	326576	18	0.3007	0.0022	28.35	0.98	0.684	0.023	0.977	3474	11	3360	88	3
Nov 18 2021	OG1-7	692888	37	0.2990	0.0022	28.83	0.98	0.700	0.023	0.976	3465	11	3420	88	1
Nov 18 2021	OG1-8	722600	24	0.2989	0.0022	28.84	0.97	0.700	0.023	0.976	3465	11	3421	87	1
Nov 18 2021	OG1-9	721825	49	0.2983	0.0022	28.76	0.98	0.700	0.023	0.977	3462	11	3419	88	1
Nov 18 2021	OG1-10	378895	48	0.2993	0.0022	28.61	0.96	0.694	0.023	0.976	3467	11	3396	86	2
Feb 28 2022	OG1-1	357765	4	0.2997	0.0021	29.62	0.97	0.717	0.023	0.977	3469	11	3486	86	0
Feb 28 2022	OG1-2	600975	1	0.2991	0.0021	29.47	0.97	0.715	0.023	0.977	3465	11	3477	86	0
Feb 28 2022	OG1-4	579432	92	0.2981	0.0021	29.22	1.01	0.711	0.024	0.979	3460	11	3463	90	0
Feb 28 2022	OG1-5	670769	86	0.2976	0.0021	29.11	0.98	0.710	0.023	0.978	3458	11	3457	88	0
Feb 28 2022	OG1-6	811195	77	0.2986	0.0021	29.37	1.04	0.714	0.025	0.980	3463	11	3472	92	0
Feb 28 2022	OG1-7	703516	61	0.2983	0.0021	29.23	1.00	0.711	0.024	0.979	3461	11	3462	89	0
Feb 28 2022	OG1-1	683739	108	0.2997	0.0022	28.31	1.06	0.685	0.025	0.981	3469	11	3365	95	3
Feb 28 2022	OG1-2	693805	137	0.2985	0.0021	29.12	1.04	0.708	0.025	0.980	3463	11	3451	93	0
Feb 28 2022	OG1-3	570537	118	0.2999	0.0021	28.28	1.02	0.684	0.024	0.980	3470	11	3360	92	3
Feb 28 2022	OG1-4	642505	82	0.2993	0.0021	29.55	1.01	0.716	0.024	0.978	3466	11	3482	89	0
Feb 28 2022	OG1-5	634841	63	0.2994	0.0022	28.88	1.03	0.700	0.024	0.980	3467	11	3421	92	1
Feb 28 2022	OG1-6	546090	30	0.2996	0.0022	29.32	1.02	0.710	0.024	0.978	3468	11	3458	90	0
Feb 28 2022	OG1-7	582174	113	0.2992	0.0021	29.80	1.04	0.723	0.025	0.979	3466	11	3507	91	-1
Feb 28 2022	OG1-8	756297	111	0.2985	0.0021	30.26	1.08	0.735	0.026	0.980	3463	11	3554	95	-3
Feb 28 2022	OG1-9	993793	46	0.2983	0.0021	29.69	1.06	0.722	0.025	0.980	3462	11	3504	94	-1
Mar 1 2022	OG1-1	543608	49	0.3004	0.0021	28.66	0.94	0.692	0.022	0.976	3473	11	3391	83	2
Mar 1 2022	OG1-2	537361	107	0.2991	0.0021	28.37	0.90	0.688	0.021	0.974	3465	11	3376	81	3
Mar 1 2022	OG1-3	508596	58	0.3005	0.0022	27.99	0.97	0.676	0.023	0.978	3473	11	3329	87	4
Mar 1 2022	OG1-4	611916	42	0.2986	0.0022	28.88	1.03	0.702	0.025	0.979	3463	11	3427	92	1
Mar 1 2022	OG1-5	735784	121	0.2979	0.0022	29.67	1.00	0.723	0.024	0.976	3459	11	3506	88	-1
Mar 1 2022	OG1-6	540286	131	0.2991	0.0022	27.97	0.93	0.679	0.022	0.976	3466	11	3339	84	4
Mar 1 2022	OG1-7	607198	158	0.3012	0.0022	28.01	0.93	0.675	0.022	0.976	3477	11	3324	84	5
Mar 1 2022	OG1-8	543770	127	0.2991	0.0022	27.94	0.97	0.678	0.023	0.978	3465	11	3336	87	4
Mar 1 2022	OG1-1	888503	54	0.2984	0.0022	28.99	0.93	0.705	0.022	0.974	3462	11	3440	83	1
Mar 1 2022	OG1-2	929771	109	0.2979	0.0022	29.67	0.93	0.723	0.022	0.973	3459	11	3506	82	-1
Mar 1 2022	OG1-3	927484	163	0.2974	0.0021	29.99	0.94	0.732	0.022	0.973	3457	11	3540	83	-2
Mar 1 2022	OG1-4	563020	96	0.2978	0.0022	29.07	0.94	0.708	0.022	0.975	3459	11	3451	84	0
Mar 1 2022	OG1-5	519824	64	0.2986	0.0021	28.79	0.93	0.700	0.022	0.975	3463	11	3419	83	1
Mar 2 2022	OG1-1	478476	92	0.2995	0.0022	28.82	0.91	0.698	0.021	0.973	3468	11	3414	81	2
Mar 2 2022	OG1-2	668743	1	0.2977	0.0021	28.16	0.89	0.686	0.021	0.973	3458	11	3369	80	3
Mar 2 2022	OG1-3	696715	28	0.2975	0.0022	28.75	0.92	0.701	0.022	0.973	3457	11	3425	82	1

Session	Spot ID	Ratios									Dates (Ma)				Disc. %
		206Pb		207Pb		207Pb		206Pb		ρ	207Pb		206Pb		
		cps	204	206Pb	2 σ	235U	2 σ	238U	2 σ		206Pb	2 σ	238U	2 σ	
Mar 2 2022	OG1-4	352702	101	0.2974	0.0024	27.40	0.86	0.669	0.020	0.965	3457	13	3300	77	5
Mar 2 2022	OG1-5	581312	87	0.2985	0.0022	27.83	0.87	0.676	0.020	0.971	3462	11	3331	78	4
Mar 2 2022	OG1-1	673962	108	0.2991	0.0022	29.55	0.96	0.717	0.023	0.973	3465	12	3485	84	-1
Mar 2 2022	OG1-2	486184	82	0.2994	0.0022	28.38	0.89	0.688	0.021	0.972	3467	11	3373	80	3
Mar 2 2022	OG1-4	706210	17	0.2985	0.0022	28.83	0.89	0.701	0.021	0.970	3462	12	3424	79	1
Mar 2 2022	OG1-5	616629	82	0.2989	0.0022	29.75	0.93	0.722	0.022	0.970	3464	12	3504	81	-1
Mar 2 2022	OG1-6	582676	75	0.2982	0.0022	28.39	0.90	0.691	0.021	0.974	3461	11	3386	81	2
Mar 2 2022	OG1-7	758952	76	0.2987	0.0022	28.49	0.89	0.692	0.021	0.971	3464	12	3391	80	2
April 25 2022	OG1-1	276340	132	0.2998	0.0022	29.57	1.00	0.716	0.024	0.976	3469	11	3480	88	0
April 25 2022	OG1-2	418102	95	0.2999	0.0022	29.68	0.98	0.718	0.023	0.975	3470	11	3488	86	-1
April 25 2022	OG1-3	557883	112	0.2977	0.0022	30.05	1.00	0.732	0.024	0.976	3459	11	3542	88	-2
April 25 2022	OG1-4	286451	81	0.2990	0.0022	30.08	0.99	0.730	0.023	0.973	3465	12	3533	86	-2
April 25 2022	OG1-5	380600	60	0.3003	0.0022	29.04	0.93	0.702	0.022	0.973	3472	11	3428	82	1
April 25 2022	OG1-6	388362	117	0.2994	0.0022	29.19	0.91	0.707	0.022	0.972	3467	11	3448	81	1
April 25 2022	OG1-7	453548	78	0.2988	0.0022	29.30	0.96	0.711	0.023	0.975	3464	11	3464	85	0
April 25 2022	OG1-8	421284	68	0.2974	0.0022	29.09	0.91	0.710	0.022	0.973	3457	11	3458	81	0
April 25 2022	OG1-9	426917	71	0.2993	0.0022	28.86	0.92	0.700	0.022	0.973	3467	11	3419	82	1
April 25 2022	OG1-10	627570	63	0.2974	0.0022	29.13	0.94	0.711	0.022	0.974	3456	11	3461	84	0
April 25 2022	OG1-11	640182	77	0.2979	0.0022	28.96	0.90	0.705	0.021	0.972	3459	11	3441	80	1
April 25 2022	OG1-12	589393	41	0.2975	0.0021	28.75	0.91	0.701	0.022	0.974	3457	11	3425	81	1
April 25 2022	OG1-13	564505	87	0.2974	0.0021	28.44	0.89	0.694	0.021	0.973	3457	11	3397	80	2
April 25 2022	OG1-14	703386	42	0.2974	0.0021	28.83	0.90	0.704	0.021	0.973	3457	11	3434	80	1
April 25 2022	OG1-15	870804	147	0.2970	0.0021	28.98	0.89	0.708	0.021	0.972	3455	11	3451	79	0
April 25 2022	OG1-16	533518	128	0.2975	0.0022	28.21	0.89	0.688	0.021	0.973	3457	11	3375	80	2
April 26 2022	OG1-1	424647	47	0.2986	0.0022	28.05	0.91	0.682	0.021	0.974	3463	11	3350	82	3
April 26 2022	OG1-2	258369	44	0.2991	0.0022	28.27	0.92	0.686	0.022	0.974	3465	11	3367	82	3
April 26 2022	OG1-3	359383	102	0.2987	0.0022	28.48	0.94	0.692	0.022	0.974	3463	11	3390	84	2
April 26 2022	OG1-4	512538	55	0.2978	0.0021	28.57	0.89	0.696	0.021	0.973	3459	11	3406	79	2
April 26 2022	OG1-5	376165	72	0.2980	0.0022	28.65	0.92	0.698	0.022	0.974	3460	11	3412	82	1
April 26 2022	OG1-6	276506	63	0.2984	0.0022	28.24	0.94	0.687	0.022	0.975	3462	11	3370	84	3
April 26 2022	OG1-7	518546	45	0.2975	0.0022	28.29	0.90	0.690	0.021	0.973	3457	11	3383	81	2
April 26 2022	OG1-8	816137	57	0.2981	0.0022	28.89	0.92	0.703	0.022	0.972	3460	12	3433	82	1
April 26 2022	OG1-9	432335	64	0.2989	0.0022	28.23	0.92	0.685	0.022	0.974	3465	11	3364	82	3
April 26 2022	OG1-10	476664	95	0.2987	0.0022	28.47	0.90	0.692	0.021	0.973	3464	11	3389	80	2
April 26 2022	OG1-11	487707	71	0.2982	0.0022	28.42	0.90	0.692	0.021	0.973	3461	11	3389	81	2
April 27 2022	OG1-1	626038	56	0.2993	0.0022	28.88	1.05	0.700	0.025	0.980	3466	11	3421	94	1
April 27 2022	OG1-2	705335	57	0.2990	0.0022	29.20	1.05	0.709	0.025	0.980	3465	11	3453	94	0
April 27 2022	OG1-3	639800	9	0.2990	0.0022	29.89	1.06	0.725	0.025	0.979	3465	11	3516	94	-1
April 27 2022	OG1-4	414258	0	0.2987	0.0022	29.13	1.03	0.708	0.025	0.979	3463	11	3450	92	0
April 27 2022	OG1-5	256900	72	0.3010	0.0022	30.48	1.17	0.735	0.028	0.981	3475	11	3552	102	-2
April 27 2022	OG1-6	593954	74	0.2997	0.0022	29.22	1.05	0.707	0.025	0.978	3469	11	3449	93	1
April 27 2022	OG1-7	648738	45	0.2970	0.0022	29.60	1.05	0.723	0.025	0.979	3454	11	3508	94	-2
April 27 2022	OG1-8	561282	51	0.2995	0.0022	30.01	1.07	0.727	0.025	0.979	3468	11	3522	94	-2
April 27 2022	OG1-9	619701	57	0.2982	0.0022	30.22	1.09	0.735	0.026	0.979	3461	11	3553	96	-3
April 27 2022	OG1-10	440660	39	0.2989	0.0022	28.35	1.02	0.688	0.024	0.978	3465	11	3376	92	3
April 27 2022	OG1-11	442582	71	0.2992	0.0022	29.38	1.06	0.713	0.025	0.979	3466	11	3468	94	0
April 28 2022	OG1-1	547769	41	0.3000	0.0021	27.97	0.96	0.677	0.023	0.978	3470	11	3331	87	4
April 28 2022	OG1-2	577563	52	0.2997	0.0022	28.15	0.97	0.682	0.023	0.978	3469	11	3350	87	4
April 28 2022	OG1-3	744983	34	0.2988	0.0022	28.48	1.03	0.692	0.024	0.979	3464	11	3389	92	2
April 28 2022	OG1-4	650948	19	0.2991	0.0022	28.30	1.00	0.686	0.024	0.978	3466	11	3369	90	3
April 28 2022	OG1-5	589980	54	0.2998	0.0022	29.14	1.02	0.705	0.024	0.978	3469	11	3441	91	1
April 28 2022	OG1-6	248999	35	0.3008	0.0022	30.16	1.10	0.728	0.026	0.979	3474	11	3524	96	-1
April 28 2022	OG1-7	499953	20	0.3003	0.0022	29.67	1.05	0.717	0.025	0.978	3472	11	3484	92	0
Aug 8 2022	OG1-1	263294	91	0.3006	0.0023	30.10	0.95	0.727	0.022	0.969	3473	12	3521	82	-1
Aug 8 2022	OG1-2	234388	101	0.2996	0.0023	30.22	0.95	0.732	0.022	0.969	3468	12	3540	82	-2
Aug 8 2022	OG1-3	503424	71	0.2983	0.0023	29.79	0.92	0.725	0.022	0.970	3461	12	3514	81	-1
Aug 8 2022	OG1-4	225281	31	0.2996	0.0023	29.72	0.96	0.720	0.022	0.970	3468	12	3496	84	-1
Aug 8 2022	OG1-5	395230	42	0.2983	0.0023	29.94	0.94	0.728	0.022	0.971	3461	12	3527	82	-2
Aug 8 2022	OG1-6	408997	24	0.2979	0.0023	29.13	0.89	0.710	0.021	0.968	3459	12	3458	79	0
Aug 8 2022	OG1-7	412096	57	0.2976	0.0023	29.06	0.86	0.709	0.020	0.966	3458	12	3453	76	0
Aug 8 2022	OG1-8	455930	107	0.2969	0.0023	28.96	0.88	0.708	0.021	0.968	3454	12	3450	78	0
Aug 8 2022	OG1-9	398321	75	0.2991	0.0023	28.61	0.85	0.694	0.020	0.967	3466	12	3397	75	2
Aug 8 2022	OG1-10	411395	63	0.2985	0.0023	28.76	0.84	0.699	0.020	0.966	3463	12	3417	75	1
Aug 8 2022	OG1-12	263203	30	0.3002	0.0023	29.44	0.93	0.712	0.022	0.970	3471	12	3464	82	0
Aug 8 2022	OG1-13	510797	107	0.2979	0.0022	29.68	0.89	0.723	0.021	0.968	3459	12	3507	78	-1
Aug 8 2022	OG1-14	392541	56	0.2979	0.0023	28.96	0.90	0.705	0.021	0.968	3459	12	3441	79	1
Aug 8 2022	OG1-15	283577	71	0.2989	0.0023	29.51	0.91	0.716	0.021	0.969	3465	12	3482	80	0
Aug 8 2022	OG1-16	278582	25	0.2983	0.0023	29.48	0.91	0.717	0.021	0.968	3461	12	3485	80	-1

Session	Spot ID	206Pb cps	204 cps	Ratios						Dates (Ma)				Disc. %	
				207Pb 206Pb	2σ	207Pb 235U	2σ	206Pb 238U	2σ	ρ	207Pb 206Pb	2σ	206Pb 238U		2σ
Aug 9 2022	OG1-1	436445	107	0.2978	0.0023	29.03	0.83	0.707	0.019	0.962	3458	12	3448	73	0
Aug 9 2022	OG1-2	263926	97	0.2988	0.0024	29.53	0.88	0.717	0.021	0.963	3464	12	3485	77	-1
Aug 9 2022	OG1-3	270892	70	0.2985	0.0023	29.78	0.88	0.724	0.021	0.964	3462	12	3511	77	-1
Aug 9 2022	OG1-4	266156	40	0.3012	0.0024	29.09	0.97	0.701	0.023	0.972	3476	12	3423	86	2
Aug 9 2022	OG1-5	364119	61	0.3000	0.0024	28.73	0.83	0.695	0.019	0.962	3470	12	3401	73	2
Aug 9 2022	OG1-6	428880	129	0.2985	0.0023	28.74	0.83	0.699	0.019	0.963	3462	12	3416	73	1
Aug 9 2022	OG1-7	407554	81	0.2999	0.0023	29.19	0.83	0.706	0.019	0.962	3469	12	3444	73	1
Aug 9 2022	OG1-8	446227	86	0.2992	0.0023	29.48	0.86	0.715	0.020	0.965	3465	12	3477	75	0
Aug 9 2022	OG1-9	414101	60	0.3008	0.0024	29.59	0.86	0.714	0.020	0.962	3473	12	3473	75	0
Aug 9 2022	OG1-10	416401	100	0.2991	0.0023	29.05	0.83	0.705	0.019	0.963	3465	12	3439	73	1
Aug 9 2022	OG1-11	410710	54	0.2996	0.0023	29.21	0.92	0.707	0.022	0.970	3468	12	3449	81	1
Aug 9 2022	OG1-12	369518	58	0.3004	0.0024	29.23	0.94	0.706	0.022	0.969	3471	12	3443	82	1
Aug 9 2022	OG1-13	406995	47	0.2991	0.0023	28.91	0.87	0.701	0.020	0.967	3465	12	3425	77	1
Aug 11 2022_R	OG1-1	71452	68	0.3002	0.0025	28.61	0.74	0.692	0.017	0.946	3471	13	3389	64	2
Aug 11 2022_R	OG1-2	73491	63	0.3006	0.0028	29.88	0.83	0.721	0.019	0.941	3474	14	3501	70	-1
Aug 11 2022_R	OG1-3	85090	114	0.2999	0.0030	30.51	0.83	0.738	0.019	0.927	3470	16	3564	68	-3
Aug 11 2022_R	OG1-4	97043	53	0.3010	0.0028	29.80	0.77	0.718	0.017	0.933	3476	14	3490	65	0
Aug 11 2022_R	OG1-5	106821	54	0.3011	0.0025	30.10	0.77	0.725	0.018	0.945	3476	13	3516	65	-1
Aug 11 2022_R	OG1-6	134123	46	0.2997	0.0025	28.73	0.73	0.696	0.017	0.945	3469	13	3404	63	2
Aug 11 2022_R	OG1-7	160355	54	0.2987	0.0024	29.60	0.75	0.719	0.017	0.948	3464	12	3493	65	-1
Aug 11 2022_R	OG1-8	117242	57	0.2985	0.0024	29.36	0.75	0.714	0.017	0.947	3462	13	3473	64	0
Aug 11 2022_R	OG1-9	148967	35	0.2989	0.0024	29.43	0.74	0.714	0.017	0.946	3464	13	3475	64	0
Aug 11 2022_R	OG1-10	114883	67	0.3005	0.0025	29.41	0.75	0.710	0.017	0.945	3473	13	3459	64	0
Aug 11 2022_R	OG1-11	116382	73	0.2980	0.0026	29.04	0.74	0.707	0.017	0.941	3460	13	3447	64	0
Oct 24 2022	OG1-1	319566	97	0.3000	0.0023	28.64	0.82	0.693	0.019	0.962	3470	12	3393	73	2
Oct 24 2022	OG1-2	306831	81	0.2988	0.0023	28.79	0.81	0.699	0.019	0.962	3464	12	3418	71	1
Oct 24 2022	OG1-3	364899	62	0.2987	0.0023	29.13	0.83	0.708	0.019	0.964	3463	12	3450	73	0
Oct 24 2022	OG1-4	306928	94	0.2986	0.0022	29.03	0.86	0.706	0.020	0.968	3463	12	3442	76	1
Oct 24 2022	OG1-5	481262	80	0.2983	0.0022	28.83	0.88	0.701	0.021	0.969	3462	12	3426	78	1
Oct 24 2022	OG1-6	416072	101	0.2979	0.0023	28.81	0.85	0.702	0.020	0.966	3459	12	3427	76	1
Oct 24 2022	OG1-7	204134	110	0.2992	0.0024	29.45	0.88	0.714	0.021	0.962	3466	13	3474	77	0
Oct 24 2022	OG1-1	445226	98	0.2989	0.0022	28.23	0.99	0.685	0.023	0.979	3464	11	3365	89	3
Oct 24 2022	OG1-2	416818	74	0.2988	0.0022	28.31	0.97	0.687	0.023	0.977	3464	11	3373	87	3
Oct 24 2022	OG1-3	366716	81	0.2996	0.0022	28.50	0.97	0.690	0.023	0.977	3468	11	3383	87	3
Oct 24 2022	OG1-4	407452	76	0.2981	0.0022	28.82	0.95	0.702	0.023	0.975	3461	11	3427	85	1
Oct 24 2022	OG1-5	444315	89	0.2985	0.0022	29.02	0.97	0.705	0.023	0.976	3463	11	3441	87	1
Oct 24 2022	OG1-1	488015	81	0.2986	0.0022	28.36	0.94	0.689	0.022	0.975	3463	11	3379	84	2
Oct 24 2022	OG1-2	485235	70	0.2989	0.0022	27.96	0.91	0.679	0.022	0.974	3464	12	3340	82	4
Oct 24 2022	OG1-3	485636	104	0.2994	0.0023	28.16	0.92	0.682	0.022	0.973	3467	12	3353	83	3
Oct 24 2022	OG1-4	490530	41	0.3002	0.0023	27.74	0.93	0.670	0.022	0.974	3471	12	3308	84	5
Oct 24 2022	OG1-5	440198	113	0.2983	0.0022	27.88	0.91	0.678	0.022	0.974	3461	11	3337	83	4
Oct 25 2022	OG1-1	379731	100	0.2991	0.0022	29.04	0.86	0.704	0.020	0.967	3466	12	3437	76	1
Oct 25 2022	OG1-2	352459	75	0.2990	0.0022	29.38	0.88	0.713	0.021	0.968	3465	11	3470	77	0
Oct 25 2022	OG1-3	373239	105	0.3000	0.0023	29.17	0.90	0.706	0.021	0.969	3470	12	3442	79	1
Oct 25 2022	OG1-4	335957	52	0.2996	0.0023	28.47	0.86	0.690	0.020	0.968	3468	12	3381	77	3
Oct 25 2022	OG1-5	326952	88	0.2974	0.0022	29.22	0.89	0.713	0.021	0.969	3457	12	3469	78	0
Mar 20 2023	OG1-1	407247	55	0.2993	0.0021	29.21	0.84	0.708	0.020	0.969	3467	11	3452	74	0
Mar 20 2023	OG1-2	324848	63	0.2992	0.0022	29.11	0.83	0.706	0.019	0.967	3466	11	3444	73	1
Mar 20 2023	OG1-3	463109	60	0.2986	0.0021	29.07	0.80	0.706	0.019	0.967	3463	11	3445	71	1
Mar 20 2023	OG1-4	465334	87	0.2978	0.0021	29.01	0.84	0.707	0.020	0.970	3459	11	3447	75	0
Mar 20 2023	OG1-5	356190	117	0.2975	0.0021	29.38	0.84	0.717	0.020	0.970	3457	11	3483	74	-1
Mar 20 2023	OG1-6	304166	92	0.2980	0.0021	30.45	0.92	0.741	0.022	0.972	3460	11	3575	80	-3
Mar 20 2023	OG1-7	361379	69	0.2999	0.0021	29.75	0.86	0.720	0.020	0.970	3470	11	3495	75	-1
Mar 20 2023	OG1-8	337449	125	0.2987	0.0021	29.52	0.88	0.717	0.021	0.971	3463	11	3485	77	-1
Mar 20 2023	OG1-9	552811	71	0.2984	0.0021	29.55	0.91	0.719	0.022	0.974	3462	11	3491	80	-1
Mar 20 2023	OG1-10	610090	112	0.2978	0.0021	30.04	0.92	0.732	0.022	0.974	3459	11	3541	81	-2
Mar 20 2023	OG1-11	438351	92	0.2979	0.0021	30.30	0.86	0.738	0.020	0.970	3459	11	3563	75	-3
Mar 20 2023	OG1-12	376647	71	0.2997	0.0021	28.78	0.85	0.697	0.020	0.971	3469	11	3409	75	2
Mar 20 2023	OG1-13	369213	90	0.2990	0.0021	28.22	0.80	0.685	0.019	0.969	3465	11	3363	71	3
Mar 20 2023	OG1-14	340139	100	0.2996	0.0021	28.44	0.81	0.689	0.019	0.969	3468	11	3378	72	3
Mar 20 2023	OG1-15	414720	104	0.2985	0.0021	29.08	0.83	0.707	0.020	0.970	3463	11	3447	74	0
Mar 20 2023	OG1-16	244229	127	0.2995	0.0021	28.49	0.80	0.690	0.019	0.967	3468	11	3384	71	2
Mar 20 2023	OG1-17	269600	73	0.2995	0.0021	28.35	0.78	0.687	0.018	0.966	3468	11	3371	69	3
Sep 14 2023	OG1-1	601365	64	0.2991	0.0021	29.60	0.97	0.718	0.023	0.976	3466	11	3489	85	-1
Sep 14 2023	OG1-2	626425	64	0.2986	0.0021	29.46	0.95	0.716	0.023	0.975	3463	11	3481	84	-1
Sep 14 2023	OG1-4	307508	36	0.2994	0.0022	28.70	0.92	0.696	0.022	0.974	3467	11	3404	82	2
Sep 14 2023	OG1-5	467854	21	0.2992	0.0022	29.29	1.01	0.710	0.024	0.978	3466	11	3460	89	0

Session	Spot ID	206Pb cps	204 cps	Ratios						Dates (Ma)				Disc. %	
				207Pb		207Pb		206Pb		207Pb		206Pb			
				206Pb	2σ	235U	2σ	238U	2σ	ρ	206Pb	2σ	238U		2σ
Sep 14 2023	OG1-6	538339	62	0.2980	0.0022	29.08	0.94	0.708	0.022	0.975	3460	11	3451	84	0
Sep 14 2023	OG1-7	662018	67	0.2983	0.0021	30.67	1.10	0.746	0.026	0.980	3461	11	3593	96	-4
April 13 2021	FC1-1	135834	46	0.07630	0.00061	1.943	0.061	0.1848	0.0056	0.967	1103	16	1093	31	1
April 13 2021	FC1-2	119808	32	0.07563	0.00066	1.932	0.060	0.1854	0.0055	0.959	1085	17	1096	30	-1
April 13 2021	FC1-3	143359	49	0.07594	0.00064	1.928	0.058	0.1842	0.0053	0.960	1093	17	1090	29	0
April 13 2021	FC1-4	163622	52	0.07620	0.00059	1.968	0.057	0.1874	0.0052	0.964	1100	15	1107	28	-1
April 13 2021	FC1-5	178943	35	0.07652	0.00063	1.976	0.062	0.1873	0.0056	0.964	1109	16	1107	31	0
April 13 2021	FC1-6	193310	40	0.07700	0.00060	2.015	0.061	0.1899	0.0055	0.966	1121	15	1121	30	0
April 13 2021	FC1-7	172495	41	0.07626	0.00060	2.010	0.059	0.1912	0.0054	0.964	1102	16	1128	29	-2
April 13 2021	FC1-8	181069	35	0.07644	0.00058	1.946	0.060	0.1848	0.0055	0.969	1107	15	1093	30	1
April 13 2021	FC1-9	276736	43	0.07607	0.00056	1.982	0.061	0.1890	0.0056	0.970	1097	15	1116	30	-2
April 13 2021	FC1-10	166712	86	0.07625	0.00061	1.926	0.059	0.1833	0.0054	0.966	1102	16	1085	30	2
April 15 2021	FC1-1	136400	16	0.07621	0.00059	1.948	0.060	0.1855	0.0055	0.968	1101	15	1097	30	0
April 15 2021	FC1-2	108454	7	0.07614	0.00060	1.929	0.060	0.1838	0.0055	0.967	1099	16	1088	30	1
April 15 2021	FC1-3	93522	46	0.07628	0.00064	1.917	0.061	0.1824	0.0056	0.965	1102	17	1080	31	2
April 15 2021	FC1-4	405243	60	0.07567	0.00056	1.998	0.061	0.1915	0.0057	0.971	1086	15	1130	31	-4
April 15 2021	FC1-5	105674	28	0.07615	0.00066	1.972	0.062	0.1879	0.0057	0.961	1099	17	1110	31	-1
April 15 2021	FC1-6	106247	34	0.07666	0.00068	1.934	0.062	0.1831	0.0057	0.961	1112	18	1084	31	3
April 15 2021	FC1-7	80473	62	0.07625	0.00082	1.911	0.063	0.1818	0.0057	0.946	1102	21	1077	31	2
April 15 2021	FC1-8	66894	45	0.07563	0.00070	2.052	0.063	0.1969	0.0058	0.954	1085	18	1159	31	-6
April 15 2021	FC1-9	92281	55	0.07617	0.00062	1.903	0.063	0.1813	0.0058	0.969	1099	16	1074	32	2
April 20 2021	FC1-1	217599	24	0.07613	0.00067	1.982	0.058	0.1889	0.0053	0.954	1098	18	1115	29	-2
April 20 2021	FC1-2	177024	29	0.07645	0.00060	1.931	0.053	0.1833	0.0048	0.958	1107	16	1085	26	2
April 20 2021	FC1-3	154522	41	0.07665	0.00062	1.941	0.053	0.1837	0.0048	0.955	1112	16	1087	26	2
April 20 2021	FC1-4	154781	65	0.07651	0.00067	1.911	0.055	0.1812	0.0049	0.952	1109	17	1074	27	3
April 20 2021	FC1-5	178973	46	0.07678	0.00062	1.899	0.057	0.1795	0.0052	0.963	1115	16	1064	28	5
April 20 2021	FC1-6	171107	11	0.07573	0.00068	1.871	0.051	0.1793	0.0046	0.945	1088	18	1063	25	2
April 20 2021	FC1-7	129095	14	0.07606	0.00064	1.939	0.055	0.1850	0.0050	0.956	1097	17	1094	27	0
April 20 2021	FC1-8	116787	19	0.07656	0.00069	1.968	0.054	0.1865	0.0049	0.946	1110	18	1103	26	1
April 20 2021	FC1-9	128674	76	0.07888	0.00071	2.042	0.058	0.1878	0.0051	0.950	1169	18	1110	28	5
April 20 2021	FC1-10	134746	43	0.07718	0.00066	1.960	0.060	0.1842	0.0054	0.960	1126	17	1090	29	3
April 20 2021	FC1-11	203440	32	0.07679	0.00057	1.977	0.058	0.1868	0.0053	0.968	1116	15	1104	29	1
April 21 2021	FC1-1	123436	49	0.07606	0.00064	1.920	0.051	0.1832	0.0047	0.949	1097	17	1084	25	1
April 21 2021	FC1-2	267972	91	0.07795	0.00060	1.938	0.057	0.1804	0.0051	0.965	1146	15	1069	28	7
April 21 2021	FC1-3	271475	68	0.07604	0.00058	1.954	0.056	0.1864	0.0052	0.965	1096	15	1102	28	-1
April 21 2021	FC1-4	312896	31	0.07585	0.00059	1.920	0.057	0.1837	0.0052	0.965	1091	15	1087	29	0
April 21 2021	FC1-5	253461	49	0.07640	0.00059	2.036	0.057	0.1934	0.0052	0.961	1105	15	1140	28	-3
April 21 2021	FC1-6	162952	45	0.07603	0.00060	1.995	0.058	0.1904	0.0053	0.963	1096	16	1124	29	-2
April 21 2021	FC1-7	143601	139	0.07627	0.00064	1.962	0.058	0.1866	0.0053	0.960	1102	17	1103	29	0
April 21 2021	FC1-8	138261	62	0.07662	0.00059	1.967	0.056	0.1862	0.0051	0.962	1111	15	1101	28	1
April 21 2021	FC1-9	129657	92	0.08536	0.00074	2.249	0.065	0.1912	0.0052	0.954	1324	17	1128	28	17
April 21 2021	FC1-10	113041	34	0.07637	0.00071	1.912	0.055	0.1816	0.0050	0.947	1105	18	1076	27	3
April 21 2021	FC1-11	181816	43	0.07650	0.00060	1.970	0.055	0.1868	0.0050	0.960	1108	16	1104	27	0
Nov 16 2021	FC1-1	548907	48	0.07606	0.00057	1.990	0.063	0.1899	0.0058	0.971	1097	15	1121	31	-2
Nov 16 2021	FC1-2	532826	45	0.07582	0.00057	1.967	0.060	0.1882	0.0056	0.969	1090	15	1112	30	-2
Nov 16 2021	FC1-3	524456	50	0.07611	0.00063	1.921	0.057	0.1831	0.0052	0.960	1098	16	1084	28	1
Nov 16 2021	FC1-4	526616	24	0.07620	0.00058	1.940	0.060	0.1848	0.0056	0.969	1100	15	1093	30	1
Nov 16 2021	FC1-5	517758	27	0.07561	0.00055	1.938	0.058	0.1860	0.0054	0.970	1085	15	1100	29	-1
Nov 16 2021	FC1-6	512973	47	0.07572	0.00057	1.933	0.057	0.1852	0.0053	0.967	1088	15	1095	29	-1
Nov 16 2021	FC1-1	535149	76	0.07596	0.00057	1.984	0.053	0.1896	0.0048	0.959	1094	15	1119	26	-2
Nov 16 2021	FC1-2	521042	51	0.07581	0.00056	1.949	0.053	0.1866	0.0049	0.962	1090	15	1103	26	-1
Nov 16 2021	FC1-3	508161	39	0.07598	0.00057	1.911	0.050	0.1825	0.0046	0.958	1095	15	1081	25	1
Nov 16 2021	FC1-4	533957	99	0.07575	0.00056	1.947	0.052	0.1865	0.0048	0.961	1089	15	1102	26	-1
Nov 16 2021	FC1-5	524625	79	0.07558	0.00056	1.922	0.051	0.1845	0.0048	0.961	1084	15	1091	26	-1
Nov 16 2021	FC1-6	527708	100	0.07561	0.00056	1.922	0.052	0.1844	0.0048	0.963	1085	15	1091	26	-1
Nov 17 2021	FC1-1	531654	13	0.07612	0.00059	1.970	0.057	0.1878	0.0053	0.964	1098	15	1109	28	-1
Nov 17 2021	FC1-2	540317	19	0.07595	0.00059	1.978	0.058	0.1890	0.0053	0.964	1094	15	1116	29	-2
Nov 17 2021	FC1-3	536851	67	0.07617	0.00059	1.931	0.057	0.1839	0.0053	0.966	1099	15	1088	29	1
Nov 17 2021	FC1-4	540520	68	0.07580	0.00057	1.946	0.057	0.1863	0.0053	0.966	1090	15	1101	29	-1
Nov 17 2021	FC1-5	548765	27	0.07583	0.00058	1.912	0.058	0.1830	0.0053	0.967	1091	15	1083	29	1
Nov 17 2021	FC1-6	202339	68	0.07659	0.00068	1.938	0.058	0.1836	0.0052	0.955	1110	18	1086	28	2
Nov 17 2021	FC1-7	153325	25	0.07640	0.00064	1.975	0.057	0.1876	0.0051	0.956	1106	17	1108	28	0
Nov 17 2021	FC1-8	136678	33	0.07593	0.00060	1.931	0.056	0.1846	0.0051	0.961	1093	16	1092	28	0
Nov 17 2021	FC1-10	188096	52	0.07598	0.00061	1.956	0.057	0.1867	0.0053	0.961	1095	16	1104	28	-1
Nov 17 2021	FC1-11	201044	58	0.07605	0.00058	1.937	0.055	0.1848	0.0051	0.964	1096	15	1093	28	0
Nov 17 2021	FC1-12	238911	57	0.07584	0.00064	1.981	0.057	0.1895	0.0052	0.955	1091	17	1119	28	-3
Nov 17 2021	FC1-13	212017	49	0.07598	0.00061	1.955	0.055	0.1867	0.0050	0.958	1095	16	1104	27	-1

Session	Spot ID	206Pb cps	204 cps	Ratios						Dates (Ma)				Disc. %	
				207Pb		207Pb		206Pb		207Pb		206Pb			
				206Pb	2σ	235U	2σ	238U	2σ	ρ	206Pb	2σ	238U		2σ
Nov 17 2021	FC1-14	150210	72	0.07649	0.00063	1.905	0.056	0.1807	0.0051	0.960	1108	16	1071	28	3
Nov 17 2021	FC1-15	134867	79	0.07617	0.00067	1.931	0.058	0.1839	0.0053	0.956	1100	18	1088	29	1
Feb 28 2022	FC1-1	306182	176	0.07629	0.00067	2.029	0.067	0.1929	0.0061	0.964	1103	17	1137	33	-3
Feb 28 2022	FC1-2	248253	58	0.07653	0.00061	2.013	0.067	0.1908	0.0061	0.970	1109	16	1126	33	-2
Feb 28 2022	FC1-3	216717	0	0.07620	0.00064	1.885	0.063	0.1795	0.0059	0.969	1100	17	1064	32	3
Feb 28 2022	FC1-4	635651	82	0.07645	0.00058	2.006	0.069	0.1904	0.0064	0.976	1107	15	1124	35	-1
Feb 28 2022	FC1-5	632876	51	0.07616	0.00056	2.064	0.071	0.1967	0.0067	0.977	1099	15	1157	36	-5
Feb 28 2022	FC1-1	700726	68	0.07629	0.00059	1.944	0.066	0.1849	0.0061	0.973	1103	15	1094	33	1
Feb 28 2022	FC1-2	738539	56	0.07603	0.00056	1.966	0.068	0.1877	0.0063	0.977	1096	15	1109	34	-1
Feb 28 2022	FC1-3	740128	90	0.07613	0.00057	1.987	0.068	0.1893	0.0064	0.976	1098	15	1118	34	-2
Feb 28 2022	FC1-4	724935	52	0.07600	0.00055	1.982	0.068	0.1892	0.0063	0.977	1095	15	1117	34	-2
Feb 28 2022	FC1-5	733868	39	0.07619	0.00056	1.989	0.068	0.1894	0.0063	0.977	1100	15	1118	34	-2
Feb 28 2022	FC1-6	710975	46	0.07623	0.00057	1.947	0.068	0.1853	0.0064	0.977	1101	15	1096	35	0
Feb 28 2022	FC1-7	719637	26	0.07595	0.00057	2.026	0.071	0.1935	0.0066	0.977	1094	15	1140	36	-4
Feb 28 2022	FC1-8	719770	64	0.07595	0.00055	2.037	0.071	0.1946	0.0066	0.978	1094	14	1146	36	-5
Feb 28 2022	FC1-9	698371	44	0.07592	0.00055	1.994	0.069	0.1905	0.0065	0.978	1093	14	1124	35	-3
Mar 1 2022	FC1-1	692072	40	0.07636	0.00058	1.975	0.064	0.1877	0.0059	0.973	1105	15	1109	32	0
Mar 1 2022	FC1-2	661728	136	0.07592	0.00056	1.953	0.063	0.1867	0.0059	0.974	1093	15	1103	32	-1
Mar 1 2022	FC1-3	670000	65	0.07614	0.00058	2.017	0.066	0.1922	0.0061	0.973	1099	15	1133	33	-3
Mar 1 2022	FC1-4	646149	82	0.07594	0.00057	1.946	0.064	0.1860	0.0060	0.974	1093	15	1099	32	-1
Mar 1 2022	FC1-5	620068	126	0.07644	0.00058	1.935	0.064	0.1837	0.0059	0.973	1107	15	1087	32	2
Mar 1 2022	FC1-1	638084	22	0.07621	0.00056	1.997	0.064	0.1901	0.0060	0.973	1100	15	1122	32	-2
Mar 1 2022	FC1-2	642491	95	0.07579	0.00059	1.999	0.066	0.1914	0.0061	0.971	1089	16	1129	33	-4
Mar 1 2022	FC1-3	647379	96	0.07563	0.00059	2.031	0.066	0.1948	0.0061	0.971	1085	15	1148	33	-5
Mar 1 2022	FC1-4	644196	57	0.07585	0.00056	1.975	0.067	0.1890	0.0062	0.976	1091	15	1116	34	-2
Mar 2 2022	FC1-1	664632	71	0.07606	0.00058	1.983	0.063	0.1892	0.0058	0.970	1097	15	1117	32	-2
Mar 2 2022	FC1-2	653421	42	0.07613	0.00060	1.991	0.063	0.1897	0.0058	0.968	1099	16	1120	31	-2
Mar 2 2022	FC1-3	680380	63	0.07582	0.00056	2.007	0.063	0.1920	0.0059	0.972	1090	15	1132	32	-4
Mar 2 2022	FC1-4	644623	73	0.07607	0.00062	1.958	0.065	0.1868	0.0060	0.970	1097	16	1104	32	-1
Mar 2 2022	FC1-5	632423	39	0.07592	0.00060	1.956	0.065	0.1870	0.0060	0.971	1093	16	1105	32	-1
Mar 2 2022	FC1-1	661041	105	0.07597	0.00060	1.983	0.064	0.1894	0.0059	0.970	1094	16	1118	32	-2
Mar 2 2022	FC1-2	647089	81	0.07593	0.00059	1.966	0.063	0.1879	0.0058	0.970	1093	15	1110	32	-2
Mar 2 2022	FC1-3	616360	12	0.07579	0.00057	1.990	0.062	0.1905	0.0057	0.970	1089	15	1124	31	-3
Mar 2 2022	FC1-4	627871	71	0.07639	0.00058	2.005	0.062	0.1904	0.0057	0.969	1105	15	1124	31	-2
Mar 2 2022	FC1-5	547731	97	0.07588	0.00057	1.966	0.061	0.1880	0.0057	0.971	1092	15	1110	31	-2
Mar 2 2022	FC1-6	825212	62	0.07572	0.00057	1.979	0.061	0.1897	0.0056	0.970	1088	15	1119	31	-3
April 25 2022	FC1-1	502827	72	0.07580	0.00057	1.972	0.065	0.1888	0.0061	0.973	1090	15	1115	33	-2
April 25 2022	FC1-2	414345	85	0.07584	0.00058	1.963	0.062	0.1878	0.0057	0.970	1091	15	1110	31	-2
April 25 2022	FC1-3	404090	87	0.07566	0.00056	1.953	0.061	0.1873	0.0057	0.972	1086	15	1107	31	-2
April 25 2022	FC1-4	392719	61	0.07587	0.00057	1.953	0.061	0.1868	0.0057	0.971	1092	15	1104	31	-1
April 25 2022	FC1-5	388813	25	0.07582	0.00059	1.949	0.061	0.1865	0.0057	0.968	1090	16	1102	31	-1
April 25 2022	FC1-6	434739	77	0.07570	0.00057	1.967	0.062	0.1886	0.0057	0.971	1087	15	1114	31	-2
April 25 2022	FC1-7	391939	44	0.07581	0.00058	1.945	0.061	0.1861	0.0056	0.969	1090	15	1100	31	-1
April 25 2022	FC1-8	370041	62	0.07571	0.00058	1.916	0.061	0.1836	0.0056	0.970	1087	15	1087	31	0
April 25 2022	FC1-9	539445	48	0.07582	0.00059	1.953	0.064	0.1869	0.0059	0.972	1090	15	1105	32	-1
April 25 2022	FC1-11	424594	111	0.07594	0.00056	1.948	0.061	0.1862	0.0056	0.971	1093	15	1101	30	-1
April 26 2022	FC1-1	376589	114	0.07615	0.00059	1.943	0.062	0.1851	0.0057	0.970	1099	15	1095	31	0
April 26 2022	FC1-2	443410	104	0.07574	0.00057	1.967	0.062	0.1884	0.0058	0.971	1088	15	1113	31	-2
April 26 2022	FC1-3	516682	117	0.07560	0.00056	1.951	0.061	0.1873	0.0057	0.972	1084	15	1107	31	-2
April 26 2022	FC1-4	136603	73	0.07566	0.00063	1.935	0.061	0.1856	0.0057	0.965	1086	16	1098	31	-1
April 26 2022	FC1-5	141071	77	0.07612	0.00066	1.957	0.061	0.1866	0.0056	0.960	1098	17	1103	30	0
April 26 2022	FC1-6	565169	93	0.07589	0.00056	1.982	0.063	0.1895	0.0059	0.972	1092	15	1119	32	-2
April 26 2022	FC1-7	570897	44	0.07585	0.00056	1.995	0.063	0.1908	0.0058	0.972	1091	15	1126	32	-3
April 26 2022	FC1-8	551487	37	0.07593	0.00060	1.963	0.063	0.1876	0.0058	0.969	1093	16	1108	31	-1
April 26 2022	FC1-9	552951	43	0.07575	0.00058	1.981	0.063	0.1897	0.0059	0.971	1089	15	1120	32	-3
April 26 2022	FC1-10	570460	44	0.07567	0.00057	1.968	0.063	0.1887	0.0058	0.972	1086	15	1114	32	-3
April 27 2022	FC1-1	176626	82	0.07687	0.00065	1.936	0.070	0.1827	0.0065	0.973	1118	17	1082	35	3
April 27 2022	FC1-2	159587	31	0.07684	0.00069	1.976	0.071	0.1866	0.0065	0.968	1117	18	1103	35	1
April 27 2022	FC1-3	670320	6	0.07593	0.00058	2.017	0.073	0.1927	0.0068	0.978	1093	15	1136	37	-4
April 27 2022	FC1-4	651897	53	0.07583	0.00057	2.032	0.081	0.1944	0.0076	0.982	1091	15	1145	41	-5
April 27 2022	FC1-5	608814	50	0.07569	0.00056	1.972	0.074	0.1890	0.0070	0.981	1087	15	1116	38	-3
April 27 2022	FC1-6	614816	79	0.07581	0.00057	2.028	0.074	0.1942	0.0069	0.978	1090	15	1144	37	-5
April 27 2022	FC1-7	541049	20	0.07614	0.00059	1.995	0.075	0.1901	0.0070	0.979	1099	15	1122	38	-2
April 27 2022	FC1-8	461737	51	0.07670	0.00057	1.975	0.071	0.1869	0.0065	0.978	1113	15	1104	35	1
April 27 2022	FC1-9	463913	61	0.07583	0.00058	2.021	0.073	0.1934	0.0068	0.977	1091	15	1140	37	-4
April 28 2022	FC1-1	562716	74	0.07586	0.00057	1.955	0.067	0.1870	0.0063	0.976	1091	15	1105	34	-1

Session	Spot ID	206Pb cps	204 cps	Ratios						Dates (Ma)				Disc. %	
				207Pb		207Pb		206Pb		207Pb		206Pb			
				206Pb	2σ	235U	2σ	238U	2σ	ρ	206Pb	2σ	238U		2σ
April 28 2022	FC1-2	644123	75	0.07598	0.00057	1.943	0.066	0.1856	0.0062	0.976	1095	15	1097	34	0
April 28 2022	FC1-3	783083	54	0.07567	0.00056	1.985	0.069	0.1904	0.0065	0.977	1086	15	1123	35	-3
April 28 2022	FC1-4	804167	73	0.07586	0.00056	1.996	0.069	0.1909	0.0065	0.977	1091	15	1126	35	-3
April 28 2022	FC1-5	804288	57	0.07582	0.00055	1.973	0.070	0.1888	0.0066	0.979	1090	15	1115	35	-2
April 28 2022	FC1-6	887858	73	0.07603	0.00056	2.033	0.071	0.1940	0.0067	0.978	1096	15	1143	36	-4
Sep 14 2023	FC1-1	672375	28	0.07594	0.00055	1.969	0.061	0.1881	0.0057	0.972	1093	14	1111	31	-2
Sep 14 2023	FC1-2	694774	113	0.07574	0.00055	2.004	0.061	0.1920	0.0057	0.972	1088	14	1132	31	-4
Sep 14 2023	FC1-3	267526	92	0.07677	0.00063	1.975	0.059	0.1867	0.0054	0.962	1115	16	1103	29	1
Sep 14 2023	FC1-4	700958	100	0.07555	0.00055	2.003	0.063	0.1924	0.0059	0.973	1083	14	1134	32	-5
Sep 14 2023	FC1-5	184039	83	0.07626	0.00059	1.928	0.059	0.1834	0.0054	0.967	1102	15	1086	30	1
Sep 14 2023	FC1-6	181488	99	0.07637	0.00057	1.915	0.059	0.1819	0.0054	0.970	1105	15	1077	29	3
Sep 14 2023	FC1-7	181720	76	0.07616	0.00061	1.923	0.059	0.1832	0.0054	0.965	1099	16	1085	30	1
Sep 14 2023	FC1-8	171887	69	0.07656	0.00060	1.917	0.058	0.1817	0.0053	0.965	1110	16	1076	29	3
Nov 18 2021	Kara-1	168813	54	0.1791	0.0014	12.02	0.40	0.487	0.016	0.972	2644	13	2558	67	3
Nov 18 2021	Kara-2	196005	44	0.1783	0.0014	12.19	0.40	0.496	0.016	0.972	2637	13	2598	68	2
Nov 18 2021	Kara-3	212306	48	0.1779	0.0014	12.18	0.40	0.497	0.016	0.972	2633	13	2600	67	1
Nov 18 2021	Kara-4	218471	31	0.1782	0.0013	12.22	0.39	0.498	0.016	0.973	2636	12	2603	67	1
Nov 18 2021	Kara-5	147430	34	0.1788	0.0015	11.95	0.40	0.485	0.016	0.971	2642	13	2548	69	4
Nov 18 2021	Kara-6	141848	42	0.1788	0.0014	11.78	0.40	0.478	0.016	0.975	2642	12	2520	68	5
Nov 18 2021	Kara-7	151405	20	0.1776	0.0013	11.71	0.40	0.478	0.016	0.975	2630	13	2520	69	4
Nov 18 2021	Kara-8	126853	40	0.1782	0.0015	11.62	0.40	0.473	0.016	0.970	2636	14	2498	69	6
Aug 8 2022	kara-1	143609	40	0.1797	0.0014	12.14	0.38	0.490	0.015	0.969	2650	13	2571	64	3
Aug 8 2022	kara-2	153313	73	0.1788	0.0014	12.32	0.37	0.500	0.015	0.966	2642	13	2614	63	1
Aug 8 2022	kara-3	154253	76	0.1783	0.0014	12.39	0.38	0.504	0.015	0.968	2637	13	2633	65	0
Aug 8 2022	kara-4	144220	27	0.1779	0.0014	12.16	0.38	0.496	0.015	0.968	2633	13	2596	65	1
Aug 8 2022	kara-5	148257	7	0.1777	0.0014	12.26	0.39	0.500	0.015	0.969	2632	13	2616	66	1
Aug 8 2022	kara-6	138039	18	0.1781	0.0015	12.07	0.37	0.492	0.014	0.962	2635	14	2579	62	2
Aug 8 2022	kara-7	96144	42	0.1780	0.0014	12.12	0.36	0.494	0.014	0.962	2635	13	2587	60	2
Aug 8 2022	kara-8	144802	71	0.1766	0.0014	12.00	0.37	0.493	0.015	0.968	2621	13	2584	63	1
Aug 8 2022	kara-9	109950	53	0.1781	0.0014	11.96	0.38	0.487	0.015	0.967	2635	13	2558	65	3
Aug 8 2022	kara-10	112239	40	0.1775	0.0014	11.90	0.36	0.487	0.014	0.965	2629	13	2556	61	3
Aug 8 2022	kara-11	100395	46	0.1794	0.0015	12.00	0.36	0.485	0.014	0.963	2647	14	2550	61	4
Aug 8 2022	kara-12	130388	25	0.1784	0.0014	12.02	0.35	0.489	0.014	0.964	2638	13	2567	60	3
Aug 8 2022	kara-13	131254	77	0.1784	0.0014	12.29	0.37	0.500	0.015	0.965	2638	13	2613	62	1
Aug 8 2022	kara-14	136328	35	0.1778	0.0014	12.02	0.36	0.491	0.014	0.964	2632	13	2574	60	2
Aug 8 2022	kara-15	131652	33	0.1773	0.0014	12.12	0.35	0.496	0.014	0.961	2627	13	2598	60	1
Aug 8 2022	kara-16	139847	6	0.1777	0.0014	11.96	0.35	0.488	0.014	0.964	2632	13	2563	59	3
Aug 9 2022	kara-1	196168	106	0.1778	0.0014	12.15	0.37	0.496	0.015	0.966	2631	13	2596	62	1
Aug 9 2022	kara-2	204403	85	0.1776	0.0014	12.20	0.36	0.498	0.014	0.962	2630	13	2607	61	1
Aug 9 2022	kara-3	193243	74	0.1778	0.0014	12.31	0.39	0.502	0.015	0.968	2632	13	2623	66	0
Aug 9 2022	kara-4	179732	21	0.1792	0.0014	12.37	0.38	0.501	0.015	0.967	2644	13	2618	64	1
Aug 9 2022	kara-5	172639	63	0.1786	0.0014	12.24	0.37	0.497	0.015	0.966	2639	13	2601	62	1
Aug 9 2022	kara-6	169038	93	0.1783	0.0014	12.31	0.38	0.501	0.015	0.965	2636	13	2618	63	1
Aug 9 2022	kara-8	109086	70	0.1794	0.0014	12.33	0.37	0.498	0.014	0.963	2647	13	2607	61	2
Aug 9 2022	kara-9	137323	49	0.1791	0.0015	11.92	0.34	0.483	0.013	0.955	2643	14	2541	57	4
Aug 9 2022	kara-10	137833	16	0.1795	0.0015	12.17	0.36	0.492	0.014	0.962	2648	14	2579	61	3
Aug 9 2022	kara-11	87313	27	0.1791	0.0015	11.95	0.41	0.484	0.016	0.969	2644	14	2545	69	4
Aug 9 2022	kara-12	114278	34	0.1783	0.0015	12.11	0.38	0.493	0.015	0.965	2636	14	2583	64	2
Aug 9 2022	kara-13	87260	30	0.1786	0.0015	12.03	0.37	0.489	0.014	0.962	2639	14	2565	62	3
Aug 9 2022	kara-14	141430	29	0.1777	0.0015	12.02	0.36	0.491	0.014	0.961	2630	14	2575	61	2
Aug 11 2022_R	kara-1	44952	18	0.1776	0.0017	11.78	0.31	0.481	0.012	0.934	2631	15	2532	51	4
Aug 11 2022_R	kara-2	45498	26	0.1774	0.0018	12.06	0.33	0.493	0.012	0.928	2628	17	2586	54	2
Aug 11 2022_R	kara-3	61395	32	0.1762	0.0016	12.05	0.32	0.496	0.012	0.936	2618	15	2598	53	1
Aug 11 2022_R	kara-4	63972	24	0.1771	0.0016	12.00	0.32	0.492	0.012	0.944	2626	15	2578	53	2
Aug 11 2022_R	kara-5	55150	24	0.1774	0.0016	12.37	0.33	0.506	0.013	0.943	2628	15	2640	54	0
Aug 11 2022_R	kara-6	49167	24	0.1777	0.0017	12.06	0.31	0.492	0.012	0.932	2632	15	2581	51	2
Aug 11 2022_R	kara-7	38905	49	0.1766	0.0018	11.67	0.31	0.480	0.012	0.929	2621	16	2525	52	4
Aug 11 2022_R	kara-8	59505	25	0.1761	0.0015	11.68	0.30	0.481	0.012	0.945	2617	14	2533	50	3
Aug 11 2022_R	kara-9	58967	19	0.1768	0.0015	11.84	0.31	0.486	0.012	0.943	2623	14	2554	51	3
Aug 11 2022_R	kara-10	38821	20	0.1764	0.0017	11.83	0.31	0.487	0.012	0.932	2619	16	2557	52	2
Aug 11 2022_R	kara-11	48070	17	0.1769	0.0016	12.09	0.32	0.496	0.012	0.942	2624	15	2596	53	1
Oct 24 2022	kara-1	188867	98	0.1781	0.0013	11.89	0.41	0.484	0.016	0.975	2635	13	2547	70	3
Oct 24 2022	kara-2	172562	76	0.1787	0.0015	12.02	0.39	0.488	0.015	0.967	2641	14	2563	66	3
Oct 24 2022	kara-3	115906	72	0.1780	0.0014	11.88	0.38	0.484	0.015	0.971	2635	13	2546	66	3
Oct 24 2022	kara-4	144737	65	0.1780	0.0013	12.08	0.40	0.493	0.016	0.973	2634	12	2582	68	2
Oct 24 2022	kara-5	107820	85	0.1786	0.0014	12.25	0.39	0.498	0.015	0.967	2640	13	2604	66	1
Oct 24 2022	kara-6	106697	34	0.1778	0.0014	11.94	0.38	0.487	0.015	0.968	2632	13	2558	64	3

Session	Spot ID	Ratios									Dates (Ma)				Disc. %
		206Pb	204	207Pb	207Pb		206Pb	207Pb		ρ	207Pb	206Pb		2σ	
		cps	cps	206Pb	2σ	235U	2σ	238U	2σ		206Pb	2σ	238U		
Oct 24 2022	kara-7	117740	62	0.1778	0.0014	11.69	0.37	0.477	0.015	0.969	2632	13	2514	64	5
Oct 24 2022	kara-8	107436	57	0.1788	0.0014	11.87	0.38	0.481	0.015	0.970	2642	13	2534	65	4
Oct 24 2022	kara-9	175500	69	0.1787	0.0013	11.80	0.40	0.479	0.016	0.975	2641	12	2523	68	5
Oct 24 2022	kara-10	163215	93	0.1782	0.0013	11.65	0.39	0.474	0.015	0.974	2636	12	2502	67	5
Oct 24 2022	kara-11	136401	39	0.1779	0.0014	11.70	0.39	0.477	0.015	0.972	2633	13	2516	66	5
Oct 24 2022	kara-12	193361	64	0.1781	0.0014	12.01	0.36	0.489	0.014	0.964	2636	13	2568	61	3
Oct 24 2022	kara-13	208458	69	0.1775	0.0014	12.20	0.35	0.499	0.014	0.964	2630	13	2608	59	1
Oct 24 2022	kara-14	178935	50	0.1781	0.0014	12.13	0.35	0.494	0.014	0.964	2635	13	2590	60	2
Oct 24 2022	kara-15	241488	60	0.1793	0.0014	12.49	0.36	0.506	0.014	0.962	2646	13	2638	60	0
Oct 24 2022	kara-16	215036	67	0.1784	0.0014	12.57	0.37	0.511	0.014	0.963	2638	13	2661	61	-1
Oct 24 2022	kara-17	224470	49	0.1778	0.0014	12.44	0.35	0.508	0.014	0.961	2633	13	2647	58	-1
Oct 24 2022	kara-18	106826	58	0.1771	0.0014	11.62	0.35	0.476	0.014	0.962	2626	13	2510	59	5
Oct 24 2022	kara-19	98438	54	0.1776	0.0015	11.95	0.36	0.488	0.014	0.959	2631	14	2563	61	3
Oct 25 2022	kara-1	124058	52	0.1790	0.0014	12.04	0.37	0.488	0.014	0.965	2643	13	2562	62	3
Oct 25 2022	kara-2	194230	60	0.1778	0.0013	11.87	0.38	0.484	0.015	0.972	2633	12	2546	65	3
Oct 25 2022	kara-3a	227140	97	0.1792	0.0014	11.96	0.37	0.484	0.014	0.966	2646	13	2546	63	4
Oct 25 2022	kara-4	229328	75	0.1776	0.0014	12.02	0.37	0.491	0.015	0.968	2630	13	2576	62	2
Oct 25 2022	kara-5	149574	123	0.1773	0.0014	12.18	0.37	0.498	0.015	0.966	2628	13	2607	63	1
Mar 20 2023	Kara-1	144182	67	0.1790	0.0013	12.17	0.34	0.493	0.013	0.963	2643	12	2585	57	2
Mar 20 2023	Kara-2	160471	58	0.1784	0.0014	12.11	0.34	0.493	0.013	0.960	2638	13	2582	57	2
Mar 20 2023	Kara-3	163301	92	0.1779	0.0013	12.29	0.35	0.501	0.014	0.967	2634	12	2618	59	1
Mar 20 2023	Kara-4	129085	68	0.1792	0.0013	11.96	0.33	0.484	0.013	0.963	2646	12	2545	55	4
Mar 20 2023	Kara-5	250238	128	0.1776	0.0013	12.32	0.36	0.503	0.014	0.970	2631	12	2629	61	0
Mar 20 2023	Kara-6	146739	77	0.1778	0.0014	12.10	0.34	0.494	0.013	0.962	2632	13	2587	58	2
Mar 20 2023	Kara-7	163674	63	0.1778	0.0013	12.45	0.36	0.508	0.014	0.970	2632	12	2649	61	-1
Mar 20 2023	Kara-8	220391	100	0.1778	0.0012	12.02	0.34	0.490	0.014	0.969	2633	12	2572	58	2
Mar 20 2023	Kara-9	142310	95	0.1794	0.0013	11.18	0.33	0.452	0.013	0.968	2647	12	2406	58	10
Mar 20 2023	Kara-10	202130	113	0.1793	0.0013	11.33	0.33	0.458	0.013	0.967	2647	12	2432	57	9
Mar 20 2023	Kara-11	175093	120	0.1780	0.0013	12.01	0.36	0.490	0.014	0.967	2634	12	2569	60	3
Mar 20 2023	Kara-12	193767	81	0.1778	0.0013	12.06	0.37	0.492	0.015	0.972	2632	12	2580	64	2
Mar 20 2023	Kara-13	143615	60	0.1776	0.0013	12.22	0.37	0.499	0.015	0.972	2631	12	2610	64	1
Mar 20 2023	Kara-14	163534	89	0.1772	0.0013	12.34	0.37	0.505	0.015	0.969	2627	12	2637	62	0
Mar 20 2023	Kara-15	210018	87	0.1779	0.0013	12.26	0.36	0.500	0.014	0.969	2633	12	2614	61	1
Mar 20 2023	Kara-16	145267	75	0.1791	0.0013	12.02	0.35	0.487	0.014	0.969	2644	12	2558	60	3
Mar 20 2023	Kara-17	120490	118	0.1783	0.0013	12.08	0.36	0.491	0.014	0.969	2637	12	2577	61	2
Mar 20 2023	Kara-18	111956	106	0.1785	0.0014	11.95	0.34	0.486	0.013	0.960	2639	13	2552	57	3
Mar 20 2023	Kara-19	158779	76	0.1785	0.0014	12.08	0.35	0.491	0.014	0.964	2639	13	2575	59	2
Sep 14 2023	kara-1	227808	46	0.1784	0.0013	12.04	0.39	0.489	0.015	0.974	2638	12	2568	67	3
Sep 14 2023	kara-2	209134	60	0.1782	0.0013	12.25	0.40	0.499	0.016	0.975	2636	12	2609	68	1
Sep 14 2023	kara-3	203149	28	0.1782	0.0013	11.96	0.39	0.487	0.015	0.974	2636	12	2558	66	3
Sep 14 2023	kara-4	194015	41	0.1779	0.0013	12.08	0.41	0.492	0.016	0.975	2634	12	2581	70	2
Sep 14 2023	kara-5	190401	58	0.1777	0.0013	11.98	0.40	0.489	0.016	0.973	2631	13	2568	68	2
Sep 14 2023	kara-6	197210	79	0.1776	0.0013	12.01	0.40	0.491	0.016	0.975	2631	12	2573	69	2
Sep 14 2023	kara-7	170297	12	0.1783	0.0013	12.08	0.38	0.492	0.015	0.971	2637	12	2578	65	2
Sep 14 2023	kara-8	168881	52	0.1781	0.0013	12.05	0.39	0.491	0.015	0.973	2635	12	2576	66	2
Sep 14 2023	kara-9	175946	32	0.1782	0.0014	12.21	0.39	0.497	0.016	0.971	2636	13	2601	67	1
Sep 14 2023	kara-10	208257	32	0.1786	0.0013	12.07	0.39	0.491	0.016	0.973	2640	12	2573	67	3
Sep 14 2023	kara-11	204505	69	0.1773	0.0013	12.20	0.38	0.499	0.015	0.970	2628	13	2611	64	1
Sep 14 2023	kara-12	226314	61	0.1779	0.0013	12.33	0.39	0.503	0.015	0.971	2633	12	2626	65	0
Sep 14 2023	kara-13	233426	30	0.1778	0.0013	12.26	0.37	0.500	0.015	0.971	2633	12	2614	63	1
Nov 19 2021	TG09-1	1896194	71	0.1703	0.0017	11.07	0.35	0.471	0.014	0.947	2561	17	2489.8	61	3
Nov 19 2021	TG09-2	1919237	57	0.1692	0.0017	11.28	0.35	0.484	0.014	0.948	2550	17	2544.2	62	0
Nov 19 2021	TG09-3	1971366	48	0.1693	0.0017	11.26	0.36	0.482	0.015	0.949	2551	17	2538	63	1
Nov 19 2021	TG09-4	2057518	53	0.1688	0.0017	11.33	0.36	0.487	0.015	0.948	2546	17	2557.5	63	0
Nov 19 2021	TG09-5	1929914	99	0.1693	0.0017	11.16	0.35	0.478	0.014	0.948	2551	17	2519.5	62	1
Nov 19 2021	TG09-6	1951664	48	0.1692	0.0017	11.25	0.35	0.483	0.014	0.948	2549	17	2539.2	62	0
Nov 19 2021	TG09-7	1909939	65	0.1698	0.0017	11.10	0.36	0.474	0.014	0.950	2556	17	2502.4	63	2
Nov 19 2021	TG09-8	2034902	78	0.1690	0.0017	11.12	0.35	0.477	0.014	0.948	2547	17	2515.8	62	1
Nov 19 2021	TG09-9	1996553	62	0.1687	0.0017	11.19	0.35	0.481	0.014	0.948	2545	17	2531.9	62	1
Nov 19 2021	TG09-10	1935491	47	0.1687	0.0017	11.18	0.35	0.481	0.014	0.948	2544	17	2531.9	62	0

Table A-15. Secondary reference material U-Pb data for the split-steam LA-ICPMS U-Pb-Hf method (section A.6).

Session	Spot ID	206Pb cps	204 cps	Ratios						Dates (Ma)				Disc. %	
				207Pb 206Pb	2σ	207Pb 235U	2σ	206Pb 238U	2σ	ρ	207Pb 206Pb	2σ	206Pb 238U		2σ
June 25 2021	OG1-1	7.03E+05	36	0.2981	0.0021	29.92	1.04	0.726	0.025	0.980	3460	11	3518	92	-2
June 25 2021	OG1-2	6.78E+05	4	0.2997	0.0021	29.56	1.01	0.714	0.024	0.980	3469	11	3473	89	0
June 25 2021	OG1-3	5.82E+05	40	0.2993	0.0023	28.61	0.99	0.692	0.024	0.976	3467	12	3392	89	2
June 25 2021	OG1-4	5.33E+05	0	0.2974	0.0021	29.54	1.02	0.720	0.024	0.978	3457	11	3497	91	-1
June 25 2021	OG1-5	4.32E+05	1	0.2963	0.0021	29.21	1.00	0.713	0.024	0.978	3451	11	3471	90	-1
June 25 2021	OG1-6	4.09E+05	0	0.2977	0.0023	29.65	1.03	0.722	0.024	0.976	3458	12	3502	91	-1
June 25 2021	OG1-7	4.30E+05	0	0.2979	0.0025	29.11	1.03	0.709	0.024	0.972	3459	13	3456	91	0
June 25 2021	OG1-8	4.74E+05	0	0.2969	0.0020	29.82	1.02	0.728	0.024	0.980	3454	11	3525	91	-2
June 25 2021	OG1-9	4.53E+05	9	0.2979	0.0021	29.42	1.01	0.715	0.024	0.979	3459	11	3475	90	0
June 25 2021	OG1-10	4.47E+05	8	0.2966	0.0020	29.84	1.02	0.729	0.024	0.980	3453	11	3530	91	-2
June 25 2021	OG1-11	4.48E+05	0	0.2981	0.0022	28.83	1.01	0.702	0.024	0.978	3460	11	3427	90	1
June 25 2021	OG1-12	5.40E+05	28	0.2994	0.0021	29.46	1.07	0.715	0.025	0.982	3467	11	3477	95	0
June 25 2021	OG1-13	6.82E+05	0	0.2992	0.0021	29.65	1.04	0.719	0.025	0.980	3466	11	3493	92	-1
June 25 2021	OG1-14	5.88E+05	27	0.2971	0.0021	29.09	1.03	0.708	0.025	0.980	3455	11	3451	92	0
June 25 2021	OG1-15	6.05E+05	81	0.2979	0.0021	29.78	1.02	0.723	0.024	0.979	3459	11	3505	90	-1
June 25 2021	OG1-16	5.04E+05	0	0.2967	0.0021	28.81	0.98	0.700	0.023	0.978	3453	11	3420	88	1
June 25 2021	OG1-17	4.40E+05	0	0.2983	0.0023	28.92	1.00	0.699	0.024	0.974	3461	12	3418	89	1
June 25 2021	OG1-18	5.07E+05	11	0.2961	0.0022	29.98	1.04	0.733	0.025	0.976	3450	12	3545	92	-3
June 25 2021	OG1-19	6.30E+05	13	0.2976	0.0023	29.38	1.02	0.714	0.024	0.976	3458	12	3472	90	0
June 25 2021	OG1-20	5.60E+05	0	0.2972	0.0025	29.24	1.04	0.715	0.025	0.972	3456	13	3477	92	-1
June 25 2021	OG1-21	5.79E+05	14	0.2973	0.0026	29.26	1.04	0.715	0.025	0.969	3456	14	3475	92	-1
July 7 2021	OG1-1	6.46E+05	0	0.2995	0.0021	30.37	1.04	0.738	0.025	0.979	3467	11	3562	91	-3
July 7 2021	OG1-2	2.80E+05	8	0.2974	0.0022	30.14	1.04	0.734	0.025	0.977	3457	11	3547	91	-3
July 7 2021	OG1-3	5.38E+05	0	0.2985	0.0021	29.53	1.01	0.721	0.024	0.978	3462	11	3499	90	-1
July 7 2021	OG1-4	5.64E+05	0	0.2987	0.0021	29.69	1.01	0.725	0.024	0.979	3463	11	3514	90	-1
July 7 2021	OG1-5	6.55E+05	127	0.2996	0.0021	29.59	1.01	0.715	0.024	0.980	3468	11	3478	90	0
July 7 2021	OG1-6	5.11E+05	2	0.2979	0.0020	29.52	1.00	0.716	0.024	0.979	3459	11	3482	89	-1
July 7 2021	OG1-7	9.06E+05	15	0.2976	0.0026	28.89	1.02	0.697	0.024	0.970	3458	13	3409	90	1
July 7 2021	OG1-8	5.70E+05	0	0.2979	0.0022	29.11	1.00	0.704	0.024	0.977	3459	11	3436	89	1
July 7 2021	OG1-9	8.17E+05	16	0.2970	0.0020	29.87	1.03	0.733	0.025	0.980	3455	11	3545	91	-3
July 7 2021	OG1-10	7.14E+05	82	0.2959	0.0021	29.39	1.00	0.724	0.024	0.979	3449	11	3512	90	-2
July 7 2021	OG1-11	5.00E+05	0	0.2969	0.0026	28.76	1.01	0.709	0.024	0.968	3454	14	3456	90	0
July 7 2021	OG1-12	5.26E+05	42	0.2965	0.0024	28.92	1.04	0.716	0.025	0.975	3452	12	3479	93	-1
July 7 2021	OG1-13	7.99E+05	48	0.2972	0.0021	30.00	1.02	0.734	0.025	0.979	3455	11	3548	91	-3
July 7 2021	OG1-14	5.98E+05	0	0.2971	0.0022	29.37	1.01	0.718	0.024	0.977	3455	11	3488	90	-1
July 7 2021	OG1-15	4.31E+05	0	0.2971	0.0022	29.82	1.04	0.726	0.025	0.977	3455	11	3518	91	-2
July 7 2021	OG1-16	5.58E+05	26	0.2979	0.0020	29.68	1.01	0.721	0.024	0.980	3459	11	3498	90	-1
July 7 2021	OG1-17	5.00E+05	5	0.2980	0.0021	29.67	1.06	0.721	0.025	0.981	3460	11	3500	94	-1
July 7 2021	OG1-18	6.67E+05	0	0.2951	0.0024	29.84	1.04	0.733	0.025	0.972	3445	13	3545	92	-3
July 9 2021	OG1-1	4.08E+05	33	0.2960	0.0023	27.98	0.98	0.685	0.023	0.975	3449	12	3365	89	3
July 9 2021	OG1-2	4.18E+05	0	0.2962	0.0025	29.50	1.04	0.722	0.025	0.970	3450	13	3505	92	-2
July 9 2021	OG1-3	6.52E+05	26	0.2973	0.0022	28.64	1.00	0.698	0.024	0.976	3456	12	3414	90	1
July 9 2021	OG1-4	2.43E+05	4	0.2976	0.0023	29.36	1.02	0.715	0.024	0.976	3458	12	3478	90	-1
July 9 2021	OG1-5	2.47E+05	39	0.2966	0.0024	29.23	1.02	0.713	0.024	0.974	3453	12	3470	91	-1
July 9 2021	OG1-6	3.74E+05	0	0.2975	0.0022	29.21	1.02	0.715	0.024	0.977	3457	11	3479	91	-1
July 9 2021	OG1-7	3.94E+05	41	0.2978	0.0027	29.44	1.06	0.721	0.025	0.968	3459	14	3500	94	-1
July 9 2021	OG1-8	5.80E+05	8	0.2978	0.0025	28.97	1.01	0.704	0.024	0.971	3459	13	3437	90	1
July 9 2021	OG1-9	6.85E+05	0	0.2984	0.0021	30.20	1.06	0.733	0.025	0.979	3462	11	3545	93	-2
July 9 2021	OG1-10	5.75E+05	0	0.2969	0.0021	29.10	1.01	0.709	0.024	0.980	3454	11	3455	91	0
July 9 2021	OG1-11	6.68E+05	53	0.2959	0.0024	29.01	1.01	0.709	0.024	0.974	3449	12	3456	90	0
July 9 2021	OG1-12	5.26E+05	0	0.2963	0.0022	28.48	0.98	0.696	0.023	0.977	3451	11	3404	88	1
July 9 2021	OG1-13	3.95E+05	0	0.2964	0.0024	28.89	1.00	0.706	0.024	0.973	3452	12	3443	89	0
July 9 2021	OG1-14	4.28E+05	7	0.2956	0.0021	29.05	1.00	0.714	0.024	0.980	3447	11	3472	90	-1
July 9 2021	OG1-15	4.49E+05	16	0.2968	0.0021	28.78	0.99	0.705	0.024	0.979	3454	11	3438	89	0
July 12 2021	OG1-1	6.56E+05	0	0.2984	0.0021	29.56	1.01	0.721	0.024	0.979	3462	11	3500	90	-1
July 12 2021	OG1-2	5.32E+05	0	0.2989	0.0021	29.90	1.03	0.729	0.024	0.978	3464	11	3529	91	-2
July 12 2021	OG1-3	5.58E+05	10	0.2990	0.0021	28.70	0.98	0.700	0.023	0.978	3465	11	3422	88	1
July 12 2021	OG1-4	4.37E+05	0	0.3000	0.0022	29.65	1.02	0.720	0.024	0.978	3470	11	3496	90	-1
July 12 2021	OG1-5	3.63E+05	0	0.2983	0.0021	30.15	1.04	0.735	0.025	0.978	3461	11	3552	92	-3
July 12 2021	OG1-6	4.26E+05	18	0.2980	0.0021	29.92	1.04	0.729	0.025	0.978	3460	11	3528	92	-2
July 12 2021	OG1-7	3.72E+05	0	0.2981	0.0021	29.10	1.00	0.707	0.024	0.978	3460	11	3446	89	0
July 12 2021	OG1-8	5.97E+05	14	0.2985	0.0022	28.86	1.00	0.704	0.024	0.977	3462	11	3436	90	1
July 12 2021	OG1-9	6.14E+05	0	0.2987	0.0023	30.23	1.17	0.739	0.028	0.980	3463	12	3567	103	-3
July 12 2021	OG1-10	6.00E+05	6	0.2981	0.0022	29.34	1.01	0.716	0.024	0.977	3460	11	3480	90	-1
July 12 2021	OG1-11	2.83E+05	7	0.2970	0.0022	29.10	1.00	0.712	0.024	0.976	3455	11	3464	89	0
July 12 2021	OG1-12	4.46E+05	0	0.2961	0.0021	28.42	0.98	0.693	0.023	0.978	3450	11	3393	88	2
July 12 2021	OG1-13	3.64E+05	0	0.2993	0.0023	28.55	0.99	0.691	0.023	0.975	3467	12	3386	89	2
July 12 2021	OG1-14	4.69E+05	8	0.2973	0.0022	28.22	0.97	0.690	0.023	0.976	3456	12	3381	88	2
July 12 2021	OG1-15	3.92E+05	2	0.2971	0.0022	31.10	1.12	0.759	0.027	0.978	3455	12	3641	97	-5
July 12 2021	OG1-16	1.02E+06	8	0.2975	0.0023	28.78	1.01	0.703	0.024	0.975	3457	12	3431	90	1

Table A-16. Secondary reference material Hf isotope data for the split-stream LA-ICPMS U-Pb-Hf method (section A.6).

Session	Spot ID	¹⁷⁶ Lu ¹⁷⁷ Hf	2SE	¹⁷⁶ Hf ¹⁷⁷ Hf	2SE	¹⁷⁶ Yb ¹⁷⁷ Hf	2SE	¹⁷⁸ Hf ¹⁷⁷ Hf	2SE	Total Hf (V)	Age (Ma)	¹⁷⁶ Hf ¹⁷⁷ Hf (i)	2SE	εHf(i)	2SE
June 25 2021	MUN1-1	0.001044	0.000033	0.282120	0.000030	0.03340	0.00150	1.467207	0.000041	12					
June 25 2021	MUN1-2	0.001466	0.000009	0.282140	0.000045	0.04859	0.00042	1.467138	0.000060	11					
June 25 2021	MUN1-3	0.001682	0.000004	0.282132	0.000039	0.05670	0.00029	1.467191	0.000045	11					
June 25 2021	MUN1-4	0.001192	0.000020	0.282113	0.000038	0.03850	0.00042	1.467157	0.000047	11					
June 25 2021	MUN1-5	0.000875	0.000043	0.282139	0.000032	0.02770	0.00110	1.467187	0.000041	12					
June 25 2021	MUN1-6	0.000652	0.000006	0.282164	0.000034	0.02132	0.00009	1.467159	0.000039	13					
June 25 2021	MUN1-7	0.001159	0.000033	0.282144	0.000046	0.03810	0.00160	1.467186	0.000055	12					
June 25 2021	MUN1-8	0.000657	0.000008	0.282130	0.000026	0.02184	0.00021	1.467155	0.000047	13					
June 25 2021	MUN1-9	0.000690	0.000038	0.282120	0.000026	0.02090	0.00100	1.467150	0.000039	12					
June 25 2021	MUN1-10	0.000630	0.000003	0.282132	0.000023	0.02030	0.00016	1.467153	0.000037	14					
June 25 2021	MUN3-1	0.002250	0.000036	0.282143	0.000037	0.06929	0.00077	1.467108	0.000039	13					
June 25 2021	MUN3-2	0.003577	0.000029	0.282147	0.000036	0.11700	0.00091	1.467173	0.000039	13					
June 25 2021	MUN3-3	0.002827	0.000031	0.282162	0.000037	0.09206	0.00059	1.467118	0.000046	14					
June 25 2021	MUN3-4	0.002857	0.000045	0.282164	0.000043	0.09060	0.00260	1.467202	0.000043	14					
June 25 2021	MUN3-5	0.003107	0.000049	0.282128	0.000047	0.10000	0.00170	1.467185	0.000056	10					
June 25 2021	MUN3-6	0.001335	0.000048	0.282131	0.000034	0.03910	0.00110	1.467189	0.000046	14					
June 25 2021	MUN3-7	0.003286	0.000008	0.282157	0.000072	0.09887	0.00088	1.467155	0.000052	9					
June 25 2021	MUN3-8	0.003580	0.000110	0.282138	0.000045	0.11580	0.00490	1.467144	0.000041	13					
June 25 2021	MUN3-9	0.002010	0.000190	0.282096	0.000061	0.05530	0.00550	1.467203	0.000055	9					
June 25 2021	MUN3-10	0.001680	0.000130	0.282090	0.000038	0.04560	0.00320	1.467225	0.000046	11					
July 7 2021	MUN1-1	0.000771	0.000060	0.282151	0.000031	0.02610	0.00230	1.467151	0.000028	13					
July 7 2021	MUN1-2	0.001185	0.000030	0.282138	0.000033	0.03967	0.00067	1.467153	0.000051	12					
July 7 2021	MUN1-3	0.000738	0.000036	0.282131	0.000027	0.02300	0.00150	1.467182	0.000048	11					
July 7 2021	MUN1-4	0.001146	0.000045	0.282130	0.000030	0.03740	0.00190	1.467123	0.000054	11					
July 7 2021	MUN1-5	0.001290	0.000022	0.282139	0.000042	0.04352	0.00044	1.467217	0.000044	12					
July 7 2021	MUN1-6	0.000960	0.000100	0.282141	0.000036	0.03270	0.00370	1.467150	0.000048	12					
July 7 2021	MUN1-7	0.000492	0.000018	0.282149	0.000033	0.01486	0.00032	1.467183	0.000041	13					
July 7 2021	MUN1-8	0.000983	0.000041	0.282159	0.000024	0.03430	0.00160	1.467204	0.000060	11					
July 7 2021	MUN3-1	0.003054	0.000035	0.282112	0.000042	0.09703	0.00047	1.467182	0.000048	12					
July 7 2021	MUN3-2	0.001099	0.000044	0.282149	0.000028	0.03270	0.00200	1.467133	0.000038	14					
July 7 2021	MUN3-3	0.003012	0.000019	0.282130	0.000043	0.09120	0.00150	1.467134	0.000042	9					
July 7 2021	MUN3-4	0.002796	0.000014	0.282113	0.000046	0.08540	0.00100	1.467166	0.000050	9					
July 7 2021	MUN3-5	0.003525	0.000026	0.282126	0.000043	0.11230	0.00200	1.467146	0.000051	11					
July 7 2021	MUN3-6	0.003608	0.000026	0.282101	0.000051	0.11912	0.00043	1.467143	0.000041	12					
July 7 2021	MUN3-7	0.002744	0.000010	0.282110	0.000037	0.08761	0.00083	1.467183	0.000043	13					
July 7 2021	MUN3-8	0.001810	0.000160	0.282140	0.000035	0.05720	0.00620	1.467204	0.000051	15					
July 9 2021	MUN1-1	0.000717	0.000004	0.282119	0.000033	0.02355	0.00016	1.467129	0.000047	13					
July 9 2021	MUN1-2	0.000953	0.000015	0.282166	0.000042	0.03006	0.00035	1.467172	0.000053	12					
July 9 2021	MUN1-3	0.000907	0.000016	0.282138	0.000029	0.02874	0.00093	1.467188	0.000034	13					
July 9 2021	MUN1-4	0.000664	0.000018	0.282154	0.000033	0.01983	0.00038	1.467158	0.000049	11					
July 9 2021	MUN1-5	0.001278	0.000021	0.282179	0.000041	0.04174	0.00037	1.467158	0.000051	11					
July 9 2021	MUN1-6	0.000494	0.000043	0.282147	0.000026	0.01480	0.00160	1.467186	0.000041	12					
July 9 2021	MUN1-7	0.000479	0.000033	0.282125	0.000029	0.01447	0.00096	1.467245	0.000044	14					
July 9 2021	MUN3-1	0.003967	0.000029	0.282135	0.000052	0.13045	0.00031	1.467131	0.000058	12					
July 9 2021	MUN3-2	0.002850	0.000016	0.282154	0.000033	0.09270	0.00110	1.467123	0.000054	13					
July 9 2021	MUN3-3	0.002814	0.000030	0.282119	0.000041	0.09122	0.00070	1.467088	0.000047	14					
July 9 2021	MUN3-4	0.004250	0.000061	0.282118	0.000049	0.13910	0.00110	1.467167	0.000056	12					
July 9 2021	MUN3-5	0.002545	0.000024	0.282123	0.000044	0.07437	0.00026	1.467177	0.000061	9					
July 9 2021	MUN3-6	0.004900	0.001100	0.282020	0.000130	0.18100	0.04700	1.467292	0.000085	7					
July 9 2021	MUN3-7	0.002969	0.000007	0.282154	0.000049	0.09650	0.00140	1.467165	0.000050	14					
July 12 2021	MUN1-1	0.000671	0.000002	0.282138	0.000027	0.02200	0.00016	1.467123	0.000045	13					

Session	Spot ID	¹⁷⁶ Lu 177Hf	2SE	¹⁷⁶ Hf 177Hf	2SE	¹⁷⁶ Yb 177Hf	2SE	¹⁷⁸ Hf 177Hf	2SE	Total Hf (V)	Age (Ma)	¹⁷⁶ Hf 177Hf (i)	2SE	εHf(i)	2SE
July 12 2021	MUN1-2	0.000779	0.000006	0.282123	0.000043	0.02393	0.00013	1.467183	0.000046	11					
July 12 2021	MUN1-3	0.000613	0.000004	0.282132	0.000028	0.02026	0.00015	1.467132	0.000043	13					
July 12 2021	MUN1-4	0.000459	0.000017	0.282130	0.000029	0.01399	0.00036	1.467187	0.000060	13					
July 12 2021	MUN1-5	0.000703	0.000002	0.282134	0.000032	0.02301	0.00016	1.467182	0.000046	12					
July 12 2021	MUN1-6	0.000647	0.000007	0.282131	0.000030	0.02124	0.00012	1.467141	0.000045	13					
July 12 2021	MUN1-7	0.000606	0.000009	0.282105	0.000025	0.01965	0.00018	1.467163	0.000045	13					
July 12 2021	MUN3-1	0.003896	0.000049	0.282144	0.000049	0.12830	0.00130	1.467150	0.000044	13					
July 12 2021	MUN3-2	0.003487	0.000024	0.282128	0.000037	0.11260	0.00210	1.467183	0.000050	13					
July 12 2021	MUN3-3	0.002516	0.000034	0.282134	0.000034	0.07817	0.00075	1.467167	0.000049	13					
July 12 2021	MUN3-4	0.004254	0.000007	0.282189	0.000054	0.13370	0.00140	1.467142	0.000045	11					
July 12 2021	MUN3-5	0.002981	0.000009	0.282126	0.000046	0.09167	0.00042	1.467185	0.000048	11					
July 12 2021	MUN3-6	0.001187	0.000088	0.282133	0.000042	0.03720	0.00260	1.467129	0.000064	10					
July 12 2021	MUN3-7	0.002853	0.000023	0.282185	0.000052	0.08388	0.00040	1.467193	0.000051	9					
June 25 2021	OG1-1	0.002000	0.000110	0.280667	0.000054	0.05960	0.00310	1.467151	0.000062	10	3467	0.280533	0.000054	-0.2	1.9
June 25 2021	OG1-2	0.001930	0.000140	0.280711	0.000041	0.05680	0.00440	1.467180	0.000044	8	3467	0.280582	0.000042	1.6	1.5
June 25 2021	OG1-3	0.001260	0.000190	0.280635	0.000041	0.03740	0.00600	1.467211	0.000043	9	3467	0.280551	0.000043	0.4	1.5
June 25 2021	OG1-4	0.001320	0.000034	0.280662	0.000051	0.03735	0.00085	1.467183	0.000059	9	3467	0.280574	0.000051	1.3	1.8
June 25 2021	OG1-5	0.001033	0.000027	0.280656	0.000039	0.02999	0.00080	1.467217	0.000052	10	3467	0.280587	0.000039	1.7	1.4
June 25 2021	OG1-6	0.001210	0.000110	0.280625	0.000043	0.03590	0.00340	1.467150	0.000062	9	3467	0.280544	0.000044	0.2	1.6
June 25 2021	OG1-7	0.001270	0.000130	0.280619	0.000045	0.03850	0.00400	1.467197	0.000053	10	3467	0.280534	0.000046	-0.1	1.6
June 25 2021	OG1-8	0.001345	0.000058	0.280688	0.000046	0.03900	0.00200	1.467181	0.000053	8	3467	0.280598	0.000046	2.1	1.6
June 25 2021	OG1-9	0.001286	0.000074	0.280663	0.000036	0.03660	0.00270	1.467148	0.000052	8	3467	0.280577	0.000036	1.4	1.3
June 25 2021	OG1-10	0.000780	0.000060	0.280644	0.000036	0.02010	0.00160	1.467152	0.000048	9	3467	0.280592	0.000036	1.9	1.3
June 25 2021	OG1-11	0.001316	0.000068	0.280687	0.000042	0.03670	0.00210	1.467217	0.000064	8	3467	0.280599	0.000042	2.2	1.5
June 25 2021	OG1-12	0.001638	0.000064	0.280675	0.000042	0.04870	0.00220	1.467158	0.000055	8	3467	0.280565	0.000042	1.0	1.5
June 25 2021	OG1-13	0.001860	0.000170	0.280721	0.000053	0.05580	0.00600	1.467145	0.000059	9	3467	0.280597	0.000054	2.1	1.9
June 25 2021	OG1-14	0.001620	0.000150	0.280712	0.000049	0.04800	0.00530	1.467183	0.000061	9	3467	0.280604	0.000050	2.3	1.8
June 25 2021	OG1-15	0.001660	0.000130	0.280633	0.000050	0.04930	0.00400	1.467231	0.000061	9	3467	0.280522	0.000051	-0.6	1.8
June 25 2021	OG1-16	0.001541	0.000075	0.280653	0.000044	0.04550	0.00220	1.467161	0.000067	9	3467	0.280550	0.000044	0.4	1.6
June 25 2021	OG1-17	0.001301	0.000051	0.280652	0.000047	0.03870	0.00150	1.467152	0.000043	9	3467	0.280565	0.000047	1.0	1.7
June 25 2021	OG1-18	0.001169	0.000044	0.280601	0.000045	0.03260	0.00140	1.467207	0.000053	9	3467	0.280523	0.000045	-0.5	1.6
June 25 2021	OG1-19	0.001722	0.000059	0.280694	0.000045	0.05100	0.00290	1.467156	0.000060	9	3467	0.280579	0.000045	1.4	1.6
June 25 2021	OG1-20	0.001371	0.000083	0.280652	0.000038	0.04060	0.00320	1.467175	0.000045	9	3467	0.280560	0.000038	0.8	1.4
June 25 2021	OG1-21	0.001330	0.000100	0.280616	0.000048	0.03980	0.00360	1.467175	0.000055	9	3467	0.280527	0.000048	-0.4	1.7
July 7 2021	OG1-1	0.000963	0.000077	0.280631	0.000042	0.02530	0.00230	1.467149	0.000047	9	3467	0.280567	0.000042	1.0	1.5
July 7 2021	OG1-2	0.000643	0.000038	0.280582	0.000039	0.01820	0.00130	1.467151	0.000057	10	3467	0.280539	0.000039	0.0	1.4
July 7 2021	OG1-3	0.001470	0.000110	0.280660	0.000055	0.04320	0.00310	1.467170	0.000049	8	3467	0.280562	0.000055	0.8	2.0
July 7 2021	OG1-4	0.001607	0.000098	0.280643	0.000056	0.04800	0.00320	1.467157	0.000073	8	3467	0.280536	0.000056	-0.1	2.0
July 7 2021	OG1-5	0.001780	0.000068	0.280672	0.000049	0.05320	0.00180	1.467173	0.000046	8	3467	0.280553	0.000049	0.5	1.8
July 7 2021	OG1-6	0.001229	0.000009	0.280631	0.000044	0.03363	0.00033	1.467175	0.000051	8	3467	0.280549	0.000044	0.4	1.6
July 7 2021	OG1-7	0.002070	0.000190	0.280630	0.000086	0.06460	0.00540	1.467177	0.000064	11	3467	0.280492	0.000087	-1.7	3.1
July 7 2021	OG1-8	0.001621	0.000091	0.280726	0.000052	0.04810	0.00270	1.467268	0.000059	8	3467	0.280618	0.000052	2.8	1.9
July 7 2021	OG1-9	0.001710	0.000170	0.280660	0.000045	0.05020	0.00630	1.467189	0.000048	9	3467	0.280546	0.000046	0.3	1.7
July 7 2021	OG1-10	0.001510	0.000110	0.280706	0.000041	0.04380	0.00390	1.467230	0.000058	9	3467	0.280605	0.000042	2.4	1.5
July 7 2021	OG1-11	0.001206	0.000084	0.280662	0.000058	0.03720	0.00240	1.467216	0.000055	10	3467	0.280581	0.000058	1.5	2.1
July 7 2021	OG1-12	0.000863	0.000090	0.280622	0.000040	0.02580	0.00290	1.467150	0.000055	10	3467	0.280564	0.000040	0.9	1.4
July 7 2021	OG1-13	0.001365	0.000093	0.280626	0.000045	0.03620	0.00280	1.467160	0.000068	8	3467	0.280535	0.000045	-0.1	1.6
July 7 2021	OG1-14	0.001437	0.000063	0.280630	0.000056	0.04340	0.00190	1.467187	0.000046	9	3467	0.280534	0.000056	-0.2	2.0
July 7 2021	OG1-15	0.001103	0.000098	0.280603	0.000044	0.03170	0.00300	1.467215	0.000049	9	3467	0.280529	0.000044	-0.3	1.6
July 7 2021	OG1-16	0.001371	0.000057	0.280626	0.000055	0.03990	0.00180	1.467163	0.000052	8	3467	0.280534	0.000055	-0.1	2.0
July 7 2021	OG1-17	0.001380	0.000140	0.280640	0.000040	0.04090	0.00450	1.467220	0.000057	8	3467	0.280548	0.000041	0.3	1.5
July 7 2021	OG1-18	0.001091	0.000028	0.280625	0.000065	0.03130	0.00100	1.467197	0.000067	11	3467	0.280552	0.000065	0.5	2.3
July 9 2021	OG1-1	0.001230	0.000110	0.280645	0.000045	0.03580	0.00310	1.467205	0.000049	9	3467	0.280563	0.000046	0.9	1.6
July 9 2021	OG1-2	0.001018	0.000048	0.280597	0.000033	0.03030	0.00140	1.467180	0.000056	10	3467	0.280529	0.000033	-0.3	1.2
July 9 2021	OG1-3	0.001880	0.000180	0.280668	0.000057	0.05650	0.00550	1.467143	0.000058	9	3467	0.280542	0.000058	0.1	2.1

Session	Spot ID	¹⁷⁶ Lu ¹⁷⁷ Hf	2SE	¹⁷⁶ Hf ¹⁷⁷ Hf	2SE	¹⁷⁶ Yb ¹⁷⁷ Hf	2SE	¹⁷⁸ Hf ¹⁷⁷ Hf	2SE	Total Hf (V)	Age (Ma)	¹⁷⁶ Hf ¹⁷⁷ Hf (i)	2SE	εHf(i)	2SE
July 9 2021	OG1-4	0.00060	0.00003	0.280638	0.000045	0.01590	0.00110	1.467150	0.000051	10	3467	0.280598	0.000045	2.1	1.6
July 9 2021	OG1-5	0.00060	0.00004	0.280593	0.000049	0.01610	0.00130	1.467089	0.000076	10	3467	0.280553	0.000049	0.5	1.7
July 9 2021	OG1-6	0.00115	0.00007	0.280649	0.000056	0.03330	0.00190	1.467130	0.000055	9	3467	0.280572	0.000056	1.2	2.0
July 9 2021	OG1-7	0.00103	0.00008	0.280628	0.000037	0.02970	0.00230	1.467141	0.000038	9	3467	0.280559	0.000037	0.8	1.3
July 9 2021	OG1-8	0.00159	0.00006	0.280701	0.000049	0.04860	0.00170	1.467127	0.000059	10	3467	0.280595	0.000049	2.0	1.8
July 9 2021	OG1-9	0.00176	0.00014	0.280698	0.000043	0.04960	0.00470	1.467133	0.000058	8	3467	0.280580	0.000044	1.5	1.6
July 9 2021	OG1-10	0.00157	0.00021	0.280662	0.000046	0.04490	0.00670	1.467166	0.000051	9	3467	0.280557	0.000048	0.7	1.7
July 9 2021	OG1-11	0.00168	0.00021	0.280671	0.000048	0.04830	0.00670	1.467158	0.000056	9	3467	0.280559	0.000050	0.7	1.8
July 9 2021	OG1-12	0.00145	0.00008	0.280669	0.000048	0.04090	0.00250	1.467164	0.000066	9	3467	0.280572	0.000048	1.2	1.7
July 9 2021	OG1-13	0.00082	0.00005	0.280652	0.000050	0.02170	0.00130	1.467165	0.000051	9	3467	0.280597	0.000050	2.1	1.8
July 9 2021	OG1-14	0.00112	0.00003	0.280584	0.000040	0.03070	0.00100	1.467209	0.000043	9	3467	0.280509	0.000040	-1.0	1.4
July 9 2021	OG1-15	0.00146	0.00007	0.280676	0.000050	0.04320	0.00190	1.467158	0.000062	8	3467	0.280578	0.000050	1.4	1.8
July 12 2021	OG1-1	0.00181	0.00010	0.280708	0.000039	0.05250	0.00390	1.467181	0.000055	8	3467	0.280587	0.000040	1.7	1.4
July 12 2021	OG1-2	0.00146	0.00006	0.280682	0.000053	0.04190	0.00190	1.467195	0.000064	9	3467	0.280585	0.000053	1.7	1.9
July 12 2021	OG1-3	0.00183	0.00018	0.280673	0.000048	0.05400	0.00520	1.467136	0.000053	9	3467	0.280551	0.000049	0.4	1.8
July 12 2021	OG1-4	0.00149	0.00009	0.280651	0.000043	0.04370	0.00250	1.467155	0.000055	8	3467	0.280551	0.000043	0.5	1.5
July 12 2021	OG1-5	0.00118	0.00009	0.280639	0.000040	0.03430	0.00280	1.467175	0.000054	8	3467	0.280560	0.000040	0.8	1.4
July 12 2021	OG1-6	0.00131	0.00010	0.280635	0.000045	0.03780	0.00310	1.467118	0.000049	8	3467	0.280548	0.000045	0.3	1.6
July 12 2021	OG1-7	0.00083	0.00007	0.280591	0.000045	0.02170	0.00170	1.467133	0.000064	10	3467	0.280535	0.000045	-0.1	1.6
July 12 2021	OG1-8	0.00188	0.00012	0.280716	0.000051	0.05670	0.00330	1.467265	0.000051	9	3467	0.280590	0.000052	1.9	1.8
July 12 2021	OG1-9	0.00162	0.00019	0.280681	0.000039	0.04850	0.00600	1.467186	0.000064	8	3467	0.280573	0.000041	1.2	1.5
July 12 2021	OG1-10	0.00174	0.00008	0.280689	0.000047	0.05150	0.00250	1.467166	0.000057	8	3467	0.280573	0.000047	1.2	1.7
July 12 2021	OG1-11	0.00072	0.00004	0.280603	0.000039	0.01890	0.00120	1.467210	0.000053	9	3467	0.280555	0.000039	0.6	1.4
July 12 2021	OG1-12	0.00135	0.00005	0.280655	0.000041	0.03910	0.00140	1.467152	0.000064	9	3467	0.280565	0.000041	0.9	1.5
July 12 2021	OG1-13	0.00109	0.00004	0.280633	0.000055	0.03206	0.00091	1.467184	0.000057	9	3467	0.280560	0.000055	0.8	2.0
July 12 2021	OG1-14	0.00130	0.00006	0.280695	0.000059	0.03710	0.00180	1.467234	0.000048	8	3467	0.280608	0.000059	2.5	2.1
July 12 2021	OG1-15	0.00101	0.00012	0.280640	0.000046	0.02960	0.00400	1.467219	0.000048	9	3467	0.280572	0.000047	1.2	1.7
July 12 2021	OG1-16	0.00204	0.00026	0.280707	0.000051	0.06010	0.00890	1.467133	0.000061	10	3467	0.280571	0.000054	1.2	1.9
June 25 2021	91500-1	0.00034	0.00000	0.282290	0.000051	0.00986	0.00008	1.467180	0.000074	6	1065	0.282283	0.000051	6.1	1.8
June 25 2021	91500-2	0.00034	0.00000	0.282333	0.000055	0.00989	0.00009	1.467175	0.000072	6	1065	0.282326	0.000055	7.7	1.9
June 25 2021	91500-3	0.00034	0.00000	0.282315	0.000052	0.00979	0.00006	1.467122	0.000054	6	1065	0.282308	0.000052	7.0	1.8
June 25 2021	91500-4	0.00034	0.00000	0.282314	0.000040	0.01012	0.00006	1.467180	0.000069	6	1065	0.282307	0.000040	7.0	1.4
June 25 2021	91500-5	0.00034	0.00000	0.282306	0.000045	0.01022	0.00009	1.467162	0.000062	6	1065	0.282299	0.000045	6.7	1.6
June 25 2021	91500-6	0.00034	0.00000	0.282292	0.000048	0.01017	0.00006	1.467221	0.000060	6	1065	0.282285	0.000048	6.2	1.7
June 25 2021	91500-7	0.00034	0.00000	0.282339	0.000046	0.01039	0.00008	1.467054	0.000054	6	1065	0.282332	0.000046	7.9	1.6
June 25 2021	91500-8	0.00035	0.00000	0.282349	0.000041	0.01036	0.00008	1.467172	0.000075	6	1065	0.282342	0.000041	8.2	1.5
June 25 2021	91500-9	0.00034	0.00000	0.282300	0.000050	0.01024	0.00008	1.467180	0.000064	6	1065	0.282293	0.000050	6.5	1.8
June 25 2021	91500-10	0.00034	0.00000	0.282328	0.000041	0.01004	0.00009	1.467213	0.000057	6	1065	0.282321	0.000041	7.5	1.5
June 25 2021	91500-11	0.00035	0.00000	0.282309	0.000055	0.01012	0.00010	1.467156	0.000061	6	1065	0.282302	0.000055	6.8	1.9
June 25 2021	91500-12	0.00036	0.00000	0.282310	0.000051	0.01043	0.00008	1.467191	0.000055	6	1065	0.282303	0.000051	6.8	1.8
June 25 2021	91500-13	0.00035	0.00000	0.282339	0.000043	0.01024	0.00009	1.467218	0.000058	6	1065	0.282332	0.000043	7.9	1.5
June 25 2021	91500-14	0.00035	0.00000	0.282333	0.000048	0.01036	0.00006	1.467189	0.000076	6	1065	0.282326	0.000048	7.6	1.7
June 25 2021	91500-15	0.00034	0.00000	0.282312	0.000040	0.01012	0.00007	1.467203	0.000059	6	1065	0.282305	0.000040	6.9	1.4
June 25 2021	91500-16	0.00035	0.00000	0.282248	0.000052	0.01021	0.00006	1.467198	0.000050	6	1065	0.282241	0.000052	4.6	1.8
June 25 2021	91500-17	0.00034	0.00000	0.282275	0.000048	0.01027	0.00006	1.467205	0.000068	7	1065	0.282268	0.000048	5.6	1.7
June 25 2021	91500-18	0.00035	0.00000	0.282262	0.000046	0.01066	0.00009	1.467212	0.000064	6	1065	0.282255	0.000046	5.1	1.6
June 25 2021	91500-19	0.00035	0.00000	0.282311	0.000053	0.01045	0.00007	1.467157	0.000067	6	1065	0.282304	0.000053	6.9	1.9
July 7 2021	91500-1	0.00034	0.00000	0.282358	0.000060	0.01049	0.00013	1.467084	0.000065	6	1065	0.282351	0.000060	8.5	2.1
July 7 2021	91500-2	0.00034	0.00000	0.282328	0.000050	0.01019	0.00011	1.467165	0.000064	6	1065	0.282321	0.000050	7.5	1.8
July 7 2021	91500-3	0.00035	0.00000	0.282362	0.000052	0.01029	0.00013	1.467158	0.000057	6	1065	0.282355	0.000052	8.7	1.8
July 7 2021	91500-4	0.00035	0.00000	0.282301	0.000069	0.01047	0.00009	1.467123	0.000051	6	1065	0.282294	0.000069	6.5	2.4
July 7 2021	91500-5	0.00035	0.00000	0.282295	0.000048	0.01046	0.00008	1.467164	0.000063	6	1065	0.282288	0.000048	6.3	1.7
July 7 2021	91500-6	0.00034	0.00000	0.282287	0.000065	0.01055	0.00014	1.467174	0.000076	6	1065	0.282280	0.000065	6.0	2.3
July 7 2021	91500-7	0.00033	0.00000	0.282362	0.000064	0.01012	0.00011	1.467159	0.000072	6	1065	0.282355	0.000064	8.7	2.3
July 7 2021	91500-8	0.00035	0.00000	0.282225	0.000050	0.01067	0.00008	1.467167	0.000068	6	1065	0.282218	0.000050	3.8	1.8
July 7 2021	91500-9	0.00036	0.00000	0.282289	0.000058	0.01085	0.00008	1.467170	0.000071	6	1065	0.282282	0.000058	6.1	2.1

Session	Spot ID	¹⁷⁶ Lu ¹⁷⁷ Hf	2SE	¹⁷⁶ Hf ¹⁷⁷ Hf	2SE	¹⁷⁶ Yb ¹⁷⁷ Hf	2SE	¹⁷⁸ Hf ¹⁷⁷ Hf	2SE	Total Hf (V)	Age (Ma)	¹⁷⁶ Hf ¹⁷⁷ Hf (i)	2SE	εHf(i)	2SE
July 7 2021	91500-10	0.000363	0.000001	0.282328	0.000057	0.01096	0.00008	1.467110	0.000064	6	1065	0.282321	0.000057	7.5	2.0
July 7 2021	91500-11	0.000364	0.000001	0.282294	0.000054	0.01091	0.00009	1.467180	0.000054	6	1065	0.282287	0.000054	6.3	1.9
July 7 2021	91500-12	0.000349	0.000001	0.282296	0.000037	0.01065	0.00013	1.467116	0.000055	6	1065	0.282289	0.000037	6.3	1.3
July 7 2021	91500-13	0.000340	0.000001	0.282295	0.000064	0.01038	0.00010	1.467157	0.000056	6	1065	0.282288	0.000064	6.3	2.3
July 7 2021	91500-14	0.000337	0.000001	0.282306	0.000042	0.01021	0.00009	1.467182	0.000078	6	1065	0.282299	0.000042	6.7	1.5
July 7 2021	91500-15	0.000331	0.000001	0.282293	0.000048	0.00993	0.00008	1.467151	0.000052	6	1065	0.282286	0.000048	6.2	1.7
July 7 2021	91500-16	0.000330	0.000001	0.282330	0.000060	0.00993	0.00010	1.467264	0.000056	6	1065	0.282323	0.000060	7.6	2.1
July 7 2021	91500-17	0.000325	0.000001	0.282339	0.000051	0.00976	0.00012	1.467147	0.000073	6	1065	0.282332	0.000051	7.9	1.8
July 7 2021	91500-18	0.000346	0.000001	0.282299	0.000046	0.01053	0.00009	1.467213	0.000063	6	1065	0.282292	0.000046	6.4	1.6
July 7 2021	91500-19	0.000335	0.000001	0.282298	0.000045	0.01008	0.00007	1.467150	0.000042	6	1065	0.282291	0.000045	6.4	1.6
July 9 2021	91500-1	0.000334	0.000001	0.282302	0.000060	0.00991	0.00010	1.467126	0.000060	6	1065	0.282295	0.000060	6.6	2.1
July 9 2021	91500-2	0.000325	0.000001	0.282315	0.000047	0.00962	0.00009	1.467098	0.000060	6	1065	0.282308	0.000047	7.0	1.7
July 9 2021	91500-3	0.000330	0.000001	0.282304	0.000052	0.00985	0.00007	1.467177	0.000057	6	1065	0.282297	0.000052	6.6	1.8
July 9 2021	91500-4	0.000324	0.000001	0.282319	0.000043	0.00975	0.00017	1.467188	0.000059	6	1065	0.282312	0.000043	7.2	1.5
July 9 2021	91500-5	0.000327	0.000001	0.282305	0.000045	0.00958	0.00009	1.467203	0.000061	6	1065	0.282298	0.000045	6.7	1.6
July 9 2021	91500-6	0.000331	0.000001	0.282314	0.000049	0.00954	0.00008	1.467071	0.000069	6	1065	0.282307	0.000049	7.0	1.7
July 9 2021	91500-7	0.000331	0.000001	0.282345	0.000051	0.00972	0.00012	1.467156	0.000058	6	1065	0.282338	0.000051	8.1	1.8
July 9 2021	91500-8	0.000328	0.000001	0.282374	0.000045	0.00948	0.00010	1.467137	0.000059	6	1065	0.282367	0.000045	9.1	1.6
July 9 2021	91500-9	0.000328	0.000001	0.282297	0.000048	0.00957	0.00008	1.467120	0.000065	6	1065	0.282290	0.000048	6.4	1.7
July 9 2021	91500-10	0.000327	0.000001	0.282333	0.000043	0.00964	0.00016	1.467220	0.000066	6	1065	0.282326	0.000043	7.7	1.5
July 9 2021	91500-11	0.000327	0.000001	0.282371	0.000049	0.00946	0.00011	1.467193	0.000066	6	1065	0.282364	0.000049	9.0	1.7
July 9 2021	91500-12	0.000318	0.000001	0.282291	0.000049	0.00921	0.00012	1.467153	0.000054	6	1065	0.282285	0.000049	6.2	1.7
July 9 2021	91500-13	0.000317	0.000001	0.282321	0.000040	0.00919	0.00011	1.467139	0.000067	6	1065	0.282315	0.000040	7.2	1.4
July 9 2021	91500-14	0.000317	0.000001	0.282331	0.000060	0.00931	0.00013	1.467149	0.000067	7	1065	0.282325	0.000060	7.6	2.1
July 9 2021	91500-15	0.000318	0.000001	0.282271	0.000039	0.00926	0.00010	1.467169	0.000068	6	1065	0.282265	0.000039	5.5	1.4
July 12 2021	91500-1	0.000316	0.000001	0.282286	0.000045	0.00905	0.00008	1.467147	0.000070	6	1065	0.282280	0.000045	6.0	1.6
July 12 2021	91500-2	0.000314	0.000001	0.282329	0.000045	0.00893	0.00007	1.467164	0.000047	6	1065	0.282323	0.000045	7.5	1.6
July 12 2021	91500-3	0.000314	0.000001	0.282266	0.000051	0.00896	0.00008	1.467166	0.000059	6	1065	0.282260	0.000051	5.3	1.8
July 12 2021	91500-4	0.000318	0.000001	0.282361	0.000040	0.00918	0.00014	1.467233	0.000068	7	1065	0.282355	0.000040	8.7	1.4
July 12 2021	91500-5	0.000325	0.000001	0.282329	0.000047	0.00931	0.00007	1.467132	0.000060	7	1065	0.282322	0.000047	7.5	1.7
July 12 2021	91500-6	0.000328	0.000001	0.282326	0.000057	0.00945	0.00011	1.467169	0.000077	6	1065	0.282319	0.000057	7.4	2.0
July 12 2021	91500-7	0.000320	0.000001	0.282253	0.000049	0.00926	0.00010	1.467144	0.000065	7	1065	0.282247	0.000049	4.8	1.7
July 12 2021	91500-8	0.000328	0.000001	0.282279	0.000041	0.00959	0.00011	1.467203	0.000053	6	1065	0.282272	0.000041	5.7	1.5
July 12 2021	91500-9	0.000327	0.000001	0.282325	0.000045	0.00960	0.00007	1.467210	0.000055	6	1065	0.282318	0.000045	7.4	1.6
July 12 2021	91500-10	0.000326	0.000001	0.282352	0.000048	0.00963	0.00009	1.467190	0.000085	6	1065	0.282345	0.000048	8.3	1.7
July 12 2021	91500-11	0.000318	0.000001	0.282339	0.000041	0.00921	0.00010	1.467220	0.000060	6	1065	0.282333	0.000041	7.9	1.5
July 12 2021	91500-12	0.000320	0.000001	0.282282	0.000050	0.00925	0.00012	1.467128	0.000063	6	1065	0.282276	0.000050	5.9	1.8
July 12 2021	91500-13	0.000323	0.000001	0.282270	0.000057	0.00943	0.00009	1.467185	0.000064	6	1065	0.282264	0.000057	5.4	2.0
July 12 2021	91500-14	0.000316	0.000001	0.282306	0.000051	0.00929	0.00020	1.467218	0.000064	7	1065	0.282300	0.000051	6.7	1.8
July 12 2021	91500-15	0.000322	0.000001	0.282291	0.000060	0.00946	0.00012	1.467137	0.000072	6	1065	0.282285	0.000060	6.2	2.1
July 12 2021	91500-16	0.000321	0.000001	0.282316	0.000051	0.00940	0.00009	1.467194	0.000042	6	1065	0.282310	0.000051	7.1	1.8

Table A-17. Secondary reference material data for the single-stream LA-MC-ICPMS Hf isotope method (section A.7).

Session	Spot ID	¹⁷⁶ Lu 177Hf	2SE	¹⁷⁶ Hf 177Hf	2SE	¹⁷⁶ Yb 177Hf	2SE	¹⁷⁸ Hf 177Hf	2SE	Total Hf (V)	Age (Ma)	¹⁷⁶ Hf/ 177Hf (i)	2SE	εHf(i)	2SE
July 6 2022	MUN1-1	0.000384	0.000021	0.282151	0.000029	0.00920	0.00049	1.467134	0.000043	9					
July 6 2022	MUN1-2	0.000663	0.000008	0.282112	0.000039	0.01833	0.00016	1.467182	0.000038	9					
July 6 2022	MUN1-3	0.000590	0.000017	0.282125	0.000034	0.01593	0.00043	1.467199	0.000040	9					
July 6 2022	MUN1-4	0.000573	0.000029	0.282169	0.000039	0.01546	0.00079	1.467172	0.000049	9					
July 6 2022	MUN3-1	0.003300	0.000110	0.282140	0.000051	0.08950	0.00340	1.467176	0.000048	9					
July 6 2022	MUN3-2	0.002442	0.000071	0.282134	0.000036	0.06500	0.00190	1.467150	0.000054	10					
July 6 2022	MUN3-3	0.003107	0.000098	0.282132	0.000038	0.08390	0.00330	1.467178	0.000051	9					
July 6 2022	MUN3-4	0.003290	0.000110	0.282126	0.000050	0.09090	0.00350	1.467175	0.000052	9					
Dec 20 2022	MUN1-1	0.003284	0.000050	0.282139	0.000017	0.01830	0.00019	1.467176	0.000034	21					
Dec 20 2022	MUN1-2	0.002876	0.000036	0.282134	0.000023	0.01461	0.00026	1.467172	0.000030	19					
Dec 20 2022	MUN1-3	0.003121	0.000038	0.282119	0.000019	0.01717	0.00013	1.467151	0.000034	21					
Dec 20 2022	MUN1-4	0.003115	0.000048	0.282124	0.000022	0.01623	0.00033	1.467160	0.000029	19					
Dec 20 2022	MUN1-5	0.003202	0.000068	0.282137	0.000017	0.01748	0.00031	1.467159	0.000026	22					
Dec 20 2022	MUN1-6	0.003149	0.000068	0.282129	0.000018	0.01698	0.00035	1.467153	0.000028	22					
Dec 20 2022	MUN1-7	0.003081	0.000049	0.282142	0.000020	0.01734	0.00016	1.467161	0.000025	22					
Dec 20 2022	MUN1-8	0.002974	0.000042	0.282128	0.000017	0.01663	0.00020	1.467162	0.000033	23					
Dec 20 2022	MUN3-1	0.003402	0.000027	0.282117	0.000021	0.02677	0.00037	1.467177	0.000031	23					
Dec 20 2022	MUN3-2	0.003340	0.000120	0.282141	0.000016	0.02790	0.00100	1.467164	0.000025	31					
Dec 20 2022	MUN3-3	0.002752	0.000018	0.282132	0.000014	0.02282	0.00014	1.467164	0.000023	31					
Dec 20 2022	MUN3-4	0.002854	0.000025	0.282128	0.000016	0.02321	0.00020	1.467129	0.000033	29					
Dec 20 2022	MUN3-5	0.002600	0.000300	0.282147	0.000016	0.02160	0.00260	1.467149	0.000025	27					
Dec 20 2022	MUN3-6	0.003686	0.000014	0.282153	0.000018	0.03017	0.00016	1.467176	0.000031	26					
Dec 20 2022	MUN3-7	0.003098	0.000029	0.282136	0.000021	0.02490	0.00027	1.467169	0.000033	24					
Dec 20 2022	MUN3-8	0.003545	0.000017	0.282149	0.000017	0.02859	0.00018	1.467151	0.000026	24					
Dec 21 2022	MUN1-1	0.002070	0.000140	0.282120	0.000021	0.01033	0.00070	1.467188	0.000036	19					
Dec 21 2022	MUN1-2	0.001360	0.000044	0.282140	0.000019	0.00689	0.00024	1.467164	0.000028	19					
Dec 21 2022	MUN1-3	0.001136	0.000061	0.282145	0.000017	0.00564	0.00033	1.467173	0.000034	22					
Dec 21 2022	MUN1-4	0.001169	0.000089	0.282106	0.000018	0.00602	0.00051	1.467206	0.000035	22					
Dec 21 2022	MUN1-5	0.001032	0.000031	0.282140	0.000020	0.02754	0.00087	1.467137	0.000033	22					
Dec 21 2022	MUN1-6	0.001086	0.000022	0.282146	0.000022	0.02901	0.00064	1.467138	0.000023	22					
Dec 21 2022	MUN1-7	0.000831	0.000039	0.282118	0.000016	0.02270	0.00110	1.467162	0.000028	23					
Dec 21 2022	MUN1-8	0.000780	0.000029	0.282164	0.000017	0.02183	0.00082	1.467212	0.000031	24					
Dec 21 2022	MUN1-9	0.000650	0.000003	0.282166	0.000022	0.01727	0.00005	1.467173	0.000032	24					
Dec 21 2022	MUN3-1	0.004650	0.000220	0.282120	0.000028	0.03780	0.00200	1.467179	0.000028	19					
Dec 21 2022	MUN3-2	0.003552	0.000058	0.282131	0.000021	0.02656	0.00022	1.467176	0.000027	20					
Dec 21 2022	MUN3-3	0.003760	0.000130	0.282127	0.000022	0.02900	0.00120	1.467141	0.000035	18					
Dec 21 2022	MUN3-4	0.004414	0.000066	0.282124	0.000023	0.03566	0.00080	1.467206	0.000034	18					
Dec 21 2022	MUN3-5	0.004450	0.000120	0.282113	0.000032	0.12360	0.00330	1.467126	0.000029	24					
Dec 21 2022	MUN3-6	0.002985	0.000018	0.282160	0.000023	0.08076	0.00058	1.467143	0.000032	26					
Dec 21 2022	MUN3-7	0.002950	0.000013	0.282104	0.000025	0.08027	0.00040	1.467196	0.000031	25					
Dec 21 2022	MUN3-8	0.002884	0.000020	0.282142	0.000024	0.07854	0.00062	1.467167	0.000029	26					
Dec 21 2022	MUN3-9	0.002762	0.000022	0.282160	0.000026	0.07452	0.00067	1.467165	0.000030	26					
Dec 21 2022	MUN3-10	0.002543	0.000051	0.282127	0.000019	0.06800	0.00140	1.467172	0.000026	27					
July 6 2022	OG1-1	0.001120	0.000110	0.280626	0.000044	0.02630	0.00290	1.467198	0.000045	7	3467	0.280551	0.000045	0.5	1.6
July 6 2022	OG1-2	0.001130	0.000120	0.280645	0.000043	0.02670	0.00320	1.467165	0.000061	7	3467	0.280569	0.000044	1.1	1.6
July 6 2022	OG1-3	0.001030	0.000150	0.280601	0.000038	0.02520	0.00400	1.467172	0.000053	7	3467	0.280532	0.000039	-0.2	1.4
July 6 2022	OG1-4	0.000832	0.000069	0.280641	0.000043	0.01870	0.00170	1.467209	0.000058	7	3467	0.280585	0.000043	1.7	1.5
July 6 2022	OG1-5	0.001590	0.000140	0.280644	0.000057	0.03690	0.00370	1.467183	0.000064	6	3467	0.280538	0.000058	0.0	2.1
July 6 2022	OG1-6	0.001130	0.000130	0.280635	0.000067	0.02600	0.00330	1.467129	0.000076	6	3467	0.280559	0.000068	0.8	2.4
July 6 2022	OG1-7	0.000745	0.000063	0.280586	0.000047	0.01640	0.00160	1.467122	0.000054	8	3467	0.280536	0.000047	-0.1	1.7
July 6 2022	OG1-8	0.001024	0.000027	0.280640	0.000045	0.02359	0.00052	1.467209	0.000066	8	3467	0.280572	0.000045	1.2	1.6
July 6 2022	OG1-9	0.001434	0.000074	0.280633	0.000055	0.03330	0.00200	1.467199	0.000051	6	3467	0.280537	0.000055	0.0	2.0

Session	Spot ID	¹⁷⁶ Lu 177Hf	2SE	¹⁷⁶ Hf 177Hf	2SE	¹⁷⁶ Yb 177Hf	2SE	¹⁷⁸ Hf 177Hf	2SE	Total Hf (V)	Age (Ma)	¹⁷⁶ Hf 177Hf (i)	2SE	εHf(i)	2SE
Dec 20 2022	OG1-1	0.001066	0.000057	0.280608	0.000022	0.02440	0.00130	1.467184	0.000031	16	3467	0.280537	0.000022	-0.1	0.8
Dec 20 2022	OG1-2	0.001235	0.000033	0.280639	0.000022	0.02862	0.00079	1.467189	0.000036	18	3467	0.280556	0.000022	0.7	0.8
Dec 20 2022	OG1 - 3	0.001336	0.000026	0.280679	0.000030	0.03190	0.00110	1.467154	0.000030	20	3467	0.280590	0.000030	1.8	1.1
Dec 20 2022	OG1 - 4	0.001253	0.000038	0.280641	0.000031	0.02970	0.00140	1.467140	0.000043	20	3467	0.280557	0.000031	0.7	1.1
Dec 20 2022	OG1 - 5	0.001400	0.000110	0.280645	0.000028	0.03260	0.00350	1.467196	0.000066	21	3467	0.280551	0.000029	0.5	1.0
Dec 20 2022	OG1 - 6	0.001065	0.000098	0.280620	0.000017	0.02410	0.00260	1.467151	0.000030	19	3467	0.280549	0.000018	0.4	0.6
Dec 20 2022	OG1 - 7	0.001021	0.000097	0.280625	0.000024	0.02340	0.00260	1.467146	0.000031	20	3467	0.280557	0.000025	0.7	0.9
Dec 20 2022	OG1 - 8	0.001370	0.000140	0.280640	0.000030	0.03340	0.00380	1.467150	0.000034	18	3467	0.280548	0.000031	0.4	1.1
Dec 20 2022	OG1 - 9	0.001523	0.000067	0.280643	0.000023	0.03600	0.00190	1.467148	0.000027	16	3467	0.280541	0.000023	0.1	0.8
Dec 21 2022	OG1-1	0.001657	0.000006	0.280623	0.000040	0.04174	0.00018	1.467214	0.000044	18	3467	0.280512	0.000040	-0.9	1.4
Dec 21 2022	OG1-2	0.000828	0.000071	0.280606	0.000028	0.01890	0.00190	1.467153	0.000034	20	3467	0.280551	0.000028	0.4	1.0
Dec 21 2022	OG1-3	0.001578	0.000059	0.280640	0.000028	0.03880	0.00180	1.467146	0.000044	16	3467	0.280534	0.000028	-0.1	1.0
Dec 21 2022	OG1-4	0.000929	0.000055	0.280616	0.000022	0.02060	0.00150	1.467160	0.000038	16	3467	0.280554	0.000022	0.6	0.8
Dec 21 2022	OG1-5	0.001680	0.000100	0.280650	0.000030	0.04160	0.00270	1.467123	0.000033	16	3467	0.280538	0.000031	0.0	1.1
Dec 21 2022	OG1-6	0.001200	0.000130	0.280620	0.000023	0.02920	0.00320	1.467123	0.000034	16	3467	0.280540	0.000025	0.1	0.9
Dec 21 2022	OG1-7	0.000605	0.000019	0.280616	0.000018	0.01399	0.00047	1.467187	0.000034	17	3467	0.280576	0.000018	1.3	0.6
Dec 21 2022	OG1-8	0.001120	0.000062	0.280633	0.000031	0.02620	0.00190	1.467169	0.000042	18	3467	0.280558	0.000031	0.7	1.1
Dec 21 2022	OG1-9	0.001108	0.000041	0.280628	0.000026	0.02510	0.00096	1.467140	0.000040	15	3467	0.280554	0.000026	0.6	0.9
Dec 21 2022	OG1-10	0.001370	0.000220	0.280645	0.000024	0.03260	0.00580	1.467176	0.000033	20	3467	0.280553	0.000028	0.5	1.0
Dec 21 2022	OG1-11	0.001220	0.000120	0.280626	0.000022	0.03040	0.00310	1.467182	0.000043	17	3467	0.280544	0.000023	0.2	0.8
Dec 21 2022	OG1-12	0.002270	0.000170	0.280716	0.000034	0.05630	0.00480	1.467206	0.000038	16	3467	0.280564	0.000036	0.9	1.3
Dec 21 2022	OG1-13	0.001392	0.000074	0.280617	0.000029	0.03270	0.00210	1.467193	0.000035	16	3467	0.280524	0.000029	-0.5	1.0
Dec 21 2022	OG1-14	0.001452	0.000058	0.280661	0.000028	0.03560	0.00170	1.467187	0.000040	16	3467	0.280564	0.000028	0.9	1.0
July 6 2022	91500-1	0.000332	0.000001	0.282304	0.000049	0.00821	0.00006	1.467114	0.000071	5	1065	0.282297	0.000049	6.6	1.7
July 6 2022	91500-2	0.000332	0.000001	0.282361	0.000050	0.00818	0.00006	1.467170	0.000083	5	1065	0.282354	0.000050	8.7	1.8
July 6 2022	91500-3	0.000321	0.000004	0.282266	0.000053	0.00791	0.00010	1.467210	0.000066	5	1065	0.282260	0.000053	5.3	1.9
July 6 2022	91500-4	0.000333	0.000001	0.282282	0.000053	0.00821	0.00005	1.467090	0.000083	5	1065	0.282275	0.000053	5.9	1.9
July 6 2022	91500-5	0.000330	0.000001	0.282305	0.000059	0.00813	0.00007	1.467154	0.000060	5	1065	0.282298	0.000059	6.7	2.1
July 6 2022	91500-6	0.000331	0.000001	0.282334	0.000057	0.00824	0.00007	1.467182	0.000059	5	1065	0.282327	0.000057	7.7	2.0
July 6 2022	91500-7	0.000329	0.000001	0.282290	0.000047	0.00807	0.00004	1.467185	0.000049	5	1065	0.282283	0.000047	6.1	1.7
July 6 2022	91500-8	0.000330	0.000001	0.282311	0.000058	0.00816	0.00007	1.467165	0.000067	5	1065	0.282304	0.000058	6.9	2.1
July 6 2022	91500-9	0.000329	0.000001	0.282322	0.000065	0.00811	0.00006	1.467137	0.000074	5	1065	0.282315	0.000065	7.3	2.3
Dec 20 2022	91500-1	0.000327	0.000003	0.282296	0.000029	0.00793	0.00006	1.467205	0.000036	12	1065	0.282289	0.000033	6.4	1.2
Dec 20 2022	91500-2	0.000331	0.000000	0.282296	0.000024	0.00821	0.00003	1.467134	0.000032	12	1065	0.282289	0.000029	6.3	1.0
Dec 20 2022	91500-3	0.000332	0.000001	0.282300	0.000027	0.00825	0.00003	1.467159	0.000036	13	1065	0.282293	0.000031	6.5	1.1
Dec 20 2022	91500-4	0.000332	0.000001	0.282321	0.000024	0.00826	0.00002	1.467139	0.000040	13	1065	0.282314	0.000029	7.2	1.0
Dec 20 2022	91500-5	0.000331	0.000001	0.282317	0.000023	0.00831	0.00003	1.467178	0.000035	12	1065	0.282310	0.000028	7.1	1.0
Dec 20 2022	91500-6	0.000332	0.000000	0.282295	0.000025	0.00827	0.00005	1.467134	0.000043	13	1065	0.282288	0.000030	6.3	1.1
Dec 20 2022	91500-7	0.000331	0.000001	0.282314	0.000024	0.00842	0.00005	1.467166	0.000039	13	1065	0.282307	0.000029	7.0	1.0
Dec 20 2022	91500-8	0.000329	0.000003	0.282297	0.000029	0.00840	0.00004	1.467161	0.000039	12	1065	0.282290	0.000033	6.4	1.2
Dec 20 2022	91500-9	0.000335	0.000001	0.282300	0.000027	0.00845	0.00004	1.467205	0.000047	13	1065	0.282293	0.000031	6.5	1.1
Dec 21 2022	91500-1	0.000343	0.000000	0.282277	0.000023	0.00828	0.00003	1.467170	0.000038	11	1065	0.282270	0.000023	5.7	0.8
Dec 21 2022	91500-2	0.000338	0.000001	0.282299	0.000026	0.00817	0.00003	1.467148	0.000047	12	1065	0.282292	0.000026	6.5	0.9
Dec 21 2022	91500-3	0.000338	0.000001	0.282321	0.000025	0.00830	0.00003	1.467157	0.000038	12	1065	0.282314	0.000025	7.2	0.9
Dec 21 2022	91500-4	0.000336	0.000000	0.282278	0.000028	0.00828	0.00003	1.467206	0.000045	12	1065	0.282271	0.000028	5.7	1.0
Dec 21 2022	91500-5	0.000331	0.000001	0.282316	0.000024	0.00827	0.00002	1.467162	0.000035	12	1065	0.282309	0.000024	7.1	0.9
Dec 21 2022	91500-6	0.000330	0.000001	0.282318	0.000022	0.00826	0.00004	1.467177	0.000047	12	1065	0.282311	0.000022	7.1	0.8
Dec 21 2022	91500-7	0.000329	0.000001	0.282329	0.000027	0.00822	0.00006	1.467174	0.000034	12	1065	0.282322	0.000027	7.5	1.0
Dec 21 2022	91500-8	0.000327	0.000000	0.282318	0.000023	0.00808	0.00002	1.467152	0.000040	11	1065	0.282311	0.000023	7.1	0.8
Dec 21 2022	91500-9	0.000324	0.000000	0.282288	0.000025	0.00808	0.00004	1.467208	0.000035	12	1065	0.282281	0.000025	6.1	0.9
Dec 21 2022	91500-10	0.000329	0.000000	0.282318	0.000030	0.00828	0.00003	1.467211	0.000036	12	1065	0.282311	0.000030	7.1	1.1

Table A-18. Secondary reference material U-Pb data for the LA-ICPMS U-Pb-TE method (section A.8).

Session	Spot ID	206Pb cps	204 cps	Ratios					Dates (Ma)				Disc. %		
				207Pb 206Pb	2σ	207Pb 235U	2σ	206Pb 238U	2σ	ρ	207Pb 206Pb	2σ		206Pb 238U	2σ
April 07 2022	OG1-1	1.84E+05	0	0.2996	0.0040	28.94	1.22	0.723	0.029	0.949	3468	21	3507	107	-1
April 07 2022	OG1-2	1.51E+05	0	0.2994	0.0037	29.51	1.24	0.712	0.029	0.955	3467	19	3466	107	0
April 07 2022	OG1-3	1.86E+05	0	0.2991	0.0035	29.16	1.15	0.704	0.027	0.955	3466	18	3434	100	1
April 07 2022	OG1-4	1.74E+05	0	0.2994	0.0040	29.56	1.27	0.720	0.029	0.950	3467	21	3496	109	-1
April 07 2022	OG1-5	1.93E+05	0	0.3005	0.0043	29.17	1.24	0.707	0.028	0.943	3473	22	3447	106	1
April 07 2022	OG1-6	1.97E+05	0	0.3006	0.0046	29.36	1.34	0.727	0.031	0.942	3473	24	3522	115	-1
April 07 2022	OG1-7	1.78E+05	0	0.2986	0.0043	29.54	1.34	0.716	0.031	0.948	3463	23	3481	115	-1
April 07 2022	OG1-8	1.83E+05	0	0.2983	0.0041	30.00	1.26	0.733	0.029	0.946	3461	21	3545	108	-2
April 07 2022	OG1-9	1.75E+05	0	0.2999	0.0036	27.66	1.17	0.636	0.026	0.959	3470	18	3173	101	9
April 08 2022	OG1-1	9.40E+04	0	0.2992	0.0046	28.32	1.34	0.686	0.031	0.945	3466	24	3367	116	3
April 08 2022	OG1-2	1.13E+05	27	0.2994	0.0046	29.51	1.35	0.719	0.031	0.942	3467	24	3492	115	-1
April 08 2022	OG1-3	1.27E+05	0	0.3017	0.0041	29.25	1.33	0.699	0.030	0.955	3479	21	3417	114	2
April 08 2022	OG1-4	1.02E+05	0	0.2988	0.0047	29.37	1.35	0.712	0.031	0.940	3464	24	3466	115	0
April 08 2022	OG1-5	9.34E+04	0	0.3000	0.0045	30.67	1.36	0.750	0.031	0.941	3470	23	3608	114	-4
April 08 2022	OG1-6	1.19E+05	0	0.2970	0.0039	30.93	1.47	0.753	0.034	0.961	3455	20	3619	125	-5
April 08 2022	OG1-7	8.14E+04	15	0.2987	0.0046	29.24	1.34	0.716	0.031	0.942	3463	24	3481	115	-1
April 11 2022	OG1-1	1.91E+05	0	0.3002	0.0043	30.07	1.41	0.726	0.032	0.953	3471	22	3518	120	-1
April 11 2022	OG1-2	1.53E+05	0	0.3004	0.0043	29.03	1.26	0.701	0.029	0.945	3472	22	3424	108	1
April 11 2022	OG1-3	1.70E+05	0	0.2997	0.0042	29.86	1.35	0.724	0.031	0.951	3469	22	3511	115	-1
April 11 2022	OG1-4	1.32E+05	0	0.3012	0.0047	30.26	1.48	0.729	0.034	0.947	3476	24	3530	124	-2
April 11 2022	OG1-5	2.32E+05	0	0.2968	0.0044	29.69	1.25	0.723	0.028	0.935	3454	23	3507	106	-2
April 11 2022	OG1-6	2.59E+05	0	0.2951	0.0036	29.58	1.30	0.721	0.030	0.960	3445	19	3500	113	-2
April 11 2022	OG1-7	2.59E+05	0	0.2975	0.0048	28.26	1.23	0.687	0.028	0.930	3457	25	3371	105	3
April 11 2022	OG1-8	1.78E+05	0	0.2977	0.0040	29.48	1.27	0.715	0.029	0.950	3458	21	3477	109	-1
April 11 2022	OG1-9	1.56E+05	6	0.2934	0.0048	28.49	1.34	0.701	0.031	0.939	3436	25	3424	117	0
April 11 2022	OG1-10	1.56E+05	0	0.2950	0.0037	28.22	1.16	0.691	0.027	0.952	3444	20	3386	102	2
April 11 2022	OG1-11	1.03E+05	0	0.2955	0.0044	29.61	1.39	0.728	0.032	0.948	3447	23	3526	120	-2
April 11 2022	OG1-12	1.84E+05	7	0.2977	0.0055	28.64	1.47	0.701	0.034	0.933	3458	29	3424	126	1
April 12 2022	OG1-1	1.41E+05	2	0.2964	0.0042	29.12	1.40	0.705	0.032	0.955	3452	22	3440	121	0
April 12 2022	OG1-2	2.07E+05	23	0.3005	0.0056	29.03	1.50	0.700	0.034	0.932	3473	29	3421	126	2
April 12 2022	OG1-3	1.35E+05	5	0.3024	0.0053	29.14	1.39	0.697	0.031	0.929	3483	27	3409	116	2
April 12 2022	OG1-4	1.38E+05	8	0.2955	0.0049	29.66	1.46	0.724	0.034	0.942	3447	26	3511	124	-2
April 12 2022	OG1-5	1.15E+05	0	0.2929	0.0052	29.76	1.47	0.733	0.034	0.933	3433	28	3545	125	-3
April 12 2022	OG1-6	2.27E+05	0	0.2917	0.0045	28.55	1.41	0.706	0.033	0.950	3427	24	3443	124	0
April 07 2022	FC1-1	1.03E+05	0	0.0759	0.0012	1.948	0.089	0.1862	0.0080	0.936	1092	32	1101	43	-1
April 07 2022	FC1-2	1.32E+05	7	0.0767	0.0011	1.947	0.082	0.1859	0.0074	0.945	1113	28	1099	40	1
April 07 2022	FC1-3	8.18E+04	0	0.0770	0.0020	1.923	0.096	0.1868	0.0081	0.859	1121	51	1104	44	2
April 07 2022	FC1-4	1.25E+05	0	0.0769	0.0010	1.929	0.078	0.1801	0.0069	0.941	1119	27	1068	37	5
April 07 2022	FC1-5	7.78E+04	0	0.0758	0.0014	1.882	0.081	0.1787	0.0069	0.903	1090	37	1060	38	3
April 07 2022	FC1-6	1.26E+05	0	0.0761	0.0012	1.945	0.085	0.1838	0.0075	0.930	1098	32	1088	41	1
April 07 2022	FC1-7	1.08E+05	0	0.0753	0.0014	1.981	0.087	0.1880	0.0075	0.905	1077	37	1111	40	-3
April 07 2022	FC1-8	1.09E+05	0	0.0765	0.0011	1.953	0.081	0.1860	0.0072	0.934	1108	30	1100	39	1
April 08 2022	FC1-1	8.10E+04	0	0.0767	0.0015	2.019	0.104	0.1908	0.0090	0.924	1113	39	1126	49	-1
April 08 2022	FC1-2	9.25E+04	0	0.0765	0.0015	1.962	0.094	0.1879	0.0082	0.912	1108	39	1110	44	0
April 08 2022	FC1-3	9.45E+04	0	0.0765	0.0012	1.903	0.085	0.1800	0.0075	0.934	1108	32	1067	41	4
April 08 2022	FC1-4	6.26E+04	0	0.0778	0.0017	1.920	0.101	0.1813	0.0087	0.910	1142	43	1074	47	6
April 08 2022	FC1-5	6.27E+04	0	0.0761	0.0014	1.921	0.097	0.1829	0.0086	0.931	1098	37	1083	47	1
April 08 2022	FC1-6	5.99E+04	0	0.0761	0.0012	1.967	0.087	0.1868	0.0077	0.932	1098	32	1104	42	-1
April 08 2022	FC1-7	5.40E+04	0	0.0769	0.0017	2.093	0.109	0.1990	0.0094	0.907	1119	44	1170	50	-4
April 11 2022	FC1-1	7.75E+04	0	0.0767	0.0014	1.950	0.085	0.1843	0.0073	0.908	1113	37	1090	40	2
April 11 2022	FC1-2	7.96E+04	0	0.0783	0.0012	2.019	0.088	0.1870	0.0076	0.932	1154	31	1105	41	4
April 11 2022	FC1-3	7.96E+04	16	0.0761	0.0012	1.982	0.084	0.1891	0.0074	0.926	1098	32	1116	40	-2
April 11 2022	FC1-4	7.30E+04	3	0.0750	0.0015	1.952	0.091	0.1890	0.0080	0.905	1069	40	1116	43	-4
April 11 2022	FC1-5	7.37E+04	0	0.0764	0.0014	1.973	0.090	0.1865	0.0078	0.916	1106	37	1102	42	0
April 11 2022	FC1-6	7.32E+04	0	0.0764	0.0013	1.886	0.081	0.1772	0.0070	0.916	1106	34	1052	38	5
April 11 2022	FC1-7	7.59E+04	15	0.0770	0.0014	2.006	0.088	0.1872	0.0075	0.909	1121	36	1106	40	1
April 11 2022	FC1-8	7.49E+04	4	0.0734	0.0016	1.928	0.092	0.1898	0.0080	0.890	1025	44	1120	43	-9
April 11 2022	FC1-9	7.86E+04	0	0.0764	0.0014	1.903	0.090	0.1797	0.0079	0.922	1106	37	1065	43	4
April 11 2022	FC1-10	8.81E+04	0	0.0749	0.0013	1.886	0.085	0.1823	0.0076	0.922	1066	35	1080	41	-1
April 11 2022	FC1-11	8.62E+04	0	0.0776	0.0011	1.944	0.088	0.1828	0.0078	0.946	1137	29	1082	42	5
April 11 2022	FC1-12	1.04E+05	1	0.0766	0.0015	1.967	0.093	0.1881	0.0081	0.911	1111	39	1111	44	0
April 12 2022	FC1-1	5.81E+04	0	0.0747	0.0015	1.902	0.095	0.1840	0.0084	0.916	1060	40	1089	46	-3
April 12 2022	FC1-2	5.61E+04	0	0.0760	0.0017	1.991	0.101	0.1897	0.0087	0.900	1095	44	1120	47	-2
April 12 2022	FC1-3	5.86E+04	0	0.0758	0.0016	1.972	0.108	0.1885	0.0095	0.924	1090	42	1113	52	-2
April 12 2022	FC1-4	5.28E+04	28	0.0766	0.0019	2.033	0.121	0.1921	0.0105	0.912	1111	49	1133	56	-2
April 12 2023	FC1-5	4.96E+04	0	0.0750	0.0020	1.988	0.113	0.1916	0.0096	0.886	1069	53	1130	52	-5
April 12 2024	FC1-6	4.88E+04	0	0.0757	0.0018	1.945	0.100	0.1869	0.0085	0.889	1087	47	1105	46	-2

Table A-19. Secondary reference material trace-element data for the LA-ICPMS U-Pb-TE method (section A.8).

Session	Spot ID	Ti ppm	2SE	Gd ppm	2SE	Yb ppm	2SE	Th ppm	2SE	U ppm	2SE	$\frac{Th}{U}$
April 7 2022	91500-1	7.2	2.5	1.90	0.43	56.7	2.7	26.07	0.93	71.4	2.1	0.37
April 7 2022	91500-2	6.3	1.8	2.19	0.55	59.8	2.1	27.3	1.2	73.4	2.6	0.37
April 7 2022	91500-3	6.1	2.6	1.89	0.43	59.9	2.7	26.8	1.0	73.4	2.7	0.36
April 7 2022	91500-4	6.1	2.3	2.48	0.66	61.0	2.9	26.6	1.1	71.9	2.5	0.37
April 7 2022	91500-5	6.2	2.2	1.68	0.39	55.8	3.8	23.4	1.1	67.3	3.0	0.35
April 7 2022	91500-6	3.7	1.8	2.29	0.40	60.9	3.5	26.2	1.0	73.5	2.5	0.36
April 7 2022	91500-7	5.8	1.7	1.69	0.45	54.2	2.7	23.78	0.92	68.8	2.7	0.35
April 7 2022	91500-8	5.4	1.9	1.73	0.38	55.5	2.7	26.17	0.89	70.2	2.4	0.37
April 8 2022	91500-1	5.2	2.0	1.92	0.34	60.6	2.9	26.38	0.96	72.0	2.0	0.37
April 8 2022	91500-2	4.8	2.2	1.62	0.50	60.7	3.6	25.8	1.4	73.4	3.3	0.35
April 8 2022	91500-3	5.1	1.8	2.02	0.43	60.9	3.2	25.5	1.1	71.8	2.9	0.36
April 8 2022	91500-4	4.0	1.9	2.51	0.59	60.7	2.8	26.4	1.1	71.1	2.4	0.37
April 8 2022	91500-5	5.8	2.0	1.80	0.43	59.3	3.2	26.6	1.4	73.5	3.2	0.36
April 8 2022	91500-6	6.2	2.5	2.00	0.44	60.4	3.1	24.9	1.1	71.6	3.1	0.35
April 8 2022	91500-7	6.9	2.3	2.44	0.60	59.4	2.8	26.9	1.1	72.0	2.9	0.37
April 11 2022	91500-1	4.3	1.5	1.85	0.41	59.8	2.4	26.15	0.83	70.7	2.5	0.37
April 11 2022	91500-2	4.2	1.8	1.82	0.44	59.4	2.6	26.4	1.0	71.1	2.6	0.37
April 11 2022	91500-3	7.0	1.8	1.86	0.37	58.5	2.5	25.90	0.93	70.2	2.1	0.37
April 11 2022	91500-4	6.8	2.3	2.10	0.40	59.1	2.7	26.8	1.0	72.7	2.5	0.37
April 11 2022	91500-5	3.5	1.6	1.96	0.41	61.2	2.7	26.5	1.0	72.1	2.3	0.37
April 11 2022	91500-6	4.4	1.8	2.18	0.44	59.1	2.6	26.0	1.2	70.1	2.6	0.37
April 11 2022	91500-7	6.2	2.5	1.84	0.45	61.6	2.7	26.3	1.0	72.1	2.5	0.37
April 11 2022	91500-8	5.0	2.3	2.31	0.50	60.8	3.5	26.5	1.1	71.8	2.7	0.37
April 11 2022	91500-9	7.6	2.3	2.36	0.56	61.5	3.0	26.5	1.0	70.2	2.5	0.38
April 11 2022	91500-10	4.1	1.8	1.87	0.39	59.4	3.4	26.6	1.1	73.2	2.6	0.36
April 11 2022	91500-11	5.9	2.0	2.11	0.44	59.4	2.7	26.7	1.0	74.7	2.4	0.36
April 11 2022	91500-12	7.3	3.1	1.71	0.39	58.9	2.8	26.7	1.1	71.6	2.5	0.37
April 12 2022	91500-1			1.65	0.43	56.4	2.7	24.5	1.3	68.2	3.2	0.36
April 12 2022	91500-2			1.69	0.48	53.8	3.1	24.1	1.2	69.2	3.5	0.35
April 12 2022	91500-3			1.36	0.39	52.2	2.9	23.35	0.93	66.8	2.1	0.35
April 12 2022	91500-4			1.78	0.51	54.0	2.6	23.0	1.0	66.1	2.7	0.35
April 12 2022	91500-5			1.86	0.46	53.3	2.8	23.2	1.3	66.6	3.0	0.35
April 12 2022	91500-6			2.13	0.54	59.2	3.0	26.58	0.91	73.3	2.9	0.36

No Ti data for April 12 2022 session due to an analytical error.

Table A-20. Secondary reference material (zircon 91500) trace-element data for the LA-ICPMS trace-element method (section A.9).

Session	Dec 6					Oct					Mar																							
	2021	2021	2021	2021	2021	2022	2022	2022	2024	2024	2024	2024	2024	2024	2024	2024	2024	2024	2024	2024	2024	2024	2024	2024	2024	2024	2024	2024	2024	2024	2024	2024	2024	2024
Spot#	1	2	3	4	5	1	2	3	1	2	3	4	5	6	7	8	9	10	1	2	3	4	5	6	7	8	9	10	11					
P	25.5	20.9	14.6	14.8	20.2			8.4	14.4	15.4	14.6	15.0	14.4	10.5	21.9	21.0	11.8	23.2	22.2	22.8	17.4	24.3	18.6	9.3	18.4	14.7	21.7	22.2	21.4					
2SE	8.4	3.9	3.1	3.5	2.6			4.9	3.5	2.9	3.5	2.9	3.6	2.8	3.2	3.9	2.8	4.7	6.1	4.3	3.4	5.3	4.0	4.9	4.2	3.9	4.2	4.9	3.8					
Ca													221						272		192													
2SE												84							106		78													
Ti	6.3	3.0	4.0	3.0	4.6	5.5	3.2	4.2	4.32	4.22	4.43	5.11	4.27	3.40	5.21	4.78	4.31	4.82	4.93	5.03	4.59	4.19	4.14	4.60	4.36	4.66	4.00	3.62	4.86					
2SE	2.2	1.1	1.0	1.0	0.9	1.2	1.0	1.3	0.56	0.65	0.76	0.73	0.59	0.68	0.67	0.65	0.65	0.61	0.72	0.61	0.66	0.72	0.60	0.60	0.50	0.53	0.58	0.51	0.51					
Ce	2.64	2.270	2.177	2.161	2.190			2.03	2.04	2.00	2.05	2.17	2.04	2.07	2.177	2.07	2.09	2.04	2.06	2.16	2.17	2.13	2.030	1.93	2.10	2.07	2.05	2.04						
2SE	0.13	0.093	0.081	0.085	0.088			0.11	0.11	0.10	0.11	0.11	0.11	0.11	0.10	0.094	0.11	0.11	0.12	0.10	0.11	0.10	0.12	0.080	0.12	0.12	0.11	0.11	0.10					
Pr		0.0061	0.0082	0.0122	0.0062							0.016																						
2SE		0.0036	0.0036	0.0049	0.0038							0.006																						
Nd	0.146	0.165	0.169	0.149	0.157	0.107		0.197	0.127	0.127	0.108	0.104	0.187				0.125	0.123	0.146	0.152	0.275	0.158	0.118	0.147	0.187	0.120	0.150	0.158	0.151	0.160				
2SE	0.053	0.036	0.037	0.035	0.038	0.090		0.121	0.050	0.047	0.061	0.062	0.058				0.042	0.060	0.062	0.055	0.057	0.060	0.043	0.061	0.068	0.060	0.062	0.073	0.068	0.051				
Sm	0.371	0.362	0.324	0.327	0.335	0.36	0.25	0.18	0.378	0.352	0.372	0.314	0.292	0.366	0.242	0.380	0.272	0.305	0.352	0.344	0.298	0.300	0.372	0.298	0.206	0.373	0.396	0.281	0.291					
2SE	0.085	0.057	0.059	0.061	0.060	0.10	0.10	0.14	0.090	0.084	0.060	0.078	0.076	0.094	0.065	0.067	0.094	0.068	0.133	0.072	0.077	0.084	0.094	0.081	0.074	0.075	0.077	0.067	0.064					
Eu	0.169	0.208	0.193	0.194	0.202	0.173	0.112	0.213	0.192	0.183	0.205	0.179	0.178	0.171	0.178	0.195	0.186	0.188	0.190	0.159	0.143	0.179	0.174	0.171	0.174	0.154	0.144	0.166	0.165					
2SE	0.031	0.021	0.022	0.027	0.022	0.034	0.033	0.061	0.028	0.029	0.028	0.028	0.029	0.027	0.029	0.025	0.035	0.028	0.028	0.016	0.022	0.025	0.027	0.021	0.029	0.020	0.021	0.026	0.029					
Gd	2.54	1.97	2.00	1.96	1.83	1.50	1.53	1.46	1.59	1.79	1.75	1.77	1.78	1.82	1.56	1.74	1.59	1.84	1.66	1.86	1.76	1.83	1.68	1.84	1.78	1.78	1.68	1.68	1.71					
2SE	0.21	0.13	0.15	0.13	0.15	0.20	0.23	0.30	0.15	0.15	0.17	0.21	0.15	0.18	0.16	0.16	0.15	0.16	0.18	0.19	0.17	0.17	0.18	0.13	0.20	0.18	0.19	0.14	0.15					
Tb	0.918	0.759	0.776	0.711	0.729	0.678	0.592	0.674	0.662	0.654	0.686	0.659	0.692	0.684	0.670	0.650	0.644	0.660	0.659	0.681	0.691	0.664	0.697	0.703	0.617	0.628	0.697	0.647	0.687					
2SE	0.055	0.047	0.036	0.035	0.033	0.056	0.069	0.086	0.057	0.042	0.046	0.045	0.043	0.043	0.046	0.045	0.042	0.046	0.047	0.048	0.048	0.049	0.055	0.042	0.049	0.048	0.044	0.046	0.057					
Dy	11.86	9.90	9.97	9.07	9.24	10.03	7.38	8.50	8.82	8.32	8.64	8.33	8.90	8.73	8.71	8.62	8.54	8.44	8.82	8.73	8.96	8.87	8.67	8.78	8.49	8.91	8.61	8.69	8.67					
2SE	0.52	0.32	0.33	0.34	0.39	0.59	0.46	0.51	0.50	0.46	0.40	0.49	0.47	0.48	0.55	0.53	0.48	0.44	0.50	0.46	0.40	0.38	0.42	0.52	0.46	0.43	0.43	0.37	0.36					
Ho	4.98	4.16	4.08	3.96	3.96	4.08	3.43	3.73	3.72	3.62	3.71	3.48	3.66	3.49	3.63	3.66	3.50	3.61	3.67	3.69	3.72	3.74	3.74	3.72	3.63	3.72	3.63	3.59	3.58					
2SE	0.15	0.16	0.14	0.14	0.14	0.20	0.20	0.25	0.21	0.20	0.19	0.20	0.15	0.18	0.18	0.19	0.17	0.20	0.21	0.16	0.21	0.16	0.20	0.19	0.18	0.19	0.17	0.19	0.18					
Er	27.03	22.04	22.56	21.23	21.56	20.86	17.45	21.95	19.87	19.24	19.89	19.58	19.82	18.88	19.95	20.23	20.18	19.75	19.46	19.79	20.35	20.32	19.56	19.88	19.77	20.32	19.21	19.5	19.70					
2SE	0.76	0.70	0.67	0.58	0.77	0.95	1.05	1.21	0.98	0.93	0.84	0.97	0.96	0.91	0.93	0.88	0.90	0.93	0.98	0.87	0.99	0.81	0.85	0.97	0.93	0.99	0.90	1.0	0.85					
Tm	6.59	5.50	5.54	5.15	5.46	5.46	4.45	5.06	4.68	4.80	4.81	4.72	4.83	4.70	4.75	5.00	4.89	4.92	4.87	4.89	5.03	4.92	4.83	4.90	4.73	4.99	4.91	4.78	4.84					
2SE	0.19	0.19	0.15	0.17	0.18	0.28	0.28	0.31	0.21	0.24	0.25	0.22	0.25	0.24	0.23	0.25	0.25	0.25	0.29	0.20	0.24	0.23	0.24	0.23	0.24	0.23	0.23	0.23	0.21					
Yb	69.8	56.7	56.4	53.6	54.9	57.0	45.6	53.1	52.0	49.3	51.5	50.3	50.0	49.0	50.4	50.6	49.6	50.3	50.5	51.5	52.3	51.2	49.9	50.1	50.3	51.7	50.2	51.1	51.0					
2SE	1.4	1.6	1.4	1.7	1.9	2.8	2.4	2.9	2.5	2.2	2.4	2.7	2.4	2.4	2.4	2.4	2.7	2.5	2.7	2.4	2.5	2.4	2.2	2.1	2.5	2.2	2.1	2.4	2.1					
Lu	14.82	11.50	11.66	11.20	11.46	11.17	9.33	10.72	10.42	10.05	10.49	10.24	10.31	10.16	10.32	10.26	10.30	10.23	10.47	10.36	10.68	10.49	10.21	10.40	10.30	10.44	10.36	10.37	10.44					
2SE	0.30	0.34	0.27	0.32	0.35	0.46	0.53	0.59	0.51	0.46	0.47	0.47	0.47	0.51	0.49	0.45	0.49	0.52	0.54	0.43	0.45	0.43	0.42	0.49	0.49	0.41	0.45	0.45	0.49					
Hf	6169	4754	4900	4778	4683	5422	4452	5458	4456	4230	4418	4343	4470	4327	4480	4408	4463	4385	4367	4418	4505	4474	4392	4510	4426	4522	4500	4520	4405					
2SE	77	118	127	126	140	206	201	173	210	195	205	211	209	209	204	189	208	209	213	175	196	197	185	205	206	201	199	214	191					
Th	31.99	26.59	26.95	24.94	25.86	24.92	20.6	22.5	23.5	22.99	23.7	23.4	23.9	23.4	23.9	23.72	23.5	23.00	23.8	24.23	24.6	23.9	23.8	24.3	23.2	24.1	23.6	23.4	23.8					
2SE	0.53	0.69	0.68	0.73	0.77	0.92	1.0	1.2	1.1	0.94	1.1	1.0	1.1	1.2	1.0	0.93	1.0	0.94	1.2	0.95	1.0	1.0	1.0	1.0	1.0	1.0	1.0	1.0	1.0					
U	84.0	70.1	71.9	67.9	68.2	70.9	58.6	67.0	65.5	63.4	65.9	65.0	65.4	63.6	66.4	64.9	64.7	64.2	65.4	66.2	67.1	66.7	66.0	65.8	65.4	67.3	65.1	65.2	65.7					
2SE	1.2	2.1	1.8	1.9	1.9	2.6	2.6	2.9	3.0	2.8	2.8	2.9	2.8	2.9	2.9	2.6	2.8	3.0	3.2	2.7	2.9	2.6	2.9	3.0	2.9	2.9	2.8	2.8	2.9					

Analyses below detection limit are left blank. All La analyses were below detection limit.

Table A-21. Secondary reference material (TEM2) data for the SIMS zircon O isotope method (section A.10).

Session	Spot ID	$\delta^{18}\text{O}$				Session	Spot ID	$\delta^{18}\text{O}$			
		$\frac{^{18}\text{O}}{^{16}\text{O}}$	1 σ %	(VSMOW) ‰	2 σ ‰			$\frac{^{18}\text{O}}{^{16}\text{O}}$	1 σ %	(VSMOW) ‰	2 σ ‰
IP21007	TEM2-1	0.00202155	0.013	8.16	0.26	IP21012	TEM2-1	0.00202149	0.010	8.12	0.20
IP21007	TEM2-2	0.00202163	0.010	8.19	0.20	IP21012	TEM2-2	0.00202189	0.011	8.32	0.21
IP21007	TEM2-3	0.00202173	0.010	8.24	0.20	IP21012	TEM2-3	0.00202160	0.011	8.18	0.23
IP21007	TEM2-4	0.00202181	0.011	8.28	0.23	IP21012	TEM2-4	0.00202168	0.010	8.22	0.19
IP21007	TEM2-5	0.00202164	0.010	8.20	0.20	IP21012	TEM2-5	0.00202177	0.012	8.26	0.23
IP21007	TEM2-6	0.00202179	0.009	8.27	0.18	IP21012	TEM2-6	0.00202168	0.009	8.22	0.18
IP21007	TEM2-7	0.00202224	0.009	8.50	0.18	IP21012	TEM2-7	0.00202212	0.009	8.44	0.18
IP21007	TEM2-8	0.00202123	0.010	7.99	0.20	IP21012	TEM2-8	0.00202187	0.010	8.31	0.21
IP21007	TEM2-9	0.00202177	0.009	8.26	0.18	IP21012	TEM2-9	0.00202187	0.009	8.31	0.18
IP21007	TEM2-10	0.00202161	0.009	8.18	0.19	IP21012	TEM2-10	0.00202135	0.010	8.05	0.19
IP21007	TEM2-11	0.00202147	0.009	8.11	0.18	IP21012	TEM2-11	0.00202180	0.010	8.28	0.20
IP21007	TEM2-12	0.00202158	0.011	8.17	0.21	IP21012	TEM2-12	0.00202192	0.010	8.34	0.20
IP21007	TEM2-13	0.00202154	0.010	8.15	0.20	IP21012	TEM2-13	0.00202182	0.010	8.29	0.19
IP21007	TEM2-14	0.00202194	0.014	8.35	0.28	IP21012	TEM2-14	0.00202194	0.009	8.35	0.18
IP21007	TEM2-15	0.00202137	0.010	8.07	0.21	IP21012	TEM2-15	0.00202171	0.009	8.23	0.18
IP21007	TEM2-16	0.00202190	0.010	8.33	0.19	IP21012	TEM2-16	0.00202174	0.011	8.25	0.23
IP21007	TEM2-17	0.00202155	0.009	8.15	0.18	IP21012	TEM2-17	0.00202214	0.009	8.45	0.18
IP21007	TEM2-18	0.00202179	0.009	8.27	0.19	IP21012	TEM2-18	0.00202180	0.010	8.28	0.20
IP21007	TEM2-19	0.00202153	0.009	8.14	0.18	IP21012	TEM2-19	0.00202166	0.011	8.21	0.23
IP21007	TEM2-20	0.00202180	0.009	8.28	0.18	IP21012	TEM2-20	0.00202160	0.010	8.18	0.19
IP21007	TEM2-21	0.00202178	0.010	8.27	0.20	IP21012	TEM2-21	0.00202155	0.009	8.16	0.19
						IP21012	TEM2-22	0.00202160	0.010	8.18	0.20
						IP21012	TEM2-23	0.00202151	0.010	8.13	0.19
						IP21012	TEM2-24	0.00202146	0.010	8.11	0.21

VSMOW: Vienna standard mean ocean water

Appendix B: Supporting information for chapter 2

B.1 The data set

Chapter 2 includes new whole-rock Sm-Nd isotope data for 82 (meta)plutonic rocks. In addition, a subset of samples known or expected to be older than 3.0 Ga were analyzed for all of, or some combination of, whole-rock elemental, and zircon U-Pb, Hf and O isotope data. The methods through which these data were acquired are described in appendix A. Table B-1 summarizes what data were collected, or were previously available, from metaplutonic rocks in the western Rae craton with crystallization ages >3.0 Ga. Sections B.2 and B.3 of this appendix describe the interpretation of the new zircon U-Pb-Hf and O isotope data in detail.

Table B-1. A summary of the data that was collected or was previously available for pre-3.0 Ga metaplutonic rocks in the western Rae craton. Numbers 1–8 indicate the data source.

Abbreviated sample ID	Sample ID	Lat. (°N)	Long. (°W)	Whole-rock elemental	Whole-rock Sm-Nd isotope	Zircon U-Pb age	Zircon Hf isotope	Zircon O isotope
S1	QM2C	67.8312	-102.3724	1	1	1	1	1
S2	QM7C	67.7851	-102.0548	1	1	1	1	1
S3	QM10A	67.7847	-101.2144	1	1	1	1	1
S4	QM10B	67.7847	-101.2144	1	1	1		
S5	QM17C	67.8502	-100.6521	1	1	1	1	1
S6	RF-86-49A	65.6833	-102.0583	1	2	1	1	1
S7	HBA-J-692-A-92	63.1400	-106.612	1		1 & 3	1	1
S8	TX08-027	62.6544	-101.199	1	1	1	1	
S9	19BN59A	61.8085	-108.9588	1	1	1	1	1
S10	21BN05H	61.8093	-108.9579	1	1	1		
S11	MSB93-139	59.4707	-110.4058		4	1 & 4	1	1
	12NK-L031a	65.7703	-103.774	8		6		
	12NK-L033A2	65.8458	-103.256	8		6		
	12NK-L038a	66.0481	-104.7079	8		6		
	62-FD-125	66.2639	-104.0199			5		
	MSB93-02	59.7413	-105.1152		4	5		
	4706-0327b	59.4104	-107.7142			7		

Data source:

1: This study; 2: Thériault et al. (1994); 3: Henderson and Thériault (1994); 4: McNicoll et al. (2000); 5: Davis et al. (2013); 6: Davis et al. (2014); 7: Ashton et al. (2014); 8: Whalen et al. (2018).

Abbreviated sample IDs correspond to those on figure 2-1 and in table 2-1 of chapter 2

The reader should note that the zircon U-Pb-Hf isotope data in this study were acquired using two different approaches. For all samples, some U-Pb isotope data were acquired with the *single-stream* LA-MC-ICPMS technique (section A.5, Appendix A). For seven samples, those U-Pb data were combined with *split-stream* LA-ICPMS U-Pb-Hf isotope data (section A.6, Appendix A). For two samples (RF-86-49A and TX08-027), those U-Pb data were combined with *single-stream* LA-MC-ICPMS Hf isotope data (section A.7, Appendix A). The advantage of the former is that the Hf isotope data are coupled to U-Pb isotope data acquired from the exact same volume of zircon. With the latter approach one must be careful when collecting and reducing the data that the Hf and U-Pb isotope measurements are representative of the same zircon growth domain. However, there are also two advantages to the latter approach. The first is that there is more space available on the zircon grains for *single-stream* U-Pb analyses, which compared to the *split-stream* U-Pb analyses, yield better internal (2SE) precision and are less affected by laser induced U/Pb fractionation (due to a shallower pit depth). The second is that the *single-stream* Hf isotope data are comparatively precise. In this case the 2SE on ϵ_{Hf} values obtained by the *single-stream* method are approximately half those obtained by the *split-stream* method (Tables B-5 and B-7). Comparing the results for samples analyzed with the two different approaches (Figure B-1), it is my opinion (in hindsight) that overall greater data quality can be achieved by carefully combining *single-stream* U-Pb data with *single-stream* Hf isotope data.

B.2 Approach to zircon U-Pb-Hf-O isotope data interpretation

The general approach taken in the interpretation of the zircon U-Pb-Hf and O isotope was as follows. The data were first screened for quality, and low-quality analyses were excluded for the reasons stated in the analytical methods sections (Appendix A). The excluded analyses can be found in the data tables (section B.7) with a note stating the reason for their exclusion. Zircon domains were then classified as having an inherited, igneous or metamorphic origin based on their characteristics in cathodoluminescence (CL) and/or backscattered electron (BSE) images, and in some cases their Th/U ratios. When the origin of a zircon domain was ambiguous, a judgment was made by comparing its characteristics and $^{207}\text{Pb}/^{206}\text{Pb}$ date to domains with a more clear origin. These classifications can be found in the data tables. All zircon CL and/or BSE images, and analytical spot locations, are given in section B.8 of this appendix.

After identifying and excluding inherited or metamorphic zircon analyses, which were typically rare, igneous crystallization ages were assigned from the oldest group of concordant to near concordant igneous zircon $^{207}\text{Pb}/^{206}\text{Pb}$ dates that yield a weighted mean with an MSWD that, for the sample size (n), is consistent with a single statistical population (Wendt and Carl, 1991). The assumption behind this approach is that any younger igneous zircon dates, even if overlapping the concordia curve, are

a product of ancient Pb-loss. For samples with coupled U-Pb-Hf isotope data, this assumption was tested by plotting $^{207}\text{Pb}/^{206}\text{Pb}$ date vs. ϵHf_t (where t is the measured $^{207}\text{Pb}/^{206}\text{Pb}$ date). In all cases, the igneous zircon data yield arrays in $^{207}\text{Pb}/^{206}\text{Pb}$ date vs. ϵHf_t space that are consistent with ancient Pb-loss from a single igneous zircon population. For samples with both single-stream U-Pb and split-stream U-Pb-Hf data, the two data sets were treated separately to arrive at the best possible crystallization age constraint; they were not combined for any weighted mean age calculations.

Initial ϵHf (ϵHf_i) values were determined by calculating all igneous zircon ϵHf values at the assigned crystallization age of the rock (not at the measured $^{207}\text{Pb}/^{207}\text{Pb}$ dates), and then taking a weighted mean of those analyses. All but one sample in this study yield weighted mean ϵHf_i values with MSWDs that are consistent with a single statistical population. For one sample (S6. RF-86-49A), there is slight over-dispersion in the ϵHf_i values ($n=29$, $\text{MSWD}=1.9$), but this over-dispersion is eliminated if only two of twenty-nine analyses are excluded. Also, the 2SD on the ϵHf_i values from all samples are 1–2 ϵHf units, which is the same amount of dispersion that is observed in the analyzed homogeneous reference materials (91500 and OG1). This means that at the precision level of the data, there is no (or virtually no) resolvable intra-sample variation in the initial zircon Hf isotope compositions. For that reason, only the weighted mean ϵHf_i values are used in interpreting the Hf isotope data, and only the weighted mean values are shown in the main text. In contrast to the zircon Hf isotope data, igneous zircon $\delta^{18}\text{O}$ values from a single sample often do not comprise a single statistical population (i.e., $\text{MSWD} \gg 1$). Therefore, all individual igneous zircon $\delta^{18}\text{O}$ measurements were plotted in the main text, along with the median rather than weighted mean $\delta^{18}\text{O}$ value.

For one sample (S11. MSB93-139), the U-Pb-Hf isotope data are comparatively complex, and I deviated from the general approach described above. The interpretation of this sample is described in detail in its respective sub-section of section B.3.

B.3 Sample-by-sample description of results

This section contains rock descriptions and analytical results for samples with new zircon U-Pb-Hf-O isotope data. Mineral modifiers in rock names are listed in order of increasing abundance. Zircon grain and spot numbers referred to in this section correspond to spot IDs in the data tables (section B.7) and on the CL and BSE images (section B.8). All dates and weighted mean dates referred to are $^{207}\text{Pb}/^{206}\text{Pb}$ dates and weighted mean $^{207}\text{Pb}/^{206}\text{Pb}$ dates.

Samples labelled “QM” and “RF” are from the Queen Maud block (Figure 2-1) and those labelled “QM” were originally described and dated in petrographic thin section by Tersmette (2012). The Queen Maud block was affected by granulite-facies metamorphism during the Arrowsmith orogeny

(Schultz et al., 2007; Tersmette, 2012; Berman et al., 2013). Four of the samples from the Queen Maud block contain pyroxene (QM2C, QM10A, QM17C and RF-86-49A), which is interpreted to be of metamorphic rather than igneous origin. This interpretation is consistent with the TTG (tonalite-trondhjemite-granodiorite) like composition of QM2C, QM17C and RF-86-49A (QM10A is a mafic rock), as TTG's typically do not contain primary igneous pyroxene (Moyen and Martin, 2012). It is also consistent the presence of Arrowsmith-aged (ca. 2.4–2.3 Ga) metamorphic zircon in the three of the pyroxene-bearing samples (QM2C, QM10A and QM17C).

S1. QM2C

This sample is a medium-grey, medium-grained, gneissic, orthopyroxene tonalite. Gneissic layering is ~0.5 cm thick. Biotite and hornblende are secondary minerals after orthopyroxene.

Zircon grains from this sample are of good quality and generally prismatic with well-defined oscillatory zoning. A number of zircon grains and domains are classified as metamorphic, including unzoned rims (e.g., grain 5), unzoned spherical grains (e.g., grain 39), irregularly zoned grains (e.g., grain 13) and unzoned domains with low Th/U (e.g., grain 108). Following data reduction, 20/22 single-stream U-Pb and 33/43 split-stream U-Pb-Hf isotope measurements were retained. After screening domains with >40 ppm Ca, 31/43 O isotope measurements were retained.

The zircon images and U-Pb-Hf isotope data are consistent with ancient Pb loss from a single igneous zircon population (Figure B-1). Weighted mean $^{207}\text{Pb}/^{206}\text{Pb}$ dates calculated from the single- and split-stream data sets are indistinguishable from each other (Figure B-1), and the single-stream date of 3225 ± 8 Ma (MSWD=1.7, n=8) is quoted as the crystallization age hereafter. When all ϵ_{Hf} values are calculated at the crystallization age, they yield a weighted mean ϵ_{Hf} of 2.66 ± 0.41 (MSWD=1.3, n=30). All igneous zircon analyses yield $\delta^{18}\text{O}$ values within the mantle zircon field (Valley et al., 1998) and a median $\delta^{18}\text{O}$ of 5.5‰. Metamorphic zircon yield $\delta^{18}\text{O}$ values above, but typically within uncertainty of, the mantle zircon field. Approximate metamorphic ages of 3085 ± 20 Ma (MSWD=1.6, n=3) and 2345 ± 23 Ma (MSWD=2.2, n=3) are calculated from the single-stream data.

S2. QM7C

This sample is a dark-grey, medium-grained, strongly-foliated biotite tonalite. The foliation is defined by aligned biotite and deformed/recrystallized quartz. Actinolite and chlorite are also present as secondary minerals.

Zircon grains from this sample are of poor quality. They are typically prismatic with poorly preserved fine-scale oscillatory zoning and moderate to extensive radiation damage. Following data reduction, 16/17 single-stream U-Pb and 16/40 split-stream U-Pb-Hf isotope measurements were retained.

After screening domains with >40 ppm Ca, only 5/28 O isotope measurements were retained. However, it is important to note that the O isotope data from high (>40 ppm) and low (<40 ppm) Ca domains in this sample are mostly consistent (Figure A-2).

The oldest group of single- and split-stream dates yield weighted means of 3089 ± 7 Ma (MSWD=1.4, n=8) and 3123 ± 7 Ma (MSWD=0.34, n=5), respectively (Figure B-1). This discrepancy is not entirely surprising, considering the poor quality of zircon grains from this sample. When calculated at 3089 and 3123 Ma, the ϵ_{Hf} values yield weighted means of $-0.26 + 0.50$ (MSWD=0.65, n=16) and $0.51 + 0.50$ (MSWD=0.66; n=16), respectively. Given that there is no evidence for inherited zircon, and that the U-Pb-Hf isotope data are consistent with ancient Pb loss from a single igneous zircon population (Figure B-1), I take 3123 ± 7 Ma and 0.51 ± 0.50 as the best estimate of the rocks crystallization age and ϵ_{Hf_i} . In either case, the rock is ca. 3.1 Ga with a chondritic Hf isotope composition. Zircon $\delta^{18}\text{O}$ values are within the mantle zircon field and yield a median $\delta^{18}\text{O}$ of 5.6‰.

S3. QM10A and S4. QM10B

These samples were collected from the same outcrop, where a brownish grey granitoid gneiss is crosscut by sheets of pink granitoid gneiss (Tersmette, 2012). Sample QM10A is from the former and sample QM10B is from the latter. QM10A is a medium-grained, gneissic, clinopyroxene-orthopyroxene quartz-diorite with hornblende and biotite after pyroxene. Gneissic layering is poorly defined and <0.5 cm thick. QM10B is a medium-grained, gneissic, orthopyroxene tonalite with biotite after orthopyroxene. Gneissic layering is well defined and ~0.5–1 cm thick.

S3. QM10A

Zircon grains from this sample are of excellent quality. They are generally prismatic with broad- to fine-scale oscillatory zoning and rare unzoned metamorphic rims. Following data reduction, 23/23 single-stream U-Pb and 20/27 split-stream U-Pb-Hf isotope measurements were retained. After screening domains with >40 ppm Ca, 19/26 O isotope measurements were retained.

The oldest group of igneous single- and split-stream dates yield weighted mean dates of 3224 ± 9 Ma (MSWD=1.7, n=6) and 3202 ± 9 Ma (MSWD=1.5, n=7), respectively. The zircon images and U-Pb-Hf isotope data (Figure B-1) are consistent with ancient Pb loss from a single igneous zircon population. Therefore, the older single-stream date is interpreted as the crystallization age. The oldest single-stream dates were also replicated in two separate analytical sessions. When all ϵ_{Hf} values are calculated at the crystallization age, they yield a weighted mean ϵ_{Hf_i} of 0.59 ± 0.46 (MSWD=1.3, n=20). All igneous zircon $\delta^{18}\text{O}$ values lie within the mantle zircon field and yield a

median $\delta^{18}\text{O}$ of 5.7‰. One unzoned metamorphic rim (spot 62.2) yields a date of 2408 ± 20 Ma and a $\delta^{18}\text{O}$ of 5.7‰.

S4. QM10B

Zircon grains from this sample are of moderate quality. They are typically prismatic with fine-scale oscillatory zoning. All 27 single-stream U-Pb isotope measurements were retained.

The U-Pb data define what is interpreted as an ancient Pb loss array along concordia from ~3.2 to 3.0 Ga (Figure B-1). The three oldest analyses yield a weighted mean date of 3200 ± 23 Ma (MSWD=2.4), which is interpreted as a minimum age of the sample. The maximum age of this sample is constrained by the crystallization age of QM10A (3227 ± 7 Ma). A single inherited core (spot 57.1) yields a date of 3316 ± 12 Ma (Figure B-1).

S5. QM17C

This sample is a medium-grey, medium-grained, gneissic, orthopyroxene granodiorite. Gneissic layering is very well defined and ~0.5 cm thick. Biotite is a secondary mineral after orthopyroxene.

Zircon grains from this sample are of moderate quality. They generally display broad- to fine-scale oscillatory zoning and are prismatic with rare unzoned metamorphic rims. Following data reduction, 18/18 single-stream U-Pb and 27/40 split-stream U-Pb-Hf isotope measurements were retained. After screening domains with >40 ppm Ca, 16/32 O isotope measurements were retained.

The U-Pb-Hf isotope data and zircon images are consistent with ancient Pb loss from a single igneous zircon population (Figure B-1). Weighted mean dates calculated from the single- and split-stream data are indistinguishable (Figure B-1). The split-stream date of 3140 ± 9 Ma (MSWD=1.4, n=7) is quoted as the crystallization age hereafter. When all ϵHf_i values are calculated at the crystallization age, they yield a weighted mean ϵHf_i of -0.02 ± 0.30 (MSWD=1.0, n=27). All $\delta^{18}\text{O}$ values are within, or within uncertainty of, the mantle field and yield a median of 5.7 ‰. Three spots on unzoned metamorphic rims (spots 40.1, 53.2 and 94.2) give dates of 2384 ± 13 , 2376 ± 13 and 1962 ± 17 Ma.

S6. RF-86-49A

This sample is a dark grey, medium-grained, foliated to weakly-gneissic, orthopyroxene-clinopyroxene tonalite. Gneissic layering is poorly defined and <0.5 cm thick. Amphibole and biotite are secondary phases after pyroxene.

Zircon grains from this sample are of excellent quality. They range from equant to prismatic and typically display faint and broad, or clear and fine oscillatory zoning. Following data reduction, 41/47 single-stream U-Pb and 29/29 single-stream Hf isotope measurements were retained.

The U-Pb-Hf isotope data and zircon images are consistent with ancient Pb loss from a single igneous zircon population (Figure B-1). The oldest group of analyses yield a weighted mean age of 3314 ± 6 Ma (MSWD=1.7, n=8), which is interpreted as the crystallization age of the rock. When all ϵ_{Hf} values are calculated at the crystallization age, they produce a weighted mean ϵ_{Hf_i} of 0.54 ± 0.22 (MSWD=1.9, n=29).

S7. HBA-J-692-A-92

This sample was originally dated via ID-TIMS (isotope dilution – thermal ionization mass spectrometry) by Henderson and Thériault (1994). Henderson and Thériault described the rock as a strongly-foliated to gneissic, white to grey, medium-grained biotite tonalite, with abundant epidote and minor muscovite. They obtained an upper intercept age of $3129 +13/-11$ Ma from four single grain fractions.

The zircon grains from this sample are of excellent quality. They are generally prismatic with broad oscillatory zoning. Less commonly, grains are equant or have fine-scale oscillatory zoning. Following data reduction, 21/22 single-stream U-Pb and 36/43 split-stream U-Pb-Hf isotope measurements were retained. After screening domains with >40 ppm Ca, 33/41 O isotope analyses were retained.

The U-Pb-Hf isotope data are consistent with minor ancient Pb loss from a single igneous zircon population (Figure B-1). Weighted mean dates calculated from the single- and split-stream data are indistinguishable from each other and from the original ID-TIMS age. The split-stream date of 3124 ± 6 Ma is quoted as the crystallization age hereafter. When all igneous zircon ϵ_{Hf} values are calculated at the crystallization age, they yield a weighted mean ϵ_{Hf_i} of -0.01 ± 0.35 (MSWD=1.3, n=35). All igneous zircon $\delta^{18}\text{O}$ values are within the mantle zircon field and yield a median $\delta^{18}\text{O}$ of 5.5 ‰. Two core domains with bright CL response (grains 28 and 104) yield dates that are older than the main zircon population and are interpreted as inherited. This interpretation is supported by an oscillatory zoned rim on grain 28 that has a date of 3110 ± 10 Ma. Two rim domains (grains 34 and 46) have lower U contents (<100 ppm, determined via electron microprobe; Appendix A) than the rest of the zircon domains and yield a weighted mean of 2419 ± 8 Ma (MSWD=1.2), which is interpreted as a metamorphic age. This interpretation is supported by the rounded, ovoid nature of grain 34 and its unzoned rim.

S8. TX08-027

This sample is a beige, medium-grained, gneissic, feldspar porphyroclastic, biotite-hornblende tonalite. The rock is strongly deformed. Gneissic layering is well-defined and ~0.75–1 cm thick. There are rare <0.25 cm thick leucocratic layers, which could represent transposed leucosome (*in situ* melt) or transposed small leucogranitic intrusions. Accessory zircon and opagues are present.. Abundant epidote is present in association with biotite and hornblende.

Zircon grains recovered from this sample are of good quality. They are typically prismatic to sub-equant and characterized by fine- to broad-scale oscillatory zoning. Following data reduction, 35/35 single-stream U-Pb and 35/36* single-stream Hf isotope measurements were retained. *Two Hf isotope measurements in the same domain (52_1 and 52_2) are correlated to the same U-Pb analyses (52.1).

The majority of the U-Pb data comprise a restricted range of concordant to near concordant dates between ~3.25 and 3.10 Ga. With the exception of two grains discussed below, the zircon images and U-Pb-Hf isotope data are consistent with ancient Pb loss from a single igneous zircon population (Figure B-1). The oldest group of analyses yield a weighted mean date of 3215 ± 6 Ma (MSWD = 1.05, n = 10), which is interpreted as the crystallization age of the rock. When all igneous zircon ϵ_{Hf} values are calculated at the crystallization age, they yield a weighted mean ϵ_{Hf} of 1.18 ± 0.27 (MSWD=0.77, n=32). Grains 88 and 112 yield three distinctly younger dates of 2406, 2395 and 2381 Ma (Figure B-1). Grain 88 displays fine-scale oscillatory zoning whereas grain 112 is unzoned. The Hf isotope compositions of these grains are consistent with a mixture of zircon recrystallization and new zircon growth within the rock (Figure B-1). These grains are therefore interpreted as metamorphic or leucosome zircon that were crystallized or recrystallized during the formation of the leucocratic layers described above.

S9. 19BN59A and S10. 21BN05H

These samples were collected from the same outcrop, ~100 metres apart. Both samples are medium-grey, medium-grained, equigranular, deformed hornblende- and biotite-bearing granitoids, and are interpreted to be part of the same unit. 19BN59A is a foliated to gneissic, biotite-hornblende tonalite, whereas 20BN05H is a foliated, hornblende-biotite quartz-monzodiorite.

S9. 19BN59A

Zircon grains from this sample are of good quality. They are generally prismatic with well-defined fine scale oscillatory zoning. Several grains are ovoid to spherical with irregularly zoned rims (e.g., grains 30 and 55) that are interpreted as metamorphic. Following data reduction, 38/45 single-stream U-Pb

isotope and 30/48 split-stream U-Pb-Hf isotope measurements were retained. After screening domains with >40 ppm Ca, 27/58 O isotope measurements were retained.

The oldest group of igneous single- and split-stream analyses yield weighted mean dates of 3238 ± 8 Ma (MSWD=1.5, n=7) and 3205 ± 7 Ma (MSWD=1.9, n=11), respectively. The zircon images and U-Pb-Hf isotope data are consistent with ancient Pb loss from a single igneous zircon population. Therefore, the older single-stream date is interpreted as the crystallization age of the rock. The oldest single-stream dates were also replicated in two separate analytical sessions. When all igneous zircon ϵ_{Hf} values are calculated at the crystallization age, they yield a weighted mean ϵ_{Hf} of 1.64 ± 0.36 (MSWD=1.3, n=30). The igneous zircon $\delta^{18}\text{O}$ values yield a median of 5.1‰ and all but two individual analyses are within the mantle zircon field. Metamorphic zircon domains typically have $\delta^{18}\text{O}$ values below the mantle field and they yield an approximate metamorphic age of 2423 ± 22 Ma (MSWD=5.2, n=5).

S10. 21BN05H

Zircon grains from this sample are of moderate to poor quality. They are mostly prismatic with faint oscillatory zoning. Following data reduction, 21/22 single-stream U-Pb isotope measurements were retained.

The U-Pb data are spread along concordia from ~3200 to 2850 Ma (Fig. S3). There is no evidence of multiple age populations in the zircon images. The spread of the U-Pb data is therefore interpreted as a product of ancient Pb loss. The weighted mean of the two oldest analyses provides a minimum age of 3185 ± 11 Ma (MSWD=0.59). The true crystallization age of this sample is probably the same as 19BN59A (3238 ± 8 Ma).

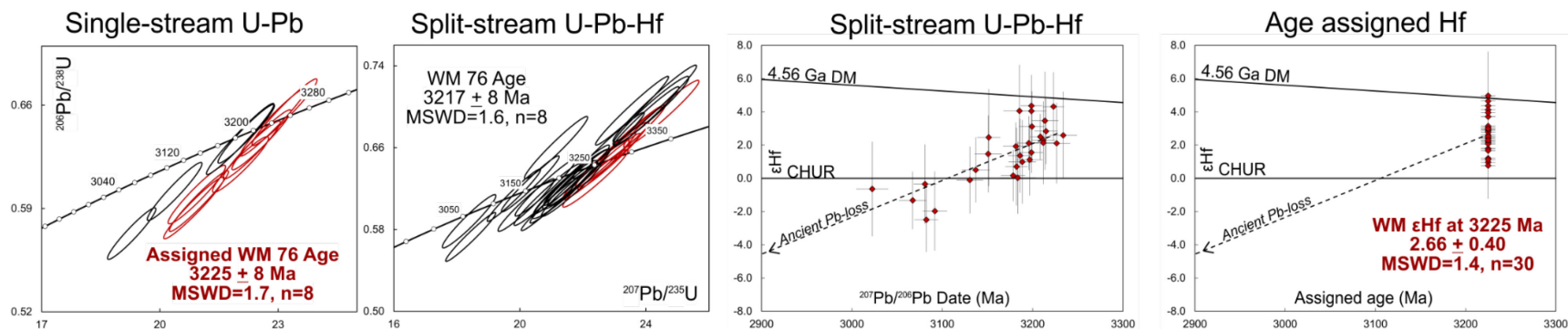
S11. MSB93-139

This sample was originally dated via ID-TIMS by McNicoll et al. (2000). McNicoll et al. described the rock as a ptygmatically folded, biotite-rich tonalite gneiss, with gneissic layering on the cm scale. The ID-TIMS data from this sample are complex. Based on two concordant to near-concordant single grain fractions, McNicoll et al. estimated the age of the sample to be $3076 \pm 15/-5$ Ma.

The zircon grains recovered from this sample are of excellent quality, but have variable morphologies and sometimes complex internal zoning. Morphologies include equant, irregular and prismatic varieties. Internal zoning ranges from homogeneous and oscillatory (e.g., grain 66) to irregular (e.g., grain 67). Several grains have what appear to be magmatic rims on inherited cores (e.g., grains 5, 17, 26, 92). Following data reduction, 22/27 single-stream U-Pb isotope and 40/53 split-stream U-Pb-Hf isotope measurements were retained. After screening domains with >40 ppm Ca, 40/53 zircon O isotope measurements were retained.

Distinguishing which analyses are from inherited or magmatic grains/domains is difficult in this sample because not all grains display clear core-overgrowth relationships and there is (with one exception noted below) no clear relationship between zircon age and composition (e.g., Th/U). It could therefore be the case that some inherited domains that underwent ancient Pb loss yield $^{207}\text{Pb}/^{206}\text{Pb}$ dates that overlap with those from magmatic domains. To estimate the crystallization age, I took a weighted mean of the oldest $^{207}\text{Pb}/^{206}\text{Pb}$ dates from igneous rims or grains that yield a single statistical population, but are themselves not older than the youngest inherited core date, unless that inherited core date was younger than its corresponding rim date (spots 37_1 and 70_1) and clearly influenced by ancient Pb loss. For the single- and split-stream data, this approach yields identical weighted mean dates of 3071 ± 7 Ma (MSWD=0.72, n=7) and 3074 ± 7 Ma (MSWD=1.6, n=14), respectively. The latter is quoted as the crystallization age of the sample hereafter. Support for this crystallization age interpretation comes from dominant probability density peaks at 3.07 Ga in both the single- and split-stream data sets (Figure B-1). This result is also consistent with the original ID-TIMS age. Due to the complexity of the zircon in this sample, only Hf and O isotope data from domains corresponding to the 7 single-stream and 14 split-stream analyses used in the above weighted mean date calculations are used to estimate the isotopic composition of the magma. The $\delta^{18}\text{O}$ values yield a median of 5.5 ‰ and all individual values are within, or within uncertainty of, the mantle zircon field. When all ϵ_{Hf} values from those domains are calculated at the crystallization age (3074 Ma), they yield a weighted mean ϵ_{Hf_i} of -1.71 ± 0.48 (MSWD=1.7, n=14). Zircon domains with dates older than those included in the weighted mean age calculations above are regarded as inherited (Figure B-1). One unzoned grain (grain 47) with a low Th/U yields a metamorphic date of 2377 ± 11 .

S1. QM2C



S2. QM7C

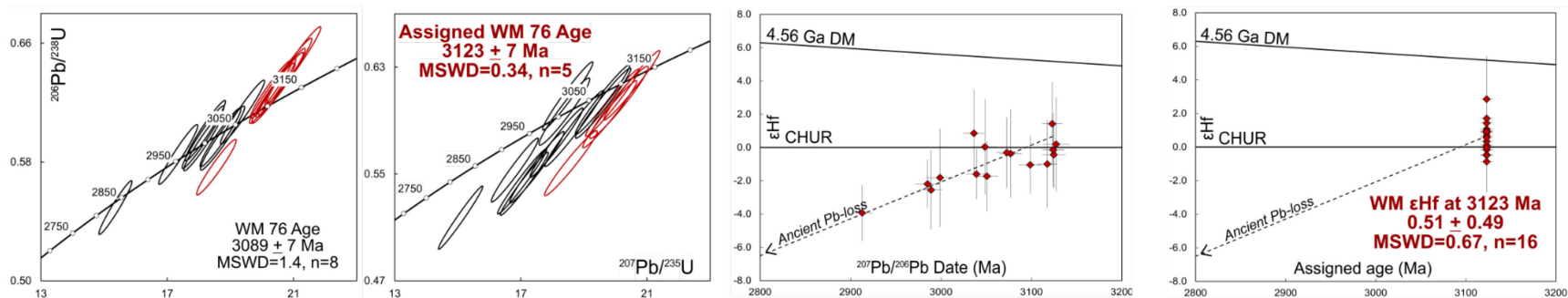
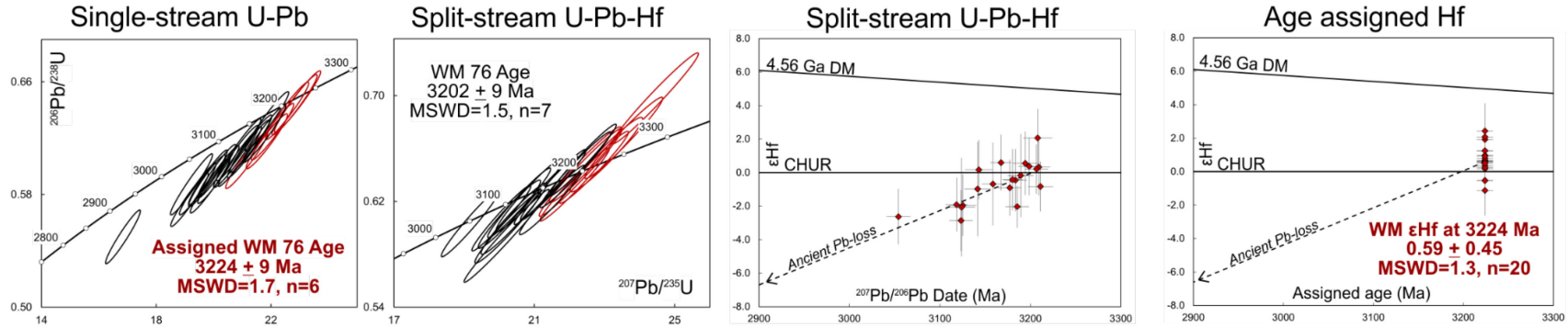
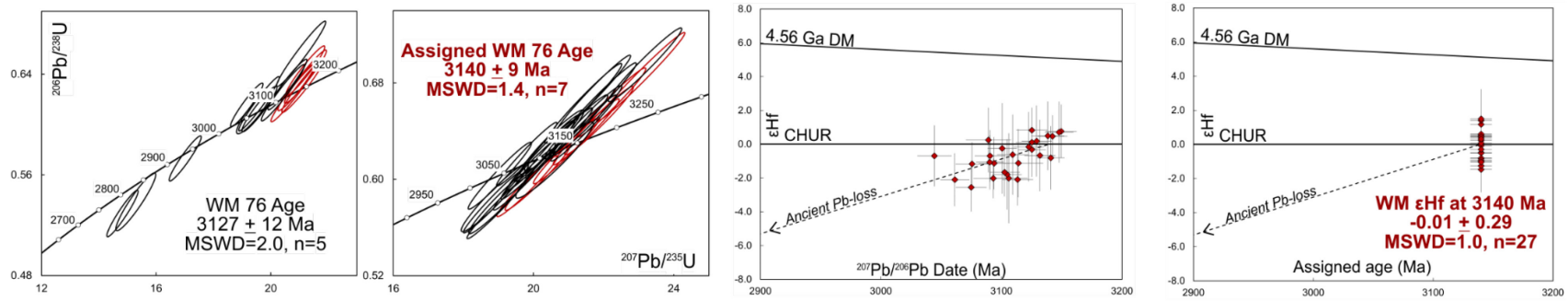


Figure B-1. Zircon U-Pb-Hf isotope data for pre-3.0 Ga granitoids from the PRT. U-Pb uncertainty ellipses are 2σ . ϵ_{Hf} uncertainty bars are 2SE . U-Pb data are plotted on Wetherill concordia diagrams. Ancient Pb loss vectors on the Hf isotope plots are the time integrated evolution of ϵ_{Hf} with a $^{176}\text{Lu}/^{177}\text{Hf}$ of 0.001. Data points in red are included in weighted mean $^{207}\text{Pb}/^{206}\text{Pb}$ ages and ϵ_{Hf} calculations. Bold red text indicates the interpreted crystallization age and ϵ_{Hf} of the sample. Uncertainties on weighted mean $^{207}\text{Pb}/^{206}\text{Pb}$ ages are 2σ and include the long-term external reproducibility of the *weighted mean* $^{207}\text{Pb}/^{206}\text{Pb}$ ratio ($\sim 0.3\%$ 2σ ; section A.13, Appendix A). Metamorphic zircon analyses are excluded for clarity. WM: Weighted Mean, DM: Depleted Mantle, CHUR: Chondritic Uniform Reservoir. 4.56 Ga DM model line from Fisher and Vervoort (2018).

S3. QM10A



S5. QM17C



S7.HBA-J-692-A-92

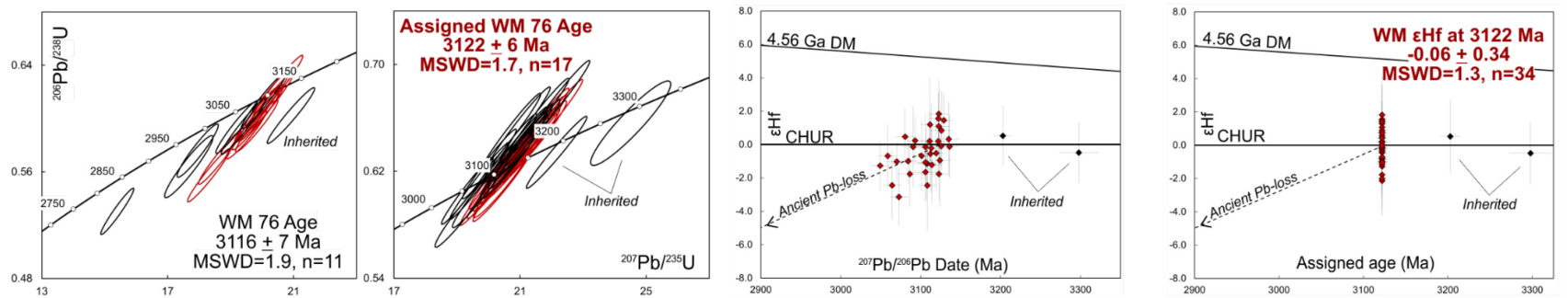
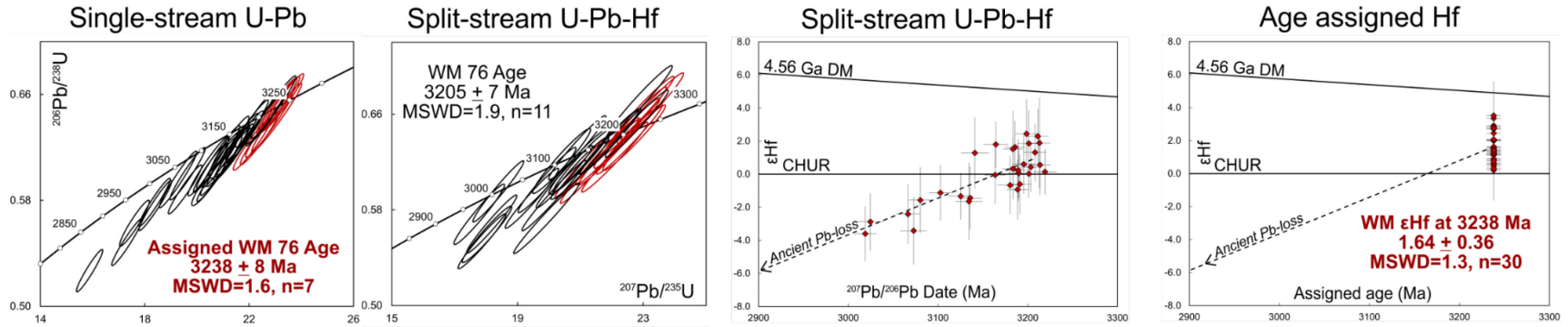


Figure B-1. Continued.

S9. 19BN59A



S11. MSB93-139

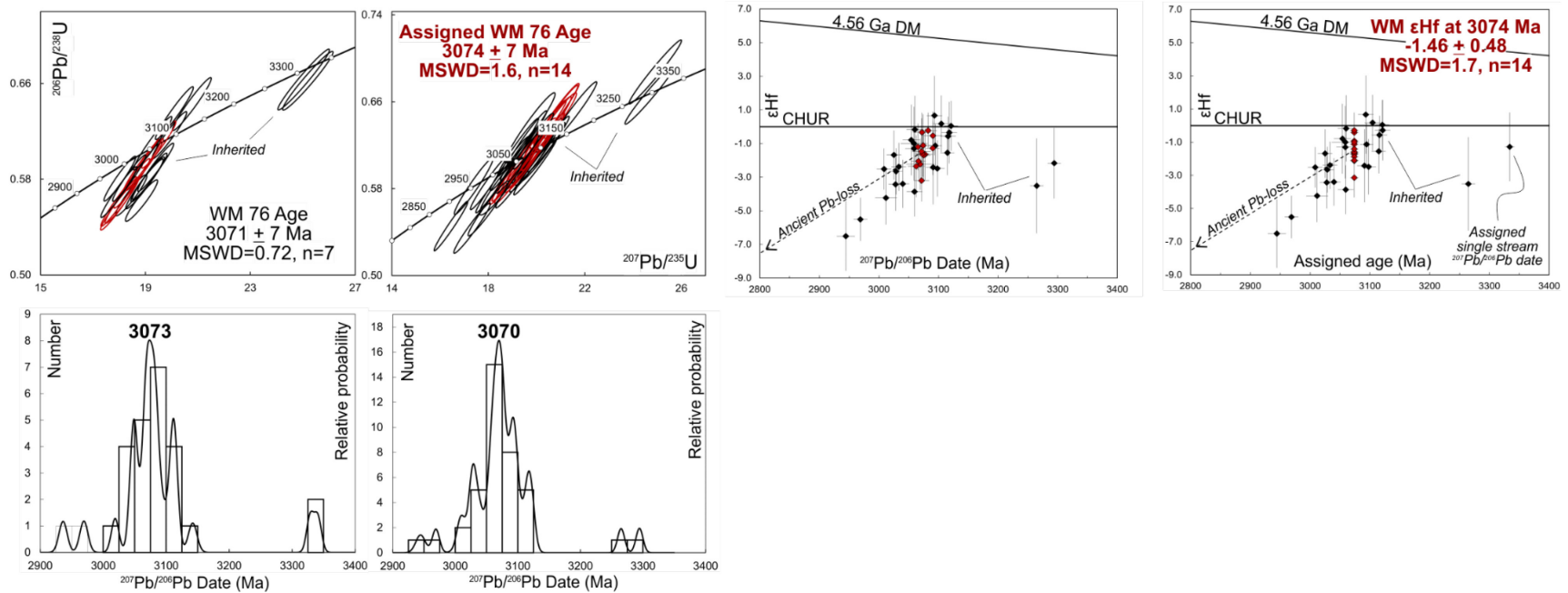


Figure B-1. Continued.

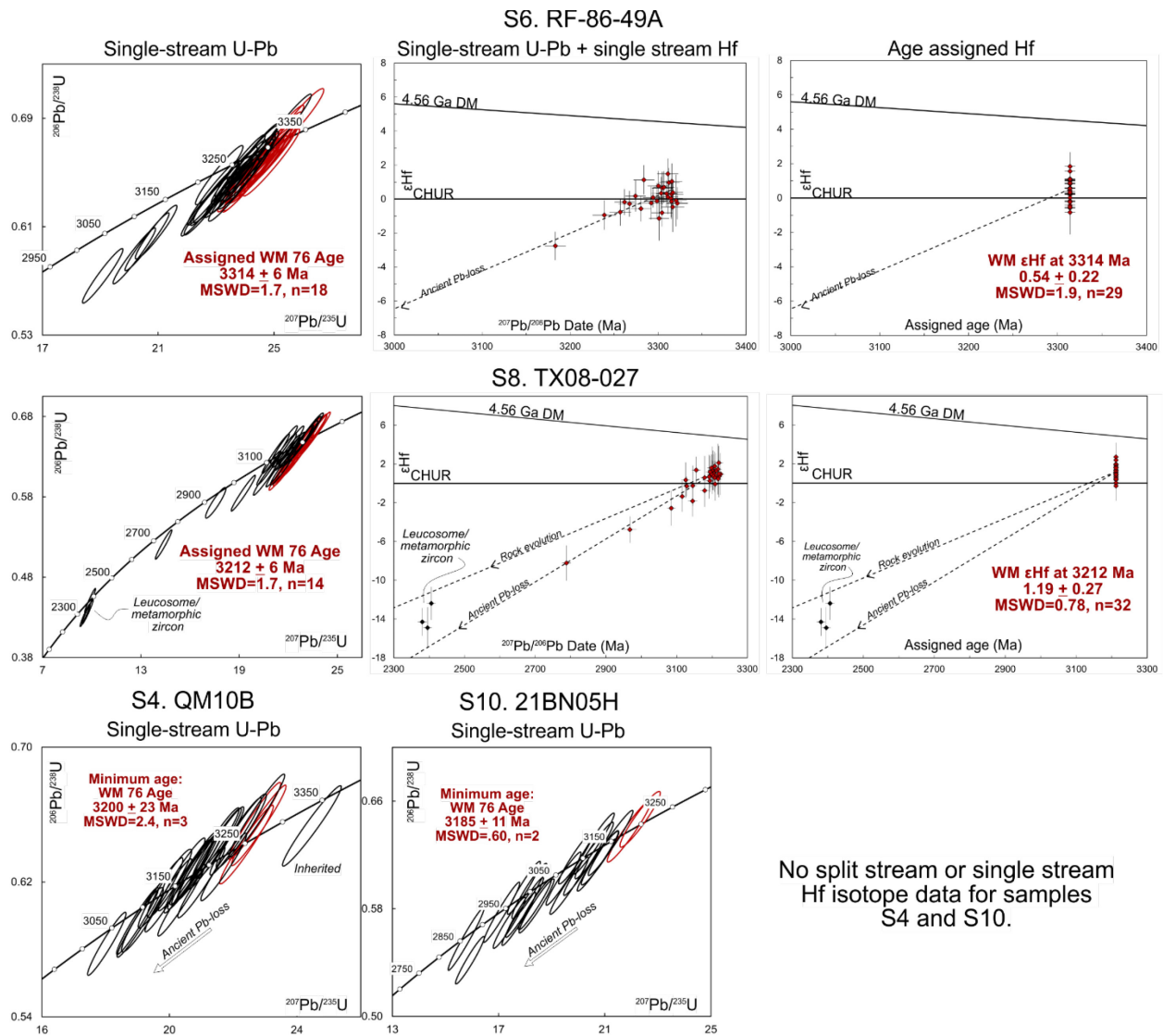


Figure B-1. Continued.

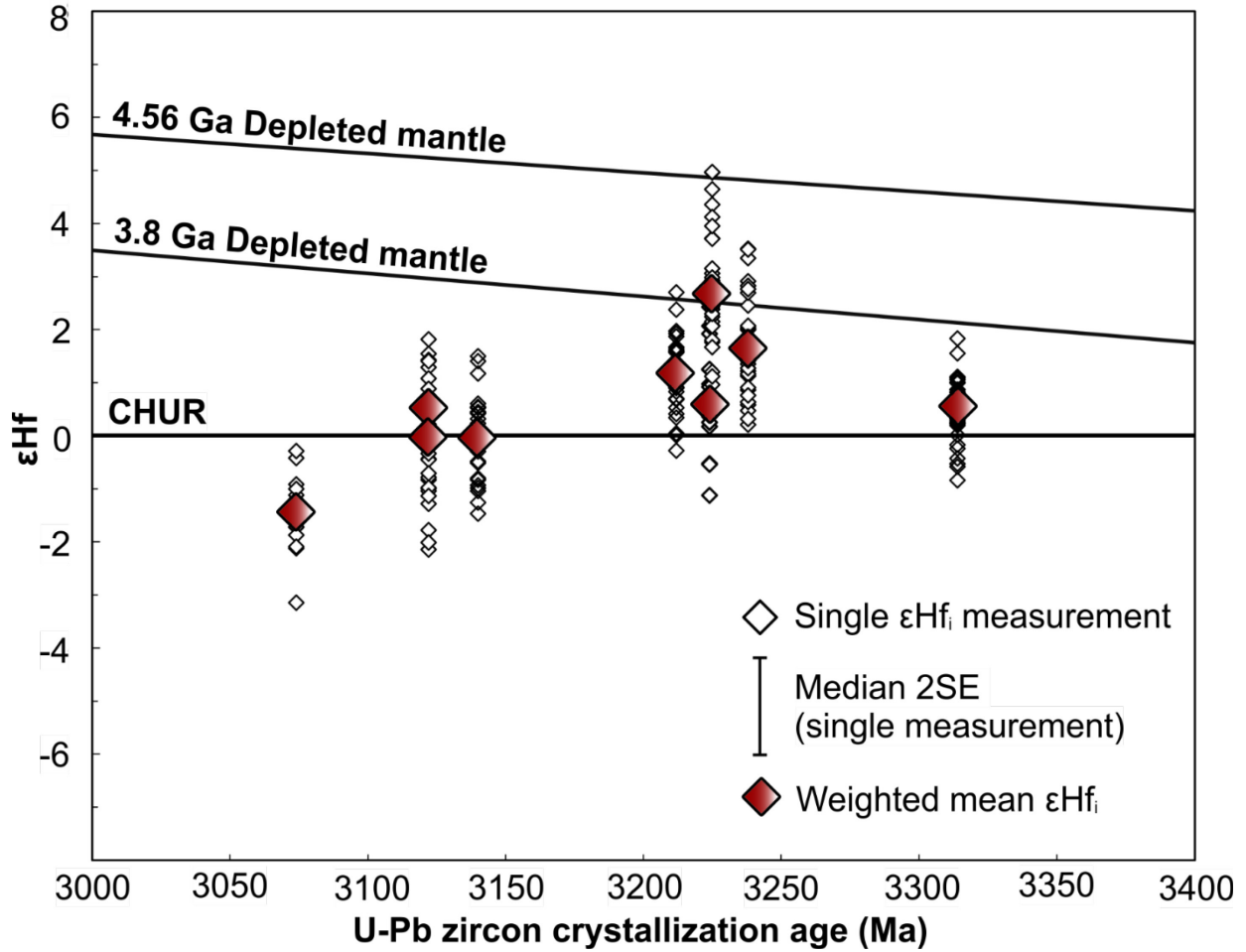


Figure B-2. All igneous zircon Hf isotope data from this study, with each individual ϵ_{Hf_i} value calculated at the interpreted crystallization age of the rock. 2SE uncertainties on weighted mean ϵ_{Hf_i} values are approximately the same size as the data point symbols. CHUR: chondritic uniform reservoir; DM: depleted mantle. DM models are from Vervoort et al. (2018) and Fisher and Vervoort (2018).

B.4 Whole-rock Sm-Nd isotope compilation (figure 2-1)

Whole-rock Sm-Nd isotope data were compiled for (meta)igneous rocks of the Rae craton. Sedimentary rocks, metasedimentary rocks, ultramafic rocks, and rocks thought to have been derived from an enriched mantle source, such as minettes or lamprophyres, were excluded from the compilation. The compiled data and associated references are available in a data repository that was published with the Geology paper: <https://doi.org/10.1130/G51110.1>

B.5 Igneous zircon Hf isotope compilation (figure 2-3)

Zircon Hf isotope data were compiled for 3.6–3.0 Ga (meta)igneous rocks globally (Figs. 2-3 and B-2). Mean, weighted mean or median zircon ϵHf_i values calculated at the crystallization age of the rock were compiled, such that each sample is represented by a single data point. It is important to compile igneous zircon Hf isotope in this way, rather than compiling individual zircon ϵHf_i values, to avoid weighting samples by the number of zircon measurements made. Whenever possible, the ϵHf_i value reported by the original authors was compiled, whether that value was a mean, weighted mean or median. If the original authors did not report a mean, weighted mean or median ϵHf_i value, I calculated mean and median values from the individual ϵHf_i values, using the original authors interpreted rock age. The median values are used in figures 2-3 and B-2, but the difference between them and the mean values is typically negligible. In very rare cases, where the original authors did not report a crystallization age of the rock, or it was unclear which zircon Hf isotope measurements could be assigned to the rocks crystallization age, the data were not compiled. Where necessary, ϵHf values were recalculated using the decay constant of Söderlund et al. (2004) and the CHUR values of Bouvier et al. (2008). The compiled data and associated references can be found in a data repository that was published with the Geology paper: <https://doi.org/10.1130/G51110.1>

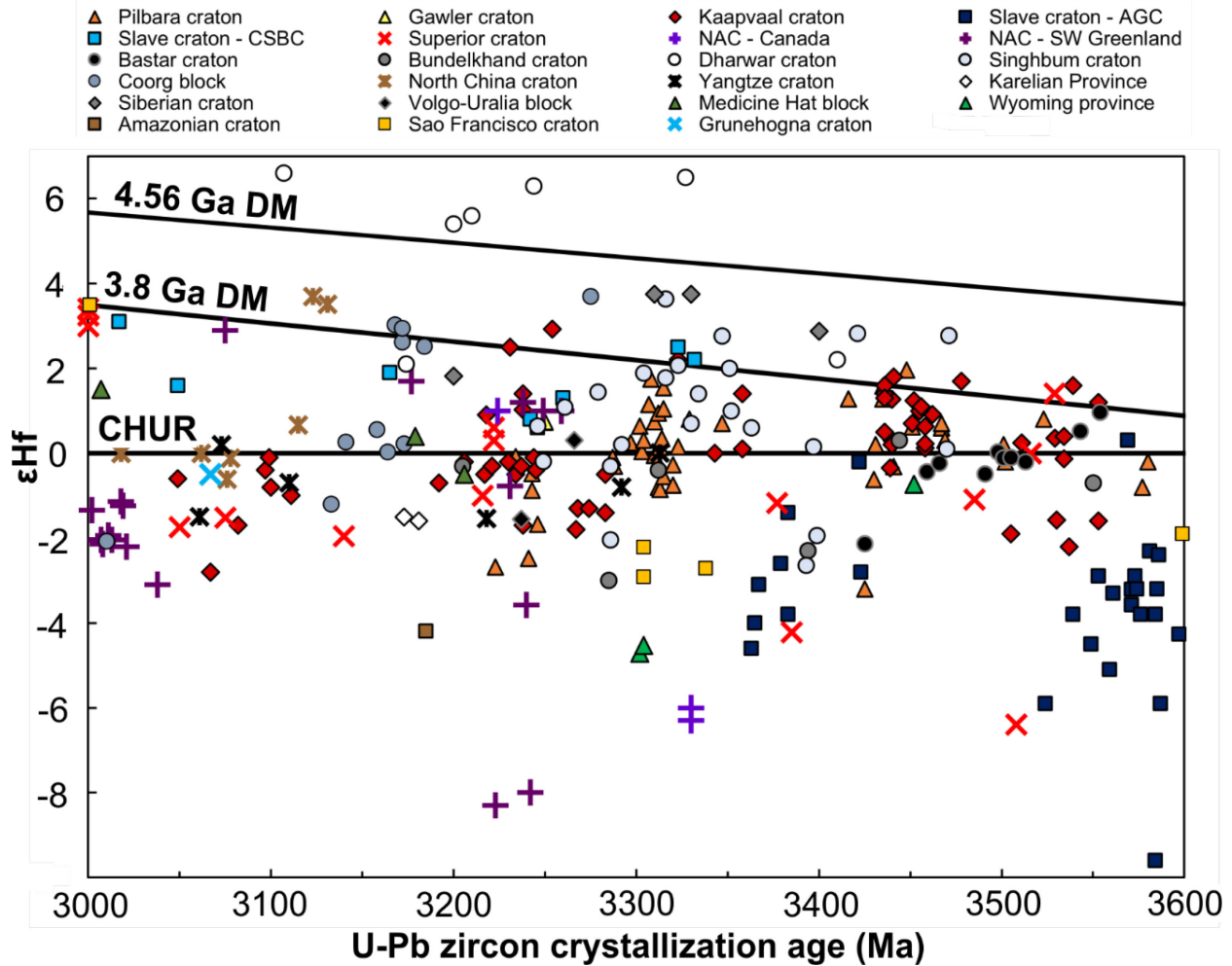


Figure B-3. Global compilation zircon Hf isotope data for 3.6–3.0 Ga igneous rocks. Each data point represents the weighted mean, mean or median zircon ϵ_{Hf} value of one rock. Data are coded by craton or crustal block. CHUR: chondritic uniform reservoir; DM: depleted mantle. 4.56 Ga and 3.8 Ga DM model lines are from Vervoort et al. (2018) and Fisher and Vervoort (2018). CSBC: Central Slave basement complex; NAC: North Atlantic craton; AGC: Acasta gneiss complex.

B.6 Hafnium mass balance of ancient continental crust

Table B-2 provides the theoretical mass balance of Hf in ancient (>3.0 Ga) continental crust, which may have been more mafic, on average, than modern continental crust (e.g., Tang et al., 2016; Hawkesworth and Jaupart, 2021; cf. Garcon, 2021). We have assumed that ancient continental crust was ~70% mafic (<57 wt.% SiO₂) and ~30% felsic (>57 wt.% SiO₂) (Hawkesworth and Jaupart, 2021). A simple subdivision of ancient continental crust into a mafic component and a felsic component is reasonable because Archean igneous rocks yield a bimodal distribution, with modes at ~50 wt.% SiO₂ and 70 wt.% SiO₂ (Taylor and McLennan, 1985; Kamber, 2015). The Hf ppm and ¹⁷⁶Lu/¹⁷⁷Hf of the mafic component are estimated from the average Hf and Lu content of mafic (<57 wt.% SiO₂) volcanic rocks from the Pilbara craton (Smithies et al., 2007). The Hf ppm and ¹⁷⁶Lu/¹⁷⁷Hf of the felsic component are estimated from the average Hf and Lu content of Archean grey gneisses (Moyen and Martin, 2012). The Archean grey gneiss compilation (Moyen and Martin, 2012) includes a variety of rock types, but is dominated by TTG (tonalite-trondhjemite-granodiorite) and potassic granitoids, and yields an average SiO₂ content of 68 wt.%. Mass balance calculations indicate that even if ~70% of ancient continental crust was mafic, ~49% of the total Hf in ancient continental crust would reside in the felsic component (Table B-2). The mafic component would have a comparatively high average ¹⁷⁶Lu/¹⁷⁷Hf of ~0.021, whereas the felsic component would have a low average ¹⁷⁶Lu/¹⁷⁷Hf ratio of ~0.007 (Table B-2).

Table B-2. Theoretical mass balance of Hafnium in ancient continental crust.

	Proportion of ancient CC	Estimated Hf (ppm)	Proportion of Hf in ancient CC	Estimated ¹⁷⁶ Lu/ ¹⁷⁷ Hf
Mafic Crust	70%	2.1 ppm	51%	0.021
Felsic Crust	30%	4.7 ppm	49%	0.007

CC: continental crust

Mafic and felsic crustal proportions from Hawkesworth et al. (2021)

Estimated Hf ppm and ¹⁷⁶Lu/¹⁷⁷Hf of mafic Archean CC is from the average Hf and Lu content of mafic volcanic rocks in the Pilbara craton (Smithies et al., 2007)

Estimated Hf ppm and ¹⁷⁶Lu/¹⁷⁷Hf in felsic Archean continental crust is from the average Hf and Lu content of Archean grey gneisses (Moyen and Martin, 2012)

The ¹⁷⁶Lu/¹⁷⁷Hf ratios for ancient mafic, felsic and bulk continental crust determined here are very similar to the ratios used by other authors to represent mafic and felsic continental crust of any age (e.g., Kemp et al., 2015; Vervoort and Kemp, 2016). The Hf contents used to represent the mafic and felsic components of ancient continental crust are also similar to the Hf contents of mafic and felsic Archean continental crust estimated by Taylor and McLennan (1985), which are 2 and 4 ppm, respectively.

The conclusion of these mass balance considerations is that, even if ~70% of ancient continental crust was mafic, approximately one half the Hf in the continental crust would reside in the felsic component, and that felsic component would typically have low $^{176}\text{Lu}/^{177}\text{Hf}$ ratios, and would therefore evolve to very unradiogenic Hf isotope compositions (low ϵHf values) with time, as shown in Figure 2-3. Therefore, if large volumes of continental crust existed by ~3.6 Ga (Dhuime et al., 2012), then a significant fraction of igneous rocks emplaced from ~3.5 to 3.0 Ga are expected to have quite negative ϵHf_i values consistent with reworking of that voluminous pre-3.6 Ga continental crust. However, as shown on figure 2-3 of the main text, this is not what is observed in the global igneous zircon Hf isotope record. It is important to use the 3.5–3.0 Ga igneous rock record to evaluate the extent of pre-3.6 Ga continental crust because, if large volumes of pre-3.6 Ga continental crust did exist, then most of that continental crust has since been recycled to the mantle, and Dhuime et al. (2018) argue that recycling took place at a rapid pace between ~3.0 and 2.5 Ga.

B.7 Data tables

Table B-3. Whole-rock Sm-Nd isotope data.

Sample ID	Easting	Northing	UTM Zone	Rock type	Sm ppm	Nd ppm	$\frac{^{147}\text{Sm}}{^{144}\text{Nd}}$	$\frac{^{143}\text{Nd}}{^{144}\text{Nd}(0)}$	2SE	$\epsilon\text{Nd}(0)$	T_{DM} (Ga)
17-13B	576424	6877575	12	Foliated granite	12.46	98.98	0.076099	0.510480	0.000010	-41.9	2.95
18-002E	576031	6877567	12	Foliate granite	16.35	104.5	0.094631	0.510610	0.000008	-39.4	3.24
18BN01C	588018	6827539	12	Foliated granite	4.167	19.26	0.130815	0.511494	0.000008	-22.2	3.05
18BN113A	576215	6877586	12	Foliated granodiorite	2.156	13.99	0.093164	0.510914	0.000010	-33.5	2.83
18BN114A	569670	6879842	12	Foliated/gneissic diorite	12.72	65.87	0.116796	0.511327	0.000009	-25.4	2.87
18BN14B	590700	6827611	12	Lineated quartz-diorite	3.382	17.67	0.115708	0.511280	0.000011	-26.3	2.91
18BN20B	578638	6877062	12	Foliated monzodiorite	8.366	46.03	0.109901	0.511207	0.000009	-27.8	2.86
18BN20C	578608	6877076	12	Foliated granite	20.99	158.0	0.080343	0.510366	0.000007	-44.2	3.17
18BN31A	576567	6877070	12	Quartz-ribbon granite	3.019	21.08	0.086601	0.510836	0.000009	-35.0	2.77
18BN38B	589824	6875569	12	Foliated metagabbro	4.696	22.09	0.128560	0.511507	0.000007	-21.9	2.95
18BN56A	575831	6880633	12	Foliated diorite	6.675	33.31	0.121153	0.511408	0.000008	-23.8	2.87
18BN94A	566912	6800513	12	Gneissic quartz-monzodiorite	7.077	38.87	0.110081	0.511169	0.000009	-28.5	2.91
18EM28B	527411	6906278	12	Foliated quartz-monzodiorite	6.306	30.92	0.123322	0.511528	0.000008	-21.5	2.74
18EM31B	602152	6869953	12	Foliated granodiorite	6.726	47.27	0.086044	0.510744	0.000007	-36.8	2.87
18EM35B	634658	6852872	12	Foliated leucotrochjemitite	0.565	6.56	0.052069	0.510051	0.000012	-50.3	2.92
19BC52A	648869	6867703	12	Foliated quartz-monzodiorite	6.926	48.21	0.086871	0.510719	0.000007	-37.3	2.92
19BC53A	652294	6869486	12	mixed tonalitic gneiss	6.797	36.56	0.112402	0.511271	0.000009	-26.5	2.83
19BN01A	641790	6862129	12	Foliated/gneissic granodiorite	4.529	33.36	0.082081	0.510587	0.000007	-39.9	2.96
19BN07A	637640	6854834	12	Granite	1.980	13.94	0.085854	0.510691	0.000008	-37.8	2.93
19BN07B	637652	6854840	12	Foliated/gneissic granodiorite	4.959	32.86	0.091246	0.510752	0.000007	-36.6	2.98
19BN106B	596654	6863093	12	Foliated quartz-monzodiorite	6.286	42.01	0.090489	0.510858	0.000010	-34.6	2.83
19BN123A	562017	6836435	12	Foliated granite	2.722	21.44	0.076765	0.510722	0.000010	-37.2	2.70
19BN126B	563443	6835534	12	Foliated granodiorite	7.158	50.54	0.085632	0.510825	0.000010	-35.2	2.77
19BN128B	531109	6899873	12	Foliated monzodiorite	4.850	24.95	0.117565	0.511403	0.000008	-23.9	2.77
19BN150A	589293	6876240	12	Foliated leucogranite	6.901	50.66	0.082355	0.510760	0.000007	-36.5	2.77
19BN154A	589895	6875584	12	Foliated quartz-monzodiorite	8.136	60.15	0.081797	0.510749	0.000008	-36.7	2.77
19BN154C	589894	6875568	12	Foliated leucogranite	2.984	25.33	0.071241	0.510558	0.000008	-40.4	2.77
19BN166A	592089	6877082	12	Foliated/gneissic granodiorite	7.714	44.72	0.104303	0.511099	0.000010	-29.9	2.86
19BN168A	592218	6875600	12	Foliated granite	7.046	48.50	0.087848	0.510409	0.000007	-43.3	3.31
19BN173A	576422	6877692	12	Foliated quartz-monzodiorite	7.052	39.75	0.107276	0.511141	0.000006	-29.0	2.88
19BN18A	641417	6865897	12	Granite	2.515	14.46	0.105155	0.511074	0.000007	-30.4	2.92
19BN32A	634585	6852789	12	Foliated leucotrochjemitite	0.711	7.70	0.055801	0.510147	0.000012	-48.4	2.89
19BN38A	634468	6852910	12	Foliated tonalite	4.842	32.28	0.090682	0.510759	0.000007	-36.5	2.96
19BN42A	655984	6869180	12	Granodiorite sill	1.996	10.17	0.118694	0.511014	0.000014	-31.5	3.42
19BN43B	653821	6871804	12	Foliated granite	15.56	85.53	0.109967	0.510809	0.000009	-35.5	3.43
19BN51A	626451	6851686	12	Lineated granite	9.390	84.16	0.067459	0.510392	0.000007	-43.7	2.87
19BN53A	622613	6854520	12	Foliated/gneissic granodiorite	6.844	36.92	0.112094	0.511245	0.000011	-27.0	2.86
19BN61A	610276	6854509	12	Foliated granite	2.178	15.75	0.083630	0.510642	0.000012	-38.8	2.94
19BN45A	640309	6859894	12	Granodiorite	1.743	10.49	0.100413	0.510852	0.000012	-34.7	3.09

Samples labelled "16DRxxxx" and "QMxx" originally described in Regis et al. (2017a) and Tersmette (2012), respectively $\epsilon\text{Nd}(0)$ values calculated with the CHUR values of Bouvier et al. (2008).

T_{DM} calculated from the linear depleted mantle model of Goldstein et al. (1984).

Sample ID	Easting	Northing	UTM Zone	Rock type	Sm ppm	Nd ppm	¹⁴⁷ Sm/ ¹⁴⁴ Nd	¹⁴³ Nd/ ¹⁴⁴ Nd (0)	2SE	εNd(0)	T _{DM} (Ga)
19BN78A	623652	6851824	12	Granite	5.329	42.19	0.076378	0.510653	0.000016	-38.6	2.77
19BN79A	620700	6853131	12	Foliated quartz-monzodiorite	17.29	100.9	0.103586	0.511088	0.000007	-30.1	2.86
19BN88A	622311	6853061	12	Foliated quartz-monzodiorite	9.789	56.30	0.105133	0.511141	0.000006	-29.1	2.82
20BC04A	595506	6798477	12	Gneissic granitoid	3.896	24.38	0.096635	0.510940	0.000008	-33.0	2.88
20EM08A	632445	6824327	12	Gneissic quartz-monzodiorite	3.666	22.90	0.096780	0.510920	0.000011	-33.4	2.91
20EM09A	636220	6822683	12	Foliated/gneissic granitoid	4.407	22.49	0.118474	0.511278	0.000011	-26.4	3.00
20EM17F	657221	6766266	12	Quartz-ribbon granite	3.979	24.69	0.097454	0.510916	0.000011	-33.4	2.93
20EM18A	649824	6769623	12	Garnet-bearing tonalite	2.714	14.90	0.110138	0.511078	0.000012	-30.3	3.05
20EM22C	629842	6782581	12	Leucogranite	1.221	10.66	0.069204	0.510438	0.000013	-42.8	2.86
20EM57D	608315	6772172	12	Leucogranite	4.181	22.35	0.113128	0.511051	0.000012	-30.8	3.18
TX08-055	624354	6899250	12	Foliated granite	3.746	24.21	0.093567	0.510917	0.000010	-33.4	2.83
TX09-052	619578	6943169	12	Foliated/gneissic granite	1.388	7.94	0.105718	0.511072	0.000012	-30.4	2.93
21BN05H	607612	6854633	12	Foliated quartz-monzodiorite	3.165	14.76	0.129645	0.511191	0.000010	-28.1	3.55
19BN59A	607568	6854540	12	Foliated/gneissic tonalite	3.287	20.06	0.099052	0.510719	0.000006	-37.3	3.23
16BK374A	345204	6853739	13	Foliated granodiorite	5.614	33.98	0.099903	0.511007	0.000010	-31.7	2.87
16DR1000C	352541	6867975	13	Foliated tonalite	4.196	22.28	0.113852	0.511171	0.000007	-28.5	3.02
16DR1001C	367625	6860488	13	Foliated granodiorite	1.363	8.61	0.095669	0.510939	0.000007	-33.0	2.86
16DR1001F	367535	6860460	13	Foliated granite	4.301	29.08	0.089430	0.510819	0.000009	-35.3	2.86
19BC02A	345748	6871676	13	Foliated quartz-diorite	5.243	30.35	0.104444	0.511107	0.000007	-29.7	2.85
KIA12-14	459384	7019081	13	Mixed granitic gneiss	1.257	8.16	0.093156	0.510604	0.000012	-39.5	3.21
KIA12-76	450425	6988941	13	Foliated granite	8.565	43.50	0.119061	0.510892	0.000007	-33.9	3.63
QM1A	603141	7526087	13	Gneissic granitoid	1.943	13.58	0.086502	0.510457	0.000009	-42.4	3.22
QM5B	604346	7483471	13	Gneissic granitoid	10.13	59.20	0.103435	0.510664	0.000006	-38.4	3.43
QM6B	619583	7543641	13	Gneissic granitoid	10.67	54.89	0.117556	0.511449	0.000008	-23.0	2.70
TX08-036	369611	6929938	13	Foliated granite	12.04	80.06	0.090927	0.510542	0.000010	-40.7	3.23
TX08-038	379113	6929726	13	Foliated granite	8.157	43.38	0.113709	0.510820	0.000009	-35.3	3.54
TX08-070	360241	6895958	13	Foliated granite	14.00	102.6	0.082463	0.510795	0.000007	-35.8	2.73
TX08-072	349371	6895823	13	Quartz-ribbon granodiorite	0.565	4.85	0.070547	0.510418	0.000013	-43.2	2.91
TX09-002	378569	6979867	13	Gneissic granodiorite	11.06	58.56	0.114193	0.511291	0.000008	-26.1	2.85
TX08-027	387322	6949010	13	Gneissic tonalite	4.449	23.13	0.116314	0.511009	0.000009	-31.6	3.35
QM2C	610617	7526394	13	Gneissic tonalite	1.991	12.68	0.094959	0.510545	0.000005	-40.7	3.34
QM7C	624225	7521866	13	Foliated tonalite	4.640	27.82	0.100855	0.510635	0.000005	-38.9	3.39
QM13A	504832	7514573	14	Gneissic granodiorite	3.859	28.95	0.080581	0.510718	0.000009	-37.3	2.78
QM13F	504832	7514573	14	Gneissic granitoid	5.488	41.76	0.079456	0.510766	0.000007	-36.4	2.71
QM13G	504832	7514573	14	Lineated monzogranite	0.667	7.98	0.050503	0.510279	0.000012	-45.9	2.68
QM13H	504832	7514573	14	Lineated diorite	8.466	46.52	0.110037	0.511272	0.000010	-26.5	2.76
QM14A	483447	7519721	14	Gneissic granite	1.799	13.99	0.077754	0.510732	0.000009	-37.0	2.71
QM15A	465274	7522240	14	Gneissic granodiorite	5.141	32.76	0.094897	0.511060	0.000006	-30.6	2.68
QM16A	447206	7529605	14	Foliated granodiorite	2.580	19.53	0.079903	0.510546	0.000008	-40.6	2.96
QM8B	385512	7514675	14	Granite	15.26	88.96	0.103694	0.510924	0.000006	-33.3	3.08
QM10A	406585	7520532	14	Gneissic quartz-diorite	3.567	19.05	0.113229	0.510912	0.000006	-33.5	3.39
QM10B	406585	7520532	14	Gneissic tonalite	3.634	22.56	0.097409	0.510563	0.000007	-40.3	3.38
QM17C	430495	7527086	14	Gneissic granodiorite	3.110	20.27	0.092786	0.510548	0.000007	-40.6	3.27

Table B-4. Single-stream LA-MC-ICPMS zircon U-Pb isotope data.

Session	Spot ID	Screen	Class	In Age	206Pb cps	204 cps	206 204	Ratios						Dates (Ma)				Disc. %	
								207Pb 206Pb	2σ	207Pb 235U	2σ	206Pb 238U	2σ	ρ	207Pb 206Pb	2σ	206Pb 238U		2σ
April 20 2021	HBA-28.1		inhrt		294864	18	16002	0.2520	0.0018	20.92	0.62	0.602	0.017	0.968	3197	12	3039	69	5
April 20 2021	HBA-8.2		ign	x	349249	68	5165	0.2420	0.0018	19.83	0.55	0.595	0.016	0.964	3133	12	3008	64	4
April 20 2021	HBA-60.1		ign	x	289109	36	7951	0.2405	0.0020	19.50	0.53	0.588	0.015	0.951	3124	13	2982	61	5
April 20 2021	HBA-8.3		ign	x	541106	37	14589	0.2401	0.0017	19.80	0.61	0.598	0.018	0.972	3121	11	3023	72	3
April 20 2021	HBA-8.1		ign	x	785476	20	38917	0.2399	0.0018	20.25	0.61	0.612	0.018	0.969	3119	12	3080	71	1
April 20 2021	HBA-44.2		ign	x	540158	22	24934	0.2398	0.0017	19.97	0.59	0.604	0.017	0.970	3119	11	3047	69	2
April 20 2021	HBA-75.1		ign	x	991980	0		0.2388	0.0018	19.82	0.57	0.602	0.017	0.967	3112	12	3040	67	2
April 20 2021	HBA-60.2		ign	x	619446	43	14419	0.2387	0.0017	19.90	0.55	0.605	0.016	0.965	3112	11	3049	65	2
April 20 2021	HBA-28.2		ign	x	880519	28	31227	0.2385	0.0017	19.85	0.56	0.604	0.016	0.966	3110	12	3045	65	2
April 20 2021	HBA-26.1		ign	x	1009088	13	78054	0.2384	0.0017	20.50	0.65	0.624	0.019	0.974	3109	11	3126	76	-1
April 20 2021	HBA-77.1		ign	x	234575	10	24289	0.2383	0.0018	18.31	0.56	0.557	0.016	0.969	3109	12	2856	67	9
April 20 2021	HBA-44.3		ign	x	1151038	22	51392	0.2380	0.0017	20.17	0.58	0.615	0.017	0.968	3107	11	3090	68	1
April 20 2021	HBA-40.1		ign	x	516566	77	6712	0.2372	0.0017	18.66	0.55	0.571	0.016	0.969	3102	12	2911	67	7
April 20 2021	HBA-76.1		ign		1231228	0		0.2372	0.0018	20.06	0.59	0.614	0.017	0.968	3101	12	3084	69	1
April 20 2021	HBA-46.1		ign		388688	13	29200	0.2371	0.0017	19.41	0.58	0.594	0.017	0.970	3100	11	3006	69	3
April 20 2021	HBA-37.1		ign		1006249	10	104131	0.2345	0.0017	19.18	0.53	0.593	0.016	0.966	3083	12	3003	64	3
April 20 2021	HBA-44.1		ign		328132	20	16475	0.2274	0.0026	17.67	0.63	0.564	0.019	0.946	3034	18	2883	78	5
April 20 2021	HBA-78.1		ign		532492	43	12402	0.2262	0.0021	17.96	0.53	0.576	0.016	0.949	3025	15	2932	66	3
April 20 2021	HBA-74.1		ign		753193	13	56463	0.2107	0.0015	15.40	0.43	0.530	0.014	0.965	2911	12	2743	60	6
April 20 2021	HBA-46.2		met		179184	38	4667	0.1570	0.0012	9.09	0.26	0.420	0.012	0.962	2424	13	2260	53	7
April 20 2021	HBA-34.2		met		123748	46	2700	0.1562	0.0012	9.37	0.27	0.435	0.012	0.963	2415	13	2329	54	4
April 20 2021	HBA-34.1	mix	ign/met		418401	83	5012	0.1886	0.0046	12.66	0.64	0.487	0.022	0.879	2730	39	2558	94	7
April 20 2021	19BN59A-70-1		ign	x	318997	45	7151	0.2604	0.0020	23.06	0.78	0.643	0.021	0.975	3249	12	3199	83	2
April 20 2021	19BN59A-59-1		ign	x	475154	71	6708	0.2593	0.0019	22.41	0.61	0.627	0.016	0.965	3242	11	3138	65	3
April 20 2021	19BN59A-77-1		ign	x	286165	50	5729	0.2593	0.0020	22.75	0.73	0.637	0.020	0.971	3242	12	3176	77	2
Nov 16 2021	19BN59A-77-2		ign	x	375966	135	2787	0.2584	0.0019	23.30	0.65	0.654	0.018	0.964	3237	12	3245	68	0
April 20 2021	19BN59A-65-1		ign	x	335886	27	12625	0.2578	0.0020	22.12	0.59	0.622	0.016	0.958	3233	12	3120	63	4
Nov 16 2021	19BN59A-70-4		ign	x	438124	138	3172	0.2576	0.0019	23.15	0.65	0.652	0.018	0.965	3232	12	3236	68	0
Nov 16 2021	19BN59A-70-5		ign	x	403395	182	2222	0.2569	0.0019	23.07	0.63	0.652	0.017	0.962	3228	12	3235	66	0
April 20 2021	19BN59A-58-1		ign		568960	108	5247	0.2559	0.0019	22.93	0.70	0.650	0.019	0.970	3222	12	3230	75	0
Nov 16 2021	19BN59A-70-3		ign		413348	132	3120	0.2559	0.0019	22.62	0.60	0.641	0.016	0.962	3222	12	3195	64	1
Nov 16 2021	19BN59A-65-3		ign		818047	159	5151	0.2555	0.0019	22.65	0.60	0.643	0.016	0.962	3219	11	3201	64	1
Nov 16 2021	19BN59A-29-1		ign		491134	141	3480	0.2523	0.0019	21.83	0.58	0.628	0.016	0.959	3199	12	3142	63	2
Nov 16 2021	19BN59A-12-2		ign		252340	121	2091	0.2521	0.0019	21.36	0.59	0.615	0.016	0.962	3198	12	3088	64	4
Nov 16 2021	19BN59A-107-2		ign		617289	199	3110	0.2519	0.0020	21.47	0.57	0.619	0.016	0.956	3197	12	3104	62	3
April 20 2021	19BN59A-107-1		ign		990258	92	10768	0.2516	0.0018	22.26	0.63	0.642	0.018	0.968	3195	11	3196	69	0
Nov 16 2021	19BN59A-13-1		ign		264932	121	2193	0.2513	0.0019	21.92	0.67	0.633	0.019	0.970	3193	12	3162	73	1
April 20 2021	19BN59A-23-1		ign		344767	99	3469	0.2508	0.0020	21.02	0.83	0.608	0.024	0.980	3190	12	3062	94	4
Nov 16 2021	19BN59A-59-2		ign		694054	153	4532	0.2507	0.0018	21.62	0.59	0.626	0.016	0.963	3189	12	3132	65	2

Spots labelled as "Sample ID-grain#-spot#.

Screen: Analysis screened for high common-Pb content (cPb), mixed isotope ratio signals (mix) or discordance (disc).

Class: Analysis classified as igneous (ign) or metamorphic (met).

In Age: An "x" indicates analyses included in the weighted mean 207Pb/206Pb date calculation.

Disc.: Percent discordance calculated as [(207Pb/206Pb date/ 206Pb/238U date)-1]*100.

Session	Spot ID	Screen	Class	In Age	Ratios										Dates (Ma)				Disc.	%	
					206Pb	204	206	207Pb		207Pb		206Pb		206Pb		207Pb		206Pb			
					cps	cps	204	206Pb	2σ	235U	2σ	238U	2σ	ρ	206Pb	2σ	238U	2σ			
April 20 2021	19BN59A-33-1		ign		516625	55	9477	0.2506	0.0019	21.17	0.65	0.613	0.018	0.971	3189	12	3082	73	3		
April 20 2021	19BN59A-12-1		ign		228466	100	2294	0.2505	0.0019	20.93	0.65	0.606	0.018	0.971	3188	12	3055	73	4		
April 20 2021	19BN59A-35-1		ign		217656	92	2353	0.2500	0.0024	20.47	0.54	0.594	0.015	0.931	3185	15	3006	59	6		
April 20 2021	19BN59A-5-1		ign		414010	51	8082	0.2499	0.0034	21.20	0.60	0.616	0.015	0.882	3184	21	3093	61	3		
Nov 16 2021	19BN59A-65-2		ign		452361	162	2792	0.2489	0.0019	20.90	0.57	0.609	0.016	0.961	3178	12	3067	64	4		
Nov 16 2021	19BN59A-80-1		ign		367568	163	2249	0.2477	0.0019	21.28	0.59	0.623	0.017	0.961	3170	12	3123	66	1		
April 20 2021	19BN59A-109-1		ign		467117	37	12786	0.2465	0.0019	20.82	0.68	0.613	0.019	0.972	3162	12	3081	77	3		
April 20 2021	19BN59A-87-1		ign		581903	32	18310	0.2463	0.0019	20.53	0.54	0.605	0.015	0.959	3161	12	3049	61	4		
Nov 16 2021	19BN59A-23-2		ign		629120	186	3384	0.2448	0.0021	20.45	0.65	0.606	0.018	0.963	3152	13	3054	74	3		
Nov 16 2021	19BN59A-70-2		ign		387932	128	3033	0.2410	0.0018	19.55	0.52	0.588	0.015	0.961	3127	12	2983	61	5		
Nov 16 2021	19BN59A-75-1		ign		418890	144	2915	0.2375	0.0018	19.64	0.55	0.600	0.016	0.963	3103	12	3031	65	2		
Nov 16 2021	19BN59A-109-3		ign		446370	189	2367	0.2348	0.0018	19.28	0.58	0.596	0.017	0.968	3085	12	3013	70	2		
April 20 2021	19BN59A-40-1		ign		565618	105	5411	0.2318	0.0017	18.41	0.51	0.576	0.015	0.964	3064	12	2933	63	4		
Nov 16 2021	19BN59A-22-1		ign		1472831	170	8670	0.2305	0.0017	18.38	0.49	0.579	0.015	0.962	3055	12	2943	60	4		
Nov 16 2021	19BN59A-43-1		ign		568256	170	3345	0.2291	0.0017	17.32	0.47	0.548	0.014	0.963	3046	12	2819	60	8		
April 20 2021	19BN59A-40-2		ign		1046140	39	26513	0.2270	0.0020	17.61	0.47	0.563	0.014	0.945	3031	14	2878	58	5		
April 20 2021	19BN59A-6-1		ign		390253	120	3252	0.2188	0.0017	15.89	0.41	0.527	0.013	0.954	2972	12	2729	55	9		
April 20 2021	19BN59A-17-1		met		55596	107	518	0.1589	0.0015	9.27	0.23	0.423	0.010	0.930	2444	15	2275	44	7		
April 20 2021	19BN59A-58-2		met		55050	34	1628	0.1580	0.0013	9.32	0.25	0.428	0.011	0.946	2435	14	2297	48	6		
April 20 2021	19BN59A-6-2		met		50633	96	526	0.1560	0.0014	9.55	0.29	0.444	0.013	0.955	2413	15	2369	56	2		
April 20 2021	19BN59A-30-1		met		56336	37	1504	0.1559	0.0014	8.89	0.24	0.414	0.010	0.946	2411	15	2233	48	8		
April 20 2021	19BN59A-55-1		mix		35740	33	1087	0.1543	0.0021	9.97	0.57	0.469	0.026	0.971	2394	23	2479	113	-3		
April 20 2021	19BN59A-71-2		disc		42576	58	739	0.1623	0.0014	9.10	0.27	0.407	0.011	0.958	2479	14	2202	52	13		
April 20 2021	19BN59A-39-1		disc,mix		224784	78	2889	0.2546	0.0021	17.59	1.00	0.501	0.028	0.989	3214	13	2619	120	23		
April 20 2021	19BN59A-29-2		disc,mix		64778	86	756	0.1643	0.0024	8.21	0.54	0.363	0.023	0.975	2500	24	1995	108	25		
April 20 2021	19BN59A-33-2		disc		69990	99	710	0.1688	0.0019	7.99	0.21	0.343	0.008	0.900	2546	19	1903	39	34		
April 20 2021	19BN59A-71-1		disc		310277	119	2608	0.2314	0.0019	10.54	0.62	0.331	0.019	0.990	3062	13	1841	92	66		
Nov 16 2021	19BN59A-109-2		cPb		248851	130	1913	0.2497	0.0019	21.69	0.57	0.630	0.016	0.958	3183	12	3151	63	1		
April 21 2021	QM7C-11-1		ign	x	1379237	52	26295	0.2362	0.0017	20.60	0.58	0.633	0.017	0.966	3095	12	3160	67	-2		
April 21 2021	QM7C-64-1		ign	x	1432265	28	51096	0.2362	0.0018	21.01	0.70	0.645	0.021	0.975	3094	12	3210	82	-4		
April 21 2021	QM7C-49-1		ign	x	1235022	50	24943	0.2360	0.0017	20.59	0.64	0.633	0.019	0.972	3093	12	3162	75	-2		
April 21 2021	QM7C-14-1		ign	x	1170659	37	31625	0.2359	0.0017	20.37	0.56	0.626	0.017	0.964	3093	12	3135	66	-1		
April 21 2021	QM7C-34-1		ign	x	2346041	66	35732	0.2358	0.0017	20.83	0.61	0.641	0.018	0.969	3092	11	3193	71	-3		
April 21 2021	QM7C-93-1		ign	x	1869376	35	53151	0.2350	0.0017	20.34	0.60	0.628	0.018	0.970	3087	11	3142	71	-2		
April 21 2021	QM7C-75-1		ign	x	4909780	50	98071	0.2341	0.0017	20.29	0.54	0.629	0.016	0.962	3080	12	3145	63	-2		
April 21 2021	QM7C-79-1		ign	x	319824	42	7685	0.2336	0.0018	18.56	0.51	0.577	0.015	0.960	3077	12	2935	62	5		
April 21 2021	QM7C-62-1		ign		1240153	40	30636	0.2292	0.0017	19.38	0.57	0.614	0.018	0.969	3047	12	3085	70	-1		
April 21 2021	QM7C-105-1		ign		1543403	75	20626	0.2283	0.0019	18.75	0.57	0.596	0.018	0.963	3040	13	3014	71	1		
April 21 2021	QM7C-100-1		ign		1539903	37	41821	0.2273	0.0018	18.69	0.53	0.596	0.016	0.960	3033	13	3016	65	1		
April 21 2021	QM7C-30-1		ign		2053558	51	40552	0.2218	0.0016	18.12	0.49	0.593	0.016	0.963	2994	12	3002	63	0		
April 21 2021	QM7C-105-2		ign		1355288	28	48423	0.2206	0.0017	18.14	0.54	0.597	0.017	0.968	2985	12	3016	69	-1		
April 21 2021	QM7C-45-1		ign		1634883	31	52705	0.2198	0.0016	18.21	0.52	0.601	0.017	0.966	2979	12	3034	66	-2		
April 21 2021	QM7C-87-1		ign		1230505	34	35778	0.2152	0.0017	17.35	0.51	0.585	0.016	0.964	2945	13	2970	67	-1		
April 21 2021	QM7C-48-1		ign		1894024	40	47752	0.2029	0.0015	15.36	0.43	0.549	0.015	0.965	2850	12	2822	61	1		
April 21 2021	QM7C-63-1		disc		1669597	3757	444	0.2459	0.0054	17.40	0.88	0.513	0.023	0.902	3159	34	2672	99	18		
April 21 2021	QM10A-15-1		ign	x	336305	42	8016	0.2575	0.0019	22.92	0.66	0.646	0.018	0.965	3231	12	3213	70	1		
April 21 2021	QM10A-35-1		ign	x	268164	13	19890	0.2573	0.0019	22.82	0.64	0.644	0.018	0.964	3230	12	3204	68	1		
April 21 2021	QM10A-11-1		ign	x	163772	49	3351	0.2567	0.0020	21.85	0.59	0.618	0.016	0.958	3226	12	3101	63	4		

Session	Spot ID	Screen	Class	In Age	206Pb cps	204 cps	206 204	Ratios						Dates (Ma)				Disc. %	
								207Pb		207Pb		206Pb		207Pb		206Pb			
								206Pb	2σ	235U	2σ	238U	2σ	p	206Pb	2σ	238U		2σ
Nov 16 2021	QM10A-35-2		ign	x	409050	113	3605	0.2562	0.0019	22.05	0.60	0.625	0.016	0.962	3223	12	3128	65	3
Nov 16 2021	QM10A-15-2		ign	x	533852	153	3494	0.2560	0.0019	22.57	0.61	0.639	0.017	0.963	3222	12	3187	65	1
April 21 2021	QM10A-32-1		ign	x	298100	19	15635	0.2539	0.0020	21.16	0.60	0.605	0.017	0.962	3209	12	3048	66	5
Nov 16 2021	QM10A-16-1		ign		388391	160	2428	0.2534	0.0019	21.77	0.61	0.623	0.017	0.964	3206	12	3123	66	3
Nov 16 2021	QM10A-29-2		ign		283616	93	3059	0.2514	0.0019	21.21	0.60	0.612	0.017	0.966	3193	12	3079	67	4
April 21 2021	QM10A-56-1		ign		328258	26	12645	0.2510	0.0019	21.86	0.62	0.632	0.017	0.965	3191	12	3157	68	1
Nov 16 2021	QM10A-20-2		ign		253404	116	2183	0.2509	0.0019	21.30	0.60	0.616	0.017	0.963	3190	12	3094	66	3
April 21 2021	QM10A-20-1		ign		203171	15	13795	0.2500	0.0019	20.91	0.61	0.607	0.017	0.968	3185	12	3058	69	4
April 21 2021	QM10A-29-1		ign		329329	31	10520	0.2484	0.0020	20.78	0.64	0.607	0.018	0.965	3175	13	3058	72	4
April 21 2021	QM10A-1-1		ign		196739	42	4710	0.2476	0.0018	20.88	0.63	0.612	0.018	0.970	3169	12	3077	72	3
April 21 2021	QM10A-24-1		ign		163344	32	5166	0.2463	0.0018	20.17	0.59	0.594	0.017	0.968	3161	12	3006	68	5
April 21 2021	QM10A-21-1		ign		267037	38	6969	0.2459	0.0018	19.88	0.57	0.587	0.016	0.965	3159	12	2976	65	6
Nov 16 2021	QM10A-32-2		ign		372919	106	3530	0.2446	0.0018	20.11	0.54	0.597	0.016	0.963	3150	12	3016	63	4
Nov 16 2021	QM10A-56-2		ign		542922	138	3923	0.2433	0.0019	19.77	0.52	0.590	0.015	0.957	3142	12	2988	60	5
April 21 2021	QM10A-62-1		ign		425879	37	11544	0.2426	0.0018	19.80	0.55	0.592	0.016	0.965	3137	12	2998	64	5
Nov 16 2021	QM10A-11-2		ign		400059	166	2406	0.2416	0.0018	19.45	0.52	0.584	0.015	0.961	3131	12	2965	61	6
Nov 16 2021	QM10A-21-2		ign		356565	97	3668	0.2413	0.0018	19.16	0.53	0.576	0.015	0.963	3128	12	2934	63	7
April 21 2021	QM10A-5-1		ign		190749	35	5473	0.2376	0.0019	19.23	0.60	0.587	0.018	0.968	3104	13	2978	72	4
April 21 2021	QM10A-38-1		ign		391319	44	8821	0.2222	0.0018	16.84	0.50	0.550	0.016	0.960	2997	13	2825	64	6
April 21 2021	QM10A-62-2		met		26350	26	1005	0.1555	0.0018	9.11	0.28	0.425	0.012	0.927	2408	20	2284	55	5
April 21 2021	QM2C-98-2		ign	x	68779	40	1709	0.2581	0.0022	22.05	0.58	0.620	0.015	0.948	3235	13	3109	61	4
April 21 2021	QM2C-100-1		ign	x	140155	47	2953	0.2574	0.0020	22.33	0.59	0.630	0.016	0.958	3231	12	3148	63	3
April 21 2021	QM2C-59-1		ign	x	267972	35	7664	0.2573	0.0019	22.58	0.61	0.637	0.017	0.962	3230	12	3175	65	2
April 21 2021	QM2C-71-1		ign	x	670322	63	10567	0.2565	0.0019	23.16	0.68	0.655	0.018	0.966	3225	12	3249	71	-1
April 21 2021	QM2C-6-1		ign	x	112808	32	3493	0.2564	0.0020	20.86	0.63	0.590	0.017	0.965	3225	12	2991	69	8
April 21 2021	QM2C-8-1		ign	x	151181	40	3755	0.2560	0.0019	20.99	0.61	0.595	0.017	0.966	3222	12	3010	68	7
April 21 2021	QM2C-99-1		ign	x	717296	41	17376	0.2560	0.0019	22.88	0.69	0.649	0.019	0.970	3222	12	3223	74	0
April 21 2021	QM2C-7-1		ign	x	98264	27	3622	0.2535	0.0022	20.94	0.59	0.599	0.016	0.954	3207	13	3027	65	6
April 21 2021	QM2C-57-1		ign		1090380	61	17836	0.2514	0.0018	22.19	0.59	0.641	0.016	0.961	3193	11	3191	64	0
April 21 2021	QM2C-5-1		ign		508375	41	12330	0.2510	0.0019	22.04	0.70	0.637	0.020	0.972	3191	12	3178	77	0
April 21 2021	QM2C-12-1		ign		179540	37	4884	0.2457	0.0020	20.37	0.57	0.602	0.016	0.958	3158	13	3036	64	4
April 21 2021	QM2C-98-1		ign		181699	33	5438	0.2442	0.0019	19.28	0.50	0.573	0.014	0.953	3148	12	2920	58	8
April 21 2021	QM2C-39-1		met		852797	52	16362	0.1495	0.0011	9.38	0.25	0.455	0.012	0.962	2340	12	2419	51	-3
April 21 2021	QM2C-5-2		met		730171	89	8211	0.1495	0.0011	8.67	0.25	0.421	0.012	0.965	2340	13	2264	52	3
April 21 2021	QM2C-57-2		met		1485581	59	24983	0.1509	0.0011	9.46	0.25	0.455	0.011	0.959	2356	13	2416	51	-2
April 21 2021	QM2C-11-1		met		257645	42	6110	0.1583	0.0014	9.53	0.27	0.437	0.012	0.950	2438	15	2336	53	4
April 21 2021	QM2C-99-2	mix	ign/met		1150444	56	20374	0.1932	0.0020	14.33	0.39	0.538	0.014	0.925	2770	17	2776	56	0
April 21 2021	QM2C-35-1		met		2728443	51	53671	0.2066	0.0015	16.58	0.44	0.582	0.015	0.961	2879	12	2959	60	-3
April 21 2021	QM2C-71-2		met		384108	51	7505	0.2340	0.0019	19.67	0.56	0.610	0.017	0.959	3079	13	3070	67	0
April 21 2021	QM2C-13-2		met		245339	50	4891	0.2344	0.0018	19.47	0.54	0.603	0.016	0.961	3082	12	3041	64	1
April 21 2021	QM2C-13-1		met		612844	55	11196	0.2363	0.0020	19.42	0.49	0.596	0.014	0.943	3095	13	3015	57	3
April 21 2021	QM2C-49-1	mix	ign/met		1320593	52	25636	0.1522	0.0013	9.19	0.23	0.438	0.010	0.941	2370	14	2343	46	1
April 21 2021	QM17C-19-1		ign	x	782326	60	12985	0.2429	0.0018	21.12	0.60	0.631	0.017	0.966	3139	12	3153	68	0
April 21 2021	QM17C-57-1		ign	x	666215	97	6875	0.2414	0.0018	20.81	0.65	0.626	0.019	0.971	3129	12	3132	75	0
April 21 2021	QM17C-72-1		ign	x	714897	135	5306	0.2412	0.0018	21.21	0.60	0.638	0.017	0.966	3128	12	3181	68	-2
April 21 2021	QM17C-82-1		ign	x	1227647	51	24072	0.2408	0.0018	20.90	0.53	0.630	0.015	0.958	3125	12	3149	60	-1
April 21 2021	QM17C-29-1		ign	x	1798589	126	14316	0.2393	0.0018	21.20	0.56	0.643	0.016	0.959	3115	12	3199	63	-3
April 21 2021	QM17C-70-1		ign		841765	123	6858	0.2370	0.0018	20.42	0.62	0.625	0.018	0.968	3100	12	3131	72	-1
April 21 2021	QM17C-94-1		ign		1442138	83	17423	0.2363	0.0017	20.58	0.56	0.632	0.016	0.963	3095	12	3157	64	-2

Session	Spot ID	Screen	Class	In Age	Ratios									Dates (Ma)				Disc. %	
					206Pb	204	206	207Pb		207Pb		206Pb		207Pb		206Pb			
					cps	cps	204	206Pb	2σ	235U	2σ	238U	2σ	ρ	206Pb	2σ	238U		2σ
April 21 2021	QM17C-2-1		ign		1848787	48	38230	0.2329	0.0018	21.06	0.70	0.656	0.021	0.972	3072	13	3252	82	-6
April 21 2021	QM17C-76-2		ign		1751590	46	37736	0.2323	0.0019	19.60	0.50	0.612	0.015	0.948	3068	13	3079	59	0
April 21 2021	QM17C-87-1		ign		1959061	49	39903	0.2310	0.0025	19.43	0.51	0.610	0.015	0.910	3059	17	3071	58	0
April 21 2021	QM17C-14-1		ign		2899798	164	17733	0.2305	0.0017	19.59	0.58	0.616	0.018	0.969	3056	12	3096	70	-1
April 21 2021	QM17C-53-1		ign		939342	133	7078	0.2259	0.0017	19.16	0.46	0.616	0.014	0.952	3023	12	3092	56	-2
April 21 2021	QM17C-32-1		ign		2752585	212	13007	0.2155	0.0018	17.02	0.46	0.573	0.015	0.950	2947	14	2920	60	1
April 21 2021	QM17C-21-1		ign		381695	116	3296	0.2060	0.0027	15.29	0.57	0.539	0.019	0.936	2874	21	2778	78	3
April 21 2021	QM17C-38-1		ign		600891	50	11905	0.2032	0.0019	14.83	0.45	0.529	0.015	0.949	2852	15	2739	63	4
April 21 2021	QM17C-94-2		met		271324	37	7247	0.1204	0.0011	5.81	0.16	0.350	0.009	0.940	1962	17	1935	43	1
April 21 2021	QM17C-40-1		met		235000	145	1625	0.1526	0.0012	9.34	0.26	0.444	0.012	0.962	2376	13	2369	53	0
April 21 2021	QM17C-53-2		met		158227	129	1229	0.1534	0.0012	9.26	0.26	0.438	0.012	0.961	2384	13	2342	54	2
April 21 2021	MSB-1-3		inhrt		442015	26	17325	0.2760	0.0020	25.19	0.79	0.662	0.020	0.971	3340	12	3276	77	2
April 21 2021	MSB-1-1		inhrt		353743	24	14440	0.2739	0.0020	25.04	0.81	0.663	0.021	0.974	3328	11	3280	80	1
April 21 2021	MSB-27-1		inhrt		179602	26	6781	0.2433	0.0021	18.85	0.50	0.562	0.014	0.944	3142	14	2876	58	9
April 21 2021	MSB-52-1		inhrt		256526	71	3588	0.2389	0.0018	19.06	0.50	0.579	0.015	0.957	3112	12	2945	59	6
April 21 2021	MSB-100-1		inhrt		183519	34	5338	0.2388	0.0020	18.99	0.60	0.577	0.018	0.966	3112	13	2936	72	6
April 21 2021	MSB-26-1		inhrt		191420	20	9548	0.2388	0.0018	19.16	0.54	0.582	0.016	0.962	3112	12	2959	64	5
April 21 2021	MSB-90-1		inhrt		174601	27	6410	0.2385	0.0018	19.39	0.56	0.590	0.016	0.966	3110	12	2989	66	4
April 21 2021	MSB-94-1		inhrt		156990	20	7890	0.2364	0.0021	18.46	0.49	0.567	0.014	0.941	3096	14	2894	58	7
April 21 2021	MSB-4-1		inhrt		1325784	41	32337	0.2345	0.0017	20.77	0.60	0.643	0.018	0.967	3083	12	3200	71	-4
April 21 2021	MSB-84-1		inhrt		1988375	84	23772	0.2343	0.0017	19.92	0.54	0.617	0.016	0.962	3082	12	3097	64	0
April 21 2021	MSB-69-1		ign	x	190900	38	5032	0.2337	0.0018	17.93	0.52	0.557	0.016	0.966	3078	12	2852	64	8
April 21 2021	MSB-66-1		ign	x	134960	25	5388	0.2336	0.0018	18.11	0.53	0.562	0.016	0.964	3077	12	2877	65	7
April 21 2021	MSB-39-1		ign	x	230815	32	7235	0.2327	0.0017	18.49	0.56	0.576	0.017	0.969	3071	12	2934	69	5
April 21 2021	MSB-29-2		ign	x	1453451	41	35038	0.2325	0.0017	19.51	0.53	0.609	0.016	0.964	3069	12	3066	64	0
April 21 2021	MSB-26-2		ign	x	419013	44	9517	0.2325	0.0017	17.98	0.56	0.561	0.017	0.971	3069	12	2872	69	7
April 21 2021	MSB-4-2		ign	x	344895	30	11324	0.2324	0.0017	18.97	0.58	0.592	0.018	0.971	3069	12	2999	71	2
April 21 2021	MSB-17-1		ign	x	502307	35	14214	0.2316	0.0017	18.89	0.59	0.592	0.018	0.971	3063	12	2997	72	2
April 21 2021	MSB-16-1		ign		1024086	29	35474	0.2297	0.0017	20.10	0.59	0.635	0.018	0.967	3050	12	3170	71	-4
April 21 2021	MSB-68-1		ign		566270	11	50352	0.2296	0.0017	18.38	0.52	0.581	0.016	0.965	3049	12	2953	64	3
April 21 2021	MSB-1-2		ign		626486	35	17703	0.2293	0.0018	19.28	0.60	0.610	0.018	0.969	3047	12	3070	73	-1
April 21 2021	MSB-9-1		ign		168846	26	6549	0.2293	0.0018	17.99	0.56	0.569	0.017	0.968	3047	13	2905	71	5
April 21 2021	MSB-29-1		ign		783470	96	8194	0.2253	0.0017	18.02	0.50	0.581	0.015	0.962	3019	12	2951	62	2
April 21 2021	MSB-84-2	cPb	ign		224927	174	1294	0.2347	0.0033	18.13	0.58	0.560	0.016	0.900	3085	22	2868	66	8
April 21 2021	MSB-88-2	disc	ign		229368	60	3795	0.2346	0.0019	17.51	0.45	0.542	0.013	0.949	3084	13	2791	55	10
April 21 2021	MSB-52-2	disc	ign		286805	44	6504	0.2184	0.0018	15.61	0.40	0.519	0.012	0.948	2969	13	2694	53	10
April 21 2021	MSB-88-1	disc	inhrt		628508	46	13729	0.2140	0.0017	15.12	0.43	0.513	0.014	0.958	2936	13	2668	59	10
April 21 2021	MSB-28-1	mix	ign		717104	154	4649	0.2197	0.0028	15.86	0.44	0.524	0.013	0.889	2978	20	2716	54	10
Nov 16 2021	TX08027-137-1		ign	x	539084	10	52098	0.2564	0.0019	23.01	0.86	0.651	0.024	0.981	3225	11	3233	93	0
Nov 16 2021	TX08027-140-1		ign	x	626074	18	34396	0.2556	0.0019	21.98	0.69	0.624	0.019	0.972	3220	12	3126	75	3
Nov 16 2021	TX08027-102-1		ign	x	545386	42	12912	0.2556	0.0019	22.21	0.68	0.631	0.019	0.970	3220	12	3152	74	2
Nov 16 2021	TX08027-37-1		ign	x	435917	12	35923	0.2555	0.0019	22.96	0.73	0.652	0.020	0.973	3219	12	3237	78	-1
Nov 16 2021	TX08027-115-1		ign	x	868917	34	25627	0.2552	0.0019	21.94	0.70	0.624	0.019	0.974	3217	11	3126	77	3
Nov 16 2021	TX08027-65-1		ign	x	1610130	27	59783	0.2551	0.0018	23.01	0.69	0.655	0.019	0.971	3216	11	3246	74	-1
Nov 16 2021	TX08027-37-2		ign	x	363014	10	35469	0.2542	0.0019	21.39	0.65	0.611	0.018	0.971	3211	11	3072	72	5
Nov 16 2021	TX08027-52-1		ign	x	661479	50	13272	0.2538	0.0019	21.91	0.67	0.626	0.019	0.969	3209	12	3136	73	2
Nov 16 2021	TX08027-98-1		ign	x	712667	62	11423	0.2536	0.0019	21.59	0.62	0.618	0.017	0.967	3208	12	3101	69	3
Nov 16 2021	TX08027-105-1		ign	x	730710	43	16899	0.2536	0.0019	22.48	0.71	0.643	0.020	0.971	3207	12	3202	77	0
Nov 16 2021	TX08027-83-1		ign	x	392587	13	29409	0.2532	0.0018	21.12	0.65	0.605	0.018	0.972	3205	11	3051	72	5

Session	Spot ID	Screen	Class	In	Age	Ratios								Dates (Ma)				Disc.		
						206Pb	204	206	207Pb		207Pb		206Pb		207Pb		206Pb			
						cps	cps	204	206Pb	2σ	235U	2σ	238U	2σ	ρ	206Pb	2σ		238U	2σ
Nov 16 2021	TX08027-5-1		ign	x		609870	30	20115	0.2530	0.0019	22.59	0.73	0.648	0.021	0.974	3204	12	3220	80	-1
Nov 16 2021	TX08027-134-1		ign	x		1122496	25	44713	0.2528	0.0019	21.48	0.67	0.616	0.019	0.972	3203	12	3096	74	3
Nov 16 2021	TX08027-81-1		ign	x		849844	29	29611	0.2528	0.0018	21.38	0.67	0.614	0.019	0.973	3202	11	3085	74	4
Nov 16 2021	TX08027-51-1		ign			1393054	52	26853	0.2524	0.0019	22.66	0.70	0.651	0.019	0.970	3200	12	3234	76	-1
Nov 16 2021	TX08027-6-1		ign			824270	40	20746	0.2522	0.0019	22.78	0.71	0.655	0.020	0.969	3198	12	3249	76	-2
Nov 16 2021	TX08027-128-1		ign			637428	58	10915	0.2521	0.0019	22.37	0.76	0.644	0.021	0.976	3198	12	3205	83	0
Nov 16 2021	TX08027-55-1		ign			757070	45	16802	0.2515	0.0019	22.26	0.65	0.642	0.018	0.964	3195	12	3197	70	0
Nov 16 2021	TX08027-125-1		ign			444641	25	17772	0.2514	0.0018	21.18	0.63	0.611	0.018	0.969	3194	12	3075	70	4
Nov 16 2021	TX08027-32-1		ign			2092776	52	40011	0.2511	0.0018	22.10	0.70	0.639	0.020	0.974	3192	11	3183	78	0
Nov 16 2021	TX08027-90-1		ign			914373	24	37667	0.2491	0.0018	20.90	0.62	0.609	0.017	0.970	3179	11	3065	70	4
Nov 16 2021	TX08027-28-1		ign			697396	29	23720	0.2491	0.0019	21.74	0.65	0.633	0.018	0.966	3179	12	3162	71	1
Nov 16 2021	TX08027-17-1		ign			983143	51	19116	0.2470	0.0018	21.44	0.63	0.630	0.018	0.969	3166	11	3149	71	1
Nov 16 2021	TX08027-31-1		ign			1284907	41	31574	0.2454	0.0019	21.62	0.68	0.639	0.020	0.971	3155	12	3186	77	-1
Nov 16 2021	TX08027-29-1		ign			391519	51	7732	0.2439	0.0018	20.15	0.63	0.599	0.018	0.972	3146	12	3027	74	4
Nov 16 2021	TX08027-130-1		ign			938722	42	22525	0.2438	0.0020	21.26	0.61	0.633	0.017	0.957	3145	13	3161	68	0
Nov 16 2021	TX08027-109-1		ign			1306010	45	29061	0.2413	0.0018	20.32	0.60	0.611	0.017	0.968	3128	12	3074	70	2
Nov 16 2021	TX08027-8-1		ign			2017619	47	43146	0.2409	0.0020	21.24	0.66	0.640	0.019	0.966	3126	13	3189	75	-2
Nov 16 2021	TX08027-117-1		ign			1913722	48	39710	0.2393	0.0017	20.74	0.68	0.629	0.020	0.976	3116	11	3145	80	-1
Nov 16 2021	TX08027-116-1		ign			908926	47	19435	0.2348	0.0017	18.75	0.61	0.580	0.018	0.973	3085	12	2947	74	5
Nov 16 2021	TX08027-71-1		ign			1139308	26	43360	0.2182	0.0025	17.07	0.51	0.568	0.015	0.921	2968	19	2898	63	2
Nov 16 2021	TX08027-124-1		ign			2178015	379	5743	0.1954	0.0015	13.89	0.41	0.516	0.015	0.968	2788	12	2681	63	4
Nov 16 2021	TX08027-112-1		met?			384558	39	9803	0.1554	0.0012	9.25	0.28	0.432	0.013	0.968	2406	13	2314	56	4
Nov 16 2021	TX08027-88-2		met?			1053738	39	26753	0.1544	0.0011	9.10	0.26	0.428	0.012	0.965	2395	12	2296	52	4
Nov 16 2021	TX08027-88-1		met?			2200318	23	94784	0.1531	0.0011	9.40	0.27	0.446	0.013	0.967	2381	13	2376	56	0
Nov 17 2021	QM10B-57-1		inhrt			333638	37	8949	0.2718	0.0020	24.47	0.75	0.653	0.019	0.970	3316	12	3241	76	2
Nov 17 2021	QM10B-61-1		ign	x		1005371	48	20891	0.2533	0.0019	22.42	0.69	0.642	0.019	0.968	3206	12	3198	75	0
Nov 17 2021	QM10B-19-1		ign	x		1966954	36	54062	0.2531	0.0018	22.80	0.70	0.654	0.020	0.972	3205	11	3242	76	-1
Nov 17 2021	QM10B-68-1		ign	x		2878432	55	52740	0.2507	0.0018	22.68	0.67	0.656	0.019	0.968	3189	12	3252	72	-2
Nov 17 2021	QM10B-21-1		ign			1227751	131	9368	0.2504	0.0018	21.70	0.59	0.629	0.016	0.962	3187	12	3145	64	1
Nov 17 2021	QM10B-20-2		ign			611403	19	33001	0.2503	0.0019	22.74	0.72	0.659	0.020	0.971	3186	12	3264	78	-2
Nov 17 2021	QM10B-21-2		ign			1962940	37	53203	0.2483	0.0021	22.25	0.64	0.650	0.018	0.958	3174	13	3229	70	-2
Nov 17 2021	QM10B-38-2		ign			2362774	67	35118	0.2476	0.0018	22.08	0.66	0.647	0.019	0.969	3169	12	3217	73	-1
Nov 17 2021	QM10B-54-1		ign			965045	51	18766	0.2458	0.0019	21.00	0.60	0.620	0.017	0.965	3158	12	3109	68	2
Nov 17 2021	QM10B-37-1		ign			2771746	34	82046	0.2435	0.0019	21.59	0.61	0.643	0.017	0.961	3143	12	3202	68	-2
Nov 17 2021	QM10B-73-1		ign			2008590	62	32200	0.2429	0.0018	21.42	0.68	0.640	0.020	0.972	3139	12	3188	77	-2
Nov 17 2021	QM10B-19-2		ign			1262378	22	56474	0.2427	0.0018	20.38	0.60	0.609	0.017	0.969	3138	12	3067	69	2
Nov 17 2021	QM10B-20-1		ign			3669398	29	127524	0.2421	0.0018	21.45	0.60	0.643	0.017	0.963	3134	12	3200	68	-2
Nov 17 2021	QM10B-38-1		ign			1915728	73	26175	0.2413	0.0018	20.99	0.59	0.631	0.017	0.965	3129	12	3155	67	-1
Nov 17 2021	QM10B-33-2		ign			1389790	64	21794	0.2413	0.0018	20.98	0.61	0.631	0.018	0.968	3128	12	3153	70	-1
Nov 17 2021	QM10B-40-1		ign			2052361	28	74158	0.2404	0.0018	20.80	0.59	0.628	0.017	0.967	3123	12	3140	68	-1
Nov 17 2021	QM10B-37-2		ign			2872822	45	64181	0.2400	0.0019	20.66	0.59	0.625	0.017	0.962	3120	12	3129	67	0
Nov 17 2021	QM10B-12-1		ign			2215860	48	46017	0.2397	0.0018	20.75	0.60	0.628	0.018	0.967	3118	12	3142	70	-1
Nov 17 2021	QM10B-51-1		ign			2347984	28	83547	0.2396	0.0018	20.59	0.61	0.624	0.018	0.966	3117	12	3124	71	0
Nov 17 2021	QM10B-49-1		ign			3372591	38	88938	0.2368	0.0020	20.38	0.60	0.625	0.018	0.959	3099	13	3128	70	-1
Nov 17 2021	QM10B-30-1		ign			5261738	89	59431	0.2367	0.0017	19.97	0.60	0.612	0.018	0.969	3098	12	3078	70	1
Nov 17 2021	QM10B-1-1		ign			1596963	38	42204	0.2344	0.0022	20.00	0.57	0.619	0.017	0.942	3082	15	3107	66	-1
Nov 17 2021	QM10B-1-2		ign			1493044	25	60046	0.2333	0.0021	19.72	0.57	0.613	0.017	0.953	3075	14	3084	68	0
Nov 17 2021	QM10B-33-1		ign			3398014	55	61446	0.2326	0.0023	19.15	0.53	0.598	0.016	0.936	3070	16	3020	63	2
Nov 17 2021	QM10B-30-2		ign			4776662	108	44089	0.2318	0.0018	19.11	0.61	0.598	0.019	0.971	3065	12	3022	75	1
Nov 17 2021	QM10B-16-1		ign			2453139	96	25529	0.2310	0.0017	19.00	0.54	0.597	0.016	0.965	3059	12	3017	65	1

Session	Spot ID	Screen	Class	In Age	206Pb cps	204 cps	206 204	Ratios						Dates (Ma)				Disc. %					
								207Pb		207Pb		206Pb		207Pb		206Pb			p	207Pb 206Pb	2σ	206Pb 238U	2σ
								206Pb	2σ	235U	2σ	238U	2σ										
Nov 17 2021	QM10B-11-1		ign		2933932	211	13901	0.2244	0.0017	18.04	0.49	0.583	0.015	0.961	3012	12	2962	62	2				
Nov 17 2021	21BN05H-32-1		ign	x	961944	42	22859	0.2506	0.0023	22.33	0.62	0.647	0.017	0.943	3189	15	3215	66	-1				
Nov 17 2021	21BN05H-7-1		ign	x	475077	29	16176	0.2494	0.0022	21.92	0.67	0.638	0.019	0.958	3181	14	3180	74	0				
Nov 17 2021	21BN05H-10-1		ign		427248	29	14686	0.2448	0.0019	21.22	0.69	0.629	0.020	0.972	3152	12	3145	78	0				
Nov 17 2021	21BN05H-27-1		ign		503199	25	20389	0.2446	0.0019	20.82	0.58	0.618	0.016	0.959	3150	12	3101	65	2				
Nov 17 2021	21BN05H-55-1		ign		469193	55	8592	0.2445	0.0018	20.74	0.64	0.616	0.018	0.970	3149	12	3093	73	2				
Nov 17 2021	21BN05H-44-1		ign		1014167	43	23475	0.2398	0.0019	20.60	0.59	0.623	0.017	0.962	3119	12	3123	68	0				
Nov 17 2021	21BN05H-56-1		ign		923539	41	22482	0.2396	0.0018	20.23	0.63	0.613	0.019	0.970	3117	12	3080	74	1				
Nov 17 2021	21BN05H-54-1		ign		370987	26	14229	0.2389	0.0018	19.66	0.59	0.597	0.017	0.968	3113	12	3018	70	3				
Nov 17 2021	21BN05H-51-1		ign		525701	33	15891	0.2377	0.0018	20.59	0.62	0.629	0.018	0.970	3105	12	3144	73	-1				
Nov 17 2021	21BN05H-49-1		ign		636447	165	3852	0.2342	0.0017	19.45	0.54	0.602	0.016	0.964	3081	12	3040	65	1				
Nov 17 2021	21BN05H-35-1		ign		1474842	40	37186	0.2339	0.0019	19.92	0.54	0.618	0.016	0.955	3079	13	3102	64	-1				
Nov 17 2021	21BN05H-23-1		ign		618410	34	18282	0.2297	0.0019	18.43	0.54	0.582	0.016	0.962	3050	13	2958	67	3				
Nov 17 2021	21BN05H-64-1		ign		702383	47	15092	0.2285	0.0017	18.37	0.51	0.583	0.015	0.961	3042	12	2962	63	3				
Nov 17 2021	21BN05H-25-1		ign		314031	24	12922	0.2251	0.0017	17.77	0.52	0.573	0.016	0.966	3018	12	2918	66	3				
Nov 17 2021	21BN05H-3-1		ign		769329	33	23643	0.2245	0.0017	17.98	0.58	0.581	0.018	0.971	3013	12	2953	74	2				
Nov 17 2021	21BN05H-8-1		ign		1083836	26	40913	0.2222	0.0020	18.16	0.54	0.593	0.017	0.952	2996	15	3002	68	0				
Nov 17 2021	21BN05H-73-1		ign		767769	50	15458	0.2217	0.0018	17.41	0.50	0.570	0.016	0.958	2993	13	2906	63	3				
Nov 17 2021	21BN05H-33-1		ign		936978	48	19535	0.2188	0.0017	17.96	0.50	0.596	0.016	0.960	2972	13	3012	65	-1				
Nov 17 2021	21BN05H-34-1		ign		425316	87	4867	0.2151	0.0017	17.12	0.56	0.577	0.018	0.972	2944	12	2938	74	0				
Nov 17 2021	21BN05H-47-1		ign		345976	65	5360	0.2132	0.0016	15.92	0.44	0.542	0.014	0.962	2930	12	2791	60	5				
Nov 17 2021	21BN05H-39-1		ign		468970	41	11542	0.2053	0.0016	15.78	0.56	0.558	0.019	0.974	2869	13	2857	79	0				
Nov 17 2021	21BN05H-24-1	mix	ign		207552	31	6612	0.1895	0.0032	13.14	0.52	0.503	0.018	0.902	2738	28	2628	76	4				
Oct 24 2022	RF8649A-3-1		ign	x	209198	22	9694	0.2749	0.0022	24.91	0.79	0.657	0.020	0.968	3334	13	3257	78	2				
Oct 24 2022	RF8649A--21-2		ign	x	214131	21	10294	0.2733	0.0020	24.96	0.70	0.663	0.018	0.965	3325	12	3277	69	1				
Oct 24 2022	RF8649A--1-1		ign	x	236487	23	10338	0.2727	0.0021	24.85	0.74	0.661	0.019	0.966	3322	12	3272	74	2				
Oct 24 2022	RF8649A--39-1		ign	x	224014	20	11358	0.2725	0.0021	24.59	0.71	0.655	0.018	0.963	3321	12	3247	70	2				
Oct 24 2022	RF8649A-40-1		ign	x	188231	28	6670	0.2719	0.0020	24.16	0.73	0.645	0.019	0.969	3317	12	3208	74	3				
Oct 24 2022	RF8649A-27-1		ign	x	647382	29	22240	0.2718	0.0023	25.88	0.68	0.691	0.017	0.947	3317	13	3386	66	-2				
Oct 24 2022	RF8649A-20-1		ign	x	203216	39	5199	0.2717	0.0021	24.10	0.72	0.644	0.019	0.967	3316	12	3204	73	3				
Oct 24 2022	RF8649A-16-1		ign	x	98311	68	1449	0.2716	0.0023	24.35	0.73	0.650	0.019	0.958	3315	13	3230	72	3				
Oct 24 2022	RF8649A-35-1		ign	x	333681	38	8797	0.2716	0.0022	25.00	0.73	0.668	0.019	0.963	3315	12	3298	73	1				
Oct 24 2022	RF8649A-34-1		ign	x	196924	46	4312	0.2715	0.0023	24.62	0.80	0.658	0.021	0.965	3315	13	3259	80	2				
Oct 24 2022	RF8649A-2-1		ign	x	180335	13	13711	0.2711	0.0021	24.40	0.72	0.653	0.019	0.965	3312	12	3240	72	2				
Oct 24 2022	RF8649A-18-1		ign	x	200007	50	4017	0.2709	0.0021	24.27	0.71	0.650	0.018	0.964	3311	12	3228	71	3				
Oct 24 2022	RF8649A-19-1		ign	x	227126	40	5700	0.2709	0.0020	24.37	0.72	0.653	0.019	0.967	3311	12	3239	72	2				
Oct 24 2022	RF8649A-24-1		ign	x	183664	21	8746	0.2706	0.0020	25.04	0.74	0.671	0.019	0.967	3310	12	3311	73	0				
Oct 24 2022	RF8649A-26-1		ign	x	230661	13	18090	0.2701	0.0021	24.69	0.71	0.663	0.018	0.963	3307	12	3280	70	1				
Oct 24 2022	RF8649A-11-1		ign	x	227165	21	4405	0.2698	0.0020	23.94	0.72	0.644	0.019	0.968	3305	12	3204	73	3				
Oct 24 2022	RF8649A-6-1		ign	x	202990	34	6031	0.2697	0.0020	24.19	0.72	0.651	0.019	0.967	3305	12	3231	73	2				
Oct 24 2022	RF8649A-9-1		ign	x	603251	67	8955	0.2696	0.0020	25.18	0.69	0.678	0.018	0.962	3304	12	3336	69	-1				
Oct 24 2022	RF8649A-36-1		ign		221597	40	5608	0.2692	0.0021	23.99	0.74	0.647	0.019	0.969	3301	12	3215	75	3				
Oct 24 2022	RF8649A-33-1		ign		884789	60	14697	0.2692	0.0020	25.37	0.75	0.684	0.020	0.969	3301	11	3359	75	-2				
Oct 24 2022	RF8649A-28-1		ign		228238	32	7157	0.2690	0.0022	23.61	0.71	0.637	0.019	0.964	3300	13	3176	73	4				
Oct 24 2022	RF8649A-14-1		ign		202205	97	2085	0.2688	0.0022	24.13	0.72	0.651	0.019	0.963	3299	13	3234	73	2				
Oct 24 2022	RF8649A-31-1		ign		176352	24	7495	0.2680	0.0020	24.29	0.71	0.658	0.019	0.967	3294	12	3258	72	1				
Oct 24 2022	RF8649A-37-1		ign		229121	35	6612	0.2676	0.0020	24.19	0.71	0.656	0.019	0.967	3292	12	3251	72	1				
Oct 24 2022	RF8649A-21-3		ign		202771	19	10707	0.2671	0.0020	23.61	0.68	0.641	0.018	0.964	3289	12	3194	69	3				
Oct 24 2022	RF8649A-32-1		ign		256862	42	6183	0.2662	0.0020	23.43	0.68	0.639	0.018	0.965	3284	12	3183	70	3				

Session	Spot ID	Screen	Class	In Age	206Pb cps	204 cps	206 204	Ratios						Dates (Ma)				Disc. %	
								207Pb		207Pb		206Pb		207Pb		206Pb			
								206Pb	2σ	235U	2σ	238U	2σ	ρ	206Pb	2σ	238U		2σ
Oct 24 2022	RF8649A-18-2		ign		394156	37	10621	0.2661	0.0020	24.29	0.69	0.662	0.018	0.965	3283	12	3276	70	0
Oct 24 2022	RF8649A-15-1		ign		122289	86	1419	0.2658	0.0020	23.82	0.74	0.650	0.020	0.970	3282	12	3229	76	2
Oct 24 2022	RF8649A-30-1		ign		353598	20	17700	0.2657	0.0019	24.24	0.75	0.662	0.020	0.971	3281	11	3275	76	0
Oct 24 2022	RF8649A-10-1		ign		592788	44	13339	0.2646	0.0020	23.62	0.65	0.648	0.017	0.962	3274	12	3220	67	2
Oct 24 2022	RF8649A-35-2		ign		398526	55	7208	0.2640	0.0020	23.83	0.71	0.655	0.019	0.967	3271	12	3247	73	1
Oct 24 2022	RF8649A-25-1		ign		230611	21	11022	0.2635	0.0021	22.71	0.67	0.626	0.018	0.962	3268	13	3132	70	4
Oct 24 2022	RF8649A-13-1		ign		182881	65	2825	0.2633	0.0024	23.01	0.66	0.634	0.017	0.948	3267	14	3166	67	3
Oct 24 2022	RF8649A-4-1		ign		190982	35	5434	0.2630	0.0020	22.93	0.67	0.633	0.018	0.964	3265	12	3160	70	3
Oct 24 2022	RF8649A-22-1		ign		205913	15	13623	0.2625	0.0019	22.60	0.65	0.625	0.017	0.967	3262	12	3128	69	4
Oct 24 2022	RF8649A-29-1		ign		222613	36	6219	0.2617	0.0021	22.91	0.73	0.635	0.020	0.969	3257	12	3170	77	3
Oct 24 2022	RF8649A-23-1		ign		247068	22	11333	0.2587	0.0022	23.11	0.67	0.648	0.018	0.955	3239	14	3221	70	1
Oct 24 2022	RF8649A-41-1		ign		235516	31	7540	0.2506	0.0021	20.93	0.59	0.606	0.016	0.953	3188	13	3054	65	4
Oct 24 2022	RF8649A-8-1		ign		166080	57	2931	0.2497	0.0019	20.62	0.62	0.599	0.017	0.968	3183	12	3026	70	5
Oct 24 2022	RF8649A-17-1		ign		148967	40	3733	0.2488	0.0019	20.18	0.60	0.588	0.017	0.966	3177	12	2983	68	6
Oct 24 2022	RF8649A-5-1		ign		153472	26	5895	0.2414	0.0020	19.09	0.57	0.574	0.016	0.961	3129	13	2923	67	7
Oct 24 2022	RF8649A-6-2	mix	ign		179900	40	4455	0.2480	0.0024	20.38	0.69	0.596	0.019	0.958	3172	15	3015	77	5
Oct 24 2022	RF8649A-7-1	mix	ign		290411	29	10084	0.2442	0.0025	20.71	0.65	0.616	0.018	0.944	3147	16	3092	73	2
Oct 24 2022	RF8649A-11-2	mix	ign		297320	43	6924	0.2641	0.0028	23.07	0.65	0.634	0.016	0.925	3271	17	3165	64	3
Oct 24 2022	RF8649A-21-1	mix	ign		195901	39	5087	0.2567	0.0028	21.65	0.62	0.612	0.016	0.924	3227	17	3078	65	5
Oct 24 2022	RF8649A-38-1	mix	ign		240812	39	6179	0.2418	0.0029	19.41	0.58	0.583	0.016	0.915	3132	19	2959	64	6
Oct 24 2022	RF8649A-12-1	mix	ign		2140994	66	32319	0.2323	0.0018	20.24	0.58	0.632	0.018	0.961	3068	13	3158	69	-3

Table B-5. Single-stream LA-MC-ICPMS zircon Hf isotope data.

Session	Spot ID	Class	In WM	At 207Pb/206Pb Date				At Rock Age												
				¹⁷⁶ Lu/ ¹⁷⁷ Hf	2SE	¹⁷⁶ Yb/ ¹⁷⁷ Hf	2SE	¹⁷⁶ Hf/ ¹⁷⁷ Hf	2SE	¹⁷⁸ Hf/ ¹⁷⁷ Hf	2SE	Total Hf (V)	Date (Ma)	2σ	εHf(t)	2SE	Age (Ma)	2σ	εHf(i)	2SE
July 6 2022	TX08027-137-1	ign	x	0.00122	0.00026	0.0300	0.0068	0.280803	0.000056	1.467143	0.000082	8	3225	11	1.0	2.1	3212	6	0.7	2.1
July 6 2022	TX08027-140-1	ign	x	0.00103	0.00012	0.0240	0.0028	0.280787	0.000058	1.467195	0.000071	7	3220	12	0.7	2.1	3212	6	0.5	2.1
July 6 2022	TX08027-102-1	ign	x	0.001038	0.000084	0.0248	0.0021	0.280796	0.000056	1.467119	0.000066	8	3220	12	1.0	2.0	3212	6	0.8	2.0
July 6 2022	TX08027-37-1	ign	x	0.000911	0.000098	0.0213	0.0025	0.280820	0.000047	1.467141	0.000069	7	3219	12	2.1	1.7	3212	6	2.0	1.7
July 6 2022	TX08027-115-1	ign	x	0.000791	0.000068	0.0184	0.0016	0.280767	0.000043	1.467174	0.000059	8	3217	11	0.5	1.5	3212	6	0.3	1.5
July 6 2022	TX08027-65-1	ign	x	0.00133	0.00030	0.0304	0.0073	0.280829	0.000069	1.467232	0.000087	11	3216	11	1.5	2.5	3212	6	1.4	2.5
July 6 2022	TX08027-37-2	ign	x	0.00095	0.00011	0.0224	0.0029	0.280804	0.000049	1.467143	0.000071	8	3211	11	1.3	1.8	3212	6	1.3	1.8
July 6 2022	TX08027-52-1	ign	x	0.000622	0.000036	0.0142	0.00083	0.280747	0.000047	1.467165	0.000051	8	3209	12	-0.1	1.7	3212	6	0.0	1.7
July 6 2022	TX08027-52-2	ign	x	0.000669	0.000041	0.0155	0.00092	0.280775	0.000041	1.467189	0.000048	9	3209	12	0.8	1.5	3212	6	0.9	1.5
July 6 2022	TX08027-98-1	ign	x	0.001229	0.000051	0.0296	0.0014	0.280837	0.000041	1.467199	0.000046	8	3208	12	1.8	1.5	3212	6	1.9	1.5
July 6 2022	TX08027-105-1	ign	x	0.000954	0.000071	0.0216	0.0016	0.280787	0.000040	1.467128	0.000058	7	3207	12	0.6	1.4	3212	6	0.7	1.4
July 6 2022	TX08027-83-1	ign	x	0.000723	0.000054	0.0172	0.0013	0.280790	0.000051	1.467254	0.000086	8	3205	11	1.1	1.8	3212	6	1.3	1.8
July 6 2022	TX08027-5-1	ign	x	0.00066	0.00015	0.0150	0.0036	0.280786	0.000030	1.467141	0.000076	12	3204	12	1.1	1.1	3212	6	1.3	1.1
July 6 2022	TX08027-134-1	ign	x	0.001103	0.000050	0.0258	0.0012	0.280821	0.000056	1.467164	0.000069	6	3203	12	1.4	2.0	3212	6	1.6	2.0
July 6 2022	TX08027-81-1	ign	x	0.000840	0.000031	0.0192	0.00071	0.280790	0.000042	1.467172	0.000056	7	3202	11	0.8	1.5	3212	6	1.1	1.5
July 6 2022	TX08027-51-1	ign	x	0.00160	0.00019	0.0380	0.0049	0.280853	0.000066	1.467169	0.000051	7	3200	12	1.4	2.4	3212	6	1.6	2.4
July 6 2022	TX08027-6-1	ign	x	0.00090	0.00011	0.0229	0.0035	0.280818	0.000036	1.467181	0.000084	13	3198	12	1.6	1.3	3212	6	1.9	1.3
July 6 2022	TX08027-128-1	ign	x	0.000685	0.000047	0.0158	0.0013	0.280788	0.000038	1.467242	0.000064	8	3198	12	1.0	1.4	3212	6	1.3	1.4
July 6 2022	TX08027-55-1	ign	x	0.00082	0.00010	0.0193	0.0027	0.280804	0.000044	1.467203	0.000055	9	3195	12	1.2	1.6	3212	6	1.6	1.6
July 6 2022	TX08027-125-1	ign	x	0.0002567	0.0000044	0.005070	0.000085	0.280744	0.000032	1.467230	0.000048	9	3194	12	0.3	1.1	3212	6	0.7	1.1
July 6 2022	TX08027-32-1	ign	x	0.001384	0.000091	0.0320	0.0022	0.280826	0.000062	1.467195	0.000070	7	3192	11	0.7	2.2	3212	6	1.1	2.2
July 6 2022	TX08027-90-1	ign	x	0.000930	0.000043	0.0217	0.0010	0.280804	0.000062	1.467225	0.000069	9	3179	11	0.6	2.2	3212	6	1.4	2.2
July 6 2022	TX08027-28-1	ign	x	0.000345	0.000028	0.00716	0.00061	0.280731	0.000046	1.467274	0.000067	11	3179	12	-0.7	1.6	3212	6	0.0	1.6
July 6 2022	TX08027-31-1	ign	x	0.000531	0.000076	0.0130	0.0026	0.280817	0.000037	1.467170	0.000090	12	3155	12	1.4	1.3	3212	6	2.7	1.3
July 6 2022	TX08027-29-1	ign	x	0.00107	0.00010	0.0257	0.0024	0.280811	0.000057	1.467220	0.000058	8	3146	12	-0.2	2.0	3212	6	1.3	2.0
July 6 2022	TX08027-130-1	ign	x	0.00080	0.00011	0.0187	0.0029	0.280750	0.000042	1.467203	0.000060	10	3145	13	-1.8	1.5	3212	6	-0.3	1.5
July 6 2022	TX08027-109-1	ign	x	0.000464	0.000044	0.0098	0.0010	0.280784	0.000027	1.467213	0.000068	10	3128	12	-0.3	1.0	3212	6	1.7	1.0
July 6 2022	TX08027-8-1	ign	x	0.000257	0.000035	0.00538	0.00092	0.280791	0.000050	1.467256	0.000058	13	3126	13	0.3	1.8	3212	6	2.4	1.8
July 6 2022	TX08027-117-1	ign	x	0.000531	0.000033	0.01216	0.00075	0.280767	0.000044	1.467160	0.000057	10	3116	11	-1.3	1.6	3212	6	0.9	1.6
July 6 2022	TX08027-116-1	ign	x	0.000550	0.000021	0.01227	0.00060	0.280754	0.000050	1.467129	0.000056	10	3085	12	-2.6	1.8	3212	6	0.4	1.8
July 6 2022	TX08027-71-1	ign	x	0.000669	0.000042	0.0151	0.0010	0.280775	0.000031	1.467157	0.000051	7	2968	19	-4.8	1.1	3212	6	0.9	1.1
July 6 2022	TX08027-124-1	ign	x	0.00072	0.00014	0.0183	0.0040	0.280797	0.000048	1.467159	0.000079	10	2788	12	-8.2	1.7	3212	6	1.6	1.7

Spots labeled as sample ID-grain#-spot#. 207Pb/206Pb dates are from the closest U-Pb spot.

Class: Analyses classified as igneous (ign) or metamorphic (met).

In WM: An "x" indicates analyses included in the WM initial εHf calculation. Analysis TX08027-17-1 screened for 2SE >3 εHf units.

εHf values calculated using the CHUR values of Bouvier et al. (2008) and the ¹⁷⁶Lu decay constant of Söderlund et al. (2004).

Session	Spot ID	Class	In WM											At 207Pb/206Pb Date				At Rock Age			
				<u>176Lu</u>		<u>176Yb</u>		<u>176Hf</u>		<u>178Hf</u>		Total Hf (V)	Date (Ma)	2σ	εHf(t)	2SE	Age (Ma)	2σ	εHf(i)	2SE	
				177Hf	2SE	177Hf	2SE	177Hf	2SE	177Hf	2SE										
July 6 2022	TX08027-112-1	met		0.000671	0.000055	0.0150	0.0013	0.280924	0.000045	1.467219	0.000065	11	2406	13	-12.4	1.6	2406	13	-12.4	1.6	
July 6 2022	TX08027-88-2	met		0.000715	0.000052	0.0157	0.0012	0.280862	0.000057	1.467238	0.000050	11	2395	12	-14.9	2.0	2395.3	12	-14.9	2.0	
July 6 2022	TX08027-88-1	met		0.000682	0.000068	0.0151	0.0016	0.280887	0.000036	1.467232	0.000063	12	2381	13	-14.3	1.3	2380.5	13	-14.3	1.3	
July 6 2022	TX08027-17-1	ign		0.00153	0.00023	0.0378	0.0058	0.28088	0.00010	1.467225	0.000089	8	3166	11	1.7	3.6	3165.6	11	1.7	3.6	
Dec 20 2022	RF8649A-1-1	ign	x	0.000559	0.000039	0.0142	0.0011	0.280664	0.000025	1.467266	0.000056	19	3322	12	-0.2	0.9	3314	6	-0.4	0.9	
Dec 20 2022	RF8649A-2-1	ign	x	0.0002876	0.0000061	0.00691	0.00022	0.280687	0.000023	1.467201	0.000041	20	3312	12	1.0	0.8	3314	6	1.0	0.8	
Dec 20 2022	RF8649A-6-1	ign	x	0.0002641	0.0000060	0.0066	0.00015	0.280641	0.000022	1.467244	0.000044	22	3305	12	-0.8	0.8	3314	6	-0.6	0.8	
Dec 20 2022	RF8649A-8-1	ign	x	0.000291	0.000012	0.00726	0.00027	0.280668	0.000022	1.467219	0.000052	19	3183	12	-2.8	0.8	3314	6	0.3	0.8	
Dec 20 2022	RF8649A-9-1	ign	x	0.000331	0.000017	0.00813	0.00048	0.280678	0.000026	1.467237	0.000049	16	3304	12	0.3	0.9	3314	6	0.6	0.9	
Dec 20 2022	RF8649A-10-1	ign	x	0.000398	0.000039	0.0099	0.0012	0.280697	0.000024	1.467173	0.000041	18	3274	12	0.2	0.9	3314	6	1.1	0.9	
Dec 20 2022	RF8649A-11-1	ign	x	0.000270	0.000005	0.00671	0.00010	0.280682	0.000026	1.467231	0.000031	19	3305	12	0.6	0.9	3314	6	0.9	0.9	
Dec 20 2022	RF8649A-14-1	ign	x	0.000419	0.000034	0.01059	0.00096	0.280674	0.000028	1.467125	0.000029	18	3299	13	-0.1	1.0	3314	6	0.2	1.0	
Dec 20 2022	RF8649A-16-1	ign	x	0.000323	0.000025	0.00818	0.00065	0.280668	0.000025	1.46717	0.000044	18	3315	13	0.3	0.9	3314	6	0.2	0.9	
Dec 20 2022	RF8649A-18-1	ign	x	0.0002340	0.0000014	0.005174	0.000045	0.280699	0.000024	1.467205	0.000035	26	3311	12	1.5	0.9	3314	6	1.6	0.9	
Dec 20 2022	RF8649A-19-1	ign	x	0.000411	0.000020	0.0106	0.00056	0.280672	0.000027	1.467177	0.000044	18	3311	12	0.1	1.0	3314	6	0.2	1.0	
Dec 20 2022	RF8649A-20-1	ign	x	0.000309	0.000009	0.00772	0.00025	0.280688	0.000029	1.467172	0.000053	18	3316	12	1.0	1.0	3314	6	1.0	1.0	
Dec 20 2022	RF8649A-22-1	ign	x	0.000267	0.000015	0.00665	0.00042	0.280687	0.000020	1.467202	0.000036	19	3262	12	-0.2	0.7	3314	6	1.1	0.7	
Dec 20 2022	RF8649A-23-1	ign	x	0.000275	0.000015	0.00682	0.00033	0.280681	0.000022	1.467200	0.000053	23	3239	14	-0.9	0.8	3314	6	0.8	0.8	
Dec 20 2022	RF8649A-24-1	ign	x	0.000296	0.000014	0.00739	0.0003	0.280671	0.000021	1.46721	0.000039	17	3310	12	0.3	0.7	3314	6	0.4	0.7	
Dec 20 2022	RF8649A-25-1	ign	x	0.000373	0.000028	0.00938	0.00072	0.280687	0.000019	1.467164	0.000034	21	3268	13	-0.3	0.7	3314	6	0.8	0.7	
Dec 20 2022	RF8649A-26-1	ign	x	0.000285	0.000016	0.00676	0.00032	0.280683	0.000025	1.467209	0.000036	25	3307	12	0.7	0.9	3314	6	0.9	0.9	
Dec 20 2022	RF8649A-27-1	ign	x	0.000790	0.000150	0.0207	0.0042	0.280676	0.000037	1.467302	0.000072	22	3317	13	-0.5	1.4	3314	6	-0.5	1.4	
Dec 20 2022	RF8649A-28-1	ign	x	0.000282	0.000014	0.00704	0.00031	0.280689	0.000023	1.467239	0.000053	25	3300	13	0.8	0.8	3314	6	1.1	0.8	
Dec 20 2022	RF8649A-29-1	ign	x	0.0001941	0.0000049	0.00453	0.00010	0.280669	0.000021	1.467178	0.000037	21	3257	12	-0.8	0.7	3314	6	0.6	0.7	
Dec 20 2022	RF8649A-30-1	ign	x	0.0002400	0.0000042	0.00565	0.00012	0.280662	0.000020	1.467193	0.000032	22	3281	11	-0.6	0.7	3314	6	0.2	0.7	
Dec 20 2022	RF8649A-31-1	ign	x	0.0003146	0.0000073	0.00783	0.00019	0.280676	0.000015	1.467169	0.000052	22	3294	12	0.1	0.5	3314	6	0.6	0.5	
Dec 20 2022	RF8649A-32-1	ign	x	0.0003615	0.0000074	0.00908	0.00011	0.280715	0.000023	1.467192	0.000049	21	3284	12	1.1	0.8	3314	6	1.8	0.8	
Dec 20 2022	RF8649A-34-1	ign	x	0.000536	0.000038	0.0136	0.0010	0.280675	0.000029	1.467168	0.000044	17	3315	13	0.0	1.0	3314	6	0.0	1.0	
Dec 20 2022	RF8649A-35-1	ign	x	0.000304	0.000052	0.0073	0.0014	0.280655	0.000027	1.46725	0.000074	24	3315	12	-0.1	1.0	3314	6	-0.2	1.0	
Dec 20 2022	RF8649A-37-1	ign	x	0.000593	0.000028	0.01506	0.00077	0.280686	0.000026	1.467171	0.000041	17	3292	12	-0.2	0.9	3314	6	0.3	0.9	
Dec 20 2022	RF8649A-39-1	ign	x	0.000492	0.000028	0.01237	0.00077	0.280665	0.000042	1.467087	0.000048	22	3321	12	-0.1	1.5	3314	6	-0.2	1.5	
Dec 20 2022	RF8649A-40-1	ign	x	0.000307	0.000010	0.00766	0.00025	0.280669	0.000020	1.467127	0.000032	17	3317	12	0.4	0.7	3314	6	0.3	0.7	
Dec 20 2022	RF8649A-33-1	ign	x	0.000346	0.000017	0.00892	0.00049	0.280639	0.000036	1.467321	0.000086	18	3301	11	-1.1	1.3	3314	6	-0.8	1.3	

Table B-6. Split-stream LA-ICPMS zircon U-Pb isotope data. Acquired in the same ablation as the Hf isotope data in Table B-7.

Session	Spot ID	Screen	Class	In Age	206Pb cps	204Pb cps	fPbc %	Th U	Ratios						Dates (Ma)				Disc. %					
									207Pb		207Pb		206Pb		207Pb		206Pb			p	206Pb	206Pb	238U	206Pb
									206Pb	2σ	235U	2σ	238U	2σ	206Pb	2σ	238U	2σ						
June 25 2021	HBA-104-1		inhrt		4.06E+05	58	0.2	0.45	0.2686	0.0043	24.51	1.04	0.656	0.026	0.927	3298	25	3252	100	1				
June 25 2021	HBA-28-1		inhrt		6.86E+05	0	0.0	0.82	0.2529	0.0018	22.16	0.79	0.634	0.022	0.979	3203	11	3166	86	1				
June 25 2021	HBA-14-1		ign	x	2.05E+06	56	0.0	1.09	0.2424	0.0016	21.28	0.72	0.637	0.021	0.981	3136	11	3178	83	-1				
June 25 2021	HBA-4-1		ign	x	2.00E+06	1389	0.9	1.95	0.2423	0.0020	20.43	0.76	0.609	0.022	0.974	3135	13	3068	87	2				
June 25 2021	HBA-1-1		ign	x	1.88E+06	64	0.0	2.07	0.2414	0.0016	22.03	0.78	0.661	0.023	0.982	3129	11	3269	89	-4				
June 25 2021	HBA-21-1		ign	x	2.05E+06	134	0.1	0.93	0.2409	0.0022	21.49	0.81	0.644	0.023	0.971	3126	14	3205	91	-2				
June 25 2021	HBA-23-1		ign	x	1.46E+06	111	0.1	1.15	0.2409	0.0017	21.52	0.75	0.649	0.022	0.979	3126	11	3225	86	-3				
June 25 2021	HBA-18-1		ign	x	1.31E+06	157	0.2	1.08	0.2406	0.0023	20.43	0.74	0.612	0.021	0.965	3124	15	3077	85	2				
June 25 2021	HBA-40-1		ign	x	7.17E+05	224	0.4	0.93	0.2404	0.0018	21.36	0.74	0.641	0.022	0.977	3123	12	3191	85	-2				
June 25 2021	HBA-12-1		ign	x	9.35E+05	19	0.0	1.06	0.2404	0.0020	20.81	0.75	0.626	0.022	0.974	3123	13	3133	86	0				
June 25 2021	HBA-10-1		ign	x	5.89E+05	408	0.9	16.0	0.2404	0.0019	20.53	0.76	0.622	0.023	0.977	3123	13	3117	89	0				
June 25 2021	HBA-55-1		ign	x	9.70E+05	189	0.2	0.84	0.2403	0.0017	20.85	0.72	0.628	0.021	0.977	3122	12	3142	83	-1				
June 25 2021	HBA-20-1		ign	x	1.37E+06	137	0.1	1.38	0.2403	0.0017	20.19	0.70	0.610	0.021	0.978	3122	12	3071	83	2				
June 25 2021	HBA-26-1		ign	x	1.28E+06	81	0.1	1.32	0.2399	0.0020	20.92	0.80	0.632	0.024	0.976	3119	13	3157	92	-1				
June 25 2021	HBA-59-1		ign	x	1.36E+06	136	0.1	1.22	0.2391	0.0018	20.42	0.75	0.617	0.022	0.978	3114	12	3100	87	0				
June 25 2021	HBA-72-1		ign	x	1.80E+06	0	0.0	1.22	0.2390	0.0017	20.76	0.73	0.629	0.021	0.979	3113	11	3144	84	-1				
June 25 2021	HBA-30-1		ign	x	9.70E+05	22	0.0	1.13	0.2388	0.0017	21.59	0.78	0.654	0.023	0.980	3112	12	3243	90	-4				
June 25 2021	HBA-90-1		ign	x	1.12E+06	415	0.5	1.17	0.2388	0.0018	20.00	0.73	0.606	0.022	0.979	3112	12	3056	87	2				
June 25 2021	HBA-3-1		ign	x	1.06E+06	8	0.0	1.13	0.2387	0.0017	20.64	0.72	0.628	0.021	0.979	3111	11	3143	84	-1				
June 25 2021	HBA-2-1		ign		1.42E+06	221	0.2	1.20	0.2383	0.0017	20.30	0.75	0.620	0.023	0.982	3108	11	3108	89	0				
June 25 2021	HBA-31-1		ign		1.73E+06	1	0.0	1.02	0.2382	0.0016	21.00	0.72	0.639	0.021	0.980	3108	11	3184	84	-2				
June 25 2021	HBA-93-1		ign		1.52E+06	45	0.0	0.89	0.2381	0.0017	21.35	0.75	0.647	0.022	0.979	3107	11	3215	87	-3				
June 25 2021	HBA-76-1		ign		1.49E+06	99	0.1	0.63	0.2379	0.0017	22.25	0.79	0.674	0.023	0.980	3106	11	3322	89	-7				
June 25 2021	HBA-75-1		ign		8.77E+05	66	0.1	1.16	0.2379	0.0018	20.90	0.73	0.633	0.022	0.977	3106	12	3162	85	-2				
June 25 2021	HBA-77-1		ign		6.01E+05	150	0.3	1.16	0.2379	0.0022	20.64	0.75	0.626	0.022	0.966	3106	15	3133	86	-1				
June 25 2021	HBA-42-1		ign		1.50E+06	74	0.1	1.43	0.2372	0.0018	21.10	0.77	0.642	0.023	0.979	3101	12	3198	90	-3				
June 25 2021	HBA-101-1		ign		1.15E+06	25	0.0	1.22	0.2360	0.0016	20.95	0.76	0.641	0.023	0.982	3093	11	3191	89	-3				
June 25 2021	HBA-29-1		ign		1.10E+06	188	0.2	0.40	0.2356	0.0021	19.73	0.71	0.604	0.021	0.970	3090	14	3045	85	1				
June 25 2021	HBA-24-1		ign		1.81E+06	219	0.2	1.41	0.2350	0.0023	19.18	0.72	0.589	0.021	0.966	3086	15	2987	86	3				
June 25 2021	HBA-62-1		ign		1.72E+06	213	0.2	0.42	0.2347	0.0017	21.58	0.79	0.661	0.024	0.981	3084	11	3269	92	-6				
June 25 2021	HBA-58-1		ign		1.40E+06	15	0.0	1.01	0.2341	0.0016	20.66	0.71	0.637	0.021	0.980	3081	11	3177	84	-3				
June 25 2021	HBA-36-1		ign		9.43E+05	100	0.1	0.61	0.2330	0.0016	19.72	0.77	0.613	0.024	0.983	3073	11	3082	93	0				
June 25 2021	HBA-7-1		ign		6.26E+05	8	0.0	1.54	0.2326	0.0018	20.97	0.81	0.653	0.025	0.980	3070	12	3240	95	-5				
June 25 2021	HBA-98-1		ign		1.18E+06	34	0.0	1.01	0.2318	0.0017	20.03	0.70	0.626	0.021	0.978	3064	12	3132	84	-2				
June 25 2021	HBA-74-1		ign		1.74E+06	60	0.0	4.58	0.2310	0.0017	19.33	0.67	0.606	0.021	0.978	3059	12	3052	82	0				
June 25 2021	HBA-86-1		ign		8.92E+05	276	0.4	1.24	0.2296	0.0017	20.70	0.78	0.649	0.024	0.980	3049	12	3224	93	-5				
June 25 2021	HBA-37-1	mix	ign		7.36E+05	88	0.2	0.53	0.2208	0.0019	16.56	0.62	0.543	0.020	0.975	2987	14	2796	83	7				
June 25 2021	HBA-53-1	mix	ign		1.22E+06	80	0.1	0.96	0.2279	0.0019	18.91	0.80	0.594	0.025	0.981	3037	13	3006	99	1				
June 25 2021	HBA-70-1	mix	ign		6.79E+05	119	0.2	0.76	0.2084	0.0043	16.79	0.70	0.576	0.021	0.869	2893	34	2932	85	-1				

Spots labelled as "Sample ID-grain#-spot#".

Screen: Analysis screened for high common-Pb content (cPb), mixed isotope ratio signals (mix), discordance (disc) or εHf 2SE>3 (2SE>3)

Class: Analysis classified as igneous (ign), inherited (inhrt) or metamorphic (met).

In Age: An "x" indicates analyses included in the weighted mean 207Pb/206Pb date calculation.

Disc.: Percent discordance calculated as [(207Pb/206Pb date/ 206Pb/238U date)-1]*100.

fPbc: Fraction of 206Pb that is common, calculated using the 204Pb method and the Stacey and Kramers (1975) common Pb model.

Session	Spot ID	Screen	Class	Age	In	Ratios										Dates (Ma)				Disc.	
						206Pb	204Pb	fPbc	Th	207Pb		207Pb		206Pb		207Pb		206Pb			
						cps	cps	%	U	206Pb	2σ	235U	2σ	238U	2σ	ρ	206Pb	2σ	238U		2σ
June 25 2021	HBA-78-1	mix	ign			8.00E+05	318	0.5	0.58	0.2281	0.0020	19.70	0.71	0.623	0.022	0.971	3039	14	3120	86	-3
June 25 2021	HBA-94-1	mix	ign			9.95E+05	121	0.2	0.91	0.2226	0.0023	17.34	0.67	0.562	0.021	0.964	3000	17	2875	86	4
June 25 2021	HBA-103-1	2SE>3	ign			2.26E+06	915	0.5	1.61	0.2359	0.0017	21.75	0.90	0.664	0.027	0.984	3092	12	3283	104	-6
June 25 2021	HBA-80-1	cPb	ign			6.24E+05	550	1.1	0.86	0.2419	0.0020	19.44	0.77	0.582	0.023	0.979	3133	13	2957	92	6
June 25 2021	MSB-1-1		inhrt			6.56E+05	9	0.0	0.60	0.2680	0.0019	24.70	0.85	0.667	0.022	0.978	3294	11	3294	86	0
June 25 2021	MSB-92-1		inhrt			8.51E+05	283	0.4	0.61	0.2630	0.0019	24.92	0.89	0.687	0.024	0.980	3265	11	3373	91	-3
June 25 2021	MSB-76-1		inhrt			6.85E+05	281	0.5	0.80	0.2402	0.0020	21.54	0.78	0.650	0.023	0.975	3121	13	3229	89	-3
June 25 2021	MSB-61-1		inhrt			1.64E+06	576	0.4	1.20	0.2401	0.0018	19.95	0.73	0.601	0.022	0.980	3121	12	3032	86	3
June 25 2021	MSB-79-1		inhrt			2.38E+05	99	0.5	0.47	0.2394	0.0019	20.27	0.75	0.614	0.022	0.975	3116	13	3086	87	1
June 25 2021	MSB-26-1		inhrt			3.19E+05	46	0.2	0.92	0.2392	0.0018	20.49	0.71	0.621	0.021	0.977	3115	12	3114	83	0
June 25 2021	MSB-90-1		inhrt			3.46E+05	123	0.4	0.45	0.2377	0.0020	19.74	0.70	0.602	0.021	0.971	3105	13	3038	82	2
June 25 2021	MSB-27-1		inhrt			3.37E+05	41	0.2	0.53	0.2367	0.0018	20.00	0.72	0.609	0.021	0.977	3098	12	3067	85	1
June 25 2021	MSB-4-1		inhrt			2.30E+06	121	0.1	0.68	0.2362	0.0016	20.19	0.71	0.619	0.021	0.980	3094	11	3105	84	0
June 25 2021	MSB-2-1		inhrt			4.85E+05	111	0.3	0.52	0.2360	0.0019	19.86	0.71	0.611	0.021	0.974	3093	13	3074	85	1
June 25 2021	MSB-22-1		inhrt			9.52E+05	459	0.6	0.52	0.2357	0.0018	19.17	0.71	0.588	0.021	0.978	3091	12	2982	86	4
June 25 2021	MSB-39-1		ign	x		2.88E+05	89	0.4	0.38	0.2356	0.0023	19.52	0.69	0.602	0.021	0.962	3090	15	3036	82	2
June 25 2021	MSB-64-1		ign	x		9.00E+05	84	0.1	0.49	0.2356	0.0017	20.27	0.73	0.623	0.022	0.980	3090	11	3123	86	-1
June 25 2021	MSB-70-2		ign	x		2.61E+05	0	0.0	0.42	0.2344	0.0022	20.73	0.76	0.641	0.023	0.967	3082	15	3192	88	-3
June 25 2021	MSB-10-1		ign	x		8.05E+05	299	0.5	0.47	0.2337	0.0018	19.60	0.70	0.605	0.021	0.976	3078	12	3051	84	1
June 25 2021	MSB-36-1		ign	x		1.25E+06	0	0.0	0.49	0.2333	0.0017	20.80	0.74	0.647	0.023	0.979	3075	12	3218	88	-4
June 25 2021	MSB-103-1		ign	x		8.39E+05	525	0.8	0.39	0.2332	0.0020	19.57	0.68	0.610	0.021	0.970	3074	14	3069	82	0
June 25 2021	MSB-59-1		ign	x		4.24E+05	0	0.0	0.62	0.2330	0.0017	20.37	0.71	0.635	0.022	0.979	3073	11	3171	84	-3
June 25 2021	MSB-69-1		ign	x		2.29E+05	20	0.1	0.40	0.2329	0.0022	20.42	0.83	0.634	0.025	0.973	3072	15	3165	99	-3
June 25 2021	MSB-9-1		ign	x		4.25E+05	102	0.3	0.39	0.2328	0.0019	20.82	0.77	0.648	0.023	0.976	3071	13	3222	91	-5
June 25 2021	MSB-73-1		ign	x		7.10E+05	236	0.4	0.94	0.2328	0.0023	19.11	0.87	0.598	0.027	0.977	3071	16	3022	107	2
June 25 2021	MSB-17-1		ign	x		2.73E+05	41	0.2	0.45	0.2325	0.0034	19.85	0.82	0.616	0.024	0.933	3069	24	3094	93	-1
June 25 2021	MSB-66-1		ign	x		2.38E+05	12	0.1	1.30	0.2321	0.0017	19.20	0.66	0.600	0.020	0.976	3066	12	3029	81	1
June 25 2021	MSB-67-1		ign	x		9.30E+05	186	0.3	0.28	0.2319	0.0017	18.96	0.66	0.593	0.020	0.979	3065	11	3002	82	2
June 25 2021	MSB-5-1		ign	x		3.24E+05	0	0.0	0.44	0.2315	0.0020	19.11	0.69	0.592	0.021	0.970	3062	14	2996	84	2
June 25 2021	MSB-44-1		ign			9.90E+05	95	0.1	1.27	0.2312	0.0020	19.22	0.73	0.603	0.022	0.973	3060	14	3042	89	1
June 25 2021	MSB-3-1		ign			9.02E+05	436	0.6	0.16	0.2311	0.0019	19.86	0.69	0.624	0.021	0.971	3060	13	3125	83	-2
June 25 2021	MSB-37-2		ign			2.21E+05	61	0.4	0.93	0.2310	0.0033	18.54	0.73	0.582	0.022	0.935	3059	23	2957	87	3
June 25 2021	MSB-65-1		ign			3.99E+05	227	0.7	0.39	0.2310	0.0022	18.00	0.68	0.562	0.021	0.969	3059	15	2874	85	6
June 25 2021	MSB-92-2		ign			5.83E+05	123	0.3	0.40	0.2303	0.0020	17.33	0.62	0.544	0.019	0.969	3054	14	2799	79	9
June 25 2021	MSB-18-1		ign			2.12E+06	0	0.0	0.19	0.2283	0.0015	19.31	0.66	0.613	0.021	0.980	3040	11	3080	82	-1
June 25 2021	MSB-50-1		ign			5.62E+05	74	0.2	0.35	0.2273	0.0017	18.88	0.66	0.603	0.020	0.976	3033	12	3042	82	0
June 25 2021	MSB-70-1		inhrt			9.73E+05	18	0.0	0.40	0.2267	0.0016	19.59	0.68	0.626	0.021	0.979	3029	11	3133	83	-3
June 25 2021	MSB-16-1		ign			2.31E+06	53	0.0	0.35	0.2266	0.0016	18.28	0.65	0.583	0.020	0.979	3028	12	2959	83	2
June 25 2021	MSB-40-1		ign			5.00E+05	78	0.2	0.24	0.2262	0.0017	19.23	0.70	0.618	0.022	0.978	3025	12	3102	87	-2
June 25 2021	MSB-4-2		ign			3.93E+05	298	1.0	0.38	0.2243	0.0025	19.73	0.85	0.636	0.026	0.965	3012	18	3173	103	-5
June 25 2021	MSB-37-1		inhrt			9.53E+05	97	0.1	0.29	0.2239	0.0017	18.03	0.63	0.585	0.020	0.976	3009	12	2970	81	1
June 25 2021	MSB-1-2		ign			1.03E+06	84	0.1	0.16	0.2184	0.0016	16.45	0.57	0.546	0.019	0.979	2969	12	2806	77	6
June 25 2021	MSB-68-1		ign			1.16E+06	0	0.0	0.20	0.2151	0.0020	17.39	0.65	0.582	0.021	0.968	2944	15	2957	86	0
June 25 2021	MSB-47-1		met			1.32E+06	0	0.0	0.19	0.1528	0.0011	10.04	0.34	0.477	0.016	0.980	2377	12	2513	70	-5
June 25 2021	MSB-94-1	cPb	inhrt			4.71E+05	654	1.7	0.55	0.2438	0.0023	19.95	0.73	0.595	0.021	0.966	3145	15	3009	85	5
June 25 2021	MSB-22-2	cPb,disc,mix	ign			5.40E+05	1378	3.2	0.28	0.2420	0.0034	17.47	0.78	0.526	0.022	0.950	3133	22	2725	94	15
June 25 2021	MSB-36-2	cPb,mix	ign			5.91E+05	1366	2.9	0.29	0.2390	0.0111	18.60	1.26	0.552	0.027	0.726	3113	74	2833	111	10

Session	Spot ID	Screen	Class	Age	In	Ratios										Dates (Ma)				Disc.	
						206Pb	204Pb	fPbc	Th	207Pb		207Pb		206Pb		207Pb		206Pb			
						cps	cps	%	U	206Pb	2σ	235U	2σ	238U	2σ	ρ	206Pb	2σ	238U		2σ
June 25 2021	MSB-104-1	2SE>3	ign			6.18E+05	36	0.1	0.96	0.2366	0.0018	20.01	0.69	0.616	0.021	0.975	3097	12	3093	82	0
June 25 2021	MSB-26-2	cPb	ign			1.85E+05	241	1.7	0.47	0.2352	0.0022	18.14	0.75	0.561	0.023	0.974	3088	15	2871	93	8
June 25 2021	MSB-24-2	cPb	ign			2.41E+05	238	1.3	0.43	0.2333	0.0021	18.45	0.72	0.574	0.022	0.973	3075	14	2924	89	5
June 25 2021	MSB-80-1	mix	ign			1.20E+06	291	0.3	0.50	0.2315	0.0020	19.09	0.69	0.597	0.021	0.972	3062	14	3017	84	2
June 25 2021	MSB-100-1	mix	inhrt			3.90E+05	275	0.9	0.68	0.2304	0.0026	18.84	0.68	0.592	0.020	0.951	3055	18	2997	81	2
June 25 2021	MSB-29-1	mix	ign			1.20E+06	741	0.8	0.36	0.2262	0.0024	17.59	0.70	0.564	0.022	0.964	3025	17	2883	89	5
June 25 2021	MSB-89-1	cPb,mix	ign			1.33E+06	1172	1.1	0.22	0.2250	0.0020	17.34	0.76	0.555	0.024	0.979	3017	14	2846	97	6
June 25 2021	MSB-24-1	cPb,mix	ign			2.79E+05	488	2.3	0.36	0.2133	0.0033	14.09	0.68	0.475	0.022	0.947	2931	25	2505	94	17
June 25 2021	MSB-28-1	disc	ign			5.72E+05	198	0.5	0.61	0.2093	0.0027	14.01	0.55	0.491	0.018	0.942	2900	21	2575	78	13
June 25 2021	MSB-77-1	cPb,mix,2SE>3	ign			5.58E+05	958	2.3	0.21	0.2065	0.0059	14.90	1.11	0.516	0.035	0.922	2878	47	2682	149	7
July 7 2021	QM17C-61-1		ign	x		1.47E+06	947	0.8	0.57	0.2445	0.0020	21.87	0.80	0.649	0.023	0.976	3149	13	3224	90	-2
July 7 2021	QM17C-60-1		ign	x		4.17E+05	18	0.1	0.91	0.2442	0.0018	21.50	0.77	0.639	0.022	0.978	3148	12	3187	87	-1
June 25 2021	QM17C-19-1		ign	x		1.82E+06	187	0.1	0.30	0.2434	0.0019	20.94	0.77	0.624	0.022	0.977	3142	12	3125	89	1
June 25 2021	QM17C-8-1		ign	x		1.42E+06	106	0.1	0.68	0.2432	0.0018	23.06	1.03	0.685	0.030	0.987	3141	11	3364	114	-7
July 7 2021	QM17C-103-1		ign	x		2.32E+06	311	0.2	0.52	0.2428	0.0021	20.11	0.75	0.601	0.022	0.973	3138	14	3034	88	3
July 7 2021	QM17C-57-1		ign	x		1.41E+06	23	0.0	0.75	0.2418	0.0020	19.82	0.71	0.594	0.021	0.974	3132	13	3007	83	4
June 25 2021	QM17C-5-1		ign	x		2.13E+06	32	0.0	0.99	0.2414	0.0019	22.22	0.80	0.664	0.023	0.976	3129	12	3282	90	-5
July 7 2021	QM17C-38-1		ign			1.39E+06	0	0.0	0.23	0.2408	0.0017	21.43	0.76	0.643	0.022	0.979	3125	11	3199	87	-2
July 7 2021	QM17C-87-1		ign			2.00E+06	234	0.1	0.33	0.2408	0.0020	21.77	0.95	0.662	0.028	0.981	3125	13	3275	109	-5
July 7 2021	QM17C-41-1		ign			9.75E+05	217	0.3	0.26	0.2408	0.0020	23.18	0.86	0.695	0.025	0.976	3125	13	3402	94	-8
July 7 2021	QM17C-54-1		ign			3.39E+06	187	0.1	0.82	0.2404	0.0019	21.54	0.80	0.649	0.024	0.977	3123	13	3224	92	-3
June 25 2021	QM17C-22-1		ign			8.78E+05	0	0.0	0.34	0.2391	0.0031	20.60	0.91	0.616	0.026	0.955	3114	21	3094	102	1
June 25 2021	QM17C-21-1		ign			1.05E+06	248	0.3	0.32	0.2390	0.0019	21.22	0.74	0.644	0.022	0.972	3113	13	3203	85	-3
July 7 2021	QM17C-80-1		ign			3.91E+06	358	0.1	0.74	0.2384	0.0019	20.73	0.78	0.631	0.023	0.976	3109	13	3154	91	-1
July 7 2021	QM17C-84-1		ign			2.79E+06	300	0.1	0.91	0.2379	0.0024	19.07	0.75	0.582	0.022	0.968	3106	16	2957	90	5
June 25 2021	QM17C-23-1		ign			5.07E+06	1492	0.4	0.37	0.2377	0.0018	18.96	0.70	0.576	0.021	0.978	3105	12	2933	84	6
July 7 2021	QM17C-98-1		ign			2.32E+06	173	0.1	0.18	0.2374	0.0019	19.99	0.75	0.611	0.022	0.977	3103	13	3074	89	1
June 25 2021	QM17C-6-1		ign			4.86E+06	152	0.0	0.91	0.2371	0.0018	19.71	0.69	0.600	0.021	0.976	3101	12	3029	82	2
July 7 2021	QM17C-91-1		ign			2.26E+06	103	0.1	0.30	0.2361	0.0019	18.88	0.72	0.582	0.022	0.978	3094	13	2957	88	5
July 7 2021	QM17C-72-1		ign			1.39E+06	19	0.0	0.22	0.2360	0.0024	20.53	0.74	0.631	0.022	0.959	3093	16	3153	86	-2
July 7 2021	QM17C-47-1		ign			3.11E+06	382	0.2	0.48	0.2356	0.0019	20.21	0.79	0.620	0.024	0.979	3090	13	3110	94	-1
June 25 2021	QM17C-12-1		ign			2.13E+06	163	0.1	0.37	0.2356	0.0017	20.39	0.75	0.626	0.023	0.981	3090	11	3133	90	-1
July 7 2021	QM17C-95-1		ign			3.04E+06	138	0.1	0.56	0.2354	0.0027	18.90	0.78	0.585	0.023	0.960	3089	19	2969	94	4
July 7 2021	QM17C-50-1		ign			1.79E+06	53	0.0	0.53	0.2334	0.0020	21.42	0.89	0.663	0.027	0.979	3076	14	3279	104	-6
June 25 2021	QM17C-2-1		ign			2.04E+06	50	0.0	0.39	0.2333	0.0019	21.71	0.87	0.671	0.026	0.980	3075	13	3310	100	-7
July 7 2021	QM17C-53-1		ign			2.84E+06	130	0.1	0.42	0.2313	0.0017	19.81	0.70	0.621	0.022	0.977	3061	12	3113	85	-2
July 7 2021	QM17C-52-1		ign			1.43E+06	115	0.1	0.73	0.2289	0.0020	19.04	0.74	0.603	0.023	0.974	3044	14	3042	91	0
June 25 2021	QM17C-14-1	mix	ign			2.45E+06	308	0.2	0.81	0.2324	0.0023	19.45	0.74	0.605	0.022	0.965	3069	16	3050	89	1
June 25 2021	QM17C-24-1	mix	ign			2.18E+06	73	0.0	0.55	0.2341	0.0052	19.58	0.94	0.606	0.026	0.884	3080	36	3054	102	1
July 7 2021	QM17C-42-1	mix	ign			2.48E+06	93	0.0	0.51	0.2289	0.0025	18.65	0.78	0.589	0.024	0.966	3044	17	2985	96	2
July 7 2021	QM17C-44-1	mix	ign			1.04E+06	56	0.1	0.57	0.2009	0.0048	15.48	0.76	0.551	0.024	0.874	2834	39	2829	97	0
July 7 2021	QM17C-70-1	mix	ign			2.47E+06	232	0.1	0.52	0.2261	0.0029	18.48	0.71	0.594	0.021	0.943	3025	20	3004	86	1
July 7 2021	QM17C-79-1	mix	ign			2.43E+06	621	0.3	0.46	0.2257	0.0035	18.49	0.79	0.594	0.024	0.931	3022	25	3006	94	1
July 7 2021	QM17C-82-1	mix	ign			1.69E+06	63	0.0	0.59	0.2371	0.0034	19.51	0.80	0.599	0.023	0.939	3101	23	3026	93	2
July 7 2021	QM17C-105-1	mix	ign			2.30E+06	239	0.1	0.51	0.2326	0.0024	19.89	0.84	0.620	0.025	0.969	3070	17	3110	100	-1
June 25 2021	QM17C-9-1	mix	ign			3.73E+06	85	0.0	0.67	0.2097	0.0019	15.70	0.59	0.538	0.020	0.971	2903	14	2777	82	5
June 25 2021	QM17C-16-1	disc	ign			4.68E+06	39	0.0	0.60	0.2415	0.0018	16.64	0.71	0.501	0.021	0.985	3130	12	2618	90	20
July 7 2021	QM17C-78-1	disc	ign			3.42E+06	344	0.1	1.05	0.2376	0.0024	17.52	1.04	0.540	0.032	0.986	3104	16	2783	131	12
July 7 2021	QM17C-65-1	disc	ign			2.90E+06	190	0.1	0.36	0.2322	0.0020	16.40	0.63	0.516	0.019	0.975	3067	14	2682	81	14

Session	Spot ID	Screen	Class	In Age	206Pb cps	204Pb cps	fPbc %	Th U	Ratios						Dates (Ma)				Disc. %	
									207Pb		207Pb		206Pb		207Pb		206Pb			
									206Pb	2σ	235U	2σ	238U	2σ	ρ	206Pb	2σ	238U		2σ
July 7 2021	QM17C-62-1	disc	ign		2.62E+06	179	0.1	0.38	0.2027	0.0020	12.03	0.49	0.433	0.017	0.970	2848	16	2318	76	23
July 7 2021	19BN59A-35-1		ign	x	6.11E+05	232	0.5	0.60	0.2555	0.0021	22.71	0.82	0.640	0.022	0.974	3219	13	3190	88	1
July 7 2021	19BN59A-117-1		ign	x	7.93E+05	122	0.2	0.63	0.2546	0.0020	21.94	0.81	0.629	0.023	0.978	3214	12	3144	89	2
July 7 2021	19BN59A-14-1		ign	x	1.04E+06	204	0.2	0.39	0.2545	0.0019	22.56	0.86	0.639	0.024	0.980	3213	12	3185	93	1
July 7 2021	19BN59A-12-1		ign	x	5.05E+05	74	0.2	0.49	0.2542	0.0019	22.09	0.86	0.624	0.024	0.981	3211	12	3126	94	3
July 7 2021	19BN59A-70-1		ign	x	7.18E+05	65	0.1	0.53	0.2537	0.0020	21.85	0.82	0.629	0.023	0.977	3208	13	3146	91	2
July 7 2021	19BN59A-59-1		ign	x	7.43E+05	171	0.3	0.48	0.2530	0.0019	21.34	0.80	0.613	0.023	0.980	3203	12	3082	90	4
July 7 2021	19BN59A-3-1		ign	x	7.43E+05	43	0.1	0.61	0.2526	0.0018	22.75	0.81	0.655	0.023	0.979	3201	11	3248	88	-1
July 7 2021	19BN59A-37-1		ign	x	1.21E+06	334	0.3	0.51	0.2526	0.0021	22.48	0.86	0.644	0.024	0.976	3201	13	3205	93	0
July 7 2021	19BN59A-28-1		ign	x	6.22E+05	4	0.0	0.46	0.2522	0.0020	23.23	0.86	0.665	0.024	0.977	3199	13	3287	93	-3
July 7 2021	19BN59A-61-1		ign	x	6.99E+05	70	0.1	0.49	0.2517	0.0020	22.98	0.81	0.664	0.023	0.976	3195	12	3281	88	-3
July 7 2021	19BN59A-86-1		ign	x	9.81E+05	365	0.5	0.46	0.2510	0.0020	21.25	0.87	0.620	0.025	0.981	3191	13	3110	98	3
July 7 2021	19BN59A-109-1		ign		1.02E+06	411	0.5	0.58	0.2508	0.0019	20.16	0.83	0.592	0.024	0.982	3190	12	2998	97	6
July 7 2021	19BN59A-13-1		ign		6.75E+05	170	0.3	0.55	0.2507	0.0019	19.92	0.85	0.573	0.024	0.983	3189	12	2920	98	9
July 7 2021	19BN59A-36-1		ign		7.16E+05	70	0.1	0.47	0.2506	0.0019	22.79	0.82	0.652	0.023	0.978	3189	12	3236	89	-1
July 7 2021	19BN59A-7-1		ign		1.33E+06	168	0.2	0.38	0.2502	0.0017	21.96	0.79	0.637	0.022	0.981	3186	11	3178	88	0
July 7 2021	19BN59A-77-1		ign		5.94E+05	81	0.2	0.49	0.2498	0.0019	22.90	0.84	0.671	0.024	0.977	3183	12	3311	92	-4
July 7 2021	19BN59A-57-1		ign		1.08E+06	120	0.1	0.50	0.2498	0.0018	21.91	0.78	0.637	0.022	0.980	3183	11	3177	87	0
July 7 2021	19BN59A-89-1		ign		8.59E+05	276	0.4	0.57	0.2493	0.0023	20.98	0.75	0.615	0.021	0.967	3180	14	3090	84	3
July 7 2021	19BN59A-110-1		ign		7.92E+05	56	0.1	0.35	0.2468	0.0021	21.05	0.75	0.621	0.022	0.971	3164	14	3113	85	2
July 7 2021	19BN59A-103-1		ign		7.74E+05	206	0.3	0.43	0.2467	0.0018	20.49	0.73	0.608	0.021	0.978	3164	12	3061	85	3
July 7 2021	19BN59A-52-1		ign		6.32E+05	64	0.1	0.42	0.2432	0.0024	20.97	0.80	0.621	0.023	0.966	3141	16	3114	90	1
July 7 2021	19BN59A-83-1		ign		3.92E+05	17	0.1	0.48	0.2424	0.0020	20.90	0.74	0.632	0.022	0.974	3136	13	3157	86	-1
July 7 2021	19BN59A-76-1		ign		4.56E+05	44	0.1	0.36	0.2422	0.0023	20.40	0.75	0.621	0.022	0.966	3134	15	3113	88	1
July 7 2021	19BN59A-73-1		ign		5.05E+05	130	0.3	0.38	0.2408	0.0021	19.94	0.76	0.605	0.022	0.974	3125	14	3050	89	2
July 7 2021	19BN59A-21-1		ign		5.68E+05	128	0.3	0.50	0.2374	0.0019	19.46	0.69	0.590	0.021	0.975	3103	13	2988	83	4
July 7 2021	19BN59A-80-1		ign		7.55E+05	179	0.3	0.51	0.2341	0.0019	18.18	0.65	0.568	0.020	0.975	3080	13	2900	81	6
July 7 2021	19BN59A-51-1		ign		1.03E+06	71	0.1	0.48	0.2330	0.0022	18.03	0.64	0.560	0.019	0.965	3073	15	2865	79	7
July 7 2021	19BN59A-23-1		ign		8.92E+05	97	0.1	0.67	0.2321	0.0020	17.87	0.63	0.554	0.019	0.970	3067	14	2841	78	8
July 7 2021	19BN59A-75-1		ign		3.09E+05	59	0.2	0.36	0.2261	0.0021	17.78	0.66	0.576	0.021	0.968	3025	15	2934	84	3
July 7 2021	19BN59A-104-1		ign		1.50E+06	45	0.0	0.36	0.2253	0.0018	18.39	0.66	0.595	0.021	0.976	3019	12	3011	84	0
July 7 2021	19BN59A-5-1	disc,mix	ign		1.05E+06	501	0.6	0.45	0.2500	0.0031	16.92	0.83	0.495	0.024	0.967	3185	20	2592	101	23
July 7 2021	19BN59A-32-1	mix	ign		6.36E+05	43	0.1	0.46	0.2372	0.0026	20.00	0.73	0.607	0.021	0.954	3101	17	3056	84	1
July 7 2021	19BN59A-39-1	disc,mix	ign		7.11E+05	651	1.1	0.44	0.2466	0.0038	12.40	1.19	0.370	0.035	0.987	3163	25	2029	163	56
July 7 2021	19BN59A-42-1	mix	ign		4.58E+05	376	1.0	0.49	0.2310	0.0033	20.60	2.15	0.633	0.065	0.991	3059	23	3161	253	-3
July 7 2021	19BN59A-44-1	mix	ign		5.89E+05	2037	4.2	0.73	0.2665	0.0100	24.10	1.38	0.659	0.028	0.751	3286	59	3263	109	1
July 7 2021	19BN59A-55-1	mix	met		1.73E+05	94	0.7	2.82	0.1847	0.0038	12.52	0.65	0.490	0.023	0.919	2696	34	2571	101	5
July 7 2021	19BN59A-69-1	disc,mix	ign		1.02E+06	4015	4.9	0.59	0.2480	0.0151	17.70	1.57	0.519	0.034	0.730	3172	96	2695	141	18
July 7 2021	19BN59A-98-1	mix	ign		6.26E+05	131	0.3	0.39	0.1974	0.0027	13.27	0.51	0.492	0.018	0.935	2805	22	2579	77	9
July 7 2021	19BN59A-101-1	disc,mix	ign		4.26E+05	227	0.7	0.44	0.2283	0.0040	16.38	0.83	0.523	0.025	0.939	3040	28	2712	105	12
July 7 2021	19BN59A-71-1	disc,mix	ign		6.19E+05	891	1.8	0.57	0.2432	0.0019	17.85	0.97	0.539	0.029	0.990	3141	12	2779	121	13
July 7 2021	19BN59A-43-1	disc	ign		7.25E+05	265	0.5	0.30	0.2389	0.0019	18.14	0.64	0.549	0.019	0.973	3113	13	2822	79	10
July 7 2021	19BN59A-116-1	disc	ign		9.71E+05	169	0.2	0.46	0.2374	0.0018	16.87	0.66	0.520	0.020	0.981	3103	12	2699	84	15
July 7 2021	19BN59A-88-1	disc	ign		9.17E+05	125	0.2	0.46	0.2516	0.0020	19.10	0.90	0.555	0.026	0.985	3195	13	2846	106	12
July 7 2021	19BN59A-24-1	disc	ign		4.96E+05	105	0.3	0.48	0.2530	0.0023	20.02	0.93	0.571	0.026	0.980	3204	15	2912	106	10
July 7 2021	19BN59A-34-1	disc	ign		1.00E+06	250	0.3	0.31	0.2126	0.0020	15.23	0.58	0.511	0.019	0.968	2925	15	2660	79	10
July 7 2021	19BN59A-22-1	disc	ign		1.70E+06	606	0.5	0.45	0.2099	0.0018	14.48	0.53	0.497	0.018	0.972	2905	14	2602	76	12
July 7 2021	19BN59A-50-1	2SE>3	ign		6.73E+05	389	0.7	0.53	0.2558	0.0020	23.49	0.84	0.666	0.023	0.977	3221	12	3289	90	-2
July 7 2021	19BN59A-65-1	2SE>3	ign		2.83E+05	194	0.9	0.49	0.2510	0.0024	21.65	0.80	0.633	0.023	0.966	3191	15	3162	89	1

Session	Spot ID	Screen	Class	In Age	206Pb cps	204Pb cps	fPbc %	Th U	Ratios					Dates (Ma)				Disc.		
									207Pb		206Pb		207Pb	206Pb		207Pb	206Pb			
									206Pb	2σ	235U	2σ	238U	2σ	ρ	206Pb	2σ		238U	2σ
July 7 2021	QM10A-32-1		ign	x	4.61E+05	20	0.1	0.70	0.2542	0.0022	23.55	0.91	0.668	0.025	0.974	3211	14	3298	96	-3
July 7 2021	QM10A-47-1		ign	x	5.48E+05	34	0.1	1.33	0.2539	0.0020	22.70	0.80	0.646	0.022	0.974	3209	13	3212	86	0
July 7 2021	QM10A-35-1		ign	x	5.84E+05	68	0.1	1.19	0.2537	0.0026	23.05	0.84	0.655	0.023	0.961	3208	16	3249	89	-1
July 7 2021	QM10A-10-1		ign	x	4.96E+05	21	0.1	1.32	0.2535	0.0020	24.45	1.00	0.698	0.028	0.981	3207	13	3413	106	-6
July 7 2021	QM10A-29-1		ign	x	5.07E+05	0	0.0	0.28	0.2522	0.0020	22.15	0.81	0.633	0.023	0.977	3199	12	3161	89	1
July 7 2021	QM10A-20-1		ign	x	5.32E+05	0	0.0	1.15	0.2515	0.0022	22.32	0.96	0.642	0.027	0.979	3194	14	3197	106	0
July 7 2021	QM10A-15-1		ign	x	7.85E+05	47	0.1	1.56	0.2507	0.0023	22.45	0.84	0.648	0.023	0.970	3189	14	3220	91	-1
July 7 2021	QM10A-16-1		ign		5.47E+05	0	0.0	0.25	0.2501	0.0021	21.51	0.76	0.621	0.021	0.973	3185	13	3114	85	2
July 7 2021	QM10A-2-1		ign		5.07E+05	10	0.0	1.29	0.2498	0.0020	20.21	0.99	0.594	0.029	0.987	3183	13	3006	115	6
July 7 2021	QM10A-58-1		ign		4.77E+05	0	0.0	1.25	0.2493	0.0018	22.38	0.78	0.651	0.022	0.978	3180	12	3233	86	-2
July 7 2021	QM10A-39-1		ign		1.00E+06	20	0.0	0.39	0.2488	0.0020	22.17	0.83	0.644	0.023	0.977	3177	13	3205	91	-1
July 7 2021	QM10A-4-1		ign		3.78E+05	0	0.0	0.68	0.2473	0.0018	21.33	0.74	0.628	0.021	0.977	3167	12	3143	83	1
July 7 2021	QM10A-34-1		ign		6.93E+05	0	0.0	1.45	0.2459	0.0019	21.54	0.76	0.633	0.022	0.975	3159	12	3159	86	0
July 7 2021	QM10A-11-1		ign		3.47E+05	0	0.0	0.54	0.2435	0.0023	20.42	0.77	0.607	0.022	0.968	3143	15	3058	88	3
July 7 2021	QM10A-21-1		ign		6.28E+05	6	0.0	1.18	0.2433	0.0022	20.24	0.76	0.600	0.022	0.970	3142	15	3030	88	4
July 7 2021	QM10A-18-1		ign		4.81E+05	0	0.0	0.70	0.2408	0.0023	20.87	0.79	0.625	0.023	0.968	3125	15	3130	90	0
July 7 2021	QM10A-56-1		ign		5.96E+05	45	0.1	1.07	0.2406	0.0022	20.29	0.73	0.610	0.021	0.966	3124	15	3071	84	2
July 7 2021	QM10A-6-1		ign		6.18E+05	0	0.0	0.99	0.2405	0.0020	20.57	0.73	0.619	0.022	0.974	3123	13	3106	85	1
July 7 2021	QM10A-45-1		ign		4.27E+05	8	0.0	1.56	0.2398	0.0018	20.06	0.69	0.607	0.020	0.975	3118	12	3059	81	2
July 7 2021	QM10A-5-1		ign		7.47E+05	0	0.0	0.98	0.2303	0.0019	19.18	0.68	0.604	0.021	0.973	3054	13	3044	83	0
July 7 2021	QM10A-33-1	mix	ign		8.36E+05	0	0.0	1.58	0.2393	0.0021	20.06	0.72	0.606	0.021	0.968	3115	14	3053	84	2
July 7 2021	QM10A-38-1	disc,mix	ign		1.02E+06	78	0.1	1.61	0.2472	0.0032	18.10	1.41	0.535	0.041	0.986	3167	21	2762	170	15
July 7 2021	QM10A-42-1	disc,mix	ign		5.90E+05	0	0.0	1.47	0.2588	0.0037	20.30	1.83	0.568	0.051	0.987	3239	22	2900	205	12
July 7 2021	QM10A-60-1	mix	ign		5.52E+05	20	0.0	0.32	0.2314	0.0072	19.26	1.46	0.605	0.042	0.914	3062	49	3050	167	0
July 7 2021	QM10A-25-1	mix,2SE>3	ign		1.00E+06	0	0.0	1.65	0.2475	0.0023	21.41	0.78	0.623	0.022	0.968	3169	14	3123	86	1
July 7 2021	QM10A-43-1	disc	ign		4.37E+05	13	0.0	1.18	0.2560	0.0021	18.07	0.66	0.511	0.018	0.975	3222	13	2661	77	21
July 7 2021	QM10A-1-1	disc	ign		8.90E+05	0	0.0	1.37	0.2495	0.0020	18.96	0.93	0.560	0.027	0.987	3182	13	2867	112	11
July 9 2021	QM2C-68-1		ign	x	1.17E+06	232	0.2	0.74	0.2579	0.0025	22.40	0.85	0.630	0.023	0.966	3234	15	3150	91	3
July 7 2021	QM2C-6-1		ign	x	4.05E+05	24	0.1	0.44	0.2567	0.0024	24.49	0.98	0.693	0.027	0.971	3227	15	3394	101	-5
July 9 2021	QM2C-93-1		ign	x	1.61E+06	0	0.0	0.54	0.2561	0.0019	22.83	0.81	0.647	0.022	0.977	3223	12	3215	87	0
July 9 2021	QM2C-65-1		ign	x	7.77E+05	10	0.0	0.52	0.2548	0.0021	22.65	0.84	0.647	0.023	0.975	3215	13	3215	91	0
July 9 2021	QM2C-67-1		ign	x	4.39E+05	0	0.0	0.64	0.2546	0.0024	22.41	0.86	0.638	0.024	0.969	3214	15	3181	93	1
July 7 2021	QM2C-7-1		ign	x	4.40E+05	0	0.0	0.43	0.2543	0.0021	23.57	0.85	0.673	0.024	0.974	3212	13	3316	91	-3
July 9 2021	QM2C-105-1		ign	x	1.07E+06	85	0.1	0.50	0.2543	0.0026	22.93	0.95	0.653	0.026	0.970	3212	16	3240	102	-1
July 9 2021	QM2C-24-1		ign	x	1.31E+06	39	0.0	0.57	0.2538	0.0019	23.56	0.83	0.672	0.023	0.977	3209	12	3312	88	-3
July 9 2021	QM2C-34-1		ign		6.72E+05	0	0.0	0.26	0.2523	0.0023	21.63	0.77	0.619	0.021	0.968	3199	14	3105	85	3
July 9 2021	QM2C-111-1		ign		3.53E+05	0	0.0	0.49	0.2522	0.0019	24.01	0.85	0.690	0.024	0.977	3199	12	3384	90	-5
July 9 2021	QM2C-89-1		ign		4.43E+05	11	0.0	0.50	0.2522	0.0026	24.16	0.99	0.696	0.027	0.966	3199	17	3405	103	-6
July 9 2021	QM2C-102-1		ign		2.30E+06	258	0.1	0.24	0.2522	0.0021	21.35	0.84	0.615	0.024	0.976	3199	13	3090	93	4
July 9 2021	QM2C-76-1		ign		3.01E+05	0	0.0	0.67	0.2519	0.0023	21.87	0.82	0.631	0.023	0.970	3197	14	3153	90	1
July 9 2021	QM2C-100-1		ign		4.16E+05	0	0.0	0.50	0.2518	0.0019	20.95	0.74	0.604	0.021	0.977	3196	12	3047	83	5
July 9 2021	QM2C-74-1		ign		6.02E+05	26	0.1	0.63	0.2506	0.0024	24.28	1.08	0.703	0.031	0.976	3189	15	3432	115	-7
July 9 2021	QM2C-81-1		ign		2.49E+05	30	0.2	0.65	0.2502	0.0021	21.38	0.77	0.622	0.022	0.973	3186	13	3116	86	2
July 9 2021	QM2C-48-1		ign		4.04E+05	0	0.0	0.47	0.2501	0.0028	21.78	0.87	0.629	0.024	0.959	3185	18	3146	94	1
July 9 2021	QM2C-33-1		ign		3.77E+05	0	0.0	0.58	0.2498	0.0031	21.43	0.85	0.619	0.023	0.948	3183	20	3106	92	2
July 9 2021	QM2C-18-1		ign		8.89E+05	6	0.0	0.54	0.2496	0.0019	22.81	0.93	0.662	0.026	0.982	3182	12	3275	102	-3
July 9 2021	QM2C-70-1		ign		1.44E+06	198	0.2	0.25	0.2495	0.0023	21.80	0.85	0.633	0.024	0.973	3182	14	3161	94	1
July 9 2021	QM2C-49-1		ign		1.21E+06	94	0.1	0.57	0.2490	0.0021	21.37	0.76	0.622	0.021	0.971	3178	13	3116	84	2

Session	Spot ID	Screen	Class	Age	In	206Pb cps	204Pb cps	fPbc %	Th U	Ratios					Dates (Ma)				Disc. %		
										207Pb		207Pb		206Pb		207Pb		206Pb			
										206Pb	2σ	235U	2σ	238U	2σ	ρ	206Pb	2σ		238U	2σ
July 9 2021	QM2C-46-1		ign			4.38E+05	17	0.0	0.57	0.2448	0.0020	23.56	0.95	0.696	0.027	0.980	3151	13	3405	103	-7
July 9 2021	QM2C-9-1		ign			1.13E+06	9	0.0	0.50	0.2447	0.0023	20.87	0.86	0.614	0.025	0.973	3151	15	3086	98	2
July 9 2021	QM2C-83-1		ign			7.70E+05	0	0.0	0.37	0.2426	0.0024	20.20	0.73	0.604	0.021	0.962	3137	16	3045	84	3
July 9 2021	QM2C-17-1		ign			4.72E+05	66	0.2	0.45	0.2416	0.0022	20.81	0.79	0.621	0.023	0.970	3131	15	3113	90	1
July 9 2021	QM2C-64-1		ign			1.21E+06	13	0.0	0.31	0.2358	0.0020	20.33	0.75	0.625	0.022	0.973	3092	13	3128	88	-1
July 7 2021	QM2C-8-1		ign			2.84E+05	35	0.2	0.47	0.2344	0.0019	18.44	0.65	0.573	0.020	0.973	3082	13	2918	80	6
July 9 2021	QM2C-72-1		ign			9.61E+05	0	0.0	0.38	0.2342	0.0019	19.81	0.69	0.613	0.021	0.974	3081	13	3084	83	0
July 9 2021	QM2C-53-1		ign			6.66E+05	0	0.0	0.38	0.2322	0.0022	21.15	0.82	0.660	0.025	0.970	3067	15	3267	96	-6
July 9 2021	QM2C-23-1		ign			4.15E+05	2	0.0	0.46	0.2258	0.0025	18.39	0.69	0.588	0.021	0.957	3023	18	2981	86	1
July 9 2021	QM2C-90-1		met			2.47E+06	0	0.0	0.14	0.2151	0.0016	16.86	0.62	0.570	0.020	0.978	2944	12	2906	84	1
July 9 2021	QM2C-108-1		met			1.40E+06	27	0.0	0.11	0.2130	0.0016	16.31	0.58	0.555	0.019	0.979	2928	12	2847	80	3
July 9 2021	QM2C-61-1		met			5.98E+05	0	0.0	0.10	0.1592	0.0016	11.00	0.42	0.501	0.019	0.966	2447	17	2617	79	-6
July 9 2021	QM2C-26-1	disc,mix	ign			1.33E+06	306	0.3	0.15	0.1666	0.0043	8.67	0.38	0.379	0.013	0.805	2524	44	2073	62	22
July 9 2021	QM2C-45-1	mix	ign			2.29E+05	0	0.0	0.54	0.2427	0.0025	22.84	1.15	0.684	0.034	0.978	3138	17	3360	128	-7
July 9 2021	QM2C-69-1	mix	ign			1.34E+06	76	0.1	0.47	0.2332	0.0037	20.77	0.85	0.645	0.024	0.922	3074	25	3209	95	-4
July 9 2021	QM2C-98-1	mix	ign			3.01E+05	6	0.0	0.56	0.2555	0.0032	19.20	1.28	0.550	0.036	0.982	3219	20	2825	148	14
July 9 2021	QM2C-109-1	mix	ign			1.76E+06	163	0.1	0.54	0.2431	0.0028	20.37	0.91	0.609	0.026	0.967	3140	18	3066	105	2
July 9 2021	QM2C-110-1	mix	ign			1.09E+06	5	0.0	0.26	0.2096	0.0025	15.95	0.69	0.552	0.023	0.962	2902	19	2833	95	2
July 7 2021	QM2C-2-1	disc,mix,2SE>3	ign			1.94E+05	124	0.8	0.44	0.2542	0.0023	27.37	1.13	0.784	0.032	0.976	3211	14	3732	113	-14
July 9 2021	QM2C-52-1	2SE>3	ign			3.65E+05	89	0.3	0.66	0.2525	0.0031	21.57	0.98	0.621	0.027	0.962	3201	20	3114	108	3
July 9 2021	QM2C-85-1	2SE>3	ign			1.10E+06	0	0.0	0.54	0.2483	0.0023	23.06	0.98	0.674	0.028	0.975	3174	15	3321	107	-4
July 9 2021	QM2C-107-1	cPb	ign			1.36E+06	1874	1.7	0.51	0.2703	0.0022	23.73	0.86	0.636	0.022	0.974	3308	13	3175	88	4
July 9 2021	QM7C-4e		ign	x		4.33E+06	1858	0.5	0.63	0.2411	0.0023	20.11	0.76	0.604	0.022	0.968	3127	15	3045	88	3
July 12 2021	QM7C-38-1		ign	x		6.91E+06	151	0.0	0.58	0.2407	0.0020	18.59	0.68	0.558	0.020	0.974	3125	13	2859	82	9
July 12 2021	QM7C-64-1		ign	x		4.26E+06	34	0.0	0.58	0.2406	0.0018	19.82	0.70	0.595	0.021	0.976	3124	12	3009	82	4
July 12 2021	QM7C-49-1		ign	x		2.36E+06	10	0.0	0.49	0.2404	0.0017	20.52	0.72	0.617	0.021	0.979	3123	11	3096	84	1
July 12 2021	QM7C-4-1		ign	x		2.72E+06	819	0.4	0.45	0.2396	0.0017	19.90	0.70	0.603	0.021	0.979	3118	11	3044	83	2
July 12 2021	QM7C-13e		ign			3.98E+06	106	0.0	0.39	0.2368	0.0019	19.61	0.72	0.603	0.021	0.976	3099	13	3042	86	2
July 9 2021	QM7C-11e		ign			2.38E+06	119	0.1	0.44	0.2336	0.0018	19.59	0.70	0.606	0.021	0.977	3077	12	3053	85	1
July 12 2021	QM7C-22e		ign			3.20E+06	0	0.0	0.16	0.2330	0.0018	18.69	0.76	0.584	0.023	0.982	3073	12	2965	94	4
July 12 2021	QM7C-79-1		ign			1.08E+06	88	0.1	0.19	0.2298	0.0018	18.13	0.69	0.574	0.021	0.979	3051	12	2922	87	4
July 12 2021	QM7C-15e		ign			3.34E+06	479	0.2	0.45	0.2295	0.0020	17.51	0.71	0.555	0.022	0.977	3049	14	2846	90	7
July 12 2021	QM7C-20-1		ign			3.42E+06	232	0.1	0.21	0.2281	0.0016	17.11	0.62	0.543	0.019	0.980	3039	12	2794	80	9
July 12 2021	QM7C-20e		ign			2.00E+06	76	0.0	0.23	0.2278	0.0017	17.04	0.64	0.544	0.020	0.980	3036	12	2802	83	8
July 12 2021	QM7C-60-1		ign			2.30E+06	47	0.0	0.05	0.2225	0.0021	18.38	0.66	0.597	0.021	0.963	2999	15	3017	82	-1
July 12 2021	QM7C-21e		ign			2.99E+06	0	0.0	0.15	0.2211	0.0017	18.49	0.65	0.609	0.021	0.976	2989	12	3064	83	-2
July 9 2021	QM7C-7e		ign			2.82E+06	487	0.2	0.38	0.2206	0.0019	16.81	0.61	0.553	0.020	0.973	2985	14	2837	81	5
July 12 2021	QM7C-48-1		ign			3.35E+06	74	0.0	0.09	0.2109	0.0015	15.09	0.58	0.517	0.019	0.983	2913	11	2688	82	8
July 9 2021	QM7C-2e	mix	ign			3.19E+06	360	0.1	0.30	0.2205	0.0017	16.43	0.85	0.540	0.028	0.988	2984	13	2783	114	7
July 9 2021	QM7C-5e	disc,mix	ign			4.10E+06	1725	0.6	0.56	0.2043	0.0056	13.47	0.87	0.476	0.028	0.907	2861	44	2510	121	14
July 9 2021	QM7C-8e	mix	ign			3.18E+06	238	0.1	0.30	0.2149	0.0034	16.61	0.79	0.557	0.025	0.944	2943	25	2854	103	3
July 9 2021	QM7C-9e	cPb,disc,mix	ign			3.13E+06	75933	26.7	0.27	0.3620	0.0451	76.00	19.25	1.330	0.293	0.871	3758	189	5453	764	-31
July 9 2021	QM7C-10e	disc,mix	ign			2.84E+06	126	0.1	0.51	0.2211	0.0023	13.66	0.68	0.450	0.022	0.978	2989	17	2395	96	25
July 12 2021	QM7C-19e	disc,mix	ign			4.43E+06	2104	0.6	0.39	0.2195	0.0035	13.79	0.72	0.462	0.023	0.952	2977	26	2448	100	22
July 12 2021	QM7C-28-1	mix	ign			2.50E+06	48	0.0	0.09	0.2102	0.0090	16.81	0.95	0.579	0.022	0.656	2907	69	2945	87	-1
July 12 2021	QM7C-48-2	disc,mix	ign			4.61E+06	3058	0.8	0.64	0.2306	0.0031	13.37	0.85	0.421	0.026	0.977	3056	21	2265	117	35
July 12 2021	QM7C-59-1	disc,mix	ign			4.15E+06	690	0.2	0.62	0.2358	0.0028	13.83	0.62	0.428	0.019	0.966	3092	19	2297	83	35
July 12 2021	QM7C-67-1	disc,mix	ign			7.27E+06	458	0.1	0.36	0.2023	0.0017	12.04	0.46	0.430	0.016	0.976	2845	14	2304	72	23
July 12 2021	QM7C-93-1	cPb,mix	ign			3.48E+06	13536	4.8	0.34	0.2560	0.0111	23.30	1.43	0.678	0.029	0.706	3222	69	3337	112	-3

Session	Spot ID	Screen	Class	Age	In	206Pb cps	204Pb cps	fPbc %	Th U	Ratios						Dates (Ma)				Disc.					
										207Pb		207Pb		206Pb		207Pb		206Pb			p	207Pb		206Pb	
										206Pb	2σ	235U	2σ	238U	2σ	206Pb	2σ	238U	2σ			206Pb	2σ	238U	2σ
July 12 2021	QM7C-14e	mix	ign			3.52E+06	117	0.0	0.37	0.2236	0.0019	16.27	0.83	0.530	0.027	0.985	3007	14	2741	111	10				
July 12 2021	QM7C-96-1	disc	ign			3.91E+06	141	0.0	0.28	0.2301	0.0020	17.03	0.63	0.535	0.019	0.973	3053	14	2763	81	10				
July 12 2021	QM7C-16e	disc	ign			4.37E+06	578	0.2	0.35	0.2152	0.0022	15.09	0.67	0.510	0.022	0.973	2945	16	2657	93	11				
July 12 2021	QM7C-100-1	disc	ign			2.30E+06	35	0.0	0.31	0.2317	0.0023	16.90	0.84	0.533	0.026	0.981	3064	16	2754	108	11				
July 12 2021	QM7C-17e	disc	ign			2.93E+06	164	0.1	0.49	0.2310	0.0018	16.58	0.66	0.523	0.020	0.982	3059	12	2712	86	13				
July 9 2021	QM7C-6-1	disc	ign			5.01E+06	352	0.1	0.44	0.2215	0.0021	15.27	0.68	0.499	0.022	0.976	2992	16	2609	92	15				
July 12 2021	QM7C-83-1	disc	ign			3.94E+06	242	0.1	0.51	0.2315	0.0020	15.49	0.69	0.483	0.021	0.980	3062	14	2540	92	21				
July 9 2021	QM7C-1e	disc,2SE>3	ign			6.20E+06	640	0.1	0.57	0.2340	0.0018	17.37	0.66	0.537	0.020	0.980	3080	12	2769	84	11				
July 12 2021	QM7C-18e	2SE>3	ign			4.74E+06	399	0.1	0.50	0.2269	0.0019	17.20	0.75	0.549	0.024	0.980	3030	14	2821	97	7				
July 9 2021	QM7C-3e	2SE>3	ign			3.83E+06	81	0.0	0.47	0.2361	0.0020	19.88	0.84	0.608	0.025	0.980	3094	13	3062	100	1				
July 12 2021	QM7C-12e	2SE>3	ign			2.73E+06	82	0.0	0.41	0.2265	0.0028	17.46	0.85	0.561	0.027	0.967	3027	20	2871	109	5				
July 12 2021	QM7C-34-1	2SE>3	ign			3.54E+06	213	0.1	0.36	0.2320	0.0020	19.13	0.70	0.596	0.021	0.972	3066	14	3014	85	2				
July 12 2021	QM7C-75-1	2SE>3	ign			4.43E+06	256	0.1	0.49	0.2345	0.0021	19.26	0.69	0.593	0.020	0.967	3083	14	3003	82	3				

Spots labelled QM7C-#, indicate analyses of the extra grains mounted for LASS-U-Pb-Hf. See zircon images.

Session	Spot ID	Scn	Class	In WM	At 207Pb/206Pb Date								At Rock Age								
					176Lu 177Hf	2SE	176Yb 177Hf	2SE	176Hf 177Hf	2SE	178Hf 177Hf	2SE	Total Hf (V)	Date (Ma)	2σ	εHf(t)	2SE	Age (Ma)	2σ	εHf(i)	2SE
June 25 2021	HBA-7-1		ign	x	0.000980	0.000059	0.0303	0.0021	0.280832	0.000031	1.467244	0.000045	11	3070	12	-1.0	1.1	3122	6	0.2	1.1
June 25 2021	HBA-98-1		ign	x	0.00146	0.00011	0.0438	0.0034	0.280824	0.000056	1.467191	0.000054	10	3064	12	-2.4	2.0	3122	6	-1.1	2.0
June 25 2021	HBA-74-1		ign	x	0.001904	0.000067	0.0574	0.0021	0.280903	0.000052	1.467105	0.000065	8	3059	12	-0.7	1.9	3122	6	0.7	1.9
June 25 2021	HBA-86-1		ign	x	0.000647	0.000056	0.0197	0.0019	0.280819	0.000040	1.467192	0.000059	12	3049	12	-1.3	1.4	3122	6	0.4	1.4
June 25 2021	HBA-37-1	x	ign		0.00070	0.00010	0.0204	0.0033	0.280758	0.000042	1.467200	0.000049	11	2987	14	-5.0	1.5				
June 25 2021	HBA-53-1	x	ign		0.001408	0.000081	0.0439	0.0021	0.280790	0.000065	1.46724	0.00012	15	3037	13	-4.2	2.3				
June 25 2021	HBA-70-1	x	ign		0.001010	0.000087	0.0289	0.0027	0.280771	0.000049	1.467227	0.000084	9	2893	34	-7.3	1.8				
June 25 2021	HBA-78-1	x	ign		0.000914	0.000057	0.0270	0.0018	0.280808	0.000033	1.467126	0.000057	10	3039	14	-2.5	1.2				
June 25 2021	HBA-94-1	x	ign		0.00079	0.00013	0.0231	0.0038	0.280850	0.000036	1.467137	0.000038	11	3000	17	-1.6	1.3				
June 25 2021	HBA-103-1	x	ign		0.00227	0.00018	0.0733	0.0058	0.280945	0.000097	1.46727	0.00012	9	3092	12	0.8	3.5				
June 25 2021	HBA-80-1	x	ign		0.000955	0.000068	0.0281	0.0021	0.280871	0.000055	1.467185	0.000077	8	3133	13	1.9	2.0				
June 25 2021	MSB-1-1		inhrt		0.00199	0.00014	0.0635	0.0048	0.280719	0.000057	1.467163	0.000068	9	3294	11	-2.2	2.1				
June 25 2021	MSB-92-1		inhrt		0.00233	0.00019	0.0716	0.0058	0.280721	0.000077	1.467208	0.000082	6	3265	11	-3.5	2.8				
June 25 2021	MSB-76-1		inhrt		0.00115	0.00015	0.0346	0.0047	0.280830	0.000048	1.467204	0.000041	9	3121	13	-0.4	1.7				
June 25 2021	MSB-61-1		inhrt		0.001510	0.000085	0.0479	0.0026	0.280861	0.000040	1.467171	0.000049	10	3121	12	0.0	1.4				
June 25 2021	MSB-79-1		inhrt		0.000526	0.000012	0.01440	0.00032	0.280788	0.000031	1.467186	0.000052	10	3116	13	-0.5	1.1				
June 25 2021	MSB-26-1		inhrt		0.001157	0.000048	0.0358	0.0014	0.280799	0.000036	1.467202	0.000060	9	3115	12	-1.5	1.3				
June 25 2021	MSB-90-1		inhrt		0.000574	0.000018	0.01594	0.00055	0.280819	0.000046	1.467175	0.000052	10	3105	13	0.2	1.6				
June 25 2021	MSB-27-1		inhrt		0.000579	0.000019	0.01650	0.00051	0.280749	0.000046	1.467206	0.000075	13	3098	12	-2.5	1.6				
June 25 2021	MSB-4-1		inhrt		0.001483	0.000030	0.04377	0.00085	0.280843	0.000035	1.467204	0.000063	10	3094	11	-1.1	1.2				
June 25 2021	MSB-2-1		inhrt		0.000958	0.000062	0.0269	0.0019	0.280863	0.000065	1.467126	0.000065	7	3093	13	0.7	2.3				
June 25 2021	MSB-22-1		inhrt		0.001229	0.000023	0.03774	0.00079	0.280794	0.000061	1.467251	0.000071	11	3091	12	-2.4	2.2				
June 25 2021	MSB-39-1		ign	x	0.000366	0.000011	0.00977	0.00030	0.280796	0.000038	1.467189	0.000050	10	3090	15	-0.5	1.4	3074	7	-0.9	1.4
June 25 2021	MSB-64-1		ign	x	0.000731	0.000028	0.02025	0.00081	0.280797	0.000044	1.467122	0.000059	11	3090	11	-1.3	1.6	3074	7	-1.7	1.6
June 25 2021	MSB-70-2		ign	x	0.0003665	0.0000069	0.00990	0.00026	0.280810	0.000027	1.467178	0.000042	10	3082	15	-0.2	1.0	3074	7	-0.4	1.0
June 25 2021	MSB-10-1		ign	x	0.000953	0.000024	0.02754	0.00075	0.280808	0.000042	1.467191	0.000069	12	3078	12	-1.6	1.5	3074	7	-1.7	1.5
June 25 2021	MSB-36-1		ign	x	0.001423	0.000049	0.0415	0.0014	0.280836	0.000041	1.467156	0.000068	8	3075	12	-1.7	1.5	3074	7	-1.7	1.5
June 25 2021	MSB-103-1		ign	x	0.000445	0.000023	0.01214	0.00066	0.280795	0.000051	1.467161	0.000049	9	3074	14	-1.1	1.8	3074	7	-1.1	1.8
June 25 2021	MSB-59-1		ign	x	0.000955	0.000058	0.0279	0.0019	0.280812	0.000040	1.467179	0.000065	8	3073	11	-1.6	1.4	3074	7	-1.6	1.4
June 25 2021	MSB-69-1		ign	x	0.000320	0.000005	0.00862	0.00016	0.280811	0.000030	1.467204	0.000045	11	3072	15	-0.3	1.1	3074	7	-0.3	1.1
June 25 2021	MSB-9-1		ign	x	0.000576	0.000043	0.0167	0.0012	0.280746	0.000033	1.467241	0.000057	11	3071	13	-3.2	1.2	3074	7	-3.1	1.2
June 25 2021	MSB-73-1		ign	x	0.00092	0.000031	0.0262	0.0092	0.280815	0.000045	1.467151	0.000071	9	3071	16	-1.5	1.7	3074	7	-1.4	1.7
June 25 2021	MSB-17-1		ign	x	0.0003769	0.0000028	0.01057	0.00011	0.280763	0.000029	1.467251	0.000077	13	3069	24	-2.2	1.0	3074	7	-2.1	1.0
June 25 2021	MSB-66-1		ign	x	0.000616	0.000029	0.01862	0.00082	0.280784	0.000028	1.467163	0.000052	10	3066	12	-2.1	1.0	3074	7	-1.9	1.0
June 25 2021	MSB-67-1		ign	x	0.000319	0.000010	0.00890	0.00039	0.280791	0.000038	1.467186	0.000055	12	3065	11	-1.2	1.4	3074	7	-1.0	1.4
June 25 2021	MSB-5-1		ign	x	0.000481	0.000032	0.0139	0.0011	0.280770	0.000050	1.467170	0.000070	13	3062	14	-2.4	1.8	3074	7	-2.1	1.8
June 25 2021	MSB-44-1		ign		0.00193	0.00017	0.0588	0.0050	0.280918	0.000052	1.467139	0.000070	8	3060	14	-0.2	1.9				

Session	Spot ID	Scn	Class	In WM									At 207Pb/206Pb Date				At Rock Age				
					176Lu 177Hf	2SE	176Yb 177Hf	2SE	176Hf 177Hf	2SE	178Hf 177Hf	2SE	Total Hf (V)	Date (Ma)	2σ	εHf(t)	2SE	Age (Ma)	2σ	εHf(i)	2SE
June 25 2021	MSB-3-1		ign		0.000609	0.000010	0.01744	0.00041	0.280737	0.000040	1.467161	0.000048	8	3060	13	-3.9	1.4				
June 25 2021	MSB-37-2		ign		0.0005779	0.0000065	0.01721	0.00025	0.280816	0.000054	1.467185	0.000064	9	3059	23	-1.0	1.9				
June 25 2021	MSB-65-1		ign		0.000381	0.000023	0.01033	0.00069	0.280796	0.000037	1.467218	0.000039	15	3059	15	-1.3	1.3				
June 25 2021	MSB-92-2		ign		0.0005763	0.0000063	0.01696	0.00037	0.280825	0.000058	1.467193	0.000089	13	3054	14	-0.8	2.1				
June 25 2021	MSB-18-1		ign		0.002032	0.000049	0.0593	0.0018	0.280846	0.000039	1.467139	0.000049	10	3040	11	-3.4	1.4				
June 25 2021	MSB-50-1		ign		0.000373	0.000016	0.00991	0.00048	0.280782	0.000039	1.467116	0.000051	9	3033	12	-2.4	1.4				
June 25 2021	MSB-70-1		inhrt		0.000555	0.000064	0.0153	0.0019	0.280788	0.000037	1.467149	0.000049	10	3029	11	-2.7	1.3				
June 25 2021	MSB-16-1		ign		0.001366	0.000092	0.0413	0.0028	0.280814	0.000042	1.467187	0.000053	10	3028	12	-3.4	1.5				
June 25 2021	MSB-40-1		ign		0.000389	0.000022	0.01080	0.00050	0.280808	0.000040	1.467207	0.000058	10	3025	12	-1.7	1.4				
June 25 2021	MSB-4-2		ign		0.0004040	0.0000027	0.01114	0.00015	0.280746	0.000040	1.467204	0.000042	12	3012	18	-4.2	1.4				
June 25 2021	MSB-37-1		inhrt		0.000469	0.000012	0.01297	0.00045	0.280800	0.000033	1.467164	0.000046	11	3009	12	-2.5	1.2				
June 25 2021	MSB-1-2		ign		0.000487	0.000014	0.01344	0.00049	0.280743	0.000035	1.467128	0.000051	11	2969	12	-5.5	1.2				
June 25 2021	MSB-68-1		ign		0.001018	0.000011	0.02970	0.00046	0.280761	0.000056	1.467227	0.000083	13	2944	15	-6.5	2.0				
June 25 2021	MSB-47-1		met		0.000636	0.000020	0.01903	0.00075	0.280940	0.000042	1.467165	0.000042	9	2377	12	-12.4	1.5				
June 25 2021	MSB-94-1	x	inhrt		0.000820	0.000120	0.0246	0.0039	0.280860	0.000042	1.467179	0.000068	8	3145	15	2.0	1.5				
June 25 2021	MSB-22-2	x	ign		0.000430	0.000011	0.0123	0.0004	0.280781	0.000031	1.467200	0.000048	11	3133	22	-0.2	1.1				
June 25 2021	MSB-36-2	x	ign		0.000721	0.000094	0.0214	0.0031	0.280833	0.000042	1.467159	0.000058	10	3113	74	0.6	1.5				
June 25 2021	MSB-104-1	x	ign		0.00205	0.00016	0.0614	0.0047	0.28093	0.00010	1.467142	0.000079	6	3097	12	0.8	3.6				
June 25 2021	MSB-26-2	x	ign		0.0004365	0.0000038	0.01176	0.00014	0.280730	0.000076	1.467183	0.000094	7	3088	15	-3.1	2.7				
June 25 2021	MSB-24-2	x	ign		0.000441	0.000017	0.01229	0.00032	0.280792	0.000038	1.467146	0.000053	10	3075	14	-1.2	1.4				
June 25 2021	MSB-80-1	x	ign		0.000747	0.000038	0.0217	0.0013	0.280769	0.000045	1.467090	0.000080	12	3062	14	-3.0	1.6				
June 25 2021	MSB-100-1	x	inhrt		0.001432	0.000076	0.0429	0.0023	0.280832	0.000049	1.467172	0.000064	8	3055	18	-2.3	1.8				
June 25 2021	MSB-29-1	x	ign		0.000871	0.000081	0.0247	0.0023	0.280804	0.000037	1.467183	0.000051	11	3025	17	-2.8	1.3				
June 25 2021	MSB-89-1	x	ign		0.001123	0.000083	0.0343	0.0028	0.280876	0.000059	1.467159	0.000088	9	3017	14	-1.0	2.1				
June 25 2021	MSB-24-1	x	ign		0.00103	0.00013	0.0344	0.0059	0.280749	0.000041	1.46714	0.00011	7	2931	25	-7.3	1.5				
June 25 2021	MSB-28-1	x	ign		0.00102	0.00012	0.0293	0.0034	0.280825	0.000059	1.467162	0.000062	9	2900	21	-5.2	2.1				
June 25 2021	MSB-77-1	x	ign		0.00082	0.00022	0.0296	0.0099	0.28057	0.00036	1.46744	0.00048	8	2878	47	-14.4	12.8				
July 7 2021	QM17C-61-1		ign	x	0.000949	0.000089	0.0267	0.0027	0.280829	0.000042	1.467132	0.000076	11	3149	13	0.8	1.5	3140	6	0.5	1.5
July 7 2021	QM17C-60-1		ign	x	0.000808	0.000092	0.0247	0.0030	0.280820	0.000049	1.467208	0.000056	8	3148	12	0.7	1.8	3140	6	0.5	1.8
June 25 2021	QM17C-19-1		ign	x	0.000513	0.000051	0.0134	0.0018	0.280799	0.000033	1.467220	0.000061	18	3142	12	0.5	1.2	3140	6	0.4	1.2
June 25 2021	QM17C-8-1		ign	x	0.000091	0.00016	0.0273	0.0049	0.280788	0.000050	1.467184	0.000057	12	3141	11	-0.8	1.8	3140	6	-0.8	1.8
July 7 2021	QM17C-103-1		ign	x	0.00104	0.00013	0.0323	0.0043	0.280834	0.000054	1.467126	0.000051	14	3138	14	0.5	1.9	3140	6	0.5	1.9
July 7 2021	QM17C-57-1		ign	x	0.00128	0.00012	0.0368	0.0032	0.280820	0.000057	1.467217	0.000055	10	3132	13	-0.7	2.0	3140	6	-0.5	2.0
June 25 2021	QM17C-5-1		ign	x	0.00165	0.00017	0.0497	0.0055	0.280868	0.000056	1.467172	0.000084	11	3129	12	0.2	2.0	3140	6	0.4	2.0
July 7 2021	QM17C-38-1		ign	x	0.000512	0.000024	0.01449	0.00079	0.280788	0.000029	1.467192	0.000070	15	3125	11	-0.3	1.0	3140	6	0.0	1.0
July 7 2021	QM17C-87-1		ign	x	0.000728	0.000055	0.0203	0.0019	0.280813	0.000056	1.467070	0.000060	10	3125	13	0.1	2.0	3140	6	0.5	2.0
July 7 2021	QM17C-41-1		ign	x	0.000426	0.000026	0.01261	0.00076	0.280815	0.000036	1.467257	0.000066	14	3125	13	0.8	1.3	3140	6	1.2	1.3

Session	Spot ID	Scn	Class	In WM									At 207Pb/206Pb Date				At Rock Age				
					176Lu 177Hf	2SE	176Yb 177Hf	2SE	176Hf 177Hf	2SE	178Hf 177Hf	2SE	Total Hf (V)	Date (Ma)	2σ	εHf(t)	2SE	Age (Ma)	2σ	εHf(i)	2SE
July 7 2021	QM17C-54-1		ign	x	0.00174	0.00034	0.0520	0.0100	0.280868	0.000050	1.467095	0.000060	12	3123	13	-0.2	1.9	3140	6	0.2	1.9
June 25 2021	QM17C-22-1		ign	x	0.000430	0.000087	0.0131	0.0028	0.280768	0.000049	1.467244	0.000064	17	3114	21	-1.1	1.8	3140	6	-0.5	1.8
June 25 2021	QM17C-21-1		ign	x	0.000561	0.000018	0.0159	0.0006	0.280749	0.000042	1.467174	0.000055	11	3113	13	-2.1	1.5	3140	6	-1.5	1.5
July 7 2021	QM17C-80-1		ign	x	0.00190	0.00025	0.0593	0.0084	0.280873	0.000062	1.467129	0.000072	11	3109	13	-0.6	2.3	3140	6	0.1	2.3
July 7 2021	QM17C-84-1		ign	x	0.00197	0.00021	0.0616	0.0070	0.280840	0.000070	1.467155	0.000073	11	3106	16	-2.0	2.5	3140	6	-1.3	2.5
June 25 2021	QM17C-23-1		ign	x	0.00163	0.00014	0.0502	0.0040	0.280827	0.000056	1.467197	0.000067	15	3105	12	-1.8	2.0	3140	6	-1.0	2.0
July 7 2021	QM17C-98-1		ign	x	0.000930	0.000069	0.0250	0.0018	0.280790	0.000038	1.467144	0.000067	12	3103	13	-1.7	1.4	3140	6	-0.8	1.4
June 25 2021	QM17C-6-1		ign	x	0.00281	0.00041	0.0870	0.0130	0.280943	0.000068	1.467224	0.000063	10	3101	12	-0.2	2.6	3140	6	0.6	2.6
July 7 2021	QM17C-91-1		ign	x	0.00107	0.00013	0.0291	0.0036	0.280819	0.000040	1.467185	0.000063	10	3094	13	-1.1	1.5	3140	6	-0.1	1.5
July 7 2021	QM17C-72-1		ign	x	0.00044	0.00001	0.01158	0.00040	0.280757	0.000029	1.467243	0.000055	17	3093	16	-2.0	1.0	3140	6	-0.9	1.0
July 7 2021	QM17C-47-1		ign	x	0.00108	0.00011	0.0325	0.0038	0.280834	0.000040	1.467168	0.000054	12	3090	13	-0.7	1.4	3140	6	0.4	1.4
June 25 2021	QM17C-12-1		ign	x	0.001121	0.000056	0.0329	0.0015	0.280826	0.000044	1.467201	0.000058	11	3090	11	-1.1	1.6	3140	6	0.1	1.6
July 7 2021	QM17C-95-1		ign	x	0.00128	0.00024	0.0392	0.0078	0.280873	0.000042	1.467132	0.000099	11	3089	19	0.2	1.6	3140	6	1.4	1.6
July 7 2021	QM17C-50-1		ign	x	0.00084	0.00014	0.0256	0.0049	0.280816	0.000031	1.467180	0.000079	12	3076	14	-1.2	1.1	3140	6	0.3	1.1
June 25 2021	QM17C-2-1		ign	x	0.00076	0.00019	0.0190	0.0064	0.280773	0.000035	1.467149	0.000074	12	3075	13	-2.5	1.3	3140	6	-1.0	1.3
July 7 2021	QM17C-53-1		ign	x	0.001009	0.000080	0.0296	0.0026	0.280809	0.000042	1.467189	0.000055	12	3061	12	-2.1	1.5	3140	6	-0.3	1.5
July 7 2021	QM17C-52-1		ign	x	0.00112	0.00013	0.0320	0.0038	0.280866	0.000047	1.467180	0.000058	9	3044	14	-0.7	1.7	3140	6	1.5	1.7
June 25 2021	QM17C-14-1	x	ign		0.00179	0.00033	0.053	0.010	0.280873	0.000062	1.467227	0.000079	10	3069	16	-1.3	2.3				
June 25 2021	QM17C-24-1	x	ign		0.000998	0.000062	0.0308	0.0020	0.280796	0.000046	1.467129	0.000082	15	3080	36	-2.1	1.6				
July 7 2021	QM17C-42-1	x	ign		0.001030	0.000170	0.0305	0.0060	0.280813	0.000035	1.467160	0.000057	11	3044	17	-2.4	1.3				
July 7 2021	QM17C-44-1	x	ign		0.000719	0.000042	0.0207	0.0014	0.280800	0.000041	1.467183	0.000059	9	2834	39	-7.1	1.5				
July 7 2021	QM17C-70-1	x	ign		0.00125	0.00023	0.0354	0.0078	0.280820	0.000047	1.467165	0.000066	11	3025	20	-3.0	1.7				
July 7 2021	QM17C-79-1	x	ign		0.00126	0.00012	0.0359	0.0032	0.280834	0.000040	1.467180	0.000056	10	3022	25	-2.6	1.4				
July 7 2021	QM17C-82-1	x	ign		0.00117	0.00012	0.0348	0.0037	0.280834	0.000051	1.467182	0.000059	11	3101	23	-0.7	1.8				
July 7 2021	QM17C-105-1	x	ign		0.00105	0.00011	0.0316	0.0036	0.280860	0.000060	1.46718	0.00012	15	3070	17	-0.2	2.1				
June 25 2021	QM17C-9-1	x	ign		0.00170	0.00013	0.0532	0.0037	0.280787	0.000058	1.467221	0.000051	13	2903	14	-7.9	2.1				
June 25 2021	QM17C-16-1	x	ign		0.001346	0.000044	0.0408	0.0015	0.280845	0.000039	1.467261	0.000066	12	3130	12	0.0	1.4				
July 7 2021	QM17C-78-1	x	ign		0.00129	0.00027	0.0409	0.0093	0.280828	0.000056	1.467127	0.000055	11	3104	16	-1.0	2.1				
July 7 2021	QM17C-65-1	x	ign		0.00104	0.00014	0.0301	0.0044	0.280831	0.000036	1.467204	0.000063	11	3067	14	-1.2	1.3				
July 7 2021	QM17C-62-1	x	ign		0.001032	0.000065	0.0310	0.0018	0.280790	0.000029	1.467162	0.000058	12	2848	16	-7.7	1.0				
July 7 2021	19BN59A-35-1		ign	x	0.00115	0.00012	0.0335	0.0042	0.280779	0.000035	1.467201	0.000056	9	3219	13	0.1	1.3	3238	8	0.6	1.3
July 7 2021	19BN59A-117-1		ign	x	0.00129	0.00013	0.0382	0.0042	0.280803	0.000049	1.467171	0.000062	9	3214	12	0.6	1.8	3238	8	1.1	1.8
July 7 2021	19BN59A-14-1		ign	x	0.00138	0.00028	0.0394	0.0081	0.280846	0.000073	1.467119	0.000071	8	3213	12	1.9	2.7	3238	8	2.5	2.7
July 7 2021	19BN59A-12-1		ign	x	0.000852	0.000038	0.0249	0.0014	0.280826	0.000046	1.467222	0.000088	10	3211	12	2.3	1.6	3238	8	2.9	1.6
July 7 2021	19BN59A-70-1		ign	x	0.001165	0.000075	0.0341	0.0023	0.280820	0.000047	1.467197	0.000057	10	3208	13	1.3	1.7	3238	8	2.0	1.7
July 7 2021	19BN59A-59-1		ign	x	0.00115	0.00016	0.0336	0.0049	0.280797	0.000039	1.467139	0.000056	9	3203	12	0.4	1.4	3238	8	1.2	1.4
July 7 2021	19BN59A-3-1		ign	x	0.001342	0.000063	0.0388	0.0020	0.280799	0.000039	1.467129	0.000059	8	3201	11	0.0	1.4	3238	8	0.9	1.4

Session	Spot ID	Scn	Class	In WM									At 207Pb/206Pb Date				At Rock Age				
					176Lu 177Hf	2SE	176Yb 177Hf	2SE	176Hf 177Hf	2SE	178Hf 177Hf	2SE	Total Hf (V)	Date (Ma)	2σ	εHf(t)	2SE	Age (Ma)	2σ	εHf(i)	2SE
July 7 2021	19BN59A-37-1		ign	x	0.00140	0.00013	0.0411	0.0045	0.280854	0.000054	1.467165	0.000048	9	3201	13	1.9	1.9	3238	8	2.7	1.9
July 7 2021	19BN59A-28-1		ign	x	0.001025	0.000076	0.0295	0.0024	0.280849	0.000057	1.467178	0.000061	9	3199	13	2.4	2.0	3238	8	3.3	2.0
July 7 2021	19BN59A-61-1		ign	x	0.001295	0.000040	0.0368	0.0011	0.280816	0.000049	1.467121	0.000049	8	3195	12	0.6	1.7	3238	8	1.6	1.7
July 7 2021	19BN59A-86-1		ign	x	0.00123	0.00017	0.0357	0.0053	0.280781	0.000047	1.467192	0.000064	11	3191	13	-0.6	1.7	3238	8	0.5	1.7
July 7 2021	19BN59A-109-1		ign	x	0.00140	0.00015	0.0415	0.0046	0.280811	0.000039	1.467174	0.000042	9	3190	12	0.1	1.4	3238	8	1.2	1.4
July 7 2021	19BN59A-13-1		ign	x	0.001236	0.000075	0.0364	0.0024	0.280806	0.000051	1.467151	0.000065	9	3189	12	0.2	1.8	3238	8	1.3	1.8
July 7 2021	19BN59A-36-1		ign	x	0.001221	0.000086	0.0348	0.0028	0.280773	0.000049	1.467149	0.000051	8	3189	12	-0.9	1.8	3238	8	0.2	1.8
July 7 2021	19BN59A-7-1		ign	x	0.00131	0.00014	0.0386	0.0043	0.280852	0.000042	1.467150	0.000056	10	3186	11	1.6	1.5	3238	8	2.8	1.5
July 7 2021	19BN59A-77-1		ign	x	0.001229	0.000049	0.0344	0.0015	0.280812	0.000051	1.467217	0.000058	8	3183	12	0.3	1.8	3238	8	1.6	1.8
July 7 2021	19BN59A-57-1		ign	x	0.001515	0.000042	0.0438	0.0012	0.280863	0.000064	1.467128	0.000055	8	3183	11	1.5	2.3	3238	8	2.8	2.3
July 7 2021	19BN59A-89-1		ign	x	0.00154	0.00013	0.0457	0.0040	0.280805	0.000046	1.467208	0.000053	10	3180	14	-0.7	1.7	3238	8	0.6	1.7
July 7 2021	19BN59A-110-1		ign	x	0.00053	0.00013	0.0150	0.0044	0.280823	0.000035	1.467197	0.000068	14	3164	14	1.8	1.3	3238	8	3.5	1.3
July 7 2021	19BN59A-103-1		ign	x	0.00154	0.00012	0.0444	0.0036	0.280833	0.000047	1.467253	0.000045	9	3164	12	0.0	1.7	3238	8	1.6	1.7
July 7 2021	19BN59A-52-1		ign	x	0.001032	0.000060	0.0300	0.0018	0.280854	0.000058	1.467155	0.000065	9	3141	16	1.3	2.1	3238	8	3.5	2.1
July 7 2021	19BN59A-83-1		ign	x	0.000985	0.000031	0.02759	0.00082	0.280778	0.000052	1.467106	0.000058	7	3136	13	-1.4	1.9	3238	8	0.9	1.9
July 7 2021	19BN59A-76-1		ign	x	0.000697	0.000026	0.01942	0.00084	0.280756	0.000064	1.467134	0.000075	9	3134	15	-1.6	2.3	3238	8	0.8	2.3
July 7 2021	19BN59A-73-1		ign	x	0.000804	0.000053	0.0230	0.0018	0.280777	0.000037	1.467185	0.000071	10	3125	14	-1.3	1.3	3238	8	1.3	1.3
July 7 2021	19BN59A-21-1		ign	x	0.000994	0.000045	0.0281	0.0013	0.280809	0.000046	1.467200	0.000069	10	3103	13	-1.1	1.6	3238	8	2.0	1.6
July 7 2021	19BN59A-80-1		ign	x	0.00120	0.00015	0.0354	0.0047	0.280823	0.000053	1.467174	0.000068	10	3080	13	-1.6	1.9	3238	8	2.0	1.9
July 7 2021	19BN59A-51-1		ign	x	0.00154	0.00017	0.0445	0.0053	0.280796	0.000053	1.467127	0.000056	9	3073	15	-3.4	1.9	3238	8	0.3	1.9
July 7 2021	19BN59A-23-1		ign	x	0.001503	0.000040	0.0444	0.0013	0.280826	0.000049	1.467170	0.000059	8	3067	14	-2.4	1.7	3238	8	1.5	1.7
July 7 2021	19BN59A-75-1		ign	x	0.000652	0.000043	0.0181	0.0012	0.280790	0.000046	1.467153	0.000067	8	3025	15	-2.9	1.6	3238	8	2.1	1.6
July 7 2021	19BN59A-104-1		ign	x	0.00111	0.00014	0.0321	0.0044	0.280800	0.000043	1.467234	0.000058	12	3019	12	-3.6	1.6	3238	8	1.4	1.6
July 7 2021	19BN59A-5-1	x	ign		0.00121	0.00020	0.0365	0.0063	0.280803	0.000046	1.467169	0.000078	11	3185	20	0.1	1.7				
July 7 2021	19BN59A-32-1	x	ign		0.001053	0.000033	0.0303	0.0012	0.280786	0.000065	1.467196	0.000073	11	3101	17	-2.1	2.3				
July 7 2021	19BN59A-39-1	x	ign		0.00121	0.00029	0.0377	0.0091	0.280826	0.000063	1.467167	0.000094	12	3163	25	0.4	2.3				
July 7 2021	19BN59A-42-1	x	ign		0.00123	0.00015	0.0355	0.0046	0.280823	0.000060	1.467219	0.000065	6	3059	23	-2.1	2.2				
July 7 2021	19BN59A-44-1	x	ign		0.00099	0.00014	0.0296	0.0048	0.280814	0.000054	1.467162	0.000075	10	3286	59	3.3	1.9				
July 7 2021	19BN59A-55-1	x	met		0.000416	0.000007	0.01352	0.00012	0.280877	0.000041	1.467238	0.000065	12	2696	34	-6.9	1.5				
July 7 2021	19BN59A-69-1	x	ign		0.00072	0.00021	0.0227	0.0068	0.280802	0.000050	1.467212	0.000093	12	3172	96	0.8	1.8				
July 7 2021	19BN59A-98-1	x	ign		0.000887	0.000073	0.0251	0.0022	0.280801	0.000042	1.467191	0.000076	8	2805	22	-8.0	1.5				
July 7 2021	19BN59A-101-1	x	ign		0.000932	0.000069	0.0268	0.0020	0.280825	0.000061	1.467263	0.000080	8	3040	28	-1.9	2.2				
July 7 2021	19BN59A-71-1	x	ign		0.00130	0.00014	0.0385	0.0045	0.280871	0.000057	1.467183	0.000064	8	3141	12	1.3	2.1				
July 7 2021	19BN59A-43-1	x	ign		0.00054	0.00014	0.0152	0.0042	0.280782	0.000057	1.467183	0.000064	11	3113	13	-0.9	2.1				
July 7 2021	19BN59A-116-1	x	ign		0.00142	0.00013	0.0407	0.0042	0.280833	0.000047	1.467195	0.000080	10	3103	12	-1.2	1.7				
July 7 2021	19BN59A-88-1	x	ign		0.001467	0.000059	0.0436	0.0020	0.280816	0.000046	1.467257	0.000074	10	3195	13	0.2	1.6				
July 7 2021	19BN59A-24-1	x	ign		0.000926	0.000058	0.0265	0.0018	0.280806	0.000045	1.467183	0.000048	8	3204	15	1.2	1.6				
July 7 2021	19BN59A-34-1	x	ign		0.001216	0.000054	0.0340	0.0015	0.280868	0.000054	1.467148	0.000065	11	2925	15	-3.5	1.9				

Session	Spot ID	Scn	Class	In WM									At 207Pb/206Pb Date				At Rock Age				
					176Lu 177Hf	2SE	176Yb 177Hf	2SE	176Hf 177Hf	2SE	178Hf 177Hf	2SE	Total Hf (V)	Date (Ma)	2σ	εHf(t)	2SE	Age (Ma)	2σ	εHf(i)	2SE
July 7 2021	19BN59A-22-1	x	ign		0.00134	0.00012	0.0394	0.0035	0.280785	0.000053	1.467204	0.000080	12	2905	14	-7.2	1.9				
July 7 2021	19BN59A-50-1	x	ign		0.00126	0.00023	0.0368	0.0071	0.280746	0.000088	1.46715	0.00010	6	3221	12	-1.2	3.2				
July 7 2021	19BN59A-65-1	x	ign		0.00090	0.00010	0.0247	0.0029	0.280815	0.000086	1.467141	0.000084	5	3191	15	1.3	3.1				
July 7 2021	QM10A-32-1		ign	x	0.000327	0.000035	0.00854	0.00090	0.280706	0.000040	1.467230	0.000060	13	3211	14	-0.8	1.4	3224	9	-0.5	1.4
July 7 2021	QM10A-47-1		ign	x	0.001399	0.000073	0.0447	0.0023	0.280806	0.000046	1.467189	0.000069	11	3209	13	0.3	1.6	3224	9	0.7	1.6
July 7 2021	QM10A-35-1		ign	x	0.001328	0.000037	0.0429	0.0017	0.280851	0.000046	1.467288	0.000088	12	3208	16	2.1	1.6	3224	9	2.4	1.6
July 7 2021	QM10A-10-1		ign	x	0.00052	0.00017	0.0144	0.0054	0.280750	0.000037	1.467145	0.000077	11	3207	13	0.2	1.4	3224	9	0.6	1.4
July 7 2021	QM10A-29-1		ign	x	0.0002778	0.0000088	0.00679	0.00011	0.280745	0.000048	1.467269	0.000056	14	3199	12	0.4	1.7	3224	9	1.0	1.7
July 7 2021	QM10A-20-1		ign	x	0.00072	0.00027	0.0210	0.0083	0.280780	0.000046	1.467273	0.000072	11	3194	14	0.6	1.7	3224	9	1.2	1.7
July 7 2021	QM10A-15-1		ign	x	0.00196	0.00020	0.0642	0.0064	0.280839	0.000066	1.467199	0.000077	10	3189	14	-0.2	2.4	3224	9	0.6	2.4
July 7 2021	QM10A-16-1		ign	x	0.000243	0.000004	0.00632	0.00012	0.280684	0.000034	1.467215	0.000086	14	3185	13	-2.0	1.2	3224	9	-1.1	1.2
July 7 2021	QM10A-2-1		ign	x	0.00082	0.00016	0.0220	0.0047	0.280765	0.000049	1.467236	0.000063	10	3183	13	-0.4	1.8	3224	9	0.5	1.8
July 7 2021	QM10A-58-1		ign	x	0.00131	0.00012	0.0415	0.0041	0.280798	0.000049	1.467204	0.000062	9	3180	12	-0.4	1.8	3224	9	0.6	1.8
July 7 2021	QM10A-39-1		ign	x	0.00088	0.00021	0.0255	0.0071	0.280760	0.000042	1.467229	0.000081	13	3177	13	-0.9	1.6	3224	9	0.2	1.6
July 7 2021	QM10A-4-1		ign	x	0.000414	0.000024	0.01047	0.00069	0.280780	0.000046	1.467131	0.000052	10	3167	12	0.6	1.6	3224	9	1.9	1.6
July 7 2021	QM10A-34-1		ign	x	0.001779	0.000091	0.0578	0.0034	0.280833	0.000068	1.467201	0.000061	11	3159	12	-0.7	2.4	3224	9	0.8	2.4
July 7 2021	QM10A-11-1		ign	x	0.000313	0.000032	0.0084	0.0011	0.280778	0.000048	1.467305	0.000098	11	3143	15	0.2	1.7	3224	9	2.1	1.7
July 7 2021	QM10A-21-1		ign	x	0.00093	0.00023	0.0294	0.0074	0.280784	0.000075	1.467273	0.000077	13	3142	15	-1.0	2.7	3224	9	0.9	2.7
July 7 2021	QM10A-18-1		ign	x	0.000460	0.000046	0.0136	0.0015	0.280739	0.000049	1.467202	0.000094	14	3125	15	-2.0	1.7	3224	9	0.4	1.7
July 7 2021	QM10A-56-1		ign	x	0.00088	0.00020	0.0274	0.0071	0.280762	0.000079	1.467186	0.000066	12	3124	15	-2.1	2.8	3224	9	0.2	2.8
July 7 2021	QM10A-6-1		ign	x	0.00098	0.00014	0.0303	0.0050	0.280746	0.000048	1.467209	0.000077	10	3123	13	-2.9	1.7	3224	9	-0.5	1.7
July 7 2021	QM10A-45-1		ign	x	0.001300	0.000026	0.0414	0.0013	0.280795	0.000044	1.467215	0.000049	9	3118	12	-1.9	1.6	3224	9	0.5	1.6
July 7 2021	QM10A-5-1		ign	x	0.00115	0.00020	0.0350	0.0063	0.280807	0.000041	1.467159	0.000065	10	3054	13	-2.6	1.5	3224	9	1.3	1.5
July 7 2021	QM10A-33-1	x	ign		0.001979	0.000079	0.0636	0.0026	0.280789	0.000059	1.46720	0.00012	10	3115	14	-3.6	2.1				
July 7 2021	QM10A-38-1	x	ign		0.00089	0.00023	0.0255	0.0070	0.280783	0.000043	1.467252	0.000077	13	3167	21	-0.3	1.6				
July 7 2021	QM10A-42-1	x	ign		0.00119	0.00055	0.038	0.018	0.280692	0.000058	1.467279	0.000061	14	3239	22	-2.6	2.4				
July 7 2021	QM10A-60-1	x	ign		0.000294	0.000029	0.00765	0.00056	0.280698	0.000082	1.46734	0.00016	14	3062	49	-4.5	2.9				
July 7 2021	QM10A-25-1	x	ign		0.002349	0.000062	0.0777	0.0026	0.28083	0.00013	1.467119	0.000095	12	3169	14	-1.8	4.6				
July 7 2021	QM10A-43-1	x	ign		0.00096	0.00027	0.0290	0.0081	0.280735	0.000071	1.467267	0.000085	13	3222	13	-0.9	2.6				
July 7 2021	QM10A-1-1	x	ign		0.00081	0.00011	0.0220	0.0030	0.280742	0.000039	1.467224	0.000069	11	3182	13	-1.3	1.4				
July 9 2021	QM2C-68-1		ign	x	0.00218	0.00013	0.0623	0.0036	0.280902	0.000071	1.46709	0.00010	11	3234	15	2.6	2.5	3225	8	2.4	2.5
July 7 2021	QM2C-6-1		ign	x	0.00084	0.00014	0.0246	0.0046	0.280810	0.000065	1.467192	0.000073	11	3227	15	2.1	2.3	3225	8	2.1	2.3
July 9 2021	QM2C-93-1		ign	x	0.002238	0.000052	0.0627	0.0020	0.280961	0.000057	1.467156	0.000062	10	3223	12	4.3	2.0	3225	8	4.4	2.0
July 9 2021	QM2C-65-1		ign	x	0.00139	0.00014	0.0380	0.0045	0.280872	0.000053	1.467167	0.000075	10	3215	13	2.8	1.9	3225	8	3.1	1.9
July 9 2021	QM2C-67-1		ign	x	0.00161	0.00038	0.048	0.012	0.280904	0.000075	1.467098	0.000068	11	3214	15	3.5	2.8	3225	8	3.7	2.8
July 7 2021	QM2C-7-1		ign	x	0.00123	0.00011	0.0350	0.0036	0.280849	0.000036	1.467162	0.000077	9	3212	13	2.3	1.3	3225	8	2.6	1.3

Session	Spot ID	Scn	Class	In WM									At 207Pb/206Pb Date				At Rock Age				
					176Lu 177Hf	2SE	176Yb 177Hf	2SE	176Hf 177Hf	2SE	178Hf 177Hf	2SE	Total Hf (V)	Date (Ma)	2σ	εHf(t)	2SE	Age (Ma)	2σ	εHf(i)	2SE
July 9 2021	QM2C-105-1		ign	x	0.00140	0.00024	0.0394	0.0075	0.280855	0.000064	1.467108	0.000081	12	3212	16	2.1	2.3	3225	8	2.4	2.3
July 9 2021	QM2C-24-1		ign	x	0.00164	0.00019	0.0460	0.0059	0.280882	0.000034	1.467203	0.000049	10	3209	12	2.5	1.3	3225	8	2.9	1.3
July 9 2021	QM2C-34-1		ign	x	0.000920	0.000050	0.0251	0.0015	0.280861	0.000058	1.467186	0.000067	12	3199	14	3.1	2.1	3225	8	3.7	2.1
July 9 2021	QM2C-111-1		ign	x	0.001401	0.000041	0.0380	0.0013	0.280926	0.000043	1.467165	0.000053	7	3199	12	4.4	1.5	3225	8	5.0	1.5
July 9 2021	QM2C-89-1		ign	x	0.00135	0.00012	0.0383	0.0040	0.280914	0.000057	1.467173	0.000080	9	3199	17	4.0	2.0	3225	8	4.6	2.0
July 9 2021	QM2C-102-1		ign	x	0.00127	0.00013	0.0358	0.0042	0.280839	0.000030	1.467088	0.000064	13	3199	13	1.5	1.1	3225	8	2.2	1.1
July 9 2021	QM2C-76-1		ign	x	0.00143	0.00016	0.0410	0.0049	0.280838	0.000057	1.467133	0.000062	9	3197	14	1.1	2.1	3225	8	1.8	2.1
July 9 2021	QM2C-100-1		ign	x	0.001666	0.000075	0.0460	0.0020	0.280881	0.000044	1.467154	0.000052	8	3196	12	2.1	1.6	3225	8	2.8	1.6
July 9 2021	QM2C-74-1		ign	x	0.00201	0.00022	0.0591	0.0072	0.280875	0.000066	1.467138	0.000072	10	3189	15	1.0	2.4	3225	8	1.8	2.4
July 9 2021	QM2C-81-1		ign	x	0.001584	0.000083	0.0445	0.0023	0.280861	0.000061	1.467209	0.000059	8	3186	13	1.4	2.2	3225	8	2.2	2.2
July 9 2021	QM2C-48-1		ign	x	0.00098	0.00012	0.0279	0.0037	0.280900	0.000074	1.46712	0.00012	11	3185	18	4.1	2.6	3225	8	5.0	2.6
July 9 2021	QM2C-33-1		ign	x	0.00184	0.00015	0.0523	0.0039	0.280841	0.000053	1.46718	0.00014	10	3183	20	0.0	1.9	3225	8	1.0	1.9
July 9 2021	QM2C-18-1		ign	x	0.00149	0.00018	0.0406	0.0055	0.280839	0.000063	1.467224	0.000072	8	3182	12	0.7	2.3	3225	8	1.7	2.3
July 9 2021	QM2C-70-1		ign	x	0.00066	0.00015	0.0186	0.0046	0.280823	0.000035	1.467145	0.000059	16	3182	14	1.9	1.3	3225	8	2.9	1.3
July 9 2021	QM2C-49-1		ign	x	0.001907	0.000078	0.0528	0.0022	0.280852	0.000041	1.467231	0.000076	8	3178	13	0.2	1.5	3225	8	1.2	1.5
July 9 2021	QM2C-46-1		ign	x	0.00149	0.00014	0.0425	0.0040	0.280908	0.000080	1.467193	0.000099	10	3151	13	2.5	2.9	3225	8	4.1	2.9
July 9 2021	QM2C-9-1		ign	x	0.00148	0.00037	0.042	0.011	0.280880	0.000055	1.46714	0.00010	12	3151	15	1.5	2.1	3225	8	3.1	2.1
July 9 2021	QM2C-83-1		ign	x	0.001089	0.000026	0.02918	0.00078	0.280838	0.000053	1.467156	0.000098	10	3137	16	0.5	1.9	3225	8	2.5	1.9
July 9 2021	QM2C-17-1		ign	x	0.001068	0.000024	0.0295	0.0013	0.280824	0.000055	1.467176	0.000082	13	3131	15	-0.1	2.0	3225	8	2.1	2.0
July 9 2021	QM2C-64-1		ign	x	0.000690	0.000013	0.01994	0.00060	0.280774	0.000066	1.46721	0.00010	13	3092	13	-2.0	2.4	3225	8	1.1	2.4
July 7 2021	QM2C-8-1		ign	x	0.00119	0.00010	0.0338	0.0031	0.280795	0.000052	1.46713	0.00010	9	3082	13	-2.5	1.9	3225	8	0.8	1.9
July 9 2021	QM2C-72-1		ign	x	0.000831	0.000037	0.0239	0.0012	0.280835	0.000066	1.467183	0.000066	12	3081	13	-0.3	2.4	3225	8	3.0	2.4
July 9 2021	QM2C-53-1		ign	x	0.001028	0.000050	0.0288	0.0015	0.280828	0.000046	1.467154	0.000063	10	3067	15	-1.3	1.6	3225	8	2.3	1.6
July 9 2021	QM2C-23-1		ign	x	0.00139	0.00012	0.0390	0.0043	0.280897	0.000076	1.467163	0.000078	10	3023	18	-0.6	2.7	3225	8	4.0	2.7
July 9 2021	QM2C-90-1		met		0.000641	0.000037	0.0192	0.0016	0.280930	0.000047	1.467187	0.000048	14	2944	12	0.3	1.7				
July 9 2021	QM2C-108-1		met		0.000233	0.000019	0.00710	0.00064	0.280861	0.000039	1.467131	0.000053	12	2928	12	-1.7	1.4				
July 9 2021	QM2C-61-1		met		0.000072	0.000013	0.00243	0.00037	0.280801	0.000051	1.467134	0.000078	12	2447	17	-14.8	1.8				
July 9 2021	QM2C-26-1	x	ign		0.00031	0.00017	0.0091	0.0052	0.280875	0.000057	1.467247	0.000091	12	2524	44	-10.8	2.1				
July 9 2021	QM2C-45-1	x	ign		0.00112	0.00013	0.0311	0.0043	0.280865	0.000083	1.467151	0.000079	8	3138	17	1.4	3.0				
July 9 2021	QM2C-69-1	x	ign		0.00095	0.00022	0.0273	0.0066	0.280818	0.000033	1.467160	0.000054	12	3074	25	-1.4	1.3				
July 9 2021	QM2C-98-1	x	ign		0.00094	0.00027	0.0272	0.0080	0.280844	0.000059	1.467120	0.000090	10	3219	20	2.9	2.2				
July 9 2021	QM2C-109-1	x	ign		0.00151	0.00025	0.0457	0.0082	0.280920	0.000054	1.467199	0.000082	13	3140	18	2.6	2.0				
July 9 2021	QM2C-110-1	x	ign		0.000597	0.000081	0.0173	0.0028	0.280810	0.000038	1.46714	0.00010	14	2902	19	-4.9	1.4				
July 7 2021	QM2C-2-1	x	ign		0.000865	0.000035	0.0235	0.0012	0.28084	0.00010	1.46708	0.00011	6	3211	14	2.8	3.6				
July 9 2021	QM2C-52-1	x	ign		0.001680	0.000130	0.0496	0.0043	0.28087	0.00010	1.46715	0.00010	10	3201	20	1.8	3.6				
July 9 2021	QM2C-85-1	x	ign		0.00201	0.00017	0.0596	0.0059	0.280902	0.000092	1.467144	0.000090	12	3174	15	1.6	3.3				
July 9 2021	QM2C-107-1	x	ign		0.00129	0.00024	0.0367	0.0075	0.280813	0.000036	1.467057	0.000072	13	3308	13	3.1	1.4				

Session	Spot ID	Scn	Class	In WM	At 207Pb/206Pb Date								At Rock Age								
					176Lu 177Hf	2SE	176Yb 177Hf	2SE	176Hf 177Hf	2SE	178Hf 177Hf	2SE	Total Hf (V)	Date (Ma)	2σ	εHf(t)	2SE	Age (Ma)	2σ	εHf(i)	2SE
July 9 2021	QM7C-4e		ign	x	0.00259	0.00022	0.0821	0.0076	0.280926	0.000075	1.467197	0.000073	11	3127	15	0.2	2.7	3123	7	0.1	2.7
July 12 2021	QM7C-38-1		ign	x	0.00249	0.00022	0.0792	0.0075	0.280904	0.000052	1.467268	0.000043	14	3125	13	-0.4	1.9	3123	7	-0.5	1.9
July 12 2021	QM7C-64-1		ign	x	0.002283	0.000095	0.0713	0.0027	0.280900	0.000061	1.467233	0.000078	13	3124	12	-0.1	2.2	3123	7	-0.2	2.2
July 12 2021	QM7C-49-1		ign	x	0.001205	0.000029	0.03611	0.00077	0.280880	0.000070	1.467181	0.000048	12	3123	11	1.4	2.5	3123	7	1.4	2.5
July 12 2021	QM7C-4-1		ign	x	0.00153	0.00018	0.0460	0.0059	0.280835	0.000072	1.467153	0.000062	13	3118	11	-1.0	2.6	3123	7	-0.9	2.6
July 12 2021	QM7C-13e		ign	x	0.00147	0.00019	0.0456	0.0065	0.280842	0.000045	1.467154	0.000082	12	3099	13	-1.0	1.7	3123	7	-0.5	1.7
July 9 2021	QM7C-11e		ign	x	0.00166	0.00012	0.0494	0.0044	0.280886	0.000073	1.467280	0.000067	10	3077	12	-0.4	2.6	3123	7	0.7	2.6
July 12 2021	QM7C-22e		ign	x	0.001111	0.000083	0.0305	0.0027	0.280858	0.000058	1.46712	0.00012	13	3073	12	-0.3	2.1	3123	7	0.8	2.1
July 12 2021	QM7C-79-1		ign	x	0.000508	0.000027	0.01440	0.00092	0.280797	0.000058	1.467186	0.000085	10	3051	12	-1.7	2.1	3123	7	0.0	2.1
July 12 2021	QM7C-15e		ign	x	0.001824	0.000094	0.0560	0.0031	0.280925	0.000079	1.467222	0.000071	11	3049	14	0.0	2.8	3123	7	1.7	2.8
July 12 2021	QM7C-20-1		ign	x	0.000985	0.000058	0.0299	0.0022	0.280836	0.000041	1.467137	0.000075	13	3039	12	-1.6	1.5	3123	7	0.3	1.5
July 12 2021	QM7C-20e		ign	x	0.000820	0.000150	0.0254	0.0048	0.280897	0.000071	1.46712	0.00018	15	3036	12	0.9	2.5	3123	7	2.9	2.5
July 12 2021	QM7C-60-1		ign	x	0.000588	0.000003	0.01486	0.00038	0.280833	0.000082	1.467169	0.000089	15	2999	15	-1.8	2.9	3123	7	1.1	2.9
July 12 2021	QM7C-21		ign	x	0.000627	0.000014	0.01636	0.00014	0.280821	0.000066	1.46706	0.00012	13	2989	12	-2.6	2.4	3123	7	0.6	2.4
July 9 2021	QM7C-7e		ign	x	0.00121	0.00024	0.0378	0.0074	0.280867	0.000033	1.467170	0.000065	11	2985	14	-2.2	1.3	3123	7	1.0	1.3
July 12 2021	QM7C-48-1		ign	x	0.000759	0.000025	0.0204	0.0011	0.280839	0.000046	1.467154	0.000052	13	2913	11	-3.9	1.6	3123	7	0.9	1.6
July 9 2021	QM7C-2e	x	ign		0.00111	0.00024	0.0338	0.0079	0.280854	0.000066	1.467256	0.000087	13	2984	13	-2.5	2.4				
July 9 2021	QM7C-5e	x	ign		0.00201	0.00042	0.064	0.014	0.280933	0.000040	1.467239	0.000078	11	2861	44	-4.2	1.6				
July 9 2021	QM7C-8e	x	ign		0.00121	0.00035	0.037	0.012	0.280898	0.000059	1.467270	0.000069	13	2943	25	-2.1	2.2				
July 9 2021	QM7C-9e	x	ign		0.000886	0.000082	0.0263	0.0033	0.280836	0.000036	1.467284	0.000065	13	3758	189	15.3	1.3				
July 9 2021	QM7C-10e	x	ign		0.00165	0.00025	0.0528	0.0082	0.280889	0.000059	1.467294	0.000066	11	2989	17	-2.2	2.2				
July 12 2021	QM7C-19e	x	ign		0.00125	0.00017	0.0395	0.0054	0.280886	0.000041	1.467254	0.000060	13	2977	26	-1.8	1.5				
July 12 2021	QM7C-28-1	x	ign		0.000768	0.000067	0.0208	0.0029	0.280885	0.000073	1.46732	0.00015	15	2907	69	-2.4	2.6				
July 12 2021	QM7C-48-2	x	ign		0.00208	0.00027	0.0671	0.0093	0.280928	0.000052	1.467232	0.000072	12	3056	21	-0.2	1.9				
July 12 2021	QM7C-59-1	x	ign		0.00227	0.00037	0.0740	0.0130	0.280849	0.000064	1.467149	0.000066	12	3092	19	-2.6	2.4				
July 12 2021	QM7C-67-1	x	ign		0.002137	0.000081	0.0684	0.0022	0.280924	0.000039	1.467246	0.000090	16	2845	14	-5.2	1.4				
July 12 2021	QM7C-93-1	x	ign		0.00108	0.00018	0.0327	0.0058	0.280852	0.000050	1.467163	0.000061	13	3222	69	3.0	1.8				
July 12 2021	QM7C-14e	x	ign		0.00121	0.00027	0.0382	0.0092	0.280849	0.000052	1.467275	0.000060	14	3007	14	-2.3	1.9				
July 12 2021	QM7C-96-1	x	ign		0.00112	0.00018	0.0328	0.0059	0.280877	0.000058	1.467234	0.000079	15	3053	14	-0.1	2.1				
July 12 2021	QM7C-16e	x	ign		0.001332	0.000074	0.0394	0.0029	0.280888	0.000055	1.46703	0.00017	13	2945	16	-2.6	2.0				
July 12 2021	QM7C-100-1	x	ign		0.00087	0.00015	0.0254	0.0048	0.280826	0.000042	1.467221	0.000089	12	3064	16	-1.1	1.5				
July 12 2021	QM7C-17e	x	ign		0.00179	0.00018	0.0553	0.0061	0.280851	0.000047	1.467118	0.000097	11	3059	12	-2.3	1.7				
July 9 2021	QM7C-6-1	x	ign		0.00190	0.00035	0.060	0.012	0.280942	0.000047	1.467161	0.000098	13	2992	16	-0.8	1.8				
July 12 2021	QM7C-83-1	x	ign		0.002243	0.000067	0.0705	0.0022	0.280910	0.000070	1.46707	0.00021	13	3062	14	-1.1	2.5				
July 9 2021	QM7C-1e	x	ign		0.00307	0.00033	0.098	0.010	0.28102	0.00010	1.467156	0.000071	12	3080	12	1.5	3.6				
July 12 2021	QM7C-18e	x	ign		0.00212	0.00024	0.0651	0.0070	0.280927	0.000082	1.46726	0.00011	12	3030	14	-0.9	3.0				
July 9 2021	QM7C-3e	x	ign		0.00199	0.00019	0.0595	0.0060	0.280894	0.000094	1.46715	0.00018	12	3094	13	-0.4	3.4				
July 12 2021	QM7C-12e	x	ign		0.00110	0.00041	0.035	0.014	0.280883	0.000091	1.467219	0.000094	14	3027	20	-0.4	3.3				
July 12 2021	QM7C-34-1	x	ign		0.00164	0.00031	0.051	0.011	0.28088	0.00011	1.467125	0.000098	14	3066	14	-0.8	4.0				
July 12 2021	QM7C-75-1	x	ign		0.00211	0.00025	0.0643	0.0077	0.280909	0.000091	1.46715	0.00011	11	3083	14	-0.4	3.3				

Spots labelled QM7C-#e, indicate analyses of the extra grains mounted for LASS-U-Pb-Hf. See zircon images.

Table B-8. SIMS zircon O isotope data and electron microprobe zircon trace-element data.

Session	Spot ID	Class	In Median	SIMS O Isotope Data				EPMA Trace-element Data		
				¹⁸ O ¹⁶ O	1σ %	δ ¹⁸ O (VSMOW) ‰	2σ ‰	Hf ppm	U ppm	Ca ppm
IP21012	MSB-36-1	ign	x	0.00201452	0.0093	4.65	0.19		343	35
IP21012	MSB-70-2	ign	x	0.00201571	0.0105	5.24	0.21	10330		37
IP21012	MSB-10-1	ign	x	0.00201598	0.0113	5.38	0.23	10059	263	19
IP21007	MSB-9-1	ign	x	0.00201601	0.0116	5.39	0.23	10048	226	19
IP21007	MSB-103-1	ign	x	0.00201611	0.0105	5.44	0.21	11906	324	22
IP21007	MSB-66-1	ign	x	0.00201612	0.0098	5.45	0.20	10260		18
IP21007	MSB-5-1	ign	x	0.00201614	0.0108	5.46	0.22	9471	63	
IP21012	MSB-69-1	ign	x	0.00201626	0.0095	5.51	0.19	11375	130	29
IP21012	MSB-73-1	ign	x	0.00201633	0.0099	5.55	0.20	8197	262	39
IP21007	MSB-26-2	ign	x	0.00201635	0.0106	5.56	0.21	11135	136	21
IP21007	MSB-64-1	ign	x	0.00201644	0.0124	5.61	0.25	10466	208	33
IP21007	MSB-39-1	ign	x	0.00201649	0.0099	5.63	0.20	11340	103	21
IP21007	MSB-17-1	ign	x	0.00201650	0.0096	5.63	0.19	11416	180	
IP21012	MSB-16-1	ign		0.00201632	0.0094	5.55	0.19	9331	696	
IP21012	MSB-76-1	inhrt		0.00201570	0.0123	5.24	0.25	10717	447	
IP21012	MSB-94-1	inhrt		0.00201480	0.0104	4.79	0.21	9102	70	
IP21012	MSB-50-1	ign		0.00201573	0.0092	5.25	0.18	9035	200	14
IP21007	MSB-37-2	ign		0.00201600	0.0103	5.38	0.21	10146		16
IP21012	MSB-79-1	inhrt		0.00201565	0.0129	5.21	0.26	10523	52	17
IP21007	MSB-100-1	ign		0.00201623	0.0111	5.50	0.22	9050	78	18
IP21012	MSB-89-1	ign		0.00201658	0.0114	5.68	0.23	9572	424	19
IP21012	MSB-90-1	inhrt		0.00201618	0.0111	5.47	0.22	10356	72	20
IP21007	MSB-1-1	inhrt		0.00201597	0.0109	5.37	0.22	8669	161	20
IP21012	MSB-24-2	ign		0.00201613	0.0096	5.45	0.19	10205	80	21
IP21007	MSB-27-1	inhrt		0.00201585	0.0098	5.31	0.20	9599	60	21
IP21007	MSB-65-1	ign		0.00201579	0.0117	5.28	0.23	10530	62	22
IP21007	MSB-18-1	ign		0.00201588	0.0102	5.33	0.20	10611	971	22
IP21007	MSB-2-1	inhrt		0.00201571	0.0106	5.24	0.21	8645	79	24
IP21007	MSB-22-1	inhrt		0.00201620	0.0108	5.49	0.22	9587	372	24
IP21012	MSB-88-2	ign		0.00201596	0.0106	5.37	0.21	9804	137	26
IP21012	MSB-70-1	inhrt		0.00201546	0.0092	5.12	0.18	14571	625	29
IP21012	MSB-28-1	ign		0.00201667	0.0108	5.72	0.22	9486	295	30
IP21012	MSB-1-2	ign		0.00201593	0.0108	5.35	0.22	11441	327	30
IP21012	MSB-61-1	inhrt		0.00201610	0.0104	5.44	0.21	8331	334	30
IP21012	MSB-52-2	ign		0.00201626	0.0119	5.52	0.24	11551	141	31
IP21012	MSB-26-1	inhrt		0.00201673	0.0096	5.75	0.19	9959	64	32
IP21012	MSB-3-1	ign		0.00201538	0.0099	5.08	0.20	11300	507	33
IP21012	MSB-92-2	ign		0.00201637	0.0095	5.57	0.19	10622	170	33
IP21007	MSB-29-1	ign		0.00201618	0.0116	5.47	0.23	11801	457	33
IP21012	MSB-104-1	ign		0.00201639	0.0100	5.58	0.20	11949	214	35
IP21007	MSB-77-1	ign		0.00201618	0.0129	5.48	0.26	12005	296	36
IP21012	MSB-80-1	ign		0.00201558	0.0096	5.17	0.19	12403	435	37
IP21007	MSB-24-1	ign		0.00201565	0.0106	5.21	0.21	11734	184	38
IP21012	MSB-47-1	met		0.00201609	0.0104	5.43	0.21	10677	773	17
IP21007	MSB-59-1	ign		0.00201607	0.0103	5.42	0.21	8707	142	43
IP21012	MSB-88-1	inhrt		0.00201621	0.0103	5.49	0.21	10471	438	43
IP21012	MSB-44-1	ign		0.00201609	0.0092	5.43	0.18	10134	151	59
IP21007	MSB-37-1	inhrt		0.00201573	0.0098	5.25	0.20	11822	317	71
IP21007	MSB-40-1	ign		0.00201530	0.0092	5.03	0.18	12475	461	100
IP21007	MSB-92-1	inhrt		0.00201618	0.0104	5.48	0.21	8090	254	140
IP21012	MSB-68-1	ign		0.00201656	0.0123	5.67	0.25	9456	379	145
IP21007	MSB-36-2	ign		0.00201583	0.0105	5.30	0.21	11082	167	389
IP21007	MSB-84-1	inhrt		0.00201557	0.0168	5.17	0.34	8439	814	422
IP21012	MSB-84-2	ign		0.00201605	0.0092	5.41	0.18	10828	196	700
IP21012	MSB-52-1	inhrt		0.00201616	0.0107	5.46	0.21	9638	529	1142
IP21007	MSB-22-2	ign		0.00201642	0.0107	5.59	0.21	11042	444	1428
IP21012	MSB-4-1	inhrt		0.00201574	0.0098	5.25	0.20	10424	750	1588

Spots labelled as sampleID-grain#-spot#.

Class: Analyses classified as igneous (ign), inherited (inhrt) or metamorphic (met).

In Median: An "X" indicates analyses plotted on Figure 2-2C of the main text and included in the median δ¹⁸O values for the sample.

Only O isotope data from domains with <40 ppm Ca were used.

Blank cells indicate EPMA trace-element analyses that were below detection limits.

VSMOW: Vienna Standard Mean Ocean Water.

Session	Spot ID	Class	In Median	SIMS O Isotope Data				EPMA Trace-element Data		
				18O	1σ	δ18O (VSMOW)	2σ	Hf	U	Ca
				16O	%	‰	‰	ppm	ppm	ppm
IP21007	QM17C-53-1	ign	x	0.00201648	0.0098	5.62	0.20	11570	804	
IP21007	QM17C-14-1	ign	x	0.00201678	0.0101	5.78	0.20	9746	417	16
IP21007	QM17C-60-1	ign	x	0.00201685	0.0131	5.81	0.26	8942	55	17
IP21012	QM17C-80-1	ign	x	0.00201662	0.0098	5.69	0.20	9286	1103	17
IP21012	QM17C-76-2	ign	x	0.00201586	0.0113	5.31	0.23	13944	1001	20
IP21007	QM17C-29-1	ign	x	0.00201654	0.0095	5.66	0.19	10245	317	21
IP21012	QM17C-65-1	ign	x	0.00201603	0.0103	5.40	0.21	12631	360	22
IP21007	QM17C-21-1	ign	x	0.00201621	0.0134	5.49	0.27	11065	265	24
IP21007	QM17C-94-1	ign	x	0.00201690	0.0091	5.83	0.18	12365	881	26
IP21007	QM17C-32-1	ign	x	0.00201653	0.0090	5.65	0.18	11715	706	27
IP21007	QM17C-95-1	ign	x	0.00201594	0.0088	5.36	0.18	11272	1008	27
IP21007	QM17C-2-1	ign	x	0.00201748	0.0108	6.13	0.22	9566	1186	30
IP21012	QM17C-42-1	ign	x	0.00201701	0.0106	5.89	0.21	9662	679	38
IP21007	QM17C-53-2	met		0.00201707	0.0115	5.92	0.23	12218	145	24
IP21007	QM17C-32-2	met		0.00201709	0.0106	5.93	0.21	12101	300	24
IP21007	QM17C-94-2	met		0.00201690	0.0102	5.83	0.20	12699	298	28
IP21012	QM17C-61-1	ign		0.00201559	0.0091	5.18	0.18	9074	367	48
IP21007	QM17C-87-1	ign		0.00201674	0.0092	5.75	0.18	9983	1290	49
IP21007	QM17C-38-1	ign		0.00201603	0.0095	5.40	0.19	13415	315	54
IP21012	QM17C-6-1	ign		0.00201663	0.0110	5.70	0.22	11747	162	55
IP21012	QM17C-72-1	ign		0.00201568	0.0101	5.22	0.20	14646	580	64
IP21007	QM17C-57-1	ign		0.00201632	0.0096	5.55	0.19	8643	325	70
IP21012	QM17C-82-1	ign		0.00201641	0.0091	5.59	0.18	8403	775	97
IP21007	QM17C-54-1	ign		0.00201697	0.0091	5.87	0.18	12069	401	110
IP21007	QM17C-8-1	ign		0.00201626	0.0104	5.52	0.21	12603	407	132
IP21007	QM17C-40-1	met		0.00201704	0.0095	5.91	0.19	12024	157	139
IP21007	QM17C-19-1	ign		0.00201568	0.0105	5.23	0.21	14004	423	187
IP21012	QM17C-35-1	ign		0.00201570	0.0106	5.24	0.21	12721	804	425
IP21012	QM17C-76-1	ign		0.00201655	0.0097	5.66	0.19	11639	1171	477
IP21007	QM17C-91-1	ign		0.00201602	0.0108	5.39	0.22	11348	879	1349
IP21007	QM17C-70-1	ign		0.00201581	0.0104	5.29	0.21	11203	1149	3749
IP21012	QM17C-84-1	ign		0.00201639	0.0098	5.58	0.20	10464	1012	6331
IP21012	QM17C-33-1	ign		0.00201652	0.0099	5.64	0.20		not measured	
IP21012	QM17C-22-1	ign		0.00201628	0.0101	5.53	0.20		not measured	
IP21007	19BN59A-13-1	ign	x	0.00201633	0.0109	5.55	0.22	8021		17
IP21007	19BN59A-103-1	ign	x	0.00201480	0.0104	4.79	0.21	8009	70	20
IP21012	19BN59A-87-1	ign	x	0.00201578	0.0115	5.27	0.23	12754	270	21
IP21007	19BN59A-116-1	ign	x	0.00201480	0.0089	4.79	0.18	8250	107	22
IP21007	19BN59A-44-1	ign	x	0.00201489	0.0095	4.83	0.19	8346	184	23
IP21007	19BN59A-39-1	ign	x	0.00201563	0.0092	5.20	0.18	8109	136	25
IP21007	19BN59A-35-1	ign	x	0.00201593	0.0098	5.35	0.20	8264	71	26
IP21012	19BN59A-80-1	ign	x	0.00201461	0.0120	4.69	0.24	8623	127	26
IP21007	19BN59A-59-1	ign	x	0.00201577	0.0101	5.27	0.20	9357	431	28
IP21012	19BN59A-77-1	ign	x	0.00201556	0.0103	5.17	0.21	9109	179	28
IP21007	19BN59A-12-1	ign	x	0.00201598	0.0111	5.37	0.22	10123	101	28
IP21012	19BN59A-5-1	ign	x	0.00201626	0.0104	5.52	0.21	8614	144	29
IP21007	19BN59A-65-1	ign	x	0.00201579	0.0097	5.28	0.19	8175	139	31
IP21007	19BN59A-107-2	ign	x	0.00201393	0.0121	4.35	0.24	9925	406	31
IP21012	19BN59A-36-1	ign	x	0.00201595	0.0104	5.36	0.21	8240	231	32
IP21012	19BN59A-83-1	ign	x	0.00201533	0.0092	5.05	0.18	8213	116	32
IP21007	19BN59A-70-1	ign	x	0.00201497	0.0100	4.87	0.20	8058	171	34
IP21012	19BN59A-57-1	ign	x	0.00201368	0.0116	4.23	0.23	9292	269	35
IP21012	19BN59A-24-1	ign	x	0.00201522	0.0092	5.00	0.18	8402		36
IP21007	19BN59A-51-1	ign	x	0.00201537	0.0113	5.07	0.23	9477	374	36
IP21012	19BN59A-17-2	ign	x	0.00201444	0.0102	4.61	0.20	6310		
IP21007	19BN59A-30-3	met		0.00201340	0.0106	4.09	0.21	10972		16
IP21007	19BN59A-55-1	met		0.00201389	0.0092	4.33	0.18	10609		19
IP21007	19BN59A-17-1	met		0.00201394	0.0110	4.36	0.22	11146		31
IP21007	19BN59A-6-2	met		0.00201272	0.0092	3.75	0.18	10819		31
IP21007	19BN59A-30-1	met		0.00201295	0.0089	3.87	0.18	11131		31
IP21012	19BN59A-76-2	met		0.00201432	0.0118	4.55	0.24	11219	49	31
IP21012	19BN59A-88-1	ign		0.00201570	0.0104	5.24	0.21	9073	146	45
IP21007	19BN59A-33-1	ign		0.00201386	0.0093	4.32	0.19	12839	55	50

Session	Spot ID	Class	In Median	SIMS O Isotope Data				EPMA Trace-element Data		
				¹⁸ O	1σ	δ ¹⁸ O (VSMOW)	2σ	Hf	U	Ca
				16O	%	‰	‰	ppm	ppm	ppm
IP21012	19BN59A-52-1	ign		0.00201465	0.0092	4.71	0.18	8946	122	55
IP21012	19BN59A-86-1	ign		0.00201578	0.0095	5.28	0.19	9402	226	60
IP21012	19BN59A-28-1	ign		0.00201628	0.0101	5.53	0.20	9147	240	61
IP21012	19BN59A-75-1	ign		0.00201478	0.0112	4.78	0.22	9578	59	62
IP21012	19BN59A-58-2	met		0.00201419	0.0105	4.48	0.21	10989	66	64
IP21007	19BN59A-109-1	ign		0.00201505	0.0094	4.91	0.19	8947	114	79
IP21007	19BN59A-6-1	ign		0.00201390	0.0111	4.34	0.22	9601	173	81
IP21012	19BN59A-22-1	ign		0.00201564	0.0093	5.21	0.19	11299	461	81
IP21012	19BN59A-104-1	ign		0.00201458	0.0110	4.68	0.22	9400	345	91
IP21012	19BN59A-110-1	ign		0.00201434	0.0095	4.56	0.19	8399	134	94
IP21012	19BN59A-76-1	ign		0.00201517	0.0111	4.97	0.22	8684	168	105
IP21007	19BN59A-23-1	ign		0.00201550	0.0126	5.14	0.25	8585	147	114
IP21007	19BN59A-71-2	met		0.00201370	0.0119	4.24	0.24	10468		138
IP21007	19BN59A-29-2	met		0.00201311	0.0093	3.94	0.19	11048	54	151
IP21012	19BN59A-58-1	ign		0.00201443	0.0092	4.60	0.18	10304	111	152
IP21012	19BN59A-117-1	ign		0.00201500	0.0102	4.89	0.20	8990	200	159
IP21007	19BN59A-33-2	met		0.00201339	0.0089	4.08	0.18	10886	79	203
IP21007	19BN59A-107-1	ign		0.00201387	0.0101	4.33	0.20	8473	458	245
IP21007	19BN59A-30-2	ign		0.00201344	0.0195	4.11	0.39	9273	239	258
IP21012	19BN59A-40-2	ign		0.00201437	0.0104	4.57	0.21	10042	111	289
IP21012	19BN59A-43-1	ign		0.00201574	0.0093	5.26	0.19	9046	242	300
IP21007	19BN59A-21-1	ign		0.00201600	0.0097	5.39	0.19	8273	106	301
IP21012	19BN59A-42-1	ign		0.00201367	0.0092	4.22	0.18	8288	234	411
IP21012	19BN59A-3-1	ign		0.00201592	0.0094	5.35	0.19	8177	171	503
IP21012	19BN59A-40-1	ign		0.00201386	0.0094	4.32	0.19	10067	926	725
IP21012	19BN59A-50-1	ign		0.00201461	0.0109	4.69	0.22	8396	407	1108
IP21007	19BN59A-71-1	ign		0.00201375	0.0097	4.26	0.19	8083	290	1556
IP21012	19BN59A-7-1	ign		0.00201427	0.0098	4.52	0.20	8727	247	3010
IP21007	19BN59A-29-1	ign		0.00201412	0.0093	4.45	0.19	9328	192	3403
IP21012	HBA-23-1	ign	x	0.00201628	0.0108	5.52	0.22	11079	472	
IP21007	HBA-8-2	ign	x	0.00201626	0.0089	5.52	0.18	12399	191	12
IP21012	HBA-24-1	ign	x	0.00201623	0.0099	5.50	0.20	8589	272	13
IP21012	HBA-4-1	ign	x	0.00201596	0.0099	5.37	0.20	10832	414	14
IP21007	HBA-74-1	ign	x	0.00201702	0.0090	5.89	0.18	11500	409	16
IP21007	HBA-7-1	ign	x	0.00201647	0.0089	5.62	0.18	8417	225	17
IP21007	HBA-53-1	ign	x	0.00201628	0.0090	5.53	0.18	9502	175	18
IP21007	HBA-37-1	ign	x	0.00201617	0.0102	5.47	0.20	11404	364	19
IP21007	HBA-55-1	ign	x	0.00201634	0.0100	5.56	0.20	10133	181	19
IP21007	HBA-3-1	ign	x	0.00201661	0.0104	5.69	0.21	8746	188	20
IP21007	HBA-60-2	ign	x	0.00201649	0.0098	5.63	0.20	12900	337	20
IP21007	HBA-20-1	ign	x	0.00201623	0.0089	5.50	0.18	9130	329	21
IP21007	HBA-93-1	ign	x	0.00201579	0.0113	5.28	0.23	10832	621	21
IP21007	HBA-26-1	ign	x	0.00201664	0.0092	5.70	0.18	9725	426	23
IP21007	HBA-77-1	ign	x	0.00201644	0.0112	5.60	0.22	9269	164	23
IP21007	HBA-76-1	ign	x	0.00201604	0.0090	5.41	0.18	11200	443	24
IP21012	HBA-40-1	ign	x	0.00201628	0.0116	5.53	0.23	9481	210	25
IP21012	HBA-90-1	ign	x	0.00201669	0.0117	5.73	0.23	9388	542	25
IP21012	HBA-59-1	ign	x	0.00201628	0.0092	5.53	0.18	10648	312	26
IP21007	HBA-78-1	ign	x	0.00201595	0.0103	5.36	0.21	11595	205	26
IP21007	HBA-12-1	ign	x	0.00201635	0.0097	5.56	0.19	8661	292	27
IP21007	HBA-8-1	ign	x	0.00201662	0.0089	5.70	0.18	10236	383	29
IP21007	HBA-44-3	ign	x	0.00201626	0.0104	5.52	0.21	10578	569	29
IP21012	HBA-21-1	ign	x	0.00201641	0.0110	5.59	0.22	10961	556	30
IP21007	HBA-46-1	ign	x	0.00201600	0.0109	5.39	0.22	9347	252	34
IP21012	HBA-18-1	ign	x	0.00201641	0.0100	5.59	0.20	9743	165	36
IP21007	HBA-44-2	ign	x	0.00201648	0.0106	5.63	0.21	8938	311	36
IP21007	HBA-44-1	ign	x	0.00201662	0.0102	5.70	0.20	11383	219	37
IP21007	HBA-72-1	ign	x	0.00201603	0.0101	5.40	0.20	12310	133	37
IP21007	HBA-34-2	met		0.00201678	0.0122	5.78	0.24	11372	86	20
IP21007	HBA-46-2	met		0.00201671	0.0099	5.74	0.20	11530	55	35
IP21007	HBA-34-1	met?		0.00201636	0.0090	5.57	0.18	11582	412	22
IP21007	HBA-28-1	inhrt		0.00201734	0.0099	6.06	0.20	8250	227	35
IP21012	HBA-29-1	ign		0.00201649	0.0106	5.63	0.21	9335	473	46

Session	Spot ID	Class	In Median	SIMS O Isotope Data				EPMA Trace-element Data		
				18O	1σ	δ18O (VSMOW)	2σ	Hf	U	Ca
				16O	%	‰	‰	ppm	ppm	ppm
IP21007	HBA-8-3	ign		0.00201579	0.0098	5.28	0.20	12185	273	76
IP21007	HBA-75-1	ign		0.00201652	0.0091	5.65	0.18	10132	363	84
IP21012	HBA-30-1	ign		0.00201632	0.0100	5.54	0.20	10320	537	99
IP21007	HBA-28-2	ign		0.00201636	0.0096	5.56	0.19	12318	338	282
IP21007	HBA-36-1	ign		0.00201641	0.0095	5.59	0.19	10244	501	136
IP21012	HBA-42-1	ign		0.00201675	0.0109	5.76	0.22	9151	541	103
IP21007	HBA-60-1	ign		0.00201669	0.0100	5.73	0.20	10786	98	102
IP21007	QM10A-11-2	ign	x	0.00201695	0.0108	5.86	0.22	8939	110	16
IP21012	QM10A-10-1	ign	x	0.00201685	0.0108	5.81	0.22	9037	150	17
IP21007	QM10A-29-1	ign	x	0.00201664	0.0091	5.71	0.18	11249	182	20
IP21007	QM10A-35-1	ign	x	0.00201671	0.0091	5.74	0.18	8717	266	21
IP21012	QM10A-43-1	ign	x	0.00201663	0.0096	5.70	0.19	11080	102	21
IP21007	QM10A-47-1	ign	x	0.00201693	0.0106	5.85	0.21	8267	171	23
IP21012	QM10A-5-1	ign	x	0.00201667	0.0109	5.72	0.22	9837	80	24
IP21007	QM10A-32-1	ign	x	0.00201617	0.0106	5.47	0.21	12140	97	26
IP21012	QM10A-24-1	ign	x	0.00201680	0.0120	5.78	0.24	8708	165	27
IP21007	QM10A-11-1	ign	x	0.00201688	0.0090	5.82	0.18	9303	165	29
IP21007	QM10A-20-1	ign	x	0.00201621	0.0106	5.49	0.21	9856	164	29
IP21007	QM10A-42-1	ign	x	0.00201677	0.0091	5.77	0.18	9894	101	29
IP21007	QM10A-58-1	ign	x	0.00201662	0.0105	5.70	0.21	8832	154	30
IP21007	QM10A-15-1	ign	x	0.00201672	0.0101	5.75	0.20	8911	206	30
IP21007	QM10A-25-1	ign	x	0.00201672	0.0090	5.75	0.18	8554	274	31
IP21007	QM10A-45-1	ign	x	0.00201664	0.0099	5.70	0.20	8638	157	32
IP21012	QM10A-60-1	ign	x	0.00201675	0.0101	5.76	0.20	9986	82	32
IP21007	QM10A-56-1	ign	x	0.00201692	0.0102	5.84	0.20	8910	230	35
IP21007	QM10A-21-1	ign	x	0.00201635	0.0100	5.56	0.20	9944	94	39
IP21007	QM10A-18-1	ign		0.00201642	0.0112	5.60	0.22	10565	144	44
IP21007	QM10A-62-1	ign		0.00201643	0.0091	5.60	0.18	9268	186	51
IP21012	QM10A-38-1	ign		0.00201665	0.0101	5.71	0.20	11026	126	72
IP21007	QM10A-8-1	ign		0.00201703	0.0095	5.90	0.19	8437	310	122
IP21007	QM10A-1-1	ign		0.00201624	0.0098	5.51	0.20	11515	189	208
IP21007	QM10A-8-2	met		0.00201700	0.0091	5.88	0.18	1746		
IP21007	QM10A-62-2	met		0.00201655	0.0093	5.66	0.19	7338		219
IP21007	QM7C-48-1	ign	x	0.00201640	0.0097	5.59	0.19	11027	882	19
IP21007	QM7C-100-1	ign	x	0.00201647	0.0100	5.62	0.20	9406	780	27
IP21007	QM7C-30-1	ign	x	0.00201624	0.0091	5.50	0.18	10975	1036	32
IP21007	QM7C-87-1	ign	x	0.00201669	0.0097	5.73	0.19	8814	397	34
IP21007	QM7C-105-1	ign	x	0.00201652	0.0092	5.65	0.18	8357	528	37
IP21007	QM7C-6-2	ign		0.00201571	0.0105	5.24	0.21	10479	705	41
IP21007	QM7C-62-1	ign		0.00201641	0.0097	5.59	0.19	13047	650	50
IP21007	QM7C-79-1	ign		0.00201703	0.0089	5.90	0.18	10279	188	52
IP21007	QM7C-105-2	ign		0.00201689	0.0089	5.83	0.18	9833	547	53
IP21012	QM7C-14-1	ign		0.00201643	0.0103	5.60	0.21	10227	760	55
IP21007	QM7C-11-1	ign		0.00201613	0.0097	5.45	0.19	11904	866	56
IP21012	QM7C-59-1	ign		0.00201591	0.0095	5.34	0.19	8992	780	96
IP21007	QM7C-96-1	ign		0.00201615	0.0089	5.46	0.18	10653	1039	97
IP21007	QM7C-20-1	ign		0.00201641	0.0110	5.59	0.22	8571	640	953
IP21007	QM7C-34-1	ign		0.00201633	0.0099	5.55	0.20	10012	1144	3000
IP21012	QM7C-38-1	ign		0.00201633	0.0112	5.55	0.22	5290	415	1242
IP21012	QM7C-45-1	ign		0.00201653	0.0102	5.65	0.20	9303	732	463
IP21007	QM7C-49-1	ign		0.00201666	0.0101	5.71	0.20	9928	549	167
IP21007	QM7C-60-1	ign		0.00201573	0.0091	5.25	0.18	10926	601	171
IP21007	QM7C-63-1	ign		0.00201662	0.0089	5.70	0.18	8893	929	733
IP21007	QM7C-64-1	ign		0.00201655	0.0107	5.66	0.21	10023	1151	2218
IP21012	QM7C-67-1	ign		0.00201586	0.0107	5.31	0.21	10464	1184	4416
IP21007	QM7C-75-1	ign		0.00201637	0.0095	5.57	0.19	8074	661	350
IP21007	QM7C-83-1	ign		0.00201628	0.0100	5.53	0.20	8740	1116	3686
IP21007	QM7C-93-1	ign		0.00201625	0.0089	5.51	0.18	8747	1217	342
IP21007	QM7C-4-1	ign		0.00201673	0.0093	5.75	0.19	9762	753	186
IP21007	QM7C-6-1	ign		0.00201545	0.0091	5.11	0.18	8789	1928	1607
IP21007	QM7C-13-1	ign		0.00201627	0.0096	5.52	0.19	10280	1513	2385

Session	Spot ID	Class	In Median	SIMS O Isotope Data				EPMA Trace-element Data		
				18O	1σ	δ18O (VSMOW)	2σ	Hf	U	Ca
				16O	%	‰	‰	ppm	ppm	ppm
IP21007	QM2C-45-1	ign	x	0.00201629	0.0088	5.53	0.18	8655	74	16
IP21007	QM2C-7-1	ign	x	0.00201639	0.0090	5.58	0.18	7796	59	23
IP21007	QM2C-67-1	ign	x	0.00201611	0.0100	5.44	0.20	7836	175	23
IP21007	QM2C-6-1	ign	x	0.00201601	0.0090	5.39	0.18	7717	72	24
IP21007	QM2C-98-2	ign	x	0.00201631	0.0109	5.54	0.22	9969	157	24
IP21007	QM2C-2-1	ign	x	0.00201634	0.0098	5.56	0.20	8246	82	25
IP21007	QM2C-57-1	ign	x	0.00201599	0.0088	5.38	0.18	11737	397	25
IP21012	QM2C-110-1	ign	x	0.00201601	0.0127	5.39	0.25	11742	1102	25
IP21012	QM2C-12-1	ign	x	0.00201656	0.0093	5.67	0.19	7517		26
IP21012	QM2C-52-1	ign	x	0.00201610	0.0113	5.44	0.23	7402	94	26
IP21012	QM2C-18-1	ign	x	0.00201668	0.0093	5.72	0.19	14054	376	27
IP21007	QM2C-59-1	ign	x	0.00201618	0.0088	5.48	0.18	7896	247	28
IP21012	QM2C-74-1	ign	x	0.00201632	0.0101	5.55	0.20	8716	151	29
IP21012	QM2C-76-1	ign	x	0.00201613	0.0107	5.45	0.21	7674	84	29
IP21007	QM2C-8-1	ign	x	0.00201607	0.0090	5.42	0.18	8393	178	30
IP21007	QM2C-98-1	ign	x	0.00201635	0.0115	5.56	0.23	7472	75	30
IP21007	QM2C-100-1	ign	x	0.00201625	0.0109	5.51	0.22	7857	87	37
IP21007	QM2C-111-1	ign	x	0.00201581	0.0088	5.29	0.18	8159	172	37
IP21007	QM2C-49-1	ign?		0.00201738	0.0090	6.08	0.18	11993	515	21
IP21007	QM2C-11-1	met		0.00201678	0.0100	5.77	0.20	11530	209	25
IP21007	QM2C-5-2	met		0.00201716	0.0090	5.97	0.18	11885	975	28
IP21012	QM2C-90-1	met		0.00201713	0.0108	5.95	0.22	11424	758	31
IP21007	QM2C-35-1	met		0.00201725	0.0109	6.01	0.22	12826	1693	33
IP21007	QM2C-13-2	met		0.00201766	0.0111	6.21	0.22	10874	136	34
IP21007	QM2C-99-2	ign?		0.00201748	0.0088	6.13	0.18	12484	523	35
IP21007	QM2C-39-1	met		0.00201722	0.0099	5.99	0.20	12267	681	41
IP21007	QM2C-72-1	ign		0.00201756	0.0098	6.16	0.20	10178	304	49
IP21012	QM2C-71-2	met		0.00201703	0.0106	5.90	0.21	9828	229	51
IP21007	QM2C-23-1	ign		0.00201713	0.0089	5.95	0.18	7698	158	55
IP21007	QM2C-81-1	ign		0.00201661	0.0104	5.69	0.21	7634	100	56
IP21007	QM2C-13-1	met		0.00201741	0.0107	6.09	0.21	10742	112	111
IP21007	QM2C-11-2	met		0.00201689	0.0090	5.83	0.18	11428	587	118
IP21007	QM2C-57-2	met		0.00201761	0.0113	6.19	0.23	11656	723	131
IP21012	QM2C-71-1	ign		0.00201581	0.0100	5.29	0.20	8581	591	190
IP21007	QM2C-99-1	ign		0.00201627	0.0095	5.52	0.19	8594	654	209
IP21007	QM2C-59-2	met		0.00201576	0.0088	5.27	0.18	11366	361	295
IP21007	QM2C-5-1	ign		0.00201658	0.0108	5.68	0.22	13410	665	825

Table B-9. Whole-rock major- and trace-element data.

	3.3-3.1 Ga Perry River terrane granitoids								HBAJ692	
	19BN59A	TX08027	21BN05H	QM10A	QM2C	QM10B	QM17C	QM7C	A92	RF8649A
ICP-OES (wt.%)										
SiO ₂	67.05	67.53	60.17	52.88	70.44	70.12	71.03	68.01	63.22	65.11
Al ₂ O ₃	16.57	14.76	18.36	16.68	15.64	15.88	15.19	16.14	19.39	15.70
FeO(T)	4.03	5.14	6.16	11.59	3.02	2.87	2.62	4.06	4.52	4.32
MnO	0.059	0.077	0.101	0.125	0.052	0.041	0.035	0.065	0.039	0.064
MgO	1.35	1.84	2.73	3.60	0.91	1.01	1.00	1.42	1.16	2.77
CaO	4.61	4.46	4.60	8.65	3.99	3.51	3.21	4.50	4.35	4.55
Na ₂ O	4.69	3.81	4.81	3.85	4.34	4.26	4.05	3.81	5.49	4.67
K ₂ O	0.97	1.58	2.17	0.89	1.16	1.80	2.38	1.41	1.40	1.87
TiO ₂	0.546	0.662	0.742	1.554	0.327	0.405	0.358	0.446	0.309	0.682
P ₂ O ₅	0.13	0.14	0.15	0.18	0.12	0.11	0.11	0.13	0.12	0.27
LOI	0.35	0.83	0.68	0.14	0.27	0.3	0.36	1.13	0.72	0.43
Total	99.10	98.86	99.37	100.7	100.4	100.6	100.5	100.6	100.1	99.53
ICP-MS (ppm)										
Sc	9	12	16	20	4	6	5	8	3	8
V	56	100	115	367	33	43	39	41	36	68
Ga	21	18	24	26	19	18	20	19	25	17
Rb	22	44	55	4	28	26	54	33	62	68
Sr	276	216	193	393	234	244	408	233	663	593
Y	11.2	16.0	15.4	22.3	6.3	9.1	5.5	19.6	9.2	10.1
Zr	195	134	175	137	137	180	125	238	698	161
Nb	4.7	5.0	4.9	7.0	3.7	4.5	3.1	7.8	3.5	7.4
Cs	0.7	0.7	1.1		0.2	0.1	0.1	0.1	1.6	0.7
Ba	605	801	1253	514	451	1010	1489	1032	1334	723
La	35.8	30.2	21.6	31.5	25.1	50.2	30.6	54.6	288	41.1
Ce	58.2	56.4	38.5	61.9	40.3	87.3	53.9	91.1	439	77.5
Pr	6.05	6.23	4.32	7.01	3.86	8.53	5.63	9.11	40.3	8.47
Nd	20.6	23.8	16.3	26.0	12.9	29.00	19.3	30.8	123	30.6
Sm	3.58	4.70	3.59	5.35	2.10	4.55	2.97	5.44	11.9	4.85
Eu	1.06	1.09	1.21	1.17	0.76	0.842	0.905	1.08	1.80	1.15
Gd	2.82	3.50	3.16	4.57	1.59	3.26	1.88	4.17	4.97	3.19
Tb	0.40	0.50	0.48	0.73	0.22	0.43	0.25	0.62	0.46	0.42
Dy	2.16	3.10	2.78	4.31	1.20	2.06	1.27	3.63	1.99	2.17
Ho	0.42	0.60	0.58	0.84	0.21	0.37	0.20	0.70	0.33	0.35
Er	1.13	1.60	1.66	2.39	0.60	0.89	0.55	1.98	0.89	0.93
Tm	0.155	0.230	0.234	0.332	0.093	0.109	0.074	0.281	0.146	0.124
Yb	0.97	1.50	1.36	1.99	0.56	0.64	0.44	1.93	1.04	0.77
Lu	0.155	0.23	0.204	0.304	0.079	0.097	0.057	0.283	0.173	0.113
Hf	4.5	3.0	4.1	3.2	3.3	3.7	3.1	5.3	14.4	3.3
Pb	6	8	6	6	7	12	17	13	18	11
Th	4.8	12.0	3.1	0.7	1.4	15.0	8.6	19.0	70.2	4.6
U	0.26	0.40	0.25	0.06	0.22	0.60	0.50	1.11	1.68	0.31

Major elements are normalized to 100%, loss on ignition (LOI) excluded. Totals are reported as measured, with all Fe as Fe₂O₃.

ICP-OES major- and ICP-MS trace-element data acquired at Actlabs, with the 4Lithoresearch analytical package.

Analyses below detection limit left blank.

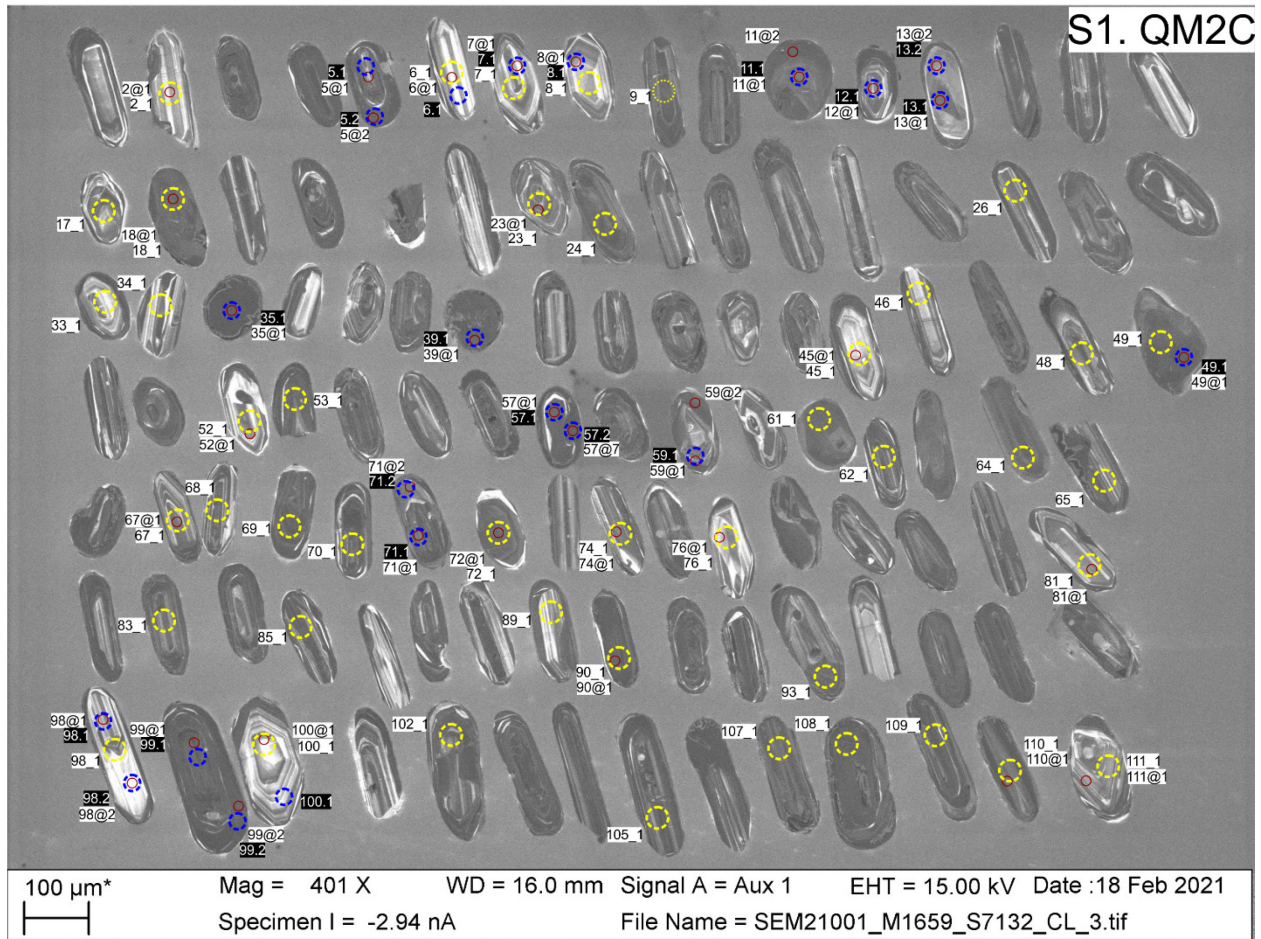
B.8 Zircon images and analytical spot locations

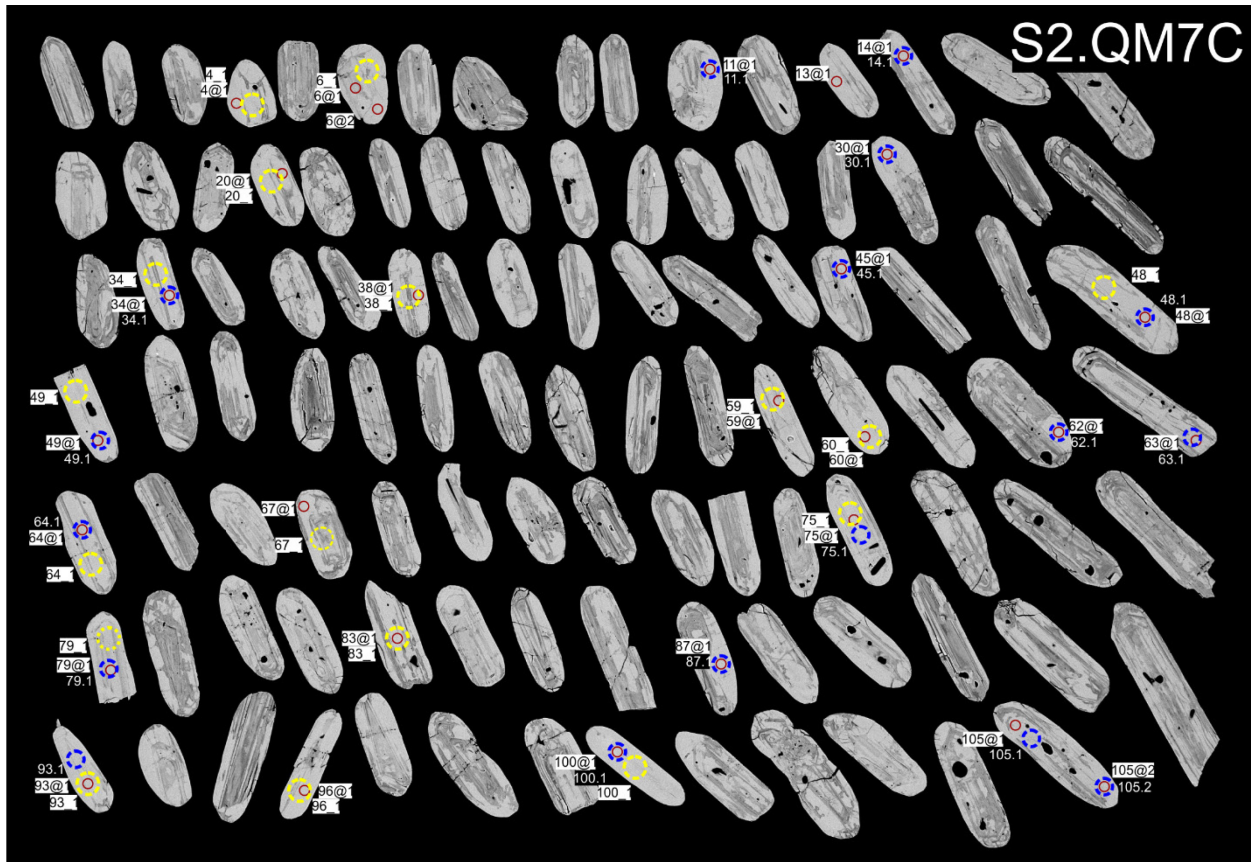
40@1  10 μm SIMS O spot

40_1  33 μm single stream LA-ICPMS Hf spot

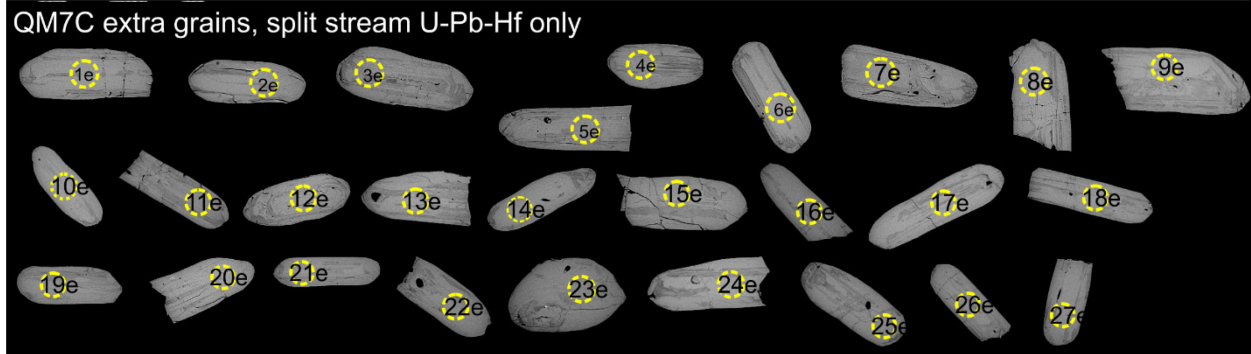
40.1  25 μm single stream LA-MC-ICPMS U-Pb spot

40_1  33 μm split stream LA-ICPMS U-Pb-Hf spot

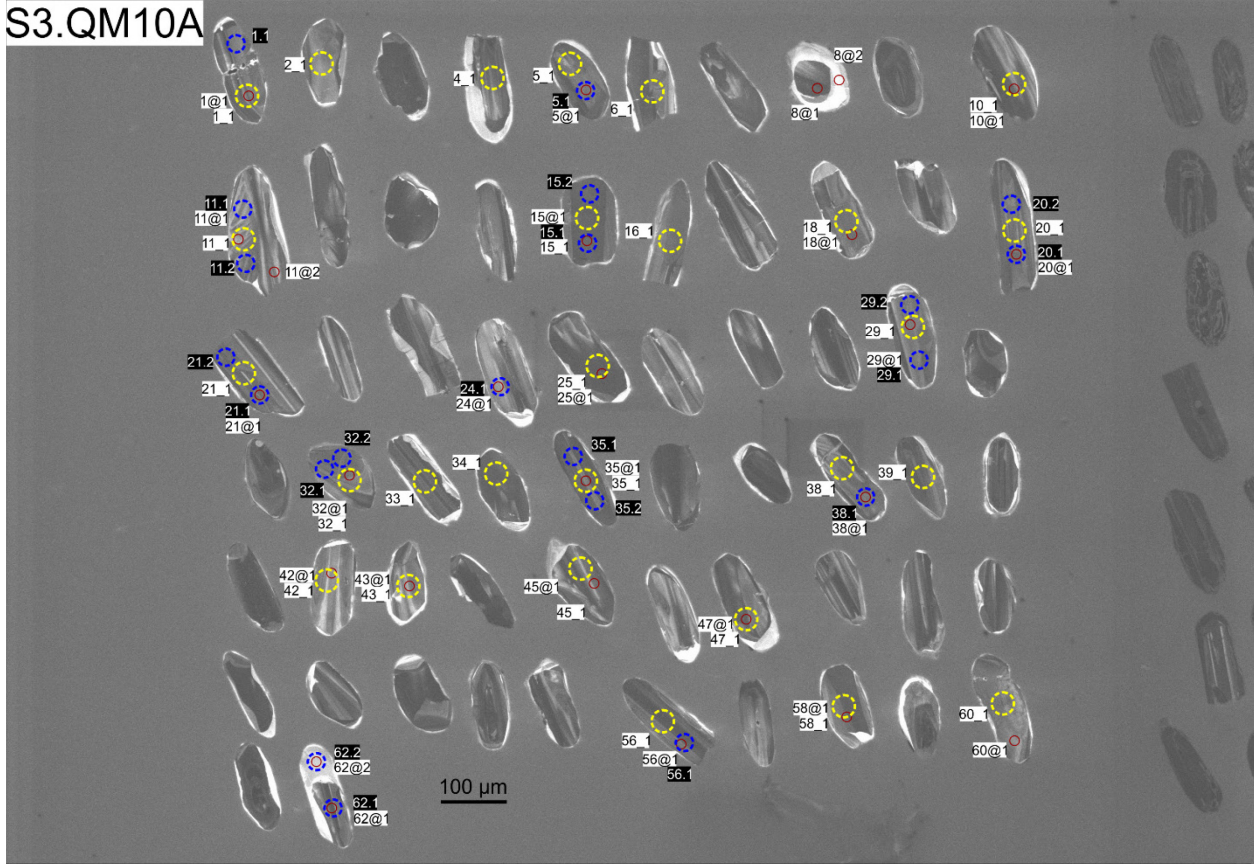




200 μm^* Mag = 411 X WD = 10.0 mm Signal A = NTS BSD EHT = 20.00 kV Date : 18 Feb 2021
 Specimen I = -3.82 nA File Name = SEM21001_M1659_S7131_BS_1.tif

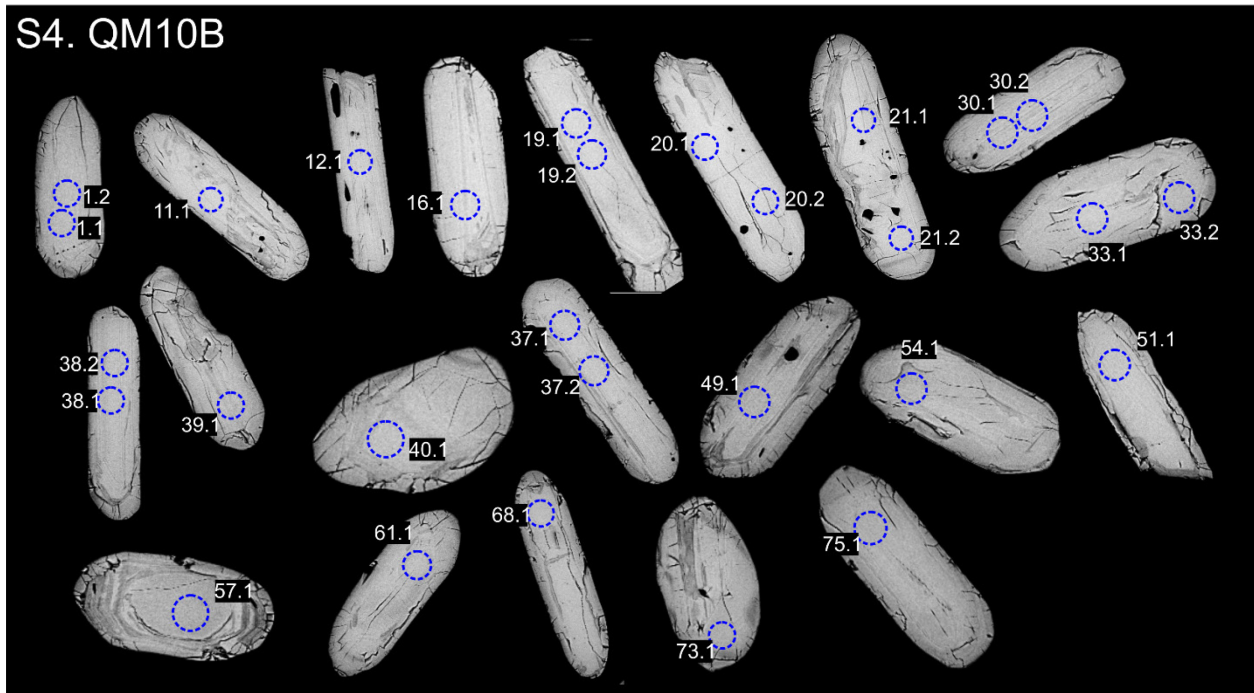


S3.QM10A



100 µm* Mag = 401 X WD = 16.0 mm Signal A = Aux 1 EHT = 15.00 kV Date : 18 Feb 2021
Specimen I = -2.74 nA File Name = SEM21001_M1659_S7130_CL_2.tif

S4.QM10B



S5. QM17C



200 μm*
|-----|

Mag = 302 X

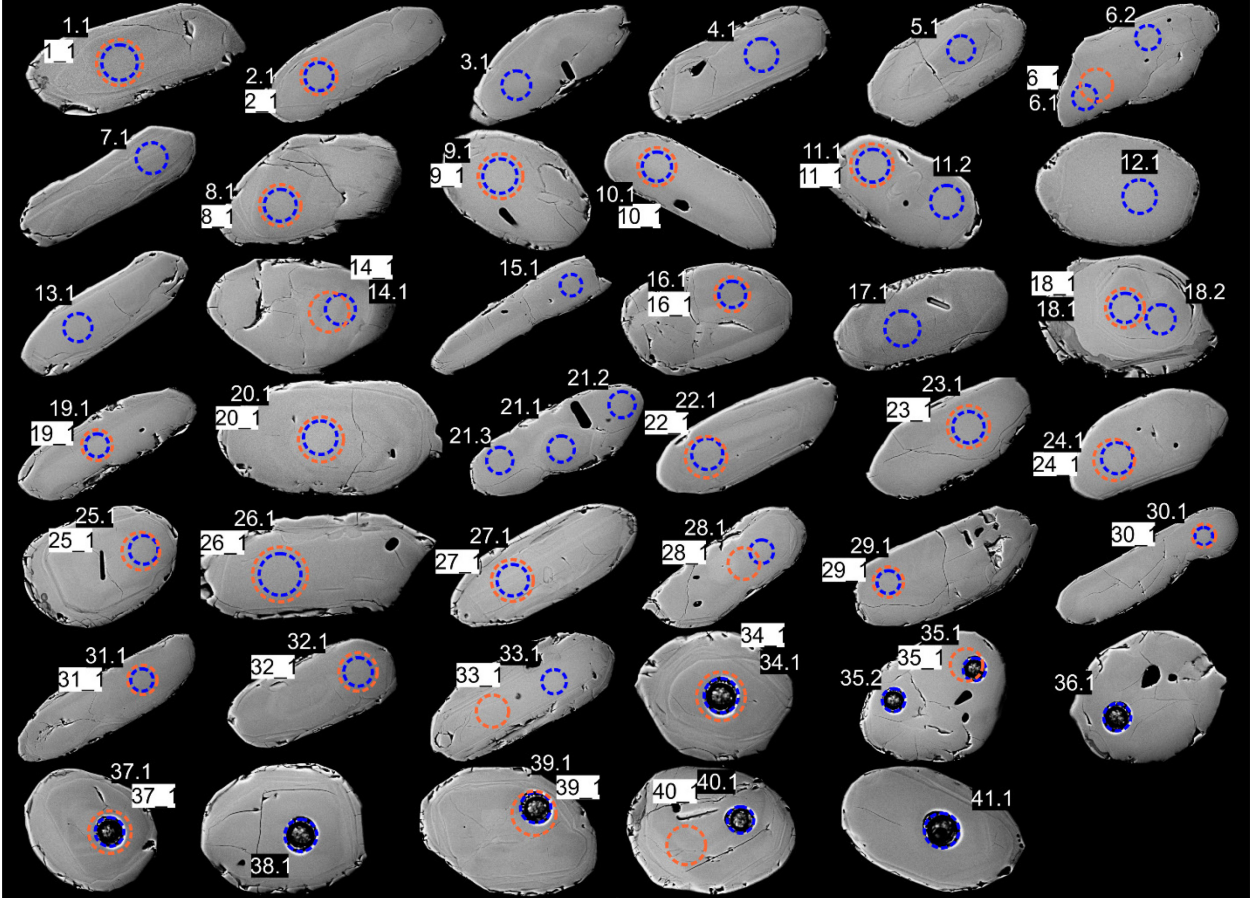
WD = 10.5 mm

Signal A = NTS BSD EHT = 20.00 kV Date :18 Feb 2021

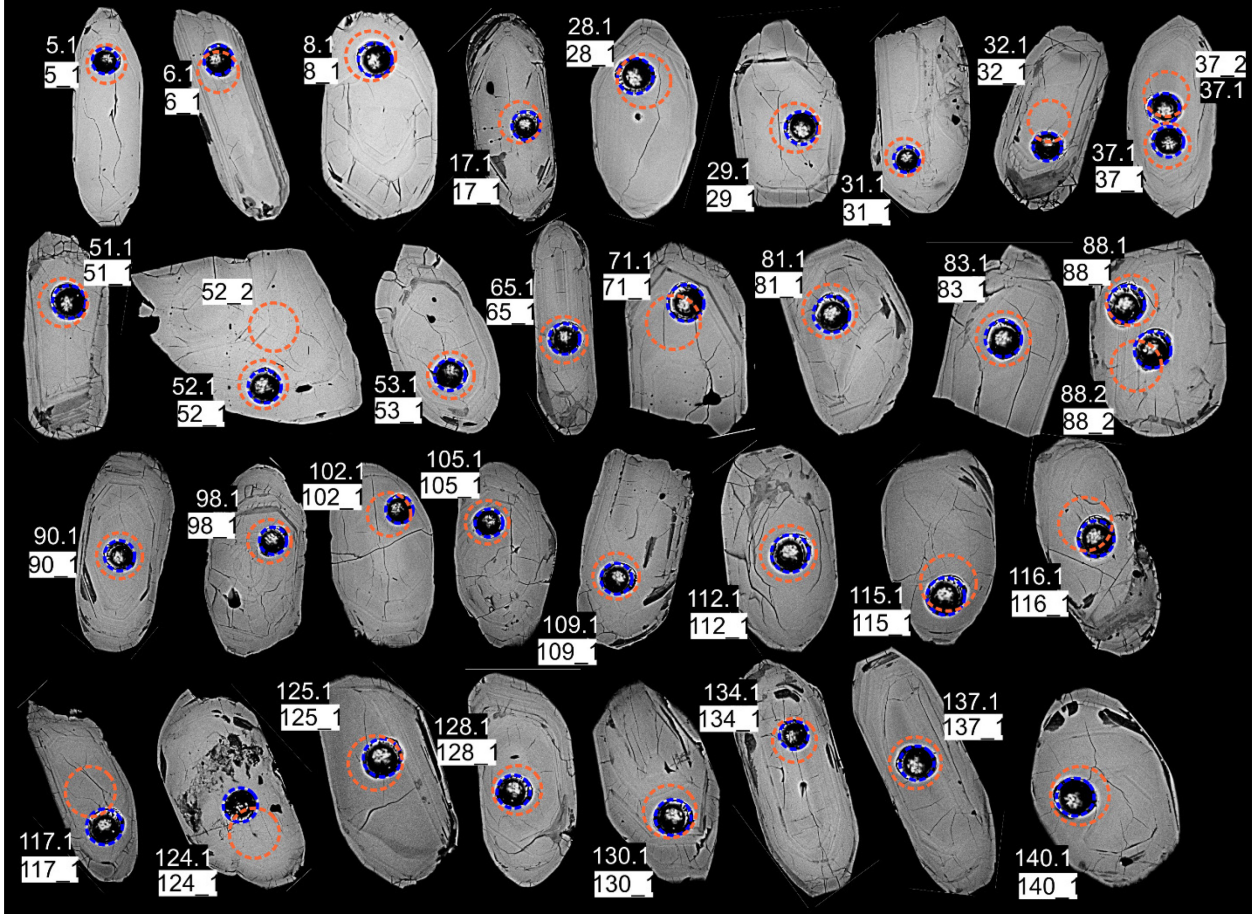
Specimen I = -3.79 nA

File Name = SEM21001_M1659_S7127_BS_1.tif

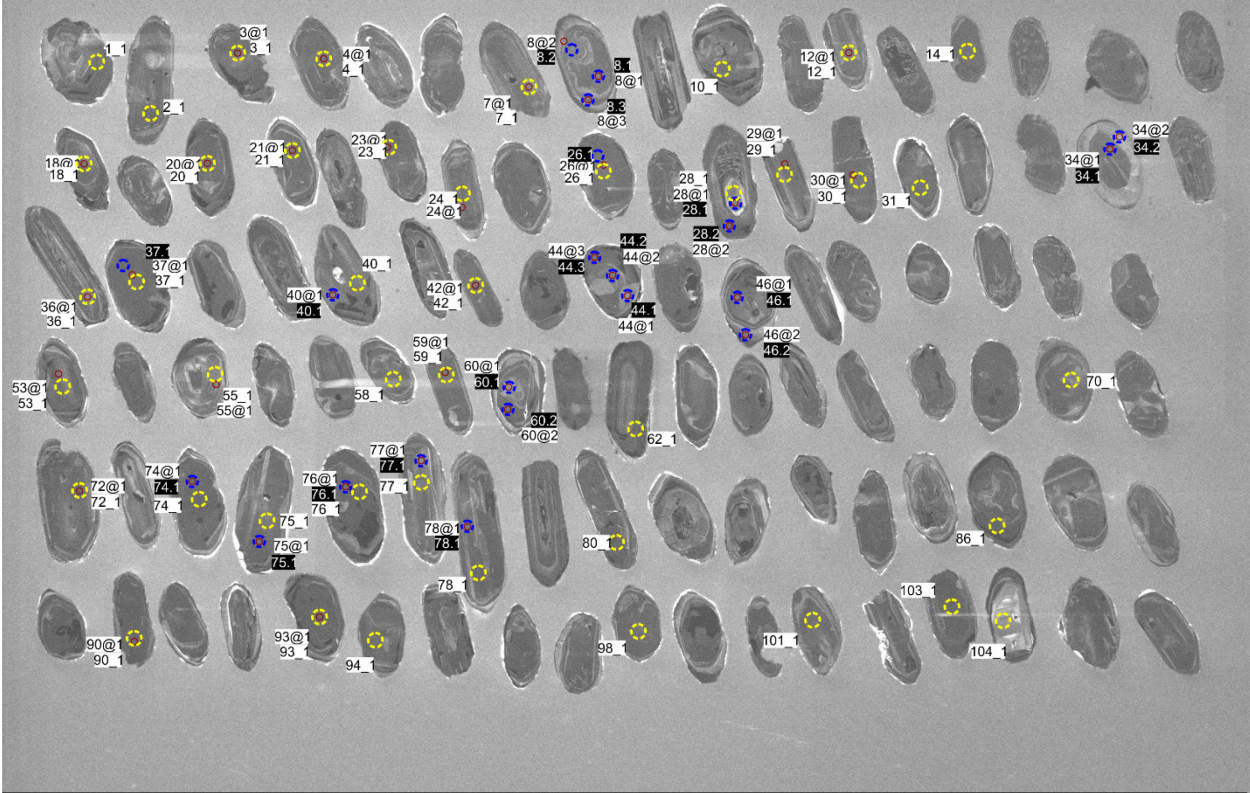
S6. RF-86-49A



S7. TX08-027

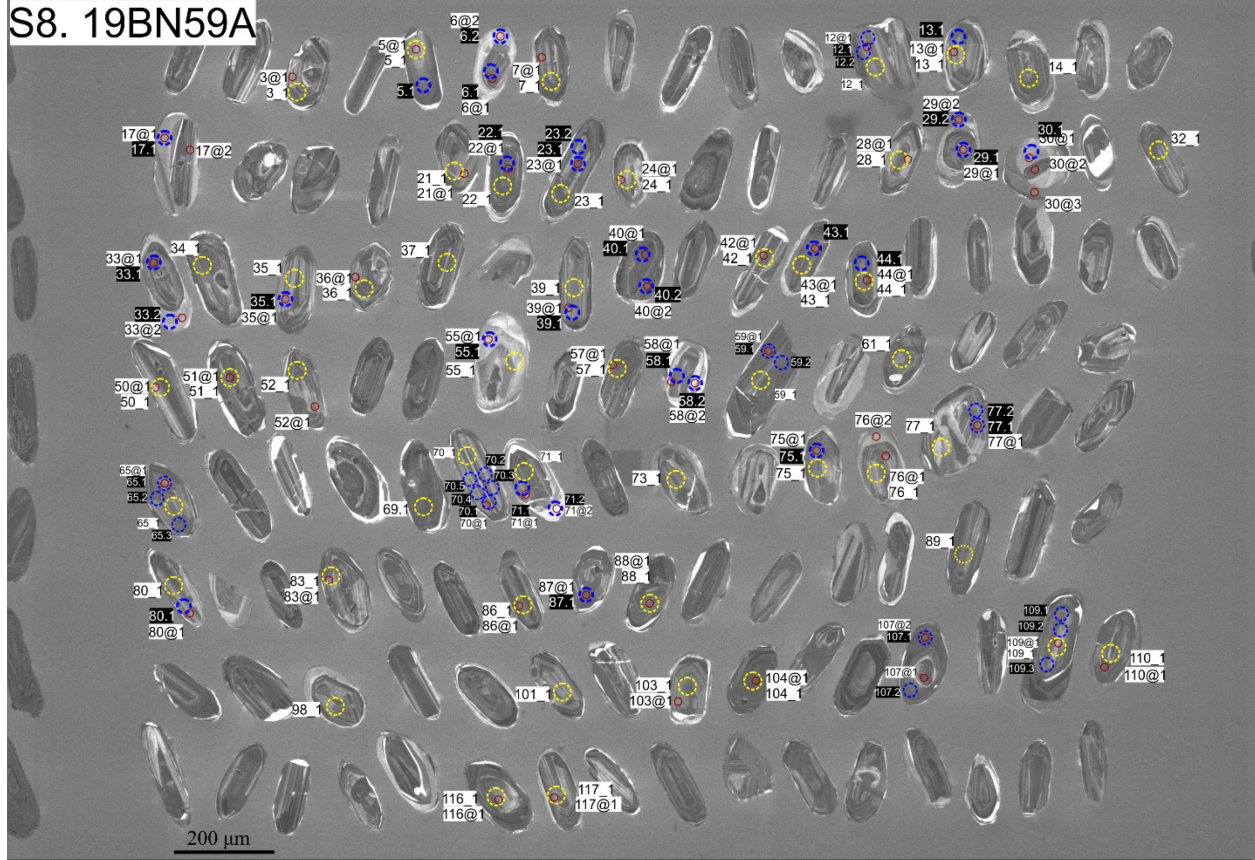


S6. HBA-J-692-A-92



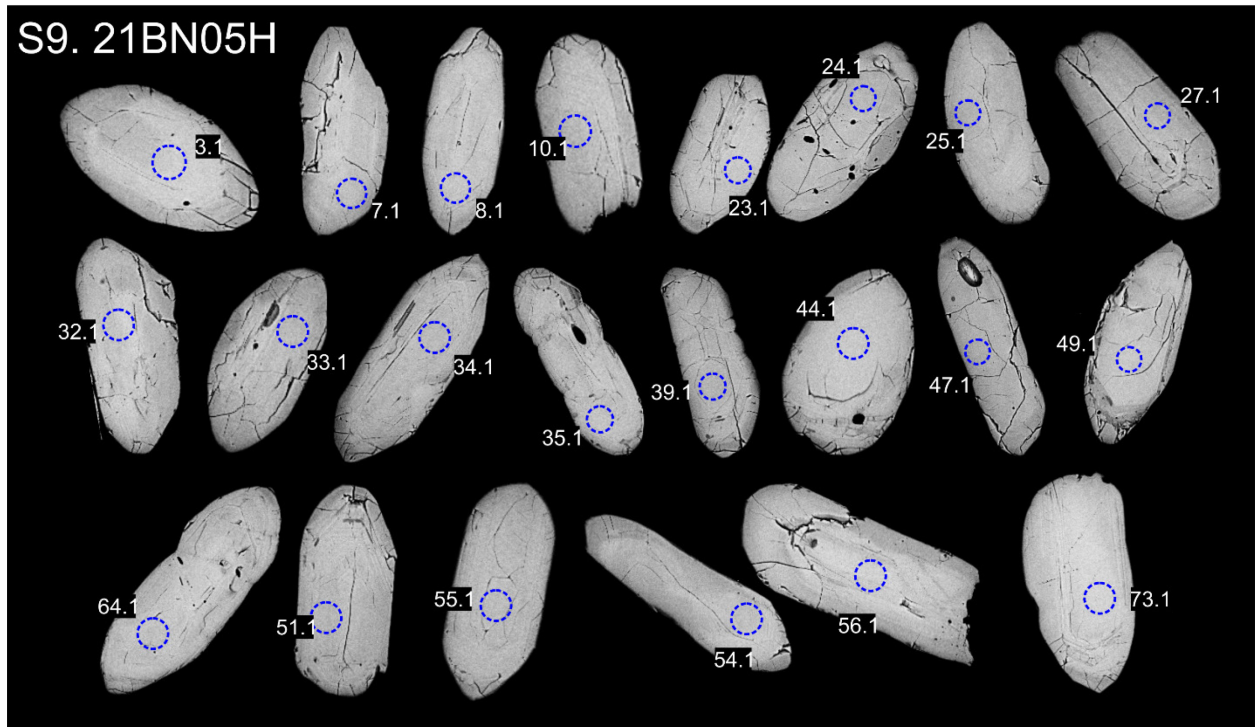
200 μm* Mag = 268 X WD = 16.0 mm Signal A = Aux 1 EHT = 15.00 kV Date : 18 Feb 2021
Specimen I = -2.71 nA File Name = SEM21001_M1659_S7129_CL_2.tif

S8. 19BN59A

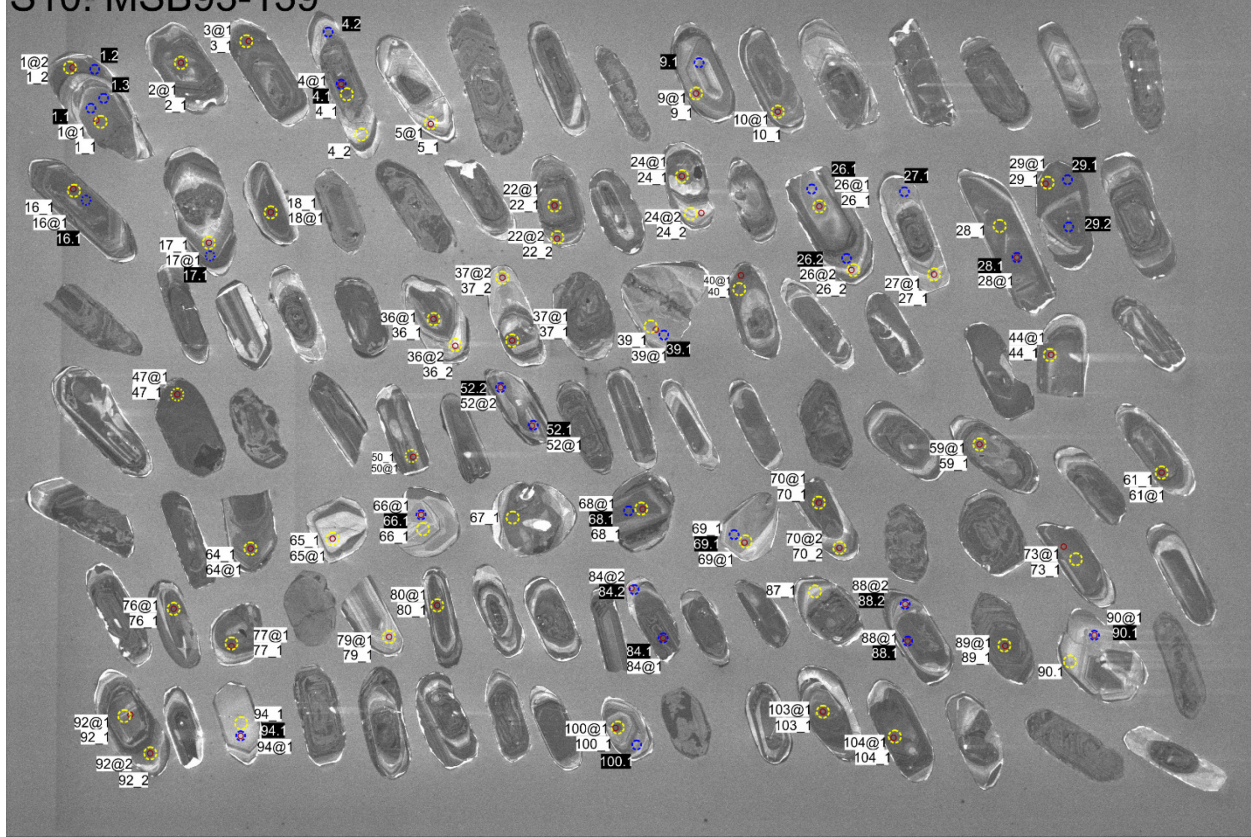


200 μm* Mag = 312 X WD = 16.0 mm Signal A = Aux 1 EHT = 15.00 kV Date :18 Feb 2021
Specimen I = -2.87 nA File Name = SEM21001_M1659_S7128_CL_2.tif

S9. 21BN05H



S10. MSB93-139



200 μm*
|-----|

Mag = 224 X

WD = 16.0 mm

Signal A = Aux 1

EHT = 15.00 kV Date :18 Feb 2021

Specimen I = -2.92 nA

File Name = SEM21001_M1659_S7125_CL_2.tif

Appendix C: Supporting information for chapter 3

C.1 Sample descriptions

Root rock names are from the geochemical Q-ANOR diagram (Streckeisen and LeMaitre, 1979). The major and accessory minerals are listed in decreasing abundance. Colours are from the weathered rock surface.

2.7 Ga granitoids

19BN01A: Medium-grey, medium-grained, strongly-foliated to gneissic, equigranular, biotite granodiorite. The foliation is defined by deformed quartz and aligned biotite. Accessory minerals include: titanite, opaques (rimmed by titanite), allanite (rimmed by epidote), zircon and apatite. Alteration is minimal. Secondary minerals include minor amounts of sericite (after feldspar), chlorite (after biotite) and epidote.

19BN38A: Medium-grey, medium-grained, moderately-foliated, equigranular, biotite tonalite. The foliation is defined by deformed quartz and aligned biotite. Accessory minerals include: titanite, oxides, zircon and apatite. Alteration is minimal. Secondary minerals include minor amounts sericite (after feldspar), chlorite (after biotite) and actinolite.

19BN45B: Medium-grey, medium-grained, weakly-foliated, equigranular biotite granodiorite. The foliation is defined by deformed quartz and aligned biotite. Accessory minerals include: titanite, oxides, allanite (rimmed by epidote), zircon and apatite. Alteration is very minimal. Secondary minerals include trace amounts of sericite (after feldspar), chlorite (after biotite), actinolite and epidote.

19BN07B: Medium-grey, medium-grained, moderately-foliated, equigranular biotite-hornblende granodiorite. Accessory minerals include titanite, oxides, apatite, zircon and allanite. Alteration is minimal. Secondary minerals include minor amounts of sericite (after feldspar), actinolite (after hornblende) and epidote.

19BC52A: Light-pink, medium- to coarse-grained, weakly-foliated, equigranular biotite-hornblende quartz monzodiorite. The weak foliation is defined by aligned biotite. Accessory minerals include titanite (abundant), oxides, zircon, allanite (rimmed by epidote) and apatite. Alteration is moderate. Secondary minerals include moderate amounts of sericite (after feldspar) and epidote.

2.6 Ga granitoids

18EM31B: Light-grey, strongly-foliated, medium-grained, K-feldspar-phyric, biotite granodiorite. K-feldspar phenocrysts are ~2–5 cm. Foliation is defined by aligned biotite and deformed quartz. No thin section made.

19BN106B: Light-grey, strongly-foliated, medium-grained, weakly K-feldspar-phyric, biotite quartz monzodiorite. K-feldspar phenocrysts are ~1 cm. Foliation is defined by aligned biotite and deformed quartz. Alteration is moderate. Secondary minerals include chlorite (after biotite), sericite (after feldspar), minor calcite and minor epidote. Accessory minerals include zircon, apatite, allanite and opaques.

19BN98A: Dark-grey, weakly-foliated, equigranular, biotite-hornblende diorite. Foliation is defined by aligned biotite. Hornblende is commonly rimmed by biotite. Accessory minerals include titanite and zircon. Alteration is moderate. Secondary minerals include moderately abundant epidote and chlorite (after biotite), and minor calcite and sericite (after feldspar).

16BK374A: Light-grey to light-pink, moderately foliated, K-feldspar-phyric, hornblende-biotite clinopyroxene granodiorite. K-feldspar phenocrysts are ~1–3 cm. Foliation is defined by aligned hornblende and biotite, and deformed quartz. Clinopyroxene occurs as relict cores in hornblende. Accessory minerals include opaques, titanite, allanite, zircon and apatite. Alteration is minor. Secondary minerals include moderate sericite (after feldspar) and minor chlorite (after biotite).

16BK366A: Same as 16BK374A.

2.5 Ga granitoids

21BN34A: Medium-grey, moderately-foliated, medium-grained, biotite-hornblende monzodiorite. Accessory minerals include opaques (commonly rimmed by titanite), titanite, apatite and zircon. Alteration is minor. Secondary minerals include minor sericite (after feldspar), chlorite (after biotite) and epidote.

21BN34C: Dark-grey, moderately-foliated, fine-grained, hornblende-biotite diorite. The foliation is defined by aligned hornblende and biotite. Accessory minerals include opaques, apatite, titanite and zircon. Alteration is minor. Secondary minerals include minor sericite (after feldspar), chlorite (after biotite) and epidote.

Samples 21BN34A and 21BN34C are from the same outcrop, where a foliated ~30cm wide dark-grey and fine-grained mafic dyke (sample 21BN34C) cross cuts at a shallow angle a foliated and light grey monzodiorite (sample 21BN34A).

18BN114A: Dark-grey, moderately-foliated to gneissic, medium-grained, hornblende-biotite diorite. The foliation is defined by aligned amphibole and biotite and deformed quartz. Accessory minerals

include opaques, titanite, apatite and zircon. Alteration is minor. Secondary minerals include minor sericite (after feldspar), and chlorite (after biotite).

18BN27A: Dark-grey, moderately-foliated to weakly-gneissic, medium-grained, hornblende-biotite monzodiorite. The foliation is defined by aligned amphibole and biotite and deformed quartz.

Accessory minerals include opaques, titanite, apatite and zircon. Alteration is moderate.

18BN56A: Dark-grey, moderately-foliated, medium-grained hornblende-biotite diorite. The foliation is defined by aligned amphibolite and biotite. Accessory minerals include titanite, opaques and zircon. Alteration is moderate. Secondary minerals include moderate amounts of sericite (after feldspar) and chlorite (after biotite). Actinolite replacement of hornblende is extensive.

18BN18B-M: Dark-grey, moderately-foliated, fine-grained hornblende-biotite quartz diorite. No thin section made.

18BN31A: Light-grey to pink, strongly-foliated, coarse-grained, equigranular, biotite granite. The foliation is defined by deformed quartz (quartz ribbons). Accessory minerals include zircon, opaques and apatite. Zircon is abundant and large (up to ~400 µm). Alteration is moderate. Secondary minerals include moderate sericite (after feldspar), and minor chlorite (after biotite) and epidote.

18BN113A: Light-grey, strongly-foliated, medium-grained, equigranular, biotite granodiorite. The foliation is defined by aligned biotite and deformed quartz. Accessory minerals include opaques, apatite, zircon and titanite. Alteration is very minor. Secondary minerals include minor sericite (after feldspar), chlorite (after biotite) and epidote.

18BN18B-F: Same as 18BN113A. No thin section made.

19BN173A: Medium- to dark-grey, strongly-foliated, medium-grained, equigranular, biotite-hornblende quartz monzodiorite. The foliation is defined by aligned biotite and hornblende, and deformed quartz. Accessory minerals include titanite, zircon and opaques. Alteration is very minor. Secondary minerals include minor sericite (after feldspar) and chlorite (after biotite).

18BN20B: Dark-grey, strongly-foliated, equigranular, medium-grained, biotite-hornblende quartz monzodiorite. The foliation is defined by aligned biotite and hornblende, and deformed quartz. Accessory minerals include titanite (abundant), opaques, zircon and apatite. Alteration is moderate to strong. Secondary minerals include abundant chlorite (after hornblende and biotite), and moderately abundant sericite (after feldspar) and epidote.

19BN154A: Light-grey, strongly-foliated, medium-grained, K-feldspar-phyric biotite granodiorite. The foliation is defined by aligned biotite and deformed quartz. Accessory minerals include titanite,

allanite, opaques, zircon and apatite. Alteration is minor. Secondary minerals include minor sericite (after feldspar), chlorite (after biotite), epidote and calcite.

19BN166A: Light-grey, strongly-foliated to gneissic, medium-grained, equigranular biotite granodiorite. The foliation is defined by aligned biotite and deformed quartz. Accessory minerals include opaques, titanite, zircon, apatite and allanite. Alteration is minor. Secondary minerals include minor amounts of sericite (after feldspar), chlorite (after biotite) and epidote.

21BN32A: Medium-grey, weakly-foliated, medium-grained, equigranular, hornblende quartz diorite. The foliation is defined by aligned hornblende and biotite. Accessory minerals include zircon, titanite, allanite and opaques. Alteration is moderate. Secondary minerals include sericite (after feldspar), chlorite (after hornblende) and epidote (after hornblende).

21BN15A: Dark-grey, very weakly-foliated, medium-grained, equigranular hornblende diorite. The foliation defined by aligned hornblende. Accessory minerals include titanite, opaques and zircon. Alteration is moderate to strong. Secondary minerals include abundant sericite (after feldspar), and moderately abundant epidote (after hornblende) and chlorite (after hornblende).

19BN79A: Dark-grey, moderately-foliated, fine-grained, equigranular, biotite-hornblende quartz monzodiorite. Foliation is defined by aligned biotite and amphibole. Accessory minerals include titanite, apatite, zircon and opaques. The sample is virtually unaltered without any noteworthy secondary minerals.

21BN09A: Same as 19BN79A

21BN16A: Medium-grey, moderately-foliated, medium-grained, equigranular, hornblende-biotite quartz monzodiorite. The foliation is defined by aligned hornblende and biotite. Accessory minerals include apatite, opaques and zircon. Alteration is minor. Secondary minerals include minor sericite (after feldspar), chlorite (after biotite) and epidote.

19BN88A: Medium-grey, moderately foliated, fine-grained, equigranular, biotite-hornblende quartz monzodiorite. The foliation is defined by aligned biotite and hornblende and deformed quartz. Accessory minerals include opaques, titanite, allanite, apatite and zircon. The sample is virtually unaltered without any noteworthy secondary minerals.

21BN28A: Light-grey, moderately-foliated, medium-grained, K-feldspar-phyric, biotite granodiorite. K-feldspar phenocrysts are ~2 to 5 cm. Foliation is defined by aligned biotite. Accessory minerals include zircon, titanite, allanite, apatite and opaques. Alteration is moderate. Secondary minerals include sericite (after feldspar) and epidote.

21BN29A: Light-pink, moderately-foliated, medium-grained, weakly K-feldspar-phyric, biotite monzogranite. K-feldspar phenocrysts are up to ~3 cm. Foliation is defined by aligned biotite. Alteration consists of only minor chloritization of biotite and sericitization of feldspar.

21BN20D: Same as 21BN29A.

21BN30A: Same as 21BN29A.

21BN20C: Dark-grey, moderately-foliated, fine-grained hornblende biotite quartz monzodiorite. No thin section was made.

19BN53A: Light-grey, strongly-foliated to gneissic, medium-grained, equigranular biotite granodiorite. The foliation is defined by aligned biotite and deformed quartz. Accessory minerals include allanite (rimmed by epidote), zircon and apatite. Alteration is very minor. Secondary minerals include minor sericite (after feldspar), chlorite (after biotite) and epidote.

19BC02A: Dark-grey, moderately-foliated, medium-grained, equigranular, hornblende-biotite diorite. Foliation is defined by aligned hornblende and biotite. Minor chloritization of biotite, minor sericitization of feldspar and minor epidote. Accessory phases include zircon, apatite and opaques. This sample was collected from a thin (~30 cm thick) layer in an outcrop of granulite-facies orthogneisses. The surrounding gneisses contain orthopyroxene, clinopyroxene and garnet, which are replaced by amphibole, biotite and chlorite to varying degrees. This sample is therefore interpreted as a retrogressed mafic granulite.

19BN126B: Light-grey, moderately-foliated, medium-grained, k-feldspar phyric, biotite granodiorite. The foliation is defined by aligned biotite and deformed quartz. K-feldspar phenocrysts are ~3 cm. Accessory minerals include zircon, apatite, opaques, allanite (rimmed by epidote) and titanite. Alteration is minor. Secondary minerals include minor amounts of sericite (after feldspar), chlorite (after biotite), epidote and calcite.

19BN127A: Dark-grey, moderately-foliated, fine-grained, equigranular, hornblende-biotite monzodiorite. The foliation is defined by aligned biotite and amphibole. Accessory minerals include apatite and zircon. Alteration is very minor. Secondary minerals include trace amounts of sericite (after feldspar), chlorite (after biotite) and epidote. Moderate amounts of actinolite are also present as rims on the hornblende.

18BN14B: Beige, strongly-lineated, medium-grained, equigranular, hornblende quartz diorite. The lineation is defined by aligned hornblende.

21BN45A: Light-beige, strongly-foliated, medium-grained, equigranular, biotite monzodiorite. Accessory minerals include apatite, opaques (commonly rimmed by titanite), zircon and titanite.

Alteration is minor to moderate. Secondary minerals include moderate sericite (after feldspar), and minor chlorite (after biotite) and epidote.

18EM33A: Dark-grey, strongly foliated to gneissic, medium-grained, equigranular, biotite monzodiorite. The foliation is defined by aligned biotite. Approximately 1-3 cm biotite and quartz-feldspar rich layers in hand sample. Accessory minerals include opaques, apatite and zircon. Alteration is moderate. Secondary minerals include epidote, chlorite (after biotite) and sericite (after feldspar).

C.2 Modelling parameters

Table C-1. Parameters used in batch melt, fractional crystallization and assimilation fractional crystallization (AFC) models in figure 3-10.

	Mineral Partition Coefficients			Primitive Mantle ppm	Bulk D			Batch melt of PM		Bulk D FC 35Ol65Cpx	Fractional crystallization of batch melt					
	Olivine	Opx	Cpx		Lherzolite Residue	5% BM		10% FC			20% FC		30% FC			
				58Ol29Opx13Cpx	ppm	/PM	ppm	/PM	ppm	/PM	ppm	/PM	ppm	/PM		
Rb	0.0007	0.003	0.01	0.635	0.00258	19.5	30.8	0.00675	21.7	34.2	24.4	38.4	27.8	43.9		
Ba	0.00023	0.00006	0.0002	6.989	0.000411	232.7	33.3	0.00138	258.5	37.0	290.8	41.6	332.4	47.6		
Th	0.0018	0.00002	0.013	0.085	0.00274	2.6	30.6	0.00908	2.9	34.0	3.2	38.2	3.7	43.6		
Nb	0.004	0.0013	0.0037	0.713	0.00318	21.6	30.2	0.00381	23.9	33.6	26.9	37.8	30.7	43.1		
La	0.000022	0.0008	0.086	0.687	0.0114	16.7	24.3	0.0559	18.5	26.9	20.6	30.0	23.4	34.1		
Ce	0.000045	0.0016	0.175	1.775	0.0232	33.8	19.0	0.114	37.1	20.9	41.2	23.2	46.3	26.1		
Sr	0.00138	0.0012	0.088	21.1	0.0126	499.9	23.7	0.0577	552.0	26.2	616.8	29.2	699.6	33.2		
Nd	0.0002	0.0056	0.47	1.354	0.0628	14.9	11.0	0.306	16.0	11.8	17.4	12.8	19.1	14.1		
Hf	0.008	0.06	0.383	0.309	0.0718	3.1	10.0	0.252	3.4	10.9	3.7	11.9	4.0	13.1		
Sm	0.000636	0.015	0.81	0.444	0.110	3.2	7.3	0.527	3.4	7.7	3.6	8.1	3.8	8.7		
Eu	0.0012	0.03	1	0.168	0.139	1.0	6.1	0.650	1.1	6.3	1.1	6.5	1.2	6.9		
Gd	0.0018	0.034	1.04	0.596	0.146	3.5	5.8	0.677	3.6	6.0	3.7	6.3	3.9	6.5		
Yb	0.0188	0.22	1.42	0.493	0.259	1.8	3.6	0.930	1.8	3.6	1.8	3.6	1.8	3.6		
Sc	0.12	1.29	1.75	16.2	0.671	23.8	1.5	1.18	23.3	1.4	22.9	1.4	22.3	1.4		
V	0.0896	0.856	2.9	82	0.677	119.4	1.5	1.92	108.4	1.3	97.3	1.2	86.1	1.0		
Cr	1.18	3.52	8.1	2625	2.76	970.3	0.4	5.68	592.7	0.2	341.6	0.1	182.9	0.1		
Ni	24.01	7.38	2.6	1960	16.4	122.9	0.1	10.1	47.2	0.0	16.2	0.0	4.8	0.0		

Mineral partition coefficients are the basaltic partition coefficients from Rollinson and Pease (2021).

Primitive mantle composition from Sun and McDonough (1989).

BM: batch melt; FC: fractional crystallization; D: bulk partition coefficient; /PM: primitive mantle normalized

Batch melt equation: $C_L = C_o / (D + F(1 - D))$, where D is the bulk D for the Lherzolite residue (58% olivine, 29% orthopyroxene, 13% clinopyroxene),

F is the fraction of melt generated, C_o is the concentration in the source rock (primitive mantle), and C_L is the concentration in the melt.

C_L is the concentration in the melt.

Fractional crystallization equation: $C_L = C_o * F(D - 1)$, where D is the bulk D for the crystallizing assemblage (35% olivine, 65% clinopyroxene),

F is the fraction of liquid remaining, C_o is the concentration in the parent magma (5% BM of PM) and C_L is the concentration in the liquid.

AFC calculations used the same C_o and bulk D values as the FC calculations, R (mass cumulates/mass assimilants) values of 1.5 and 3, and the median local 2.7 and 2.6 Ga crust (34 ppm Nd, 24 ppm Ni) as the assimilant. AFC equations from DePaolo (1981b).

Table C-2. Parameters used for AFC models in figure 3-11.

	Parent magmas		Assimilants		
	Depleted mantle/ Primitive CAB	18BN56A Most primitive 2.5 Ga sample	Median 2.6 Ga crust	Median 2.7 Ga crust	Median >3 Ga crust
Nd ppm	15	35	39	34	21
$^{143}\text{Nd}/^{144}\text{Nd}$ at 2.5 Ga	0.5095301	0.5094111	0.5093545	0.5092641	0.5090183
ϵNd at 2.5 Ga	2.6	0.2	-0.9	-2.7	-7.5

One set of models assumes a parent magma with the Nd isotopic composition of depleted mantle at 2.5 Ga (DePaolo, 1981a)

and the Nd content (15 ppm) of an average primitive continental arc basalt (CAB; Kelemen et al., 2014). The other set of models assumes a parent magma with the composition of the most primitive 2.5 Ga sample (18BN56A). Median compositions for 2.6 and 2.7 Ga crust are from data for 2.6 and 2.7 Ga granitoids in chapter 3. Median compositions for >3 Ga crust are from data for 3.3–3.1 Ga PRT granitoids in chapter 2. AFC calculations assumed R values (mass of cumulates/mass of assimilants) of 1.5 and 3.

AFC equations from DePaolo (1981b).

C.3 References for data compilations

U-Pb crystallization age and Sm-Nd isotope composition for meta(igneous) rocks of the Rae craton, shown on figures 3-1 and 3-9:

Acosta-Góngora et al. (2018); Ashton (1988); Ashton et al. (2007); Ashton et al. (2009); Ashton et al. (2014); Ashton et al. (2016); Ashton et al. (2017a); Ashton et al. (2017b); Ashton et al. (2017c); Baldwin et al. (2003); Berman and Camacho (2020); Berman et al. (2013); Berman et al. (2015); Bethune and Scammell (2003); Bostock and Loveridge (1988); Card et al. (2014); Card et al. (2016); Cloutier et al. (2021); Davis and Zaleski (1998); Davis et al. (2006); Davis et al. (2013); Davis et al. (2014); Davis et al. (2015); Davis et al. (2021); Dudas et al. (1991); Frisch and Hunt (1988); Frisch and Hunt (1993); Frisch and Parrish (1992); Ganderton (2013); Hanmer et al. (1994); Hartlaub et al. (2005); Hinchey et al. (2011); Hunter et al. (2018); Hunter et al. (2021); Jackson et al. (1990); Johnstone (2002); LaFlamme et al. (2014a); LaFlamme et al. (2014b); LeCheminant and Roddick (1991); MacHattie (2008); MacLachlan et al. (2005); Martel et al. (2008); McNicoll et al. (2000); Mills et al. (2007); Neil et al. (2023); Peterson (2006); Peterson et al. (2010); Peterson et al. (2024); Rayner et al. (2011); Regan et al. (2017); Regis and Sanborn-Barrie (2022); Regis and Sanborn-Barrie (2023); Regis et al. (2017a); Regis et al. (2017b); Regis et al. (2019); Regis et al. (2022); Roddick et al. (1992); Sanborn-Barrie et al. (2015); Sandeman et al. (2006); Schultz (2007); Schultz et al. (2007); Sherlock et al. (2004); Skipton et al. (2019); Skulski et al. (2003); Stern et al. (2003); Tersmette (2012); Thiessen et al. (2017); Thiessen et al. (2022); van Breemen et al. (1990); van Breemen et al. (2007); Whalen et al. (2011); Wodicka et al. (2002).

Geochemical data for Archean and Phanerozoic granitoid fields shown on figures 3-5 through 3-11:

N = number of samples in the dataset or sub-dataset

Archean TTG (N=1454): compilation of Moyen (2020)

Archean Sanukitoid s.l (N=653): compilation of Moyen (2020), minus data from the ferroan Matok pluton (Laurent et al., 2014b), plus sanukitoid data from the Slave craton (Davis et al., 1994).

Post-collisional I-type (N=1606):

Caledonian orogen (N=487): Clemens et al. (2009); Fowler et al. (2001, 2008); Nielson (2008); compilation of Gómez-Frutos et al. (2023).

Variscan orogen (N=1119): Castro et al. (2023); Donaire et al. (1999; 2005); Gómez-Frutos and Castro (2023); Janoušek et al. (2000); Slaby and Martin (2008); compilation of Moyen et al. (2017); compilation of Jacob et al. (2021).

Continental Arc I-type (N=5163):

Western North America (Coast Mountains batholith, Sierra Nevada batholith; Peninsula Ranges batholith, Cascades, N=1149): GEOROC database; Barth et al. (2011); Cecil et al. (2012); Chapman et al. (2014); Coleman et al. (2012); Girardi et al. (2012); Holland et al. (2013); Klein and Jagoutz (2021); Lackey et al. (2008); Lackey et al. (2012); Lee et al. (2007); Nelson et al. (2013); Putirka et al. (2014); Tepper et al. (1993).

Central America (N=137): GEOROC database

Andes (N=1233): GEOROC database; Pitcher et al. (1985); Herve et al. (2007)

Trans-Himalayan batholith (N=121): Ahmad et al. (1998); Crawford and Searle (1992); Debon et al. (1986, 1987); Honegger et al. (1982).

Honshu Arc, Japan (N=2523): GEOROC database.

When combining other compilations (e.g., compilation of Jacob et al., 2021) with my own, care was taken to avoid sample duplication. Sensitivity tests were performed to see how the removal or addition of large amounts of data from certain areas (e.g., Honshu Arc, Japan) influenced the compositional fields (75% Kernel density contours) shown in the main text. The removal or addition of such data has a negligible impact on the compositional fields. See examples in figured C-1.

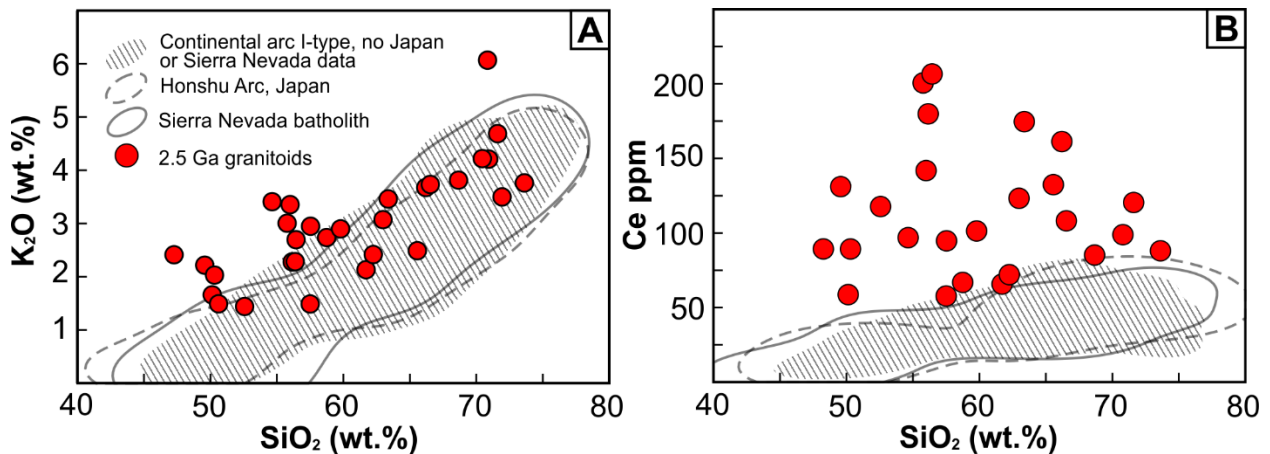


Figure C-1. Plots illustrating that the continental arc I-type fields are not sensitive to the removal or addition of data from the Honshu Arc (Japan) or the Sierra Nevada batholith, for example. (A) SiO₂ wt.% vs. K₂O wt.%. (B) SiO₂ wt.% vs. Ce ppm. Data fields are 75% Kernel density contours.

C.4 Another (ca. 2.78 Ga) component of map unit 1

An additional sample from map unit 1 (Figure 3-2B) was processed for U-Pb zircon geochronology. Sample 19BC54C (655967E, 6869185N, UTM zone 12) was collected from an outcrop of heterogeneous straight gneisses near the east end of Gray Lake. The outcrop consists of amphibolitic, tonalitic and granitic gneisses that are interlayered on a decimetre to metre scale. The sample was taken from a layer of mylonitic (quartz-ribbon) granitic gneiss that is strongly altered, as evidenced by pervasive pink and green (epidote) staining in outcrop (Figure C-2A). This sample was originally processed for zircon geochronology because a cross-cutting granitic dyke yielded >3.0 Ga inherited zircon (Canam, 2023). As such, it was thought that 19BC54C could represent a component of the >3 Ga Perry River terrane (Neil et al., 2023). No whole-rock geochemical or isotopic data were acquired from this sample, because of its strongly altered nature.

The zircon grains recovered from 19BC54C range from prismatic with fine-scale oscillatory zoning to equant with no apparent zoning (Figure C-2B). Several grains contain cores with fine-scale oscillatory zoning and rims that are unzoned (Figure C-2B). The domains with fine-scale oscillatory zoning are interpreted as igneous in origin, whereas the unzoned domains are interpreted as metamorphic. U-Pb age data were acquired from these zircon grains via LA-MC-ICPMS (Appendix A). Seventeen of 33 igneous domain analyses yield a weighted mean $^{207}\text{Pb}/^{206}\text{Pb}$ date of 2776 ± 6 Ma, which is interpreted as the crystallization age of the sample (Figure C-2C). This interpretation is supported by a prominent probability density peak in the $^{207}\text{Pb}/^{206}\text{Pb}$ dates at ~ 2.78 Ga (Figure C-2C). A single older (2810 ± 12 Ma) core analysis may reflect inheritance, and several younger igneous domain analyses are attributed to Pb-loss (Figure C-2C). The $^{207}\text{Pb}/^{206}\text{Pb}$ dates from the metamorphic domains range from ~ 2.45 to 2.39 Ga; and yield a probability density peak of ~ 2.42 Ga. The U-Pb data from this sample demonstrate that some components of map unit 1 (Figure 3-2C) are ca. 2.78 Ga in age, and provide further evidence of an Arrowsmith-aged (ca. 2.4 Ga) metamorphic overprint in the Nonacho Lake area.

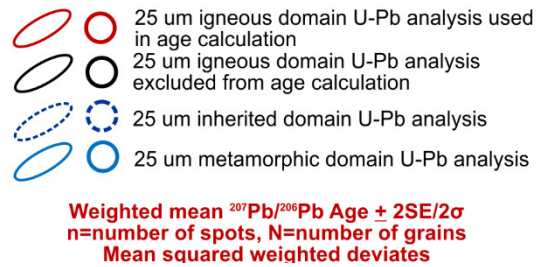
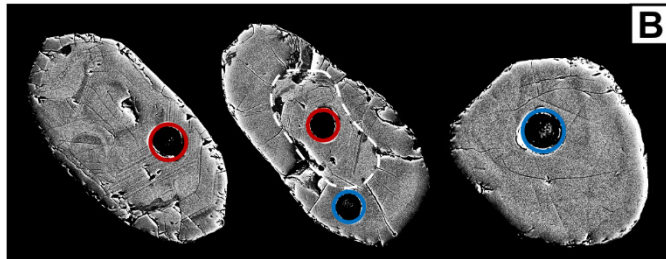
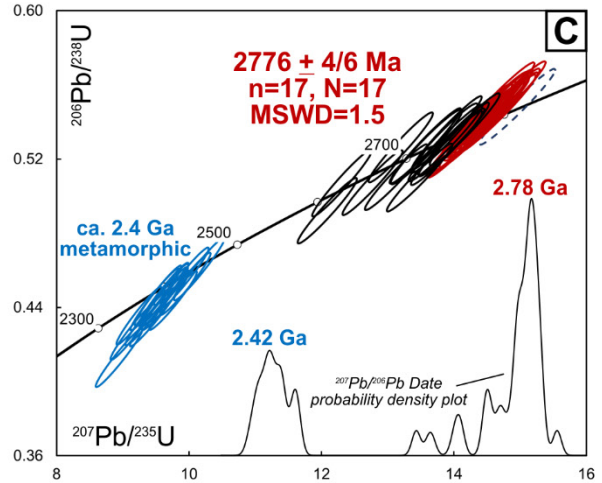
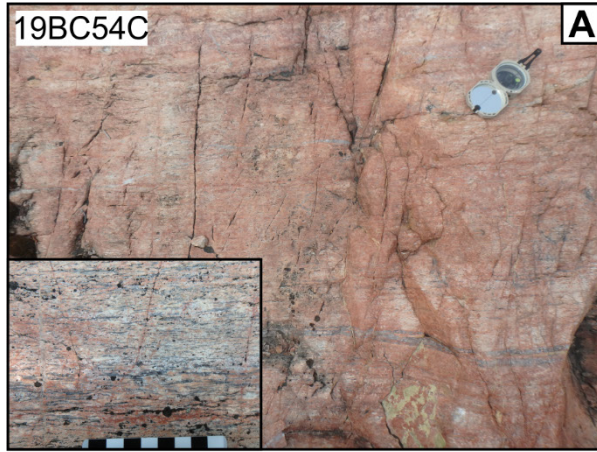


Figure C-2. (A) Outcrop photographs for sample 19BC54C. (C) Representative BSE images of zircon from 19BC54C. (B) Wetherill concordia diagram of LA-MC-ICPMS U-Pb zircon data from 19BC54C.

C.5 Data tables

Table C-3. LA-MC-ICPMS zircon U-Pb isotope data.

Session	Spot ID	Screen	Class	238U cps	206Pb cps	204 cps	Ratios						Dates (Ma)				Disc. %	
							207Pb 206Pb	2σ	207Pb 235U	2σ	206Pb 238U	2σ	ρ	207Pb 206Pb	2σ	206Pb 238U		2σ
Mar 20 2023	19BN07B-6-1		ign	748795	326261	59	0.1873	0.0013	12.92	0.37	0.500	0.014	0.970	2718	12	2616	60	4
Mar 20 2023	19BN07B-9-1		ign	561246	244286	35	0.1870	0.0013	12.89	0.39	0.500	0.014	0.970	2716	12	2614	62	4
Mar 20 2023	19BN07B-13-2		ign	781901	342650	85	0.1866	0.0013	13.06	0.36	0.508	0.014	0.967	2712	12	2648	58	2
Mar 20 2023	19BN07B-22-1		ign	906334	403515	57	0.1860	0.0013	13.19	0.40	0.515	0.015	0.973	2707	12	2677	65	1
Mar 20 2023	19BN07B-4-1		ign	830197	367079	59	0.1859	0.0013	12.89	0.38	0.503	0.014	0.970	2706	12	2627	61	3
Mar 20 2023	19BN07B-17-1		ign	940334	414428	58	0.1858	0.0013	13.05	0.38	0.510	0.014	0.969	2705	12	2655	60	2
Mar 20 2023	19BN07B-13-1		ign	747638	323737	53	0.1855	0.0013	12.83	0.36	0.502	0.014	0.968	2703	12	2622	58	3
Mar 20 2023	19BN07B-20-1		ign	1148687	507636	19	0.1851	0.0013	13.03	0.38	0.511	0.014	0.970	2699	12	2661	61	1
Mar 20 2023	19BN07B-2-1		ign	1120239	484361	61	0.1845	0.0013	12.51	0.35	0.492	0.013	0.966	2694	12	2579	58	4
Mar 20 2023	19BN07B-11-1		ign	1185704	521106	58	0.1845	0.0013	12.95	0.36	0.509	0.014	0.968	2694	11	2654	58	1
Mar 20 2023	19BN07B-21-1		ign	1173254	504625	20	0.1841	0.0013	12.62	0.37	0.497	0.014	0.970	2691	12	2602	61	3
Mar 20 2023	19BN07B-8-1		ign	880076	375198	58	0.1830	0.0014	12.35	0.35	0.490	0.013	0.964	2680	12	2569	57	4
Mar 20 2023	19BN07B-18-1		ign	1003603	435991	63	0.1827	0.0013	12.65	0.37	0.502	0.014	0.970	2677	12	2624	61	2
Mar 20 2023	19BN07B-8-2		ign	1381992	605528	108	0.1823	0.0013	12.73	0.37	0.507	0.014	0.968	2674	12	2642	61	1
Mar 20 2023	19BN07B-26-1		ign	1273294	563849	61	0.1817	0.0013	12.82	0.37	0.512	0.015	0.970	2668	12	2665	62	0
Mar 20 2023	19BN07B-19-1		ign	697456	300649	42	0.1815	0.0014	12.47	0.37	0.498	0.014	0.968	2667	12	2607	62	2
Mar 20 2023	19BN07B-16-1		ign	1424350	621084	61	0.1813	0.0013	12.60	0.37	0.504	0.014	0.970	2665	12	2632	61	1
Mar 20 2023	19BN07B-23-1		ign	747239	326734	51	0.1810	0.0013	12.61	0.36	0.506	0.014	0.967	2662	12	2638	60	1
Mar 20 2023	19BN07B-3-1		ign	691329	292654	70	0.1806	0.0013	11.99	0.36	0.482	0.014	0.969	2658	12	2534	60	5
Mar 20 2023	19BN07B-1-1		ign	1208161	510719	74	0.1803	0.0013	11.95	0.33	0.481	0.013	0.967	2656	12	2531	56	5
Mar 20 2023	19BN07B-24-1		ign	928691	394674	34	0.1794	0.0013	12.15	0.36	0.491	0.014	0.971	2647	12	2577	61	3
Mar 20 2023	19BN07B-11-2		ign	1299188	542945	101	0.1787	0.0013	11.93	0.35	0.484	0.014	0.966	2641	12	2546	59	4
Mar 20 2023	19BN07B-7-1		ign	759465	319103	44	0.1784	0.0014	11.87	0.35	0.483	0.014	0.965	2638	13	2539	59	4
Mar 20 2023	19BN07B-5-1		ign	1433417	635576	69	0.1773	0.0013	12.33	0.37	0.504	0.015	0.971	2628	12	2633	63	0
Mar 20 2023	19BN07B-25-1		ign	1231553	523269	67	0.1770	0.0013	11.98	0.36	0.491	0.014	0.971	2625	12	2576	61	2
Mar 20 2023	19BN07B-12-1		ign	834627	347358	37	0.1754	0.0014	11.66	0.34	0.482	0.013	0.963	2609	13	2538	58	3
Mar 20 2023	19BN07B-10-1		met	7587154	3090562	57	0.1557	0.0011	10.04	0.29	0.468	0.013	0.970	2409	12	2474	57	-3
Mar 20 2023	19BN07B-14-1		met	1053309	402138	63	0.1547	0.0011	9.43	0.28	0.443	0.013	0.972	2398	12	2362	57	2
Mar 20 2023	19BN07B-15-1	cPb	ign	504282	207084	122	0.1851	0.0016	12.11	0.35	0.475	0.013	0.954	2699	14	2505	57	8
Mar 20 2023	19BN07B-6-2	cPb	ign	1049272	451478	158	0.1832	0.0013	12.56	0.35	0.497	0.013	0.967	2682	12	2603	58	3

Spots labelled as "Sample ID-grain#-spot#"

Class: Analysis classified as igneous (ign), metamorphic (met), inherited (inhrt) or ambiguous (amb).

Screen: Analysis screened for high common-Pb contents (cPb), mixed isotope ratio signals (mix) or discordance (disc).

Disc.: Percent discordance calculated as $[(207\text{Pb}/206\text{Pb date} / 206\text{Pb}/238\text{U date}) - 1] * 100\%$

Session	Spot ID	Screen	Class	238U cps	206Pb cps	204 cps	Ratios						Dates (Ma)				Disc. %	
							207Pb		207Pb		206Pb		207Pb		206Pb			
							206Pb	2σ	235U	2σ	238U	2σ	ρ	206Pb	2σ	238U		2σ
Mar 20 2023	19BN01A-1-1		ign	661976	286640	49	0.1862	0.0014	12.85	0.39	0.501	0.015	0.971	2709	12	2617	63	4
Mar 20 2023	19BN01A-11-1		ign	916243	395909	82	0.1854	0.0013	12.77	0.41	0.500	0.016	0.976	2702	12	2612	67	3
Mar 20 2023	19BN01A-19-1		ign	791982	351624	30	0.1845	0.0013	13.26	0.38	0.522	0.015	0.968	2693	12	2706	62	0
Mar 20 2023	19BN01A-2-1		ign	919226	412788	76	0.1842	0.0013	13.18	0.39	0.519	0.015	0.969	2691	12	2696	62	0
Mar 20 2023	19BN01A-21-1		ign	796594	348098	31	0.1854	0.0014	13.11	0.37	0.513	0.014	0.966	2701	12	2671	60	1
Mar 20 2023	19BN01A-24-1		ign	1282627	553217	67	0.1843	0.0013	12.87	0.41	0.507	0.016	0.974	2692	12	2642	66	2
Mar 20 2023	19BN01A-3-1		ign	691233	293552	77	0.1867	0.0014	12.63	0.38	0.491	0.014	0.966	2713	13	2575	61	5
Mar 20 2023	19BN01A-30-1		ign	745741	324483	46	0.1837	0.0013	12.94	0.41	0.511	0.016	0.973	2686	12	2661	66	1
Mar 20 2023	19BN01A-31-1		ign	1269399	578638	111	0.1842	0.0013	13.59	0.39	0.535	0.015	0.969	2691	12	2764	62	-3
Mar 20 2023	19BN01A-34-1		ign	618134	272882	74	0.1845	0.0013	13.19	0.38	0.519	0.014	0.968	2694	12	2693	61	0
Mar 20 2023	19BN01A-35-1		ign	767540	344458	60	0.1853	0.0013	13.46	0.42	0.527	0.016	0.974	2701	12	2729	67	-1
Mar 20 2023	19BN01A-37-1		ign	502578	215170	61	0.1844	0.0014	12.78	0.37	0.503	0.014	0.963	2693	13	2626	60	3
Mar 20 2023	19BN01A-5-1		ign	690603	301056	53	0.1842	0.0014	12.79	0.39	0.504	0.015	0.970	2691	12	2631	63	2
Mar 20 2023	19BN01A-7-1		ign	552528	239280	78	0.1855	0.0014	12.80	0.41	0.501	0.015	0.972	2702	12	2617	66	3
Mar 20 2023	19BN01A-8-1		ign	1019272	444921	104	0.1858	0.0013	12.92	0.37	0.505	0.014	0.968	2705	12	2634	60	3
Mar 20 2023	19BN01A-9-1		ign	732873	319369	68	0.1855	0.0013	12.88	0.39	0.504	0.015	0.971	2703	12	2630	63	3
Mar 20 2023	19BN01A-28-1		ign	1121370	483918	82	0.1822	0.0013	12.73	0.36	0.507	0.014	0.969	2673	12	2643	59	1
Mar 20 2023	19BN01A-39-1		ign	651149	284309	69	0.1822	0.0013	12.88	0.38	0.513	0.015	0.969	2673	12	2669	63	0
Mar 20 2023	19BN01A-25-1		ign	515005	222628	43	0.1821	0.0014	12.74	0.38	0.508	0.015	0.965	2672	13	2647	62	1
Mar 20 2023	19BN01A-38-1		ign	1015073	447336	75	0.1817	0.0013	12.97	0.35	0.518	0.013	0.965	2669	12	2689	57	-1
Mar 20 2023	19BN01A-22-1		ign	1730148	749411	146	0.1812	0.0013	12.71	0.35	0.509	0.014	0.965	2664	12	2651	58	0
Mar 20 2023	19BN01A-36-1		ign	2550178	1117212	89	0.1811	0.0013	12.84	0.40	0.515	0.015	0.972	2663	12	2676	65	-1
Mar 20 2023	19BN01A-23-1		ign	1162053	491306	106	0.1807	0.0015	12.37	0.35	0.497	0.014	0.956	2659	14	2599	58	2
Mar 20 2023	19BN01A-33-1		ign	1317931	570710	87	0.1806	0.0014	12.66	0.35	0.509	0.014	0.962	2658	12	2651	58	0
Mar 20 2023	19BN01A-26-1		ign	1128512	484373	84	0.1798	0.0013	12.49	0.36	0.504	0.014	0.968	2651	12	2632	60	1
Mar 20 2023	19BN01A-20-1		ign	1200514	516090	22	0.1797	0.0013	12.51	0.35	0.505	0.014	0.969	2650	12	2635	59	1
Mar 20 2023	19BN01A-18-1		ign	1661430	689629	101	0.1787	0.0013	11.82	0.34	0.480	0.013	0.965	2641	12	2527	57	5
Mar 20 2023	19BN01A-32-1		ign	1079197	464021	89	0.1771	0.0013	12.33	0.37	0.505	0.015	0.971	2626	12	2635	62	0
Mar 20 2023	19BN01A-12-1		ign	884023	367533	68	0.1762	0.0014	11.67	0.36	0.481	0.014	0.969	2618	13	2530	63	3
Mar 20 2023	19BN01A-24-2		met	533076	201878	66	0.1576	0.0012	9.66	0.29	0.445	0.013	0.970	2431	13	2372	58	2
Mar 20 2023	19BN01A-17-1		met	1230832	485271	24	0.1573	0.0011	9.88	0.29	0.456	0.013	0.969	2426	12	2421	57	0
Mar 20 2023	19BN01A-29-1		met	395772	149621	60	0.1572	0.0012	9.62	0.28	0.444	0.013	0.967	2425	13	2369	56	2
Mar 20 2023	19BN01A-14-1		met	546488	205008	25	0.1570	0.0011	9.38	0.29	0.434	0.013	0.971	2423	12	2323	57	4
Mar 20 2023	19BN01A-16-1		met	1383941	536867	45	0.1565	0.0012	9.67	0.29	0.449	0.013	0.968	2418	13	2389	58	1
Mar 20 2023	19BN01A-10-1		met	657722	251703	53	0.1563	0.0011	9.53	0.28	0.442	0.013	0.969	2416	12	2362	56	2
Mar 20 2023	19BN01A-6-1		met	832676	317386	80	0.1562	0.0011	9.49	0.28	0.441	0.012	0.970	2415	12	2354	55	3
Mar 20 2023	19BN01A-4-1		met	902641	349649	49	0.1558	0.0011	9.62	0.29	0.448	0.013	0.972	2411	12	2386	58	1
Mar 20 2023	19BN01A-15-1		mix	1038831	438703	42	0.1752	0.0017	11.79	0.35	0.488	0.014	0.949	2608	16	2563	60	2
Mar 20 2023	19BN01A-13-1		cPb	464891	178014	115	0.1633	0.0012	9.97	0.30	0.443	0.013	0.968	2490	13	2363	58	5
Mar 20 2023	19BN01A-20-2		cPb	789687	299361	116	0.1588	0.0011	9.75	0.28	0.445	0.012	0.969	2443	12	2374	56	3
Mar 20 2023	19BN01A-27-1		cPb	510588	193195	106	0.1559	0.0012	9.55	0.28	0.444	0.012	0.964	2412	13	2371	55	2
Mar 20 2023	19BN01A-15-2		mix	1213854	519153	15	0.1810	0.0018	12.34	0.39	0.494	0.015	0.952	2662	16	2590	64	3
July 13 2020	18EM31B-4-1		ign	950986	427152	90	0.1740	0.0012	11.05	0.34	0.461	0.014	0.972	2596	12	2443	60	6
July 13 2020	18EM31B-13-1		ign	1037529	452396	69	0.1739	0.0013	11.84	0.37	0.494	0.015	0.971	2595	12	2589	64	0
July 13 2020	18EM31B-10-1		ign	898127	396446	74	0.1733	0.0013	11.28	0.34	0.472	0.014	0.969	2590	12	2493	60	4
July 13 2020	18EM31B-6-1		ign	553606	246842	40	0.1733	0.0013	11.39	0.36	0.477	0.014	0.971	2589	12	2514	63	3

Session	Spot ID	Screen	Class	238U cps	206Pb cps	204 cps	Ratios					Dates (Ma)			Disc. %			
							207Pb	2σ	207Pb	2σ	206Pb	2σ	ρ	207Pb		206Pb	2σ	
							206Pb		235U		238U			206Pb		238U		
July 13 2020	18EM31B-22-1		ign	796959	363910	45	0.1732	0.0013	11.66	0.38	0.488	0.016	0.975	2589	12	2564	67	1
July 13 2020	18EM31B-1-1		ign	1220040	539517	61	0.1731	0.0012	11.29	0.35	0.473	0.014	0.972	2588	12	2497	62	4
July 13 2020	18EM31B-34-1		ign	995577	457096	102	0.1730	0.0013	11.57	0.36	0.485	0.015	0.972	2587	12	2550	63	1
July 13 2020	18EM31B-21-1		ign	883025	403589	16	0.1729	0.0013	11.65	0.37	0.489	0.015	0.973	2586	12	2566	65	1
July 13 2020	18EM31B-15-1		ign	1182631	548094	54	0.1727	0.0013	11.80	0.40	0.496	0.016	0.975	2584	13	2596	71	0
July 13 2020	18EM31B-25-1		ign	768323	339821	18	0.1723	0.0013	11.23	0.34	0.473	0.014	0.971	2580	12	2497	61	3
July 13 2020	18EM31B-24-1		ign	816074	367674	29	0.1722	0.0012	11.44	0.36	0.482	0.015	0.973	2579	12	2536	63	2
July 13 2020	18EM31B-8-1		ign	733952	327381	41	0.1721	0.0013	11.32	0.35	0.477	0.014	0.970	2579	12	2515	62	3
July 13 2020	18EM31B-11-1		ign	1212929	549086	76	0.1721	0.0013	11.49	0.35	0.484	0.014	0.971	2578	12	2546	62	1
July 13 2020	18EM31B-9-1		ign	1015629	466236	43	0.1721	0.0013	11.65	0.36	0.491	0.015	0.972	2578	12	2575	64	0
July 13 2020	18EM31B-32-1		ign	606274	269359	32	0.1719	0.0013	11.26	0.35	0.475	0.014	0.971	2576	12	2507	63	3
July 13 2020	18EM31B-17-1		ign	1040215	474131	16	0.1717	0.0012	11.54	0.37	0.488	0.015	0.974	2575	12	2560	66	1
July 13 2020	18EM31B-30-1		ign	931752	418062	69	0.1716	0.0012	12.03	0.38	0.509	0.015	0.973	2574	12	2651	66	-3
July 13 2020	18EM31B-16-1		ign	1318759	595402	18	0.1716	0.0013	11.42	0.36	0.483	0.015	0.973	2574	12	2540	64	1
July 13 2020	18EM31B-31-1		ign	1452725	666605	47	0.1713	0.0012	11.59	0.36	0.491	0.015	0.973	2570	12	2575	63	0
July 13 2020	18EM31B-7-1		ign	1010035	449737	48	0.1711	0.0012	11.23	0.35	0.476	0.014	0.973	2569	12	2511	63	2
July 13 2020	18EM31B-19-1		ign	1200593	555824	18	0.1704	0.0012	11.63	0.37	0.495	0.015	0.974	2561	12	2593	66	-1
July 13 2020	18EM31B-20-1		ign	745272	347885	27	0.1700	0.0012	11.70	0.38	0.499	0.016	0.974	2558	12	2611	67	-2
July 13 2020	18EM31B-35-1		ign	1889523	837435	54	0.1692	0.0012	11.72	0.37	0.502	0.015	0.974	2550	12	2624	66	-3
July 13 2020	18EM31B-18-1		amb	1628432	764101	31	0.1637	0.0012	10.86	0.34	0.481	0.015	0.971	2494	13	2534	64	-2
July 13 2020	18EM31B-5-1	mix	ign	105471	45689	12	0.1678	0.0015	10.71	0.33	0.463	0.014	0.956	2535	15	2455	60	3
July 13 2020	18EM31B-2-1	cPb,mix	ign	2004242	773109	224	0.1613	0.0014	9.18	0.28	0.413	0.012	0.961	2470	14	2227	55	11
July 13 2020	18EM31B-12-1	mix, disc	ign	1859234	688281	53	0.1646	0.0014	8.98	0.35	0.396	0.015	0.976	2504	14	2151	69	16
July 13 2020	18EM31B-14-1	cPb,mix	ign	1282274	589466	253	0.1780	0.0013	12.07	0.37	0.492	0.015	0.969	2635	12	2578	63	2
July 13 2020	18EM31B-23-1	cPb,mix	ign	851611	390414	352	0.1837	0.0026	12.42	0.41	0.490	0.015	0.902	2687	23	2573	63	4
July 13 2020	18EM31B-26-1	mix	ign	417071	189590	85	0.1762	0.0014	11.81	0.38	0.486	0.015	0.970	2618	13	2555	65	2
July 13 2020	18EM31B-27-1	cPb, disc	ign	745587	296814	118	0.1761	0.0014	10.34	0.38	0.426	0.015	0.976	2616	13	2287	68	14
July 13 2020	18EM31B-28-1	cPb,mix	ign	764873	334205	172	0.1782	0.0014	11.48	0.36	0.467	0.014	0.966	2636	13	2472	61	7
July 13 2020	18EM31B-29-1	cPb	ign	887593	399840	162	0.1758	0.0013	11.67	0.38	0.482	0.015	0.974	2614	12	2536	65	3
July 13 2020	18EM31B-33-1	cPb	ign	1331927	590632	264	0.1769	0.0013	11.56	0.37	0.474	0.015	0.973	2624	12	2503	64	5
April 13 2021	16BK374A-14-2		ign	750227	328735	98	0.1736	0.0013	11.89	0.35	0.497	0.014	0.967	2593	12	2601	61	0
April 13 2021	16BK374A-20-1		ign	1031186	451600	80	0.1735	0.0013	11.88	0.34	0.497	0.014	0.967	2592	12	2600	60	0
April 13 2021	16BK374A-30-2		ign	818012	358631	63	0.1733	0.0013	11.88	0.38	0.497	0.016	0.974	2590	12	2602	67	0
April 13 2021	16BK374A-3-1		ign	350712	151010	28	0.1732	0.0013	11.66	0.39	0.488	0.016	0.976	2588	12	2564	69	1
April 13 2021	16BK374A-23-1		ign	1300855	573623	52	0.1728	0.0012	11.92	0.37	0.500	0.015	0.973	2585	12	2615	64	-1
April 13 2021	16BK374A-28-1		ign	1150829	488308	35	0.1727	0.0012	11.46	0.34	0.481	0.014	0.970	2584	12	2533	60	2
April 13 2021	16BK374A-30-1		ign	921875	395611	53	0.1727	0.0012	11.59	0.35	0.487	0.014	0.970	2584	12	2557	61	1
April 13 2021	16BK374A-19-2		ign	834068	365999	43	0.1724	0.0013	11.82	0.37	0.498	0.015	0.971	2581	12	2604	64	-1
April 13 2021	16BK374A-18-1		ign	622259	272953	37	0.1723	0.0012	11.82	0.35	0.498	0.014	0.969	2580	12	2603	61	-1
April 13 2021	16BK374A-29-2		ign	590652	245788	30	0.1723	0.0012	11.21	0.34	0.472	0.014	0.971	2580	12	2493	61	4
April 13 2021	16BK374A-9-1		ign	623541	271490	26	0.1722	0.0013	11.72	0.36	0.494	0.015	0.971	2580	12	2588	64	0
April 13 2021	16BK374A-6-1		ign	1839043	807894	63	0.1722	0.0012	11.83	0.33	0.498	0.013	0.966	2579	12	2607	58	-1
April 13 2021	16BK374A-22-1		ign	1121649	513342	49	0.1722	0.0012	12.32	0.45	0.519	0.019	0.981	2579	12	2696	79	-4
April 13 2021	16BK374A-27-1		ign	2207963	951962	55	0.1721	0.0013	11.60	0.36	0.489	0.015	0.971	2578	12	2567	63	0
April 13 2021	16BK374A-13-1		ign	624239	265979	42	0.1721	0.0012	11.46	0.38	0.483	0.016	0.977	2578	12	2542	68	1
April 13 2021	16BK374A-7-1		ign	794791	356764	31	0.1721	0.0012	12.07	0.38	0.509	0.016	0.974	2578	12	2653	66	-3
April 13 2021	16BK374A-2-2		ign	452909	197945	33	0.1720	0.0013	11.75	0.39	0.496	0.016	0.974	2578	12	2596	68	-1

Session	Spot ID	Screen	Class	238U cps	206Pb cps	204 cps	Ratios						Dates (Ma)			Disc. %		
							207Pb		207Pb		206Pb		207Pb		206Pb			
							206Pb	2σ	235U	2σ	238U	2σ	ρ	206Pb	2σ		238U	2σ
April 13 2021	16BK374A-19-1		ign	805689	348900	55	0.1720	0.0012	11.65	0.36	0.491	0.015	0.973	2577	12	2576	63	0
April 13 2021	16BK374A-10-1		ign	601547	258388	18	0.1720	0.0013	11.55	0.37	0.487	0.015	0.974	2577	12	2559	66	1
April 13 2021	16BK374A-21-1		ign	1568284	697618	43	0.1719	0.0012	11.96	0.37	0.505	0.015	0.973	2577	12	2634	66	-2
April 13 2021	16BK374A-17-1		ign	826434	348097	49	0.1719	0.0012	11.32	0.36	0.478	0.015	0.974	2576	12	2518	65	2
April 13 2021	16BK374A-26-1		ign	599316	259376	31	0.1718	0.0013	11.63	0.34	0.491	0.014	0.968	2576	12	2575	59	0
April 13 2021	16BK374A-2-1		ign	2018157	916546	21	0.1718	0.0012	12.20	0.37	0.515	0.015	0.971	2575	12	2679	64	-4
April 13 2021	16BK374A-31-1		ign	1524029	677782	43	0.1718	0.0012	11.94	0.37	0.504	0.015	0.974	2575	12	2633	65	-2
April 13 2021	16BK374A-4-1		ign	2185569	987397	26	0.1717	0.0012	12.13	0.40	0.512	0.017	0.977	2574	12	2667	71	-3
April 13 2021	16BK374A-20-2		ign	690538	298556	37	0.1717	0.0013	11.60	0.35	0.490	0.014	0.968	2574	12	2573	61	0
April 13 2021	16BK374A-5-1		ign	1482675	662518	36	0.1716	0.0012	11.99	0.40	0.507	0.016	0.977	2573	12	2643	70	-3
April 13 2021	16BK374A-11-1		ign	655092	289745	17	0.1716	0.0012	11.87	0.38	0.502	0.016	0.974	2573	12	2621	67	-2
April 13 2021	16BK374A-25-1		ign	1932404	848389	43	0.1715	0.0012	11.77	0.34	0.498	0.014	0.968	2573	12	2605	59	-1
April 13 2021	16BK374A-15-2		ign	748990	318149	35	0.1715	0.0013	11.39	0.35	0.482	0.014	0.971	2572	12	2535	62	1
April 13 2021	16BK374A-8-1		ign	1275177	562222	25	0.1714	0.0012	11.82	0.36	0.500	0.015	0.971	2572	12	2614	63	-2
April 13 2021	16BK374A-24-2		ign	1107790	488293	35	0.1714	0.0012	11.81	0.35	0.500	0.014	0.971	2572	12	2614	62	-2
April 13 2021	16BK374A-14-1		ign	1669001	747712	47	0.1714	0.0012	12.00	0.37	0.508	0.015	0.973	2571	12	2649	66	-3
April 13 2021	16BK374A-12-1		ign	1744175	760214	51	0.1714	0.0013	11.68	0.43	0.494	0.018	0.980	2571	12	2590	76	-1
April 13 2021	16BK374A-10-2		ign	2174623	994401	41	0.1712	0.0012	12.24	0.43	0.519	0.018	0.979	2569	12	2694	75	-5
April 13 2021	16BK374A-15-1		ign	2641437	1188542	40	0.1712	0.0012	12.04	0.36	0.510	0.015	0.971	2569	12	2658	63	-3
April 13 2021	16BK374A-4-2		ign	1941388	865770	40	0.1711	0.0012	11.93	0.37	0.506	0.015	0.973	2569	12	2639	65	-3
April 13 2021	16BK374A-16-1		ign	1872325	786461	55	0.1695	0.0012	11.13	0.32	0.476	0.013	0.968	2552	12	2512	57	2
April 13 2021	16BK374A-6-2	disc	ign	655353	244370	70	0.1731	0.0013	10.09	0.42	0.423	0.017	0.985	2588	12	2274	78	14
April 13 2021	16BK374A-29-1	cPb,mix	ign	1205035	498245	123	0.1752	0.0013	11.32	0.31	0.469	0.012	0.962	2607	13	2479	54	5
April 13 2021	16BK374A-26-2	mix	ign	2155817	837921	61	0.1698	0.0013	10.32	0.30	0.441	0.012	0.967	2556	12	2355	55	9
April 13 2021	16BK374A-23-2	cPb,mix	ign	547108	208606	447	0.1971	0.0066	11.75	0.53	0.433	0.013	0.680	2802	53	2317	60	21
April 13 2021	16BK374A-24-1	cPb,mix	ign	1295750	562086	237	0.1768	0.0018	11.99	0.35	0.492	0.013	0.933	2623	17	2580	57	2
April 13 2021	16BK374A-1-1	disc	ign	1999322	759515	49	0.1714	0.0012	10.18	0.31	0.431	0.013	0.973	2571	12	2310	58	11
April 15 2021	19BN106B-1-1		ign	600186	273903	25	0.1745	0.0013	11.95	0.40	0.497	0.016	0.975	2601	12	2601	69	0
April 15 2021	19BN106B-10-1		ign	324065	143263	24	0.1719	0.0013	11.41	0.38	0.481	0.016	0.973	2576	13	2534	67	2
April 15 2021	19BN106B-10-2		ign	413007	186809	22	0.1718	0.0012	11.67	0.38	0.493	0.015	0.975	2576	12	2582	66	0
April 15 2021	19BN106B-11-1		ign	655101	287486	53	0.1740	0.0013	11.46	0.36	0.478	0.015	0.973	2597	12	2518	64	3
April 15 2021	19BN106B-11-3		ign	668266	299036	57	0.1727	0.0013	11.60	0.38	0.487	0.016	0.975	2584	12	2559	68	1
April 15 2021	19BN106B-14-1		ign	1533811	700238	106	0.1725	0.0012	11.82	0.37	0.497	0.015	0.972	2582	12	2602	64	-1
April 15 2021	19BN106B-17-1		ign	1244292	588237	32	0.1710	0.0012	11.66	0.35	0.495	0.014	0.970	2567	12	2592	61	-1
April 15 2021	19BN106B-18-1		ign	556969	250429	30	0.1721	0.0013	11.62	0.38	0.490	0.015	0.974	2579	12	2569	66	0
April 15 2021	19BN106B-18-2		ign	530624	235658	34	0.1728	0.0013	11.52	0.36	0.484	0.015	0.971	2585	12	2543	63	2
April 15 2021	19BN106B-20-1		ign	516617	225891	35	0.1726	0.0013	11.32	0.36	0.476	0.015	0.973	2583	12	2511	64	3
April 15 2021	19BN106B-21-1		ign	512322	215138	34	0.1730	0.0013	11.39	0.34	0.478	0.014	0.969	2587	12	2517	61	3
April 15 2021	19BN106B-21-2		ign	480916	208866	38	0.1729	0.0013	11.27	0.36	0.473	0.015	0.974	2586	12	2497	64	4
April 15 2021	19BN106B-22-1		ign	1928351	851039	36	0.1710	0.0013	11.83	0.37	0.502	0.015	0.972	2567	12	2622	65	-2
April 15 2021	19BN106B-23-1		ign	1245292	563789	46	0.1711	0.0012	11.62	0.37	0.493	0.015	0.974	2568	12	2584	65	-1
April 15 2021	19BN106B-26-1		ign	510893	219899	65	0.1723	0.0013	11.62	0.35	0.490	0.014	0.967	2580	13	2569	61	0
April 15 2021	19BN106B-27-1		ign	949994	431871	37	0.1712	0.0012	11.68	0.36	0.495	0.015	0.973	2569	12	2593	64	-1
April 15 2021	19BN106B-30-1		ign	674215	301605	41	0.1733	0.0012	11.64	0.37	0.487	0.015	0.975	2590	12	2558	65	1
April 15 2021	19BN106B-30-2		ign	861631	385147	39	0.1736	0.0012	11.65	0.37	0.487	0.015	0.974	2593	12	2557	65	1
April 15 2021	19BN106B-31-1		ign	492009	216231	44	0.1718	0.0012	11.33	0.36	0.479	0.015	0.975	2576	12	2521	64	2
April 15 2021	19BN106B-32-1		ign	552685	240623	53	0.1720	0.0012	11.24	0.36	0.474	0.015	0.975	2577	12	2502	65	3

Session	Spot ID	Screen	Class	238U cps	206Pb cps	204 cps	Ratios						Dates (Ma)				Disc. %	
							207Pb		206Pb		ρ	207Pb		206Pb				
							206Pb	2σ	235U	2σ		206Pb	2σ	206Pb	2σ			
April 15 2021	19BN106B-33-1		ign	1370514	619868	44	0.1712	0.0012	11.62	0.37	0.493	0.015	0.975	2569	12	2582	66	0
April 15 2021	19BN106B-35-1		ign	1073474	483469	106	0.1727	0.0012	11.68	0.40	0.490	0.017	0.978	2584	12	2573	71	0
April 15 2021	19BN106B-36-1		ign	351687	157032	71	0.1718	0.0013	11.51	0.38	0.486	0.016	0.974	2575	12	2555	67	1
April 15 2021	19BN106B-37-1		ign	593356	248750	64	0.1728	0.0013	11.36	0.32	0.477	0.013	0.966	2585	12	2513	57	3
April 15 2021	19BN106B-38-1		ign	349072	154999	74	0.1726	0.0013	11.50	0.39	0.484	0.016	0.974	2583	13	2543	68	2
April 15 2021	19BN106B-39-1		ign	490311	210876	65	0.1721	0.0013	11.11	0.35	0.468	0.014	0.972	2579	12	2476	63	4
April 15 2021	19BN106B-4-1		ign	297807	134810	19	0.1716	0.0013	11.66	0.38	0.493	0.016	0.973	2573	13	2584	67	0
April 15 2021	19BN106B-7-1		ign	1590488	715452	134	0.1729	0.0012	11.67	0.36	0.490	0.015	0.974	2586	12	2570	64	1
April 15 2021	19BN106B-7-2		ign	629541	273620	17	0.1716	0.0013	11.69	0.33	0.494	0.014	0.963	2573	13	2589	58	-1
April 15 2021	19BN106B-8-1		ign	512390	230417	7	0.1724	0.0013	11.63	0.38	0.490	0.016	0.975	2581	12	2570	68	0
April 15 2021	19BN106B-9-1		ign	939194	424125	24	0.1720	0.0012	11.66	0.37	0.492	0.015	0.975	2577	12	2578	66	0
April 15 2021	19BN106B-13-1		ign	1516955	679715	61	0.1702	0.0012	11.45	0.37	0.488	0.015	0.975	2560	12	2562	66	0
April 15 2021	19BN106B-28-1		ign	650161	274052	55	0.1652	0.0013	10.91	0.34	0.479	0.015	0.970	2509	13	2525	63	-1
April 15 2021	19BN106B-25-1		ign	586835	251255	63	0.1651	0.0012	10.61	0.34	0.466	0.014	0.974	2509	12	2467	63	2
April 15 2021	19BN106B-24-1	mix	ign	2345513	1078434	33	0.1690	0.0012	11.67	0.36	0.501	0.015	0.974	2548	12	2617	65	-3
April 15 2021	19BN106B-12-1	mix	ign	1859192	850238	39	0.1682	0.0012	11.54	0.38	0.498	0.016	0.976	2539	12	2605	68	-3
April 15 2021	19BN106B-6-1	mix	ign	1816346	832907	9	0.1648	0.0012	11.34	0.36	0.499	0.016	0.975	2506	12	2611	66	-4
April 15 2021	19BN106B-34-1	mix	ign	2081252	939135	120	0.1644	0.0012	11.13	0.35	0.491	0.015	0.974	2501	12	2577	65	-3
April 15 2021	19BN106B-11-2	mix	ign	3997405	1647658	78	0.1601	0.0015	9.91	0.29	0.449	0.013	0.947	2457	16	2390	56	3
April 15 2021	19BN106B-3-1	mix	ign	1989515	925982	21	0.1682	0.0013	11.75	0.36	0.507	0.015	0.966	2539	13	2643	64	-4
April 15 2021	19BN106B-2-1	mix,cPb	ign	3355515	1306833	1529	0.1685	0.0022	9.85	0.39	0.424	0.016	0.944	2543	22	2279	72	12
April 15 2021	19BN106B-5-1	mix,cPb	ign	4914734	1693227	465	0.1444	0.0042	7.47	0.36	0.375	0.014	0.794	2281	49	2054	66	11
April 15 2021	19BN106B-5-2	mix,cPb	ign	535657	234985	186	0.1829	0.0018	12.04	0.37	0.478	0.014	0.947	2679	16	2517	60	6
April 15 2021	19BN106B-29-1	mix,cPb	ign	1420316	651730	726	0.1886	0.0047	12.99	0.52	0.500	0.016	0.784	2730	40	2613	67	4
April 15 2021	19BN106B-9-2	mix,cPb	ign	636028	277820	339	0.1873	0.0027	12.28	0.42	0.476	0.015	0.908	2718	24	2509	64	8
April 15 2021	19BN106B-15-1	mix,cPb	ign	1072043	494032	361	0.1793	0.0019	12.40	0.40	0.502	0.015	0.943	2646	18	2622	66	1
April 15 2021	19BN106B-16-1	mix,cPb	ign	631316	290415	167	0.1775	0.0014	12.26	0.41	0.501	0.016	0.972	2630	13	2618	70	0
April 15 2021	19BN106B-16-2	mix,cPb	ign	1235856	574050	1223	0.2020	0.0026	14.08	0.48	0.506	0.016	0.929	2842	20	2639	69	8
April 15 2021	19BN106B-16-3	mix,cPb	ign	426652	194125	492	0.2076	0.0033	14.18	0.52	0.496	0.016	0.899	2887	26	2594	70	11
April 15 2021	19BN106B-19-1	cPb	ign	764327	342947	107	0.1748	0.0013	11.77	0.37	0.489	0.015	0.972	2604	12	2565	64	2
April 15 2021	16BK366A-1-1		ign	1927588	886552	23	0.1712	0.0012	11.91	0.38	0.505	0.016	0.975	2569	12	2634	68	-2
April 15 2021	16BK366A-2-1		ign	485750	213813	32	0.1714	0.0013	11.41	0.36	0.483	0.015	0.973	2572	12	2540	65	1
April 15 2021	16BK366A-3-1		ign	920302	412380	33	0.1716	0.0012	11.63	0.37	0.492	0.015	0.973	2573	12	2578	65	0
April 15 2021	16BK366A-4-1		ign	1559573	690804	26	0.1707	0.0012	12.14	0.44	0.516	0.018	0.980	2565	12	2682	77	-4
April 15 2021	16BK366A-4-2		ign	543423	239929	22	0.1715	0.0013	11.45	0.36	0.485	0.015	0.973	2573	12	2547	64	1
April 15 2021	16BK366A-5-1		ign	461272	202735	83	0.1733	0.0013	11.52	0.37	0.482	0.015	0.973	2590	12	2537	66	2
April 15 2021	16BK366A-6-1		ign	2512325	1137459	65	0.1705	0.0012	11.68	0.35	0.497	0.014	0.972	2563	12	2600	62	-1
April 15 2021	16BK366A-7-1		ign	1952891	873609	80	0.1708	0.0012	11.56	0.34	0.491	0.014	0.971	2566	12	2575	60	0
April 15 2021	16BK366A-8-1		ign	1138824	518360	61	0.1707	0.0012	11.75	0.35	0.499	0.015	0.972	2564	12	2612	62	-2
April 15 2021	16BK366A-9-1		ign	1288637	592645	82	0.1717	0.0012	11.94	0.39	0.505	0.016	0.975	2574	12	2634	69	-2
April 15 2021	18BK366A-10-1		ign	3688082	1663484	82	0.1696	0.0012	11.57	0.34	0.495	0.014	0.970	2554	12	2592	60	-1
April 15 2021	18BK366A-11-1		ign	2045270	899655	101	0.1708	0.0013	11.39	0.33	0.484	0.013	0.963	2565	13	2544	58	1
April 15 2021	18BK366A-12-1		ign	739181	323103	71	0.1708	0.0012	11.29	0.33	0.480	0.014	0.969	2565	12	2526	60	2
April 15 2021	18BK366A-13-1		ign	465646	194037	77	0.1719	0.0013	10.86	0.33	0.458	0.013	0.967	2576	13	2433	59	6
April 15 2021	18BK366A-14-1		ign	716300	316231	25	0.1715	0.0012	11.45	0.37	0.484	0.015	0.975	2572	12	2547	65	1
April 15 2021	18BK366A-15-1		ign	623457	285454	24	0.1715	0.0012	11.87	0.38	0.502	0.016	0.974	2572	12	2624	67	-2
April 15 2021	18BK366A-16-1		ign	1898010	873529	69	0.1710	0.0012	11.90	0.37	0.505	0.015	0.973	2568	12	2635	65	-3

Session	Spot ID	Screen	Class	238U cps	206Pb cps	204 cps	Ratios						Dates (Ma)				Disc. %					
							207Pb		207Pb		206Pb		207Pb		206Pb			ρ	207Pb 206Pb	2σ	238U	2σ
							206Pb	2σ	235U	2σ	238U	2σ	206Pb	2σ								
April 15 2021	18BK366A-17-1		ign	406635	178773	28	0.1716	0.0013	11.41	0.40	0.482	0.017	0.977	2573	13	2538	72	1				
April 15 2021	18BK366A-18-1		ign	361921	160569	21	0.1715	0.0013	11.51	0.39	0.487	0.016	0.975	2573	12	2557	69	1				
April 15 2021	18BK366A-19-1		ign	853684	368639	27	0.1708	0.0012	11.15	0.34	0.474	0.014	0.972	2565	12	2501	62	3				
April 15 2021	16BK366A-20-1		ign	450724	197139	38	0.1720	0.0013	11.37	0.36	0.480	0.015	0.972	2577	12	2526	64	2				
April 15 2021	16BK366A-21-1		ign	836439	383732	46	0.1716	0.0012	11.90	0.40	0.503	0.016	0.977	2573	12	2629	70	-2				
April 15 2021	16BK366A-22-1		ign	665197	289994	36	0.1714	0.0014	11.43	0.35	0.484	0.014	0.966	2571	13	2545	62	1				
July 10 2020	19BC02A-5-2		ign	1369862	740885	67	0.1674	0.0012	11.15	0.42	0.483	0.018	0.982	2531	12	2542	77	0				
July 10 2020	19BC02A-10-1		ign	1240607	643345	23	0.1666	0.0015	10.74	0.38	0.468	0.016	0.969	2524	15	2474	70	2				
July 10 2020	19BC02A-9-2		ign	2106408	1138747	13	0.1664	0.0012	11.19	0.43	0.488	0.019	0.984	2522	12	2561	80	-2				
July 10 2020	19BC02A-1-1		ign	2531271	1390656	50	0.1662	0.0012	11.25	0.48	0.491	0.021	0.986	2519	12	2575	89	-2				
July 10 2020	19BC02A-9-6		ign	960919	461406	77	0.1659	0.0012	10.59	0.40	0.463	0.017	0.981	2517	12	2453	75	3				
July 10 2020	19BC02A-2-1		ign	3306799	1799169	21	0.1657	0.0012	11.11	0.43	0.486	0.019	0.983	2515	12	2555	80	-2				
July 10 2020	19BC02A-5-1		ign	1575417	805187	33	0.1655	0.0012	10.42	0.37	0.457	0.016	0.980	2513	12	2426	71	4				
July 10 2020	19BC02A-9-4		ign	3384916	1833607	4	0.1655	0.0012	11.15	0.39	0.489	0.017	0.978	2513	12	2565	72	-2				
July 10 2020	19BC02A-7-1		ign	369611	187013	49	0.1654	0.0012	10.31	0.39	0.452	0.017	0.982	2512	12	2405	75	4				
July 10 2020	19BC02A-9-5		ign	376502	199838	4	0.1650	0.0012	10.89	0.46	0.479	0.020	0.985	2508	12	2522	86	-1				
July 10 2020	19BC02A-9-3		ign	2789598	1402084	76	0.1648	0.0013	11.01	0.39	0.485	0.017	0.977	2505	13	2548	73	-2				
July 10 2020	19BC02A-6-2		ign	1160541	610983	29	0.1636	0.0012	10.61	0.40	0.471	0.017	0.981	2494	12	2486	75	0				
July 10 2020	19BC02A-8-1		ign	551073	287773	48	0.1629	0.0015	10.58	0.40	0.471	0.017	0.970	2486	15	2488	75	0				
July 10 2020	19BC02A-9-1		ign	2403720	1248351	87	0.1629	0.0011	10.52	0.37	0.468	0.016	0.980	2486	12	2477	71	0				
July 10 2020	19BC02A-6-1		ign	1650500	888815	20	0.1626	0.0012	10.79	0.41	0.481	0.018	0.982	2483	12	2533	77	-2				
July 10 2020	19BC02A-11-2		ign	1719254	908794	59	0.1621	0.0012	10.66	0.41	0.477	0.018	0.983	2478	12	2513	79	-1				
July 10 2020	19BC02A-11-3		ign	1327756	683419	57	0.1615	0.0012	10.33	0.40	0.464	0.018	0.980	2471	13	2459	77	1				
July 10 2020	19BC02A-11-1		ign	1203272	608586	15	0.1609	0.0011	10.12	0.38	0.456	0.017	0.982	2465	12	2423	74	2				
July 10 2020	19BC02A-25		ign	451889	214251	25	0.1609	0.0013	10.14	0.42	0.457	0.018	0.981	2465	14	2427	81	2				
July 10 2020	19BC02A-6-4		ign	481102	239567	54	0.1605	0.0012	9.84	0.38	0.445	0.017	0.980	2461	13	2373	74	4				
July 10 2020	19BC02A-10-2		met?	89127	41411	7	0.1560	0.0016	9.01	0.38	0.419	0.017	0.969	2413	17	2257	77	7				
July 10 2020	19BC02A-9-7		met?	81787	35380	14	0.1526	0.0016	8.77	0.36	0.417	0.016	0.967	2375	17	2248	74	6				
July 10 2020	19BC02A-3-1	mix	ign	3814596	2051060	325	0.1632	0.0012	10.81	0.43	0.481	0.019	0.983	2489	12	2530	81	-2				
July 10 2020	19BC02A-4-1	mix	ign	1526983	713315	97	0.1596	0.0014	9.18	0.38	0.418	0.017	0.977	2451	15	2249	77	9				
July 10 2020	19BC02A-6-4	mix,cPb	ign	423330	207678	96	0.1609	0.0014	9.72	0.36	0.439	0.016	0.971	2465	15	2344	70	5				
Mar 2 2022	19BN154A_16-1		ign	2709153	1163111	89	0.1637	0.0016	10.04	0.32	0.445	0.014	0.953	2494	16	2372	60	5				
Mar 2 2022	19BN154A_17-1		ign	1816462	826986	23	0.1639	0.0015	10.65	0.34	0.472	0.014	0.956	2496	16	2491	62	0				
Mar 2 2022	19BN154A_18-1		ign	2247471	1038193	15	0.1634	0.0015	10.78	0.37	0.479	0.016	0.962	2491	16	2521	69	-1				
Mar 2 2022	19BN154A_19-1		ign	1247547	596585	56	0.1652	0.0016	11.10	0.36	0.488	0.015	0.957	2510	16	2560	66	-2				
Mar 2 2022	19BN154A_20-1		ign	2898754	1330935	69	0.1641	0.0015	10.76	0.36	0.476	0.015	0.960	2498	16	2509	67	0				
Mar 2 2022	19BN154A_22-1		ign	2135482	960293	128	0.1642	0.0016	10.82	0.37	0.478	0.016	0.960	2500	16	2518	68	-1				
Mar 2 2022	19BN154A_23-1		ign	2413986	1095638	92	0.1657	0.0016	10.74	0.33	0.470	0.014	0.950	2515	16	2485	60	1				
Mar 2 2022	19BN154A_24-1		ign	1961516	922078	34	0.1644	0.0015	11.04	0.35	0.487	0.015	0.955	2502	16	2558	63	-2				
Mar 2 2022	19BN154A_26-1		ign	2467595	1141433	27	0.1639	0.0015	10.82	0.35	0.479	0.015	0.957	2496	16	2524	64	-1				
Mar 2 2022	19BN154A_27-1		ign	1845978	857800	67	0.1645	0.0016	10.91	0.37	0.481	0.015	0.957	2502	16	2534	67	-1				
Mar 2 2022	19BN154A_28-1		ign	2666906	1191907	98	0.1641	0.0015	10.74	0.36	0.475	0.015	0.961	2498	16	2505	67	0				
Mar 2 2022	19BN154A_29-1		ign	3028538	1415203	61	0.1634	0.0015	10.91	0.35	0.484	0.015	0.958	2492	16	2545	64	-2				
Mar 2 2022	19BN154A_30-1		ign	1426336	645527	45	0.1651	0.0016	10.67	0.36	0.469	0.015	0.960	2509	16	2479	66	1				
Mar 2 2022	19BN154A_31-1		ign	2420653	1105674	101	0.1635	0.0015	10.66	0.34	0.473	0.015	0.958	2492	16	2498	64	0				

Session	Spot ID	Screen	Class	238U cps	206Pb cps	204 cps	Ratios						Dates (Ma)				Disc. %	
							207Pb		206Pb		ρ	207Pb		206Pb				
							206Pb	2σ	235U	2σ		238U	2σ	207Pb	2σ	206Pb		2σ
Mar 2 2022	19BN154A_8-2		ign	2155151	1004510	45	0.1638	0.0015	10.90	0.35	0.483	0.015	0.957	2496	16	2540	65	-2
Mar 2 2022	19BN154A_9-2		ign	1329598	600454	61	0.1646	0.0016	10.62	0.34	0.468	0.014	0.955	2504	16	2474	63	1
May 28 2021	19BN154A_1-1		ign	1728677	837545	146	0.1654	0.0015	10.97	0.40	0.481	0.017	0.969	2512	15	2532	73	-1
May 28 2021	19BN154A_10-1		ign	1640330	751943	50	0.1647	0.0015	10.55	0.36	0.465	0.015	0.965	2505	15	2461	67	2
May 28 2021	19BN154A_11-1		ign	1187243	536175	51	0.1651	0.0015	10.42	0.38	0.458	0.016	0.968	2509	15	2430	71	3
May 28 2021	19BN154A_12-1		ign	1382397	621008	44	0.1657	0.0015	10.40	0.36	0.455	0.015	0.967	2514	15	2420	68	4
May 28 2021	19BN154A_13-1		ign	1962528	883556	58	0.1663	0.0015	10.46	0.37	0.457	0.015	0.966	2521	15	2424	68	4
May 28 2021	19BN154A_14-1		ign	1358392	635063	67	0.1640	0.0015	11.01	0.40	0.487	0.017	0.968	2497	15	2558	73	-2
May 28 2021	19BN154A_2-1		ign	1815491	892355	170	0.1652	0.0015	11.11	0.39	0.488	0.017	0.967	2509	15	2563	72	-2
May 28 2021	19BN154A_3-1		ign	2324687	1128427	59	0.1644	0.0015	10.92	0.40	0.482	0.017	0.970	2502	15	2536	74	-1
May 28 2021	19BN154A_4-1		ign	1809201	875327	49	0.1633	0.0015	10.82	0.40	0.480	0.017	0.969	2491	15	2529	74	-2
May 28 2021	19BN154A_5-1		ign	1376731	670979	50	0.1660	0.0015	11.07	0.41	0.484	0.017	0.970	2518	15	2545	75	-1
May 28 2021	19BN154A_6-1		ign	1946977	952484	108	0.1662	0.0015	11.13	0.43	0.486	0.018	0.972	2519	15	2553	78	-1
May 28 2021	19BN154A_6-2		ign	2805915	1307941	78	0.1654	0.0015	10.55	0.35	0.463	0.015	0.962	2512	15	2452	65	2
May 28 2021	19BN154A_8-1		ign	1907434	841901	124	0.1658	0.0015	10.23	0.32	0.448	0.013	0.958	2516	15	2384	60	6
May 28 2021	19BN154A_9-1		ign	787589	345802	48	0.1659	0.0015	10.18	0.38	0.445	0.016	0.970	2517	15	2374	71	6
May 28 2021	19BN154A_7-1	cPb,mix	ign	1318499	605360	140	0.1665	0.0015	10.68	0.39	0.466	0.016	0.967	2523	15	2464	71	2
Mar 2 2022	19BN154A_15-1	cPb,mix	ign	2900889	1303700	278	0.1668	0.0016	10.70	0.35	0.466	0.015	0.957	2526	16	2464	65	2
Mar 2 2022	19BN154A_21-1	cPb	ign	1477296	670661	369	0.1713	0.0017	11.10	0.35	0.470	0.014	0.952	2570	16	2485	61	3
Mar 2 2022	19BN154A_25-1	cPb,mix	ign	2510269	1136869	1595	0.1908	0.0082	12.34	0.68	0.469	0.016	0.627	2749	69	2480	71	11
Feb 28 2022	19BN173A_33-1		ign	208162	100906	15	0.1677	0.0015	10.85	0.38	0.469	0.016	0.969	2535	14	2481	70	2
Feb 28 2022	19BN173A_8-1		ign	831323	403380	58	0.1663	0.0012	10.77	0.38	0.470	0.016	0.979	2520	12	2483	71	2
Feb 28 2022	19BN173A_21-1		ign	167804	78938	25	0.1658	0.0013	10.41	0.37	0.455	0.016	0.974	2516	13	2420	70	4
Feb 28 2022	19BN173A_10-2		ign	278758	134031	49	0.1657	0.0013	10.90	0.38	0.477	0.016	0.973	2515	14	2516	71	0
Feb 28 2022	19BN173A_31-1		ign	267195	128258	51	0.1654	0.0013	10.60	0.36	0.465	0.016	0.973	2512	13	2461	68	2
Feb 28 2022	19BN173A_54-1	ign?		234646	112398	67	0.1652	0.0013	10.01	0.36	0.440	0.015	0.974	2510	13	2349	68	7
Feb 28 2022	19BN173A_49-1		ign	238182	114646	49	0.1651	0.0013	10.05	0.36	0.442	0.016	0.977	2508	13	2358	69	6
Feb 28 2022	19BN173A_12-2		ign	540920	246303	0	0.1649	0.0012	10.02	0.37	0.441	0.016	0.981	2506	12	2355	72	6
Feb 28 2022	19BN173A_19-1		ign	1983296	995542	22	0.1647	0.0012	11.03	0.39	0.486	0.017	0.980	2505	12	2554	72	-2
Feb 28 2022	19BN173A_17-1		ign	266512	122434	7	0.1646	0.0012	10.09	0.35	0.445	0.015	0.976	2504	12	2372	66	6
Feb 28 2022	19BN173A_1-1		ign	290010	134402	44	0.1645	0.0012	10.43	0.37	0.460	0.016	0.977	2502	13	2441	69	3
Feb 28 2022	19BN173A_35-1		ign	2330521	1181128	67	0.1643	0.0012	11.11	0.40	0.491	0.017	0.981	2501	12	2574	75	-3
Feb 28 2022	19BN173A_14-1		ign	1779710	790436	0	0.1642	0.0012	9.97	0.34	0.440	0.015	0.978	2500	12	2352	65	6
Feb 28 2022	19BN173A_27-2		ign	316858	147271	13	0.1642	0.0013	10.18	0.35	0.450	0.015	0.974	2499	13	2395	67	4
Feb 28 2022	19BN173A_56-2		ign	1576506	794484	57	0.1640	0.0012	10.46	0.37	0.463	0.016	0.980	2498	12	2451	71	2
Feb 28 2022	19BN173A_44-1		ign	3219663	1613145	122	0.1639	0.0013	10.79	0.36	0.478	0.016	0.970	2497	14	2517	67	-1
Feb 28 2022	19BN173A_12-1		ign	2157777	994722	0	0.1639	0.0012	10.34	0.35	0.458	0.015	0.977	2497	12	2430	66	3
Feb 28 2022	19BN173A_43-1		ign	3202594	1644809	314	0.1638	0.0012	10.82	0.40	0.479	0.017	0.980	2495	12	2524	75	-1
Feb 28 2022	19BN173A_48-1		ign	2048378	1020251	95	0.1636	0.0012	10.31	0.36	0.457	0.016	0.978	2493	12	2427	69	3
Feb 28 2022	19BN173A_2-1		ign	209637	88900	87	0.1634	0.0013	9.79	0.32	0.435	0.014	0.970	2492	13	2327	62	7
Feb 28 2022	19BN173A_4-1		ign	156088	74008	0	0.1632	0.0015	10.93	0.37	0.486	0.016	0.965	2489	15	2554	69	-3
Feb 28 2022	19Bn173A_28-1		ign	325594	150271	42	0.1632	0.0012	10.05	0.35	0.447	0.015	0.976	2489	13	2381	67	5
Feb 28 2022	19BN173A_18-1		ign	3526503	1831939	76	0.1632	0.0011	11.31	0.37	0.503	0.016	0.977	2489	12	2627	69	-5
Feb 28 2022	19BN173A_32-1		ign	3655202	1818935	70	0.1626	0.0011	10.79	0.36	0.482	0.016	0.978	2482	12	2535	68	-2
Feb 28 2022	19BN173A_41-1		ign	1073954	535879	2	0.1619	0.0012	10.39	0.45	0.466	0.020	0.985	2476	13	2465	87	0
Feb 28 2022	19BN173A_47-1		ign	1285852	623007	48	0.1618	0.0011	9.92	0.36	0.445	0.016	0.981	2475	12	2371	70	4
Feb 28 2022	19BN173A_3-1		ign	3139918	1497647	155	0.1615	0.0012	10.89	0.35	0.489	0.015	0.975	2472	12	2566	66	-4

Session	Spot ID	Screen	Class	238U cps	206Pb cps	204 cps	Ratios						Dates (Ma)				Disc. %					
							207Pb		207Pb		206Pb		207Pb		206Pb			p	207Pb 206Pb	2σ	206Pb 238U	2σ
							206Pb	2σ	235U	2σ	238U	2σ	206Pb	2σ	206Pb	2σ						
Feb 28 2022	19BN173A_27-1		ign	1130106	510011	101	0.1615	0.0012	10.30	0.33	0.463	0.014	0.971	2471	13	2451	64	1				
Feb 28 2022	19BN173A_36-1		ign	3235352	1623363	37	0.1614	0.0011	10.81	0.37	0.486	0.016	0.979	2470	12	2553	70	-3				
Feb 28 2022	19BN173A_42-1		ign	3345981	1620960	58	0.1605	0.0012	10.00	0.35	0.452	0.015	0.978	2461	12	2405	67	2				
Feb 28 2022	19BN173A_6-1		ign	2006309	961315	35	0.1599	0.0012	10.48	0.34	0.476	0.015	0.976	2454	12	2509	66	-2				
Feb 28 2022	19BN173A_5-2		ign	2864309	1394872	11	0.1590	0.0011	10.60	0.36	0.484	0.016	0.976	2445	12	2543	68	-4				
Feb 28 2022	19BN173A_15-2		ign?	256349	113939	16	0.1586	0.0013	9.41	0.32	0.430	0.014	0.972	2441	13	2307	64	6				
Feb 28 2022	19BN173A_51-1		ign	2841318	1461564	90	0.1569	0.0011	10.21	0.36	0.472	0.016	0.979	2423	12	2493	71	-3				
Feb 28 2022	19BN173A_53-1		met	209386	99340	72	0.1563	0.0012	9.38	0.36	0.435	0.017	0.980	2416	13	2330	74	4				
Feb 28 2022	19BN173A_46-1		met	163940	73298	21	0.1562	0.0019	9.17	0.36	0.426	0.016	0.951	2414	20	2289	71	5				
Feb 28 2022	19BN173A_24-1		met	164205	72232	44	0.1561	0.0012	9.16	0.32	0.426	0.014	0.974	2414	13	2287	65	6				
Feb 28 2022	19BN173A_45-1		met	170457	79176	9	0.1559	0.0013	9.32	0.34	0.434	0.015	0.975	2412	14	2322	68	4				
Feb 28 2022	19BN173A_23-1		met	135992	60242	28	0.1552	0.0014	9.18	0.33	0.429	0.015	0.966	2404	16	2301	67	4				
Feb 28 2022	19BN173A_38-1		met	456272	208729	70	0.1550	0.0011	9.12	0.32	0.427	0.015	0.977	2402	13	2292	65	5				
Feb 28 2022	19BN173A_9-1		met	339891	149022	69	0.1549	0.0012	9.29	0.31	0.435	0.014	0.973	2400	13	2330	63	3				
Feb 28 2022	19BN173A_39-1		met	266658	121562	45	0.1547	0.0012	9.07	0.33	0.425	0.015	0.977	2398	13	2285	68	5				
Feb 28 2022	19BN173A_6-2	cPb	ign	193744	93010	129	0.1648	0.0013	10.83	0.40	0.477	0.017	0.975	2506	14	2513	74	0				
Feb 28 2022	19BN173A_7-1	cPb	ign?	250950	120296	104	0.1648	0.0013	10.81	0.47	0.476	0.020	0.984	2506	13	2510	88	0				
Feb 28 2022	19BN173A_20-1	cPb	ign	896030	431964	148	0.1673	0.0013	11.40	0.38	0.494	0.016	0.974	2531	12	2589	68	-2				
Feb 28 2022	19BN173A_22-1	mix	ign	2152372	1049726	945	0.1767	0.0027	11.50	0.43	0.472	0.016	0.913	2623	25	2493	71	5				
Feb 28 2022	19BN173A_47-2	mix	ign	375309	189426	87	0.1690	0.0016	10.79	0.42	0.463	0.018	0.972	2547	15	2454	77	4				
Feb 28 2022	19BN173A_55-1	mix	ign	841631	419481	101	0.1680	0.0013	10.59	0.39	0.457	0.017	0.976	2538	13	2428	73	5				
Feb 28 2022	19BN173A_56-1	mix	ign	1251041	627934	146	0.1643	0.0012	10.43	0.39	0.461	0.017	0.980	2500	12	2442	74	2				
Feb 28 2022	19BN173A_5-1	mix,cPb	ign	2531396	1225892	175	0.1624	0.0016	10.76	0.36	0.481	0.015	0.958	2481	16	2531	67	-2				
Feb 28 2022	19BN173A_10-1	mix,cPb	ign	1846239	873170	379	0.1646	0.0013	10.66	0.37	0.470	0.016	0.975	2504	13	2482	70	1				
Feb 28 2022	19BN173A_10-3	mix,cPb	ign?	181752	79610	219	0.1924	0.0032	11.53	0.44	0.435	0.015	0.896	2763	27	2328	66	19				
Feb 28 2022	19BN173A_11-1	mix,cPb	ign	3313923	1562112	661	0.1697	0.0018	10.95	0.38	0.468	0.016	0.954	2555	17	2475	68	3				
Feb 28 2022	19BN173A_13-1	mix,cPb	ign	1270506	601332	1397	0.2052	0.0057	12.96	0.61	0.458	0.017	0.806	2868	45	2432	76	18				
Feb 28 2022	19BN173A_15-1	mix,cPb	ign	2125993	896573	2551	0.2015	0.0087	11.34	0.63	0.408	0.014	0.629	2838	69	2207	65	29				
Feb 28 2022	19BN173A_16-1	mix,cPb	ign	1661627	811574	565	0.1723	0.0013	11.23	0.40	0.473	0.016	0.978	2580	12	2496	72	3				
Feb 28 2022	19BN173A_25-1	mix,cPb	ign	1810055	858110	177	0.1569	0.0013	9.93	0.34	0.459	0.015	0.969	2423	14	2435	67	-1				
Feb 28 2022	19BN173A_26-1	mix,cPb	ign	1735954	835113	522	0.1686	0.0018	10.82	0.37	0.466	0.015	0.951	2544	18	2465	66	3				
Feb 28 2022	19BN173A_29-1	mix,cPb	ign	1917141	955639	271	0.1663	0.0012	11.06	0.40	0.483	0.017	0.979	2520	12	2539	73	-1				
Feb 28 2022	19BN173A_30-1	mix,cPb	ign	1822616	900903	676	0.1715	0.0025	11.31	0.42	0.479	0.016	0.919	2573	24	2521	71	2				
Feb 28 2022	19BN173A_34-1	mix,cPb	ign	2618003	1340634	355	0.1670	0.0014	11.41	0.42	0.496	0.018	0.974	2528	14	2596	77	-3				
Feb 28 2022	19BN173A_36-2	mix,cPb	ign	548709	263439	222	0.1734	0.0014	11.11	0.42	0.465	0.017	0.977	2591	13	2461	75	5				
Feb 28 2022	19BN173A_37-1	mix,cPb	ign	1885024	976679	510	0.1726	0.0013	11.94	0.45	0.502	0.019	0.979	2583	13	2621	79	-1				
Feb 28 2022	19BN173A_40-1	mix,cPb	ign	2649640	1372772	1256	0.1722	0.0018	11.48	0.43	0.484	0.018	0.962	2579	17	2543	76	1				
Feb 28 2022	19BN173A_50-1	mix,cPb	ign	1268884	652374	386	0.1744	0.0025	11.34	0.44	0.472	0.017	0.930	2600	24	2492	75	4				
Feb 28 2022	19BN173A_52-1	mix,cPb	ign	3271193	1714910	665	0.1657	0.0016	10.99	0.42	0.481	0.018	0.970	2515	16	2532	78	-1				
Mar 1 2022	19BN166A_1-1		ign	3970758	1961685	104	0.1644	0.0012	11.07	0.39	0.489	0.017	0.978	2502	12	2565	73	-2				
Mar 1 2022	19BN166A_2-1		ign	4049301	1805906	132	0.1624	0.0014	9.87	0.37	0.441	0.016	0.974	2480	14	2356	72	5				
Mar 1 2022	19BN166A_2-2		amb	1237022	558532	18	0.1550	0.0011	9.54	0.31	0.447	0.014	0.974	2402	12	2380	63	1				
Mar 1 2022	19BN166A_3-1		ign	932406	425656	164	0.1660	0.0012	10.33	0.40	0.452	0.017	0.981	2518	12	2402	75	5				
Mar 1 2022	19BN166A_4-1		ign	1965868	895839	40	0.1653	0.0012	10.27	0.34	0.451	0.015	0.977	2510	12	2399	64	5				
Mar 1 2022	19BN166A_4-2		ign	4357831	2024143	41	0.1630	0.0012	10.32	0.35	0.459	0.015	0.977	2487	12	2437	66	2				
Mar 1 2022	19BN166A_5-1		ign	1129251	492837	235	0.1639	0.0013	9.75	0.33	0.432	0.014	0.974	2497	13	2313	64	8				
Mar 1 2022	19BN166A_6-1		ign	3145916	1446218	306	0.1625	0.0012	10.18	0.36	0.455	0.016	0.976	2482	13	2416	69	3				

Session	Spot ID	Screen	Class	238U cps	206Pb cps	204 cps	Ratios						Dates (Ma)				Disc. %	
							207Pb		207Pb		206Pb		207Pb		206Pb			
							206Pb	2σ	235U	2σ	238U	2σ	206Pb	2σ	238U	2σ		
Mar 1 2022	19BN166A_7-1		ign	974781	447602	250	0.1661	0.0012	10.40	0.36	0.454	0.015	0.978	2519	12	2414	68	4
Mar 1 2022	19BN166A_8-1		ign	2331716	1091599	250	0.1644	0.0012	10.49	0.35	0.463	0.015	0.976	2502	12	2453	65	2
Mar 1 2022	19BN166A_9-1		ign	726627	335121	98	0.1642	0.0012	10.32	0.34	0.456	0.015	0.974	2500	13	2423	65	3
Mar 1 2022	19BN166A_10-1		ign	2485162	1184870	46	0.1645	0.0012	10.69	0.35	0.472	0.015	0.976	2502	12	2491	67	0
Mar 1 2022	19BN166A_10-2		ign	2818331	1343004	35	0.1641	0.0012	10.66	0.37	0.471	0.016	0.979	2498	12	2489	70	0
Mar 1 2022	19BN166A_11-1		amb	764398	327235	49	0.1563	0.0012	9.12	0.32	0.423	0.015	0.978	2416	12	2276	66	6
Mar 1 2022	19BN166A_12-1		ign	3843900	1828802	59	0.1647	0.0012	10.68	0.37	0.471	0.016	0.978	2505	12	2486	69	1
Mar 1 2022	19BN166A_12-2		amb	1455208	662993	92	0.1548	0.0011	9.62	0.34	0.451	0.015	0.978	2400	12	2398	68	0
Mar 1 2022	19BN166A_13-1		ign	1929329	899374	39	0.1660	0.0012	10.55	0.34	0.461	0.015	0.974	2518	12	2444	64	3
Mar 1 2022	19BN166A_14-1		ign	4768817	2280669	33	0.1639	0.0012	10.69	0.36	0.473	0.016	0.977	2497	12	2497	68	0
Mar 1 2022	19BN166A_15-1		inhrt	1304111	645044	117	0.1707	0.0012	11.51	0.39	0.489	0.016	0.977	2564	12	2567	70	0
Mar 1 2022	19BN166A_16-1		ign	1599020	775150	173	0.1648	0.0012	10.89	0.37	0.480	0.016	0.977	2505	12	2525	69	-1
Mar 1 2022	19BN166A_17-1		ign	2469400	1192724	87	0.1638	0.0012	10.79	0.35	0.478	0.015	0.976	2496	12	2517	66	-1
Mar 1 2022	19BN166A_17-2		ign	2423548	1195586	62	0.1644	0.0012	11.05	0.37	0.488	0.016	0.977	2501	12	2562	68	-2
Mar 1 2022	19BN166A_18-1		ign	2111068	1017583	73	0.1639	0.0012	10.77	0.39	0.477	0.017	0.980	2496	12	2513	73	-1
Mar 1 2022	19BN166A_19-1		inhrt	800150	364035	47	0.1674	0.0013	10.38	0.35	0.450	0.015	0.975	2532	13	2395	66	6
Mar 1 2022	19BN166A_19-2		ign	1331042	620431	34	0.1646	0.0012	10.46	0.35	0.461	0.015	0.976	2504	12	2444	66	2
Mar 1 2022	19BN166A_20-1		ign	1771094	808979	733	0.1772	0.0023	11.03	0.38	0.452	0.014	0.929	2627	21	2403	63	9
Mar 1 2022	19BN166A_20-2		ign	2761799	1317614	182	0.1658	0.0013	10.78	0.36	0.472	0.016	0.975	2515	13	2492	68	1
Mar 1 2022	19BN166A_21-1		ign	1529015	728773	43	0.1651	0.0012	10.73	0.36	0.471	0.015	0.976	2509	12	2490	67	1
Mar 1 2022	19BN166A_22-1		ign	1723409	826584	63	0.1633	0.0012	10.67	0.35	0.474	0.015	0.975	2490	12	2503	67	-1
Mar 1 2022	19BN166A_23-1		ign	898691	429297	51	0.1644	0.0012	10.71	0.35	0.473	0.015	0.975	2502	12	2495	66	0
Mar 1 2022	19BN166A_24-1		inhrt	2705945	1350058	131	0.1706	0.0012	11.60	0.38	0.494	0.016	0.975	2564	12	2586	67	-1
Mar 1 2022	19BN166A_25-1		ign	1082191	501012	37	0.1650	0.0012	10.42	0.35	0.458	0.015	0.975	2508	12	2430	66	3
Mar 1 2022	19BN166A_26-1		ign	3068383	1476829	74	0.1646	0.0012	10.80	0.37	0.476	0.016	0.978	2503	12	2510	69	0
Mar 1 2022	19BN166A_26-2		ign	3172635	1555742	215	0.1636	0.0012	10.94	0.39	0.485	0.017	0.979	2494	12	2549	73	-2
Mar 1 2022	19BN166A_27-1		ign	1237159	578969	52	0.1636	0.0012	10.44	0.36	0.463	0.015	0.976	2493	12	2452	67	2
Mar 1 2022	19BN166A_27-2		ign	2059709	980107	32	0.1638	0.0012	10.62	0.34	0.471	0.015	0.973	2495	12	2487	64	0
Mar 1 2022	19BN166A_28-1		ign	882701	410853	28	0.1646	0.0012	10.45	0.37	0.460	0.016	0.978	2504	12	2441	70	3
Mar 1 2022	19BN166A_29-1		ign	897655	444945	33	0.1651	0.0012	11.15	0.40	0.490	0.017	0.979	2508	12	2572	74	-2
Mar 1 2022	19BN166A_29-2		ign	2513879	1221071	36	0.1635	0.0012	10.83	0.37	0.480	0.016	0.976	2492	12	2529	69	-1
Mar 1 2022	19BN166A_30-1		ign	4797918	2280875	62	0.1642	0.0012	10.64	0.34	0.470	0.015	0.974	2499	12	2485	64	1
Mar 1 2022	19BN166A_31-1		ign	3867234	1890813	42	0.1635	0.0012	10.90	0.37	0.484	0.016	0.978	2492	12	2543	70	-2
Mar 1 2022	19BN166A_32-1		ign	4797758	2404889	29	0.1624	0.0012	11.10	0.38	0.496	0.017	0.977	2481	12	2596	71	-4
Mar 1 2022	19BN166A_33-1		ign	1154041	549772	54	0.1641	0.0012	10.66	0.37	0.471	0.016	0.977	2499	13	2489	70	0
Mar 1 2022	19BN166A_34-1		ign	1476565	702277	67	0.1618	0.0012	10.49	0.36	0.470	0.016	0.976	2475	12	2486	68	0
Mar 1 2022	19BN166A_34-2		ign	2575100	1260291	60	0.1602	0.0011	10.69	0.35	0.484	0.016	0.976	2458	12	2545	67	-3
Mar 1 2022	19BN166A_35-1		ign	2051378	993527	77	0.1625	0.0012	10.73	0.35	0.479	0.015	0.975	2482	12	2523	66	-2
Mar 1 2022	19BN166A_35-2		ign	4168139	2022147	126	0.1544	0.0011	10.21	0.34	0.480	0.016	0.976	2395	12	2527	68	-5
Mar 1 2022	19BN166A_36-1		ign	2133850	1015866	61	0.1595	0.0012	10.35	0.37	0.471	0.016	0.978	2451	12	2488	71	-1
Mar 2 2022	19BN126B_2-1		ign	1305854	581305	90	0.1654	0.0013	10.45	0.35	0.458	0.015	0.974	2511	13	2432	67	3
Mar 2 2022	19BN126B_4-1		ign	1089461	492818	36	0.1643	0.0012	10.54	0.35	0.466	0.015	0.974	2500	13	2465	67	1
Mar 2 2022	19BN126B_5-1		ign	1682054	746579	30	0.1628	0.0012	10.25	0.33	0.457	0.014	0.974	2485	12	2426	63	2
Mar 2 2022	19BN126B_5-2		ign	1517760	682974	29	0.1635	0.0012	10.44	0.35	0.463	0.015	0.975	2492	12	2454	66	2
Mar 2 2022	19BN126B_6-1		ign	2086762	946452	39	0.1634	0.0012	10.52	0.36	0.467	0.015	0.975	2492	13	2470	68	1
Mar 2 2022	19BN126B_7-1		ign	1665819	737057	77	0.1644	0.0012	10.32	0.32	0.456	0.014	0.972	2502	12	2420	60	3
Mar 2 2022	19BN126B_8-1		ign	1557763	703413	51	0.1639	0.0012	10.50	0.35	0.465	0.015	0.975	2496	12	2461	66	1

Session	Spot ID	Screen	Class	238U cps	206Pb cps	204 cps	Ratios						Dates (Ma)				Disc. %	
							207Pb		207Pb		206Pb		207Pb		206Pb			
							206Pb	2σ	235U	2σ	238U	2σ	ρ	206Pb	2σ	238U		2σ
Mar 2 2022	19BN126B_9-1		ign	2495971	1180475	61	0.1640	0.0012	11.00	0.35	0.487	0.015	0.973	2497	12	2557	65	-2
Mar 2 2022	19BN126B_10-1		ign	1604264	752804	59	0.1623	0.0012	10.81	0.35	0.483	0.015	0.975	2480	12	2541	66	-2
Mar 2 2022	19BN126B_11-1		ign	1359037	589028	57	0.1600	0.0013	9.84	0.31	0.446	0.014	0.965	2456	14	2378	60	3
Mar 2 2022	19BN126B_12-1		ign	1293264	576109	39	0.1640	0.0012	10.36	0.34	0.459	0.015	0.975	2497	12	2433	65	3
Mar 2 2022	19BN126B_13-1		ign	1281577	565642	28	0.1640	0.0012	10.27	0.34	0.454	0.015	0.973	2497	13	2415	64	3
Mar 2 2022	19BN126B_14-1		ign	684826	308461	46	0.1654	0.0013	10.57	0.35	0.464	0.015	0.972	2512	13	2456	65	2
Mar 2 2022	19BN126B_14-2		ign	1473681	652892	92	0.1607	0.0012	10.10	0.31	0.456	0.014	0.971	2463	12	2422	61	2
Mar 2 2022	19BN126B_15-1		ign	2207602	1029691	81	0.1631	0.0012	10.79	0.35	0.480	0.015	0.975	2488	12	2528	66	-2
Mar 2 2022	19BN126B_16-1		ign	990966	450918	58	0.1642	0.0012	10.60	0.36	0.468	0.015	0.975	2500	13	2477	67	1
Mar 2 2022	19BN126B_17-1		ign	1166543	527368	79	0.1645	0.0012	10.55	0.33	0.465	0.014	0.972	2502	12	2463	63	2
Mar 2 2022	19BN126B_18-1		ign	1152694	507166	56	0.1644	0.0012	10.26	0.34	0.453	0.015	0.974	2501	13	2408	64	4
Mar 2 2022	19BN126B_19-1		ign	1120040	519998	52	0.1641	0.0012	10.81	0.37	0.478	0.016	0.975	2498	13	2518	69	-1
Mar 2 2022	19BN126B_20-1		ign	2037575	913093	53	0.1629	0.0012	10.36	0.33	0.461	0.014	0.973	2486	12	2446	63	2
Mar 2 2022	19BN126B_21-1		ign	1555046	725105	71	0.1641	0.0012	10.85	0.37	0.480	0.016	0.975	2498	13	2528	69	-1
Mar 2 2022	19BN126B_22-1		ign	1225561	561093	38	0.1639	0.0012	10.65	0.35	0.471	0.015	0.974	2496	13	2489	67	0
Mar 2 2022	19BN126B_23-1		amb	922536	392696	121	0.1570	0.0014	9.48	0.31	0.438	0.014	0.961	2424	15	2343	61	3
Mar 2 2022	19BN126B_24-1		ign	1993149	920551	82	0.1621	0.0012	10.62	0.37	0.475	0.016	0.977	2478	12	2508	70	-1
Mar 2 2022	19BN126B_25-1		ign	1071348	507846	69	0.1649	0.0012	11.09	0.38	0.488	0.016	0.976	2507	12	2562	70	-2
Mar 2 2022	19BN126B_26-1		ign	989748	448446	85	0.1648	0.0013	10.59	0.34	0.466	0.015	0.971	2505	13	2468	64	2
Mar 2 2022	19BN126B_1-1		cPb ign	2030205	912933	255	0.1677	0.0012	10.70	0.33	0.463	0.014	0.972	2535	12	2453	62	3
Mar 2 2022	19BN126B_3-1		mix,cPb ign	1757150	818059	280	0.1670	0.0015	11.03	0.34	0.479	0.014	0.960	2528	15	2524	62	0
April 25 2022	18BN14B-1-1		ign	674371	333801	56	0.1660	0.0012	10.99	0.36	0.480	0.015	0.975	2518	12	2528	67	0
April 25 2022	18BN14B-3-1		ign	717573	364719	56	0.1663	0.0012	11.30	0.40	0.493	0.017	0.979	2521	12	2584	74	-2
April 25 2022	18BN14B-5-1		ign	689540	351819	34	0.1653	0.0013	11.28	0.39	0.495	0.017	0.975	2511	13	2592	71	-3
April 25 2022	18BN14B-10-1		ign	646081	308967	51	0.1671	0.0012	11.22	0.36	0.487	0.015	0.973	2529	12	2559	65	-1
April 25 2022	18BN14B-11-1		ign	505104	234243	89	0.1671	0.0013	10.88	0.35	0.472	0.015	0.971	2529	13	2494	65	1
April 25 2022	18BN14B-12-1		ign	584106	271055	76	0.1669	0.0012	10.87	0.35	0.473	0.015	0.973	2527	12	2496	65	1
April 25 2022	18BN14B-13-1		ign	801453	380278	82	0.1663	0.0012	11.08	0.35	0.483	0.015	0.973	2521	12	2542	65	-1
April 25 2022	18BN14B-14-1		ign	675765	318465	77	0.1658	0.0012	10.97	0.34	0.480	0.014	0.970	2516	13	2528	62	0
April 25 2022	18BN14B-15-1		ign	941131	446495	29	0.1656	0.0012	11.03	0.35	0.483	0.015	0.972	2514	13	2542	65	-1
April 25 2022	18BN14B-16-1		ign	473902	219034	37	0.1660	0.0013	10.77	0.36	0.471	0.015	0.973	2517	13	2488	66	1
April 25 2022	18BN14B-17-1		ign	725034	335752	34	0.1661	0.0012	10.80	0.34	0.472	0.015	0.973	2519	12	2492	64	1
April 25 2022	18BN14B-18-1		ign	329150	153863	48	0.1679	0.0015	11.02	0.38	0.476	0.016	0.967	2537	15	2511	69	1
April 25 2022	18BN14B-19-1		ign	615124	279545	16	0.1668	0.0012	10.64	0.33	0.463	0.014	0.971	2525	13	2453	62	3
April 25 2022	18BN14B-20-1		ign	469890	214957	25	0.1655	0.0013	10.63	0.34	0.466	0.014	0.971	2512	13	2466	63	2
April 25 2022	18BN14B-21-1		ign	553595	260255	44	0.1664	0.0013	10.98	0.36	0.479	0.015	0.972	2522	13	2523	66	0
April 25 2022	18BN14B-22-1		ign	812329	380090	92	0.1657	0.0012	10.88	0.35	0.477	0.015	0.972	2514	13	2513	64	0
April 25 2022	18BN14B-23-1		ign	517079	246617	66	0.1657	0.0013	11.10	0.36	0.486	0.015	0.971	2515	13	2553	65	-1
April 25 2022	18BN14B-24-1		ign	441409	207625	60	0.1664	0.0013	10.99	0.35	0.479	0.015	0.971	2522	13	2524	64	0
April 25 2022	18BN14B-25-1		ign	853385	410750	81	0.1651	0.0013	11.16	0.36	0.490	0.015	0.971	2508	13	2572	66	-2
April 25 2022	18BN14B-26-1		ign	711964	335071	67	0.1662	0.0012	10.98	0.34	0.480	0.015	0.971	2520	12	2525	63	0
April 25 2022	18BN14B-27-1		ign	1009676	470927	52	0.1651	0.0012	10.82	0.33	0.475	0.014	0.970	2509	13	2506	62	0
April 25 2022	18BN14B-28-1		ign	731982	346633	59	0.1663	0.0012	11.06	0.35	0.482	0.015	0.972	2520	12	2538	64	-1
April 25 2022	18BN14B-29-1		ign	342597	159131	32	0.1670	0.0014	10.89	0.35	0.473	0.015	0.968	2527	14	2498	64	1
April 25 2022	18BN14B-30-1		ign	464480	212111	57	0.1659	0.0013	10.64	0.34	0.465	0.014	0.969	2517	13	2463	63	2
April 25 2022	18BN14B-31-1		ign	759724	342693	53	0.1665	0.0013	10.55	0.33	0.460	0.014	0.971	2523	13	2438	62	3
April 25 2022	18BN14B-32-1		ign	496454	228574	41	0.1663	0.0013	10.75	0.34	0.469	0.014	0.970	2521	13	2480	62	2

Session	Spot ID	Screen	Class	238U cps	206Pb cps	204 cps	Ratios						Dates (Ma)				Disc. %	
							207Pb		207Pb		206Pb		207Pb		206Pb			ρ
							206Pb	2σ	235U	2σ	238U	2σ	206Pb	2σ	206Pb	2σ		
April 25 2022	18BN14B-33-1		ign	513586	238274	66	0.1657	0.0013	10.79	0.34	0.473	0.014	0.970	2515	13	2495	63	1
April 25 2022	18BN14B-34-1		ign	699145	332293	66	0.1659	0.0012	11.07	0.35	0.484	0.015	0.971	2517	12	2546	64	-1
April 25 2022	18BN14B-35-1		ign	505886	238259	67	0.1655	0.0013	10.94	0.36	0.480	0.015	0.973	2513	13	2527	66	-1
April 25 2022	18BN14B-36-1		ign	811733	386367	61	0.1658	0.0012	11.08	0.35	0.485	0.015	0.973	2516	12	2549	65	-1
April 25 2022	18BN14B-40-1		ign	642434	298170	71	0.1655	0.0012	10.78	0.38	0.473	0.016	0.977	2512	13	2496	70	1
April 25 2022	18BN14B-41-1		ign	833564	400519	51	0.1654	0.0012	11.16	0.34	0.490	0.015	0.971	2512	12	2569	63	-2
April 25 2022	18BN14B-39-1		ign	2155548	1007254	70	0.1599	0.0012	10.49	0.38	0.476	0.017	0.978	2455	13	2510	74	-2
April 25 2022	18BN14B-2-1	mix,cPb	ign	1333492	704346	1127	0.1865	0.0019	13.17	0.48	0.512	0.018	0.959	2711	17	2667	75	2
April 25 2022	18BN14B-4-1	mix,cPb	ign	868366	453131	402	0.1762	0.0014	12.29	0.42	0.506	0.017	0.971	2617	14	2640	72	-1
April 25 2022	18BN14B-6-1	mix,cPb	ign	1006347	528012	915	0.1753	0.0091	12.29	0.77	0.509	0.018	0.563	2609	84	2652	76	-2
April 25 2022	18BN14B-7-1	cPb	ign	541099	282862	252	0.1657	0.0012	11.58	0.45	0.507	0.019	0.981	2515	12	2644	82	-5
April 25 2022	18BN14B-8-1	cPb	ign	744706	382066	279	0.1655	0.0012	11.35	0.42	0.498	0.018	0.980	2512	13	2604	78	-4
April 25 2022	18BN14B-9-1	cPb	ign	990872	514969	372	0.1680	0.0013	11.67	0.39	0.504	0.016	0.974	2537	13	2632	70	-4
April 25 2022	18BN14B-37-1	cPb	ign	865771	401388	206	0.1697	0.0013	11.05	0.35	0.472	0.014	0.969	2555	13	2494	62	2
April 25 2022	18BN14B-38-1	cPb	ign	769271	336568	127	0.1676	0.0013	10.30	0.32	0.446	0.013	0.968	2534	13	2376	59	7
April 25 2022	21BN32A-1-1		ign	695544	320867	30	0.1647	0.0013	10.67	0.34	0.470	0.014	0.967	2504	13	2484	63	1
April 25 2022	21BN32A-2-1		ign	1236885	569579	55	0.1636	0.0012	10.58	0.34	0.469	0.015	0.973	2493	12	2480	64	1
April 25 2022	21BN32A-3-1		ign	614147	289643	44	0.1634	0.0012	10.82	0.35	0.481	0.015	0.971	2491	13	2529	65	-2
April 25 2022	21BN32A-4-1		ign	854355	405417	48	0.1638	0.0012	10.92	0.36	0.483	0.015	0.975	2496	12	2542	67	-2
April 25 2022	21BN32A-5-1		ign	1494147	725608	51	0.1624	0.0012	11.07	0.36	0.495	0.016	0.974	2481	12	2591	68	-4
April 25 2022	21BN32A-6-1		ign	1991521	960370	117	0.1623	0.0012	10.99	0.36	0.491	0.016	0.975	2480	12	2576	67	-4
April 25 2022	21BN32A-8-1		ign	627626	287335	71	0.1638	0.0013	10.53	0.33	0.466	0.014	0.971	2495	13	2468	63	1
April 25 2022	21BN32A-9-1		ign	777297	353581	68	0.1640	0.0012	10.48	0.34	0.463	0.014	0.972	2497	13	2455	63	2
April 25 2022	21BN32A-10-1		ign	490197	232474	42	0.1650	0.0013	10.99	0.37	0.483	0.016	0.971	2507	13	2541	69	-1
April 25 2022	21BN32A-11-1		ign	1344591	633606	35	0.1640	0.0012	10.85	0.38	0.480	0.016	0.976	2497	13	2528	71	-1
April 25 2022	21BN32A-12-1		ign	1493080	698034	37	0.1635	0.0012	10.73	0.35	0.476	0.015	0.973	2492	12	2511	65	-1
April 25 2022	21BN32A-13-1		ign	2319622	1111207	34	0.1625	0.0012	10.93	0.35	0.488	0.015	0.974	2482	12	2562	65	-3
April 25 2022	21BN32A-14-1		ign	1800424	838185	42	0.1631	0.0012	10.66	0.34	0.474	0.015	0.972	2488	12	2503	63	-1
April 25 2022	21BN32A-15-1		ign	786204	362975	36	0.1642	0.0012	10.64	0.33	0.470	0.014	0.972	2499	12	2485	62	1
April 25 2022	21BN32A-16-1		ign	1096031	524494	53	0.1638	0.0012	11.01	0.36	0.488	0.016	0.975	2495	12	2560	68	-3
April 25 2022	21BN32A-17-1		ign	1339271	638753	34	0.1632	0.0012	10.93	0.34	0.486	0.015	0.973	2489	12	2553	64	-2
April 25 2022	21BN32A-19-1		ign	903317	444163	33	0.1635	0.0012	11.29	0.40	0.501	0.017	0.978	2492	13	2618	75	-5
April 25 2022	21BN32A-20-1		ign	1933365	933840	33	0.1624	0.0012	11.01	0.38	0.492	0.016	0.977	2481	12	2580	70	-4
April 25 2022	21BN32A-21-1		ign	233453	108030	59	0.1663	0.0013	10.81	0.34	0.471	0.015	0.969	2521	13	2490	63	1
April 25 2022	21BN32A-22-1		ign	931736	430172	56	0.1644	0.0012	10.66	0.33	0.470	0.014	0.972	2502	12	2485	62	1
April 25 2022	21BN32A-23-1		ign	644704	300830	60	0.1642	0.0013	10.76	0.35	0.475	0.015	0.971	2500	13	2507	65	0
April 25 2022	21BN32A-24-1		ign	490749	227264	45	0.1644	0.0012	10.69	0.35	0.472	0.015	0.974	2502	13	2492	66	0
April 25 2022	21BN32A-25-1		ign	1080395	490484	45	0.1638	0.0012	10.44	0.32	0.463	0.014	0.971	2496	12	2451	61	2
April 25 2022	21BN32A-26-1		ign	395280	180451	55	0.1648	0.0013	10.57	0.35	0.465	0.015	0.974	2506	13	2462	66	2
April 25 2022	21BN32A-27-1		ign	2007885	960605	46	0.1627	0.0012	10.93	0.35	0.487	0.015	0.974	2484	12	2560	65	-3
April 25 2022	21BN32A-28-1		ign	2220344	1072942	30	0.1630	0.0012	11.06	0.36	0.492	0.016	0.974	2487	12	2581	67	-4
April 25 2022	21BN32A-29-1		ign	1036846	486343	15	0.1632	0.0012	10.75	0.34	0.478	0.015	0.971	2489	13	2518	64	-1
April 25 2022	21BN32A-30-1		ign	1438769	706347	23	0.1638	0.0012	11.29	0.39	0.500	0.017	0.978	2495	12	2615	73	-5
April 25 2022	21BN32A-31-1		ign	733413	340048	28	0.1635	0.0012	10.64	0.35	0.472	0.015	0.974	2492	12	2494	66	0
April 25 2022	21BN32A-32-1		ign	987719	459208	27	0.1633	0.0012	10.66	0.36	0.474	0.016	0.975	2490	12	2500	68	0
April 25 2022	21BN32A-7-1	mix	ign	1580026	813034	101	0.1621	0.0012	11.72	0.40	0.524	0.017	0.976	2478	12	2717	73	-9
April 25 2022	21BN32A-18-1	cPb	ign	1684133	777420	392	0.1701	0.0022	11.03	0.38	0.470	0.015	0.925	2559	22	2485	65	3

Session	Spot ID	Screen	Class	238U cps	206Pb cps	204 cps	Ratios						Dates (Ma)				Disc. %	
							207Pb		206Pb		ρ	207Pb		206Pb				
							206Pb	2σ	235U	2σ		206Pb	2σ	206Pb	2σ			
April 25 2022	21BN15A-1-1		ign	3567017	1744708	19	0.1630	0.0012	11.19	0.35	0.498	0.015	0.974	2487	12	2607	66	-5
April 25 2022	21BN15A-2-1		ign	1813513	881556	24	0.1634	0.0012	11.15	0.35	0.495	0.015	0.973	2491	12	2593	64	-4
April 25 2022	21BN15A-2-2		ign	2420232	1170477	6	0.1632	0.0012	11.08	0.34	0.493	0.015	0.973	2489	12	2583	64	-4
April 25 2022	21BN15A-3-1		ign	2022048	980588	1	0.1637	0.0012	11.15	0.36	0.494	0.015	0.975	2494	12	2588	66	-4
April 25 2022	21BN15A-4-1		ign	369150	170353	44	0.1650	0.0012	10.69	0.34	0.470	0.015	0.972	2508	13	2484	64	1
April 25 2022	21BN15A-5-1		ign	1244180	606992	58	0.1641	0.0012	11.24	0.41	0.497	0.018	0.979	2498	13	2601	76	-4
April 25 2022	21BN15A-6-1		ign	456978	215953	83	0.1649	0.0012	10.94	0.38	0.481	0.016	0.976	2507	13	2534	70	-1
April 25 2022	21BN15A-7-1		ign	870259	415380	71	0.1648	0.0012	11.05	0.36	0.486	0.015	0.974	2506	12	2555	67	-2
April 25 2022	21BN15A-10-1		ign	290776	135232	70	0.1660	0.0014	10.84	0.36	0.474	0.015	0.970	2518	14	2500	67	1
April 25 2022	21BN15A-11-1		ign	497985	220842	30	0.1656	0.0013	10.31	0.33	0.452	0.014	0.969	2514	13	2403	62	5
April 25 2022	21BN15A-8-1	mix,cPb	ign	1248641	592065	875	0.1845	0.0040	12.28	0.46	0.483	0.015	0.810	2693	35	2541	63	6
April 25 2022	21BN15A-9-1	mix,cPb	ign	2080713	1040122	294	0.1664	0.0013	11.68	0.37	0.509	0.016	0.969	2521	13	2654	66	-5
April 25 2022	21BN15A-10-2	mix,cPb	ign	376086	162231	98	0.1693	0.0013	10.25	0.33	0.439	0.014	0.972	2550	13	2348	62	9
April 26 2022	18BN114A-11-1		ign	1914573	903728	94	0.1608	0.0012	10.70	0.35	0.483	0.015	0.974	2464	12	2539	66	-3
April 26 2022	18BN114A-12-1		ign	654370	291933	48	0.1607	0.0012	10.10	0.33	0.456	0.014	0.972	2463	13	2423	64	2
April 26 2022	18BN114A-21-1		ign	1402767	676948	19	0.1619	0.0012	11.01	0.37	0.493	0.016	0.975	2476	12	2585	69	-4
April 26 2022	18BN114A-22-1		amb	748473	353031	2	0.1630	0.0012	10.83	0.39	0.482	0.017	0.977	2487	13	2537	73	-2
April 26 2022	18BN114A-24-1		amb	1996576	940913	159	0.1625	0.0013	10.79	0.35	0.482	0.015	0.968	2481	14	2535	66	-2
April 26 2022	18BN114A-24-2		amb	1933452	889513	189	0.1617	0.0012	10.48	0.36	0.470	0.016	0.976	2474	13	2485	69	0
April 26 2022	18BN114A-27-1		amb	533426	240465	82	0.1619	0.0012	10.28	0.33	0.461	0.014	0.972	2475	13	2444	64	1
April 26 2022	18BN114A-28-1		amb	532935	242467	69	0.1625	0.0012	10.42	0.35	0.465	0.015	0.974	2482	13	2462	67	1
April 26 2022	18BN114A-29-1		ign	945856	441437	78	0.1612	0.0012	10.60	0.37	0.477	0.016	0.978	2468	12	2515	71	-2
April 26 2022	18BN114A-34-1		amb	893041	410856	87	0.1630	0.0012	10.56	0.34	0.470	0.015	0.972	2487	13	2485	64	0
April 26 2022	18BN114A-35-1		ign	1217883	587089	76	0.1619	0.0012	11.00	0.37	0.493	0.016	0.976	2476	12	2583	70	-4
April 26 2022	18BN114A-37-1		ign	470563	214810	56	0.1618	0.0012	10.41	0.34	0.467	0.015	0.972	2474	13	2469	64	0
April 26 2022	18BN114A-41-1		ign	1136121	525227	2	0.1627	0.0012	10.60	0.35	0.473	0.015	0.975	2484	12	2495	66	0
April 26 2022	18BN114A-43-1		ign	864116	396060	5	0.1617	0.0012	10.44	0.34	0.469	0.015	0.974	2473	12	2478	65	0
April 26 2022	18BN114A-46-1		amb	371012	168577	9	0.1635	0.0013	10.47	0.35	0.465	0.015	0.973	2492	13	2460	66	1
April 26 2022	18BN114A-48-1		ign	1927517	933022	18	0.1612	0.0012	11.00	0.38	0.495	0.017	0.977	2469	12	2592	71	-5
April 26 2022	18BN114A-51-1		ign	1138878	527034	40	0.1613	0.0012	10.52	0.35	0.473	0.015	0.972	2470	13	2497	66	-1
April 26 2022	18BN114A-51-2		ign	1510435	695551	60	0.1610	0.0012	10.45	0.33	0.471	0.015	0.973	2466	12	2487	64	-1
April 26 2022	18BN114A-53-1		ign	1491604	692106	32	0.1621	0.0012	10.60	0.33	0.474	0.014	0.970	2477	13	2503	62	-1
April 26 2022	18BN114A-53-2		ign	1952623	938251	67	0.1621	0.0012	10.98	0.38	0.491	0.017	0.978	2478	12	2576	72	-4
April 26 2022	18BN114A-6-1		amb	678830	310751	81	0.1625	0.0012	10.48	0.35	0.468	0.015	0.975	2482	12	2475	66	0
April 26 2022	18BN114A-20-1		amb	1130788	536707	10	0.1605	0.0012	10.74	0.37	0.485	0.016	0.977	2461	12	2550	71	-3
April 26 2022	18BN114A-50-1		ign	465920	216941	36	0.1605	0.0012	10.53	0.35	0.476	0.016	0.974	2461	13	2510	68	-2
April 26 2022	18BN114A-5-1		amb	961584	444028	26	0.1604	0.0012	10.43	0.33	0.472	0.015	0.973	2459	12	2493	64	-1
April 26 2022	18BN114A-4-1		ign	2096094	949551	23	0.1599	0.0012	10.21	0.33	0.463	0.014	0.972	2455	13	2454	63	0
April 26 2022	18BN114A-39-1		ign	3688836	1787975	10	0.1597	0.0012	10.91	0.35	0.496	0.016	0.974	2453	12	2595	67	-5
April 26 2022	18BN114A-30-1		ign	2864635	1318354	91	0.1589	0.0011	10.31	0.32	0.471	0.014	0.972	2444	12	2486	62	-2
April 26 2022	18BN114A-18-1		ign	1403473	680368	6	0.1584	0.0012	10.82	0.35	0.496	0.016	0.973	2438	13	2595	67	-6
April 26 2022	18BN114A-23-1		amb	1224198	561732	1	0.1575	0.0012	10.18	0.36	0.469	0.016	0.977	2429	13	2480	70	-2
April 26 2022	18BN114A-14-1		ign	1542937	693161	42	0.1573	0.0011	9.96	0.32	0.459	0.014	0.974	2427	12	2437	62	0
April 26 2022	18BN114A-19-1		ign	664774	305957	42	0.1570	0.0012	10.18	0.38	0.471	0.017	0.978	2423	13	2486	74	-3
April 26 2022	18BN114A-36-1		ign	1559159	732147	102	0.1567	0.0011	10.37	0.34	0.480	0.015	0.975	2421	12	2528	66	-4
April 26 2022	18BN114A-49-1		ign	1451628	677909	19	0.1565	0.0011	10.30	0.39	0.477	0.018	0.982	2418	12	2516	77	-4

Session	Spot ID	Screen	Class	238U cps	206Pb cps	204 cps	Ratios						Dates (Ma)				Disc. %	
							207Pb 206Pb		207Pb 235U		206Pb 238U		p	207Pb 206Pb		206Pb 238U		
							2σ	2σ	2σ	2σ	2σ	2σ		2σ	2σ			
April 26 2022	18BN114A-2-1		met	330332	142965	18	0.1563	0.0013	9.53	0.34	0.443	0.015	0.973	2416	14	2362	69	2
April 26 2022	18BN114A-40-1		met	368930	157666	8	0.1551	0.0012	9.34	0.31	0.437	0.014	0.974	2403	13	2337	63	3
April 26 2022	18BN114A-7-1		amb	623711	273015	55	0.1547	0.0012	9.54	0.31	0.448	0.014	0.971	2399	13	2384	62	1
April 26 2022	18BN114A-31-1		amb	3738933	1688630	74	0.1544	0.0011	9.83	0.32	0.462	0.015	0.975	2395	12	2447	65	-2
April 26 2022	18BN114A-47-1		amb	3796703	1698542	8	0.1544	0.0011	9.73	0.32	0.457	0.015	0.975	2395	12	2428	65	-1
April 26 2022	18BN114A-32-1		amb	377082	163919	84	0.1541	0.0012	9.44	0.32	0.444	0.015	0.972	2392	14	2371	65	1
April 26 2022	18BN114A-38-2		amb	1327792	614866	11	0.1541	0.0011	10.05	0.35	0.473	0.016	0.978	2392	12	2499	71	-4
April 26 2022	18BN114A-13-1		met	525360	224477	14	0.1540	0.0012	9.27	0.31	0.437	0.014	0.974	2390	13	2337	64	2
April 26 2022	18BN114A-26-1		ign	2130738	982167	100	0.1536	0.0011	9.98	0.31	0.471	0.014	0.972	2387	12	2489	63	-4
April 26 2022	18BN114A-15-1		ign	2799824	1281690	34	0.1534	0.0011	9.89	0.32	0.468	0.015	0.974	2384	13	2475	64	-4
April 26 2022	18BN114A-3-1		met	1218723	534305	18	0.1532	0.0011	9.46	0.30	0.448	0.014	0.973	2382	12	2388	62	0
April 26 2022	18BN114A-42-1		amb	601989	257424	7	0.1531	0.0011	9.22	0.29	0.437	0.013	0.972	2381	13	2338	60	2
April 26 2022	18BN114A-45-1		met	825775	366966	15	0.1531	0.0011	9.58	0.33	0.454	0.015	0.976	2380	13	2415	68	-1
April 26 2022	18BN114A-25-1		met	2167067	999739	90	0.1524	0.0011	9.91	0.33	0.472	0.015	0.976	2373	12	2491	66	-5
April 26 2022	18BN114A-8-1		met	1819179	811913	104	0.1523	0.0011	9.58	0.31	0.456	0.014	0.975	2372	12	2423	63	-2
April 26 2022	18BN114A-33-1		amb	2063806	949328	124	0.1521	0.0011	9.86	0.34	0.470	0.016	0.977	2369	12	2485	69	-5
April 26 2022	18BN114A-52-1		amb	1784740	791009	27	0.1521	0.0011	9.50	0.30	0.453	0.014	0.973	2369	13	2409	62	-2
April 26 2022	18BN114A-44-1		met	829261	368696	15	0.1517	0.0011	9.50	0.32	0.455	0.015	0.976	2365	12	2416	65	-2
April 26 2022	18BN114A-10-1		met	810894	356150	66	0.1515	0.0011	9.38	0.31	0.449	0.015	0.976	2363	12	2391	65	-1
April 26 2022	18BN114A-38-1		amb	2097893	941749	72	0.1501	0.0011	9.50	0.32	0.459	0.015	0.977	2347	12	2435	67	-4
April 26 2022	18BN114A-1-1	mix	amb	2769090	1228461	68	0.1597	0.0016	9.99	0.41	0.454	0.018	0.969	2453	17	2411	79	2
April 26 2022	18BN114A-9-1	mix,cPb	amb	5739958	1875353	839	0.1326	0.0024	6.10	0.32	0.334	0.016	0.938	2132	32	1858	79	15
April 27 2022	21BN45A-2-1		ign	485589	256390	13	0.1654	0.0013	10.81	0.39	0.474	0.017	0.977	2512	13	2501	72	0
April 27 2022	21BN45A-4-1		ign	1387947	787207	25	0.1642	0.0012	11.41	0.41	0.504	0.018	0.979	2499	12	2633	76	-5
April 27 2022	21BN45A-5-1		ign	374116	200076	33	0.1651	0.0012	10.92	0.40	0.480	0.017	0.978	2508	13	2528	74	-1
April 27 2022	21BN45A-6-1		ign	825501	456378	32	0.1652	0.0012	11.31	0.41	0.496	0.018	0.979	2510	12	2598	76	-3
April 27 2022	21BN45A-7-1		ign	692486	374460	18	0.1657	0.0012	11.09	0.39	0.486	0.017	0.978	2515	13	2551	73	-1
April 27 2022	21BN45A-8-1		ign	900762	518123	64	0.1652	0.0012	11.65	0.42	0.512	0.018	0.980	2509	12	2663	77	-6
April 27 2022	21BN45A-9-1		ign	674744	370764	50	0.1627	0.0012	11.07	0.41	0.493	0.018	0.979	2484	13	2585	77	-4
April 27 2022	21BN45A-10-1		ign	641571	347332	44	0.1638	0.0012	10.97	0.40	0.486	0.018	0.979	2495	13	2554	76	-2
April 27 2022	21BN45A-11-1		ign	872115	479438	29	0.1653	0.0012	11.24	0.42	0.494	0.018	0.981	2510	12	2586	78	-3
April 27 2022	21BN45A-12-1		ign	719235	406551	23	0.1649	0.0012	11.42	0.42	0.503	0.018	0.980	2506	12	2626	78	-5
April 27 2022	21BN45A-14-1		ign	625036	332290	6	0.1658	0.0012	10.90	0.40	0.477	0.017	0.979	2515	13	2516	74	0
April 27 2022	21BN45A-18-1		ign	513927	267173	67	0.1653	0.0012	10.64	0.39	0.467	0.017	0.980	2511	12	2469	74	2
April 27 2022	21BN45A-20-1		ign	1072901	566545	77	0.1651	0.0012	10.79	0.41	0.474	0.018	0.981	2509	12	2502	76	0
April 27 2022	21BN45A-22-1		ign	1130312	581588	0	0.1643	0.0012	10.46	0.38	0.462	0.017	0.979	2501	12	2448	73	2
April 27 2022	21BN45A-23-1		ign	825387	424490	0	0.1650	0.0012	10.50	0.39	0.462	0.017	0.980	2508	12	2447	74	2
April 27 2022	21BN45A-24-1		ign	1138400	615606	0	0.1652	0.0012	11.05	0.41	0.486	0.018	0.981	2509	12	2551	77	-2
April 27 2022	21BN45A-25-1		ign	372188	193853	1	0.1654	0.0013	10.66	0.45	0.468	0.019	0.984	2512	13	2473	85	2
April 27 2022	21BN45A-26-1		ign	509189	262099	53	0.1638	0.0012	10.43	0.39	0.462	0.017	0.979	2495	13	2449	73	2
April 27 2022	21BN45A-28-1		ign	972323	499463	27	0.1648	0.0012	10.47	0.40	0.461	0.017	0.982	2505	12	2445	77	2
April 27 2022	21BN45A-29-1		ign	924020	487234	21	0.1654	0.0012	10.79	0.40	0.473	0.017	0.981	2512	12	2499	75	1
April 27 2022	21BN45A-30-1		ign	748157	382164	21	0.1651	0.0012	10.44	0.42	0.459	0.018	0.983	2508	12	2434	79	3
April 27 2022	21BN45A-31-1		ign	569833	288824	14	0.1656	0.0013	10.39	0.39	0.455	0.017	0.979	2514	13	2418	73	4
April 27 2022	21BN45A-32-1		ign	940217	471800	31	0.1650	0.0012	10.24	0.37	0.451	0.016	0.979	2507	12	2398	70	5
April 27 2022	21BN45A-33-1		ign	707580	351012	26	0.1647	0.0012	10.11	0.36	0.445	0.016	0.979	2504	12	2375	69	5
April 27 2022	21BN45A-34-1		ign	650202	322441	18	0.1655	0.0012	10.16	0.36	0.445	0.015	0.978	2513	12	2374	68	6

Session	Spot ID	Screen	Class	238U cps	206Pb cps	204 cps	Ratios						Dates (Ma)				Disc. %	
							207Pb		207Pb		206Pb		207Pb		206Pb			
							206Pb	2σ	235U	2σ	238U	2σ	ρ	206Pb	2σ	238U		2σ
April 27 2022	21BN45A-35-1		ign	731279	362236	59	0.1657	0.0012	10.15	0.36	0.445	0.015	0.977	2514	13	2372	68	6
April 27 2022	21BN45A-36-1		ign	690189	342476	29	0.1633	0.0012	10.02	0.36	0.446	0.016	0.979	2490	13	2375	70	5
April 27 2022	21BN45A-3-1		ign	888765	461419	5	0.1609	0.0012	10.24	0.38	0.462	0.017	0.980	2465	12	2447	73	1
April 27 2022	21BN45A-13-1		ign	736125	383308	17	0.1624	0.0012	10.46	0.39	0.468	0.017	0.980	2480	12	2473	74	0
April 27 2022	21BN45A-21-1		ign	541838	266223	0	0.1622	0.0013	9.86	0.38	0.441	0.017	0.980	2478	13	2356	74	5
April 27 2022	21BN45A-27-1		ign	657559	335985	55	0.1615	0.0012	10.21	0.39	0.459	0.017	0.981	2471	13	2434	75	2
April 27 2022	21BN45A-37-1		ign	649160	319398	40	0.1580	0.0013	9.62	0.37	0.442	0.016	0.978	2434	13	2359	73	3
April 27 2022	21BN45A-1-1	mix,cPb	ign	1108736	593527	185	0.1650	0.0012	10.93	0.39	0.481	0.017	0.979	2507	12	2530	72	-1
April 27 2022	21BN45A-15-1	mix,cPb	ign	458788	255970	133	0.1649	0.0013	11.28	0.42	0.496	0.018	0.977	2507	13	2598	77	-3
April 27 2022	21BN45A-16-1	mix,cPb	ign	629142	342131	144	0.1658	0.0012	11.16	0.42	0.488	0.018	0.980	2516	12	2563	77	-2
April 27 2022	21BN45A-17-1	mix,cPb	ign	973423	507365	123	0.1557	0.0012	10.34	0.37	0.482	0.017	0.977	2409	13	2535	73	-5
April 27 2022	21BN45A-19-1	mix, disc	ign	3733250	1617838	189	0.1542	0.0037	8.27	0.51	0.389	0.022	0.923	2393	40	2119	102	13
April 27 2022	19BN88A-27-1		ign	273997	143785	35	0.1665	0.0013	10.81	0.39	0.471	0.017	0.977	2522	13	2489	73	1
April 27 2022	19BN88A-28-1		ign	1475675	805612	106	0.1654	0.0012	11.17	0.40	0.490	0.017	0.979	2512	12	2571	75	-2
April 27 2022	19BN88A-25-1		ign	446078	253052	48	0.1654	0.0012	11.61	0.48	0.509	0.021	0.984	2511	13	2654	89	-5
April 27 2022	19BN88A-19-1		ign	183173	90949	29	0.1653	0.0014	10.16	0.38	0.446	0.016	0.974	2511	14	2377	72	6
April 27 2022	19BN88A-31-1		ign	315723	157228	43	0.1653	0.0014	10.49	0.37	0.460	0.016	0.970	2511	15	2441	70	3
April 27 2022	19BN88A-34-1		ign	629280	337399	72	0.1653	0.0012	10.97	0.39	0.481	0.017	0.978	2510	12	2533	73	-1
April 27 2022	19BN88A-35-1		ign	923286	501102	59	0.1653	0.0012	11.10	0.41	0.487	0.018	0.980	2510	12	2559	76	-2
April 27 2022	19BN88A-30-1		ign	1573703	873598	127	0.1652	0.0012	11.35	0.41	0.498	0.018	0.979	2509	12	2607	75	-4
April 27 2022	19BN88A-22-1		ign	602443	314346	28	0.1650	0.0012	10.66	0.41	0.469	0.018	0.980	2508	13	2477	77	1
April 27 2022	19BN88A-32-1		ign	812885	433867	71	0.1650	0.0012	10.90	0.39	0.479	0.017	0.978	2508	13	2524	73	-1
April 27 2022	19BN88A-9-1		ign	655568	354721	96	0.1649	0.0012	11.04	0.40	0.486	0.017	0.979	2506	12	2553	74	-2
April 27 2022	19BN88A-33-1		ign	904687	486531	49	0.1649	0.0012	10.97	0.40	0.483	0.017	0.979	2506	12	2540	75	-1
April 27 2022	19BN88A-16-1		ign	991255	505252	150	0.1648	0.0012	10.39	0.37	0.458	0.016	0.978	2505	12	2429	69	3
April 27 2022	19BN88A-14-1		ign	1105540	574925	66	0.1646	0.0012	10.59	0.40	0.467	0.017	0.980	2504	12	2470	75	1
April 27 2022	19BN88A-24-1		ign	693338	370295	37	0.1646	0.0012	10.88	0.41	0.480	0.018	0.980	2503	13	2525	77	-1
April 27 2022	19BN88A-36-1		ign	930858	496319	41	0.1646	0.0012	10.86	0.40	0.479	0.017	0.980	2503	12	2522	75	-1
April 27 2022	19BN88A-10-1		ign	721143	380950	53	0.1646	0.0012	10.76	0.40	0.474	0.018	0.981	2503	12	2502	76	0
April 27 2022	19BN88A-17-1		ign	1067067	545822	79	0.1645	0.0012	10.41	0.37	0.459	0.016	0.978	2503	12	2436	71	3
April 27 2022	19BN88A-18-1		ign	1221331	649403	78	0.1644	0.0012	10.72	0.38	0.473	0.016	0.979	2501	12	2496	71	0
April 27 2022	19BN88A-2-1		ign	1364651	698867	103	0.1644	0.0012	10.42	0.36	0.460	0.016	0.977	2501	12	2439	68	3
April 27 2022	19BN88A-13-1		ign	957853	496106	20	0.1643	0.0012	10.53	0.40	0.465	0.017	0.981	2501	12	2462	76	2
April 27 2022	19BN88A-20-1		ign	763916	393689	35	0.1642	0.0012	10.47	0.38	0.463	0.016	0.979	2499	12	2452	72	2
April 27 2022	19BN88A-23-1		ign	840428	448253	25	0.1640	0.0012	10.83	0.39	0.479	0.017	0.979	2498	12	2523	74	-1
April 27 2022	19BN88A-5-1		ign	1087809	585617	73	0.1639	0.0012	10.92	0.41	0.483	0.018	0.981	2496	12	2542	76	-2
April 27 2022	19BN88A-4-1		ign	953221	508005	81	0.1638	0.0012	10.80	0.44	0.479	0.019	0.983	2496	12	2521	83	-1
April 27 2022	19BN88A-6-1		ign	1850802	982067	95	0.1638	0.0013	11.07	0.45	0.491	0.019	0.981	2495	13	2573	83	-3
April 27 2022	19BN88A-15-1		ign	1231544	664443	56	0.1637	0.0012	10.93	0.42	0.484	0.018	0.981	2495	13	2547	79	-2
April 27 2022	19BN88A-8-1		ign	1590768	846244	29	0.1635	0.0012	10.77	0.38	0.478	0.016	0.978	2493	12	2517	71	-1
April 27 2022	19BN88A-7-1		ign	1141064	592492	88	0.1635	0.0013	10.82	0.40	0.480	0.018	0.978	2492	13	2527	76	-1
April 27 2022	19BN88A-1-1		ign	2718875	1481492	105	0.1634	0.0012	11.01	0.40	0.489	0.017	0.979	2491	12	2567	74	-3
April 27 2022	19BN88A-3-1		ign	2818852	1486072	54	0.1631	0.0012	10.64	0.38	0.473	0.016	0.979	2489	12	2498	71	0
April 27 2022	19BN88A-12-1		ign	1568713	816749	23	0.1631	0.0012	10.51	0.36	0.467	0.016	0.978	2488	12	2473	69	1
April 27 2022	19BN88A-11-1		ign	4387215	2356460	35	0.1625	0.0012	10.80	0.38	0.482	0.017	0.978	2482	12	2537	72	-2
April 27 2022	19BN88A-26-1		ign	1191107	627670	66	0.1621	0.0012	10.57	0.41	0.473	0.018	0.981	2477	13	2497	79	-1
April 27 2022	19BN88A-29-1	disc	ign	657907	403661	29	0.1636	0.0012	12.30	0.48	0.546	0.021	0.982	2493	12	2807	86	-11

Session	Spot ID	Screen	Class	238U cps	206Pb cps	204 cps	Ratios						Dates (Ma)				Disc. %	
							207Pb		207Pb		206Pb		207Pb		206Pb			
							206Pb	2σ	235U	2σ	238U	2σ	ρ	207Pb	2σ	206Pb		2σ
April 28 2022	21BN34A-19-1		inhrt	2023093	1102163	18	0.1717	0.0013	11.56	0.40	0.489	0.017	0.977	2575	12	2564	72	0
April 28 2022	21BN34A-19-2		inhrt	2146773	1184089	21	0.1712	0.0013	11.67	0.40	0.495	0.017	0.977	2570	12	2591	71	-1
April 28 2022	21BN34A-1-1		ign	1915359	956919	4	0.1632	0.0012	10.27	0.36	0.456	0.016	0.978	2489	12	2424	70	3
April 28 2022	21BN34A-1-4		ign	1372146	679593	50	0.1651	0.0012	10.38	0.36	0.456	0.016	0.979	2508	12	2422	69	4
April 28 2022	21BN34A-11-1		ign	2233230	1202291	27	0.1644	0.0012	10.94	0.44	0.483	0.019	0.984	2502	12	2539	82	-1
April 28 2022	21BN34A-15-1		ign	3203141	1764484	94	0.1632	0.0012	11.11	0.40	0.494	0.018	0.980	2489	12	2588	75	-4
April 28 2022	21BN34A-17-1		ign	1306601	679548	37	0.1635	0.0012	10.51	0.39	0.466	0.017	0.981	2492	12	2468	74	1
April 28 2022	21BN34A-19-3		ign	2287310	1235721	22	0.1646	0.0012	10.99	0.39	0.484	0.017	0.979	2504	12	2547	73	-2
April 28 2022	21BN34A-2-2		ign	3574534	1860312	11	0.1638	0.0012	10.54	0.38	0.467	0.016	0.980	2495	12	2469	72	1
April 28 2022	21BN34A-21-1		ign	907085	455545	54	0.1648	0.0012	10.23	0.36	0.450	0.015	0.978	2506	12	2397	68	5
April 28 2022	21BN34A-23-1		ign	1145675	646336	46	0.1650	0.0012	11.20	0.43	0.493	0.018	0.980	2508	13	2582	79	-3
April 28 2022	21BN34A-24-1		ign	788077	411435	41	0.1657	0.0012	10.41	0.40	0.456	0.017	0.981	2515	13	2421	75	4
April 28 2022	21BN34A-25-1		ign	1080101	586701	30	0.1631	0.0012	10.66	0.43	0.474	0.019	0.983	2488	12	2503	81	-1
April 28 2022	21BN34A-28-1		ign	1106595	595926	64	0.1644	0.0012	10.66	0.39	0.470	0.017	0.981	2502	12	2485	74	1
April 28 2022	21BN34A-29-1		ign	2319780	1198209	172	0.1648	0.0012	10.52	0.38	0.463	0.016	0.979	2506	12	2454	72	2
April 28 2022	21BN34A-36-1		ign	2601522	1326098	0	0.1640	0.0012	10.33	0.37	0.457	0.016	0.979	2497	12	2427	70	3
April 28 2022	21BN34A-37-1		ign	2322615	1208343	0	0.1642	0.0012	10.56	0.38	0.467	0.017	0.980	2499	12	2468	73	1
April 28 2022	21BN34A-38-1		ign	1681177	878315	9	0.1644	0.0012	10.61	0.45	0.468	0.020	0.985	2501	12	2477	86	1
April 28 2022	21BN34A-4-1		ign	993150	507420	0	0.1641	0.0012	10.36	0.42	0.458	0.018	0.984	2498	12	2431	81	3
April 28 2022	21BN34A-40-1		ign	2983590	1504151	34	0.1654	0.0012	10.30	0.37	0.452	0.016	0.979	2511	12	2405	70	4
April 28 2022	21BN34A-41-1		ign	2318763	1206936	1	0.1650	0.0013	10.62	0.38	0.467	0.016	0.976	2508	13	2469	71	2
April 28 2022	21BN34A-42-1		ign	2543994	1337757	2	0.1639	0.0012	10.65	0.40	0.472	0.017	0.980	2497	12	2490	75	0
April 28 2022	21BN34A-43-1		ign	2745669	1462491	7	0.1635	0.0012	10.77	0.41	0.478	0.018	0.981	2493	13	2517	78	-1
April 28 2022	21BN34A-44-1		ign	2506599	1281886	3	0.1636	0.0012	10.34	0.37	0.459	0.016	0.980	2493	12	2433	70	2
April 28 2022	21BN34A-45-1		ign	2337102	1195791	2	0.1634	0.0012	10.33	0.38	0.459	0.016	0.980	2492	12	2434	72	2
April 28 2022	21BN34A-46-1		ign	3451956	1926154	6	0.1645	0.0012	11.34	0.41	0.500	0.018	0.980	2502	12	2615	75	-4
April 28 2022	21BN34A-46-2		ign	3364922	1877261	17	0.1642	0.0012	11.32	0.40	0.500	0.017	0.979	2500	12	2615	74	-4
April 28 2022	21BN34A-47-1		ign	2601821	1434453	53	0.1628	0.0012	11.09	0.39	0.494	0.017	0.977	2485	13	2590	74	-4
April 28 2022	21BN34A-47-2		ign	2623834	1416119	35	0.1645	0.0012	10.97	0.38	0.484	0.016	0.978	2503	12	2545	71	-2
April 28 2022	21BN34A-5-1		ign	2115958	1144430	65	0.1644	0.0012	10.99	0.39	0.485	0.017	0.979	2502	12	2549	73	-2
April 28 2022	21BN34A-6-1		ign	2660285	1430298	61	0.1649	0.0012	11.44	0.49	0.504	0.021	0.984	2506	13	2630	90	-5
April 28 2022	21BN34A-7-1		ign	2559152	1363240	31	0.1638	0.0012	10.79	0.39	0.478	0.017	0.980	2496	12	2517	73	-1
April 28 2022	21BN34A-9-1		ign	2822589	1498949	50	0.1653	0.0012	10.85	0.38	0.476	0.016	0.977	2510	12	2511	71	0
April 28 2022	21BN34A-1-2		ign	3010750	1531541	20	0.1626	0.0012	10.50	0.37	0.468	0.016	0.978	2483	12	2477	70	0
April 28 2022	21BN34A-18-1		ign	3024151	1589353	39	0.1626	0.0012	10.56	0.37	0.471	0.016	0.976	2483	13	2489	70	0
April 28 2022	21BN34A-26-1		ign	2446396	1341163	121	0.1624	0.0012	10.72	0.41	0.479	0.018	0.981	2481	12	2522	78	-2
April 28 2022	21BN34A-20-1		ign	1625818	830158	32	0.1624	0.0012	10.25	0.37	0.458	0.016	0.978	2481	12	2430	70	2
April 28 2022	21BN34A-1-3		ign	2255945	1138480	28	0.1620	0.0012	10.29	0.35	0.461	0.015	0.977	2476	12	2444	68	1
April 28 2022	21BN34A-10-1		ign	2947291	1606137	32	0.1619	0.0012	10.91	0.40	0.489	0.017	0.981	2476	12	2565	75	-3
April 28 2022	21BN34A-22-1		ign	3495080	1769438	90	0.1619	0.0012	10.58	0.38	0.474	0.017	0.980	2475	12	2502	73	-1
April 28 2022	21BN34A-32-1		ign	3169075	1626043	6	0.1616	0.0012	10.25	0.36	0.460	0.016	0.979	2472	12	2440	69	1
April 28 2022	21BN34A-35-1		ign	1635942	859785	14	0.1615	0.0012	10.49	0.38	0.471	0.017	0.979	2472	12	2489	73	-1
April 28 2022	21BN34A-16-1		ign	2922343	1480046	2	0.1612	0.0012	10.09	0.35	0.454	0.016	0.979	2468	12	2414	69	2
April 28 2022	21BN34A-3-1		ign	2357040	1206349	1	0.1608	0.0012	10.17	0.38	0.459	0.017	0.981	2464	12	2435	75	1
April 28 2022	21BN34A-31-1		ign	1909485	956652	0	0.1608	0.0012	9.96	0.35	0.449	0.016	0.978	2464	12	2392	69	3
April 28 2022	21BN34A-33-1		ign	1130236	555511	8	0.1607	0.0012	9.76	0.34	0.441	0.015	0.978	2463	12	2354	68	5
April 28 2022	21BN34A-16-2		ign	743261	339587	0	0.1603	0.0012	9.45	0.33	0.428	0.015	0.977	2458	13	2297	66	7

Session	Spot ID	Screen	Class	238U cps	206Pb cps	204 cps	Ratios						Dates (Ma)				Disc. %	
							207Pb		207Pb		206Pb		207Pb		206Pb			ρ
							206Pb	2σ	235U	2σ	238U	2σ	206Pb	2σ	206Pb	2σ		
April 28 2022	21BN34A-2-1		ign	2593545	1214814	90	0.1600	0.0012	9.95	0.33	0.451	0.015	0.975	2456	12	2401	65	2
April 28 2022	21BN34A-13-1		ign	2104547	1150798	85	0.1594	0.0011	10.77	0.39	0.490	0.017	0.980	2450	12	2572	74	-5
April 28 2022	21BN34A-8-1		ign	2188556	1147359	9	0.1584	0.0012	10.26	0.37	0.470	0.017	0.979	2439	13	2484	73	-2
April 28 2022	21BN34A-26A-1		ign	2347730	1243507	123	0.1584	0.0012	10.09	0.40	0.463	0.018	0.983	2438	12	2451	80	-1
April 28 2022	21BN34A-30-1		ign	928214	464563	20	0.1576	0.0012	9.75	0.34	0.449	0.015	0.978	2430	12	2390	68	2
April 28 2022	21BN34A-27-1		ign	1045897	571589	65	0.1549	0.0011	10.19	0.46	0.477	0.021	0.987	2401	13	2515	93	-5
April 28 2022	21BN34A-34-1		ign	3180660	1558698	20	0.1546	0.0011	9.36	0.34	0.439	0.015	0.980	2397	12	2348	69	2
April 28 2022	21BN34A-12-1	mix	ign	3332939	1730225	115	0.1541	0.0011	9.89	0.37	0.466	0.017	0.981	2392	12	2464	75	-3
April 28 2022	21BN34A-14-1	mix	ign	2956838	1482706	158	0.1587	0.0012	10.28	0.34	0.470	0.015	0.974	2442	13	2483	67	-2
Oct 25 2022	19BN53A-1-1		ign	2131525	964742	34	0.1648	0.0012	10.99	0.36	0.484	0.015	0.974	2505	12	2545	67	-2
Oct 25 2022	19BN53A-10-1		ign	1426067	625091	90	0.1644	0.0012	10.62	0.35	0.469	0.015	0.973	2501	13	2478	65	1
Oct 25 2022	19BN53A-11-1		ign	1977315	888365	36	0.1643	0.0012	10.88	0.34	0.480	0.014	0.972	2501	12	2529	63	-1
Oct 25 2022	19BN53A-12-1		ign	304638	135419	23	0.1655	0.0013	10.84	0.38	0.475	0.016	0.973	2513	13	2507	70	0
Oct 25 2022	19BN53A-13-1		ign	1752102	772150	64	0.1647	0.0012	10.69	0.34	0.471	0.015	0.973	2504	12	2489	64	1
Oct 25 2022	19BN53A-13-2		ign	1795135	799067	57	0.1638	0.0012	10.75	0.33	0.476	0.014	0.971	2496	12	2510	62	-1
Oct 25 2022	19BN53A-14-1		ign	2549387	1139607	58	0.1636	0.0012	10.78	0.35	0.478	0.015	0.974	2493	12	2518	65	-1
Oct 25 2022	19BN53A-15-1		ign	972010	429119	70	0.1652	0.0012	10.75	0.33	0.472	0.014	0.970	2510	13	2493	62	1
Oct 25 2022	19BN53A-16-1		ign	1840965	816011	84	0.1642	0.0012	10.72	0.36	0.474	0.016	0.976	2499	12	2501	68	0
Oct 25 2022	19BN53A-17-1		ign	2333406	1020679	44	0.1645	0.0012	10.61	0.33	0.468	0.014	0.970	2503	12	2474	61	1
Oct 25 2022	19BN53A-18-1		ign	1214754	525452	98	0.1658	0.0012	10.57	0.35	0.463	0.015	0.975	2515	13	2451	66	3
Oct 25 2022	19BN53A-18-2		ign	2948884	1355947	40	0.1634	0.0012	11.07	0.34	0.492	0.014	0.970	2491	12	2578	62	-3
Oct 25 2022	19BN53A-19-1		ign	1460105	653305	71	0.1643	0.0012	10.83	0.37	0.478	0.016	0.976	2500	12	2520	69	-1
Oct 25 2022	19BN53A-22-1		ign	1582407	723119	30	0.1627	0.0013	10.95	0.35	0.489	0.015	0.971	2484	13	2565	66	-3
Oct 25 2022	19BN53A-23-1		ign	2935722	1286189	27	0.1633	0.0012	10.55	0.32	0.468	0.014	0.968	2491	13	2477	60	1
Oct 25 2022	19BN53A-25-1		ign	1908348	842809	108	0.1643	0.0012	10.70	0.34	0.472	0.015	0.973	2501	13	2493	64	0
Oct 25 2022	19BN53A-26-1		ign	1457857	637484	73	0.1637	0.0012	10.55	0.34	0.468	0.015	0.974	2494	12	2473	64	1
Oct 25 2022	19BN53A-27-1		ign	1833621	798850	78	0.1640	0.0012	10.53	0.32	0.466	0.014	0.971	2498	12	2465	61	1
Oct 25 2022	19BN53A-28-1		ign	1776514	809372	53	0.1638	0.0012	10.99	0.36	0.487	0.015	0.974	2495	12	2558	66	-2
Oct 25 2022	19BN53A-28-2		ign	3623602	1619870	24	0.1633	0.0012	10.76	0.33	0.478	0.014	0.971	2490	12	2519	62	-1
Oct 25 2022	19BN53A-29-1		ign	3005174	1363070	26	0.1632	0.0012	10.91	0.34	0.485	0.015	0.972	2489	12	2549	64	-2
Oct 25 2022	19BN53A-3-1		ign	3570317	1645490	51	0.1634	0.0012	11.10	0.36	0.493	0.015	0.974	2491	12	2583	66	-4
Oct 25 2022	19BN53A-30-1		ign	2326887	954200	70	0.1635	0.0013	10.12	0.35	0.449	0.015	0.975	2493	13	2391	68	4
Oct 25 2022	19BN53A-31-1		ign	2585592	1072135	53	0.1633	0.0012	10.22	0.33	0.454	0.014	0.973	2490	13	2413	63	3
Oct 25 2022	19BN53A-32-1		ign	2096015	946216	13	0.1636	0.0012	10.89	0.35	0.483	0.015	0.973	2493	12	2539	65	-2
Oct 25 2022	19BN53A-4-1		ign	3130149	1454777	119	0.1633	0.0012	11.19	0.42	0.497	0.018	0.980	2491	12	2601	78	-4
Oct 25 2022	19BN53A-5-1		ign	3234999	1469199	95	0.1628	0.0012	10.89	0.33	0.486	0.014	0.970	2485	12	2552	61	-3
Oct 25 2022	19BN53A-5-2		ign	3782615	1702319	84	0.1626	0.0012	10.78	0.36	0.481	0.016	0.975	2483	12	2533	68	-2
Oct 25 2022	19BN53A-6-1		ign	1030827	445991	67	0.1659	0.0012	10.58	0.35	0.463	0.015	0.975	2516	12	2451	66	3
Oct 25 2022	19BN53A-7-1		ign	1502867	670352	83	0.1641	0.0012	10.79	0.35	0.477	0.015	0.973	2499	12	2514	65	-1
Oct 25 2022	19BN53A-9-1		ign	1624966	734167	105	0.1638	0.0012	10.90	0.36	0.483	0.016	0.974	2495	12	2541	67	-2
Oct 25 2022	19BN53A-9-2		ign	1819222	804621	42	0.1642	0.0012	10.70	0.34	0.473	0.014	0.972	2499	12	2496	63	0
Oct 25 2022	19BN53A-1-2	cPb,mix	ign	1224540	488682	2955	0.2401	0.0156	14.12	1.05	0.427	0.015	0.484	3121	100	2291	69	36
Oct 25 2022	19BN53A-32-2	cPb,mix	ign	1953940	857982	192	0.1665	0.0013	10.77	0.34	0.470	0.014	0.969	2523	13	2481	63	2
Oct 25 2022	19BN53A-20-1	cPb,mix	ign	1490526	654838	424	0.1704	0.0014	11.03	0.36	0.470	0.015	0.970	2562	13	2483	65	3
Oct 25 2022	19BN53A-21-1	cPb,mix	ign	1255584	547787	333	0.1689	0.0015	10.86	0.35	0.467	0.015	0.960	2546	15	2468	64	3
Oct 25 2022	19BN53A-24-1	cPb,mix	ign	1801120	765520	303	0.1693	0.0016	10.60	0.32	0.454	0.013	0.951	2551	16	2415	58	6
Oct 25 2022	19BN53A-31-2	cPb,mix	ign	2286340	1005567	302	0.1673	0.0014	10.84	0.36	0.470	0.015	0.966	2531	14	2485	66	2

Session	Spot ID	Screen	Class	238U cps	206Pb cps	204 cps	Ratios						ρ	Dates (Ma)				Disc. %
							207Pb		207Pb		206Pb			207Pb		206Pb		
							206Pb	2 σ	235U	2 σ	238U	2 σ		206Pb	2 σ	238U	2 σ	
Oct 25 2022	19BN53A-8-1	cPb,mix	ign	1875820	853972	291	0.1667	0.0014	11.18	0.34	0.487	0.014	0.963	2525	14	2557	62	-1
Aug 8 2022	21BN34C-9-1		ign	231277	95406	47	0.1623	0.0013	10.26	0.31	0.458	0.013	0.964	2480	14	2432	59	2
Aug 8 2022	21BN34C-42-1		ign	171528	69441	22	0.1644	0.0014	10.19	0.31	0.450	0.013	0.957	2501	15	2395	58	4
Aug 8 2022	21BN34C-41-1		ign	403176	168037	26	0.1645	0.0013	10.50	0.32	0.463	0.014	0.966	2503	13	2453	60	2
Aug 8 2022	21BN34C-4-1		ign	400003	163840	62	0.1625	0.0013	10.19	0.31	0.455	0.013	0.962	2482	14	2418	59	3
Aug 8 2022	21BN34C-37-1		ign	265118	110224	65	0.1630	0.0013	10.38	0.32	0.462	0.014	0.965	2487	14	2448	60	2
Aug 8 2022	21BN34C-36-1		ign	295202	121210	85	0.1630	0.0014	10.25	0.33	0.456	0.014	0.964	2487	14	2423	62	3
Aug 8 2022	21BN34C-34-1		ign	362854	151054	49	0.1636	0.0013	10.43	0.33	0.463	0.014	0.968	2494	13	2451	62	2
Aug 8 2022	21BN34C-32-1		ign	190915	78887	35	0.1651	0.0014	10.45	0.32	0.459	0.014	0.963	2509	14	2436	59	3
Aug 8 2022	21BN34C-29-1		ign	216492	85664	51	0.1648	0.0014	9.99	0.31	0.440	0.013	0.960	2505	15	2349	59	7
Aug 8 2022	21BN34C-27-1		ign	234948	98972	35	0.1655	0.0014	10.68	0.37	0.468	0.016	0.972	2513	14	2475	70	2
Aug 8 2022	21BN34C-26-1		ign	234834	95197	23	0.1650	0.0014	10.24	0.32	0.450	0.013	0.963	2507	14	2397	59	5
Aug 8 2022	21BN34C-25-2		ign	200146	81781	39	0.1653	0.0014	10.34	0.32	0.454	0.014	0.965	2511	14	2413	60	4
Aug 8 2022	21BN34C-24-1		ign	283047	115780	28	0.1646	0.0013	10.31	0.34	0.455	0.014	0.970	2504	13	2415	63	4
Aug 8 2022	21BN34C-23-1		ign	244722	99819	39	0.1642	0.0014	10.26	0.31	0.453	0.013	0.963	2499	14	2410	59	4
Aug 8 2022	21BN34C-22-1		ign	147628	58437	23	0.1638	0.0014	9.93	0.31	0.440	0.013	0.961	2495	14	2350	58	6
Aug 8 2022	21BN34C-2-1		ign	370782	153844	54	0.1632	0.0013	10.37	0.33	0.461	0.014	0.969	2489	13	2444	62	2
Aug 8 2022	21BN34C-18-1		ign	479359	200689	50	0.1644	0.0012	10.54	0.33	0.465	0.014	0.970	2502	13	2463	62	2
Aug 8 2022	21BN34C-17-1		ign	215439	89008	46	0.1642	0.0013	10.39	0.33	0.459	0.014	0.969	2500	13	2436	62	3
Aug 8 2022	21BN34C-16-1		ign	179652	73729	62	0.1653	0.0014	10.39	0.32	0.456	0.014	0.965	2510	14	2422	61	4
Aug 8 2022	21BN34C-15-1		ign	431350	173134	90	0.1636	0.0013	10.06	0.29	0.446	0.012	0.963	2493	13	2377	55	5
Aug 8 2022	21BN34C-13-1		ign	223704	90865	63	0.1634	0.0014	10.16	0.32	0.451	0.014	0.963	2491	14	2401	61	4
Aug 8 2022	21BN34C-12-1		ign	161191	64975	60	0.1644	0.0013	10.15	0.34	0.448	0.014	0.969	2502	14	2386	64	5
Aug 8 2022	21BN34C-11-1		ign	195205	79465	64	0.1650	0.0013	10.29	0.32	0.452	0.014	0.965	2508	14	2406	60	4
Aug 8 2022	21BN34C-10-1		ign	162022	66548	51	0.1652	0.0014	10.39	0.36	0.456	0.015	0.971	2509	14	2424	67	4
Aug 8 2022	21BN34C-38-1		ign	345639	137450	34	0.1622	0.0013	9.88	0.30	0.442	0.013	0.966	2479	13	2359	58	5
Aug 8 2022	21BN34C-30-1		ign	275890	109274	17	0.1621	0.0013	9.83	0.30	0.440	0.013	0.961	2478	14	2351	57	5
Aug 8 2022	21BN34C-19-1		ign	350773	147943	25	0.1619	0.0013	10.46	0.33	0.469	0.014	0.968	2476	13	2478	62	0
Aug 8 2022	21BN34C-31-1		ign	378507	153938	22	0.1615	0.0013	10.06	0.30	0.452	0.013	0.967	2471	13	2404	59	3
Aug 8 2022	21BN34C-1-1		ign	256151	102195	67	0.1603	0.0013	9.79	0.30	0.443	0.013	0.966	2458	13	2366	59	4
Aug 8 2022	21BN34C-8-1		ign	576910	240261	51	0.1602	0.0012	10.22	0.32	0.463	0.014	0.969	2458	13	2452	61	0
Aug 8 2022	21BN34C-39-1		ign	110741	43969	25	0.1598	0.0014	9.72	0.31	0.441	0.014	0.960	2454	15	2356	60	4
Aug 8 2022	21BN34C-21-1		ign	222081	87627	28	0.1593	0.0014	9.63	0.29	0.438	0.013	0.960	2449	14	2344	57	4
Aug 8 2022	21BN34C-40-1		ign	196351	78969	28	0.1593	0.0013	9.81	0.31	0.447	0.014	0.967	2449	14	2381	61	3
Aug 8 2022	21BN34C-7-1		ign	227333	94027	49	0.1587	0.0014	10.05	0.33	0.460	0.015	0.962	2442	15	2438	64	0
Aug 8 2022	21BN34C-14-1		ign	573483	226592	86	0.1586	0.0012	9.60	0.30	0.439	0.013	0.968	2441	13	2346	60	4
Aug 8 2022	21BN34C-33-1		ign	426294	171286	35	0.1582	0.0012	9.73	0.29	0.446	0.013	0.966	2436	13	2380	58	2
Aug 8 2022	21BN34C-5-1		ign	200314	79808	51	0.1578	0.0013	9.63	0.31	0.443	0.014	0.966	2432	14	2363	62	3
Aug 8 2022	21BN34C-35-1		ign	297113	116692	74	0.1567	0.0015	9.43	0.30	0.436	0.013	0.953	2420	16	2335	59	4
Aug 8 2022	21BN34C-28-1		ign	174361	67772	30	0.1564	0.0013	9.31	0.31	0.432	0.014	0.967	2417	14	2314	62	4
Aug 8 2022	21BN34C-43-1		ign	266605	104363	30	0.1556	0.0014	9.33	0.30	0.435	0.013	0.960	2408	15	2328	59	3
Aug 8 2022	21BN34C-3-1		ign	376003	145997	35	0.1552	0.0012	9.23	0.29	0.431	0.013	0.969	2404	13	2312	59	4
Aug 8 2022	21BN34C-6-1		ign	501669	201337	59	0.1537	0.0012	9.45	0.29	0.446	0.013	0.968	2388	13	2377	58	0
Aug 8 2022	21BN34C-20-1		ign	504825	200648	57	0.1512	0.0012	9.20	0.28	0.442	0.013	0.967	2360	13	2358	58	0
Aug 8 2022	21BN34C-25-1	disc	ign	143548	46695	37	0.1341	0.0013	6.68	0.22	0.361	0.011	0.954	2152	17	1989	53	8
Feb 28 2022	18BN113A_1-2		ign	2016658	1079388	155	0.1661	0.0013	11.24	0.40	0.491	0.017	0.975	2519	13	2576	73	-2

Session	Spot ID	Screen	Class	238U cps	206Pb cps	204 cps	Ratios						Dates (Ma)				Disc. %	
							207Pb		207Pb		206Pb		207Pb		206Pb			
							206Pb	2σ	235U	2σ	238U	2σ	ρ	206Pb	2σ	238U		2σ
Feb 28 2022	18BN113A_3-1		ign	633641	313720	68	0.1661	0.0012	10.40	0.40	0.454	0.017	0.982	2518	12	2415	75	4
Feb 28 2022	18BN113A_5-1		ign	1642858	845923	121	0.1644	0.0012	10.71	0.41	0.473	0.018	0.981	2502	12	2495	78	0
Feb 28 2022	18BN113A_7-1		met	509721	237714	25	0.1554	0.0011	9.16	0.34	0.428	0.016	0.981	2406	12	2297	71	5
Feb 28 2022	18BN113A_9-1		ign	2125763	1069150	169	0.1666	0.0012	10.60	0.39	0.462	0.016	0.980	2523	12	2447	72	3
Feb 28 2022	18BN113A_9-2		ign	3467349	1751538	50	0.1638	0.0012	10.46	0.38	0.464	0.017	0.979	2495	13	2455	73	2
Feb 28 2022	18BN113A_10-1		met	606356	287525	13	0.1571	0.0012	9.42	0.37	0.435	0.017	0.980	2425	13	2329	74	4
Feb 28 2022	18BN113A_11-1		ign	4032773	2082419	99	0.1608	0.0011	10.50	0.39	0.474	0.017	0.982	2464	12	2501	75	-1
Feb 28 2022	18BN113A_13-1		ign	3912287	2086503	156	0.1648	0.0012	11.11	0.40	0.489	0.017	0.980	2505	12	2568	74	-2
Feb 28 2022	18BN113A_15-1		ign	3597463	1900226	61	0.1623	0.0012	10.85	0.39	0.485	0.017	0.979	2480	12	2548	74	-3
Feb 28 2022	18BN113A_16-1		ign	3651142	1870522	303	0.1646	0.0012	10.67	0.38	0.470	0.016	0.979	2504	12	2484	71	1
Feb 28 2022	18BN113A_18-1		met	429550	201269	46	0.1569	0.0012	9.30	0.34	0.430	0.016	0.979	2422	13	2306	70	5
Feb 28 2022	18BN113A_20-1		ign	2170466	1144024	94	0.1648	0.0012	10.98	0.41	0.484	0.018	0.982	2505	12	2544	76	-2
Feb 28 2022	18BN113A_21-1		met	519662	244571	22	0.1551	0.0012	9.23	0.36	0.432	0.017	0.982	2403	13	2314	74	4
Feb 28 2022	18BN113A_22-1		met	482061	225351	30	0.1562	0.0012	9.23	0.36	0.429	0.016	0.981	2415	13	2301	73	5
Feb 28 2022	18BN113A_23-1		met	267503	122143	9	0.1571	0.0012	9.07	0.34	0.419	0.015	0.980	2425	13	2256	69	7
Feb 28 2022	18BN113A_25-1		met	579906	270321	7	0.1560	0.0011	9.20	0.35	0.428	0.016	0.982	2413	12	2296	72	5
Feb 28 2022	18BN113A_26-1		met	422692	197467	13	0.1547	0.0012	9.14	0.34	0.429	0.016	0.979	2399	13	2300	71	4
Feb 28 2022	18BN113A_27-1		ign	3954200	2096477	73	0.1631	0.0012	10.94	0.42	0.487	0.018	0.983	2488	12	2556	79	-3
Feb 28 2022	18BN113A_28-1		ign	1325345	685721	69	0.1661	0.0012	10.87	0.41	0.475	0.018	0.982	2519	12	2505	76	1
Feb 28 2022	18BN113A_29-1		met	565078	276136	46	0.1570	0.0012	9.71	0.36	0.448	0.016	0.980	2424	13	2388	72	1
Feb 28 2022	18BN113A_30-1		met	430182	202974	45	0.1555	0.0011	9.28	0.36	0.433	0.017	0.982	2408	12	2319	74	4
Feb 28 2022	18BN113A_31-2		ign	541330	268509	48	0.1626	0.0012	10.20	0.39	0.455	0.017	0.981	2483	13	2418	76	3
Feb 28 2022	18BN113A_32-1		ign	1723525	913014	54	0.1648	0.0012	11.04	0.42	0.486	0.018	0.982	2506	12	2554	79	-2
Feb 28 2022	18BN113A_33-1		ign	2403924	1306507	98	0.1644	0.0012	11.30	0.43	0.499	0.018	0.983	2501	12	2609	79	-4
Feb 28 2022	18BN113A_35-1		ign	713891	357171	76	0.1652	0.0012	10.46	0.38	0.459	0.016	0.981	2510	12	2436	72	3
Feb 28 2022	18BN113A_36-1		ign	3186381	1650344	57	0.1594	0.0011	10.44	0.38	0.475	0.017	0.980	2449	12	2507	73	-2
Feb 28 2022	18BN113A_37-1		ign	531376	278845	94	0.1664	0.0012	11.04	0.42	0.482	0.018	0.981	2522	12	2534	77	0
Feb 28 2022	18BN113A_38-1		ign	2267852	1249330	192	0.1653	0.0012	11.52	0.44	0.506	0.019	0.982	2510	12	2638	80	-5
Feb 28 2022	18BN113A_39-1		ign	2986080	1626383	94	0.1626	0.0012	11.20	0.40	0.500	0.018	0.980	2483	12	2613	75	-5
Feb 28 2022	18BN113A_40-2		ign	545249	271677	65	0.1671	0.0013	10.53	0.36	0.457	0.015	0.976	2528	13	2428	68	4
Feb 28 2022	18BN113A_41-1		ign	2714042	1450302	89	0.1637	0.0012	11.06	0.42	0.490	0.018	0.982	2494	12	2572	79	-3
Feb 28 2022	18BN113A_43-1		ign	1495728	813335	182	0.1661	0.0012	11.43	0.43	0.499	0.019	0.983	2519	12	2610	80	-3
Feb 28 2022	18BN113A_43-2		ign	593803	306628	73	0.1614	0.0013	10.54	0.44	0.474	0.019	0.981	2470	14	2501	84	-1
Feb 28 2022	18BN113A_45-1		ign	2944678	1564584	37	0.1620	0.0012	10.88	0.40	0.488	0.018	0.981	2476	12	2560	76	-3
Feb 28 2022	18BN113A_46-1		ign	3077610	1631221	39	0.1618	0.0011	10.85	0.42	0.486	0.019	0.983	2474	12	2555	80	-3
Feb 28 2022	18BN113A_47-1		ign	1872994	1016362	45	0.1630	0.0012	11.19	0.46	0.498	0.020	0.984	2487	12	2605	86	-5
Feb 28 2022	18BN113A_47-2		inhrt?	743957	357361	95	0.1682	0.0012	10.22	0.37	0.441	0.016	0.980	2540	12	2354	70	8
Feb 28 2022	18BN113A_48-1		met	798914	392291	17	0.1584	0.0011	9.84	0.40	0.451	0.018	0.985	2439	12	2398	81	2
Feb 28 2022	18BN113A_48-2		met	492514	232417	42	0.1564	0.0012	9.34	0.35	0.433	0.016	0.979	2417	13	2320	71	4
Feb 28 2022	18BN113A_49-1		ign	2267303	1202634	51	0.1625	0.0012	10.90	0.40	0.487	0.017	0.980	2482	12	2557	75	-3
Feb 28 2022	18BN113A_50-1		ign	1216164	621933	53	0.1651	0.0012	10.68	0.39	0.469	0.017	0.980	2508	12	2481	73	1
Feb 28 2022	18BN113A_51-1		ign	3318250	1741102	79	0.1606	0.0011	10.66	0.42	0.482	0.019	0.984	2461	12	2534	81	-3
Feb 28 2022	18BN113A_1-1	cPb	ign	1772871	926385	458	0.1708	0.0013	11.29	0.42	0.480	0.017	0.978	2565	13	2525	75	2
Feb 28 2022	18BN113A_4-1	cPb	ign	1931672	984538	406	0.1690	0.0014	10.89	0.42	0.468	0.018	0.977	2547	14	2474	78	3
Feb 28 2022	18BN113A_6-1	cPb	ign	586334	286986	111	0.1676	0.0013	10.38	0.43	0.449	0.018	0.983	2534	13	2392	80	6
Feb 28 2022	18BN113A_8-1	cPb	ign	3695301	1992337	552	0.1652	0.0012	11.26	0.41	0.495	0.018	0.980	2509	12	2591	75	-3
Feb 28 2022	18BN113A_12-1	cPb	ign	1307082	643200	319	0.1696	0.0013	10.55	0.41	0.452	0.017	0.980	2553	13	2402	75	6

Session	Spot ID	Screen	Class	238U cps	206Pb cps	204 cps	Ratios						Dates (Ma)				Disc. %	
							207Pb		207Pb		206Pb		207Pb		206Pb			
							206Pb	2σ	235U	2σ	238U	2σ	206Pb	2σ	238U	2σ		
Feb 28 2022	18BN113A_14-1	cPb	ign	710186	333500	176	0.1665	0.0013	9.89	0.38	0.431	0.016	0.980	2523	13	2310	73	9
Feb 28 2022	18BN113A_34-1	cPb	ign	2228641	1175704	333	0.1623	0.0011	10.83	0.42	0.484	0.018	0.983	2480	12	2545	79	-3
Feb 28 2022	18BN113A_36-2	cPb	ign	424445	212563	103	0.1656	0.0013	10.49	0.38	0.460	0.016	0.978	2514	13	2438	72	3
Feb 28 2022	18BN113A_41-2	cPb	met	583886	288867	349	0.1796	0.0015	11.24	0.42	0.454	0.016	0.974	2649	14	2413	72	10
Feb 28 2022	18BN113A_53-1	mix	ign	4582381	2191740	58	0.1511	0.0018	9.14	0.55	0.439	0.026	0.980	2358	21	2346	116	1
Feb 28 2022	18BN113A_17-1	mix,cPb	met	583090	239614	292	0.1715	0.0016	8.91	0.35	0.377	0.014	0.971	2572	16	2063	67	25
Feb 28 2022	18BN113A_19-1	mix,cPb	ign	10295312	4116645	153	0.1431	0.0020	7.24	0.32	0.367	0.015	0.949	2265	24	2015	72	12
Feb 28 2022	18BN113A_24-1	mix,cPb	ign	2285380	1139195	1018	0.1763	0.0047	11.12	0.51	0.457	0.017	0.819	2619	44	2428	76	8
Feb 28 2022	18BN113A_31-1	mix,cPb	ign	2133409	1108153	303	0.1662	0.0016	10.92	0.40	0.477	0.017	0.963	2520	16	2513	73	0
Feb 28 2022	18BN113A_40-1	mix,cPb	ign	5473266	2715985	275	0.1576	0.0015	9.89	0.47	0.455	0.021	0.978	2430	16	2419	92	0
Feb 28 2022	18BN113A_42-1	mix,cPb	ign	4130952	2283090	597	0.1661	0.0018	11.61	0.41	0.507	0.017	0.953	2519	18	2645	72	-5
Feb 28 2022	18BN113A_44-1	mix,cPb	ign	3923741	2075524	596	0.1686	0.0016	11.28	0.41	0.485	0.017	0.964	2544	16	2551	73	0
Feb 28 2022	18BN113A_44-2	mix,cPb	met	712844	360053	187	0.1725	0.0020	11.02	0.47	0.464	0.019	0.961	2582	19	2455	83	5
Feb 28 2022	18BN113A_52-1	mix,cPb	ign	2065161	1083974	461	0.1657	0.0016	11.00	0.41	0.482	0.017	0.965	2515	16	2535	74	-1
Mar 20 2023	19BC52A-10-2		ign	964420	421791	17	0.1837	0.0013	12.92	0.37	0.510	0.014	0.970	2687	12	2658	60	1
Mar 20 2023	19BC52A-13-1		ign	1941501	885755	25	0.1834	0.0013	13.46	0.40	0.532	0.015	0.971	2684	12	2751	65	-2
Mar 20 2023	19BC52A-15-1		ign	1140433	501501	43	0.1824	0.0013	12.90	0.38	0.513	0.015	0.971	2675	12	2670	62	0
Mar 20 2023	19BC52A-16-1		ign	639078	278168	51	0.1845	0.0013	12.91	0.37	0.508	0.014	0.968	2694	12	2647	61	2
Mar 20 2023	19BC52A-17-1		ign	1041681	457654	70	0.1855	0.0014	13.10	0.39	0.513	0.015	0.970	2702	12	2668	63	1
Mar 20 2023	19BC52A-17-2		ign	1031512	454796	63	0.1845	0.0013	13.08	0.39	0.514	0.015	0.970	2694	12	2675	63	1
Mar 20 2023	19BC52A-18-1		ign	1278260	549871	70	0.1844	0.0013	12.75	0.38	0.502	0.015	0.971	2693	12	2622	63	3
Mar 20 2023	19BC52A-19-1		ign	1333334	575666	30	0.1827	0.0013	12.69	0.37	0.504	0.014	0.971	2678	12	2630	61	2
Mar 20 2023	19BC52A-20-1		ign	850830	372831	34	0.1838	0.0013	12.95	0.37	0.511	0.014	0.969	2688	12	2662	61	1
Mar 20 2023	19BC52A-20-3		ign	793175	351793	40	0.1837	0.0013	13.10	0.37	0.517	0.014	0.967	2686	12	2688	59	0
Mar 20 2023	19BC52A-4-1		ign	801770	340087	48	0.1831	0.0013	12.49	0.35	0.495	0.013	0.965	2681	12	2592	57	3
Mar 20 2023	19BC52A-6-1		ign	1087406	487800	90	0.1846	0.0014	13.31	0.40	0.523	0.015	0.967	2694	13	2714	64	-1
Mar 20 2023	19BC52A-6-2		ign	1102908	498795	29	0.1844	0.0013	13.41	0.39	0.528	0.015	0.970	2692	12	2732	63	-1
Mar 20 2023	19BC52A-9-1		ign	1079891	471256	65	0.1835	0.0014	12.88	0.38	0.509	0.014	0.967	2685	12	2653	61	1
Mar 20 2023	19BC52A-1-2		ign	946253	404499	53	0.1818	0.0014	12.49	0.36	0.499	0.014	0.962	2669	13	2608	58	2
Mar 20 2023	19BC52A-16-2		ign	657982	283607	40	0.1817	0.0013	12.59	0.36	0.503	0.014	0.967	2668	12	2626	59	2
Mar 20 2023	19BC52A-2-1		ign	964841	414084	38	0.1814	0.0013	12.52	0.38	0.501	0.015	0.971	2666	12	2617	63	2
Mar 20 2023	19BC52A-19-2		ign	1184857	516416	4	0.1813	0.0013	12.71	0.38	0.509	0.015	0.971	2665	12	2650	62	1
Mar 20 2023	19BC52A-10-1		ign	1299862	555352	41	0.1812	0.0013	12.68	0.35	0.508	0.013	0.963	2664	12	2648	57	1
Mar 20 2023	19BC52A-1-1		ign	834605	357732	56	0.1807	0.0013	12.69	0.37	0.510	0.014	0.968	2659	12	2655	61	0
Mar 20 2023	19BC52A-20-2		ign	730940	312125	91	0.1807	0.0013	12.40	0.35	0.498	0.013	0.967	2659	12	2606	58	2
Mar 20 2023	19BC52A-15-2		ign	967812	422196	36	0.1790	0.0013	12.56	0.38	0.509	0.015	0.972	2644	12	2652	63	0
Mar 20 2023	19BC52A-14-1		ign	858889	360872	14	0.1789	0.0013	12.32	0.37	0.499	0.014	0.969	2643	12	2612	62	1
Mar 20 2023	19BC52A-3-1		ign	720455	302644	66	0.1741	0.0012	11.76	0.35	0.490	0.014	0.970	2598	12	2571	60	1
Mar 20 2023	19BC52A-12-1		ign	908009	371111	31	0.1740	0.0014	11.43	0.34	0.477	0.014	0.964	2596	13	2514	59	3
Mar 20 2023	19BC52A-11-1		ign	797708	326342	29	0.1706	0.0013	11.22	0.34	0.477	0.014	0.968	2563	13	2516	61	2
Mar 20 2023	19BC52A-5-1		met	368447	143542	29	0.1599	0.0012	9.92	0.30	0.450	0.013	0.966	2455	13	2396	58	2
Mar 20 2023	19BC52A-8-2		met	486069	183463	36	0.1587	0.0014	9.91	0.28	0.453	0.012	0.951	2442	15	2410	53	1
Mar 20 2023	19BC52A-8-1		met	415084	156942	85	0.1586	0.0012	9.64	0.30	0.441	0.013	0.970	2440	13	2356	60	4
Mar 20 2023	19BC52A-7-1		met	974156	381312	36	0.1581	0.0011	9.95	0.29	0.457	0.013	0.969	2435	12	2425	57	0
Mar 20 2023	19BC52A-13-2		met	249831	93736	12	0.1561	0.0013	9.42	0.29	0.438	0.013	0.966	2414	14	2341	59	3
Mar 20 2023	19BC52A-18-2		met	253637	93624	38	0.1539	0.0012	9.14	0.27	0.431	0.012	0.964	2390	13	2309	55	4

Session	Spot ID	Screen	Class	238U cps	206Pb cps	204 cps	Ratios						Dates (Ma)				Disc. %	
							207Pb		207Pb		206Pb		207Pb		206Pb			p
							206Pb	2σ	235U	2σ	238U	2σ	206Pb	2σ	206Pb	2σ		
Mar 20 2023	19BN127A-1-1		ign	335675	138640	62	0.1639	0.0012	10.89	0.33	0.482	0.014	0.969	2497	13	2535	62	-2
Mar 20 2023	19BN127A-10-1		ign	1146800	464351	78	0.1643	0.0012	10.70	0.31	0.472	0.013	0.970	2500	12	2494	58	0
Mar 20 2023	19BN127A-11-1		ign	214230	82235	30	0.1656	0.0013	10.12	0.30	0.444	0.013	0.965	2513	13	2367	57	6
Mar 20 2023	19BN127A-11-2		ign	268633	105027	46	0.1653	0.0013	10.29	0.29	0.452	0.012	0.962	2510	13	2403	55	4
Mar 20 2023	19BN127A-12-1		ign	174947	67729	42	0.1660	0.0015	10.24	0.30	0.447	0.013	0.955	2518	15	2383	56	6
Mar 20 2023	19BN127A-13-2		ign	579209	232184	65	0.1636	0.0012	10.55	0.33	0.468	0.014	0.971	2493	12	2473	61	1
Mar 20 2023	19BN127A-14-2		ign	1170514	476391	90	0.1642	0.0012	10.75	0.32	0.475	0.014	0.972	2500	12	2505	61	0
Mar 20 2023	19BN127A-14-3		ign	1293359	514768	97	0.1637	0.0011	10.48	0.29	0.464	0.013	0.968	2494	12	2459	55	1
Mar 20 2023	19BN127A-15-1		ign	1781304	731007	54	0.1631	0.0011	10.76	0.31	0.479	0.013	0.971	2488	12	2522	58	-1
Mar 20 2023	19BN127A-15-2		ign	1779452	733790	54	0.1628	0.0011	10.80	0.31	0.481	0.013	0.970	2485	12	2532	58	-2
Mar 20 2023	19BN127A-16-1		ign	158045	59452	64	0.1649	0.0015	9.88	0.30	0.435	0.012	0.952	2506	15	2327	56	8
Mar 20 2023	19BN127A-16-2		ign	154501	60454	70	0.1648	0.0014	10.27	0.29	0.452	0.012	0.953	2506	14	2405	53	4
Mar 20 2023	19BN127A-17-1		ign	1352961	526375	77	0.1637	0.0013	10.24	0.30	0.454	0.013	0.964	2495	13	2413	56	3
Mar 20 2023	19BN127A-18-1		ign	150820	57867	48	0.1646	0.0018	10.35	0.31	0.456	0.013	0.931	2503	18	2422	56	3
Mar 20 2023	19BN127A-4-1		ign	646611	264471	43	0.1639	0.0012	10.78	0.30	0.477	0.013	0.967	2497	12	2515	56	-1
Mar 20 2023	19BN127A-4-2		ign	575290	234265	34	0.1637	0.0012	10.72	0.32	0.475	0.014	0.969	2494	12	2506	59	0
Mar 20 2023	19BN127A-4-3		ign	525092	217099	61	0.1647	0.0012	10.95	0.39	0.482	0.017	0.978	2504	12	2538	73	-1
Mar 20 2023	19BN127A-5-1		ign	1197773	485158	64	0.1640	0.0012	10.68	0.31	0.473	0.013	0.969	2498	12	2495	58	0
Mar 20 2023	19BN127A-5-2		ign	1297755	528495	38	0.1637	0.0012	10.72	0.31	0.475	0.013	0.969	2494	12	2506	57	0
Mar 20 2023	19BN127A-6-1		ign	828689	330714	96	0.1640	0.0012	10.52	0.33	0.466	0.014	0.974	2497	12	2464	63	1
Mar 20 2023	19BN127A-8-1		ign	748119	299162	85	0.1637	0.0012	10.52	0.29	0.467	0.013	0.967	2494	12	2468	55	1
Mar 20 2023	19BN127A-9-1		ign	1266191	502799	90	0.1633	0.0012	10.42	0.30	0.463	0.013	0.969	2490	12	2454	57	1
Mar 20 2023	19BN127A-9-2		ign	1402177	551431	39	0.1624	0.0013	10.27	0.30	0.459	0.013	0.963	2481	13	2434	56	2
Mar 20 2023	19BN127A-13-1		ign	2713814	1015618	136	0.1613	0.0011	9.61	0.27	0.432	0.012	0.968	2469	12	2317	53	7
Mar 20 2023	19BN127A-3-1		amb	475452	176366	52	0.1569	0.0012	9.63	0.27	0.446	0.012	0.963	2423	13	2375	54	2
Mar 20 2023	19BN127A-2-1		amb	541113	203945	60	0.1554	0.0011	9.42	0.27	0.440	0.012	0.967	2406	12	2349	54	2
Mar 20 2023	19BN127A-10-2		amb	1260804	481061	29	0.1535	0.0011	9.42	0.27	0.445	0.012	0.967	2386	12	2374	54	1
Mar 20 2023	19BN127A-7-1	mix	ign	2097104	862904	92	0.1606	0.0013	10.63	0.29	0.480	0.013	0.956	2462	14	2528	55	-3
Mar 20 2023	19BN127A-14-1	cPb	ign	1106188	450946	122	0.1649	0.0012	10.81	0.33	0.476	0.014	0.972	2507	12	2508	62	0
Sep 14 2023	21BN09A-10-1		inhrt?	594326	277326	67	0.1689	0.0012	11.00	0.35	0.473	0.015	0.973	2546	12	2495	64	2
Sep 14 2023	21BN09A-1-1		ign	548423	253050	43	0.1653	0.0013	10.65	0.34	0.467	0.015	0.971	2511	13	2472	64	2
Sep 14 2023	21BN09A-12-1		ign	1719044	734890	169	0.1633	0.0013	9.74	0.32	0.433	0.014	0.969	2490	13	2319	61	7
Sep 14 2023	21BN09A-13-1		ign	524593	232718	88	0.1652	0.0013	10.63	0.33	0.467	0.014	0.967	2510	13	2470	61	2
Sep 14 2023	21BN09A-15-1		ign	578882	253689	74	0.1652	0.0012	10.11	0.31	0.444	0.013	0.971	2510	12	2368	59	6
Sep 14 2023	21BN09A-16-1		ign	1214895	576055	62	0.1635	0.0013	11.24	0.37	0.499	0.016	0.972	2492	13	2609	69	-4
Sep 14 2023	21BN09A-18-1		ign	1222838	544795	121	0.1655	0.0013	10.69	0.34	0.469	0.014	0.969	2513	13	2478	63	1
Sep 14 2023	21BN09A-19-1		ign	272545	126324	60	0.1643	0.0013	10.63	0.47	0.469	0.021	0.985	2501	13	2481	90	1
Sep 14 2023	21BN09A-20-1		ign	630903	281072	47	0.1663	0.0012	10.34	0.33	0.451	0.014	0.972	2520	13	2401	62	5
Sep 14 2023	21BN09A-21-1		ign	584064	257747	50	0.1659	0.0012	10.22	0.32	0.447	0.014	0.973	2517	12	2382	60	6
Sep 14 2023	21BN09A-23-1		ign	1172289	515113	34	0.1629	0.0012	10.38	0.31	0.462	0.013	0.970	2486	12	2450	59	1
Sep 14 2023	21BN09A-24-1		ign	604583	280075	36	0.1648	0.0013	10.66	0.39	0.469	0.017	0.978	2505	13	2480	74	1
Sep 14 2023	21BN09A-28-1		ign	2024781	918602	118	0.1632	0.0012	10.34	0.32	0.460	0.014	0.973	2489	12	2437	62	2
Sep 14 2023	21BN09A-3-1		ign	227636	101452	32	0.1655	0.0013	10.29	0.33	0.451	0.014	0.969	2512	13	2402	62	5
Sep 14 2023	21BN09A-3-2		ign	1401507	610586	33	0.1635	0.0012	10.33	0.32	0.458	0.014	0.972	2492	12	2433	61	2
Sep 14 2023	21BN09A-30-1		ign	766709	370822	68	0.1638	0.0012	11.06	0.42	0.490	0.018	0.981	2495	12	2570	78	-3
Sep 14 2023	21BN09A-31-1		ign	1268625	554345	89	0.1638	0.0015	9.99	0.37	0.443	0.016	0.970	2495	15	2362	70	6
Sep 14 2023	21BN09A-32-1		ign	895090	400696	83	0.1654	0.0013	10.74	0.33	0.471	0.014	0.969	2512	13	2488	62	1

Session	Spot ID	Screen	Class	238U cps	206Pb cps	204 cps	Ratios						Dates (Ma)				Disc.	
							207Pb		207Pb		206Pb		207Pb		206Pb			
							206Pb	2σ	235U	2σ	238U	2σ	ρ	207Pb	2σ	206Pb		2σ
Sep 14 2023	21BN09A-33-1		ign	443333	202176	24	0.1649	0.0013	10.50	0.34	0.462	0.014	0.970	2507	13	2448	63	2
Sep 14 2023	21BN09A-34-1		ign	1631000	763209	36	0.1649	0.0012	10.77	0.36	0.474	0.015	0.977	2507	12	2501	67	0
Sep 14 2023	21BN09A-36-1		ign	1668413	782731	25	0.1645	0.0012	10.77	0.34	0.475	0.015	0.974	2502	12	2506	64	0
Sep 14 2023	21BN09A-37-1		ign	406024	179579	73	0.1649	0.0012	10.58	0.36	0.465	0.016	0.975	2507	13	2463	68	2
Sep 14 2023	21BN09A-38-1		ign	296901	129127	37	0.1646	0.0012	10.38	0.36	0.458	0.016	0.977	2503	13	2429	69	3
Sep 14 2023	21BN09A-39-1		ign	425294	181581	47	0.1651	0.0012	9.84	0.31	0.432	0.013	0.971	2508	13	2317	59	8
Sep 14 2023	21BN09A-4-1		ign	1252721	587549	60	0.1649	0.0012	10.79	0.35	0.475	0.015	0.975	2506	12	2506	65	0
Sep 14 2023	21BN09A-40-1		ign	1664272	699619	76	0.1630	0.0013	9.57	0.30	0.426	0.013	0.969	2487	13	2287	58	9
Sep 14 2023	21BN09A-5-1		ign	1112718	486427	31	0.1646	0.0012	10.44	0.32	0.460	0.014	0.972	2504	12	2440	61	3
Sep 14 2023	21BN09A-6-1		ign	454924	201924	31	0.1651	0.0012	10.23	0.35	0.450	0.015	0.976	2508	12	2393	66	5
Sep 14 2023	21BN09A-7-1		ign	614793	288946	59	0.1650	0.0012	10.82	0.35	0.476	0.015	0.973	2507	13	2510	66	0
Sep 14 2023	21BN09A-29-1		ign	2433100	1023111	144	0.1617	0.0012	9.86	0.30	0.442	0.013	0.968	2474	13	2362	57	5
Sep 14 2023	21BN09A-2-1	disc	ign	2213233	823288	133	0.1545	0.0012	8.02	0.28	0.377	0.013	0.975	2396	13	2061	59	16
Sep 14 2023	21BN09A-9-1	mix	ign	12814923	5136393	267	0.1455	0.0031	8.14	0.47	0.406	0.022	0.931	2293	36	2196	99	4
Sep 14 2023	21BN09A-25-1	cPb	ign	776903	349730	130	0.1628	0.0012	10.23	0.37	0.456	0.016	0.979	2485	12	2422	71	3
Sep 14 2023	21BN09A-14-1	cPb	ign	507995	229294	105	0.1619	0.0012	10.20	0.38	0.457	0.016	0.979	2476	13	2427	72	2
Sep 14 2023	21BN09A-35-1	cPb	ign	1096333	488187	210	0.1690	0.0014	10.50	0.33	0.451	0.014	0.964	2548	14	2400	61	6
Sep 14 2023	21BN09A-22-1	cPb,mix	ign	1649341	643302	422	0.1684	0.0014	9.17	0.34	0.395	0.014	0.976	2542	14	2146	65	18
Sep 14 2023	21BN09A-27-1	cPb	ign	1030236	459378	225	0.1674	0.0014	10.42	0.33	0.452	0.014	0.964	2531	14	2403	61	5
Sep 14 2023	21BN09A-17-1	cPb	ign	972844	447414	123	0.1670	0.0012	10.72	0.33	0.466	0.014	0.972	2528	12	2465	62	3
Sep 14 2023	21BN09A-11-1	cPb	ign	618193	279339	120	0.1669	0.0013	10.53	0.35	0.458	0.015	0.974	2527	13	2429	65	4
Sep 14 2023	21BN09A-8-1	cPb	ign	1538189	698994	311	0.1663	0.0013	10.55	0.35	0.460	0.015	0.973	2520	13	2441	66	3
Sep 14 2023	21BN09A-26-1	cPb	ign	589756	263955	150	0.1662	0.0014	10.79	0.38	0.471	0.016	0.973	2520	14	2488	71	1
April 13 2021	19BC54C-6-2		inhrt	684392	330731	31	0.1980	0.0014	14.96	0.47	0.548	0.017	0.973	2810	12	2818	69	0
April 13 2021	19BC54C-25-1		ign	990847	476914	82	0.1953	0.0014	14.70	0.44	0.546	0.016	0.972	2788	12	2808	66	-1
April 13 2021	19BC54C-1-1		ign	1724635	828994	48	0.1953	0.0014	14.67	0.49	0.545	0.018	0.976	2787	12	2805	73	-1
April 13 2021	19BC54C-12-1		ign	1471274	710772	33	0.1950	0.0015	14.72	0.47	0.548	0.017	0.971	2784	12	2817	70	-1
April 13 2021	19BC54C-10-1		ign	1542428	751398	37	0.1947	0.0014	14.83	0.45	0.553	0.016	0.972	2783	12	2836	68	-2
April 13 2021	19BC54C-30-1		ign	1232300	590798	91	0.1945	0.0014	14.58	0.46	0.544	0.017	0.973	2781	12	2800	69	-1
April 13 2021	19BC54C-39-1		ign	1523818	729175	86	0.1943	0.0014	14.53	0.44	0.543	0.016	0.972	2779	12	2795	66	-1
April 13 2021	19BC54C-26-1		ign	1671082	787046	70	0.1942	0.0014	14.30	0.43	0.534	0.015	0.970	2778	12	2759	64	1
April 13 2021	19BC54C-34-1		ign	1641032	778738	72	0.1939	0.0014	14.38	0.43	0.538	0.016	0.970	2775	12	2776	65	0
April 13 2021	19BC54C-35-1		ign	1314949	612969	104	0.1938	0.0014	14.12	0.42	0.529	0.015	0.971	2774	12	2736	64	1
April 13 2021	19BC54C-19-1		ign	1807527	873362	56	0.1938	0.0014	14.64	0.45	0.548	0.016	0.973	2774	12	2817	68	-2
April 13 2021	19BC54C-37-2		ign	1566538	745983	94	0.1938	0.0014	14.42	0.43	0.540	0.016	0.970	2774	12	2784	66	0
April 13 2021	19BC54C-17-1		ign	968514	455884	42	0.1935	0.0014	14.24	0.46	0.534	0.017	0.973	2772	12	2758	69	1
April 13 2021	19BC54C-24-1		ign	598594	279868	28	0.1933	0.0014	14.13	0.44	0.530	0.016	0.973	2770	12	2743	68	1
April 13 2021	19BC54C-3-1		ign	1643026	792453	59	0.1933	0.0014	14.57	0.45	0.547	0.016	0.972	2770	12	2813	68	-2
April 13 2021	19BC54C-16-1		ign	1190060	567382	46	0.1929	0.0014	14.38	0.46	0.541	0.017	0.974	2767	12	2787	71	-1
April 13 2021	19BC54C-4-1		ign	2190268	1064719	20	0.1928	0.0014	14.65	0.46	0.551	0.017	0.973	2766	12	2831	70	-2
April 13 2021	19BC54C-28-1		ign	1397943	666734	67	0.1924	0.0014	14.35	0.44	0.541	0.016	0.972	2763	12	2788	67	-1
April 13 2021	19BC54C-14-1		ign	540179	242877	42	0.1918	0.0014	13.48	0.41	0.510	0.015	0.971	2758	12	2657	63	4
April 13 2021	19BC54C-22-1		ign	1168496	552119	51	0.1917	0.0014	14.16	0.43	0.536	0.016	0.970	2757	12	2767	66	0
April 13 2021	19BC54C-2-1		ign	877823	406999	35	0.1916	0.0014	13.89	0.44	0.526	0.016	0.974	2756	12	2724	69	1
April 13 2021	19BC54C-36-1		ign	1236738	576763	115	0.1915	0.0014	13.96	0.41	0.529	0.015	0.969	2755	12	2737	63	1
April 13 2021	19BC54C-20-1		ign	978277	457637	39	0.1914	0.0014	14.00	0.44	0.531	0.016	0.971	2754	12	2744	68	0
April 13 2021	19BC54C-9-1		ign	749609	349358	46	0.1904	0.0014	13.87	0.46	0.529	0.017	0.973	2746	12	2736	71	0

Session	Spot ID	Screen	Class	238U cps	206Pb cps	204 cps	Ratios						Dates (Ma)				Disc. %	
							207Pb		207Pb		206Pb		207Pb		206Pb			
							206Pb	2σ	235U	2σ	238U	2σ	ρ	206Pb	2σ	238U		2σ
April 13 2021	19BC54C-33-1		ign	1090005	510461	38	0.1892	0.0015	13.85	0.41	0.531	0.015	0.965	2735	13	2747	64	0
April 13 2021	19BC54C-32-1		ign	2160533	1017508	49	0.1887	0.0013	13.89	0.43	0.534	0.016	0.973	2731	12	2759	67	-1
April 13 2021	19BC54C-27-1		ign	1895626	879926	59	0.1872	0.0016	13.59	0.44	0.527	0.017	0.963	2718	14	2727	69	0
April 13 2021	19BC54C-23-1		ign	1201826	558446	37	0.1868	0.0014	13.57	0.44	0.527	0.017	0.972	2714	13	2729	70	-1
April 13 2021	19BC54C-18-1		ign	1062245	477748	32	0.1867	0.0013	13.13	0.38	0.510	0.014	0.969	2714	12	2657	62	2
April 13 2021	19BC54C-15-1		ign	1445609	646385	129	0.1827	0.0013	12.77	0.37	0.507	0.014	0.969	2678	12	2645	61	1
April 13 2021	19BC54C-21-1		ign	1219414	565748	49	0.1820	0.0014	13.20	0.40	0.526	0.015	0.968	2671	12	2726	65	-2
April 13 2021	19BC54C-41-1		ign	1689110	732753	174	0.1782	0.0014	12.09	0.37	0.492	0.014	0.967	2637	13	2580	62	2
April 13 2021	19BC54C-19-2		ign	1677442	749759	106	0.1762	0.0013	12.31	0.37	0.507	0.015	0.971	2617	12	2644	63	-1
April 13 2021	19BC54C-15-2		met	834110	338805	36	0.1599	0.0012	10.16	0.31	0.461	0.014	0.972	2455	12	2443	61	0
April 13 2021	19BC54C-6-1		met	633448	247807	53	0.1596	0.0012	9.76	0.29	0.444	0.013	0.968	2451	13	2367	58	4
April 13 2021	19BC54C-29-1		met	497771	198644	47	0.1594	0.0012	9.95	0.31	0.453	0.014	0.970	2450	13	2407	61	2
April 13 2021	19BC54C-21-2		met	639798	257060	53	0.1580	0.0012	9.93	0.30	0.456	0.013	0.970	2435	13	2421	59	1
April 13 2021	19BC54C-5-1		met	324354	124552	56	0.1579	0.0012	9.48	0.30	0.436	0.014	0.972	2433	13	2331	61	4
April 13 2021	19BC54C-13-1		met	384044	150248	28	0.1578	0.0012	9.65	0.29	0.444	0.013	0.970	2432	12	2368	58	3
April 13 2021	19BC54C-31-1		met	336307	122420	45	0.1571	0.0013	8.94	0.29	0.413	0.013	0.969	2425	13	2228	59	9
April 13 2021	19BC54C-25-2		met	566886	222604	21	0.1567	0.0012	9.62	0.30	0.445	0.013	0.970	2420	13	2375	59	2
April 13 2021	19BC54C-38-1		met	513620	196984	75	0.1565	0.0012	9.38	0.28	0.435	0.013	0.968	2418	13	2328	57	4
April 13 2021	19BC54C-11-1		met	434106	171274	16	0.1562	0.0012	9.63	0.29	0.448	0.013	0.968	2414	13	2384	58	1
April 13 2021	19BC54C-4-2		met	503305	198376	21	0.1560	0.0012	9.62	0.31	0.447	0.014	0.970	2413	13	2382	62	1
April 13 2021	19BC54C-40-1		met	331746	124833	83	0.1555	0.0012	9.15	0.27	0.427	0.012	0.967	2408	13	2292	56	5
April 13 2021	19BC54C-8-1		met	452150	177942	33	0.1549	0.0012	9.53	0.29	0.446	0.013	0.968	2401	13	2379	58	1
April 13 2021	19BC54C-24-2		met	677091	265221	30	0.1548	0.0011	9.48	0.30	0.444	0.014	0.973	2400	12	2370	61	1
April 13 2021	19BC54C-17-2		met	217258	83406	18	0.1540	0.0012	9.25	0.28	0.435	0.013	0.968	2391	13	2330	57	3
April 13 2021	19BC54C-7-1	cPb	ign	1479295	700012	243	0.1982	0.0017	14.67	0.44	0.537	0.015	0.959	2812	14	2770	64	2
April 13 2021	19BC54C-37-1	disc	met	499789	173109	100	0.1599	0.0012	8.66	0.24	0.393	0.011	0.963	2455	13	2136	48	15

Table C-4. LA-MC-ICPMS zircon Hf isotope data.

Session	Spot ID	<u>¹⁷⁶Lu</u>		<u>¹⁷⁶Yb</u>		<u>¹⁷⁶Hf</u>		<u>¹⁷⁸Hf</u>		Total Hf (V)	At ²⁰⁷ Pb/ ²⁰⁶ Pb Date				At Rock Age			
		<u>177Hf</u>	<u>2SE</u>	<u>177Hf</u>	<u>2SE</u>	<u>177Hf</u>	<u>2SE</u>	<u>177Hf</u>	<u>2SE</u>		Date (Ma)	2σ	εHf(t)	2SE	Age (Ma)	2σ	εHf(i)	2SE
Dec 21 2022	19BN126B-4-1	0.001060	0.000070	0.0248	0.0018	0.281221	0.000022	1.467143	0.000045	14	2500	13	-0.3	1.0	2496	6	-0.4	0.8
Dec 21 2022	19BN126B-5-1	0.001185	0.000097	0.0300	0.0025	0.281239	0.000032	1.467146	0.000049	18	2485	12	-0.2	1.3	2496	6	0.0	1.2
Dec 21 2022	19BN126B-6-1	0.001240	0.000110	0.0294	0.0025	0.281238	0.000028	1.467163	0.000039	18	2492	13	-0.2	1.2	2496	6	-0.1	1.0
Dec 21 2022	19BN126B-7-1	0.001140	0.000095	0.0304	0.0028	0.281217	0.000028	1.467184	0.000041	18	2502	12	-0.6	1.2	2496	6	-0.7	1.0
Dec 21 2022	19BN126B-8-1	0.001275	0.000076	0.0313	0.0019	0.281252	0.000028	1.467153	0.000043	16	2496	12	0.3	1.2	2496	6	0.3	1.0
Dec 21 2022	19BN126B-11-1	0.001050	0.000130	0.0268	0.0033	0.281228	0.000040	1.467160	0.000051	23	2456	14	-1.1	1.6	2496	6	-0.2	1.5
Dec 21 2022	19BN126B-12-1	0.001545	0.000080	0.0383	0.0021	0.281225	0.000024	1.467170	0.000033	20	2497	12	-1.1	1.0	2496	6	-1.1	0.9
Dec 21 2022	19BN126B-13-1	0.000884	0.000096	0.0213	0.0023	0.281266	0.000028	1.467195	0.000054	20	2497	13	1.5	1.2	2496	6	1.5	1.0
Dec 21 2022	19BN126B-15-1	0.001770	0.000180	0.0442	0.0045	0.281224	0.000029	1.467160	0.000036	18	2488	12	-1.7	1.3	2496	6	-1.5	1.1
Dec 21 2022	19BN126B-16-1	0.001253	0.000054	0.0310	0.0014	0.281219	0.000028	1.467134	0.000038	16	2500	13	-0.7	1.1	2496	6	-0.8	1.0
Dec 21 2022	19BN126B-17-1	0.000902	0.000081	0.0216	0.0020	0.281234	0.000029	1.467190	0.000036	19	2502	12	0.5	1.2	2496	6	0.3	1.1
Dec 21 2022	19BN126B-18-1	0.001100	0.000250	0.0266	0.0062	0.281259	0.000024	1.467123	0.000030	18	2501	13	1.0	1.2	2496	6	0.9	1.0
Dec 21 2022	19BN126B-20-1	0.000959	0.000091	0.0235	0.0023	0.281233	0.000022	1.467127	0.000041	19	2486	12	-0.1	1.0	2496	6	0.2	0.8
Dec 21 2022	19BN126B-21-1	0.001051	0.000044	0.0253	0.0011	0.281220	0.000021	1.467157	0.000029	19	2498	13	-0.4	0.9	2496	6	-0.4	0.8
Dec 21 2022	19BN126B-24-1	0.001202	0.000084	0.0302	0.0022	0.281231	0.000025	1.467173	0.000030	18	2478	12	-0.7	1.1	2496	6	-0.3	0.9
Dec 21 2022	19BN126B-25-1	0.001100	0.000100	0.0271	0.0027	0.281225	0.000038	1.467180	0.000068	19	2507	12	-0.1	1.5	2496	6	-0.3	1.4
Dec 21 2022	19BN126B-26-1	0.001110	0.000160	0.0268	0.0039	0.281201	0.000023	1.467122	0.000041	19	2505	13	-1.0	1.1	2496	6	-1.2	0.9
Dec 21 2022	19BN154A-1-1	0.001360	0.000210	0.0322	0.0054	0.281207	0.000030	1.467140	0.000045	17	2512	12	-1.1	1.3	2505	6	-1.2	1.2
Dec 21 2022	19BN154A-2-1	0.001557	0.000052	0.0400	0.0013	0.281197	0.000028	1.467148	0.000038	15	2509	12	-1.8	1.1	2505	6	-1.9	1.0
Dec 21 2022	19BN154A-3-1	0.001239	0.000070	0.0311	0.0021	0.281203	0.000028	1.467136	0.000041	20	2502	12	-1.2	1.1	2505	6	-1.2	1.0
Dec 21 2022	19BN154A-5-1	0.002050	0.000260	0.0526	0.0069	0.281228	0.000038	1.467182	0.000035	20	2518	12	-1.4	1.6	2505	6	-1.7	1.5
Dec 21 2022	19BN154A-6-1	0.001746	0.000069	0.0413	0.0014	0.281215	0.000028	1.467160	0.000029	18	2519	12	-1.3	1.1	2505	6	-1.6	1.0
Dec 21 2022	19BN154A-8-1	0.001380	0.000190	0.0334	0.0047	0.281238	0.000030	1.467135	0.000039	19	2516	12	0.1	1.3	2505	6	-0.2	1.2
Dec 21 2022	19BN154A-13-1	0.001161	0.000082	0.0276	0.0022	0.281171	0.000024	1.467161	0.000029	17	2521	12	-1.8	1.0	2505	6	-2.2	0.9
Dec 21 2022	19BN154A-14-1	0.001700	0.000210	0.0418	0.0050	0.281230	0.000032	1.467177	0.000070	17	2497	12	-1.2	1.4	2505	6	-1.0	1.2
Dec 21 2022	19BN154A-17-1	0.001040	0.000220	0.0254	0.0052	0.281187	0.000025	1.467194	0.000061	17	2496	12	-1.6	1.2	2505	6	-1.4	1.0
Dec 21 2022	19BN154A-23-1	0.002074	0.000055	0.0538	0.0015	0.281194	0.000038	1.467172	0.000094	19	2515	13	-2.7	1.5	2505	6	-2.9	1.4
Dec 21 2022	19BN154A-24-1	0.000944	0.000044	0.0234	0.0013	0.281191	0.000022	1.467168	0.000037	18	2502	12	-1.2	0.9	2505	6	-1.1	0.8
Dec 21 2022	19BN154A-26-1	0.000945	0.000053	0.0216	0.0013	0.281223	0.000028	1.467155	0.000034	17	2496	12	-0.2	1.1	2505	6	0.1	1.0
Dec 21 2022	19BN154A-28-1	0.000950	0.000120	0.0225	0.0031	0.281220	0.000029	1.467166	0.000052	16	2498	12	-0.2	1.2	2505	6	-0.1	1.1
Dec 21 2022	19BN154A-8-2	0.001081	0.000059	0.0250	0.0015	0.281197	0.000023	1.467134	0.000039	18	2496	12	-1.3	1.0	2505	6	-1.1	0.8
Dec 21 2022	19BN154A-9-2	0.001610	0.000140	0.0411	0.0037	0.281244	0.000026	1.467137	0.000046	16	2504	13	-0.4	1.2	2505	6	-0.3	1.0

Spots are given the same ID (sample ID-grain#-spot#) as the closest U-Pb spot. ²⁰⁷Pb/²⁰⁶Pb dates are from the closest U-Pb spot.

εHf values calculated using the CHUR values of Bouvier et al. (2008) and the ¹⁷⁶Lu decay constant of Söderlund et al. (2004)

Session	Spot ID	<u>176Lu</u>		<u>176Yb</u>		<u>176Hf</u>		<u>178Hf</u>		Total Hf (V)	At 207Pb/206Pb Date				At Rock Age			
		177Hf	2SE	177Hf	2SE	177Hf	2SE	177Hf	2SE		Date (Ma)	2σ	εHf(t)	2SE	Age (Ma)	2σ	εHf(t)	2SE
Dec 21 2022	21BN45A-2-1	0.000807	0.000021	0.02055	0.00054	0.281179	0.000066	1.467252	0.000067	22	2512	13	-1.1	2.4	2507	6	-1.2	2.4
Dec 21 2022	21BN45A-5-1	0.000776	0.000084	0.01930	0.00220	0.281155	0.000030	1.467194	0.000035	20	2508	13	-2.0	1.2	2507	6	-2.0	1.1
Dec 21 2022	21BN45A-6-1	0.001220	0.000100	0.03170	0.00230	0.281212	0.000034	1.467195	0.000059	18	2510	12	-0.7	1.4	2507	6	-0.8	1.2
Dec 21 2022	21BN45A-7-1	0.001000	0.000030	0.02515	0.00068	0.281207	0.000023	1.467197	0.000051	22	2515	13	-0.4	1.0	2507	6	-0.6	0.8
Dec 21 2022	21BN45A-9-1	0.000860	0.000200	0.02170	0.00520	0.281192	0.000031	1.467149	0.000048	20	2484	13	-1.4	1.4	2507	6	-0.9	1.2
Dec 21 2022	21BN45A-10-1	0.001100	0.000210	0.02900	0.00580	0.281171	0.000044	1.467258	0.000069	23	2495	13	-2.3	1.8	2507	6	-2.0	1.6
Dec 21 2022	21BN45A-11-1	0.001097	0.000058	0.02710	0.00160	0.281190	0.000038	1.467166	0.000065	20	2510	12	-1.3	1.5	2507	6	-1.3	1.4
Dec 21 2022	21BN45A-12-1	0.000910	0.000032	0.02184	0.00079	0.281183	0.000023	1.467194	0.000055	19	2506	12	-1.3	1.0	2507	6	-1.3	0.8
Dec 21 2022	21BN45A-13-1	0.001242	0.000036	0.03074	0.00097	0.281215	0.000031	1.467179	0.000098	22	2480	12	-1.3	1.2	2507	6	-0.7	1.1
Dec 21 2022	21BN45A-18-1	0.000758	0.000046	0.01890	0.00130	0.281157	0.000030	1.467170	0.000037	18	2511	12	-1.8	1.2	2507	6	-1.9	1.1
Dec 21 2022	21BN45A-20-1	0.001740	0.000220	0.04840	0.00820	0.281190	0.000038	1.467204	0.000058	20	2509	12	-2.4	1.6	2507	6	-2.4	1.4
Dec 21 2022	21BN45A-22-1	0.001556	0.000039	0.04110	0.00130	0.281210	0.000047	1.467159	0.000040	20	2501	12	-1.5	1.8	2507	6	-1.4	1.7
Dec 21 2022	21BN45A-23-1	0.000604	0.000050	0.01470	0.00130	0.281178	0.000030	1.467178	0.000062	20	2508	12	-0.9	1.2	2507	6	-0.9	1.1
Dec 21 2022	21BN45A-25-1	0.000800	0.000190	0.02070	0.00510	0.281222	0.000033	1.467177	0.000044	22	2512	13	0.4	1.4	2507	6	0.3	1.3
Dec 21 2022	21BN45A-26-1	0.000519	0.000068	0.01220	0.00160	0.281183	0.000023	1.467174	0.000057	23	2495	13	-0.9	1.0	2507	6	-0.6	0.8
Dec 21 2022	21BN45A-29-1	0.001345	0.000043	0.03400	0.00120	0.281192	0.000034	1.467180	0.000042	18	2512	12	-1.6	1.3	2507	6	-1.7	1.2
Dec 21 2022	21BN45A-30-1	0.000700	0.000110	0.01740	0.00300	0.281173	0.000033	1.467144	0.000039	19	2508	12	-1.2	1.3	2507	6	-1.3	1.2
Dec 21 2022	18BN14B-10-1	0.001540	0.000130	0.03260	0.00310	0.281165	0.000037	1.467216	0.000047	19	2529	12	-2.5	1.5	2518	5	-2.7	1.3
Dec 21 2022	18BN14B-11-1	0.001118	0.000038	0.02458	0.00090	0.281133	0.000039	1.467123	0.000056	21	2529	13	-2.9	1.5	2518	5	-3.1	1.4
Dec 21 2022	18BN14B-15-1	0.001400	0.000220	0.02980	0.00510	0.281196	0.000022	1.467144	0.000068	18	2514	13	-1.5	1.1	2518	5	-1.4	0.9
Dec 21 2022	18BN14B-16-1	0.001117	0.000044	0.02296	0.00094	0.281200	0.000036	1.467158	0.000060	20	2517	13	-0.8	1.4	2518	5	-0.8	1.3
Dec 21 2022	18BN14B-17-1	0.001191	0.000097	0.02480	0.00240	0.281193	0.000042	1.467192	0.000053	19	2519	12	-1.1	1.6	2518	5	-1.1	1.5
Dec 21 2022	18BN14B-18-1	0.000880	0.000120	0.01950	0.00330	0.281178	0.000032	1.467225	0.000069	22	2537	15	-0.7	1.4	2518	5	-1.1	1.2
Dec 21 2022	18BN14B-19-1	0.001690	0.000210	0.03710	0.00530	0.281258	0.000047	1.467190	0.000140	17	2525	13	0.5	1.9	2518	5	0.3	1.7
Dec 21 2022	18BN14B-23-1	0.001430	0.000130	0.03070	0.00290	0.281225	0.000038	1.467175	0.000060	17	2515	13	-0.5	1.5	2518	5	-0.4	1.4
Dec 21 2022	18BN14B-24-1	0.001012	0.000025	0.02095	0.00066	0.281218	0.000041	1.467142	0.000080	18	2522	13	0.1	1.5	2518	5	0.1	1.5
Dec 21 2022	18BN14B-25-1	0.001410	0.000170	0.02940	0.00380	0.281230	0.000036	1.467133	0.000074	17	2508	13	-0.4	1.5	2518	5	-0.2	1.3
Dec 21 2022	18BN14B-26-1	0.001062	0.000065	0.02220	0.00150	0.281245	0.000051	1.467211	0.000075	22	2520	12	1.0	1.9	2518	5	0.9	1.8
Dec 21 2022	18BN14B-27-1	0.000988	0.000043	0.01985	0.00094	0.281236	0.000019	1.467183	0.000051	21	2509	13	0.5	0.9	2518	5	0.7	0.7
Dec 21 2022	18BN14B-28-1	0.001022	0.000072	0.02160	0.00170	0.281207	0.000044	1.467228	0.000041	19	2520	12	-0.3	1.7	2518	5	-0.4	1.6
Dec 21 2022	18BN14B-30-1	0.001140	0.000210	0.02420	0.00470	0.281170	0.000055	1.467254	0.000041	18	2517	13	-1.9	2.1	2518	5	-1.9	2.0
Dec 21 2022	18BN14B-35-1	0.001000	0.000022	0.02008	0.00050	0.281179	0.000074	1.467240	0.000140	21	2513	13	-1.4	2.7	2518	5	-1.3	2.6
Dec 21 2022	18BN14B-40-1	0.001344	0.000069	0.02900	0.00160	0.281262	0.000049	1.467093	0.000072	26	2512	13	0.9	1.8	2518	5	1.1	1.8
Dec 21 2022	18BN14B-41-1	0.001215	0.000098	0.02590	0.00240	0.281180	0.000052	1.467186	0.000052	26	2512	12	-1.8	1.9	2518	5	-1.6	1.9

Session	Spot ID	<u>176Lu</u>		<u>176Yb</u>		<u>176Hf</u>		<u>178Hf</u>		Total Hf (V)	At 207Pb/206Pb Date				At Rock Age			
		177Hf	2SE	177Hf	2SE	177Hf	2SE	177Hf	2SE		Date (Ma)	2σ	εHf(t)	2SE	Age (Ma)	2σ	εHf(i)	2SE
Dec 21 2022	21BN32A-1-1	0.000297	0.000075	0.00680	0.00170	0.281191	0.000032	1.467171	0.000058	21	2504	13	0.0	1.3	2494	6	-0.2	1.2
Dec 21 2022	21BN32A-2-1	0.000445	0.000062	0.00910	0.00120	0.281170	0.000024	1.467175	0.000059	22	2493	12	-1.3	1.0	2494	6	-1.2	0.9
Dec 21 2022	21BN32A-5-1	0.000475	0.000017	0.00899	0.00030	0.281200	0.000021	1.467234	0.000063	20	2481	12	-0.5	0.9	2494	6	-0.2	0.8
Dec 21 2022	21BN32A-8-1	0.000623	0.000024	0.01345	0.00048	0.281178	0.000023	1.467178	0.000063	17	2495	13	-1.2	1.0	2494	6	-1.3	0.8
Dec 21 2022	21BN32A-10-1	0.000287	0.000026	0.00551	0.00053	0.281195	0.000025	1.467261	0.000059	16	2507	13	0.2	1.1	2494	6	-0.1	0.9
Dec 21 2022	21BN32A-11-1	0.000683	0.000095	0.01350	0.00190	0.281202	0.000030	1.467129	0.000044	19	2497	13	-0.4	1.2	2494	6	-0.5	1.1
Dec 21 2022	21BN32A-17-1	0.001350	0.000170	0.02990	0.00370	0.281235	0.000040	1.467124	0.000096	17	2489	12	-0.6	1.6	2494	6	-0.5	1.5
Dec 21 2022	21BN32A-21-1	0.000362	0.000011	0.00764	0.00024	0.281152	0.000027	1.467218	0.000043	18	2521	13	-1.1	1.1	2494	6	-1.7	1.0
Dec 21 2022	21BN32A-25-1	0.000672	0.000023	0.01433	0.00054	0.281185	0.000016	1.467157	0.000040	18	2496	12	-1.0	0.8	2494	6	-1.1	0.6
Dec 21 2022	21BN32A-26-1	0.000580	0.000170	0.01280	0.00390	0.281184	0.000038	1.467176	0.000049	18	2506	13	-0.7	1.6	2494	6	-1.0	1.4
Dec 21 2022	21BN32A-27-1	0.001330	0.000190	0.02920	0.00430	0.281262	0.000036	1.467175	0.000047	17	2484	12	0.3	1.5	2494	6	0.5	1.4
Dec 21 2022	21BN32A-30-1	0.000610	0.000250	0.01350	0.00550	0.281193	0.000036	1.467238	0.000076	22	2495	12	-0.7	1.5	2494	6	-0.7	1.4
Dec 21 2022	21BN15A-2-1	0.002210	0.000210	0.04940	0.00470	0.281366	0.000049	1.467248	0.000053	15	2491	12	2.7	1.9	2500	9	2.9	1.8
Dec 21 2022	21BN15A-2-2	0.001550	0.000300	0.03420	0.00660	0.281324	0.000032	1.467169	0.000061	16	2489	12	2.3	1.5	2500	9	2.5	1.4
Dec 21 2022	21BN15A-4-1	0.000615	0.000077	0.01370	0.00190	0.281229	0.000042	1.467280	0.000037	14	2508	13	0.9	1.6	2500	9	0.7	1.5
Dec 21 2022	21BN15A-5-1	0.000846	0.000021	0.01826	0.00056	0.281272	0.000024	1.467235	0.000078	18	2498	13	1.8	1.0	2500	9	1.9	0.9
Dec 21 2022	21BN15A-6-1	0.000431	0.000068	0.00940	0.00160	0.281214	0.000040	1.467272	0.000055	20	2507	13	0.6	1.5	2500	9	0.5	1.5
Dec 21 2022	21BN15A-10-1	0.001250	0.000210	0.02830	0.00500	0.281244	0.000041	1.467226	0.000085	15	2518	14	0.6	1.7	2500	9	0.2	1.6
Dec 21 2022	19BN88A-1-1	0.002820	0.000190	0.07390	0.00520	0.281321	0.000037	1.467235	0.000052	20	2491	12	0.0	1.5	2502	6	0.3	1.4
Dec 21 2022	19BN88A-4-1	0.001645	0.000068	0.04260	0.00190	0.281331	0.000031	1.467184	0.000060	21	2496	12	2.5	1.2	2502	6	2.6	1.1
Dec 21 2022	19BN88A-6-1	0.001620	0.000170	0.04310	0.00470	0.281293	0.000042	1.467191	0.000054	21	2495	13	1.2	1.7	2502	6	1.3	1.5
Dec 21 2022	19BN88A-7-1	0.001443	0.000065	0.03700	0.00170	0.281305	0.000035	1.467191	0.000064	19	2492	13	1.8	1.4	2502	6	2.1	1.3
Dec 21 2022	19BN88A-10-1	0.002080	0.000180	0.05430	0.00490	0.281313	0.000038	1.467233	0.000068	20	2503	12	1.3	1.6	2502	6	1.3	1.4
Dec 21 2022	19BN88A-15-1	0.002290	0.000530	0.06100	0.01400	0.281301	0.000056	1.467194	0.000061	20	2495	13	0.3	2.4	2502	6	0.5	2.2
Dec 21 2022	19BN88A-22-1	0.001460	0.000290	0.04010	0.00830	0.281306	0.000063	1.467170	0.000096	19	2508	13	2.2	2.4	2502	6	2.1	2.3
Dec 21 2022	19BN88A-23-1	0.001940	0.000200	0.04980	0.00580	0.281317	0.000040	1.467254	0.000076	20	2498	12	1.5	1.6	2502	6	1.6	1.5
Dec 21 2022	19BN88A-28-1	0.001990	0.000160	0.05130	0.00430	0.281307	0.000035	1.467185	0.000050	18	2512	12	1.4	1.4	2502	6	1.2	1.3
Dec 21 2022	19BN88A-32-1	0.001277	0.000032	0.03293	0.00080	0.281249	0.000033	1.467294	0.000080	18	2508	13	0.5	1.3	2502	6	0.3	1.2
Dec 21 2022	19BN88A-33-1	0.001049	0.000066	0.02720	0.00160	0.281264	0.000043	1.467230	0.000045	19	2506	12	1.4	1.6	2502	6	1.3	1.5
Dec 21 2022	19BN88A-36-1	0.001380	0.000210	0.03530	0.00570	0.281296	0.000032	1.467197	0.000040	18	2503	12	1.9	1.4	2502	6	1.8	1.2
Dec 20 2022	19BN88A-27-1	0.000910	0.000160	0.02270	0.00420	0.281239	0.000020	1.467221	0.000046	25	2522	13	1.1	1.1	2502	6	0.6	0.8
Dec 20 2022	19BN88A-25-1	0.001056	0.000079	0.02700	0.00200	0.281237	0.000039	1.467115	0.000048	18	2511	13	0.5	1.5	2502	6	0.3	1.4
Dec 20 2022	19BN88A-13-1	0.001225	0.000048	0.03080	0.00110	0.281247	0.000025	1.467204	0.000045	18	2501	12	0.3	1.0	2502	6	0.4	0.9
Dec 20 2022	19BN88A-5-1	0.001250	0.000130	0.03230	0.00380	0.281226	0.000027	1.467198	0.000050	23	2496	12	-0.6	1.2	2502	6	-0.4	1.0

Session	Spot ID									At 207Pb/206Pb Date				At Rock Age				
		<u>176Lu</u>		<u>176Yb</u>		<u>176Hf</u>		<u>178Hf</u>		Total Hf (V)	Date (Ma)	2σ	εHf(t)	2SE	Age (Ma)	2σ	εHf(i)	2SE
		177Hf	2SE	177Hf	2SE	177Hf	2SE	177Hf	2SE									
Dec 21 2022	19BN166A-10-2	0.001140	0.000130	0.02890	0.00370	0.281241	0.000025	1.467214	0.000048	19	2498	12	0.2	1.1	2499	6	0.2	0.9
Dec 21 2022	19BN166A-12-1	0.000439	0.000013	0.01024	0.00037	0.281203	0.000019	1.467211	0.000036	24	2505	12	0.2	0.8	2499	6	0.1	0.7
Dec 21 2022	19BN166A-13-1	0.001460	0.000150	0.03690	0.00390	0.281234	0.000029	1.467171	0.000036	18	2518	12	-0.1	1.2	2499	6	-0.6	1.1
Dec 21 2022	19BN166A-16-1	0.000341	0.000038	0.00768	0.00098	0.281225	0.000022	1.467177	0.000043	26	2505	12	1.2	0.9	2499	6	1.0	0.8
Dec 21 2022	19BN166A-17-1	0.000862	0.000067	0.02170	0.00190	0.281204	0.000032	1.467215	0.000046	21	2496	12	-0.7	1.3	2499	6	-0.6	1.2
Dec 21 2022	19BN166A-18-1	0.000579	0.000074	0.01260	0.00190	0.281268	0.000038	1.467095	0.000080	20	2496	12	2.1	1.5	2499	6	2.1	1.4
Dec 21 2022	19BN166A-21-1	0.001420	0.000110	0.03670	0.00300	0.281197	0.000034	1.467193	0.000051	19	2509	12	-1.6	1.4	2499	6	-1.8	1.2
Dec 21 2022	19BN166A-22-1	0.001161	0.000056	0.02750	0.00140	0.281174	0.000035	1.467159	0.000038	19	2490	12	-2.4	1.4	2499	6	-2.2	1.3
Dec 21 2022	19BN166A-23-1	0.001260	0.000140	0.03140	0.00380	0.281166	0.000029	1.467170	0.000064	18	2502	12	-2.6	1.2	2499	6	-2.6	1.1
Dec 21 2022	19BN166A-25-1	0.000730	0.000150	0.01920	0.00410	0.281192	0.000032	1.467185	0.000045	26	2508	12	-0.6	1.3	2499	6	-0.8	1.2
Dec 21 2022	19BN166A-27-1	0.001610	0.000330	0.04410	0.00990	0.281194	0.000055	1.467092	0.000088	25	2493	12	-2.4	2.2	2499	6	-2.2	2.1
Dec 21 2022	19BN166A-28-1	0.0003680	0.0000069	0.00845	0.00021	0.281141	0.000037	1.467189	0.000034	17	2504	12	-1.9	1.4	2499	6	-2.0	1.3
Dec 21 2022	19BN166A-29-1	0.000474	0.000025	0.01168	0.00066	0.281182	0.000023	1.467185	0.000048	18	2508	12	-0.5	1.0	2499	6	-0.7	0.8
Dec 21 2022	19BN166A-30-1	0.000780	0.000140	0.02010	0.00380	0.281188	0.000035	1.467182	0.000071	20	2499	12	-1.0	1.4	2499	6	-1.0	1.3
Dec 21 2022	19BN166A-31-1	0.002630	0.000560	0.07200	0.01600	0.281264	0.000044	1.467177	0.000081	22	2492	12	-1.6	2.1	2499	6	-1.5	1.9
Dec 20 2022	19BN53A-1-1	0.001133	0.000053	0.02780	0.00120	0.281225	0.000024	1.467178	0.000044	21	2505	12	-0.2	1.0	2497	6	-0.4	0.9
Dec 20 2022	19BN53A-5-1	0.001112	0.000077	0.02740	0.00220	0.281268	0.000025	1.467181	0.000064	27	2485	12	0.9	1.1	2497	6	1.2	0.9
Dec 20 2022	19BN53A-7-1	0.001207	0.000019	0.02884	0.00051	0.281240	0.000022	1.467167	0.000051	23	2499	12	0.1	0.9	2497	6	0.0	0.8
Dec 20 2022	19BN53A-9-1	0.001360	0.000180	0.03450	0.00490	0.281260	0.000030	1.467177	0.000048	28	2495	12	0.4	1.3	2497	6	0.5	1.1
Dec 20 2022	19BN53A-10-1	0.000798	0.000047	0.01980	0.00130	0.281214	0.000036	1.467211	0.000040	29	2501	13	-0.1	1.4	2497	6	-0.2	1.3
Dec 20 2022	19BN53A-13-2	0.000954	0.000060	0.02350	0.00160	0.281232	0.000036	1.467125	0.000058	20	2496	12	0.1	1.4	2497	6	0.2	1.3
Dec 20 2022	19BN53A-14-1	0.001058	0.000038	0.02606	0.00097	0.281224	0.000021	1.467179	0.000048	30	2493	12	-0.4	0.9	2497	6	-0.3	0.8
Dec 20 2022	19BN53A-16-1	0.000728	0.000033	0.01786	0.00082	0.281231	0.000027	1.467188	0.000033	27	2499	12	0.6	1.1	2497	6	0.5	1.0
Dec 20 2022	19BN53A-17-1	0.000790	0.000160	0.01960	0.00420	0.281254	0.000026	1.467191	0.000042	31	2503	12	1.4	1.2	2497	6	1.2	1.0
Dec 20 2022	19BN53A-19-1	0.001005	0.000046	0.02500	0.00130	0.281240	0.000021	1.467157	0.000042	28	2500	12	0.4	0.9	2497	6	0.4	0.8
Dec 20 2022	19BN53A-26-1	0.001053	0.000067	0.02610	0.00180	0.281268	0.000027	1.467190	0.000041	23	2494	12	1.2	1.1	2497	6	1.3	1.0
Dec 20 2022	19BN53A-27-1	0.001410	0.000047	0.03370	0.00110	0.281267	0.000030	1.467177	0.000048	20	2498	12	0.7	1.2	2497	6	0.6	1.1
Dec 20 2022	19BN53A-30-1	0.001147	0.000041	0.02850	0.00110	0.281268	0.000030	1.467184	0.000053	23	2493	13	1.0	1.2	2497	6	1.1	1.1
Dec 20 2022	19BN53A-31-1	0.001027	0.000099	0.02620	0.00250	0.281236	0.000022	1.467169	0.000044	23	2490	13	0.0	1.0	2497	6	0.2	0.8
Dec 20 2022	19BN53A-32-1	0.000657	0.000044	0.01570	0.00130	0.281236	0.000014	1.467177	0.000048	27	2493	12	0.7	0.7	2497	6	0.8	0.5

Session	Spot ID	<u>176Lu</u>		<u>176Yb</u>		<u>176Hf</u>		<u>178Hf</u>		Total Hf (V)	At 207Pb/206Pb Date				At Rock Age			
		177Hf	2SE	177Hf	2SE	177Hf	2SE	177Hf	2SE		Date (Ma)	2σ	εHf(t)	2SE	Age (Ma)	2σ	εHf(i)	2SE
Dec 20 2022	21BN34A-1-1	0.000650	0.000020	0.01569	0.00044	0.281211	0.000020	1.467164	0.000040	23	2500	12	0.0	0.9	2500	6	0.0	0.7
Dec 20 2022	21BN34A-1-2	0.0007420	0.0000078	0.01826	0.00019	0.281199	0.000022	1.467212	0.000031	22	2483	12	-1.0	0.9	2500	6	-0.6	0.8
Dec 20 2022	21BN34A-2-1	0.000666	0.000039	0.01690	0.00100	0.281211	0.000017	1.467212	0.000034	24	2456	12	-1.0	0.8	2500	6	0.0	0.6
Dec 20 2022	21BN34A-9-1	0.001090	0.000140	0.02680	0.00370	0.281234	0.000031	1.467216	0.000045	24	2510	12	0.3	1.3	2500	6	0.1	1.2
Dec 20 2022	21BN34A-24-1	0.000910	0.000310	0.02300	0.00820	0.281219	0.000022	1.467174	0.000074	25	2515	13	0.2	1.3	2500	6	-0.1	1.0
Dec 20 2022	21BN34A-28-1	0.000920	0.000170	0.02190	0.00440	0.281201	0.000029	1.467095	0.000045	23	2502	12	-0.8	1.3	2500	6	-0.8	1.1
Dec 20 2022	21BN34A-40-1	0.001130	0.000140	0.02890	0.00380	0.281253	0.000026	1.467170	0.000070	24	2511	12	1.0	1.2	2500	6	0.7	1.0
Dec 20 2022	21BN34A-41-1	0.001010	0.000170	0.02520	0.00420	0.281208	0.000044	1.467170	0.000039	24	2508	13	-0.5	1.8	2500	6	-0.7	1.6
Dec 20 2022	21BN34A-43-1	0.000910	0.000150	0.02390	0.00420	0.281194	0.000025	1.467204	0.000090	30	2493	13	-1.2	1.1	2500	6	-1.0	1.0
Dec 20 2022	21BN34A-45-1	0.000872	0.000060	0.02080	0.00170	0.281216	0.000021	1.467180	0.000056	27	2492	12	-0.4	0.9	2500	6	-0.2	0.8
Dec 20 2022	21BN34A-47-1	0.001060	0.000220	0.02620	0.00540	0.281247	0.000030	1.467198	0.000043	22	2485	13	0.3	1.4	2500	6	0.6	1.2
Dec 20 2022	21BN34A-25-1	0.001410	0.000120	0.03510	0.00300	0.281271	0.000047	1.467234	0.000075	22	2488	12	0.6	1.8	2500	6	0.9	1.7
Dec 20 2022	21BN34C-4-1	0.000700	0.000110	0.01630	0.00290	0.281259	0.000034	1.467140	0.000066	16	2482	14	1.2	1.4	2499	6	1.6	1.2
Dec 20 2022	21BN34C-5-1	0.0002419	0.0000091	0.00543	0.00018	0.281242	0.000019	1.467196	0.000027	24	2432	14	0.2	0.9	2499	6	1.8	0.7
Dec 20 2022	21BN34C-7-1	0.000401	0.000041	0.00915	0.00094	0.281235	0.000025	1.467170	0.000060	20	2442	15	0.0	1.2	2499	6	1.3	0.9
Dec 20 2022	21BN34C-8-1	0.000910	0.000100	0.02130	0.00270	0.281248	0.000031	1.467170	0.000040	15	2458	13	-0.1	1.3	2499	6	0.9	1.1
Dec 20 2022	21BN34C-10-1	0.001010	0.000240	0.03070	0.00910	0.281210	0.000029	1.467178	0.000047	18	2509	14	-0.4	1.4	2499	6	-0.7	1.2
Dec 20 2022	21BN34C-12-1	0.001050	0.000190	0.02690	0.00610	0.281238	0.000045	1.467176	0.000054	14	2502	14	0.3	1.8	2499	6	0.3	1.7
Dec 20 2022	21BN34C-15-1	0.000740	0.000130	0.01740	0.00320	0.281256	0.000028	1.467149	0.000041	17	2493	13	1.3	1.2	2499	6	1.4	1.0
Dec 20 2022	21BN34C-17-1	0.001260	0.000150	0.03520	0.00520	0.281252	0.000029	1.467203	0.000039	17	2500	13	0.4	1.3	2499	6	0.4	1.1
Dec 20 2022	21BN34C-22-1	0.000590	0.000200	0.01640	0.00650	0.281188	0.000025	1.467208	0.000040	23	2495	14	-0.8	1.3	2499	6	-0.7	1.0
Dec 20 2022	21BN34C-25-2	0.000454	0.000049	0.01050	0.00120	0.281207	0.000033	1.467215	0.000040	17	2511	14	0.5	1.3	2499	6	0.2	1.2
Dec 20 2022	21BN34C-26-1	0.000322	0.000043	0.00741	0.00095	0.281239	0.000023	1.467188	0.000048	19	2507	14	1.7	1.0	2499	6	1.5	0.8
Dec 20 2022	21BN34C-28-1	0.000700	0.000110	0.02290	0.00450	0.281220	0.000029	1.467196	0.000059	18	2417	14	-1.7	1.3	2499	6	0.2	1.1
Dec 20 2022	21BN34C-29-1	0.001160	0.000430	0.03400	0.01400	0.281298	0.000035	1.467041	0.000076	15	2505	15	2.4	1.9	2499	6	2.2	1.5
Dec 20 2022	21BN34C-32-1	0.000589	0.000063	0.01360	0.00150	0.281229	0.000063	1.467125	0.000060	13	2509	14	1.0	2.3	2499	6	0.7	2.3
Dec 20 2022	21BN34C-34-1	0.000647	0.000072	0.01540	0.00170	0.281231	0.000024	1.467150	0.000053	15	2494	13	0.6	1.1	2499	6	0.7	0.9
Dec 20 2022	21BN34C-38-1	0.000638	0.000056	0.01400	0.00130	0.281223	0.000020	1.467181	0.000052	16	2479	13	0.0	1.0	2499	6	0.4	0.7
Dec 20 2022	21BN34C-39-1	0.000404	0.000044	0.00930	0.00100	0.281187	0.000024	1.467195	0.000066	29	2454	15	-1.5	1.1	2499	6	-0.4	0.9
Dec 20 2022	21BN34C-41-1	0.000453	0.000056	0.01130	0.00210	0.281243	0.000052	1.467222	0.000079	13	2503	13	1.6	2.0	2499	6	1.5	1.9
Dec 20 2022	21BN34C-43-1	0.000482	0.000042	0.01084	0.00098	0.281246	0.000020	1.467155	0.000053	20	2408	15	-0.6	1.1	2499	6	1.5	0.7

Table C-5. Whole-rock Sm-Nd isotope data.

Sample ID	Sm ppm	Nd ppm	$\frac{147\text{Sm}}{144\text{Nd}}$	$2\sigma^1$	$\frac{143\text{Nd}}{144\text{Nd}} (0)$	2SE	$2\sigma^1$	Age (Ma) ²	2σ	$\frac{143\text{Nd}}{144\text{Nd}} (i)$	$2\sigma^3$	$\epsilon\text{Nd}(i)$	$2\sigma^3$
19BN38A	4.842	32.28	0.09068	0.00018	0.510759	0.000007	0.000017	2700	10	0.509127	0.000018	-0.2	0.4
19BN07B	4.959	32.86	0.09125	0.00018	0.510752	0.000007	0.000017	2707	8	0.509121	0.000018	-0.2	0.3
19BN45B	4.272	30.75	0.08400	0.00017	0.510641	0.000008	0.000017	2700	10	0.509143	0.000018	0.1	0.4
19BN01A	4.529	33.36	0.08208	0.00016	0.510587	0.000007	0.000017	2698	6	0.509172	0.000017	0.6	0.3
19BC52A	6.926	48.21	0.08687	0.00017	0.510719	0.000007	0.000017	2688	7	0.509178	0.000018	0.5	0.3
19BN106B	6.286	42.01	0.09049	0.00018	0.510858	0.000010	0.000018	2580	6	0.509318	0.000019	0.5	0.4
19BN98A	4.992	24.54	0.12302	0.00025	0.511376	0.000008	0.000017	2600	10	0.509267	0.000020	0.0	0.4
18EM31B	6.726	47.27	0.08604	0.00017	0.510744	0.000007	0.000017	2582	6	0.509279	0.000017	-0.3	0.3
16BK374A	5.614	33.98	0.09990	0.00020	0.511007	0.000010	0.000018	2578	5	0.509308	0.000019	0.2	0.4
21BN34A	12.91	77.31	0.10099	0.00020	0.511060	0.000007	0.000017	2500	6	0.509396	0.000018	-0.1	0.3
21BN34C	9.598	50.90	0.11402	0.00023	0.511308	0.000009	0.000018	2499	6	0.509430	0.000019	0.6	0.4
18BN114A	12.72	65.87	0.11680	0.00023	0.511327	0.000009	0.000018	2476	6	0.509421	0.000019	-0.2	0.4
18BN27A	16.50	80.71	0.12366	0.00025	0.511417	0.000006	0.000017	2500	10	0.509379	0.000019	-0.4	0.4
18BN56A	6.675	33.31	0.12115	0.00024	0.511408	0.000008	0.000017	2500	10	0.509411	0.000020	0.2	0.4
18BN18B-M	5.838	31.46	0.11220	0.00022	0.511231	0.000008	0.000017	2500	10	0.509382	0.000019	-0.4	0.4
18BN31A	3.019	21.08	0.08660	0.00017	0.510836	0.000009	0.000018	2500	10	0.509409	0.000019	0.2	0.4
19BN173A	7.052	39.75	0.10728	0.00021	0.511141	0.000006	0.000017	2502	7	0.509372	0.000018	-0.5	0.3
18BN113A	2.156	13.99	0.09316	0.00019	0.510914	0.000010	0.000018	2512	7	0.509371	0.000019	-0.3	0.4
18BN20B	8.366	46.03	0.10990	0.00022	0.511207	0.000009	0.000018	2500	10	0.509395	0.000020	-0.1	0.4
19BN154A	8.136	60.15	0.08180	0.00016	0.510749	0.000008	0.000017	2505	6	0.509398	0.000018	0.1	0.3
19BN166A	7.714	44.72	0.10430	0.00021	0.511099	0.000010	0.000018	2499	6	0.509380	0.000019	-0.4	0.4
21BN32A	6.885	33.58	0.12398	0.00025	0.511453	0.000007	0.000017	2494	6	0.509415	0.000018	0.1	0.4
21BN15A	9.298	38.47	0.14613	0.00029	0.511819	0.000007	0.000017	2500	6	0.509411	0.000019	0.2	0.4
19BN79A	17.29	100.9	0.10359	0.00021	0.511088	0.000007	0.000017	2500	10	0.509381	0.000018	-0.4	0.4
21BN09A	16.67	96.05	0.10496	0.00021	0.511126	0.000008	0.000017	2504	6	0.509394	0.000018	0.0	0.4
21BN16A	7.466	38.26	0.11798	0.00024	0.511343	0.000011	0.000019	2500	10	0.509398	0.000021	0.0	0.4
19BN88A	9.789	56.30	0.10513	0.00021	0.511141	0.000006	0.000016	2502	6	0.509407	0.000017	0.2	0.3
21BN20D	6.255	33.68	0.11230	0.00022	0.511229	0.000009	0.000018	2500	10	0.509378	0.000019	-0.4	0.4
21BN20C	7.280	44.72	0.09843	0.00020	0.511032	0.000011	0.000019	2500	10	0.509410	0.000020	0.2	0.4
21BN28A	11.62	67.80	0.10363	0.00021	0.511125	0.000010	0.000018	2500	10	0.509417	0.000020	0.3	0.4
21BN29A	7.102	39.04	0.10998	0.00022	0.511196	0.000009	0.000018	2500	10	0.509384	0.000020	-0.3	0.4
21BN30A	7.334	45.25	0.09801	0.00020	0.511026	0.000010	0.000018	2500	10	0.509410	0.000020	0.2	0.4
19BN53A	6.844	36.92	0.11209	0.00022	0.511245	0.000011	0.000019	2497	6	0.509400	0.000020	-0.1	0.4
19BN126B	7.158	50.54	0.08563	0.00017	0.510825	0.000010	0.000018	2496	6	0.509416	0.000019	0.2	0.4
19BN127A	8.208	46.99	0.10561	0.00021	0.511155	0.000009	0.000018	2497	6	0.509417	0.000019	0.3	0.4
18BN14B	3.382	17.67	0.11571	0.00023	0.511280	0.000011	0.000019	2518	5	0.509359	0.000020	-0.3	0.4
21BN45A	14.82	73.75	0.12147	0.00024	0.511394	0.000011	0.000019	2507	6	0.509386	0.000020	-0.1	0.4
18EM33A	10.73	53.39	0.12148	0.00024	0.511380	0.000005	0.000016	2500	10	0.509377	0.000019	-0.4	0.4

¹⁴³Nd/¹⁴⁴Nd(i) and $\epsilon\text{Nd}(i)$ calculated using the decay constant of Lugmair and Marti (1978). $\epsilon\text{Nd}(i)$ values calculated with the CHUR values of Bouvier et al. (2008).

1: includes long-term external reproducibility; 2: Ages in *italics* are assumed; 3: includes long-term external reproducibility and age uncertainty.

Some of these data were published in Neil et al. (2023)/chapter 2, but have been reproduced here for clarity.

Table C-6. Whole-rock major- and trace-element data.

	2.7 Ga Granitoids					2.6 Ga Granitoids			
	19BC52A	19BN45B	19BN07B	19BN01A	19BN38A	19BN98A	19BN106B	18EM31B	16BK374A
ICP-OES (wt.%)									
SiO ₂	61.09	64.44	66.84	66.96	68.31	51.95	61.08	65.06	67.15
Al ₂ O ₃	17.74	17.06	15.04	15.41	15.50	19.99	18.28	16.72	16.05
FeO(t)	5.32	5.00	4.16	4.01	3.74	8.55	5.42	4.52	4.01
MnO	0.094	0.065	0.065	0.055	0.052	0.122	0.083	0.075	0.054
MgO	2.86	2.48	2.48	2.59	2.04	4.93	2.78	1.98	1.74
CaO	4.69	4.20	4.25	3.88	4.02	8.84	5.21	4.42	3.99
Na ₂ O	5.25	3.91	3.91	4.28	4.15	2.28	3.54	2.98	3.67
K ₂ O	1.96	2.09	2.54	2.11	1.50	2.23	2.89	3.47	2.60
TiO ₂	0.667	0.541	0.490	0.471	0.491	0.904	0.499	0.570	0.573
P ₂ O ₅	0.32	0.21	0.23	0.24	0.19	0.21	0.21	0.21	0.18
LOI	1.48	0.77	0.95	1.62	0.93	3.28	2.94	1.91	1.19
Total	100.3	99.80	99.93	100.2	99.31	99.96	100.40	99.34	100.7
ICP-MS (ppm)									
La	67.19	50.85	47.11	54.01	47.90	17.24	56.51	66.48	40.19
Ce	124.08	90.19	90.58	95.13	89.15	40.84	106.71	131.40	78.36
Pr	13.896	9.504	9.650	10.107	9.750	5.747	11.862	14.527	9.377
Nd	49.42	32.17	34.18	34.41	33.65	25.39	43.11	50.48	35.30
Sm	7.15	4.39	5.27	4.67	5.12	5.23	6.47	7.20	5.97
Eu	1.781	1.520	1.394	1.433	1.389	1.515	1.722	1.471	1.415
Gd	4.527	2.930	3.566	3.026	3.379	4.106	4.642	4.640	4.198
Tb	0.511	0.333	0.441	0.343	0.414	0.565	0.588	0.604	0.553
Dy	2.31	1.60	2.17	1.63	1.95	3.02	2.95	3.01	2.81
Ho	0.393	0.277	0.386	0.281	0.353	0.576	0.551	0.594	0.530
Er	0.928	0.698	0.997	0.734	0.883	1.491	1.434	1.531	1.392
Tm	0.1293	0.1021	0.1438	0.1056	0.1243	0.2143	0.2067	0.2247	0.2048
Yb	0.741	0.590	0.860	0.648	0.800	1.302	1.264	1.366	1.200
Lu	0.106	0.098	0.134	0.099	0.123	0.208	0.188	0.202	0.170
Ba	930.2	1247.4	1193.9	963.2	973.4	546.3	1076.0	1244.3	801.1
Th	1.53	11.52	15.76	9.19	17.82	1.50	8.64	17.68	7.33
Nb	5.80	4.03	4.18	4.58	5.49	5.24	4.84	7.98	7.69
Y	10.95	7.60	10.96	8.20	10.00	15.31	14.77	15.85	14.87
Hf	4.14	3.64	3.95	4.11	3.71	2.69	5.17	6.09	5.23
U	0.41	0.43	0.53	0.52	2.83	0.78	1.02	1.43	1.83
Pb	16.13	13.66	19.71	13.84	18.14	11.98	16.86	24.81	15.84
Rb	85.0	63.3	57.0	69.5	35.9	83.2	97.6	105.7	86.1
Cs	3.31	2.42	0.37	3.82	0.57	1.33	1.31	1.18	1.01
Sr	1091.2	553.8	585.3	456.5	528.5	675.8	679.3	511.0	487.4
Sc	9.40	8.35	8.89	8.12	7.95	23.35	15.63	11.28	7.75
Zr	173.8	146.3	149.2	159.2	136.3	97.2	196.5	235.6	195.6
XRF (ppm)									
Rb	82.1	62.8	50.1	68.1	34.9	84.0	103.5	110.2	87.8
Sr	1039	534	514	441	514	667	702	509	483
Y	10	7.1	8.3	7.5	9.9	14.4	13.7	15.5	15.1
Zr	160	140	133	143	129	102	189	200	163
V	89	80	67	69	73	205	111	72	84
Ni	30	24	33	30	25	11	6	8	8
Cr	39	36	47	53	23	<2	6	17	7
Ga	20.7	20.3	15.6	17.3	18.1	23.9	22	20	21
Nb	13.3	7.2	7.8	6.6	8.2	9.7	9.6	10.3	9.7
Cu	19	9	20	11	13	34	25	14	6
Zn	78	67	53	62	45	96	68	68	58
Ba	877	1194	1066	913	920	549	1115	1324	788
La	69	46	40	57	48	12	62	68	40
Ce	139	96	72	102	107	40	112	129	94
U	<0.5	<0.5	<0.5	<0.5	2.9	<0.5	<0.5	1.2	1.7
Th	0.8	10.5	13.5	8.3	16.4	<0.5	8.6	16.5	6.5
Sc	10	8	10	9	11	22	16	10	11
Pb	15	12	15	13	16	12	17	23	15

Major elements are normalised to 100%, loss on ignition (LOI) excluded. Totals are reported as measured, with all Fe as Fe₂O₃.

Analyses below detection limit indicated with "<".

ICP-OES major-element data from Actlabs. ICP-MS trace-element data from Washington State University.

XRF: trace-element data from Franklin & Marshall College.

2.5 Ga Granitoids

	19BN127A	18BN27A	18BN56A	21BN34C	21BN15A	18BN114A	18EM33A	19BN79A	21BN45A	21BN34A
ICP-OES (wt.%)										
SiO ₂	47.26	49.57	50.13	50.30	50.61	52.57	54.64	55.77	55.99	56.15
Al ₂ O ₃	17.89	17.86	15.96	16.38	13.66	16.80	17.75	16.35	18.55	19.91
FeO(t)	13.41	11.49	9.93	11.43	11.24	10.82	8.55	9.01	7.63	6.56
MnO	0.227	0.193	0.188	0.215	0.256	0.196	0.165	0.142	0.109	0.098
MgO	5.47	4.54	7.87	6.41	8.60	4.49	4.04	3.41	3.22	2.60
CaO	8.27	8.73	9.90	8.15	10.59	8.11	6.89	6.95	6.31	6.88
Na ₂ O	2.83	3.30	2.51	2.73	2.39	3.65	2.82	2.85	3.55	4.25
K ₂ O	2.41	2.22	1.66	2.03	1.49	1.44	3.41	3.01	3.35	2.28
TiO ₂	1.781	1.561	1.460	1.733	0.936	1.400	1.341	1.603	0.945	0.996
P ₂ O ₅	0.44	0.55	0.37	0.61	0.22	0.53	0.39	0.90	0.34	0.29
LOI	0.95	1.55	2.29	2.44	1.66	1.16	1.90	1.30	1.57	1.55
Total	99.83	99.81	100.4	100.2	100.2	99.55	99.03	100.1	98.40	98.82
ICP-MS (ppm)										
La	39.58	51.01	24.23	36.65	23.57	49.44	40.86	89.94	60.71	87.91
Ce	89.56	131.08	58.69	89.27	64.14	117.74	96.87	200.60	141.83	179.87
Pr	11.781	19.030	8.157	12.286	9.183	16.236	13.254	25.650	18.695	21.322
Nd	48.65	82.47	34.60	51.73	39.92	68.10	54.62	103.57	75.60	79.63
Sm	8.54	16.85	6.94	9.95	9.75	13.07	11.13	17.77	15.45	13.32
Eu	3.112	2.740	1.741	2.378	1.828	2.861	1.797	3.377	1.962	2.318
Gd	6.839	13.313	5.791	7.720	9.584	10.186	8.698	12.667	12.100	9.605
Tb	0.963	1.917	0.824	1.109	1.650	1.488	1.183	1.656	1.740	1.318
Dy	5.28	10.24	4.50	5.93	9.98	8.01	6.10	8.26	9.36	6.91
Ho	1.066	1.935	0.871	1.158	2.133	1.515	1.175	1.516	1.794	1.285
Er	2.935	5.126	2.281	3.093	6.453	4.051	3.059	3.905	4.779	3.433
Tm	0.4368	0.7213	0.3407	0.4504	1.0420	0.5956	0.4283	0.5353	0.7118	0.4720
Yb	2.739	4.232	2.010	2.792	6.746	3.559	2.684	3.223	4.176	2.857
Lu	0.432	0.650	0.333	0.440	1.071	0.568	0.400	0.493	0.611	0.418
Ba	1711.1	560.1	508.8	667.7	141.8	674.5	818.4	1334.3	539.9	855.1
Th	1.79	1.91	1.64	1.57	4.55	1.98	0.75	5.64	4.39	0.75
Nb	8.68	17.66	11.46	12.24	20.37	21.24	20.14	26.54	19.21	15.67
Y	28.80	54.75	24.97	30.58	63.85	43.02	32.57	41.64	50.07	35.14
Hf	5.75	3.86	2.03	4.39	3.28	7.54	6.26	8.78	4.46	7.62
U	0.44	0.74	0.34	0.62	1.72	0.77	0.40	1.18	0.34	0.57
Pb	9.12	16.60	33.54	6.82	15.03	7.89	15.38	18.35	18.58	10.79
Rb	83.4	80.8	66.8	55.5	61.9	33.6	168.3	112.8	140.6	54.6
Cs	2.00	0.43	0.49	0.43	0.64	0.45	1.45	5.11	1.20	0.78
Sr	605.4	578.2	449.8	399.9	276.6	590.8	597.7	662.0	575.2	659.6
Sc	30.71	36.28	31.38	33.52	48.87	28.77	18.62	23.76	22.95	20.26
Zr	284.6	142.0	63.6	170.9	98.5	310.1	251.4	386.5	169.3	310.1
XRF (ppm)										
Rb	83.2	77.0	63.7	56.9	63.0	31.3	12.6	108.8	140.7	53.7
Sr	581	519	401	400	263	522	612	622	559	644
Y	27.0	49.2	22.3	29.0	61.7	38.9	2.5	39.1	49.7	33.2
Zr	239	116	69	161	95	247	200	340	154	260
V	306	282	236	190	258	135	9	164	154	106
Ni	7	7	105	49	37	18	6	11	12	7
Cr	<2	<2	346	125	232	59	7	7	30	18
Ga	23	25	19	21	18	24	15	23	26	26
Nb	11.9	19.0	12.3	13.6	19.4	21.4	1.1	27.3	20.8	18.6
Cu	15	42	35	12	52	17	1	25	18	12
Zn	134	144	158	185	118	136	14	124	84	94
Ba	1628	502	462	596	138	629	320	1247	538	768
La	36	49	24	36	16	54	17	93	60	81
Ce	93	131	61	82	63	129	27	209	143	158
U	<0.5	<0.5	<0.5	<0.5	2.0	0.8	1.4	<0.5	<0.5	0.9
Th	0.8	1.4	0.9	0.8	4.2	0.7	0.7	5.6	3.5	<0.5
Sc	30	35	34	33	49	31	2	26	21	24
Pb	8	16	28	8	16	8	14	18	17	10

2.5 Ga Granitoids

	18BN14B	21BN09A	21BN32A	18BN20B	21BN16A	21BN20C	18BN18B-M	19BN173A	19BN88A	19BN154A
ICP-OES (wt.%)										
SiO ₂	56.37	56.44	57.50	57.53	58.74	59.79	61.70	62.25	62.98	63.37
Al ₂ O ₃	18.18	16.86	16.99	17.35	16.77	17.68	16.75	16.70	15.97	17.37
FeO(t)	7.90	8.98	7.63	6.93	6.23	6.24	6.47	5.64	6.14	4.80
MnO	0.159	0.138	0.139	0.164	0.113	0.125	0.108	0.105	0.117	0.091
MgO	4.98	2.82	4.63	4.30	5.22	3.19	3.39	2.67	2.07	1.60
CaO	6.34	6.82	7.70	5.76	6.19	4.77	5.10	5.59	4.94	4.78
Na ₂ O	3.04	2.80	3.11	3.77	2.90	4.30	3.45	3.59	3.42	3.62
K ₂ O	2.28	2.70	1.49	2.95	2.74	2.90	2.13	2.42	3.07	3.46
TiO ₂	0.605	1.646	0.673	0.919	0.815	0.734	0.703	0.829	0.933	0.692
P ₂ O ₅	0.13	0.81	0.14	0.32	0.29	0.29	0.18	0.21	0.36	0.20
LOI	2.75	1.13	2.08	3.45	1.79	0.83	1.32	1.29	0.53	1.48
Total	99.93	100.1	100.4	99.83	99.32	99.61	99.11	98.36	99.18	99.93
ICP-MS (ppm)										
La	11.91	94.36	20.93	43.62	27.34	55.48	30.85	33.68	57.57	97.55
Ce	30.69	206.62	57.75	94.73	66.87	101.35	65.74	72.07	123.26	174.64
Pr	4.424	26.151	8.227	12.096	9.285	12.471	8.126	9.452	15.227	18.427
Nd	18.09	102.59	34.02	47.93	39.38	46.57	32.36	38.44	58.43	61.77
Sm	3.57	17.73	7.10	8.87	7.66	7.65	6.09	7.05	10.17	8.31
Eu	1.046	3.571	1.386	1.655	1.598	1.734	1.665	1.763	2.125	1.867
Gd	2.901	12.663	5.563	6.656	6.100	5.629	4.634	4.879	7.334	5.537
Tb	0.457	1.625	0.823	0.904	0.858	0.727	0.591	0.615	0.998	0.749
Dy	2.66	8.20	4.53	4.64	4.59	3.79	3.07	2.92	5.16	3.81
Ho	0.545	1.483	0.881	0.876	0.893	0.715	0.560	0.510	0.959	0.724
Er	1.545	3.711	2.560	2.285	2.355	1.910	1.419	1.270	2.556	1.919
Tm	0.2396	0.5216	0.4082	0.3281	0.3540	0.2799	0.2065	0.1759	0.3699	0.2740
Yb	1.543	3.076	2.685	1.989	2.102	1.802	1.251	1.048	2.293	1.724
Lu	0.252	0.456	0.434	0.309	0.317	0.285	0.194	0.154	0.351	0.279
Ba	640.2	1144.6	344.2	560.2	780.0	627.7	574.4	860.6	1039.4	1525.5
Th	0.73	6.81	8.46	2.95	6.30	9.42	2.17	0.28	8.65	15.96
Nb	5.21	25.19	14.18	14.63	10.84	10.11	8.61	11.37	12.60	10.64
Y	15.57	40.70	26.59	23.86	24.23	20.36	15.17	13.46	26.90	20.53
Hf	1.97	9.39	2.57	4.79	4.75	4.84	3.82	3.80	5.44	6.27
U	0.20	1.37	2.63	1.09	1.98	1.86	0.60	0.29	1.40	1.77
Pb	10.09	14.43	16.58	14.04	12.25	18.62	14.51	12.72	17.69	20.20
Rb	73.3	154.2	65.9	138.0	116.3	244.8	76.8	90.6	108.6	142.4
Cs	0.78	7.73	0.53	1.79	2.77	19.83	0.82	0.75	3.85	1.91
Sr	557.5	630.0	612.9	429.2	474.8	481.2	532.8	552.8	598.6	613.7
Sc	24.35	23.38	24.15	20.57	23.18	14.36	15.83	17.87	17.67	13.58
Zr	76.8	397.7	77.7	184.5	178.2	190.3	135.7	150.8	203.5	258.9
XRF (ppm)										
Rb	73.6	151.2	66.6	145.9	117.1	251.7	79.6	84.9	102.6	137.4
Sr	525	605	592	429	464	489	538	519	551	555
Y	14.5	36.1	24.9	21.8	23.9	19.8	15.4	12.3	24.7	18.8
Zr	79	346	79	147	165	199	143	138	183	226
V	171	175	199	144	166	94	120	106	101	68
Ni	18	5	13	21	30	9	16	9	<2	4
Cr	114	<2	10	99	179	29	39	13	<2	<2
Ga	19	24	21	23	20	21	22	21	20	19
Nb	8.2	25.4	16.8	15.3	12.5	10.4	9.4	13.1	14.6	13.1
Cu	5	26	30	9	19	3	16	9	7	14
Zn	97	117	89	130	79	93	116	90	86	68
Ba	615	1089	330	520	743	616	573	760	993	1491
La	6	107	18	38	28	57	27	30	69	101
Ce	32	208	60	81	72	104	67	73	143	180
U	<0.5	1.5	1.9	<0.5	1.0	1.8	0.9	<0.5	1.1	1.2
Th	<0.5	5.7	7.6	2.0	5.1	9.2	2.5	<0.5	8.0	14.0
Sc	27	24	25	21	25	14	15	18	18	10
Pb	11	12	17	14	11	17	14	12	16	18

2.5 Ga Granitoids

	19BN126B	21BN28A	19BN166A	19BN53A	18BN18B-F	21BN29A	18BN31A	21BN30A	18BN113A	21BN20D
ICP-OES (wt.%)										
SiO ₂	65.56	66.20	66.54	68.66	70.45	70.79	70.84	71.60	71.94	73.62
Al ₂ O ₃	16.62	15.16	16.12	14.85	15.23	14.57	15.10	14.38	14.60	13.44
FeO(t)	4.80	5.05	4.09	3.91	2.76	3.16	1.86	2.91	2.47	2.70
MnO	0.095	0.085	0.068	0.079	0.039	0.079	0.037	0.054	0.038	0.056
MgO	1.558	2.236	1.715	1.655	1.227	0.933	0.995	0.850	1.026	0.850
CaO	4.16	3.97	3.57	3.61	2.49	2.35	2.03	2.24	2.85	1.96
Na ₂ O	3.88	2.81	3.38	2.83	3.07	3.43	2.53	2.87	3.05	3.23
K ₂ O	2.49	3.67	3.73	3.81	4.22	4.21	6.07	4.69	3.50	3.76
TiO ₂	0.610	0.643	0.584	0.453	0.379	0.385	0.343	0.342	0.449	0.324
P ₂ O ₅	0.23	0.17	0.19	0.13	0.13	0.10	0.19	0.08	0.09	0.06
LOI	0.99	1.13	1.19	0.80	1.12	0.81	1.19	1.01	0.94	0.62
Total	100.4	99.64	100.8	98.49	100.0	99.46	99.92	100.1	100.7	99.81
ICP-MS (ppm)										
La	69.05	82.79	53.36	40.91	31.87	47.59	28.09	60.72	19.93	38.82
Ce	132.40	161.29	108.16	85.20	56.95	98.87	49.27	120.44	35.64	88.05
Pr	14.832	19.227	12.622	10.177	6.269	11.553	5.654	13.379	4.047	9.753
Nd	52.02	69.51	46.34	37.76	22.14	41.05	21.60	46.26	14.85	35.21
Sm	7.32	12.13	8.07	7.12	3.25	7.54	3.17	7.50	2.30	6.62
Eu	1.962	1.664	1.503	1.128	1.515	0.971	1.731	0.959	1.320	0.913
Gd	4.713	8.924	5.827	5.284	2.150	5.806	2.008	5.164	1.441	4.970
Tb	0.559	1.262	0.809	0.798	0.233	0.879	0.229	0.711	0.170	0.791
Dy	2.73	6.91	4.22	4.33	1.08	5.01	1.04	3.64	0.75	4.29
Ho	0.499	1.310	0.781	0.841	0.181	1.042	0.190	0.652	0.133	0.854
Er	1.279	3.539	1.979	2.354	0.425	2.914	0.469	1.663	0.333	2.504
Tm	0.1766	0.5306	0.2835	0.3570	0.0616	0.4617	0.0712	0.2311	0.0454	0.4115
Yb	1.126	3.283	1.677	2.289	0.380	2.982	0.505	1.299	0.275	2.786
Lu	0.190	0.491	0.246	0.363	0.057	0.448	0.073	0.174	0.039	0.461
Ba	1632.4	934.6	880.2	821.5	1765.0	621.9	2986.6	672.8	1691.4	458.9
Th	9.19	16.37	5.60	15.55	1.53	34.10	0.21	21.91	0.57	24.17
Nb	12.37	15.79	11.82	14.55	5.47	20.14	3.68	11.66	6.57	15.49
Y	13.33	37.20	21.65	25.33	5.00	30.23	5.38	17.70	3.85	27.06
Hf	5.61	6.12	5.57	4.53	3.98	4.95	13.25	4.30	3.29	4.79
U	0.56	3.73	0.59	3.23	0.34	5.87	0.11	1.30	0.35	3.03
Pb	15.17	21.87	18.52	25.14	16.57	34.05	23.28	25.56	14.13	25.52
Rb	78.0	169.3	149.2	159.1	101.9	215.6	118.8	185.6	93.4	220.3
Cs	1.40	3.02	1.47	3.58	0.57	3.51	0.38	2.41	0.47	4.65
Sr	599.6	426.8	413.0	359.3	473.8	255.6	543.3	238.1	511.5	201.3
Sc	12.10	16.76	10.27	12.77	5.55	8.56	3.28	9.31	3.93	6.24
Zr	230.4	223.7	206.7	154.0	154.2	159.8	563.4	144.9	129.7	148.3
XRF (ppm)										
Rb	76.5	170.3	146.5	154.5	103.3	222.3	119.1	190.6	88.2	226.5
Sr	569	406	390	330	465	260	522	234	458	199
Y	12.9	37.2	21.3	24.4	3.9	29.6	4.6	18.3	3.4	28.4
Zr	213	211	180	130	138	168	475	143	113	147
V	58	76	62	68	47	37	31	37	26	32
Ni	3	10	9	6	7	2	5	2	3	4
Cr	4	51	15	22	16	7	17	<2	8	13
Ga	21	20	20	18	18	19	14	17	16	17
Nb	14.4	16.2	12.3	14.5	7.3	19.1	6.3	11.0	8.4	14.1
Cu	7	15	15	2	6	2	12	2	31	2
Zn	75	78	66	58	48	61	28	49	40	38
Ba	1545	896	857	799	1712	607	2830	653	1609	443
La	68	89	53	43	25	45	24	66	16	40
Ce	154	184	115	99	57	95	60	132	47	97
U	1.2	3.3	0.6	3.0	<0.5	5.0	<0.5	1.1	<0.5	3.0
Th	7.8	15.7	5.2	14.1	0.8	30.0	<0.5	21.7	<0.5	25.4
Sc	10	15	9	11	5	9	4	8	5	6
Pb	14	20	17	23	17	35	22	23	14	26

Appendix D: Supporting information for chapter 4

Table D-1. LA-MC-ICPMS zircon and monazite U-Pb isotope data.

Session	Spot ID	Mineral	Screen	Class	206Pb cps	204 cps	206 204	Ratios					Dates (Ma)				Disc. %		
								207Pb 206Pb	2σ	207Pb 235U	2σ	206Pb 238U	2σ	ρ	207Pb 206Pb	2σ		206Pb 238U	2σ
May 28 2021	18BN37B-66-1	Zrc		ign	316080	14	22772	0.3568	0.0026	37.31	0.68	0.759	0.013	0.917	3736	11	3639	46	3
May 28 2021	18BN37B-30-1	Zrc		ign	420477	50	8334	0.2673	0.0022	23.78	0.49	0.645	0.012	0.916	3291	13	3210	47	2
May 28 2021	18BN37B-24-1	Zrc		ign	557731	21	26683	0.2202	0.0016	17.18	0.33	0.566	0.010	0.926	2982	11	2892	41	3
May 28 2021	18BN37B-49-1	Zrc		ign	173047	40	4304	0.2086	0.0015	15.91	0.37	0.553	0.012	0.950	2895	12	2838	50	2
May 28 2021	18BN37B-57-1	Zrc		ign	197623	57	3453	0.2082	0.0016	15.32	0.25	0.534	0.008	0.891	2892	12	2758	33	5
May 28 2021	18BN37B-3-1	Zrc		ign	1052789	82	12848	0.2053	0.0015	15.83	0.26	0.559	0.008	0.901	2869	12	2864	34	0
May 28 2021	18BN37B-33-1	Zrc		ign	507529	59	8672	0.1989	0.0014	14.71	0.33	0.537	0.011	0.949	2817	11	2769	47	2
May 28 2021	18BN37B-53-1	Zrc		ign	716548	39	18578	0.1981	0.0015	14.75	0.30	0.540	0.010	0.930	2811	12	2784	43	1
May 28 2021	18BN37B-47-1	Zrc		ign	451413	37	12322	0.1882	0.0013	13.51	0.30	0.521	0.011	0.945	2726	12	2704	46	1
May 28 2021	18BN37B-87-1	Zrc		ign	697489	45	15617	0.1871	0.0013	12.97	0.20	0.503	0.007	0.897	2717	11	2627	30	3
May 28 2021	18BN37B-4-1	Zrc		ign	1072298	102	10559	0.1869	0.0013	13.78	0.31	0.535	0.012	0.952	2715	11	2763	49	-2
May 28 2021	18BN37B-72-1	Zrc		ign	447323	100	4734	0.1868	0.0013	13.20	0.20	0.512	0.007	0.881	2715	12	2667	29	2
May 28 2021	18BN37B-29-1	Zrc		ign	1477077	70	21211	0.1866	0.0015	14.10	0.34	0.548	0.012	0.939	2713	13	2818	51	-4
May 28 2021	18BN37B-93-1	Zrc		ign	695839	60	11553	0.1859	0.0013	13.18	0.21	0.515	0.008	0.899	2706	12	2676	32	1
May 28 2021	18BN37B-20-1	Zrc		ign	841737	31	27179	0.1835	0.0013	13.11	0.25	0.519	0.009	0.926	2685	12	2693	38	0
May 28 2021	18BN37B-71-1	Zrc		ign	595020	55	10746	0.1818	0.0013	13.06	0.24	0.521	0.009	0.923	2669	12	2705	38	-1
May 28 2021	18BN37B-48-1	Zrc		ign	256502	38	6755	0.1779	0.0015	11.88	0.28	0.484	0.011	0.937	2633	14	2546	47	3
May 28 2021	18BN37B-18-1	Zrc		ign	416646	54	7655	0.1751	0.0013	11.79	0.24	0.489	0.009	0.933	2607	12	2566	40	2
May 28 2021	18BN37B-17-1	Zrc		ign	829027	87	9505	0.1743	0.0013	11.91	0.23	0.496	0.009	0.929	2600	12	2595	39	0
May 28 2021	18BN37B-40-1	Zrc		ign	562949	54	10372	0.1743	0.0012	11.67	0.20	0.486	0.007	0.907	2600	12	2552	32	2
May 28 2021	18BN37B-62-1	Zrc		ign	336289	38	8867	0.1743	0.0012	11.47	0.23	0.477	0.009	0.935	2600	12	2516	39	3
May 28 2021	18BN37B-74-1	Zrc		ign	834775	39	21428	0.1742	0.0013	11.47	0.23	0.478	0.009	0.931	2599	12	2517	38	3
May 28 2021	18BN37B-7-1	Zrc		ign	698383	70	9973	0.1741	0.0012	12.15	0.26	0.506	0.010	0.945	2597	12	2641	44	-2
May 28 2021	18BN37B-77-1	Zrc		ign	924124	41	22522	0.1740	0.0012	11.53	0.20	0.481	0.008	0.917	2597	12	2531	34	3
May 28 2021	18BN37B-45-1	Zrc		ign	279187	49	5698	0.1737	0.0013	11.49	0.26	0.480	0.010	0.947	2594	12	2527	45	3
May 28 2021	18BN37B-1-1	Zrc		ign	688679	62	11090	0.1736	0.0013	12.00	0.23	0.501	0.009	0.922	2593	12	2620	37	-1
May 28 2021	18BN37B-89-1	Zrc		ign	512494	100	5127	0.1735	0.0013	11.31	0.24	0.473	0.010	0.941	2592	12	2497	42	4
May 28 2021	18BN37B-79-1	Zrc		ign	853986	55	15457	0.1732	0.0012	11.42	0.22	0.478	0.009	0.934	2589	12	2520	38	3
May 28 2021	18BN37B-60-1	Zrc		ign	716051	45	15904	0.1728	0.0012	11.85	0.26	0.498	0.010	0.947	2585	12	2603	44	-1
May 28 2021	18BN37B-8-1	Zrc		ign	674719	62	10908	0.1724	0.0013	11.74	0.26	0.494	0.011	0.947	2581	12	2589	45	0
May 28 2021	18BN37B-63-1	Zrc		ign	792502	42	18829	0.1713	0.0012	11.76	0.25	0.498	0.010	0.944	2570	12	2606	44	-1
May 28 2021	18BN37B-69-1	Zrc		ign	260981	64	4081	0.1711	0.0013	11.88	0.38	0.504	0.016	0.973	2569	12	2629	66	-2
May 28 2021	18BN37B-28-1	Zrc		ign	802764	120	6705	0.1691	0.0012	11.13	0.21	0.477	0.008	0.927	2549	12	2516	37	1
May 28 2021	18BN37B-11-1	Zrc		ign	1293492	75	17224	0.1690	0.0012	11.69	0.25	0.502	0.010	0.943	2548	12	2622	43	-3
May 28 2021	18BN37B-56-1	Zrc		ign	1020846	80	12810	0.1688	0.0012	11.05	0.20	0.475	0.008	0.923	2546	12	2505	35	2
May 28 2021	18BN37B-64-1	Zrc		ign	459599	34	13681	0.1680	0.0012	10.86	0.22	0.469	0.009	0.940	2538	12	2479	40	2
May 28 2021	18BN37B-85-1	Zrc		ign	936749	42	22384	0.1674	0.0012	10.92	0.28	0.473	0.012	0.961	2532	12	2498	51	1
May 28 2021	18BN37B-95-1	Zrc		ign	1232275	60	20631	0.1671	0.0012	10.84	0.17	0.471	0.007	0.897	2529	12	2486	29	2
May 28 2021	18BN37B-12-1	Zrc		ign	661064	68	9697	0.1665	0.0012	10.70	0.21	0.466	0.008	0.928	2523	12	2467	37	2
May 28 2021	18BN37B-59-1	Zrc		ign	555077	58	9558	0.1663	0.0012	10.69	0.19	0.466	0.007	0.911	2521	12	2468	32	2

Spots labelled as "Sample ID-grain#-spot#".

Mineral: Indicates if zircon (Zrc) or monazite (Mnz) was analyzed.

Class: Analysis classified as igneous (ign) or metamorphic (met).

Screen: Analysis screened for high common-Pb content (cPb), mixed isotope ratio signals (mix) or discordance (disc).

Disc.: Percent discordance calculated as [(207Pb/206Pb date/ 206Pb/238U date)-1]*100

Session	Spot ID	Mineral	Screen	Class	206Pb cps	204 cps	206 204	Ratios						Dates (Ma)				Disc. %	
								207Pb		207Pb		206Pb		207Pb		206Pb			
								206Pb	2σ	235U	2σ	238U	2σ	ρ	206Pb	2σ	238U		2σ
May 28 2021	18BN37B-70-1	Zrc		ign	1149555	78	14676	0.1662	0.0012	11.04	0.25	0.482	0.010	0.948	2519	12	2537	45	-1
May 28 2021	18BN37B-32-1	Zrc		ign	396086	35	11356	0.1661	0.0012	10.52	0.20	0.459	0.008	0.924	2519	12	2437	35	3
May 28 2021	18BN37B-41-1	Zrc		ign	914630	51	17970	0.1659	0.0012	11.01	0.15	0.481	0.005	0.849	2517	12	2534	24	-1
May 28 2021	18BN37B-82-1	Zrc		ign	1594616	23	69858	0.1657	0.0012	10.70	0.18	0.468	0.007	0.906	2515	12	2476	31	2
May 28 2021	18BN37B-58-1	Zrc		ign	1241537	36	34893	0.1649	0.0012	10.92	0.26	0.481	0.011	0.953	2506	12	2530	48	-1
May 28 2021	18BN37B-36-1	Zrc		ign?	1452455	70	20829	0.1601	0.0011	10.16	0.14	0.460	0.005	0.850	2457	12	2441	23	1
May 28 2021	18BN37B-80-2	Zrc		ign?	1579786	93	17046	0.1599	0.0012	9.91	0.14	0.450	0.005	0.858	2455	12	2394	24	3
May 28 2021	18BN37B-20-2	Zrc		ign?	1377232	39	34983	0.1594	0.0012	10.58	0.23	0.482	0.010	0.942	2450	12	2534	42	-3
May 28 2021	18BN37B-23-1	Zrc		ign?	1249628	132	9491	0.1580	0.0011	9.67	0.24	0.444	0.010	0.959	2435	12	2369	47	3
May 28 2021	18BN37B-86-1	Zrc		met	819637	50	16396	0.1541	0.0011	9.27	0.17	0.436	0.007	0.925	2392	12	2335	33	2
May 28 2021	18BN37B-84-1	Zrc		met	783991	32	24826	0.1538	0.0011	9.29	0.18	0.438	0.008	0.930	2388	12	2344	35	2
May 28 2021	18BN37B-42-1	Zrc		ign?	1134964	183	6211	0.1536	0.0011	9.60	0.26	0.453	0.012	0.966	2386	12	2410	53	-1
May 28 2021	18BN37B-51-1	Zrc		met	920559	42	22129	0.1535	0.0011	9.63	0.19	0.455	0.008	0.934	2386	12	2418	37	-1
May 28 2021	18BN37B-34-1	Zrc		met	645588	45	14210	0.1535	0.0011	9.47	0.19	0.448	0.008	0.932	2385	12	2386	37	0
May 28 2021	18BN37B-51-2	Zrc		met	922144	55	16814	0.1534	0.0011	9.58	0.19	0.453	0.008	0.933	2384	12	2409	37	-1
May 28 2021	18BN37B-35-1	Zrc		met	946961	63	14928	0.1534	0.0011	9.57	0.17	0.453	0.007	0.915	2384	12	2408	32	-1
May 28 2021	18BN37B-43-1	Zrc		met	858944	53	16083	0.1533	0.0011	9.77	0.20	0.462	0.009	0.937	2383	12	2450	39	-3
May 28 2021	18BN37B-15-1	Zrc		met	830329	68	12298	0.1532	0.0011	9.66	0.18	0.458	0.008	0.923	2382	12	2429	34	-2
May 28 2021	18BN37B-6-1	Zrc		met	712510	67	10684	0.1531	0.0011	9.57	0.19	0.453	0.008	0.931	2381	12	2411	36	-1
May 28 2021	18BN37B-2-2	Zrc		met	970278	89	10895	0.1530	0.0011	9.69	0.18	0.459	0.008	0.928	2379	12	2437	36	-2
May 28 2021	18BN37B-29-2	Zrc		met	891363	37	23825	0.1526	0.0011	9.49	0.18	0.451	0.008	0.925	2376	12	2401	34	-1
May 28 2021	18BN37B-55-1	Zrc	disc	ign	200735	64	3130	0.2129	0.0017	15.82	0.20	0.539	0.005	0.782	2928	13	2779	22	5
May 28 2021	18BN37B-27-1	Zrc	disc	ign	153002	24	6487	0.1877	0.0015	12.65	0.22	0.489	0.007	0.875	2722	14	2566	32	6
May 28 2021	18BN37B-94-1	Zrc	disc	ign	321887	68	4749	0.1861	0.0014	12.55	0.25	0.489	0.009	0.930	2708	12	2568	39	5
May 28 2021	18BN37B-50-1	Zrc	disc	ign	137939	39	3579	0.1861	0.0014	12.51	0.22	0.488	0.008	0.908	2708	12	2562	34	6
May 28 2021	18BN37B-90-1	Zrc	disc	ign	212673	57	3719	0.1849	0.0015	12.48	0.30	0.490	0.011	0.942	2698	13	2569	47	5
May 28 2021	18BN37B-9-1	Zrc	disc	ign	517896	72	7156	0.1793	0.0014	11.56	0.20	0.468	0.007	0.896	2646	13	2475	31	7
May 28 2021	18BN37B-81-1	Zrc	disc	ign	359428	59	6060	0.1729	0.0013	10.95	0.23	0.460	0.009	0.936	2586	13	2438	41	6
May 28 2021	18BN37B-2-1	Zrc	disc	ign	538406	133	4035	0.1727	0.0015	9.74	0.15	0.409	0.005	0.824	2584	15	2212	24	17
May 28 2021	18BN37B-76-1	Zrc	disc	ign	346478	90	3841	0.1716	0.0012	10.94	0.23	0.463	0.009	0.940	2574	12	2451	40	5
May 28 2021	18BN37B-75-1	Zrc	disc	ign	984406	50	19554	0.1710	0.0014	10.86	0.31	0.461	0.013	0.959	2568	14	2442	56	5
May 28 2021	18BN37B-39-1	Zrc	disc	ign	147657	95	1562	0.1691	0.0014	10.48	0.31	0.450	0.013	0.961	2549	14	2394	57	6
May 28 2021	18BN37B-25-1	Zrc	disc	ign	152612	21	7157	0.1677	0.0012	10.46	0.17	0.453	0.006	0.892	2535	12	2407	29	5
May 28 2021	18BN37B-80-1	Zrc	disc	ign	570636	53	10837	0.1675	0.0012	10.42	0.23	0.451	0.010	0.947	2533	12	2401	42	5
May 28 2021	18BN37B-68-1	Zrc	disc	ign	771165	78	9913	0.1604	0.0013	9.49	0.11	0.429	0.004	0.721	2460	13	2303	16	7
May 28 2021	18BN37B-27-2	Zrc	disc	ign	1232331	57	21692	0.1586	0.0012	9.43	0.12	0.431	0.004	0.792	2441	13	2312	19	6
May 28 2021	18BN37B-19-1	Zrc	cPb	ign	718446	884	813	0.2006	0.0016	14.78	0.27	0.535	0.009	0.896	2831	13	2761	37	3
May 28 2021	18BN37B-44-1	Zrc	cPb	ign	453727	159	2851	0.1895	0.0014	13.50	0.32	0.517	0.012	0.947	2738	12	2685	49	2
May 28 2021	18BN37B-14-1	Zrc	cPb	ign	803238	248	3244	0.1737	0.0013	11.37	0.28	0.475	0.011	0.950	2594	13	2505	48	4
May 28 2021	18BN37B-73-1	Zrc	cPb	ign	1246955	392	3181	0.1721	0.0012	11.20	0.25	0.472	0.010	0.949	2578	12	2494	44	3
May 28 2021	18BN37B-16-1	Zrc	disc,cPb	ign	545765	15996	34	0.8586	0.0447	8.86	8.62	0.075	0.073	0.999	5022	72	466	422	979
May 28 2021	18BN37B-31-1	Zrc	disc,cPb	ign	2079539	32398	64	0.3636	0.0337	34.62	3.89	0.691	0.044	0.564	3765	134	3386	165	11
May 28 2021	18BN37B-91-1	Zrc	disc,cPb	ign	125633	300	419	0.2354	0.0018	16.97	0.25	0.523	0.007	0.854	3089	12	2713	28	14
May 28 2021	18BN37B-54-1	Zrc	disc,cPb	ign	419187	201	2090	0.1713	0.0013	9.82	0.10	0.416	0.003	0.682	2571	12	2242	13	15
May 28 2021	18BN37B-26-1	Zrc	disc,cPb	met	573227	146	3930	0.1567	0.0013	8.15	0.14	0.377	0.006	0.889	2421	13	2063	27	17
May 28 2021	18BN37B-21-1	Zrc	mix	ign	1532278	100	15331	0.1539	0.0018	9.03	0.13	0.426	0.004	0.566	2390	20	2285	16	5
May 28 2021	18BN37B-78-1	Zrc	mix,cPb	ign	580685	242	2397	0.1765	0.0017	11.61	0.23	0.477	0.008	0.876	2620	16	2515	37	4
May 28 2021	18BN37B-88-1	Zrc	mix,disc	ign	329130	42	7757	0.2171	0.0022	15.08	0.25	0.504	0.007	0.798	2959	16	2631	29	12
May 28 2021	18BN37B-5-1	Zrc	mix,disc	ign	308115	515	598	0.2039	0.0028	14.47	0.39	0.515	0.012	0.863	2857	22	2678	51	7
May 28 2021	18BN37B-92-1	Zrc	mix,disc	ign	54452	53	1034	0.1998	0.0018	13.49	0.30	0.490	0.010	0.912	2825	15	2570	43	10

Session	Spot ID	Mineral	Screen	Class	206Pb cps	204 cps	206 204	Ratios						Dates (Ma)				Disc. %	
								207Pb		207Pb		206Pb		207Pb		206Pb			
								206Pb	2σ	235U	2σ	238U	2σ	ρ	206Pb	2σ	238U		2σ
May 28 2021	18BN37B-13-1	Zrc	mix,disc	ign	775911	1529	507	0.1869	0.0086	12.29	0.75	0.477	0.019	0.653	2715	74	2515	82	8
May 28 2021	18BN37B-37-1	Zrc	mix,disc	ign	942155	2327	405	0.1867	0.0093	11.95	0.86	0.465	0.024	0.721	2713	80	2460	105	10
May 28 2021	18BN37B-10-1	Zrc	mix,disc	ign	986072	601	1640	0.1865	0.0019	12.12	0.21	0.471	0.007	0.818	2712	16	2490	29	9
May 28 2021	18BN37B-22-1	Zrc	mix,disc	ign	1019902	1224	833	0.1841	0.0026	11.79	0.46	0.465	0.017	0.935	2690	23	2461	75	9
May 28 2021	18BN37B-61-1	Zrc	mix,disc	ign	572454	515	1111	0.1825	0.0028	12.16	0.30	0.484	0.009	0.789	2676	25	2543	41	5
May 28 2021	18BN37B-46-1	Zrc	mix,disc	ign	971822	176	5536	0.1822	0.0031	11.52	0.22	0.459	0.004	0.415	2673	28	2435	16	10
May 28 2021	18BN37B-67-1	Zrc	mix,disc	ign	308970	300	1029	0.1802	0.0021	11.74	0.21	0.473	0.006	0.737	2655	20	2496	27	6
May 28 2021	18BN37B-65-1	Zrc	mix,disc	ign	253603	48	5312	0.1761	0.0019	11.32	0.24	0.466	0.008	0.857	2617	18	2468	37	6
May 28 2021	18BN37B-83-1	Zrc	mix,disc	ign	1219215	57	21495	0.1574	0.0027	8.84	0.19	0.408	0.005	0.605	2428	28	2204	24	10
May 28 2021	18BN37B-38-1	Zrc	mix,disc	ign	1275649	588	2171	0.1539	0.0053	7.24	0.26	0.341	0.004	0.303	2389	57	1893	18	26
May 28 2021	18BN37B-52-1	Zrc	mix,disc	ign	1870796	97	19330	0.1474	0.0016	7.54	0.09	0.371	0.002	0.519	2316	18	2035	11	14
Nov 17 2021	18BN81A-9-1	Zrc		ign	1071775	41	26149	0.2568	0.0019	23.53	0.82	0.665	0.023	0.976	3227	12	3285	87	-2
Nov 17 2021	18BN81A-42-1	Zrc		ign	1234708	68	18228	0.2544	0.0019	22.44	0.71	0.640	0.020	0.971	3212	12	3189	77	1
Nov 17 2021	18BN81A-93-1	Zrc		ign	512178	54	9563	0.2035	0.0016	15.73	0.54	0.561	0.019	0.975	2854	12	2871	77	-1
Nov 17 2021	18BN81A-37-1	Zrc		ign	105682	45	2364	0.1979	0.0018	14.41	0.47	0.528	0.016	0.961	2809	15	2734	69	3
Nov 17 2021	18BN81A-45-1	Zrc		ign	224085	23	9608	0.1974	0.0019	14.50	0.53	0.533	0.019	0.966	2805	15	2753	78	2
Nov 17 2021	18BN81A-68-1	Zrc		ign	116839	61	1920	0.1966	0.0018	14.18	0.50	0.523	0.018	0.966	2798	15	2713	74	3
Nov 17 2021	18BN81A-47-1	Zrc		ign	247859	17	14180	0.1898	0.0014	13.64	0.48	0.522	0.018	0.977	2741	12	2706	75	1
Nov 17 2021	18BN81A-94-1	Zrc		ign	268851	35	7676	0.1894	0.0015	13.29	0.43	0.509	0.016	0.971	2737	13	2653	68	3
Nov 17 2021	18BN81A-24-1	Zrc		ign	234295	39	5979	0.1849	0.0015	12.80	0.43	0.502	0.016	0.970	2698	13	2623	69	3
Nov 17 2021	18BN81A-27-1	Zrc		ign	201106	20	9911	0.1841	0.0016	12.63	0.43	0.498	0.017	0.967	2690	14	2604	71	3
Nov 17 2021	18BN81A-67-1	Zrc		ign	525637	22	24202	0.1828	0.0013	12.93	0.42	0.513	0.016	0.974	2678	12	2670	68	0
Nov 17 2021	18BN81A-50-1	Zrc		ign	443200	12	37397	0.1791	0.0014	12.11	0.40	0.490	0.016	0.972	2644	13	2573	67	3
Nov 17 2021	18BN81A-20-1	Zrc		ign	769466	36	21216	0.1777	0.0015	12.27	0.38	0.501	0.015	0.963	2632	14	2619	65	0
Nov 17 2021	18BN81A-75-1	Zrc		ign	510867	100	5126	0.1759	0.0015	12.02	0.42	0.496	0.017	0.970	2615	14	2595	72	1
Nov 17 2021	18BN81A-36-1	Zrc		ign	243622	60	4084	0.1756	0.0014	11.65	0.38	0.481	0.015	0.969	2612	13	2532	66	3
Nov 17 2021	18BN81A-91-1	Zrc		ign	551523	48	11441	0.1732	0.0013	11.55	0.37	0.481	0.015	0.970	2589	13	2534	65	2
Nov 17 2021	18BN81A-6-1	Zrc		ign	632099	62	10241	0.1732	0.0013	11.75	0.42	0.492	0.017	0.977	2589	13	2581	74	0
Nov 17 2021	18BN81A-25-1	Zrc		ign	1978921	49	40467	0.1722	0.0014	11.80	0.41	0.497	0.017	0.973	2580	13	2602	71	-1
Nov 17 2021	18BN81A-22-1	Zrc		ign	506700	29	17398	0.1709	0.0012	11.71	0.40	0.497	0.017	0.977	2567	12	2601	71	-1
Nov 17 2021	18BN81A-32-1	Zrc		ign	712789	39	18421	0.1709	0.0012	11.59	0.39	0.492	0.016	0.977	2566	12	2581	70	-1
Nov 17 2021	18BN81A-88-1	Zrc		ign	771904	47	16526	0.1702	0.0012	11.44	0.39	0.488	0.016	0.977	2559	12	2561	70	0
Nov 17 2021	18BN81A-84-1	Zrc		ign	290323	40	7266	0.1701	0.0013	11.23	0.39	0.479	0.016	0.976	2559	13	2522	70	1
Nov 17 2021	18BN81A-35-1	Zrc		ign	1330648	49	27173	0.1700	0.0012	11.67	0.38	0.498	0.016	0.975	2558	12	2605	68	-2
Nov 17 2021	18BN81A-19-1	Zrc		ign	840674	46	18411	0.1695	0.0012	11.21	0.36	0.480	0.015	0.975	2553	12	2527	66	1
Nov 17 2021	18BN81A-52-1	Zrc		ign	190781	14	13218	0.1694	0.0013	10.90	0.37	0.467	0.015	0.974	2552	13	2469	67	3
Nov 17 2021	18BN81A-96-1	Zrc		ign	575511	91	6338	0.1691	0.0012	11.05	0.38	0.474	0.016	0.977	2548	12	2503	69	2
Nov 17 2021	18BN81A-99-1	Zrc		ign	639829	63	10226	0.1686	0.0012	11.37	0.39	0.489	0.017	0.977	2544	12	2567	71	-1
Nov 17 2021	18BN81A-46-1	Zrc		ign	853310	41	20578	0.1686	0.0012	11.43	0.38	0.492	0.016	0.976	2544	12	2580	68	-1
Nov 17 2021	18BN81A-87-1	Zrc		ign	277409	40	6963	0.1682	0.0013	10.79	0.35	0.465	0.015	0.973	2540	13	2462	65	3
Nov 17 2021	18BN81A-57-1	Zrc		ign	745996	27	27421	0.1682	0.0012	11.13	0.36	0.480	0.015	0.974	2540	12	2528	65	0
Nov 17 2021	18BN81A-48-1	Zrc		ign	473700	37	12739	0.1679	0.0013	11.23	0.39	0.485	0.016	0.975	2537	13	2550	71	0
Nov 17 2021	18BN81A-66-1	Zrc		ign	865901	11	78874	0.1678	0.0013	11.24	0.36	0.486	0.015	0.969	2536	13	2553	65	-1
Nov 17 2021	18BN81A-60-1	Zrc		ign	790386	43	18356	0.1669	0.0012	10.96	0.35	0.476	0.015	0.974	2527	12	2512	65	1
Nov 17 2021	18BN81A-39-1	Zrc		ign	1335763	95	14011	0.1669	0.0012	11.01	0.39	0.479	0.017	0.978	2527	12	2521	72	0
Nov 17 2021	18BN81A-34-1	Zrc		ign	472792	37	12810	0.1669	0.0012	11.03	0.38	0.480	0.016	0.977	2526	12	2526	70	0
Nov 17 2021	18BN81A-59-1	Zrc		ign	705299	48	14839	0.1668	0.0013	10.70	0.34	0.466	0.014	0.970	2526	13	2464	63	3
Nov 17 2021	18BN81A-71-1	Zrc		ign	280814	69	4055	0.1668	0.0013	10.90	0.37	0.474	0.016	0.973	2525	13	2503	68	1
Nov 17 2021	18BN81A-1-1	Zrc		ign	705360	32	22094	0.1667	0.0012	10.71	0.36	0.466	0.016	0.976	2525	12	2467	68	2
Nov 17 2021	18BN81A-23-1	Zrc		ign	262100	37	7125	0.1665	0.0012	10.74	0.37	0.468	0.016	0.976	2522	13	2475	69	2

Session	Spot ID	Mineral	Screen	Class	206Pb cps	204 cps	206 204	Ratios						Dates (Ma)				Disc. %	
								207Pb		207Pb		206Pb		207Pb		206Pb			
								206Pb	2σ	235U	2σ	238U	2σ	ρ	206Pb	2σ	238U		2σ
Nov 17 2021	18BN81A-76-1	Zrc		ign	919353	89	10337	0.1663	0.0012	11.01	0.37	0.480	0.016	0.976	2520	12	2529	68	0
Nov 17 2021	18BN81A-56-1	Zrc		ign	460812	28	16452	0.1663	0.0012	10.98	0.36	0.479	0.016	0.975	2520	12	2524	67	0
Nov 17 2021	18BN81A-21-1	Zrc		ign	1094155	46	23825	0.1661	0.0012	11.17	0.38	0.488	0.016	0.976	2518	12	2563	69	-2
Nov 17 2021	18BN81A-80-1	Zrc		ign	839857	89	9419	0.1659	0.0013	11.07	0.37	0.484	0.016	0.974	2516	13	2545	68	-1
Nov 17 2021	18BN81A-69-1	Zrc		ign	406052	76	5327	0.1658	0.0012	10.77	0.36	0.471	0.015	0.976	2515	12	2490	67	1
Nov 17 2021	18BN81A-15-1	Zrc		ign	535890	44	12194	0.1657	0.0013	11.17	0.39	0.489	0.017	0.975	2514	13	2567	72	-2
Nov 17 2021	18BN81A-82-1	Zrc		ign	515489	98	5258	0.1656	0.0012	10.89	0.37	0.477	0.016	0.976	2514	13	2515	69	0
Nov 17 2021	18BN81A-90-1	Zrc		ign	397404	21	18653	0.1656	0.0012	10.52	0.35	0.461	0.015	0.974	2513	12	2445	65	3
Nov 17 2021	18BN81A-64-1	Zrc		ign	486424	37	12979	0.1656	0.0013	10.46	0.34	0.458	0.014	0.971	2513	13	2432	63	3
Nov 17 2021	18BN81A-72-1	Zrc		ign	773153	80	9628	0.1655	0.0013	10.95	0.37	0.480	0.016	0.973	2512	13	2528	68	-1
Nov 17 2021	18BN81A-11-1	Zrc		ign	525282	42	12589	0.1651	0.0013	10.37	0.33	0.456	0.014	0.970	2509	13	2420	62	4
Nov 17 2021	18BN81A-3-1	Zrc		ign	1095217	46	23651	0.1647	0.0013	10.83	0.35	0.477	0.015	0.971	2504	13	2514	64	0
Nov 17 2021	18BN81A-92-1	Zrc		ign	760335	62	12298	0.1645	0.0012	10.63	0.35	0.469	0.015	0.975	2502	12	2479	65	1
Nov 17 2021	18BN81A-98-1	Zrc		ign	1549641	25	61285	0.1640	0.0013	10.70	0.37	0.474	0.016	0.973	2497	13	2500	69	0
Nov 17 2021	18BN81A-44-1	Zrc		ign	721701	46	15574	0.1640	0.0012	10.78	0.38	0.477	0.017	0.977	2497	13	2515	72	-1
Nov 17 2021	18BN81A-31-1	Zrc		ign	266157	12	22533	0.1638	0.0012	10.31	0.35	0.457	0.015	0.975	2496	13	2424	66	3
Nov 17 2021	18BN81A-18-1	Zrc		ign	607776	31	19539	0.1637	0.0012	10.40	0.35	0.461	0.015	0.976	2494	12	2444	66	2
Nov 17 2021	18BN81A-26-1	Zrc		ign	683007	40	16982	0.1627	0.0014	10.50	0.38	0.468	0.017	0.970	2483	15	2476	72	0
Nov 17 2021	18BN81A-79-1	Zrc		ign	735693	85	8608	0.1610	0.0012	10.50	0.35	0.473	0.015	0.976	2466	12	2497	67	-1
Nov 17 2021	18BN81A-74-1	Zrc		ign	1560484	227	6886	0.1599	0.0013	10.27	0.34	0.466	0.015	0.970	2454	14	2467	66	-1
Nov 17 2021	18BN81A-4-1	Zrc		ign	813697	65	12559	0.1591	0.0012	10.22	0.36	0.466	0.016	0.979	2446	12	2467	70	-1
Nov 17 2021	18BN81A-8-1	Zrc		ign	460772	27	16823	0.1586	0.0012	10.13	0.33	0.463	0.014	0.974	2441	12	2454	63	-1
Nov 17 2021	18BN81A-83-1	Zrc		ign	1030543	45	23050	0.1585	0.0012	10.12	0.34	0.463	0.015	0.976	2440	12	2453	66	-1
Nov 17 2021	18BN81A-2-1	Zrc		ign	1225355	76	16055	0.1575	0.0013	10.07	0.34	0.464	0.015	0.971	2429	13	2456	66	-1
Nov 17 2021	18BN81A-40-1	Zrc		ign	505554	73	6958	0.1566	0.0011	9.70	0.34	0.452	0.016	0.978	2408	12	2406	69	0
Nov 17 2021	18BN81A-73-1	Zrc		met	211164	80	2628	0.1549	0.0011	9.33	0.32	0.437	0.015	0.977	2400	12	2337	65	3
Nov 17 2021	18BN81A-49-1	Zrc		met	287608	29	10014	0.1547	0.0012	9.28	0.31	0.435	0.014	0.975	2398	13	2329	64	3
Nov 17 2021	18BN81A-78-1	Zrc		met	780789	110	7088	0.1546	0.0011	9.57	0.31	0.449	0.014	0.974	2397	12	2393	63	0
Nov 17 2021	18BN81A-38-1	Zrc		met	561888	72	7757	0.1542	0.0012	9.43	0.33	0.444	0.015	0.976	2393	13	2367	66	1
Nov 17 2021	18BN81A-86-1	Zrc		met	515065	38	13724	0.1541	0.0011	9.66	0.34	0.455	0.016	0.978	2392	12	2417	69	-1
Nov 17 2021	18BN81A-61-1	Zrc		met	481530	37	12952	0.1540	0.0012	9.56	0.32	0.450	0.015	0.975	2391	13	2397	65	0
Nov 17 2021	18BN81A-63-1	Zrc		met	483511	37	13065	0.1536	0.0011	9.52	0.34	0.450	0.015	0.978	2386	13	2394	69	0
Nov 17 2021	18BN81A-85-1	Zrc		met	482355	47	10168	0.1535	0.0011	9.46	0.34	0.447	0.016	0.979	2385	12	2382	69	0
Nov 17 2021	18BN81A-28-1	Zrc		met	988411	33	30358	0.1535	0.0011	9.65	0.32	0.456	0.015	0.976	2385	12	2423	65	-2
Nov 17 2021	18BN81A-62-1	Zrc		met	406809	36	11224	0.1535	0.0011	9.65	0.33	0.456	0.015	0.975	2385	13	2423	66	-2
Nov 17 2021	18BN81A-43-1	Zrc		met	599349	82	7282	0.1534	0.0011	9.47	0.33	0.448	0.015	0.978	2384	12	2386	67	0
Nov 17 2021	18BN81A-89-1	Zrc		met	387842	23	16800	0.1533	0.0011	9.38	0.32	0.444	0.015	0.977	2383	12	2368	66	1
Nov 17 2021	18BN81A-29-1	Zrc		met	394997	12	33632	0.1533	0.0011	9.24	0.31	0.437	0.015	0.976	2383	13	2338	65	2
Nov 17 2021	18BN81A-70-1	Zrc		met	783014	66	11920	0.1533	0.0011	9.59	0.31	0.454	0.014	0.974	2383	12	2414	63	-1
Nov 17 2021	18BN81A-95-1	Zrc		met	606998	50	12180	0.1532	0.0011	9.51	0.32	0.450	0.015	0.977	2382	12	2397	66	-1
Nov 17 2021	18BN81A-13-1	Zrc		met	441176	24	18667	0.1530	0.0011	9.28	0.31	0.440	0.014	0.975	2380	13	2352	64	1
Nov 17 2021	18BN81A-65-1	Zrc		met	868204	27	32395	0.1529	0.0012	9.56	0.34	0.454	0.016	0.975	2379	13	2411	70	-1
Nov 17 2021	18BN81A-81-1	Zrc		met	1087856	40	27502	0.1527	0.0011	9.42	0.33	0.448	0.015	0.978	2377	12	2385	67	0
Nov 17 2021	18BN81A-17-1	Zrc		met	431194	41	10528	0.1527	0.0011	9.15	0.30	0.435	0.014	0.974	2377	13	2327	62	2
Nov 17 2021	18BN81A-30-1	Zrc		met	462779	25	18619	0.1527	0.0011	9.31	0.31	0.442	0.014	0.975	2376	13	2361	64	1
Nov 17 2021	18BN81A-41-1	Zrc		met	803723	56	14339	0.1522	0.0011	9.28	0.30	0.443	0.014	0.974	2370	12	2362	62	0
Nov 17 2021	18BN81A-33-1	Zrc		met	919142	36	25555	0.1522	0.0011	9.39	0.32	0.448	0.015	0.975	2370	13	2385	65	-1
Nov 17 2021	18BN81A-5-1	Zrc		met	927307	46	20326	0.1521	0.0012	9.34	0.33	0.445	0.015	0.976	2370	13	2375	67	0
Nov 17 2021	18BN81A-7-1	Zrc		met	650424	63	10390	0.1521	0.0011	9.28	0.32	0.443	0.015	0.976	2369	13	2364	65	0
Nov 17 2021	18BN81A-14-1	Zrc	disc	met	701598	150	4681	0.1545	0.0011	8.88	0.28	0.417	0.013	0.972	2396	13	2248	58	7
Nov 17 2021	18BN81A-51-1	Zrc	disc	ign	421781	80	5301	0.1588	0.0012	9.44	0.32	0.431	0.014	0.976	2443	12	2312	63	6

Session	Spot ID	Mineral	Screen	Class	206Pb cps	204 cps	206 204	Ratios						Dates (Ma)				Disc. %	
								207Pb		207Pb		206Pb		207Pb		206Pb			
								206Pb	2σ	235U	2σ	238U	2σ	206Pb	2σ	238U	2σ		
Nov 17 2021	18BN81A-54-1	Zrc	disc	ign	754006	155	4858	0.1661	0.0013	9.14	0.39	0.399	0.017	0.984	2518	13	2166	76	16
Nov 17 2021	18BN81A-97-1	Zrc	disc	ign	399931	79	5063	0.1710	0.0013	10.84	0.34	0.460	0.014	0.972	2567	12	2440	62	5
Nov 17 2021	18BN81A-16-1	Zrc	cPb	met	361282	141	2564	0.1577	0.0012	9.73	0.34	0.448	0.015	0.978	2431	13	2386	68	2
Nov 17 2021	18BN81A-53-1	Zrc	cPb, disc	ign	1146397	318	3608	0.1584	0.0013	9.24	0.29	0.423	0.013	0.964	2439	14	2276	57	7
Nov 17 2021	18BN81A-55-1	Zrc	cPb, disc	ign	710630	1454	489	0.2003	0.0031	13.86	0.53	0.502	0.017	0.912	2828	25	2623	74	8
Nov 17 2021	18BN81A-77-1	Zrc	cPb, disc	ign	431649	776	556	0.1875	0.0070	11.87	0.58	0.459	0.014	0.638	2720	61	2436	63	12
Nov 17 2021	18BN81A-10-1	Zrc	mix	ign	209315	20	10681	0.1701	0.0018	11.35	0.42	0.484	0.017	0.957	2558	18	2545	74	1
Nov 17 2021	18BN81A-12-1	Zrc	mix, disc	ign	132605	48	2746	0.1872	0.0023	10.99	0.42	0.426	0.015	0.946	2718	20	2287	69	19
Nov 17 2021	18BN81A-58-1	Zrc	mix, disc	ign	283569	36	7905	0.2041	0.0025	14.68	0.49	0.522	0.016	0.930	2859	20	2707	68	6
Nov 19 2021	18BN81A-1.1	Mnz		met	406521	18	22002	0.1185	0.0012	5.29	0.17	0.324	0.010	0.947	1934	18	1809	47	7
Nov 19 2021	18BN81A-1.2	Mnz		met	372633	26	14560	0.1190	0.0012	5.32	0.17	0.325	0.010	0.946	1942	18	1812	46	7
Nov 19 2021	18BN81A-1.3	Mnz		met	346446	22	15440	0.1193	0.0012	5.31	0.17	0.323	0.010	0.945	1945	18	1806	46	8
Nov 19 2021	18BN81A-1.4	Mnz		met	407631	20	20054	0.1184	0.0012	5.28	0.17	0.323	0.010	0.944	1932	18	1806	46	7
Nov 19 2021	18BN81A-1.5	Mnz		met	425766	22	19145	0.1188	0.0012	5.33	0.17	0.326	0.010	0.947	1939	18	1817	47	7
Nov 19 2021	18BN81A-2.1	Mnz		met	537519	16	33170	0.1189	0.0012	5.38	0.17	0.329	0.010	0.948	1939	18	1832	47	6
Nov 19 2021	18BN81A-2.2	Mnz		met	266227	31	8659	0.1188	0.0012	5.46	0.17	0.333	0.010	0.947	1939	18	1854	48	5
Nov 19 2021	18BN81A-3.1	Mnz		met	269049	10	27827	0.1203	0.0012	5.34	0.17	0.322	0.010	0.946	1961	18	1799	46	9
Nov 19 2021	18BN81A-3.2	Mnz		met	327598	25	13355	0.1200	0.0012	5.37	0.17	0.325	0.010	0.951	1956	18	1813	49	8
Nov 19 2021	18BN81A-3.3	Mnz		met	321550	29	11123	0.1197	0.0012	5.31	0.17	0.322	0.010	0.946	1951	18	1798	46	9
Nov 19 2021	18BN81A-3.4	Mnz		met	374716	29	12953	0.1195	0.0012	5.36	0.17	0.325	0.010	0.946	1948	18	1816	47	7
Nov 19 2021	18BN81A-1.6	Mnz		met	473015	40	11772	0.1199	0.0012	5.33	0.17	0.323	0.010	0.946	1954	18	1804	46	8
June 20 2019	18BN81B-1.1	Mnz		ign	1273012	70	18232	0.1192	0.0012	5.81	0.14	0.353	0.008	0.904	1944	19	1951	37	0
June 20 2019	18BN81B-2.1	Mnz		ign	705323	63	11116	0.1192	0.0012	5.94	0.15	0.361	0.008	0.905	1945	19	1988	38	-2
June 20 2019	18BN81B-2.2	Mnz		ign	480700	22	21530	0.1196	0.0013	5.56	0.14	0.338	0.008	0.912	1950	19	1875	38	4
June 20 2019	18BN81B-3.2	Mnz		ign	1152335	30	37958	0.1185	0.0013	5.96	0.15	0.365	0.008	0.893	1933	20	2004	38	-4
June 20 2019	18BN81B-4.2	Mnz		ign	1115754	27	41874	0.1184	0.0012	5.67	0.14	0.347	0.008	0.905	1933	18	1921	37	1
June 20 2019	18BN81B-5.1	Mnz		ign	595830	49	12226	0.1193	0.0013	5.66	0.14	0.344	0.008	0.907	1946	19	1907	37	2
June 20 2019	18BN81B-6.1	Mnz		ign	1002537	79	12616	0.1187	0.0012	5.69	0.15	0.348	0.008	0.916	1936	19	1924	40	1
June 20 2019	18BN81B-7.1	Mnz		ign	1426226	27	52251	0.1176	0.0012	5.69	0.14	0.351	0.008	0.905	1921	19	1938	37	-1
June 20 2019	18BN81B-8.1	Mnz		ign	594980	55	10841	0.1192	0.0014	5.77	0.15	0.351	0.008	0.895	1945	20	1939	38	0
June 20 2019	18BN81B-9.1	Mnz		ign	1696318	64	26589	0.1179	0.0013	5.54	0.16	0.341	0.009	0.927	1925	19	1891	43	2
June 20 2019	18BN81B-10.1	Mnz		ign	758437	28	26768	0.1187	0.0013	5.52	0.14	0.337	0.008	0.910	1936	19	1874	38	3
June 20 2019	18BN81B-10.2	Mnz		ign	724638	17	43743	0.1177	0.0012	5.69	0.15	0.351	0.008	0.917	1922	18	1939	40	-1
June 20 2019	18BN81B-11.1	Mnz		ign	520768	20	26181	0.1190	0.0012	5.63	0.14	0.343	0.008	0.914	1941	19	1903	39	2
June 20 2019	18BN81B-3.1	Mnz	cPb	ign	1223112	393	3112	0.1218	0.0013	6.24	0.15	0.372	0.008	0.904	1983	19	2037	39	-3
June 20 2019	18BN81B-4.1	Mnz	cPb	ign	792040	156	5072	0.1202	0.0013	5.81	0.15	0.351	0.008	0.908	1959	19	1937	39	1

Table D-2. LA-ICPMS zircon U-Pb isotope data. Acquired in the same ablation as the trace-element data in Table D-3.

Session	Spot ID	Screen	Class	206Pb cps	204 cps	206 204	Ratios					Dates (Ma)				Disc. %		
							207Pb 206Pb	2σ	207Pb 235U	2σ	206Pb 238U	2σ	ρ	207Pb 206Pb	2σ		206Pb 238U	2σ
April 11 2022	18BN37B-27-1		ign	9.07E+04	0.00E+00		0.2170	0.0042	17.00	0.71	0.566	0.021	0.885	2959	31	2891	85	2
April 11 2022	18BN37B-53-1		ign	1.08E+05	6.40E+01	1.69E+03	0.2137	0.0034	16.50	0.68	0.558	0.021	0.924	2934	25	2858	87	3
April 11 2022	18BN37B-5-1		ign	6.99E+04	0.00E+00		0.2075	0.0036	15.72	0.63	0.550	0.020	0.903	2886	28	2825	82	2
April 11 2022	18BN37B-70-1		ign	1.65E+04	0.00E+00		0.2020	0.0057	15.64	0.82	0.559	0.025	0.843	2842	46	2862	101	-1
April 11 2022	18BN37B-29-1		ign	1.69E+05	0.00E+00		0.1975	0.0038	14.86	0.69	0.544	0.023	0.911	2806	31	2800	95	0
April 11 2022	18BN37B-14-1		ign	1.73E+05	1.60E+01	1.08E+04	0.1962	0.0030	14.51	0.59	0.536	0.020	0.925	2795	25	2767	84	1
April 11 2022	18BN37B-54-1		ign	2.07E+05	3.10E+01	6.68E+03	0.1889	0.0033	14.17	0.60	0.542	0.021	0.910	2733	29	2792	86	-2
April 11 2022	18BN37B-65-1		ign	1.08E+05	8.30E+01	1.31E+03	0.1859	0.0035	12.72	0.58	0.493	0.020	0.909	2706	31	2584	87	5
April 11 2022	18BN37B-6-1		ign	2.56E+05	0.00E+00		0.1852	0.0026	13.70	0.53	0.534	0.019	0.934	2700	23	2758	81	-2
April 11 2022	18BN37B-31-1		ign	2.57E+05	3.60E+01	7.14E+03	0.1846	0.0029	13.72	0.60	0.536	0.022	0.932	2695	26	2767	92	-3
April 11 2022	18BN37B-39-1		ign	1.11E+05	0.00E+00		0.1832	0.0030	13.22	0.55	0.519	0.020	0.917	2682	27	2695	83	0
April 11 2022	18BN37B-64-1		ign	1.09E+05	0.00E+00		0.1795	0.0028	12.99	0.52	0.521	0.019	0.918	2648	26	2703	81	-2
April 11 2022	18BN37B-37-1		ign	1.66E+05	2.70E+01	6.13E+03	0.1792	0.0026	13.10	0.49	0.526	0.018	0.920	2645	24	2725	75	-3
April 11 2022	18BN37B-19-1		ign	1.56E+05	4.70E+01	3.32E+03	0.1788	0.0029	12.48	0.53	0.507	0.020	0.924	2642	27	2644	85	0
April 11 2022	18BN37B-35-1		ign	2.35E+05	0.00E+00		0.1777	0.0031	13.17	0.59	0.534	0.022	0.922	2632	29	2758	92	-5
April 11 2022	18BN37B-67-1		ign	2.00E+05	1.60E+01	1.25E+04	0.1777	0.0028	11.90	0.49	0.483	0.018	0.921	2632	26	2540	79	4
April 11 2022	18BN37B-10-1		ign	5.58E+05	3.70E+01	1.51E+04	0.1766	0.0037	12.66	0.60	0.520	0.022	0.901	2621	34	2699	94	-3
April 11 2022	18BN37B-25-1		ign	3.61E+05	0.00E+00		0.1760	0.0034	12.14	0.60	0.498	0.023	0.921	2616	32	2605	97	0
April 12 2022	18BN37B-36-1		ign	2.74E+05	0.00E+00		0.1752	0.0040	12.41	0.71	0.512	0.027	0.917	2608	38	2665	113	-2
April 11 2022	18BN37B-41-1		ign	3.94E+05	3.30E+01	1.19E+04	0.1719	0.0023	11.64	0.48	0.489	0.019	0.946	2576	22	2566	82	0
April 11 2022	18BN37B-60-1		ign	3.23E+05	7.90E+01	4.09E+03	0.1719	0.0026	12.18	0.58	0.508	0.023	0.946	2576	26	2648	97	-3
April 11 2022	18BN37B-52-1		ign	1.37E+05	0.00E+00		0.1705	0.0031	11.38	0.50	0.483	0.019	0.911	2563	31	2540	84	1
April 11 2022	18BN37B-97-1		ign	3.34E+05	1.40E+01	2.39E+04	0.1705	0.0028	11.21	0.50	0.479	0.020	0.932	2563	27	2523	87	2
April 11 2022	18BN37B-17-1		ign	3.16E+05	4.40E+01	7.18E+03	0.1696	0.0023	11.92	0.47	0.510	0.019	0.937	2554	23	2657	80	-4
April 11 2022	18BN37B-22-1		ign	2.21E+05	3.20E+01	6.91E+03	0.1695	0.0031	11.54	0.57	0.493	0.023	0.928	2553	31	2584	97	-1
April 11 2022	18BN37B-13-1		ign	2.31E+05	4.90E+01	4.71E+03	0.1689	0.0029	11.17	0.49	0.480	0.019	0.919	2547	29	2527	84	1
April 11 2022	18BN37B-74-1		ign	2.45E+05	2.50E+01	9.80E+03	0.1681	0.0026	11.82	0.53	0.508	0.021	0.938	2539	26	2648	91	-4
April 12 2022	18BN37B-86-1		ign?	2.13E+05	3.50E+01	6.09E+03	0.1681	0.0032	11.14	0.51	0.477	0.020	0.912	2539	32	2514	87	1
April 11 2022	18BN37B-72-1		ign	2.34E+05	5.50E+01	4.25E+03	0.1676	0.0025	11.56	0.48	0.497	0.019	0.931	2534	25	2601	82	-3
April 11 2022	18BN37B-16-1		ign	3.06E+05	7.70E+01	3.97E+03	0.1674	0.0035	11.18	0.54	0.481	0.021	0.899	2532	35	2532	90	0
April 11 2022	18BN37B-48-1		ign	4.35E+05	4.50E+01	9.67E+03	0.1674	0.0026	11.34	0.48	0.485	0.019	0.928	2532	26	2549	81	-1
April 11 2022	18BN37B-57-1		ign	5.11E+04	0.00E+00		0.1673	0.0028	11.29	0.45	0.488	0.018	0.910	2531	28	2562	76	-1
April 11 2022	18BN37B-96-1		ign	2.23E+05	3.50E+01	6.37E+03	0.1670	0.0029	11.18	0.52	0.489	0.021	0.926	2528	29	2566	90	-2
April 11 2022	18BN37B-40-1		ign	5.77E+05	1.20E+01	4.81E+04	0.1668	0.0026	11.16	0.43	0.478	0.017	0.915	2526	26	2518	73	0
April 12 2022	18BN37B-109-1		ign	1.61E+05	0.00E+00		0.1667	0.0031	11.46	0.55	0.496	0.022	0.922	2525	31	2597	93	-3
April 11 2022	18BN37B-15-1		ign	2.95E+05	0.00E+00		0.1664	0.0033	10.71	0.63	0.467	0.026	0.944	2522	33	2470	114	2
April 12 2022	18BN37B-75-1		ign	9.30E+04	2.20E+01	4.23E+03	0.1662	0.0033	11.19	0.58	0.488	0.023	0.921	2520	34	2562	100	-2
April 11 2022	18BN37B-8-1		ign	3.17E+05	1.10E+01	2.88E+04	0.1645	0.0028	10.93	0.52	0.481	0.022	0.934	2502	29	2532	93	-1
April 11 2022	18BN37B-87-1		ign	4.74E+05	1.70E+01	2.79E+04	0.1645	0.0027	11.32	0.52	0.499	0.021	0.931	2502	28	2609	90	-4
April 11 2022	18BN37B-55-1		ign	2.61E+05	1.00E+00	2.61E+05	0.1636	0.0026	11.25	0.47	0.494	0.019	0.926	2493	27	2588	82	-4
April 11 2022	18BN37B-82-1		ign	3.11E+05	4.60E+01	6.76E+03	0.1627	0.0027	10.46	0.49	0.466	0.021	0.934	2484	28	2466	90	1
April 11 2022	18BN37B-69-1		ign	3.87E+05	2.50E+01	1.55E+04	0.1608	0.0029	10.21	0.54	0.457	0.023	0.940	2464	30	2426	99	2
April 11 2022	18BN37B-82-1		met?	4.03E+05	1.10E+01	3.66E+04	0.1567	0.0022	10.16	0.48	0.467	0.021	0.954	2420	24	2470	93	-2
April 11 2022	18BN37B-18-1		ign	4.28E+05	7.50E+01	5.71E+03	0.1537	0.0028	9.32	0.39	0.439	0.017	0.902	2388	31	2346	74	2
April 12 2022	18BN37B-93-1		met	2.57E+05	1.80E+01	1.43E+04	0.1557	0.0034	9.89	0.55	0.459	0.023	0.920	2409	37	2435	103	-1
April 11 2022	18BN37B-103-1		met	2.77E+05	3.70E+01	7.49E+03	0.1552	0.0025	9.45	0.39	0.442	0.017	0.917	2404	28	2360	74	2
April 12 2022	18BN37B-89.2-1		met	1.90E+05	1.00E+00	1.90E+05	0.1543	0.0024	9.49	0.42	0.445	0.019	0.935	2394	27	2373	83	1
April 12 2022	18BN37B-101-2		met	2.29E+05	0.00E+00		0.1543	0.0026	10.00	0.43	0.468	0.018	0.919	2394	29	2475	81	-3

Spots labelled as "Sample ID-grain#-spot#.

Class: Analysis classified as igneous (ign) or metamorphic (met).

Screen: Analysis screened for high common-Pb content (cPb), intersection of an inclusion (incl), mixed isotope ratio signals (mix) or discordance (disc).

Disc.: Percent discordance calculated as [(207Pb/206Pb date/ 206Pb/238U date)-1]*100.

Session	Spot ID	Screen	Class	Ratios										Dates (Ma)				Disc.
				206Pb	204	206	207Pb	207Pb	206Pb	207Pb	206Pb	207Pb	206Pb	207Pb	206Pb	207Pb	206Pb	
				cps	cps	204	206Pb	2σ	235U	2σ	238U	2σ	ρ	206Pb	2σ	238U	2σ	
April 12 2022	18BN37B-98-1		met	3.28E+05	4.20E+01	7.81E+03	0.1541	0.0029	9.94	0.52	0.464	0.023	0.936	2392	31	2457	99	-3
April 12 2022	18BN37B-100-1		met	3.19E+05	1.10E+01	2.90E+04	0.1537	0.0026	9.47	0.41	0.445	0.018	0.922	2388	29	2373	80	1
April 11 2022	18BN37B-102-1		met	6.05E+05	0.00E+00		0.1536	0.0024	9.33	0.40	0.443	0.018	0.934	2386	26	2364	80	1
April 12 2022	18BN37B-88-1		met	1.82E+05	4.00E+00	4.55E+04	0.1533	0.0024	9.58	0.41	0.449	0.018	0.930	2383	27	2391	80	0
April 12 2022	18BN37B-89-1		met	2.09E+05	0.00E+00		0.1533	0.0031	9.81	0.52	0.464	0.023	0.924	2383	34	2457	99	-3
April 11 2022	18BN37B-102-2		met	3.18E+05	1.70E+01	1.87E+04	0.1530	0.0025	9.49	0.40	0.455	0.018	0.920	2380	28	2417	77	-2
April 12 2022	18BN37B-95-1		met	2.95E+05	4.00E+00	7.38E+04	0.1528	0.0023	9.74	0.43	0.460	0.019	0.940	2377	25	2440	83	-3
April 12 2022	18BN37B-99-1		met	2.01E+05	0.00E+00		0.1527	0.0024	9.79	0.44	0.463	0.020	0.940	2376	26	2453	86	-3
April 12 2022	18BN37B-81-2		met	2.82E+05	1.80E+01	1.57E+04	0.1525	0.0031	9.78	0.46	0.459	0.020	0.903	2374	35	2435	86	-3
April 12 2022	18BN37B-94-1		met	3.36E+05	0.00E+00		0.1525	0.0028	9.94	0.50	0.468	0.022	0.930	2374	32	2475	96	-4
April 12 2022	18BN37B-92-1		met	2.25E+05	4.40E+01	5.11E+03	0.1523	0.0027	9.97	0.44	0.473	0.019	0.918	2372	30	2497	84	-5
April 11 2022	18BN37B-91-1		met?	4.66E+05	0.00E+00		0.1518	0.0021	9.50	0.43	0.455	0.020	0.950	2366	24	2417	86	-2
April 11 2022	18BN37B-81-1		met	2.89E+05	1.40E+01	2.06E+04	0.1517	0.0024	9.39	0.40	0.450	0.018	0.933	2365	26	2395	80	-1
April 11 2022	18BN37B-80-1		met?	3.46E+05	5.70E+01	6.07E+03	0.1503	0.0025	9.57	0.45	0.461	0.020	0.936	2349	28	2444	89	-4
April 11 2022	18BN37B-3-1	disc	ign	3.13E+05	2.70E+01	1.16E+04	0.1803	0.0028	14.26	0.61	0.574	0.023	0.933	2656	25	2924	93	-9
April 11 2022	18BN37B-9-1	disc	ign	8.70E+05	5.90E+01	1.47E+04	0.1619	0.0031	12.41	0.60	0.554	0.024	0.915	2476	33	2842	101	-13
April 11 2022	18BN37B-26-1	disc	ign	2.20E+05	0.00E+00		0.1647	0.0040	10.07	0.60	0.444	0.024	0.914	2504	40	2369	106	6
April 11 2022	18BN37B-32-2	disc	ign	4.80E+05	6.90E+01	6.96E+03	0.1534	0.0026	8.87	0.44	0.417	0.020	0.940	2384	29	2247	88	6
April 11 2022	18BN37B-49-1	disc	ign	1.90E+05	4.00E+00	4.75E+04	0.1654	0.0024	11.75	0.45	0.513	0.018	0.924	2512	25	2669	78	-6
April 11 2022	18BN37B-51-1	disc	ign	1.97E+05	0.00E+00		0.1830	0.0035	12.29	0.63	0.484	0.023	0.928	2680	32	2545	100	5
April 11 2022	18BN37B-56-1	disc	ign	4.89E+05	5.90E+01	8.29E+03	0.1792	0.0027	14.15	0.69	0.568	0.026	0.951	2645	25	2900	107	-9
April 11 2022	18BN37B-59-1	disc	ign	2.97E+05	4.10E+01	7.24E+03	0.1668	0.0029	11.85	0.54	0.514	0.022	0.922	2526	29	2674	91	-6
April 11 2022	18BN37B-76-1	disc	ign	2.88E+05	5.30E+01	5.43E+03	0.1520	0.0030	11.23	0.55	0.532	0.024	0.916	2369	34	2750	100	-14
April 11 2022	18BN37B-77-1	disc	ign	1.23E+05	7.70E+01	1.59E+03	0.1658	0.0030	10.24	0.45	0.446	0.018	0.912	2516	30	2377	80	6
April 11 2022	18BN37B-79-1	disc	ign	3.56E+05	1.60E+01	2.23E+04	0.1696	0.0030	9.48	0.47	0.404	0.019	0.932	2554	30	2187	84	17
April 12 2022	18BN37B-110-1	disc	ign	2.29E+05	2.70E+01	8.48E+03	0.1636	0.0029	11.60	0.50	0.508	0.020	0.912	2493	30	2648	85	-6
April 12 2022	18BN37B-108-1	disc	ign?	4.90E+05	6.00E+00	8.17E+04	0.1608	0.0032	11.08	0.60	0.499	0.025	0.928	2464	34	2609	107	-6
April 12 2022	18BN37B-108-2	disc	ign?	3.04E+05	1.10E+01	2.76E+04	0.1604	0.0031	9.18	0.50	0.412	0.021	0.937	2460	32	2224	95	11
April 12 2022	18BN37B-84-1	disc	met	1.98E+05	9.00E+00	2.20E+04	0.1536	0.0029	10.14	0.53	0.478	0.023	0.930	2386	33	2519	100	-5
April 12 2022	18BN37B-101-1	disc	met	1.86E+05	0.00E+00		0.1522	0.0024	10.47	0.44	0.493	0.019	0.924	2371	27	2584	82	-8
April 11 2022	18BN37B-4-1	cPb	ign	2.75E+05	2.85E+02	9.66E+02	0.1875	0.0043	14.09	0.71	0.545	0.024	0.888	2720	38	2804	101	-3
April 11 2022	18BN37B-7-1	cPb	ign	3.09E+05	1.25E+02	2.47E+03	0.1590	0.0033	10.04	0.51	0.460	0.021	0.911	2445	35	2440	93	0
April 11 2022	18BN37B-11-1	cPb	ign	1.78E+05	1.77E+02	1.01E+03	0.1770	0.0039	11.71	0.54	0.481	0.019	0.877	2625	37	2532	84	4
April 11 2022	18BN37B-20-1	cPb	ign	2.87E+05	2.46E+02	1.17E+03	0.1768	0.0041	11.54	0.54	0.474	0.019	0.869	2623	39	2501	84	5
April 11 2022	18BN37B-24-1	cPb	ign	3.08E+05	1.16E+02	2.66E+03	0.1621	0.0027	10.27	0.55	0.458	0.023	0.953	2478	28	2431	103	2
April 11 2022	18BN37B-32-1	cPb	ign	4.19E+05	1.32E+02	3.17E+03	0.1600	0.0032	10.32	0.47	0.466	0.019	0.897	2456	34	2466	83	0
April 11 2022	18BN37B-34-1	cPb	ign	2.48E+05	1.14E+02	2.18E+03	0.1821	0.0034	13.13	0.72	0.520	0.027	0.940	2672	31	2699	113	-1
April 11 2022	18BN37B-38-1	cPb	ign	2.51E+05	2.31E+02	1.09E+03	0.1687	0.0036	10.74	0.50	0.459	0.019	0.887	2545	36	2435	83	5
April 11 2022	18BN37B-42-1	cPb	ign	4.04E+05	1.43E+02	2.83E+03	0.1721	0.0035	12.40	0.67	0.519	0.026	0.926	2578	34	2695	110	-4
April 11 2022	18BN37B-50-1	cPb	ign	2.32E+05	2.70E+02	8.59E+02	0.1802	0.0027	12.10	0.50	0.485	0.019	0.933	2655	25	2549	81	4
April 11 2022	18BN37B-58-1	cPb	ign	2.68E+05	1.34E+02	2.00E+03	0.1783	0.0043	12.40	0.67	0.503	0.024	0.895	2637	40	2627	103	0
April 11 2022	18BN37B-63-1	cPb	ign	1.87E+05	2.09E+02	8.95E+02	0.1804	0.0033	12.19	0.56	0.485	0.020	0.914	2657	31	2549	87	4
April 11 2022	18BN37B-78-1	cPb	ign	3.13E+05	5.30E+02	5.91E+02	0.1856	0.0045	12.78	0.57	0.497	0.019	0.838	2704	40	2601	79	4
April 11 2022	18BN37B-85-1	cPb	ign	3.19E+05	1.00E+02	3.19E+03	0.1705	0.0033	11.51	0.62	0.489	0.025	0.935	2563	32	2566	106	0
April 11 2022	18BN37B-2-1	cPb,incl	ign	1.51E+07	6.10E+05	2.48E+01	0.2620	0.0800	65.00	36.03	18.200	8.418	0.834	3259	481	19049	2344	-83
April 11 2022	18BN37B-12-1	cPb	ign	3.94E+05	5.20E+02	7.58E+02	0.1930	0.0231	16.10	2.65	0.551	0.062	0.687	2768	196	2829	254	-2
April 11 2022	18BN37B-21-1	cPb	ign	5.40E+05	1.32E+04	4.09E+01	0.3580	0.0501	71.00	24.96	1.090	0.352	0.917	3741	213	4752	1002	-21
April 11 2022	18BN37B-23-1	cPb	ign	1.38E+05	1.37E+03	1.01E+02	0.2900	0.0232	24.10	2.26	0.591	0.029	0.524	3418	124	2993	117	14
April 11 2022	18BN37B-28-1	cPb	ign	2.38E+05	1.14E+03	2.09E+02	0.2260	0.0142	17.70	1.37	0.564	0.025	0.584	3024	101	2883	104	5
April 11 2022	18BN37B-43-1	cPb	ign	8.53E+04	6.80E+02	1.25E+02	0.2670	0.0133	22.10	1.47	0.592	0.026	0.662	3288	78	2998	104	10
April 11 2022	18BN37B-45-1	cPb	ign	2.37E+05	1.89E+03	1.25E+02	0.2530	0.0123	17.10	1.11	0.486	0.021	0.664	3204	77	2553	90	25
April 11 2022	18BN37B-46-1	cPb	ign	3.58E+05	1.01E+03	3.54E+02	0.2040	0.0122	14.60	1.39	0.500	0.037	0.780	2858	97	2614	158	9
April 11 2022	18BN37B-47-1	cPb	ign	2.46E+05	1.47E+03	1.67E+02	0.2309	0.0070	15.98	0.75	0.499	0.018	0.766	3058	48	2609	77	17
April 11 2022	18BN37B-66-1	cPb,incl	ign	3.70E+05	3.86E+02	9.59E+02	0.1735	0.0067	11.20	0.80	0.460	0.028	0.841	2592	65	2440	121	6
April 11 2022	18BN37B-73-1	cPb	ign	7.72E+04	9.50E+02	8.13E+01	0.3100	0.0193	24.80	2.08	0.565	0.032	0.672	3521	96	2887	130	22

Session	Spot ID	Screen	Class	Ratios										Dates (Ma)				Disc. %
				206Pb	204	206	207Pb		207Pb		206Pb		207Pb		206Pb			
				cps	cps	204	206Pb	2σ	235U	2σ	238U	2σ	ρ	206Pb	2σ	238U	2σ	
April 11 2022	18BN37B-33-1	disc,cPb	ign	3.80E+05	2.63E+02	1.44E+03	0.1731	0.0024	10.87	0.42	0.454	0.016	0.932	2588	23	2413	72	7
April 11 2022	18BN37B-44-1	cPb,incl	ign	2.93E+05	1.48E+02	1.98E+03	0.1797	0.0028	13.63	0.58	0.547	0.022	0.928	2650	26	2813	89	-6
April 11 2022	18BN37B-71-1	disc,cPb	ign	1.09E+05	3.70E+02	2.93E+02	0.2303	0.0095	17.20	1.23	0.539	0.031	0.817	3054	66	2779	130	10
April 11 2022	18BN37B-90-1	disc,cPb	ign	4.01E+05	2.05E+02	1.96E+03	0.1755	0.0032	11.08	0.53	0.459	0.020	0.924	2611	31	2435	89	7
April 11 2022	18BN37B-1-1	incl	ign	8.95E+05	4.90E+01	1.83E+04	0.1576	0.0025	9.67	0.41	0.445	0.017	0.928	2430	27	2373	77	2
April 11 2022	18BN37B-30-1	incl	ign	5.12E+05	9.30E+01	5.51E+03	0.1671	0.0045	10.89	0.66	0.471	0.025	0.893	2529	45	2488	110	2
April 11 2022	18BN37B-68-1	incl	ign	1.72E+05	3.50E+01	4.91E+03	0.2068	0.0032	16.55	0.63	0.576	0.020	0.911	2881	25	2932	81	-2
April 12 2022	18BN37B-83-2	cPb	met	2.09E+05	2.08E+02	1.00E+03	0.1654	0.0045	11.31	0.65	0.494	0.025	0.879	2512	46	2588	107	-3
April 12 2022	18BN37B-61-1	disc,cPb	ign	2.60E+05	4.56E+02	5.70E+02	0.1771	0.0050	11.13	0.57	0.454	0.020	0.835	2626	47	2413	86	9
April 12 2022	18BN37B-83-1	disc,cPb	met	2.28E+05	1.28E+03	1.78E+02	0.2320	0.0251	17.60	2.30	0.520	0.038	0.563	3066	173	2699	160	14
April 07 2022	18BN81A-36-1		ign	1.50E+05	1.90E+01	7.89E+03	0.2237	0.0031	18.63	0.68	0.595	0.020	0.923	3008	23	3011	81	0
April 08 2022	18BN81A-126-1		ign	1.14E+05	0.00E+00		0.1985	0.0039	14.56	0.68	0.528	0.023	0.907	2814	32	2733	94	3
April 07 2022	18BN81A-12-1		ign	7.55E+04	0.00E+00		0.1970	0.0032	14.58	0.59	0.548	0.020	0.917	2802	26	2817	84	-1
April 07 2022	18BN81A-14-1		ign	2.15E+05	6.10E+01	3.52E+03	0.1967	0.0031	14.12	0.56	0.524	0.019	0.918	2799	26	2716	81	3
April 07 2022	18BN81A-62-1		ign	5.42E+04	1.70E+01	3.19E+03	0.1944	0.0041	14.00	0.62	0.525	0.020	0.880	2780	34	2720	86	2
April 07 2022	18BN81A-49-1		ign	1.16E+05	1.70E+01	6.80E+03	0.1881	0.0032	12.80	0.60	0.512	0.022	0.930	2726	28	2665	94	2
April 08 2022	18BN81A-106-1		ign	2.28E+05	0.00E+00		0.1861	0.0033	13.03	0.53	0.507	0.019	0.903	2708	29	2644	80	2
April 07 2022	18BN81A-27-1		ign	1.04E+05	1.10E+01	9.45E+03	0.1843	0.0034	13.51	0.86	0.525	0.032	0.957	2692	31	2720	134	-1
April 07 2022	18BN81A-15-1		ign	1.69E+05	3.00E+00	5.63E+04	0.1827	0.0035	12.26	0.60	0.500	0.023	0.921	2678	32	2614	97	2
April 08 2022	18BN81A-89-1		ign	4.63E+05	0.00E+00		0.1821	0.0031	12.85	0.57	0.510	0.021	0.923	2672	28	2657	88	1
April 08 2022	18BN81A-124-1		ign	1.62E+05	5.00E+01	3.24E+03	0.1804	0.0035	12.97	0.63	0.519	0.023	0.916	2657	32	2695	97	-1
April 07 2022	18BN81A-11-1		ign	2.85E+05	9.90E+01	2.88E+03	0.1801	0.0029	11.74	0.48	0.489	0.018	0.918	2654	27	2566	79	3
April 08 2022	18BN81A-108-1		ign	5.47E+04	0.00E+00		0.1799	0.0042	12.56	0.61	0.504	0.021	0.875	2652	39	2631	91	1
April 07 2022	18BN81A-17-1		ign	1.77E+05	5.50E+01	3.22E+03	0.1785	0.0027	12.06	0.48	0.482	0.018	0.925	2639	25	2536	76	4
April 08 2022	18BN81A-128-1		ign	1.17E+05	1.00E+00	1.17E+05	0.1781	0.0033	12.08	0.58	0.491	0.022	0.922	2635	31	2575	93	2
April 08 2022	18BN81A-110-1		ign	1.45E+05	9.00E+00	1.61E+04	0.1749	0.0030	11.62	0.51	0.478	0.019	0.922	2605	28	2519	84	3
April 08 2022	18BN81A-113-1		ign	1.41E+05	1.20E+01	1.18E+04	0.1745	0.0030	12.08	0.55	0.506	0.021	0.924	2601	29	2640	91	-1
April 07 2022	18BN81A-78-1		ign	8.66E+04	8.00E+00	1.08E+04	0.1743	0.0030	11.82	0.53	0.494	0.020	0.924	2599	28	2588	87	0
April 07 2022	18BN81A-46-1		ign	1.89E+05	1.10E+01	1.72E+04	0.1740	0.0026	11.75	0.46	0.491	0.018	0.926	2596	25	2575	77	1
April 07 2022	18BN81A-43-1		ign	5.58E+04	0.00E+00		0.1739	0.0036	11.83	0.52	0.499	0.019	0.883	2596	34	2609	82	-1
April 08 2022	18BN81A-129-1		ign	2.17E+05	0.00E+00		0.1735	0.0038	11.66	0.56	0.489	0.021	0.890	2592	37	2566	90	1
April 08 2022	18BN81A-133-1		ign	7.10E+04	1.90E+01	3.74E+03	0.1732	0.0027	11.79	0.49	0.490	0.019	0.927	2589	26	2571	82	1
April 07 2022	18BN81A-42-1		ign	2.26E+05	2.30E+01	9.84E+03	0.1729	0.0024	11.91	0.50	0.498	0.020	0.943	2586	23	2605	85	-1
April 07 2022	18BN81A-39-1		ign	2.81E+05	0.00E+00		0.1726	0.0026	12.04	0.54	0.505	0.021	0.943	2583	25	2635	91	-2
April 07 2022	18BN81A-48-1		ign	2.08E+05	0.00E+00		0.1726	0.0027	11.59	0.47	0.492	0.018	0.922	2583	26	2579	79	0
April 07 2022	18BN81A-47-1		ign	1.28E+05	8.00E+00	1.60E+04	0.1724	0.0028	11.33	0.44	0.478	0.017	0.909	2581	27	2518	73	3
April 07 2022	18BN81A-24-1		ign	1.58E+05	3.00E+00	5.27E+04	0.1723	0.0026	11.10	0.43	0.465	0.016	0.922	2580	25	2462	72	5
April 08 2022	18BN81A-105-1		ign	1.25E+05	0.00E+00		0.1715	0.0029	11.23	0.45	0.472	0.017	0.910	2572	28	2492	75	3
April 07 2022	18BN81A-19-1		ign	2.05E+05	6.40E+01	3.20E+03	0.1712	0.0028	11.18	0.51	0.468	0.020	0.933	2569	27	2475	86	4
April 07 2022	18BN81A-68-1		ign	1.39E+05	2.00E+01	6.95E+03	0.1712	0.0024	11.73	0.48	0.497	0.019	0.939	2569	24	2601	82	-1
April 07 2022	18BN81A-57-1		ign	2.10E+05	2.60E+01	8.08E+03	0.1711	0.0027	11.63	0.50	0.496	0.020	0.929	2568	26	2597	85	-1
April 08 2022	18BN81A-96-1		ign	1.20E+05	1.40E+01	8.59E+03	0.1711	0.0029	11.29	0.47	0.482	0.018	0.910	2568	29	2536	79	1
April 07 2022	18BN81A-80-1		ign	2.98E+05	1.60E+01	1.86E+04	0.1709	0.0023	11.60	0.46	0.498	0.019	0.939	2566	23	2605	79	-1
April 07 2022	18BN81A-8-1		ign	2.83E+05	5.00E+00	5.66E+04	0.1708	0.0035	11.45	0.55	0.503	0.022	0.908	2565	34	2627	94	-2
April 07 2022	18BN81A-22-1		ign	3.36E+05	5.80E+01	5.79E+03	0.1703	0.0029	10.92	0.46	0.467	0.018	0.911	2561	29	2470	78	4
April 07 2022	18BN81A-31-1		ign	2.23E+05	0.00E+00		0.1702	0.0026	12.15	0.52	0.516	0.021	0.938	2560	25	2682	88	-5
April 07 2022	18BN81A-72-1		ign	1.60E+05	2.90E+01	5.50E+03	0.1701	0.0035	11.39	0.53	0.487	0.020	0.894	2559	35	2558	87	0
April 07 2022	18BN81A-20-1		ign	1.12E+05	0.00E+00		0.1700	0.0032	11.34	0.44	0.483	0.017	0.878	2558	31	2538	72	1
April 07 2022	18BN81A-69-1		ign	2.20E+05	0.00E+00		0.1698	0.0025	11.60	0.52	0.497	0.021	0.946	2556	24	2601	90	-2
April 08 2022	18BN81A-109-1		ign	1.72E+05	0.00E+00		0.1697	0.0031	11.24	0.51	0.479	0.020	0.916	2555	31	2523	87	1
April 08 2022	18BN81A-134-1		ign	1.22E+05	1.40E+01	8.71E+03	0.1695	0.0030	11.29	0.46	0.482	0.018	0.899	2553	30	2536	76	1
April 07 2022	18BN81A-21-1		ign	1.97E+05	1.90E+01	1.04E+04	0.1692	0.0027	11.02	0.45	0.472	0.018	0.922	2550	27	2492	78	2
April 07 2022	18BN81A-37-1		ign	5.41E+05	1.34E+02	4.04E+03	0.1692	0.0024	11.69	0.44	0.511	0.018	0.928	2550	24	2661	76	-4
April 07 2022	18BN81A-38-1		ign	2.35E+05	0.00E+00		0.1692	0.0025	11.45	0.44	0.490	0.017	0.921	2550	25	2570	75	-1

Session	Spot ID	Screen	Class	Ratios										Dates (Ma)				Disc. %
				206Pb	204	206	207Pb		207Pb		206Pb		207Pb		206Pb			
				cps	cps	204	206Pb	2σ	235U	2σ	238U	2σ	p	206Pb	2σ	238U	2σ	
April 07 2022	18BN81A-65-1		ign	1.54E+05	3.00E+00	5.12E+04	0.1688	0.0023	11.31	0.45	0.493	0.018	0.938	2546	23	2584	79	-1
April 08 2022	18BN81A-84-1		ign	8.60E+04	0.00E+00		0.1687	0.0034	11.15	0.56	0.478	0.022	0.920	2545	33	2519	96	1
April 07 2022	18BN81A-30-1		ign	2.58E+05	4.00E+01	6.45E+03	0.1677	0.0031	10.72	0.52	0.473	0.021	0.926	2535	31	2497	93	2
April 07 2022	18BN81A-53-1		ign	1.87E+05	2.10E+01	8.90E+03	0.1675	0.0027	11.09	0.61	0.486	0.026	0.957	2533	27	2553	110	-1
April 07 2022	18BN81A-66-1		ign	1.51E+05	0.00E+00		0.1673	0.0025	11.23	0.43	0.491	0.017	0.919	2531	25	2576	74	-2
April 07 2022	18BN81A-29-1		ign	1.87E+05	0.00E+00		0.1671	0.0025	11.01	0.42	0.468	0.017	0.924	2529	25	2477	72	2
April 07 2022	18BN81A-50-1		ign	2.50E+05	2.10E+01	1.19E+04	0.1670	0.0025	10.72	0.44	0.463	0.018	0.930	2528	25	2453	78	3
April 07 2022	18BN81A-71-1		ign	3.38E+05	3.30E+01	1.02E+04	0.1670	0.0028	11.24	0.55	0.490	0.022	0.941	2528	28	2571	97	-2
April 08 2022	18BN81A-81-1		ign	1.13E+05	2.60E+01	4.33E+03	0.1669	0.0033	11.43	0.56	0.500	0.023	0.918	2527	33	2614	97	-3
April 08 2022	18BN81A-100-1		ign	2.69E+05	0.00E+00		0.1669	0.0028	11.06	0.50	0.482	0.020	0.930	2527	28	2536	87	0
April 08 2022	18BN81A-92-1		ign	2.03E+05	3.20E+01	6.34E+03	0.1667	0.0026	10.80	0.46	0.474	0.019	0.929	2525	26	2501	81	1
April 07 2022	18BN81A-75-1		ign	8.15E+04	3.40E+01	2.40E+03	0.1666	0.0031	10.49	0.45	0.456	0.018	0.901	2524	31	2422	77	4
April 07 2022	18BN81A-33-1		ign	1.33E+05	0.00E+00		0.1665	0.0027	10.83	0.43	0.464	0.017	0.915	2523	27	2457	74	3
April 07 2022	18BN81A-28-1		ign	3.37E+05	5.60E+01	6.02E+03	0.1663	0.0028	11.17	0.53	0.489	0.022	0.933	2521	29	2566	93	-2
April 07 2022	18BN81A-7-1		ign	2.35E+05	0.00E+00		0.1661	0.0025	10.83	0.43	0.485	0.018	0.923	2519	26	2549	76	-1
April 07 2022	18BN81A-41-1		ign	2.53E+05	1.10E+01	2.30E+04	0.1659	0.0025	11.33	0.44	0.492	0.018	0.921	2517	26	2581	76	-2
April 08 2022	18BN81A-118-1		ign	9.80E+04	9.00E+00	1.09E+04	0.1655	0.0031	11.28	0.47	0.494	0.018	0.895	2513	31	2588	79	-3
April 07 2022	18BN81A-58-1		ign	2.95E+05	0.00E+00		0.1652	0.0022	11.05	0.43	0.492	0.018	0.940	2510	22	2579	77	-3
April 07 2022	18BN81A-63-1		ign	1.18E+05	4.10E+01	2.89E+03	0.1651	0.0028	11.45	0.47	0.504	0.019	0.908	2509	29	2631	80	-5
April 07 2022	18BN81A-51-1		ign	3.82E+05	3.20E+01	1.19E+04	0.1648	0.0026	10.61	0.44	0.490	0.019	0.927	2506	26	2571	82	-3
April 07 2022	18BN81A-59-1		ign	1.64E+05	5.00E+01	3.28E+03	0.1647	0.0030	11.17	0.50	0.503	0.021	0.914	2504	31	2627	88	-5
April 07 2022	18BN81A-74-1		ign	1.02E+05	0.00E+00	#DIV/0!	0.1645	0.0030	11.32	0.47	0.501	0.019	0.898	2502	31	2618	79	-4
April 08 2022	18BN81A-135-1		ign	2.74E+05	3.00E+01	9.13E+03	0.1642	0.0030	11.31	0.55	0.496	0.023	0.929	2499	31	2597	97	-4
April 07 2022	18BN81A-44-1		ign?	2.98E+05	1.70E+01	1.75E+04	0.1633	0.0028	11.02	0.48	0.487	0.020	0.919	2490	29	2558	84	-3
April 08 2022	18BN81A-132-1		ign	1.23E+05	0.00E+00	#DIV/0!	0.1633	0.0028	10.31	0.45	0.457	0.018	0.918	2490	29	2426	80	3
April 07 2022	18BN81A-32-1		ign	1.74E+05	2.00E+01	8.70E+03	0.1627	0.0024	10.68	0.42	0.473	0.017	0.924	2484	25	2495	74	0
April 07 2022	18BN81A-18-1		ign	1.40E+05	0.00E+00		0.1618	0.0027	10.85	0.47	0.488	0.020	0.922	2475	28	2562	84	-3
April 08 2022	18BN81A-98-1		ign	1.31E+05	0.00E+00		0.1611	0.0025	10.38	0.44	0.469	0.018	0.931	2467	26	2479	81	0
April 07 2022	18BN81A-9-1		ign	3.17E+05	0.00E+00		0.1607	0.0021	9.80	0.38	0.450	0.016	0.939	2463	22	2396	72	3
April 07 2022	18BN81A-54-1		met?	3.34E+05	2.00E+01	1.67E+04	0.1593	0.0030	10.33	0.52	0.479	0.022	0.925	2448	32	2523	96	-3
April 07 2022	18BN81A-26-1		ign	2.97E+05	0.00E+00		0.1591	0.0028	9.90	0.43	0.451	0.018	0.916	2446	30	2400	80	2
April 07 2022	18BN81A-10-1		ign	4.35E+05	1.90E+01	2.29E+04	0.1588	0.0023	9.99	0.38	0.469	0.016	0.922	2443	25	2477	71	-1
April 07 2022	18BN81A-70-1		met	2.20E+05	0.00E+00		0.1571	0.0022	9.99	0.39	0.460	0.017	0.932	2425	24	2440	74	-1
April 07 2022	18BN81A-67-1		mixed?	2.87E+05	1.00E+00	2.87E+05	0.1571	0.0023	9.86	0.38	0.457	0.016	0.922	2425	25	2427	71	0
April 08 2022	18BN81A-95-1		met	1.49E+05	0.00E+00		0.1569	0.0028	9.48	0.43	0.442	0.019	0.921	2423	30	2360	82	3
April 08 2022	18BN81A-115-1		mixed?	1.79E+05	3.40E+01	5.26E+03	0.1567	0.0025	9.94	0.43	0.464	0.018	0.925	2420	28	2457	80	-1
April 08 2022	18BN81A-122-1		met	9.72E+04	3.00E+01	3.24E+03	0.1563	0.0041	9.88	0.60	0.457	0.025	0.902	2416	45	2426	110	0
April 08 2022	18BN81A-130-1		met	1.34E+05	7.00E+00	1.92E+04	0.1562	0.0027	9.67	0.40	0.448	0.017	0.908	2415	29	2386	74	1
April 08 2022	18BN81A-136-1		met	3.81E+05	1.30E+01	2.93E+04	0.1555	0.0028	9.50	0.46	0.443	0.020	0.930	2407	30	2364	89	2
April 08 2022	18BN81A-131-1		met	1.30E+05	1.70E+01	7.67E+03	0.1551	0.0029	9.82	0.41	0.457	0.017	0.891	2403	32	2426	75	-1
April 08 2022	18BN81A-120-1		met	1.64E+05	1.50E+01	1.10E+04	0.1547	0.0028	9.55	0.45	0.450	0.019	0.924	2399	30	2395	86	0
April 08 2022	18BN81A-83-1		met	2.60E+05	1.80E+01	1.44E+04	0.1545	0.0027	10.03	0.46	0.467	0.020	0.925	2396	30	2470	86	-3
April 08 2022	18BN81A-123-1		met	1.68E+05	1.00E+01	1.68E+04	0.1545	0.0024	9.47	0.41	0.442	0.018	0.931	2396	27	2360	79	2
April 08 2022	18BN81A-91-1		met	2.34E+05	0.00E+00		0.1543	0.0038	9.49	0.62	0.452	0.028	0.926	2394	42	2404	121	0
April 08 2022	18BN81A-85-1		met	1.06E+05	1.60E+01	6.63E+03	0.1541	0.0028	9.76	0.40	0.457	0.017	0.900	2392	31	2426	75	-1
April 07 2022	18BN81A-16-1		met	3.16E+05	3.80E+01	8.32E+03	0.1538	0.0024	9.65	0.37	0.458	0.016	0.910	2389	27	2432	70	-2
April 08 2022	18BN81A-114-1		met	1.88E+05	2.60E+01	7.23E+03	0.1538	0.0028	9.80	0.47	0.466	0.021	0.926	2389	31	2466	90	-3
April 08 2022	18BN81A-103-1		met	1.13E+05	1.70E+01	6.66E+03	0.1537	0.0028	9.22	0.41	0.433	0.018	0.911	2388	32	2319	79	3
April 08 2022	18BN81A-116-1		met	2.03E+05	2.00E+00	1.02E+05	0.1537	0.0024	9.12	0.39	0.433	0.017	0.927	2388	27	2319	76	3
April 08 2022	18BN81A-111-1		met	9.98E+04	2.20E+01	4.54E+03	0.1536	0.0027	9.71	0.41	0.462	0.018	0.910	2386	30	2448	78	-3
April 08 2022	18BN81A-117-1		met	1.81E+05	5.00E+00	3.62E+04	0.1534	0.0027	9.92	0.45	0.472	0.020	0.924	2384	30	2492	87	-4
April 08 2022	18BN81A-101-1		met	1.47E+05	0.00E+00		0.1533	0.0027	9.40	0.44	0.444	0.019	0.928	2383	30	2369	86	1
April 08 2022	18BN81A-107-1		met?	2.17E+05	2.00E+00	1.09E+05	0.1533	0.0025	9.43	0.44	0.443	0.019	0.936	2383	28	2364	86	1
April 08 2022	18BN81A-102-1		met	1.16E+05	0.00E+00		0.1531	0.0023	9.21	0.35	0.434	0.015	0.920	2381	25	2322	68	3
April 08 2022	18BN81A-104-1		met	1.39E+05	1.80E+01	7.72E+03	0.1529	0.0028	9.10	0.38	0.429	0.016	0.901	2379	31	2302	72	3

Session	Spot ID	Screen	Class	Ratios										Dates (Ma)				Disc. %
				206Pb	204	206	207Pb		207Pb		206Pb		ρ	207Pb		206Pb		
				cps	cps	204	206Pb	2σ	235U	2σ	238U	2σ		206Pb	2σ	238U	2σ	
April 08 2022	18BN81A-97-1		met	2.12E+05	2.20E+01	9.64E+03	0.1528	0.0025	9.18	0.39	0.438	0.017	0.922	2377	28	2342	76	2
April 08 2022	18BN81A-86-1		met	1.74E+05	0.00E+00		0.1527	0.0030	9.81	0.47	0.464	0.020	0.913	2376	34	2457	89	-3
April 08 2022	18BN81A-125-1		met	1.27E+05	1.80E+01	7.03E+03	0.1526	0.0030	9.38	0.41	0.444	0.017	0.892	2375	34	2369	77	0
April 08 2022	18BN81A-99-1		met	1.71E+05	0.00E+00		0.1524	0.0028	9.21	0.38	0.442	0.017	0.901	2373	31	2360	74	1
April 07 2022	18BN81A-13-1		met	7.05E+05	0.00E+00		0.1497	0.0034	9.59	0.41	0.455	0.017	0.851	2343	38	2419	73	-3
April 07 2022	18BN81A-52-1		met	4.80E+05	1.10E+01	4.36E+04	0.1586	0.0022	10.14	0.38	0.472	0.016	0.929	2441	23	2494	71	-2
April 08 2022	18BN81A-90-1		met	6.54E+05	2.10E+01	3.11E+04	0.1535	0.0026	9.79	0.41	0.461	0.018	0.915	2385	29	2444	78	-2
April 08 2022	18BN81A-88-1	disc	ign	3.38E+05	0.00E+00		0.3219	0.0066	30.80	1.52	0.691	0.031	0.909	3579	32	3386	117	6
April 07 2022	18BN81A-6-1	disc	ign	2.44E+05	2.50E+01	9.77E+03	0.1693	0.0023	10.48	0.41	0.454	0.017	0.938	2551	23	2413	74	6
April 07 2022	18BN81A-34-1	disc	ign	2.34E+05	0.00E+00		0.1721	0.0050	10.23	0.61	0.425	0.022	0.872	2578	49	2283	99	13
April 07 2022	18BN81A-35-1	disc	ign	3.70E+05	0.00E+00		0.1560	0.0029	10.43	0.53	0.496	0.023	0.932	2413	31	2597	100	-7
April 07 2022	18BN81A-45-1	disc	ign	1.87E+05	3.80E+01	4.92E+03	0.1628	0.0026	10.15	0.41	0.443	0.017	0.921	2485	27	2364	74	5
April 07 2022	18BN81A-55-1	disc	ign	1.38E+05	1.20E+01	1.15E+04	0.1675	0.0028	11.86	0.47	0.513	0.018	0.908	2533	28	2669	78	-5
April 07 2022	18BN81A-60-1	disc	ign	4.18E+05	4.10E+01	1.02E+04	0.1723	0.0023	12.61	0.51	0.535	0.021	0.946	2580	22	2762	86	-7
April 07 2022	18BN81A-61-1	disc	ign	2.89E+05	6.20E+01	4.66E+03	0.1707	0.0030	12.03	0.62	0.525	0.025	0.939	2565	30	2720	107	-6
April 07 2022	18BN81A-73-1	disc	ign	2.21E+05	4.00E+00	5.53E+04	0.1701	0.0029	12.63	0.59	0.545	0.024	0.932	2559	28	2804	98	-9
April 07 2022	18BN81A-76-1	disc	ign	2.08E+05	0.00E+00		0.1701	0.0027	10.88	0.45	0.457	0.018	0.924	2559	27	2426	77	5
April 07 2022	18BN81A-77-1	disc	met	2.89E+05	7.40E+01	3.91E+03	0.1571	0.0026	8.27	0.66	0.374	0.029	0.978	2425	28	2048	136	18
April 07 2022	18BN81A-79-1	disc	ign	3.26E+05	5.90E+01	5.53E+03	0.1697	0.0025	10.74	0.41	0.457	0.016	0.924	2555	24	2427	71	5
April 08 2022	18BN81A-82-1	disc	met?	4.72E+05	4.00E+00	1.18E+05	0.1516	0.0023	10.11	0.41	0.481	0.018	0.929	2364	26	2532	78	-7
April 08 2022	18BN81A-94-1	disc	met	2.10E+05	0.00E+00		0.1517	0.0021	9.92	0.42	0.477	0.019	0.948	2365	23	2514	84	-6
April 08 2022	18BN81A-119-1	disc	ign	2.45E+05	3.70E+01	6.62E+03	0.1751	0.0033	13.08	0.57	0.545	0.022	0.902	2607	31	2804	89	-7
April 08 2022	18BN81A-121-1	disc	met	1.20E+05	2.80E+01	4.29E+03	0.1587	0.0030	9.40	0.42	0.428	0.018	0.910	2442	32	2297	79	6
April 07 2022	18BN81A-25-1	cPb	ign	2.00E+05	1.21E+02	1.66E+03	0.1782	0.0037	12.84	0.56	0.502	0.019	0.881	2636	34	2622	82	1
April 07 2022	18BN81A-40-1	cPb	ign	8.23E+05	2.38E+02	3.46E+03	0.1603	0.0025	10.90	0.62	0.482	0.026	0.962	2459	26	2536	114	-3
April 08 2022	18BN81A-93-1	cPb,incl	met	2.97E+05	2.29E+02	1.30E+03	0.1652	0.0038	9.77	0.50	0.433	0.020	0.895	2510	38	2319	89	8
April 08 2022	18BN81A-112-1	cPb,incl	met	1.60E+05	3.90E+02	4.10E+02	0.1927	0.0091	8.31	0.88	0.324	0.031	0.894	2765	78	1809	147	53
April 07 2022	18BN81A-56-1	disc,cPb	ign	9.60E+04	1.49E+02	6.44E+02	0.1963	0.0038	11.57	0.79	0.429	0.028	0.960	2796	31	2301	126	21
April 07 2022	18BN81A-64-1	cPb,incl	met	2.63E+05	1.03E+02	2.55E+03	0.1548	0.0025	7.21	0.71	0.344	0.034	0.987	2400	27	1906	159	26
April 08 2022	18BN81A-127-1	disc	ign	2.42E+05	0.00E+00		0.1899	0.0087	12.90	0.92	0.484	0.026	0.765	2741	75	2545	113	8
April 08 2022	18BN81A-87-1	incl	met	1.76E+05	0.00E+00		0.1531	0.0024	9.36	0.41	0.444	0.018	0.930	2381	27	2369	80	1
April 07 2022	18BN81A-23-1	mix	ign	4.53E+05	8.90E+01	5.09E+03	0.1746	0.0052	12.55	0.69	0.513	0.024	0.840	2602	50	2669	100	-3

Table D-3. LA-ICPMS zircon trace-element data. Acquired in the same ablation as the U-Pb isotope data in Table D-2.

Session	Spot ID	Screen	Class	Date (Ma)		Trace-elements											Th U	Gd(CN) Yb(CN)	Ti-in-zircon T °C
				207Pb	2σ	Ti	2SE	Gd	2SE	Yb	2SE	Th	2SE	U	2SE				
				206Pb	2σ	ppm	2SE	ppm	2SE	ppm	2SE	ppm	2SE	ppm	2SE				
April 11 2022	18BN37B-27-1		ign	2959	31	5.0	1.9	20.9	2.2	173.3	9.4	43.7	2.7	90.1	5.7	0.49	0.10	685	
April 11 2022	18BN37B-53-1		ign	2934	25	5.7	2.6	24.0	1.9	153	12	34.0	5.4	142.6	8.1	0.24	0.13	696	
April 11 2022	18BN37B-5-1		ign	2886	28	11.8	2.4	17.1	1.3	233.6	9.2	49.6	2.4	79.7	3.4	0.62	0.06	762	
April 11 2022	18BN37B-70-1		ign	2842	46	9.1	2.7	11.6	1.7	151	10	14.0	1.2	20.5	1.2	0.68	0.06	737	
April 11 2022	18BN37B-29-1		ign	2806	31	3.7	2.6	66.8	4.3	262	11	403	23	237	12	1.70	0.21	660	
April 11 2022	18BN37B-14-1		ign	2795	25	18.0	4.6	4.1	10	270	18	168.4	9.9	200.4	9.1	0.84	0.13	804	
April 11 2022	18BN37B-54-1		ign	2733	29	5.8	2.1	20.4	2.4	269.7	9.5	278	20	264	12	1.05	0.06	697	
April 11 2022	18BN37B-65-1		ign	2706	31	12.1	3.7	40.1	6.5	233.0	8.0	92.0	3.6	151.6	5.6	0.61	0.14	764	
April 11 2022	18BN37B-6-1		ign	2700	23	6.2	1.8	21.7	1.9	258.0	9.5	114.7	4.4	277.2	9.9	0.41	0.07	703	
April 11 2022	18BN37B-31-1		ign	2695	26	5.2	2.2	29.0	2.6	347	13	154.7	5.5	332	12	0.47	0.07	688	
April 11 2022	18BN37B-39-1		ign	2682	27	4.5	2.0	14.8	1.0	214.8	8.1	74.2	3.8	132.5	6.1	0.56	0.06	676	
April 11 2022	18BN37B-64-1		ign	2648	26	14.5	3.7	45.6	3.1	157.0	7.7	114.8	6.5	149	11	0.77	0.24	782	
April 11 2022	18BN37B-37-1		ign	2645	24	5.8	2.8	6.8	1.0	157	11	110.8	5.9	197.3	9.8	0.56	0.04	697	
April 11 2022	18BN37B-19-1		ign	2642	27	9.2	3.0	11.2	1.5	158.0	8.9	74.1	6.2	190	14	0.39	0.06	738	
April 11 2022	18BN37B-35-1		ign	2632	29	8.4	2.2	27.6	2.3	201	10	189.3	5.7	282	17	0.67	0.11	730	
April 11 2022	18BN37B-67-1		ign	2632	26	6.7	2.6	31.3	1.9	282.4	9.5	252	14	287	14	0.88	0.09	710	
April 11 2022	18BN37B-10-1		ign	2621	34	6.2	2.2	22.7	2.5	370	28	243	19	586	45	0.41	0.05	703	
April 11 2022	18BN37B-25-1		ign	2616	32	25.8	9.9	30.1	3.6	466	29	121	13	442	62	0.27	0.05	843	
April 12 2022	18BN37B-36-1		ign	2608	38			7.5	1.8	326	27	32.7	3.4	728	82	0.04	0.02		
April 11 2022	18BN37B-41-1		ign	2576	22	9.4	3.1	56.3	7.0	805	26	86.2	4.5	568	22	0.15	0.06	740	
April 11 2022	18BN37B-60-1		ign	2576	26	7.3	2.8	23.3	2.5	277	10	231.4	8.0	514	18	0.45	0.07	717	
April 11 2022	18BN37B-52-1		ign	2563	31	7.9	2.4	15.9	1.1	210.1	8.2	74.5	3.4	196.4	9.7	0.38	0.06	724	
April 11 2022	18BN37B-97-1		ign	2563	27	4.9	2.3	29.1	2.5	288	12	216.6	9.6	525	21	0.41	0.08	683	
April 11 2022	18BN37B-17-1		ign	2554	23	14.2	3.2	55	11	515	31	82.7	8.3	362	33	0.23	0.09	780	
April 11 2022	18BN37B-22-1		ign	2553	31	10.6	3.3	59.4	4.9	423	17	132.0	6.6	249.7	9.5	0.53	0.12	751	
April 11 2022	18BN37B-13-1		ign	2547	29	13.2	3.3	79.1	5.0	506	19	246	14	290	12	0.85	0.13	773	
April 11 2022	18BN37B-74-1		ign	2539	26	10.2	2.8	73.7	5.8	469	22	210.6	7.2	347	14	0.61	0.13	748	
April 12 2022	18BN37B-86-1		ign?	2539	32			68	23	326	15	98.1	5.3	395	27	0.25	0.17		
April 11 2022	18BN37B-72-1		ign	2534	25	23.4	6.9	123	24	438	15	227.5	8.7	328	12	0.69	0.23	833	
April 11 2022	18BN37B-16-1		ign	2532	35	5.7	2.3	121	23	310	16	277	17	538	25	0.51	0.32	696	
April 11 2022	18BN37B-48-1		ign	2532	26	6.8	1.9	69.9	4.1	517	19	319	14	548	22	0.58	0.11	711	
April 11 2022	18BN37B-57-1		ign	2531	28	8.5	4.2	49.5	2.9	383	14	101.5	4.0	79.8	2.6	1.27	0.11	731	
April 11 2022	18BN37B-96-1		ign	2528	29	9.4	2.6	26.6	1.9	228.7	8.5	147.2	5.8	321	15	0.46	0.10	740	
April 11 2022	18BN37B-40-1		ign	2526	26	11.7	2.7	43.4	6.3	398	20	179.2	8.7	771	26	0.23	0.09	761	
April 12 2022	18BN37B-109-1		ign	2525	31			18.5	2.5	252	12	147.0	8.7	297	17	0.49	0.06		
April 11 2022	18BN37B-15-1		ign	2522	33	13.4	4.9	67	14	329	39	110	26	511	29	0.22	0.17	774	
April 12 2022	18BN37B-75-1		ign	2520	34			33.0	7.0	260	36	98	21	157	24	0.62	0.10		
April 11 2022	18BN37B-8-1		ign	2502	29	7.6	2.4	33.9	4.7	281	29	190.2	7.7	448	41	0.42	0.10	721	
April 11 2022	18BN37B-87-1		ign	2502	28	3.4	2.1	17.3	2.1	317	28	160	32	701	83	0.23	0.05	654	
April 11 2022	18BN37B-55-1		ign	2493	27	4.5	1.9	50.2	5.2	238.6	9.3	209	10	382	13	0.55	0.17	676	
April 11 2022	18BN37B-82-1		ign	2484	28	6.4	2	94.6	7.0	596	22	390	19	441	34	0.88	0.13	706	
April 11 2022	18BN37B-69-1		ign	2464	30	20.1	8.7	36.4	5.1	396	44	51	15	540	38	0.09	0.08	816	
April 11 2022	18BN37B-62-1		met?	2420	24	27.7	5.5	61.3	6.0	358	15	118.5	5.8	609	23	0.19	0.14	852	
April 11 2022	18BN37B-18-1		ign	2388	31	14.8	4.7	27.5	5.6	326	33	136	15	612	45	0.22	0.07	784	
April 12 2022	18BN37B-93-1		met	2409	37			87	11	48.0	5.3	162	13	452	32	0.36	1.50		
April 11 2022	18BN37B-103-1		met	2404	28	7.2	2.3	15.3	1.4	13.8	1.2	135.6	7.3	429	21	0.32	0.92	716	
April 12 2022	18BN37B-89.2-1		met	2394	27			34.6	3.2	27.7	2.1	116.5	5.0	387	16	0.30	1.03		
April 12 2022	18BN37B-101-2		met	2394	29			18.8	2.0	22.9	1.8	150.6	7.1	464	20	0.32	0.68		

Spots labelled as "Sample ID-grain#-spot#".

Class: Analysis classified as igneous (ign) or metamorphic (met).

Screen: Analysis screened for high common-Pb content (cPb), intersection of an inclusion (incl), mixed isotope ratio signals (mix) or discordance (disc).

Gd(CN)/Yb(CN) ratio chondrite normalized (CN) using the chondrite value of Sun and McDonough (1989).

Ti-in-zircon temperatures (Ferry and Watson, 2007) calculated assuming a SiO2=a TiO2=1. No Ti data for April 12 2022 session.

Session	Spot ID	Screen	Class	Date (Ma)		Trace-elements												Ti-in-zircon T °C	
				207Pb		Ti		Gd		Yb		Th		U		Th	Gd(CN)		Yb(CN)
				206Pb	2σ	ppm	2SE	ppm	2SE	ppm	2SE	ppm	2SE	ppm	2SE	ppm	2SE		
April 12 2022	18BN37B-98-1		met	2392	31			35.8	5.0	62	11	115.3	8.3	645	35	0.18	0.48		
April 12 2022	18BN37B-100-1		met	2388	29			40.2	2.3	27.9	2.5	267	16	650	39	0.41	1.19		
April 11 2022	18BN37B-102-1		met	2386	26	6.0	2.4	29.2	7.9	60	16	49.9	3.5	995	87	0.05	0.40	700	
April 12 2022	18BN37B-88-1		met	2383	27			22.2	2.0	19.0	1.6	130.2	4.7	412	14	0.32	0.97		
April 12 2022	18BN37B-89-1		met	2383	34			20.4	1.6	16.9	1.4	148.3	9.4	418	27	0.35	1.00		
April 11 2022	18BN37B-102-2		met	2380	28	9.6	2.9	24.7	2.3	15.2	1.1	166.6	6.5	483	24	0.34	1.34	742	
April 12 2022	18BN37B-95-1		met	2377	25			41	3.1	43.4	2.6	270	12	577	26	0.47	0.78		
April 12 2022	18BN37B-99-1		met	2376	26			21.9	2.6	88	16	119.6	5.7	447	21	0.27	0.21		
April 12 2022	18BN37B-81-2		met	2374	35			39.3	1.8	29.5	1.6	261	14	574	28	0.45	1.10		
April 12 2022	18BN37B-94-1		met	2374	32			46.4	6.1	99	12	189.4	8.8	653	44	0.29	0.39		
April 12 2022	18BN37B-92-1		met	2372	30			24.5	2.1	26.1	2.4	121.3	4.2	416	22	0.29	0.78		
April 11 2022	18BN37B-91-1		met	2366	24	7.0	2.6	30.6	1.8	18.0	1.4	170.5	8.0	748	37	0.23	1.41	713	
April 11 2022	18BN37B-81-1		met	2365	26	6.8	2.0	26.3	2.0	26.4	2.4	143	7.6	456	28	0.31	0.82	711	
April 11 2022	18BN37B-80-1		met	2349	28	14.3	2.9	38.5	4.1	109	18	92.3	6.5	566	33	0.16	0.29	781	
April 11 2022	18BN37B-3-1	disc	ign	2656	25	13.3	2.8	28.3	2.1	289.2	9.2	123.2	6.7	344	14	0.36	0.08		
April 11 2022	18BN37B-9-1	disc	ign	2476	33	13.7	4.4	54.8	7.0	427	71	259	75	930	120	0.28	0.11		
April 11 2022	18BN37B-26-1	disc	ign	2504	40	9.5	5.0	23.2	4.1	235	13	155	13	465	34	0.33	0.08		
April 11 2022	18BN37B-32-2	disc	ign	2384	29	12.9	4.8	43	12	113	13	73.6	5.5	694	53	0.11	0.31		
April 11 2022	18BN37B-49-1	disc	ign	2512	25	10.6	3.0	46.0	4.6	566	35	118	13	237	15	0.50	0.07		
April 11 2022	18BN37B-51-1	disc	ign	2680	32	13.6	4.7	86	10	505	30	399	88	341	18	1.17	0.14		
April 11 2022	18BN37B-56-1	disc	ign	2645	25	8.7	3.1	31.1	3.1	343	27	169	11	554	35	0.31	0.08		
April 11 2022	18BN37B-59-1	disc	ign	2526	29	7.0	2.8	50.0	5.2	422	23	217	13	451	21	0.48	0.10		
April 11 2022	18BN37B-76-1	disc	ign	2369	34	12.8	5.2	49	10	302	18	104.6	7.3	486	39	0.22	0.13		
April 11 2022	18BN37B-77-1	disc	ign	2516	30	12.2	3.6	42.3	3.6	407	28	92.3	4.6	184.7	7.9	0.50	0.09		
April 11 2022	18BN37B-79-1	disc	ign	2554	30	35.0	6.1	134	19	284	21	102.3	6.9	675	29	0.15	0.39		
April 12 2022	18BN37B-110-1	disc	ign	2493	30			20	2.3	206	15	172	16	410	26	0.42	0.08		
April 12 2022	18BN37B-108-1	disc	ign?	2464	34			12.2	1.8	400	35	180	16	880	140	0.20	0.03		
April 12 2022	18BN37B-108-2	disc	ign?	2460	32			8.2	1.0	257	30	103.1	4.2	704	81	0.15	0.03		
April 12 2022	18BN37B-84-1	disc	met	2386	33			17.6	2.3	12.4	1.2	150.5	8.4	474	27	0.32	1.17		
April 12 2022	18BN37B-101-1	disc	met	2371	27			16.1	1.6	24.2	4.1	107.6	6.8	350	20	0.31	0.55		
April 11 2022	18BN37B-4-1	cPb	ign	2720	38	12.1	3.6	33.3	2.3	354	15	139.6	8.2	276	14	0.51	0.08		
April 11 2022	18BN37B-7-1	cPb	ign	2445	35	12.7	5.0	14.9	4.0	136	23	26.5	2.5	598	35	0.04	0.09		
April 11 2022	18BN37B-11-1	cPb	ign	2625	37	11.4	2.7	59	12	300	32	106	10	227	24	0.47	0.16		
April 11 2022	18BN37B-20-1	cPb	ign	2623	39	8.6	3.4	72.4	7.8	428	28	175	18	422	41	0.41	0.14		
April 11 2022	18BN37B-24-1	cPb	ign	2478	28	16.5	3.8	72.1	3.2	335	16	41.1	2.0	431	27	0.10	0.18		
April 11 2022	18BN37B-32-1	cPb	ign	2456	34	22.2	6.2	58.3	9.7	415	26	45.1	5.6	816	71	0.06	0.12		
April 11 2022	18BN37B-34-1	cPb	ign	2672	31	7.9	2.6	47.8	4.6	215	18	239.0	9.5	322	18	0.74	0.18		
April 11 2022	18BN37B-38-1	cPb	ign	2545	36	89	34	64	5.4	239	40	118	22	322	22	0.37	0.22		
April 11 2022	18BN37B-42-1	cPb	ign	2578	34	21	4.2	119	15	562	41	444	20	528	24	0.84	0.18		
April 11 2022	18BN37B-50-1	cPb	ign	2655	25	11.3	3.4	57.6	6.4	246	16	133.1	8.5	318	12	0.42	0.19		
April 11 2022	18BN37B-58-1	cPb	ign	2637	40	18.9	3.8	168	26	942	45	80.6	6.8	386	23	0.21	0.15		
April 11 2022	18BN37B-63-1	cPb	ign	2657	31	19.3	4.3	84.7	5.7	317	16	185.3	8.8	308	12	0.60	0.22		
April 11 2022	18BN37B-78-1	cPb	ign	2704	40	8.5	2.6	30.8	2.1	221	11	217	13	428	23	0.51	0.12		
April 11 2022	18BN37B-85-1	cPb	ign	2563	32	19.9	5.0	57.4	8.0	408	14	115.6	6.8	467	41	0.25	0.12		
April 11 2022	18BN37B-2-1	cPb,incl	ign	3259	481	400	160	254	28	553	80	480	110	563	85	0.85	0.38		
April 11 2022	18BN37B-12-1	cPb	ign	2768	196	12.6	3.5	40.6	3.0	422	22	178	17	511	29	0.35	0.08		
April 11 2022	18BN37B-21-1	cPb	ign	3741	213	19.1	5.4	53.5	3.3	397	21	72.3	2.7	336	17	0.22	0.11		
April 11 2022	18BN37B-23-1	cPb	ign	3418	124	10.1	2.8	39.6	6.0	143.4	7.6	79.6	3.7	156.6	7.1	0.51	0.23		
April 11 2022	18BN37B-28-1	cPb	ign	3024	101	16.5	3.3	140	26	342	26	270	40	314	32	0.86	0.34		
April 11 2022	18BN37B-43-1	cPb	ign	3288	78	11.8	2.6	48.5	5.2	265	15	70.4	3.5	90.9	5.5	0.77	0.15		
April 11 2022	18BN37B-45-1	cPb	ign	3204	77	12.2	4.0	114	12	416	18	119.3	6.8	335	16	0.36	0.23		
April 11 2022	18BN37B-46-1	cPb	ign	2858	97	8.6	2.9	38	2.9	414	20	124.4	6.7	505	35	0.25	0.08		
April 11 2022	18BN37B-47-1	cPb	ign	3058	48	18	4.2	77	13	564	63	93.4	9.6	341	41	0.27	0.11		
April 11 2022	18BN37B-66-1	cPb,incl	ign	2592	65	1560	560	113.3	6.5	381	24	221	12	575	69	0.38	0.25		
April 11 2022	18BN37B-73-1	cPb	ign	3521	96	24.9	4.3	66.8	3.0	316	11	76.9	4.1	94.2	4.6	0.82	0.17		

Session	Spot ID	Screen	Class	Date (Ma)		Trace-elements														Ti-in-zircon T °C
				207Pb		Ti		Gd		Yb		Th		U		Th	Gd(CN)			
				206Pb	2σ	ppm	2SE	ppm	2SE	ppm	2SE	ppm	2SE	ppm	2SE	ppm	2SE	U	Yb(CN)	
April 11 2022	18BN37B-33-1	disc,cPb	ign	2588	23	10.8	4.8	61.9	3.1	473	22	155	10	440	18	0.35	0.11			
April 11 2022	18BN37B-44-1	cPb,incl	ign	2650	26	450	110	103	11	398	12	102.5	3.6	360	16	0.28	0.21			
April 11 2022	18BN37B-71-1	disc,cPb	ign	3054	66	14.7	3.6	37.2	5.5	304	17	132.6	9.3	128.4	7.4	1.03	0.10			
April 11 2022	18BN37B-90-1	disc,cPb	ign	2611	31	23	4.8	88	15	307	15	90	6	633	45	0.14	0.24			
April 11 2022	18BN37B-1-1	incl	ign	2430	27	27.5	5.1	3.69	0.77	358	20	38.4	6.2	1312	63	0.03	0.01			
April 11 2022	18BN37B-30-1	incl	ign	2529	45	42.1	9.3	750	370	361	26	2900	1200	700	130	4.14	1.72			
April 11 2022	18BN37B-68-1	incl	ign	2881	25	490	200	86.6	8.4	500	21	173	10	194.1	8.8	0.89	0.14			
April 12 2022	18BN37B-83-2	cPb	met	2512	46			20.5	2.4	25.8	3.3	150.2	9.5	497	33	0.30	0.66			
April 12 2022	18BN37B-61-1	disc,cPb	ign	2626	47			33.5	2.9	21.3	1.7	117.2	9.7	511	20	0.23	1.30			
April 12 2022	18BN37B-83-1	disc,cPb	met	3066	173			32.6	3.5	33.7	3.7	149	18	452	44	0.33	0.80			
April 07 2022	18BN81A-36-1		ign	3008	23	15.8	3.1	28.2	2.2	375	15	82.6	2.7	144	10	0.57	0.06	791		
April 08 2022	18BN81A-126-1		ign	2814	32	8.1	2.7	3.38	0.88	81.4	5.8	52.6	3.0	170.2	8.2	0.31	0.03	726		
April 07 2022	18BN81A-12-1		ign	2802	26	8.3	2.3	12.2	2.3	174	17	51.4	5.4	74.0	4.9	0.69	0.06	729		
April 07 2022	18BN81A-14-1		ign	2799	26	23.4	5.8	67	14	421	67	259	56	254	43	1.02	0.13	833		
April 07 2022	18BN81A-62-1		ign	2780	34	18	4.1	27.4	2.4	290	16	55.5	5.8	77.8	6.1	0.71	0.08	804		
April 07 2022	18BN81A-49-1		ign	2726	28	11.7	2.9	8.4	1.4	135.6	5.6	111.6	3.8	137.7	4.4	0.81	0.05	761		
April 08 2022	18BN81A-106-1		ign	2708	29	12.3	2.8	15.6	1.7	227	13	278	22	371	24	0.75	0.06	766		
April 07 2022	18BN81A-27-1		ign	2692	31	17.7	2.8	16.7	2.5	137	22	55	16	126	38	0.44	0.10	803		
April 07 2022	18BN81A-15-1		ign	2678	32	12.6	3.2	34.6	2.8	313.7	6.2	75.0	3.1	175.1	7.4	0.43	0.09	768		
April 08 2022	18BN81A-89-1		ign	2672	28	23.7	5.4	68	10	696	55	443	66	779	45	0.57	0.08	834		
April 08 2022	18BN81A-124-1		ign	2657	32	10.1	3.0	33.5	6.9	250	16	164.6	8.3	277	16	0.59	0.11	747		
April 07 2022	18BN81A-11-1		ign	2654	27	12.8	3.5	78.6	6.7	371	19	494	42	298.9	9.7	1.65	0.18	770		
April 08 2022	18BN81A-108-1		ign	2652	39	9.8	3.5	2.74	0.52	53.9	2.3	44.5	2.2	93.3	5.7	0.48	0.04	744		
April 07 2022	18BN81A-17-1		ign	2639	25	18.7	5.8	37.4	3.5	281	17	259	26	222	17	1.17	0.11	808		
April 08 2022	18BN81A-128-1		ign	2635	31	11.4	3.3	22.9	2.8	225	16	109.6	4.3	200	11	0.55	0.08	758		
April 08 2022	18BN81A-110-1		ign	2605	28	9.3	2.3	33.6	1.9	301.9	8.5	137.5	6.5	247	10	0.56	0.09	739		
April 08 2022	18BN81A-113-1		ign	2601	29	18.6	3.6	44.6	4.2	341	12	158.4	8.5	249.6	9.1	0.63	0.11	808		
April 07 2022	18BN81A-78-1		ign	2599	28	15.4	4.0	26.8	1.3	278	12	62.1	3.7	134.9	8.3	0.46	0.08	788		
April 07 2022	18BN81A-46-1		ign	2596	25	16.1	3.2	50.3	2.3	437	19	134.1	7.9	244	13	0.55	0.10	793		
April 07 2022	18BN81A-43-1		ign	2596	34	16.6	3.5	36.9	1.9	338.6	8.6	49.6	1.4	68.3	2.5	0.73	0.09	796		
April 08 2022	18BN81A-129-1		ign	2592	37	13.4	3.7	20.4	2.1	279	18	187.5	9.5	374	21	0.50	0.06	774		
April 08 2022	18BN81A-133-1		ign	2589	26	11.8	3.6	11.4	1.2	162.0	5.3	67.8	2.5	146.7	5.6	0.46	0.06	762		
April 07 2022	18BN81A-42-1		ign	2586	23	24.9	3.8	90.1	3.4	592	18	191	10	313	14	0.61	0.13	839		
April 07 2022	18BN81A-39-1		ign	2583	25	13.5	2.5	28.9	2.8	319	21	123.9	7.5	340	20	0.36	0.07	775		
April 07 2022	18BN81A-48-1		ign	2583	26	10.4	3.2	41.6	2.6	441	19	79.9	5.3	280	13	0.29	0.08	750		
April 07 2022	18BN81A-47-1		ign	2581	27	21.3	4.4	18.1	2.2	176	15	84.8	6.2	170.1	9.5	0.50	0.09	822		
April 07 2022	18BN81A-24-1		ign	2580	25	13.3	3.0	46.4	4.2	286.2	9.4	58.3	2.9	187	12	0.31	0.13	773		
April 08 2022	18BN81A-105-1		ign	2572	28	11.7	2.6	29.2	2.8	240.7	9.4	122.6	6.4	215.8	9.3	0.57	0.10	761		
April 07 2022	18BN81A-19-1		ign	2569	27	28.6	5.1	100.2	8.8	505	26	360	110	268	12	1.34	0.16	855		
April 07 2022	18BN81A-68-1		ign	2569	24	14.8	3.3	32.2	2.1	329	14	101.3	4.4	192	18	0.53	0.08	784		
April 07 2022	18BN81A-57-1		ign	2568	26	13.7	2.8	29.2	4.3	196	12	156.8	5.4	295	12	0.53	0.12	776		
April 08 2022	18BN81A-96-1		ign	2568	29	11.5	3.6	41.5	3.6	174	10	198	13	195	11	1.02	0.20	759		
April 07 2022	18BN81A-80-1		ign	2566	23	65	21	92	13	496	23	620	110	473	15	1.31	0.15	958		
April 07 2022	18BN81A-8-1		ign	2565	34	14.5	2.7	58.6	6.6	666	28	77	13	301	23	0.26	0.07	782		
April 07 2022	18BN81A-22-1		ign	2561	29	13.9	2.5	32.6	5.0	262	10	183.4	5.5	414	12	0.44	0.10	778		
April 07 2022	18BN81A-31-1		ign	2560	25	15.0	2.8	75.5	8.8	267	12	180	17	274	22	0.66	0.23	785		
April 07 2022	18BN81A-72-1		ign	2559	35	15.4	3.3	29.5	2.9	312	12	109.6	4.4	256	10	0.43	0.08	788		
April 07 2022	18BN81A-20-1		ign	2558	31	9.1	2.0	17.3	1.3	158.4	5.3	49.7	2.1	130.1	5.5	0.38	0.09	737		
April 07 2022	18BN81A-69-1		ign	2556	24	21.7	4.8	88.2	5.3	668	30	319	22	359	17	0.89	0.11	824		
April 08 2022	18BN81A-109-1		ign	2555	31	9.9	2.4	27.8	2.5	355	13	97.5	4.4	287	12	0.34	0.06	745		
April 08 2022	18BN81A-134-1		ign	2553	30	15.2	3.4	46.5	5.0	275	23	114	14	218	21	0.52	0.14	787		
April 07 2022	18BN81A-21-1		ign	2550	27	14.8	2.9	29.4	2.5	188	6.6	109.6	5.5	233.4	9.6	0.47	0.13	784		
April 07 2022	18BN81A-37-1		ign	2550	24	12.1	3.2	13.0	1.1	328	17	151.9	5.0	635	22	0.24	0.03	764		
April 07 2022	18BN81A-38-1		ign	2550	25	11.8	2.8	21.7	2.3	291	22	98.2	9.7	292	35	0.34	0.06	762		

Session	Spot ID	Screen	Class	Date (Ma)		Trace-elements														Ti-in-zircon T °C
				207Pb		Ti		Gd		Yb		Th		U		Th	Gd(CN)			
				206Pb	2σ	ppm	2SE	ppm	2SE	ppm	2SE	ppm	2SE	ppm	2SE	ppm	2SE	U	Yb(CN)	
April 07 2022	18BN81A-65-1	ign	2546	23	11.2	2.8	22.9	2.1	180.9	4.9	98.1	7.1	231	13	0.42	0.10	757			
April 08 2022	18BN81A-84-1	ign	2545	33	13.9	3.8	47.8	4.6	291	15	109	10	157	11	0.69	0.14	778			
April 07 2022	18BN81A-30-1	ign	2535	31	15.7	3.1	41.0	4.3	314.4	9.8	165.7	5.3	292	11	0.57	0.11	790			
April 07 2022	18BN81A-53-1	ign	2533	27	17.3	4.3	50.7	7.9	322	38	120	17	291	41	0.41	0.13	800			
April 07 2022	18BN81A-66-1	ign	2531	25	20.7	5.0	76.3	5.0	441	19	180	12	229.3	6.6	0.78	0.14	819			
April 07 2022	18BN81A-29-1	ign	2529	25	18.2	2.6	69.0	3.9	378	12	136	12	245.4	9.1	0.55	0.15	805			
April 07 2022	18BN81A-50-1	ign	2528	25	29.2	6.0	94	20	443	24	268	19	385	15	0.70	0.18	858			
April 07 2022	18BN81A-71-1	ign	2528	28	27.1	3.9	95.9	4.7	644	21	502	27	574	25	0.87	0.12	849			
April 08 2022	18BN81A-81-1	ign	2527	33	17.7	4.3	49	18	158	10	380	200	171	11	2.22	0.26	803			
April 08 2022	18BN81A-100-1	ign	2527	28	15.3	2.7	35.3	3.0	267	13	193.6	7.5	480	22	0.40	0.11	787			
April 08 2022	18BN81A-92-1	ign	2525	26	13.0	3.3	31.4	4.3	267	17	193.1	8.5	361	15	0.53	0.10	771			
April 07 2022	18BN81A-75-1	ign	2524	31	11.6	3.3	36.5	2.6	239	12	81.4	4.3	143.8	5.9	0.57	0.13	760			
April 07 2022	18BN81A-33-1	ign	2523	27	18.7	3.1	34.5	4.7	222	18	96.2	7.1	162	10	0.59	0.13	808			
April 07 2022	18BN81A-28-1	ign	2521	29	10.5	3.2	41.0	3.7	300	19	55.5	5.4	412	27	0.13	0.11	750			
April 07 2022	18BN81A-7-1	ign	2519	26	12.2	3.6	79.6	3.8	504	43	247	33	271	31	0.91	0.13	765			
April 07 2022	18BN81A-41-1	ign	2517	26	13.7	3.0	7.95	0.91	154.6	4.3	99.1	3.4	324.3	8.4	0.31	0.04	776			
April 08 2022	18BN81A-118-1	ign	2513	31	16.1	3.5	43.7	9.1	279	25	124	12	176	13	0.70	0.13	793			
April 07 2022	18BN81A-58-1	ign	2510	22	13.8	3.3	25.6	2.5	333	22	204.3	9.1	411	14	0.50	0.06	777			
April 07 2022	18BN81A-63-1	ign	2509	29	9.5	2.8	15.1	2.6	140.8	7.1	67.2	5.2	183	15	0.37	0.09	741			
April 07 2022	18BN81A-51-1	ign	2506	26	10.5	4.9	47.7	6.5	395	28	290	12	477	38	0.61	0.10	750			
April 07 2022	18BN81A-59-1	ign	2504	31	28.0	6.1	34.6	5.4	219	16	121.1	6.8	229	15	0.53	0.13	853			
April 07 2022	18BN81A-74-1	ign	2502	31	11.1	2.7	24.2	3.4	183	15	54.2	5.9	161	15	0.34	0.11	756			
April 08 2022	18BN81A-135-1	ign	2499	31	12.6	3.8	9.2	1.2	140.1	7.5	230	13	516	29	0.45	0.05	768			
April 07 2022	18BN81A-44-1	ign?	2490	29	17.4	3.4	61	11	435	48	79.8	8.8	384	50	0.21	0.12	801			
April 08 2022	18BN81A-132-1	ign	2490	29	11.8	3.6	51.5	4.7	436	24	149	10	256	19	0.58	0.10	762			
April 07 2022	18BN81A-32-1	ign	2484	25	12.3	2.3	28.7	1.3	437	16	67.1	2.3	220.3	6.5	0.30	0.05	766			
April 07 2022	18BN81A-18-1	ign	2475	28	9.5	2.5	23.3	1.8	207.3	8.5	103.4	5.5	162.1	7.0	0.64	0.09	741			
April 08 2022	18BN81A-98-1	ign	2467	26	16.5	4.0	61.8	4.0	346	14	240	11	243	13	0.99	0.15	795			
April 07 2022	18BN81A-9-1	ign	2463	22	12.7	3.3	36.1	2.0	588	21	99.4	3.5	371	21	0.27	0.05	769			
April 07 2022	18BN81A-54-1	met?	2448	32	25.8	5.6	54.6	6.8	270	85	66	10	516	55	0.13	0.17	843			
April 07 2022	18BN81A-26-1	ign	2446	30	10.3	2.8	44.2	4.6	347	17	261	15	394	20	0.66	0.11	749			
April 07 2022	18BN81A-10-1	ign	2443	25	16.5	3.3	57	11	323	15	91.0	3.5	521	21	0.17	0.15	795			
April 07 2022	18BN81A-70-1	met	2425	24	20.9	4.3	54	5.4	104.4	7.8	60.8	6.9	393	19	0.15	0.43	820			
April 07 2022	18BN81A-67-1	mixed?	2425	25	14.0	2.8	20.3	2.4	68	25	71.3	5.9	460	39	0.16	0.25	779			
April 08 2022	18BN81A-95-1	met	2423	30	16.8	3.0	33.3	5.9	25.7	4.2	59.5	3.1	296	13	0.20	1.07	797			
April 08 2022	18BN81A-115-1	mixed?	2420	28	18.1	4.0	24.0	4.9	142	31	72.5	4.6	346	32	0.21	0.14	805			
April 08 2022	18BN81A-122-1	met	2416	45	16.2	7.0	14.0	2.3	7.6	1.8	99.9	5.7	226	18	0.44	1.52	793			
April 08 2022	18BN81A-130-1	met	2415	29	13.6	2.8	25.0	2.0	10.01	0.98	101.1	6.3	257.2	9.2	0.39	2.07	776			
April 08 2022	18BN81A-136-1	met	2407	30	13.3	3.2	27.5	4.0	195	15	81	12	822	33	0.10	0.12	773			
April 08 2022	18BN81A-131-1	met	2403	32	15.8	4.0	13.6	1.6	12.9	3.6	109.6	4.3	256.4	9.5	0.43	0.87	791			
April 08 2022	18BN81A-120-1	met	2399	30	15.1	3.6	22.0	1.9	19.1	2.7	65.7	2.5	316	13	0.21	0.95	786			
April 08 2022	18BN81A-83-1	met	2396	30	17.2	4.2	21.3	2.6	80	25	64	12	504	57	0.13	0.22	800			
April 08 2022	18BN81A-123-1	met	2396	27	12.3	3.4	29.7	2.3	93	22	102.7	6.4	344	19	0.30	0.26	766			
April 08 2022	18BN81A-91-1	met	2394	42	13.1	3.8	58	13	63	15	70.8	6.1	398	28	0.18	0.76	772			
April 08 2022	18BN81A-85-1	met	2392	31	16.0	4.0	19.8	2.0	19.1	3.4	101.2	3.7	205.1	7.0	0.49	0.86	792			
April 07 2022	18BN81A-16-1	met	2389	27	13.5	3.8	42.7	4.8	26.9	2.6	76.0	3.4	354	12	0.21	1.31	775			
April 08 2022	18BN81A-114-1	met	2389	31	10.4	2.5	24.6	1.5	21.7	2.0	72.7	3.1	341	14	0.21	0.94	750			
April 08 2022	18BN81A-103-1	met	2388	32	14.3	3.1	11.8	1.1	4.27	0.67	98.8	4.3	219.7	9.4	0.45	2.29	781			
April 08 2022	18BN81A-116-1	met	2388	27	21.1	4.7	52	12	147	43	71.5	9.4	419	34	0.17	0.29	821			
April 08 2022	18BN81A-111-1	met	2386	30	14.0	4.2	21.4	2.4	21.5	2.8	99.9	5.0	200	10	0.50	0.82	779			
April 08 2022	18BN81A-117-1	met	2384	30	21.4	4.7	30.6	4.4	50	13	67.7	1.9	362	16	0.19	0.51	823			
April 08 2022	18BN81A-101-1	met	2383	30	12.3	2.9	16.0	2.2	10.3	3.1	55.4	4.8	290	14	0.19	1.29	766			
April 08 2022	18BN81A-107-1	met?	2383	28	13.9	3.2	34.0	2.5	26	3.8	132.3	9.2	427	25	0.31	1.08	778			
April 08 2022	18BN81A-102-1	met	2381	25	11.7	2.7	13.7	1.3	10.2	0.93	98.7	3.5	219.5	7.6	0.45	1.11	761			
April 08 2022	18BN81A-104-1	met	2379	31	14.5	3.1	21.1	3.1	4.5	1.0	88.2	7.8	247	23	0.36	3.88	782			

Session	Spot ID	Screen	Class	Date (Ma)		Trace-elements														Ti-in-zircon T °C
				207Pb		Ti	Gd		Yb		Th		U		Th	Gd(CN)	Yb(CN)			
				206Pb	2σ	ppm	2SE	ppm	2SE	ppm	2SE	ppm	2SE	ppm	2SE	ppm	2SE	U	Yb(CN)	
April 08 2022	18BN81A-97-1		met	2377	28	14.6	3.4	75	20	51	11	69.7	2.9	381	14	0.18	1.22	783		
April 08 2022	18BN81A-86-1		met	2376	34	13.6	4.4	21.5	1.6	3.02	0.62	88.4	4.1	297	13	0.30	5.89	776		
April 08 2022	18BN81A-125-1		met	2375	34	12.0	3.1	16.6	1.4	7.6	1.9	85.0	4.7	223.9	8.9	0.38	1.81	763		
April 08 2022	18BN81A-99-1		met	2373	31	14.2	2.7	21.8	1.8	9.5	1.6	72.5	2.7	318	13	0.23	1.90	780		
April 07 2022	18BN81A-13-1		met	2343	38	6.4	2.3	11.3	3.2	505	26	20.94	0.89	870	47	0.02	0.02	706		
April 07 2022	18BN81A-52-1		met	2441	23	14.8	4.3	4.9	1.1	649	17	6.21	0.34	647	27	0.01	0.01	784		
April 08 2022	18BN81A-90-1		met	2385	29	12.7	3.4	7.38	0.99	566	29	17.3	1.4	1151	59	0.02	0.01	769		
April 08 2022	18BN81A-88-1	disc	ign	3579	32	16.0	3.3	10.9	2.1	138.1	7.5	57.2	4.3	391	18	0.15	0.07			
April 07 2022	18BN81A-6-1	disc	ign	2551	23	10.5	3.0	84	15	437	14	197.7	9.7	280	16	0.71	0.16			
April 07 2022	18BN81A-34-1	disc	ign	2578	49	40.3	8.0	78	14	316	52	108.1	9.2	332	36	0.33	0.20			
April 07 2022	18BN81A-35-1	disc	ign	2413	31	13.5	3.1	65.7	2.6	450	22	242	12	403	25	0.60	0.12			
April 07 2022	18BN81A-45-1	disc	ign	2485	27	14.2	4.2	40.7	2.9	309	18	168.6	8.4	261	12	0.65	0.11			
April 07 2022	18BN81A-55-1	disc	ign	2533	28	14.1	3.2	45.2	3.9	294	28	133	11	179	19	0.74	0.13			
April 07 2022	18BN81A-60-1	disc	ign	2580	22	19.9	4.3	59.3	5.5	479	29	328	13	561	29	0.58	0.10			
April 07 2022	18BN81A-61-1	disc	ign	2565	30	21.4	4.8	164	53	403	18	860	340	419	30	2.05	0.34			
April 07 2022	18BN81A-73-1	disc	ign	2559	28	210	31	40.1	4.1	227	21	112	15	321	33	0.35	0.15			
April 07 2022	18BN81A-76-1	disc	ign	2559	27	15.8	2.9	80.1	8.5	487	37	262	26	336	25	0.78	0.14			
April 07 2022	18BN81A-77-1	disc	met	2425	28	35.2	7.0	107	15	630	41	72	14	718	86	0.10	0.14			
April 07 2022	18BN81A-79-1	disc	ign	2555	24	12.3	2.9	59.0	4.9	462	19	211.7	8.7	548	21	0.39	0.11			
April 08 2022	18BN81A-82-1	disc	met?	2364	26	12.1	2.8	13.92	0.96	38.7	6.2	40.2	1.5	832	40	0.05	0.30			
April 08 2022	18BN81A-94-1	disc	met	2365	23	12.1	3.4	36.4	3.7	69	11	58.5	2.4	370	14	0.16	0.44			
April 08 2022	18BN81A-119-1	disc	ign	2607	31	40.3	9.0	17.2	2.2	205	22	157	21	373	47	0.42	0.07			
April 08 2022	18BN81A-121-1	disc	met	2442	32	17.3	3.0	28.3	1.9	22	1.8	90.3	4.5	233	15	0.39	1.06			
April 07 2022	18BN81A-25-1	cPb	ign	2636	34	11	4.5	18.9	2.0	218.8	8.8	89.0	4.5	252	10	0.35	0.07			
April 07 2022	18BN81A-40-1	cPb	ign	2459	26	15.9	4.3	15.1	2.9	649	44	64	14	1200	180	0.05	0.02			
April 08 2022	18BN81A-93-1	cPb,incl	met	2510	38	41.3	8.6	117	15	218	40	44.1	7.5	628	66	0.07	0.44			
April 08 2022	18BN81A-112-1	cPb,incl	met	2765	78	97	24	1070	280	580	120	65.2	8.1	518	58	0.13	1.53			
April 07 2022	18BN81A-56-1	disc,cPb	ign	2796	31	21.5	4.0	52.6	5.3	274	35	68	16	143	27	0.48	0.16			
April 07 2022	18BN81A-64-1	cPb,incl	met	2400	27	71	16	660	190	870	250	60	13	710	130	0.08	0.63			
April 08 2022	18BN81A-127-1	disc	ign	2741	75	12.7	3.0	12.2	1.8	216	21	36.6	4.8	410	130	0.09	0.05			
April 08 2022	18BN81A-87-1	incl	met	2381	27	1180	160	42.4	4.6	70	13	76.9	3.5	339	16	0.23	0.50			
April 07 2022	18BN81A-23-1	mix	ign	2602	50	35.4	8.9	32.4	5.4	399	78	66.5	8.8	552	32	0.12	0.07			

Table D-4. Electron microprobe compositional data and U-Th-Pb(total) dates for monazite from sample 18BN37B.

Spot ID	Element concentrations (Wt.%)															U-Th-Pb(total)
	U	Pb	Th	Ca	Si	P	S	Ce	La	Y	Pr	Nd	Sm	O	Total	Date (Ma)
18BN37B-1-1	0.401	0.708	4.772	0.695	0.280	13.740	0.0064	23.776	11.417	1.972	2.715	10.212	1.723	28.131	100.55	2367
18BN37B-1-2	0.110	0.556	4.751	0.578	0.621	13.106	0.0709	24.503	11.238	1.123	2.847	10.938	1.604	27.686	99.73	2285
18BN37B-1-3	0.331	0.819	5.848	0.545	0.555	13.075	0.0190	24.532	11.649	0.325	2.869	10.881	1.682	27.548	100.68	2425
18BN37B-1-4	0.341	0.843	5.887	0.513	0.560	13.063	0.0015	24.642	11.576	0.323	2.870	11.003	1.649	27.527	100.80	2465
18BN37B-1-5	0.342	0.852	6.229	0.538	0.587	12.939	0.0008	24.659	11.555	0.332	2.860	10.824	1.705	27.436	100.86	2388
18BN37B-1-6	0.363	0.887	6.420	0.533	0.598	12.902	0.0023	24.326	11.494	0.483	2.855	10.783	1.667	27.391	100.70	2396
18BN37B-1-7	0.355	0.833	5.993	0.522	0.572	13.164	0.0030	24.389	11.482	0.534	2.895	10.748	1.697	27.661	100.85	2393
18BN37B-1-8	0.340	0.831	5.849	0.512	0.558	13.039	0.0004	24.418	11.614	0.528	2.904	10.864	1.724	27.505	100.69	2446
18BN37B-1-9	0.335	0.756	5.532	0.483	0.517	12.877	0.0008	24.641	11.640	0.651	2.906	10.884	1.709	27.265	100.20	2347
18BN37B-1-10	0.314	0.800	5.636	0.499	0.510	13.204	0.0034	24.609	11.541	0.563	2.853	10.914	1.716	27.656	100.82	2462
18BN37B-1-11	0.309	0.775	5.606	0.519	0.518	13.253	0.0020	24.503	11.586	0.535	2.910	10.898	1.736	27.719	100.87	2409
18BN37B-1-12	0.296	0.715	5.043	0.597	0.384	13.433	0.0099	23.883	11.377	1.458	2.853	10.715	1.728	27.823	100.31	2437
18BN37B-1-13	0.293	0.675	4.952	0.546	0.380	13.613	0.0031	24.256	11.604	1.443	2.797	10.710	1.671	28.083	101.03	2351
18BN37B-1-14	0.216	0.732	5.485	0.499	0.479	13.246	0.0001	24.474	11.379	1.202	2.897	10.809	1.634	27.728	100.78	2445
18BN37B-1-15	0.351	0.991	7.143	0.476	0.794	12.862	0.0031	23.497	11.016	1.113	2.796	10.705	1.593	27.558	100.90	2459
18BN37B-1-16	0.431	0.698	4.658	0.668	0.314	13.504	0.0124	23.408	11.082	2.170	2.757	10.433	1.795	27.839	99.77	2337
18BN37B-1-17	0.339	0.801	5.590	0.510	0.508	13.189	0.0079	24.495	11.494	0.839	2.861	10.896	1.724	27.688	100.94	2446
18BN37B-1-18	0.332	0.811	6.023	0.531	0.569	12.983	0.0019	24.751	11.561	0.397	2.866	11.014	1.723	27.507	101.07	2352
18BN37B-1-19	0.372	0.834	5.852	0.546	0.542	12.960	0.0032	24.829	11.526	0.351	2.864	10.993	1.678	27.422	100.77	2414
18BN37B-1-20	0.352	0.883	5.733	0.599	0.544	13.206	0.0115	24.673	11.604	0.338	2.864	10.917	1.705	27.736	101.17	2604
18BN37B-1-21	0.289	0.698	5.036	0.542	0.410	13.491	0.0026	24.123	11.377	1.553	2.836	10.637	1.720	27.942	100.66	2396
18BN37B-1-22	0.372	0.895	6.343	0.497	0.639	13.141	0.0103	23.643	11.090	1.282	2.784	10.718	1.641	27.738	100.79	2427
18BN37B-3-1	0.613	0.908	5.799	1.178	0.113	13.808	0.0094	22.098	10.452	2.069	2.626	9.401	2.095	27.892	99.06	2351
18BN37B-3-2	0.504	0.880	5.540	1.133	0.101	13.772	0.0037	22.430	10.587	1.946	2.674	9.464	2.058	27.812	98.90	2468
18BN37B-3-3	0.546	1.061	7.308	0.504	0.838	12.852	0.0025	21.433	8.619	2.592	2.773	10.276	2.443	27.351	98.60	2381
18BN37B-4-1	0.490	0.887	5.854	0.327	0.723	12.570	0.0082	23.539	9.442	1.528	2.933	10.896	2.306	26.897	98.40	2415
18BN37B-4-1	0.579	1.176	8.051	0.530	0.900	12.625	0.0021	21.156	8.536	2.558	2.676	9.987	2.271	27.092	98.14	2412
18BN37B-4-1	0.522	0.895	5.955	0.348	0.708	12.740	0.0007	22.889	9.060	2.013	2.899	10.863	2.495	27.088	98.47	2372
18BN37B-5-1	0.552	1.716	13.227	0.371	1.820	11.284	0.0139	20.869	8.579	1.064	2.627	9.883	1.779	26.566	100.35	2367
18BN37B-5-2	0.518	1.396	10.360	0.408	1.376	11.763	0.0113	21.433	8.790	1.541	2.705	10.129	2.060	26.624	99.11	2389
18BN37B-5-3	0.533	1.042	7.123	0.471	0.853	12.876	0.0079	21.922	8.928	2.264	2.782	10.480	2.417	27.446	99.14	2396
18BN37B-5-4	0.561	1.128	7.873	0.519	0.930	12.628	0.0214	21.534	8.575	2.287	2.741	10.366	2.455	27.225	98.84	2375
18BN37B-5-5	0.492	0.976	6.670	0.456	0.785	12.894	0.0160	22.271	9.050	2.008	2.888	10.649	2.374	27.376	98.91	2403
18BN37B-5-6	0.461	1.035	7.396	0.462	0.924	12.504	0.0289	22.762	9.314	1.580	2.846	10.778	2.198	27.154	99.44	2385
18BN37B-6-1	0.387	0.930	6.909	0.714	0.582	13.027	0.0042	23.517	11.261	0.870	2.729	10.172	1.743	27.498	100.34	2347
18BN37B-6-2	0.256	0.811	6.465	0.486	0.636	12.679	0.0027	24.276	11.198	0.320	2.869	10.918	1.760	27.050	99.73	2311
18BN37B-6-3	0.228	0.785	6.339	0.442	0.627	12.789	0.0041	24.648	11.453	0.355	2.884	10.915	1.708	27.255	100.43	2309
18BN37B-6-4	0.123	0.929	7.268	0.301	0.872	12.362	0.0160	24.814	11.647	0.541	2.859	10.556	1.335	27.059	100.68	2533
18BN37B-6-5	0.135	0.732	5.582	0.446	0.543	12.875	0.0091	24.914	11.514	0.916	2.878	10.658	1.642	27.311	100.16	2530
18BN37B-6-6	0.115	0.811	6.484	0.315	0.755	12.450	0.0107	24.797	11.284	0.601	2.900	10.807	1.441	26.933	99.70	2475
18BN37B-6-7	0.122	0.819	6.551	0.353	0.756	12.474	0.0152	24.432	11.435	0.630	2.902	10.812	1.480	26.976	99.76	2468
18BN37B-6-8	0.175	0.665	5.121	0.675	0.349	13.238	0.0075	24.267	11.180	1.150	2.833	10.416	1.790	27.455	99.32	2428
18BN37B-6-9	0.199	0.671	5.138	0.623	0.345	13.110	0.0257	24.220	11.283	1.143	2.810	10.536	1.756	27.316	99.17	2402
18BN37B-6-10	0.163	0.669	5.251	0.545	0.442	13.041	0.0222	24.120	10.638	1.597	2.890	10.714	1.824	27.360	99.28	2410
18BN37B-6-11	0.160	0.673	5.141	0.546	0.409	13.143	0.0099	24.709	11.728	0.977	2.859	10.575	1.751	27.503	100.18	2466
18BN37B-6-12	0.186	0.685	5.416	0.517	0.457	12.910	0.0015	24.696	11.476	1.005	2.818	10.533	1.655	27.206	99.56	2367
18BN37B-6-13	0.132	0.808	6.442	0.339	0.728	12.392	0.0037	24.756	11.190	0.732	2.945	10.777	1.486	26.846	99.58	2459
18BN37B-6-14	0.121	0.752	6.248	0.371	0.692	12.685	0.0209	24.486	11.149	0.699	2.861	10.987	1.526	27.153	99.75	2376
18BN37B-6-15	0.134	0.772	6.362	0.408	0.709	12.549	0.0469	24.838	11.173	0.676	2.886	10.840	1.473	27.099	99.97	2381
18BN37B-6-16	0.156	0.634	4.698	0.727	0.328	13.312	0.0602	24.417	11.428	1.136	2.801	10.578	1.749	27.643	99.67	2520
18BN37B-6-17	0.188	0.689	5.129	0.675	0.327	13.420	0.0083	24.211	11.264	1.212	2.845	10.623	1.801	27.731	100.12	2484
18BN37B-6-18	0.116	0.794	6.443	0.304	0.746	12.699	0.0035	24.985	11.485	0.632	2.940	10.868	1.433	27.314	100.76	2439
18BN37B-6-19	0.116	0.788	6.343	0.348	0.715	12.754	0.0227	24.850	11.381	0.641	2.898	10.850	1.477	27.340	100.52	2455
18BN37B-6-20	0.110	0.788	6.137	0.314	0.688	12.647	0.0000	25.122	11.442	0.654	2.888	10.928	1.474	27.165	100.36	2536
18BN37B-6-21	0.110	0.717	5.900	0.423	0.630	12.821	0.0142	24.912	11.217	0.874	2.897	11.052	1.563	27.371	100.50	2403
18BN37B-6-22	0.248	0.727	5.449	0.668	0.396	13.126	0.0146	23.533	10.890	1.925	2.769	10.391	1.694	27.434	99.26	2400
18BN37B-6-23	0.184	0.686	5.173	0.603	0.346	13.227	0.0175	23.931	10.951	1.852	2.824	10.480	1.730	27.526	99.53	2464

Spots labeled as sample ID-grain#-spot#.

U-Th-Pb(total) dates calculated by iteration using the equation of Suzuki and Adachi (1991).

Spot ID	Element concentrations (Wt.%)														U-Th-Pb(total)	
	U	Pb	Th	Ca	Si	P	S	Ce	La	Y	Pr	Nd	Sm	O	Total	Date (Ma)
18BN37B-6-24	0.151	0.687	5.259	0.597	0.392	13.325	0.0110	24.053	10.922	1.733	2.803	10.758	1.755	27.731	100.18	2481
18BN37B-6-25	0.299	0.798	5.682	0.774	0.441	13.299	0.0154	23.538	11.163	1.409	2.716	10.286	1.719	27.684	99.83	2461
18BN37B-6-26	0.136	0.635	5.038	0.562	0.408	13.218	0.0127	24.279	11.058	1.456	2.927	11.008	1.678	27.601	100.02	2418
18BN37B-6-27	0.134	0.623	4.925	0.544	0.407	13.279	0.0391	24.395	11.110	1.527	2.847	10.971	1.705	27.725	100.23	2425
18BN37B-6-28	0.134	0.624	4.874	0.488	0.395	13.380	0.0065	24.333	11.108	1.707	2.917	10.907	1.699	27.803	100.38	2447
18BN37B-6-29	0.153	0.642	4.715	0.492	0.376	13.339	0.0034	24.199	11.064	1.773	2.848	10.864	1.713	27.678	99.86	2546
18BN37B-6-30	0.139	0.604	4.740	0.483	0.365	13.418	0.0027	24.483	11.034	1.785	2.847	10.816	1.763	27.807	100.29	2421
18BN37B-6-31	0.372	0.831	5.814	0.609	0.504	13.036	0.0475	23.505	11.184	1.524	2.726	10.246	1.629	27.438	99.47	2420
18BN37B-6-32	0.252	0.754	5.709	0.608	0.447	13.005	0.0022	23.904	11.065	1.295	2.804	10.555	1.718	27.293	99.41	2389
18BN37B-6-33	0.274	0.743	5.739	0.538	0.490	12.745	0.0102	24.287	11.402	0.732	2.774	10.670	1.728	26.984	99.12	2320
18BN37B-6-34	0.145	0.729	5.837	0.345	0.624	12.486	0.0108	24.889	11.225	0.819	2.912	10.952	1.524	26.854	99.35	2412
18BN37B-6-35	0.134	0.716	5.726	0.339	0.606	12.681	0.0038	24.836	11.197	0.826	2.923	10.947	1.558	27.050	99.54	2427
18BN37B-6-36	0.350	0.790	5.816	0.735	0.480	13.005	0.1114	23.938	11.372	0.848	2.805	10.279	1.708	27.467	99.70	2336
18BN37B-6-37	0.348	0.760	5.493	0.620	0.439	13.193	0.0015	24.116	11.347	1.033	2.836	10.671	1.810	27.568	100.24	2353
18BN37B-6-38	0.386	0.859	6.212	0.619	0.543	12.885	0.0127	24.259	11.351	0.580	2.858	10.540	1.687	27.282	100.07	2362
18BN37B-6-39	0.412	0.804	5.407	0.954	0.170	13.506	0.0021	23.456	11.293	1.666	2.730	10.024	1.615	27.691	99.73	2423
18BN37B-7-1	0.509	0.743	5.012	0.788	0.436	13.294	0.1114	22.401	9.855	2.742	2.754	10.216	2.152	27.755	98.77	2264
18BN37B-7-2	0.451	0.853	5.675	0.605	0.495	13.314	0.0078	23.271	10.570	1.829	2.824	10.464	1.979	27.764	100.10	2425
18BN37B-7-3	0.558	0.875	5.567	0.707	0.486	13.242	0.0409	22.189	9.675	2.905	2.675	9.987	2.120	27.620	98.65	2390
18BN37B-7-4	0.413	0.798	5.511	0.622	0.516	13.213	0.0068	24.736	11.772	0.660	2.836	10.647	1.715	27.765	101.21	2374
18BN37B-7-5	0.306	0.800	5.653	0.550	0.537	13.291	0.0093	24.568	11.636	0.639	2.888	10.874	1.749	27.864	101.37	2467
18BN37B-7-6	0.315	0.774	5.712	0.520	0.542	13.157	0.0047	24.611	11.668	0.641	2.894	10.910	1.721	27.701	101.17	2366
18BN37B-7-7	0.335	0.776	5.495	0.551	0.516	13.186	0.0381	24.772	11.511	0.573	2.881	10.747	1.757	27.703	100.84	2412
18BN37B-7-8	0.374	0.791	5.637	0.578	0.517	12.933	0.0271	24.808	11.615	0.545	2.879	10.727	1.704	27.402	100.54	2363
18BN37B-7-9	0.364	0.815	5.666	0.540	0.538	13.020	0.0049	24.508	11.650	0.571	2.847	10.813	1.725	27.468	100.53	2431
18BN37B-7-10	0.341	0.797	5.617	0.545	0.539	13.292	0.0165	24.645	11.530	0.649	2.853	10.782	1.797	27.859	101.26	2426
18BN37B-7-11	0.373	0.818	5.489	0.554	0.518	13.180	0.0109	24.315	11.295	1.009	2.893	10.604	1.796	27.651	100.51	2481
18BN37B-7-12	0.373	0.813	5.616	0.715	0.673	13.131	0.0627	24.001	11.423	0.797	2.814	10.500	1.715	27.791	100.42	2428
18BN37B-7-13	0.446	0.848	5.815	0.670	0.501	13.281	0.0211	24.016	11.243	0.935	2.829	10.456	1.768	27.760	100.59	2379
18BN37B-7-14	0.701	0.861	4.880	0.882	0.249	13.761	0.0205	22.876	10.473	2.278	2.780	9.878	1.887	28.032	99.56	2387
18BN37B-7-15	0.492	0.938	5.947	0.878	0.491	13.274	0.0531	23.982	11.158	0.764	2.801	10.555	1.811	27.855	101.00	2507
18BN37B-7-16	0.560	0.823	5.251	0.827	0.349	13.563	0.0241	23.260	10.706	1.948	2.696	10.039	1.957	27.943	99.94	2346
18BN37B-7-17	0.418	0.675	4.474	1.339	0.329	13.394	0.2063	23.346	11.151	1.683	2.689	9.854	1.778	28.002	99.34	2347
18BN37B-8-1	0.443	0.953	5.854	0.533	0.706	12.794	0.0475	22.898	9.001	1.759	2.877	10.895	2.464	27.199	98.42	2625
18BN37B-8-2	0.512	0.940	6.403	0.486	0.762	12.574	0.0321	22.389	8.881	2.128	2.890	10.771	2.440	26.990	98.20	2371

Table D-5. Whole-rock major- and trace-element data for the quartzofeldspathic gneiss samples 18BN37B and 18BN81A.

	Quartzofeldspathic gneiss	
	18BN37B	18BN81A
ICP-OES (wt.%)		
SiO ₂	73.72	71.56
Al ₂ O ₃	15.84	14.67
FeO(T)	2.77	4.54
MnO	0.0257	0.0571
MgO	1.192	2.100
CaO	0.32	1.59
Na ₂ O	1.325	1.906
K ₂ O	4.38	2.90
TiO ₂	0.407	0.657
P ₂ O ₅	0.021	0.020
LOI	2.27	1.89
Total	99.90	100.48
ICP-MS (ppm)		
Sc	6	16
V	60	82
Ga	20	19
Rb	176	107
Sr	84	209
Y	11.4	19.3
Zr	129	240
Nb	5.4	15.0
Cs	1.9	2.0
Ba	706	944
La	27.5	49.3
Ce	50.2	89.3
Pr	5.34	9.56
Nd	18.5	34.1
Sm	3.03	6.00
Eu	0.79	1.47
Gd	2.08	5.52
Tb	0.32	0.81
Dy	1.95	4.30
Ho	0.41	0.71
Er	1.26	1.85
Tm	0.190	0.231
Yb	1.25	1.35
Lu	0.211	0.205
Hf	3.2	6.6
Pb	26	11
Th	7.6	10.3
U	0.86	0.88

Major elements are normalized to 100%, loss on ignition (LOI) excluded.

Totals are reported as measured, with all Fe as Fe₂O₃.

ICP-OES major- and ICP-MS trace-element data acquired at Actlabs, with the 4Lithoresearch analytical package.

Appendix E: Supporting information for chapter 5

Table E-1. TiO₂ and SiO₂ activity values for granitoid samples with Ti-in-Zr temperature data, estimated following the recommendations of Schiller and Finger (2019).

Sample ID	18EM35B	19BN123A	19BN150A	19BN154C	18BN20C	19BN07E
Zr ppm	190	165	144	100	458	261
T _{Zr} (°C)	805	799	784	748	893	835
T _{Zr(M)} (°C)	860	820	811	785	893	844
T _{Zr/2(M)} (°C)	820	784	775	751	838	807
a TiO ₂ TZr	0.60	0.37	0.20	0.50	0.25	0.23
a SiO ₂ TZr	1.00	1.00	1.00	1.00	0.90	1.00
a TiO ₂ TZr(M)	0.31	0.30	0.13	0.40	0.25	0.22
a SiO ₂ TZr(M)	1.00	1.00	1.00	1.00	0.90	1.00
a TiO₂ TZr/2(M)	0.56	0.44	0.23	0.50	0.35	0.31
a SiO₂ TZr/2(M)	1.00	1.00	1.00	1.00	1.00	1.00
Ti-in-Zr ppm Median	8.1	3.0	3.1	5.5	14.5	9.3
Ti-in-Zr T Median (°C)	782 (n=32)	712 (n=9)	774 (n=5)	755 (n=5)	899 (n=19)	861 (n=15)
Ti-in-Zr T SD (°C)	26	34	45	38	44	51

Note:

T_{Zr}: Zircon saturation temperature of the whole-rock (crystal +melt) composition, from the calibration of Watson and Harrison (1983).

T_{Zr(M)}: Zircon saturation temperature of the melt, corrected for the removal of crystals*

T_{Zr/2(M)}: Temperature at which 50% of zircon would have crystallized from the melt, corrected for the removal of crystals*

*Equilibrium crystallization modelling conducted in Excel-based Rhyolite-MELTS 1.1 at P=4 kbar, fO₂=QFM and initial H₂O=3 wt.%

n: number of zircon analyses included in calculation, SD: standard deviation

Ti-in-Zr temperatures were calculated using the activities at T_{Zr/2(M)}

Table E-2. LA-MC-ICPMS zircon U-Pb isotope data.

Session	Spot ID	Screen	Class	206Pb cps	204 cps	206 204	Ratios						Dates (Ma)				Disc. %	
							207Pb 206Pb	2σ	207Pb 235U	2σ	206Pb 238U	2σ	ρ	207Pb 206Pb	2σ	206Pb 238U		2σ
Sep 14 2023	18EM35B-1-1		ign	337573	19	18086	0.1576	0.0011	10.02	0.33	0.461	0.015	0.975	2430	12	2446	65	-1
Sep 14 2023	18EM35B-2-1		ign	549469	23	23705	0.1572	0.0011	10.22	0.35	0.472	0.016	0.978	2426	12	2490	70	-3
Sep 14 2023	18EM35B-2-2		ign	500179	14	36270	0.1577	0.0011	10.33	0.38	0.475	0.017	0.981	2431	12	2506	75	-3
Sep 14 2023	18EM35B-4-1		ign	450756	78	5803	0.1591	0.0012	10.49	0.36	0.478	0.016	0.977	2446	12	2520	69	-3
Sep 14 2023	18EM35B-5-1		ign	553129	82	6725	0.1573	0.0011	10.29	0.33	0.475	0.015	0.975	2427	12	2504	65	-3
Sep 14 2023	18EM35B-7-1		ign	693843	41	16822	0.1578	0.0012	10.29	0.34	0.473	0.015	0.974	2432	13	2497	67	-3
Sep 14 2023	18EM35B-8-1		ign	601553	39	15535	0.1573	0.0012	10.01	0.31	0.462	0.014	0.970	2427	13	2447	61	-1
Sep 14 2023	18EM35B-9-1		ign	429937	75	5734	0.1561	0.0011	10.21	0.32	0.474	0.014	0.972	2414	12	2502	63	-4
Sep 14 2023	18EM35B-11-1		ign	656244	19	33685	0.1586	0.0011	10.60	0.33	0.485	0.015	0.974	2441	12	2550	64	-4
Sep 14 2023	18EM35B-14-1		ign	129910	36	3566	0.1586	0.0014	9.53	0.33	0.436	0.015	0.968	2441	15	2332	65	5
Sep 14 2023	18EM35B-15-1		ign	1242154	29	43156	0.1585	0.0011	10.35	0.32	0.474	0.014	0.973	2439	12	2500	62	-2
Sep 14 2023	18EM35B-16-1		ign	311457	38	8275	0.1594	0.0012	10.03	0.32	0.457	0.014	0.972	2449	12	2425	62	1
Sep 14 2023	18EM35B-17-1		ign	1127555	47	24091	0.1567	0.0012	10.32	0.34	0.478	0.015	0.975	2421	12	2516	66	-4
Sep 14 2023	18EM35B-19-1		ign	506394	21	23789	0.1584	0.0011	10.01	0.32	0.459	0.014	0.975	2439	12	2433	63	0
Sep 14 2023	18EM35B-20-1		ign	431891	6	70115	0.1584	0.0011	10.03	0.32	0.460	0.014	0.973	2438	12	2438	62	0
Sep 14 2023	18EM35B-21-1		ign	738357	21	35161	0.1570	0.0012	9.94	0.30	0.459	0.014	0.967	2424	13	2436	60	-1
Sep 14 2023	18EM35B-22-1		ign	820820	29	28495	0.1561	0.0011	9.87	0.31	0.459	0.014	0.974	2414	12	2434	62	-1
Sep 14 2023	18EM35B-23-1		ign	177603	81	2198	0.1561	0.0012	9.24	0.29	0.430	0.013	0.966	2414	13	2304	58	5
Sep 14 2023	18EM35B-24-1		ign	271234	71	3810	0.1589	0.0012	9.86	0.31	0.450	0.014	0.972	2444	12	2395	61	2
Sep 14 2023	18EM35B-25-1		ign	197560	67	2957	0.1587	0.0012	9.91	0.33	0.453	0.015	0.976	2442	12	2410	66	1
Sep 14 2023	18EM35B-26-1		ign	409419	43	9615	0.1575	0.0011	10.19	0.36	0.469	0.016	0.979	2429	12	2481	70	-2
Sep 14 2023	18EM35B-27-1		ign	137735	40	3427	0.1566	0.0012	9.68	0.32	0.448	0.015	0.972	2420	13	2388	64	1
Sep 14 2023	18EM35B-28-1		ign	207119	68	3052	0.1557	0.0012	9.48	0.32	0.442	0.014	0.973	2410	13	2359	64	2
Sep 14 2023	18EM35B-29-1		ign	113607	67	1689	0.1546	0.0012	9.30	0.32	0.437	0.014	0.973	2397	13	2335	65	3
Sep 14 2023	18EM35B-29-2		ign	126828	64	1971	0.1545	0.0011	9.27	0.31	0.435	0.014	0.975	2396	13	2330	64	3
Sep 14 2023	18EM35B-31-1		ign	378556	46	8165	0.1589	0.0011	10.13	0.33	0.463	0.015	0.975	2444	12	2451	64	0
Sep 14 2023	18EM35B-32-1		ign	637360	61	10423	0.1580	0.0011	10.20	0.32	0.468	0.014	0.974	2435	12	2477	63	-2
Sep 14 2023	18EM35B-33-1		ign	175425	45	3916	0.1568	0.0011	9.83	0.31	0.455	0.014	0.973	2422	12	2416	62	0
Sep 14 2023	18EM35B-34-1		ign	157573	55	2846	0.1572	0.0012	9.70	0.33	0.448	0.015	0.974	2426	13	2386	66	2
Sep 14 2023	18EM35B-35-1		ign	1164362	73	15864	0.1576	0.0011	10.39	0.32	0.478	0.015	0.973	2430	12	2520	63	-4
Sep 14 2023	18EM35B-36-1		ign	172136	56	3048	0.1584	0.0012	10.06	0.35	0.461	0.016	0.974	2439	13	2444	68	0
Sep 14 2023	18EM35B-37-1		ign	477655	87	5502	0.1582	0.0013	10.10	0.32	0.463	0.014	0.968	2437	13	2454	62	-1
Sep 14 2023	18EM35B-39-1		ign	488112	45	10894	0.1581	0.0011	9.89	0.34	0.454	0.015	0.978	2435	12	2412	67	1
Sep 14 2023	18EM35B-40-1		ign	440925	57	7789	0.1581	0.0011	10.35	0.37	0.475	0.016	0.979	2435	12	2506	71	-3
Sep 14 2023	18EM35B-41-1		ign	193737	47	4150	0.1588	0.0013	9.76	0.32	0.446	0.014	0.969	2443	14	2377	64	3
Sep 14 2023	18EM35B-42-1		ign	160181	38	4246	0.1582	0.0012	9.76	0.32	0.447	0.014	0.974	2437	13	2383	64	2
Sep 14 2023	18EM35B-43-1		ign	139113	54	2590	0.1555	0.0012	9.46	0.32	0.442	0.015	0.974	2407	13	2358	65	2
Sep 14 2023	18EM35B-44-1		ign	154790	76	2028	0.1570	0.0012	9.69	0.35	0.448	0.016	0.979	2423	12	2385	70	2
Sep 14 2023	18EM35B-45-1		ign	653655	89	7377	0.1583	0.0012	10.07	0.32	0.461	0.014	0.971	2438	13	2445	62	0

Spots labelled as "Sample ID-grain#-spot#.

*Note for samples 19BN154C, 150A and 123A, all mounted zircon grains were numbered, not just the analyzed grains, so the spot numbering is not sequential.

Class: Analysis classified as igneous (ign), metamorphic (met), inherited (inhrt) or ambiguous (amb).

Screen: Analysis screened for high common-Pb content (cPb), mixed isotope ratio signals (mix) or discordance (disc).

Disc.: Percent discordance calculated as $[(207\text{Pb}/206\text{Pb date}/206\text{Pb}/238\text{U date})-1]*100$

Session	Spot ID	Screen	Class	Ratios										Dates (Ma)				Disc. %
				206Pb	204	206	207Pb		207Pb		206Pb		206Pb		207Pb	206Pb		
				cps	cps	204	206Pb	2σ	235U	2σ	238U	2σ	ρ	206Pb	2σ	238U	2σ	
Sep 14 2023	18EM35B-46-1		ign	96273	77	1244	0.1551	0.0012	9.26	0.31	0.433	0.014	0.974	2403	13	2320	63	4
Sep 14 2023	18EM35B-47-1		ign	250491	61	4092	0.1572	0.0012	9.74	0.32	0.450	0.014	0.974	2426	13	2394	64	1
Sep 14 2023	18EM35B-48-1		ign	268670	74	3609	0.1575	0.0012	9.82	0.32	0.452	0.014	0.973	2429	13	2406	64	1
Sep 14 2023	18EM35B-49-1		ign	211152	48	4436	0.1563	0.0012	9.66	0.31	0.448	0.014	0.972	2416	13	2388	62	1
Sep 14 2023	18EM35B-50-1		ign	197542	71	2800	0.1578	0.0012	9.92	0.34	0.456	0.015	0.977	2432	12	2421	67	0
Sep 14 2023	18EM35B-51-1		ign	555649	38	14570	0.1579	0.0012	10.43	0.35	0.479	0.016	0.976	2434	12	2524	69	-4
Sep 14 2023	18EM35B-52-1		ign	103203	45	2283	0.1551	0.0012	9.47	0.32	0.443	0.015	0.972	2403	13	2364	65	2
Sep 14 2023	18EM35B-3-1	cPb	ign	769309	923	834	0.1712	0.0030	10.97	0.41	0.465	0.015	0.881	2569	29	2461	67	4
Sep 14 2023	18EM35B-6-1	cPb	ign	559416	287	1950	0.1637	0.0018	11.11	0.48	0.492	0.021	0.968	2495	18	2580	88	-3
Sep 14 2023	18EM35B-10-1	cPb	ign	2065536	1515	1363	0.1581	0.0017	9.73	0.40	0.446	0.018	0.966	2436	18	2379	78	2
Sep 14 2023	18EM35B-12-1	cPb	ign	445405	124	3583	0.1610	0.0012	10.37	0.34	0.467	0.015	0.975	2467	12	2472	66	0
Sep 14 2023	18EM35B-13-1	cPb	ign	682884	16063	43	0.4356	0.0626	20.05	3.14	0.334	0.021	0.397	4037	199	1857	100	117
Sep 14 2023	18EM35B-17-2	cPb	ign	435683	740	589	0.1856	0.0042	12.17	0.47	0.476	0.015	0.811	2704	36	2508	64	8
Sep 14 2023	18EM35B-18-1	cPb	ign	400872	435	921	0.1716	0.0029	11.05	0.41	0.467	0.015	0.887	2574	28	2472	67	4
Sep 14 2023	18EM35B-19-2	cPb	ign	443708	166	2669	0.1650	0.0014	10.57	0.35	0.465	0.015	0.968	2508	14	2461	65	2
Sep 14 2023	18EM35B-30-1	cPb	ign	543151	523	1039	0.1681	0.0022	10.69	0.37	0.461	0.015	0.925	2539	22	2445	64	4
Aug 11 2022_R	19BN51A-R21-2		ign	232251	74	3132	0.1582	0.0013	9.82	0.25	0.450	0.011	0.942	2437	14	2397	48	2
Aug 11 2022_R	19BN51A-R5-1		ign	129863	41	3173	0.1582	0.0014	10.17	0.26	0.467	0.011	0.939	2437	15	2468	49	-1
Aug 11 2022_R	19BN51A-R15-1		ign	53149	8	7074	0.1580	0.0015	9.96	0.28	0.457	0.012	0.940	2435	16	2427	53	0
Aug 11 2022_R	19BN51A-R6-1		ign	144603	46	3174	0.1577	0.0013	9.58	0.24	0.441	0.011	0.945	2432	14	2355	47	3
Aug 11 2022_R	19BN51A-R17-1		ign	143202	33	4392	0.1576	0.0014	9.76	0.25	0.449	0.011	0.940	2431	15	2392	48	2
Aug 11 2022_R	19BN51A-R3-1		ign	158610	21	7412	0.1569	0.0013	10.01	0.25	0.463	0.011	0.945	2423	14	2452	48	-1
Aug 11 2022_R	19BN51A-R6-2		ign	166103	59	2822	0.1568	0.0013	9.88	0.25	0.457	0.011	0.944	2422	14	2427	48	0
Aug 11 2022_R	19BN51A-R13-1		ign	131759	14	9355	0.1568	0.0013	9.34	0.25	0.460	0.011	0.946	2421	14	2440	48	-1
Aug 11 2022_R	19BN51A-R22-1		ign	89461	10	8690	0.1566	0.0014	9.68	0.25	0.449	0.011	0.941	2419	15	2389	48	1
Aug 11 2022_R	19BN51A-R16-1		ign	214297	4	55308	0.1562	0.0013	9.91	0.25	0.460	0.011	0.944	2415	14	2440	49	-1
Aug 11 2022_R	19BN51A-R20-2		ign	112572	34	3328	0.1560	0.0013	9.52	0.24	0.443	0.011	0.947	2412	14	2363	47	2
Aug 11 2022_R	19BN51A-R20-1		ign	113973	41	2803	0.1556	0.0013	9.63	0.24	0.449	0.011	0.943	2409	14	2392	48	1
Aug 11 2022_R	19BN51A-R11-1		ign	137538	14	10035	0.1556	0.0014	9.61	0.25	0.448	0.011	0.932	2408	16	2387	48	1
Aug 11 2022_R	19BN51A-R10-1		ign	187994	7	27242	0.1555	0.0013	9.82	0.25	0.458	0.011	0.944	2408	14	2431	48	-1
Aug 11 2022_R	19BN51A-R2-1		ign	182088	8	23141	0.1549	0.0013	9.66	0.25	0.452	0.011	0.942	2401	14	2406	48	0
Aug 11 2022_R	19BN51A-R9-1		ign	181453	20	9236	0.1544	0.0012	9.60	0.25	0.451	0.011	0.950	2396	14	2401	49	0
Aug 11 2022_R	19BN51A-R4-1		met?	253429	55	4581	0.1534	0.0013	9.61	0.24	0.454	0.011	0.944	2385	14	2415	48	-1
Aug 11 2022_R	19BN51A-R19-1		met?	259309	15	17609	0.1531	0.0012	9.52	0.24	0.451	0.011	0.949	2381	13	2401	48	-1
Aug 11 2022_R	19BN51A-R19-2		met?	242441	60	4063	0.1531	0.0013	9.54	0.24	0.452	0.011	0.941	2380	15	2405	48	-1
Aug 11 2022_R	19BN51A-R7-1		met?	171476	32	5337	0.1524	0.0012	9.55	0.24	0.455	0.011	0.946	2374	14	2417	48	-2
Aug 11 2022_R	19BN51A-R8-1	cPb	ign	165180	122	1357	0.1645	0.0031	10.17	0.31	0.449	0.011	0.791	2502	31	2389	48	5
Aug 11 2022_R	19BN51A-R1-1	mix	ign?	124579	56	2209	0.1622	0.0018	9.87	0.26	0.442	0.011	0.905	2478	19	2359	47	5
Aug 11 2022_R	19BN51A-R12-1	mix,disc	ign	71603	28	2517	0.1666	0.0024	9.64	0.33	0.420	0.013	0.905	2524	24	2260	59	12
Aug 11 2022_R	19BN51A-R14-1	cPb	ign	228081	391	583	0.1774	0.0034	11.00	0.34	0.450	0.011	0.778	2629	32	2395	48	10
Aug 11 2022_R	19BN51A-R18-1	mix	ign	75182	74	1013	0.1674	0.0021	9.63	0.28	0.417	0.011	0.900	2531	21	2249	50	13
Aug 11 2022_R	19BN51A-R21-1	cPb	ign	155875	315	495	0.1841	0.0087	11.21	0.59	0.442	0.011	0.451	2690	76	2360	47	14
Mar 1 2022	19BN154C-40-2		inhrt	356877	90	3971	0.1665	0.0013	11.02	0.37	0.480	0.016	0.975	2523	13	2527	69	0
Mar 1 2022	19BN154C-77-1		inhrt	659996	109	6074	0.1668	0.0013	10.26	0.32	0.446	0.013	0.968	2526	13	2378	59	6
Mar 1 2022	19BN154C-40-1		inhrt	156411	58	2696	0.1658	0.0012	10.11	0.35	0.442	0.015	0.976	2515	13	2362	66	7

Session	Spot ID	Screen	Class	Ratios										Dates (Ma)				Disc. %
				206Pb	204	206	207Pb		207Pb		206Pb		207Pb		206Pb			
				cps	cps	204	206Pb	2σ	235U	2σ	238U	2σ	ρ	206Pb	2σ	238U	2σ	
Mar 1 2022	19BN154C-77-2		inhrt	613362	44	13843	0.1650	0.0012	10.34	0.34	0.455	0.015	0.974	2508	12	2415	64	4
Mar 1 2022	19BN154C-95-1		inhrt	1013319	231	4394	0.1650	0.0012	10.57	0.35	0.465	0.015	0.976	2507	12	2462	66	2
Mar 1 2022	19BN154C-73-2		inhrt	1023164	156	6553	0.1647	0.0012	10.66	0.35	0.470	0.015	0.976	2504	12	2483	67	1
Mar 1 2022	19BN154C-73-1		inhrt	1356213	212	6409	0.1645	0.0012	10.57	0.34	0.466	0.015	0.973	2502	13	2468	65	1
Mar 1 2022	19BN154C-35-1		inhrt	818808	82	9936	0.1643	0.0012	10.95	0.41	0.484	0.018	0.981	2501	12	2543	76	-2
Mar 1 2022	19BN154C-21-1		inhrt	1027050	24	42379	0.1633	0.0013	10.48	0.36	0.466	0.016	0.975	2490	13	2465	69	1
Mar 1 2022	19BN154C-101-1		inhrt	946867	191	4957	0.1632	0.0012	9.99	0.32	0.444	0.014	0.974	2489	12	2368	62	5
Mar 1 2022	19BN154C-52-1		inhrt	1540548	144	10708	0.1632	0.0012	10.61	0.36	0.472	0.015	0.975	2489	13	2491	67	0
Mar 1 2022	19BN154C-34-2		inhrt	1183454	49	24274	0.1629	0.0012	10.85	0.38	0.483	0.017	0.979	2486	12	2541	72	-2
Mar 1 2022	19BN154C-34-1		inhrt	1633597	72	22826	0.1626	0.0012	10.84	0.36	0.484	0.015	0.975	2482	12	2543	67	-2
Mar 1 2022	19BN154C-21-2		inhrt	968135	10	94940	0.1625	0.0012	10.61	0.36	0.474	0.016	0.975	2481	13	2501	69	-1
Mar 1 2022	19BN154C-44-1		inhrt	1737543	75	23019	0.1622	0.0012	10.66	0.41	0.477	0.018	0.980	2479	13	2512	78	-1
Mar 1 2022	19BN154C-49-1		inhrt	1278117	159	8020	0.1620	0.0012	10.41	0.33	0.466	0.014	0.971	2476	13	2467	63	0
Mar 1 2022	19BN154C-101-2		inhrt	973406	147	6620	0.1618	0.0012	9.74	0.33	0.437	0.014	0.975	2475	12	2336	64	6
Mar 1 2022	19BN154C-18-1		inhrt	1207277	50	24343	0.1617	0.0012	10.72	0.35	0.481	0.015	0.975	2474	12	2531	66	-2
Mar 1 2022	19BN154C-71-1		ign	1452579	279	5202	0.1538	0.0013	9.33	0.33	0.440	0.015	0.971	2389	15	2352	68	2
Mar 1 2022	19BN154C-27-2		ign	1453750	233	6247	0.1535	0.0011	9.35	0.31	0.442	0.014	0.975	2386	13	2360	64	1
Mar 1 2022	19BN154C-25-1		ign	1372060	219	6255	0.1532	0.0011	9.38	0.32	0.445	0.015	0.976	2382	13	2371	66	0
Mar 1 2022	19BN154C-2-1		ign	1791448	46	38634	0.1532	0.0012	9.34	0.32	0.442	0.015	0.974	2382	13	2360	66	1
Mar 1 2022	19BN154C-5-1		ign	3437302	60	57131	0.1530	0.0011	9.99	0.35	0.474	0.016	0.977	2379	12	2501	70	-5
Mar 1 2022	19BN154C-99-1		ign	999303	67	14908	0.1529	0.0011	9.37	0.33	0.445	0.015	0.979	2379	12	2372	69	0
Mar 1 2022	19BN154C-99-2		ign	1086999	56	19359	0.1528	0.0012	9.57	0.30	0.455	0.014	0.967	2378	14	2416	62	-2
Mar 1 2022	19BN154C-96-1		ign	1360407	76	17818	0.1523	0.0011	9.03	0.31	0.430	0.015	0.978	2372	12	2306	66	3
Mar 1 2022	19BN154C-51-1		ign	1551570	84	18522	0.1522	0.0012	8.78	0.29	0.418	0.013	0.973	2371	13	2253	61	5
Mar 1 2022	19BN154C-33-1		ign	1653785	104	15916	0.1515	0.0011	9.32	0.31	0.447	0.015	0.977	2363	12	2380	65	-1
Mar 1 2022	19BN154C-12-1		ign	921112	47	19485	0.1514	0.0011	9.29	0.32	0.445	0.015	0.976	2362	12	2373	66	0
Mar 1 2022	19BN154C-53-1		ign	1736780	61	28369	0.1505	0.0011	9.13	0.29	0.440	0.014	0.973	2352	13	2351	61	0
Mar 1 2022	19BN154C-27-1		ign	1641750	165	9940	0.1491	0.0012	8.29	0.28	0.403	0.013	0.971	2336	14	2185	61	7
Mar 1 2022	19BN154C-6-1	cPb	inhrt	292835	116	2526	0.1679	0.0014	11.08	0.41	0.479	0.017	0.976	2537	13	2522	75	1
Mar 1 2022	19BN154C-62-1	cPb	inhrt	1544579	389	3968	0.1656	0.0016	10.23	0.35	0.448	0.015	0.961	2514	16	2388	66	5
Mar 1 2022	19BN154C-65-1	cPb	inhrt	1130281	408	2768	0.1679	0.0013	10.15	0.32	0.439	0.013	0.971	2537	13	2345	60	8
Mar 1 2022	19BN154C-87-1	cPb	inhrt	1236187	330	3749	0.1678	0.0014	10.64	0.38	0.460	0.016	0.972	2536	14	2441	71	4
Mar 1 2022	19BN154C-95-2	cPb	inhrt	1417817	1420	999	0.1682	0.0038	10.26	0.43	0.442	0.015	0.837	2540	38	2362	68	8
Mar 1 2022	19BN154C-95-3	mix	inhrt	1254860	288	4362	0.1579	0.0013	9.85	0.35	0.453	0.016	0.973	2434	14	2407	69	1
Mar 1 2022	19BN154C-94-1	disc,mix	inhrt	795991	94	8428	0.1636	0.0012	9.48	0.33	0.420	0.014	0.975	2493	13	2262	64	10
Mar 1 2022	19BN150A-3-1		inhrt	272715	33	8291	0.1689	0.0012	10.86	0.38	0.467	0.016	0.978	2546	12	2469	70	3
Mar 1 2022	19BN150A-85-2		inhrt	621916	79	7873	0.1678	0.0012	11.23	0.39	0.485	0.017	0.977	2536	12	2551	71	-1
Mar 1 2022	19BN150A-98-2		inhrt	796837	153	5218	0.1661	0.0013	10.83	0.34	0.473	0.015	0.968	2518	13	2497	63	1
Mar 1 2022	19BN150A-22-1		inhrt	815126	103	7915	0.1659	0.0012	10.81	0.36	0.473	0.016	0.977	2517	12	2496	68	1
Mar 1 2022	19BN150A-94-1		inhrt	976714	31	31393	0.1653	0.0012	10.77	0.35	0.473	0.015	0.974	2511	12	2495	66	1
Mar 1 2022	19BN150A-12-1		inhrt	681988	27	25524	0.1652	0.0012	10.97	0.37	0.482	0.016	0.977	2510	12	2535	69	-1
Mar 1 2022	19BN150A-37-2		inhrt	629467	59	10623	0.1651	0.0012	10.90	0.36	0.479	0.016	0.975	2509	12	2522	67	-1
Mar 1 2022	19BN150A-115-1		inhrt	987155	30	32377	0.1651	0.0012	11.05	0.39	0.486	0.017	0.978	2509	12	2552	72	-2
Mar 1 2022	19BN150A-67-1		inhrt	860076	36	23798	0.1650	0.0012	10.94	0.38	0.481	0.016	0.977	2508	12	2533	71	-1
Mar 1 2022	19BN150A-44-1		inhrt	362582	53	6786	0.1650	0.0013	10.78	0.35	0.474	0.015	0.972	2508	13	2500	65	0
Mar 1 2022	19BN150A-37-1		inhrt	886053	45	19734	0.1650	0.0012	10.96	0.39	0.482	0.017	0.978	2508	12	2535	73	-1

Session	Spot ID	Screen	Class	206Pb cps	204 cps	206 204	Ratios						Dates (Ma)				Disc. %	
							207Pb 206Pb		207Pb 235U		206Pb 238U		207Pb 206Pb		206Pb 238U			ρ
							2σ	2σ	2σ	2σ	2σ	2σ	2σ	2σ				
Mar 1 2022	19BN150A-91-1		inhrt	1207036	53	22815	0.1649	0.0012	11.03	0.37	0.485	0.016	0.975	2506	12	2551	68	-2
Mar 1 2022	19BN150A-44-2		inhrt	557179	47	11859	0.1648	0.0012	10.80	0.37	0.476	0.016	0.977	2505	12	2508	69	0
Mar 1 2022	19BN150A-24-1		inhrt	721309	34	21390	0.1647	0.0012	10.80	0.36	0.476	0.016	0.976	2505	12	2508	68	0
Mar 1 2022	19BN150A-41-1		inhrt	925092	46	20032	0.1645	0.0012	10.92	0.37	0.482	0.016	0.975	2503	13	2534	69	-1
Mar 1 2022	19BN150A-57-1		inhrt	940305	35	26944	0.1644	0.0012	10.91	0.38	0.481	0.016	0.978	2501	12	2533	71	-1
Mar 1 2022	19BN150A-9-1		inhrt	829873	57	14558	0.1643	0.0012	10.82	0.37	0.478	0.016	0.977	2500	12	2518	69	-1
Mar 1 2022	19BN150A-110-1		inhrt	1251595	76	16414	0.1642	0.0012	10.94	0.35	0.483	0.015	0.975	2499	12	2542	66	-2
Mar 1 2022	19BN150A-98-1		inhrt	985570	50	19556	0.1640	0.0012	10.84	0.38	0.480	0.016	0.978	2497	12	2527	71	-1
Mar 1 2022	19BN150A-76-1		inhrt	1051282	53	19686	0.1638	0.0012	10.86	0.37	0.481	0.016	0.977	2496	12	2532	70	-1
Mar 1 2022	19BN150A-25-1		inhrt	1402263	64	21887	0.1636	0.0012	11.28	0.38	0.501	0.017	0.978	2493	12	2616	71	-5
Mar 1 2022	19BN150A-6-1		inhrt	848368	27	30942	0.1634	0.0012	10.34	0.34	0.459	0.015	0.975	2491	12	2437	65	2
Mar 1 2022	19BN150A-57-2		inhrt	1182559	81	14559	0.1631	0.0012	10.82	0.35	0.481	0.015	0.975	2488	12	2533	66	-2
Mar 1 2022	19BN150A-67-2		inhrt	1127294	40	28090	0.1625	0.0012	10.84	0.35	0.484	0.015	0.975	2482	12	2545	67	-2
Mar 1 2022	19BN150A-7-1		inhrt	1408437	18	78279	0.1620	0.0012	10.65	0.37	0.477	0.016	0.977	2476	12	2516	70	-2
Mar 1 2022	19BN150A-23-1		ign	2065643	113	18341	0.1537	0.0011	9.82	0.32	0.464	0.015	0.975	2387	12	2455	64	-3
Mar 1 2022	19BN150A-77-1		ign	2246201	77	29098	0.1531	0.0011	10.04	0.37	0.476	0.017	0.980	2381	12	2509	74	-5
Mar 1 2022	19BN150A-53-1		ign	2081132	35	58719	0.1531	0.0012	9.71	0.33	0.460	0.015	0.973	2381	13	2440	66	-2
Mar 1 2022	19BN150A-97-1		ign	2438918	42	58079	0.1529	0.0011	9.64	0.32	0.458	0.015	0.977	2378	12	2429	66	-2
Mar 1 2022	19BN150A-24-2		ign	2260502	102	22176	0.1529	0.0011	9.98	0.31	0.474	0.014	0.973	2378	12	2500	63	-5
Mar 1 2022	19BN150A-5-1		ign	2699483	45	59388	0.1528	0.0011	10.03	0.33	0.476	0.015	0.976	2378	12	2511	66	-5
Mar 1 2022	19BN150A-68-2		ign	2289384	76	30255	0.1528	0.0011	9.77	0.33	0.464	0.015	0.978	2377	12	2457	68	-3
Mar 1 2022	19BN150A-78-1		ign	2186943	27	80369	0.1527	0.0013	9.38	0.30	0.446	0.013	0.961	2376	15	2376	60	0
Mar 1 2022	19BN150A-106-1		ign	2016362	39	51850	0.1527	0.0011	9.48	0.31	0.451	0.014	0.976	2376	12	2398	64	-1
Mar 1 2022	19BN150A-4-1	cPb	inhrt	2707526	1056	2564	0.1611	0.0019	10.78	0.38	0.485	0.016	0.940	2467	20	2551	70	-3
Mar 1 2022	19BN150A-13-1	cPb,disc	inhrt	1035021	1172	883	0.1796	0.0018	10.62	0.35	0.429	0.013	0.954	2650	16	2301	60	15
Mar 1 2022	19BN150A-42-1	cPb,disc	inhrt	526134	7524	70	0.3773	0.0033	34.19	1.17	0.657	0.022	0.967	3821	13	3257	84	17
Mar 1 2022	19BN150A-42-2	cPb	inhrt	518703	1078	481	0.1919	0.0062	13.31	0.59	0.503	0.015	0.681	2759	52	2627	65	5
Mar 1 2022	19BN150A-49-1	cPb,disc	inhrt	1131686	6407	177	0.2589	0.0357	18.60	2.74	0.521	0.027	0.349	3240	202	2705	113	20
Mar 1 2022	19BN150A-85-1	cPb	inhrt	550957	613	899	0.1808	0.0018	11.55	0.40	0.464	0.015	0.957	2660	16	2456	67	8
Mar 1 2022	19BN150A-93-1	cPb,disc	inhrt	862127	720	1197	0.1757	0.0030	9.87	0.43	0.407	0.016	0.915	2613	29	2203	73	19
Mar 1 2022	19BN150A-109-1	cpb	inhrt	687284	564	1218	0.1763	0.0025	11.43	0.41	0.471	0.015	0.915	2618	24	2486	67	5
Mar 1 2022	19BN150A-68-1	cPb,disc	ign	1623374	422	3849	0.1495	0.0020	7.96	0.32	0.386	0.015	0.942	2340	23	2106	68	11
Mar 1 2022	19BN150A-32-1	cPb	inhrt	736027	406	1815	0.1726	0.0018	11.51	0.43	0.484	0.017	0.960	2583	17	2545	74	1
Mar 1 2022	19BN150A-15-1	disc	inhrt	378821	83	4582	0.1681	0.0013	9.92	0.37	0.428	0.016	0.980	2539	13	2297	71	11
Mar 2 2022	19BN123A-27-1		inhrt	430071	88	4881	0.1670	0.0013	10.71	0.36	0.466	0.015	0.974	2528	13	2464	67	3
Mar 2 2022	19BN123A-28-1		inhrt	312248	65	4839	0.1658	0.0013	10.34	0.35	0.452	0.015	0.974	2516	13	2405	66	5
Mar 2 2022	19BN123A-18-2		inhrt	192580	72	2684	0.1655	0.0013	10.34	0.36	0.453	0.015	0.972	2512	14	2410	67	4
Mar 2 2022	19BN123A-1-1		inhrt	856494	99	8681	0.1654	0.0014	10.71	0.34	0.470	0.015	0.964	2511	14	2483	64	1
Mar 2 2022	19BN123A-8-1		inhrt	436895	128	3425	0.1651	0.0013	10.65	0.42	0.468	0.018	0.981	2508	13	2476	79	1
Mar 2 2022	19BN123A-111-1		inhrt	434943	116	3760	0.1650	0.0012	9.77	0.31	0.429	0.013	0.972	2508	12	2303	59	9
Mar 2 2022	19BN123A-30-1		inhrt	758232	55	13662	0.1647	0.0012	10.58	0.36	0.466	0.016	0.976	2504	13	2466	69	2
Mar 2 2022	19BN123A-38-1		inhrt	814427	69	11777	0.1645	0.0012	10.98	0.36	0.484	0.016	0.975	2502	12	2545	67	-2
Mar 2 2022	19BN123A-26-1		inhrt	448168	58	7749	0.1645	0.0013	10.73	0.34	0.473	0.015	0.970	2502	13	2498	63	0
Mar 2 2022	19BN123A-15-1		inhrt	908937	174	5228	0.1644	0.0012	10.63	0.34	0.469	0.015	0.973	2502	12	2480	64	1
Mar 2 2022	19BN123A-101-1		inhrt	363323	79	4586	0.1642	0.0012	10.37	0.34	0.458	0.015	0.975	2500	12	2432	65	3
Mar 2 2022	19BN123A-36-1		inhrt	611164	45	13702	0.1641	0.0012	10.41	0.33	0.460	0.014	0.972	2499	13	2440	62	2

Session	Spot ID	Screen	Class	206Pb cps	204 cps	206 204	Ratios						Dates (Ma)				Disc. %	
							207Pb 206Pb		207Pb 235U		206Pb 238U		207Pb 206Pb		206Pb 238U			p
							2σ	2σ	2σ	2σ	2σ	2σ	2σ	2σ				
Mar 2 2022	19BN123A-13-1		inhrt	789215	132	5998	0.1640	0.0012	10.48	0.37	0.464	0.016	0.977	2498	12	2456	70	2
Mar 2 2022	19BN123A-51-1		inhrt	464748	5	94839	0.1640	0.0012	9.78	0.31	0.433	0.014	0.974	2497	12	2318	61	8
Mar 2 2022	19BN123A-15-2		inhrt	971831	69	14186	0.1639	0.0012	10.94	0.36	0.485	0.016	0.975	2496	12	2547	67	-2
Mar 2 2022	19BN123A-84-1		inhrt	380200	73	5233	0.1637	0.0012	10.08	0.34	0.447	0.015	0.975	2494	12	2381	64	5
Mar 2 2022	19BN123A-101-2		inhrt	564052	76	7416	0.1636	0.0012	10.45	0.34	0.464	0.015	0.974	2493	12	2455	64	2
Mar 2 2022	19BN123A-104-1		inhrt	350116	63	5535	0.1636	0.0012	10.40	0.35	0.461	0.015	0.974	2493	13	2446	66	2
Mar 2 2022	19BN123A-106-1		inhrt	1189661	146	8170	0.1635	0.0012	10.57	0.32	0.469	0.014	0.970	2492	12	2480	60	0
Mar 2 2022	19BN123A-32-1		inhrt	776348	37	20903	0.1633	0.0012	10.74	0.37	0.477	0.016	0.977	2490	12	2516	70	-1
Mar 2 2022	19BN123A-61-1		inhrt	695442	53	13087	0.1630	0.0012	10.51	0.35	0.468	0.015	0.976	2488	12	2474	66	1
Mar 2 2022	19BN123A-70-1		inhrt	1460375	48	30738	0.1625	0.0012	10.80	0.36	0.482	0.016	0.976	2482	12	2538	68	-2
Mar 2 2022	19BN123A-18-1		inhrt	747758	81	9284	0.1618	0.0012	10.67	0.37	0.478	0.016	0.977	2475	12	2520	70	-2
Mar 2 2022	19BN123A-49-1		inhrt	1095954	48	22852	0.1617	0.0012	9.32	0.29	0.418	0.013	0.970	2474	13	2251	57	10
Mar 2 2022	19BN123A-76-1		inhrt	268588	34	7892	0.1613	0.0012	10.12	0.36	0.455	0.016	0.977	2470	13	2418	70	2
Mar 2 2022	19BN123A-37-1		inhrt	639643	56	11470	0.1590	0.0012	10.75	0.42	0.491	0.019	0.983	2445	12	2573	82	-5
Mar 2 2022	19BN123A-30-2		ign	1241690	66	18699	0.1548	0.0011	9.74	0.33	0.457	0.015	0.976	2399	13	2426	66	-1
Mar 2 2022	19BN123A-43-1		ign	1225547	30	41281	0.1545	0.0012	9.27	0.29	0.435	0.013	0.968	2396	13	2330	59	3
Mar 2 2022	19BN123A-7-2		ign	1312784	122	10753	0.1543	0.0011	9.86	0.31	0.464	0.014	0.972	2394	12	2456	62	-3
Mar 2 2022	19BN123A-99-1		ign	2275731	172	13239	0.1539	0.0011	9.71	0.31	0.458	0.014	0.974	2390	12	2430	63	-2
Mar 2 2022	19BN123A-31-1		ign	1123657	53	21347	0.1533	0.0011	9.83	0.35	0.465	0.016	0.979	2383	12	2463	71	-3
Mar 2 2022	19BN123A-97-1		ign	1443284	107	13483	0.1532	0.0011	9.66	0.31	0.457	0.014	0.974	2382	13	2428	64	-2
Mar 2 2022	19BN123A-112-1		ign	1657550	45	36856	0.1531	0.0011	9.69	0.31	0.459	0.014	0.973	2381	12	2437	63	-2
Mar 2 2022	19BN123A-80-1		ign	1832367	133	13796	0.1530	0.0011	9.66	0.33	0.458	0.015	0.977	2379	12	2432	67	-2
Mar 2 2022	19BN123A-79-1		ign	1838501	51	35745	0.1529	0.0011	9.75	0.34	0.463	0.016	0.978	2379	12	2451	69	-3
Mar 2 2022	19BN123A-37-2		ign	2294138	52	44024	0.1529	0.0011	10.00	0.33	0.474	0.015	0.975	2378	12	2503	67	-5
Mar 2 2022	19BN123A-60-1		ign	956365	55	17364	0.1527	0.0011	9.21	0.28	0.438	0.013	0.970	2377	13	2340	58	2
Mar 2 2022	19BN123A-53-1		ign	2264990	9	244933	0.1527	0.0011	9.79	0.32	0.465	0.015	0.974	2377	12	2461	64	-3
Mar 2 2022	19BN123A-88-1		ign	2268647	80	28474	0.1525	0.0011	9.82	0.32	0.467	0.015	0.974	2374	12	2472	64	-4
Mar 2 2022	19BN123A-71-1		ign	3078640	53	58621	0.1524	0.0011	9.79	0.32	0.466	0.015	0.974	2373	12	2466	65	-4
Mar 2 2022	19BN123A-91-1		ign	1371718	59	23277	0.1523	0.0011	9.76	0.32	0.465	0.015	0.975	2372	12	2462	65	-4
Mar 2 2022	19BN123A-41-1		ign	2392792	20	121534	0.1523	0.0011	9.69	0.33	0.462	0.015	0.976	2371	13	2448	67	-3
Mar 2 2022	19BN123A-78-1	disc	ign	1325221	67	19809	0.1548	0.0012	8.57	0.32	0.402	0.015	0.980	2400	13	2177	67	10
Mar 2 2022	19BN123A-108-1	disc	inhrt	971043	70	13777	0.1584	0.0012	7.36	0.24	0.337	0.011	0.970	2438	13	1873	51	30
Mar 2 2022	19BN123A-7-1	disc	inhrt	570711	135	4243	0.1637	0.0012	9.36	0.29	0.415	0.012	0.970	2495	12	2236	56	12
Mar 2 2022	19BN123A-23-1	disc	inhrt	365053	74	4943	0.1642	0.0013	9.22	0.29	0.408	0.012	0.967	2500	14	2204	57	13
Nov 18 2021	21BN52B-6-1		inhrt	334936	39	8641	0.1817	0.0014	13.51	0.45	0.540	0.017	0.973	2668	13	2782	72	-4
Nov 18 2021	21BN52B-21-1		inhrt	596933	23	25783	0.1668	0.0012	10.40	0.35	0.452	0.015	0.976	2526	13	2406	66	5
Nov 18 2021	21BN52B-1-1		inhrt	435352	30	14430	0.1663	0.0012	11.30	0.37	0.493	0.016	0.973	2520	13	2585	67	-2
Nov 18 2021	21BN52B-5-1		inhrt	311772	38	8119	0.1652	0.0012	10.59	0.34	0.465	0.015	0.973	2509	13	2463	64	2
Nov 18 2021	21BN52B-31-1		inhrt	911371	28	32496	0.1651	0.0013	10.57	0.35	0.465	0.015	0.973	2509	13	2460	66	2
Nov 18 2021	21BN52B-16-1		inhrt	868149	12	74948	0.1651	0.0012	10.82	0.37	0.476	0.016	0.976	2508	12	2508	68	0
Nov 18 2021	21BN52B-30-1		inhrt	1439876	22	65470	0.1642	0.0012	10.90	0.39	0.482	0.017	0.978	2499	12	2534	72	-1
Nov 18 2021	21BN52B-25-1		inhrt	1775206	103	17279	0.1610	0.0012	9.69	0.33	0.437	0.014	0.975	2466	13	2336	65	6
Nov 18 2021	21BN52B-28-1		inhrt	685996	7	96032	0.1591	0.0012	9.72	0.33	0.443	0.015	0.976	2446	13	2365	66	3
Nov 18 2021	21BN52B-27-1		inhrt	1909289	3	604219	0.1587	0.0012	9.66	0.33	0.442	0.015	0.975	2442	13	2358	65	4
Nov 18 2021	21BN52B-17-1		inhrt	1254371	11	117000	0.1586	0.0012	10.28	0.35	0.470	0.016	0.976	2441	13	2485	69	-2
Nov 18 2021	21BN52B-7-1		ign	619124	32	19155	0.1560	0.0012	10.08	0.32	0.469	0.015	0.971	2413	13	2477	63	-3

Session	Spot ID	Screen	Class	Ratios										Dates (Ma)				Disc. %		
				206Pb	204	206	207Pb		207Pb		206Pb		206Pb		p	207Pb			206Pb	
				cps	cps	204	206Pb	2σ	235U	2σ	238U	2σ	206Pb	2σ		238U	2σ			
Nov 18 2021	21BN52B-13-1		ign	180112	34	5321	0.1555	0.0012	8.96	0.28	0.418	0.013	0.972	2407	13	2251	58	7		
Nov 18 2021	21BN52B-4-1		ign	143538	83	1734	0.1545	0.0012	9.53	0.30	0.447	0.013	0.970	2396	13	2384	60	1		
Nov 18 2021	21BN52B-9-1		ign	441737	55	8081	0.1544	0.0011	9.46	0.31	0.444	0.014	0.974	2395	13	2370	63	1		
Nov 18 2021	21BN52B-5-3		ign	133814	49	2727	0.1543	0.0013	9.44	0.30	0.444	0.014	0.966	2395	14	2368	61	1		
Nov 18 2021	21BN52B-20-1		ign	155176	27	5830	0.1543	0.0012	8.95	0.31	0.421	0.014	0.973	2394	14	2265	65	6		
Nov 18 2021	21BN52B-23-1		ign	166164	12	14278	0.1542	0.0012	8.77	0.31	0.413	0.014	0.976	2393	13	2228	65	7		
Nov 18 2021	21BN52B-19-1		ign	210359	13	16119	0.1541	0.0012	9.21	0.33	0.434	0.015	0.978	2392	13	2322	67	3		
Nov 18 2021	21BN52B-24-1		ign	623834	18	34000	0.1541	0.0011	9.25	0.31	0.436	0.014	0.976	2392	13	2332	64	3		
Nov 18 2021	21BN52B-32-1		ign	125309	25	4967	0.1540	0.0012	8.87	0.31	0.418	0.014	0.973	2391	14	2250	65	6		
Nov 18 2021	21BN52B-6-2		ign	157571	34	4609	0.1538	0.0012	9.22	0.29	0.435	0.013	0.969	2388	13	2329	60	3		
Nov 18 2021	21BN52B-1-2		ign	403568	97	4167	0.1537	0.0011	9.32	0.30	0.440	0.014	0.973	2388	13	2350	61	2		
Nov 18 2021	21BN52B-12-1		ign	141367	20	7211	0.1536	0.0012	9.19	0.29	0.434	0.013	0.970	2386	13	2324	59	3		
Nov 18 2021	21BN52B-11-1		ign	244773	20	12188	0.1532	0.0012	9.16	0.30	0.434	0.014	0.972	2382	13	2322	61	3		
Nov 18 2021	21BN52B-28-2		ign	136881	5	25828	0.1532	0.0011	8.66	0.31	0.410	0.014	0.979	2382	13	2215	66	8		
Nov 18 2021	21BN52B-5-2		ign	125692	29	4299	0.1530	0.0012	9.03	0.29	0.428	0.013	0.968	2380	14	2297	59	4		
Nov 18 2021	21BN52B-6-3		ign	142089	32	4433	0.1529	0.0012	9.08	0.29	0.431	0.013	0.970	2378	13	2310	59	3		
Nov 18 2021	21BN52B-2-1		ign	192876	55	3509	0.1528	0.0012	9.27	0.29	0.440	0.014	0.971	2377	13	2352	60	1		
Nov 18 2021	21BN52B-18-1		ign	172079	12	14436	0.1528	0.0012	8.90	0.31	0.423	0.014	0.972	2377	14	2274	65	5		
Nov 18 2021	21BN52B-26-1		ign	184217	6	31533	0.1527	0.0012	8.71	0.30	0.414	0.014	0.975	2377	13	2322	63	6		
Nov 18 2021	21BN52B-25-2		ign	479894	34	14208	0.1526	0.0011	9.05	0.31	0.430	0.014	0.976	2375	13	2308	65	3		
Nov 18 2021	21BN52B-3-1		ign	164196	64	2580	0.1523	0.0012	9.33	0.30	0.445	0.014	0.970	2372	13	2371	62	0		
Nov 18 2021	21BN52B-14-1		ign	205222	12	17047	0.1520	0.0012	9.24	0.30	0.441	0.014	0.970	2368	13	2356	62	1		
Nov 18 2021	21BN52B-22-1		ign	529670	35	15334	0.1515	0.0011	8.90	0.30	0.426	0.014	0.977	2363	12	2287	63	3		
Nov 18 2021	21BN52B-10-1		ign	255972	14	18739	0.1515	0.0012	9.05	0.29	0.433	0.014	0.971	2363	13	2321	61	2		
Nov 18 2021	21BN52B-29-1	mix	inhrt	960990	22	44300	0.1576	0.0012	9.69	0.34	0.446	0.016	0.977	2431	13	2377	69	2		
Nov 18 2021	21BN52B-15-1	mix	inhrt	1255121	15	85207	0.1563	0.0012	10.08	0.34	0.468	0.015	0.974	2416	13	2475	66	-2		
Nov 18 2021	21BN52B-8-1	mix	inhrt	918874	34	27286	0.1557	0.0012	10.12	0.36	0.472	0.017	0.978	2409	13	2491	72	-3		
May 28 2021	19BN43B-14-1		inhrt	638137	51	12609	0.1781	0.0013	11.63	0.42	0.474	0.017	0.980	2635	12	2501	74	5		
May 28 2021	19BN43B-1-1		ign	1137556	104	10941	0.1497	0.0011	8.83	0.32	0.428	0.015	0.980	2342	12	2297	68	2		
May 28 2021	19BN43B-1-2		ign	860915	137	6291	0.1477	0.0010	8.61	0.31	0.423	0.015	0.980	2319	12	2275	67	2		
May 28 2021	19BN43B-1-3		ign	858346	45	18910	0.1483	0.0010	8.72	0.33	0.427	0.016	0.983	2326	12	2292	71	1		
May 28 2021	19BN43B-2-1		ign	977825	54	18002	0.1485	0.0011	9.39	0.44	0.459	0.021	0.986	2328	13	2435	92	-4		
May 28 2021	19BN43B-3-1		ign	1409760	89	15764	0.1473	0.0011	8.74	0.32	0.430	0.016	0.981	2315	12	2307	70	0		
May 28 2021	19BN43B-4-1		ign	1181084	72	16297	0.1467	0.0010	8.54	0.31	0.423	0.015	0.982	2308	12	2272	69	2		
May 28 2021	19BN43B-5-1		ign	1036675	59	17538	0.1477	0.0010	8.68	0.30	0.426	0.015	0.980	2319	12	2289	66	1		
May 28 2021	19BN43B-7-1		ign	1006821	54	18744	0.1475	0.0010	8.69	0.31	0.427	0.015	0.980	2317	12	2293	67	1		
May 28 2021	19BN43B-8-1		ign	951590	65	14541	0.1474	0.0011	8.66	0.31	0.426	0.015	0.979	2316	12	2288	66	1		
May 28 2021	19BN43B-10-1		ign	1228990	55	22321	0.1477	0.0010	8.71	0.31	0.428	0.015	0.981	2319	12	2297	67	1		
May 28 2021	19BN43B-11-1		ign	1061489	47	22770	0.1478	0.0010	8.85	0.34	0.434	0.017	0.983	2320	12	2326	74	0		
May 28 2021	19BN43B-12-1		ign	788727	107	7376	0.1481	0.0010	8.60	0.29	0.421	0.014	0.979	2324	12	2267	63	3		
May 28 2021	19BN43B-13-1		ign	956521	91	10560	0.1482	0.0010	8.83	0.34	0.432	0.016	0.983	2325	12	2316	74	0		
May 28 2021	19BN43B-13-2		ign	1053420	57	18447	0.1477	0.0010	8.59	0.31	0.422	0.015	0.980	2319	12	2270	66	2		
May 28 2021	19BN43B-15-1		ign	1451100	59	24637	0.1479	0.0010	8.59	0.31	0.422	0.015	0.980	2322	12	2268	67	2		
May 28 2021	19BN43B-16-1		ign	958734	72	13371	0.1485	0.0011	8.46	0.31	0.413	0.015	0.980	2329	12	2230	67	4		
May 28 2021	19BN43B-17-1		ign	1118495	43	26061	0.1480	0.0010	8.61	0.31	0.422	0.015	0.981	2323	12	2270	67	2		
May 28 2021	19BN43B-14-2	mix	ign	70553	45	1582	0.1612	0.0014	9.61	0.34	0.433	0.015	0.971	2468	14	2318	67	7		
May 28 2021	19BN43B-6-1	mix, disc	ign	1744376	96	18100	0.1371	0.0028	6.46	0.36	0.342	0.018	0.928	2191	35	1896	84	16		
May 28 2021	19BN43B-9-1	cPb	ign	348101	130	2687	0.1584	0.0013	9.50	0.40	0.435	0.018	0.980	2439	14	2329	80	5		

Session	Spot ID	Screen	Class	206Pb cps	204 cps	206 204	Ratios					Dates (Ma)				Disc. %		
							207Pb		207Pb		206Pb		207Pb		206Pb			
							206Pb	2σ	235U	2σ	238U	2σ	ρ	206Pb	2σ		238U	2σ
Oct 24 2022	19BN07E-21-1		inhrt	85925	45	1911	0.1896	0.0016	13.07	0.44	0.500	0.016	0.969	2739	14	2615	70	5
Oct 24 2022	19BN07E-4-2		ign	565659	109	5179	0.1489	0.0011	8.40	0.26	0.409	0.012	0.970	2334	13	2211	56	6
Oct 24 2022	19BN07E-26-1		ign	394669	5	81708	0.1488	0.0011	8.66	0.31	0.422	0.015	0.978	2332	13	2270	67	3
Oct 24 2022	19BN07E-24-1		ign	314040	37	8539	0.1487	0.0011	9.13	0.32	0.445	0.015	0.977	2331	13	2375	67	-2
Oct 24 2022	19BN07E-9-2		ign	631596	126	5016	0.1486	0.0011	8.84	0.28	0.431	0.013	0.972	2330	13	2312	60	1
Oct 24 2022	19BN07E-25-1		ign	416602	69	6050	0.1485	0.0011	8.81	0.31	0.430	0.015	0.978	2329	13	2307	67	1
Oct 24 2022	19BN07E-2-1		ign	357766	32	11162	0.1484	0.0012	9.21	0.32	0.450	0.015	0.974	2328	13	2395	68	-3
Oct 24 2022	19BN07E-28-1		ign	302021	22	13450	0.1484	0.0011	8.83	0.30	0.432	0.014	0.977	2328	12	2315	65	1
Oct 24 2022	19BN07E-3-2		ign	178854	13	13361	0.1482	0.0011	9.09	0.31	0.445	0.015	0.975	2325	13	2374	65	-2
Oct 24 2022	19BN07E-3-1		ign	219399	9	23922	0.1481	0.0011	8.89	0.30	0.435	0.014	0.975	2324	13	2330	64	0
Oct 24 2022	19BN07E-31-1		ign	577363	141	4105	0.1479	0.0011	8.63	0.28	0.423	0.013	0.974	2322	13	2276	60	2
Oct 24 2022	19BN07E-35-2		ign	378673	61	6248	0.1478	0.0011	8.58	0.27	0.421	0.013	0.973	2320	12	2267	58	2
Oct 24 2022	19BN07E-36-1		ign	441105	68	6500	0.1478	0.0012	8.67	0.28	0.426	0.013	0.970	2320	13	2286	60	1
Oct 24 2022	19BN07E-17-1		ign	331758	48	6883	0.1477	0.0011	8.18	0.26	0.402	0.013	0.973	2319	13	2178	57	6
Oct 24 2022	19BN07E-35-1		ign	462340	41	11142	0.1477	0.0011	8.88	0.30	0.436	0.015	0.977	2319	13	2334	65	-1
Oct 24 2022	19BN07E-35-3		ign	369244	54	6809	0.1476	0.0011	8.90	0.31	0.437	0.015	0.976	2318	13	2338	66	-1
Oct 24 2022	19BN07E-18-1		ign	1113980	60	18533	0.1474	0.0011	9.08	0.30	0.447	0.015	0.976	2316	12	2381	64	-3
Oct 24 2022	19BN07E-19-2		ign	633021	46	13637	0.1474	0.0011	8.83	0.31	0.435	0.015	0.978	2316	12	2327	66	0
Oct 24 2022	19BN07E-4-1		ign	1020826	13	79974	0.1472	0.0011	8.80	0.29	0.434	0.014	0.975	2314	12	2323	62	0
Oct 24 2022	19BN07E-23-1		ign	447851	46	9717	0.1471	0.0011	8.63	0.27	0.426	0.013	0.972	2312	13	2287	58	1
Oct 24 2022	19BN07E-36-3		ign	684878	27	25327	0.1471	0.0011	8.89	0.28	0.439	0.013	0.970	2312	13	2344	60	-1
Oct 24 2022	19BN07E-20-1		ign	1707583	64	26484	0.1470	0.0011	9.02	0.29	0.445	0.014	0.975	2312	12	2375	63	-3
Oct 24 2022	19BN07E-8-1		ign	732975	44	16509	0.1469	0.0011	8.94	0.31	0.441	0.015	0.977	2310	13	2357	67	-2
Oct 24 2022	19BN07E-10-1		ign	887432	46	19093	0.1469	0.0011	8.57	0.28	0.423	0.013	0.974	2310	13	2275	61	2
Oct 24 2022	19BN07E-30-1		ign	475186	71	6739	0.1469	0.0011	8.64	0.29	0.427	0.014	0.974	2310	13	2292	63	1
Oct 24 2022	19BN07E-22-1		ign	1382506	44	31411	0.1468	0.0011	9.10	0.31	0.450	0.015	0.977	2309	12	2393	65	-4
Oct 24 2022	19BN07E-32-1		ign	1501647	102	14752	0.1468	0.0011	9.17	0.31	0.453	0.015	0.974	2309	13	2410	66	-4
Oct 24 2022	19BN07E-19-1		ign	548896	77	7174	0.1468	0.0011	8.11	0.28	0.401	0.013	0.977	2309	13	2172	61	6
Oct 24 2022	19BN07E-34-1		ign	1105433	62	17839	0.1466	0.0011	8.63	0.29	0.427	0.014	0.975	2307	13	2293	63	1
Oct 24 2022	19BN07E-6-1		ign	716096	25	28146	0.1466	0.0011	9.55	0.31	0.472	0.015	0.975	2307	12	2494	65	-7
Oct 24 2022	19BN07E-12-2		ign	1001229	63	15972	0.1464	0.0011	8.95	0.29	0.443	0.014	0.975	2305	12	2366	62	-3
Oct 24 2022	19BN07E-7-1		ign	334181	36	9163	0.1464	0.0011	7.77	0.28	0.385	0.013	0.978	2305	13	2101	62	10
Oct 24 2022	19BN07E-33-1		ign	530205	69	7674	0.1463	0.0011	8.40	0.30	0.417	0.014	0.978	2304	13	2245	65	3
Oct 24 2022	19BN07E-16-1		ign	490269	76	6456	0.1463	0.0011	7.83	0.25	0.388	0.012	0.972	2303	13	2114	56	9
Oct 24 2022	19BN07E-12-1		ign	1018763	36	28563	0.1462	0.0011	8.86	0.29	0.440	0.014	0.975	2301	13	2349	64	-2
Oct 24 2022	19BN07E-5-1		ign	893153	19	46983	0.1462	0.0011	9.07	0.33	0.450	0.016	0.979	2301	12	2397	70	-4
Oct 24 2022	19BN07E-29-2		ign	1267084	67	19052	0.1462	0.0011	8.88	0.27	0.441	0.013	0.968	2301	13	2355	59	-2
Oct 24 2022	19BN07E-14-1		ign	536950	67	7992	0.1461	0.0011	8.93	0.30	0.444	0.015	0.975	2301	13	2367	65	-3
Oct 24 2022	19BN07E-11-1		ign	1245002	91	13680	0.1461	0.0011	9.02	0.30	0.448	0.014	0.975	2301	13	2387	63	-4
Oct 24 2022	19BN07E-34-2		ign	942964	55	17070	0.1458	0.0011	8.39	0.27	0.418	0.013	0.972	2297	13	2251	58	2
Oct 24 2022	19BN07E-15-1		ign	1224699	62	19734	0.1457	0.0011	8.97	0.29	0.447	0.014	0.974	2297	13	2380	63	-4
Oct 24 2022	19BN07E-36-2		ign	336813	26	13179	0.1457	0.0012	8.07	0.28	0.402	0.014	0.973	2296	14	2178	62	5
Oct 24 2022	19BN07E-29-1		ign	1002884	20	50598	0.1449	0.0011	7.96	0.31	0.399	0.015	0.982	2286	12	2163	70	6
Oct 24 2022	19BN07E-1-1	cPb	ign	437241	989	442	0.1691	0.0068	10.41	0.68	0.447	0.023	0.792	2548	66	2381	103	7
Oct 24 2022	19BN07E-9-1	cPb	ign	947079	334	2839	0.1506	0.0016	8.87	0.29	0.427	0.013	0.947	2353	18	2294	60	3
Oct 24 2022	19BN07E-13-1	disc,mix	ign	609259	52	11624	0.1446	0.0011	7.41	0.29	0.372	0.014	0.980	2283	13	2038	66	12
Oct 24 2022	19BN07E-27-1	mix	ign	2559797	69	37321	0.1407	0.0020	7.93	0.31	0.409	0.015	0.927	2236	25	2211	67	1

Session	Spot ID	Screen	Class	Ratios										Dates (Ma)				Disc. %
				206Pb	204	206	207Pb		207Pb		206Pb		p	207Pb		206Pb		
				cps	cps	204	206Pb	2σ	235U	2σ	238U	2σ		206Pb	2σ	238U	2σ	
Aug 9 2022	18EM17E-21-1		ign	577639	86	6748	0.1490	0.0012	8.97	0.26	0.437	0.012	0.964	2334	13	2336	55	0
Aug 9 2022	18EM17E-10-1		ign	670870	10	69055	0.1490	0.0012	9.42	0.31	0.459	0.015	0.971	2333	13	2434	64	-4
Aug 9 2022	18EM17E-25-1		ign	562178	63	8869	0.1489	0.0011	8.89	0.25	0.433	0.012	0.962	2333	13	2320	52	1
Aug 9 2022	18EM17E-2-1		ign	524345	70	7529	0.1489	0.0011	9.45	0.35	0.461	0.016	0.978	2332	13	2442	72	-4
Aug 9 2022	18EM17E-19-1		ign	531453	27	19448	0.1488	0.0012	9.17	0.27	0.447	0.013	0.964	2332	13	2381	56	-2
Aug 9 2022	18EM17E-11-2		ign	432308	24	17842	0.1485	0.0011	8.95	0.25	0.437	0.012	0.962	2327	13	2338	53	0
Aug 9 2022	18EM17E-23-1		ign	582472	80	7296	0.1484	0.0011	8.90	0.27	0.435	0.013	0.967	2326	13	2329	57	0
Aug 9 2022	18EM17E-12-1		ign	550652	21	26605	0.1484	0.0012	9.20	0.31	0.450	0.015	0.972	2326	13	2395	64	-3
Aug 9 2022	18EM17E-24-1		ign	455264	28	16472	0.1482	0.0011	8.99	0.27	0.440	0.013	0.968	2325	13	2350	57	-1
Aug 9 2022	18EM17E-14-1		ign	480598	8	56829	0.1482	0.0012	8.95	0.28	0.438	0.013	0.966	2324	14	2343	59	-1
Aug 9 2022	18EM17E-18-1		ign	494724	26	19291	0.1481	0.0011	9.12	0.28	0.447	0.013	0.967	2324	13	2381	58	-2
Aug 9 2022	18EM17E-26-1		ign	611270	33	18516	0.1481	0.0011	9.01	0.28	0.442	0.013	0.969	2323	13	2358	59	-1
Aug 9 2022	18EM17E-20-1		ign	689863	62	11208	0.1480	0.0011	9.24	0.27	0.453	0.013	0.967	2323	13	2408	58	-4
Aug 9 2022	18EM17E-24-2		ign	489509	29	16917	0.1480	0.0011	9.09	0.27	0.446	0.013	0.965	2322	13	2376	56	-2
Aug 9 2022	18EM17E-13-1		ign	713941	37	19230	0.1480	0.0011	9.26	0.27	0.454	0.013	0.966	2322	13	2412	57	-4
Aug 9 2022	18EM17E-11-1		ign	740534	23	32342	0.1480	0.0011	9.30	0.26	0.456	0.012	0.962	2322	13	2423	54	-4
Aug 9 2022	18EM17E-1-1		ign	583091	48	12218	0.1479	0.0011	9.15	0.28	0.449	0.013	0.968	2321	13	2389	59	-3
Aug 9 2022	18EM17E-12-2		ign	538331	44	12341	0.1479	0.0012	9.19	0.30	0.451	0.014	0.970	2321	13	2399	62	-3
Aug 9 2022	18EM17E-16-1		ign	937124	46	20269	0.1478	0.0012	9.14	0.27	0.449	0.013	0.965	2320	13	2389	58	-3
Aug 9 2022	18EM17E-15-1		ign	723086	49	14625	0.1478	0.0012	8.72	0.25	0.428	0.012	0.957	2320	14	2297	53	1
Aug 9 2022	18EM17E-5-2		ign	500287	40	12455	0.1477	0.0011	9.24	0.29	0.454	0.014	0.969	2319	13	2413	61	-4
Aug 9 2022	18EM17E-5-1		ign	369638	52	7116	0.1475	0.0013	9.06	0.27	0.446	0.013	0.956	2316	15	2377	57	-3
Aug 9 2022	18EM17E-8-1		ign	538084	35	15198	0.1474	0.0011	9.08	0.27	0.447	0.013	0.966	2315	13	2383	57	-3
Aug 9 2022	18EM17E-18-2		ign	674573	39	17213	0.1473	0.0011	9.14	0.27	0.450	0.013	0.966	2315	13	2395	56	-3
Aug 9 2022	18EM17E-7-1		ign	515652	28	18519	0.1473	0.0011	9.17	0.28	0.452	0.013	0.968	2314	13	2403	59	-4
Aug 9 2022	18EM17E-17-1		ign	652043	24	26705	0.1473	0.0011	8.98	0.29	0.442	0.014	0.970	2314	13	2361	61	-2
Aug 9 2022	18EM17E-22-1		ign	675970	59	11413	0.1471	0.0011	8.89	0.27	0.438	0.013	0.968	2312	13	2343	58	-1
Aug 9 2022	18EM17E-2-2		ign	655649	40	16519	0.1468	0.0011	9.08	0.27	0.449	0.013	0.967	2309	13	2390	58	-3
Aug 9 2022	18EM17E-4-1		ign	599205	30	19959	0.1467	0.0011	8.95	0.27	0.443	0.013	0.968	2307	13	2363	58	-2
Aug 9 2022	18EM17E-6-1		ign	772696	31	25193	0.1462	0.0011	8.90	0.26	0.442	0.013	0.965	2302	13	2359	56	-2
Aug 9 2022	18EM17E-9-1	cPb	ign	421650	114	3702	0.1498	0.0012	9.19	0.28	0.445	0.013	0.961	2343	14	2374	57	-1
Aug 9 2022	18EM17E-3-1	cPb	ign	617068	1889	327	0.1880	0.0106	12.70	0.86	0.490	0.019	0.563	2724	90	2572	81	6
Aug 9 2022	18BN31C-6-1		ign	634230	154	4123	0.1494	0.0012	8.88	0.26	0.431	0.012	0.958	2339	14	2310	53	1
Aug 9 2022	18BN31C-5-1		ign	533423	86	6213	0.1491	0.0012	8.78	0.26	0.427	0.012	0.964	2334	13	2294	55	2
Aug 9 2022	18BN31C-25-1		ign	451087	101	4449	0.1487	0.0012	8.81	0.27	0.430	0.013	0.966	2330	13	2306	56	1
Aug 9 2022	18BN31C-2-1		ign	604511	52	11644	0.1487	0.0012	8.93	0.30	0.436	0.014	0.972	2330	13	2332	63	0
Aug 9 2022	18BN31C-11-1		ign	657027	73	8967	0.1482	0.0012	8.89	0.28	0.435	0.013	0.967	2324	14	2329	60	0
Aug 9 2022	18BN31C-26-1		ign	773274	107	7206	0.1480	0.0011	8.99	0.27	0.441	0.013	0.966	2323	13	2354	56	-1
Aug 9 2022	18BN31C-24-1		ign	432255	81	5320	0.1478	0.0012	8.42	0.26	0.413	0.012	0.967	2320	13	2229	56	4
Aug 9 2022	18BN31C-4-1		ign	770356	55	14068	0.1477	0.0011	8.89	0.28	0.437	0.013	0.970	2318	13	2336	59	-1
Aug 9 2022	18BN31C-19-1		ign	630056	34	18519	0.1476	0.0011	9.01	0.28	0.443	0.013	0.969	2318	13	2364	59	-2
Aug 9 2022	18BN31C-17-1		ign	577687	23	24741	0.1476	0.0011	8.91	0.27	0.438	0.013	0.967	2318	13	2342	57	-1
Aug 9 2022	18BN31C-23-1		ign	1042628	107	9717	0.1476	0.0011	8.85	0.28	0.435	0.013	0.969	2317	13	2330	59	-1
Aug 9 2022	18BN31C-17-2		ign	544574	41	13415	0.1475	0.0011	9.08	0.28	0.446	0.014	0.970	2317	13	2380	60	-3
Aug 9 2022	18BN31C-20-1		ign	660237	48	13807	0.1474	0.0011	8.91	0.27	0.439	0.013	0.967	2315	13	2346	56	-1
Aug 9 2022	18BN31C-10-1		ign	873834	49	17913	0.1474	0.0011	9.01	0.27	0.444	0.013	0.967	2315	13	2367	57	-2
Aug 9 2022	18BN31C-15-1		ign	772473	20	38526	0.1473	0.0011	8.95	0.26	0.441	0.013	0.966	2314	13	2354	56	-2
Aug 9 2022	18BN31C-28-1		ign	830583	62	13469	0.1472	0.0011	9.03	0.26	0.445	0.013	0.965	2313	13	2373	56	-3
Aug 9 2022	18BN31C-21-1		ign	719480	55	13169	0.1472	0.0011	9.35	0.28	0.461	0.013	0.968	2313	13	2444	59	-5
Aug 9 2022	18BN31C-17-3		ign	834831	56	14820	0.1471	0.0011	9.16	0.29	0.452	0.014	0.971	2312	13	2403	62	-4

Session	Spot ID	Screen	Class	Ratios									Dates (Ma)				Disc. %	
				206Pb	204	206	207Pb		207Pb		206Pb		p	207Pb		206Pb		
				cps	cps	204	206Pb	2σ	235U	2σ	238U	2σ		206Pb	2σ	238U		2σ
Aug 9 2022	18BN31C-27-1		ign	987566	109	9024	0.1471	0.0012	9.02	0.27	0.445	0.013	0.964	2312	14	2372	57	-3
Aug 9 2022	18BN31C-25-2		ign	761510	124	6154	0.1470	0.0012	8.79	0.31	0.434	0.015	0.973	2311	14	2323	66	-1
Aug 9 2022	18BN31C-25-3		ign	888005	86	10301	0.1470	0.0011	9.03	0.29	0.446	0.014	0.970	2311	13	2376	61	-3
Aug 9 2022	18BN31C-8-1		ign	820617	79	10397	0.1470	0.0011	9.00	0.26	0.445	0.013	0.965	2310	13	2371	56	-3
Aug 9 2022	18BN31C-13-1		ign	796463	58	13619	0.1469	0.0012	8.69	0.26	0.429	0.012	0.963	2310	14	2301	56	0
Aug 9 2022	18BN31C-15-2		ign	802043	21	37702	0.1469	0.0011	8.91	0.27	0.440	0.013	0.968	2310	13	2351	57	-2
Aug 9 2022	18BN31C-20-2		ign	781208	27	28874	0.1469	0.0011	9.10	0.28	0.449	0.013	0.969	2309	13	2393	58	-3
Aug 9 2022	18BN31C-29-1		ign	976900	46	21369	0.1467	0.0011	8.99	0.27	0.445	0.013	0.968	2307	13	2371	58	-3
Aug 9 2022	18BN31C-18-1		ign	777251	66	11825	0.1466	0.0011	8.66	0.25	0.429	0.012	0.966	2306	13	2299	55	0
Aug 9 2022	18BN31C-27-2		ign	1093264	50	21966	0.1466	0.0011	9.26	0.27	0.458	0.013	0.967	2305	13	2433	58	-5
Aug 9 2022	18BN31C-12-1		ign	930323	80	11621	0.1461	0.0011	8.65	0.27	0.430	0.013	0.969	2300	13	2304	59	0
Aug 9 2022	18BN31C-3-1	cPb	ign	529238	272	1944	0.1533	0.0023	9.08	0.38	0.430	0.017	0.931	2382	26	2306	75	3
Aug 9 2022	18BN31C-9-1	cPb	ign	914231	605	1510	0.1482	0.0045	7.96	0.47	0.390	0.020	0.859	2325	51	2121	92	10
Aug 9 2022	18BN31C-12-2	cPb	ign	648473	570	1139	0.1588	0.0020	9.54	0.31	0.436	0.013	0.921	2442	21	2331	58	5
Aug 9 2022	18BN31C-16-1	cPb	ign	511507	377	1356	0.1586	0.0026	9.69	0.35	0.444	0.014	0.891	2440	27	2366	63	3
Aug 9 2022	18BN31C-22-1	cPb	ign	527156	164	3219	0.1494	0.0012	8.89	0.28	0.432	0.013	0.970	2339	13	2314	60	1
Aug 9 2022	18BN31C-7-1	cPb	ign	464751	237	1962	0.1528	0.0014	9.57	0.30	0.454	0.014	0.953	2377	16	2414	60	-2
Aug 9 2022	18002E-6-1		ign	619862	80	7727	0.1485	0.0011	8.84	0.27	0.432	0.013	0.967	2328	13	2314	56	1
Aug 9 2022	18002E-2-1		ign	803423	52	15310	0.1479	0.0011	9.06	0.28	0.444	0.013	0.969	2321	13	2371	60	-2
Aug 9 2022	18002E-1-1		ign	1012139	49	20705	0.1479	0.0011	9.00	0.28	0.442	0.013	0.969	2321	13	2359	59	-2
Aug 9 2022	18002E-22-2		ign	595050	48	12476	0.1476	0.0011	9.01	0.28	0.443	0.014	0.969	2318	13	2364	60	-2
Aug 9 2022	18002E-10-1		ign	718709	110	6532	0.1475	0.0012	8.94	0.27	0.440	0.013	0.965	2317	13	2350	57	-1
Aug 9 2022	18002E-21-1		ign	852123	55	15409	0.1475	0.0012	8.99	0.28	0.442	0.013	0.967	2316	14	2361	59	-2
Aug 9 2022	18002E-8-1		ign	1003611	63	15853	0.1474	0.0012	8.85	0.27	0.436	0.013	0.967	2315	13	2331	57	-1
Aug 9 2022	18002E-11-1		ign	720755	68	10628	0.1474	0.0011	8.92	0.28	0.439	0.013	0.970	2315	13	2348	59	-1
Aug 9 2022	18002E-22-1		ign	769281	38	20222	0.1473	0.0011	9.01	0.28	0.444	0.013	0.968	2315	13	2367	58	-2
Aug 9 2022	18002E-12-1		ign	978701	79	12402	0.1473	0.0011	8.97	0.28	0.442	0.014	0.970	2314	13	2360	60	-2
Aug 9 2022	18002E-4-1		ign	824300	15	54154	0.1473	0.0011	9.08	0.28	0.448	0.014	0.970	2314	13	2384	60	-3
Aug 9 2022	18002E-24-1		ign	795563	90	8868	0.1472	0.0011	8.79	0.25	0.433	0.012	0.962	2313	13	2320	53	0
Aug 9 2022	18002E-18-1		ign	1025332	61	16676	0.1471	0.0011	8.84	0.27	0.436	0.013	0.968	2312	13	2333	58	-1
Aug 9 2022	18002E-4-2		ign	632509	50	12531	0.1471	0.0011	9.04	0.28	0.446	0.013	0.968	2311	13	2379	59	-3
Aug 9 2022	18002E-26-1		ign	1080934	40	27346	0.1470	0.0012	9.01	0.26	0.445	0.013	0.963	2311	14	2371	56	-3
Aug 9 2022	18002E-23-2		ign	1017069	70	14462	0.1470	0.0011	9.06	0.27	0.447	0.013	0.967	2311	13	2383	57	-3
Aug 9 2022	18002E-3-1		ign	1162971	11	108229	0.1470	0.0011	9.10	0.27	0.449	0.013	0.968	2311	13	2391	58	-3
Aug 9 2022	18002E-16-1		ign	1037199	75	13794	0.1470	0.0011	9.01	0.27	0.445	0.013	0.966	2311	13	2371	56	-3
Aug 9 2022	18002E-15-1		ign	676192	48	14048	0.1470	0.0011	9.07	0.30	0.448	0.015	0.974	2310	13	2386	64	-3
Aug 9 2022	18002E-14-1		ign	928956	93	10023	0.1470	0.0011	8.91	0.29	0.440	0.014	0.970	2310	13	2351	61	-2
Aug 9 2022	18002E-20-1		ign	625565	78	8006	0.1470	0.0011	9.02	0.27	0.445	0.013	0.967	2310	13	2374	58	-3
Aug 9 2022	18002E-23-1		ign	970770	55	17609	0.1469	0.0011	9.04	0.28	0.447	0.013	0.969	2310	13	2380	60	-3
Aug 9 2022	18002E-25-1		ign	909317	89	10254	0.1469	0.0011	9.01	0.29	0.445	0.014	0.970	2309	13	2373	61	-3
Aug 9 2022	18002E-29-1		ign	587970	39	15180	0.1469	0.0011	8.94	0.27	0.442	0.013	0.968	2309	13	2358	58	-2
Aug 9 2022	18002E-7-1		ign	1050613	72	14646	0.1468	0.0011	9.12	0.29	0.451	0.014	0.971	2308	13	2399	61	-4
Aug 9 2022	18002E-27-2		ign	980027	30	32768	0.1468	0.0011	8.97	0.27	0.443	0.013	0.966	2308	13	2365	56	-2
Aug 9 2022	18002E-19-1		ign	850454	72	11866	0.1468	0.0011	8.83	0.27	0.437	0.013	0.969	2308	13	2336	58	-1
Aug 9 2022	18002E-27-1		ign	1293714	48	26953	0.1463	0.0011	9.03	0.27	0.448	0.013	0.966	2302	13	2387	56	-4
Aug 9 2022	18002E-17-1		ign	750120	80	9413	0.1462	0.0012	8.67	0.26	0.430	0.012	0.958	2301	15	2308	55	0
Aug 9 2022	18002E-5-1	mix	ign	568466	44	13032	0.1473	0.0012	9.71	0.27	0.478	0.013	0.959	2314	14	2519	56	-8
Aug 9 2022	18002E-28-1	cPb	ign	1206628	38	32025	0.1448	0.0017	8.64	0.27	0.433	0.013	0.926	2285	20	2319	56	-1

Session	Spot ID	Screen	Class	Ratios										Dates (Ma)				Disc. %
				206Pb cps	204 cps	206 204	207Pb 206Pb		207Pb 235U		206Pb		ρ	207Pb		206Pb		
							206Pb	2 σ	235U	2 σ	238U	2 σ		206Pb	2 σ	238U	2 σ	
Aug 8 2022	18BN20C-1-1		ign	132434	72	1852	0.1487	0.0013	8.93	0.30	0.436	0.014	0.967	2331	15	2333	63	0
Aug 8 2022	18BN20C-2-1		ign	197885	88	2241	0.1487	0.0012	8.76	0.29	0.428	0.014	0.971	2331	13	2295	61	2
Aug 8 2022	18BN20C-3-1		ign	168926	89	1890	0.1483	0.0012	8.59	0.26	0.420	0.012	0.964	2327	14	2262	55	3
Aug 8 2022	18BN20C-4-1		ign	289611	54	5336	0.1476	0.0011	8.62	0.26	0.424	0.012	0.966	2319	13	2278	55	2
Aug 8 2022	18BN20C-5-1		ign	253108	67	3759	0.1486	0.0011	8.79	0.28	0.429	0.013	0.970	2330	13	2302	60	1
Aug 8 2022	18BN20C-6-1		ign	207267	52	3981	0.1477	0.0012	8.81	0.29	0.433	0.014	0.971	2320	13	2319	62	0
Aug 8 2022	18BN20C-7-1		ign	175072	65	2708	0.1482	0.0012	8.64	0.26	0.423	0.012	0.967	2325	13	2274	56	2
Aug 8 2022	18BN20C-9-1		ign	178744	74	2405	0.1485	0.0012	8.63	0.26	0.422	0.012	0.963	2329	14	2268	55	3
Aug 8 2022	18BN20C-10-1		ign	196988	51	3873	0.1483	0.0012	8.73	0.26	0.427	0.012	0.963	2326	14	2293	55	1
Aug 8 2022	18BN20C-11-1		ign	196511	29	6729	0.1481	0.0011	8.76	0.29	0.429	0.014	0.973	2324	13	2303	62	1
Aug 8 2022	18BN20C-12-1		ign	144997	31	4688	0.1484	0.0012	8.72	0.27	0.427	0.013	0.965	2327	14	2290	58	2
Aug 8 2022	18BN20C-13-1		ign	179427	49	3685	0.1477	0.0012	8.81	0.30	0.433	0.014	0.971	2319	14	2318	63	0
Aug 8 2022	18BN20C-14-1		ign	247287	99	2492	0.1475	0.0012	8.79	0.27	0.432	0.013	0.966	2318	14	2316	58	0
Aug 8 2022	18BN20C-15-1		ign	426607	89	4820	0.1477	0.0011	8.88	0.28	0.436	0.013	0.969	2319	13	2334	59	-1
Aug 8 2022	18BN20C-16-1		ign	172166	78	2220	0.1479	0.0011	8.79	0.29	0.431	0.014	0.971	2322	13	2312	61	0
Aug 8 2022	18BN20C-17-1		ign	320205	94	3398	0.1474	0.0011	8.73	0.27	0.430	0.013	0.969	2316	13	2304	58	1
Aug 8 2022	18BN20C-19-1		ign	254816	73	3503	0.1476	0.0012	8.97	0.30	0.441	0.015	0.973	2319	13	2355	65	-2
Aug 8 2022	18BN20C-20-1		ign	233262	52	4463	0.1474	0.0012	8.87	0.29	0.436	0.014	0.972	2316	13	2335	62	-1
Aug 8 2022	18BN20C-21-1		ign	240446	57	4248	0.1478	0.0012	8.92	0.30	0.438	0.014	0.973	2321	13	2342	64	-1
Aug 8 2022	18BN20C-22-1		ign	540004	97	5564	0.1481	0.0011	8.87	0.26	0.434	0.012	0.966	2325	13	2326	56	0
Aug 8 2022	18BN20C-23-1		ign	243348	28	8725	0.1480	0.0012	8.77	0.27	0.430	0.013	0.965	2323	14	2306	56	1
Aug 8 2022	18BN20C-24-1		ign	173608	29	5983	0.1484	0.0012	8.73	0.27	0.427	0.013	0.966	2327	14	2292	57	2
Aug 8 2022	18BN20C-25-1		ign	227640	17	13025	0.1476	0.0011	8.70	0.26	0.428	0.012	0.965	2318	13	2295	55	1
Aug 8 2022	18BN20C-26-1		ign	163897	37	4429	0.1476	0.0012	8.75	0.27	0.430	0.013	0.967	2319	13	2307	58	1
Aug 8 2022	18BN20C-27-1		ign	212873	11	18650	0.1477	0.0012	8.81	0.27	0.433	0.013	0.967	2320	13	2318	58	0
Aug 8 2022	18BN20C-28-1		ign	161703	7	24313	0.1478	0.0012	8.75	0.28	0.429	0.013	0.968	2321	14	2303	60	1
Aug 8 2022	18BN20C-29-1		ign	142186	11	13438	0.1485	0.0013	8.74	0.27	0.427	0.013	0.962	2329	14	2292	57	2
Aug 8 2022	18BN20C-30-1		ign	233527	6	41434	0.1480	0.0012	8.70	0.27	0.427	0.013	0.968	2322	13	2291	58	1
Aug 8 2022	18BN20C-31-1		ign	189591	16	11573	0.1478	0.0012	8.69	0.28	0.427	0.013	0.970	2321	13	2291	60	1
Aug 8 2022	18BN20C-8-1	mix	ign	165234	79	2090	0.1515	0.0015	8.45	0.26	0.405	0.012	0.947	2362	16	2190	53	8
Aug 8 2022	18BN20C-18-1	cPb	ign	155400	106	1467	0.1480	0.0012	8.82	0.29	0.432	0.014	0.970	2323	14	2316	62	0
Oct 24 2022	21BN48D-1-1		ign	537816	22	24246	0.1483	0.0012	8.39	0.34	0.410	0.016	0.979	2326	14	2216	74	5
Oct 24 2022	21BN48D-18-1		ign	247690	94	2635	0.1475	0.0011	9.24	0.30	0.455	0.015	0.974	2318	13	2415	64	-4
Oct 24 2022	21BN48D-4-2		ign	1189961	33	36059	0.1470	0.0011	9.03	0.32	0.446	0.016	0.980	2311	12	2377	69	-3
Oct 24 2022	21BN48D-22-1		ign	498542	36	13848	0.1470	0.0011	8.74	0.31	0.431	0.015	0.979	2311	13	2312	67	0
Oct 24 2022	21BN48D-10-1		ign	618054	70	8829	0.1470	0.0011	8.85	0.36	0.437	0.017	0.984	2311	12	2338	77	-1
Oct 24 2022	21BN48D-17-1		ign	574379	66	8703	0.1469	0.0011	8.60	0.29	0.425	0.014	0.975	2310	13	2283	62	1
Oct 24 2022	21BN48D-16-2		ign	411831	54	7627	0.1469	0.0011	8.83	0.31	0.436	0.015	0.976	2310	13	2333	66	-1
Oct 24 2022	21BN48D-6-1		ign	1313964	50	26279	0.1466	0.0011	8.71	0.28	0.431	0.013	0.975	2307	12	2309	60	0
Oct 24 2022	21BN48D-5-1		ign	948930	31	30611	0.1466	0.0011	8.87	0.31	0.439	0.015	0.978	2307	12	2346	66	-2
Oct 24 2022	21BN48D-3-2		ign	658491	13	50653	0.1465	0.0011	8.71	0.29	0.431	0.014	0.977	2305	12	2311	63	0
Oct 24 2022	21BN48D-9-1		ign	1332920	56	23802	0.1465	0.0011	8.64	0.30	0.428	0.015	0.979	2305	12	2297	66	0
Oct 24 2022	21BN48D-2-1		ign	1326292	60	22105	0.1464	0.0011	8.93	0.29	0.442	0.014	0.972	2305	13	2361	63	-2
Oct 24 2022	21BN48D-20-1		ign	1275330	117	10900	0.1464	0.0011	8.66	0.28	0.429	0.014	0.975	2304	12	2303	61	0
Oct 24 2022	21BN48D-22-2		ign	608648	139	4379	0.1463	0.0011	7.75	0.26	0.384	0.013	0.977	2303	12	2097	59	10
Oct 24 2022	21BN48D-13-1		ign	725519	65	11105	0.1462	0.0011	8.84	0.30	0.439	0.015	0.975	2302	13	2345	65	-2
Oct 24 2022	21BN48D-23-1		ign	1059880	44	24088	0.1462	0.0011	8.73	0.29	0.433	0.014	0.975	2302	13	2321	63	-1
Oct 24 2022	21BN48D-17-2		ign	488391	73	6690	0.1461	0.0011	8.10	0.29	0.402	0.014	0.976	2301	13	2178	64	6
Oct 24 2022	21BN48D-16-1		ign	623124	64	9736	0.1461	0.0011	8.46	0.28	0.420	0.014	0.975	2301	13	2262	61	2
Oct 24 2022	21BN48D-12-1		ign	1090340	68	16034	0.1460	0.0011	8.86	0.28	0.440	0.014	0.974	2300	12	2351	61	-2

Session	Spot ID	Screen	Class	206Pb cps	204 cps	206 204	Ratios						Dates (Ma)				Disc. %					
							207Pb		207Pb		206Pb		207Pb		206Pb			p	207Pb	206Pb	207Pb	206Pb
							206Pb	2σ	235U	2σ	238U	2σ	206Pb	2σ	206Pb	2σ						
Oct 24 2022	21BN48D-22-3		ign	420885	34	12379	0.1460	0.0011	8.58	0.34	0.426	0.017	0.982	2300	13	2288	74	0				
Oct 24 2022	21BN48D-15-1		ign	1267079	62	20437	0.1458	0.0011	8.88	0.30	0.442	0.015	0.976	2298	12	2359	65	-3				
Oct 24 2022	21BN48D-11-1		ign	964417	74	13033	0.1457	0.0011	8.74	0.29	0.435	0.014	0.974	2296	13	2329	62	-1				
Oct 24 2022	21BN48D-24-1		ign	1434007	42	34143	0.1457	0.0011	8.73	0.30	0.435	0.014	0.977	2296	12	2329	64	-1				
Oct 24 2022	21BN48D-19-1		ign	710524	106	6703	0.1448	0.0011	8.03	0.29	0.402	0.014	0.979	2285	13	2180	65	5				
Oct 24 2022	21BN48D-8-1		ign	939813	78	12049	0.1437	0.0011	7.96	0.27	0.402	0.013	0.975	2273	13	2177	62	4				
Oct 24 2022	21BN48D-14-1		ign	940304	67	14119	0.1427	0.0010	7.73	0.25	0.393	0.012	0.974	2260	13	2136	58	6				
Oct 24 2022	21BN48D-4-1	mix,cPb.	ign	986876	196	5035	0.1485	0.0014	9.17	0.32	0.448	0.015	0.964	2329	16	2386	67	-2				
Oct 24 2022	21BN48D-7-1	mix,disc	ign	1390676	79	17603	0.1442	0.0013	8.43	0.27	0.424	0.013	0.961	2278	15	2279	60	0				
Oct 24 2022	21BN48D-7-2	mix,disc	ign	1118934	75	14919	0.1356	0.0029	6.79	0.34	0.363	0.016	0.899	2172	37	1997	76	9				
Oct 24 2022	21BN48D-3-1	mix,disc	ign	1336197	60	22270	0.1249	0.0028	5.14	0.31	0.299	0.017	0.932	2028	39	1685	83	20				
Oct 24 2022	21BN48D-21-1	cPb,disc	ign	1072405	350	3064	0.1426	0.0012	7.00	0.37	0.356	0.019	0.986	2258	15	1964	88	15				
May 28 2021	19BN168A-25-1		inhrt?	430417	104	4143	0.1608	0.0012	10.11	0.37	0.456	0.016	0.979	2464	13	2424	72	2				
May 28 2021	19BN168A-5-1		inhrt?	1333827	218	6132	0.1455	0.0021	6.43	0.37	0.321	0.018	0.968	2294	24	1793	87	28				
May 28 2021	19BN168A-1-1		ign	3802981	369	10299	0.1222	0.0010	5.12	0.21	0.304	0.012	0.979	1989	15	1711	61	16				
May 28 2021	19BN168A-10-2		ign	1504152	89	16967	0.1427	0.0019	7.46	0.29	0.379	0.014	0.941	2261	22	2074	64	9				
May 28 2021	19BN168A-11-1		ign	2394194	355	6745	0.1103	0.0010	3.93	0.15	0.258	0.010	0.970	1804	17	1482	49	22				
May 28 2021	19BN168A-12-1		ign	1465004	97	15149	0.1482	0.0010	9.15	0.34	0.448	0.016	0.982	2325	12	2386	73	-3				
May 28 2021	19BN168A-13-1		ign	3176884	579	5491	0.1204	0.0011	4.14	0.15	0.250	0.009	0.968	1962	16	1437	44	37				
May 28 2021	19BN168A-14-1		ign	2341770	256	9157	0.1145	0.0010	4.03	0.13	0.256	0.008	0.966	1872	15	1467	41	28				
May 28 2021	19BN168A-16-1		ign	1258909	96	13077	0.1466	0.0014	7.94	0.25	0.393	0.012	0.955	2307	16	2135	55	8				
May 28 2021	19BN168A-17-1		ign	1890570	239	7908	0.1277	0.0030	5.30	0.29	0.301	0.015	0.907	2066	40	1697	74	22				
May 28 2021	19BN168A-18-1		ign	2720924	404	6734	0.1309	0.0012	6.19	0.25	0.343	0.014	0.972	2110	17	1902	65	11				
May 28 2021	19BN168A-19-1		ign	6376839	1183	5389	0.1503	0.0010	9.12	0.31	0.440	0.014	0.978	2349	12	2352	64	0				
May 28 2021	19BN168A-2-1		ign	1454298	138	10535	0.1467	0.0015	8.67	0.29	0.429	0.014	0.951	2308	18	2301	61	0				
May 28 2021	19BN168A-20-1		ign	798744	1	605763	0.1482	0.0010	8.73	0.30	0.427	0.014	0.979	2325	12	2294	65	1				
May 28 2021	19BN168A-22-1		ign	1652946	117	14156	0.1442	0.0012	8.64	0.31	0.435	0.015	0.970	2278	15	2327	67	-2				
May 28 2021	19BN168A-23-1		ign	863888	133	6490	0.1429	0.0011	7.88	0.32	0.400	0.016	0.982	2263	13	2170	73	4				
May 28 2021	19BN168A-24-1		ign	2353723	320	7362	0.1221	0.0012	4.74	0.16	0.281	0.009	0.955	1988	18	1598	46	24				
May 28 2021	19BN168A-26-1		ign	1368251	108	12702	0.1265	0.0009	4.98	0.16	0.286	0.009	0.975	2051	13	1619	46	27				
May 28 2021	19BN168A-27-1		ign	1386179	110	12602	0.1423	0.0020	7.42	0.41	0.379	0.020	0.967	2255	24	2069	93	9				
May 28 2021	19BN168A-28-1		ign	3401063	233	14628	0.1436	0.0010	7.94	0.28	0.401	0.014	0.981	2271	12	2174	65	4				
May 28 2021	19BN168A-3-1		ign	1857461	376	4940	0.0937	0.0010	2.54	0.10	0.197	0.007	0.957	1503	21	1159	39	30				
May 28 2021	19BN168A-3-2		ign	2030397	346	5863	0.1024	0.0009	3.11	0.10	0.220	0.007	0.964	1668	16	1283	35	30				
May 28 2021	19BN168A-4-1		ign	2662523	540	4931	0.1112	0.0011	3.68	0.13	0.240	0.008	0.959	1820	18	1388	43	31				
May 28 2021	19BN168A-5-2		ign	2254921	379	5943	0.1162	0.0009	4.38	0.14	0.273	0.009	0.970	1899	14	1559	44	22				
May 28 2021	19BN168A-6-1		ign	2121676	241	8785	0.1199	0.0011	4.60	0.17	0.278	0.010	0.966	1954	17	1583	50	23				
May 28 2021	19BN168A-9-1		ign	1882755	240	7849	0.1230	0.0009	4.63	0.18	0.273	0.011	0.984	2000	13	1557	54	28				
May 28 2021	19BN168A-4-2	cPb	ign	2222335	3264	681	0.1341	0.0051	5.67	0.34	0.307	0.014	0.772	2153	65	1724	70	25				
May 28 2021	19BN168A-7-1	cPb	ign	1150182	722	1593	0.1408	0.0010	6.64	0.35	0.342	0.018	0.990	2237	13	1898	86	18				
May 28 2021	19BN168A-8-1	cPb	ign	3004543	832	3612	0.1342	0.0010	5.16	0.17	0.279	0.009	0.977	2153	13	1587	46	36				
May 28 2021	19BN168A-10-1	cPb	ign	1396684	740	1888	0.1567	0.0016	9.82	0.36	0.455	0.016	0.960	2420	17	2417	71	0				
May 28 2021	19BN168A-15-1	cPb	ign	4458008	1261	3536	0.1176	0.0009	4.73	0.18	0.292	0.011	0.981	1921	13	1650	54	16				
May 28 2021	19BN168A-21-1	cPb	ign	1222956	365	3349	0.1369	0.0012	5.52	0.38	0.293	0.020	0.992	2188	15	1655	98	32				

Table E-3. Whole-rock Sm-Nd isotope data.

Sample ID	Sm ppm	Nd ppm	$\frac{147\text{Sm}}{144\text{Nd}}$	$\frac{143\text{Nd}}{144\text{Nd}} (0)$	2SE	Age (Ma)	2 σ	$\frac{143\text{Nd}}{144\text{Nd}} (i)$	$\epsilon\text{Nd}(i)$	T_{DM} (Ga)
18EM35B	0.565	6.56	0.05207	0.510051	0.000012	2432	6	0.509216	-5.3	2.92
19BN32A	0.711	7.70	0.05580	0.510147	0.000012	2432		0.509253	-4.6	2.89
19BN51A	9.390	84.16	0.06746	0.510392	0.000007	2420	6	0.509316	-3.7	2.87
19BN123A	2.722	21.44	0.07676	0.510722	0.000010	2382	7	0.509517	-0.7	2.70
19BN150A	6.901	50.66	0.08235	0.510760	0.000007	2379	7	0.509468	-1.7	2.77
19BN154C	2.984	25.33	0.07124	0.510558	0.000008	2374	9	0.509444	-2.4	2.77
18BN20C	20.99	158.0	0.08034	0.510366	0.000007	2323	6	0.509136	-9.7	3.17
19BN43B	15.56	85.53	0.10997	0.510809	0.000009	2322	6	0.509127	-9.9	3.43
18BN17E	15.22	109.9	0.08370	0.510540	0.000009	2321	6	0.509260	-7.3	3.05
TX08-038	8.157	43.38	0.11371	0.510820	0.000009	2320		0.509082	-10.8	3.54
TX08-036	12.04	80.06	0.09093	0.510542	0.000010	2320		0.509152	-9.5	3.23
17-13A	13.15	89.36	0.08896	0.510496	0.000008	2320		0.509136	-9.8	3.24
17-13B	12.46	98.98	0.07610	0.510480	0.000010	2320		0.509317	-6.2	2.95
17-13C	13.89	100.4	0.08362	0.510434	0.000011	2320		0.509156	-9.4	3.18
21BN35A	13.63	103.6	0.07953	0.510612	0.000006	2320		0.509396	-4.7	2.88
17-12A	13.96	107.5	0.07853	0.510599	0.000010	2320		0.509399	-4.6	2.87
19BN168A	7.046	48.50	0.08785	0.510409	0.000007	2316	25	0.509068	-11.2	3.31
18BN18C	13.28	98.93	0.08119	0.510468	0.000011	2316	6	0.509229	-8.0	3.08
18BN31C	15.09	112.2	0.08131	0.510596	0.000008	2316	6	0.509356	-5.6	2.94
19BN07E	18.06	103.3	0.10570	0.510773	0.000013	2314	6	0.509161	-9.4	3.35
18-002E	16.35	104.5	0.09463	0.510610	0.000008	2312	6	0.509168	-9.3	3.24
18BN16A	12.74	89.31	0.08627	0.510437	0.000010	2320		0.509118	-10.1	3.24
18BC37A	16.74	113.1	0.08947	0.510497	0.000008	2320		0.509129	-9.8	3.25
21BN48D	17.67	120.8	0.08840	0.510691	0.000009	2305	6	0.509349	-6.0	2.99

$^{143}\text{Nd}/^{144}\text{Nd}(i)$ and $\epsilon\text{Nd}(i)$ calculated using the decay constant of Lugmair and Marti (1978).

$\epsilon\text{Nd}(i)$ values calculated with the CHUR values of Bouvier et al. (2008).

T_{DM} calculated from the linear depleted mantle model of Goldstein et al. (1984).

Ages in *italics* are assumed.

Some of these data were published in Neil et al. (2023)/chapter 2, but have been reproduced here for clarity.

Table E-4. Whole-rock major- and trace-element data.

	ca. 2.43 Ga leucotrochjemitite		ca. 2.42 & 2.38 Ga leucogranites			
	18EM35B	19BN32A	19BN51A	19BN150A	19BN123A	19BN154C
ICP-OES (wt.%)						
SiO ₂	75.89	70.94	75.08	75.96	76.65	74.69
Al ₂ O ₃	14.35	16.32	13.35	13.54	12.60	13.57
FeO(t)	0.95	1.86	1.54	0.55	1.38	1.35
MnO	0.024	0.035	0.026	0.011	0.024	0.021
MgO	0.52	0.79	0.58	0.15	0.37	0.34
CaO	3.28	2.63	1.74	0.54	0.68	1.38
Na ₂ O	4.39	5.18	2.63	3.04	2.74	2.68
K ₂ O	0.47	2.04	4.79	6.11	5.34	5.74
TiO ₂	0.127	0.159	0.215	0.063	0.178	0.188
P ₂ O ₅	0.01	0.05	0.04	0.02	0.04	0.03
LOI	0.67	0.47	0.92	0.76	0.71	0.81
Total	99.05	98.25	98.70	99.97	100.5	100.0
ICP-MS (ppm)						
La	19.10	23.91	151.88	63.82	37.81	41.60
Ce	26.35	31.75	269.02	128.49	68.20	78.89
Pr	2.269	2.736	26.992	14.594	7.230	8.299
Nd	6.41	7.92	86.10	50.08	23.80	26.68
Sm	0.57	0.77	9.44	7.08	3.01	3.16
Eu	0.898	0.974	1.402	0.753	1.421	0.845
Gd	0.255	0.332	4.489	3.537	1.592	1.543
Tb	0.027	0.038	0.376	0.341	0.172	0.160
Dy	0.14	0.16	1.34	1.32	0.76	0.63
Ho	0.033	0.032	0.184	0.196	0.144	0.106
Er	0.103	0.079	0.378	0.421	0.373	0.260
Tm	0.0191	0.0123	0.0510	0.0557	0.0562	0.0400
Yb	0.155	0.080	0.350	0.357	0.372	0.255
Lu	0.026	0.015	0.052	0.063	0.068	0.046
Ba	328.3	1694.7	1954.7	1004.9	2803.3	462.4
Th	0.12	0.09	59.29	18.43	6.81	31.86
Nb	0.93	0.81	3.39	3.91	4.73	4.01
Y	1.05	0.79	5.04	4.85	4.10	3.12
Hf	4.87	1.04	6.61	4.72	4.76	3.13
U	0.24	0.07	1.71	1.41	0.56	0.86
Pb	13.73	22.56	33.51	101.95	15.62	27.20
Rb	11.3	25.3	100.1	162.4	109.6	162.1
Cs	0.15	0.44	0.42	0.54	0.16	0.51
Sr	610.2	424.0	269.3	199.6	295.6	230.0
Sc	1.21	2.32	3.46	1.07	0.97	1.22
Zr	189.7	41.4	243.1	144.0	165.3	100.2
XRF (ppm)						
Rb	12.6	25.5	101.8	169.7	114.8	168.3
Sr	612	423	262	198	289	224
Y	3	1	5	4	4	3
Zr	200	43	227	136	147	102
V	9	20	20	5	12	17
Ni	6	5	2	<2	<2	<2
Cr	7	15	<2	<2	<2	<2
Ga	14.9	17.6	15.8	14.4	13.1	13.1
Nb	1.1	1.0	4.2	3.7	5.3	4.1
Cu	1	22	5	6	3	<2
Zn	14	33	30	60	25	20
Ba	320	1675	1915	978	2692	458
La	17	22	149	62	40	40
Ce	27	27	289	144	96	84
U	1.4	0.0	1.5	0.9	0.7	0.8
Th	0.7	1.9	61.9	19.1	6.6	31.8
Sc	2	1	3	2	<2	<2
Pb	14	23	28	97	15	25

Major elements are normalised to 100%, loss on ignition (LOI) excluded. Totals are reported as measured, with all Fe as Fe₂O₃.

ICP-OES major-element data from Actlabs. ICP-MS trace-element data from Washington State University.

XRF trace-element data from Franklin & Marshall College.

Analyses below detection limit indicated with "<".

ca. 2.32–2.31 Ga biotite granites

	18BN17E	18-002E	17-12A	18BN16A	18BN31C	17-13B	17-13A	19BC37A	21BN35A	17-13C
ICP-OES (wt.%)										
SiO ₂	69.73	70.11	70.19	70.47	70.83	71.11	71.23	71.39	71.63	71.76
Al ₂ O ₃	14.67	14.57	14.75	15.38	14.55	14.75	14.57	14.13	14.30	14.30
FeO(t)	3.52	3.30	2.74	2.72	2.80	2.51	2.79	2.99	2.80	2.71
MnO	0.039	0.040	0.039	0.022	0.032	0.031	0.035	0.044	0.031	0.035
MgO	0.85	0.76	1.26	0.61	0.78	0.58	0.64	0.57	0.80	0.68
CaO	1.54	1.80	1.47	1.24	1.57	1.77	1.55	1.61	1.78	1.61
Na ₂ O	3.13	2.94	3.22	3.29	2.88	2.84	2.93	3.26	2.69	2.52
K ₂ O	5.76	5.77	5.55	5.77	5.95	5.93	5.73	5.45	5.44	5.87
TiO ₂	0.600	0.563	0.620	0.403	0.486	0.398	0.425	0.444	0.434	0.433
P ₂ O ₅	0.16	0.15	0.17	0.10	0.11	0.09	0.10	0.12	0.10	0.09
LOI	1.17	1.39	1.35	0.00	1.26	0.96	1.36	0.00	1.10	1.15
Total	100.3	98.24	98.27	99.32	98.81	98.42	98.23	99.67	99.99	99.21
ICP-MS (ppm)										
La	171.70	161.71	157.77	160.45	170.34	170.44	154.65	186.86	179.26	177.15
Ce	339.43	306.88	324.52	287.86	319.47	308.05	283.61	357.55	345.39	323.49
Pr	35.851	32.555	34.182	29.837	33.536	31.769	29.139	37.340	36.329	33.081
Nd	116.07	107.82	112.39	96.72	109.52	100.33	93.80	120.62	116.37	105.49
Sm	16.17	17.63	14.77	13.88	15.24	12.82	13.83	18.04	15.03	14.63
Eu	1.551	1.520	1.767	1.261	1.459	1.410	1.212	1.344	1.478	1.377
Gd	10.094	13.305	7.897	9.114	9.731	7.317	9.664	13.064	8.589	9.288
Tb	1.304	1.937	0.951	1.146	1.303	0.836	1.293	1.856	1.063	1.128
Dy	6.24	10.18	4.44	5.30	6.64	3.69	6.32	9.90	5.19	5.10
Ho	1.09	1.83	0.75	0.92	1.21	0.62	1.11	1.88	0.90	0.86
Er	2.66	4.59	1.88	2.05	3.02	1.50	2.56	4.89	2.16	1.99
Tm	0.3663	0.6187	0.2610	0.2539	0.4088	0.2078	0.3310	0.6762	0.2904	0.2485
Yb	2.099	3.317	1.488	1.384	2.284	1.161	1.692	3.965	1.632	1.438
Lu	0.287	0.434	0.199	0.198	0.321	0.181	0.220	0.536	0.241	0.217
Ba	2003.1	2028.4	2120.0	2383.0	1820.8	2047.5	2013.2	1736.3	1506.3	2195.5
Th	72.81	81.91	34.01	68.22	46.91	55.79	71.23	110.84	57.77	63.81
Nb	17.21	20.59	12.05	8.35	13.51	7.28	11.06	22.55	10.45	9.74
Y	30.28	48.63	19.75	22.94	32.39	16.46	28.12	51.20	23.38	22.24
Hf	14.51	13.36	13.25	10.54	10.58	8.53	10.31	13.47	9.96	10.73
U	1.97	2.49	1.26	0.93	1.45	1.18	1.41	4.58	1.27	1.47
Pb	26.73	33.15	19.99	16.08	32.19	31.53	36.49	58.97	18.74	31.57
Rb	190.2	186.1	137.0	171.4	163.8	176.2	178.0	230.7	179.9	148.8
Cs	0.42	0.46	0.26	0.43	0.52	0.49	0.40	0.35	0.56	0.47
Sr	227.6	230.0	325.6	254.2	281.2	264.9	199.7	163.4	286.7	246.7
Sc	3.91	5.38	4.36	1.76	4.80	6.07	3.27	4.25	5.56	4.42
Zr	589.3	505.6	567.3	393.9	417.4	343.1	391.3	500.1	385.3	414.7
XRF (ppm)										
Rb	193.2	191.0	137.3	174.4	163.6	179.0	175.2	237.6	183.5	151.6
Sr	220	227	308	262	272	257	184	170	285	237
Y	29.2	45.9	16.8	22	30.6	16.2	25.5	50.5	20.9	21
Zr	495	436	496	397	335	309	328	512	355	357
V	41	34	36	28	29	25	25	29	34	25
Ni	6	6	7	6	4	4	4	4	4	5
Cr	<2	6	7	11	<2	<2	<2	12	4	3
Ga	20.1	19.9	15.4	19.3	18.0	17.9	17.7	20.7	17.9	17.3
Nb	15.9	18.9	11.9	8.4	13.0	7.3	10.1	22.6	10.4	9.4
Cu	8	6	17	5	12	4	4	5	5	5
Zn	42	45	42	26	40	34	41	49	38	37
Ba	1984	1954	1928	2368	1800	2005	1891	1723	1482	2112
La	209	180	167	159	186	205	166	185	183	203
Ce	408	317	322	287	339	388	304	349	340	362
U	1.4	2.4	1.1	<0.5	0.7	<0.5	1.4	3.5	<0.5	1.6
Th	77.8	85.4	35.2	64	47.2	58.2	73.3	110.2	59.5	69.2
Sc	3	5	3	1	4	4	2	3	4	4
Pb	21	26	19	14	26	25	27	51	16	26

ca. 2.32–2.31 Ga biotite granites

	18BN20C	18BN18C	TX08-036	21BN48D	19BN43B	21BN39A	19BN07E	19BN168A	TX08-038
ICP-OES (wt.%)									
SiO ₂	72.10	72.97	73.00	73.08	73.33	73.60	73.87	74.09	75.50
Al ₂ O ₃	14.27	13.94	13.81	14.04	13.77	13.92	13.64	13.87	13.04
FeO(t)	2.85	2.27	2.74	2.26	2.20	2.41	2.26	1.75	1.75
MnO	0.038	0.027	0.031	0.035	0.031	0.040	0.022	0.022	0.025
MgO	0.59	0.49	0.89	0.63	0.35	0.47	0.39	0.30	0.29
CaO	0.96	0.95	0.54	1.19	1.36	0.88	0.81	1.02	0.73
Na ₂ O	2.89	2.86	2.84	3.47	2.99	2.88	3.14	3.10	3.00
K ₂ O	5.82	6.04	5.75	4.84	5.64	5.46	5.62	5.67	5.52
TiO ₂	0.390	0.375	0.331	0.364	0.276	0.297	0.221	0.150	0.149
P ₂ O ₅	0.09	0.07	0.07	0.09	0.05	0.05	0.04	0.04	0.01
LOI	1.41	1.11	1.19	1.16	0.61	0.88	0.88	0.74	0.70
Total	99.90	99.84	100.19	98.89	100.0	99.74	99.21	100.37	98.62
ICP-MS (ppm)									
La	292.83	173.93	133.89	188.41	116.92	116.21	154.30	89.34	60.30
Ce	527.36	328.66	257.81	366.02	232.99	210.95	299.09	155.65	137.27
Pr	53.974	32.863	26.684	38.912	25.630	21.707	33.079	15.622	14.004
Nd	168.28	103.85	84.71	126.00	87.03	71.14	111.19	49.32	46.03
Sm	22.61	14.07	13.05	18.43	15.86	11.26	19.55	7.30	8.59
Eu	1.594	1.023	0.841	1.601	0.968	0.921	0.923	0.732	0.496
Gd	13.533	8.503	8.256	12.241	12.628	8.993	14.435	4.129	6.258
Tb	1.577	1.001	1.081	1.685	1.889	1.383	1.951	0.457	0.966
Dy	7.35	4.71	5.04	8.80	9.90	7.78	9.76	1.99	5.07
Ho	1.24	0.79	0.87	1.59	1.81	1.59	1.78	0.33	0.95
Er	3.06	1.93	2.15	4.16	4.50	4.51	4.74	0.80	2.66
Tm	0.4173	0.2662	0.2958	0.5951	0.6143	0.6892	0.7043	0.1081	0.4129
Yb	2.439	1.610	1.770	3.420	3.356	4.323	4.269	0.695	2.544
Lu	0.354	0.255	0.290	0.477	0.471	0.642	0.672	0.110	0.395
Ba	1648.5	1437.7	1460.1	1273.3	1111.3	1358.9	774.0	868.1	592.3
Th	100.44	69.14	90.59	86.95	121.75	55.67	125.92	79.63	94.85
Nb	9.40	11.72	12.63	21.85	20.87	19.94	23.68	4.58	19.42
Y	33.45	21.08	24.05	43.52	48.87	47.57	50.98	9.15	25.20
Hf	12.33	10.53	7.38	9.69	8.94	7.63	8.66	6.46	5.12
U	1.92	1.57	4.82	6.37	11.25	5.47	10.77	6.46	8.29
Pb	35.26	23.36	12.06	35.71	53.30	27.96	25.19	30.98	37.77
Rb	125.2	169.8	180.4	118.6	244.7	211.8	195.0	134.4	246.9
Cs	0.27	0.34	0.26	0.20	1.22	0.80	0.20	0.37	0.67
Sr	216.6	166.4	99.6	365.9	148.3	165.8	113.0	119.9	59.0
Sc	2.42	3.47	3.57	4.67	2.94	4.73	4.03	2.93	3.45
Zr	458.3	378.2	269.0	356.9	294.6	264.5	261.4	200.7	148.1
XRF (ppm)									
Rb	130.6	174.3	185.9	120.7	252.1	215.5	200.4	134.4	256
Sr	211	164	98	353	146	162	108	113	58
Y	33.2	20.8	24.2	42.9	50.7	46.2	49.8	8.4	24.8
Zr	430	340	285	339	295	256	271	198	159
V	25	20	26	24	15	19	10	15	8
Ni	3	3	6	3	3	4	<2	<2	<2
Cr	<2	<2	<2	<2	<2	<2	<2	<2	<2
Ga	19.2	17.3	18.4	16.5	20.2	20.7	19.9	21.3	19.2
Nb	9.3	10.1	10.9	21.6	19.1	18.2	21.4	4.0	16.4
Cu	12	3	12	7	10	<2	<2	<2	7
Zn	35	26	35	37	33	34	23	20	25
Ba	1506	1410	1366	1179	1106	1310	726	823	579
La	307	206	143	209	130	127	159	88	66
Ce	557	390	288	394	276	232	309	162	157
U	1.4	1.9	5.5	6.0	11.7	5.7	11.5	8.1	8.8
Th	106.1	74.3	97.6	93.4	128.6	56.3	132.2	80.5	102.3
Sc	2	3	2	4	2	5	3	3	4
Pb	30	19	11	34	45	26	24	27	33

Table E-5. LA-ICPMS zircon trace-element data. Concentrations in ppm.

Session	Mar 20 2024																
Sample ID	19BN126B														19BN154A		
Spot ID	3-1	5-1	5-2	8-1	10-1	11-1	12-1	13-1	15-1	17-1	18-1	20-1	24-1	25-1	1-1	4-1	
Class	ign																
P	791	627	847	342	468	348	1340	241	734	250	295	279	353	308	271	359	
2SE	48	42	20	25	57	18	114	38	94	24	25	15	47	19	36	69	
Ca					181									224			
2SE					115									70			
Ti	3.25	4.01	5.41	7.00	2.79	4.1	5.57	1.82	3.8	4.54	4.07	2.24	7.4	5.73	6.6	11.8	
2SE	0.87	0.86	0.70	0.73	0.54	1.3	0.71	0.81	1.4	0.90	0.58	0.66	1.8	0.88	1.0	5.3	
La	0.58	0.198	0.043	3.48	0.92	0.178	0.027	0.061	0.22	0.278	0.24	0.133	3.15	8.7	1.53	0.95	
2SE	0.12	0.053	0.035	0.94	0.33	0.062	0.010	0.037	0.15	0.100	0.11	0.035	0.67	2.4	0.55	0.38	
Ce	9.48	5.48	3.49	30.2	10.7	9.5	1.47	9.0	4.54	12.3	24.2	8.87	37.8	52.3	31.6	52.7	
2SE	0.88	0.44	0.32	4.8	1.7	2.1	0.38	1.9	0.69	2.5	3.8	0.78	5.8	9.3	3.8	12.8	
Pr	0.80	0.494	0.169	5.7	0.90	0.197	0.070	0.164	0.26	0.63	0.53	0.115	4.88	5.8	3.26	1.46	
2SE	0.17	0.084	0.053	1.4	0.32	0.071	0.013	0.081	0.12	0.21	0.16	0.029	0.81	1.1	0.98	0.26	
Nd	6.8	6.51	2.42	42.0	4.6	1.84	1.39	2.4	2.29	6.7	7.3	0.86	38.0	41.2	27.3	21.5	
2SE	1.4	0.86	0.42	9.4	1.5	0.60	0.24	1.0	0.74	2.1	1.9	0.21	5.9	9.4	6.4	4.8	
Sm	7.4	10.4	4.45	27.5	4.10	4.5	3.62	3.3	3.1	8.6	8.2	1.85	31.7	20.8	17.8	30.4	
2SE	1.2	1.1	0.35	4.2	0.89	1.1	0.50	1.2	1.0	2.3	1.7	0.29	3.6	3.5	2.1	7.2	
Eu	0.77	1.26	0.482	3.07	0.54	0.57	0.202	0.57	0.23	1.82	2.84	0.384	5.88	4.22	6.32	6.4	
2SE	0.10	0.17	0.071	0.45	0.13	0.19	0.034	0.21	0.11	0.50	0.60	0.057	0.94	0.77	0.71	1.8	
Gd	26.6	41.3	25.2	54.6	13.8	20.9	22.7	13.4	17.1	26.0	31.4	10.29	82.0	50.5	56.4	120	
2SE	2.8	4.2	1.1	9.8	1.0	4.1	2.3	4.0	1.7	6.7	6.3	0.85	7.5	7.7	9.8	26	
Tb	8.13	11.7	8.16	12.2	4.67	7.2	7.93	3.8	5.88	7.1	8.5	3.61	19.3	11.6	14.9	33.3	
2SE	0.45	1.1	0.36	3.4	0.23	1.2	0.64	1.0	0.28	1.7	1.7	0.19	1.4	1.8	2.9	6.3	
Dy	90.3	121	101.6	122	57.0	80	97.5	48	68.0	73	89	43.6	189	119	156	350	
2SE	3.2	12	4.2	39	2.7	12	6.9	12	6.2	16	16	1.6	16	19	31	63	
Ho	34.33	42.0	40.5	43.0	22.5	30.7	38.5	18.4	26.8	26.3	31.4	17.25	64.7	42.4	55	121	
2SE	0.85	4.0	1.7	13.9	1.1	4.7	2.5	4.4	2.3	5.5	5.6	0.59	5.1	6.2	11	19	
Er	165.3	181	195.3	192	115.7	147	188	89	131	123	144	83.1	278	191	250	525	
2SE	5.8	17	6.3	60	6.3	21	12	20	10	25	25	2.7	23	27	48	82	
Tm	32.8	33.8	38.9	37.0	24.3	29.5	38.4	18.7	27.0	25.0	29.5	17.85	52.6	37.5	51.0	102	
2SE	1.1	3.1	1.0	10.8	1.2	4.4	2.1	3.9	1.3	4.8	4.9	0.47	4.2	5.0	9.7	16	
Yb	302	296	361.5	327	237	275	351	178	251	235	279	168.2	446	336	474	890	
2SE	10	28	8.2	91	12	44	17	36	16	43	46	4.2	33	41	86	129	
Lu	62.1	58.7	75.2	66.0	51.9	55.4	74.3	35.9	54.5	49.0	59.3	36.0	88.3	68.1	100	175	
2SE	2.5	5.4	1.8	17.5	2.7	7.8	4.0	6.1	3.0	8.6	9.6	1.0	6.6	7.8	18	26	
Hf	9316	7051	7355	8743	8367	8457	8694	8031	7536	7329	7039	6742	9202	8270	7485	8051	
2SE	452	188	225	195	397	459	419	355	358	194	203	235	508	309	262	652	
Th	91.3	89.6	74.3	109	62.3	98	41.2	46	44.8	85	135	60.4	182	115	360	761	
2SE	5.0	9.5	2.5	38	3.4	17	4.3	10	3.3	18	24	3.5	31	18	91	171	
U	272	173	216.6	213	244	236	173.2	118	155	141	127	152.7	337	191	297	714	
2SE	19	16	9.5	46	12	24	9.0	13	13	13	17	4.0	39	17	52	108	
Th/U	0.34	0.52	0.34	0.51	0.26	0.42	0.24	0.39	0.29	0.60	1.06	0.40	0.54	0.60	1.21	1.07	
Ti-in-Zr	650	667	691	713	639	668	694	607	662	677	668	622	718	696	708	762	
Ti-in-Zr (corr)	720	737	761	783	709	738	764	677	732	747	738	692	788	766	778	832	
Ti-in-Zr (corr2)																	
Date (Ma)	U-Pb	2485	2492	2496	2480	2456	2497	2497	2488	2502	2501	2486	2478	2507	2512	2491	
2σ	scrn	12	12	12	12	14	12	13	12	12	13	12	12	12	15	15	

Spots labeled after the closest U-Pb analysis. Spots labeled with "a" or "b" indicate multiple trace-element analysis associated with one U-Pb analysis.

Date (Ma) is the 207Pb/206Pb date from the closest U-Pb analysis. "U-Pb scrn" indicates that the associated U-Pb data were screened.

Class: analysis classified as igneous (ign) or inherited (inhrt).

For sample 18EM35B: ign1 = domains with fine-scale zoning; ign2 = domains with broad/no zoning. See Ch5 text for further explanation.

No Ce data for Oct 28 2021 session. Analyses below detection limit left blank.

Ti-in-Zr: Ti-in-zircon temperature calculated assuming a SiO2=a TiO2=1.

Ti-in-Zr (corr): Ti-in-zircon temperature calculated assuming a SiO2=a TiO2=1, plus 70°C (Schiller and Finger, 2019).

Ti-in-Zr (corr2): For samples 19BN123A, 19BN150A, 19BN154C, 18EM35B, 18BN20C and 19BN07E, igneous zircon Ti-in-Zr temperatures corrected using the a SiO2 and a TiO2 values in Table E-1.

Session	Mar 20 2024															
Sample ID	19BN154A															
Spot ID	5-1	8-1	8-2	9-1	10-1	11-1	13-1	14-1	17-1	20-1	23-1	25-1	27-1	30-1	31-1	16-1
Class	ign															
P	272	172	191	677	914	553	362	579	517	773	462	424	3399	519	464	386
2SE	31	16	22	43	44	49	26	23	15	77	41	27	822	57	23	17
Ca	148	752									225	292	496	406		
2SE	100	227									114	124	133	114		
Ti	5.1	2.47	4.1	11.2	4.59	4.0	4.32	4.22	4.65	16.0	7.1	8.3	10.1	9.2	3.86	4.4
2SE	1.3	0.85	1.5	1.8	0.49	1.3	0.82	0.75	0.87	6.2	1.0	1.1	2.7	1.1	0.77	1.0
La	0.318	0.71	0.15	3.0	1.33	1.50	3.04	3.61	0.36	0.092	4.8	4.5	5.9	6.20	1.92	0.31
2SE	0.049	0.29	0.13	1.1	0.43	0.64	0.45	0.98	0.23	0.027	2.7	1.5	1.8	0.97	0.56	0.22
Ce	28.6	16.83	17.1	59.1	27.4	33.2	32.9	46.0	24.6	32.8	57	46.5	52.5	54.5	30.5	16.6
2SE	3.3	0.97	1.6	9.6	1.6	2.0	3.2	6.6	1.7	8.5	22	9.1	8.8	5.3	3.8	1.4
Pr	0.956	0.57	0.43	5.26	1.45	2.47	4.41	4.5	0.43	0.91	7.1	5.8	5.2	7.1	1.77	0.76
2SE	0.077	0.27	0.26	2.15	0.45	0.93	0.69	1.2	0.20	0.23	3.9	1.5	2.1	1.3	0.53	0.31
Nd	12.9	4.1	4.1	38	9.0	20.5	29.3	30.2	4.3	14.3	47	40.4	36	52.5	11.7	8.9
2SE	1.5	1.2	1.1	13	2.1	5.9	4.3	7.3	1.3	3.5	24	9.1	10	9.0	3.2	2.3
Sm	17.4	5.06	5.7	30.1	8.40	16.9	21.2	18.4	5.00	20.1	33	19.0	25.2	31.4	7.8	11.35
2SE	2.1	0.54	1.6	4.4	0.63	1.1	3.6	3.3	0.79	6.3	12	4.6	4.4	4.4	1.5	0.88
Eu	3.45	4.7	1.89	8.5	2.31	4.3	5.0	4.8	0.96	4.45	12.2	7.3	7.9	10.1	4.8	1.96
2SE	0.38	1.5	0.94	2.3	0.67	1.0	1.1	1.1	0.15	0.57	4.2	1.5	2.0	1.2	1.3	0.26
Gd	74.5	21.9	25.6	96.6	27.6	51.7	33.9	46.6	22.0	80	83	34.5	76.4	59.9	21.5	40.7
2SE	9.3	1.7	4.9	5.3	2.7	8.4	4.8	8.4	1.2	25	18	6.1	9.2	6.8	2.0	1.8
Tb	21.1	7.00	7.4	25.3	8.97	13.7	6.29	11.2	6.65	23.3	21.8	7.8	19.2	14.0	5.93	11.16
2SE	2.5	0.73	1.2	1.0	0.77	2.7	0.56	1.9	0.53	7.1	4.4	1.1	3.3	1.4	0.36	0.52
Dy	229	87.5	88	265	98.4	148	54.5	112	74.6	245	209	74.4	196	138	71.1	122.0
2SE	25	2.9	16	11	8.1	33	4.8	19	6.8	70	39	9.5	36	11	3.5	3.9
Ho	79.9	33.1	34.7	91.7	38.5	53	17.8	39.2	28.7	87	70	27.2	70	47.1	27.8	40.7
2SE	8.5	2.3	5.7	3.9	3.5	11	1.3	5.7	2.9	22	13	3.5	12	2.7	1.2	1.5
Er	345	162	173	379	173	232	84.8	186	139	400	296	128	304	219	137.0	176.8
2SE	35	10	25	21	13	47	7.4	25	16	99	56	16	55	13	5.8	3.7
Tm	66.0	38.3	38.9	71.5	35.4	46.3	17.8	37.9	29.2	83	56	28.4	59	44.5	29.8	33.5
2SE	6.4	1.0	5.4	3.8	2.6	8.8	1.7	4.4	3.4	18	11	3.4	10	2.8	1.7	1.4
Yb	577	360	374	624	328	421	178	352	275	768	491	291	533	411	300	299.6
2SE	51	19	51	32	21	68	18	36	32	152	91	32	90	34	20	8.6
Lu	114	78.0	82	119.9	67.2	83	39.0	72.1	57.9	158	97	60.4	105	81.6	63.8	57.2
2SE	10	4.1	10	6.0	4.0	13	3.8	6.5	7.0	26	17	6.8	17	6.4	3.9	2.0
Hf	7983	8226	8176	6483	8965	8966	8448	7719	8925	6469	8688	8237	6761	7889	7339	7200
2SE	507	179	210	165	484	115	530	146	311	95	307	171	213	391	200	190
Th	386	327	382	567	177	272	89	279	163	732	305	176	393	259	233	119.4
2SE	56	25	77	70	16	55	11	15	14	218	56	24	103	32	15	3.3
U	391	640	669	470	302	352	215	496	286	832	334	294	391	481	413	138.0
2SE	37	35	140	40	17	54	19	40	24	102	29	29	71	96	18	2.1
Th/U	0.99	0.51	0.57	1.21	0.58	0.77	0.41	0.56	0.57	0.88	0.91	0.60	1.01	0.54	0.56	0.87
Ti-in-Zr	686	629	668	756	677	667	672	671	678	792	714	728	747	738	664	675
Ti-in-Zr (corr)	756	699	738	826	747	737	742	741	748	862	784	798	817	808	734	745
Ti-in-Zr (corr2)																
Date (Ma)	2518	2516	2496	2517	2505	2509	2521	2497	2496	2498	2515	U-Pb	2502	2509	2492	2494
2σ	15	15	16	15	15	15	15	15	16	16	16	scm	16	16	16	16

Session	Mar 20 2024	Oct 28 2021																
Sample ID	19BN123A																	
Spot ID	1-1	101-2	18-1	27-1	30-1	38-1	61-1	76-1	8-1	84-1	112-1	31-1	37-2a	37-2b	53-1	71-1	79-1	
Class	inhrt	ign																
P	1316	769	259	305	254	1359	355	558	535	283	253							
2SE	288	28	27	24	20	520	36	15	76	24	21	165	226	147	290	176	79	
Ca						509	259											
2SE						433	80											331
Ti	2.5	4.45	4.19	6.1	3.32	2.60	4.3	2.75	4.0	2.37	3.0	2.4	2.6	2.08	4.4	4.4	6.7	
2SE	2.0	0.86	0.68	1.1	0.78	0.69	1.1	0.86	1.8	0.85	1.6	1.6	1.0	0.91	1.9	1.6	2.3	
La	2.21	0.87	2.61	7.3	0.99	0.73	2.87	0.083	1.09	0.157	0.47	0.07		2.68	0.57	0.115	3.8	
2SE	0.59	0.41	0.87	1.7	0.40	0.49	0.54	0.069	0.40	0.095	0.30	0.12		0.75	0.18	0.084	1.2	
Ce	35.6	41.9	35.5	60.8	27.0	20.5	46.7	28.2	31.6	14.9								
2SE	4.2	1.5	4.7	3.7	3.7	5.9	8.5	1.1	4.5	2.3								
Pr	2.32	0.86	2.76	5.32	1.34	0.78	2.98	0.24	1.47	0.29	0.54	0.10		0.92	0.48	0.04	4.4	
2SE	0.49	0.31	0.79	0.94	0.58	0.45	0.51	0.04	0.32	0.16	0.31	0.19		0.26	0.17	0.03	1.4	
Nd	13.0	7.8	17.5	41.5	8.5	6.3	22.4	3.62	13.3	3.0	4.5	1.1	0.48	3.6	3.8	0.54	23.0	
2SE	2.4	1.9	4.7	5.0	3.6	2.8	3.9	0.38	2.4	1.2	2.4	1.3	0.20	1.0	1.1	0.17	6.7	
Sm	8.6	8.85	11.3	34.7	7.0	6.9	17.3	5.98	13.1	3.6	2.61	1.9	1.30	1.83	2.74	1.54	12.7	
2SE	1.3	0.85	1.9	3.8	1.1	1.7	3.7	0.42	1.5	1.1	0.93	1.3	0.27	0.23	0.79	0.29	3.6	
Eu	5.49	2.92	4.13	12.0	1.95	1.31	6.41	1.12	4.9	0.79	0.98	0.30	0.148	0.72	0.82	0.146	3.68	
2SE	0.89	0.48	0.92	1.6	0.86	0.23	1.35	0.13	1.1	0.35	0.45	0.41	0.055	0.17	0.31	0.038	1.09	
Gd	31.1	33.7	34.3	104.2	29.9	24.0	41.8	24.7	46.5	12.6	9.4	7.8	10.76	9.17	12.2	10.5	16.7	
2SE	3.6	1.3	2.5	4.6	1.5	4.1	9.2	1.3	2.2	1.5	1.4	1.0	0.89	0.82	2.1	1.1	2.5	
Tb	9.80	10.27	9.95	26.3	10.7	7.2	10.5	7.39	12.71	4.36	3.36	3.06	4.14	3.71	4.69	4.14	4.31	
2SE	0.92	0.28	0.57	1.1	1.1	1.2	2.3	0.40	0.70	0.75	0.25	0.41	0.24	0.22	0.70	0.30	0.40	
Dy	109.7	117.1	105.6	252.9	130.5	73	101	80.3	133.2	52.1	42.6	39.6	54.4	46.2	58.8	52.3	46.3	
2SE	6.9	3.2	6.3	9.8	8.6	12	22	4.0	7.0	8.7	2.0	2.9	2.1	2.8	8.2	3.1	3.2	
Ho	41.1	44.4	37.6	82.8	48.0	25.3	35.0	28.8	45.6	20.0	17.27	16.7	22.13	19.1	24.8	22.2	17.99	
2SE	2.2	1.6	2.0	3.0	5.2	3.5	7.4	1.4	2.1	2.9	0.54	1.0	0.91	1.0	3.2	1.1	0.96	
Er	194	207.3	173.3	354	225	120	153	129.1	200.3	98	89.5	88.5	117.0	100.9	129	117.4	91.1	
2SE	13	7.5	7.7	13	22	18	30	6.2	9.5	12	2.0	3.8	4.1	5.9	15	6.0	3.9	
Tm	39.6	41.4	35.0	68.7	47.7	23.6	31.1	25.8	40.2	21.3	20.22	21.4	27.02	23.5	29.1	28.1	21.51	
2SE	1.5	1.9	1.6	2.5	4.8	2.6	5.7	1.3	2.1	2.5	0.45	1.2	0.89	1.3	3.3	1.4	0.94	
Yb	368	383	315	608	433	225	289	234	368	206	213.5	218.6	274.4	247	290	293	230.8	
2SE	15	16	15	19	40	25	49	12	15	22	3.9	7.6	8.7	13	29	16	8.8	
Lu	73.4	79.6	63.4	118.8	86.1	48.9	59.6	47.8	74.8	44.3	47.43	50.8	60.1	55.5	62.7	65.3	49.7	
2SE	2.9	3.8	2.6	4.1	7.0	5.2	9.1	2.4	3.4	4.4	0.93	2.9	1.8	2.8	5.4	3.8	1.8	
Hf	10929	5639	7977	7478	13801	6482	7682	7547	6334	8877	10046	12405	10562	10365	8937	10155	9336	
2SE	172	169	188	417	737	185	278	300	217	357	277	578	354	471	349	378	396	
Th	142.3	177.3	136.2	193	172	72	128	94.5	139.9	58	121.9	109.7	174.0	142.9	131	170	137.6	
2SE	7.2	4.4	9.1	16	14	12	29	3.0	8.1	11	3.7	4.9	5.0	8.8	14	11	8.8	
U	261.7	190.2	224.1	185	369	123	340	108.4	146.8	113	615	531	838	801	528	1030	625	
2SE	5.9	6.3	5.7	15	16	16	47	3.5	6.1	12	17	16	19	41	11	81	29	
Th/U	0.54	0.93	0.61	1.04	0.47	0.59	0.38	0.87	0.95	0.51	0.20	0.21	0.21	0.18	0.25	0.17	0.22	
Ti-in-Zr	630	675	670	701	652	633	671	637	667	626	645	626	633	617	674	674	709	
Ti-in-Zr (corr)	700	745	740	771	722	703	741	707	737	696	715	696	703	687	744	744	779	
Ti-in-Zr (corr2)											712	691	698	680	746	746	786	
Date (Ma)	2511	2493	2475	2528	2504	2502	2488	2470	2508	2494	2381	2383	2378	2378	2377	2373	2379	
2σ	14	12	12	13	13	12	12	13	13	12	12	12	12	12	12	12	12	

Session	Oct 28 2021	Oct 28 2021	Oct 28 2021	Mar 20 2024											
Sample ID	19BN123A			19BN150A											
Spot ID	88-1	91-1	99-1	110-1	15-1	22-1a	22-1b	24-1	25-1	3-1	32-1	37-2	41-1	42-2	44-1
Class	ign	ign	ign	inhrt											
P	662	417	536	678	332	698	733	406	382	225	201	181	210	131	355
2SE	55	40	114	55	19	87	163	79	28	14	8	7	14	6	35
Ca										174			260	251	225
2SE										108			253	110	110
Ti		3.9	2.7	18.2	4.9	6.1	9.1	14.7	21.6	4.67	3.9	2.98	3.2	4.4	4.08
2SE		2.0	1.5	2.3	1.8	2.4	2.0	6.4	2.0	0.93	1.1	0.56	1.3	1.1	0.89
La			0.79	0.97	0.88	0.35	4.04	4.9	0.106	1.63	12.6	0.03	2.33	9.03	4.4
2SE			0.22	0.44	0.32	0.10	0.81	1.4	0.026	0.37	2.7	0.01	0.74	0.76	2.8
Ce				55.4	7.8	15.3	33.1	49.0	47.7	22.3	58.2	17.32	39.0	23.1	39
2SE				4.2	1.9	3.1	7.4	7.8	3.2	2.6	8.4	0.49	5.0	1.9	19
Pr	0.023	0.030	0.35	2.02	0.94	0.64	5.26	4.40	1.36	2.19	6.9	0.429	2.15	4.64	4.8
2SE	0.020	0.028	0.13	0.28	0.39	0.17	0.96	0.88	0.13	0.38	1.2	0.036	0.66	0.40	2.6
Nd	0.42	0.35	2.31	28.8	4.6	8.6	35.5	33.9	21.2	20.4	38.3	7.3	12.6	25.6	29
2SE	0.15	0.14	0.77	3.2	2.1	2.1	9.6	6.9	2.6	2.7	8.1	0.4	3.4	1.8	13
Sm	1.71	1.16	3.08	39.5	3.26	13.7	17.9	34.5	35.5	23.2	15.2	13.15	10.1	16.7	22.3
2SE	0.31	0.28	0.67	3.7	0.50	2.8	5.1	9.0	2.8	2.1	2.4	0.50	1.6	1.4	5.0
Eu	0.186	0.150	0.54	5.97	0.77	2.69	4.36	5.6	2.37	4.49	2.31	2.04	1.30	3.93	4.7
2SE	0.070	0.085	0.18	0.68	0.15	0.50	0.88	2.0	0.24	0.25	0.34	0.10	0.22	0.40	1.0
Gd	11.04	5.76	17.0	146	11.0	53	39	120	149.1	76.8	30.1	57.1	43.3	43.9	64.4
2SE	0.87	0.53	2.9	14	2.6	11	13	28	8.8	4.8	4.2	1.6	3.2	3.5	5.5
Tb	4.18	2.23	5.82	37.7	3.21	14.3	7.5	31.8	41.3	19.1	7.11	16.00	12.35	10.95	16.9
2SE	0.23	0.17	0.80	3.5	0.40	2.7	1.3	6.9	2.5	1.0	0.70	0.46	0.85	0.89	1.4
Dy	55.2	30.2	67.0	371	35.6	146	71	304	428	185.2	63.1	167.3	135.8	102.6	172
2SE	1.8	1.4	7.5	33	2.4	26	22	54	31	8.4	3.1	4.9	4.1	7.2	12
Ho	22.26	13.08	26.3	122	14.1	51.0	22.2	106	147	61.9	21.15	58.5	48.9	33.0	57.5
2SE	0.76	0.40	2.8	12	1.2	8.6	7.3	19	12	3.0	0.95	1.8	1.9	2.3	3.1
Er	115.2	72.6	127	491	64.0	220	101	431	619	259	92.4	250.9	210.1	137.9	243
2SE	3.6	2.9	14	44	5.1	37	34	67	47	10	3.7	7.8	8.3	8.8	11
Tm	26.49	17.43	27.1	88.8	13.72	41.5	18.9	78.0	112.7	47.8	17.63	46.1	39.9	25.7	45.2
2SE	0.61	0.76	2.8	8.5	0.79	6.2	4.6	11.4	8.0	2.1	0.63	1.5	1.5	1.6	2.2
Yb	272.4	186.0	259	736	143	368	190	654	966	415	161.5	405	356	228	397
2SE	7.5	5.9	30	64	12	54	43	89	67	17	5.9	12	13	13	17
Lu	59.7	42.4	52.7	136	30.1	72.2	36.1	121	179	81.4	32.7	77.8	68.3	45.8	76.5
2SE	1.9	1.3	5.7	12	1.8	9.2	6.3	15	11	3.3	1.0	2.4	2.1	2.4	3.1
Hf	10427	11255	9628	8113	5970	5944	9916	8570	9191	6578	6389	7546	9784	5928	7520
2SE	358	347	459	388	104	171	217	870	487	298	214	278	315	315	431
Th	173.9	110.9	152	406	29.4	162	66	282	509	121.3	100.2	172.0	238	54.7	103.3
2SE	5.7	4.4	20	38	3.1	28	34	63	29	6.3	6.0	3.6	38	5.1	5.6
U	875	481	292	325	58.4	234	455	310	561	142.7	147.4	238.8	334	114	135.9
2SE	20	15	29	28	4.3	16	31	26	49	6.8	7.0	7.4	14	33	6.2
Th/U	0.20	0.23	0.52	1.25	0.50	0.69	0.15	0.91	0.91	0.85	0.68	0.72	0.71	0.48	0.76
Ti-in-Zr		665	636	805	682	701	737	783	823	679	664	643	649	674	668
Ti-in-Zr (corr)		735	706	875	752	771	807	853	893	749	734	713	719	744	738
Ti-in-Zr (corr2)		736	702												
Date (Ma)	2374	2372	2390	2499	U-Pb	2517	2517	2505	2493	2546	U-Pb	2509	2503	U-Pb	2508
2σ	12	12	12	12	scrn	12	12	12	12	12	scrn	12	13	scrn	13

Session	Mar 20 2024	Oct 28 2021														
Sample ID	19BN150A															
Spot ID	57-1	57-2	6-1	67-1	67-2	76-1	94-1	98-1	98-2	106-1a	24-2a	24-2b	5-1	68-2	77-1	
Class	inhrt	ign	ign	ign	ign	ign	ign									
P	490	272	275	588	462	461	909	728	592	411		22615	266	650	1239	
2SE	15	13	19	30	16	175	219	61	17	44		7832	20	79	178	
Ca						458	194	161					851			
2SE						196	86	91					189			
Ti	7.0	3.32	2.3	8.3	1.76	2.17	11.3	20.0	3.0	3.1		2.7	2.25	6.5	5.1	
2SE	2.0	0.69	1.0	1.8	0.50	0.81	1.9	1.6	1.2	1.9		1.1	0.85	2.2	2.2	
La	2.76	2.06	0.66	0.158	0.041	1.92	1.73	1.45	0.18	0.144	1.57	5.01	0.65	4.4	2.00	
2SE	0.78	0.15	0.31	0.063	0.025	0.86	0.73	0.27	0.19	0.078	0.87	0.99	0.24	1.4	0.60	
Ce	51.8	35.00	18.5	27.1	11.7	18.5	40.4	64.5	40.1							
2SE	3.0	0.96	1.6	3.6	0.6	2.9	4.2	3.5	1.5							
Pr	4.5	3.77	0.67	0.83	0.059	1.48	2.32	3.29	0.33	0.20	0.85	3.27	0.60	3.57	2.77	
2SE	1.1	0.32	0.28	0.18	0.018	0.36	0.52	0.28	0.12	0.10	0.44	0.60	0.23	0.64	0.79	
Nd	33.2	24.9	5.9	13.8	1.02	11.2	22.6	31.1	5.48	1.40	5.3	18.4	3.0	27.2	18.1	
2SE	6.9	1.4	1.5	2.8	0.17	2.2	3.5	1.8	0.84	0.62	2.0	3.4	1.1	4.6	4.9	
Sm	27.4	16.32	12.3	23.2	3.02	11.2	28.4	38.8	10.9	2.59	3.6	13.5	1.73	27.9	14.4	
2SE	3.1	0.88	2.0	3.5	0.24	1.8	3.7	1.4	1.9	0.69	1.1	2.4	0.44	2.5	4.2	
Eu	4.15	2.43	1.29	2.98	0.108	2.30	4.36	4.66	1.24	0.212	0.51	2.31	0.28	4.04	5.72	
2SE	0.53	0.17	0.42	0.72	0.025	0.52	0.65	0.30	0.12	0.098	0.22	0.39	0.11	0.45	1.65	
Gd	80.1	38.6	57.1	97	18.82	38.4	93	144.3	58.6	14.1	16.3	35.7	8.1	89.9	34.7	
2SE	8.8	1.7	2.6	13	0.98	5.0	16	4.5	3.6	2.3	2.1	4.4	1.0	9.2	8.3	
Tb	21.8	9.95	17.21	27.4	6.39	10.9	24.8	38.4	17.1	5.16	4.60	9.36	3.28	23.5	8.2	
2SE	2.9	0.37	0.57	2.8	0.30	1.1	4.4	1.5	1.2	0.62	0.35	0.91	0.31	2.3	1.8	
Dy	223	102.8	186.5	284	79.4	116	250	381	187	62.7	50.0	87.8	42.3	245	85	
2SE	30	4.0	5.5	26	3.4	12	45	15	11	6.7	2.4	8.5	3.7	23	16	
Ho	75.0	36.4	68.1	97.4	30.8	40.6	85	127.0	66.1	24.5	18.96	30.1	17.0	84.4	29.1	
2SE	9.8	1.6	3.5	8.5	1.2	4.0	15	5.3	4.1	2.4	0.77	2.4	1.4	8.1	5.2	
Er	321	159.1	299	413	146.2	182	359	513	284	115.4	86.1	126.8	85.6	358	124	
2SE	40	7.0	14	31	5.6	18	64	20	19	9.2	4.0	9.1	6.6	32	20	
Tm	60.3	31.0	57.9	75.7	29.8	35.7	67	93.0	54.5	25.3	17.0	23.9	19.1	67.9	24.7	
2SE	6.5	1.4	2.8	4.9	1.1	3.4	12	3.2	3.8	1.9	0.7	1.6	1.5	5.9	3.6	
Yb	515	274	505	646	276	334	583	787	474	231	152.0	203	189	589	218	
2SE	52	12	28	45	11	31	95	30	32	14	5.8	12	15	47	30	
Lu	97.9	53.6	98.1	122.1	55.0	66.3	108	146.8	90.8	49.4	31.5	41.8	38.6	112.8	44.2	
2SE	9.3	2.5	4.7	8.6	2.1	6.1	17	5.9	5.4	2.8	1.0	2.0	2.6	8.6	5.8	
Hf	9856	9282	11409	8467	9740	7760	8806	7213	9456	10408	8299	6224	10399	8447	7751	
2SE	820	684	692	908	400	190	326	355	395	532	230	311	559	839	312	
Th	342	124	189	270	144	139	266	417	327	78.8	41.5	77.9	116	235	80	
2SE	98	14	14	25	10	18	47	11	19	3.3	1.0	9.4	13	28	11	
U	404	242	335	325	335	222	528	400	435	347	102.2	147	1027	339	365	
2SE	51	11	20	27	17	31	54	11	31	79	4.9	13	57	54	18	
Th/U	0.85	0.51	0.56	0.83	0.43	0.63	0.50	1.04	0.75	0.23	0.41	0.53	0.11	0.69	0.22	
Ti-in-Zr	714	652	626	728	605	620	757	816	645	646		636	623	706	687	
Ti-in-Zr (corr)	784	722	696	798	675	690	827	886	715	716		706	693	776	757	
Ti-in-Zr (corr2)										774		761	744	853	828	
Date (Ma)	2501	2488	2491	2508	2482	2496	2511	2497	2518	2376	2378	2378	2378	2377	2381	
2σ	12	12	12	12	12	12	12	12	13	12	12	12	12	12	12	

Session	Mar 20 2024	Mar 21 2024														
Sample ID	19BN154C								18EM35B							
Spot ID	40-1	40-2	6-1	33-1	5-1	53-1	71-1	99-1	11-1	26-1	36-1	43-1	1-1	19-1	27-1	
Class	inhrt	inhrt	inhrt	ign	ign	ign	ign	ign	ing2							
P	372	512	457	613	201	312	511	478	228	268	327	331	255	166	272	
2SE	23	34	17	45	18	79	44	34	16	23	13	18	19	16	13	
Ca					4762		607									
2SE					1085		309									
Ti	6.05	3.9	2.33	5.5	4.0	7.0	9.4	3.7	4.3	6.38	6.70	7.5	8.0	8.3	8.9	
2SE	0.75	1.0	0.67	1.9	1.5	5.0	3.5	2.1	2.2	0.61	0.77	1.6	3.9	1.8	1.0	
La	0.082	1.11	0.47	0.17	2.41	4.48	4.2	3.62	0.85		0.05		0.08	0.42		
2SE	0.080	0.23	0.13	0.11	0.99	0.56	2.0	0.65	0.24		0.02		0.05	0.19		
Ce	13.55	25.4	26.0						5.8	1.33	3.03	2.12	1.44	3.06	4.55	
2SE	0.95	1.8	3.3						1.3	0.24	0.35	0.15	0.23	0.49	0.17	
Pr	0.22	2.08	0.74	0.16	1.04	5.92	5.7	4.73	0.80		0.036	0.025	0.084	0.23	0.051	
2SE	0.13	0.44	0.25	0.08	0.44	0.81	2.4	0.92	0.26	0.014	0.010	0.010	0.061	0.10	0.018	
Nd	2.61	17.31	5.62	1.70	7.3	41.2	36	25.0	4.7	0.38	0.65	0.55	0.76	1.80	1.21	
2SE	0.83	2.31	1.55	0.82	3.4	7.5	15	5.5	1.7	0.13	0.12	0.15	0.59	0.57	0.16	
Sm	4.02	15.3	6.5	3.03	2.01	19.5	22.5	4.83	1.64	0.96	1.51	0.88	1.32	1.53	2.18	
2SE	0.51	1.1	1.3	0.59	0.99	3.3	9.0	0.98	0.49	0.24	0.21	0.15	0.37	0.28	0.28	
Eu	1.03	3.89	1.73	0.15	1.38	3.24	5.5	0.86	1.87	0.179	0.132	0.085	0.31	0.72	0.085	
2SE	0.12	0.27	0.44	0.06	0.55	0.43	2.3	0.17	0.62	0.068	0.031	0.024	0.14	0.15	0.028	
Gd	15.64	48.8	21.8	14.29	6.9	25.1	28.0	14.9	4.77	6.59	7.6	6.28	5.94	8.36	11.21	
2SE	0.66	2.9	3.1	0.90	1.1	2.1	6.6	1.6	0.74	0.97	1.0	0.57	0.13	0.54	0.99	
Tb	4.62	12.30	6.11	4.94	2.38	4.96	5.15	5.00	1.62	2.16	2.46	2.18	1.95	2.63	3.31	
2SE	0.19	0.80	0.63	0.35	0.17	0.52	0.53	0.30	0.11	0.22	0.30	0.14	0.29	0.25	0.20	
Dy	51.4	125.9	64.8	60.8	34.4	43.5	50.4	60.1	14.42	25.2	27.0	28.8	22.0	28.2	37.3	
2SE	1.5	8.3	5.8	2.8	2.2	3.4	2.0	2.8	0.53	3.1	3.3	2.7	1.0	2.2	1.5	
Ho	19.16	44.1	23.3	24.27	14.80	15.28	19.00	24.2	4.59	8.7	9.9	11.9	8.24	10.17	13.62	
2SE	0.53	3.6	1.6	0.86	0.97	0.73	0.88	1.1	0.29	1.2	1.2	1.2	0.34	0.63	0.61	
Er	92.0	190	106.3	121.9	84.9	68.8	94.2	122.7	19.7	40.0	45.0	58.3	38.4	46.6	61.1	
2SE	2.6	15	6.7	3.8	5.2	4.8	5.9	5.5	1.0	6.5	5.1	6.8	2.8	2.8	2.1	
Tm	18.55	36.5	21.1	27.77	21.8	15.1	21.5	28.1	3.41	8.0	9.05	12.1	7.73	9.30	12.68	
2SE	0.54	3.2	1.1	0.97	1.3	1.1	1.3	1.3	0.18	1.6	0.96	1.4	0.32	0.71	0.38	
Yb	172.8	321	195.5	270.0	267	152.1	226	272	34.1	77	80.7	112	77.3	87.7	113.1	
2SE	5.9	30	9.0	9.8	19	3.9	23	13	3.0	15	8.0	13	3.4	7.0	5.5	
Lu	38.0	66.9	41.2	56.6	51.8	33.1	45.1	58.1	5.69	15.0	17.0	23.2	16.7	18.2	23.44	
2SE	1.2	6.7	2.0	1.9	2.9	1.9	2.1	2.9	0.49	2.9	1.6	2.6	1.2	1.3	0.67	
Hf	6284	5969	9005	11666	12198	9718	10954	9022	10409	9928	8462	8663	6839	10765	9913	
2SE	129	133	499	413	535	346	356	269	261	554	250	270	152	619	292	
Th	48.0	175	90	193.6	115.5	178.2	149.9	246	24.4	27.6	63.2	43.1	22.7	30.6	76.6	
2SE	2.7	14	11	4.8	6.6	6.2	4.1	16	1.0	3.0	6.9	2.8	0.9	3.0	3.6	
U	84.2	132	164	587	1717	481	518	568	406	316	130	76.9	213.5	283	106.7	
2SE	5.4	15	14	17	167	22	62	25	12	11	15	4.4	9.8	20	2.0	
Th/U	0.57	1.32	0.55	0.33	0.07	0.37	0.29	0.43	0.06	0.09	0.49	0.56	0.11	0.11	0.72	
Ti-in-Zr	701	665	625	693	666	714	740	660	672	705	709	719	726	728	735	
Ti-in-Zr (corr)	771	735	695	763	736	784	810	730	742	775	779	789	796	798	805	
Ti-in-Zr (corr2)				755	725	779	809	718	722	758	763	773	781	784	792	
Date (Ma)	2515	2523	U-Pb	2363	2379	2352	2389	2379	2441	2429	2439	2407	2430	2439	2420	
2σ	13	13	scrn	12	12	13	15	12	12	12	13	13	12	12	13	

Session	Mar 21 2024															
Sample ID	18EM35B															
Spot ID	24-1	46-1	33-1	41-1	9-1	47-1	48-1	52-1	49-1	50-1	28-1	39-1	4-1	35-1	45-1	32-1
Class	ing2	ign1	ign1	ign1	ign1											
P	324	361	337	412	141	339	331	289	306	318	347	240	186	210	215	297
2SE	5	9	12	23	17	31	34	17	9	24	22	9	7	19	24	17
Ca	182															
2SE	74															
Ti	8.97	9.35	9.43	9.5	9.8	9.86	10.10	10.7	11.5	12.0	13.4	5.4	5.5	6.2	6.2	6.9
2SE	0.78	0.78	0.86	1.0	1.5	0.91	0.74	2.0	1.3	1.9	1.4	1.2	1.2	1.4	2.7	1.0
La					0.091	0.0094				0.121	0.58	0.055	0.086	0.085	0.142	
2SE					0.089	0.0055				0.073	0.17	0.018	0.047	0.027	0.046	
Ce	4.05	2.95	2.76	3.82	3.3	4.02	3.92	2.45	5.28	6.47	9.99	1.68	1.71	1.38	1.77	1.17
2SE	0.19	0.16	0.17	0.26	1.8	0.64	0.92	0.21	0.47	0.30	1.05	0.14	0.30	0.19	0.23	0.10
Pr	0.044	0.037	0.040	0.066	0.038	0.071	0.059	0.027	0.050	0.145	0.543	0.056	0.062	0.060	0.089	0.026
2SE	0.010	0.012	0.011	0.019	0.025	0.017	0.019	0.014	0.021	0.072	0.140	0.024	0.032	0.035	0.043	0.013
Nd	0.86	0.81	0.64	1.42	0.64	1.09	0.94	0.52	1.00	2.6	5.5	0.42	0.62	0.69	0.57	0.311
2SE	0.12	0.09	0.13	0.29	0.28	0.22	0.26	0.19	0.30	1.8	1.4	0.14	0.25	0.21	0.18	0.095
Sm	1.51	1.83	1.72	2.56	1.44	2.03	1.98	1.19	1.90	2.90	5.58	1.19	0.73	1.09	0.80	1.28
2SE	0.17	0.16	0.16	0.46	0.20	0.33	0.51	0.43	0.49	0.39	0.42	0.20	0.22	0.30	0.16	0.30
Eu	0.096	0.074	0.091	0.147	0.226	0.127	0.114	0.062	0.134	0.197	1.43	0.298	0.26	0.33	0.255	0.263
2SE	0.019	0.018	0.025	0.035	0.068	0.043	0.027	0.035	0.029	0.045	0.47	0.035	0.14	0.12	0.059	0.073
Gd	7.83	7.71	9.51	13.09	6.76	9.7	9.5	5.44	8.9	15.7	24.0	7.13	4.25	6.9	5.8	8.04
2SE	0.64	0.78	0.80	2.43	0.68	1.5	2.0	0.52	1.2	1.1	2.2	0.43	0.51	1.2	1.2	0.60
Tb	2.56	2.49	2.98	3.80	2.21	2.91	2.82	1.77	3.11	4.25	6.96	2.25	1.22	1.97	1.94	2.64
2SE	0.15	0.21	0.24	0.53	0.25	0.41	0.62	0.10	0.47	0.27	0.49	0.13	0.06	0.21	0.23	0.12
Dy	27.4	26.6	33.2	40.9	22.7	32.2	33.0	19.9	35.6	47.3	69.2	24.6	14.6	21.3	17.7	26.0
2SE	1.6	2.2	2.6	4.2	3.0	4.6	7.3	1.1	4.1	1.6	2.2	1.3	1.0	1.5	2.6	1.3
Ho	9.67	9.74	12.42	14.1	7.5	11.3	11.9	7.08	13.1	16.4	23.16	8.82	4.90	7.59	6.6	9.71
2SE	0.52	0.81	0.92	1.3	1.3	1.6	2.6	0.37	1.6	1.3	0.61	0.54	0.34	0.58	1.2	0.43
Er	42.7	42.7	53.7	58.4	33.2	48.7	56	30.6	60.4	70.8	97.0	41.5	20.6	34.7	28.7	42.6
2SE	2.1	3.5	4.1	3.9	7.3	6.8	13	2.0	7.8	3.1	3.8	2.1	1.6	2.6	6.1	1.5
Tm	8.53	8.41	10.28	11.00	6.8	9.5	11.2	5.91	12.3	14.02	18.4	8.67	4.00	7.15	5.8	8.79
2SE	0.45	0.70	0.82	0.71	1.6	1.3	2.5	0.51	1.5	0.61	1.1	0.46	0.28	0.71	1.2	0.32
Yb	74.6	73.0	90.1	95.7	63	86	102	54.8	114	124.2	156.6	80.1	36.4	67.1	54	82.2
2SE	3.6	5.7	7.0	4.7	16	12	22	3.2	14	4.6	5.2	4.9	2.5	5.6	10	3.5
Lu	14.99	14.6	18.6	19.0	12.6	17.3	20.7	10.63	23.7	24.7	29.25	17.5	7.69	13.9	11.4	16.45
2SE	0.73	1.1	1.3	1.0	3.5	2.3	4.3	0.50	2.8	1.3	0.76	1.0	0.52	1.4	2.3	0.57
Hf	7979	8336	8540	9340	11378	8822	9656	9598	10559	10242	11255	7406	8938	7318	6833	8494
2SE	289	348	333	477	390	265	295	357	606	354	636	233	262	239	90	291
Th	63.8	54.3	58.4	88	29.5	58.0	62	37.8	81.1	104.1	149.5	27.4	37.3	22.4	19.9	28.9
2SE	3.2	3.8	5.5	10	2.6	8.4	15	2.0	6.7	9.0	8.1	1.3	2.1	2.1	2.4	1.0
U	98.8	93.9	94.5	119.3	310	105.2	114.3	71.2	121.7	131.4	166.2	252.3	287.0	211	200	268
2SE	5.1	4.6	7.9	3.6	23	7.0	12.4	3.9	5.1	3.7	6.3	10.5	9.6	17	15	11
Th/U	0.65	0.58	0.62	0.74	0.10	0.55	0.54	0.53	0.67	0.79	0.90	0.11	0.13	0.11	0.10	0.11
Ti-in-Zr	736	739	740	741	744	744	747	752	759	763	774	691	692	703	703	712
Ti-in-Zr (corr)	806	809	810	811	814	814	817	822	829	833	844	761	762	773	773	782
Ti-in-Zr (corr2)	792	796	797	798	801	802	804	810	819	823	835	742	744	755	756	765
Date (Ma)	2444	2403	2422	2443	2414	2426	2429	2403	2416	2432	2410	2435	2446	2430	2438	2435
2σ	12	13	12	14	12	13	13	13	13	12	13	12	12	12	13	12

Session	Mar 21 2024	Oct 28 2022														
Sample ID	18EM35B								18BN20C							
Spot ID	22-1	40-1	15-1b	51-1	17-1b	15-1a	16-1	20-1	1-1	2-1	3-1	7-1	22-1	21-1	10-1	
Class	ign1	ign														
P	337	275	312	263	260	296	237	237	1325	411	279	321	717	692	891	
2SE	22	18	21	28	16	25	24	39	110	25	13	16	156	129	83	
Ca												156	212	321		
2SE												64	133	127		
Ti	7.18	7.5	7.72	7.92	8.1	8.20	8.7	9.0	13.8	13.6	11.2	14.6	16.4	11.8	10.6	
2SE	0.79	1.6	0.81	0.95	1.2	0.88	3.7	1.2	1.0	1.3	1.2	1.6	1.1	1.3	3.8	
La	0.0246	0.106	0.022	0.032	0.20	0.016	0.44		0.48	0.317	0.148	0.023	3.61	0.60	0.149	
2SE	0.0076	0.033	0.010	0.030	0.25	0.012	0.10		0.12	0.077	0.058	0.010	0.61	0.23	0.069	
Ce	1.84	1.82	5.60	1.51	1.91	5.57	2.98	1.69	29.8	23.5	17.82	21.4	36.8	20.4		
2SE	0.24	0.20	0.44	0.21	0.84	0.78	0.23	0.13	1.1	1.0	0.40	2.1	3.5	1.7		
Pr	0.029	0.117	0.062	0.021	0.237	0.063	0.103	0.034	0.695	0.670	0.262	0.151	2.21	0.44	0.49	
2SE	0.012	0.042	0.015	0.011	0.268	0.018	0.048	0.018	0.056	0.052	0.049	0.035	0.36	0.12	0.13	
Nd	0.55	1.05	0.78	0.50	0.40	0.84	0.69	0.71	8.78	7.92	2.87	2.24	15.53	4.55	4.1	
2SE	0.11	0.35	0.13	0.14	0.28	0.18	0.40	0.15	0.30	0.68	0.37	0.40	2.35	0.82	1.1	
Sm	1.41	1.37	2.01	1.67	1.70	1.85	0.65	1.62	11.4	9.95	4.55	3.99	16.5	5.34	6.6	
2SE	0.17	0.31	0.23	0.16	0.43	0.31	0.21	0.27	1.4	0.86	0.44	0.73	2.1	0.82	1.7	
Eu	0.291	0.76	0.844	0.229	0.362	0.81	0.19	0.398	1.47	1.23	0.594	0.494	1.84	0.62	0.68	
2SE	0.038	0.19	0.093	0.077	0.235	0.12	0.10	0.079	0.18	0.13	0.058	0.090	0.28	0.11	0.27	
Gd	9.56	7.67	11.08	11.0	13.4	10.5	6.1	10.30	42.8	42.1	22.8	18.8	60.9	21.6	28.4	
2SE	0.82	0.61	0.70	1.2	2.3	1.2	1.0	0.82	3.5	2.9	1.1	2.6	9.1	1.4	4.0	
Tb	3.11	2.33	3.51	3.19	4.56	3.23	1.73	3.43	13.19	12.23	6.88	6.14	18.4	6.69	8.99	
2SE	0.22	0.13	0.26	0.35	0.53	0.33	0.10	0.28	0.51	0.73	0.19	0.69	2.6	0.35	1.32	
Dy	34.6	24.8	40.5	36.0	44.9	38.3	17.5	36.3	140.3	129.6	76.9	67.2	188	77.6	97	
2SE	2.5	0.9	2.2	3.7	2.4	3.8	1.4	2.8	2.4	8.3	2.1	7.9	26	3.0	11	
Ho	13.2	9.44	15.44	12.9	12.99	14.4	6.51	14.0	48.1	45.6	28.02	24.5	62.9	28.2	35.5	
2SE	1.1	0.28	0.92	1.8	0.57	1.3	0.65	1.4	1.6	2.7	0.74	2.8	8.0	1.3	4.0	
Er	62.5	41.4	74.4	56	45.5	72.2	27.6	62.9	207.7	193	119.8	109	263	122.6	152	
2SE	5.8	1.7	4.6	10	3.6	6.4	2.5	6.4	6.1	11	3.4	11	34	4.5	16	
Tm	13.1	8.94	16.0	11.2	8.33	14.9	5.16	13.8	38.6	35.1	22.57	21.0	48.0	23.35	27.3	
2SE	1.3	0.41	1.0	2.4	0.52	1.2	0.67	1.8	1.5	2.0	0.65	2.1	6.3	0.92	2.6	
Yb	129	85.6	156.0	109	69	147	46.7	136	329	304	200.9	189	404	210	250	
2SE	13	4.1	9.6	25	10	12	5.7	17	12	18	5.5	17	49	11	22	
Lu	27.1	17.5	34.0	21.5	10.8	31.7	8.9	28.3	61.6	56.2	37.9	35.7	73.1	39.9	46.5	
2SE	2.8	1.0	2.1	5.7	1.5	2.5	1.2	4.2	1.9	3.2	1.0	2.9	8.7	1.6	3.8	
Hf	8401	8546	6809	9869	15693	7237	7860	10421	8518	7489	8007	8859	9501	7406	8090	
2SE	278	132	333	355	544	465	254	687	287	232	177	275	341	229	174	
Th	37.9	29.0	60.6	42.8	53.9	64.6	38.8	39.9	186.3	205	116.7	108	310	106.1	167	
2SE	3.8	0.8	6.8	3.3	2.0	7.4	4.9	4.8	7.1	13	7.6	11	47	6.3	13	
U	317	287	167	429	898	264	164	360	113.1	122.0	98.7	90.3	179	87.7	115.3	
2SE	23	13	15	37	49	37	12	28	4.9	4.6	11.5	5.2	20	2.8	6.2	
Th/U	0.12	0.10	0.36	0.10	0.06	0.24	0.24	0.11	1.65	1.68	1.18	1.19	1.73	1.21	1.45	
Ti-in-Zr	716	720	722	724	726	727	733	736	777	775	756	783	794	762	751	
Ti-in-Zr (corr)	786	790	792	794	796	797	803	806	847	845	826	853	864	832	821	
Ti-in-Zr (corr2)	770	774	777	779	781	783	789	792	893	891	868	900	915	875	861	
Date (Ma)	2414	2435	2439	2434	2421	2439	2449	2438	2331	2331	2327	2325	2325	2321	2326	
2σ	12	12	12	12	12	12	12	12	15	13	14	13	13	13	14	

Session	Oct 28 2022	Mar 21 2024	Mar 21 2024	Mar 21 2024	Mar 21 2024											
Sample ID	18BN20C											19N07E				
Spot ID	13-1	14-1	15-1	18-1	19-1	25-1	24-1	28-1	30-1	16-1	23-1	2-1	36-1	29-2	25-1	
Class	ign															
P	355	309	112	277	370	346	445	547	725	319	383	306	338	1014	416	
2SE	49	19	20	82	35	40	49	31	121	15	22	132	48	106	27	
Ca										164	271	264				
2SE										358	246	194				
Ti	15.1	11.3	3.6	13.1	21.7	18.8	19.1	13.9	19.5	19.7	15.5	3.2	4.5	5.3	6.7	
2SE	6.1	2.2	2.1	3.4	8.9	8.1	6.4	3.1	7.2	5.8	4.5	1.2	2.1	1.4	2.0	
La	0.13	0.70	0.91	0.24	0.40	0.057	0.11	0.056	0.38		0.086	0.83	0.517	0.26	1.92	
2SE	0.10	0.14	0.29	0.18	0.15	0.053	0.10	0.056	0.10		0.046	0.40	0.086	0.48	0.24	
Ce												13.2	23.1	27.9	31.4	
2SE												3.2	3.2	3.4	3.5	
Pr	0.14	1.33	0.67	0.22	0.256	0.643	0.34	0.163	0.81	0.41	0.72	0.82	0.96	0.21	2.26	
2SE	0.10	0.12	0.34	0.11	0.076	0.069	0.16	0.045	0.17	0.13	0.13	0.35	0.19	0.30	0.55	
Nd	1.34	14.2	5.4	3.3	2.78	11.1	3.0	2.47	7.66	5.6	9.9	4.3	6.8	3.0	12.5	
2SE	0.62	1.0	2.9	2.0	0.77	1.4	1.1	0.47	0.80	1.2	1.2	1.6	2.1	2.5	2.8	
Sm	3.2	14.6	4.5	2.43	4.5	15.3	6.9	4.57	11.4	8.5	11.3	4.4	6.7	5.7	9.5	
2SE	1.0	1.3	2.1	0.65	1.1	1.2	1.5	0.84	1.3	2.1	1.3	1.5	1.3	3.2	1.5	
Eu	0.48	1.99	0.32	0.56	0.41	1.72	0.82	0.62	1.28	0.96	1.39	0.35	0.59	0.62	1.34	
2SE	0.17	0.22	0.20	0.14	0.13	0.32	0.31	0.13	0.26	0.26	0.26	0.16	0.22	0.53	0.19	
Gd	14.1	52.8	13.2	15.6	20.5	60.3	26.2	20.5	46.4	38.0	45.2	11.2	19.4	32.6	26.0	
2SE	2.6	3.9	4.5	2.8	2.1	8.2	2.2	2.1	4.1	6.5	3.0	3.3	4.9	6.9	2.8	
Tb	4.41	15.7	4.4	5.8	6.03	17.7	8.16	6.23	12.9	11.4	13.11	4.4	6.50	11.7	7.5	
2SE	0.41	1.1	1.4	1.0	0.57	1.4	0.74	0.48	1.2	2.0	0.64	1.4	0.95	2.5	1.2	
Dy	55.6	175.0	61	66	79.0	205	97.3	76.4	142.2	132	157.5	49	70.1	146	67.5	
2SE	2.1	9.7	19	11	7.6	16	7.4	3.5	7.1	20	7.1	13	9.5	19	6.6	
Ho	20.0	57.4	24.1	23.8	26.0	66.8	33.4	26.9	50.8	44.4	51.9	16.0	26.7	56.7	22.9	
2SE	1.2	2.7	6.8	3.2	1.8	4.1	2.3	1.2	3.0	6.3	2.4	3.2	3.1	5.6	2.9	
Er	79.7	229	111	94	105.8	253	130.9	111.4	210	176	202.1	70	120	269	95	
2SE	3.8	11	28	11	6.5	25	5.9	3.7	11	24	9.2	14	12	16	11	
Tm	17.7	47.0	26.6	21.2	23.0	53.8	27.7	22.94	40.6	37.6	42.3	14.9	24.3	57.1	18.6	
2SE	1.4	1.9	6.2	2.3	1.6	4.0	1.4	0.79	1.5	5.2	1.7	2.4	2.6	2.3	2.4	
Yb	143.0	361	239	173	195	437	237	201.7	360	293	345	133	217	520	161	
2SE	3.9	17	54	17	10	30	17	7.8	11	41	15	20	19	13	16	
Lu	29.7	71.9	53	33.9	38.9	83.0	45.5	39.3	65.9	59.5	66.9	25.4	43.9	103.2	31.9	
2SE	1.6	3.5	11	3.4	1.5	8.7	2.5	1.4	3.5	7.7	2.7	2.9	3.7	2.4	3.2	
Hf	7410	8849	9954	7093	7862	9889	8418	7606	7439	9251	7480	8835	8126	12539	8263	
2SE	251	372	219	246	245	1020	341	177	148	595	243	211	304	666	343	
Th	109.4	249	203	95	165.2	327	161.4	110.5	242.0	202	253	108	186	517	138	
2SE	3.4	14	69	12	7.2	26	5.7	6.3	7.5	36	11	14	17	23	12	
U	87.8	155.3	396	71.9	117.3	181	100.5	81.6	142.3	120	143.3	274	239.0	752	235	
2SE	2.2	5.4	90	5.8	3.2	17	2.5	3.0	2.9	17	4.9	19	8.1	52	21	
Th/U	1.25	1.60	0.51	1.32	1.41	1.81	1.61	1.35	1.70	1.68	1.77	0.40	0.78	0.69	0.59	
Ti-in-Zr	786	758	658	771	824	809	811	778	813	814	789	648	676	689	710	
Ti-in-Zr (corr)	856	828	728	841	894	879	881	848	883	884	859	718	746	759	780	
Ti-in-Zr (corr2)	904	870	748	887	952	933	935	894	938	939	908	748	782	799	824	
Date (Ma)	2319	2318	2319	U-Pb	2319	2318	2327	2321	2322	2322	2323	2328	2320	2301	2329	
2σ	14	14	13	scrn	13	13	14	14	13	13	14	13	13	13	13	

Session	Mar 21 2024	Dec 6 2021													
Sample ID	19N07E										21BN52B				
Spot ID	11-1	5-1	3-1	4-2	16-1	30-1	6-1	26-1	23-1	18-1	1-1	5-1	6-1	31-1	6-2
Class	ign	inhrt	inhrt	inhrt	inhrt	ign									
P	639	661	519	651	589	548	664	730	878	891	217	299	162	138	105
2SE	166	12	35	24	56	77	15	70	37	39	10	29	12	11	8
Ca	694	525	196		217	448				223	129		720		
2SE	229	132	88		73	113				116	117		168		
Ti	8.0	8.97	9.35	9.5	9.5	10.9	13.1	13.1	14.7	14.7	20.1	7.5	22.7	8.3	18.0
2SE	1.7	0.94	0.71	1.5	1.4	1.0	1.5	1.4	1.4	3.0	2.0	3.7	3.4	2.1	3.1
La	1.80	0.72	0.010	0.116	5.21	3.87	1.29	0.35	0.94	0.70	1.62	0.22	4.11		0.033
2SE	0.80	0.12	0.005	0.016	1.37	0.97	0.28	0.18	0.21	0.29	0.24	0.10	0.56		0.025
Ce	69.4	41.6	23.4	40.7	80.8	76.1	61.3	39.7	51.0	74.3	21.5	21.7	47.4	13.41	3.52
2SE	8.3	1.8	0.9	2.2	7.3	10.1	2.6	1.5	3.6	5.1	1.5	4.7	3.1	0.62	0.18
Pr	1.89	0.60	0.16	0.56	6.1	4.5	1.70	0.81	1.68	1.45	1.26	0.122	4.23	0.079	0.168
2SE	0.14	0.11	0.03	0.13	1.5	1.2	0.33	0.17	0.34	0.24	0.26	0.064	0.26	0.027	0.037
Nd	14.4	5.72	2.87	8.5	41.2	31.0	15.5	9.93	13.3	18.0	9.1	0.94	26.8	1.37	2.79
2SE	3.5	0.51	0.50	1.3	9.8	6.5	2.4	0.70	1.7	2.4	1.9	0.51	2.3	0.17	0.36
Sm	13.8	6.36	4.91	10.9	31.3	28.5	16.0	13.92	15.5	25.4	6.70	1.88	11.91	2.26	4.40
2SE	6.0	0.40	0.72	1.0	3.3	4.9	1.9	0.96	1.6	2.0	0.70	0.50	0.88	0.17	0.35
Eu	1.50	0.525	0.523	1.07	2.96	2.61	1.64	1.54	1.19	2.26	1.88	0.55	5.27	0.524	0.119
2SE	0.48	0.083	0.089	0.17	0.44	0.34	0.27	0.17	0.19	0.41	0.26	0.13	0.26	0.066	0.029
Gd	67.7	27.9	25.4	47.2	87.1	81.2	53.6	61.5	57.0	116.9	21.0	7.6	27.5	10.44	11.44
2SE	31.5	1.3	2.9	3.6	5.4	7.2	3.3	1.7	4.2	3.4	1.6	1.1	1.6	0.91	0.66
Tb	22.3	9.65	8.16	15.49	23.1	23.0	16.09	19.08	17.76	36.0	5.57	2.56	6.19	3.11	1.95
2SE	9.8	0.32	0.78	0.71	1.5	1.8	0.58	0.50	0.80	1.4	0.27	0.34	0.59	0.18	0.13
Dy	256	109.7	89.8	170	230	227	173.6	216.7	195.1	390	63.9	30.0	61.5	36.5	12.95
2SE	105	1.6	6.8	13	11	12	3.7	7.2	8.5	13	1.9	2.3	4.2	2.7	0.62
Ho	91	40.8	34.5	63.3	77.5	75.3	61.7	79.4	67.2	136.5	23.8	12.15	21.72	14.83	2.60
2SE	33	1.3	2.2	4.7	3.8	3.5	1.6	2.2	4.7	3.8	1.1	0.49	0.84	0.46	0.17
Er	404	191	151.7	282	324	304	267.3	352	292	578	117.1	70.7	113.3	72.0	7.76
2SE	131	10	9.1	15	11	11	4.1	11	18	19	4.9	1.5	4.5	3.3	0.47
Tm	77	38.9	29.1	51.0	62.4	57.8	51.3	67.1	54.9	105.6	25.5	18.7	29.0	16.38	1.151
2SE	20	3.0	1.6	3.5	2.4	2.4	1.7	2.1	3.6	2.4	1.1	1.1	1.7	0.66	0.088
Yb	687	356	253	441	555	492	438	575	476	887	247	210	326	165.4	7.97
2SE	148	33	12	33	23	16	17	20	30	31	11	14	17	6.6	0.56
Lu	131	73.6	49.0	83.7	108.7	87.0	81.9	106.6	87.4	161.5	54.6	53.0	79.0	36.6	1.19
2SE	24	8.4	2.2	6.2	3.0	2.4	2.6	4.0	5.9	2.8	2.6	3.7	6.1	1.6	0.12
Hf	12211	10054	8146	7398	11700	9814	9953	10287	10029	10381	7277	8637	11668	7655	10258
2SE	2331	684	309	115	453	533	525	592	561	489	230	482	331	187	316
Th	842	387.9	204	524	582	517	538	551	443	1171	90.8	105	82.0	100.7	20.0
2SE	373	7.5	18	48	46	36	16	72	33	34	6.1	21	6.0	4.1	3.6
U	670	516	152.5	354	536	364	426	326	326	635	190	359	303	234.0	104.9
2SE	67	67	7.5	19	21	15	34	27	16	20	12	45	28	8.8	2.0
Th/U	1.26	0.75	1.34	1.48	1.09	1.42	1.26	1.69	1.36	1.84	0.48	0.29	0.27	0.43	0.19
Ti-in-Zr	725	736	739	741	741	754	772	772	783	783	816	720	829	728	804
Ti-in-Zr (corr)	795	806	809	811	811	824	842	842	853	853	886	790	899	798	874
Ti-in-Zr (corr2)	844	856	861	863	863	879	902	902	917	917					
Date (Ma)	2301	2301	2324	2334	2303	2310	2307	2332	2312	2316	2520	2509	2668	2509	2388
2σ	13	12	13	13	13	13	12	13	13	12	13	13	13	13	13